

# **Miocene Stratigraphy**

## **An Integrated Approach**

**A. Montanari  
G.S. Odin  
R. Coccioni  
(Editors)**

---

**Developments in Palaeontology  
and Stratigraphy**

**15**

---

**Elsevier**

# Miocene Stratigraphy

## An Integrated Approach

the volume has been prepared under the aegis of the  
**Subcommission on Geochronology**



which is a body of the  
**International Commission on Stratigraphy**



itself pertaining to the  
**International Union of Geological Sciences**



## **FURTHER TITLES IN THIS SERIES**

1. A.J. Boucot  
EVOLUTION AND EXTINCTION RATE CONTROLS
2. W.A. Berggren and J.A. van Couvering  
THE LATE NEOGENE - BIOSTRATIGRAPHY, GEOCHRONOLOGY AND  
PALEOCLIMATOLOGY OF THE LAST 15 MILLION YEARS IN MARINE  
AND CONTINENTAL SEQUENCES
3. L.J. Salop  
PRECAMBRIAN OF THE NORTHERN HEMISPHERE
4. J.L. Wray  
CALCAREOUS ALGAE
5. A. Hallam (Editor)  
PATTERNS OF EVOLUTION, AS ILLUSTRATED BY THE FOSSIL RECORD
6. F.M. Swain (Editor)  
STRATIGRAPHIC MICROPALAEONTOLOGY OF ATLANTIC BASIN AND  
BORDERLANDS
7. W.C. Mahaney (Editor)  
QUATERNARY DATING METHODS
8. D. Janóssy  
PLEISTOCENE VERTEBRATE FAUNAS OF HUNGARY
9. Ch. Pomerol and I. Premoli-Silva (Editors)  
TERMINAL EOCENE EVENTS
10. J.C. Briggs  
BIOGEOGRAPHY AND PLATE TECTONICS
11. T. Hanai, N. Ikeya and K. Ishizaki (Editors)  
EVOLUTIONARY BIOLOGY OF OSTRACODA. ITS FUNDAMENTALS  
AND APPLICATIONS
12. V.A. Zubakov and I.I. Borzenkova  
GLOBAL PALAEOCLIMATE OF THE LATE CENOZOIC
13. F.P. Agterberg  
AUTOMATED STRATIGRAPHIC CORRELATION
14. J.C. Briggs  
GLOBAL BIOGEOGRAPHY

*Developments in Palaeontology and Stratigraphy, 15*

# **Miocene Stratigraphy**

## **An Integrated Approach**

Edited by

**A. Montanari**

*Osservatorio Geologico di Coldigioco, Frontale di Apero, Italy*

**G.S. Odin**

*Université Pierre et Marie Curie, Paris, France*

**R. Coccioni**

*Università degli Studi, Urbino, Italy*



1997

ELSEVIER

Amsterdam – Lausanne – New York – Oxford – Shannon – Tokyo

ELSEVIER SCIENCE B.V.  
Sara Burgerhartstraat 25  
P.O. Box 211, 1000 AE Amsterdam, The Netherlands

ISBN:0-444-82498-7

© 1997 Elsevier Science B.V. All rights reserved.

No part of this publication may be reproduced, stored in a retrieval system or transmitted in any form or by any means, electronic, mechanical, photocopying, recording or otherwise, without the prior written permission of the publisher, Elsevier Science B.V., Copyright & Permissions Department, P.O. Box 521, 1000 AM Amsterdam, The Netherlands.

Special regulations for readers in the USA. This publication has been registered with the Copyright Clearance Center Inc. (CCC), 222 Rosewood Drive Danvers, MA 01923. Information can be obtained from the CCC about conditions under which photocopies of parts of this publication may be made in the USA. All other copyright questions, including photocopying outside of the USA, should be referred to the copyright owner, Elsevier Science B.V., unless otherwise specified.

No responsibility is assumed by the publisher for any injury and/or damage to persons or property as a matter of products liability, negligence or otherwise, or from any use or operation of any methods, products, instructions or ideas contained in the material herein.

This book is printed on acid-free paper.

Printed in The Netherlands

## FOREWORD

This volume results from the enthusiastic involvement of Alessandro Montanari and Rodolfo Coccioni in the geology of the Italian Apennine area. This region is exceptional due to the presence of pelagic sediments deposited in quiet environments together with volcanic explosive activity which is the source of frequent interbedded volcanoclastic layers. These features make the area very suitable for documenting the geological history through the application of a multi-faceted approach that is the base of modern integrated stratigraphy.

The 'Miocene Project' has a great deal in common with stratigraphic geochronology, a subject in which I am particularly involved as the leader of the Subcommittee on Geochronology of the International Commission on Stratigraphy. For this reason and for having collaborated in a similar research project in the past — the Eocene/Oligocene boundary — Alessandro and Rodolfo asked for my collaboration in this project.

In this volume, I have been careful to follow certain rules. These rules result from my involvement in the search for establishing a unified 'calendar' of the historical geology, which is the main object of chronostratigraphy. This 'calendar' is a succession of Stages and groups of Stages; the latter are conventional units which combine empirical observations with subjective choices both of which need rigor if they are to be meaningful and long-lived.

### *The importance of historical stratotypes*

In my view, the use of the *Global Stratotype Section and Point* (GSSP) concept supported by the International Commission on Stratigraphy for siting Stage-boundaries is not an attempt to provide different definitions of units; these units usually exist and have been defined, although imperfectly, by their *historical stratotypes*. These are bodies of rocks containing stratigraphical signals of different type. The role of the GSSPs is to fix more precisely the fuzzy or multiple definitions of the Stage boundaries. The precision required, and attainable, is on the scale of about tens of ka in the Miocene.

Hence, chronostratigraphic units can be regarded as conventional units based on real bodies of rocks and the boundaries between them may be denoted by an error bar which corresponds to the 'thickness' of the boundary. Today, it is necessary that this thickness is reduced to the resolution obtainable by the best stratigraphical tools.

### *How to attain precision at the boundaries?*

GSSPs are designed for achieving unique and precise boundary definitions. Essentially, as the historical stratotypes, GSSPs are points which provide a local time horizon that by extrapolation may allow the recognition of an instant of geological history. Their position has to be selected by correlation, in reasonable consistency with the historical stratotypes. Their characterization must involve two factors in this order of priority, the

easiest correlation potential from a particular section and the best possible obtainable precision. The first factor is mostly determined by biostratigraphical constraints of unequivocal character; the second by lithostratigraphical and physico-chemical constraints usually of a more equivocal character. In this volume, the problem we have dealt with is to document the first point using both biostratigraphy and geochronology, in order to propose useful sections for future siting of GSSPs.

Physico-chemical data have also been considered for more precise characterization, though with less success. Additional search would still be necessary to achieve a better resolution. This resolution has ultimately to become better than the potential diachronism of the biostratigraphic markers and the current uncertainty linked to the analytical calibration of the geochronologically derived numerical ages.

### *Chronostratigraphy and biostratigraphy*

I asked the volume contributors to pay particular attention to distinguishing between the conventional and the real nature of the chronostratigraphic units, and the correlation criteria used for the recognition of the boundaries of those units. It is difficult to explain the need to avoid the confusion between any particular criterion useful for correlation and the actual, fundamentally 'lithological', definition of a boundary. One solution is to avoid the temptation to make a boundary correspond to any particular criterion which then tends to become 'the' magic criterion. The preference for multiple approaches at GSSPs is recommended by the International Commission on Stratigraphy. Multiple overlapping criteria also become necessary if a single magic criterion is rejected in favour of a set of bracketing signals that characterize a GSSP.

The problem mostly concerns biological signals. I have tried to convince colleagues that biological signals are not accurate time markers at the scale that we now deem to be necessary (high resolution  $\leq 20$  ka). This requires that chronostratigraphic units should avoid a definition at, or approximation with, the known location of a single biosignal in a section. In terms of high resolution, the location of biological signals in the field is a characteristic of a section which may or may not be widespread to other sections.

The discussion may be extended to biozones, especially those defined by first or last occurrences. It is not uncommon to see in textbooks and even in research papers that, following Eras, Periods, Epochs and Ages (Stages) the next finer time subdivision will be the biozone. This is fundamentally incorrect: the nature of units is different, the coincidence of limits between units in the two systems of subdivision is not necessary, and I dare say, not desirable. I would like to propose a relevant comparison. Chronostratigraphic units are like centuries in the occidental calendar; the biozones are like the reigns of sovereigns or dynasties. The former are conventional and useful for a number of geologists (chronostratigraphic units)/peoples (centuries). The later are particular to a section or a basin (biozones)/country (reigns). Centuries cannot be subdivided in reigns, and the limits of these two kinds of intervals do not coincide.

In short, avoiding confusion between biostratigraphic and chronostratigraphic subdivisions is mandatory for a precise definition and correct use of the Stage names. The best way to avoid such a confusion is to disconnect the limits of the two kinds of units. The data reported in this volume show that the historical definitions of Stages do not coincide with later established biozonal subdivisions useful for long-distance correlation.

*The global character of our search*

I have encouraged the enlargement of the initial number of studies (from the Northern Apennines), to strive for a global extent that chronostratigraphic subdivisions must approach. My colleagues and I were lucky to meet interested geologists working in other basins, countries, and continents; but application of our approach to other sections and basins still has to be considered even though this volume has reached its last stage toward publication.

*Geochronology in stratigraphy*

Proposals have been made during the last decade to circumvent the great difficulty of documentation of the geological time scale by focusing on physically measured ages. Mathematical treatment of data (the use of chronograms), magneto-kilometric interpolation (hypothesis of constant sea-floor spreading rate), and astrochronologic approaches have been used to propose 'reliable' age models. The experience shows that: (1) in absence of enough data, a common occurrence, mathematical treatment is not always useful to derive meaningful numbers; (2) extrapolation–interpolation procedures may lead to incorrect numbers; (3) real progress for such efforts are better based on data acquisition rather than on mathematical or modelling criteria.

Let us have a look at two examples. As early as in 1975, I emphasized (Odin, *Doct. Thesis*) that an age of 37–38 Ma (Harland et al., 1964; Palmer, 1983; and later magneto-kilometrically derived products) was too old for the Eocene/Oligocene boundary: an age at 34 Ma based on geochronological data (Odin, 1982; Odin and Odin, 1990) was proposed. This was independently supported by Glass and colleagues who dated Late Eocene North American tektites (Glass et al., 1986). But the old age was maintained in some popular syntheses favouring the interpolation approach. An extremely pernicious effect resulted from this dogmatic old age. A significant number of ages including excellent K–Ar and Rb–Sr ones at about 34 Ma for Late Eocene biotite separates was published by Montanari et al. (1985). Instead of using this set of data to document the young age favoured by Glass or myself, the authors initially preferred to question the stratigraphy of the dated section at Massignano and suggested an intermediate age at 35.4 Ma based on a single level (later shown to be problematic). I convinced Alessandro to reconsider the question and we undertook a new geochronological study. This led us to propose the section at Massignano for locating the GSSP of the Eocene/Oligocene boundary with a newly documented age at  $33.7 \pm 0.5$  Ma (Odin et al., 1991) in agreement with previous data interpreted independently from the extant time scales.

The second example concerns the Tortonian/Messinian boundary. All time scales published before 1992 have considered an age of about 6.5 Ma for this boundary. Mathematical calculation, interpolation–extrapolation, and astrochronologic approaches did not question this number (poorly constrained with direct measurements). The pioneer work by Vai et al. (1993) has shown that this age was more than 10% too young; several contributions in this volume confirm this fact.

The indirect approaches have failed to show their potential of predictability.

It may appear that the real age of this or that boundary is not important: we need only to refer to a common scale. However, the incorrect estimate of the age of the two



boundaries discussed above, particularly in the case of the Eocene/Oligocene boundary, has led to an important problem for continental geologists. In North America, the stratigraphy of the Land Mammal Ages was documented with geochronologic data, but in Europe the continental fauna was correlated to marine Stages the age of which was taken from current and biased numerical time scales. In this situation, the so-called 'Grande Coupure' at the Eocene/Oligocene boundary was supposed at a different time in the two palaeogeographic domains: intercontinental correlations resulted in artificial 'diachroneity' of the evolution of mammals. The problem is only resolved when the 3 to 4 Ma younger age has finally been agreed for the boundary. However, for the past 15 years, intercontinental correlation remained incorrect partly because priority for geochronological ages has not been rationally applied at early stage.

In this foreword I wished to demonstrate that geochronology is a necessary and integral discipline of stratigraphy. Search for application of this approach must be a priority because indirect approaches are simply subjective estimates, their use being realized only after they have been tied to a numerical time scale.

Concerning the question of time scale calibration, the main problem in the correlation between the two complementary approaches (geochronological documentation and modelling for 'continuous' scales) is commonly based on the misunderstanding of the actual meaning of the basic numerical age data. The most difficult exercise in geochronology is not to obtain an age but to correctly estimate and express a realistic geological uncertainty on the calculated analytical age. Some common language and general explanations are proposed at the end of this volume and I have attempted to suggest a unified expression of age uncertainties that, hopefully, will appear obvious to users of the information gathered in this volume.

These were some points which have been debated during the putting together of this volume. We intended to prepare more than just a simple collection of contributions with some sort of unified direction, and to influence the funding of this basic knowledge of historical geology, i.e., stratigraphy.

After many months spent in this pursuit, I hope that we have achieved at least a part of the goal of presenting an 'Integrated Approach to Miocene Stratigraphy'. We have tried.

G.S. Odin

*Chairman Subcommission on Geochronology  
Paris, 20 June 1996*

### *Acknowledgements*

This text has benefited from interesting discussions with and significant formal improvement by Silvia Gardin and Bilal Haq.

### *Additional references*

- Glass, B.P., Hall, C.M. and York, D., 1986.  $^{40}\text{Ar}/^{39}\text{Ar}$  laser probe dating of North American tektite fragments from Barbados and the age of the Eocene–Oligocene boundary. In: G.S. Odin (Editor), Calibration of the Phanerozoic Time Scale. Chem. Geol. (Isot. Geosci. Sect.), 59: 181–186.
- Odin, G.S., 1975. De glaucouiarum constitutione origine aetateque. Thèse Doctorat d'État, Université P. et M. Curie, Paris, 250 pp.
- Odin, G.S. (Editor), 1982. Numerical Dating in Stratigraphy. John Wiley, Chichester, 1040 pp.

## PREFACE

At the end of the Miocene Columbus Project (MICOP) in Portonovo (Ancona, Italy, November 11–15, 1992), there was much satisfaction and excitement, among the 100 or so participants who attended the meeting, for the positive outcome of this international scientific workshop. The MICOP was promoted under the aegis of the Subcommission on Geochronology (S.O.G., Gilles Serge Odin, Chairman) of the International Union of Geological Sciences (I.U.G.S.), and organized by the editors of this volume. It was prompted when new data and insight about the geology and palaeontology of the Miocene Epoch started to emerge from the studies by numerous European, American, and Japanese researchers. In fact, the preliminary results presented in 50 original abstracts [Montanari, Coccioni and Odin (Editors), 1992] shed some light on the many intriguing aspects of this Epoch which witnessed such extraordinary events as the upheaval of the Alpine–Himalayan orogenesis, global climatic and environmental changes, the progressive closure of the western Tethys Ocean and consequent isolation of the Mediterranean Sea from the rest of the world's oceans, and ultimately, the appearance of hominids in Africa. In a few words, the Miocene represents the prelude to modern geologic times, a Renaissance in the history of the Earth, when the biologic and physical environments of the planet reached the familiar profiles of today's world.

The positive outcome of the MICOP encouraged the organizers to propose the publication of two special issues, one that would have collected the scientific contributions relevant to the regional stratigraphy of the Miocene, and the other, in the form of a book, mainly focused on the general stratigraphic attributions of this Epoch. Our optimism, backed by the success of the MICOP workshop, led us to believe that in less than a couple of years we would have accomplished these tasks.

The publication of a special issue of the *Giornale di Geologia* entitled 'Miocene Stratigraphy of Italy and Adjacent Areas' (Coccioni, Montanari, and Odin, 1994b) was punctually accomplished about two years after the MICOP, and succeeded in documenting various aspects of Miocene regional stratigraphy of Italy and surrounding areas.

For the second issue, we engaged in the ambitious task of introducing, in the most exemplar and exhaustive way as possible, the concept of integrated stratigraphy in general, and the Miocene Integrated Stratigraphy in particular. By integrated stratigraphy, we concordantly intended the direct application of geochronology to biostratigraphically defined sedimentary sequences which could be characterized also with other time-relative tools (i.e., lithostratigraphy, magnetostratigraphy, and chemostratigraphy). The works presented at the MICOP conference showed that in Italy, Spain, and Japan there are, in fact, Miocene sedimentary sequences suitable for the application of integrated stratigraphy (i.e., marine, fossiliferous, continuous sections containing datable volcanoclastic layers). In short, integrated stratigraphy is an interdisciplinary team effort which can lead to a more reliable and cross-checked recognition of the time relations between samples collected vertically and horizontally, and provides the means for confident correlation of geological and palaeobiological events at a global scale.

Unfortunately, longer time than expected was required to accomplish the publication of this volume. As senior editor, and therefore responsible for this delay, I wish to address my personal apologies to those contributors who punctually submitted their completed works before the proposed deadline of 1994, for having to wait another three years to see their articles in print. On the other hand, this delay has been inevitable for two main reasons. One is that many of the results presented at the MICOP conference were preliminary, and required further (time-consuming and painstaking) analytical work by interdisciplinary and international research teams before being submitted in their definitive and acceptable forms. The second reason is that the book could not be launched as an unfinished ship, but required a non-trivial editorial effort to ensure internal consistency (both formal and substantial), and cross-checked verification among the innumerable and interdisciplinary data documented by 80 authors in 37 original contributions, and corroborated by 777 cited references.

Finally, I would like to stress that this volume is not simply a black on white documentation of the work done by individual participants in an international scientific workshop, but it represents a genuine team achievement of the kind that modern science needs for its fundamental process of dynamic progress. Nor it is an issue that is meant to be more or less absorbed and then archived in a bookshelf as a closed case file, but rather an honest starting point, and at the same time a stimulus, for further studies on the still unresolved mysteries of the fascinating Miocene Epoch.

#### *Acknowledgements*

I would like to thank my colleagues, friends, and co-editors Gilles Serge Odin and Rodolfo Coccioni for their firm commitment and faithful dedication in working as a team on the complex, costly, and sometime nerve-racking editorial work for this volume.

A special thanks goes to Walter Alvarez, and Bernard Beaudoin for having financially supported the editorial work which was mostly carried out at the Geological Observatory of Coldigioco. I also would like to thank Tanya Atwater, Kevin Stewart, Paul Myrow, July Maxon, Paul and Debbie Kopsick, the geology students of the Keck Program, and the students of the Carleton College who in the summer 1995 helped revising, often with useful critical remarks, most of the manuscripts of this volume.

Alessandro Montanari  
*Coldigioco, 19 May, 1996*

## LIST OF CONTRIBUTORS

- Alvarez, Walter*, Department of Geology and Geophysics, University of California, Berkeley, CA 94720, U.S.A. (permanent), and Osservatorio Geologico di Coldigioco, 62020 Frontale (MC), Italy (summer)
- Amorosi, Alessandro*, Università degli Studi di Bologna, Dipartimento di Scienze Geologiche, Via Zamboni, 67, I-40127 Bologna, Italy
- Aubry, Marie-Pierre*, Laboratoire de Géologie du Quaternaire, CNRS Luminy, Case 907, F-13288 Marseille Cedex 9, France
- Beaudoin, Bernard*, Ecole des Mines, CGGM Sedimentologie, 35, rue Saint Honoré, 77305 Fontainebleau Cedex, France
- Bice, David M.*, Department of Geology, Carleton College, Northfield, MN 55057, U.S.A. (permanent), and Osservatorio Geologico di Coldigioco, Italy (summer)
- Biolzi, Milena*, Istituto di Geologia e Paleontologia, Università di Parma, Viale della Scienze, 78, I-43100 Parma, Italy
- Bonhomme, Patricia*, Centre des Faibles Radioactivités, C.N.R.S.–C.E.A., Avenue de la Terrasse, 91198 Gif-sur-Yvette Cedex, France
- Borsetti, Anna Maria*, Istituto per la Geologia Marina del C.N.R., Via Gobetti 101, I-40127 Bologna, Italy
- Bossio, Alessandro*, Dipartimento di Scienze della Terra, Università di Pisa, Via Santa Maria, 53, 56127 Pisa, Italy
- Cahuzac, Bruno*, Laboratoire de Recherches et Applications Géologiques, Université Bordeaux I, 351, Cours de la Libération, 33405 Talence Cedex, France
- Canudo, José Ignacio*, Departamento de Ciencias de la Tierra, Facultad de Ciencias, Universidad, 50009 Zaragoza, Spain
- Capo, Rosemary*, California Institute of Technology, Division of Geological and Planetary Sciences, Pasadena, CA 91125, U.S.A.
- Carbonnel, Gilles*, Centre des Sciences de la Terre, URA 11, Université Claude Bernard Lyon 1, 43 Bd. du 11 Novembre 1918, F-69622 Villeurbanne Cedex, France
- Cati, Franco*, Dipartimento di Scienze Geologiche, Via Zamboni 65, I-40127 Bologna, Italy
- Chan, Lung S.*, Department of Geology, University of Wisconsin, Eau Claire, WI 54701, U.S.A.
- Channell, Jim*, Department of Geology, University of Florida, 1112 Turlington Hall, Gainesville, FL 32611, U.S.A.
- Cita, Maria Bianca*, Dipartimento di Scienze della Terra, Università degli Studi, Via Mangiagalli, 34 20133 Milano, Italy
- Clauzon, Georges*, Institut de Géographie, URA 903 CNRS, Université de Provence, 29 avenue R. Schuman, 13621 Aix-en-Provence Cedex, France
- Coccioni, Rodolfo*, Istituto di Geologia, Università degli Studi, Località Crocicchie, 61029 Urbino, Italy

- Colalongo, Maria Luisa*, Dipartimento di Scienze della Terra e geologico-ambientali dell'Università di Bologna, Via Zamboni 67, I-40127 Bologna, Italy
- Corfield, Richard*, Department of Earth Sciences, University of Oxford, Parks Road, Oxford OX1 3PR, England
- Cosca, Michael*, Institut de Minéralogie, Université, BFSH2, CH-1015 Lausanne, Switzerland
- Cuenca Bescós, Gloria*, Departamento de Ciencias de la Tierra, Facultad de Ciencias, Universidad, 50009 Zaragoza, Spain
- D'Atri, Anna*, Dipartimento di Scienze della Terra, Via Accademia delle Scienze 5, 10123 Torino, Italy
- De Grandis, Giuliana*, Istituto di Geocronologia e Geochimica Isotopica, CNR, Via C. Maffi, 56127 Pisa, Italy
- Deino, Alan*, Berkeley Geochronology Center, 2453 Ridge Road, Berkeley, CA 94709, U.S.A.
- Demarcq, Gérard*, Centre des Sciences de la Terre, URA 11, Université Claude Bernard Lyon 1, 43 Bd. du 11 Novembre 1918, F-69622 Villeurbanne Cedex, France
- DePaolo, Donald J.*, Department of Geology and Geophysics, University of California, Berkeley, CA 94720, U.S.A.
- Dercourt, Jean*, Laboratoire de Stratigraphie, Université P. et M. Curie, 4, Place Jussieu, 75252 Paris Cedex, France
- Emmanuel, Laurent*, Centre des Sciences de la Terre et URA 157, Univ. de Bourgogne, 6 Bd. Gabriel, F-21000 Dijon, France
- Fornaciari, Eliana*, Dipartimento di Geologia e Paleontologia, Università degli Studi Via Giotto 1, 35137 Padova, Italy
- Gautier, François*, Institut des Sciences de l'Evolution, URA 327 CNRS, Université Montpellier II, 34095 Montpellier Cedex 5, France
- Gelati, Romano*, Dipartimento di Scienze della Terra, Università degli Studi, Via Mangiagalli, 34 20133 Milano, Italy
- Gnaccolini, Mario*, Dipartimento di Scienze della Terra, Università degli Studi, Via Mangiagalli, 34 20133 Milano, Italy
- Hunziker, Johannes C.*, Institut de Minéralogie, Université, BFSH2, CH-1015 Lausanne, Switzerland
- Iaccarino, Silvia*, Istituto di Geologia, Università degli Studi, Viale delle Scienze 78, 43100 Parma, Italy
- Kruger, Michael*, Department of Geology, Southern Illinois University, Carbondale, IL 62901, U.S.A.
- Lago, M.*, Departamento de Ciencias de la Tierra, Facultad de Ciencias, Universidad, 50009 Zaragoza, Spain
- Laurenzi, Marinella A.*, Istituto di Geocronologia e Geochimica Isotopica, CNR, Via C. Maffi, 56127 Pisa, Italy
- Londeix, Laurent*, Laboratoire de Géologie et Océanographie, URA 197, Université de Bordeaux I, Avenue des Facultés, 33405 Talence, France
- Lundblad, Steve*, Department of Geology, CB#3315 University of North Carolina, Chapel Hill, NC 27599 3315, U.S.A.
- Martin-Perez, José Antonio*, Departamento de Geologia, Facultad de Ciencias, Universidad de Malaga, Malaga, Spain

- Mazzei, Roberto*, Dipartimento di Scienze della Terra, Università di Siena, Via della Cerchia 3, 53100 Siena, Italy
- Miculan, Pietro*, Dipartimento di Scienze Geologiche, Università di Bologna, via Zamboni 67, 40127 Bologna, Italy
- Monechi, Simonetta*, Dipartimento di Scienze della Terra, Università di Firenze, Via La Pira 4, 50121 Firenze, Italy
- Montanari, Alessandro*, Osservatorio Geologico di Coldigioco, 62020 Frontale di Apiro, Italy (permanent), and Ecole Supérieur des Mines, Paris
- Montenat, Christian*, Institut Géologique Albert-de-Lapparent (IGAL), Centre Polytechnique Saint-Louis 13, Boulevard de l'Hautail, F-95092 Cergy-Pontoise Cedex, France
- Mozzato, Cristina*, Dipartimento di Geologia e Paleontologia, Via Giotto 1, 35137 Padova, Italy
- Napoleone, Giovanni*, Dipartimento Scienze della Terra, Università di Firenze, Via G. La Pira 4, I-50121 Firenze, Italy
- Negri, Alessandra*, Dipartimento di Scienze dei Materiali e della Terra, Università degli Studi, Via delle Becce Bianche, I-60131 Ancona, Italy
- Oda, Motoyoshi*, Department of Earth Sciences, Kumamoto University, 2-39-1 Kurokami, Kumamoto 860, Japan
- Odin, Gilles S.*, Laboratoire de Géochronologie et Sédimentologie Océanique, Université P. et M. Curie, URA CNRS 1761, 4, Place Jussieu, Case 119A, F-75252 Paris Cedex 05, France
- Pasini, Giancarlo*, Istituto di Geologia Marina del C.N.R., Via P. Gobetti 101, I-40129 Bologna, Italy
- Pialli, Giampaolo*, Dipartimento di Scienze della Terra, Piazza dell'Università, 06100 Perugia, Italy
- Pini, Gian Andrea*, Università degli Studi di Bologna, Dipartimento di Scienze Geologiche, Via Zamboni, 67, I-40127 Bologna, Italy
- Poignant, Armelle*, Laboratoire de Micropaléontologie, URA 1761, Université P. et M. Curie, 4, Place Jussieu, 75252 Paris Cedex 05, France
- Portier, Eric*, École des Mines, CGGM Sédimentologie, 35, Rue Saint Honoré, 77305 Fontainebleau Cedex, France
- Pouyet, Simone*, Centre des Sciences de la Terre, URA 11, Université Claude Bernard Lyon 1, 43 Bd. du 11 Novembre 1918, F-69622 Villeurbanne Cedex, France
- Pujol, Claude*, Laboratoire de Géologie et Océanographie, URA 197, Université de Bordeaux I, Avenue des Facultés, 33405 Talence, France
- Renard, Maurice*, Département de Géologie Sédimentaire et URA CNRS 1761, Univ. P. et M. Curie, 4 Place Jussieu, F-75252 Paris Cedex 05, France
- Ringeade, Michel*, Laboratoire de Géologie et Océanographie, URA 197, Université de Bordeaux I, Avenue des Facultés, 33405 Talence, France
- Rio, Domenico*, Dipartimento di Geologia e Paleontologia, Università degli Studi, Via Giotto 1, 35137 Padova, Italy
- Rögl, Fred*, Naturhistorisches Museum Wien, Geol.-Paläont. Abteilung, Postfach 417, Burgring 7, A-1014 Wien, Austria
- Rörtzel, Reinhard*, Geologische Bundesanstalt, Postfach 154, Rasumofskygasse 23, 1031 Wien, Austria

- Saito, Kazuo*, Department of Earth Sciences, Yamagata University, 1-4-12, Koshi-rakawa, Yamagata 990, Japan
- Salvatorini, Gianfranco*, Dipartimento di Scienze della Terra, Università di Siena, Via della Cerchia 3, 53100 Siena, Italy
- Sandroni, Paolo*, Osservatorio Geologico di Coldigioco, 62020 Frontale di Apiro, Italy
- Serrano, Francisco*, Departamento de Geologia, Facultad de Ciencias Universidad de Malaga, Malaga, Spain
- Spezzaferri, Silvia*, Dipartimento di Scienze della Terra, Università degli Studi, Via Mangiagalli, 34 20133 Milano, Italy
- Stankiewicz, Arthur*, Department of Geology, Southern Illinois University, Carbondale, IL 62901, U.S.A.
- Steininger, Fritz F.*, Institut für Paläontologie, Universität Wien, Universitätsstr. 7/II, A-1010 Wien, Austria
- Suc, Jean-Pierre*, Institut des Sciences de l'Evolution, URA 327 CNRS, Université Montpellier II, 34095 Montpellier Cedex 5, France
- Takahashi, Masaki*, Geological Survey of Japan, 1-1-3 Higashi, Tsukuba, Ibaraki 305, Japan
- Tateo, Fabio*, Università degli Studi di Bologna, Dipartimento di Scienze Mineralogiche, Piazza di Porta San Donato 1, I-40127 Bologna, Italy
- Turpin, Laurent*, Centre des Faibles Radioactivités, C.N.R.S.-C.E.A., Avenue de la Terrasse, 91198 Gif-sur-Yvette Cedex, France
- Vai, Gian Battista*, Università degli Studi di Bologna, Dipartimento di Scienze Geologiche, Via Zamboni, 67, I-40127 Bologna, Italy
- Vigliotti, Luigi*, Istituto di Geologia Marina del CNR, Via Zamboni 65, 40127 Bologna, Italy
- Villa, Igor M.*, Istituto di Geocronologia e Geochimica Isotopica, CNR, Via C. Maffi 36, 56127 Pisa, Italy
- Vrielynck, Bruno*, Laboratoire de Stratigraphie, Université P. et M. Curie, CNRS URA 1761, 4, Place Jussieu, 75252 Paris Cedex, France
- Zevenboom, Daan*, Laboratory of Paleobotany and Palynology, University of Utrecht, Heidelberglaan 2, 3584 CS Utrecht, The Netherlands

# CONTENTS

Foreword . . . . .	v
Preface . . . . .	ix
List of Contributors . . . . .	xi
<b>Part A. The historical stratotypes . . . . .</b>	<b>1</b>
Chronostratigraphic units: historical stratotypes and global stratotypes . . . . .	3
<i>G.S. Odin</i>	
A1 The Aquitanian historical stratotype . . . . .	9
<i>A. Poignant, C. Pujol, M. Ringeade and L. Londeix</i>	
A2 The Burdigalian historical stratotype . . . . .	17
<i>A. Poignant, C. Pujol, M. Ringeade and L. Londeix</i>	
A3 The Burdigalian historical stratotype in the Rhodanian area . . . . .	25
<i>S. Pouyet, G. Carbonnel and G. Demarcq</i>	
A4 Sr isotope record in the area of the Lower Miocene historical stratotypes of the Aquitaine basin (France) . . . . .	33
<i>B. Cahuzac, L. Turpin and P. Bonhomme</i>	
A5 Langhian, Serravallian, and Tortonian historical stratotypes . . . . .	57
<i>D. Rio, M.B. Cita, S. Iaccarino, R. Gelati and M. Gnaccolini</i>	
A6 Calcareous plankton biostratigraphy of the Langhian historical stratotype . . . . .	89
<i>E. Formaciari, S. Iaccarino, R. Mazzei, D. Rio, G. Salvatorini, A. Bossio and B. Monteforti</i>	
A7 Planktonic foraminiferal biostratigraphy of the Tortonian historical stratotype, Rio Mazzapiedi–Castellania Section, northwestern Italy . . . . .	97
<i>P. Miculan</i>	
A8 The Messinian historical stratotype and the Tortonian/Messinian boundary . . . . .	107
<i>M.L. Colalongo and G. Pasini</i>	
A9 Proposal for the global stratotype section and point (GSSP) for the base of the Neogene (the Palaeogene/Neogene Boundary) . . . . .	125
<i>F.F. Steininger, M.P. Aubry, M. Biolzi, A.M. Borsetti, F. Cati, R. Corfield, R. Gelati, S. Iaccarino, C. Napoleone, F. Rögl, R. Rötzel, S. Spezzaferri, F. Tateo, G. Villa and D. Zeevenboom</i>	
A10 The Miocene/Pliocene boundary: present and future . . . . .	149
<i>J.-P. Suc, G. Clauzon and F. Gautier</i>	
<b>Part B. Geology of the two main study areas . . . . .</b>	<b>155</b>
B1 Miocene palaeogeography of the Tethys Ocean; potential global correlations in the Mediterranean . . . . .	157
<i>B. Vrielynck, G.S. Odin and J. Dercourt</i>	
B2 Tectonic setting of the Miocene northern Apennines: the problem of contemporaneous compression and extension . . . . .	167
<i>G. Pialli and W. Alvarez</i>	
B3 Geology, tectonics, and integrated stratigraphy potential of Japan . . . . .	187
<i>M. Takahashi and M. Oda</i>	



<b>Part C. Studies relevant to the Lower Miocene subseries</b> . . . . .	203
Introduction: the Lower Miocene . . . . .	205
<i>A. Montanari and R. Coccioni</i>	
C1 Integrated stratigraphy near the Oligocene/Miocene boundary in the Piedmont basin (Italy): biostratigraphy and geochronology . . . . .	209
<i>G.S. Odin, A. d'Atri, F. Tateo, M. Cosca and J.C. Hunziker</i>	
C2 Integrated stratigraphy (biostratigraphy and geochronology) of the Early Miocene sequence from the Emilian Apennines (Italy) . . . . .	221
<i>G.S. Odin, A. Amorosi, F. Tateo, R. Coccioni, M. Cosca, A. Negri, G.A. Pini and J.C. Hunziker</i>	
C3 Integrated stratigraphy of the Chattian to mid-Burdigalian pelagic sequence of the Contessa valley (Gubbio, Italy) . . . . .	249
<i>A. Montanari, D.M. Bice, R. Capo, R. Coccioni, A. Deino, D.J. DePaolo, L. Emmanuel, S. Monechi, M. Renard and D. Zevenboom</i>	
C4 Potential integrated stratigraphy of the Aquitanian to upper Burdigalian section at Santa Croce di Arcevia (NE Apennines, Italy) . . . . .	279
<i>R. Coccioni, A. Montanari, E. Fornaciari, D. Rio and D. Zevenboom</i>	
C5 Biostratigraphy and geochronology of a Miocene continental volcanoclastic layer from the Ebro basin, Spain . . . . .	297
<i>G.S. Odin, G. Cuenca Bescós, J.I. Canudo, M. Cosca and M. Lago</i>	
<b>Part D. Studies relevant to the Middle Miocene subseries</b> . . . . .	311
Introduction: the Middle Miocene . . . . .	313
<i>A. Montanari and R. Coccioni</i>	
D1 Integrated stratigraphy of the upper Burdigalian–lower Langhian section at Moria (Marche region, Italy) . . . . .	315
<i>A. Deino, J. Channell, R. Coccioni, G. De Grandis, D.J. DePaolo, E. Fornaciari, L. Emmanuel, M.A. Laurenzi, A. Montanari, D. Rio and M. Renard</i>	
D2 Potential integrated stratigraphy in the Langhian l'Annunziata section near Apiro (Marche region, Italy) . . . . .	343
<i>A. Montanari, R. Coccioni, E. Fornaciari and D. Rio</i>	
D3 Biostratigraphy and geochronology of an early Serravallian volcanoclastic layer from Sicily <i>G.S. Odin, P. Miculan, M. Cosca, F. Tateo, A. Amorosi and J.C. Hunziker</i>	351
D4 Potential integrated Middle Miocene stratigraphy in southeastern Spain . . . . .	363
<i>Ch. Montenat, F. Serrano and J.A. Martín-Perez</i>	
D5 The potential for integrated stratigraphic studies of Middle Miocene sequences in central Japan . . . . .	371
<i>M. Takahashi and M. Oda</i>	
D6 Radiometric age of the first occurrence of <i>Globigerina nepenthes</i> in the Tomioka sequence, central Japan . . . . .	381
<i>M. Takahashi and K. Saito</i>	
D7 Géochronologie de niveaux situés autour de l'apparition de <i>Globigerina nepenthes</i> au Japon et en Italie: âge de la limite Serravallien/Tortonien . . . . .	395
<i>G.S. Odin, M. Takahashi, R. Coccioni et M. Cosca</i>	

<b>Part E. Studies relevant to the Upper Miocene subseries</b> . . . . .	403
Introduction: the Upper Miocene . . . . .	405
<i>A. Montanari and R. Coccioni</i>	
E1 Integrated stratigraphy of the Middle to Upper Miocene pelagic sequence of the Cònero Riviera (Marche region, Italy) . . . . .	409
<i>A. Montanari, B. Beaudoin, L.S. Chan, R. Coccioni, A. Deino, D.J. DePaolo, L. Emmanuel, E. Fornaciari, M. Kruge, S. Lundblad, C. Mozzato, E. Portier, M. Renard, D. Rio, P. Sandroni and A. Stankiewicz</i>	
E2 Integrated stratigraphy of the late Tortonian Pieve di Gesso section (Romagna, Italy) . . . . .	451
<i>G.S. Odin, M. Cosca, F. Tateo, A. Negri, G.B. Vai and J.C. Hunziker</i>	
E3 Cyclostratigraphic estimate of the Messinian stage duration . . . . .	463
<i>G.B. Vai</i>	
E4 Calcareous nannofossil biostratigraphy and palaeomagnetism of the Monte Tondo and Monte del Casino sections (Romagna Apennine, Italy) . . . . .	477
<i>A. Negri and L. Vigliotti</i>	
E5 New radiometric datings bracketing the Tortonian/Messinian boundary in the Romagna potential stratotype sections (northern Apennines, Italy) . . . . .	493
<i>M.A. Laurenzi, F. Tateo, I.M. Villa and G.B. Vai</i>	
E6 Contribution to the geochronology of the Tortonian/Messinian boundary in the Faenza area (Romagna, Italy) . . . . .	521
<i>G.S. Odin, G.B. Vai, M. Cosca, F. Tateo and J.C. Hunziker</i>	
E7 Integrated stratigraphy of the Maccarone section, late Messinian (Marche region, Italy) . . . . .	531
<i>G.S. Odin, F. Ricci Lucchi, F. Tateo, M. Cosca and J.C. Hunziker</i>	
E8 Potential integrated Upper Miocene stratigraphy in southeastern Spain . . . . .	547
<i>Ch. Montenat and F. Serrano</i>	
E9 A review of geological, biostratigraphical, and geochronological studies of the Miura peninsula (central Japan) . . . . .	553
<i>K. Saito, C. Inoue and Y. Kanie</i>	
E10 Preliminary results and potential for integrated stratigraphy of the volcano-sedimentary sequence in the Boso peninsula, central Japan . . . . .	575
<i>M. Takahashi, M. Oda and E. Uchida</i>	
<b>Part F.</b> . . . . .	581
F1 Miocene geochronology: methods, techniques, and results . . . . .	583
<i>G.S. Odin, A. Deino, M. Cosca, M.A. Laurenzi and A. Montanari</i>	
F2 Chronostratigraphy of Miocene Stages: a proposal for the definition of precise boundaries . . . . .	597
<i>G.S. Odin, A. Montanari and R. Coccioni</i>	
References . . . . .	631
Author Index . . . . .	665
Paleontologic Index . . . . .	677
Geography and Geology Index . . . . .	683

This Page Intentionally Left Blank

**Part A**

**THE HISTORICAL STRATOTYPES**

This Page Intentionally Left Blank

*Introduction to Part A*

## **CHRONOSTRATIGRAPHIC UNITS: HISTORICAL STRATOTYPES AND GLOBAL STRATOTYPES**

G.S. Odin

### **DEFINITION OF CHRONOSTRATIGRAPHIC UNITS**

In agreement with common usage, the word Stage is used in this presentation both for the actual rocks deposited during an interval of time, and for the interval of time itself (sometimes called Age). Designation of Stages (and Ages) is the purpose of chronostratigraphy. Stages are the fundamental and smallest subdivisions used for most of the Phanerozoic (i.e., from Cambrian to Pliocene). Definition of these units is thus of primary interest for stratigraphers. The main purpose of this volume is to improve the knowledge and definition of the Stages for the Miocene Epoch.

Stages have been defined referring to a lithologic unit with particular palaeontologic content usually deposited in a shallow water shelf or platform environment usually rich in macrofossils. Therefore, a Stage is usually defined by a body of rocks with a characterizing fossil content. Where palaeontology and lithology were different at a given time over a broad area, different Stages were defined. The resulting chronostratigraphy has long been dependent on basal or broader palaeogeographic areas with difficulties when correlations had to be drawn over greater distances.

In Europe, the widely used subdivision for the Miocene Epoch comprises three sub-Epochs (Early, Middle, and Late), each divided into two Stages; the sequence is from older to younger: Aquitanian, Burdigalian, Langhian, Serravallian, Tortonian and Messinian. These six Stages were originally defined in three areas: the oldest two in Aquitaine (western France), the next three in the Piedmont region of northwestern Italy, and the youngest in the island of Sicily (southern Italy). Later, the Burdigalian Stage of Aquitaine (the lower portion of the Stage) has been supplemented with a type section in a fourth area: the Rhône Valley (higher portion of the Stage).

These historical definitions use bodies of rock for the definition of the Stages; in modern terms the Stages are defined by the various characteristics of a body of rock which can be used for correlation purposes: petrographical, chemical, physical and biological. This means that the Stages are defined by a *content* which is chronologically significant — as documented by numerical dating: geochronology. Their practical use is as wide as correlation can be made. This principle has to remain consistent and thus, the main definition of a Stage is a 'type section' (sometimes supplemented with annex sections) comprising rocks deposited during the main portion of time represented by the Stage itself.

In the last few decades, geologists have included consideration of a global practice when recommending chronostratigraphic conventions. In addition, a more precise definition than in previous time may now be useful — if not necessary — for these

conventional units because modern approaches sometimes allow a greatly improved resolution of time. With this purpose in mind, the Commission on Stratigraphy has recommended that historical stratotype sections be supplemented by a new concept aimed at defining precise boundaries between Stages. This concept is the Global Stratotype Section and Point (later abbreviated GSSP; Cowie et al., 1986).

Two aspects must be emphasized: in the preferred view supported here, (1) GSSP is aimed at giving additional information for supplementing historical stratotypes, and (2) it practically defines a boundary between two Stages and not particularly the base of the next Stage.

(1) The Stage definition must primarily — and always — be defined in terms of actual content since earth scientists are primarily concerned with the study of actual rocks. In this situation, the instant defined by a GSSP (or the interval of time defined between two GSSP) is not self-sufficient for defining a Stage: the latter must correspond — at least in part — to a geological object. In other words, one may consider that Stage boundaries are already defined by historical stratotypes but that they are at present rather poorly defined by these stratotypes, and must be improved with the use of the GSSP concept.

(2) The Stage boundary itself must be defined using changes in characteristics observed within a section. The priority given to the base of a Stage comes from an ancient concept of Stages still supported by some stratigraphers. They used the principle of historical stratotype and, in order to eliminate the real problem of imprecise Stage boundaries, they recommended an additional convention which was to select the Stage boundary at the base of the younger Stage in the historical stratotype. In this convention, everything located below the base of the historical stratotype must be accepted to be part of the preceding Stage. With this solution, it is clear that the term 'next Stage' is actually defined by actual rocks with a given geologic and/or palaeontologic content but the 'former Stage' is only theoretical, and concretely undefined due to the (common) sedimentary break located below the first rocks of the historical stratotype. Here again, the GSSP concept emphasizes the presence of concrete material (for both the older and younger Stages) for defining the basic units of chronostratigraphy.

If one accepts the above-proposed concepts, it must be emphasized that the aim of a study for proposal of a GSSP is not to change the definitions of Stages. GSSP must be located to be consistent with the previous definitions of the bracketing historical stratotypes.

In other words, the aim of this study is to elaborate Stages of global use defined by a combination of historical stratotypes and GSSP. In this situation, improvement of Stage definition using GSSP necessarily requires a good knowledge of the historical stratotypes, the use of the most recent stratigraphic tools in these classic sections, as well as the sections where GSSP are proposed to be located.

In agreement with this prerequisite, I have encouraged experts to summarize the classical data on what may be considered 'historical stratotypes', and to try to obtain additional information on these sections that are comparable to data from studies recently undertaken on potential GSSP sections.

Part A of this volume presents the data available from the four historical areas quoted in the beginning of this introduction: Aquitaine, Rhône Valley, Italian Piedmont, and Sicily, as well as from some nearby areas where additional data have been recently considered for Stage definitions. The authors were requested to present their data

following an organization and content similar to the one suggested for submission of GSSPs. These comprise ten points, not necessarily of equal importance, two of which concern access and study, four on the quality of the geological record, and four other points on the availability of correlation tools (adapted from Odin, 1992).

(1) *Accessibility*. The GSSP has to be accessible to investigators without politic or social restrictions, excessive effort or expense.

(2) *Permanent artificial marker*. A permanent artificial marker should highlight the GSSP in the outcrop to insure its easy identification, uniqueness, and constancy. Designation of an official responsible for preservation of the site is suggested.

(3) *Marine character*. Within the Miocene, GSSPs should be selected within a marine, pelagic depositional environment allowing correlations over large areas. Non-pelagic deposits may be more useful for some intervals of time, and the potential for correlation into continental deposits must be generally considered.

(4) *Continuous deposition and thickness (applicability of sequence stratigraphy)*. The GSSP has to be chosen within a section with continuous deposition across the boundary. The sedimentation rate should be sufficiently high (5 to 50 m per Ma) in order to register environmental variations in detail. The thickness of the section below and above the GSSP should be great enough to record the eustatic cycles preceding and following the boundary (i.e., thicknesses corresponding to approximately 1 to 2 Ma on each side of the boundary).

(5) *Quiet history (no tectonics, strong diagenesis or bioturbation)*. The section should be free of structural complication, strong diagenetic alteration, and redeposition. Tectonic activity may change the original succession of the strata whereas strong diagenetic changes may destroy or alter the magnetic, geochemical, and biological record. The record and resolution of palaeontologic, magnetic, and geochemical events have to be undisturbed, without excessive bioturbation, reworking or vertical mixing.

(6) *No facies change*. The absence of a facies change across the boundary should reduce the presence of depositional hiatuses (see point 4) and insure the representativity of the variations characterised by the stratigraphic tools (see points 7–10).

(7) *Applicability of biostratigraphy (the first order condition)*. A good palaeontologic record should enable biostratigraphic correlations based on several groups of fossils. For the Miocene, significant calcareous nannofossils and planktonic Foraminifera must be present.

(8) *Applicability of magnetostratigraphy*. The applicability of magnetostratigraphy is particularly important for the last 150 Ma. For the Miocene Epoch, the complexity of the magnetic polarity record requires thick sections to allow analysis of significantly long records.

(9) *Applicability of chemostratigraphy*. The composition of the marine water masses (trace elements, stable and unstable isotopes) changes with time and chemostratigraphic signals have an excellent correlation potential. Sr isotopes are of special interest for the Miocene Epoch, and pelagic carbonates seem to be most favourable for the application of this tool.

(10) *Applicability of geochronology*. The possibility of direct numerical dating of the GSSP by the presence of geochronometers is important for the definition of the numerical time scale. This is particularly feasible for the Miocene Epoch.

More general conditions/recommendations may be added. The most important is the one already quoted in this introduction: a GSSP should be consistent with previous



historical stratotypes — i.e., when possible, the point should not be located at a time clearly identified as or suspected to be within the previously defined Stages. This means that, when data are collected for the establishment of an appropriate GSSP, the main question to be answered will be: *where are the layers equivalent to those of the historical stratotypes in the candidate section?* The limits for location of the GSSP first depends on the answer to this question.

A second recommendation concerns the criteria used for selecting a particular point in the section for location of the global stratotype point (GSP). A number of previous proposals for GSSP have been based upon only one (palaeontological) criterion. In some cases, the criterion of correlation is taken itself as the criterion of definition; for example, the last occurrence of a fossil — coinciding with the level where the GSSP has been selected — is the only criterion considered for characterizing the limit. This is a source of considerable error and arises from a lack of understanding of the concept. A GSSP must strictly remain a point, the lateral extension of which separates a content below from a content above. The sum of the characteristics of the rocks below and above gives the means for correlating the point. In this view, a fundamental rule for the precise location of a GSSP within the interval not defined by the historical stratotypes will be: *'the best location of a GSSP is with respect to a series (a maximum number) of potential correlation criteria'*. This excludes, at least formally, the use of — or dependence upon — a single criterion.

In the search for and description of sections able to host GSSP, data to be gathered should address the ten recommendations described above. Thus the plan suggested in this volume for each study comprises three sections:

- (1) in the introduction, an answer to the first two questions (for access and study),
- (2) then a discussion of the four points concerning the quality of the geological record, and
- (3) finally the description of the four points regarding availability of correlation tools.

For the latter, it has generally been accepted that five main groups of tools should be considered successively during these studies in the following natural order: (i) field observations followed by more and more precise examination of the rock; (ii) time characterization of the rock.

The first point includes the 'equivocal' tools related to the lithology of the rock. These include lithostratigraphical approaches, chemostratigraphical investigation, and then magnetostratigraphic investigation. The second point includes the 'unequivocal' tools; firstly, the most commonly used and practical tool, which is the relative dating of the rock by mean of fossils. Finally, as a crown on the work (or as the cherry on the cake), the numerical dating using geochronology, which is more globally valid although not commonly applicable.

Following the description of data for historical stratotypes, this first part also includes the present situation related to the proposal for GSSP at the upper and lower limits of the Miocene Series.

## SOMMAIRE — UNITÉS CHRONOSTRATIGRAPHIQUES: STRATOTYPES HISTORIQUES ET STRATOTYPES GLOBAUX

L'élaboration d'une échelle chronostratigraphique de validité internationale nécessite une définition précise des unités fondamentales que sont les Étages. Ceux-ci peuvent être conçus, aujourd'hui, comme la combinaison: (1) de leur définition classique par le stratotype historique qui détermine l'essentiel de leur contenu concret; et (2) de leurs limites précisées par le concept de point stratotypique global (les PSG). Dans cette vue, une bonne connaissance des stratotypes historiques est une condition sine qua non pour le progrès des conventions. En effet, l'amélioration de la définition des Étages ne passe pas par un changement mais par un complément de cette définition par l'ajout de points stratotypiques compatibles avec les conventions déjà en usage.

La contribution à l'élaboration de ces PSG — pour les temps miocènes — est l'objectif de ce travail; il importait donc de débiter cet ouvrage par un rappel et, lorsque cela fut possible, des résultats nouveaux sur les stratotypes historiques. Ces exposés sont suivis par les propositions de PSG en cours d'élaboration pour les limites inférieure et supérieure de la Série. Ces synthèses, conçues pour aider à la présentation de coupes susceptibles d'accueillir un PSG sont l'occasion de rappeler ou de présenter les caractères qui permettront d'utiliser les PSG pour des corrélations aussi larges que possibles.

### ACKNOWLEDGEMENTS

The author and editors acknowledge the help of Tanya Atwater (University of California at Santa Barbara) for kindly improving the form of this introduction.

This Page Intentionally Left Blank

## Chapter A1

### THE AQUITANIAN HISTORICAL STRATOTYPE

A. Poignant, C. Pujol, M. Ringeade and L. Londeix

#### HISTORY OF THE DEFINITION

##### *Origin of the term (Mayer-Eymar, 1858)*

The Aquitanian stratotype (from *Aquitania*, the Latin name for Aquitaine) has been defined ('Aquitansische Stufe') by Mayer-Eymar near the Saucats village (Gironde) in the valley of the Saint-Jean-d'Etampes brook, between La Brède and the Moulin de l'Eglise. Later on, Dollfus (1909) specified and precisely indicated the geographical location of the stratotype. The stratotype was ratified and confirmed during international congresses on the Mediterranean Neogene (Vienna 1959, Bologna 1967).

##### *Historical stratotype definition and usage*

To define the stratotype, Mayer-Eymar (1858) used three sections (Fig. 1) located along the edges of the Saint-Jean-d'Etampes brook (called the Saucats on the IGN topographic map). They are: the Moulin de Bernachon section ( $x = 370.01$ ;  $y = 266.67$ ) (Figs. 2 and 3), the L'Ariey section ( $x = 369.57$ ;  $y = 266.37$ ) (Fig. 4) and the Moulin de l'Eglise section ( $x = 369.20$ ;  $y = 266.70$ ). These coordinates refer to the following topographic maps: IGN topographic map 'Pessac' 1 : 50,000–1 : 25,000; geological maps 'La Teste de Buch' 1 : 80,000, No. 191, 2nd edition, 1966; 'Pessac' 1:50,000, No. 827, first edition 1976.

Nowadays, the Moulin de Bernachon and the L'Ariey sections are the object of a geological itinerary proposed by the Management Association of the Geological Natural Reserve following the decree of creation of this Reserve by the Ministère de l'Environnement (September 1, 1982, and publication in the Journal Officiel on September 5, 1982).

A trail allows one to reach the L'Ariey section from the Moulin de Bernachon. The access is free but regulated with signs prohibiting sampling. On both sections, each level is marked by a numbered plaque. A notice board located at the right of the exposures gives a brief description of the section and the location of the fossiliferous layers, with just a few comments. The protected site is regularly patrolled and maintained by the Reserve officers.

Conversely, the Moulin de L'Eglise section, located on a private fenced property, is now covered by vegetation and is no longer visible (see editorial note at the end of the chapter).

The contact with the Oligocene is not visible at Moulin de Bernachon. However, according to Mayer-Eymar's description, it is exposed at the base of Coteau d'Avignon, south-southeast of Bordeaux (La Brède village). It is composed of white marls covered

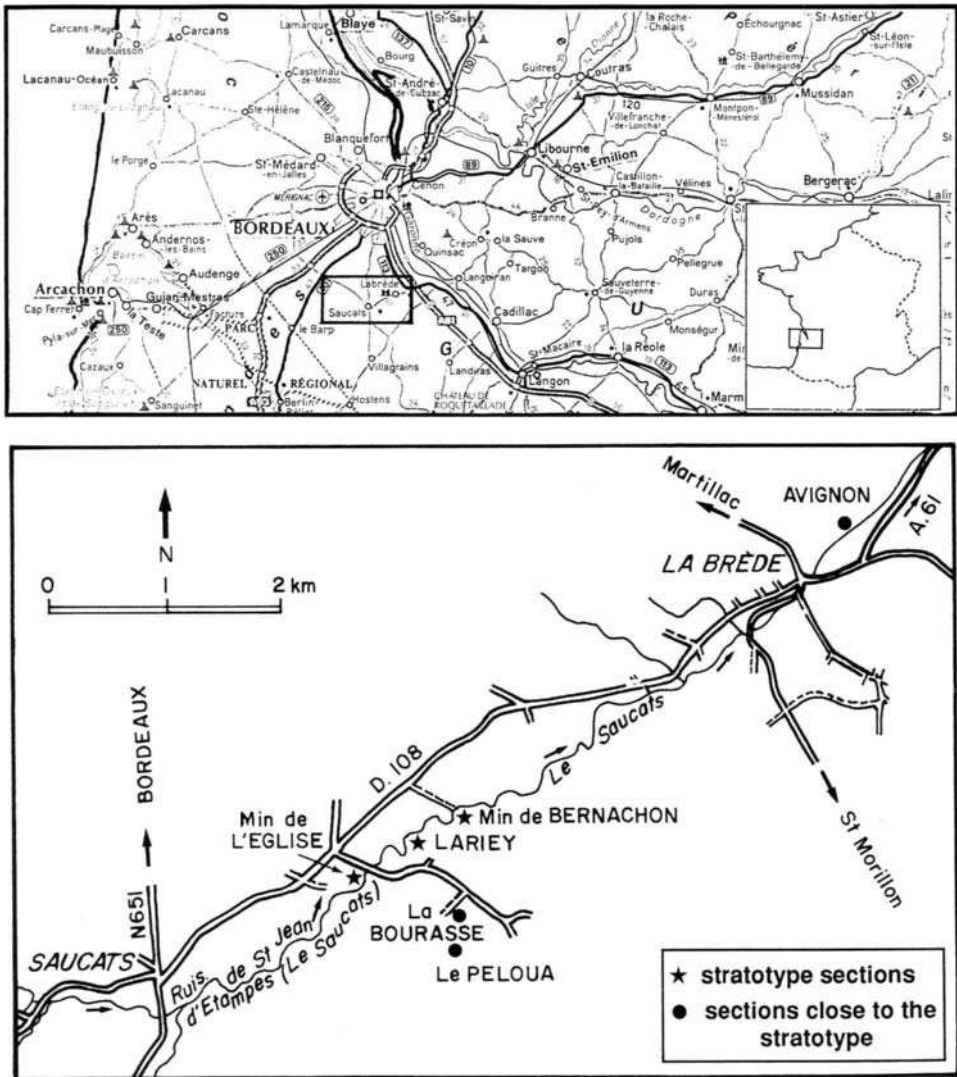


Fig. 1. Locations of the historical Aquitanian exposures.

by green marine clays which constitute the first unit of the Miocene marine sequence in this area.

The upper contact can be seen at Peloua, near the Moulin de Bernachon section. The parcel of land enclosing the historical level of Peloua was bought by the Municipality of Saucats where this site is illustrated in a permanent exhibit in the local Museum. In situ, the visible section allows one to make a correlation with L'Ariey, as well as to point out the Aquitanian/Burdigalian contact.

The Aquitanian fossiliferous marine deposits underlie a dark grey limestone with *Planorbis* and *Limnaea*. This unit is considered to be the top of the Aquitanian in

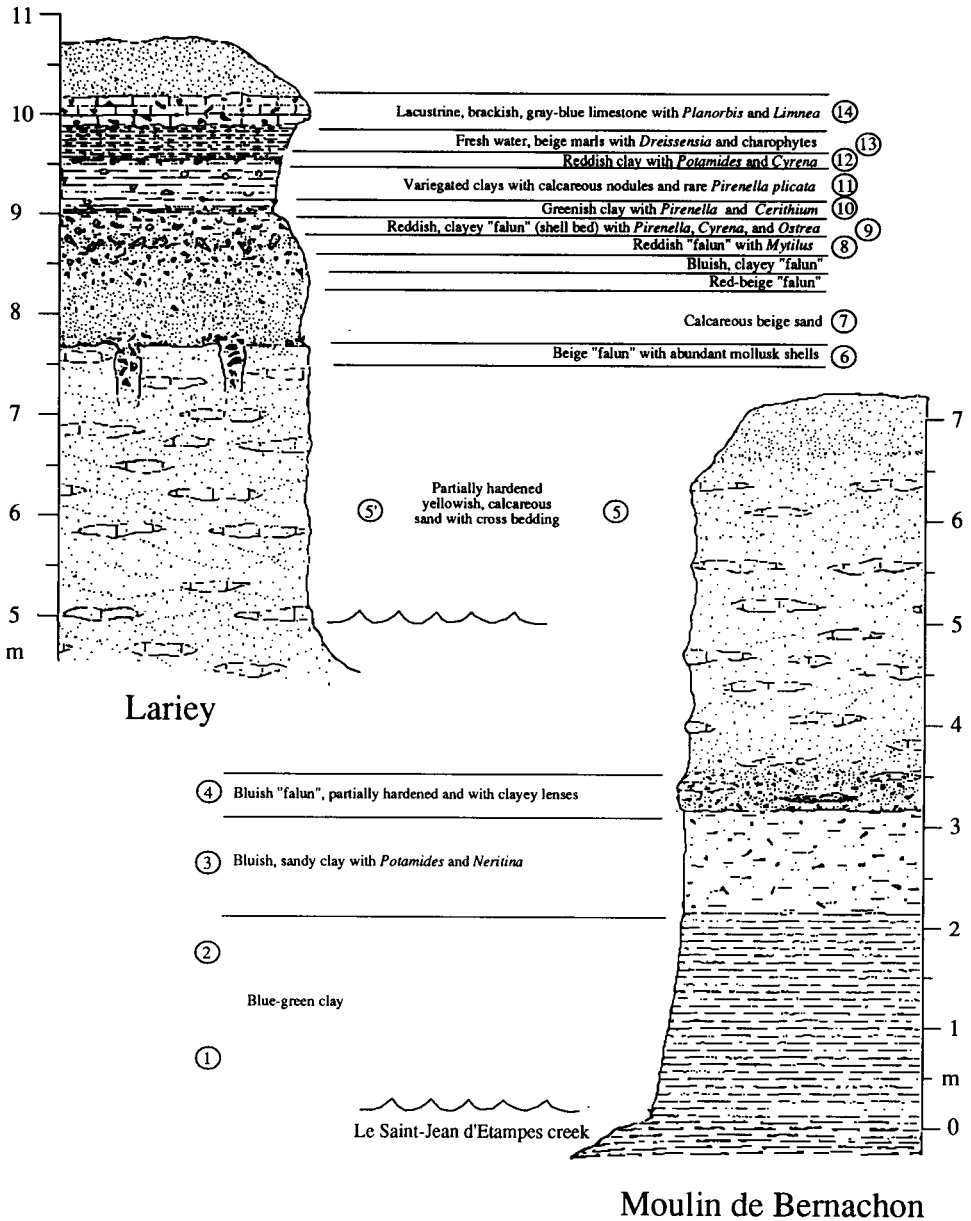


Fig. 2. Lithostratigraphic sections of the Aquitanian stratotype (modified after Londeix, 1991).

this area. A level with *Pecten beudanti* is found above it, and contains a new fauna characteristic of the Burdigalian. This transition was studied in a section called 'La Bourasse', quarried in a field nearby ( $x = 369.97$ ;  $y = 265.80$ ;  $z = 43$  m), and situated about 600 m from the Son village (Ringade, 1978; Poignant and Pujol, 1978; Londeix, 1991). La Bourasse excavations are no longer visible but breaks in the local overgrowth

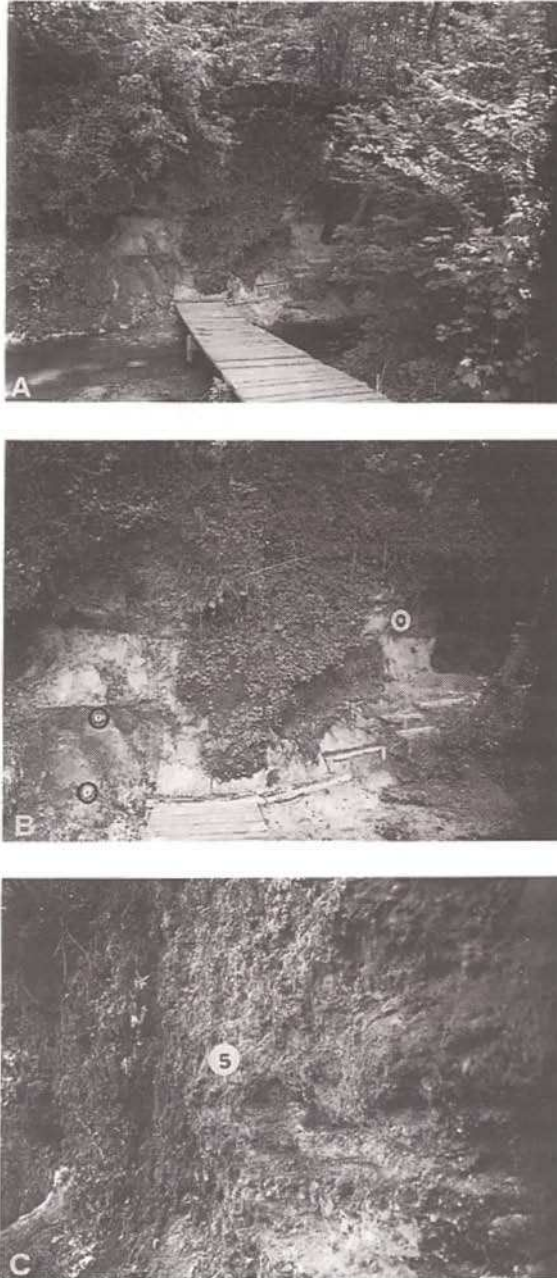


Fig. 3. The Moulin de Bernachon section with numbered levels. (A) General view of the outcrop on the stream bank. (B) Close-up of the same outcrop showing levels 1 and 2 (Marnes Bleues), 3 (Marnes Beiges) and the talus cover (4); close-up of level 5 (calcareous sandstones).



Fig. 4. The protected site of L'Ariey.

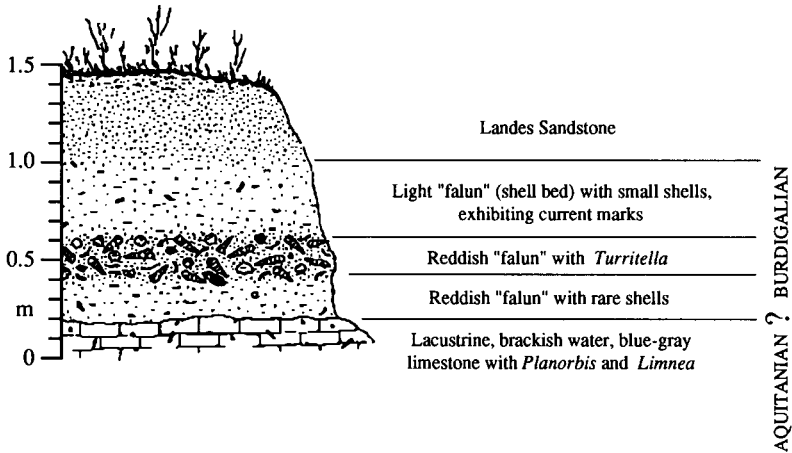


Fig. 5. Lithologic section of the 'La Bourasse' outcrop (after Londeix, 1991).

still allows one to trace again the same horizons and to see the Aquitanian/Burdigalian boundary (Fig. 5).

### STRATIGRAPHY

#### *Lithostratigraphy*

The first marine Miocene layers are transgressive over white, non-fossiliferous marls which rest on green azoic clays. The latter are superposed on the 'Calcaire à Astéries' (Stampian).

The lithologic succession of the Moulin de Bernachon and L'Ariey sections (Londeix, 1991) is summarized in Fig. 2. The sediments are mainly sandy clays, crags (lagoon



deposits — outer zone opened towards the sea), and sand or cross-bedded sandstone (deposits of a zone of lagoons connected to the ocean and subject to tides). The sedimentological analysis of the stratotype sections are indicative of a marine littoral to sublittoral environment. The faunal assemblages are typical of a subtropical to tropical climate.

### *Biostratigraphy*

The fauna and flora in these sediments are generally well preserved, which makes their specific identifications, and relative biostratigraphic assignments easy. Well diversified bivalves and gastropods have been described by Cossmann and Peyrot (1909–1933); this study was completed and revised in Alvinerie et al. (1977). The other organisms, including macro- and microfossils, pollens, and microplankton, have been listed in various works: Vigneaux (1949) for Bryozoa, Drooger et al. (1955) for Foraminifera, Moyes (1966) for Ostracoda, Caratini and Sivak (1971) for palynoplankton. The microfauna of small Foraminifera has been described and illustrated by Poignant and Pujol (1976). This microfauna is abundant: more than 150 species of benthonic Foraminifera have been collected, and among them 61 porcelaneous forms. Planktonic Foraminifera and calcareous nannoplankton are scarcer and less diversified (Müller and Pujol, 1979).

### *Biostratigraphic definition*

The study of planktonic Foraminifera and calcareous nannoplankton allows one to place the beginning of the Aquitanian near the base of the N4 Zone of Blow (1969), and the top in the lower part of the N5 Zone. The calcareous nannoplankton studied by Müller and Pujol (1979) allows the recognition of the NN1 Zone of Martini (1971) (Table 1).

As far as biostratigraphy is concerned, the most characteristic species are as following.

Planktonic Foraminifera: *Globigerinoides primordius*, *G. immaturus*, *Globoquadrina dehiscens*, *Globigerina woodi*, and *Globorotalia kugleri* (very rare).

Calcareous nannoplankton: *Braarudosphaera bigelowi*, *Coronocyclus nitescens*, *Cycli-cargolithus abisectus*, *C. floridanus*, *Discolithina desueta*, *D. enormis*, *Helicosphaera carteri*, *H. euphratis*, and *Sphenolithus moriformis*. The ubiquitous character of the planktonic microfauna, and nanoflora as a function of environment, does not allow one to clearly distinguish the succession of biozones between the sections.

### *Chemostratigraphy*

The  $^{87}\text{Sr}/^{86}\text{Sr}$  values of  $0.708440 \pm 23$ , and  $0.708493 \pm 20$  in biogenic calcite from two samples in the lower (La Brède) and middle (L'Ariey) part of the Aquitanian, respectively, were measured by DePaolo and Ingram (1985) who proposed an age of 21.5 Ma for the base of the Aquitanian, and 20 Ma for l'Ariey based on the time scale of Berggren (1972).

## CONCLUSIONS AND RECOMMENDATIONS

The Aquitanian stratotype is now protected and maintained within a context of the Geological Natural Reserve. The Moulin de Bernachon and L'Ariey sections,

Table 1

Distribution of nannoplankton and planktonic Foraminifera from the Bernachon and Lariery sections as shown in Fig. 2

5	5'	9	Levels	
•			<i>Coccolithus pelagicus</i>	NANNOPLANKTON
•			<i>Coronocyclus nitescens</i>	
•			<i>Cyclicargolithus abisectus</i>	
•			<i>Cyclicargolithus floridanus</i>	
•			<i>Sphenolithus moriformis</i>	
•			<i>Helicosphaera carteri</i>	
•			<i>Helicosphaera euphratis</i>	
•			<i>Discolithina desueta</i>	
•			<i>Discolithina enormis</i>	
NN1			ZONE	
•	•		<i>Globorotalia kugleri</i>	PLANKTONIC FORAMINIFERA
•			<i>Globorotalia obesa</i>	
•			<i>Globorotalia siakensis</i>	
•	•		<i>Globigerina angustiumbilicata</i>	
•	•		<i>Globigerina praebulloides</i>	
•	•		<i>Globigerina woodi</i>	
•	•		<i>Globigerinoides primordius</i>	
•	•		<i>Globigerinoides aff. immaturus</i>	
•	•		<i>Globoquadrina dehiscens</i>	
•	•		<i>Globorotaloides testarugosa</i>	
N4-N5 (base ?)			ZONE	


Blow (1969)	Martini (1971)	Aquitaine Basin (Bordeaux area)	Series
N5	NN2		Lower Miocene
N4	NN1		
	NP25		
			Oligocene

Fig. 6. Biostratigraphic range of the Aquitanian stratotype.

representing almost the entire Aquitanian Stage, remain accessible. The numerous palaeontological studies allow the placement of the historical stratotype at the base of the Miocene (Fig. 6).

## SOMMAIRE — LE STRATOTYPE HISTORIQUE AQUITANIEN

*(Manuscrit soumis: Avril 1993, révisé: Janvier 1994; rédacteur responsable: GSO)*

Le stratotype historique de l'Aquitainien (de Aquitania pour la province romaine d'Aquitaine) est situé à près de 20 km de Bordeaux (SO France). Il fut désigné par Mayer-Eymar en 1858. Il se compose de trois sections exposées le long d'un ruisseau entre La Brède et Saucats. A ce jour, deux affleurements seulement peuvent être visités: le Moulin de Bernachon et l'Ariey qui sont protégés par une réserve géologique. Les limites inférieure et supérieure du stratotype sont visibles dans des affleurements voisins. Les dépôts furent étudiés dans de nombreuses investigations sédimentologiques et paléontologiques; ils représentent un environnement marin peu profond en climat subtropical. Les sédiments correspondent à la zone de nannoplancton calcaire NN1 et aux zones de foraminifères planctoniques N4 et N5 (en partie). La limite Aquitainien/Burdigalien est visible près du stratotype de l'Aquitainien et est marquée par des niveaux de calcaires lacustres. La connaissance de ce stratotype peut être améliorée.

*(Sommaire adapté par les rédacteurs d'après un résumé des auteurs, GSO)*

### EDITORIAL NOTE

Since the submission of this manuscript in 1993, the outcropping conditions have been improved in the area; the series is now exposed again along the river with a thickness of 4 m (communication by B. Cahuzac). See also the most recent contribution of Cahuzac et al. in Chapter A3 for the description of recent outcrops.

## Chapter A2

### THE BURDIGALIAN HISTORICAL STRATOTYPE

A. Poignant, C. Pujol, M. Ringeade and L. Londeix

#### HISTORY OF THE DEFINITION

##### *Origin of the term Burdigalian*

The term Burdigalian (from *Burdigala*, Latin name for the city of Bordeaux in the Roman time) was proposed as a stage name by Depéret (1892) in two distinct French areas, the Bordeaux area and the Rhône valley: "... on doit distinguer dans le Miocène marin un grand étage inférieur avec l'horizon des faluns de Saucats et de Léognan à la base et celui de la molasse calcaire du bassin du Rhône à *Pecten praescabriusculus* au sommet".

As far as the Bordelais is concerned, later on Dollfus (1909) designated the typical crag of Coquillat at Léognan as the stratotype of the Burdigalian. In the proceedings of the Mediterranean Neogene Congress held in Vienna (1959), Coquillat is indicated as the type locality for the Burdigalian. Following these recommendations, Vigneaux (1971) described the Coquillat exposure at Léognan as the stratotype for Burdigalian in the descriptive sheets of the Mediterranean stages. This exposure shows a yellowish crag, about 50 cm thick, with shelly remains, and Foraminifera. At the present time, however, this outcrop is practically inaccessible because it is situated in a private property. Therefore, Poignant and Pujol (1978) referred to the Pont-Pourquey exposure as the 'substitution stratotype'. This exposure was already cited by Vigneaux (1971) who indicated it as a subsequent reference for the stratotype, admitting that it was as valid as the stratotype itself (Mediterranean Neogene Congress of Vienna, 1959).

##### *Historical stratotype, definition, and usage*

The Coquillat exposure ( $x = 366.59$ ;  $y = 273.25$ ), as designated by Dollfus (1909), is located about 1 km WSW of the Léognan village (Gironde) in the vicinity of the small brook L'Eau Blanche (Fig. 1).

The Pont-Pourquey exposure, cited and described by Poignant and Pujol (1978) as the substitution stratotype ( $x = 366.48$ ;  $y = 265.37$ ), is located about 1 km WSW of the Saucats village along the Saint-Jean-d'Etampes brook (Fig. 2).

The available topographic documents are: IGN topographic map 'Pessac' 5-6, 1:25,000; geological maps: 'La Teste de Buch', 1:80,000, No. 191, 2nd ed., 1966; 'Pessac', 1:50,000, No. 827, 1st ed., 1976.

Unfortunately, the substitution stratotype is no longer exposed because it has been buried under detritus by the riverside residents. Nevertheless, an identical section is exposed about 50 m upstream from the bridge over the Saint-Jean-d'Etampes brook,

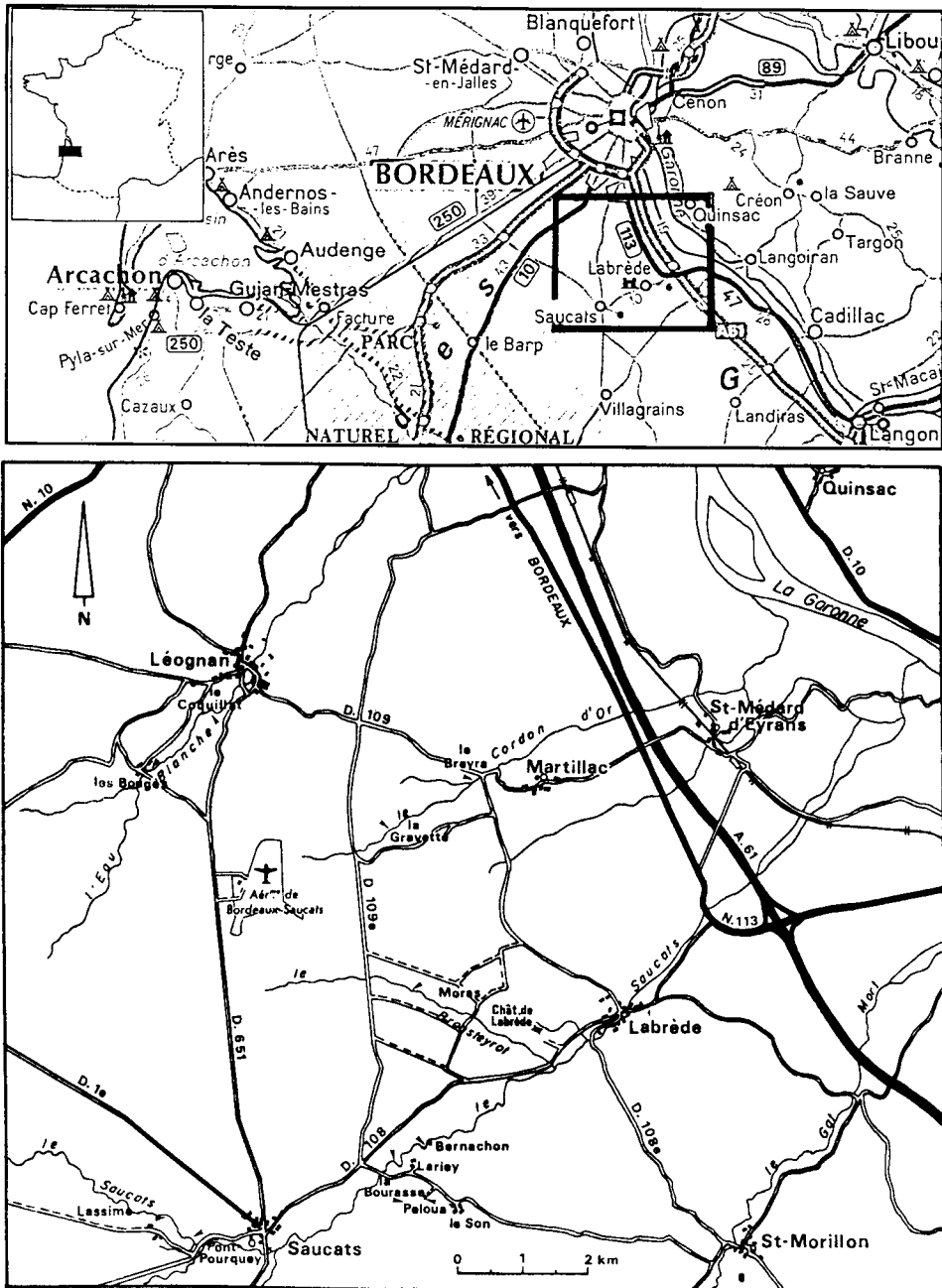


Fig. 1. Location of the historical Burdigalian stratotype exposures in the Bordeaux area.

while the classic (i.e. standard) section was situated at the same distance downstream from the bridge. This exposure, well maintained and easily accessible, is now located in a 'Natural Reserve' (Figs. 3 and 4).

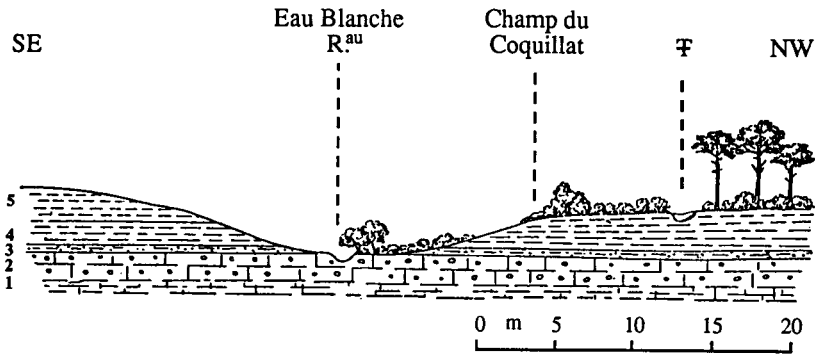


Fig. 2. Schematic section of 'Le Coquillat' at Léognan (Gironde, France, after Daguin, 1948). (1) Upper Aquitanian fresh-water limestone; (2) bone-bearing molasses with *Scutella leognanensis* and *Squalodon grateloupi*; (3) sandstones with Operculines and *Echinolampas richardi*; (4) horizon with *Pectunculus*; (5) Coquina deposit with *Euthriofusus burdigalensis*, *Cancellaria acutangulata*, *Turritella terebralis* and *Meretrix erycinoides*.

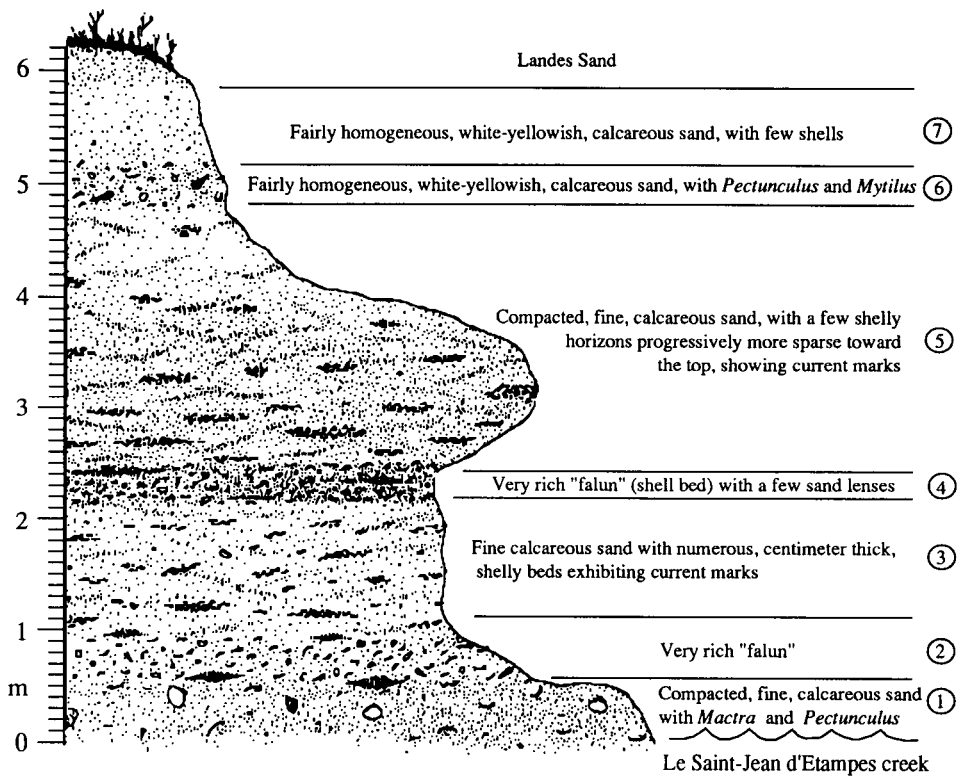


Fig. 3. Lithologic section of the 'Pont-Pourquey' outcrop (after Londeix, 1991).

The lower contact was not visible at the Coquillat outcrop. On the contrary, in the village of Léognan, just east of the Pirègues locality, it was noticed by Malvesin-Fabre (1939). This contact is marked by a level of lacustrine limestone, sometimes perforated



Fig. 4. The riverbank exposure of Pont-Pourquey.

or destroyed, covered by a Burdigalian horizon with *Maetra* (op. cit. p. 166), and a thick layer (about 5 m) of a shallow-water calcareous sand (= *molasse ossifère de Léognan*). Consequently, the Burdigalian rests on top of a lacustrine horizon terminating the Aquitanian.

The upper contact was unknown at Coquillat, and is not visible at Pont-Pourquey. However, slightly upstream from Pont-Pourquey, along the Saint-Jean-d'Etampes brook, the La Sime section (Fig. 5) exhibits the Burdigalian/Middle Miocene contact (Poignant and Pujol, 1978; Londeix, 1991). These authors describe a hiatus between the Burdigalian calcareous sand unit and the Serravallian clayey sand unit; on the basis of microfauuna and calcareous nannoflora analyses (Müller and Pujol, 1979), this hiatus represents an estimated missing interval of about 4–5 Ma.

## STRATIGRAPHY

### *Lithostratigraphy*

The sediments at Léognan (Coquillat), as well as Saucats (Pont-Pourquey), are crags containing a rich mollusk macrofauna. The Pont-Pourquey section (Figs. 3 and 4), which consists of a 6 m thick exposure above the river bed (Fig. 4), exhibits an alternation of crags containing abundant marine mollusk shells (Fig. 6), and calcareous sand showing frequent palaeocurrent marks. These sediments represent shallow-marine deposits in the far end of a bay, not far from river outlets.

### *Biostratigraphy*

*Palaeontological content.* The faunal and floral content of these sediments exhibit a good state of preservation favouring an easy taxonomic identification.

Very abundant and diversified mollusks have been mainly reported by Cossmann and

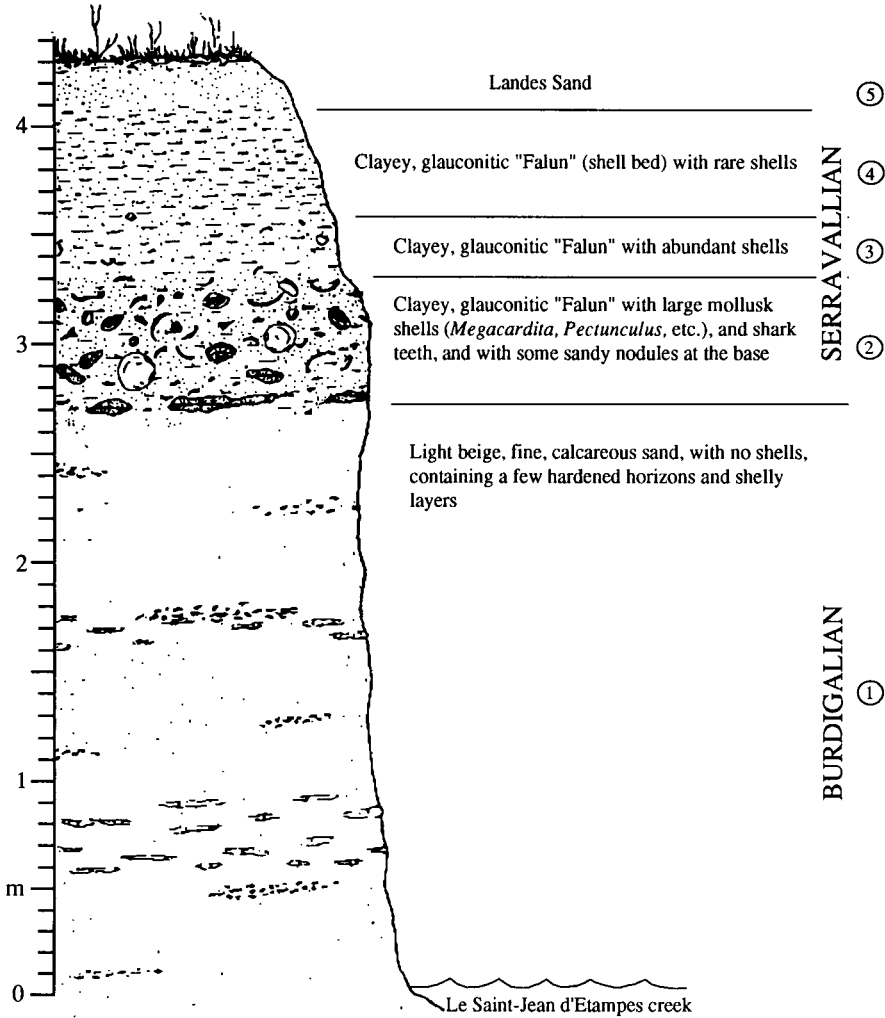


Fig. 5. Lithologic section of 'La Sime'.

Peyrot (1909–1933). About 90 species of Bryozoa have been described by Vigneaux (1949). The rich ostracod fauna has been studied by Keij (in Drooger et al., 1955), and Moyes (1965). Drooger et al. (1955) and Poignant and Pujol (1978) examined the Foraminifera, identifying more than 250 species of benthonic Foraminifera, and more than 25 species of planktonic Foraminifera. Müller and Pujol (1979) observed the nannoplankton, Caratini and Sivak (1971) the palynoflora, and Jan du Chêne and Londeix (1987) the palynoplankton.

*Biostratigraphic location.* The detailed analysis of the planktonic microfauna, more abundant and diversified than the Aquitanian one (Poignant and Pujol, 1978), indicates that the Burdigalian of the Bordeaux area covers on the whole, or in part, the N5–N6 zonal interval of Blow (1969) (Fig. 7).





Fig. 6. The crag exposed in the Pont-Pourquey section, exhibiting abundant marine mollusk shells.


Blow (1969)	Martini (1971)	Aquitaine Basin (Bordeaux area)	Series
N6	NN3	 Burdigalian stratotype	Lower Miocene
N5	NN2		
N4	NN1		
	NP25		
			Oligocene

Fig. 7. Biostratigraphic assignment of the Burdigalian stratotype in the Bordeaux area.

As far as biostratigraphy is concerned, the most interesting species are the following: *Globigerina ciperoensis*, *G. gr. bulloides*, *G. woodi*, *Globigerinoides altiapertura*, *G. trilobus*, *G. sacculifer*, *G. subquadratus*, *Globoquadrina dehiscens*, *G. globosa*, *G.*

Table 1

Distribution of calcareous nannofossils and planktonic Foraminifera from the Pont-Pourquey section in levels as shown in Fig. 3

1	2	3	4	5	Levels	
•	•	•	•	•	<i>Braarudosphaera bigelowii</i>	Calcareous nannofossils
•	•	•	•	•	<i>Coccolithus pelagicus</i>	
•	•	•	•	•	<i>Coronocyclus nitescens</i>	
•	•	•	•	•	<i>Discoaster deflandrei</i>	
•	•	•	•	•	<i>Discolithina multipora</i>	
•	•	•	•	•	<i>Helicosphaera ampliaperta</i>	
•	•	•	•	•	<i>Helicodphaera carteri</i>	
•	•	•	•	•	<i>Reticulofenestra</i> sp.	
•	•	•	•	•	<i>Sphenolithus moriformis</i>	
NN2 Zone						
•	•	•	•	•	<i>Globorotalia birnageae</i>	Planktonic Foraminifera
•	•	•	•	•	<i>Globorotalia continuosa</i>	
•	•	•	•	•	<i>Globorotalia obesa</i>	
•	•	•	•	•	<i>Globorotalia saginata</i>	
•	•	•	•	•	<i>Globorotalia siakensis</i>	
•	•	•	•	•	<i>Globigerina angustumbilicata</i>	
•	•	•	•	•	<i>Globigerina</i> gr. <i>bulloides</i>	
•	•	•	•	•	<i>Globigerina ciproensis</i>	
•	•	•	•	•	<i>Globigerina</i> aff. <i>venezuelana</i>	
•	•	•	•	•	<i>Globigerina woodi</i>	
•	•	•	•	•	<i>Globigerinoides altiaperturaus</i>	
•	•	•	•	•	<i>Globigerinoides sacculifer</i>	
•	•	•	•	•	<i>Globigerinoides immaturus</i>	
•	•	•	•	•	<i>Globigerinoides</i> gr. <i>quadrilobatus</i>	
•	•	•	•	•	<i>Globigerinoides subquadratus</i>	
•	•	•	•	•	<i>Globigerinoides trilobus</i>	
•	•	•	•	•	<i>Globigerinita</i> sp.	
•	•	•	•	•	<i>Catapsydrax</i> sp.	
•	•	•	•	•	<i>Globoquadrina altispira globosa</i>	
•	•	•	•	•	<i>Globoquadrina dehiscens</i>	
•	•	•	•	•	<i>Globoquadrina globularis</i>	
N5-N6 Zone						

*globularis*, *Globorotalia birnageae*, *G. continuosa*, *G. obesa*, *G. saginata*, and *G. siakensis*. The qualitative distributions of the different species do not show any significant evolution from the base to the top of the section.

The nannoflora studied at Pont-Pourquey by Müller and Pujol (1979) shows that these marly sediments belong to the NN2 Zone of Martini (1971), although very few specimens of *Helicosphaera ampliaperta* are found in this interval (Table 1).

### Chemostratigraphy and geochronology

Mollusk-bearing layers at Saucats and Léognan were indirectly dated by DePaolo and Ingram (1985) who measured the <sup>87</sup>Sr/<sup>86</sup>Sr ratio in biogenic carbonate from several samples spanning the Burdigalian (i.e., lower, middle and upper parts of the stratotype), and utilized the resulting values to construct a Tertiary isotopic curve which was dated using the time scale of Berggren (1972). The inferred numerical ages obtained with this method are 17 Ma for Saucats, and 19 to 18 Ma for Léognan. Likewise, preliminary results from Sr isotopic analysis (Londeix and Grousset, in progress) on selacian fish teeth collected at Pont-Pourquey, suggest an age of about 18 Ma for this unit.

A glauconite sample taken at 195 m depth (*Globorotalia peripheroronda* Zone according to Pujol, 1970, is N5 Zone) in the Soustons dwelling, provided an apparent age between 19.7 and 19.3 Ma, thus indicative of the basal part of Burdigalian (Alvinerie et al., 1974). This dwelling, which is located in the southern part of the Aquitaine Basin, is biostratigraphically equivalent to the Burdigalian of Pont-Pourquey (Pujol, 1970).

## CONCLUSION AND RECOMMENDATIONS

The Pont-Pourquey section is nowadays protected and will be maintained in the framework of the 'Natural Reserve' of Saucats–La Brède.<sup>1</sup> The numerous palaeontological studies have permitted to make a comprehensive assessment of the highly abundant and diversified marine fossils contained therein, and to correlate the Burdigalian historical stratotype of the Bordelais with the commonly used Lower Miocene biozonations.

## SOMMAIRE — LE STRATOTYPE HISTORIQUE BURDIGALIEN

(Manuscrit soumis: Avril 1993, révisé: Janvier 1994; rédacteur responsable: GSO)

Le stratotype historique du Burdigalien (de *Burdigala*, nom romain de Bordeaux) est situé à près de 20 km de Bordeaux (SO France); il fut proposé par Dollfus en 1909. Auparavant, en 1892, Depéret avait proposé de définir l'étage Burdigalien dans deux régions: celle de Bordeaux et la vallée du Rhône. Dans la région bordelaise, le stratotype est situé dans les bourgs de Léognan et Saucats (Congrès sur le Néogène Méditerranéen de Vienne, 1959). Les couches burdigaliennes sont visibles au dessus des affleurements aquitaniens et sont surtout bien exposées à Saucats (section de Pont-Pourquey protégée maintenant par une réserve géologique). La section de Pont-Pourquey a à peu près 6 m d'épaisseur et est constituée de faluns et sables calcaires alternés. Ces sédiments indiquent un environnement côtier. La faune et la flore, exceptionnellement abondantes et bien préservées, permettent d'attribuer les dépôts burdigaliens de la région bordelaise aux zones de nannoplancton calcaire NN2 et de foraminifères planctoniques N5 et N6 (pro parte). La limite supérieure du Burdigalien est présente au sommet de la section de Pont-Pourquey. Les sédiments sus jacents sont supposés d'âge serravallien à la Sime dénotant un hiatus de dépôt. La connaissance de ce stratotype pourrait être améliorée par de nouvelles recherches.

(Sommaire adapté par les rédacteurs d'après un résumé des auteurs, GSO)

<sup>1</sup> Association pour la Réserve géologique de Saucats–La Brède, Mairie de Saucats, 33650 La Brède.

Chapter A3

**THE BURDIGALIAN HISTORICAL STRATOTYPE IN THE RHODANIAN AREA**

S. Pouyet, G. Carbonnel and G. Demarcq

HISTORY OF THE DEFINITION

*Location*

The Rhodanian stratotype established by Demarcq and Carbonnel (1975, p. 51) is represented by the Saint-Paul-Trois-Châteaux section in the Valréas basin (Drôme), 120 m thick exposed along Road D859 (= D59a): Bollène-Saint-Restitut ( $x = 795.76$ ;  $y = 228.46$ ). Access is free and easy at any time during the year (Figs. 1, 2, and 3). In the Alpine foothills of the same basin, 10 km further to the northeast, the Montbrison-Fontbonau (Drôme) section ( $x = 814.80$ ;  $y = 240.86$ , sometimes called Prieuré section) was established by Demarcq as the parastratotype of the Rhodanian Burdigalian (Figs. 1 and 2). In this section, the Burdigalian bordering the first subalpine Cretaceous hills dips 15–30° WSW. The bed succession is visible along the small Aigue Longue stream.

*Topographic maps.* IGN maps 1 : 25,000 Bollène-Pierrelatte (Serie bleue Nr. 3039 West), Valréas (Serie bleue Nr. 3039 East), and Nyons (Serie bleue Nr. 3139 West).

*Geologic maps.* Map 1 : 50,000 Valreas Nr. XXX-39 and Nyons XXXI-39.

The Saint-Paul-Trois-Châteaux section (Fig. 2) is located on the southern side of the Saint-Restitut hill. It is visible on both sides of road D59a, and starts in the 'Les

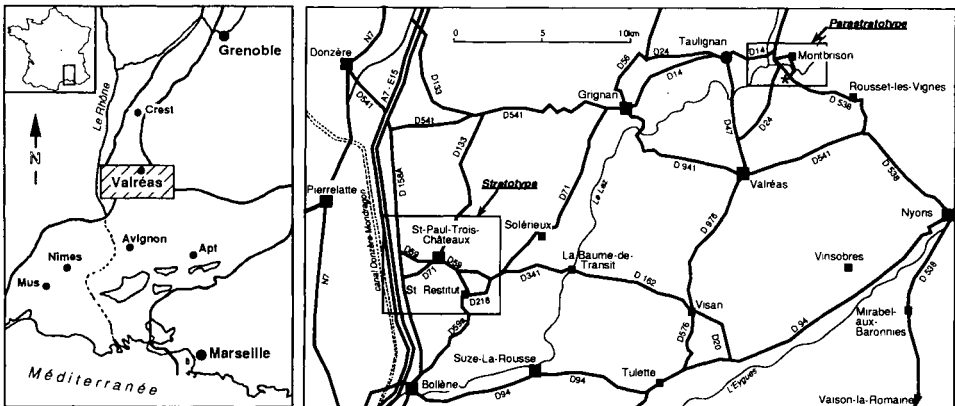


Fig. 1. Location map of the Rhodanian stratotype and parastratotype.

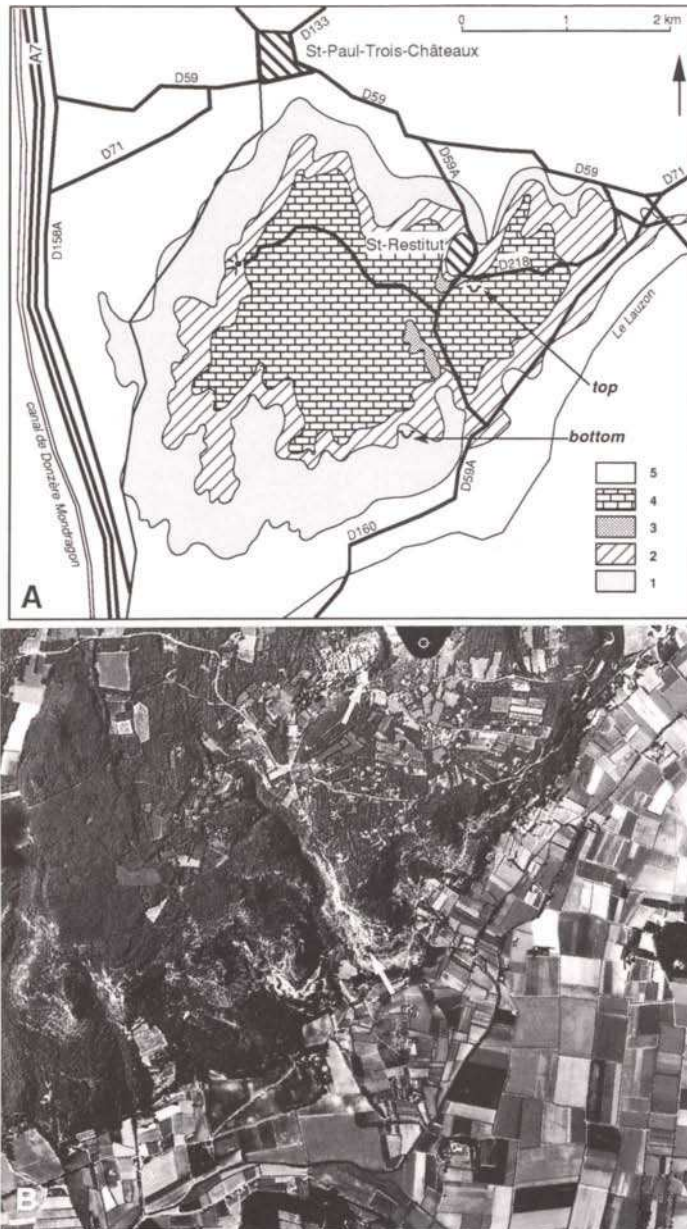


Fig. 2. (A) Simplified geologic map of the Saint-Paul-Trois-Châteaux area showing the location of the limits of the Rhodanian stratotype section. 1 = Upper Cretaceous; 2 = Greenish molasse of Saint-Restitut; 3 = Salles marls; 4 = Calcareous molasse of Saint-Paul-Trois-Châteaux; 5 = post-Miocene. (B) Air photo of the Saint-Paul-Trois-Châteaux area. The white arrows indicate the top and bottom of the stratotype section (see also Fig. 3). Photographie aérienne de l'IGN, © IGN – PARIS 1996 – Autorisation No. 50–6118.

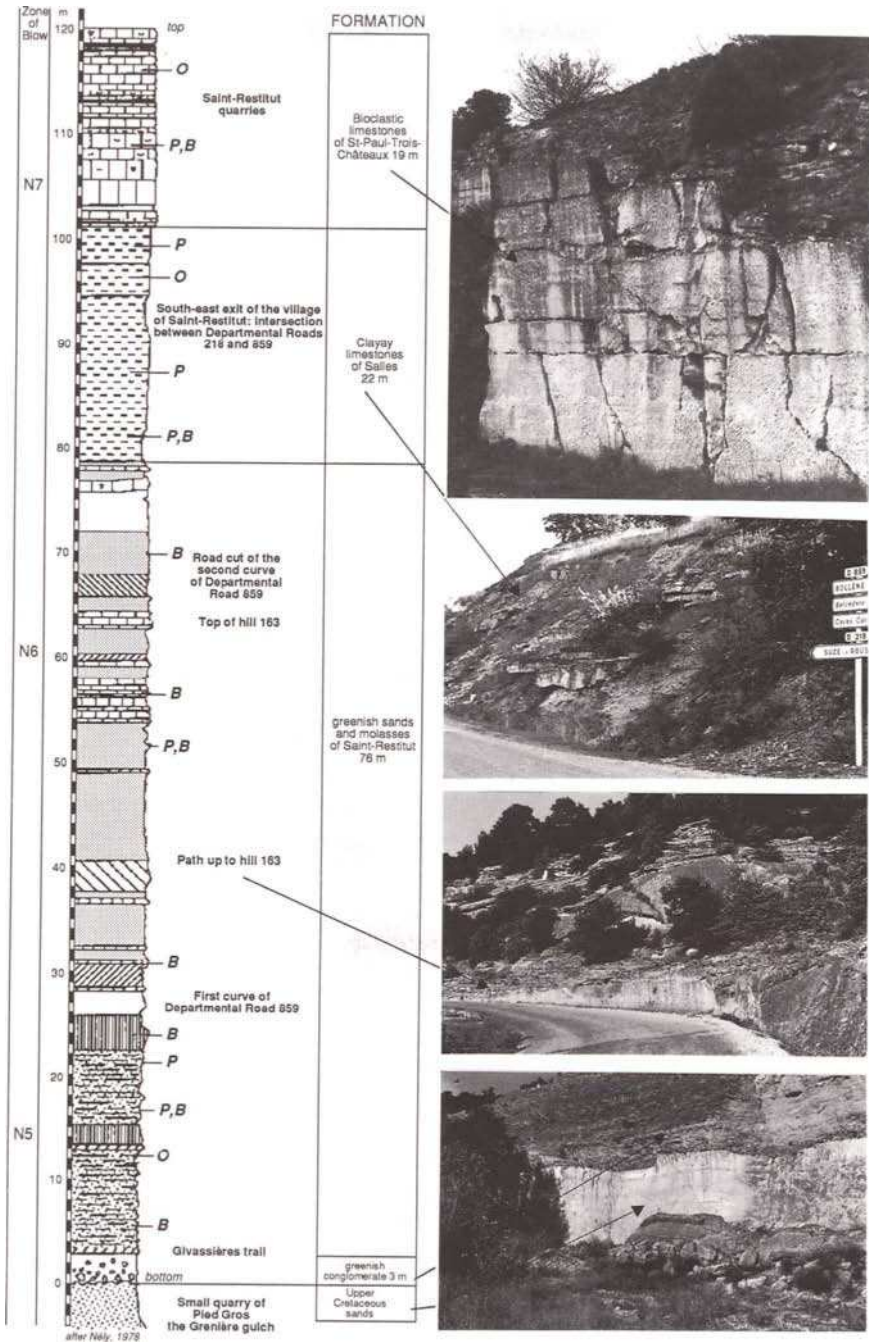


Fig. 3. Stratigraphic column of the Rhodanian stratotype, and precise location of fossiliferous levels: O = Ostracoda; P = Pectinidae; B = Bryozoa.

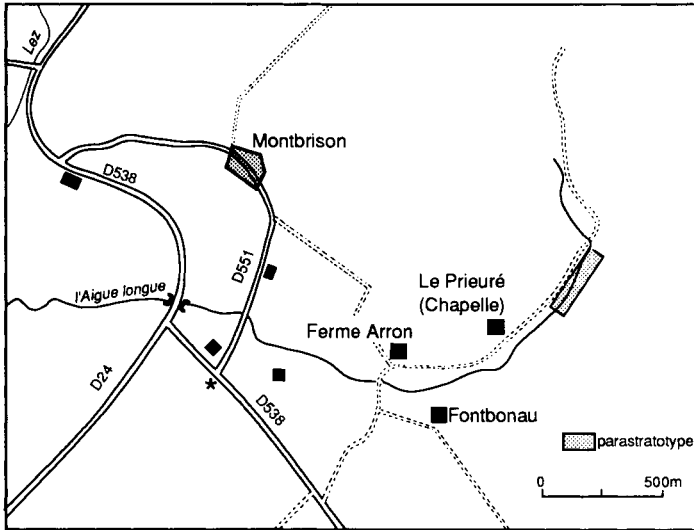


Fig. 4. Detailed access map to the site of the Rhodanian parastratotype.

Givassières'. The Montbrison-Fontbonau section (Fig. 3) is located on the left side of the Aigue Longue stream, approx. 800 m off the Arron farm.

#### *Lower limit*

In the stratotype, on top of the Upper Cretaceous channelized white sands (Pied Cros quarry) the basal conglomerate with perforated greenish clasts marking the beginning of the Burdigalian transgression is easily visible (Fig. 4).

In Montbrison-Fontbonau, the clay-rich Oligocene sands have been partially eroded and gullied out. The contact is less abrupt. The transgressive conglomerate is for the most part made-up of these sands mixed with limestone, siliceous clasts, and angular flints of smaller size than those of the stratotype.

#### *Upper limit*

The upper limit in the stratotype is absent due to an erosional surface. The uppermost beds of whitish bioclastic limestone of the Saint-Paul-Trois-Châteaux section can be observed in the quarries of the Saint-Restitut village.

In Montbrison-Fontbonau on top of the bioclastic limestones a succession of marly and sandy molasses (30 m thick) can be seen on the right side of the stream at the level of the Prieuré ruins. A 9.5 m deep borehole and two small drill holes permit to attribute this succession to the N8 zone of Blow (1969) (Langhian, Demarcq et al., 1974) defined by the presence of *Praeorbulina sicana*.

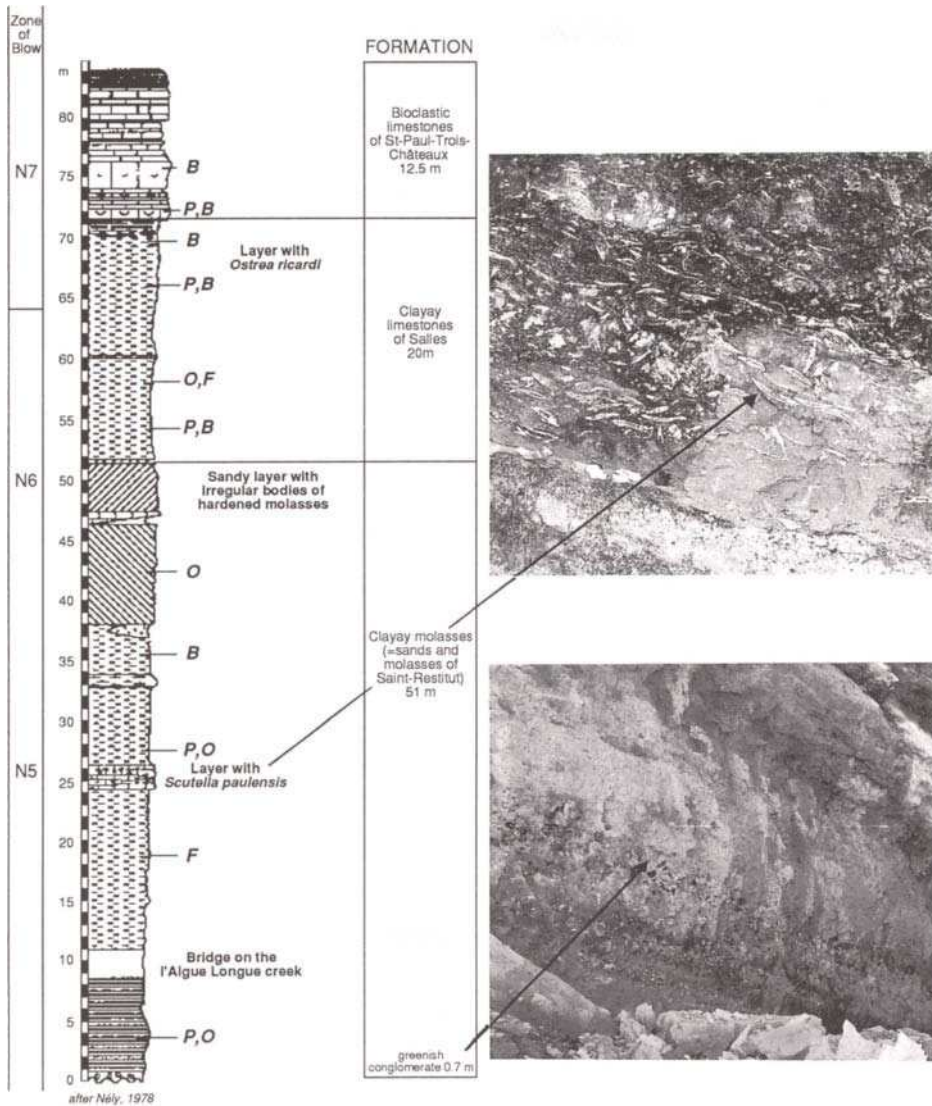


Fig. 5. Stratigraphic column of the Rhodanian parastratotype, and precise location of fossiliferous levels: *O* = Ostracoda; *P* = Pectinidae; *B* = Bryozoa.

## STRATIGRAPHY

### Lithostratigraphy

Four formations are present in both sections (Figs. 4 and 5). From bottom to top in the sequence these units are:

(1) A basal greenish conglomerate containing glauconite; this unit is 3 m thick in the stratotype but thins to 70 cm in the parastratotype.



(2) Molassic sands and molasses with oblique lenticular stratification. This formation is called Saint Restitut Greenish Molasse. It is 76 m thick in the stratotype and 50 m thick in the parastratotype. The influence of tidal currents in the deposition of this unit has been described by Lesueur et al. (1990) in the type section.

(3) Marls and argillaceous limestones called Salles Calcareous Marls, 22 m thick in the stratotype, and 20 m in Montbrison.

(4) The uppermost formation in the sequence is called Saint-Paul-Trois-Châteaux Calcareous Molasse, and consists of a massive bioclastic limestone, quarried since ancient times, and locally known as the *Pierre du Midi*. Its thickness is 19 m in the stratotype, and 12.5 m in the parastratotype.

According to Lesueur et al. (1990), these four formations correspond to a highstand transgressive sequence as defined by Vail et al. (1987).

Sedimentological analyses in the two sections (Nely, 1978) indicate a clastic input of 35–40% sand, 50–55% carbonate, and 5–10% clay at the base of the Burdigalian Saint Restitut molasse.

The overlying finer terrigenous sediments were deposited more slowly, and the sand content decreases significantly up section. These terrigenous sediments constitute the Salles Calcareous Marls and Sands unit, and are made-up of 2–5% sand, 75–85% carbonate, and 15–20% clay. The bioclastic sands marking the top of the Burdigalian have only 2–3% sand, and 4–5% clay, whereas limestone represents 92–95% of the unit.

The enclosed, shallow water basin of Valréas was influenced by circular currents. In the western part of the basin (Saint-Paul-Trois-Châteaux), the environment was wave-dominated, and poorer in fauna than the one represented by the parastratotype to the northeast (Monbrison), which was characterized by quite waters, and abundant prolific macrofauna associations indicate a temperate to warm water platform environment (> –60 m). The presence of Ostracoda indicates an intertidal (infralittoral) environment with algal mats.

### Biostratigraphy

*Microfauna.* No exhaustive studies on Foraminifera are available for these sections. This group is mainly represented by benthic forms which are particularly abundant in detrital facies. Their association is rather homogeneous. According to R. Anglada (unpubl. data) the benthonic foraminiferal assemblage is represented by about 60 species mainly belonging to the genera *Ammonia*, *Astrononion*, *Brizalina*, *Cibicides*, *Florilus*, *Elphidium*. Planktonic Foraminifera are scarce and poorly diversified.

The calcareous nannoplankton content of the Rhodanian sections was studied by Martini (1988) in the same sites of sampling the Ostracoda. The assemblages are relatively poor in both sections. *Coccolithus pelagicus* and *Reticulofenestra* sp. are the most abundant species and particularly predominant in the conglomerate of the Saint-Paul-Trois-Châteaux section. Sporadic *C. abisectus*, *Cyclococcolithus floredanus*, *Helicospaera ampliapertura*, *H. carteri*, *Reticulofenestra pseudoumbilica*, *Sphenolithus cf. belemnus*, and *S. moriformis* are also present.

Ostracoda are represented by many species but few individuals (Carbonnel, 1969). Characteristic species at this biostratigraphic location, which is included in the biozone A of Carbonnel (1969), are: *Cytheridea acuminata caumontensis*, *C. fourmiei*, *Hemicythere triangularis triangularis*, *H. notata costulata*, *Aurila cauditoiles*, *A. vauchusi*, *A.*

*ventroinflata*, *A. cicatricosa lauzea*, *Leguminocythereis elongata restitutensis*, *Loxoconcha linearis linearis*, *Ruggiera carinata fongolini*, *Quadracythere bavarica rhodanica*, and *Q. polygonata*.

In Saint-Paul-Trois-Châteaux, the Ostracoda indicate a littoral biotope around 10 to 50 m water depth with abundant algal vegetation. There is a slight deepening (= 50 m) towards Montbrison-Fontbonau.

**Macrofauna.** The malacofauna is abundant but scarcely diversified and more dispersed than in the Bordelais region; fossils in particular are scarce in detrital facies. Bivalves are more abundant than Gastropoda, and among them Pectinidae are the most common. Other bivalve species worth mentioning are: *Arca diluvii*, *Anadara turonica*, *Ostrea ricardi*, *O. offreti*, *Anomia*, *Cardium*, *Corbula*, *Panopea*, *Pinna*, and *Tapes*.

F. Fontannes, who was a pioneer in studying the stratotypes, gave a complete list of Gastropoda. Among these the following species are the most representative of the assemblage: *Fasciolaria tarbelaria*, *Ficula condita*, *Natica*, and *Turritella vermicularis*.

The Bryozoa of the Saint-Paul-Trois-Châteaux section have been partially studied by Mongereau (1970), whereas those from the parastratotype have been studied by Li (1990). In addition to the small branching forms, large, celled pores are present including *Celleporaria palmata* which is a symbiotic of the madreporide *Culicia parasitica*.

The Bryozoa are abundant (130 species and several thousand individuals in 1500 cm<sup>3</sup>), and their palaeoecological importance is significant. According to Li (1990), in Montbrison all the species indicate an average depth between 40 and 60 m, normal salinity, and a water temperature higher than the actual Mediterranean.

Echinoids are represented by approx. ten taxa but with few specimens. Only two taxa are abundant: the small *Psammechinus dubius*, and the genus *Scutella* which, in the Scutelles sandstone unit of the parastratotype, is represented by at least six species.

The remaining part of the macrofauna is made-up of Brachiopoda, essentially represented by thecideides, and balanids (*Balanus tulipiformis*), and a few madrepora, serpulids, and algae.

**Biostratigraphic location.** Analyses of the planktonic Foraminifera indicate that in the Rhodanian basin the Burdigalian starts in Zone N5 and ends in Zone N7 of Blow (1969). The most diagnostic species are: *Globigerinoides quadrilobatus* and its subspecies *altiapertus*, *sacculifer* and *trilobus*, together with *Globigerina praebulloides*, *G. ciproensis*, *Globoquadrina altispira*, and *G. dehiscens*.

The only index species of calcareous nannofossils found in both sections is *Helicosphaera ampliapertura*, which is present in the Calcareous Marls of the Salles formation. On basis of the scarce nannoplankton assemblage, and the presence of *H. ampliapertura* in particular, Martini (1988) placed the bases of the stratotype and the parastratotype in the NN2 Zone, and the upper parts of both sections in the NN2–NN3 Zone of the standard zonation of Martini (1971).

Among the Ostracoda, *Loxoconcha linearis* is the type species of biozone A of Carbonnel (1969) extending from the Aquitanian to the end of the Burdigalian.

The Pectinidae show that the Burdigalian belongs to the PN3 (Demarcq, 1990). In Saint-Restitut, index species found are: *Chlamys praescabriuscula* and *Pecten subbenedictus* along with *Chlamys palmata* (rare), *C. justiana* (types and varieties), *C. davidi*,

*C. tournali*, *C. pavonacea*, *C. gentoni*, *C. multistriata*, *C. subholgeri*, *Gigantopecten latissima restitutensis*, *Pecten paulensis*, *P. pseudobeudanti*, *P. josslingi*, *P. ziziniæ*, and *Flabellipecten galloprovincialis*.

Among the Bryozoa *Hornera dorsocavata* is considered as the characteristic species of the Burdigalian, and is present in both sections associated with *Pseudofrondipora davidi* and *Frondipora verrucosa*.

#### *Physico-chemical stratigraphy*

No geochemical data are presently available for either sections. Nevertheless fish teeth are present in the Saint-Restitut greenish molasse (Saint-Paul-Trois-Châteaux section), and glauconite is found in the basal conglomerate at both locations. These may be potentially useful for strontium isotope chemostratigraphic determination, and radioisotope dating.

#### CONCLUSIONS

The Burdigalian stratotype of the Rhône valley, as well as the parastratotype are very fossiliferous and of easy access. To complement our palaeontological knowledge, further studies on Foraminifera and calcareous nannofossils are needed. In the Burdigalian stratotype in the Bordelais region, dating would allow to localize both sections in a precise chronological context.

#### SOMMAIRE — LE STRATOTYPE HISTORIQUE BURDIGALIEN DANS LA VALLÉE DU RHÔNE

(Manuscrit soumis: Avril 1993, révisé: Janvier 1994; rédacteur responsable: GSO)

Le stratotype historique du Burdigalien de la Vallée du Rhône est situé à Saint-Paul-Trois-Châteaux et un parastratotype existe à Montbrison-Fontbonau (Drôme, SE France). Les sédiments conglomératiques de la base du Burdigalien du stratotype transgressent sur le Crétacé supérieur. Dans le parastratotype, les sédiments burdigaliens débutent par un conglomérat remaniant des sables argileux de l'Oligocène. Ces sédiments, très fossilifères et épais de près de 120 m dans le stratotype, ont un caractère littoral; ils correspondraient à des dépôts de séquence transgressive de haut niveau. La microfaune de foraminifères n'a pas encore fait l'objet de publication mais une étude d'Anglada a identifié les zones N5 à N7 dans le stratotype tandis qu'un sondage dans l'unité sus-jacente indique déjà la zone N8. La nannoflore calcaire été étudiée par Martini qui a reconnu les zones NN2 à la base et les zones NN2–NN3 au sommet. La connaissance de ce stratotype devrait être mise à jour.

(Sommaire proposé par les rédacteurs, GSO)

#### ACKNOWLEDGEMENTS

We would like to thank Philippe Claeys (U.C. Berkeley), and A. Montanari for translating into English the original French manuscript.

*Chapter A4*

**Sr ISOTOPE RECORD IN THE AREA OF THE LOWER MIOCENE  
HISTORICAL STRATOTYPES OF THE AQUITAINE BASIN (FRANCE)**

B. Cahuzac, L. Turpin and P. Bonhomme

**INTRODUCTION**

During the Miocene, the Aquitaine Basin was a large embayment opening westward into the Atlantic Ocean. Several transgressions extended more or less eastward, with facies of mainly shallow to infralittoral types. These deposits are generally very fossiliferous, which led earlier authors to define the Aquitanian and Burdigalian stages there.

Among the undertaken studies, the  $^{87}\text{Sr}/^{86}\text{Sr}$  chemostratigraphic tool has been used to characterize these reference exposures. In the past decade, improvements in analytical techniques as well as in the stratigraphic coverage from ODP sites have made possible high resolution Sr isotope stratigraphy of marine sections. During geological periods of high  $^{87}\text{Sr}/^{86}\text{Sr}$  slope, such as the Miocene, the resolution can be theoretically better than 0.5 Ma.

In this study, we present the Sr isotope record of the Aquitanian and Burdigalian stratotypes area. Samples were collected in historical as well as new outcrops described here. Among these sections, a few are protected and have been cleaned and set off in the framework of the 'Réserve Naturelle Géologique de Saucats–La Brède'. Analyses were performed on well preserved macrofossils only, preferably on aragonitic bivalves. Some years ago, a few preliminary Sr isotope ratios of the Miocene historical stratotypes in the Bordeaux area have been documented by DePaolo and Ingram (1985). More precise and numerous analyses have been undertaken today, with the goal to determine the minimum range of  $^{87}\text{Sr}/^{86}\text{Sr}$  ratio values for the Aquitanian and Burdigalian deposits of the Aquitaine Basin from the historical stratotype sections, and from some geographically close outcrops. These deposits have been well dated on the basis of their microfaunas. With this aim in view, we have revised and sampled many outcrops throughout the whole palaeobasin.

In this study, we also compare the Sr isotope ratios from Aquitaine samples, and from ODP deep-sea deposits, based on the same biostratigraphic calibration. We made also preliminarily such a comparison between Aquitaine samples and Italian samples for the Lower Miocene. At last, for Aquitaine levels, we propose estimated Sr ages with the aim of providing good relative datings for the stratotypic sequences on one hand, and to supply an indication about the sedimentation rate in these stratotypes on the other hand.

**DESCRIPTION OF THE ANALYSED SAMPLES**

For this study, we have preferably chosen samples from the stratotype area (i.e. the Bordeaux area, North Aquitaine, in the vicinity of Saucats and Léognan villages), but

we recognized also many Miocene outcrops (under Sr-study) elsewhere in the Aquitaine Basin.

*Aquitanian from the Saucats area (Fig. 1)*

*Historical stratotype.* The Aquitanian stratotype stretches along the Saucats brook, from La Brède to Saucats, in accordance with Mayer-Eymar's original description (1858). Usually, the Aquitanian Stage has been mainly studied on the three classic sections of Bernachon, L'Ariey, and Moulin de l'Eglise because of their easy access. However, these sections do not represent the entire stratotype. This stratotype was very well described by Mayer-Eymar (1858) in a figure redrawn by Dollfus (1909). The whole of the deposits constituting this stage stretch from the first marine layer overlying the Late Oligocene continental clays (at La Brède) onto the lacustrine limestone (included) situated at the top of L'Ariey and Moulin de l'Eglise sections (at Saucats). These continental (Late Oligocene) lower clays with concretions are cited by Mayer-Eymar (1858) above his 'marine Tongrian' (= Rupelian) of La Brède. This author specifies: "... Near the mill (now called Moulin de la Maule, Moulin du Malcomptant), as near the second (Moulin du Battant [= Augey]) (...), this clay is covered by: 1) a clayey marl either blue or whitish-blue, with numerous *Cerithium*..., *Turritella*..., *Lucina*..., *Cyrena*..." etc. Mayer-Eymar obviously made the Aquitanian stratotype begin with this first marine level (cf. his figure, 1858).

Our recent and detailed field study of the outcrops along the Saucats river has allowed us to observe many exposures along the stream, from La Brède (Moulin de la Mole = 'Maule' in Mayer-Eymar, 1858) to Saucats (L'Ariey; see Fig. 1A). As a start, the Sr-analyses of some of them are presented herein.

At La Brède, the marine Lower Oligocene (Rupelian = regional 'Stampian' with 'calcaire à Astéries' facies) is exposed under the Avignon locality. Upstream, as indicated by Mayer-Eymar (1858), we observe green (then whitish above) continental clays, today attributed to the Chattian. Above these clays, the first marine layer that overlies the Chattian can be presently observed between 'Moulin de la Mole' and 'Moulin d'Augey', on the right bank of the Saucats brook (municipality of La Brède). This layer is a grey to beige, argillaceous shelly coastal marl (Sr-analysed, No. 1; Fig. 1A). Also at this site, the Chattian consists of whitish to greenish azoic marly clays that contain calcareous nodules and concretions, as formerly described by Mayer-Eymar (1858).

Going upstream along the Saucats brook to the 'Pont de Lassus' (going past the 'Moulin du Bois Partus', now entirely ruined, cf. Mayer-Eymar's description), we saw a few outcropping marly levels, of either margino-littoral or coastal facies. At Lassus (on the right bank), a sample of grey-beige sandy marls with mollusks was collected for Sr-analysis (No. 2; Fig. 1A). Upstream, between Lassus and Moulin de l'Eglise (going past the Bernachon and L'Ariey sections, see locations 3 and 4 in Fig. 1A), we observed almost continuous outcrops (cf. also Poignant and Pujol, 1976). We took samples at Bernachon (layer 3, upper part, and layer 5, upper part), and L'Ariey (layers 6, 8 and 12, which is a brackish lagunal clay); this numbering of layers is according to Poignant et al. (Chapter A1 in this volume).

Nowadays, the complete sequence of the typical Aquitanian of Mayer-Eymar is therefore still mostly visible. Only the upper levels (Bernachon, L'Ariey) belong to the

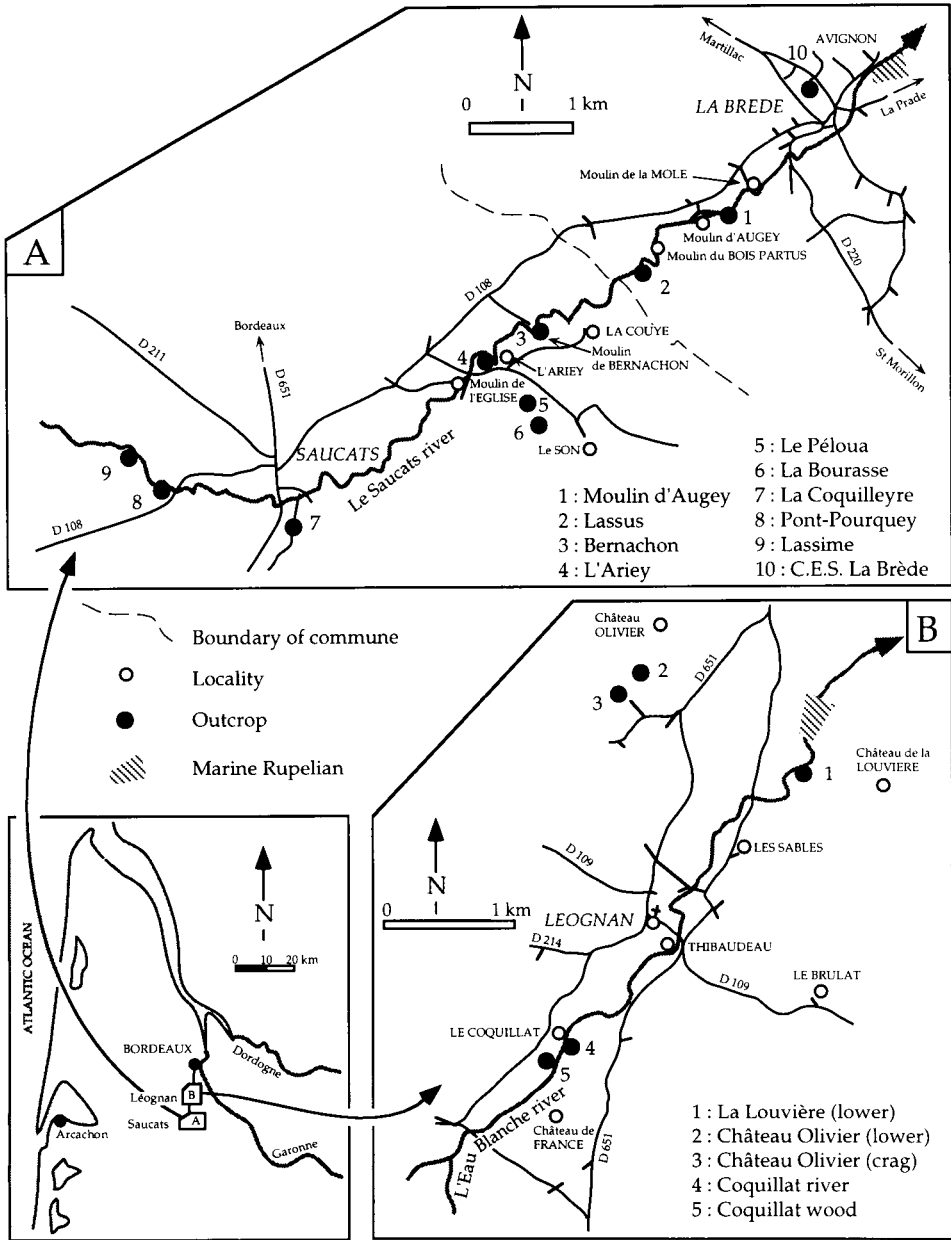


Fig. 1. Maps of the northern Aquitaine Basin, with location of some exposures in the Saucats–La Brède area (A) and Léognan area (B). In (A), the Aquitanian historical stratotype is located between Moulin de la Mole and Moulin de l'Eglise, along the Saucats river.

'Réserve Naturelle Géologique' and have been declared protected area. They have been described in detail by Pognant et al. (Chapter A1 in this volume), and Cahuzac et al. (1996). These profiles have been recently cleaned to be presented to the public.

*Other exposures (Fig. 1A).* Near the historical stratotype valley, we sampled a layer of light beige to reddish shelly marls from the lower part of the La Bourasse section (No. 6 in Fig. 1A and cf. Fig. 2). This layer is overlain by lacustrine marls, then by a lacustrine limestone (which is located at the bottom of the section as figured by Poignant et al. in Chapter A1). The La Bourasse section is at about 800 m from the Saucats brook (Fig. 1A). At La Brède, on the Avignon hillside (about 500 m to the north of the Saucats brook, on the left bank of the stream), we sampled greenish fossiliferous marls in the exposure of the 'Collège' (= C.E.S. = secondary school; No. 10 in Fig. 1A). These marls, which in this site overlie whitish marlstones, crop out at an altitude of about 33–34 m, and contain brackish and marine mollusks (*Ostrea*, Potamididae, *Loripes*, *Barbatia*).

### *Burdigalian from the Saucats area*

The Saucats area exhibits several sections of the 'faluns de Saucats et de Léognan' which constitute the stratotypical formation of the Burdigalian (lower part of the stage), as described in the author's definition (Depéret, 1892).

On the framework of the project 'Réserve Naturelle Géologique', the Péloua section has recently been set up for visitors. This section is at about 500 m from the Saucats brook on the right bank of the stream (No. 5 in Fig. 1A and cf. Fig. 2). It is exposed on the surface – a classic Burdigalian layer which consists of a sandy 'falun' (crag) very rich in hermatypic corals and mollusks. The layers underlying this crag have been made visible thanks to the creation of this new exposure. We dug a trench about 3 m deep. Lacustrine marls and limestones occur at the bottom of this section (Fig. 2). They correspond to the terminal phase of the lacustrine episode of the latest Aquitanian (this episode is also observed at the top of L'Ariey section, cf. Poignant et al., Chapter A1). These lacustrine layers are overlain by the Burdigalian marine series. The bottom of this series consists of marls which contain brackish to marine fauna (Sr-analysis of a sample of *Anadara* from the upper part of this layer), overlain by fine sands, then followed by the crag (cf. detailed figure of the section: L. Londeix in Cahuzac et al., 1996).

Nearby, in the La Bourasse section (6 in Fig. 1A), we sampled the outcropping classic Burdigalian crag which is particularly abundant in large specimens of *Turritella terebralis* (up to 10 cm long), *Euthriofusus*, *Anadara*, with *Trigonostoma*, *Xenophora*, etc.

In the Saucats brook, several Burdigalian outcrops occur between the Moulin de l'Eglise and the village of Saucats, and farther upstream. We analysed samples from: (1) the La Coquilleyre section, located in a little brook, tributary in the right bank (7 in Fig. 1A), sample from light beige shelly sands in the lower part of the outcropping cliff; (2) the new Pont-Pourquey section, one of the exposures designated to illustrate the Burdigalian stratotype (8 in Fig. 1A; cf. discussion in Poignant et al., Chapter A2 in this volume, samples from layers 4 and 6 in the figure of these authors); (3) the Lassime exposure (9 in Fig. 1A), sample from upper part of layer 1 (op. cit.); moreover, we analysed also a sample from layer 2 (above No. 1), which corresponds to Serravallian deposits (within zones NN7 Martini, N13–14 Blow; cf. Müller and Pujol, 1979) overlying directly the Burdigalian ones in this area.

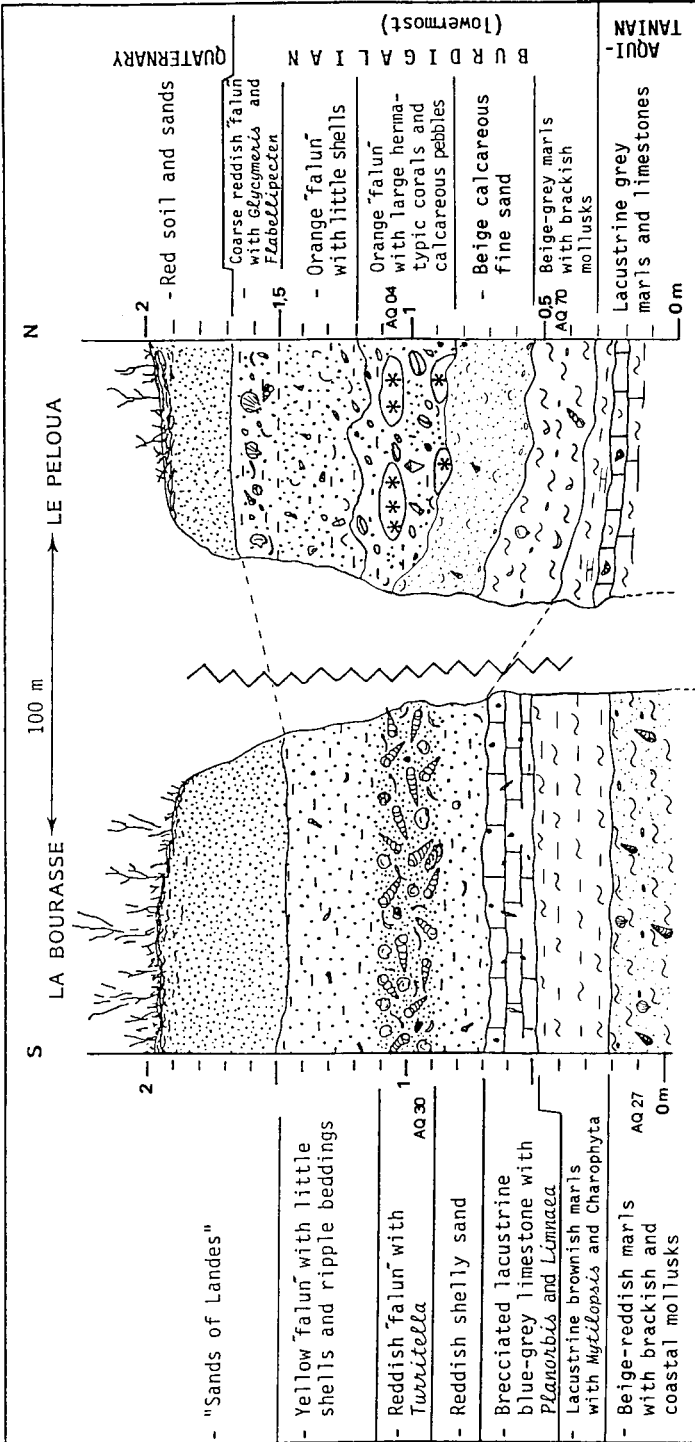


Fig. 2. Schematic sections of the La Bourrasse exposure (partly from Chapter A2) and Le Péloua (new trench outcrop) in Saucats, with location of the Sr-analyzed samples (numbers 'AQ').



### Lower Miocene from the Léognan area

*Overview and Aquitanian samples.* Léognan village is located 8 km to the north of Saucats (see Fig. 1). Numerous classic Miocene outcrops have been mentioned at Léognan. We rediscovered and sampled several sections with more or less fossiliferous layers. Preliminary data are presented here. As at La Brède, the basement consisting of Rupelian marine layers can be observed. These layers occur downstream from La Louvière in the 'L'Eau Blanche' valley (Fig. 1B). Upstream, and stratigraphically above the Rupelian beds, there are white clays (continental Chattian), which are overlain by greyish marls with brackish mollusks, of Aquitanian age (we made a Sr-analysis of a sample from the La Louvière Aquitanian lower section: 1 in Fig. 1B).

*Burdigalian samples.* According to numerous early authors (ref. in Daguin, 1948), it has been classically admitted that at Léognan, the Burdigalian series begins with the 'molasse ossifère' which was quarried in this area. This marine formation consists of fine, beige, sometimes slightly indurated, calcareous sands, containing abundant bones of marine mammals. The Burdigalian age of this deposit has been confirmed by Drooger (in Drooger et al., 1955) based on evolutionary stages of the Miogypsinidae nepionic apparatus. The presence of a lacustrine limestone layer at the top of the Aquitanian as seen in Saucats cannot be confirmed here, because the Miocene series is not fully exposed presently. Tournouer (1862, p. 1047) and Dollfus (1920, p. 145) emphasize its absence, whereas other authors mention few pieces, which may not be in situ, of such a limestone (ref. in Malvesin-Fabre, 1939; Daguin, 1948). At Léognan, the Burdigalian classic 'faluns' facies ('formation-type' of which the stage is made up) occurs at places within the 'molasse ossifère', but mainly above this basal 'molasse'. For example, the 'falun' (crag) of the Le Coquillat historical section was designated to define the Burdigalian stratotype.

Thus for a start we analysed few representative levels of the Léognan Burdigalian, including the 'stratotypic faluns' (crag). From bottom to top, we sampled first the basal sandy 'molasse' layer near the base of the now visible section of Château Olivier, in abandoned quarries (at about 1.2 km from the L'Eau Blanche river; 2 in Fig. 1B). This 'molasse' contains sand dollar urchins, *Echinolampas richardi* and some internal molds of mollusks. Close by, towards the southwest, this sandy formation contains abundant mollusk (mainly *Bivalvia*) shells; we analysed this 'Château Olivier crag', which is very rich in the *Bivalvia Glycymeris cor* (bivalve specimens), with *G. bimaculata*, *Flabellipecten burdigalensis*, etc. (3 in Fig. 1B).

Another good sequence of Burdigalian age occurs presently in the L'Eau Blanche river, upstream from the Léognan bridge located on road D 109. Going upstream, at the base of the Burdigalian series, the first exposed unit is the sandy 'molasse'. In this site, this unit formerly contained the 'falun de Thibaudeau', on the left bank, as Daguin (1948) indicates: "La molasse n'a pas une composition homogène; parfois très sableuse, elle passe latéralement à un falun (falun de Thibaudeau) ..." A sample from this crag was Sr-analysed by DePaolo and Ingram (1985; cf. Table 1b and Fig. 1B). Far upstream, under the locality Le Coquillat, the upper part of the sandy 'molasse' is a bioclastic beige sand with numerous Pectinidae (*Flabellipecten burdigalensis*), which occurs in the river (4 in Fig. 1B). Above the sand, we observed the classic yellow-rust crag of Le Coquillat on both the left and right banks. For instance, there is currently a good outcrop of this crag in the Coquillat wood (Sr-sample 5 in Fig. 1B, from the left bank).

Table 1a

 $^{87}\text{Sr}/^{86}\text{Sr}$  analytical data from some Chattian–Miocene samples of Aquitaine Basin

Reference	$^{87}\text{Sr}/^{86}\text{Sr}$ (SRM = 0.710254)	Biozones	Sample / section	Locality	Analysed fossil	Other indications	
*AQ 01	0.708237	P22/NP25	Abesse river: GA.38522	St Paulès-Dax (40)	<i>Glycymeris</i> sp. (= " <i>G. poustagnacensis</i> ") [a]	SW Aquitaine	
AQ 17	0.708262	P22/NP25	Abesse upper cliff	St Paulès-Dax (40)	<i>Cardium</i> sp. [a]	Chattian	
AQ 21 ♦	0.708340		Moulin Augey: GA.34412	La Brède	<i>Miltha incrassata subscopulorum</i> [a]	♦ Aquitanian stratotype (Saucats - La Brède)	
AQ 22 ♦	0.708377		Lassus: GA.34401	Saucats	<i>Miltha incrassata subscopulorum</i> [a]		
AQ 23 ♦	0.708392		Bernachon 3 (upper)	Saucats	<i>Corbula</i> sp. [a]		
*AQ 12/AQ 63 ♦	0.708405		Bernachon 5 (upper)	Saucats	<i>Glycymeris</i> cor [a]		
*AQ 02 ♦	0.708399		L'Arçay 6 (lower)	Saucats	<i>Glycymeris</i> cor [a]		
AQ 27	0.708413		Bourasse-lower: GA.34419	Saucats	<i>Chione (Clausinella) sacyi</i> [a]		
AQ 64	0.708415		GA.34403 (C.E.S.)	La Brède	<i>Barbatia barbata</i> [a]		
AQ 51 ♦	0.708420		L'Arçay 8	Saucats	<i>Timoclea subspadicea</i> [a]		
(AQ 52) ♦	(0.708457)		L'Arçay 12 (lagoonal)	Saucats	<i>Polymesoda (=Cyrena) brogniantii</i> [a]		
AQ 70	0.708460	#	Péloua lower: GA.39095	Saucats	<i>Anadara</i> gr. <i>cardififormis</i> [a]		Burdigalian of Saucats
*AQ 04	0.708478	N5	Péloua (coral crag)	Saucats	<i>Glycymeris</i> cor [a]		
*AQ 11	0.708502	N5-low/N6/NN2	Pont-Pourquey 4	Saucats	<i>Glycymeris</i> cor [a]		
AQ 30	0.708517	N5-low/N6	Bourasse-crag: GA.34413	Saucats	<i>Turritella terebralis</i> [b]		
*AQ 05	0.708541	N5-low/N6/NN2	Pont-Pourquey 6	Saucats	<i>Glycymeris</i> cor [a]		
AQ 33	0.708543	N5-low/N6	Lassime-1 (upper): GA.34418	Saucats	<i>Donax transversa</i> [a]		
AQ 78	0.708559	N5-low/N6	Coquilleyre: GA.39096	Saucats	<i>Glycymeris</i> cor [a]		
AQ 39	0.708851	N13-N14/NN7	Lassime-2: GA.34420	Saucats	<i>Glycymeris bimaculata</i> [a]	Serravallian of Saucats	
AQ 19	0.708384	N4	La Louvière-lower: GA.34405	Léognan	<i>Veneridae</i> (cf. <i>Tapes</i> sp.) [a]	Aquitainian	
AQ 71	0.708446	#	Olivier-lower molasse: GA.39065	Léognan	<i>Parasutella</i> gr. <i>bonati</i> [echinoid]	Léognan area	
AQ 74	0.708450	#	Château Olivier crag: GA.39094	Léognan	<i>Glycymeris</i> cor [a]		
AQ 73	0.708488	N5-low/N6/NN2	Coquillat-wood: GA.34406	Léognan	<i>Glycymeris bimaculata</i> [a]		
AQ 32	0.708631	N6	Magomy lower: GA.34408	Pessac	<i>Glycymeris</i> cor [a]	Other areas of Aquitaine	
*AQ 07	0.708643	NN4	Le Brugas: GA.34467	St Jean-de-Marsacq (40)	<i>Glycymeris</i> cor [a]		
AQ 96	0.708750	upper N9/NN5	Lafaurie: GA.34479	Saubrigues (40)	<i>Anadara dilevii</i> [a]		
** Toul.	0.708619	N5-low/N6/NN2	Pont-Pourquey 4	Saucats	Shark tooth	Burdigalian	

\* analyses H. ELDERFIELD (Cambridge University); \*\* analysis Toulouse University; [a] = Bivalves; [b] = Gastropods; # Stratigraphic confirmation by Micropalaeontology study; [(AQ 52) sample: see discussion in the text].  
 - Confidence intervals on Sr isotope ratios: 2  $\sigma$  external on SRM 987 ( $\sim 1.6 \cdot 10^{-4}$ , see text). - Among the Saucats Aquitanian samples, those belonging to the historical stratotype are marked with a black diamond ♦.  
 - All the samples are in Gironde ("département" n°33, North Aquitaine), except a few ones from Landes ("département" n°40, South Aquitaine).

Table 1b

<sup>87</sup>Sr/<sup>86</sup>Sr analytical data from some Chattian–Miocene samples, from DePaolo and Ingram (1985)

Reference of sample	<sup>87</sup> Sr/ <sup>86</sup> Sr (SRM = 0.710254)	(±10 <sup>-6</sup> ) <sup>a</sup>	Section	Locality	Fossil
<i>Aquitanian</i>					
A1	0.708384	23		'La Brède'	<i>Corbulomya tournoueri</i> <sup>b</sup>
A2	0.708437	20	L'Ariey	Saucats	<i>Timoclea subspadicea</i> <sup>b</sup>
<i>Burdigalian</i>					
Burd2	0.708449	24	Thibaudeau	Léognan	<i>Nuculana emarginata</i> <sup>b</sup>
M7	0.708489	27		'Léognan'	<i>Dentalium exlamarcki</i> <sup>d</sup>
Burd3	0.708491	31		'Léognan'	<i>Oxysteles burdigalensis</i> <sup>c</sup>
M6	0.708520	32		'Saucats'	Scaphopoda <sup>d</sup>
<i>Chattian</i>					
O4	0.708227	35		Germany	<i>Dentalium</i> <sup>d</sup>

<sup>a</sup> Uncertainty is two internal standard errors on individual measurements. <sup>b</sup> Bivalves. <sup>c</sup> Gastropods.<sup>d</sup> Scaphopods.

This new outcrop, very near the historical stratotypic exposure of Le Coquillat which is now inaccessible (see discussion in Poignant et al., in Chapter A2), may, in our opinion, correctly replace the latter one, and be considered as a useful neostratotype.

#### *A few other samples from the Aquitaine Basin*

In order to document the Sr isotopic ratio range throughout the Oligocene and Miocene in Aquitaine, we also investigated some other localities well dated by palaeontology. Those localities are in stratigraphic continuity with the Saucats–Léognan sequence.

*Examples of Chattian exposures.* The Upper Oligocene (Chattian Stage) marine series is exposed only in southwestern Aquitaine, with various, often reefal facies. Several exposures are known, for example, in St-Paul-lès-Dax (Landes Department); they contain bioclastic sands and crags which are very rich in larger benthic Foraminifera (cf. sections in Cahuzac and Poignant, 1988; Cahuzac and Roman, 1994; stratigraphic data in Müller and Pujol, 1979; Cahuzac et al., 1995). We present here the analytical results from two samples collected in the upper part of the Chattian series recognized in this area: the Abesse river outcrop (with e.g. numerous *Nummulites bouillei*, *Cycloclypeus*, *Miogypsinoides*), and the Abesse upper cliff exposure.

*Examples of Burdigalian/Langhian exposures.* In some regions, Burdigalian deposits which are younger than in the stratotypic area of Saucats and Léognan, have been evidenced.

In northern Aquitaine, 6 km southwest of Bordeaux, the new Pessac–Magonty section shows a Burdigalian sandy bioclastic sequence, which is overlain by marine Middle Miocene deposits; we analysed a sample from a grey crag from the lower part of this Burdigalian section.

In southwestern Aquitaine, the Saubrigues Gulf (140 km of Bordeaux) constitutes the western part of a palaeocanyon, the eastern part of which was filled in during the Chattian (see Cahuzac et al., 1995). This Saubrigues Gulf was filled in with Lower

Miocene, mostly marly deposits, representing a continuous Aquitanian–Burdigalian series. Some borehole sections yielded a thickness of about 400 m for the Lower Miocene. Several outcrops (grey marls more or less rich in mollusks) have been allocated to Zone NN4 of Martini (1971). We present a Sr-analysis of a sample from one of these outcrops, at St-Jean-de-Marsacq/Le Bragas. Towards the northwest, this gulf shows deposits related to plankton Zones NN5, upper part of N8, and of a Langhian age (Müller and Pujol, 1979; Cahuzac et al., 1995 and ref. therein; these sediments contain *Praeorbulina sicana* and *P. curva* among others), for example the Saubrigues/Lafaurie shell-bearing marls, which have been analysed from Sr isotopes.

### *Biostratigraphic and palaeogeographic overview*

Ages for the Aquitaine samples were determined, along with lithostratigraphic criteria, on the basis of planktonic microfaunas and nannofloras, as well as other biostratigraphic data. In Table 1a we indicated the planktonic biozones, either directly evidenced (as published previously) or presumed when a biomarker has been cited (ref. in Jenkins, 1966b; Drooger et al., 1976; Pognant and Pujol, 1976, 1978; Benda et al., 1977; Müller and Pujol, 1979; Cahuzac et al., 1995; foraminiferal zonation: Blow, 1969; nannoplankton zonation: Martini, 1971).

Concerning the nannoplankton, which is very scarce in all the Aquitanian exposures, only one sample from the Aquitanian stratotype could be allocated to a biozone, namely NN1. This is the ‘La Couye’ sample, collected downstream from Bernachon, i.e. between our ‘Lassus’ and Bernachon samples (GA 101 sample, cf. Müller and Pujol, 1979). However, it can be noted that “la détermination de cette zone dans la région méditerranéenne n’est pas très sûre” (Müller and Pujol, 1979), and is based on the absence of certain tropical index species. Therefore, a confirmation would have to be found in other Aquitanian stratotypic samples. In the Burdigalian stratotype formations, the NN2–NN3 zonal interval has been recognized at the base of Pont-Pourquey section with the presence notably of *Discoaster druggii* (Benda et al., 1977), whereas Müller and Pujol (1979) allocated this section to Zone NN2 based on the presence of *Helicosphaera ampliaperata*. *D. druggii* is the index fossil for the base of Zone NN2, while *H. ampliaperata* appears within Zone NN2.

For the Chattian samples of Aquitaine, and for those of the Aquitanian–Burdigalian at Saucats and Léognan, the biostratigraphic position was confirmed by the study of Miogypsinidae (larger benthic Foraminifera) populations (cf. Drooger et al., 1955; Drooger, 1964; and our personal observations). The Miogypsinidae, which are generally abundant in most of these deposits in littoral facies, are known to be very good markers for dating, thanks to their rapid evolution as evidenced in the characteristics of the nepionic spirals. For the new Burdigalian samples Saucats AQ 70 and Léognan AQ 71/74, no planktonic studies are yet available; therefore, their age was determined by Miogypsinidae stratigraphy, with presence of the taxa *Miogypsina globulina*.

Based on these stratigraphic datings, the recognition of the Miocene deposits in the whole Aquitaine Basin (from outcrops and boreholes) led palaeogeographic interpretations. In the Lower Miocene for example, two main transgressive phases occurred, during which the sea extended far eastward (see Alvinerie et al., 1992). The first one is mainly developed in the upper part of the Aquitanian Stage. The

facies are shallow everywhere; this sequence contains marine deposits interfingering with brackish and lacustrine sediments. In the central and eastern Aquitaine Basin, we generally observed lagunal deposits (lower ‘marnes à *Ostrea aginensis*’, of Aquitanian age), which overlie the regionally classic, lacustrine ‘calcaire blanc de l’Agenais’ (of Chattian/lowermost Aquitanian age). The second main transgression occurred during the lower Burdigalian and extended locally a bit farther than the Aquitanian one in southern and northeastern Aquitaine. In comparison with the data concerning the Aquitanian, the lower Burdigalian faunal assemblages are generally more stenohaline, coral reef build-ups are more widely developed (Cahuzac and Chaix, 1996) and the marine palaeoenvironments are more open to oceanic influences.

## Sr ISOTOPE ANALYSIS

### *Materials and analytical techniques*

Only pristine-like shells, i.e. those not cemented and without traces of secondary incrustation, were selected for analysis. When available, initially aragonitic bivalves were preferred. X-ray diffractograms of a few samples chosen following the same criteria showed 100% aragonite, i.e. these shells have preserved their initial mineralogic composition without significant recrystallization. The following results were obtained (analyses by G.S. Odin):

Chattian: *Glycymeris abessensis*, GA 38522 (St-Paul-lès-Dax), max. 79 mm high (peak at 3.40 Å)

Aquitanian: *Anadara cardiiformis* (Toulouzette), max. 93 mm high

Burdigalian: *Glycymeris cor*, Pont-Pourquey (Saucats), max. 79 mm high

Burdigalian: *Glycymeris cor*, GA 39094 (Léognan), max. 92 mm high

Serravallian: *Megacardita jouanneti*, Salles, max. 90 mm high

Serravallian: *Glycymeris bimaculata*, Lassime (Saucats), max. 91 mm high

Recent: *Cardium*, Atlantic beach, max. 64 mm high

Recent: *Venus verrucosa*, Atlantic beach, max. 71 mm high

It is worth noting that the two Recent bivalve shells analyses gave a main peak of 10% to 30% lower than those obtained from the fossil shells.

These aragonitic mollusks were also used in Aquitaine for Sr isotope analyses by DePaolo (1986, p. 104) who emphasizes that these “macrofossil samples have high Sr concentrations, have never been deeply buried, and thus are unlikely to be modified”.

Well preserved shells were broken with steel scissors and the harder fragments selected for analysis. Fragments were then sonicated in 18 MΩ water, the eventual traces of clay minerals removed by suspension in 1M NaPO<sub>3</sub>, and the sample cleaned again in 18 MΩ water. Fragments were then reacted with 20% acetic acid, centrifuged at 14,000 rpm, and the supernatant was dried and subsequently dissolved in 4M HNO<sub>3</sub>. Sr was isolated by reverse phase chromatography on 20 μl SrSpec<sup>®</sup> columns held in the Luer end of a polyethylene syringe closed by a 4 mm diameter Millex<sup>®</sup> filter. Recovery was better than 90% and blank was ~20 pg. All operations were done in a clean lab with class 10 laminar flow hoods. Sr was loaded on a single W filament with TaF5/phosphoric acid (Birck, 1986) and analysed in static multicollection mode on a Finnigan MAT 262 (C.F.R., Gif-sur-Yvette). Mean value of NIST SRM (Standard Reference Material) 987

is 0.710237,  $2\sigma$  external absolute = 0.000016. The latter (external reproducibility) has been preferred to the within-run statistics as the best estimate of confidence interval on the result (not taken up in Tables 1 and 2).

### Results

Analytical data from the present study are reported in Table 1a, together with a few performed in the Cambridge laboratory (H. Elderfield) and which will be included in a paper by N. Goldsmith et al. (paper in progress). A single analysis of a shark tooth made in the lab at Toulouse University (cf. Poignant et al., Chapter A2) has been included. For comparison, we have also included in Table 1b the Sr ratios given by DePaolo and Ingram (1985) from the Aquitaine Miocene and from the German Chattian. All these  $^{87}\text{Sr}/^{86}\text{Sr}$  values (normalized to  $^{86}\text{Sr}/^{88}\text{Sr} = 0.1194$ ) have been normalized to the SRM 987 = 0.710254 (cf. Oslick et al., 1994, in order to use easily the equations of these authors). For information, the respective SRM 987 at the time of the analyses, and which we took into account, were: 0.710237 (nobis, Gif-sur-Yvette), 0.710254 (Elderfield), 0.710250 (Toulouse), 0.710310 (DePaolo and Ingram, 1985). (For the standard of these latter authors, if a value of 0.710330 should have to be adopted instead of 0.710310 as indicated by McArthur (1994), the concerned Sr ratios values which are included in Table 1b would have to be lowered by  $2 \times 10^{-5}$ .)

Estimated ages, calculated from the linear regressions given by Oslick et al., 1994 (based on ODP 747A hole data and using the numerical ages estimated by Cande and Kent, 1992, in their geomagnetic polarity time scale), are reported in Table 2, although as pointed out by McArthur (1994), there are no reasons for the  $^{87}\text{Sr}/^{86}\text{Sr}$  of the ocean to follow a linear evolution (Fig. 3).

Confidence intervals on the ages are thus critical to evaluate: as a first approximation, we only propagated the confidence interval ( $2\sigma$ ) of the measurement in the equations given by Oslick et al. (1994). These equations do not cover the whole time interval: as it appears in Figs. 3 and 4, a plateau occurs in the long-term  $^{87}\text{Sr}/^{86}\text{Sr}$  evolution at the Chattian/Aquitainian boundary (cf. also Hodell and Woodruff, 1994). As a consequence, there is a gap in the linear regression coverage. For sample AQ 21, close to the bottom of the Aquitainian stratotype, no age has thus been calculated and included in Table 2.

## DISCUSSION OF RESULTS: $^{87}\text{Sr}/^{86}\text{Sr}$ RATIOS

### *Consistency and evolution in the Sr isotope ratios from Aquitaine Basin*

*Overview.* A significant evolution can be noted in the  $^{87}\text{Sr}/^{86}\text{Sr}$  ratios from bottom to top of the studied samples series. In a first examination, most samples give in general  $^{87}\text{Sr}/^{86}\text{Sr}$  increasing with stratigraphic height (Table 1, Figs. 4 and 6), indicating good stratigraphic continuity. Also in most individual outcrops, this evolution agrees well with the superposition order of the deposits observed in the field: a trend of increasing Sr values towards higher stratigraphic levels can be observed in these outcrops.

From these data, we can determine the range of the  $^{87}\text{Sr}/^{86}\text{Sr}$  ratios for the different stages (Table 1). Ranges are minima and a little approximate, notably because the analysed samples are not necessarily the closest ones to the stage boundaries; further

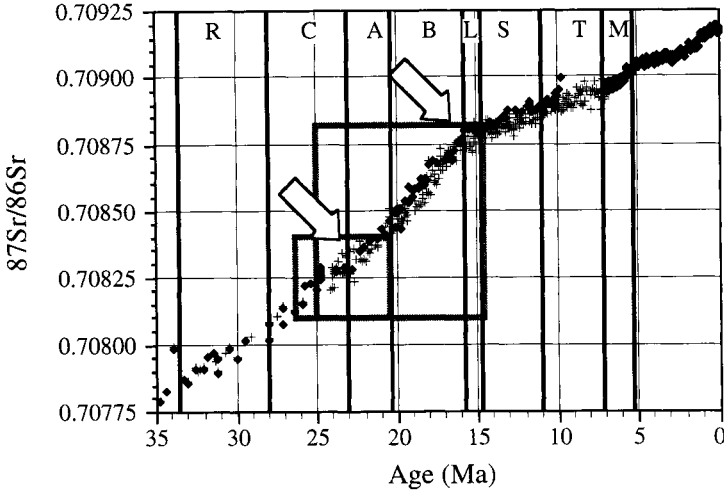


Fig. 3. Synthesis of ODP data for the period 0–35 Ma. Filled diamonds represent data from Holes 758 and 747A with the highest quality time scale (Oslick et al., 1994; Farrel et al., 1995), crosses represent Holes 522 (Miller et al., 1988), 289 (Hodell and Woodruff, 1994) and 588 (Hodell et al., 1991). Arrows show the periods of change in the evolution slope, boxes show the plotting areas of Figs. 4 and 5. All data have been normalized to NIST SRM 987 = 0.710254 and to the GPTS from Cande and Kent (1992). The ages of the stage boundaries are from Odin (1994) and this volume; for the legibility of this figure, only the mean value of these ages has been represented (see the uncertainties in the cited ref.). Stage abbreviations: *R* = Rupelian, *C* = Chattian, *A* = Aquitanian, *B* = Burdigalian, *L* = Langhian, *S* = Serravallian, *T* = Tortonian, *M* = Messinian.

analyses, currently in progress, will complete this first set of data. We can first emphasize that our Sr ratios are very consistent with those of DePaolo and Ingram (1985) for the Aquitaine Lower Miocene, even if the precise outcrops of the samples analysed by these authors are unfortunately not always indicated (D. DePaolo could not provide such information: written commun., 1993).

**Chattian Sr ratios range.** The exposed Chattian marine deposits are those of southwestern Aquitaine only. Table 1a shows two analyses from the upper part of the Chattian series. In fact, in Aquitaine, the Sr ratios range from at least 0.708150 in St-Etienne-d'Orthe exposure (P22/NP25 Zones, under study, and cf. Cahuzac et al., 1995) to about 0.708262.

**Aquitanian Sr ratios.** From the stratotype area (Saucats–La Brède, Tables 1a and 1b), we consider that the Sr ratios range from about 0.708340 (sample AQ 21) to 0.708420 (AQ 51)/0.708430 (sample A2).

Sample AQ 21 from the lowermost layer at Moulin d'Augey, gives a value of 0.708340. It is worth noting that both brackish and shallow-marine faunas have been observed in this level. In near-shore environment or lagunal conditions,  $^{87}\text{Sr}/^{86}\text{Sr}$  of seawater may experience a continental imprint (Mc Culloch et al., 1989; Ingram and DePaolo, 1992; Ingram et al., 1996). Provided the riverine input had a  $^{87}\text{Sr}/^{86}\text{Sr}$  higher than seawater, which is the case in all non-volcanic conditions, the  $^{87}\text{Sr}/^{86}\text{Sr}$  in carbonate is being increased. This possibility will be carefully examined in the Moulin d'Augey level in further studies. (The outlier position of sample AQ 52, sampled in a fully

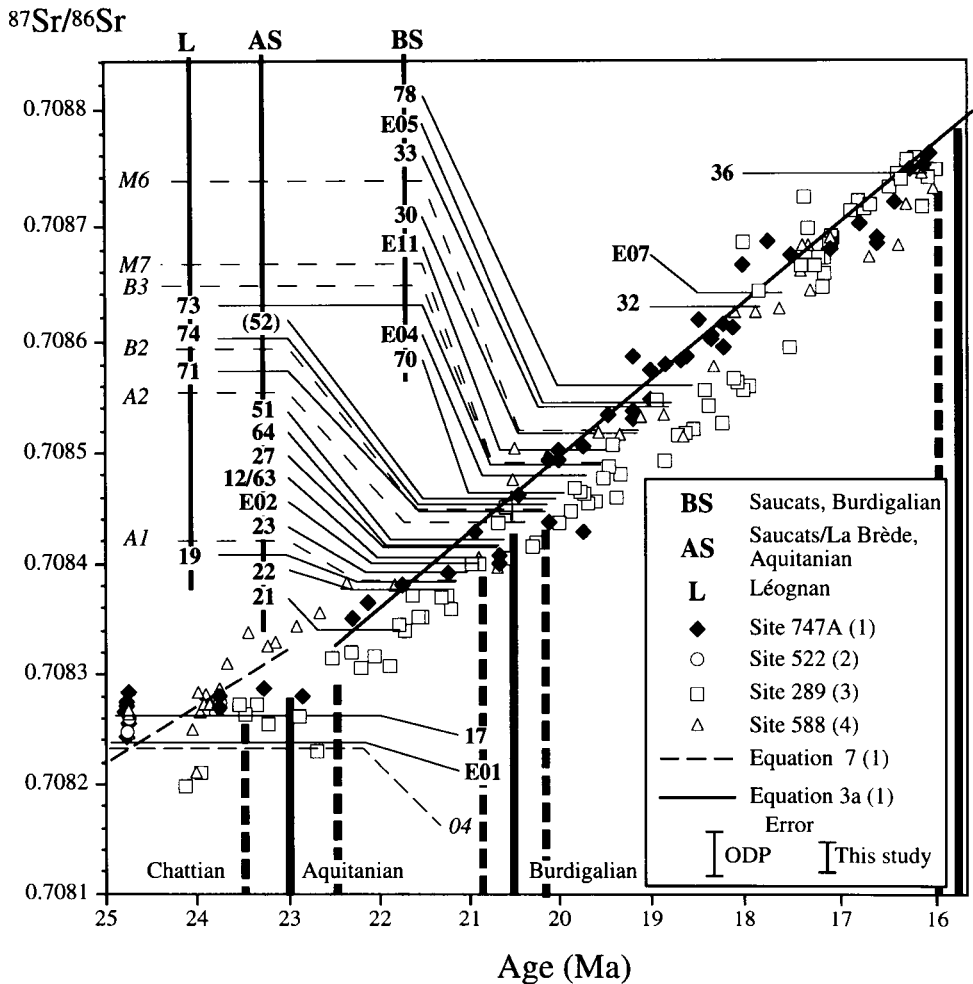


Fig. 4. Synthesis of  $^{87}\text{Sr}/^{86}\text{Sr}$  ratios for the Chattian, Aquitanian and Burdigalian of the Aquitaine Basin (especially the Saucats-Léognan area) plotted with data from ODP sites (CK92 time scale); (1) Oslick et al., 1994; (2) Miller et al., 1988; (3) Hodell and Woodruff, 1994; (4) Hodell et al., 1991. The two regression lines are those given in Oslick et al. (1994). Thick lines are best estimate for stage boundaries (based on extrapolated radiometric ages, as proposed in this volume); the thick dashed lines show the confidence interval of the age of these limits. References in italics (left of the figure) are from DePaolo and Ingram (1985). *E05* = Elderfield's analyses (cf. N. Goldsmith et al., to be published). Sample data are figured as a horizontal thin line. The two error bars ( $2\sigma$  = external reproducibility) are those for ODP results ( $\pm 2 \times 10^{-5}$ ) and the present study ( $\pm 1.6 \times 10^{-5}$ ). Most samples plot in agreement with their stratigraphic order; No. (52) sample ratio: see text. There is also good agreement between the intervals covered by the  $^{87}\text{Sr}/^{86}\text{Sr}$  vs time CK92 of ODP points, and by the stratotypic data points when plotted within radiometric age boundaries, respectively.

lagunal level, can be unambiguously attributed to such a near-continental imprint: see below). Otherwise, the Sr ratio value of this AQ 21 sample needs re-evaluation of its deduced chemostratigraphic age estimate (cf. below).



The overlying samples (AQ 22 to AQ 51 and A2) show a progression, very consistent with the field data, in the Sr isotopic ratios (Figs. 4 and 6), leading to the following remark. Concerning both the Bernachon 5 and L'Ariey 6 samples, the L'Ariey 6 (level just above Bernachon 5) Sr ratio seems somewhat low (even if these two ratios are not significantly different). Perhaps the origin of this sample, from a crag deposit filling in vortical cavities (thanatocoenose accumulation with shells not surely in place, possibly reworked from neighbouring slightly older layers) may explain this fact.

The AQ 52 upper sample comes from the upper part of the L'Ariey section, from a very lagunal clay with only brackish fauna, such as the mollusks *Granulolabium plicatum* and *Polymesoda brongniarti*. Thus, we think that its ratio (0.708457, in brackets in Table 1a) is probably too high (and the estimated age a bit too young, Table 2) and that this sample is a kind of outlier.

*Burdigalian Sr ratios range from the stratotypic area.* For the Bordeaux stratotypic area (Léognan/Saucats), the Sr ratios range from about 0.708440 (AQ 71 and 'Burd2' samples) to 0.708560 (AQ 78). The Burdigalian transgression may have occurred a little earlier at Léognan than at Saucats. At Saucats, an emersion time permitted locally the deposition of a lacustrine limestone near the Aquitanian/Burdigalian boundary; this limestone is well evidenced everywhere in the Saucats area.

Concerning the AQ 71 and AQ 74 samples in the Léognan lowermost Burdigalian (the AQ 71 level just under AQ 74), their Sr ratios are very close to each other, as it was to be expected. But it is worth to point out the original calcitic composition of the AQ 71 analysed fossil, a sand dollar echinoid, compared with the other samples, which are mostly originally aragonitic.

An interesting comparison can be made between the analysis of the two samples AQ 11 and 'Toul', from exactly the same layer, No. 4, of Pont-Pourquey (one of the stratotypic exposures): their Sr ratios are significantly different, respectively 0.708502 for an aragonitic bivalve, and 0.708619 for a phosphatic shark tooth. Phosphatic teeth are known to form in vivo with lower Sr content than commonly observed in sediments (e.g., Grandjean et al., 1987; see also Staudigel et al., 1985/86). In phosphatic material, the maximum Sr content is reached after diagenetic uptake of interstitial Sr in sediments. The phosphatic remains can indeed incorporate alkaline-earth elements such as Sr in exchangeable sites. This leads some authors (e. g., Smalley et al., 1994) to consider such remains to be 'of low reliability' in Sr isotope stratigraphy. In fact, it is more exact to say that the reliability of such remains is dependent upon their immediate environment. The Sr content of sediments may vary over an order of magnitude from one locality to another. The  $^{87}\text{Sr}/^{86}\text{Sr}$  of interstitial water will be buffered by marine Sr in sediments rich in carbonate. But in cases where interstitial waters are buffered by volcanogenic material with low-radiogenic Sr (e.g., Elderfield et al., 1982; Blanc et al., 1995), the  $^{87}\text{Sr}/^{86}\text{Sr}$  of phosphates will experience decrease with time. The opposite, i.e. increase with time, may be observed when interstitial waters are buffered by continental clay minerals which have a  $^{87}\text{Sr}/^{86}\text{Sr}$  higher than seawater, which could have occurred in the 'Toul' sample.

*Sr isotope ratios from few other samples.* In addition to the stratotype area, there are various deposits in the Aquitaine Basin allocated to middle and upper parts of the Burdigalian Stage. Preliminary data concerning such deposits are included in Table 1a (Sr ratios of about 0.708640: AQ 32, AQ 07). Another sample (AQ 36) allocated to the

calcareous plankton Zones N8 (upper part) and NN5, (i.e. dated as Langhian or near the Burdigalian/Langhian boundary, depending on the criterion chosen for the definition of this boundary) has a Sr ratio of about 0.708750.

At last, a sample from the Mid Miocene deposits which directly overlie the Burdigalian ones in Saucats (Lassime outcrop), gave a Sr isotopic ratio of 0.708851; this sample has a Serravallian age. In this outcrop, we noticed a Sr ratio of 0.708543 from a Burdigalian sample (AQ 33), which gives an idea of the large extent of the sedimentary break existing locally in this area.

### *Consistency of the Sr isotopes between Aquitaine and oceanic deep-sea sediments*

We now compare the Sr isotope ratio values from Aquitaine levels with the ones from deep-sea boreholes sequences, for samples which can be allocated to the same planktonic biozone. So, it is the biostratigraphic tool which allows to correlate directly these typical landsections and the oceanic sediments. (In the following comparative data, all Sr ratios have been normalized to SRM 987 = 0.710254.)

*Aquitanian stratotype.* In the Aquitanian stratotype, two studies quote the presence (although very rare) of the index taxon *Globorotalia kugleri* at L'Ariey (lower part of the section; Poignant and Pujol, 1976) and in the three outcrops of Bernachon, Moulin de l'Eglise and L'Ariey (Drooger et al., 1976). Another index planktonic foraminifer, *Globoquadrina dehiscens*, is present in the sediments immediately underlying the Bernachon section, and above (Poignant and Pujol, 1976). With these species (in addition to *Globigerinoides primordius*, also present), these deposits can be allocated to Zone N4 of Blow (1969).

The two former taxa (*G. kugleri* and *G. dehiscens*) are often quoted from deep-sea borehole sediments, where the FO (First Occurrence) of *G. kugleri* has particularly been looked for, and is used to define the base of N4. In some ODP sites (cf. Hess et al., 1989), isotopic analyses of deposits allocated to Zone N4 gave approximate Sr ratio ranges of about: 0.708310 to 0.708450 in Site 292 (West Pacific); 0.708268 to 0.708457 in Site 529 (South Atlantic); 0.708300 to 0.708457 in Site 77B (Pacific).

Elsewhere, the base of Zone N4 has been recognized in sediments with Sr ratios of about 0.708290 in Site 516F (South Atlantic), 0.708328 in Site 563 (North Atlantic, see Hess et al., 1989 and ref. herein), 0.708292 in Site 608 (North Atlantic, see Miller et al., 1991b) and slightly lower (0.708240) in Site 289 (West Pacific, see Hodell and Woodruff, 1994). In Site 747A (Southern Indian Ocean, see Oslick et al., 1994), the base of the equivalent of Zone N4 (the classic index taxa being absent) is related to a Sr ratio of about 0.708280. In Site 588C (Southwest Pacific, see Hodell et al., 1991), some levels containing index taxa of N4 gave Sr ratios between about 0.708250 and 708405. Otherwise, the lower N4 zone corresponds to a ratio of 0.708282 in a borehole in the Gulf of Mexico (Atlantic, see Zhang et al., 1993).

The comparison between these ODP data and the ratios of 0.708340 to 0.708420/0.708430 in the series of the Aquitanian stratotype (Table 1) shows that the Sr ratio ranges are consistent and generally very similar in these two domains, taken into account the diverse uncertainties in these results. Otherwise, the Sr model ages calculated for these stratotypic exposures corroborate very well this consistency evidenced in the Sr ratios (see below and Fig. 5).

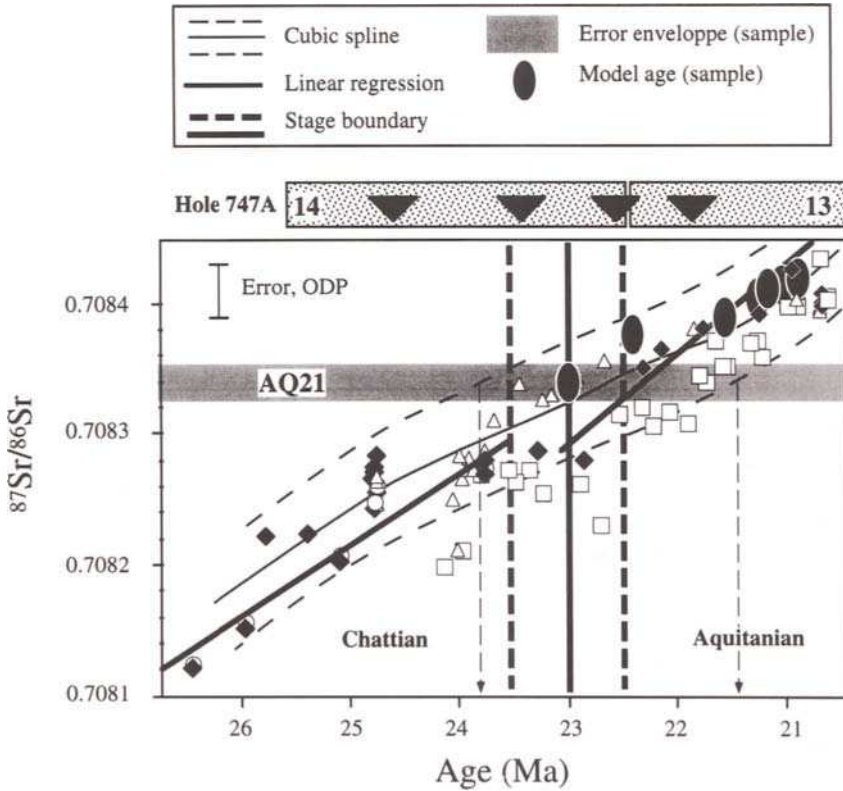


Fig. 5. Detail of the interval corresponding to the Chattian/Aquitanian boundary; symbols as in Fig. 4. The cubic spline smoothing is calculated with ISOPLOT (Ludwig, 1992) on data from Hole 747A (Oslick et al., 1994). The synthetic log of Hole 747A is also shown at the top of the figure, with reference to drill core sections 13 and 14; magnetostratigraphic tie points are represented by black triangles. Some scatter appears in the ODP data at this period, and unfortunately the presumably Chattian/Aquitanian limit was encountered not far from a core limit in Hole 747A. Taking into account all the uncertainties, i.e. concerning  $^{87}\text{Sr}/^{86}\text{Sr}$  as well as concerning the actual distribution of ODP data as illustrated by the confidence interval envelope on the cubic spline, the  $^{87}\text{Sr}/^{86}\text{Sr}$  age (ODP 747A/CK92, cubic spline) of sample 21 (bottom of the historical stratotype) and the extrapolated radiometric age proposed in the present volume for the Chattian/Aquitanian boundary are in agreement within their respective confidence intervals. If AQ 21 is taken as the lowermost Aquitanian sample and is assigned an age of  $23 \pm 0.5$  Ma, then model ages calculated for Saucats–La Brède samples (plotted as black ellipse of which the size gives the error) assuming a constant sedimentation rate, give an independent estimate of  $^{87}\text{Sr}/^{86}\text{Sr}$  vs time, which is in excellent agreement with ODP data.

*Burdigalian stratotype.* The index species *Globigerinoides altiapertura* is often used, among other useful criteria, to correlate the base of the Burdigalian (see Iaccarino, 1985; Montanari et al., 1991; Berggren et al., 1995; see also Chapter F2). In the stratotype deposits of Saucats–Léognan, it is present right at their base (Coquillat sands: Jenkins, 1966b), as well as higher up in the sections (Pont-Pourquey, Lassime sections: Poignant and Pujol, 1978), together with *G. trilobus*. These formations have been allocated to zones N5–lower N6 of Blow (1969), and to Zone NN2 of Martini

(1971; see also Chapter A2). In this lower Burdigalian stratotype series, the Sr ratios range from about 0.708440 to 0.708560 (Table 1).

In ODP sections (see references above), the base of Zone N5 corresponds approximately to Sr ratio values of 0.708450 (Site 292) or 0.708457 (Sites 529, 77B); in Site 608, the Sr ratios in deposits allocated to Zone N5 range from about 0.708400 to 0.708580, and for Zone N6 they range from 0.708580 to 0.708640. In Site 516, sediments allocated to Zones N5/N6 gave a Sr ratio range from about 0.708450 (with presence, as FO in this level, of *Globigerinoides altiapertura*) to 0.708590. In Site 289, in sediments close to the N5/N6 zonal boundary, Sr ratios of about 0.708530 are recorded. In some Southwest Pacific ODP sections, in samples allocated to Zone NN2, Sr ratios of about 0.708470 and 0.708480 (Site 590B, see DePaolo, 1986), of 0.708496 to 0.708532 (Site 588C, see Hodell et al., 1991), and of 0.708549 (Site 593, see Hess et al., 1986), have been measured. Otherwise, the Sr ratios in layers allocated to Zone N5 range from 0.708479 to 0.708589 in borehole E68-151 in the Gulf of Mexico (Zhang et al., 1993). These comparative data show that also for the stratotypic Burdigalian there is a good consistency in Sr ratio values from the Aquitaine Basin, and from oceanic sequences, based on biostratigraphic calibration of the samples.

*Other data and conclusions.* Consistent data occur also for other Aquitaine samples presented in Table 1a, for instance:

(1) In deposits related to the upper parts of Zones P22 and NP25: from the Latest Oligocene of Aquitaine, the Sr ratios are about 0.708230–0.708260 (Table 1a). These ratios are close to the ones recorded in ODP sections, as about 0.708220–0.708247 in Site 608, 0.708250–0.708280 in Site 747A, 0.708270 in Site 563, etc.

(2) In deposits allocated on the whole to Zone N8: in Aquitaine, a Sr ratio of about 0.708750 is recorded (Table 1a). In ODP boreholes, the Sr ratios in sediments corresponding to N8 range, for example, between 0.708745 and 0.708800 in Site 608, and between 0.708670 and 0.708790 in Site 289.

In conclusion, the regular evolution evidenced in the  $^{87}\text{Sr}/^{86}\text{Sr}$  ratios as well as the ranges of values of these Sr ratios in the Lower Miocene of the Aquitaine Basin are very consistent with the data recorded in deep-sea oceanic sediments. Therefore, the mollusk shells from the Aquitanian and Burdigalian stratotype areas are good indicators of the composition of the marine waters at the time of deposition. Particularly, the aragonitic samples which have been principally analysed here are reliable materials for such a characterization.

#### *Comparison with Mediterranean data*

Preliminary and approximate elements of comparison can be provided between Aquitaine and Italian Sr isotopic data. We consider samples allocated to a same planktonic biozone (Blow zonation). For instance, in the Chattian, analyses of samples corresponding to Zone P22 gave Sr isotope ratios of about 0.708150 to 0.708262 in Aquitaine, 0.708227 in the Chattian stratotypic area in Germany (DePaolo and Ingram, 1985, and Table 1b), and 0.708199 (sample CQ 292.4 m) to 0.708274 (sample CQ 298.0 m) in the Italian Contessa section (Montanari et al., 1991, and Chapter C3); all the data are adjusted to SRM 987 = 0.710254 and we took into account here the value (0.710248) of the SRM standard relating to the Italian analyses as indicated by A.

Montanari (pers. commun., 1996). For the Chattian, these analyses show Sr ratio values very close in the samples from these three regions.

On the other hand, for the Lower Miocene,  $^{87}\text{Sr}/^{86}\text{Sr}$  ratios significantly lower than those recorded in both the oceanic deep sea and the Aquitaine Basin have been obtained by Montanari et al. (Chapter D1) in the Contessa section. Thus, in the Aquitanian, analyses of samples on the whole allocated to Zone N4 gave Sr ratios of about 0.708340 to 0.708420/0.708430 in Aquitaine, and 0.708315 (N4 zone, CQ 304.0 m. sample) to 0.708338 (top N4, CT 306.6 m. sample) in Italy. In the lower Burdigalian, analyses of samples related to N5/6 Zones gave Sr ratios of about 0.708440 to 0.708560 in Aquitaine, and 0.708305 to 0.708387 in Italy. In 'mid-upper' Burdigalian, the Italian Sr ratios remain again lower than values from Aquitaine and/or oceanic sequences (for instance 0.708643 in Aquitaine and 0.708569–0.708539 for Zone N7 from the Italian Moria section; see Chapter D1). However, some data from other areas of the Mediterranean realm (Rhône valley, see Goldsmith et al., 1994) are close to those from Aquitaine in mid-upper Burdigalian deposits. Similarly, analyses of samples corresponding to upper Zone N8 gave similar Sr ratios, of 0.708750 in Aquitaine (Table 1a) and 0.708769 in Mediterranean Spain (Goldsmith et al., 1994), whereas a Sr value (significantly lower) of 0.708651 has been obtained from the Moria section (Zone N8) by Montanari et al. (see Chapter D1).

Further studies (particularly geochemical investigations) are necessary for better specifying and explaining these data. Perhaps the nature of the analysed samples in the Italian Contessa and Moria sections (phosphatic material and bulk carbonate), and/or the presence of volcanic material in these rocks may be taken into consideration. In spite of the care taken in sample selection, it remains that both phosphatic fish bones and bulk carbonate can sometimes experience more or less diagenetic exchange with interstitial waters: in some ODP sites, whole core sections showed interstitial water with 'modified'  $^{87}\text{Sr}/^{86}\text{Sr}$  ratios (Koepnick et al., 1985). As we have no objective arguments to discuss neither the reliability of Contessa data nor that of the Mediterranean record, we just want to outline the discrepancy between the results from the present study and those from Italy concerning the  $^{87}\text{Sr}/^{86}\text{Sr}$  composition of Lower Miocene biogenic material.

## Sr ISOTOPE STRATIGRAPHY

### *Basic principles and limitations*

The analysis of foraminiferal calcite gives the  $^{87}\text{Sr}/^{86}\text{Sr}$  of sea water at the time it precipitated, under the condition that any diagenetic transformations are postulated to be negligible. Consequently, the best ODP records, i.e. those in which the stratigraphic succession is documented at its best, allow to calibrate the  $^{87}\text{Sr}/^{86}\text{Sr}$  of ocean water against the time scale used in the log description. Magnetostratigraphically interpolated time scales are commonly used, for example the geomagnetic polarity time scale (GPTS) of Cande and Kent (1992, hereafter referred to as CK92; later slightly modified by Cande and Kent, 1995), or many others before and after based on the same principle. This GPTS relies on a sound basis, that is a rigorous statistical analysis of ridge expansion rates based on a certain number of independent radiometric age determinations.

The statistical notion of confidence interval on GPTS ages lacks mathematical sense

Table 2

Estimated ages, on the Sr stratigraphy basis, of the samples from Aquitaine Basin (based on calibration proposed for ODP 747A/CK 92 and the equations of Oslick et al., 1994)

Reference of sample	<sup>87</sup> Sr/ <sup>86</sup> Sr (SRM = 0.710254)	Estimated ages (Ma) [Equations of Oslick et al., 1994]			Geographic and stratigraphic indications	
				± 2σ		
*AQ 01	0.708237	9	24.6	0.31	SW Aquitaine Chattian	
AQ 17	0.708262	9	24.1	0.31		
AQ 21 ♦	0.708340	#	#		♦ Aquitanian stratotype (Saucats-La Brède)	
AQ 22 ♦	0.708377	4a	21.6	0.23		
AQ 23 ♦	0.708392	4a	21.4	0.23		
*AQ 12/AQ 63 ♦	0.708405	4a	21.2	0.23		
*AQ 02 ♦	0.708399	4a	21.3	0.23		
AQ 27	0.708413	4a	21.1	0.23		
AQ 64	0.708415	4a	21.1	0.23		
AQ 51 ♦	0.708420	4a	21.0	0.23		
(AQ 52) ♦	(0.708457)	(4a)	(20.5)	(0.23)		
AQ 70	0.708460	4a	20.4	0.23		Burdigalian of Saucats
*AQ 04	0.708478	4a	20.2	0.23		
*AQ 11	0.708502	4a	19.8	0.23		
AQ 30	0.708517	4a	19.6	0.23		
*AQ 05	0.708541	4a	19.2	0.23		
AQ 33	0.708543	4a	19.2	0.23		
AQ 78	0.708559	4a	19.0	0.23		
AQ 39	0.708851	2a	12.9	0.72	Serravallian of Saucats	
AQ 19	0.708384	4a	21.5	0.23	Aquitanian	Léognan area
AQ 71	0.708446	4a	20.6	0.23	Burdigalian	
AQ 74	0.708450	4a	20.6	0.23		
AQ 73	0.708488	4a	20.0	0.23		
AQ 32	0.708631	4a	17.9	0.23	Other areas of Aquitaine	
*AQ 07	0.708643	4a	17.7	0.23		
AQ 36	0.708750	4a	16.2	0.72		
A1	0.708384	4a	21.5	0.23	Aquitanian	<i>in</i> DePaolo & Ingram, 1985
A2	0.708437	4a	20.8	0.23		
Burd2	0.708449	4a	20.6	0.23	Burdigalian	
M7	0.708489	4a	20.0	0.23		
Burd3	0.708491	4a	20.0	0.23		
M6	0.708520	4a	19.5	0.23		
O4	0.708227	9	24.8	0.31	Chattian	
** Toul.	0.708619	4a	18.1	0.23	Burdigalian	

- Ages of AQ 21 (#) and (AQ 52) samples: see discussion in text; - symbols as in Table 1

for two reasons: (1) there is no way to propagate error in non-parametric estimators; (2) as a consequence, the GPTS can be used as it stands as an intercalibration tool which gives best estimated ages for geomagnetic events without bearing any inference about stage boundaries (the same applies with astronomic polarity time scale, APTS). A parallel can be made with radiometric disintegration constants whose best estimated central values are accepted by the radiochronology community: confidence intervals for these constants are not propagated in radiometric age calculations.

The derivation of  $^{87}\text{Sr}/^{86}\text{Sr}$  'ages' against GPTS is so made possible as long as a parametric expression linking  $^{87}\text{Sr}/^{86}\text{Sr}$  to geomagnetic age can be made available. The evolution shown by Foraminifera data in the interval of 22.8–15.5 Ma CK92 (see Fig. 3) allowed Oslick et al. (1994) to propose a simple linear regression as a possible age determination. Although there are no reasons for nature to follow such a regular evolution, this procedure allows to determine ages (in Ma CK92) relative to Hole 747A magnetostratigraphic model points. A seemingly more rigorous treatment would be the use of a non-parametric cubic spline with associated error envelopes (as in Fig. 5). Such a technique allows to take into account the actual geological dispersion of data points, but makes any mathematical derivation of age impossible: only a graphic treatment is made possible (Smalley et al., 1994), and thus this technique must be restricted to the evaluation of the quality of data. The division of the long-term evolution of oceanic  $^{87}\text{Sr}/^{86}\text{Sr}$  in straight line sections remains a good way to determine ages. High-order polynomials could be applied to longer time periods but their mathematical resolution by means of iterative algorithms is not so trivial. The important points in Sr isotope stratigraphy are: (1) to always include the actual NIST SRM 987 value used, and (2) to give the time scale and ODP composite used in the calculation.

In a field study with distant and generally not-continuous exposures as in the present work, the  $^{87}\text{Sr}/^{86}\text{Sr}$  ratios can particularly lead to 'relative ages' with a precision which is better than the direct geochronologic and/or biostratigraphic datings since the evolution of the Sr ratios with age is well known in this part of the Miocene.

### *Sr chemostratigraphic discussion*

On the basis as above specified (ODP 747A/CK92), the estimated Sr ages of the analysed Aquitaine samples are presented in Table 2 (confidence intervals,  $2\sigma$ , on these ages: see explanations above, and Table 2). These ages range between 24.6 Ma to 12.9 Ma (from Chattian to Serravallian). The uppermost Chattian AQ 17 sample has an assigned age of 24.1 Ma.

The estimated age of the lowermost Aquitanian sample (AQ 21) that we analysed has to be discussed. As pointed out above, a plateau in the oceanic  $^{87}\text{Sr}/^{86}\text{Sr}$  occurs at the top of the Chattian. From equation 3a/4a of Oslick et al. (1994), an age of 22.5 Ma CK92 could be calculated from the  $^{87}\text{Sr}/^{86}\text{Sr}$  ( $= 0.708340$ ) of AQ 21, but such an age is at the lower limit of validity of the linear regression. Taking into account the ODP Holes 608 and 747A, which are assumed to have a very good magnetostratigraphic record, Miller et al. (1991b; Hole 608) indicate ages of 22.69 and 22.97 Ma, respectively, for Sr ratios of 0.708353 and 0.708347 (values adjusted to SRM 987  $= 0.710254$ ), and Oslick et al. (1994; Hole 747A) an age of 22.37 Ma for a Sr ratio of 0.708349. A cubic spline treatment (Ludwig, 1992; McArthur, 1994) of the ODP Site 747A data shows a

smooth evolution of  $^{87}\text{Sr}/^{86}\text{Sr}$  vs age (Fig. 5), and assigns an age of 22.7 ( $-1.2 + 1.1$ ) Ma CK92, i.e. between 21.5 and 23.8, to the central value of AQ 21. The confidence interval on the cubic spline age changes to  $+1.3 - 1.5$ , i.e. between 21.2 and 24.0 Ma, when the confidence interval on the  $^{87}\text{Sr}/^{86}\text{Sr}$  is taken into account. AQ 21 age is thus not significantly different from either the geochronologically derived age of  $23 \pm 0.5$  Ma assigned to the Chattian/Aquitainian boundary by Odin (1994), or the age of  $23.5 \pm 1$  Ma proposed for the base of the Aquitainian in this volume (see Chapter F2).

An approached Sr age for the top of the Aquitainian is provided by the samples AQ 51 and A2 (21.0 and 20.8 Ma CK92), but in the Saucats area, the uppermost Aquitainian levels consist of lacustrine layers, which are not Sr-datable.

The lowermost Burdigalian stratotype formations of Saucats–Léognan we analysed yield an estimated Sr age of 20.5–20.6 Ma CK92 (Table 2). They contain the index taxon *Globigerinoides altiaperturus*. The FO of this species might be one of the criteria useful for correlating the base of the Burdigalian Stage (see Chapter F2). It is worth noting that the general FO of this species seems to be located at the top of chronozone C6An (20.52 Ma CK92, in DSDP Hole 516 F, cf. Berggren et al., 1995, and references herein) and in the older part of chron C6r (20.5 Ma, in the Contessa Highway section, see Montanari et al., 1991). So, as a first approximation, there is a good consistency between these data and our Sr estimated ages.

The estimated age of the outcropping Burdigalian stratotype sequence ranges from about 20.5–20.6 to 19 Ma CK92 in Saucats–Léognan (Table 2). In southwestern Aquitaine, the sample AQ 07 shows an example of Burdigalian deposit which is more recent than the Aquitaine lower Burdigalian stratotype; a Sr age of 17.7 Ma CK92 is herein assigned to this sample. Otherwise, a Sr age of 12.9 Ma CK92 is assigned to the Serravallian Saucats sample (AQ 39).

In conclusion, it is worth noting that there is a good agreement between these estimated Sr ages of our analysed samples and the geochronologically derived ages of stage boundaries as proposed in this volume.

### Sr 'age' models

Fig. 6 gives approximate data about the thickness of the Saucats Aquitainian–Burdigalian series. The sedimentation rate for Lower Miocene deposits (spanning from about 23 Ma to about 19 Ma) in the Saucats brook area is about 8–9 m/Ma, if we consider hypothetically that these deposits are strictly horizontal, and that no tectonic accident disrupts their geometry. In this region, data from a few boreholes provide a thickness of about 40 to 50 m for the marine Lower Miocene of Saucats–Léognan, which corresponds to a sedimentation rate of about 10 m/Ma. On a larger scale in the Aquitaine Basin, this thickness increases regularly toward the west, i.e. toward the more open oceanic conditions of sedimentation (see Alvinerie et al., 1992).

Sr model ages can be calculated for the historical Aquitainian stratotype of Saucats–La Brède by assigning stratigraphic ages to the stage boundary levels. The Chattian/Aquitainian boundary would be at an altitude of about 17.5 m, and the Aquitainian/Burdigalian boundary at about 41 m (Fig. 6). Assuming a constant sedimentation rate, a set of model ages is calculated based on the age considered there for the Chattian/Aquitainian boundary ( $23 \pm 0.5$  Ma). Results are given in Fig. 5 and show a



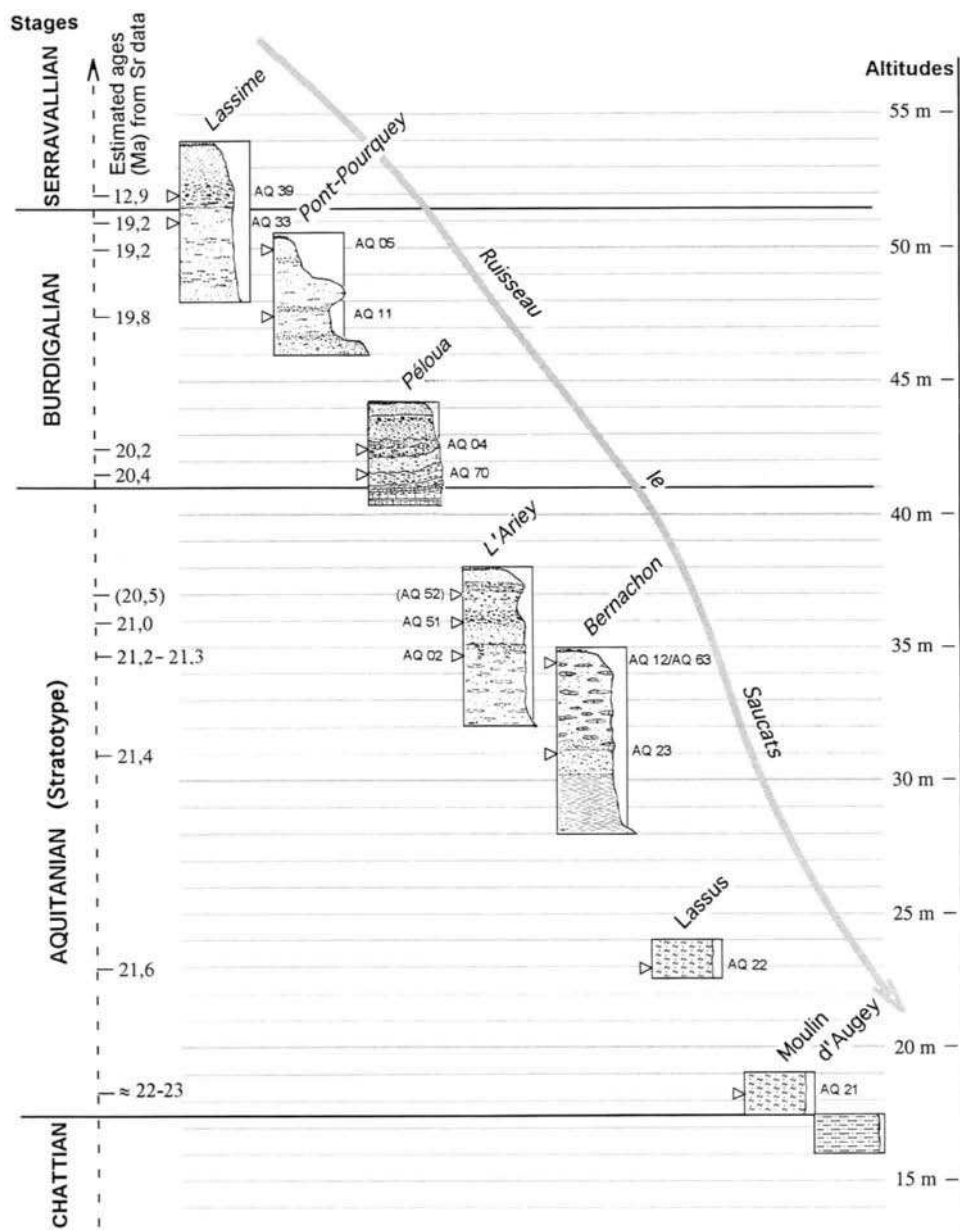


Fig. 6. Synthetic representation of some sections located on the right bank of Le Saucats river. They are arranged according to their altitude in the field, with indication of the estimated ages of the Sr-analyzed samples (from Cahuzac et al., 1996, supplemented); these ages are established on the basis of ODP 747A data normalized to CK92's GPTS. We estimate that sample AQ 21 is about 22–23 Ma CK92 old; see discussion in the text.

good agreement with ODP data: data from the Atlantic province can thus be directly compared with the deep-sea record. Provided an independent time scale would be assigned to continental sections,  $^{87}\text{Sr}/^{86}\text{Sr}$  ratios of aragonitic macrofauna would even be more reliable than those of the calcitic microfauna. (Indeed, if ODP sites have the advantage of combining continuous marine sections with biozonal stratigraphic as well as magnetostratigraphic tie points, foraminiferal tests often experience minute recrystallization or isotope exchange; moreover, the microfauna in ODP sediments, which have been generally deeply buried, may have suffered diagenesis; see Elderfield et al., 1982; Richter and Liang, 1993.)

## CONCLUSIONS

In this paper, updated information on the available outcrops related to the Aquitanian and Burdigalian historical stratotypes in the Aquitaine Basin was collected and presented. These historical stratotypes are represented by deposits rich in very well preserved, aragonitic mollusk shells, which constitute particularly suitable material for Sr isotopic analyses. The set of data presented here allows to specify the minimum  $^{87}\text{Sr}/^{86}\text{Sr}$  ranges in these stratotypes, and in the Chattian–Miocene series from neighbouring areas of Aquitaine, thanks to a revision of numerous exposures. Especially for the Aquitanian, we considered and sampled several new outcrops which encompass in its entirety the historical stratotype as originally described by Mayer-Eymar (1858). These Sr analyses gave reliable values which are very consistent with field data, and with the stratigraphy of the deposits. A good consistency is obtained in Sr isotopic ratios between Aquitaine and (ODP and DSDP) oceanic sequences, which were correlated on the basis of biostratigraphic criteria; this is in agreement with the position of the Aquitaine Basin which was still well connected with the Atlantic Ocean and was even widely open toward this ocean during the Miocene. If such an agreement of Sr stratigraphy between land sections and deep-sea sites is considered as a key quality for stratotype deposits, this agreement reinforces the interest of these historical typical layers, and their usefulness as reference sections.

From the present study (and at least for the samples analysed herein), the base of the Aquitanian Stage corresponds to a  $^{87}\text{Sr}/^{86}\text{Sr}$  ratio of about 0.708340, and the Chattian/Aquitainian boundary would occur in a  $^{87}\text{Sr}/^{86}\text{Sr}$  interval of 0.708260–0.708340. The Aquitanian/Burdigalian boundary corresponds to a  $^{87}\text{Sr}/^{86}\text{Sr}$  interval of about 0.708420/0.708430 to 0.708440. (All these ratios have been normalized to SRM 987 = 0.710254.)

We have also indicated and discussed the deduced Sr chemostratigraphic ages, which are on the whole very consistent with the geochronologically derived ages specified in this volume. Alternatively, a (preliminary) comparison with some Lower Miocene Italian sections gives significantly lower  $^{87}\text{Sr}/^{86}\text{Sr}$  ratios compared to the Aquitaine deposits and deep-sea sites. It would indeed be very useful to undertake also Sr analyses in the upper part of the Burdigalian stratotype (Rhône Valley), in order to specify the range of Sr isotopic ratios in these typical deposits and to compare them with the Sr data from the land sections in Aquitaine and Italy.

## SOMMAIRE — RAPPORTS ISOTOPIQUES $^{87}\text{Sr}/^{86}\text{Sr}$ DANS LA RÉGION DES STRATOTYPES HISTORIQUES MIOCÈNES D'AQUITAINE

(Manuscrit soumis: Mars 1996, révisé: Avril 1996; rédacteur responsable: GSO)

Les stratotypes de l'Aquitainien et du Burdigalien d'Aquitaine font l'objet d'une mise en valeur active depuis quelques années. Des affleurements ont été recherchés dans la région bordelaise (entre La Brède et Saucats) et de nouvelles coupes proches (Léognan) ou plus lointaines ont été étudiées par comparaison pour couvrir l'intervalle Chattien à Serravallien. Parmi les études entreprises, l'outil chimiostratigraphique  $^{87}\text{Sr}/^{86}\text{Sr}$  a été utilisé pour les caractériser. Le présent travail fait le point sur quelques affleurements disponibles. Pour l'essentiel, des mollusques ont été choisis parmi ceux dont le test était initialement aragonitique et riche en strontium. On a vérifié que le minéral original avait été préservé dans ces sédiments jamais enfouis profondément. La corrélation entre les coupes types et les séries océaniques a pu être proposée par l'outil biostratigraphique (microfaune et nannoflore planctoniques). L'analyse isotopique a été réalisée sur 26 coquilles et un oursin; l'analyse d'une dent de requin a été prise en compte pour comparaison. Les rapports isotopiques précis obtenus ont permis de déceler une évolution régulière. De même que cette évolution, les valeurs des rapports isotopiques sont tout à fait compatibles avec les observations réalisées dans les sédiments océaniques profonds. Ainsi, les coquilles de mollusques de la région-type sont-elles de bons indicateurs de la composition des eaux marines contemporaines avec des rapports isotopiques croissant de 0,70834 à 0.70864 de la base de l'Aquitainien présent dans la région au sommet des niveaux burdigaliens analysés dans la région et ne comprenant pas les horizons très supérieurs. La limite Aquitainien/Burdigalien correspond à un intervalle d'environ 0.708420 à 0.708440 (rapports normalisés au standard SRM 987 = 0.710254). Selon les auteurs, les coquilles aragonitiques utilisées paraissent plus fidèles que les dents de requin ou les 'carbonates totaux' pour caractériser la composition de l'eau de mer dans laquelle ont vécu les fossiles. Des calculs sont proposés pour estimer la durée de dépôt des sédiments présents d'après l'ampleur de l'intervalle de variation des rapports isotopiques observés. Les âges chimiostratigraphiques (Sr) estimés des échantillons s'accordent avec les âges des limites d'Etages géochronologiquement déduits par ailleurs dans ce volume.

(Manuscrit soumis: Mars 1996, révisé: Avril 1996; rédacteur responsable: GSO) (Sommaire proposé par les rédacteurs, GSO)

### ACKNOWLEDGEMENTS

We thank N. Goldsmith, Chairman of Anthracothere Hill Project, who has initiated and organized the first Sr analyses made by H. Elderfield, G.S. Odin for review and for the X-ray analyses, F. Grousset and L. Londeix for the information concerning the 'Toul' Sr analysis, A. Montanari and H. Elderfield for discussions, M. Ringeade, A. Cluzaud and L. Londeix for their help with the sampling in the field. This work is part of the framework of the 'Réserve Naturelle Géologique de Saucats-La Brède'. We thank the management Association of this "Réserve Géologique" which has financially supported several Sr analyses, and Y. Gilly, curator of the "Réserve", who has obtained funds.

## Chapter A5

# LANGHIAN, SERRAVALLIAN, AND TORTONIAN HISTORICAL STRATOTYPES

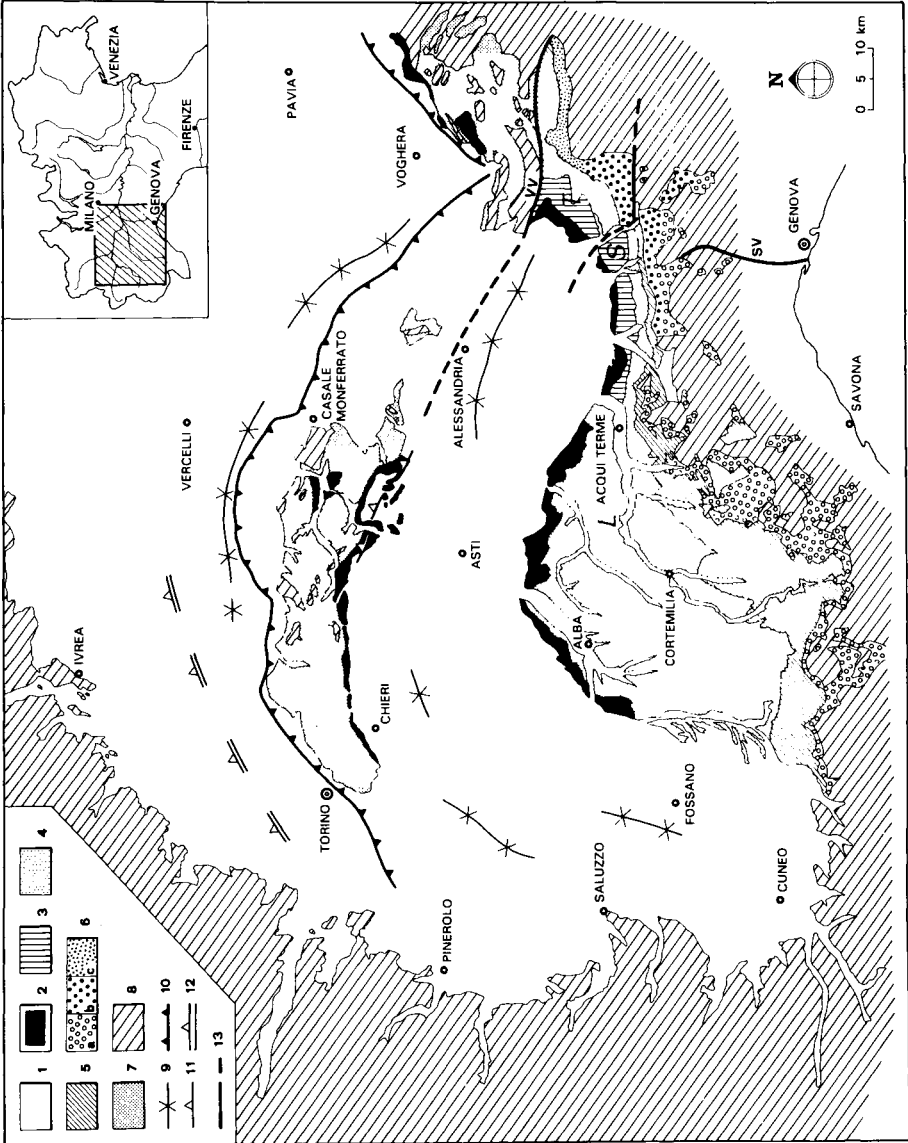
D. Rio, M.B. Cita, S. Iaccarino, R. Gelati and M. Gnaccolini

## INTRODUCTION

Chronostratigraphy does represent a basic common language of communication in Earth Sciences. However, most chronostratigraphic units of the standard Geologic Time Scale lack an appropriate, and rigid definition in the rock stratigraphic record usable on a global basis, severely hampering the reason of being of the Chronostratigraphy. Specifically, the standard Neogene (Miocene, Pliocene and Pleistocene) stages, defined in the Mediterranean marine stratigraphic record, are rarely used in practical work outside the type region (see, for example Barron et al., 1985a, and most volumes of DSDP and ODP Scientific Results). And even in the Mediterranean domain, Neogene stages and subdivisions are often intended in a different and conflicting manner, with deleterious consequences in scientific communication. One of the most urgent tasks of the International Commission of Stratigraphy (ICS) is to prompt an international agreement on the subdivision of the Chronostratigraphic Scale and the establishment of rigorous definitions of the boundaries between the various rank subdivisions. To this purpose the ICS has recommended that stages, the basic chronostratigraphic unit of the standard Chronostratigraphic Scale, in prospect recognizable worldwide (Hedberg, 1976, p. 71), be defined by using Global Stratotype Section and Point (GSSP) of their bases (Cowie et al., 1986). The critical factors in selecting the GSSP is its amenability to worldwide correlations. However, for the chronostratigraphic nomenclature it is of equal importance that the GSSP be defined in such a manner that the historical concepts of the defined chronostratigraphic unit are respected as far as possible (Hedberg, 1976). In this paper we review the state of the art of our knowledge on the historical Langhian, Serravallian, and Tortonian stratotypes, as a contribution to the selection of the GSSP of their bases.

In order to make our discussion and conclusions more clear, it is necessary to state some of our guidelines in chronostratigraphic procedures:

- historical stages have their definition in the rock stratigraphic record;
- for reasons of stability, the criteria which have been used for its recognition outside the type area are important;
- in the absence of a proposed GSSP, it is considered that the boundary between stages is defined by the base of the overlying stage (Hedberg, 1976);
- the most important reason to re-define the base of a stage is its worldwide correlatability; it would be stultifying to maintain a unit in the chronostratigraphic scale only for historical reasons without considering its practical applicability.



## THE TERTIARY PIEDMONT BASIN

The stratotypes of the Langhian, of the Serravallian and of the Tortonian are all located in the Piedmont region (northwestern Italy, Fig. 1), which is known in the regional geological literature as the 'Tertiary Piedmont Basin' (TPB). To avoid repetition we give here some general information on the geological setting, and on the Middle to Upper Miocene stratigraphy of the TPB, where conspicuously thick sequences of Cenozoic sediments are housed, which have been studied for more than a century and have served as the basis for defining numerous, more or less successful, chronostratigraphic units (Bormidian, Langhian, Serravallian, Tortonian, Cessolian, Cortemilian, Bubbian, Perletian, Castellanian, Fossanian, Astian, Villafranchian; see Carloni et al., 1971).

The TPB, bounded southward and westward by the Western Alps, and northward by the northwestern termination of the Apennines, is located in a critical boundary-sector between the Alps and the Apennines. It developed, on top of a substratum represented by allochthonous Alpine and Apenninic units, internally to a south-dipping suture zone (Fig. 1). Its depositional history started in the Late Eocene, after a major palaeogeographic reorganization of the Alps–Apennines orogenic system (the so-called 'Ligurian Phase'). The basin fill is represented by more than 4000 m of mainly siliciclastic sediments, deposited under varying local tectonic setting. Prevailing extensional and compressional tectonic regimes have been recognized during the Oligocene and during the Miocene, respectively. The TPB can be considered as an episutural basin (Fig. 2), developed in a collisional regime, behind the thrust front of the mesoalpine belt overthrust on top of the Adria microplate (Gelati and Gnaccolini, 1980; Hunziker and Martinotti, 1987; Gnaccolini et al., 1990; Boccaletti et al., 1990).

The sedimentary history has been highly articulated, with the deposition of vastly different facies sediments, from continental alluvial fans to deep-water turbidites. Unconformities, rapid subsidence events, migration of depocentres and complex facies relationships are common. Gnaccolini et al. (in press) recognized fourteen depositional sequences in the Langhe region, in the Late Eocene–Tortonian interval. In Fig. 3, we present a simplified stratigraphic sketch of the latero-vertical facies relationships between the western and the eastern sectors of the TPB during late Burdigalian–Tortonian times. The area of Cessole, where the Langhian stratotype is located, acted as a basin while the area of Serravalle–Gavi, where the Serravallian stratotype is located, acted as a basin margin.

---

Fig. 1. Geological sketch map of the Tertiary Piedmont Basin (BTP). 1 = Pliocene to Recent deposits; 2 = Messinian deposits; 3 = Langhian to Tortonian siliciclastic and carbonates; 4 = late Burdigalian to Tortonian mainly turbiditic successions (only Burdigalian in the eastern sector of the area); 5 = Late Oligocene to Burdigalian turbidite systems and hemipelagic mudstones; 6 = Late Eocene to Early Oligocene deposits (*a*, alluvial to coastal conglomerates, shallow-marine sandstones and hemipelagic mudstones; *b*, slope and base-of-slope, resedimented conglomerates; *c*, mainly turbidites); 7 = Late Eocene to Tortonian siliciclastic deposits of the NW Apennines–Basso Monferrato–Collina di Torino wedge; 8 = Alpine and Apenninic allochthonous units; 9 = depocentre axis of the Pliocene–Quaternary basins; 10 = buried thrust-fronts of the Collina di Torino–Basso Monferrato–NW Apennines wedge; 11 = buried, south-vergent backthrusts of the Basso Monferrato, active from the Messinian onward; 12 = buried, pre-Burdigalian backthrusts of the Western Alps (as inferred by Roure et al., 1990b); 13 = tectonic lines. SV = Sestri-Voltaggio; VV = Villavernia-Varzi. Modified after Gnaccolini et al. (in press). Type areas: L = Langhian; S = Serravallian; T = Tortonian.

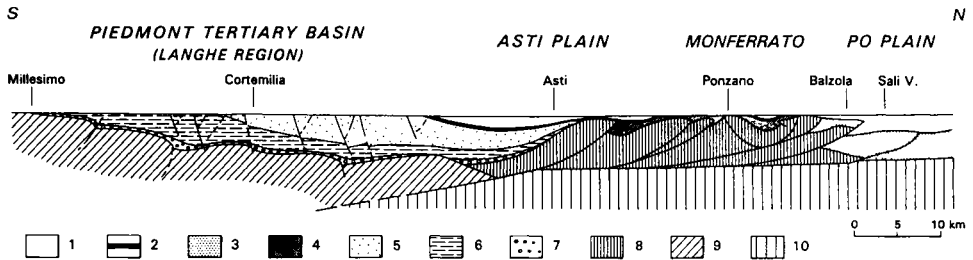


Fig. 2. Geologic section through the Tertiary Piedmont Basin (TPB) and the Po Plain. 1 = Pliocene and Quaternary; 2 = Messinian; 3 = Oligocene–Miocene foredeep succession of the Po Plain; 4 = Monferrato succession; 5 = late Burdigalian to Tortonian turbidites; 6 = Late Oligocene to Burdigalian turbidite systems and hemipelagic mudstones; 7 = Late Oligocene to Early Oligocene alluvial to coastal conglomerates, shallow-water sandstones and hemipelagic mudstones; 8 = Ligurian units; 9 = Insubrian units.

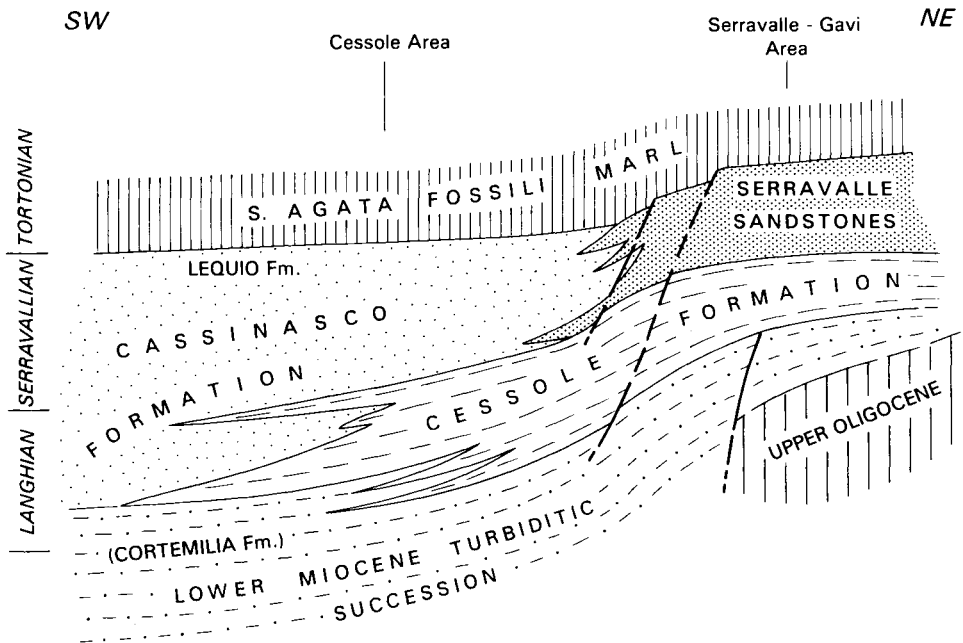


Fig. 3. Schematic stratigraphic relationship between the eastern and central TPB during Middle to Late Miocene times.

## THE LANGHIAN

### *History of definition*

The term Langhian was introduced in the geological literature by Lorenzo Pareto, a geologist and politician belonging to a noble family from Genova, who was a minister under King Carlo Alberto di Savoia. The publication (Pareto, 1865) had a well focused character and appeared in the Bulletin of the Société Géologique de France. The type

area is clearly and unambiguously indicated: “L’ensemble des couches que je considère comme constituant la subdivision moyenne du terrain Miocène, que je nommerai étage Langhien ... se montre sur une grande étendue dans les hautes collines appelées Langhe, traversées par les vallées supérieures de la Bormida et du Belbo.” “... Les localités où cet étage paraît plus développé sont les hautes collines au N de Ceva ... dans les vallées de la Bormida vers Ponti, Bistagno et Acqui, ce que l’on appelle les Langhe.”

No precise type locality or type section was given by the marquis de Pareto, who died the same year when his publication appeared. The dominant lithology was described as consisting of sandy marls, generally greyish in colour, associated with molasses and occasionally with ophiolitic sand layers transitional to conglomerates.

Pareto introduced the Langhian as the second stage of the Miocene, above the Bormidian (Vervloet, 1966; Cita, 1971a) and below the Serravallian (Fig. 4a). He considered the Tortonian (introduced by Mayer-Eymar in 1858) as belonging to the Pliocene Series). The term Langhian was rapidly adopted in the Italian stratigraphic literature (i.e., Omboni, 1869; Stoppani, 1873). In 1868, Mayer modified the concept of the Langhian as typified by Pareto limiting the term to the upper part of the stratigraphic succession indicated originally, mainly represented by marly lithologies with common Pteropods (‘Pteropod Marls’), ascribing to the Aquitanian the lower terrigenous part.

Mayer’s chronostratigraphic system was well advertised, and not surprisingly his concept of the Langhian was soon adopted, even in the Piedmont region, as testified by the fundamental geological and palaeontological work of Sacco (in Bellardi and Sacco, 1872–1904). The ‘Pteropod Marls’ of the Piedmont region have become synonym of the Langhian, and the designation of a stratotype section (see below) was done in the light of this widely accepted practice. In 1892, Depéret introduced the Burdigalian to which the Langhian has long been held to be correlative and virtually synonymous. While in Italy the name Langhian continued to be used, in most international time scales (i.e., De Lapparent, 1906; Haug, 1927; Gignoux, 1950; Fig. 4a), the name Burdigalian was adopted, notwithstanding that it is defined in poorly outcropping shallow-water marine sediments of the Aquitaine basin (SW France; see Selli, 1957). We now know that the type Burdigalian is considerably older (!) than the type Langhian *sensu* Sacco (1889) and Mayer-Eymar (1868) (but not *sensu* Pareto, 1865).

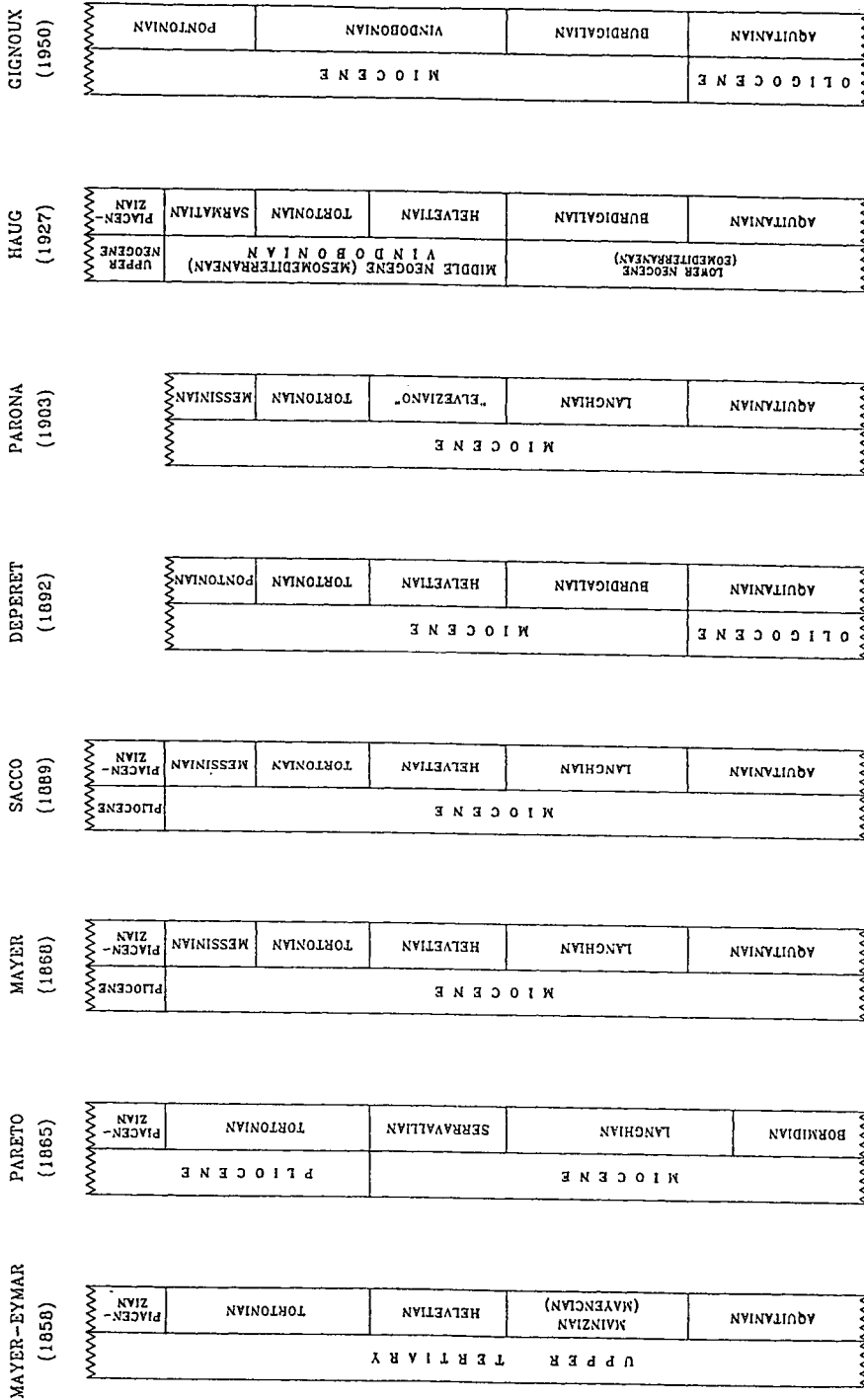
### *The Langhian stratotype: definition and geological setting*

The type section of the Langhian was proposed by Cita and Premoli Silva (1960) near the village of Cessole, in the heart of the Langhe, in the Bormida valley (Piedmont, northern Italy; Fig. 1), mentioned by Pareto when introducing the Langhian stage.

Detailed information on the geologic setting of the stratotype area is provided by Gelati (1968), Gnaccolini (1960, 1968, 1969), and Gelati et al. (1993). The Langhe region during Langhian times was acting as depocentre in the Tertiary Piedmont Basin (TPB), being infilled by a thick succession of hemipelagic to terrigenous sediments (Fig. 3).

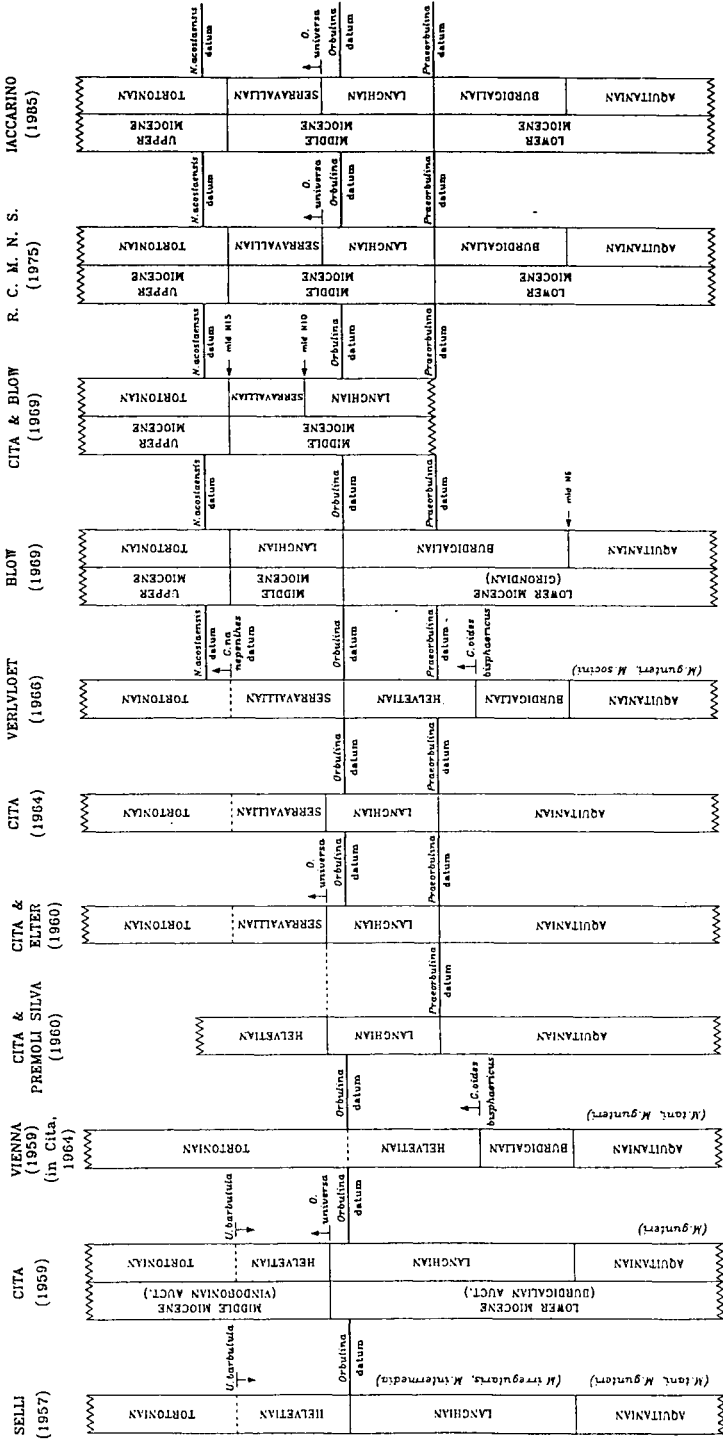
The stratotype section is composed of two-component segments, named Bricco del Moro and Bricco della Croce sections (Figs. 5, 6, 7, 8). The type Langhian is represented by mainly marly sediments (‘Pteropod Marls’ *Auctorum*) known in the most recent geologic literature as Cessole Formation (Vervloet, 1966) or Cessole Marls (Boni,





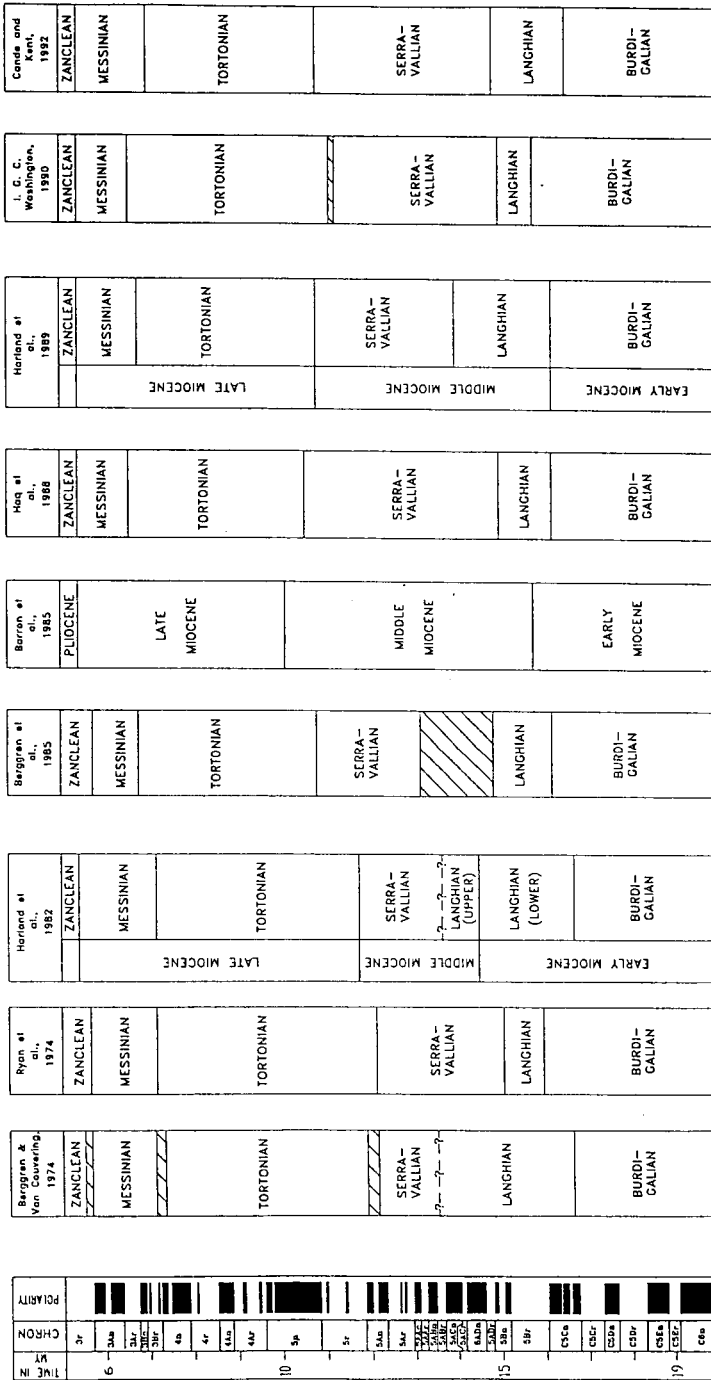
(a)

Fig. 4. Historical review of the Miocene chronostratigraphic subdivision. (a) Chronostratigraphic proposals before the development of calcareous plankton biostratigraphy.



(b)

Fig. 4 (continued). (b) Chronostratigraphic proposals using planktonic foraminifer biostratigraphy.



(c)

Fig. 4 (continued). (c) Position of the Miocene stages versus magnetostratigraphy in the most widely used chronostratigraphic schemes proposed in the last 20 years.

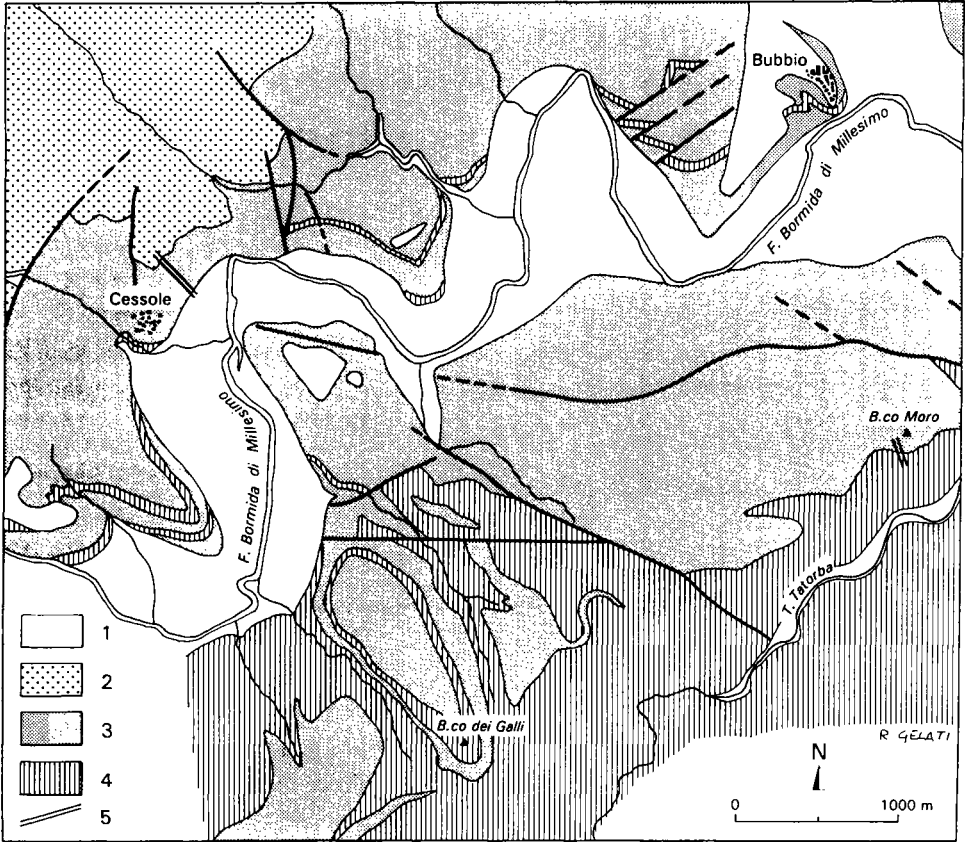


Fig. 5. Geological map of the type area of the Langhian stage, in central eastern TPB. 1 = alluvial deposits; 2 = Cassinasco Formation; 3 = Cessole Formation; 4 = Cortemilia Formation; 5 = Location of the Langhian stratotype composite section of Bricco del Moro and Bricco della Croce.

1967; Gelati, 1968). The type Langhian is comprised between two, mainly arenaceous, turbiditic formations: the Cortemilia Formation below and the Cassinasco Formation above (Vervloet, 1966; Gelati, 1968). The base of the Langhian is exposed in the Bricco del Moro section, located on a hill south of the Bormida river (Fig. 5), where the transition from the Cortemilia Formation to the Cessole Marls is gradational. The main part of the Langhian and its top are exposed in the Bricco della Croce section outcropping on the slope north of the Bormida river (Fig. 5). The transition from the Cessole Marls to the overlying Cassinasco Formation is abrupt.

Recently, Gelati et al. (1993) have ascribed the stratotype Langhian to a single depositional sequence (their sequence C2), which has been correlated on the basis of planktonic Foraminifera to the 3rd-order cycle 2.3, supercycle TB2, of the Global Cycle Chart of Haq et al. (1988). In turn, this 3rd-order cycle correlates with the interval of minimum values of  $\delta^{18}\text{O}$  in benthonic Foraminifera of the entire Miocene (Miller et al., 1991a, b), which probably testifies to the maximum sea level stand in the Miocene and a sort of 'climatic optimum'. These findings are in agreement with the



Fig. 6. Langhian historical stratotype near Cessole (Langhe). The exposure shows the lower part of the Bricco della Croce section, on the left bank of the river Bormida di Millesimo.

well known subtropical character of the planktonic foraminiferal assemblages present in the Mediterranean, and the ‘transgressive’ nature of Langhian sediments in Italy.

#### *International use of the term Langhian*

After the clarification in the sixties of the position in time of the Burdigalian and the Langhian, the use of the term Langhian has become firmly established in the international literature (Van Eysinga, 1975; Harland et al., 1982, 1990; Berggren et al., 1985a,b; Haq et al., 1988; etc). The base of the Langhian (the generally accepted definition of the Early/Middle Miocene boundary) has been generally approximated by the *Praeorbulina* datum (Fig. 4b). With reference to the Geomagnetic Polarity Time Scale (GPTS), the base of the Langhian has been associated to Chron C5Cn or to the lower part of Chron C5Br (Fig. 4c). However, a formal definition of the base of the Langhian by a GSSP has not yet been proposed.

#### *Timing of the Langhian stratotype*

Out of the different methods available for positioning in time and correlate worldwide the Langhian stratotype, only calcareous plankton biostratigraphy and biochronology can be utilized. Magnetostratigraphy was established by Nakagawa et al. (1974) in a composite section in the stratotype area near Cessole, but it appears of limited utility. To our knowledge, no radiometric or stable isotope study is available from the stratotype or from the type area.

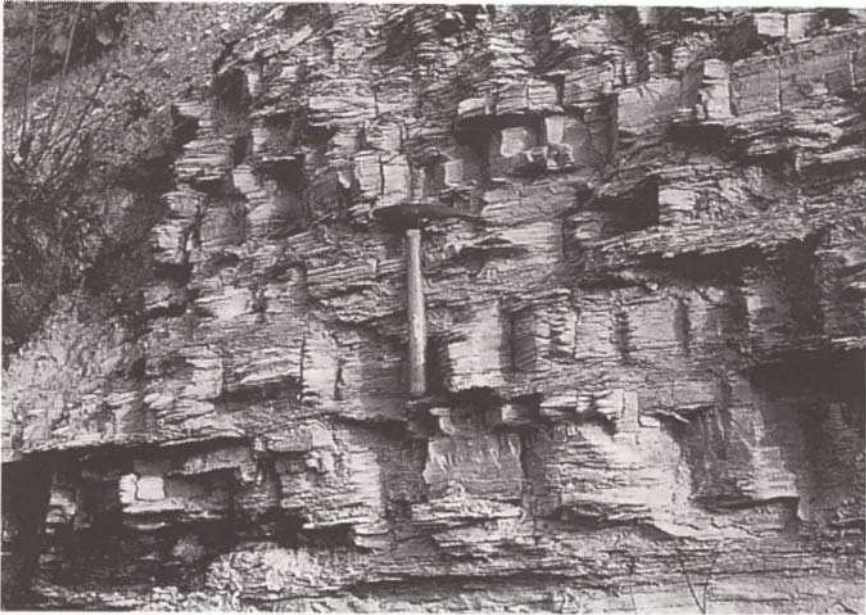


Fig. 7. Close-up of the Pteropod Marls (lower part of the Cessole Formation) in the type area.

*Calcareous plankton biostratigraphy.* Cita and Premoli Silva (1960) in their original study which led to the designation of the Langhian stratotype evidenced its rich contents in planktonic Foraminifera, and recognized the various steps of the now well established evolutionary *Globigerinoides–Orbulina* lineage (Fig. 8). Specifically, the first evolutionary appearance of *Praeorbulina glomerosa* at the base of the type Langhian at the very base of the ‘Cessole Marls’ (Fig. 8), and the first evolutionary appearance of *Orbulina suturalis* (N8/N9 boundary in the zonal scheme of Blow, 1969) in its upper part were detected. Both these biohorizons have been (and are) of momentous importance for the worldwide correlatability of the Langhian stage.

Calcareous nannofossils were first studied by Martini (1968, 1971) in the same set of samples utilized by Cita and Premoli Silva (1960) as reported in Fig. 8. The base of the Langhian (Bricco del Moro section) predates the last occurrence (LO) of *Helicosphaera ampliapertura* and contains *Sphenolithus heteromorphus*, and hence is referable to Zone NN4 of Martini (1971).

The indications provided by the two calcareous plankton groups for positioning in time the base of the Langhian are consistent. In fact the *Praeorbulina* datum is normally associated with the upper part of Zone NN4 (see, for example, Berggren et al., 1985b). Martini associated the top of the Langhian with the NN6/NN7 zonal boundary of the calcareous nannofossil zonation of Martini (1971). This result is strongly conflicting with the evidence provided by planktonic Foraminifera. In fact, plenty of data in oceanic areas indicate that the entire Zone N9 falls within Zone NN5. Indeed, the recent integrated calcareous plankton study of the Langhian stratotype carried out by Fornaciari et al. (Chapter A6), indicates that the results of Martini need to be rectified. The top of the Langhian lies well within the range of *S. heteromorphus*

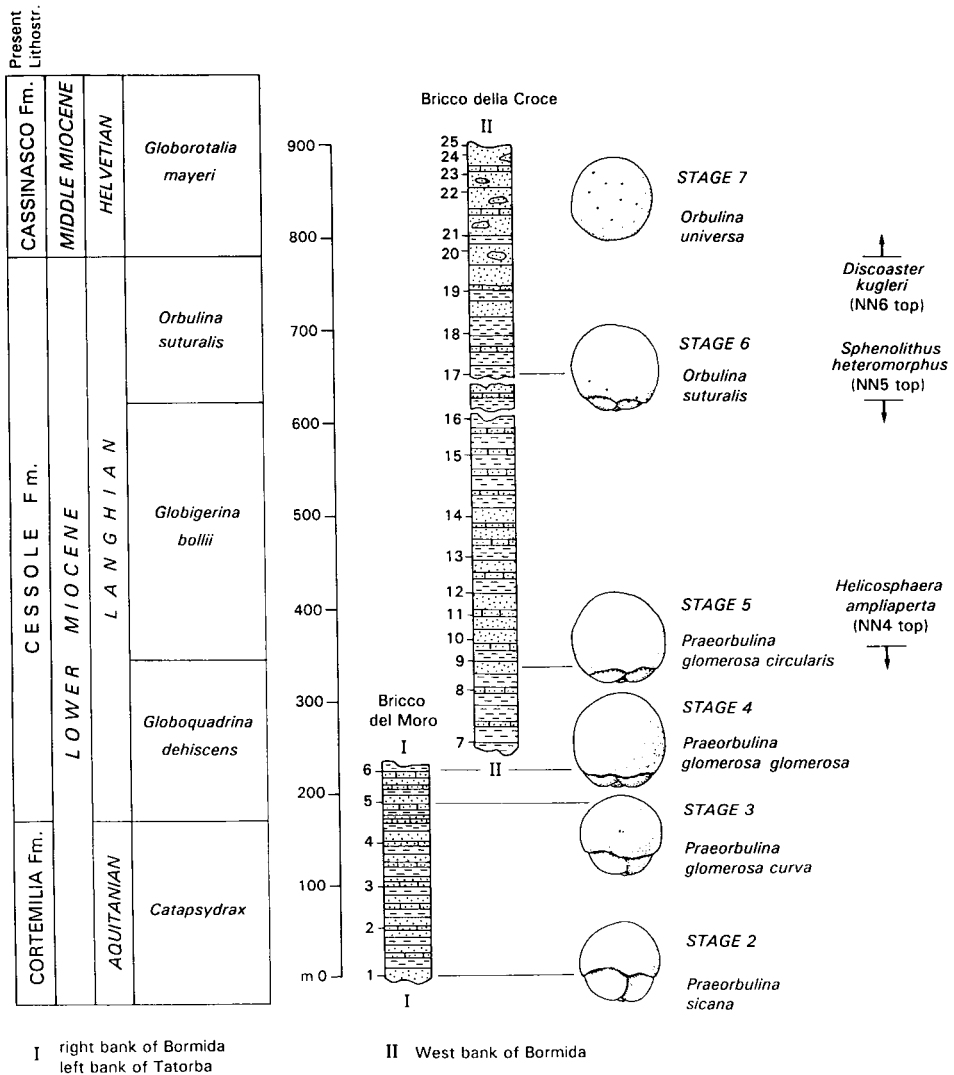


Fig. 8. The original columnar log of the Langhian stratotype as proposed by Cita and Premoli Silva (1960). The main stages of the evolution of *Orbulina universa* from *Globigerinoides bisphericus* via *Praeorbulina* spp. is shown. Note that the taxonomy of planktonic Foraminifera has been updated. Nannofossil data after Martini (1968, 1971).

(within Zone NN5), and the relative order of the calcareous plankton biohorizons observed in the stratotype is the same detected all over the world (Fornaciari et al., Chapter A6). Other results of this recent study of Fornaciari et al. (Chapter A6) which deserve attention are the findings that: (1) the *Praeorbulina* datum (*Praeorbulina sicana* FO; see Jenkins et al., 1981) actually occurs some 100 m below the base of the Langhian stratotype, within the turbiditic Cortemilia Formation; (2) the top of the Langhian is virtually coincident with the first occurrence (FO) of *Orbulina universa*

and the first common and continuous occurrence (FCO) of *Helicosphaera walbersdorfensis* (Fig. 9).

*Calcareous plankton biochronology.* The above commented biostratigraphic events allow wide correlation of the Langhian, although a precise placement of the unit in geologic time is prevented by the lack of magnetostratigraphic data. However, its approximate position in time can be inferred by using the calcareous plankton biochronology established in oceanic areas. We are confident that the considered calcareous plankton biohorizons should not be affected by major diachroneities between the mid- and low-latitude oceanic areas and the Mediterranean because their relative order is the same in the two areas. The base of the Langhian, bracketed by the FO of *Praeorbulina* and the LO of *H. ampliapertura*, should be correlated with Chron C5n, considering the available calibrations of these events (Berggren et al., 1985a, b; Miller et al., 1991a; Fig. 9). The top of the Langhian is bracketed by the FO of *O. suturalis* and the LO of *S. heteromorphus*. The two events are widely spaced, the former being associated with Chron C5Bn, and the latter with Chron C5ABr (Fig. 9; Berggren et al., 1985b; Backman et al., 1990).

As is well known, the chronometric calibration of the Miocene Geomagnetic Polarity Time Scale (GPTS) is in a flux state (Baksi, 1993), and we refrain here, and throughout this paper, from giving absolute age evaluations.

#### *Relationship with the Burdigalian*

The Burdigalian stage (Depéret, 1892) is defined by shallow-water, difficult-to-date, poorly outcropping marine sediments located in the Aquitaine basin, in southwestern France (Berggren, 1971). It is generally held that the type Burdigalian is correlative with foraminiferal Zones N5, N6, and possibly lower, N7 (Berggren et al., 1985b; Iaccarino, 1985). In terms of the calcareous nannofossil standard zonation of Martini (1971), the type Burdigalian would correlate to Zone NN2 according to Müller (in Bizon and Müller, 1979). It appears that no overlap should exist between the type Burdigalian and the type Langhian, and that most probably a time gap is present between the two stages.

#### *Concluding remarks on the Langhian stage*

We consider that Pareto's (1865) concept of a Middle Miocene Langhian stage represented by the marly unit cropping out in the Langhe is valid, and that the stratotype section defined by Cita and Premoli Silva (1960) faithfully substantiates this concept, which is well calibrated by at least two fossil groups: planktonic Foraminifera and calcareous nannofossils.

The international use of the Langhian is widespread and consistent in the last several years, because the biostratigraphy is sufficiently well established. However, a precise definition of its base by a GSSP is lacking, and should be designated. We suggest to locate the GSSP of the base of the Langhian in the lithologic record in a position in time close to Chron C5Cn and to the *Praeorbulina* datum, in agreement with a well consolidated practice (Figs. 4B and 4C). The Langhian historical stratotype at Cessole, characterized in its lower part by terrigenous and turbiditic sedimentation, appears as



unsuitable for establishing the detailed chronology which is needed for serving as GSSP, and the search for a pelagic–hemipelagic section for defining the base of the Langhian is recommended.

## THE SERRAVALLIAN

### *History of definition*

In his paper introducing the Langhian in the geological literature, Pareto (1865) also introduced the term Serravallian. Unfortunately, the author died the same year the paper was published and so could not further improve, reiterate, and extend the definition with subsequent studies, and defend the new name against potential competitors.

As follows, the type area, as well as the stratigraphic position in relation to the underlying Langhian, is clearly indicated: “vers la partie supérieure de l’étage langhien on voit commencer l’alternance de marnes grisâtres avec des couches plus sableuses jaunâtres qui commencent à prendre l’aspect de dépôts qui se sont formés dans une mer moins profonde et moins loin de la côte. C’est au commencement de ces alternances sableuses grisâtres et de sables jaunes que je place la limite inférieure de la troisième subdivision du terrain miocène, qui est celle du miocène supérieur que j’appellerai l’étage serravallien du bourg de Serravalle, près duquel l’étage est bien marqué et où il forme une rangée de hautes collines géologique particulière.”

Therefore, the lower boundary of the stage coincides with the lithologic change from prevailing marls to prevailing sandstones.

The term Serravallian was used only for a short time in Italy after its introduction (Omboni, 1869; Stoppani, 1873), and it was abandoned in favour of the Helvetian introduced by Mayer-Eymar (1858), the type of which is older than the Langhian (Marks and Webbs, 1966). Even Sacco (1889), the greatest authority for the Cenozoic of the Piedmont Basin, used the Helvetian as the stage intermediate between the Langhian and the Tortonian, followed by the generality of geologists and stratigraphers. The name Serravallian was entirely forgotten for a long time. In the 1960s, with the realization that the Helvetian was time-equivalent to the Burdigalian (Congress of the Regional Committee on the Mediterranean Neogene Stratigraphy — RCMNS — Vienna, 1959), the term Serravallian was revived by several authors (Cita and Elter, 1960; Cita, 1964; Vervloet, 1966) although with different meanings (Fig. 4b). At the RCMNS Congress held in Bratislava in 1975, a proposal was made to adopt the Serravallian in the standard Chronostratigraphic Scale as the second upper subdivision of the Middle Miocene, above the Langhian and below the Tortonian. Since then the term Serravallian has been adopted in all most recent Geologic Time Scales (Fig. 4c).

### *The Serravallian stratotype: definition and geologic setting*

A stratotype section for the Serravallian stage was designated by Vervloet (1966) along the western bank of the Scrivia river, in the proximity of the village of Serravalle Scrivia, in agreement with the indications of Pareto (1865; Fig. 10). Vervloet (1966) equated the Serravallian with his Serravalle Formation, a mainly shallow-water sandy unit, overlying the mainly marly and deeper-water Cessole Formation.

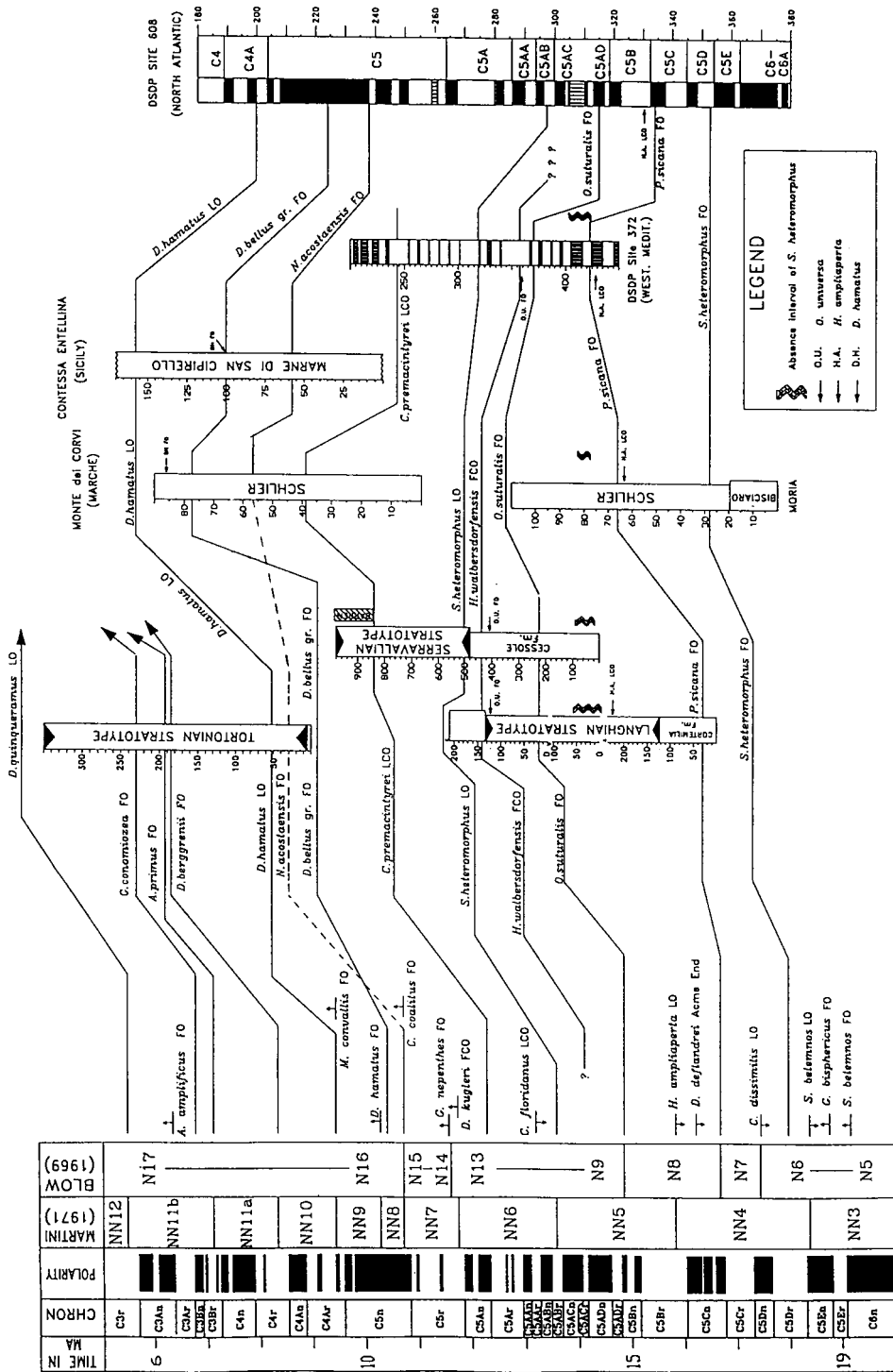


Fig. 9. Calcareous plankton biostratigraphic correlations among the Langhian, Serravallian and Tortonian stratotype sections and other Mediterranean reference sections. To the left: correlations to DSDP Site 608 (North Atlantic), proposed as a deep-sea Miocene reference section (Miller et al., 1991b). To the right: calcareous plankton biochronology developed in low- and mid-latitude oceanic sediments. Geomagnetic Polarity Time Scale after Cande and Kent (1992). Biochronologic data after Berggren et al. (1985), Backman et al. (1990), Raffi et al. (1995). (After Fornaciari et al., submitted.)

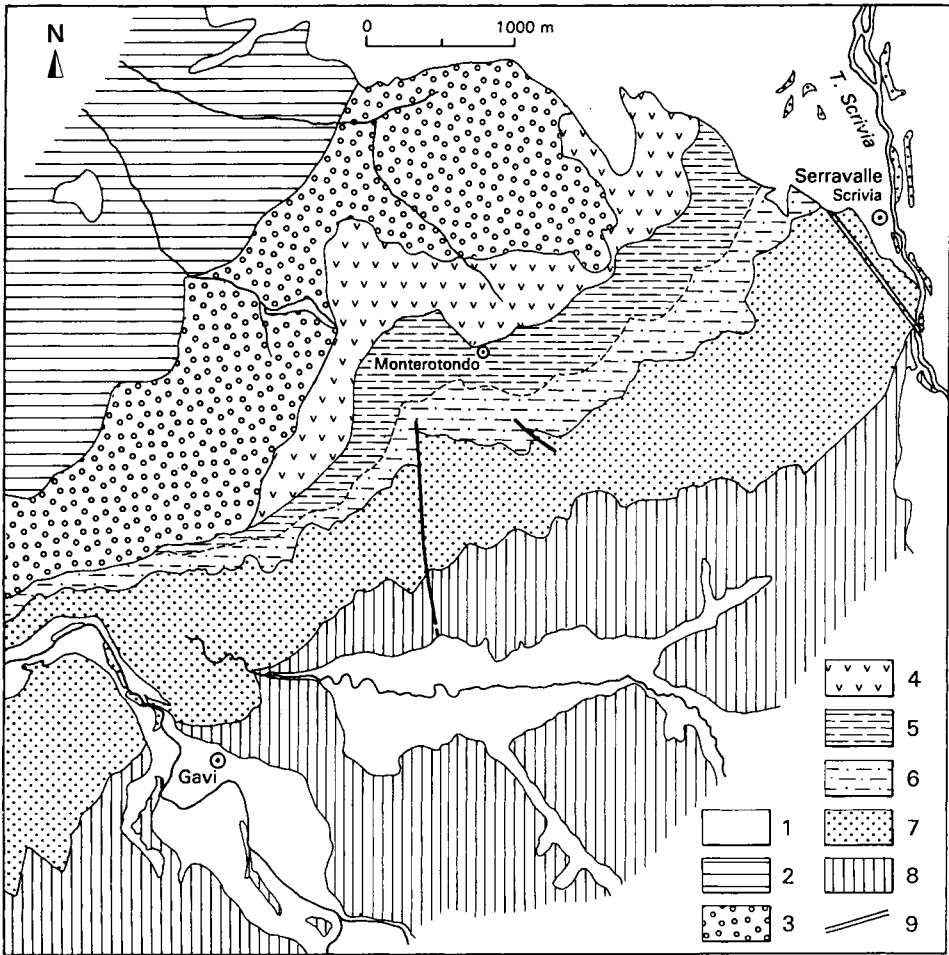


Fig. 10. Geologic sketch map of the Serravallian type area and location of the Serravallian stratotype section designated by Vervloet (1966). 1 = alluvial deposits; 2 = Lugagnano Clays; 3 = Cassano Spinola Conglomerates; 4 = 'Gessoso-Solfifera' Formation; 5 = Sant'Agata Fossili Marl (lower member); 6 = Sant'Agata Fossili Marl (upper member); 7 = Serravalle Sandstone; 8 = Cessole Formation; 9 = Location of the Serravallian stratotype (after Ghibaudo et al., 1985, modified).

The thickness of the Serravalle Formation, and hence of the Serravallian stratotype was stated to be about 150 m by Vervloet. Actually, careful measuring along the same section track followed by Vervloet carried out by Massari and Ghibaudo (in Fornaciari et al., submitted) indicates a thickness of about 400 m for the Serravallian stratotype.

Since the Serravalle Scrivia section was considered to be a poor stratotype because of its shallow-water depositional environment, and the scarcity of planktonic Foraminifera, an alternative stratotype section was proposed by Boni (1967) at Gavi, a few kilometres from Serravalle Scrivia, and a deep-water parastratotype section was proposed by Cita and Premoli Silva (1968) near the villages of Arguello and Lequio, in the western Tertiary Piedmont Basin, some 60 km from Serravalle Scrivia (Fig. 1).

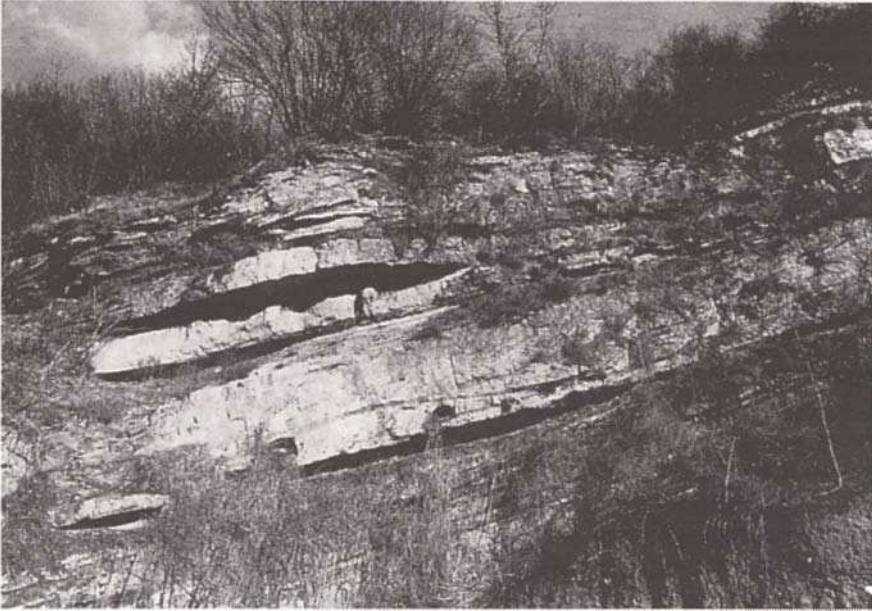


Fig. 11. Outcrop of Serravallian sandstones near Gavi Ligure, showing cross-lamination.

Since these various sections may not be entirely time-equivalent, for priority reasons, we will regard the Serravallian stratotype section designated by Vervloet (1966) as the unique valid stratotype and as the definition of the Serravallian.

Facies analysis by Ghibaudo et al. (1985), Caprara et al. (1985) and Gnaccolini (1989) have clearly demonstrated that the ‘Serravallian Sandstones’ in the area of Serravalle Scrivia represent a shelf deposit, probably interrupted by unconformities. The lower part of this formation (70–75 m) is characterized by a high variability of lithofacies: extensively bioturbated siltstones prevail and rhythmically alternate with normally graded or large-scale cross-laminated hybrid arenites. The main body of the formation is mostly represented by medium- to large-scale cross-laminated hybrid sandstones. The lower part of the ‘Serravalle Sandstones’ testifies the transition area between a prograding platform and a basinal plain located northwestwards (Figs. 3, 11 and 12). Upward, the formation represents a well developed shallow-water area characterized by sand waves consisting of mixed bioclastic and siliciclastic sandstones.

#### *International use of the term Serravallian*

The Serravallian stage is adopted in all the Geological Time Scales proposed after the RCMNS Congress of Bratislava (1975) (Fig. 4c). However, the term is rarely used outside the Mediterranean area (see for example most scientific reports of DSDP and ODP). Certainly this derives from the fact that until quite recently the Serravallian has been poorly constrained in time as testified by the different interpretations proposed for the position of the Langhian/Serravallian boundary versus the GPTS (Fig. 4c).

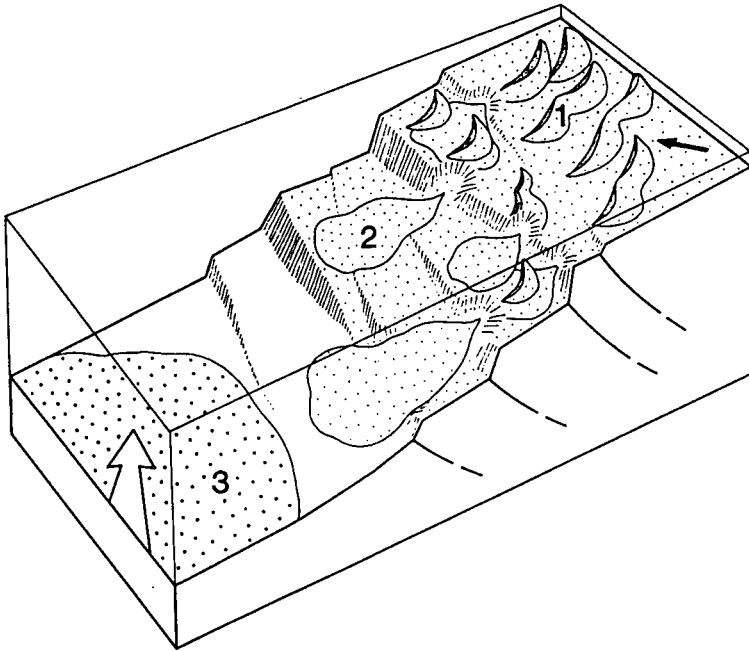


Fig. 12. Palaeogeographic restoration of the area between Gavi (Serravallian type area) and Acqui (central TPB, close to the Langhian type area) during the Serravallian. 1 = hybrid arenites, sand waves; 2 = resedimented hybrid arenites; 3 = turbidite lithoarenites (white arrow indicates palaeocurrent direction). The black arrow points to the north. (After Gnaccolini, 1989.)

In the Mediterranean area, where it is routinely recognized, it is generally approximated by the FO of *O. universa* (Iaccarino, 1985). We will show that this practice is at odds with the real age of the base of the Serravallian stratotype. So far no proposal has been made for a GSSP of the base of the Serravallian.

#### *Timing of the Serravallian stratotype*

Out of the different methods available for positioning in time and to correlate worldwide the Serravallian stratotype, only calcareous plankton biostratigraphy and biochronology can be utilized. Some magnetostratigraphic data are available from the Serravallian sediments in the Rio Mazzapiedi–Castellania section (Tortonian stratotype) and in the area of the type Langhian in western TPB (Nakagawa et al., 1974), but they are difficult to interpret and of limited utility for timing the Serravallian stratotype. To our knowledge, no radiometric or stable isotope studies are available from the stratotype or from the type area.

*Calcareous plankton biostratigraphy.* The planktonic foraminiferal contents of the Serravallian stratotype were studied by Vervloet (1966), Cita and Blow (1969) and in recent times by Miculan (1992), Foresi (1993), and by Fornaciari et al. (submitted), who agree in considering that the planktonic Foraminifera are poorly preserved and not very diagnostic. Because of this fact, the position in time of the Serravallian has been based on the foraminiferal contents of other reference sections (Gavi, Vignole

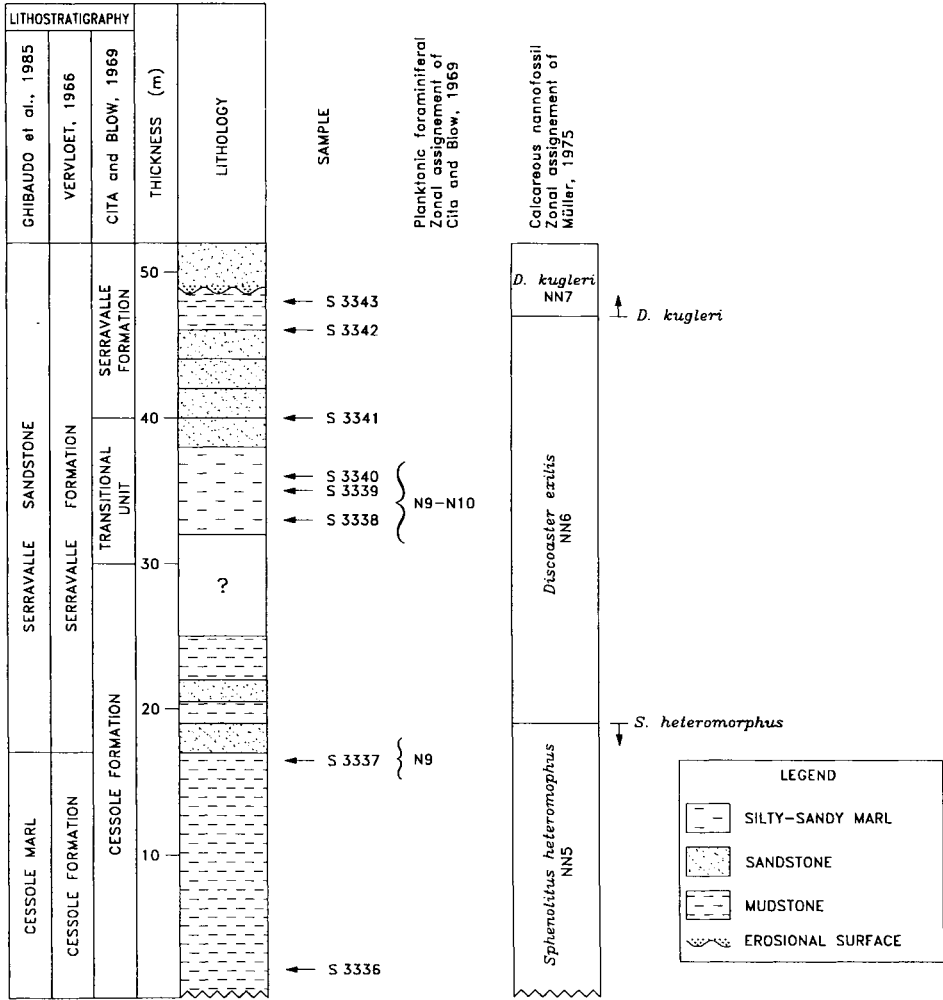


Fig. 13. Summary of calcareous plankton data on the Serravallian stratotype section provided by Cita and Blow (1969) and by Müller (1975).

Borbera, Arguello-Lequio, etc.) considered as time-equivalent to the Serravallian stratotype.

Integrating the available data, Cita and Blow (1969) and Foresi (1993) correlated the basal part of the Serravallian with the base of Zone N10 (FO of *Globorotalia praemenardii*), while Iaccarino (1985) and Miculan (1992) located it within Zone N9. Most importantly, all the authors agree that the base of the Serravallian stratotype postdates the FO of *O. universa*.

Calcareous nannofossils from the stratotype were studied by Müller (1975) in a limited set of samples (Fig. 13) and by Fornaciari et al. (submitted, Fig. 14). Müller concluded that the base of the Serravallian is approximated by the FO of *Discoaster kugleri* (NN6/NN7 boundary). It is important to remark that Müller (1975) considered

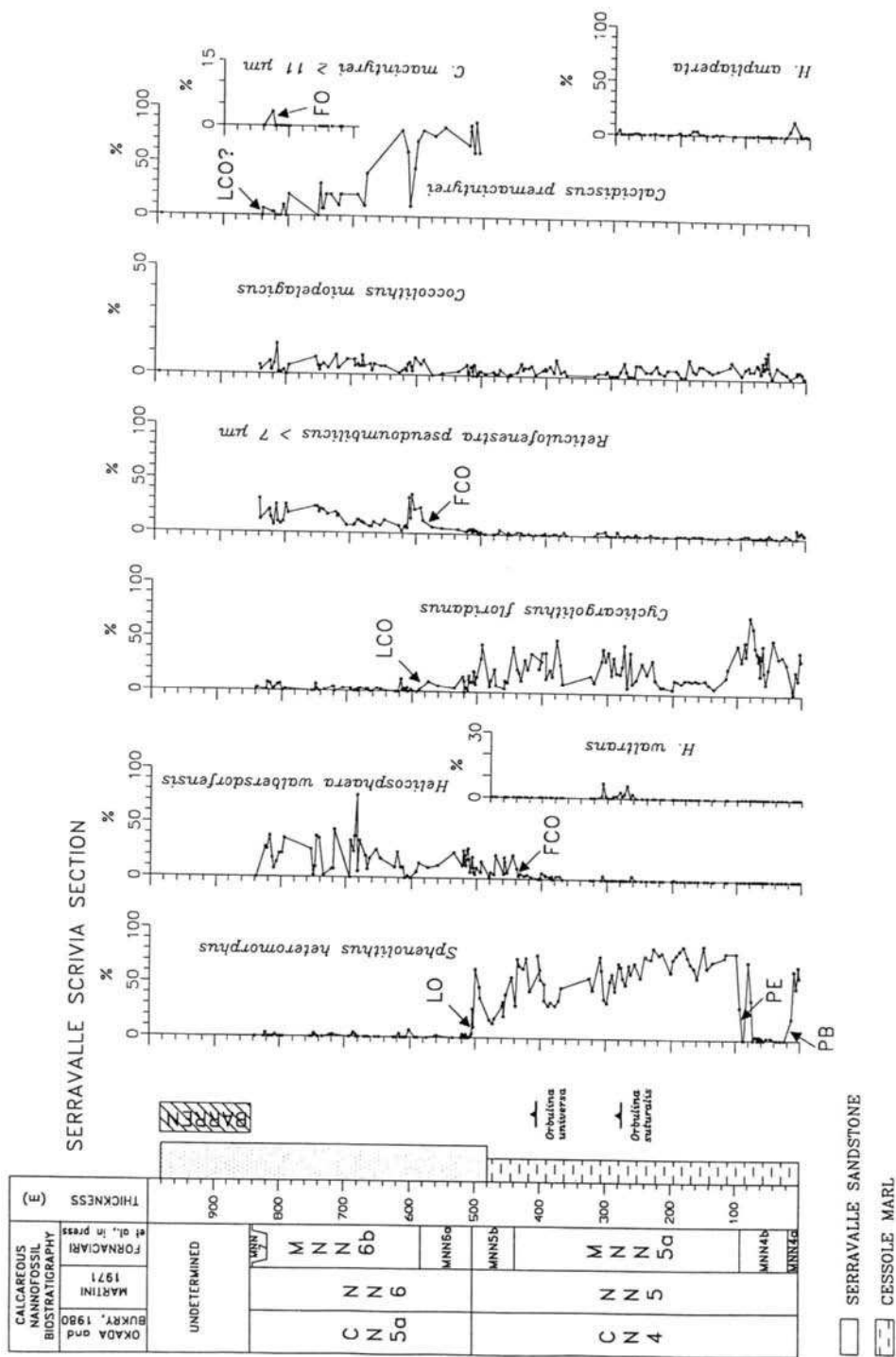


Fig. 14. Calcareous nannofossil quantitative distribution patterns and biostratigraphy in the Serravallian stratotype section provided by Formaciari et al. (submitted).

in a restrictive sense the Serravallian stratotype ascribing the 'transitional unit' reported in Fig. 13 to the Langhian, while it belongs to the Serravallian stratotype as designated by Vervloet (1966) (see Fornaciari et al., 1996). The results of the recent high-resolution study of Fornaciari et al. (submitted, Fig. 14) indicate that the base of the Serravallian is located in the top part of the NN5 Zone, i.e., just below the LO of *S. heteromorphus*.

On the base of these recent calcareous nannofossil data, it can be stated that now the position in time of the base of the Serravallian is fairly well constrained. In fact the LO of *S. heteromorphus* is one of the most easily recognized and correlated biohorizon of the Cenozoic (Fornaciari et al., 1996; Raffi et al., 1995). The LO of *S. heteromorphus* has been calibrated to Chron C5ABr (Backman et al., 1990; Olafsson, 1991) and is associated with one of the major changes in the palaeoclimatic–palaeoceanographic history of the Cenozoic, the so called 'mid-Miocene' event (base of the oxygen stable isotope Zone Mi3 of Miller et al., 1991a, b). This event consists in a major  $\delta^{18}\text{O}$  increase of the benthonic Foraminifera record interpreted as related to a combination of an increased production of high-latitude, cold deep waters and increased East Antarctic ice-sheet growth (Shackleton and Kennett, 1975a,b; Kennett, 1985; Miller et al., 1985, 1987; Woodruff and Savin, 1989, 1991; Wright et al., 1992). The evaluation of the extension in time of the Serravallian and the precise pinpoint of its top is precluded by the fact that about the upper 150 m of the stratotype are barren of calcareous plankton microfossils (Fig. 12). However, the presence of secondary calcareous nannofossil markers allows to infer that the fossiliferous lower–middle part of the type Serravallian is correlated to Zone NN6 (Fornaciari et al., 1996; Fig. 14).

### *Relationships with the Langhian*

The relationships between the type Langhian (Cessole Marls in the Langhe region) and the type Serravallian is equivocal in the existing literature (Berggren et al., 1985b, p. 221). Müller (1975) inferred that the shallow-water Serravalle Sandstones do correlate in time with the deep-water Cassinasco Formation. Actually, as documented in Fig. 9, calcareous nannofossils allow a straightforward correlation between the two stratotypes, which is not contradicted by planktonic Foraminifera; this correlation indicates that a time gap exists between the top of the Langhian and the base of the Serravallian. Specifically, the first common and continuous occurrence (FCO) of *H. walberdorsfensis* and the FO of *O. universa*, at the top of the Langhian (at the transition from the Cessole Marls to the Cassinasco Formation), are recorded some 30 m below the base of the Serravallian stratotype.

### *Concluding remarks on the Serravallian stage*

We have noted above that the Serravallian is rarely used outside the Mediterranean, probably because of the lack of a precise perception of its position in time. The practical criterion most frequently used in the Mediterranean region for its recognition, the FO of *O. universa*, is not used as a zonal marker in the standard zonation, has not been calibrated to GPTS and is rarely reported in the range charts of oceanic sediments. Indeed, some authors (i.e., Stainforth et al., 1975) used the FO of *O. suturalis* (*Orbulina datum*) as boundary criterion. Actually, both events predate the base of the Serravallian



stratotype, which in the absence of a GSSP of the base of the Serravallian, is the working definition of the Langhian/Serravallian boundary. The recent study of Fornaciari et al. (submitted; Fig. 14) indicates that the base of the Serravallian stratotype is remarkably close to the LO of *S. heteromorphus*, which is the best biostratigraphic tool for its correlation.

The Serravallian stratotype is represented by shallow-water sediments unsuitable for defining the GSSP of its base, which must be looked for in another area. In agreement with the position in time of the base of the historical stratotype, we propose the driving criterion to follow in designating the GSSP be the LO of *S. heteromorphus*. This event is known to occur, as commented previously, in a critical interval of the Miocene climatic history, and would provide a 'natural' divide in the Miocene chronostratigraphy.

## THE TORTONIAN

### *History of definition*

The term Tortonian was introduced in the geological literature by Mayer-Eymar (1858) in one of his numerous time scales published in the form of tables that provide very little information concerning the fossiliferous beds that substantiate the nominate time interval. Indeed, only ten words define the Tortonian as follows: "Blau Mer gel mit *Conus canaliculatus* und *Ancillaria glandiformis* von Tortona". Mayer being (or Mayer-Eymar, as he often called himself) a Privat Dozent at the polytechnical school of Zurich since 1857, and a professor of Stratigraphy and Palaeontology at the Zurich University from 1875 to 1906, he was able to publish several times his time scale and to indoctrinate generations of geologists. In particular the stage name Tortonian was used in the last century by Omboni (1869), Stoppani (1873), Sacco (1889), Issel (1897), and, in our century, by De Lapparent (1906), Parona (1903), and Haug (1927).

### *The Tortonian stratotype: definition and geological setting*

The stratotype of the Tortonian was designated by Gianotti (1953) in the section outcropping in the valley of Rio Mazzapiedi and Rio Castellania, between the village of Sant'Agata Fossili and the town of Alessandria, some 10 km south of Tortona (Fig. 15). Gianotti studied the foraminiferal contents (basically benthonic Foraminifera) of the stratotype section, which was designated on basis of the geological study of the area by Gino (1953).

Recent relevant geologic-stratigraphic studies in the area of the Tortonian stratotype have been carried out by Vervloet (1966), Clari and Ghibaudo (1979), and by Ghibaudo et al. (1985), to which the reader is referred for detailed information. The Rio Mazzapiedi-Castellania section has a monoclinial setting, gently dipping to the north, toward the Po Plain. The simplified original columnar log of the section as described by Gino (1963) and Gianotti (1953) is shown in Fig. 16, where successive lithostratigraphic terminology is reported. The Tortonian stratotype is mainly represented by marly sediments (the Sant'Agata Fossili Marls of Ghibaudo et al., 1985) which lie over the shallow-water marine Serravalle Sandstones. Clari and Ghibaudo (1979) subdivided the Sant'Agata Fossili Marls into two members. The lower member, 180 m thick, consists

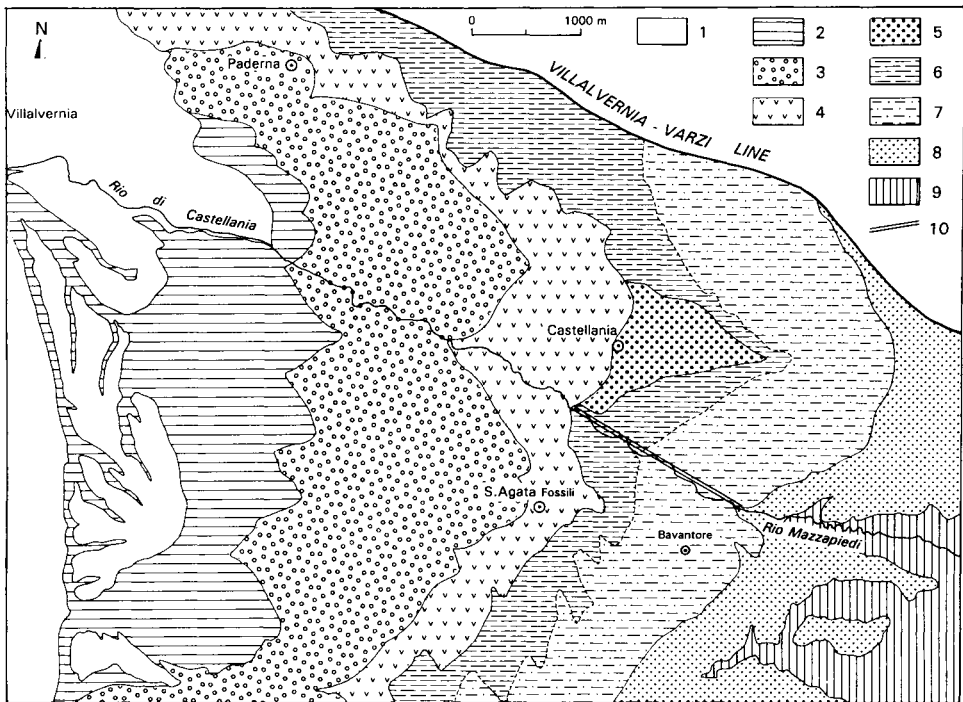


Fig. 15. Geologic map of the Tortonian type area and location of the Tortonian stratotype section. 1 = alluvial deposits; 2 = Lugagnano Clays; 3 = Cassano Spinola Conglomerate; 4 = Gessoso-Solfifera Formation; 5 = S. Alosio Conglomerate; 6 = S. Agata Fossili Marl (upper member); 7 = S. Agata Fossili Marl (lower member); 8 = Serravalle Sandstone; 9 = Apennine units; 10 = trace of the Tortonian stratotype section. (After Clari and Ghibaud, 1979.)

of alternating beds of bioturbated fine sandstones and muddy siltstones occasionally displaying faint horizontal laminae. These sediments are rich in fine carbonaceous matter and plant debris. Multiple intraformational discordances which are cut in the topmost part of the sequence, represent scars left by repeated downslope sliding, probably triggered by tectonic oversteepening (Fig. 17). The upper member consists of about 80 m of blue-grey hemipelagic silty marls, with thin-bedded turbidites in the upper part. Both the biota and facies associations are indicative of an outer shelf and a slope environment for the lower and upper member, respectively.

#### *The international use of the term Tortonian*

In spite of the fact that no formal and official decision has been taken by the International Commission of Stratigraphy concerning the definition of the Tortonian, the Rio Mazzapiedi–Rio Castellania section has been unanimously considered as the reference for the nominate time interval. However, it should be noted that the original extension of the Tortonian of Gianotti has been severely decapitated because of the successive lowering of the base of the Messinian (Cita et al., 1965; D’Onofrio et al., 1975; Fig. 16).

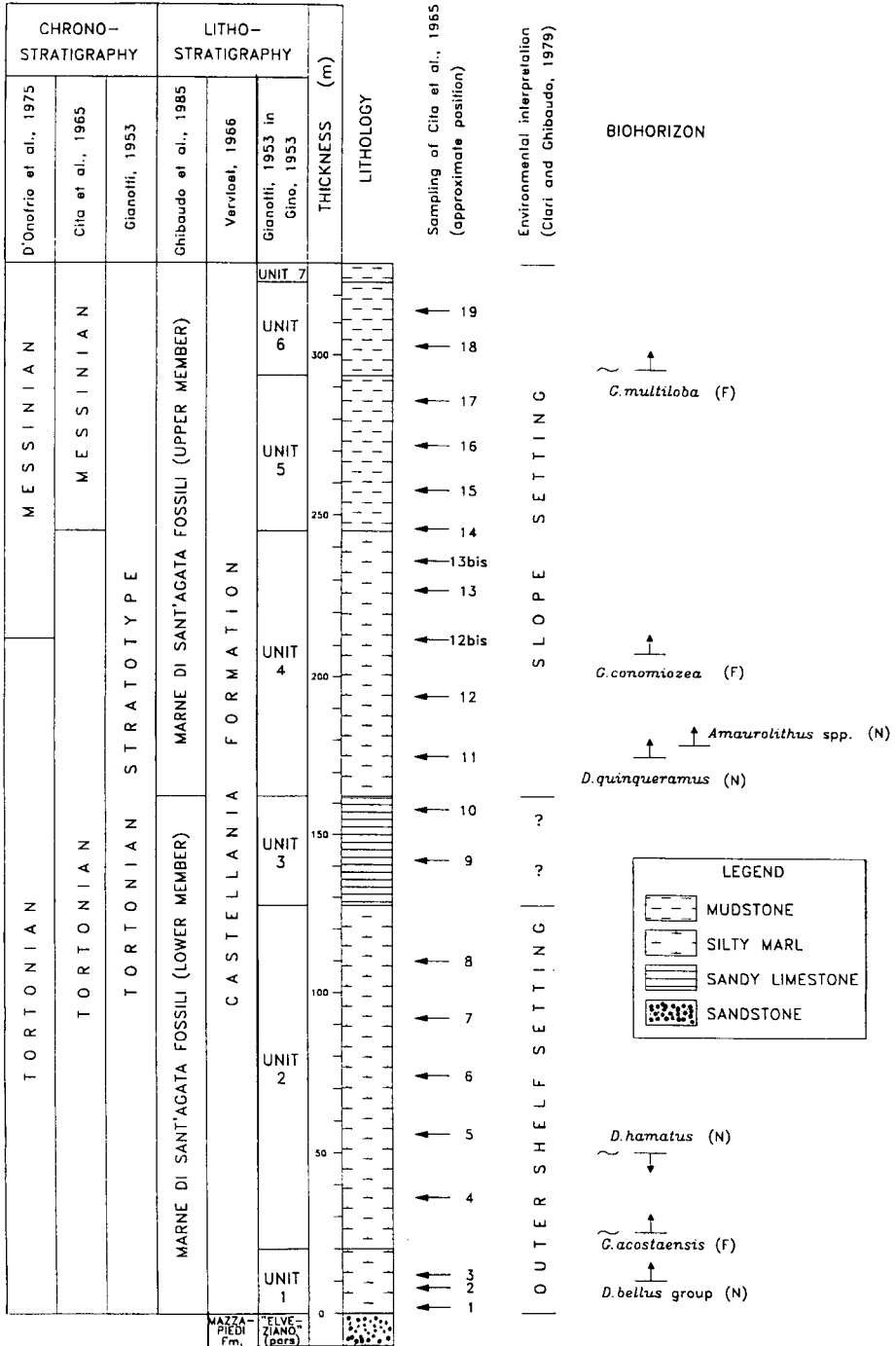


Fig. 16. Summary of the calcareous plankton biostratigraphic data available on the Tortonian stratotype (Cita and Blow, 1969; Martini, 1975; D'Onofrio et al., 1975; Mazzei, 1977). The original columnar log of Gino (1963) is utilized and the lithostratigraphic terminology used by various authors is shown.



Fig. 17. Tortonian historical stratotype: upper part of the section east of Castellania, showing slump scars.

The Tortonian is consistently reported as a global (not regional) stage in all the recently published geologic time scales (Fig. 4c). In spite of the problems (discussed below) concerning the position in time of the base of the Tortonian stratotype, there has been a general consensus in approximating the base of the Tortonian by the FO of the planktonic foraminifer *Neogloboquadrina acostaensis* (Fig. 4b)

#### *Timing of the Tortonian stratotype*

Out of the different methods available for positioning in time the Tortonian stratotype section, only calcareous plankton biostratigraphy and magnetostratigraphy are available. To our knowledge, no radiometric or stable isotope study has been carried out in the stratotype or in the type area.

*Calcareous plankton biostratigraphy.* The rich and well diversified contents in planktonic Foraminifera from the Tortonian stratotype have been studied by Cita et al. (1965), Cita and Blow (1969), and for the upper part, by D'Onofrio et al. (1975). The calcareous nannofossil contents have been studied by Martini (1975) and Mazzei (1977). Calcareous nannofossil assemblages are well diversified, partly preserved but affected by reworking. It should be noted that in the Mediterranean area many calcareous nannofossil marker species utilized for zoning on a global base in the time interval of interest are either rare (*Amaurolithus* spp., *Discoaster hamatus*), present with atypical forms (*Discoaster kugleri*, *D. quinqueramus*, and *D. berggrenii*), or are missing (*Catinaster coalitus*).

The most relevant calcareous plankton biohorizons, useful for long-distance correlations, are shown in Fig. 14. The base of the Tortonian stratotype is considered

as belonging to the foraminiferal Zone N15 of Blow (Cita and Blow, 1969) and to nannofossil Zone NN9 of Martini (Martini, 1975; Mazzei, 1977). As discussed by Rio et al. (1990a,c) these zonal assignments are conflicting since the FO of *Neogloboquadrina acostaensis* (N15/N16 zonal boundary definition) is in mid-latitude areas (i.e., Berggren et al., 1985b; Miller et al., 1985) and in the Mediterranean region (Rio et al., 1990c) close to the base of nannofossil Zone NN8 (Fig. 8). The available studies on the stratotype are based on a limited number of samples and, therefore, the issue cannot be satisfactorily settled. However, most probably the local FO of *N. acostaensis* in the Rio Mazzapiedi–Castellania section does represent a delayed entrance, possibly related to the unfavourable ecologic conditions (the depositional environment of the basal part of the section is an inner shelf). In order to definitively solve the problem, a high-resolution integrated (physical stratigraphy and calcareous plankton biostratigraphy) study at the transition from the Serravalle Sandstones to the Sant'Agata Fossili Marls is necessary.

Other bioevents detected in the section, of great importance for long-distance correlation are the FOs of *D. berggrenii*, *D. quinquaramus*, *Amaurolithus primus*, *A. delicatus*, and of *Globorotalia conomiozea* (Fig. 14). On the basis of these biostratigraphic elements, it can be concluded that the upper part of the original stratotype of the Tortonian overlaps considerably with the Messinian, as recently redefined by Colalongo et al. (1979a, b), with its base at the FO of *G. conomiozea* (Fig. 14).

**Magnetostratigraphy.** Magnetostratigraphic investigations in the Tortonian stratotype (Mazzapiedi Formation in the terminology of Vervloet, 1966) were carried out by Nakagawa et al. (1974; Fig. 18). The magnetostratigraphic results obtained by Nakagawa and co-workers in the 1970s in the Mediterranean Neogene and Pleistocene sediments are generally considered not to be very reliable (i.e., Channell et al., 1994), and we do not know the value of the data obtained of the Tortonian stratotype in the Castellania–Rio Mazzapiedi section. In Fig. 15 we compare the bio-magnetostratigraphy available in this section with the biomagnetostratigraphy established in oceanic areas. The magnetic polarity history derived by Nakagawa et al. (1974) from the Tortonian stratotype does not show a good pattern fit to the standard Geomagnetic Polarity Time Scale (GPTS). However, considering the available biostratigraphic constraints, the following interpretation can be tentatively proposed (Fig. 18):

- the basal positive magnetozones D and E correlate most probably with Chron C5n because of the scattered presence of *Discoaster hamatus*, known to appear within this Chron, and becoming extinct during Chron C4Ar;

- the thick negative interval of magnetozone B, in the upper part of the section, might correlate with Chron C3Ar, because of the presence of *Amaurolithus* spp. and of *Globorotalia conomiozea*;

- the long positive interval of magnetozone C is difficult to correlate; it might correlate with Chron C4n, and in this case a hiatus would be present in correspondence with Chron C4An, and the local entrance of *D. quinquaramus* would be delayed with respect to the oceanic areas (Fig. 18); or it might correlate to Chron C4An, and a hiatus would be present in correspondence with Chron C4n.

In this section, the FO of *N. acostaensis* is approximately at the top of a positive interval apparently correlatable with Chron C5n, while in extra-Mediterranean sections the FO is at the base of this Chron (Fig. 8; see Miller et al., 1985). This would confirm

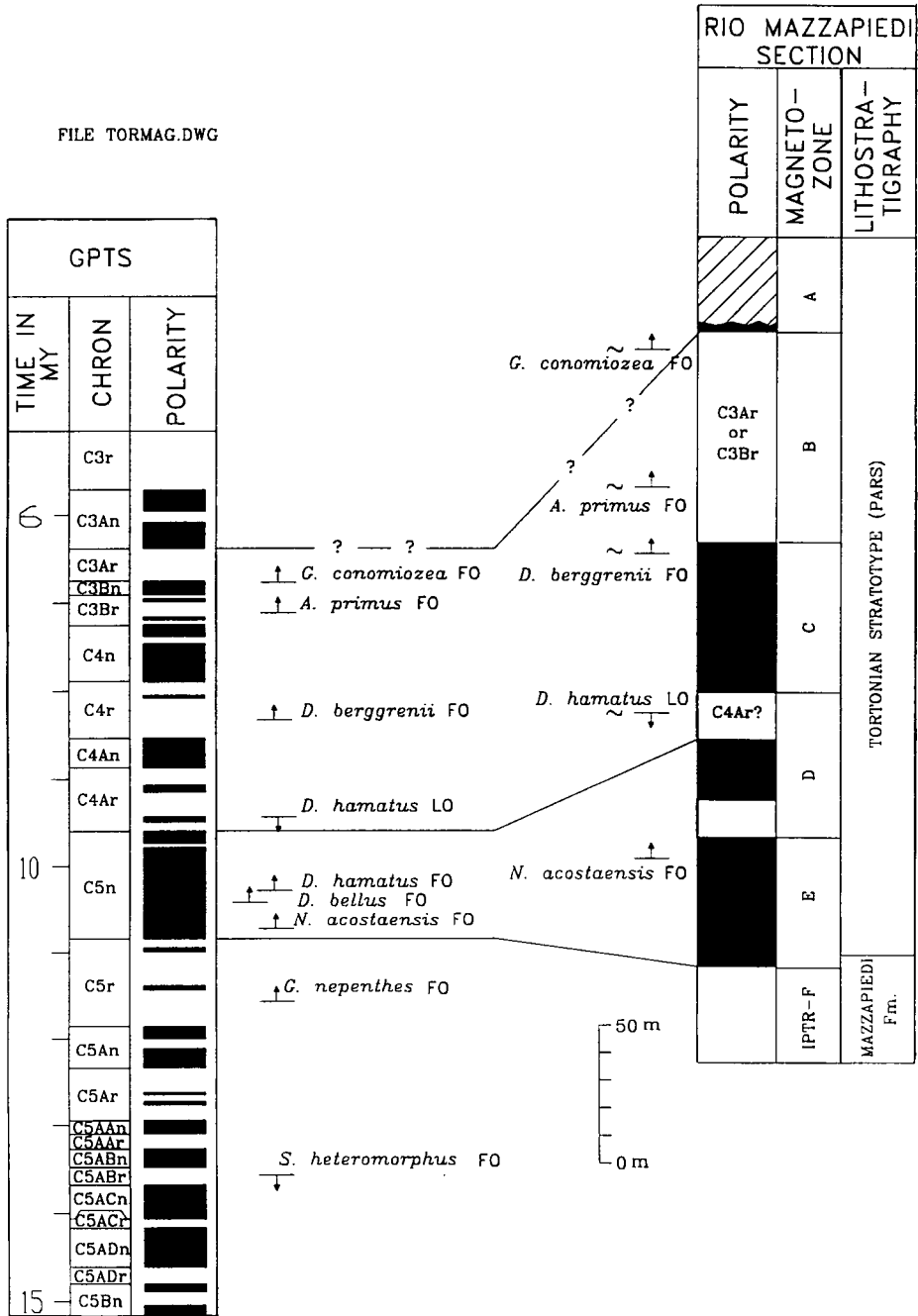


Fig. 18. Tentative correlation of the magnetic polarity history determined by Nakagawa et al. (1974) in the Tortonian stratotype section (Rio Mazzapiedi-Castellania section) with the standard Geomagnetic Polarity Time Scale of Cande and Kent (1992). See the text for discussion.

the indication obtained above, integrating nannofossil and planktonic foraminifer data, that entrance of this taxon into the Tortonian stratotype is delayed.

### *Relationships with the Serravallian and the Messinian*

The Serravallian stratotype section at Serravalle Scrivia (Vervloet, 1966; Boni and Selli, 1971) is located in the same area of the Tortonian stratotype, some 15–20 km to the southwest (Fig. 1). The Middle and Late Miocene sedimentary histories in these two localities, although similar, differ in the details (Ghibaud et al., 1985). Specifically, the ‘Sant’Agata Fossili Marls’ are thicker in the area of the Tortonian stratotype with respect to the area of the Serravallian stratotype. A detailed physical correlation between the successions outcropping in the two areas is lacking. As discussed in the previous pages, the top 150 m of the Serravallian stratotype lack planktonic microfossils, and cannot be dated. However, the onset of a mainly pelitic sedimentation (the Tortonian) above the sandy sedimentation of the Serravallian is a general feature of the eastern TPB, and most probably does represent a correlatable event related to the regional tectonic evolution and/or to a global eustatic variation. Considering the shallow-water depositional environment of both the upper part of the Serravallian stratotype and the lower part of the Tortonian stratotype, it is well possible that hiatuses are present. But it appears as highly improbable that an overlap exists between the top Serravallian and the basal Tortonian.

As anticipated, there is a considerable overlap between the Tortonian and the Messinian as recently redefined in the Falconara section (see Colalongo et al., 1979b). Indeed the newly proposed definition of the base of the Messinian with the appearance of *G. conomiozea* has resulted in defining the beginning of the Messinian, historically intended as the interval of restricted communication between the Mediterranean and the Atlantic, leading to the deposition of evaporites well within the normal-marine Tortonian, and to a considerable shortening of the latter (Fig. 16).

### *Concluding remarks on the Tortonian stage*

The original definition of the Tortonian by Mayer-Eymar (1858) was outrageously simple and showed lack of information, but it defined, in a non-ambiguous manner, the locality (Tortona) and the lithology (marls). The use of the term Tortonian is deeply entrenched in the stratigraphic literature since the last century, and its use has not been controversial, even if its positioning in time has been variously interpreted (Fig. 4). The base of the Tortonian was not defined palaeontologically (which is correct), but for correlation purposes the biohorizon most used has been the FO of *N. acostaensis* (Fig. 4b, even if this biohorizon may be older than the base of the stratotype. The range of *N. acostaensis* in itself versus the range of *Globorotalia siakensis* (or *G. mayeri*) is a very controversial point among biostratigraphers (see discussion in Cita and Blow, 1969) and has not been assessed with certainty, even in oceanic sediments, because of the widespread dissolution in the time interval of interest.

The designation of a stratotype section (Gianotti, 1953) in the Rio Mazzapiedi–Castellania section has not been particularly fortunate for the quality of the exposure, the shallow-water depositional environment and the continuity of the succession. The designation of a GSSP in a continuous deep-marine section seems mandatory for

anchoring in a stable and unequivocal manner the base of the Tortonian stage. For reasons of stability and correlatability, it is recommended that the driving criterion in selecting the GSSP for the base of the Tortonian be the first evolutionary appearance of *N. acostaensis*. This biohorizon has been calibrated as occurring in mid-latitude areas close to the base of Chron C5n (Berggren et al., 1985b; Fig. 9). Approximately at this time, a major turnover in calcareous nannofossils occurred with the appearance of the five-ray discoasterids (*Discoaster bellus* group sensu Rio et al., 1990a; see also Raffi et al., 1995). Apparently, associated with the lower part of ChronC5n, is also the appearance of *Hipparion* in the Indian subcontinent (Barry et al., 1982; Tauxe and Opdyke, 1982), a major event in the continental stratigraphy. All these elements should ensure a wide correlatability of the base of the Tortonian, and facilitate its use on an international basis.

## GENERAL CONCLUSIONS

We have reviewed the state of the art of our knowledge on the historical stratotypes of the Langhian, the Serravallian, and the Tortonian, all of which have been designated in the lithostratigraphic record of the Tertiary Piedmont Basin, in NW Italy. Although the lack of unequivocal magnetostratigraphic data prevents a precise timing of the stratotype sections of the nominate units, integrated calcareous plankton biostratigraphy allows to evaluate their mutual relationships and, at least grossly, to correlate them on global scale. We have shown that the three stratotypes do not overlap each other and time gaps exist between them (Figs. 9 and 19). Biostratigraphic events close to their bases and useful for long-distance correlations are the *Praeorbulina* datum (base of the Langhian), the LO of *S. heteromorphus* (base of the Serravallian) and the FO of *N. acostaensis* (base of the Tortonian).

In order to meet with the needs of precision and accuracy in time correlations, which can be achieved in modern stratigraphy (and especially in the Neogene), the practice of defining stages by the GSSP of their bases has become widely accepted. We have discussed the suitability of the stratotype sections of the three nominate stages to serve as GSSPs of their bases. The Langhian, the Serravallian and the Tortonian (as well as virtually all the stages of the standard Geologic Time Scale) have been introduced, and later 'stratotypified' in a cultural context different from the present one, and often with regional (and not global) scopes. Not surprisingly their stratotypes fail to meet the requirements of the GSSP. Specifically, the facies of the stratotype sections are unsuitable for obtaining the precise chronology which is needed in defining the GSSPs of the Neogene stages. The search for suitable marine pelagic sequences is under way by members of the Subcommittee of the Neogene Stratigraphy (Leader: M.B. Cita) and of the Miocene Columbus Project (MICOP, Leaders: A. Montanari, R. Coccioni, and G.S. Odin).

Finally, we have discussed the criteria which should guide in selecting the boundary points in the fossil record for defining the GSSPs of the bases of the stages under discussion. The potential of worldwide correlatability has been the most critical part of our work, and in line with this reasoning our main concern is to propose that: (1) the base of the Langhian be defined close to (not necessarily coincident with) the *Praeorbulina* datum; (2) the base of the Serravallian be defined close to the LO of *S.*



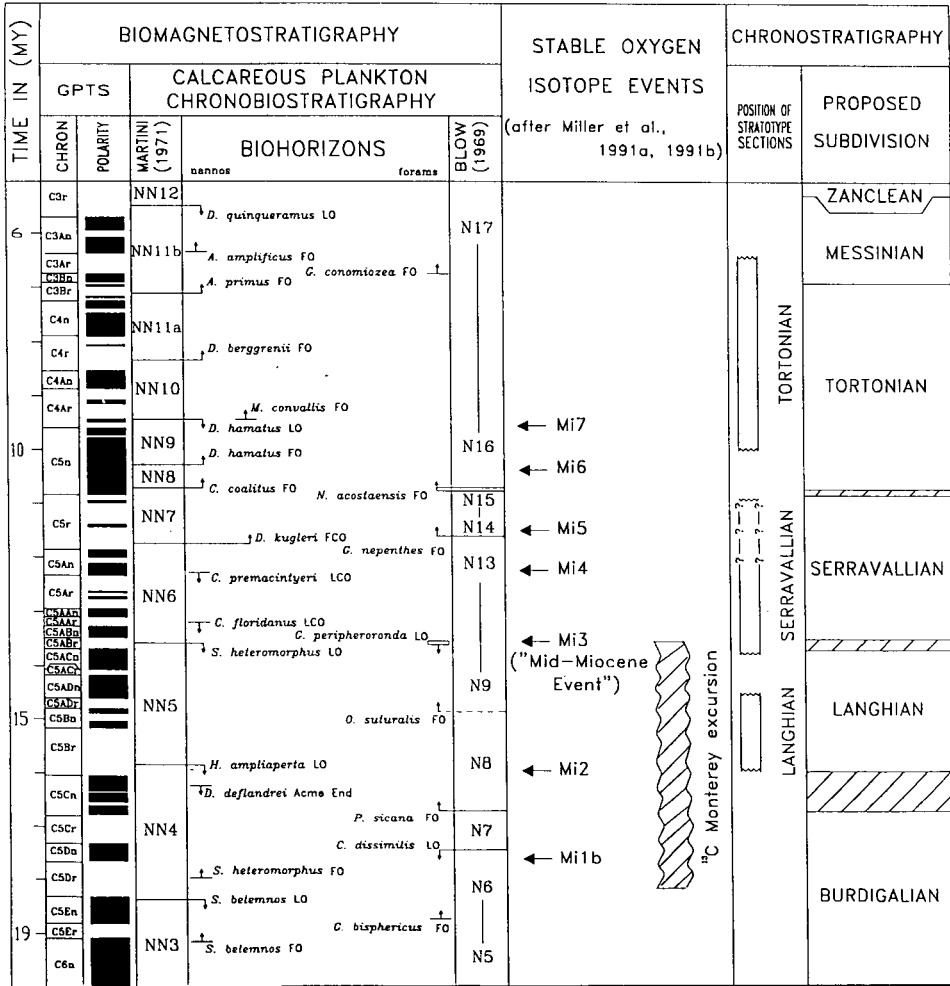


Fig. 19. Early to Late Miocene time framework and the proposal of chronostratigraphic subdivision discussed in this work. Geomagnetic Polarity Time Scale after Cande and Kent (1992). Biochronologic data after Berggren et al. (1985), Backman et al. (1990), Raffi et al. (1995). Position of the  $\delta^{13}C$  Monterey excursion after Woodruff and Savin (1991).

*heteromorphus*; (3) the base of the Tortonian close to the FO of *N. acostaensis*. This proposal, summarized in Fig. 16, does not violate the position in time of the historical stratotypes and results in a balanced subdivision of the Miocene Series. The bases of the Serravallian and the Tortonian are positioned in times of high climatic instability, which should facilitate their global recognition. The Langhian, which is deeply entrenched in the stratigraphic literature, corresponds with the maximum Miocene sea-level stand (Miller et al., 1991a, b; Wright et al., 1992), but its base apparently does not correspond with a major climatic threshold.

**SOMMAIRE — LES STRATOTYPES HISTORIQUES LANGHIEN, SERRAVALLIEN ET TORTONIEN**

(Manuscrit soumis: Janvier 1994, révisé: Juin 1994; rédacteurs responsables: GSO, AM & RC)

Cette contribution fait le point de notre connaissance sur les sections stratotypiques historiques des Étages Langhien, Serravallien et Tortonien toutes trois situées dans le Bassin Tertiaire du Piémont au NO de l'Italie. En dépit de l'absence de données radiométriques, géochimiques et magnétostratigraphiques directes, la biostratigraphie du plancton calcaire (foraminifères et nannofossiles) permet leur corrélation sur une large portion du globe et l'évaluation de leurs relations mutuelles. Les trois stratotypes historiques ne se recouvrent pas dans le temps et des lacunes temporelles existent entre ces Étages tels que définis actuellement. Des événements utiles pour leur reconnaissance globale sont l'apparition évolutive — émergence — de *Praeorbulina* spp. (près de la base du Langhien), la disparition évolutive — extinction — de *Sphenolithus heteromorphus* (près de la base du Serravallien) et l'émergence de *Neogloboquadrina acostaensis* (près de la base du Tortonien). Des conditions de faciès défavorables ne permettent pas d'utiliser ces sections stratotypiques historiques pour une définition précise des limites; dans ce but, des Points et Sections Stratotypes Globaux sont à l'étude. En tenant compte de la position temporelle des stratotypes historiques, de l'utilisation pratique des unités qui a été faite au cours des années et du potentiel de corrélation globale, une proposition de critères est faite pour guider le choix des points limites dans l'enregistrement lithologique. Concrètement, il est proposé de définir: (1) la limite Burdigalien/Langhien près du biopère *Praeorbulina* (magnétozone C5Cn), en relation avec le début du maximum de niveau marin du Miocène moyen; (2) la limite Langhien/Serravallien près de l'extinction de *S. heteromorphus* (magnétozone C5AB), en relation avec un changement majeur dans l'histoire climatico-océanique du Cénozoïque; (3) la limite Serravallien/Tortonien près de l'émergence de *N. acostaensis* (base de la magnétozone C5n) au moment où se déroulent des changements majeurs dans le système climatique, dans les associations de nannofossiles calcaires et dans les faunes de vertébrés.  
(Sommaire proposé par les rédacteurs d'après un résumé des auteurs, GSO)

**ACKNOWLEDGMENTS**

We thank Eliana Fornaciari (Padova University), who has studied carefully calcareous nannofossils from the Mediterranean stratigraphic record and graciously allowed us to utilize her data not yet fully published. Financial support has been provided by the CNR 'Centro per la Geodinamica Alpina' (Padova) and MURST (40%) grants (responsibles F. Proto Decima, S. Iaccarino, and M.B. Cita).

This Page Intentionally Left Blank

Chapter A6

**CALCAREOUS PLANKTON BIOSTRATIGRAPHY OF THE LANGHIAN HISTORICAL STRATOTYPE**

E. Fornaciari, S. Iaccarino, R. Mazzei, D. Rio, G. Salvatorini, A. Bossio and B. Monteforti

INTRODUCTION

The Langhian Stage, introduced by Pareto in 1865, is the currently accepted chronostratigraphic unit for indicating the lower part of the Middle Miocene (Berggren et al., 1985a, b). The published calcareous plankton (planktonic Foraminifera and calcareous nannofossils) biostratigraphic data on the stratotype of the Langhian are contradictory (Berggren et al., 1985a, b). Specifically, the upper part of the Langhian has been ascribed to the planktonic foraminiferal Zone N9 of Blow (1969) by Cita and Blow (1969) and to the uppermost part of the calcareous nannofossil Zone NN6 of Martini (1971) by Martini (1971) and Müller (1975). Indeed, plenty of data in oceanic areas (i.e. Berggren et al., 1985a, b) indicate that the entire Zone N9 falls within NN5. In order to clarify this contrast and to better constrain the type Langhian in terms of calcareous plankton biostratigraphy, we have undertaken an integrated study of planktonic Foraminifera and calcareous nannofossils from the stratotype section designated by Cita and Premoli Silva (1960) near the village of Cessole in the Langhe region (Piedmont, northwest Italy, Fig. 1). We will show that while the planktonic foraminiferal results of Cita and Premoli Silva (1960) are substantially in agreement with our findings, the position of the top of the Langhian as indicated by Martini (1971) and Müller (1975) needs to be rectified. Specifically, the top of the Langhian stratotype falls well within the range of *Sphenolithus heteromorphus* (Zone NN5 of Martini) and no contrast exists in the succession of the calcareous plankton biohorizons observed in the stratotype area and in the global oceanic sedimentary record.

SAMPLING

The reader is referred to the papers of Cita and Premoli Silva (1960), Cita (1971a), Gnaccolini (1960, 1968), Gelati (1968), and Gelati et al. (1993) for information on the geologic setting of the area of the Tertiary Piedmont Basin where the Langhian stratotype section is located. It is sufficient to recall here that the stratotype section is composed of two component segments, named Bricco del Moro and Bricco della Croce sections (Fig. 2). The type Langhian is represented by mainly marly sediments (Pteropod Marls Auctorum) known in the most recent geologic literature as Cessole Formation (Vervloet, 1966) or Cessole Marls (Boni, 1967; Gelati, 1968). The Cessole Marls (type Langhian) are located between two, mainly arenaceous, turbiditic formations: the Cortemilia Formation below and the Cassinasco Formation above (Vervloet, 1966; Gelati, 1968).

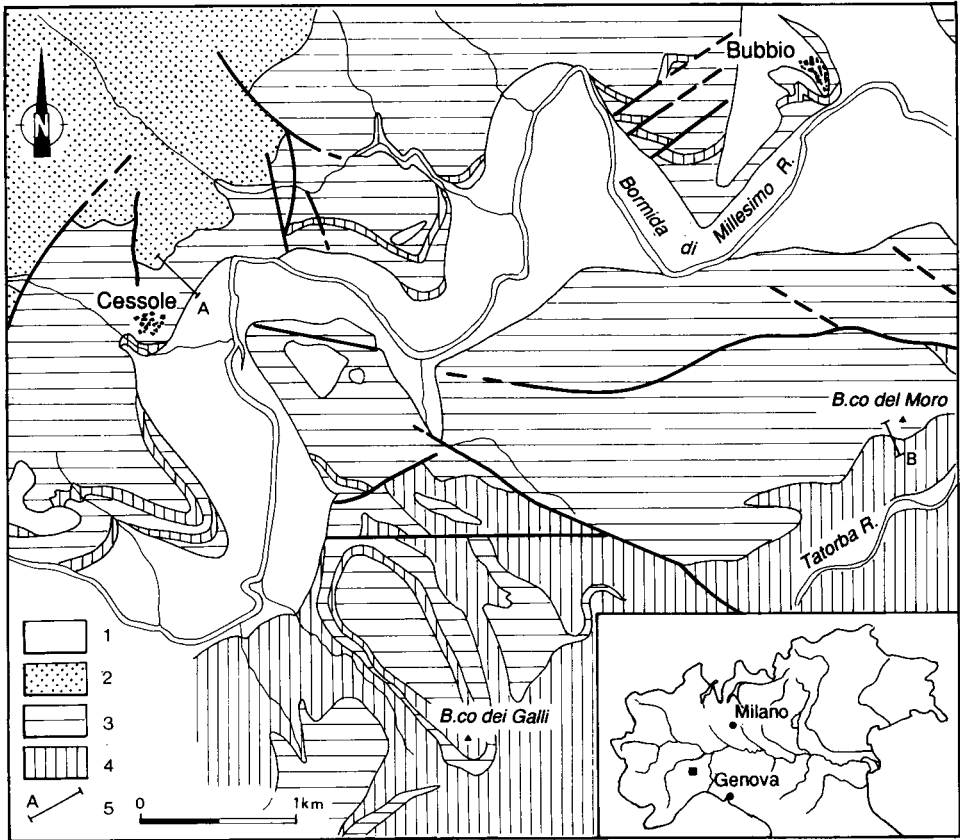


Fig. 1. Geological map of the area of the Langhian historical stratotype: 1 = alluvial deposits; 2 = Cassinasco Formation; 3 = Cessole Formation; 4 = Cortemilia Formation. The two component segments of the stratotype are indicated: A = Bricco della Croce section; B = Bricco del Moro section.

The base of the Langhian is exposed in the Bricco del Moro section, located on a hill south of the Bormida river, where the transition from the Cortemilia Formation to the Cessole Marls is gradational. We collected 20 samples in this section (Fig. 3). The main part of the Langhian and its top are exposed in the Bricco della Croce section outcropping on the slope north of the Bormida river (Fig. 1). The transition from the Cessole Marls to the overlying Cassinasco Formation is abrupt. We collected 60 samples, 49 from the Cessole Marls throughout a composite section consisting of three segments, and 11 from the first 50 m of the overlying Cassinasco Formation (Fig. 3).

#### CALCAREOUS NANNOFOSSIL BIOSTRATIGRAPHY

Standard techniques ('smear slides') were used for preparing calcareous nannofossils, which were studied in the light microscope. We examined a total of 80 samples in search for marker species utilized in the standard zonations of Martini (1971) and Okada

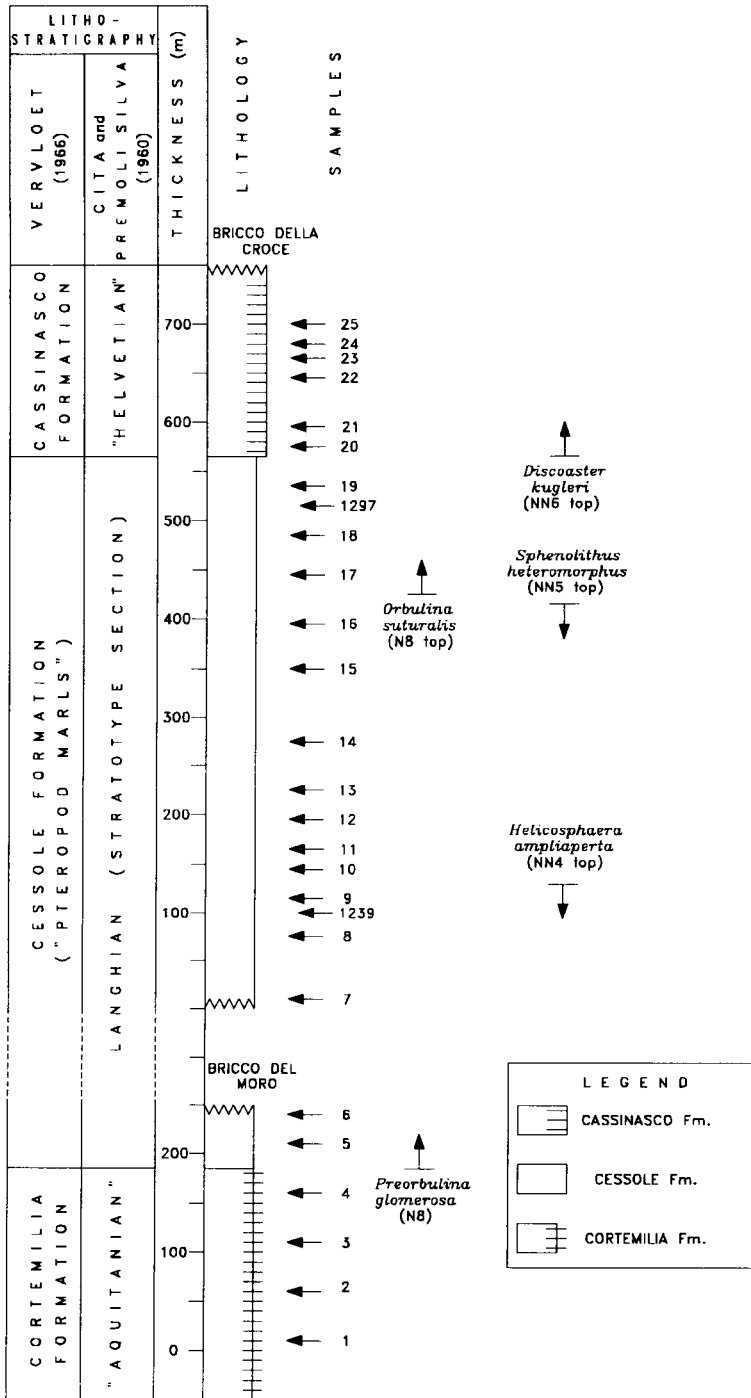


Fig. 2. The Langhian stratotype section: lithostratigraphy and summary of calcareous plankton biohorizons indicated by Cita and Premoli Silva (1960) and by Martini (1968, 1971).

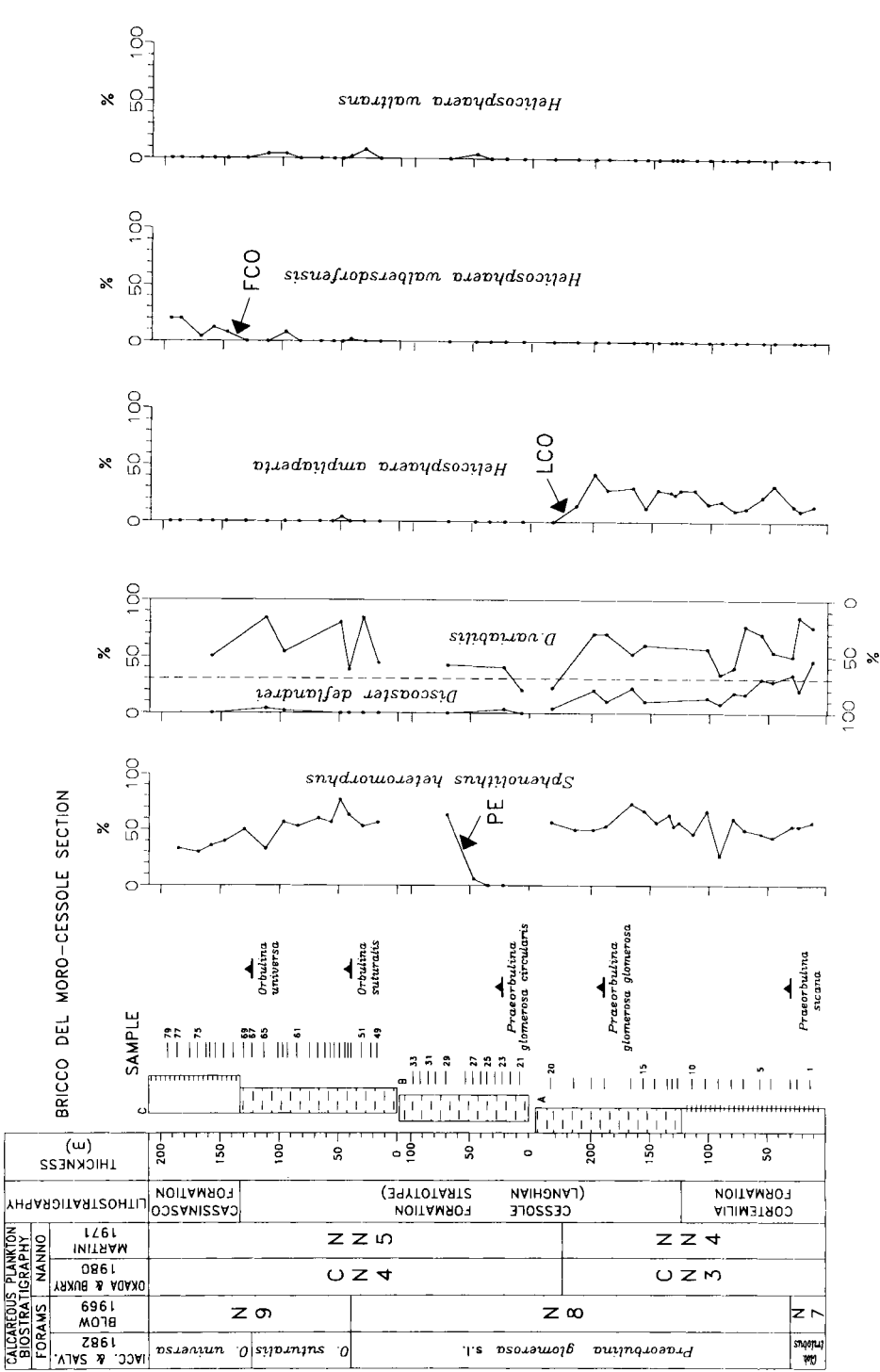


Fig. 3. Lithology, sampling, and calcareous plankton biostratigraphy of the Langhian stratotype section. The distribution patterns of the most indicative calcareous nanofossils are shown.

and Bukry (1980). In a set of 38 samples quantitative analysis for establishing the distribution patterns of indicative forms was carried out following the methods of Rio et al. (1990b).

Specifically, we established the frequency of *S. heteromorphus* in a count of 100 sphenoliths, the frequencies of *Helicosphaera ampliaperta*, *Helicosphaera waltrans* and *Helicosphaera walbersdorfensis* in a count of 50 helicoliths and the frequencies of *Discoaster deflandrei* and of *Discoaster exilis* and *Discoaster variabilis* in a count of 100 discoasterids. Results are reported in Fig. 3 together with the biostratigraphic classification in terms of the Martini (1971) and Okada and Bukry (1980) standard zonation.

The Bricco del Moro section, and hence the base of the Langhian, where *S. heteromorphus* and *H. ampliaperta* are common and continuously present, is ascribed to Zones NN4/CN3, in agreement with the previous assignment of Martini (1971). *Discoaster deflandrei*, *D. variabilis* and *D. exilis* (the latter two plotted together because poor preservation prevents their confident distinction) are common throughout. In sample 15 the FO of *Calcidiscus macintyre* sensu Bukry (1973) and Mazzei (1985) (not sensu Fornaciari et al., 1990; Raffi and Rio, 1979; Backman and Shackleton, 1983) has been observed.

In the Bricco della Croce section *H. ampliaperta* is missing and the discoasterid assemblage is dominated by free-ray forms (*D. exilis* and *D. variabilis*) as *D. deflandrei* is missing or in very low abundance. *Sphenolithus heteromorphus* is absent or in very low abundance in the lowermost 30 m samples of the section; thereafter, it is the dominant form within the sphenolith assemblage up to the top of the section, and above the top of the Langhian stratotype (Fig. 3).

Martini (1968) also found an interval of reduced abundance of *S. heteromorphus* and considered it as representing the true extinction of the species, and related the (abundant) presence of *S. heteromorphus* in the upper part of the stratotype to reworking. We disagree with this interpretation and we consider as genuine the presence of *S. heteromorphus* in the upper part of the Langhian stratotype (and above) because its high abundance is difficult to explain as due to reworking and because no other forms co-distributed with *S. heteromorphus* in the Miocene (like *D. deflandrei* and *H. ampliaperta*) are present. Furthermore, an interval of temporary absence of *S. heteromorphus* in the Mediterranean region within the middle part of the Langhian is a general feature in this region as documented by Fornaciari et al. (1996). We therefore ascribe the entire section of the Bricco della Croce and the top of the Langhian to Zone NN5.

Martini (1968, 1971) also claimed to have found the *Discoaster kugleri* FO (and hence the NN6/NN7 zonal boundary) at the base of the Cassinascio Formation, i.e. just above the top of the Langhian stratotype. *D. kugleri* is difficult to recognize, and its presence in the Mediterranean region is questionable (Müller, 1978). We did not find *D. kugleri* in our material, but we detected the presence in several samples starting from the top part of the Cessole Marls of *Discoaster musicus* Stradner, 1959 (*Discoaster sanmiguelensis* of Bukry, 1981), which is similar to *D. kugleri*, from which it is differentiated by the presence of a button in the central area. The appearance of this form is known to occur within Zone NN5 (Perch-Nielsen, 1985; Rio et al., 1990a).



## PLANKTONIC FORAMINIFERA BIOSTRATIGRAPHY

Planktonic foraminiferal analysis was carried out in a total of 80 samples. The ranges of the most important taxa are reported in Table 1 and the position of significant biohorizons are summarized in Fig. 3. Our results are basically in agreement with the previous study of Cita and Premoli Silva (1960) which was based on a more limited set of samples. The most outstanding feature of the Langhian stratotype is the presence of the various evolutionary steps of the well known *Globigerinoides bisphericus*–*Praeorbulina*–*Orbulina* lineage.

At the very base of the Bricco del Moro section, within the turbiditic Cortemilia Formation, some 100 m below the base of the Cessole Marls, we detected the FO of *Praeorbulina sicana* (*Praeorbulina* datum, Jenkins et al., 1981). In agreement with Cita and Premoli Silva (1960), we found the FO of *P. glomerosa glomerosa* in the basal Cessole Marls. The other steps of the evolution of the lineage have been recorded in the Bricco della Croce section: *P. circularis* first occurs in sample 23, *O. suturalis* in sample 52 and the FO of *O. universa* is in sample 67 (Fig. 3). The latter biohorizon, occurring about 10 m below the top of the Langhian, was not mentioned by Cita and Premoli Silva (1960) who did not have samples available in the top part of the Cessole Marls (Fig. 2). On the basis of these results, it can be concluded that the lower and upper boundaries of the Langhian historical stratotype fall within Zones N8 and N9 of Blow (1969), respectively.

## RELATIONSHIP WITH THE BURDIGALIAN

The Burdigalian stage (Depéret, 1892) is defined by shallow-water, difficult to date, poorly outcropping marine sediments located in the Aquitaine basin, in southwestern France (Vigneaux, 1971). It is generally held that the type Burdigalian is correlated with foraminiferal Zones N5, N6, and possibly lower N7 (Poignant and Pujol, 1978; Berggren et al., 1985a, b; Iaccarino, 1985). In terms of the calcareous nannofossil standard zonation of Martini (1971) the type Burdigalian would correlate to Zone NN2 according to Müller (in Bizon and Müller, 1979). It appears unlikely that an overlap exists between the type Burdigalian and the type Langhian and that most probably a time gap is present between the two stages.

## CONCLUSIONS

We have studied the calcareous plankton contents (calcareous nannofossils and planktonic Foraminifera) from the composite Langhian stratotype section (Bricco del Moro and Bricco della Croce sections), proposed by Cita and Premoli Silva (1960). Our results indicate that the base of the Langhian, lithologically corresponding with the base of the Cessole Marls, is located some 100 m above the FO of *Praeorbulina sicana* (*Praeorbulina* datum), within planktonic Foraminifera Zone N8 of Blow (1969) and within calcareous nannofossil Zone NN4 of Martini (1971). Within the Langhian the well known evolution of *Orbulina* (*Orbulina* datum) from *Globigerinoides* via *Preorbulina* occurs, which ensures a wide correlatability of the nominate chronostratigraphic unit. At the top of the Langhian the FO of *O. universa*, known to occur within Zone

Table 1

Range chart of selected planktonic Foraminifera from the Langhian historical stratotype

CORTEMILIA Fm.		CESSOLE Fm.		CASSINASCO Fm.		LITOSTRATIGRAPHY
		LANGHIAN STRATOTYPE				CHRONOSTRATIGRAPHY
N 7	N 8	N 8	N 9	O. suturalis		Blow, 1969
G. trii	Praeorbulina glomerosa s. l.		O. suturalis		Iaccarino and Salvatorini, 1982	
				O. universon		Iaccarino, 1985
80						80
79						79
78						78
77						77
76						76
75						75
74						74
73						73
72						72
71						71
70						70
69						69
68						68
67						67
66						66
65						65
64						64
63						63
62						62
61						61
60						60
59						59
58						58
57						57
56						56
55						55
54						54
53						53
52						52
51						51
50						50
49						49
48						48
47						47
46						46
45						45
44						44
43						43
42						42
41						41
40						40
39						39
38						38
37						37
36						36
35						35
34						34
33						33
32						32
31						31
30						30
29						29
28						28
27						27
26						26
25						25
24						24
23						23
22						22
21						21
20						20
19						19
18						18
17						17
16						16
15						15
14						14
13						13
12						12
11						11
10						10
9						9
8						8
7						7
6						6
5						5
4						4
3						3
2						2
1						1

R = rare; P = present; C = common.

N9 of Blow (1969), is recorded. Contrary to the statement of Martini (1971) the top of the Langhian stratotype falls entirely within calcareous nannofossil Zone NN5 of Martini (1971). Plenty of data in oceanic areas (i.e. Berggren et al., 1985a, b) and in the

Mediterranean (Mazzei, 1985; Bossio et al., 1992b) indicate that *O. universa* first occurs within Zones NN5/CN3.

Modern chronostratigraphic practice demands that chronostratigraphic boundaries be defined by the GSSP of the base of the overlying unit. The *Praeorbulina* datum, notwithstanding the fact that it occurs below the base of the historical stratotype, is suggested as the best criterion to utilize in defining the GSSP of the base of the Langhian, which should also serve to define the Early/Middle Miocene boundary. This biohorizon occurs in the area of the Langhian stratotype in a terrigenous turbiditic formation (the Cortemilia Formation), and therefore the selection of a GSSP in areas of hemipelagic to pelagic sedimentation, suitable for detailed chronostratigraphic studies, is suggested.

## SOMMAIRE — BIOSTRATIGRAPHIE DU PLANCTON CALCAIRE DU STRATOTYPE HISTORIQUE LANGHIEN

(Manuscrit soumis: Avril 1995, révisé: Juin 1995; rédacteurs responsables: AM et RC)

L'étude biostratigraphique du stratotype historique du Langhien (Formation de Cessole, NO Italie) a été entreprise pour lever les contradictions de la littérature sur l'attribution des niveaux sédimentaires classiques aux biozones de foraminifères planctoniques et de nannofossiles calcaires. En particulier, la correspondance entre ces deux systèmes de corrélation était discutable à la lumière des connaissances acquises dans d'autres domaines. Cette étude réconcilie les résultats. Elle a permis de localiser la base du Langhien clairement au dessus (100 m) de l'émergence — apparition phylétique — de *Praeorbulina sicana* (ou biorepère *Praeorbulina* donc bien à l'intérieur de la zone N8 des foraminifères planctoniques de Blow) et à l'intérieur de la biozone NN 4 des nannofossiles calcaires de Martini. Le biorepère émergence de *Orbulina* dans l'évolution classique *Globigerinoides*–*Praeorbulina*–*Orbulina*, est bien localisé à l'intérieur du stratotype. Le sommet du stratotype historique est situé un peu au-dessus de l'émergence de *Orbulina universa* (dans la biozone N9 de Blow) et nettement à l'intérieur de l'intervalle d'existence de *Sphenolithus heteromorphus* (dans la biozone NN 5 de Martini). L'absence de biosignaux indicatifs ne permet pas de supposer le voisinage de la biozone suivante au sommet de ce stratotype.

(Sommaire proposé par les rédacteurs, GSO)

## ACKNOWLEDGEMENTS

Financial support has been provided by the "Centro CNR di Studio per la Geodinamica Alpina" (University of Padova and MURST (40%) grants, responsables F. Proto Deuma, S. Iaccarino, and H.B. Cita).

Chapter A7

**PLANKTONIC FORAMINIFERAL BIOSTRATIGRAPHY OF  
THE TORTONIAN HISTORICAL STRATOTYPE, RIO MAZZAPIEDI-  
CASTELLANIA SECTION, NORTHWESTERN ITALY**

P. Miculan

INTRODUCTION

Karl Mayer (also cited as Mayer) first proposed the Tortonian Stage ('Tortonische Stufe') in 1858. The stratigraphic unit, publicized by the author in his subsequent works (Mayer-Eymar, 1858, 1868; Mayer, 1867, 1877), was rapidly adopted by European stratigraphers working on the Miocene (e.g., Pareto, 1865; Sacco, 1890; Depéret, 1892).

On the basis of Mayer's rather general original definition ("Blaue mergel mit *Conus canaliculatus* und *Ancillaria glandiformis* von Tortona" — Mayer-Eymar, 1858, Tabelle), Gianotti (1953) proposed the Rio Mazzapiedi section near Castellania (Alessandria province) as the stratotype for the Tortonian Stage. This section has been traditionally accepted as the type for the stage but it was never ratified as the standard for the definition of the Tortonian by a recognized stratigraphical authority.

In the past 40 years, many efforts have been made to elucidate the stratigraphic and palaeontologic characters of this famous section (e.g., Gino, 1953; Gianotti, 1953; Dieci and Russo, 1965; Cita et al., 1965, 1966; Cita, 1967, 1971b; Ascoli, 1968; Robba, 1968, 1970; Cita and Blow, 1969; Ryan et al., 1974; Nakagawa et al., 1974; Martini, 1975; D'Onofrio et al., 1976; Mazzei, 1977; Ciampo, 1986).

Nevertheless, some questions are still open. In particular, the biostratigraphic data presently available for the lower part of the section (Cita and Blow, 1969; Martini, 1975; Mazzei, 1977), are rather conflicting (see also Berggren et al., 1985b; Rio et al., 1990a, c). For this reason, the section was closely sampled and a biostratigraphic study on planktonic Foraminifera has been performed. The results of this study are presented herein.

THE RIO MAZZAPIEDI-CASTELLANIA SECTION

The studied section corresponds to the lower and middle parts of the classic Tortonian stratotype proposed by Gianotti (1953) and described by Gino (1953), but the sampling route is not precisely the same. Gino (1953) and Gianotti (1953) measured and sampled their section along the Rio Mazzapiedi and Rio Castellania. At present, the Tortonian stratigraphic succession is discontinuously exposed on the banks of these streams. Probably, the exposure was not better in 1964 when Bayliss surveyed the section; as a matter of fact, he was not able to precisely register the stratigraphic position of

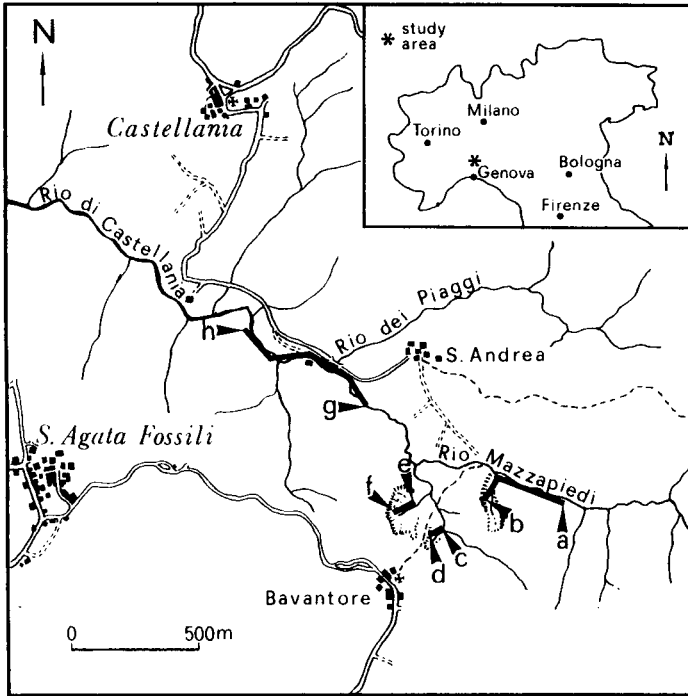


Fig. 1. Location of the studied section in sheet 70 II NE Villalvernia of the Carta d'Italia, scale of 1 : 25,000, edited by the Istituto Geografico Militare.

many samples he collected. These samples were studied by Cita and Blow (1969). I measured the section mainly in the deep gullies which cut the left side of the Rio Mazzapiedi–Castellama valley. It is made up of four subsections whose exact location is shown in Fig. 1. (The studied area falls within sheet 70 II NE Villalvernia of the Carta d'Italia, scale of 1 : 25,000, edited by the Istituto Geografico Militare.)

The covered stratigraphic interval spans the uppermost portion of the Serravalle Sandstone, and the largest part of the S. Agata Fossili Formation. The S. Agata Fossili Formation of the present work exactly corresponds to the Marne di S. Agata Fossili (= S. Agata Fossili Marl) of Beatrizotti et al. (1965), as described by Ghibaudo et al. (1986). It is nearly equivalent to Vervloet's (1966) Castellania Formation.

I partially change the former name introduced by Beatrizotti et al. (1965) because it is rather misleading. The lithostratigraphic unit is made up of argillaceous marls only in its upper part — upper member of Ghibaudo et al. (1986). The lower part consists of siltstone and very fine-grained sandstone.

I divide the Formation into three informal members (Fig. 2):

(1) A lower member which comprises the lower part of the Formation, from its base up to the erosional surfaces described by Clari and Ghibaudo (1979).

(2) A middle member which consists of hard bioclastic sandstones (lower part) and sandy siltstones or fine-grained sandstone (upper part). Its base is the aforementioned erosional unconformity. This part of the Formation equates with Gino's (1953) unit 3.

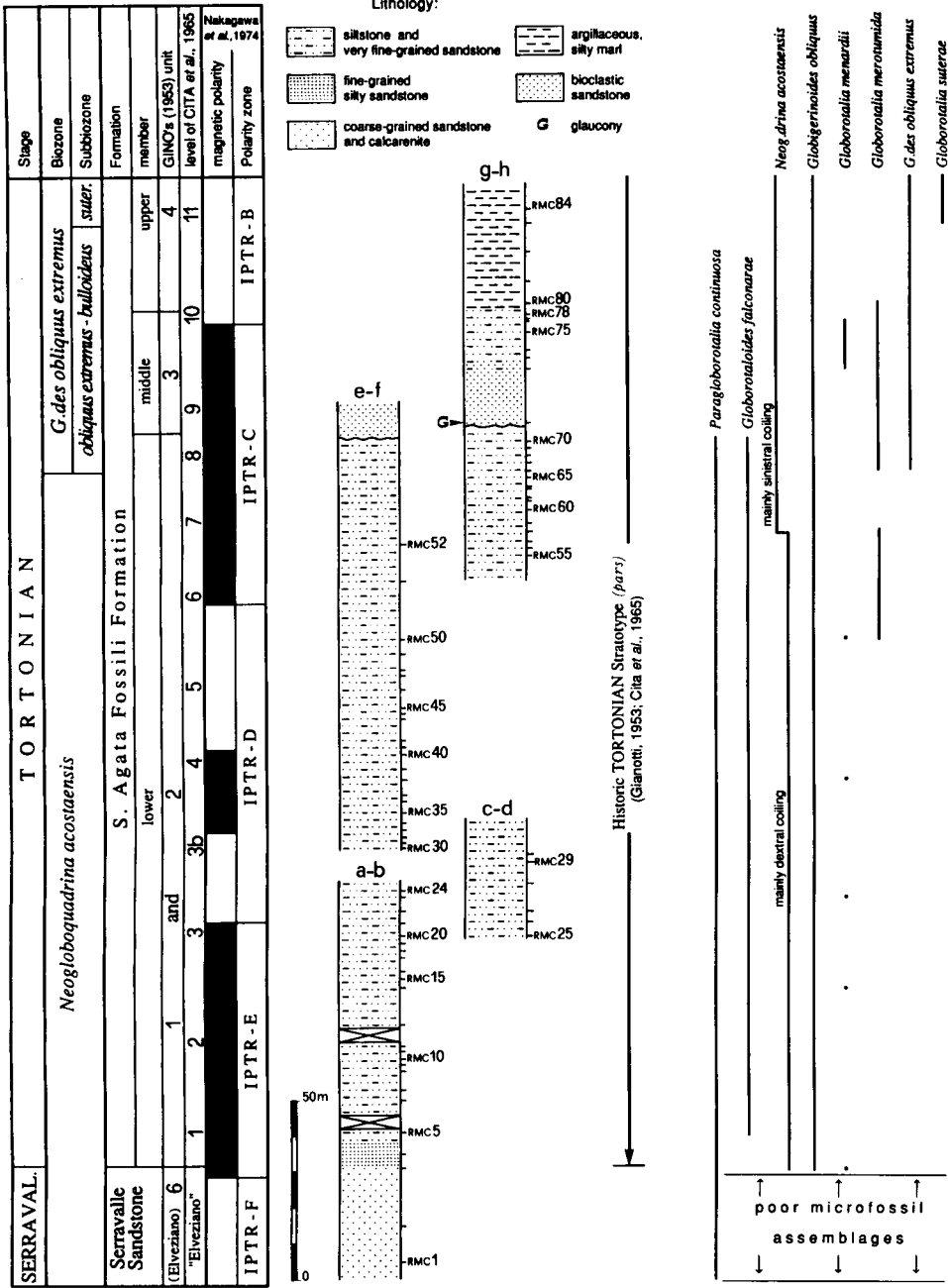


Fig. 2. Lithological log of the Rio Mazzapiedi-Castellania section and ranges of selected planktonic foraminiferal species.

(3) An upper member which corresponds to the upper member of the S. Agata Fossili Marl as defined by Ghibaudo et al. (1986).

Taking into account the biostratigraphic interpretation presented here, the unconformity at the lower boundary of the middle member easily correlates with the base of the so-called 'Sahelian Cycle' (Ruggieri, 1956, 1958; Ricci Lucchi, 1986; Borsetti et al., 1990; Patacca et al., 1992). Probably it records a geodynamic event whose signs are wide-spread in the western Mediterranean area.

The interval measured for this study (Fig. 2) corresponds to units 1, 2, 3 and 4 (pars) of Gino (1953) and to levels 1 to 11 of Cita et al. (1965). The upper member of the Formation was reviewed from a biostratigraphical standpoint by D'Onofrio et al. (1976) and a re-examination appears unnecessary.

## BIOSTRATIGRAPHY

A total of 82 samples were collected from the section and processed for micropalaeontological analysis. For each sample, approximately 250 g of dried rock was soaked in tap water and wet sieved over a 125 mm cloth. Washing residues contain variable but always high amounts of sand grains (except for samples collected in the marls of the upper member of the S. Agata Fossili Formation). Interspersed microfossils (planktonic and benthonic foraminifers, ostracods, otoliths and fish teeth, molluscan shell fragments) are scarce to moderately abundant. Their preservation is rather poor to fairly good (very good in the upper member of the S. Agata Fossili Formation).

The planktonic foraminiferal species recognized in the studied samples are listed in Tables 1A and B, where the species occurrences are recorded for each sample. The stratigraphic distribution of some selected taxa is also displayed in Fig. 2.

The planktonic foraminiferal zonal scheme adopted in the present work is that of D'Onofrio et al. (1976) as modified by Iaccarino and Salvatorini (see Iaccarino and Salvatorini, 1982; Iaccarino, 1985; Miculan, 1994).

The first three samples (RMC1, RMC2 and RMC3 from the Serravalle Sandstone) yielded rare planktonic foraminifers forming low-diversity assemblages. However, rare specimens of *Neogloboquadrina acostaensis* have been recognized in sample RMC3, immediately below the upper limit of the Serravalle Sandstone. Consequently, the uppermost part of this formation and the lower one of the S. Agata Fossili Formation are certainly referable to the *N. acostaensis* Zone of Iaccarino and Salvatorini (1982).

Taking into account the rather poor microfossil record of the Serravalle Sandstone (the lithofacies is clearly unfavourable for precisely recording planktonic foraminiferal events) it seems highly improbable that the first recognized occurrence of the *N. acostaensis* documents the first evolutionary appearance of the species. As a consequence, a significant stratigraphic interval of unknown thickness below level RMC3 has to be referred to the *N. acostaensis* Zone. (Level RMC3 is the level where sample RMC3 was collected.)

Foraminifers are more abundant and diversified in the S. Agata Fossili Formation. Nevertheless, no reliable biostratigraphic event has been detected in the lower part of the Formation, up to level RMC66.

In the RMC66 sample, the first occurrence of *Globigerinoides obliquus extremus* was recognized. Its phyletic predecessor, *Globigerinoides obliquus obliquus*, is discontinu-





Table 1B

Occurrence of planktonic Foraminifera in samples from the Rio Mazzapedi–Castellania section

samples:	RMC53	RMC56	RMC57	RMC58	RMC59	RMC60	RMC61	RMC62	RMC63	RMC64	RMC65	RMC66	RMC67	RMC68	RMC69	RMC70	RMC71	RMC72	RMC73	RMC74	RMC75	RMC76	RMC77	RMC78	RMC80	RMC81	RMC82	RMC83	RMC84			
species:																																
1. <i>Globigerinoides trilobus</i>	x	x	x	x	x	x	x	x	x	x	x	x	x	x	x	x	x	x	x	x	x	x	x	x	x	x	x	x	x			
2. <i>Paragloborotalia continuosa</i>	x	x	x	x	x	x	x	x	x	x	x	x	x	x	x	x																
3. <i>Globigerina praebulloides</i>																																
4. <i>Globigerinita glutinata</i>					x	x	x	x			x	x	x			x	x	x	x	x	x	x	x									
5. <i>Globigerina woodi</i>	x	x	x	x	x	x	x	x			x	x	x	x	x	x	x															
6. <i>Globigerina nepenthes</i>	x	x			x	x	x	x	x	x	x	x	x	x	x	x																
7. <i>Globigerinella obesa</i>	x	x	x	x								x																				
8. <i>Globigerinoides bulloides</i>			x												x																	
9. <i>Turborotalia quinqueloba</i>	x	x	x	x	x	x	x	x	x	x	x	x	x	x	x	x	x	x	x	x	x	x	x	x	x	x	x	x	x			
10. <i>Globorotalia scitula</i>	x	x	x	x	x	x	x	x	x	x	x	x	x	x	x	x	x	x	x	x	x	x	x	x	x	x	x	x	x			
11. <i>Neogloboquadrina acostaensis</i> *	D	D	D	S	S	S	S	S	S	S	S	S	S	S	D	S	S	S	S	S	S	S	S	S	S	S	S	S	S			
12. <i>Orbulina universa</i>	x	x	x	x	x	x	x	x	x	x	x	x	x	x	x	x	x	x	x	x	x	x	x	x	x	x	x	x	x			
13. <i>Globigerinoides obliquus</i>		x	x	x	x	x	x	x	x	x	x	x						x	x	x	x	x	x	x	x	x	x	x	x			
14. <i>Globorotalia menardii</i>			x	x																												
15. <i>Globoquadrina dehiscens</i>												x																				
16. <i>Globigerina falconensis</i>																																
17. <i>Orbulina suturalis</i>	x	x	x	x	x	x	x	x	x						x	x	x	x	x	x	x	x	x	x	x	x	x	x	x			
18. <i>Globigerina decoraperta</i>		x	x	x	x							x							x	x							x	x	x			
19. <i>Globorotaloides falconarae</i>	x	x	x	x	x	x	x	x	x	x	x	x			x																	
20. <i>Globigerinella siphonifera</i>	x		x						x						x											x	x	x	x			
21. <i>Globigerina bulloides</i>	x	x	x	x	x	x	x	x	x	x	x	x	x	x	x	x	x	x	x	x	x	x	x	x	x	x	x	x	x			
22. <i>Globigerinita uvula</i>											x																					
23. <i>Globorotalia languaensis</i>																																
24. <i>Globigerina foliata</i>												x																	x			
25. <i>Globigerinoides bollii</i>										x	x																					
26. <i>Globigerina apertura</i>											cf																					
27. <i>Globorotalia merotumida</i>		x	x											x	x	x	x	x	x	x	x	x	x	x								
28. <i>Globigerinoides obliquus extremus</i>														x																		
29. <i>Neogloboquadrina praeumerosa</i>																																
30. <i>Sphaeroidinellopsis subdehiscens</i>																																
31. <i>Globorotalia suterae</i>																																
32. <i>Globoquadrina altispira</i>																																
<i>Paragloborotalia mayeri</i> **							x																									
<i>Globoquadrina baroemoenensis</i> **												x																				
<i>Paragloborotalia parimlabiata</i> **																																
<i>Globigerinoides subquadratus</i> **																																
ZONE											<i>N. acostaensis</i>										<i>Globigerinoides obliquus extremus</i>											
SUBZONE																					<i>G. obliquus extremus</i> / <i>G. bulloides</i>						<i>suterae</i>					
STAGE	TORTONIAN																															
*dominant direction of coiling: D - Dextral ; S - Sinistral ** species interpreted as reworked																																

ously present in the lower part of the section. Therefore we may confidently assume that the first local occurrence of *G. obliquus extremus* approximates its first evolutionary appearance. The base of the *G. obliquus extremus* Zone of Iaccarino and Salvatorini (1982) is taken as coincident with level RMC66.

The last occurrences of *Paragloborotalia continuosa* and *Globorotaloides falconarae* are in sample RMC70, which was collected below the erosional surface at the base of the middle member of the S. Agata Fossili Formation. According to qualified literature the disappearances of the two species are not synchronous (Colalongo et al., 1979b; Iaccarino, 1985; etc.). Apparently the unconformity below level RMC71 represents a significant hiatus in the local stratigraphic record. Grains of glaucony are present in

the coarse-grained bioclastic sandstone of level RMC71 and the thickness of the *G. obliquus extremus* Zone seems rather reduced (considering that the sedimentation rate was probably high).

*Globorotalia suterae* is first recorded in sample RMC83; the first appearance of the species marks the lower boundary of the *G. suterae* Subzone (D'Onofrio et al., 1976).

Keeled globorotaliids, represented by *Globorotalia menardii*, have been scantily detected in the lower part of the section. They become more common from sample RMC50 upwards. In this sample *Globorotalia merotumida* first occurs. The first local occurrence of the species does not seem reliable for correlation, because the lower stratigraphic succession probably records environmental conditions not favourable for keeled globorotaliids.

*G. menardii* and *G. merotumida* disappear some metres below the first occurrence of *G. suterae* (in sample RMC76 and in sample RMC80, respectively) and lack in the upper part of the studied section. These (temporary) disappearances match well with Event 1 of Sierro (1985) and Sierro et al. (1993).

The coiling direction of *N. acostaensis* was followed in detail and results mostly as dextral in the lower member of the S. Agata Fossili Formation. It turns to dominantly sinistral in the uppermost part of the *N. acostaensis* Zone (from level RMC58). This coiling change is a promising biostratigraphic event, probably valuable for correlation. However, its usefulness has to be tested in a convenient number of different sections.

Rare specimens of *Paragloborotalia mayeri* have been sporadically recorded throughout the section. Similarly, I registered the occasional occurrence of Serravallian species currently considered not to be present in the Tortonian (e.g. *Globigerinoides subquadratus*, *Paragloborotalia partimlabiata*, *Globoquadrina baroemoensis*). All these species are interpreted as reworked because their presence is irregular and scanty. The occurrence of reworked microfossil tests is to be expected in the studied samples, since they always contain a significant fraction of sand-size terrigenous clasts.

## DISCUSSION

The biostratigraphic interpretation of the Rio Mazzapiedi–Castellania section presented in this work differs from that of Cita and Blow (1969) mainly in the evaluation of the lower part of the section. This part contains the lithostratigraphic boundary between the Serravalle Sandstone and the S. Agata Fossili Formation which was taken as the lower limit of the historical 'Tortonian stratotype', following a long-standing tradition (Gianotti, 1953; Cita et al., 1965; Cita, 1967, 1971; Ryan et al., 1974).

According to Cita and Blow (1969, p. 582; see also Ryan et al., 1974) the first evolutionary appearance of *N. acostaensis* occurs in the lower part of the S. Agata Fossili Formation (named Castellania Formation in the quoted work), about 35 m above its base. As a consequence the base of the Formation (lower limit of the 'Tortonian stratotype') would fall within Blow's (1969) zone N15. It is worth noting that Cita and Blow (1969) recognized the first occurrence of *N. acostaensis* in sample By261 and considered it as lying immediately above level 3 of Cita et al. (1965). However, Bayliss, who had collected the sample, had not reported its actual stratigraphic height (Cita and Blow, 1969, appendix II). Cita et al. (1965, 1966) placed level 3 and level 4 respectively 15 m and 40 m above the top of the Serravalle Sandstone ('Elveziano' Auctt.). These

values were corrected by Cita and Blow (1969) and increased to 30 m and 50 m, respectively (see their fig. 9) but still seem too low: compare the columnar section of Nakagawa et al. (1974, fig. 6), where level 4 of Cita et al. was placed roughly half-way between the base of the S. Agata Fossili Formation and the bioclastic sandstones of the middle member of the Formation.

I have found *N. acostaensis* immediately below the boundary between the Serravalle Sandstone and the S. Agata Fossili Formation. Therefore, I conclude that the boundary is referable to the *N. acostaensis* Zone and to Zone N16 of Blow (1969).

These data and interpretations match better with those of Martini (1975) and Mazzei (1977). Both of them reported the occurrence of *Discoaster hamatus* Martini and Bramlette in the lower part of the S. Agata Fossili Formation, up to level 4 of Cita et al. (1965) included. As a consequence, this stratigraphic interval belongs to the *D. hamatus* Total-range-zone (Zone NN9 of Martini, 1971) and is 90 m thick at the least (taking the value reported by Nakagawa et al., 1974). Zone NN9 is currently correlated with the middle part of Blow's Zone N16 (Miller et al., 1985; Berggren et al., 1985b; Rio et al., 1990a, c; Miller et al., 1991b; etc.).

It follows that the traditional lower boundary of the 'Tortonian stratotype' (base of the S. Agata Fossili Formation in the Rio Mazzapiedi–Castellania section) is neither approximated by the first evolutionary appearance of *N. acostaensis* (as Rio et al., 1990a have correctly pointed out) nor by the disappearance of *Discoaster hamatus* which occurs more than 90 m above the base of the S. Agata Fossili Formation.

According to Nakagawa et al. (1974), the base of the S. Agata Fossili Formation is in the lower part of a normal magnetic polarity zone.

## CONCLUSIONS

The detailed biostratigraphic study of planktonic foraminifers collected in the Rio Mazzapiedi–Castellania section allows a general reappraisal of the stratigraphic information on this classic section, which is commonly accepted as the 'Tortonian stratotype'. The attention has been focused on the lower part of the section in order to single out valuable criteria for a proper definition of the lower boundary of the Tortonian Stage.

Main results are as follows:

(1) The lower boundary of the Tortonian Stage in the Rio Mazzapiedi–Castellania type-section was taken as coincident with the lithostratigraphic limit between the Serravalle Sandstone and the S. Agata Fossili Formation. It follows that the boundary interval does not record homogeneous depositional conditions. Moreover it is not well exposed.

(2) Both the upper part of the Serravalle Sandstone and the lower one of the S. Agata Fossili Formation yielded rather poor planktonic foraminiferal assemblages. Time-significant species are exceedingly rare or lacking throughout the Sandstone.

(3) The base of the historical 'Tortonian stratotype' falls within the *N. acostaensis* Zone of Iaccarino and Salvatorini (1982) and within Zone N16 of Blow (1969). It is referable to Zone NN9 of Martini (1971).

(4) No significant biostratigraphic event has been recognized near the proposed chronostratigraphic boundary.

The Rio Mazzapiedi–Castellania section seems unsuitable for an appropriate definition of the base of the Tortonian Stage (Serravallian/Tortonian boundary).

SOMMAIRE — BIOSTRATIGRAPHIE DES FORAMINIFÈRES PLANCTONIQUES  
DU STRATOTYPE HISTORIQUE TORTONIEN, SECTION RIO  
MAZZAPIEDI–CASTELLANIA, NO ITALIE

(Manuscrit soumis: Février 1994, révisé: Juin 1994; rédacteur responsable: GSO)

Notre connaissance sur la biostratigraphie des foraminifères planctoniques de la section Rio Mazzapiedi–Castellania (stratotype historique du Tortonien) est rassemblée ici. Quatre-vingt deux échantillons rapprochés ont été étudiés dans les parties basse et moyenne de la section. La répartition locale des espèces est présentée. Cette étude est l'occasion d'une mise à jour générale des données biostratigraphiques sur la section. Une attention particulière a été portée sur la question de la définition précise de la limite inférieure de l'Étage Tortonien. Il en résulte que cette limite inférieure se trouve au dessus de l'apparition de *Neogloboquadrina acostaensis* (*N. acostanesis* Zone) dans le stratotype historique du Tortonien. Aucun événement significatif des foraminifères planctoniques n'a été reconnu au voisinage immédiat de la limite qui ne doit donc pas être confondue avec un événement biostratigraphique particulier.

(Sommaire proposé par les rédacteurs, GSO)

ACKNOWLEDGEMENTS

Many thanks to Profs. M.L. Colalongo, S. Sartoni and R. Barbieri (Dipartimento di Scienze Geologiche, Università di Bologna) for their critical reading of the manuscript and helpful comments. Financial support of the Italian Ministero dell'Università e della Ricerca Scientifica e Tecnologica (MURST 40%) is acknowledged.

TAXONOMIC REFERENCES

- Globigerina bulloides* d'Orbigny, 1826 — d'Orbigny, 1826, Ann. Sci. Nat. Paris, ser. 1, 7, p. 277; Banner and Blow, 1960, Contrib. Cushman Found. Foram. Res., 11 (1), p. 3–4; tav. 1, fig. 1,4 (lectotype).  
*Globigerina praebulloides* Blow, 1959 — Blow, 1959, Bull. Am. Paleontol., 39 (178), pp. 180–181, tav. 8, fig. 47a–c; tav. 9, fig. 48.  
*Globigerina foliata* Bolli, 1957 — Bolli, 1957, U.S. Nat. Mus. Bull., 215, p. 111, tav. 24, fig. 1a–c.  
*Globigerina falconensis* Blow, 1959 — Blow, 1959, Bull. Am. Paleontol., 39 (178), p. 177, tav. 9, figs. 40–41.  
*Globigerina woodi* Jenkins, 1960 — Jenkins, 1960, Micropaleontology, 6 (4), p. 352, tav. 2, fig. 2a–c.  
*Globigerina apertura* Cushman, 1918 — Cushman, 1918, U.S. Geol. Surv. Bull., 676, p. 57, tav. 12, fig. 8a–c.  
*Globigerina nepenthes* Todd, 1957 — Todd, 1957, U.S. Geol. Surv. Prof. Pap., 280-H, p. 301, tav. 78, fig. 7a–b.  
*Globigerina decoraperta* Takayanagi and Saito, 1962 — Takayanagi and Saito, 1962, Sci. Rep. Tohoku Univ., ser. 2 (Geol.), Spec. Vol. 5, p. 85, tav. 28, fig. 10a–c (*Globigerina druryi decoraperta*).  
*Turborotalita quinqueloba* (Natland, 1938) — Natland, 1938, California Univ. Inst. Oceanogr. Bull. Tech. Ser., 4 (5), p. 149, tav. 6, fig. 7a–c (*Globigerina*).  
*Globigerinoides obliquus* Bolli, 1957 — Bolli, 1957, U.S. Nat. Mus. Bull., 215, p. 113, tav. 25, fig. 10a–c, text-fig. 21, 5.  
*Globigerinoides obliquus* Bolli *extremus* Bolli and Bermudez, 1965 — Bolli and Bermudez, 1965, Bol. Infor. Asoc. Venez. Geol. Miner. Petrogr., 8 (5), p. 139, tav. 1, fig. 10–12.  
*Globigerinoides bulloideus* Crescenti, 1966 — Crescenti, 1966, Geol. Rom., 5, p. 43, text-fig. 8 (3–3a) and 9.

- Globigerinoides trilobus* (Reuss, 1850) — Reuss, 1850, K. Akad. Wiss. Wien, 1, p. 374, tav. 47, fig. 11a–d (*Globigerina triloba*).
- Globigerinoides subquadratus* Brönnimann, 1954 — Brönnimann, 1954, in Todd, Cloud, Low and Schmidt, Am. J. Sci., 252 (11), pp. 680–681, tav. 1, fig. 8a–c and fig. 5.
- Globigerinoides bollii* Blow, 1959 — Blow, 1959, Bull. Am. Paleontol., 39 (178), pp. 189–191, tav. 10, fig. 65a–c.
- Sphaeroidinellopsis subdehiscens* (Blow, 1959) — Blow, 1959, Bull. Am. Paleontol., 39 (178), pp. 195–196, tav. 12, figs. 71a–c, 72 (*Sphaeroidinella dehiscens subdehiscens*).
- Globigerinella obesa* (Bolli, 1957) — Bolli, 1957, U.S. Nat. Mus. Bull., 215, p. 119, tav. 29, figs. 2–3 (*Globorotalia*).
- Globigerinella siphonifera* (D'Orbigny, 1926) — d'Orbigny, 1826, Ann. Sci. Nat. Paris, ser.1, 7, p. 278; Banner and Blow, 1960, Contrib. Cushman Found. Foramin. Res., 11 (1), p. 3–4, tav. 1, fig. 1,4 (lectotype).
- Orbulina universa* d'Orbigny, 1839 — d'Orbigny, 1839, in De la Sagra, Histoire physique, politique et naturelle de l'île de Cuba, 8, p. 2, tav. 1, fig. 1; Blow, 1956, Micropaleontology, 2 (1), p. 66, tav. 2, figs. 8–9.
- Orbulina suturalis* Brönnimann, 1951 — Brönnimann, 1951, Contrib. Cushman Found. Foramin. Res., 2(4), p. 135, fig. 2, nrs. 1–2, 5–8, 10; fig. 3, nrs. 3–8, 11, 13–16, 18, 20–22; fig. 4, nrs. 2–4, 7–12, 15–16, 19–22.
- Globorotalia scitula* (Brady, 1882) — Brady, 1882, R. Soc. Edinburgh, Proc. II (III) pp. 716–717, (*Pulvinulina*); Brady, 1882, Rep. Voyage Challenger, Zool., tav. 103, fig. 7a–c; Banner and Blow, 1960, Contrib. Cushman Found. Foramin. Res., 11 (1), p. 27, tav. 5, fig. 5 (lectotype).
- Globorotalia suterae* Catalano and Sprovieri, 1971 — Catalano and Sprovieri, 1971 in A. Farinacci (ed.) Proceedings of the II Planktonic Conference, pp. 241–242, tav. 1, figs. 1a–d, 2 and fig. 18 n.t.
- Globorotalia menardii* (Parker, Jones and Brady, 1865) — Parker, Jones and Brady, 1865, Ann. Mag. Nat. Hist., London, ser.3, 16, pp. 20, tav. 3, fig. 81 (*Rotalia*); Stainforth, Lamb and Jeffords, 1978, Bull. Zool. Nomenclature, 34, pp. 252–262 (neotype).
- Globorotalia linguaensis* Bolli, 1957 — Bolli, 1957, U.S. Nat. Mus. Bull., 215, pp. 120–121, tav. 29, fig. 5a–c.
- Globorotalia merotumida* Blow and Banner, 1965 — Banner and Blow, 1965, Nature, 207 (5004), p. 1352, text-figs. 1a–c.
- Paragloborotalia continuosa* (Blow, 1959) — Blow, 1959, Bull. Am. Paleontol., 39 (178), p. 218, tav. 19, fig. 125a–c (*Globorotalia*).
- Paragloborotalia mayeri* (Cushman and Ellisor, 1939) — Cushman and Ellisor, 1939, Contrib. Cushman Lab. Foramin. Res., 15 (1), p. 11, tav. 2, fig. 4a–c (*Globorotalia*); Bolli and Saunders, 1982, J. Foramin. Res., 12 (1), tav. 1, figs. 7–15 (holotype redrawn).
- Paragloborotalia partimlabiata* (Ruggieri and Sprovieri, 1970) — Ruggieri and Sprovieri, 1970, Lav. Ist. Geol. Univ. Palermo, 10, pp. 22–24, figs. 3–4 (*Globorotalia*).
- Neogloboquadrina acostaensis* (Blow, 1959) — Blow, 1959, Bull. Am. Paleontol., 39 (178), pp. 208–210, tav. 17, figs. 106a–c, 107 (*Globorotalia*).
- Neogloboquadrina praeumerosa* (Natori, 1976) — Natori, 1976, in Takayanagi and Saito, Progress in Micropaleontology, Micropaleontology Press, 227 pp., tav. 2, figs. 1a–c, 3a–c (*Globorotalia humerosa praeumerosa*).
- Globoquadrina dehiscens* (Chapman, Parr and Collins, 1934) — Chapman, Parr and Collins, 1934, Linn. Soc. London, J. Zool., 38, (262), p. 569, tav. 11, fig. 36a–c (*Globorotalia*).
- Globoquadrina baroemoensis* (LeRoy, 1939) — LeRoy, 1939, Natuurk. Tijdschr. Nederl.-Indie, 99 (6), p. 263, tav. 6, figs. 1–2 (*Globigerina*).
- Globoquadrina altispira* (Cushman and Jarvin, 1936) — Cushman and Jarvin, 1936, Contrib. Cushman Lab. For. Res., 12 (1), p. 5, tav. 1, figs. 13a–c, 14 (*Globigerina*).
- Globorotaloides falconarae* Giannelli and Salvatorini, 1976 — Giannelli and Salvatorini, 1976, Boll. Soc. Paleontol. Ital., 15 (2), pp. 170–172, tav. 2, figs. 1–6.
- Globigerinita glutinata* (Egger, 1895) — Egger, 1895, K. Bayer. Akad. Wiss. Munchen, Math. Phys. Kl., Abh., 18 (2), p. 371, tav. 13, figs. 19–21 (*Globigerina*).
- Globigerinita uvula* (Ehrenberg, 1861) — Ehrenberg, 1861, K. Preuss. Akad. Wiss. Berlin, pp. 276–277, 308 (*Pyloedexia*); the type was fig. d in Ehrenberg, 1893, K. Akad. Wiss. Berlin, Abh., Jahrg. 1872, tav. 2, figs. 24–25.

*Chapter A8*

**THE MESSINIAN HISTORICAL STRATOTYPE AND THE  
TORTONIAN/MESSINIAN BOUNDARY**

M.L. Colalongo and G. Pasini

**THE MESSINIAN STRATOTYPE: HISTORY OF THE DEFINITION**

*Origin of the term Messinian*

In 1867, K. Mayer-Eymar proposed the Messinian Stage which included open-marine, brackish and fresh-water sediments. The name of the stage is derived from the town of Messina in Sicily, in the neighbourhood of which this stage, according to Mayer-Eymar, is represented by marine facies. In 1868 Mayer-Eymar clarified that the Messinian Stage is located between the Tortonian and the Astian stages (since 1867 Mayer-Eymar gave the name Astian to the whole Pliocene).

*Historical stratotype definition*

In 1960, Selli, entrusted by the Mediterranean Neogene Committee (Vienna, 1959) to re-examine the Messinian of Mayer-Eymar, corrected some inconsistencies and gave the following definition: “(il Messiniano è l’) intervallo di tempo compreso fra il Tortoniano (strati di Tortona) e il Pliocene (strati di Tabiano), caratterizzato in tutto il Mediterraneo e nella Paratetide da una crisi di salinità e in Italia essenzialmente da un ambiente iperalino e da sedimenti evaporitici” (the Messinian is the time interval stretching from the Tortonian (Tortona beds) to the Pliocene (Tabiano beds), characterized in the whole Mediterranean and in the Parathetys by a salinity crisis and in Italy essentially by a hypersaline environment and by evaporitic sediments). Whereas Mayer-Eymar did not propose any stratotype, and from his papers it is not possible to choose a section suitable for this purpose, Selli (1960) proposed the ‘Pasquasia–Capodarso section’ as the neostatotype for the Messinian Stage.

Selli’s neostatotype can be considered as the initial reference section, i.e., as the ‘historical stratotype’.

The Pasquasia–Capodarso section is located in Sicily (Figs. 1 and 2), between Enna and Caltanissetta (Atlante Stradale d’Italia of the Touring Club Italiano, 1:200,000, Sud, plate 52; Italy, topographic map 1:25,000, sheet 268-IV-SE, Stazione di Imera). The section is easily accessible from the Strada Statale Agrigentina No. 122 through good secondary roads (Fig. 3).

The Messinian sediments in the Pasquasia–Capodarso section have a thickness of about 180 m. In 1960 the section was well exposed, continuously so from the Tortonian (outcropping for about 130 m) to the Lower Pliocene (outcropping for about 80 m). No permanent artificial marker is present in the Pasquasia–Capodarso section.

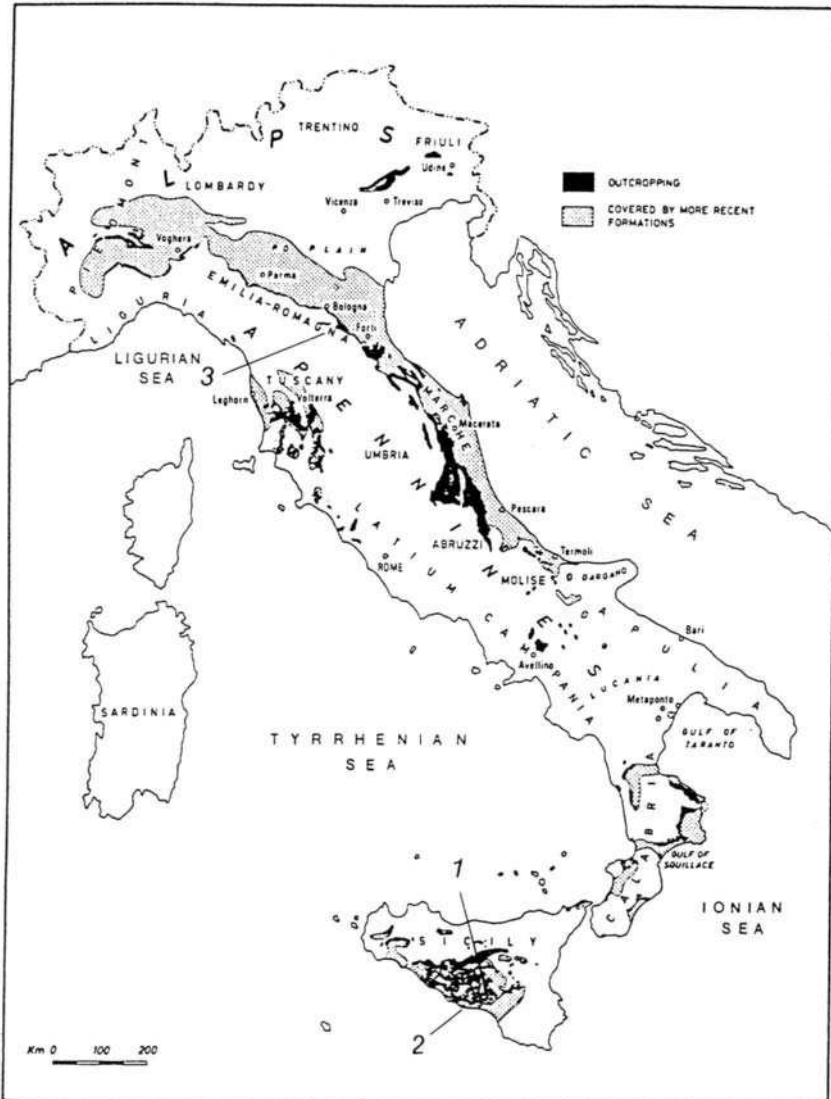


Fig. 1. The extent of Messinian sediments in Italy (from Selli 1973, modified). 1 = Pasquasia–Capodarso section; 2 = Falconara section; 3 = Monte del Casino and Monte Tondo sections.

From the tectonic point of view, the Pasquasia–Capodarso sediments are part of a regular monocline, dipping about  $30^{\circ}\text{SSE}$ . The section is free from structural complications, metamorphism and excessive bioturbation. Unfortunately, the condition of the outcrop of the Capodarso section today is very different from that indicated by Selli in 1960, because the lower part of the section has been buried by an extensive landslide, which covers also the Tortonian/Messinian boundary (R. Sprovieri, pers. commun., December, 1993).



Fig. 2. The Capodarso section. (Photo by G. Lo Cicero.)

### *Stratigraphy*

*Lithostratigraphy.* According to Selli (1971), the lowermost part of the Pasquasia–Capodarso section is represented by ‘clayey marls’ (formation 1 in Fig. 3), which near the top indicate a hypersaline environment. The marly diatomites overlying these marls (‘Tripoli’, formation 2 in Fig. 3) are also indicative of a hypersaline environment. The evaporitic limestones, the gypsum and the clayey marls (formations 3–7) clearly indicate a strongly hypersaline environment. Formation 8 of the Pasquasia–Capodarso section consists of white marls with Foraminifera (‘Trubi’) which were deposited in an open but not very deep sea, with normal salinity. The paucity of benthonic foraminifers and the absence of macrofossils in formation 8 would indicate that the conditions near the bottom of this sea were not yet normal during its deposition. The condition became normal, with the introduction of abundant benthonic organisms, during the deposition of formation 9 (marly clays). There are no significant hiatuses at the base, at the top or inside the section (Selli, 1971).

The ‘historical stratotype’ is a regional facies, which is represented only in the Mediterranean Sea. According to Selli (1960, 1971), formation 1 (‘marne argillose’ in Fig. 3) is primarily Tortonian in age. However, in the upper 25 m of this formation and at the bottom of the overlying marly diatomites (‘Tripoli’, formation 2) the microfaunas show a rapid impoverishment in the species number, and a dominance of dystrophic forms. According to Selli this indicates the onset of the environmental change leading to the deposition of evaporites. According to Selli (1960, 1971), the Tortonian/Messinian boundary should be placed about 25 m below the top of the clayey marls (formation 1)



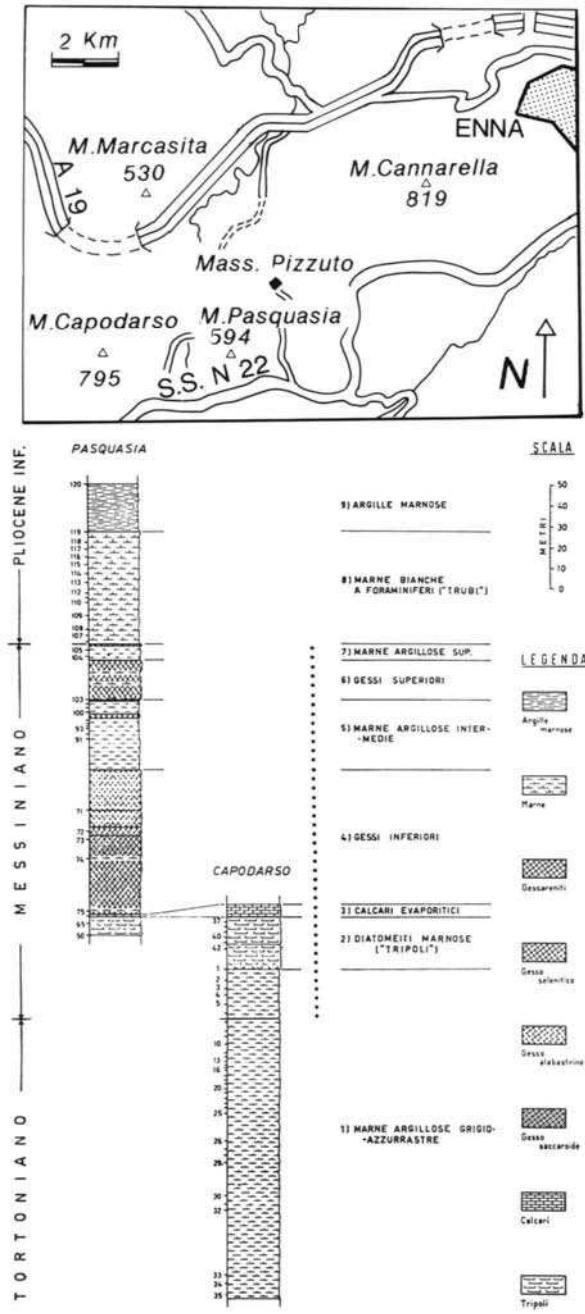


Fig. 3. The Pasquasia–Capodarso composite-section (from Selli, 1960, modified). The dotted line indicates the interval of the section characterized — according to Selli 1960 — by hyperhaline environment.

underlying the 'Tripoli formation' of the Pasquasia–Capodarso section (and not 40 m below the top of these clayey marls, as quoted erroneously by Ryan et al., 1974, p. 650), at the beginning of the Mediterranean salinity crisis. According to Selli (1960, 1971), the beginning of this crisis is marked by a rapid drop in the number of species and the dominance of dystrophic forms. This is demonstrated by a sentence of Selli (1960, p. 24), which affirms that this rapid drop is determined by the increase of salinity in the western Mediterranean. According to Selli (1971), the upper boundary of the Messinian has to be placed between formations 7 and 8, at the base of the 'Trubi' (Fig. 3).

In summary, during the Messinian the Mediterranean underwent a widespread salinity crisis. The sediments resulting from this dramatic event constitute the Messinian stratigraphic record (Selli, 1971).

There are three main models for explaining this salinity crisis. A first 'open sea' model (Selli, 1954, 1973) proposes that the communication between the Mediterranean and the Atlantic Ocean continued without interruption during the whole Messinian. Restriction by sills connecting the innermost basins, and a high evaporation rate in the Mediterranean caused an increasing salinity leading to the deposition of limestone, gypsum and other evaporite sediments. The level of this hypersaline Messinian sea, according to Selli (1973), was the same as that of the Atlantic Ocean.

A second model proposed by Ruggieri (1958), Hsü et al. (1973, 1978), Ruggieri and Sprovieri (1976), envisions a 'deep basin' desiccation. During the Messinian, the western Mediterranean was first an open-marine basin connected with the Atlantic through the Betic-Riff straits. In a second stage, the communication of the Mediterranean with the Atlantic was interrupted, and the Mediterranean became a partly desiccated deep depression whose deepest parts were occupied by endorheic lakes with brackish water. The water level of these lakes (similar to those of the Paratethys located to the east) during the late Messinian was conspicuously lower than that of the Atlantic Ocean (Ruggieri and Sprovieri, 1976). The Messinian change from normal-marine to evaporite-forming conditions was not a response to climatic factors, but rather was a consequence of the closure of the western straits, which during the Tortonian connected the Mediterranean with the Atlantic Ocean (Hsü et al., 1978). According to this second model, the Pliocene sediments should be interpreted as the result of a sudden flooding of Mediterranean depressions by Atlantic waters (Ruggieri and Sprovieri, 1976). The sediments of the late Messinian shallow and fresh or brackish water lakes ('Lago-Mare', Hsü et al., 1978) contain reworked Tortonian and lower Messinian marine faunas together with hyposaline and fresh-water or mesosaline faunas. The first Pliocene sediments (the 'Trubi' formation) immediately above the Messinian lacustrine deposits are deep- and open-marine hemipelagic sediments. The sharp contact between lacustrine Messinian and deep-sea Pliocene sediments can be explained "if the Pliocene transgression is considered to be a consequence of the re-establishment of communications with the open sea" (Ruggieri and Sprovieri, 1976). Benson et al. (1991, p. 184) suggested "a version of the historical scenario for the Salinity Crisis [...] modified from that proposed by Hsü et al. (1978) and adjusted toward that of Muller and Hsü (1987)": "Pericontinental evaporite deposition in the west [Mediterranean], and basin deposition in the east, preceded marine deep-water/deep-basin evaporite deposition [...] in the west; all of which preceded the deposition of the shallow-water/deep-basin, desiccation phase [...]. The evaporite deposition in deep basins with deep water ended with the last of the recorded influx through the [Rifian] cor-

ridor. The evaporite deposition that followed, that associated with 'lago mare' deposits, is principally of continental origin in isolated basins. [...] This composite scenario fits better with Longinelli's (1979/1980) analysis of the upper gypsum layers, the record of impoverished fauna 'marine' evaporites followed by an unconformity, and then evaporites with interbedded 'lago mare' deposits as found in Sicily [...] and northern Italy (Emilia; G. Ruggieri, personal communication, 1989), and our present data."

A third model or 'shallow-basin desiccation model', was proposed by Nesteroff (1973). According to this author the Mediterranean Messinian evaporites were deposited in shallow basins. During the Messinian the Mediterranean underwent several desiccation episodes, which transformed it into deserts and salt lakes. These desiccations alternated with marine transgressions, during which marine marls were deposited. As for Messinian palaeotopography, evaporite sedimentation occurred in different Mediterranean basins which were 200 m to 500 m deep, thus much shallower than the present Mediterranean basins.

Further information and discussion on the Messinian salinity crisis are provided by Drooger (1973), and Kastens (1992).

*Biostratigraphy.* D'Onofrio (1964) and Colalongo (1970) studied the planktonic and benthonic Foraminifera of the Pasquasia–Capodarso section from the Tortonian to the Pliocene. Unfortunately, as demonstrated in successive studies by the same authors, the investigated faunas appeared to be reworked, in particular in the stratigraphic interval including the middle and upper parts of the Messinian. Nevertheless, the biostratigraphic considerations made by these authors for the lower portion of the Messinian neostrototype (i.e., below the evaporitic limestones) are still valid. In particular, D'Onofrio (1964) pointed out the scarcity of planktonic faunas from sample 12 upwards in the Pasquasia–Capodarso section (Fig. 3), and proposed the *Bulimina echinata* subzone, coincident with formation 2 (marly diatomites or 'Tripoli'); this regional subzone is still utilized nowadays in Italy. Colalongo (1970) reported the absence of typical *Globorotalia menardii* in the lower Messinian of the Pasquasia–Capodarso section, recently confirmed by Sierro (1985), and Calieri (1992), as well as the first appearance of *Globorotalia conomiozea*, 43 m below the evaporitic limestones (formation 3, Fig. 3) (i.e., only 2 m above the Tortonian/Messinian boundary proposed by Selli in 1960).

D'Onofrio et al. (1975) specifically studied the Capodarso section from a biostratigraphic point of view in order to identify the Tortonian/Messinian boundary. The results of this latter study are summarized below, in the section on the biostratigraphy of the Tortonian/Messinian boundary.

*Physico-chemical stratigraphy.* Chemostratigraphic research on the Pasquasia–Capodarso section was never performed, as far as we know. However the section should be suitable for this kind of research ( $^{18}\text{O}/^{16}\text{O}$ ,  $^{13}\text{C}/^{12}\text{C}$ , etc.).

### Conclusions

According to Selli (1960, 1971) the Tortonian/Messinian boundary should be located at the beginning of the Mediterranean salinity crisis as evidenced in the microfaunas by a rapid impoverishment in the number of species, and by a dominance of dystrophic forms. In the Pasquasia–Capodarso section this boundary is located about 25 m below the base of the 'Tripoli' formation.

Moreover at Pasquasia–Capodarso, 2 m above the boundary proposed by Selli, there is the first occurrence (FO) of *G. conomiozea*, which is the biostratigraphic event that best approximates the beginning of the Mediterranean salinity crisis sensu Selli (Colalongo, 1970).

Currently, it is impossible to locate the ‘golden spike’ for the Tortonian/Messinian boundary in the Pasquasia–Capodarso section because, as noted previously, the lower part of this section, including the boundary, is covered by a landslide.

According to Selli (1971, p. 130) the Miocene/Pliocene boundary (which is not the objective of this paper) should be placed in the Pasquasia section between formations 7 and 8, that is, at the base of the ‘Trubi’. However, Cita et al. (1973) affirmed that the Miocene/Pliocene boundary “. . . cannot be investigated in detail in the Pasquasia section” because “the contact between the ‘Trubi’ Formation and the ‘Gessoso-solfifera’ Formation being obscured.” Furthermore, according to Sprovieri (1975, p. 77), in the Pasquasia section the contact between the Messinian and the Pliocene sediments is poorly exposed.

Numerous sections were studied in Sicily (e.g., Sprovieri, 1975), where the Miocene/Pliocene boundary is better exposed, and it has been proposed to locate the boundary stratotype in the Capo Rossello section, near Realmonte (Agrigento) (Cita, 1975). According to Cita and McKenzie (1986, p. 129) “The lago-mare biotope was destroyed by the basal Pliocene ‘transgression’ [the inverted commas are ours], which reintroduced the marine fauna from the Atlantic into the Mediterranean. The Miocene/Pliocene boundary, as defined at the base of the ‘Trubi’ Formation at Capo Rossello (Cita, 1975), records the reestablishment of open-marine conditions in the Mediterranean after the Messinian salinity crisis. The change was drastic, and no survivors of the Paratethyan fauna have been reported anywhere in the Mediterranean realm [. . .]. The Pliocene transgression is a pan-Mediterranean event and is usually marked by an abrupt lithologic change, both in the deep-sea record and in the record from land”. Nevertheless, studies on the Miocene/Pliocene boundary are still in progress.

## THE TORTONIAN/MESSINIAN BOUNDARY

### *History of the definition*

In connection with the Italian Research Program ‘The geodynamic significance of the Late Miocene salinity crisis in the Mediterranean’, a working group composed of D’Onofrio, Giannelli, Iaccarino, Morlotti, Romeo, Salvatorini, Sampò, and Sprovieri, was directed in 1974 to study the problem of the lower boundary of the Messinian, in order to identify and correlate this boundary by means of planktonic Foraminifera. The above-mentioned working group sampled several Italian sections, including the Tortonian stratotype and the Capodarso section, where the lower part of the Messinian neostratotype was defined. In summary, these authors showed that: (1) it is impossible to detect the Tortonian/Messinian boundary in the neostratotype section, because the lower part of the section has been buried by a landslide; (2) the first appearance of *G. conomiozea* is the reliable biostratigraphic event closest to the three proposed upper boundaries of the Tortonian (Mayer-Eymar, 1858; Giannotti, 1953; Gino, 1953; Mayer-Eymar, 1868; Cita et al., 1965; see Fig. 6) located in the Tortonian type section (Piedmont). Therefore the



Fig. 4. The Falconara section. (Photo by R. Sprovieri.)

Tortonian/Messinian boundary should be placed at the lithological level in which the first appearance of *G. conomiozea* occurs (D'Onofrio et al., 1975; see Fig. 6).

Colalongo et al. (1979a) proposed to place the Tortonian/Messinian boundary-stratotype in correspondence with the lithologic level of first appearance of *G. conomiozea* in the Falconara section (southern Sicily, Figs. 1, 4, and 5), in the uppermost part of the 'Marne a Globigerine' formation, 6 m below the base of the 'Tripoli' unit.

The proposed boundary-stratotype (Colalongo et al., 1979a) is located in the southern slope of Monte Cantigaglione, about 3.5 km NW of Castello di Falconara on the southern coast of Sicily, between Licata and Gela (Atlante Stradale d'Italia of the Touring Club Italiano, 1:200,000, Sud, plate 52; Italy, topographic map 1:25,000, sheet 272-III-NW; coordinates of the extremes of the boundary-stratotype section: (A) lat. 37°07'32"N, long. 1°34'12"E of Monte Mario Meridian; (B) lat. 37°07'38"N, long. 1°34'08"E of Monte Mario Meridian). The Falconara section can be easily reached by a road connected to the Highway 115 (Gela–Licata) near the km 238 road marker. The geological features of the Falconara section area are shown in fig. 1 of Colalongo et al. (1979b). The Falconara section is well preserved, but is disturbed by faults (G.B. Vai, pers. commun., December, 1993).

## STRATIGRAPHY

*Lithostratigraphy.* The Falconara section, about 112 m thick, consists of 'Argille scagliose' at the base (belonging to the 'Sicilide Nappe'), above which the Neogene

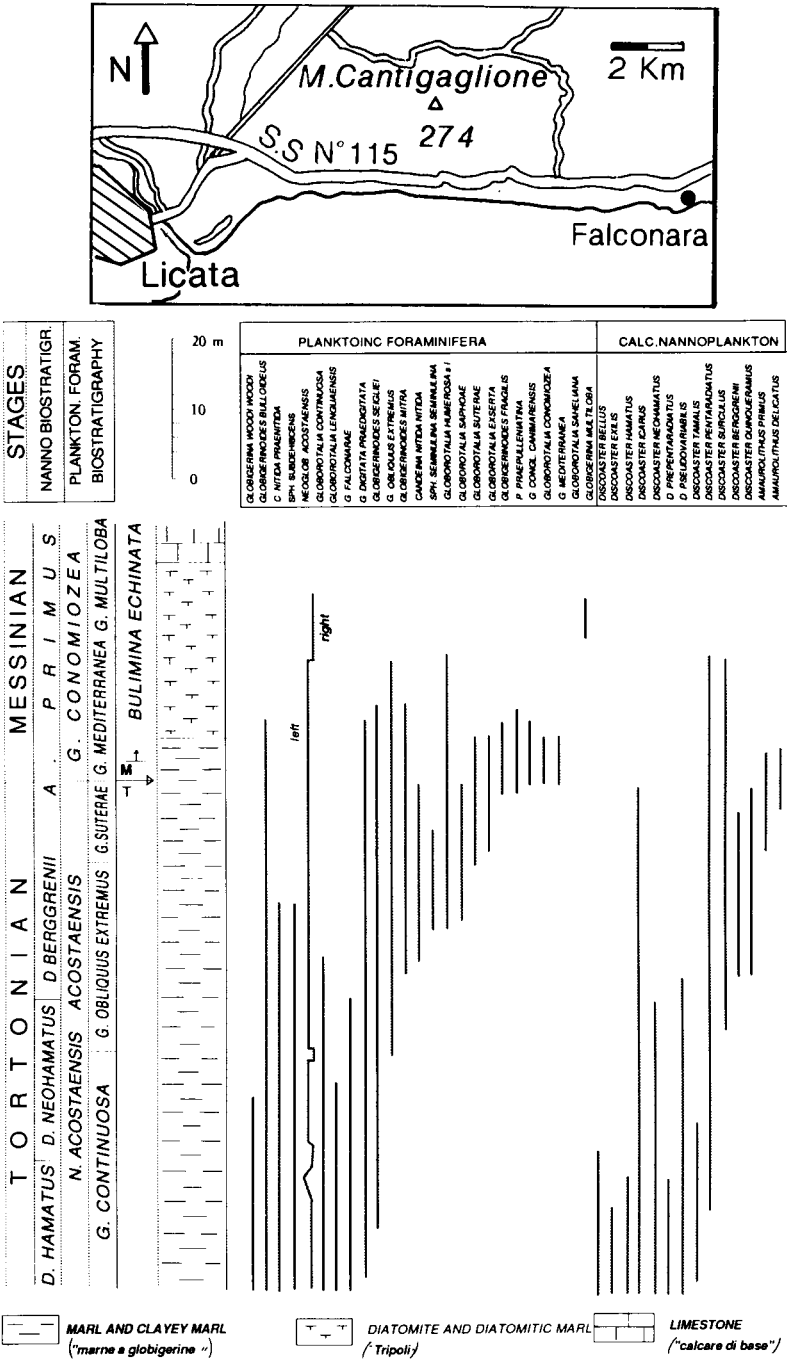


Fig. 5. Schematic stratigraphic column of the Falconara section, with the biostratigraphic zones and the distribution of the most significant taxa (from Colalongo 1979a, modified).

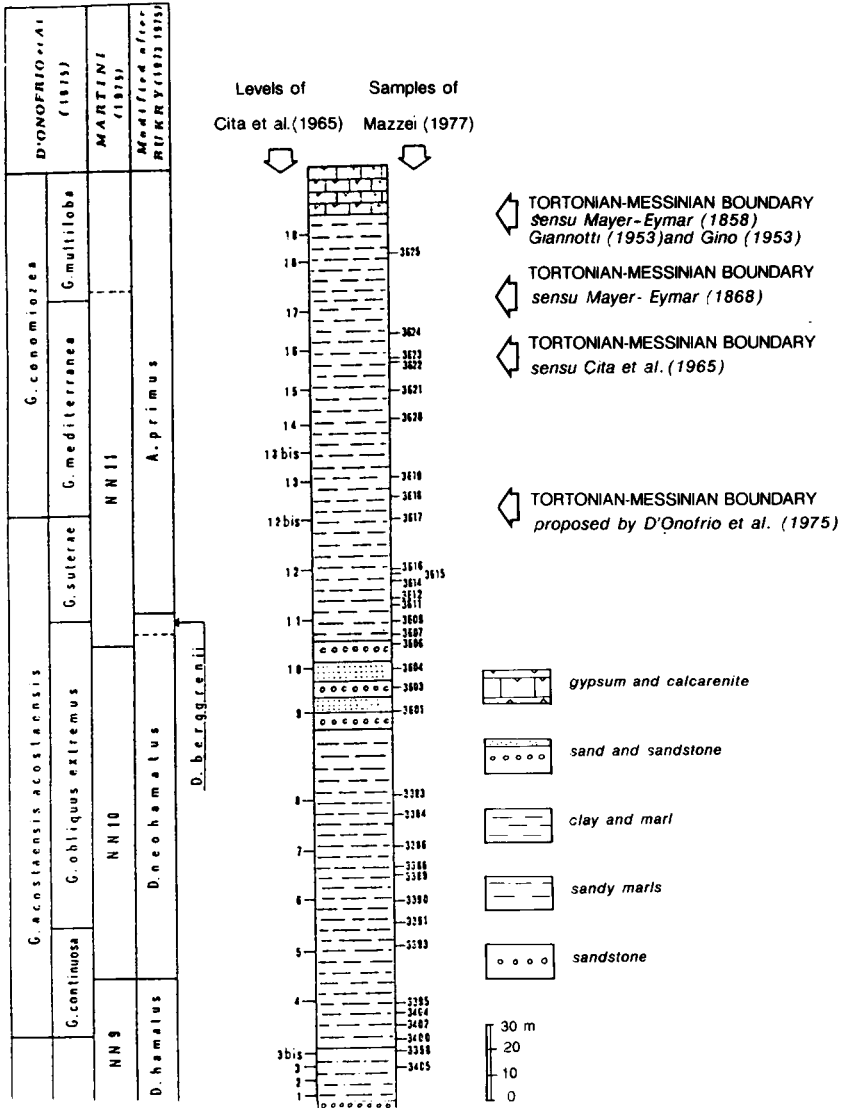


Fig. 6. Planktonic Foraminifera Zones and calcareous nannoplankton Zones of the Tortonian stratotype section (Rio Mazzapedi–Castellania section, Piedmont) (from Mazzei 1977, modified). The positions of the Tortonian/Messinian boundary according to some authors are shown.

sequence is outcropping: this sequence includes, from bottom to top, the ‘Marne a Globigerine’, the ‘Tripoli’, the ‘Calcare di Base’, the Gypsum, and the ‘Trubi’ units (Fig. 5). The Neogene sequence is continuous and well exposed; the open-marine sediments accumulated at considerable depths (Van der Zwaan, 1982, p. 80). The sequence does not show metamorphism. However, minor flat-lying thrust surfaces (i.e., the front of the Gela Nappe), and a dense system of normal faults related

to the transtensional belt of the Strait of Sicily, intersect the section. Furthermore, from a recent survey on the section, volcanoclastic horizons are absent (G.B. Vai, pers. commun., 1992). Planktonic Foraminifera and calcareous nannofossils are very abundant throughout the section. No permanent artificial markers are present in the Falconara section.

At Mediterranean ODP Site 654 (Glaçon et al., 1990), Late Miocene sediments were recovered, consisting of (from top to bottom): interbedded gypsum and carbonate layers, 69.9 m thick; dolomitic laminated dark shales (suggesting an anoxic environment), 36.3 m thick; a fining-upward sequence, 55 m thick, with sediments finer than 125  $\mu\text{m}$ , passing from shallow-water sands to deep-water nannofossil oozes and characterizing a prograding transgression; fine glauconitic sand, 11.8 m thick, containing *Operculina*, and some Ostreid-rich levels, both suggesting a deposition in near-shore deltaic environment; a 8.1 m thick conglomerate surrounded by red beds (interpreted as continental sediments).

In DSDP Site 610 (Atlantic Ocean) the Lower to Upper Miocene sediments consist of nannofossil chalk (more than 400 m thick), overlain by nannofossil ooze (about 150 m thick), which represents also the Lower Pliocene. The lithology of DSDP Site 611 (Atlantic Ocean) is reported to be very similar to DSDP site 610 (see fig. 2 in Hill, 1987).

*Biostratigraphy.* The Tortonian/Messinian boundary proposed by Colalongo et al. (1979a) in the Falconara section which coincides with the lithologic level in which the first appearance of *G. conomiozea* occurs, is easily correlatable both in the Mediterranean and the extra-Mediterranean areas, because *G. conomiozea* has a wide geographical distribution. Moreover, even when *G. conomiozea* is missing, the boundary is easily recognizable because there are many other biostratigraphic events closely preceding it, among which are, from bottom to top in the Falconara section, the first appearances of *G. suteræ*, *G. exserta*, *Amaurolithus primus*, *A. amplificus*, *Globorotalia mediterranea*, and *Amaurolithus delicatus*. Among the events following the FO of *G. conomiozea* there are the appearances of *Bulimina echinata* and *Globorotalia nicolae*, the sinistral to dextral coiling change of *Neogloboquadrina acostaensis*, and finally the appearance of *Globigerina multiloba* (Fig. 5) (Colalongo et al., 1979a, b). Some authors, except for Channel et al. (1990), and Benson and Rakic-El-Bied (1991), affirm that the first appearance of *G. conomiozea* occurs within a reversed polarity interval.

Several authors working in the Mediterranean area report on a distinctive change in the assemblages of keeled globorotaliids coinciding with the FO of *G. conomiozea*. This change consists of the abrupt disappearance of the *G. menardii* group (dextral coiled specimens), which is replaced by the *Globorotalia miotumida* group (sinistral coiled specimens). This replacement is recognized in several Atlantic Ocean areas, and is proposed by Sierró (1985) as a criterion useful to recognize the Tortonian/Messinian boundary in the regions where *G. conomiozea* is sporadic or absent.

Glaçon et al. (1990) studied a Miocene interval of the Tyrrhenian ODP Site 654. In this interval the above-mentioned authors found the first appearance of *G. conomiozea* and recognized the Mediterranean Late Miocene biozonation, identifying the *G. suteræ* Subzone, and the *G. conomiozea* Zone. "Other paleontologic events such as the LO of sinistral keeled globorotaliids (Event I), the FO and LO of dextral keeled globorotaliids (Events II and III), the sinistral to dextral (Event A) and dextral to sinistral (Event B) coiling changes in 'scutiform' globorotaliids and the increase in abundance of left



planoconvex keeled *Globorotalia miotumida* group (Event IV) have been identified. These events are well correlatable with similar events reported from southern Spain, Northern Morocco, and North Atlantic Ocean. In particular, Event IV [which predates the *G. conomiozea* FO] is very close to the FO of *G. conomiozea*, and we therefore suggest that it might be used to recognize the Tortonian/Messinian boundary in areas where *G. conomiozea* is absent or very rare" (p. 426).

The palaeontologic events reported by Glaçon et al. (1990) have been recognized in the same stratigraphic position by Calieri et al. (1992) in the Monte del Casino and the Monte Tondo sections (Romagna, Italy; see also Negri and Vigliotti in Chapter E4, and Laurenzi et al., in Chapter E5).

According to Glaçon et al. (1990, p. 426), "Some differences exist in the taxonomic concept of *Globorotalia conomiozea*." According to Scott (1980) and Zachariasse (1979b) "*G. conomiozea* s.s. does not exist in the Mediterranean." According to Zachariasse (1975, 1979b), "Mediterranean *G. conomiozea* refers to left-coiled planoconvex keeled globorotaliids having on average 4.5 crescent shape chambers in the last whorl". However, conical forms with only four chambers in the last whorl as *G. conomiozea* are documented by D'Onofrio et al. (1975), Colalongo et al. (1979b) and Bossio et al (1977). Different opinions exist also about the taxonomy of *G. conoidea* and *G. conomiozea*: "[...] A biometric study comparing Mediterranean and Atlantic forms of *G. conomiozea* and *G. conoidea* with the Pacific ones is in progress (G.G.), in order to clarify if we are dealing with different ecophenotypes of a single species reflecting environmental variations (different water masses) as suggested by Sierro et al. (1987)." (Glaçon et al., 1990).

Channell et al. (1990, p. 681) say that "The correlation of the Messinian/Tortonian boundary both in the Mediterranean and in the open ocean remains problematic due, at least in part, to the unsatisfactory nature of the FAD of *Globorotalia conomiozea* as a marker for this boundary. This biostratigraphic event is not widely recognized in open ocean sections. [...] However, the correlation at Site 654 of various events [...] close to the Tortonian/Messinian boundary, including *Globorotalia conomiozea* FAD and *Amaurolithus delicatus* FAD, to the GRTS helps to refine the correlation of this boundary to the open ocean".

According to Gartner (1992, p. 320) in the North Atlantic DSDP Site 608 the three biohorizons containing *Discoaster loeblichii*, *D. pentaradiatus*, *Dictyococcites productus*, and the *Gephyrocapsa* lowest occurrences "coincide with the limits of sample spacing and occur at 190.26 m (21–4,46). Such coincidence is suspicious and may suggest a minor hiatus, although the abrupt appearance of large numbers of very small placoliths here assigned to *D. productus*, and some of which clearly are *Gephyrocapsa*, must signal an important change in surface water properties that might effect productivity. This biohorizon is within the uppermost normal polarity interval of Chron 4A and has an age of 8.1 m.y.". *Discoaster berggreni* lowest occurrence "is within the upper part of Chron 4 and has an age of 6.9 m.y."; the *Minylitha convallis* highest occurrence "is near the top of Chron 4 and is assigned an age of 6.8 m.y."; the *Discoaster surculus* lowest occurrence is situated at "the very top of Chron 4 and has an age of 6.7 m.y."; the *Discoaster loeblichii* highest occurrence "is within the lower part of Chron 3A and is tentatively assigned an age of 6.4 m.y."; "the lowest occurrence of species of the genus *Amaurolithus*", which "may be very rare and occasionally are not

to be found in samples within their range [...] is within Chron 3A and is estimated to have an age of about 6.4 m.y.” (p. 321).

According to Bessedik (1985) the climatic conditions recorded by the flora in western Mediterranean during the Late Miocene were from subtropical to warm-temperate. Palynologic research carried out in the upper Neogene of Sicily (Suc and Bessais, 1990) demonstrates that in the central Mediterranean the climate was thermo-xeric, similar to the present climate of the Red Sea. Bertolani Marchetti (1984) asserts that during the lower and middle Messinian there were in the Mediterranean cold climate peaks. According to Bertini (1992), on the ground of pollen analyses carried out in four sections located in the Adriatic slope of the central-northern Apennines, it is possible: (1) to affirm that in this area there were only environmental oscillations, tied also to eustatic phenomena, simulating cooling events; (2) to hypothesize for this area the presence of subtropical–warm-temperate conditions in the Messinian.

## PHYSICO-CHEMICAL STRATIGRAPHY

*Magnetostratigraphy.* Langereis and Dekkers (1992, p. 100) demonstrated that “The Tortonian/Messinian boundary stratotype at Stazione Falconara (Sicily) yields normal remanent magnetization of post-tilting age, implying that the entire section is (sub)recently remagnetized.”

Channell et al. (1990) affirm that at ODP Site 654 the Tortonian/Messinian boundary occurs in a normal polarity zone correlated to Chron 6n (Chron 3B). However the magnetostratigraphy of Site 654 may not be very reliable, because the cores of this site were recovered by means of rotary drilling technique.

According to Krijgsman et al. (1994) “The recognition of two additional short subchrons in the CK92 [Cande and Kent, 1992] time scale, not recorded before in the commonly used time scales, solves the previous correlation problem of the late Miocene Cretan polarity sequence to the GPTS [...]. Straightforward correlation to CK92 implies that the FOD of *G. conomiozea* and hence the Tortonian/Messinian boundary occurs in the short reversed polarity subchron C3Bn.1r. [...]. Incorporating an astronomical age of 6.287 [Ma] for the younger reversal boundary of chron C3An.2n (y) (Shackleton et al., 1993) and a radiometric age of 9.66 for C5n (o) (Baksi et al., 1993, Krijgsman et al., in press) as age calibration points in the CK92 time scale enables us to re-estimate the ages of the polarity reversals. If we use linear interpolation between the two new calibration points, the correlation of the Cretan polarity sequence to the modified polarity pattern [...] results in an age of 7.10 Ma for the FOD of *G. conomiozea* and hence also the Tortonian/Messinian boundary.” This agrees with radiometric datings from the northern Apennines, where Vai et al. (1992) obtained an age of  $7.37 \pm 0.13$  Ma for biotite-rich ash layers a few metres below the Tortonian/Messinian boundary, and with the new results quoted in the present volume.

*Chemostratigraphy.* Stable isotope analyses ( $\delta^{13}\text{C}$  and  $\delta^{18}\text{O}$ ) of planktonic foraminifers from several section of Sicily — including the Falconara section — were performed by Van der Zwaan and Gudjonsson (1986), and yielded a detailed Middle Miocene to Upper Pliocene record. Only the upper part of the Messinian sequence, consisting of limestones and evaporites, was omitted from the analyses. “A comparison between this record and previously published stable isotope records from the Pacific and Atlantic

Oceans suggests that, at least during the time span considered, the Mediterranean had a palaeoclimatic and palaeoceanographic history that bears a close resemblance to that of the world's oceans" (Van der Zwaan and Gudjonsson, 1986). However, different local Mediterranean overprints superimposed on the general isotope signal were recognized. In particular these authors (p. 82) assert that "From 7–5.6 Ma a marked shift to light values can be observed in the Pacific Site [289]; this event is recognized in other oceans as well (e.g. Bender and Keigwin, 1979; Keigwin and Shackleton, 1980; Vincent et al., 1980; Bender and Graham, 1981) and is known as the 6.3 Ma carbon shift. It can be seen however, that both in the record of Site 289 and in the Mediterranean the shift starts already earlier (at about 7.2 Ma) and seems to culminate at 5.6 Ma. In the Mediterranean this culmination is characterized by the entry of *Globorotalia conomiozea*".

The mean salinity (Na + Cl) in intraevaporitic marls collected at Borgo Tossignano (northern Apennines, near Imola) is 153 ppm. These marls exhibit wide variations of total salinity (Coradossi and Corazza, 1980).

Glaçon et al. (1990), in their study on the Tyrrhenian ODP Site 654, emphasize that "the parallelism between the occurrence of low salinity species (*G. sacculifer*) and peaks of low  $\delta^{18}\text{O}$  values as well as that of normal salinity species (*Globigerinoides obliquus*) and peaks of high  $\delta^{18}\text{O}$  values, suggests strong local changes of environmental conditions".

According to Kastens (1992, p. 346), "in oxygen isotope records from the late Miocene at open ocean DSDP/ODP sites, one frequently observes two or three brief intervals during which  $^{18}\text{O}$  is enriched in both benthonic and planktonic Foraminifera [Shackleton and Cita, 1979; Shackleton and Kennett, 1975; McKenzie and Oberhansly, 1985; Hodell and Kennett, 1986; Keigwin et al., 1987]. A possible interpretation is that these  $^{18}\text{O}$  maxima record increased glaciation, probably in the southern hemisphere [Keigwin, 1987, and references therein]. If so, the  $^{18}\text{O}$  maxima should be accompanied by a drop in global sea level. [. . .]. Hodell et al. [1986] suggested that the glacio-eustatic sea level fluctuations indicated by these  $\delta^{18}\text{O}$  events severed the connection between the Mediterranean and the Atlantic and thus triggered the Mediterranean salinity crisis". The magnitude of the latest Miocene sea-level drop has been estimated as about 75 m relative to present sea level (Lincoln and Schlanger, 1987, 1991).

Kastens (1992, p. 352) affirms also what follows: "Although this paper has emphasized glacio-eustatic effects as the immediate trigger for beginning and ending the salinity crisis, I nonetheless agree with previous workers who envisioned that tectonically driven convergence of Africa/Eurasia established the necessary preconditions for the salinity crisis by squeezing the Mediterranean/Atlantic passageways into narrow, shallow-silled straits".

Muller and Mueller (1991) state: "Strontium isotope ratios from the Messinian [. . .] evaporites of the Mediterranean basin [. . .] support a subdivision into stratigraphically lower, predominantly marine deposits (lower evaporites [. . .]: lower gypsum and main salt) characterized by Sr isotopic ratios generally equivalent to those of Messinian seawater, and stratigraphically higher deposits (upper evaporites [. . .]) with  $^{87}\text{Sr}/^{86}\text{Sr}$  ratios lower than Messinian seawater. [. . .] Strontium isotopic ratios measured from the upper evaporites [. . .] are lower, and high proportion of this Sr was probably derived from low  $^{87}\text{Sr}/^{86}\text{Sr}$  continental runoff that characterizes much of this basin [. . .]. These results, therefore, strongly support depositional models utilizing a deep desiccated basin [. . .]

with a constant marine inflow during the early stages, including salt formation, followed by a series of long-lasting and sometimes isolated desiccation events that produced a strong, but variable, continental influence on the Sr isotopic composition of the upper evaporites”.

*Geochronology.* There are no absolute age determinations, as far as we know, on the Falconara section. New studies on the Vena del Gesso basin (Northern Apennines, Romagna, Imola area) made by Gandolfi et al. (1983) and Marabini and Vai (1985) revealed for the first time that in this area there are some thin, volcanogenic, biotite-rich horizons intercalated in a continuous, marine, very fossiliferous sequence spanning the Tortonian/Messinian boundary, as it was defined by Colalongo et al. (1979a).

Vai et al. (1993) showed that the datable minerals of this sequence are of first-order quality and preservation; they dated four biotite samples (K/Ar), which allowed the distinction of two late to latest Tortonian levels in the sequence ( $7.72 \pm 0.15$  and  $7.35 \pm 0.08$  Ma); a fifth biotite–plagioclase sample provided an excellent control (K/Ar and Ar/Ar) of the age of the second volcanic cycle at  $7.33 \pm 0.08$  Ma. M.L. Colalongo (in Vai et al., 1993) carried out a detailed biostratigraphic study of Foraminifera straddling the Tortonian/Messinian boundary in the Imola area. These authors calculated that the extrapolated age of the Tortonian/Messinian boundary should be  $7.26 \pm 0.10$  Ma, and proposed one of the well exposed sections in the Imola area (Monte del Casino or Monte Tondo sections, having a thickness of 35 to 52 m, respectively; for the locations of these section see Negri and Vigliotti in Chapter E4, Vai in Chapter E3, and Laurenzi et al., in Chapter E5) as a candidate for the Global Stratotype Section and Point for the Tortonian/Messinian boundary. Vai et al. (1993) affirm that the basal lithofacies of these sections is “made of massive, light-grey [...] heavily bioturbated mudstone rich in Foraminifera with scattered echinoids, pelagic bathyal to epibathyal molluscs [lithofacies A 1]; fossils indicate normal marine water conditions. Lithofacies A 1 passes upwards to a centimetre banded dark-grey to green-brown mudstone with higher organic matter content and scattered thin partings enriched in forams, pteropods, otoliths, a.o. (mass extinction levels) (E 2); oligotypic fauna may be abundant bearing witness to severe euxinic environment; pyrite lenses and laminae along with plant debris are frequently associated with the lithofacies in the upper part of the section.”

## CONCLUSIONS AND RECOMMENDATIONS

In order to respect the historical concept of the Tortonian/Messinian boundary, the GSSP for the Tortonian/Messinian boundary should correspond to a level time equivalent to the one located 25 m below the transition from the grey-bluish marls to the ‘Tripoli’ (marly diatomites) formation in the Pasquasia–Capodarso section, which was considered as the beginning of the Mediterranean ‘salinity crisis’ by Selli (1960, 1971). The *G. conomiozea* FO was found in this section only 2 m above the boundary proposed by Selli (coinciding with the beginning of the salinity crisis). Moreover Colalongo et al. (1979b) demonstrated that the *G. conomiozea* FO is the reliable biostratigraphic event closest to the three upper boundaries of the Tortonian (located in the Tortonian type section, Piedmont) proposed by Mayer-Eymar (1858, 1868), Giannotti (1953), Gino (1953) and Cita et al. (1965) (Fig. 6). Therefore the *G.*

*conomiozea* FO is very useful to choose the lithological level within which to locate the Tortonian/Messinian boundary, as evidenced by Colalongo et al. (1979a, b). Moreover this FO is accompanied by several close biostratigraphic events (concerning nannofossils and planktonic Foraminifera) very suitable for long-range correlations. Obviously the GSSP for the Tortonian/Messinian boundary should contain several of these events; it should have a reliable magnetostratigraphic record, and be possibly suitable to chemostratigraphic investigations and radiometric age determinations. Several authors affirm that the first appearance of *G. conomiozea* occurs within a reversed chron, except for Channel et al. (1990), and Benson and Rakic-El-Bied (1991).

In the Pasquasia–Capodarso section the fossils are scarce. The portion of the section not covered by the landslide is well exposed, and could be suitable for palaeomagnetic and chemostratigraphic investigations. A magnetostratigraphic research on this section (and on other sections of Sicily and Andalusia) was performed by Gautier et al. (1994).

The Falconara section seemed not suitable as Miocene/Pliocene boundary stratotype section because it is plagued by faults and was recently remagnetized. Therefore Vai et al. (1993) proposed the Monte del Casino or Monte Tondo sections in Romagna (northern Italy) as candidates for the GSSP of the Tortonian/Messinian boundary because these sections are well exposed, very rich in well preserved fossils — including the main taxa utilized for the correlation of the Tortonian/Messinian boundary (among which the FO of *G. conomiozea*) — and show some biotite-rich ash layers very close to the Tortonian/Messinian boundary, which yielded some reliable absolute age determinations. These sections encompass the beginning of the Mediterranean salinity crisis (sensu Selli), documented by the appearance of oligotypic and dystrophic forms. “High frequency palaeoclimatic cycles (including the equivalent of early Messinian  $^{13}\text{C}$  negative shift) recognized on the basis of changing relative abundance of different forms of Foraminifera have been found in our sections”; these cycles are reliably “correlated with  $\delta^{18}\text{O}$  cycles from well known sections in and outside the Mediterranean (Calieri, 1992)” (Vai et al., 1993). Studies on nannofossil, stable isotope and magnetostratigraphy of the Monte del Casino and Monte Tondo sections are in progress.

## SOMMAIRE — LE STRATOTYPE HISTORIQUE MESSINIEN ET LA LIMITE TORTONIEN/MESSINIEN

(Manuscrit soumis: Juillet 1993, révisé: Juin 1994; rédacteurs responsables: GSO, AM et RC)

L'Étage fut proposé par Mayer-Eymar en 1867 mais le stratotype historique du Messinien (nom dérivé de la ville de Messine, Sicile) fut proposé par Selli (1960) dans le profil de Pasquasia–Capodarso (Sicile). Epais de 180 m, le stratotype recouvrait à l'époque tout l'intervalle entre le Tortonien supérieur et le Pliocène inférieur et comprenait 7 unités: (1) marnes argileuses (seuls les 25 m supérieurs de cette unité sont 'messiniens'), (2) diatomite marneuse ('Tripoli'), (3) calcaire évaporitique, (4) gypse inférieur, (5) marne argileuse intermédiaire, (6) gypse supérieur, (7) marne argileuse supérieure. Dès l'unité 1, le faciès est interprété comme hyperhalin, caractère distinctif du Messinien. Le tout était recouvert de marnes blanches à foraminifères marines ('Trubi') qui marque le début du Pliocène. On souligne que la 'crise de salinité', au sens

initial de Selli, débute bien avant l'apparition du gypse. Trois modèles d'explication de cette 'crise de salinité' sont exposés. Le plus notable biosignal, très proche et plus jeune que la limite inférieure du stratotype est l'apparition de *Globorotalia conomiozea*, 2 m au dessus de la limite lithologique proposée par Selli. Cet auteur a considéré comme limite inférieure, un niveau situé 25 m sous la limite avec l'unité 2 d'après l'observation d'un appauvrissement du nombre d'espèces et de la dominance des formes mal nourries qui dénotent la sursalure.

Du fait de la disparition de la base de l'affleurement de Capodorso, Colalongo et al. (1979) ont proposé de localiser la limite Tortonien/Messinien dans la coupe Falconara. La limite, approchée là grâce à l'apparition de *G. conomiozea*, un taxon de large répartition, peut aussi être caractérisée par divers autres marqueurs biostratigraphiques proches (foraminifères et nannofossiles calcaires). Ces derniers sont aussi présents dans les coupes de Romagne étudiées dans ce volume. L'apparition de *G. conomiozea* a été localisée en Crête dans la courte magnétozone inverse C3Bn. 1r. En Romagne, elle a été datée directement par géochronologie aux alentours de 7,3 Ma.

*(Sommaire proposé par les rédacteurs, GSO)*

#### ACKNOWLEDGEMENTS

The authors thank G.S. Odin (Université P. & M. Curie, Paris) and P. Myrow (Colorado College, Boulder) for the critical review of this paper. Special thanks are due to G.B. Vai (Dipartimento di Scienze della Terra e geologico-ambientali dell'Università di Bologna) for the very useful discussions and for the bibliographic material placed at our disposal. G. Lo Cicero and R. Sprovieri (Dipartimento di Geologia e Geodesia dell'Università di Palermo) kindly permitted the use of their photographic material. We are grateful also to A. Bellanca (Istituto di Mineralogia, Petrografia e Geochimica dell'Università di Palermo), F.P. Bonadonna (Dipartimento di Scienze della Terra dell'Università di Pisa), N. Coradossi (Dipartimento di Scienze della Terra dell'Università di Firenze), E. Corazza (Laboratorio di Geocronologia del CNR di Pisa) and A. Longinelli (Istituto di Mineralogia e Petrografia dell'Università di Trieste) for the useful discussions.

This Page Intentionally Left Blank

Chapter A9

**PROPOSAL FOR THE GLOBAL STRATOTYPE SECTION AND POINT  
(GSSP) FOR THE BASE OF THE NEOGENE (THE PALAEOGENE/NEOGENE  
BOUNDARY)**

F.F. Steininger, M.P. Aubry, M. Biolzi, A.M. Borsetti, F. Cati, R. Corfield, R. Gelati, S. Iaccarino, C. Napoleone, F. Rögl, R. Rötzel, S. Spezzaferri, F. Tateo, G. Villa and D. Zevenboom

INTRODUCTION (F.F. Steininger)

The historical concepts of 'stratigraphic units' (chronostratigraphic units of modern usage) have been based mainly on two observations: (1) major or minor discontinuities (or facies changes) in rock sequences, and (2) major or minor changes in the overall biotic content, or within a specific taxonomic group.

Hörnes (1853) defined the Neogene in exactly the same way. In his 1853 publication on p. 806, he discussed his 'organic'-palaeontologic-reasons for combining Lyell's (1833) Miocene and Pliocene into his Neogene by referring to the mollusc fauna: "die Verschiedenheit der [of the mollusc] Fauna der Eozän- und Miozän-Epoche" of Lyell, and in 1864, p. 510, he pointed out the widespread discontinuities: "Unstreitig haben zwischen der Eozän- und Neogenzeit gewaltige Schichtstörungen in Europa stattgefunden".

The Working Group on the Palaeogene/Neogene Boundary was established at the IGC in Sydney 1976. Since then the Working Group held several meetings, discussing the general philosophy to be followed and the possible GSSP candidates; field meetings have been organized in Italy, Spain, Greece, Romania, where GSSP candidates have been sampled by the members of the group; the achieved results have been presented at successive Neogene meetings (Bologna, Vienna, Athens, Milano, Granada, Parma, Utrecht, Budapest, etc.) and at the IGC congresses in Paris, 1980, Washington, 1989 and Kyoto, 1992. Two volumes containing the evolution of the general approach and the results of the potential GSSP sections studied were published under the heading: 'In search of the Palaeogene/Neogene Boundary Stratotype' (Cati et al., 1981; Gelati and Steininger, 1983).

The first step was achieved in Vienna in 1979, with all votes of the Working Group members in favour of the following points.

(1) The base of the Neogene and the base of the Miocene corresponding to the Palaeogene/Neogene Boundary must be situated between the Chattian and the Aquitanian Stages, with the goal to include the total Aquitanian Stage in the Neogene.

(2) The Palaeogene/Neogene Boundary coincides with the Oligocene/Miocene Boundary.

(3) A possible GSSP candidate for the base of the Neogene (base of the Miocene and the Palaeogene/Neogene corresponding to the Oligocene/Miocene Boundary) would be ideal when covering in one continuous outcropping section the so-called 'critical time span'. This 'critical time span' was defined at that time by the biostratigraphic interval



between planktonic foraminiferal Zones P 22 and N 5 of Blow (1969) and Berggren and Miller (1988); this corresponds to the base of the *Globorotalia opima opima* Zone and top of the *Catapsydrax dissimilis* Zone of Bolli (1957, 1966) and Bizon and Bizon (1972) and Zones P21 to M 2 of Berggren et al. (1995) (Fig. 1); in terms of nannofossil zonation from NP 25, *Spenolithus ciperoensis* Zone, to NN 2, *Discoaster druggi* Zone according to Martini (1971) and Martini and Müller (1986).

Following the evaluation of the proposed GSSP section candidates from all over the world, several sections in the Mediterranean area (Italy, Spain and Greece), and the Paratethys (Romania) were studied in detail. Finally the proponents of the Working Group decided in 1988 to concentrate their efforts on two sections already studied in 1978 and published in 1981: (1) The Ca' Fusconi section in the Marche region (central Italy), and (2) the Carrosio–Lemme section in the Piedmont Basin (northern Italy). The two sections were deeply cleaned from scree in order to reach unaltered sediments and completely resampled in 1988.

The preliminary biostratigraphic results were presented at the IGC in Washington (1989), the magnetostratigraphic results were ready in 1990 and at the Working Group meeting in Vienna 1991 the results were thoroughly discussed. This discussion excluded the Ca' Fusconi section as a potential GSSP because it did not cover the entire 'critical time span'. After resampling and marking the Carrosio–Lemme section in 1991 the Working Group last met in Parma in April 1992 and it was decided to propose the Carrosio–Lemme section as the official candidate for the definition of the GSSP of the base of the Neogene (base of the Miocene and the Palaeogene/Neogene resp. the Oligocene/Miocene Boundary). It was also decided to place the GSSP within the Carrosio–Lemme section near to a group of prominent biostratigraphic events and near to resp. within a prominent magnetic reversal pattern. Therefore meter 35 of the Carrosio–Lemme section was chosen as the GSSP for the base of the Neogene (the Miocene and the Palaeogene/Neogene, corresponding to the Oligocene/Miocene Boundary). This point in the section is bracketed by a number of prominent biostratigraphic events within the calcareous nannofossils, the planktonic Foraminifera, the benthic Foraminifera and the dinoflagellate cysts, and marked by the distinct pattern of chron C6Cn, specifically the base of chron C6Cn.2n.

The results achieved to date have been presented orally and in a poster at the IGC in Kyoto 1992, where they were discussed with the geologic community interested in this subject. This proposal was approved at the International Geologic Congress 1996 in Beijing, China by IUGS.

## THE PROPOSED GSSP FOR THE BASE OF THE NEOGENE

- Name of the boundary: base of the Neogene (base of the Miocene and the Palaeogene/Neogene, corresponding to the Oligocene/Miocene Boundary).
- Rank of the boundary: System, resp. Period.
- Name of the locality of the Global Stratotype Section and Point: Carrosio–Lemme Section, Italy, Europe (Fig. 2).
- Geographic position of the Global Stratotype Section and Point: longitude 8°50'11"E, latitude 44°39'32"N.
- Position of the Global Boundary Stratotype Point: meter 35.00 of the Lemme Carrosio Section.

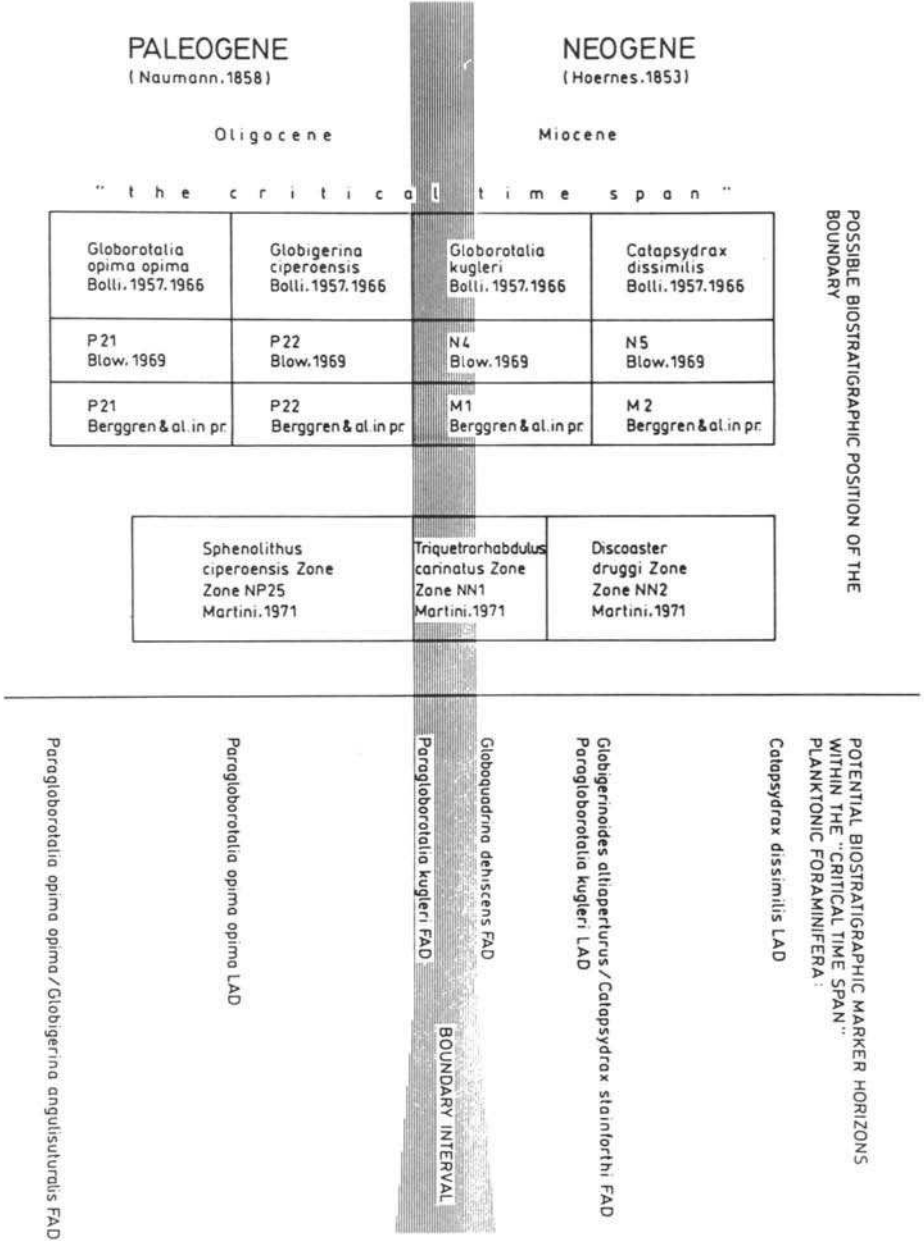


Fig. 1. The 'critical time span' concept and the 'boundary interval' concept of the IUGS-ICS Working Group on the Palaeogene/Neogene Boundary.

- Sedimentological marker of the GSSP section (R. Rötzel): an excellent sedimentological marker for recognition of meter 35, the GSSP for the base of the Neogene (base of the Miocene and the Palaeogene/Neogene, corresponding to the Oligocene/Miocene Boundary), is the prominent sedimentological change between Unit A (the more mas-

sive part of the section) and Unit B-1 (the more layered part of the section) at meter 50, marked also by a horizon with yellowish nodules. Meter 35, the GSSP for the base of the Neogene, is exactly 15 m above this sedimentological marker. The next layer with yellowish nodules follows in sedimentological Subunit B 2 just 1 m below meter 35, the GSSP of the base of the Neogene.

- Artificial markings of the GSSP of the section: meter 0.00 of the section is marked at the top by a metal stick driven into the marls of the Rigoroso Formation just 0.50 m below the top of the Rigoroso Formation because of technical reasons.

- From meter 0.00, a steel cable runs down the entire section. Each meter of the section is marked by a metal tag (with the meter number). These tags are fixed at the cable and additionally in the formation. In addition meter 35.00 is marked by a metal plaque fixed in the section with the following text:

IUGS ICS  
GSSP  
PALAEOGENE  
NEOGENE  
BOUNDARY AT  
METER 35  
1993

- Geographical location (R. Gelati and F.F. Steininger). Europe: northern Italy, Province Alessandria, village of Carrosio south of the town of Gavi, resp. north of Voltaggio. The section is situated east of Carrosio village, on the right bank of the Lemme river, on the cliff above and on the property of Case Carrezzani (Fig. 2).

- Map: official topographic map: Foglio Genova No. 82 (1 : 100,000); Tav. Voltaggio I NE (1 : 25,000).

- Access (Fig. 2): the village of Carrosio can be reached by public and private transportation, cars can cross the bridge on the Lemme river and drive up to the house 'Case Carrezzani'. From there the section is accessible by 10 minutes walk. The cliff where the section is situated is relatively steep; however, this guarantees an excellent, permanent outcrop situation. The present owner of the property, Mr. Nando Traverso, agreed to give access to the section chosen as an international point of geologic interest.

- Geology (R. Gelati): the area of the Carrosio–Lemme section is situated within the Piedmont Tertiary Basin, in southern Piedmont, northwestern Italy. The basin itself is bordered by the arc of the Western Alps and by the northwestern end of the northern Apennines. The basement of this basin consists of Penninic and Ligurian tectonic units (Fig. 3). The Late Eocene to Late Miocene succession forms a large homocline, gently dipping to the northwest. The basin formed during the Late Eocene/Early Oligocene as an extensional basin behind the arc of the Western Alps. Since the Late Oligocene it is involved in the Apennine compressional history, in more recent times (after the Late Miocene) evidences of an extensional tectonic are clearly recorded (Falletti et al., 1994). The facies evolution of the Piedmont Tertiary Basin is strongly controlled by the syndimentary tectonic activity and allows the recognition of three large-scale facies belts from west to east: the Langhe, the Visone–Lemme and the Borbera–Staffora facies belts (Fig. 4).

The GSSP section is situated within the Visone–Lemme facies belt in the upper part of the Rioroso Formation which overlies the Molare Formation (Oligocene fan delta conglomerates with sandy shallow-marine intercalations yielding micro- and macrofauna).

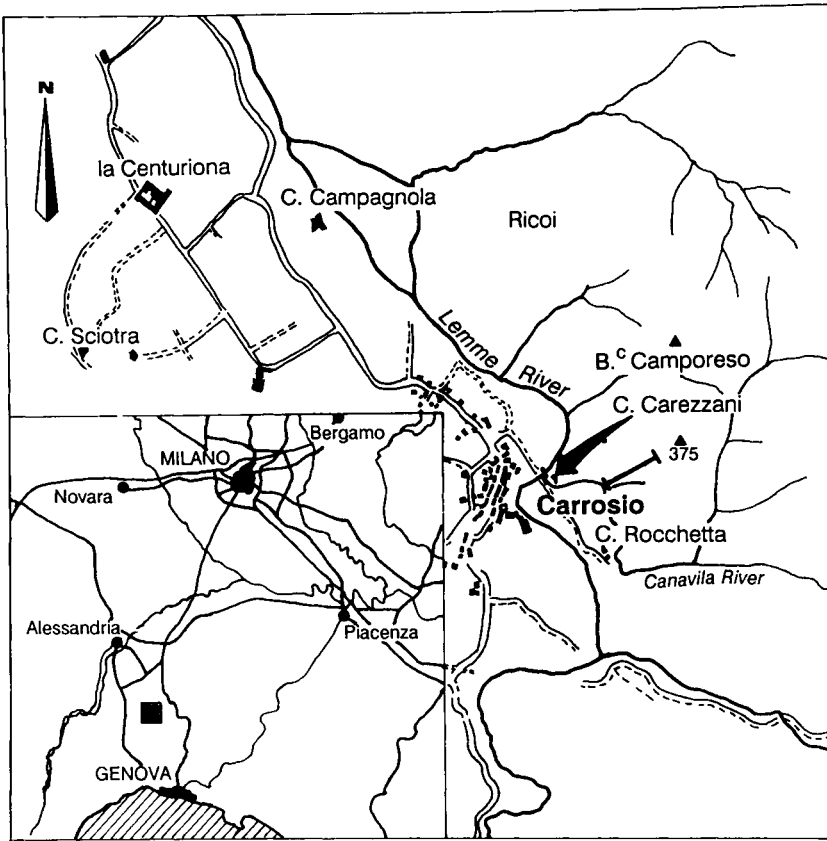


Fig. 2. Geographic location of the Carrosio-Lemme Section.

The Molare Formation lies unconformably on Pre-Cenozoic substratum (Gnaccolini, 1978a, b). The Rigoroso Formation itself is overlain by the upper Early Miocene Costa Montada Formation (Vervloet, 1966; Galbiati, 1976; Andreoni et al., 1981).

#### LITHOLOGY (R. Rötzel)

From bottom to top the measured section can be divided into three lithologic units:

##### *Unit A*

The basal Unit A (approximately 13.00 m exposed in the section) (Fig. 5) is characterized by bluish-grey, massive, partly indistinct, fine-bedded, clayey to fine sandy silt. Observed yellow to orange spots and nodules could relate to bioturbation structures.

##### *Unit B*

Unit B is approximately 45.50 m thick. This noticeable more fine-grained part of the section makes up the main part and can be further subdivided into three subunits (Fig. 5).

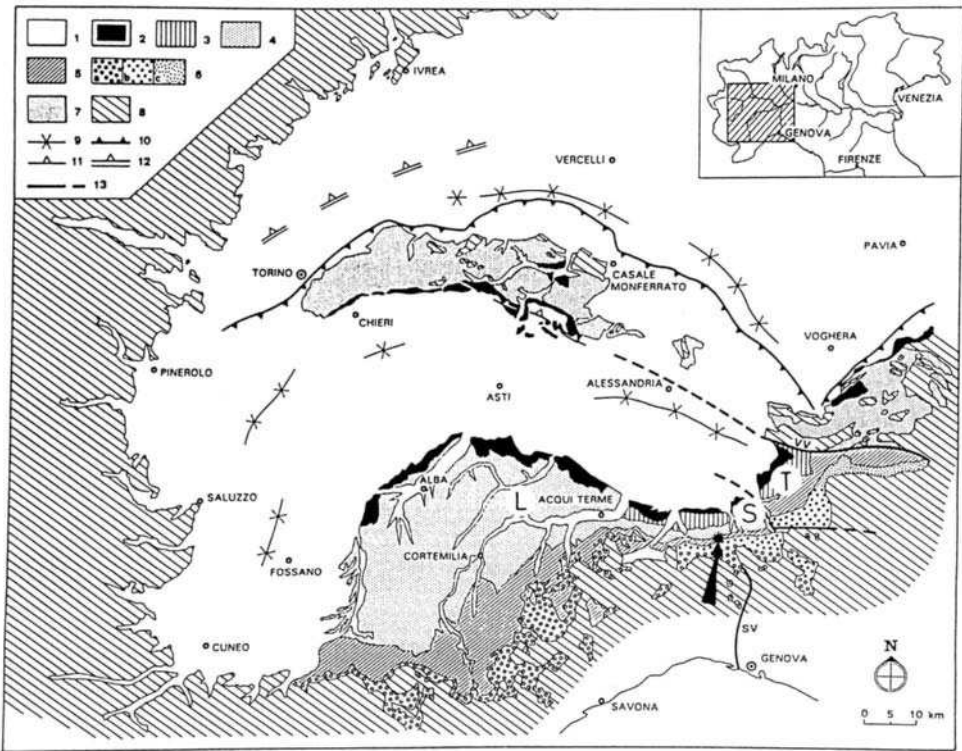


Fig. 3. The geologic frame of the Piedmont Tertiary Basin: \* = location of the Neogene GSSP, the Carrosio–Lemme Section; L = location of the Langhian type section; S = location of the Serravallian type section; T = location of the Tortonian type section. (1) Pliocene to Recent deposits. (2) Messinian deposits. (3) Langhian to Tortonian siliciclastics and carbonates; shelf and slope deposits. (4) Late Burdigalian to Tortonian mainly turbiditic succession; only Burdigalian in the eastern sector of this figure. (5) Late Oligocene to Burdigalian turbidite systems and hemipelagic mudstones. (6) Late Eocene to Early Oligocene deposits: (a) alluvial to coastal conglomerates, shallow-water sandstones and hemipelagic mudstones; (b) slope and base-of-slope, resedimented conglomerates; (c) mainly turbidites. (7) Late Eocene to Tortonian mainly siliciclastic deposits of the NW Apennines–Basso Monferrato–Collina di Torino wedge. (8) Alpine and Apennine allochthonous units. (9) Depocentre axis of the Plio–Quaternary basins. (10) Buried thrust front of the Collina di Torino–Basso Monferrato–NW Apennine wedge. (11) Buried, south-vergent backthrust of the Basso Monferrato, active from Messinian onward. (12) Buried, pre-Burdigalian backthrust of the Western Alps (as inferred from Roure et al., 1990a, b). (13) Tectonic lines: SV = Sestri–Voltaggio, VV = Villalvernia–Varzi.

*Subunit B1*, the basal unit, approximately 12.20 m thick: massive to indistinctly bedded, bluish-grey, clayey silt with few, thin-laminated, more clayey pelitic layers. Again yellow to orange spots and nodules.

*Subunit B2*, approximately 13.5 m thick: this characteristic sequence is made up by massive, indistinctly bedded, silty parts and thin-bedded, wavy laminated, more clayey pelitic layers. Within the massive bluish-grey silt marker horizons are characterized by yellowish to orange coloured nodules. This unit with fining-upward cycles is probably influenced by turbidites. The GSSP of the base of the Neogene (base of the Miocene and the Palaeogene/Neogene, resp. the Oligocene/Miocene Boundary) was defined 2 m

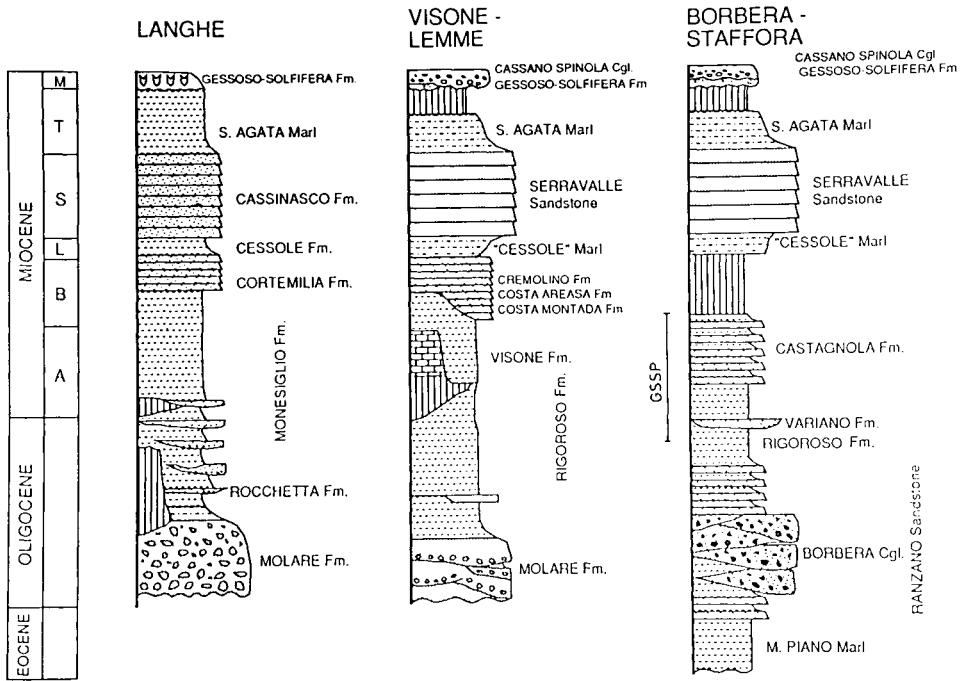


Fig. 4. Generalized lithologic and lithostratigraphic sections of the Langhe, Visone-Lemme and Borbera-Staffora areas.

above the base of Subunit B2, just 1 m above a very distinct layer with yellowish to orange coloured nodules.

*Subunit B3*, approximately 19.8 m thick: alternating sedimentation characterized by massive, indistinctly bedded bluish-grey silt with wavy laminated more clayey pelitic intercalations and several meters of thin-laminated, mostly clayey pelites.

*Unit C*

Unit C is approximately 4.4 m thick. In general massive bluish-grey silt layers with only a few laminated and more clayey pelitic intercalations. The silts change towards the top of Unit C into fine-sandy silt. The Costa Montada Formation overlies unconformably Unit C.

*General remarks*

The section is characterized by poorly to very poorly sorted sediments which can be classified as fine- and medium-grained silt with fine silt dominating. The CaCO<sub>3</sub> content (Fig. 6) shows a prominent decrease at meter 35.00.

*Mineral content (F. Tateo)*

The total mineral content is dominated by phyllosilicates and quartz, with various amounts of feldspar, calcite, dolomite, serpentine and pyrite. The main part of the clay fraction consists of a high amount of smectite, and minor parts of illite, kaolinite, chlorite and even serpentine.

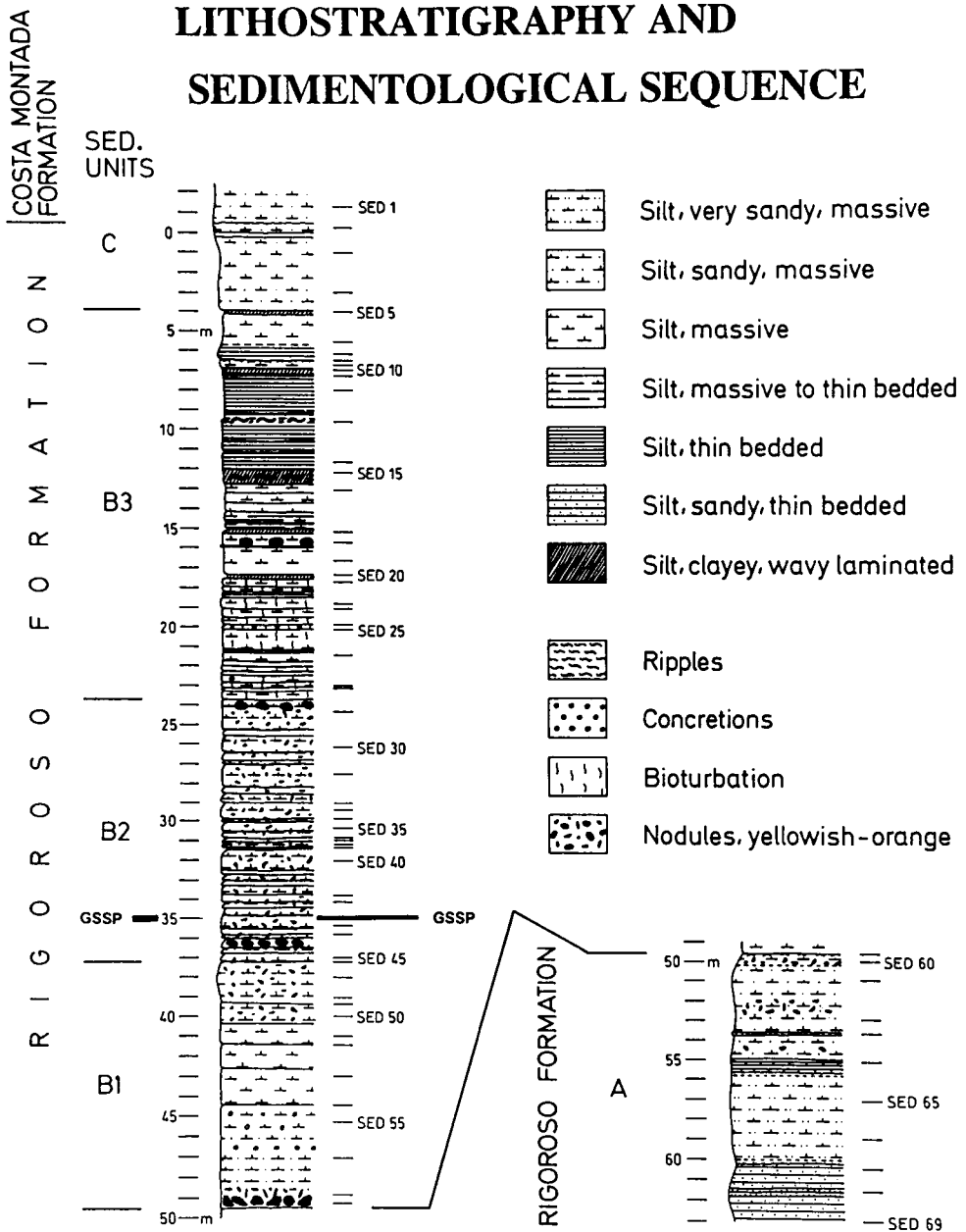


Fig. 5. Sedimentologic sequence and lithostratigraphy of the Carrosio-Lemme Section.

### BIOSTRATIGRAPHY

Only the most important biostratigraphic markers are discussed here. In general the preservation of planktonic foraminifera and calcareous microfossils is moderate to poor;

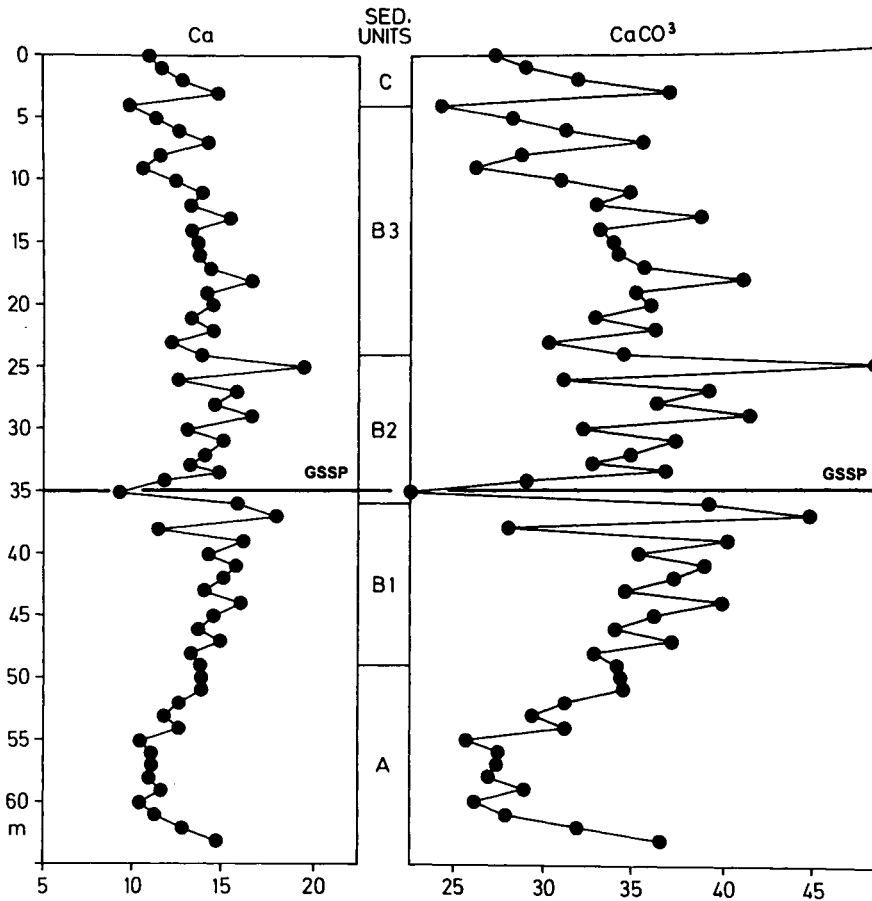


Fig. 6. Calcium and calcium carbonate content of the Carrosio-Lemme Section.

the dinocyst preservation is good to excellent. The abbreviations FAD and LAD indicate first and last appearance date(s) (Fig. 7).

*Calcareous nannofossils* (M.P. Aubry and G. Villa)

FAD of *Sphenolithus delphix* 12 m below meter 35.00; FAD and LAD of *Sphenolithus capricornutus* within one meter above meter 35.00 and LAD of *Sphenolithus delphix* 4 m above meter 35.00.

*Planktonic Foraminifera* (Fig. 8) (S. Iaccarino in collaboration with M. Biolzi, A.M. Borsetti, F. Rögl, S. Spezzaferri)

FAD of *Paragloborotalia kugleri* 2 m above meter 35.00, LAD of *Paragloborotalia kugleri* 25 m above meter 35.00; FAD of *Globoquadrina dehiscens* 12 m above meter 35.00, FAD of *Globigerinoides altiaperturus* 22 m above meter 35.00.



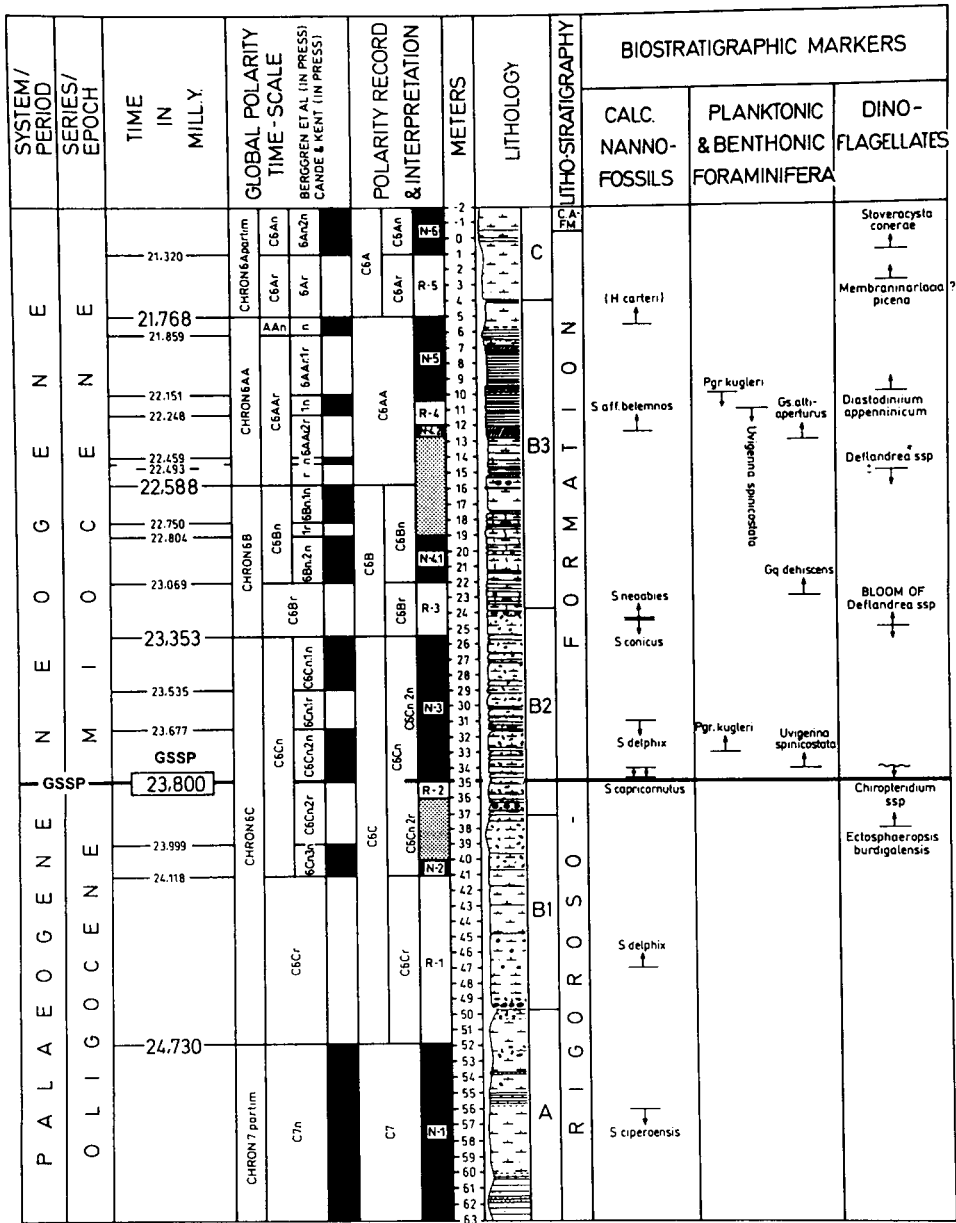


Fig. 7. Chronostratigraphy, geochronology, magnetostratigraphy, litho-stratigraphy and biostratigraphy of the Carrosio-Lemme Section: black = normal polarity; white = reversed polarity; grey = undetermined polarity.

#### Benthonic Foraminifera (M. Biolzi and F. Rögl)

FAD of *Uvigerina spinicostata* 1 m above meter 35.00 and its LAD 21 m above meter 35.00 might be a useful biostratigraphic event. The rich assemblages of benthic Foraminifera are characteristic of an upper bathyal environment.

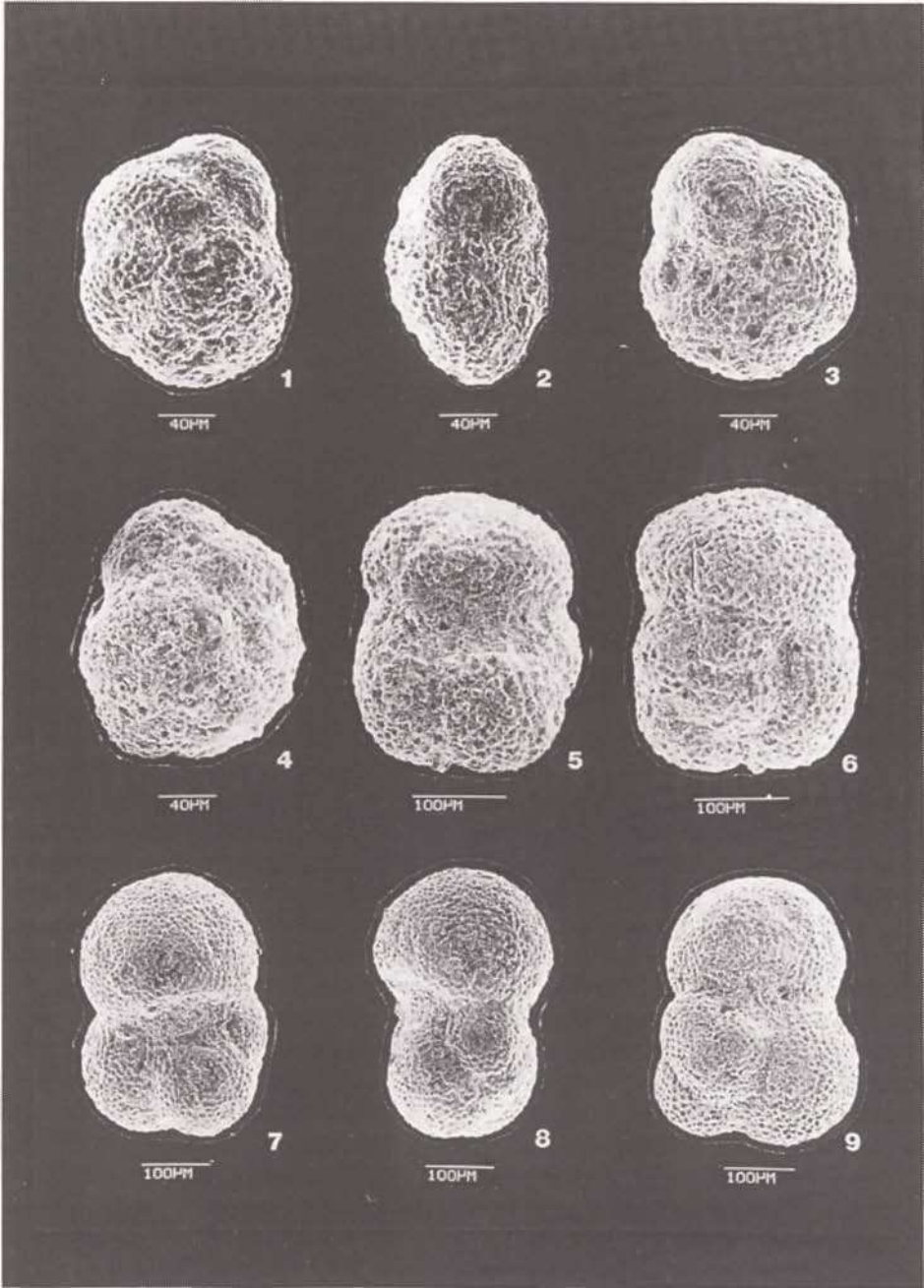


Fig. 8. Planktonic Foraminifera of the Carrosio-Lemme Section: (1-3) *Paragloborotalia kugleri*, sample LE III, meter 33 (1 spiral view, 2 side view, 3 umbilical view); (4) *Paragloborotalia kugleri*, sample LE III, meter 27, spiral view; (5-6) *Globoquadrina dehiscens*, sample LE III, meter 23 (5 umbilical view, 6 spiral view); (7-9) *Globigerinoides altiapertura*, sample LE III, meter 13 (7 umbilical view, 8 side view, 9 spiral view).

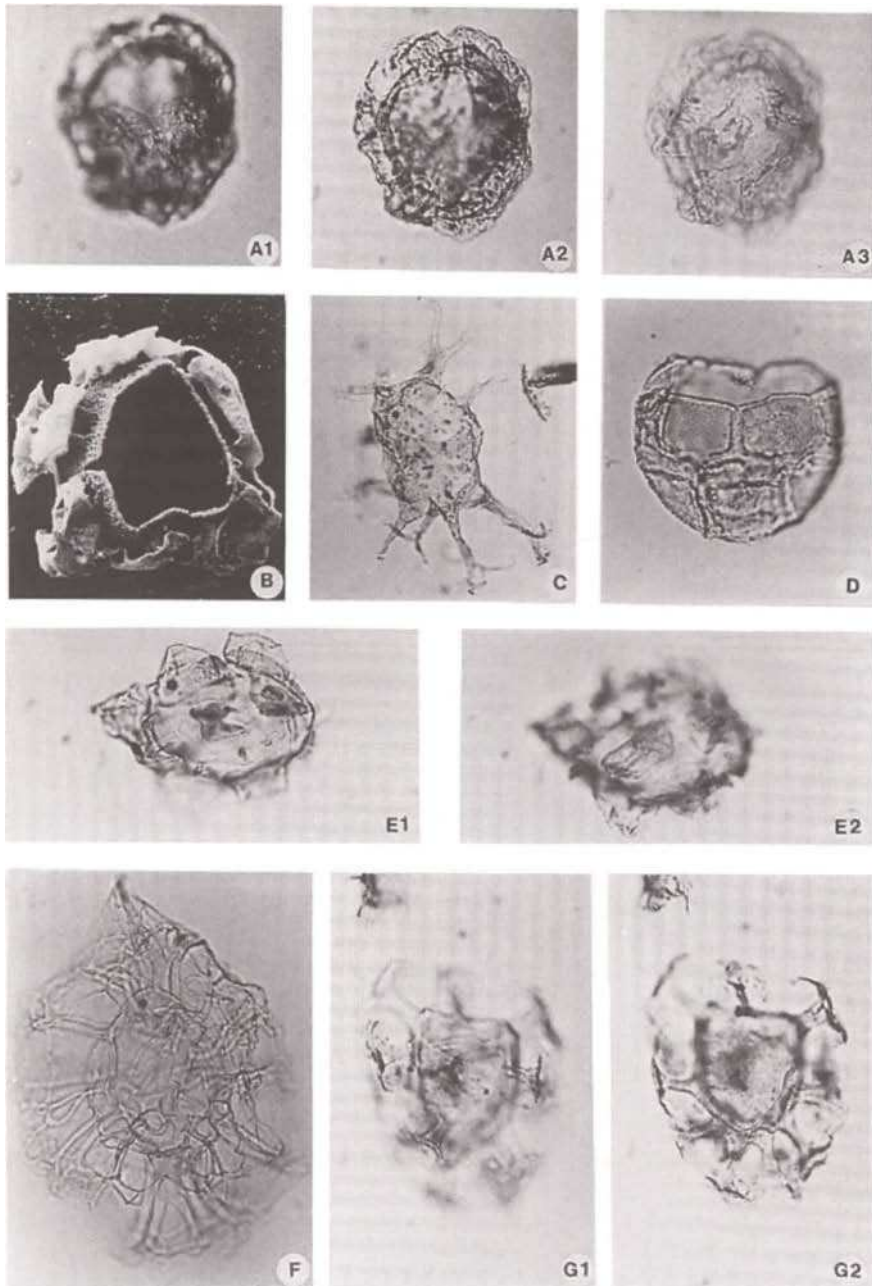


Fig. 9. Dinoflagellate cysts of the Carrosio–Lemme Section. (A1–A3) *Membranilarnacia? picena* (Biffi and Manum, 1988). Sample LE III A/1. EF: T 32/3. (B) *Membranilarnacia? picena* (Biffi and Manum, 1988). Sample H 365/366, Heumensoord Well, The Netherlands. (This species is added to clarify the complex nature of the processes.) (C) *Distatodinium biffi* (Brinkhuis et al., 1992). Sample LE III 44/1. EF: 0 40. (D) *Stoveracysta conerae* (Biffi and Manum, 1988). Sample LE III A 0 bis/2. EF: V 37/2. (E1–E2) *Hystrichokolpoma truncata* (Biffi and Manum, 1988). Sample LE III A 0 bis/1. EF: S 33/2.

*Dinoflagellate cysts* (Fig. 9) (D. Zevenboom)

FAD of *Ectosphaeropsis burdigalensis* at meter 38.00; last abundant *Chiropteridium* spp. at meter 39.00 and approximate LAD of *Chiropteridium* spp. 1 m above meter 35.00; bloom of *Deflandrea* spp. about 10 m above meter 35.00 and last abundant *Deflandrea* at meter 15.00; FAD of *Distatodinium apenninicum* at meter 10; FAD of *Membraninarlacia ?picena* at meter 3.00 and FAD of *Stoveracysta conerae* at meter 1.00.

*General remarks*

From the base of the section to meter 34.00 the planktonic foraminiferal assemblage is poorly diversified. From meter 33.00 up to meter 23.00 a remarkable change in the diversification of this assemblage has been recorded with an acme of the genus *Globigerinoides* comparable to the extra Mediterranean deep-sea record (Keller, 1981; Spezzaferri, 1991, 1994). From meter 21 up to the top of the section the foraminiferal assemblage is still well diversified. However, from meter 11 up to the top of the section a great abundance of radiolaria well known in this stratigraphic position of the region and the Mediterranean is remarkable (Sanfilippo et al., 1973).

*Interpretations on depositional environment, palaeoclimatology, and palaeotemperature*

The lithology and the microfossil content indicate an upper bathyal environment.

*Planktonic Foraminifera* (Fig. 10) (S. Spezzaferri)

Interpretation of planktonic foraminiferal data suggests that warmer conditions characterize the lower part of the section (up to meter 40), where the higher upwelling intensity is also registered. In general cooler conditions and palaeoclimatic instability with low-magnitude cool water fluctuations persists up to 10 m. Warmer conditions apparently stabilize in the uppermost part of the section. This palaeoclimatic trend is consistent with that observed in the open ocean. Finally, the palaeoclimatic instability may be responsible for the discrepancies of the range of several species.

*Dinoflagellate cysts* (Fig. 11) (D. Zevenboom)

The oceanic species *Impagidinium* div. sp. and *Nematosphaeropsis* div. sp. are used to approximate the sea surface temperature conditions. They show a cooling trend within the lower part of the section up to meters 40/39; a 'sudden' warming pulse up to meter 36/35; a relative cool pulse up to meter 24/23; a warming pulse up to meter 15/14 and a relative cool pulse upwards, briefly interrupted at meter 4/3 to meter 2/1 of the section.

---

(F) *Ectosphaeropsis burdigalensis* (Londeix and Jan du Chene, 1988). Sample LE III A 14/2. EF: E 47/4. (G1-G2) *Distatodinium apenninicum* (Brinkhuis et al., 1992). Sample LE III A 1/1. EF: T 44. (EF stands for England Finder coordinates.)

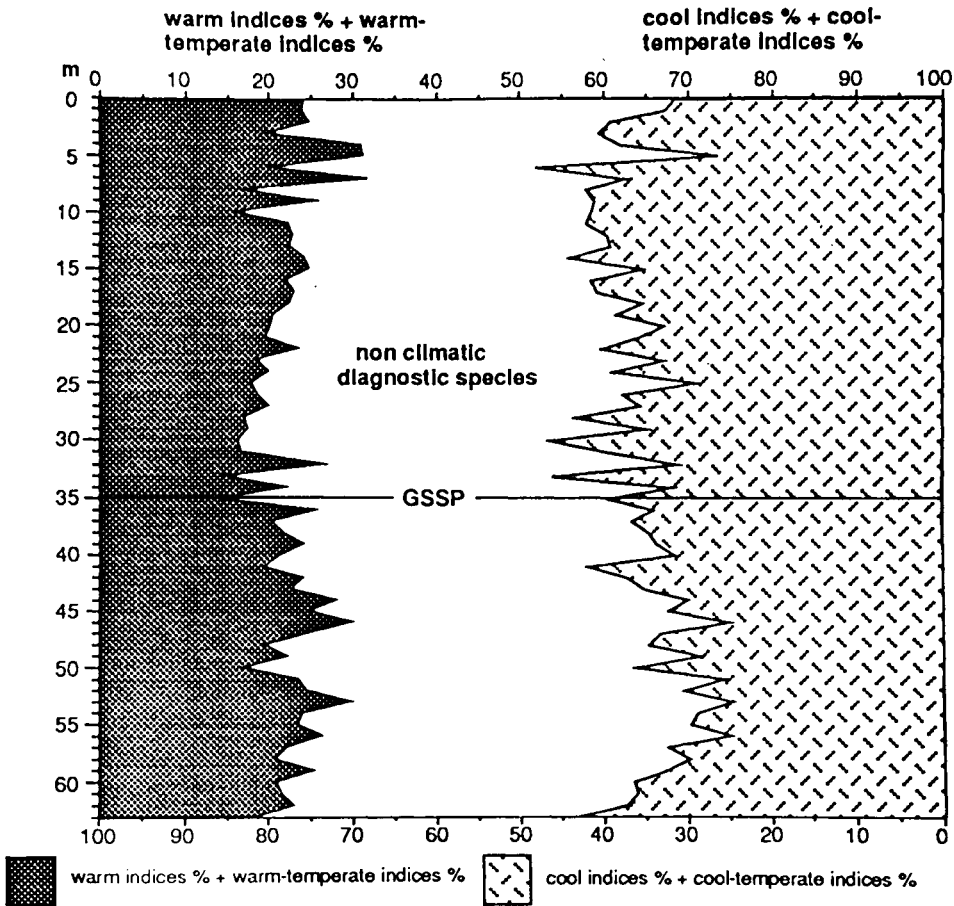


Fig. 10. Palaeoclimatology based on planktonic foraminifera of the Carrosio-Lemme Section.

#### MAGNETOSTRATIGRAPHY (G. Napoleone and F.F. Steininger)

The magnetostratigraphy is the result of two successive magnetic sampling campaigns to improve and propose a stable geomagnetic record for this section. Both sets of samples (circles LE II-1989, and squares LE III-1991) of the Carrosio-Lemme section gave a consistent geomagnetic pattern of at least six normal and five reversed polarity periods (Fig. 12). The section starts at the base with a longer normal part from meter 63 up to meter 52 (Magnetozone N-1), followed by a distinct reversed part from meter 52/51 up to meter 41 (Magnetozone R-1), followed by a short prominent normal part from meter 41 to meter 39.3 (Magnetozone N-2). Now the magnetic signal becomes disturbed up to meter 36.5. Just in one sample of LE II-1989 a fair normal polarity was measured. This is followed at meter 36 by a clear reversed polarity lasting up to meter 35: Magnetozone R-2. From meter 35 up to meter 25.6 the section is in a normal period: Magnetozone N-3. Only at meter 31 we do have perhaps a fair indication for a short reversal. This normal polarity changes at meter 25.6 up to meter 22.3 to a

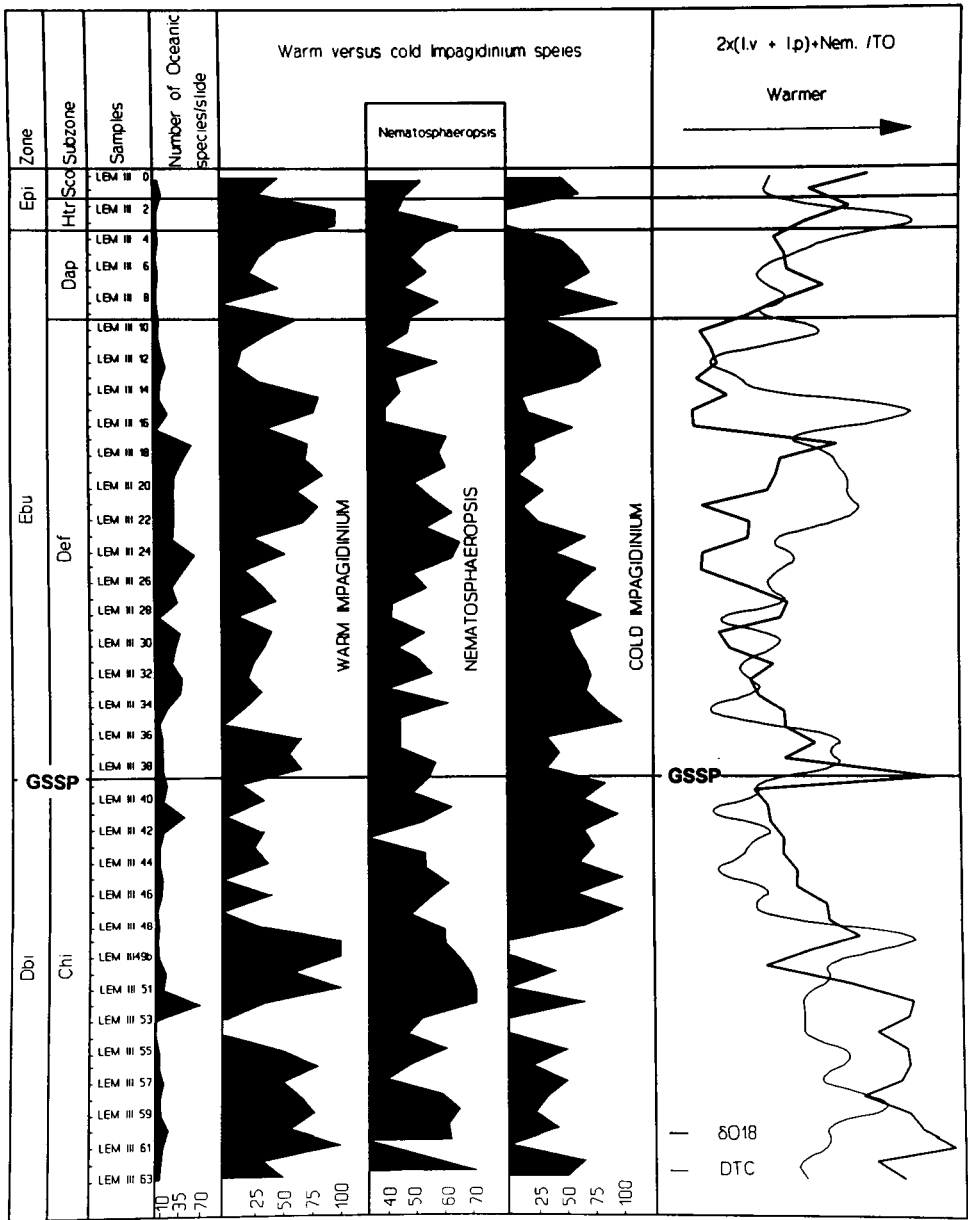


Fig. 11. Palaeoclimatology based on dinoflagellate cysts of the Carroisio-Lemme Section.

reversed magnetization (Magnetozone R-3), followed from meter 22.3 up to 18.7 by a clear normal period (Magnetozone N-4.1), which continues from meter 12.8 to meter 12 (Magnetozone N-4.2). In between, from meter 18.7 to meter 12.8, the measured polarity record is obscured and we find indications for normal and reversed polarities. From meter 12 to meter 10.5 we have a good indication for a reversed period (Magnetozone

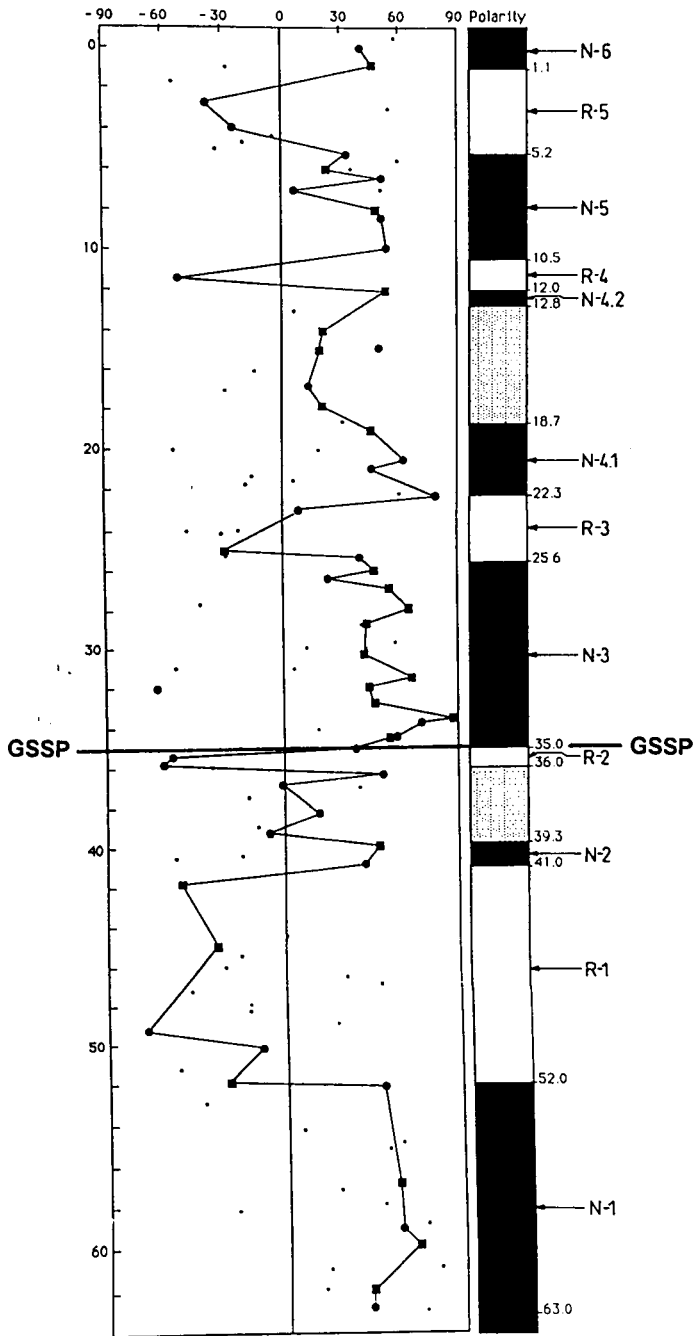


Fig. 12. The measured and interpreted polarity distribution. Virtual geomagnetic pole (VGP) latitudes are shown for all selected samples and the accuracy of each measured value is represented by the size of the symbols: full circles correspond to the first set of samples (LE II-1989), full squares to the second one (LE III-1991). Where latitudes are too low or values are less reliable, the dubious interpretation is marked by shadowed intervals.

R-4), followed by a clear normal period from 10.5 up to meter 5.2 (Magnetozone N-5). From meter 5.2 up to meter 1.1 the section falls into a clear reversed polarity (Magnetozone R-5), and the rest of the section till the measured top falls into a clear normal polarity period (Magnetozone N-6).

Biostratigraphic correlation tie points allow the interpretation and comparison of the geomagnetic pattern of this section with the geomagnetic time scales of Cande and Kent (1992) and Berggren et al. 1985b, 1995): Magnetozone N-1 can be correlated by the LAD of *Sphenolithus ciperoensis* with the upper part of chron C7n, Magnetozone R-1 with the FAD of *Sphenolithus delphix*, and the questionable presence of *Reticulofenestra bisecta* (? reworking) is correlated with chron C6r. The geomagnetic pattern of Magnetozones N-2, R-2 and R-3 can be correlated by the FAD and LAD of *Sphenolithus capricornutus* (at meter 35, resp. 34), the LAD of *S. delphix* (at meter 31) and the FAD of *Globorotalia kugleri* (at meter 33) with chron C6C. The distinct polarity change at meter 35 from Magnetozone R-2 to Magnetozone N-3 with the biostratigraphic markers cited above gives a clear indication of the correlation of these magnetozones with chron C6Cn.2r and with chron C6Cn.2n, respectively. This clear geomagnetic pattern and the excellent biostratigraphic markers have been one of the reasons to define the base of the Neogene (base of the Miocene and the Palaeogene/Neogene, corresponding to the Oligocene/Miocene Boundary) at meter 35 of the Carrosio–Lemme section. Within Magnetozone N-3 there is also a good indication at meter 31 for a short reversed part which might indicate chron C6Cn.1r. The LAD of *Sphenolithus conicus* and the FAD of *S. neoabies* (at meter 24.5) as well as the FAD of *Globoquadrina dehiscens* (at meter 23) and the bloom of *Deflandrea* spp. are recognized within Magnetozone R-3, which is therefore correlated to chron C6Br. Magnetozones R-3 (see above), N-4.1 to N-4.2, R-4 and N-5 are tentatively correlated to chrons C6B and C6AA. Magnetozone R-5 is interpreted as chron C6Ar and the uppermost measured part of the section (Magnetozone N-6) is correlated tentatively with chron C6An.

#### STABLE ISOTOPE STRATIGRAPHY (Fig. 13) (R. Corfield)

The stable isotope studies were performed on whole-rock carbonates.

The oxygen isotope record shows a systematic enrichment in  $^{18}\text{O}$  from the base of the section to approximately meter 15 of the section. This may correlate in whole or in part with the cooling trend identified by foraminiferal abundance analyses, or may reflect the ice-volume growth event labelled Mi-1 by Miller et al. (1991a, b) and Oslik et al. (1994).

Carbon isotope signals of  $-1.5\%$  are recognized between 40 and 35 m. These signals can be well compared in position to the carbon signals shown by Miller et al. (1991) and Oslik et al. (1994).

#### SEQUENCE STRATIGRAPHY AND SEA-LEVEL CHANGES (F.F. Steininger and D. Zevenboom)

Planktonic foraminiferal biostratigraphy and the geomagnetic polarity time scale allow an accurate correlation with the eustatic sea-level fluctuations and the sequence stratigraphy of Haq et al. (1988), respectively. Through the planktonic Foraminifera



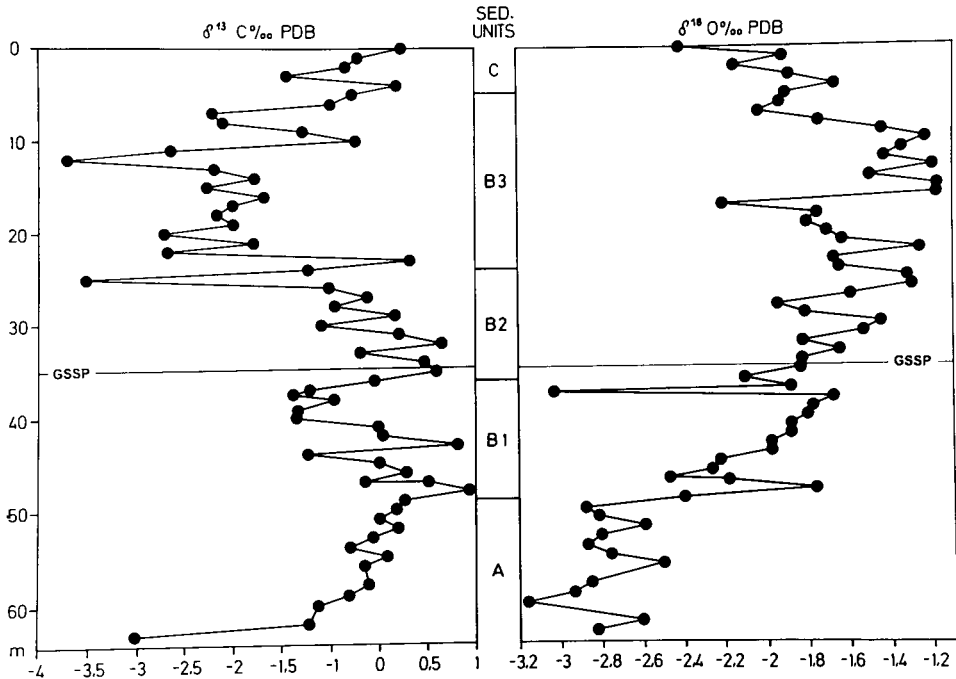


Fig. 13. Carbon isotope and oxygen isotope stratigraphy of the Carrosio-Lemme Section.

(FAD of *P. kugleri*) the section appears to coincide with the MFS of TB 1.4 given an age of 24.8 Ma by Haq et al. (1988). The section would fall into the Supercycle TB 1, the GSSP within the lower part of the highstand of TB 1.4.

Also the abundance of oceanic dinoflagellate cysts can be interpreted in terms of sea-level fluctuations. According to their distribution it is likely that the lower part of the section up to meter 39/38 was deposited during a sea-level fall (upper part of Dbi Zone corresponding to Chi Subzone) = TB 1.3, changing to a sea-level rise up to meter 10/9 (lower part of Ebu Zone corresponding to the entire Def Subzone) = TB 1.4, followed by a sea-level fall (upper part of Ebu Zone, corresponding to the entire Dap Subzone) = TB 1.4 to TB 1.5.

**REASONS FOR THE CHOICE OF THE GSSP OF THE BASE OF THE NEOGENE**  
(base of the Miocene and the Palaeogene/Neogene corresponding to the Oligocene/Miocene Boundary at the Carrosio-Lemme section (F.F. Steininger)

#### *Geographic position*

The chosen Global Stratotype Section and Point at the Carrosio-Lemme section is within the area already considered in history by Lyell (1833), Bronn (1838), Hörnes (1853 and 1864) and Naumann (1858) when defining their terms Eocene and Miocene (Lyell, 1833), 'Neogen' (Hörnes, 1853) and 'Paläogen' (Naumann, 1858).

### *Quality of the section*

Excellent exposure, continuous sedimentation without major structural complications or unconformities within the so called 'critical time span' (see above and Fig. 1), adequate thickness of the sediments, favourable facies, rather good possibilities to apply planktonic and benthic microfossil biostratigraphies, magnetostratigraphy, stable isotope stratigraphy and for the future eventually also cyclostratigraphy.

### *Biostratigraphy*

The GSSP for the base of the Neogene (base of the Miocene and the Palaeogene/Neogene, resp. the Oligocene/Miocene Boundary) at meter 35.00 is bracketed by a set of biostratigraphic events of planktonic microfossil groups (calcareous nannofossils, planktonic foraminifera and dinoflagellate cysts). The preservation of fossils is medium, the dinocyst preservation is good to excellent. The planktonic microfossil groups exhibit a moderate diversity and the abundance of index fossils is in relation with preservation medium good to excellent. In the calcareous nannofossil associations, reworking prevents using datums which elsewhere have proven to be useful markers such as the highest occurrence of *Zygrhablithus bijugatus* and the highest occurrence of *Reticulofenestra bisecta*. However, major biostratigraphic groups occur rather uniformly throughout the section and biostratigraphically equivalent results have been achieved accordingly by all specialists working on the same set of samples collected first in 1978, then in 1988 and finally in 1991.

### *Magnetostratigraphy and stable isotope stratigraphy*

Magnetostratigraphy and stable isotope stratigraphy have provided good and coherent results, which can be relatively unequivocally interpreted.

### *Correlation of GSSP*

Meter 35.00 (marked by a metal tag in the section) is proposed as the Global Stratotype Section and Point for the base of the Neogene (base of the Miocene and the Palaeogene/Neogene, respectively the Oligocene/Miocene Boundary) because this level offers several excellent possibilities for a worldwide correlation by means of several biostratigraphically relevant marine planktonic microfossil groups, magnetostratigraphy and stable isotope stratigraphy. Magnetostratigraphy allows further to tie this boundary into the continental record, respectively to correlate continental biostratigraphic zonations and events with the marine record.

### *Accessibility and conservation*

The section is easily accessible for public and private transportation and the present owner of the property, Mr. Nando Traverso, has agreed to provide access to colleagues interested in visiting and sampling the section and to conserve the section as an international geological point of prime interest.

THE POSITION OF THE GSSP OF THE BASE OF THE NEOGENE (BASE OF THE MIOCENE AND THE PALAEOGENE/NEOGENE, RESPECTIVELY THE OLIGOCENE/MIOCENE BOUNDARY) IN RELATION TO GLOBAL BIOSTRATIGRAPHIC ZONATIONS, MAGNETOSTRATIGRAPHY, STABLE ISOTOPES, SEQUENCE STRATIGRAPHY GEOCHRONOLOGY AND REGIONAL CHRONOSTRATIGRAPHIC TIME SCALES (F.F. Steininger)

*Biostratigraphic zonations*

*Calcareous nannofossils.* Approximately base of Zone NN 1 (Martini, 1971; Martini and Müller, 1986); approximately base of Subzone CN 1A (Bukry, 1973, 1975; Okada and Bukry, 1980).

*Planktonic foraminifera.* Base of the '*Globorotalia kugleri* Zone (Bolli, 1957; Bolli and Saunders, 1985) and close to the base of the *G. dehiscens* Subzone for the Mediterranean (Iaccarino and Salvatorini, 1982; Iaccarino, 1985); base M 1 Zone (Berggren et al., 1985a); base of M 1 resp. Mt 1 (Berggren et al., 1995); base of the (Sub)Antarctic Zone AN 1 (Berggren et al., 1995).

*Radiolaria.* Base of the *Lychnocanoma elongata* Zone; uppermost part of Zone 14 (= *Dorcadospyrus ateuchus* Zone) (Riedel and Sanfilippo, 1970, 1971, 1978; Sanfilippo and Nigrini, 1994).

*Diatoms.* North Pacific: lowermost portion of the *Thalassiosira spinosa* Partial Range Zone of Gladenkov and Barron (in prep.). Southern Ocean/Antarctic: upper part of the *Rocella gelida* Zone of Baldauf and Barron (1994). Low latitudes: within the *Rocella gelida* Partial Range Zone of Barron (1983; see also Barron et al., 1985a, Fenner, 1985, and Bolli and Saunders, 1985). The consensus for all three areas is that the GSSP for the base of the Neogene falls within the *Rocella gelida* PRZ (? near the top of the Zone).

*Silicoflagellates.* Within the *Distephanus speculum haliomma* Subzone of the *Naviculopsis biapiculata* Zone (Bukry, 1981; Perch-Nielsen, 1985).

*Dinoflagellate cysts.* Base of the *Cordosphaeridium canthaerellum* Zone (Williams, 1977); DO-3B Subzone at the uppermost part of the DO-3 Zone (Biffi and Manum, 1988); Def Subzone within the lowermost Ebu Zone (Brinkhuis et al., 1992).

*Mammals.* European Mammal Zonation: within and at the base of the MN 1 Zone (according to Burbank et al., 1992, and Agusti et al., 1994); within the Agenian mammal faunal unit, in the 'unnamed' continental stage below the Ramblian Stage of the European Continental Stage concept (de Bruijn et al., 1992; Steininger et al., 1989, 1995).

*North American land mammal 'ages'.* Within the late early-Arikareean to the base of the early late-Arikareean (Tedford, 1987).

*Pollen.* East Mediterranean: above the Kale Pollen Zone (Steininger et al., 1989; Benda and Meulenkamp, 1990); Central Paratethys: approximately between the NGZ I and NGZ II Zones (Hochuli, 1978; Steininger et al., 1989)

*Charophyte.* Base of the *Rantzieniella nitida* Zone (Riveline, 1986), respectively top of the *Stephanochara berdotensis* Zone of Feist et al., (1994).

### *Magnetostratigraphy*

By biostratigraphic correlations, the position of the base of the Neogene GSSP at meter 35, the base of the Miocene and the Palaeogene/Neogene, corresponding to the Oligocene/Miocene Boundary is situated at the boundary between chrons C6Cn.2r and C6Cn.2n (Berggren et al., 1955; Cande and Kent, 1992, 1995).

### *Stable isotopes*

The prominent oxygen spike recognized at meter 35 — the GSSP of the base of the Neogene and the Miocene, the Palaeogene/Neogene, resp. the Oligocene/Miocene Boundary — is correlated to/interpreted as spike Mi-1 named by Miller et al. (1991a, b).

Carbon shifts of  $-1.5\%$  are recognized between meters 40 and 35 of the Neogene GSSP. These shifts can be well compared in position to the carbon shifts recognized by Miller et al. (1991a, b).

### *Sequence stratigraphy*

Supercycle TB 1 at the highstand of TB 1.4 (Haq et al. 1988).

### *Geochronology*

The estimated numerical age for the proposed GSSP is 23.8 Ma (see also Berggren et al., 1995; Odin, 1992; Odin and Luterbacher, 1992).

### *Regional chronostratigraphic scales*

*Mediterranean.* At or just below the base of the type section of the Aquitanian Stage.

*Northern Europe.* Probably within the uppermost part of the (Neo-) Chattian Stage. Paratethys: Central: within the uppermost Egerian Stage; Eastern: within the uppermost Caucasian Stage (Kalmykian/Karadzhalgian Stage boundary).

*North America.* East coast (Gulf coast): uppermost Hackberryian Stage; West coast: uppermost Zemorrian Stage.

*New Zealand.* Upper Duntroonian Stage. East Indian Letter Stages: uppermost e4/lowermost e5.

## SOMMAIRE — PROPOSITION DE POINT STRATOTYPE GLOBAL POUR LA BASE DU NEOGÈNE (LA LIMITE PALÉOGÈNE/NÉOGÈNE)

(Manuscrit soumis: Février 1995, révisé: Juillet 1995; rédacteurs responsables: AM et RC)

La limite Paléogène/Néogène qui correspond à la limite Oligocène/Miocène est proposée dans la section de Carrosio–Lemme, au sud de la ville de Gavi et au Nord de celle de Voltaggio, Italie du Nord. La section est située à l'Est de Carrosio, sur la rive droite de la rivière Lemme, sur la falaise et dans la propriété Case Carezzani. La position

du Point Stratotypique Global (PSG) est fixée au niveau du mètre 35 qui est repéré par une plaque métallique dans la coupe. Les principales possibilités de corrélation du PSG proposé sont les suivantes.

Biostratigraphie: le biorepère d'apparition (BRA) de *Sphenolithus delphix*, 12 m sous le niveau 35; le BRA et le biorepère d'extinction (BRE) de *Sphenolithus capricornutus* tous deux compris dans le mètre suivant le niveau 35; le BRE de *Sphenolithus delphix* 4 m au dessus du niveau 35. Le BRA et le BRE de *Paragloborotalia kugleri*, respectivement 2 m et 25 m au dessus du niveau 35, le BRA de *Globoquadrina dehiscens*, 12 m au dessus du niveau 35, le BRA de *Globigerinoides altiapertura* 22 m au dessus du niveau 35. Le BRA et le BRE de *Uvigerina spinicostata*, respectivement 1 m et 24 m au dessus du niveau 35. Le BRA de *Ectosphaeropsis burdigalensis*, 3 m sous le niveau 35; l'appauvrissement phylétique et le BRE approché de *Chiropteridium* spp., respectivement 4 m au dessous et 1 m au dessus du niveau 35; l'épanouissement et l'appauvrissement phylétique de *Deflandrea* spp., respectivement environ 10 m et 20 m au dessus du niveau 35; le BRA de *Distatodinium apenninicum*, 25 m au dessus du niveau 35; le BRA de *Membranaralacia ? picena*, 32 m au dessus du niveau 35 et le BRA de *Stoveracysta conerae*, 34 m au dessus du niveau 35.

Magnétostratigraphie: le diagramme d'inversions magnétiques analysé au niveau 35,00, est interprété par les auteurs comme la limite entre les magnétozones C6Cn2r et C6Cn2n.

Chimiostratigraphie: pour les isotopes de l'oxygène, le signal montre un enrichissement progressif en isotope lourd de la base jusqu'au niveau 13 m. Une partie ou l'ensemble de cette tendance peut être mise en parallèle avec l'événement Mi-1 de Miller et al. (1991). Cet événement a été corrélé avec la magnétozone C6Cn par Hodell et Woodruff (1994). Pour les isotopes du carbone, il est à noter que les variations isotopiques du C et de l'O ne sont pas synchrones dans les échantillons du profil de Lemme suggérant ainsi que ces variations ne sont pas liées à la diagenèse. Des excursions négatives du delta <sup>13</sup>C ont été reconnues près de la limite et se corrélaient avec des observations obtenues par ailleurs.

Lithostratigraphie, interprétation séquentielle: l'intervalle comprenant la limite est interprété comme tombant dans le Supercycle TB 1 et, d'après les résultats biostratigraphiques (BRA *P. kugleri*) et magnétostratigraphiques, au haut niveau marin TB 1.4 de Haq et al. (1988). Cette interprétation semble corroborée par l'interprétation des associations de kystes de Dinoflagellés.

(Sommaire proposé par les rédacteurs d'après résumé des auteurs, GSO)

## ACKNOWLEDGEMENTS

This work was carried out in cooperation with IUGS-ICS-SNS, 'Working Group on the Palaeogene/Neogene Boundary', and IGCP Project 329: 'Oligocene-Miocene Transition in the Northern Hemisphere'. We are grateful to Mr. Nando Traverso, the owner of the property, for his continuous help, his understanding and patience during the years (1978 to 1993) we were studying this section.

We acknowledge the help of numerous colleagues over the years for their critical views on the subject and developing therewith the concept we followed. Numerous colleagues gave us their help in arranging our field meetings and our conferences. Finally

we are grateful for the financial aid we received over the years from the International Union of Geological Sciences via the International Commission on Stratigraphy.

The Austrian part was supported financially by the Austrian Academy of Science, the Austrian National Committee for the International Geological Correlation Program (IGCP Project No. 326: 'Oligocene–Miocene Transition in the Northern Hemisphere'), the Institute for Palaeontology of the University of Vienna, the Geological–Palaeontological Department of the Natural History Museum in Vienna and the Geological Survey of Austria.

The Italian part was financially supported by the Ministero Università e Ricerca Scientifica (MURST 40% and MURST 60%) and by Consiglio Nazionale delle Ricerche–Istituto per la Geologia Marina of Bologna (CNR–IGN).

The following colleagues are thanked for providing to us most valuable unpublished information, for reviews and for their help with the correction of this proposal: A. Albanelli (Firenze), J. Barron (Menlo Park), W.A. Berggren (Woods Hole), P. Falietti (Milano), S. Landi (Firenze), F. Lévêque (Marseille), L. Martellini (Milano), G.S. Odin (Paris), F. Ottner (Vienna), A. Sanfilippo (San Diego) and F. Woodruff (Los Angeles).

This Page Intentionally Left Blank

## Chapter A10

# THE MIOCENE/PLIOCENE BOUNDARY: PRESENT AND FUTURE

J.-P. Suc, G. Clauzon and F. Gautier

## INTRODUCTION

Until recently, the definition and the chronostratigraphic location of the Miocene/Pliocene boundary has not been the subject of intense discussion. A complete review of its history was made by Cita (1975), who also provided the modern definition of the boundary in the light of the deep-sea drilling project (DSDP Leg 13) in the Mediterranean Sea. It corresponds to the renewal of marine conditions in the Mediterranean Sea after the Messinian Salinity Crisis. The *Sphaeroidinellopsis* Acme-Zone followed by the first appearance of *Globorotalia margaritae* in the Mediterranean marked the boundary (Fig. 1).

Aside from the fact that the definition and the location of a chronostratigraphic boundary is in the first place a matter of nomenclature, one must not neglect its global importance as a reference point. In this way, the choice of a continuous boundary stratotype is a real scientific question. Nevertheless, such a choice is not devoid of a geopolitical aspect, all the Neogene stratotypes (including the boundary ones) being located in the northwestern and central Mediterranean region, and mostly in Italy.

Recent progress in integrated stratigraphy, both in the Mediterranean (Hilgen and Langereis, 1993; Gautier et al., 1994) and in the Atlantic Morocco (Benson et al., 1991), requires reconsideration of the problem. However, one must bear in mind that, in dating and identifying the lowermost Pliocene deposits, the problem was touched upon in the Mediterranean only because of the Salinity Crisis.

The topic has been recently discussed in detail in several papers (Hilgen and Langereis, 1993; Benson and Hodell, 1994). As a consequence, this paper does not aim to examine again all the aspects of the question, but to emphasize the main ones taking into account recent progress in chronostratigraphy in order to synthesize the debate for the emergence of the best solution. The time scale adopted here is that of Cande and Kent (1995) who have revised their earlier magnetostratigraphic chronology (Cande and Kent, 1992) to be consistent with astronomic chronology.

## THE PRESENT-DAY CONVENTIONAL BOUNDARY AND ITS PROBLEMS

The first problem concerning the Miocene/Pliocene boundary, but not the least, is the large diachronism of the first appearance datum (FAD) of *Globorotalia margaritae* between the Atlantic Ocean and the Mediterranean Sea (Figs. 1 and 2). In the Atlantic Ocean, at Mediterranean latitudes (i.e., Bou Regreg section in Morocco), the FAD of *Globorotalia margaritae* occurs within mid Subchron CA3n.2n (Benson and Rakic-El Bied, 1991; Fig. 2). In the Mediterranean (i.e., Capo Rossello, Singa, Eraclea Minoa sections), the massive increase in abundance of *Globorotalia margaritae* occurs in mid



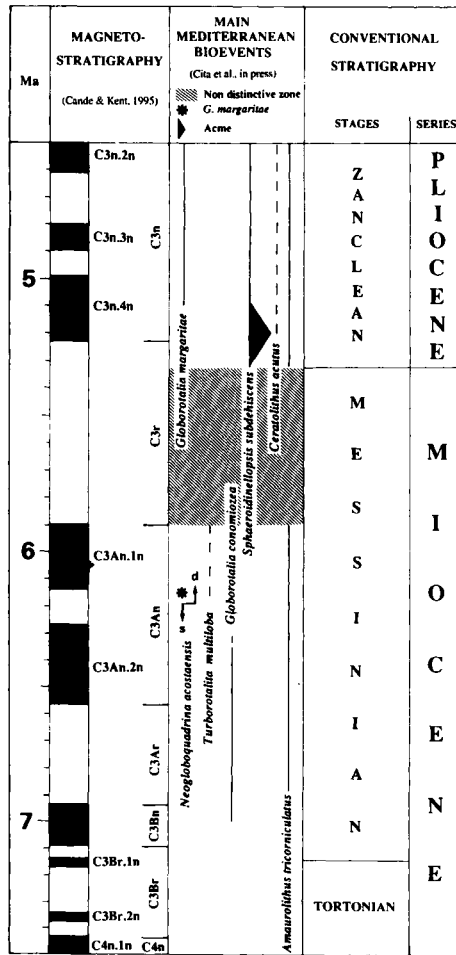


Fig. 1. Conventional status of the Miocene/Pliocene boundary with respect to the Mediterranean biostratigraphy and the modern magnetostratigraphic scale.

Subchron C3n.4n (Thvera) (Hilgen and Langereis, 1988; Langereis and Hilgen, 1991; Fig. 1). This represents a diachronism of about 1.3 Ma in spite of some isolated records in the lower Messinian Tripoli in Sicily (Colalongo et al., 1979a, b; D. Violanti, R. Sprovieri, oral commun.) (Fig. 1). Thus, there is no direct possibility of correlating the Mediterranean and the Atlantic stratigraphies using this biostratigraphic event.

The FAD of *Ceratolithus acutus* (calcareous nannoplankton) has been used also (Cita and Gartner, 1973), but the species is very rare in the Mediterranean Pliocene (Rio et al., 1984). This bioevent follows the Miocene/Pliocene boundary by about 0.1 Ma (early Subchron C3n.4n), such a difference being too large in comparison with the desired precision for the chronologic definition of the Miocene/Pliocene boundary (Figs. 1 and 2). In addition, a rare appearance of this species has been found near the Chron C3An/C3r boundary (Benson and Hodell, 1994), denoting a

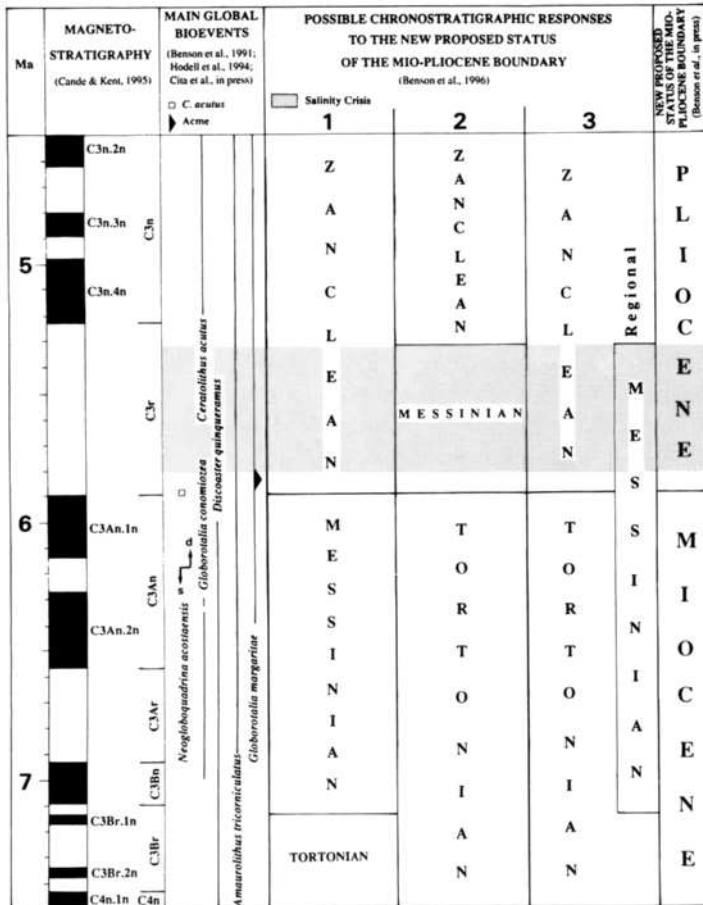


Fig. 2. The proposed new definition of the Miocene/Pliocene boundary and its inference on the Messinian Stage according to the recent chronologic location of the Salinity Crisis.

diachronism of about 0.7 Ma between the Atlantic and the Mediterranean.

There is no possibility to use the same biostratigraphic markers both in the Mediterranean and in the Atlantic for the recognition of the Miocene/Pliocene boundary. As a consequence, the present-day definition of the boundary in the Mediterranean region cannot have a worldwide significance. Two options are to be discussed: either to change the chronologic location (and the definition) of the boundary outside the Mediterranean, or to modify its definition (without changing its chronologic location).

THE PROPOSED NEW LOCATION OF THE BOUNDARY AT THE C3An/C3r CHRON BOUNDARY

This solution at the topmost Chron C3An, proposed by Benson et al. (1996) would present the advantage of a global significance of the boundary (Fig. 2). Indeed, the top of

Chron C3An.1n is relatively easy to determine in long, continuous sedimentary records, even without a detailed biostratigraphy. Such a definition of the boundary contains two major disadvantages: (1) there is no significant biostratigraphic event at the boundary level; and (2) according to its new magnetostratigraphic assignment in the early Chron C3r (Gautier et al., 1994), the Messinian Salinity Crisis would belong to the Pliocene (Fig. 2).

Three stratigraphic responses can be advanced to such a modified definition of the Miocene/Pliocene boundary (Fig. 2):

(1) To retain the Messinian Stage as the last stage of the Miocene. In this way, it would have a reduced duration, from about 7.0 to ca. 5.9 Ma, and would be separated from the Salinity Crisis which formed an integral part of its origin characterization. This would raise an erroneous situation vis à vis accepted stratigraphic principles.

(2) To transfer the Messinian Stage to the lowermost Pliocene (from ca. 5.9 to 5.32 Ma). It would then almost exactly correspond to the Salinity Crisis; this situation would give to the Messinian Stage a regional (i.e., non-global) significance.

(3) To delete the Messinian Stage from the global stratigraphic scale as already proposed by Berggren (1971), to become a regional stage. In that case the Tortonian would be the terminal stage of the Miocene, and the Zanclean the first of the Pliocene. The regional Messinian Stage would have exactly the same chronologic definition as at present.

It is clear that the main obstruction for solving the Miocene/Pliocene boundary question is the sedimentary hiatus in the Mediterranean caused by the Salinity Crisis.

#### DOES AN ACCURATE CHRONOLOGY OF THE MESSINIAN SALINITY CRISIS ALLOW A NEW DEFINITION OF THE CLASSICAL BOUNDARY?

An accurate chronology of the Messinian Salinity Crisis is proposed by Clauzon et al. (1996) (Fig. 3), who consider three newly gathered sets of data.

(1) The Salinity Crisis occurred entirely during the magnetostratigraphic 'quiet zone' Chron C3r (Gautier et al., 1994; Fig. 2).

(2) On the basis of new geomorphological observations, the evaporites can be separated into (older) marginal, including the Sicilian evaporites, and (younger) deep basin evaporites (Clauzon et al., 1996; Fig. 3).

(3) The astronomically calibrated  $\delta^{18}\text{O}$  curves of ODP Site 846 (eastern equatorial Pacific; Shackleton et al., 1995) and the Salé core (Morocco; Hodell et al., 1994) yield a ca. 20 ka subdivision of Chron C3r (Fig. 3). Twenty two isotopic stages (TG1–TG22) ran between Subchrons C3n.4n and C3An.1n. Some peaks (glacials: TG22, TG20, TG14, TG12; interglacials: TG15, TG11, TG9, TG5), offer a very similar feature in these distant regions and can be used as chronostratigraphic datums.

The Miocene/Pliocene boundary should be drawn at a stratigraphic level representative of a rise in sea-level, i.e., in correspondence with an interglacial peak. Peaks TG15, TG11 and TG9 cannot be selected because they are coeval with the Salinity Crisis and such a boundary would not have a global significance. In addition, they are devoid of any bioevent. Only peak TG5, which appears the most intense in the Salé section, occurred near the end of the Salinity Crisis. Its age is certainly very close to that of the lowermost Sicilian Trubi layers. The sudden Zanclean transgression

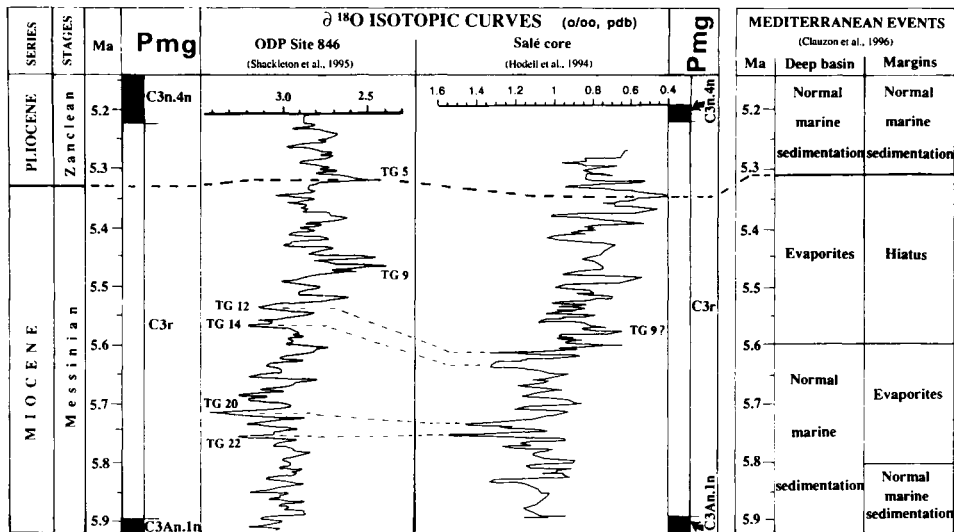


Fig. 3. Proposal for a newly defined Miocene/Pliocene boundary at 5.32 Ma, based on isotopic stratigraphy. Pmg = palaeomagnetism.

in the Mediterranean was probably caused by a global sea-level rise connected with a change in the tectonic activity in the Alboran Sea. Such a definition based on the isotopic stratigraphy needs a new intensive biostratigraphic effort both in the Atlantic Morocco and in the Mediterranean. The detailed study of dinocysts from the Bou Regreg section and in the reference Mediterranean sections could provide an appropriate response.

### THE ELECTION OF THE CORRESPONDING STRATOTYPE

The Bou Regreg section (including the Salé core) would appear to offer all the appropriate advantages to become elected as the Global Stratotype Section and Point (GSSP) for the Miocene/Pliocene boundary. Peak TG5 is easily identifiable in field (Rakic-El Bied, 1990; Hodell et al., 1994). This could constitute the reference section for the passage from the Messinian to the Zanclean in continuous sedimentary areas.

The Zanclean stratotype, in Sicily (the Capo Rossello section or the complementary Eraclea Minoa section), should offer a very precise datation of the base of the Pliocene considering the astronomic cycles.

We consider that the Carmona section (Guadalquivir basin, Spain), is inappropriate because an important unconformity seems to be present near the Miocene/Pliocene boundary in the boreholes cored in 1991 (Clauzon et al., to be published).

In conclusion, this proposal, characterized by the stability of the Miocene/Pliocene boundary, offers several advantages among which the most relevant are: (1) it preserves the historical argument in the Mediterranean where the boundary has a biostratigraphic basis; and (2) it provides a modern definition (isotopic stage) as well as a global significance to the boundary.

The question was greatly debated during the 10th RCMNS Congress (Bucharest, Sept. 1995) on the occasion of two meetings organized by Prof. M.B. Cita: the Workshop on the Miocene/Pliocene boundary and the session of the Subcommittee of Neogene Stratigraphy. At the end of these meetings, large consensus appeared among the members of the SNS despite any official decision. The Miocene/Pliocene boundary should be maintained at 5.32 Ma. R.H. Benson announced his intention to abandon the proposal to place the boundary at the top of the C3An.1n Chron and to investigate new biostratigraphic markers within the Bou Regreg section near isotopic stage TG5. In this way, we can conclude that our proposal (see above), presented at Bucharest, has been considered as the best solution.

## SOMMAIRE — LA LIMITE MIOCÈNE/PLIOCÈNE: PRÉSENT ET FUTUR

(Manuscrit soumis: Février 1995, révisé: Octobre 1995; rédacteurs responsables: AM et RC)

La définition chronostratigraphique de la limite Miocène/Pliocène correspond au rétablissement des conditions marines en Méditerranée après la 'crise de salinité messinienne'. La zone d'abondance de *Sphaeroidinellopsis* suivie de l'apparition de *Globorotalia margaritae* en Méditerranée marquent la limite en biostratigraphie.

La définition de la limite chronostratigraphique est une convention; son application globale est un problème qui fut discuté récemment par divers experts; les auteurs soulignent les principaux aspects de ce problème afin de conduire vers la meilleure solution pour le choix d'un point stratotypique dans un dépôt continu. Longtemps, le problème de la localisation de la limite a été circonscrit à la Méditerranée à cause de la 'crise de Salinité'. Mais l'étage a une validité globale par sa durée et la question doit être examinée dans cette optique globale.

Des progrès récents sur la stratigraphie intégrée à la fois en Méditerranée et au Maroc atlantique requièrent un réexamen du problème. Le diachronisme des biosignaux entre l'Atlantique et la Méditerranée est une difficulté fondamentale (par exemple on a estimé celui du biosignal apparition de *Globorotalia margaritae* à environ 1,3 Ma). Pour s'abstraire du problème biostratigraphique, 2 solutions ont été proposées: (1) faire correspondre la limite avec l'inversion N/I magnétostratigraphique C3An/C3r 'facile' à repérer; (2) faire correspondre la limite avec une élévation du niveau marin (un pic interglaciaire) dénoté par la courbe d'évolution des isotopes de l'oxygène. La seconde solution semble la plus appropriée, elle est seule compatible avec la chronostratigraphie traditionnelle du Messinien et du Zancéen. Le choix du niveau précis se porterait sur le pic TG5 de la courbe des isotopes de l'oxygène, particulièrement intense dans les séries du Maroc où le PSG pourrait être localisé. Ce niveau se situerait dans le quart supérieur de la magnétozone C3r.

(Sommaire proposé par les rédacteurs, GSO)

## ACKNOWLEDGEMENTS

The help of W.A. Berggren and M.-P. Aubry is highly appreciated in reviewing and correcting the paper.

## **Part B**

### **GEOLOGY OF THE TWO MAIN STUDY AREAS**

This Page Intentionally Left Blank

*Chapter B1*

**MIOCENE PALAEOGEOGRAPHY OF THE TETHYS OCEAN; POTENTIAL GLOBAL CORRELATIONS IN THE MEDITERRANEAN**

B. Vrielynck, G.S. Odin and J. Dercourt

**INTRODUCTION**

The two main areas where integrated stratigraphy has been applied to Miocene sediments, as reported in this volume, are Japan and the Mediterranean region. The former is connected to the Pacific super-basin, the latter is mostly related to the Atlantic super-basin. If correlation of sections between these two study areas were possible, then similar correlations might be practical on a global scale. This is of primary interest for proposal of global stratotype sections. Given the importance of pelagic fossils for the correlations, it is clear that correlation between the two study areas (and the global application of our study) will heavily depend on the possibility for continuous and easy faunal exchanges between Japan and the Mediterranean basin. The natural means for such exchanges would have been through the Tethys Ocean for which a recent synthetic reconstruction is available (Dercourt et al., 1993). This reconstruction will be used throughout this paper.

**HISTORY OF THE TETHYS OCEAN**

The palaeoenvironmental atlas of the Tethys Ocean by Dercourt et al. (1993) reconstructs the palaeogeographies of that ocean for the last 260 Ma. In agreement with previous reconstructions (Scotese and Mc Kerrow, 1990; Scotese, 1991), the maps show that the opening of the Atlantic Ocean during Jurassic time, is the primary factor in the break-up of the Pangea. The Tethys Ocean reaches its maximum extent during Cretaceous time.

From the Maastrichtian to the Present, the Tethys Ocean decreases in width. Circum-oceanic circulations are threatened in three regions: between Australia and Asia (present tropical connection between the Indian and Pacific Oceans), between Arabia and Asia (connection between the Mediterranean Tethys and Eastern Tethys — Indian — Oceans: Camoin et al. 1993) and between South America and North America (between the tropical Atlantic and Pacific Oceans). For example, between the Mediterranean Tethys and Eastern Tethys, ophiolites are obducted along the margin of Arabia and the remaining domains are subducting below the Pontids and Iran. In this region, the ocean becomes narrow; however, sea-water still flows from the Eastern Tethys to the Atlantic Ocean through deep basins.

Palaeoenvironmental maps for Cenozoic time illustrate, in part, the evolution of these connections (Fig. 1). The key area between the Eastern Tethys and Eastern



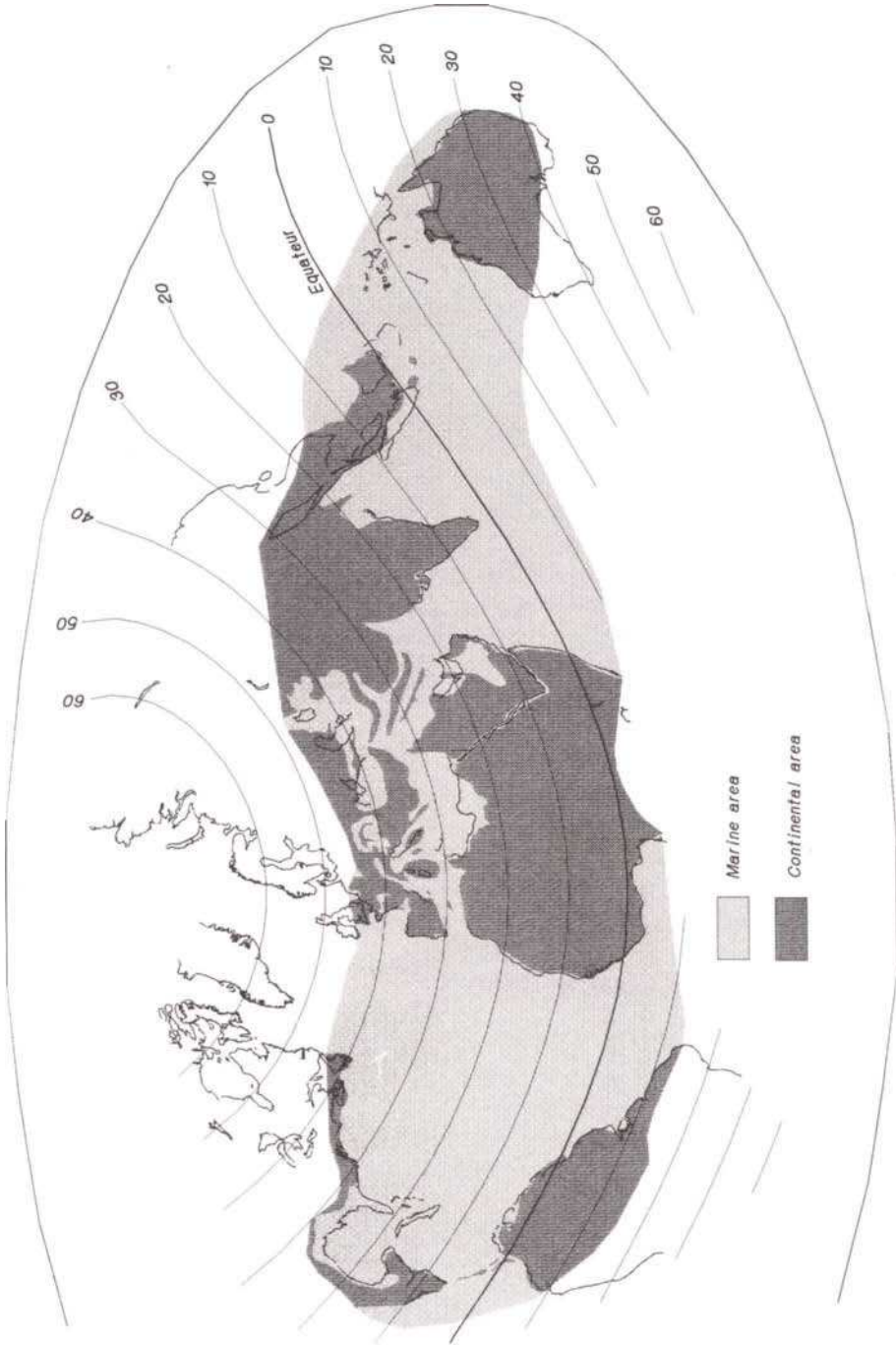


Fig. 1. General palaeoenvironmental map (late Burdigalian, about 18 Ma ago). Mollweide projection centered on 20°N. Adapted from data by Cavelier et al., 1993; reconstructed using original unpublished software of B. Vrielynck. Possible exchange of planktonic material is underlined by arrows, the sense of which is uncertain.

Mediterranean is the region where Arabia collides with Asia during Oligocene time. Yet in Rupelian time (Lorenz et al., 1993), this region shows no oceanic basin connecting the Mediterranean Tethys basin and the Indian Ocean, of which the northern portion is a remnant of the Eastern Tethys. The easternmost deep trough of the Mediterranean domain was very narrow and recorded deposition of the marls of the Pabdeh Formation (Borzonio et al., 1964; Sampo, 1969; Bizon et al., 1972). This trough did not reach the Indian Ocean. It was fringed to the north and to the south and it was closed to the east by a shallow carbonate platform which, in some areas, was emergent (e.g., Fars area according to Braud, 1989). During Miocene time, this landscape with marine and continental areas evolved toward a fully continental facies which disconnected the east and west portions of the Tethys. This resulted in poor faunal exchanges, and as a result, biostratigraphic correlations become difficult.

### MIOCENE HISTORY OF THE PACIFIC–INDIAN–MEDITERRANEAN–ATLANTIC CONNECTIONS

During the Miocene and up to the present time, the Pacific–Indian connection (Indonesian–Australian Lithospheric Seuil of Vrielynck et al., 1994) remained open in tropical latitudes. This area did not generally prevent longitudinal faunal exchanges. However, let us consider the streams (counter-clockwise streams to the north plus clockwise ones to the south of the Equator), and the distribution of land masses (Indonesian emerged blocks are known to have existed down to the Equator) at this seuil; due to dextral streams south of the Equator this combination of streams and land masses is presumed to favour the faunal exchanges from Indian to Pacific Ocean, better than the reverse way. Therefore, at this seuil, it is possible to imagine some sort of Equatorial stream-dependent barrier for surface waters which might have resulted in diachronism and endemism in the microfaunal record, while the geochemical properties of the oceanic masses would have remained homogeneous.

At the other tip of the Tethys, the west Atlantic–East Pacific connection (Caribbean Lithospheric Seuil of Vrielynck et al., 1994) had an influence on pelagic faunal exchanges due to the progressive closure of this seuil during Miocene time. In late Burdigalian time, the global sea-level was high, the area was under the northern tropical latitude, and the Caribbean Seuil was open in spite of the already building Isthmus of Panama. Faunal exchanges were possible mostly through tropical carbonate platforms which were, however, restricted in width. On the other hand, the counter-clockwise streams on both sides of the Isthmus would have favoured faunal exchanges from Atlantic to Pacific more than the reverse; this would have reinforced the effect of ‘isolation’ of the Pacific quoted above at the Indonesian–Australian Seuil leading to potential endemism of the planktonic faunas. Later in Tortonian time the sea-level was low and there is no longer sediment of an open marine character preserved in the area of the present Isthmus of Panama. A continental barrier is probable, at least during most of the Tortonian and younger times. In addition, it is known that mammalian faunas were able to cross the Isthmus Strait between North and South America in Tortonian time. Later in Messinian time, palaeogeographic data support the closure of the connection.

Concerning the Mediterranean Seuil, there were two (groups of) gates: the Mediterranean–Atlantic connection between Spain and North Africa (Alboran gate) which

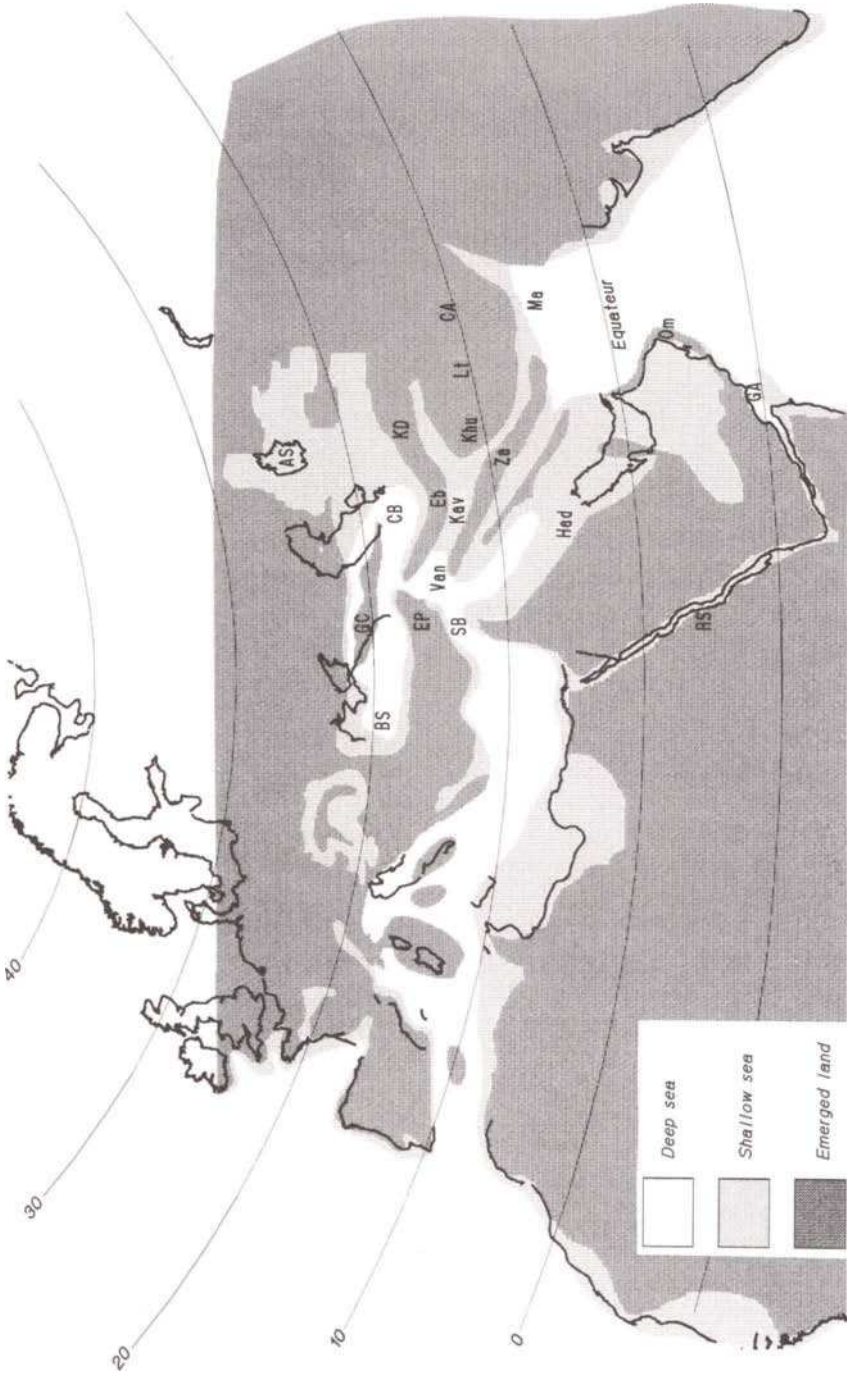


Fig. 2. Palaeoenvironmental map of the Arabian key area (late Burdigalian; about 18 Ma ago). Projection as for Fig. 1. Abbreviations: AS = Aral Sea; BS = Black Sea; CA = Central Afghanistan; CB = Caspian Basin; EB = Elburz; EP = Eastern Pontids; FA = Fars area; GA = Gulf of Aden; GC = Great Caucasus; HAD = Hadrukh; KAV = Kavir; KD = Kopet Dagh; KHU = Khur; LI = Lut; M = Moesia; MA = Makran margin; OM = Oman Mountain belt; RA = Razak Formation; RS = Red Sea; SB = Sivas Basin; VAN = Van area; ZA = Zagros. Note the possible marine exchanges through the Arabian gates.

was always more or less open up to the present time, and the Indian–Mediterranean connection (let us say the Arabian gates) which will be considered in the next section.

## PALAEOGEOGRAPHY OF THE INDIAN–MEDITERRANEAN CONNECTION

The probability of faunal exchanges can be deduced from examination of the two maps drawn for late Burdigalian and Tortonian times (Dercourt et al., 1993).

### *Burdigalian reconstruction (Fig. 2)*

The distribution of late Burdigalian palaeoenvironments (Cavelier et al., 1993) is significant for our purpose because the Neogene sea-level is at its maximum at the Early/Middle Miocene boundary (Haq et al., 1987). At that time, the Arabian block was in contact with Eurasia along the Zagros (Za) which was overthrusting. To the east, the remaining Tethys Ocean disappeared below Iran and Afghanistan (CA) along the Makran subduction zone (Ma). To the west, the East Mediterranean basin was similarly subducting below Eurasia. To the south, the opening of the Gulf of Aden (GA) was increasing and the volcanism of the Arabian coast of the Red Sea (RS) ceased (Brown et al., 1989). A complex palaeogeographic situation resulted from the marine transgression over the whole area as summarized below.

The Great Caucasus was emergent to the north of the Black Sea (BS) and Caspian Basin (CB), which were connected. The deepest-water deposits are fine-grained clastics and clays corresponding to more or less normal marine salinity conditions (Neveskaya et al., 1984). The surrounding belt of shallower deposits indicates a terrigenous shelf facies extending to the east as far as the Aral Sea (AS) where deltaic facies are observed. This Black Sea (BS) and Caspian Basin (CB) marine domain (Paratethys) was connected to the Eastern Mediterranean Sea by a corridor opened toward the Sivas Basin (SB), which is well documented by the marine deposits of the Lake of Van area (Van) as described by Erentoz and Oztemar (1964).

More to the south, a continental domain comprises Eastern Pontids (EP), Elburz (Eb), Kopet Dagh (KD), Khur (Khu), Lut (Lt) and Central Afghanistan (CA). This domain comprises intramontane basins filled by ‘red beds’ type deposits (Lang, 1975).

To the south of the above continental domain, there is an E–W marine corridor documented by locally reef-forming limestone facies. West of Kavir (Kav), this corridor is connected to the Qum Basin towards the northwest, and to the Indian Ocean eastward. The corresponding very shallow water channel disappears at the end of the Burdigalian. The Qum Basin also disappears at this time as shown by the deposition of the ‘Upper Red Beds’.

To the south, the Zagros area (Za: Reyre and Mohafez, 1970) emerged and a tectonic zone begins south of the Zagros where it thrusts over the Arabian Platform. This platform is covered by shallow platform carbonate to the north and the east with terrigenous components in the vicinity of the tectonic contact.

Increased uplift and erosion of the western and southern domains of the Arabian Shield and the Oman mountain belt (Om) led to detritus accumulation (Hadruk-Had Formation, Powers et al., 1966; Ghar Formation, Milton, 1967) that restricted the extent of the carbonate platform. To the east and southeast, the uplift of the Oman mountain

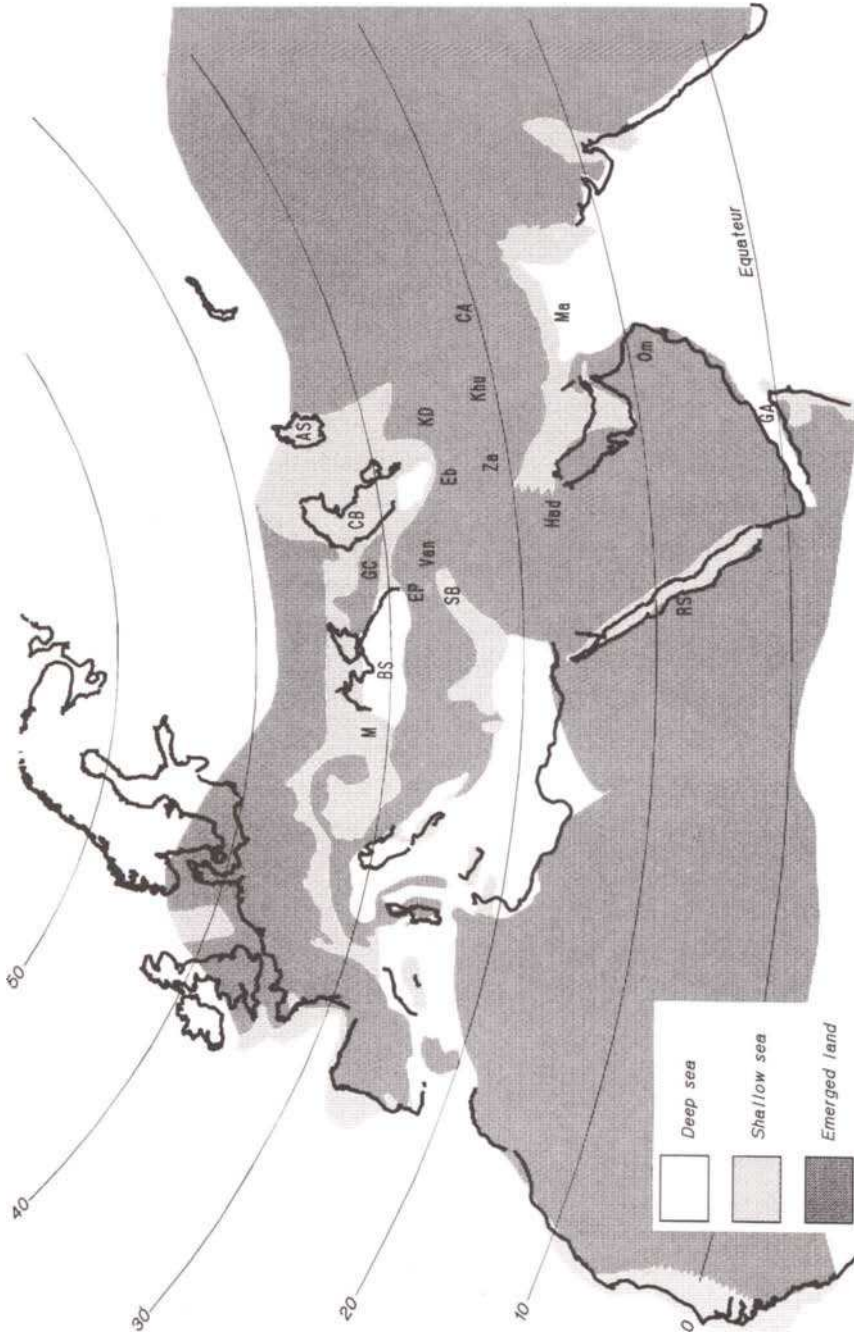


Fig. 3. Palaeoenvironmental map of the Arabian key area (Tortonian). Adapted from data by Orszag et al., 1993; Projection as for Fig. 1. For abbreviation see Fig. 2. Note the stop of possible marine exchanges between the Mediterranean and the Indian Ocean through the Arabian gates. Note also the reduced gates between the Mediterranean and the Atlantic Ocean.

(Om) acts as a morphological barrier between this platform and the slope towards the Indian Ocean. However, a local link with the Indian Ocean is documented by the Razak Formation (Ra) which accumulated to the south edge of the Zagros area (James and Wynd, 1965). On the western and southern parts of the Arabian Shield, along the Red Sea (RS) and the opening Gulf of Aden (GA), a fringe of platform carbonates denotes an additional continuous passage from the Indian Ocean to the Mediterranean Sea.

In short there are three Indian–Mediterranean sea-ways open: the Kavin–Makram corridor, the South Zagros–North Arabian Platform corridor, and the Red Sea–Gulf of Aden corridor.

#### *Tortonian reconstruction* (Fig. 3)

The distribution of the Tortonian palaeoenvironments is significant for our purpose because the sea-level is at one of its lowest stands of the Miocene (Haq et al., 1987). The plate organization is similar to the present-day one and the advanced collision within the Mediterranean Tethys resulted in the sealing of this previously major sea-way. The main marine facies are flysch and molasse deposits (Orszag-Sperber et al., 1993).

The domain which appears now as the Middle East was essentially characterized by a continental environment. To the north, the previously wide marine area was then restricted to the Black Sea (BS) and Caspian Basin (CB). From the Moesia (M) to the Aral Sea (AS), evaporites or lacustrine deposits accumulated in depressions abandoned by the previous sea (Ricou et al., 1977; Braud, 1989; Wang et al., 1992).

Further to the south, emerged lands were predominant from the Eastern Pontids (EP) to Central Afghanistan (CA). Continental deposits accumulated there on braided alluvial plains and in large lacustrine basins. In some of these basins such as the Sivas Basin (SB), continental marl, limestone, and coal can be observed with conglomerate and sand. The connection between the Paratethys and Eastern Mediterranean had vanished by this time.

South to Zagros (Za), between the Arabian-Persian Gulf and Eastern Mediterranean, land drainage led to alluvial fan deltaic deposits filling gulfs located in the present Turkey area (Bizon et al., 1972; Akay et al., 1985). To the east, the drainage flowed toward the Makran margin (Ma). Active rifting followed on the western margin of the Arabian Plate (Purser et al., 1986; Jarrige et al., 1986; Montenat et al., 1986).

To the south of Arabia, the previous Red Sea–Gulf of Aden corridor was closed. The main deposits were salt; however, rare shallow-marine deposits are known from the Ethiopian and Yemeni regions suggesting a short connection with the Gulf of Aden (GA) which was characterized by deep-marine conditions.

In short the three Indian–Mediterranean sea-ways quoted above were closed.

#### APPROPRIATENESS OF MEDITERRANEAN OUTCROPS FOR SELECTION OF STRATOTYPE SECTIONS

As will be shown in this volume, some outcrops from the present Mediterranean area contain appropriate sediments for multi-method stratigraphic characterization. In light of the above reconstruction, it is possible to comment on the a-priori appropriateness of these outcrops for selection as stratotype sections. If one looks for a global use of

stratotype sections, potential faunal exchanges are of major importance for the use of biostratigraphical correlation tools, and oceanic circulation is necessary for application of chemostratigraphical correlation tools.

The above description indicates that Mediterranean outcrops will be a priori appropriate for locating GSSPs for the Early Miocene stages. The Caribbean and Indonesian–Australian Seuil were open. In addition to the Alboran gate, the longitudinal corridors of the Arabian–Asian key area were also open; they were located in tropical latitudes and the same pelagic faunas were able to circulate from the Indian to the Atlantic Ocean. In general, chemical equilibration was insured through rather deep-water corridors but planktonic faunal endemism may have existed in the Pacific Ocean.

One may infer that, during Middle Miocene time, the situation was less favourable with the Arabian gates closing quickly, an Alboran gate still open, and a Caribbean Seuil progressively closing. In this situation, connection with the Pacific became more and more difficult; faunal diachronism became possible between the Japanese and the Mediterranean areas. If faunal exchanges occurred as long as surface water circulated at least from time to time, the problem becomes more important for geochemical characteristics. Elementary and isotopic equilibria will have been lost as soon as the Mediterranean Sea became a cul-de-sac. To the west, at the Alboran gate, a selection of elements and isotopes coming from the Atlantic Ocean may have begun to occur. But, more clearly, the influence of regional factors increased because, within this tectonically active area, the abundant material brought to the sea modified its composition before equilibrium could have been reached through the narrowing Alboran gate.

During Late Miocene time the situation became worse ... for stratigraphers. Planktonic faunal exchanges were still possible between the Atlantic Ocean and the Mediterranean during Tortonian time. The environmental problem was important during Messinian time with sea-water composition and salinity becoming specific. Faunas similar to the Atlantic were still able to be present at least at times when salinity was consistent with their life conditions (at the Tortonian/Messinian boundary) but the geochemical equilibria with the open Ocean were no longer possible, making the Mediterranean an area of poor potential for geochemical global correlation.

## CONCLUSIONS

Thanks to palaeogeographic reconstructions we may suggest that outcrops from inside the Mediterranean appear a priori favourable for location of GSSPs and to provide precise definition of Early Miocene Stage boundaries. For younger stage boundaries the appropriateness of the area progressively decreases and finally becomes quite poor for some correlation tools, with firstly a probable loss of the global-scale utility of the chemostratigraphic study as soon as in Mid-Miocene time and, later on, a loss of biostratigraphic correlatability at least in Messinian time.

In this situation, and for younger stage boundaries, the quality of stratigraphic tools not sensitive to the progressive closure of the Mediterranean area (e.g. magnetostratigraphy for plurivocal tools and geochronology for unequivocal tools as defined by Odin and Odin, 1990) should be considered more carefully than for older stages. Good data will become essential in these fields. When sections within the Mediterranean area will be considered for proposal of GSSP of Late Miocene Stage boundaries, it is suggested that

comparison with and examination of nearby outcrops from the open Atlantic domain be considered for a better guarantee of the significance of the correlation tools applied and significant application of the biostratigraphic and chemostratigraphic correlation criteria.

## SOMMAIRE — PALÉOGÉOGRAPHIE MIOCÈNE DE LA TÉTHYS; POTENTIEL DE CORRÉLATION GLOBALE DE LA RÉGION MÉDITERRANÉENNE

*(Manuscrit soumis: Novembre 1994; révisé: Mai 1995; rédacteur responsable: GSO)*

La connaissance de la paléogéographie de la Téthys a fait des progrès récemment. Nous avons utilisé les données rassemblées dans l'Atlas Téthys pour tenter d'estimer les qualités des profils destinés à abriter des points stratotypes globaux dans la région méditerranéenne. Pour le Miocène, la qualité de ces points dépend de façon cruciale des échanges possibles dans la Téthys à l'échelon mondial. L'histoire des trois seuils lithosphériques: Indonésien, Méditerranéen et Caraïbe, de l'est vers l'ouest, est déterminante à la fois pour les échanges de faunes planctoniques utilisées lors des corrélations biostratigraphiques et pour les équilibres géochimiques considérés lors des corrélations chemostratigraphiques. Encore ouvert au Miocène inférieur, le Seuil Méditerranéen se ferme à l'est au Miocène moyen et les eaux de la Méditerranée se confinent au Miocène supérieur. Pour ces raisons, les divers outils géochimiques, dès le Miocène moyen et l'outil paléontologique, au Miocène supérieur, donneront des informations susceptibles d'être déformées par des influences régionales entraînant des problèmes de corrélation avec l'Océan global. Dans cette mesure, il deviendra important que les autres outils plurivoques (magnétostratigraphie, séquences de dépôt) et l'autre outil univoque (géochronologie) suppléent aux déficiences notées. La possibilité d'utilisation de ces derniers outils de corrélation est donc cardinale pour que les coupes méditerranéennes soient favorables pour abriter des points stratotypes d'application globale.

*(Sommaire des auteurs)*

## ACKNOWLEDGEMENTS

The authors and editors acknowledge the help of Dr. Paul Myrow (Colorado College at Boulder) who kindly improved the language of this paper.



This Page Intentionally Left Blank

Chapter B2

**TECTONIC SETTING OF THE MIOCENE NORTHERN APENNINES: THE PROBLEM OF CONTEMPORANEOUS COMPRESSION AND EXTENSION**

G. Pialli and W. Alvarez

INTRODUCTION

The sedimentary rocks of the Northern Apennines (hereinafter NA, see Fig. 1) contain a wealth of stratigraphic information about the Miocene Epoch which is relevant to Earth history on a global scale. To understand the deposition of these sedimentary rocks requires an investigation of the tectonic evolution of the NA, which leads to questions and interpretations relevant to tectonic questions on a global scale

The Alps–Apennines system is forming in the broad context of collision between the irregular fronts of Africa and Europe, an ongoing polyphased process of suturing which began in the Cretaceous. The Alps developed, beginning in the mid-Cretaceous, as a direct result of this suturing and display, from bottom to top, a tectonic sequence of (1) European continental crust and cover, (2) remnants of Tethyan oceanic crust, oceanic sediments and microcontinental fragments, and (3) Italian continental crust and

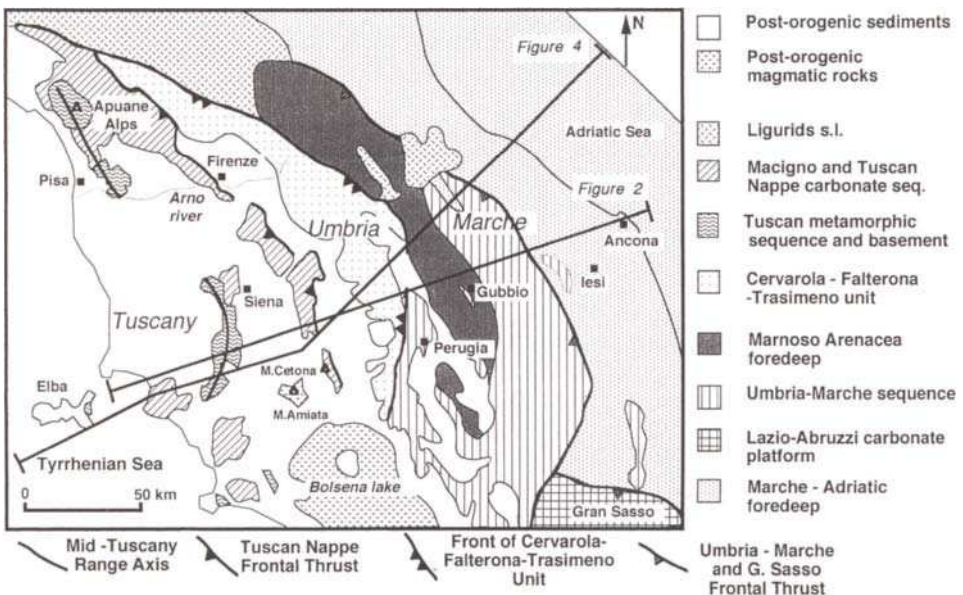


Fig. 1. Simplified tectonic map of the NA region showing the principal tectonic units and their frontal thrusts. The locations of the profiles of Figs. 2 and 4 are also shown.

its cover, representing the leading edge of Africa. It is generally accepted by Alpine geologists that this pile resulted from the subduction of the Ligurian–Piedmont oceanic crust underneath the African plate along one or more south- and southeast-dipping planes.

The history of the NA partially overlaps that of the Western and Central Alps and has strong similarities with the evolution of the Southern Alps (Alvarez, 1991).

After the Ligurian phase of the Lower–Middle Eocene, which corresponds to the mesoalpine deformations of Corsica and the Western Alps, the NA mountain chain has developed since Late Oligocene–Early Miocene times as the front of the African plate has collided with the already formed Alpine chain, acting as a wedge and causing its backthrusting over the Italian continental margin.

This wedging occurred as an obductional response to a new subduction, now following a west- and northwest-dipping plane (as indicated by calc-alkaline volcanism in western Sardinia and southern France), concurrently with the rotation of the Corsica–Sardinia block. Thus the tectonic pile of the NA consists of (1) Alpine units at its top (Schistes Lustrés and crystalline nappes), (2) oceanic crust and pelagic sedimentary cover (Ligurids *sensu lato*) in the middle and (3) African continental crust with its basement and cover (Tuscan and Umbro–Marchean units) at the bottom.

During the Miocene and Pliocene the NA orogenesis propagated toward the Adriatic foreland, generating foredeeps that were progressively incorporated in the tectonic pile. The present-day Adriatic Sea is the expression of the latest foredeep, now in the making.

A major problem in understanding the NA arises because this fold-and-thrust belt is still actively advancing toward the Adriatic Sea, but is no longer being pushed from behind by the Corsica–Sardinia microplate. In fact, there is a wave of compressional deformation, moving northeastward, followed by a wave of extension. The leading belt of compression currently runs along the Adriatic offshore while extension characterizes all the region between the Tyrrhenian Sea and the main Apennine divide. This pattern of coupled compression and extension seems to have endured from the Middle Miocene (or Early Miocene, beginning in the Corsica basin, according to Carmignani et al., 1994) to the present, and it is difficult to see what would drive the fold-and-thrust belt forward while extension is going on just to the rear.

In the present paper we review existing and new geophysical data on the NA, summarize the geological history, and propose a deep crustal and mantle behaviour which could account for the contemporaneous extension and compression.

## GEOPHYSICAL DATA

### *Gravimetric, aeromagnetic and heat flow data*

Bouguer and free-air gravity anomalies display positive values, although not uniformly distributed, all over the northern Tyrrhenian Sea (NTS) and western Tuscany, while the Po Valley and the Romagna–Marche Apennine foothills show strong negative values. Still farther east, in the northern and central Adriatic, values trend to rise and become positive again (Fig. 2). The transition from western, positive, to eastern negative values occurs in a narrow strip which includes the zero-mGal contour, where the decrease is more than 100 mGal. This strip is arc-shaped with an eastward convexity,

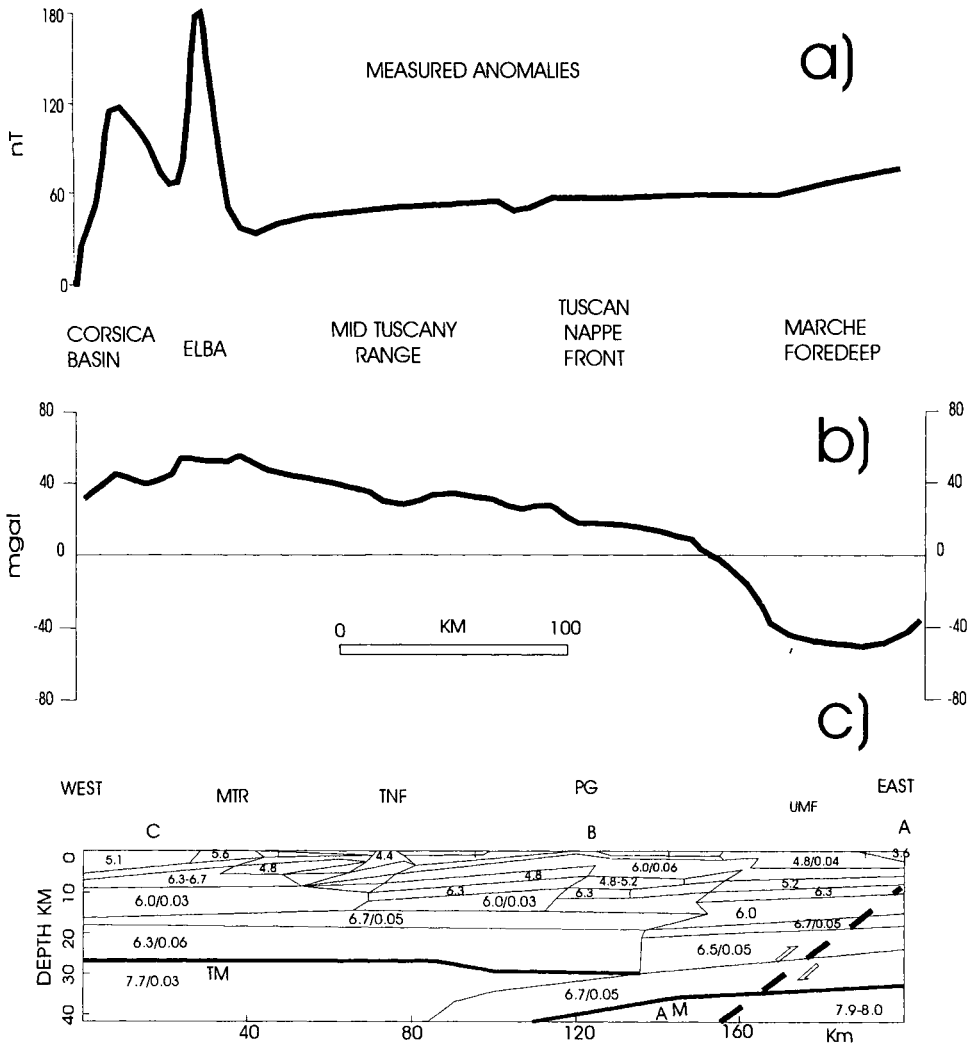


Fig. 2. Aeromagnetic (a), gravimetric (b), and seismic refraction (c) profiles across the NA from the Tyrrhenian coast to Ancona. Vp values in km/s, gradients in  $\text{km s}^{-1} \text{km}^{-1}$ . Heavy dashed line on the right marks the plane where 'deep' compressive earthquakes occur (see Fig. 3E). TM = Tuscan Moho; AM = Adriatic Moho. A, B, C = shot points; (a): after Cassano, 1991; (b): after Cassinis et al., 1991; (c): after Ponziani et al. 1994, modified.

and runs roughly parallel to the main Northern Apennine Ridge. The transition to the positive values of the Adriatic Sea from the negative ones of the Apennine foothills is less abrupt.

A recent interpretation of the gravity anomalies (Cassinis et al., 1991), integrated with other geophysical and geological data, attributes the positive values of the northern Tyrrhenian Sea (NTS) and Tuscany to an asthenospheric uplift, initiated since the Middle Miocene, that stretched the lithosphere, particularly the lower crust, and probably led to

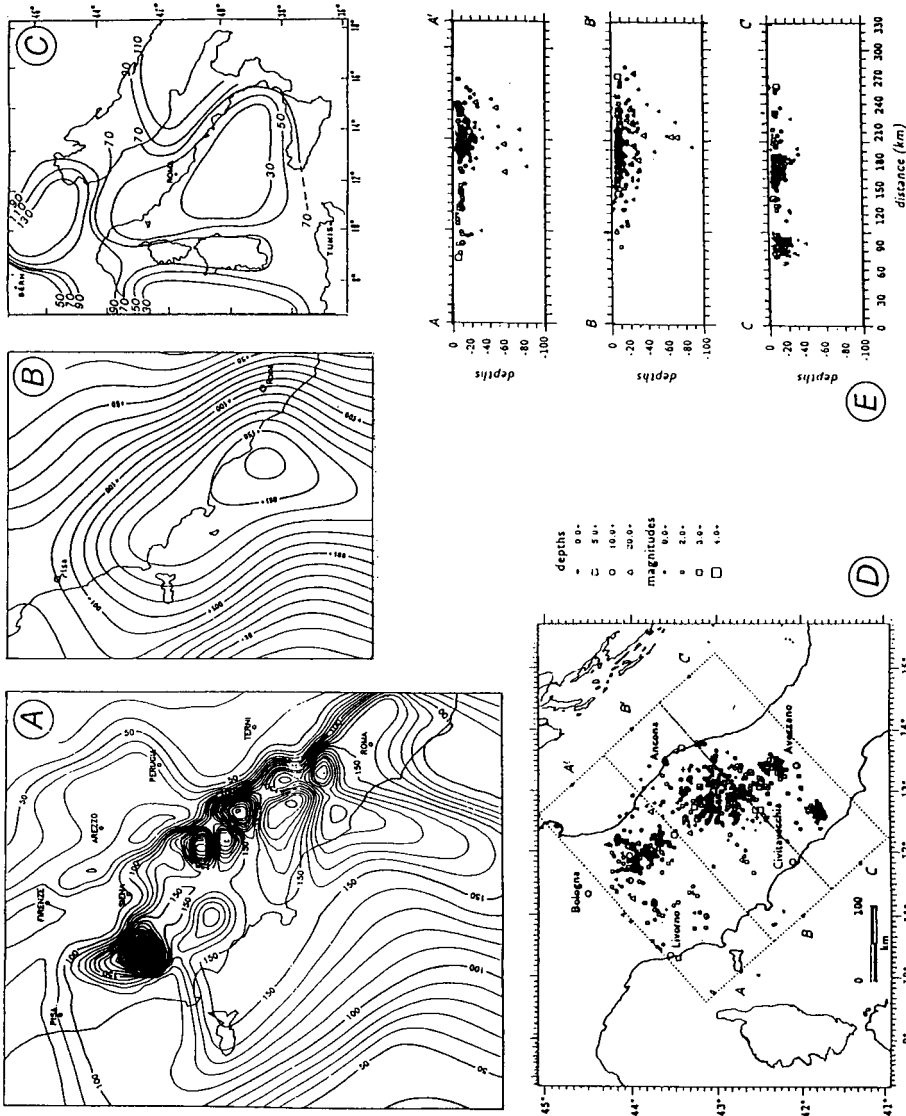


Fig. 3. Heat flow, lithospheric thicknesses and seismicity of the NA region. (A) Map of the observed heat flow and (B) of the corresponding regional heat flow, using a filter of 150 km wavelength. Values in  $mW/m^2$ , after Mongelli and Zito (1991); (C) map of lithospheric thicknesses (in km) around the Tyrrhenian Sea, after Calcagnile and Panza (1980); (D) map of epicentres and (E) profiles showing 'deep' earthquakes occurring along a west-dipping plane underneath the NA, after Amato and Selvaggi (1991).

the formation of a new Moho. These authors interpret the transition zone from positive to negative anomalies as the expression of a crustal doubling of regional extent caused by compressive stresses in Late Miocene–Pliocene times.

The magnetic anomaly map (Agip, 1983) shows high positive values all over the northern Tyrrhenian Sea, with a long, intense anomaly (around 200 nT) corresponding to the Gorgona–Pianosa Ridge (Fig. 3), and positive values in the northern Adriatic offshore as well. In between the two areas the magnetic field is gently sloping, with values rising gradually from 40 nT at the Tuscan coast to 80 nT in the Adriatic. Evaluations of these data (Cassano, 1991; Bartole et al., 1991), along with seismic lines and dredgings in the Tyrrhenian Sea, stress the correspondence of the positive peak of the Gorgona–Pianosa Ridge to the Alpine units of Schistes Lustrés and make it possible to interpret this positive anomaly as the uppermost tectonic unit of the Apennine pile.

Magnetic data also distinguish (Cassano, 1991) the basement of the Marche–Adriatic region (medium magnetic susceptibility) from that of Tuscany–Umbria (low magnetic susceptibility) and suggest that both were involved during compressive phases.

The map of observed heat flow (Fig. 3) in the NA and northern Tyrrhenian Sea (Mongelli and Zito, 1991) shows peaks of anomalously high values (concentrated in the geothermal fields of Larderello, Monte Amiata, Alfina and other centres of the Roman Magmatic Province) aligned along an Apennine trend and lying inside the 100-mW/m<sup>2</sup> contour line which encompasses all the eastern side of the northern Tyrrhenian Sea, almost all of Tuscany, and the northwestern part of Latium (Fig. 3A). The regional field of the heat flow, derived from that map, smoothes the peaks and shows a plateau of high values (more than 90 mW/m<sup>2</sup>) centred in the Tyrrhenian area, elongated NW–SE, with a steep northeastern flank running from about Rome to Pisa and more gently dipping flanks on the other sides (Fig. 3B). Most of this heat flow is thought to have an asthenospheric origin and to be the result of asthenospheric uplift and lithosphere stretching which occurred about 6 Ma with a beta factor of around 3 (Mongelli and Zito, 1991). It is not clear how the stretching is partitioned between the crust and the rest of the lithosphere. Recent geologic data of areas around the western part of the NTS (Bartole et al., 1991), however, show that stretching began earlier than 6 Ma, in the late Burdigalian–Langhian (around 15 Ma); in that case, the present measurements of the heat flow indicate that the corresponding beta value of lithospheric stretching is 4, a value which seems unrealistic.

It is interesting to note that the boundaries of the high heat flow plateau in NA and NTS almost match those of areas where the lithospheric thicknesses of the Apulian plate (Fig. 3C) are attenuated (Calcagnile and Panza, 1980). In addition, the sharp northeast boundary of the high heat flow plateau runs almost parallel to, and about 70 km in the rear of, the steep slope of the gravimetric gradient which separates the regions with positive and negative anomalies.

#### *Active and passive seismic data*

The Northern Apennines were actively explored by deep seismic refraction profiling (DSS) in 1974 and 1978 (Letz et al., 1977; Wigger, 1984). A recent complete revision of the 1978 data and of part of the 1974 data, based on converting analog to digital data (Ponziani et al., 1994) shows that the crust of the NA includes, from the Moho upward,

two pairs of layers, with each pair displaying a velocity inversion (Fig. 2c). The lower pair has a low-velocity layer (6.4 km/s) overlain by a high-velocity layer (6.7 km/s). The upper pair has again a slow layer (6.2 km/s) at the base overlain by a faster layer of 6.7 km/s. The thickness of the entire crust is about 25 km across the Tuscan sector, reaches 35 km in the pre-Apennine foothills and decreases again to about 30 km around the Adriatic coast. Rocks of the upper mantle in Tuscany have a slower velocity than the equivalent rocks of the Adriatic sector (7.8 vs. 8.0 km/s). Across the geothermal field of Larderello, both upper mantle and crustal rocks show a decrease of 10% in velocity in a zone about 50 km in diameter.

The region where crust has its maximum thickness displays two Mohos which overlap over a width of more than 30 km. The upper Moho continues to the west, by means of a small step, into the Moho of Tuscany, which stands in a higher position, while the lower Moho is continuous with the Adriatic Moho. This Moho doubling is the result of an east-verging crustal thrust and shows that the footwall rocks of the Adriatic lower crust dip westward and extend down to at least 40 km, the depth to which information is available.

In central-western Tuscany and in the NTS both mantle and lower-crust rocks display anomalously low values of compressional velocity. In this area Bouguer anomalies are positive and the regional field of heat flow has its plateau of high values. In addition, magmatic activity since 6.2 Ma (15 Ma, considering eastern Corsica), testifies to the presence of magma sources at depth (Serri et al., 1991). These observations suggest that in Tuscany and the NTS an asthenospheric uplift in an extensional regime occurred along with a strong asthenosphere–lithosphere interaction which could have affected the old Apulian Moho and transformed it, so that the present Tuscan Moho is completely new (Cassinis et al., 1991).

The 1974 data led Letz et al. (1977) to hypothesize the existence of an east-dipping European Moho which, from Corsica, reaches the depth of about 60 km in the area of Elba Island, underneath a Tuscan Moho about 25 km deep. This overlapping was thought to be caused by a lithospheric west-verging, 'Alpine' thrust. Revision of those data (Ponziani et al., 1994), although not yet complete, seems to preclude the presence of a European Moho at 60 km depth and an overlapping of the two Mohos for more than 40 km, but does not preclude a partial Moho doubling. If so, to satisfy ray-tracing models, the European Moho, starting from Corsica, should dip very steeply eastward below the Tuscan Moho, ending up at the longitude of Elba Island, because no trace of it has been found under mainland Tuscany.

Passive seismic studies of the NA region yield data on two topics: seismic tomography and seismogenic zones. Spakman (1986) first recognized the existence of cold, fast and deep lithospheric bodies beneath all of peri-Adriatic mountains. A recent study by Amato et al. (1991) confirms that underneath the NA a high-velocity anomaly is present which reaches a depth of about 200 km. In a two-layer model of the Italian Peninsula, this fast anomaly is seen to coincide with the Apennine arc from the Western Alps to Sicily, bordered on the east and south by a slow anomaly which corresponds to the thickened crust of the external foredeep basins. A more elaborate five-layer model confirms the positive anomaly and shows that it deepens towards the southeast along the peninsula and ties into the active seismicity of the Aeolian arc. These data agree with independent seismological data coming from surface wave dispersion (Suhadolc

and Panza, 1989) and imply the existence of an active or remnant subducting slab of continental lithosphere beneath the entire Apennine system.

Most of the NA seismicity is of crustal origin and occurs at depths of less than 15 km (Fig. 3D). A seismic macrozonation of this region (Amato and Selvaggi, 1991) shows: (1) an inner area (western and central Tuscany) with very shallow (less than 7 km), weak seismicity, extensional in character, in some cases associated with volcanism; (2) an Apennine ridge area with strong earthquakes (7–15 km deep) showing extensional or transtensive focal mechanisms; and (3) a peri-Adriatic area where strike-slip and thrust fault-plane solutions prevail. In geodynamic terms this zonation means that at the present time two adjacent sectors of the Apennines: the western, from the Tyrrhenian Sea to the Apennine ridge, and the eastern, including the foothills and the Adriatic coast area are simultaneously subjected to extension and compression, respectively.

Underneath the Northern Apennines there is also a well documented subcrustal seismicity (Fig. 3D). According to Amato and Selvaggi (1991) it occurs below the Apennine ridge down to a depth of about 90 km, with foci roughly aligned along a westward-dipping plane, inclined 45°, which can be traced from the Adriatic coast to the Umbrian and Tuscan pre-Apennines. This plane is deeper and placed further toward the foreland than the one responsible for the Moho doubling underneath the Umbrian and Tuscan pre-Apennines. Although ill defined, due to their low magnitude, these earthquakes show thrust focal mechanisms (A. Amato, pers. comm., 1993). This kind of seismicity is completely absent in central and western Tuscany. In a vertical section across the Apennine ridge (Fig. 4), therefore, there are two seismogenetic zones acting simultaneously: (1) a crustal zone (less than 15 km deep) which accommodates extensional processes, and (2) a deep, subcrustal or lithospheric, zone (reaching 90 km), which is due to compressive stresses.

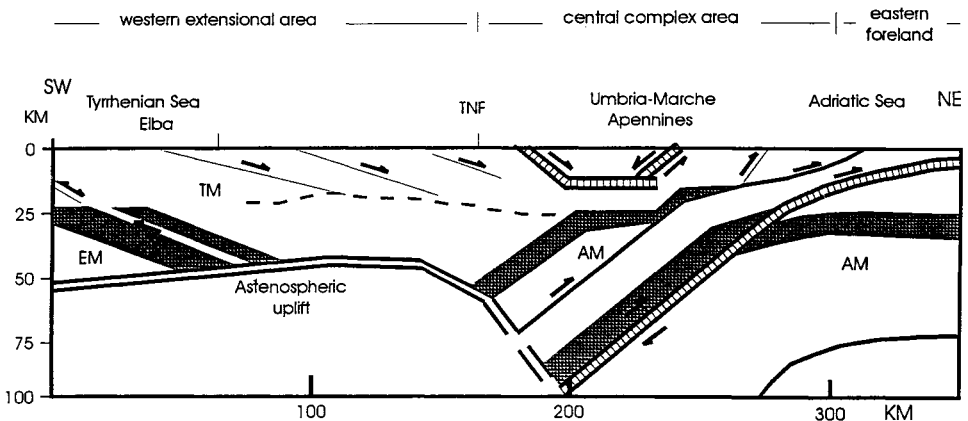


Fig. 4. Present geodynamic model of the NA region in a cross-section from the Corsica basin to the northern Adriatic Sea. Double lines mark structural elements presently active, single lines refer to fossil elements; grey indicates lower crust. EM = European Moho; TM = new Moho of the northern Tyrrhenian Sea and western Tuscany; AM = Adriatic Moho.



### *Geologic consequences of the geophysical data*

To synthesize the regional geophysical data of the NA and surrounding areas, it is useful to consider a geotraverse, running from eastern Corsica to the northern Adriatic Sea (Fig. 4) and crossing all the structural provinces of the NA chain, south of the Arno river, from the hinterland to the foreland. In that section there are the following three major structural provinces:

(1) A western area consists of the NTS and central-western Tuscany. Here crust and lithosphere are very thin, the asthenosphere is uplifted and the dominant dynamic processes are extensional in character.

(2) A central, complex area is composed of the NA ridge, including the pre-Apenines and the foothills. Here crust appears to be thickened by thrusts which occurred in the recent past bringing the lower crust of the footwall down to an estimated depth of more than 40 km, and the lithosphere displays deep, almost vertical roots. Geodynamically this large province is characterized by extensional and transtensive processes in its upper part (less than 15 km deep) and by compressional processes from there down to a depth of about 90 km.

(3) An eastern foreland province lies to the east of the Adriatic coast with both crust and lithosphere showing normal thicknesses. This province is linked to the central area by the westward-dipping plane where 'deep' earthquakes occur.

This cross-sectional pattern implies several geological consequences. Among them, we stress the following:

(1) Most of the original lithospheric base of the crust of the western area has subsided and rolled back eastward so that it now lies beneath the NA and has been replaced by the new thin lithosphere of the NTS and western-central Tuscany.

(2) The asthenosphere intrusion of western Tuscany cannot have commenced earlier than the late Burdigalian because before that period the Apulian lithosphere was actively subducting under the Corsica–Sardinia microplate, as calc-alkaline volcanism of that area shows; the Sisco basic dyke (Serri et al., 1991) seems to mark, at 15 Ma, the beginning of asthenospheric intrusion and of the extensional processes that led to the present Tyrrhenian Sea.

(3) If the northern Tyrrhenian lithosphere began to stretch 15 million years ago and the present heat flow values are correct, then, as noted before, the corresponding beta value (Mongelli and Zito, 1991) based on McKenzie's equations is 4, not 3. This result is hardly credible because it means that, assuming the present crustal thickness of 25 km in Tuscany is correct, before extension it was about 100 km (i.e. twice the present thickness of the Alps) with no substantial indication of an emerging thrust belt, since the Epiligurid sequences (top of Apennine pile) are formed by marine sediments. Either the stratigraphic and experimental data are not correct (which seems unrealistic) or the method for calculating the beta value is inadequate for the Tyrrhenian–Tuscany region (which is again improbable), or the thermal and extensional history of this area has to be re-evaluated.

(4) Of the several deformational events that affected the NA, only those that occurred before 15 Ma were accomplished during active subduction; the others occurred while the Apulian lithosphere was retreating and rolling back toward its present position. To explain these other events we have to search for a mechanism different from pure subduction.

(5) There is no doubt that during the compressive events the lower crust and upper mantle were involved; the lower crust of the footwall of each thrust system (along with the uppermost part of the mantle) underwent a process of delamination and was carried at least to a depth of 40 km. The concept of a single regional monocline applied to the NA chain (Bally et al., 1986) needs a correction since geophysical data show that in the area between the pre-Apennines and the Adriatic coast there are two deep thrust systems. Rather it seems reasonable to hypothesize that a few deep thrust systems have contributed to the construction of the NA (Ponziani et al., 1994) and that these systems were active in sequence.

(6) If we apply the present geodynamic scenario of the NA to their post-early Burdigalian history, then for each tectonic phase we have to conclude that, while extension took place at upper crustal levels, in a given place compression was going on underneath. This means that extension and uplift took place in the upper plate, in the hanging wall of a deep-seated thrust fault that involved upper mantle and lower crust, while the thrust itself was acting. In the case of the Elba–Mid-Tuscany Range (and, probably, the Apuane Alps), we conclude that extension began there when the adjacent thrust (toward the foreland) was active, and exhumation of the metamorphic core occurred during the hanging-wall uplift caused by the movement of the thrust itself. Elba and the Mid-Tuscany Range therefore cannot be considered true metamorphic core complexes, *sensu* Basin and Range, because extension in that case post-dates compression. This concept of the NA belt implies that the transport of the Ligurids toward the foreland occurred mainly by means of extensional processes in the hanging wall of deep-seated thrusts. In modern terms, this corresponds to Merla's (1951) idea of the orogenic landslides.

#### STRATIGRAPHY OF NORTHERN APENNINES MIOCENE FORELAND BASINS AND RELATED COMPRESSIVE PHASES

Three major foreland basin sequences have been deposited in the NA on the continental crust of the Apulian plate (Fig. 1): (1) the Macigno, which includes the Falterona–Trasimeno tectonic unit (Late Oligocene to Early–Middle Miocene); (2) the Marnoso–Arenacea (Burdigalian–Tortonian); and (3) the Marcheana–Romagnan foredeep sequence (Messinian–Pliocene). Each has developed in a system with a tectonic nappe pile at the rear and a peripheral bulge in front. This system has migrated progressively toward the Adriatic foreland during the Neogene, reducing the Adriatic Sea to the present narrow corridor.

##### *Macigno foredeep basin*

The Macigno foredeep started to develop during the Late Oligocene in front of an advancing tectonic pile of Alpine units, Ligurids and Subligurids. Its peripheral bulge was located about underneath the present-day structure of Monte Leoni. The Macigno sequence rests on top of pelagic Scaglia-type limestones (Upper Cretaceous–Middle Eocene) that progressively grade upward to red and grey shales (Late Eocene–Oligocene) of a deep-water environment of deposition, close to the CCD. From the bottom upwards, it abruptly starts with proximal turbidites consisting of massive, amal-

gamated sandstones (Monte Falterona Formation) that evolve to more distal turbidites made up by an alternation of sandstones and shales (Monte Cervarola Formation) containing in their upper part several calcarenitic-marly levels. One of these latter marks the Oligo/Miocene boundary. A thin interval of black shales and cherts of Aquitanian age follows; the sequence ends with a thick deck of light hemipelagic marls (Vicchio Formation) of Middle Miocene age. The from the west advancing, Liguride nappe progressively covers the foredeep reaching the eastern sectors during the Langhian-lower Serravallian.

As a whole the Macigno sequence is of the fining-upward type; its vertical evolution reflects a rapid basin filling followed by a condition of pelagic plateau. In tectonic terms this means that soon after its infilling the Macigno foredeep was embodied in the tectonic pile so that a new foreland basin was formed adjacent to it (the Marnoso-Arenacea) while it retained the condition of a piggy-back basin.

The deformation of the Macigno basin (Fig. 5) occurred in three events starting in early Burdigalian time (D'Offizi et al., 1994); first the foredeep was reached by the advancing pile of Ligurids, then a deep thrust brought the basement over the already emplaced Ligurids (Keller and Pialli, 1990). This huge pile generated the Barrovia metamorphism of Complex II of Elba, whose age has been established at 19.6 Ma (Deino et al., 1994). Eventually all the Elba-Mid-Tuscany Range building was refolded and rethrust with an opposite (westward) vergence as it is clearly shown in central Elba.

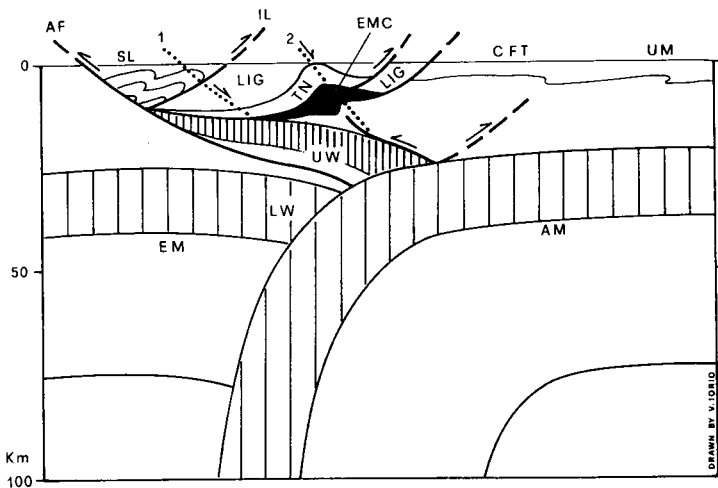


Fig. 5. Cartoon showing the tight Alps-NA system during the early Burdigalian phase (19.6 Ma) in an idealized Corsica-northern Adriatic Sea section: *UW* = upper wedge of Adriatic upper mantle and lower crust obducted during Late Oligocene-Early Miocene; *LW* = lower wedge consisting of European upper mantle and lower crust; *AF* = Alpine front of Corsica; *SL* = Schistes Lustrés; *IL* = Insubric Line; *LIG* = Ligurids l.s.; *TN* = Tuscan nappe; *EMC* = Elba metamorphic core (black); *CFT* = Cervarola-Falterona-Trasimeno basin; *UM* = Umbria-Marche domain; *EM* = European Moho; *AM* = Adriatic Moho; *1, 2* = future normal fault systems of the Corsica basin and of Elba, respectively. Vertically ruled lower Adriatic crust, down to a depth of more than 100 km, is referred to subsequent phases: it will balance during Middle-Upper Miocene the shortening of the Cervarola and UM Apennines thrust systems. Not to scale.

This early Burdigalian phase is well recorded also in the Southwestern Alps (Roure et al., 1990b), where an Adriatic-verging thrust emplaced the crystalline basement on top of the Oligo–Aquitainian Gonfolite Group; it is also probable that this phase may be recognized on the Tyrrhenian side of Calabria (G.P. Pialli, unpublished data). We hypothesize that this phase affected the entire western and northern boundary of the Apulian plate because it occurred almost simultaneously with the rotation of the Corsica–Sardinia microplate (Rehault et al., 1987) and during eruption of calc-alkaline volcanics in Sardinia, i.e. during active subduction of the Apulian lithosphere. Among the Apenninic phases this is the only one which surely occurred before the extensional movements that led to the opening of the Tyrrhenian Sea, in a linked Alps–Apennines system. The recent findings in the Alpine region of the EGT; NFP 20 and CROP–ECORS research projects (Freeman et al., 1990; Roure et al., 1990a) in fact substantiate, in agreement with Reutter et al. (1980), an obduction of the Apulian crust and upper mantle toward the north and west over the European lithosphere that caused the already formed Alpine chain to backthrust over South Alpine and Apennine units.

When the early Burdigalian phase came to an end, the NTS began to develop, starting in the late Burdigalian–Langhian (Bartole et al., 1991), due to extensional movements that created the Corsica basin. From this moment on, the Alps–Apennines linkage terminates, pure subduction ceases, and the Apulian lithosphere begins to retreat and roll back. It is in these new conditions that the other Miocene and Pliocene foredeeps of the NA evolved.

#### *Marnoso–Arenacea foredeep basin*

The Marnoso–Arenacea foredeep basin characterizes the Umbria–Romagna domain of the NA. It rests on top of a pelagic Mesozoic–Palaeogene sequence and displays a maximum thickness of about 3500 m (about 1000 m more than that of the Macigno). It developed from the Burdigalian to the late Tortonian adjacent to the former Macigno trough and had its peripheral bulge roughly aligned with the present-day Apennine ridge.

The Marnoso–Arenacea rests on a pre-flysch sequence consisting of pelagic limestones and marls with black cherts and thin tuff levels (Bisciario Formation) of Aquitanian age overlain by hemipelagic marls (Schlier Formation) whose age progressively becomes younger from the inner to the outer sectors of the foredeep (Burdigalian to Tortonian). In the Umbria–Romagna area, which corresponds to the basin depocentre, the Marnoso–Arenacea shows a very transitional passage to the underlying Schlier Formation. It starts with distal turbidites and evolves upward to more proximal deposits (Premilcuore member, lower Serravallian) forming a thickening-upward cycle. Again distal sandy–marly turbidites follow, containing several calcarenite–marl key-beds of regional importance (i.e. Contessa and Colombine of the lower Serravallian).

The same lithology, devoid of calcarenitic key-beds, continues upward till the late Tortonian. An unconformity of regional importance within the late Tortonian, separates such a sequence from an overlying sandy body (Fontanelice member) that evolves upward to hemipelagic marly deposits. A paraconformable surface again separates these marls from the overlying Gessoso–Solifera Formation of Messinian age.

The evolution of the Marnoso–Arenacea basin shows marked differences with that of the Macigno. A first difference lies in the transition pre-flysch/flysch which is abrupt

in the Macigno and gradual in the Marnoso–Arenacea. A second one is the almost continuous fining- and thinning-upward sequence, with minor episodes of thickening up, of the Macigno, whereas the Marnoso–Arenacea shows a composite evolution where thickening-up cycles are of primary importance, being linked to materials that come from the tectonic pile adjacent to its basin. The main similarity in the evolution of both basins is the presence of hemipelagic marls that drape the turbiditic deposits testifying to a common condition of piggy-back basin at the end of their sedimentary history.

The paroxysm of the deformation of the Marnoso–Arenacea basin occurred mainly in the late Tortonian–Messinian (pre-evaporitic stage) but synsedimentary tectonics began earlier. In fact, during Langhian–Serravallian time its basin was reached by a number of olisthostromes consisting of Ligurian materials that slid from the advancing front of the Cervarola–Trasimeno thrust sheet, on top of which the Ligurid nappes were passively transported. It is therefore mainly in the Langhian–Serravallian that the emplacement of the most external part of the Macigno onto its former peripheral bulge and into the inner part of the Marnoso–Arenacea trough occurred. The thrust system responsible for this emplacement is a set of shallow imbricates (Fig. 6) that join into a master thrust which deepens below the Monte Cetona structure, where it involves basement and upper crustal levels (Ponziani et al., 1994). Geophysical data do not establish whether the continuation at depth of this thrust system did or did not involve the ancient Tuscan Moho; very probably it did, but the subsequent extensional phase has removed any evidence.

A late Tortonian thrust system refolded the thin-skin imbricates of the Cervarola–Trasimeno nappe. This thrust nucleated below the inner domain of Umbria–Romagna where it put basement rocks over Triassic evaporites (Anelli et al., 1992) creating the Perugia Mesozoic Massifs. Eastward, its advanced section broke up into a sequence of shallow imbricates in the Marnoso–Arenacea cover, known in the literature as Signorini's (1941) Umbro–Romagnan structure. No trace at depth of an involvement of the ancient Moho in this thrust system can be read in seismic refraction data, although upper crustal levels are probably involved (Ponziani et al., 1994).

#### *Messinian and Pliocene foredeep basins*

The Messinian and Pliocene foredeeps developed in front of the main Apennine ridge and had their peripheral bulge in the modern Adriatic Sea. They form a bundle of eastward-convex arcs with a general alignment parallel to the main NA Ridge, from the Po Valley to the Southern Apennines. Their depocentres roughly coincide with the principal negative Bouguer anomalies. The earliest of these foredeeps is the Messinian–Lower Pliocene Laga basin (about 4000 m thick), in front of the Sibillini Mountains at the southern end of the NA, which formed soon after the NA Ridge underwent its first compressive event. It was subsequently deformed at the end of the Lower Pliocene when the NA Ridge underwent a second event that brought Mesozoic rocks over the Laga flysch itself. The deep traces of the thrusts responsible for both events may be recognized in the Moho doubling shown by refraction seismics (Ponziani et al., 1994) beneath the area of eastern Tuscany and western Umbria.

The Pliocene troughs show a greater stratigraphic thickness than does the Laga basin. The thickest of them do not crop out at the surface, but are hidden below the Po Valley

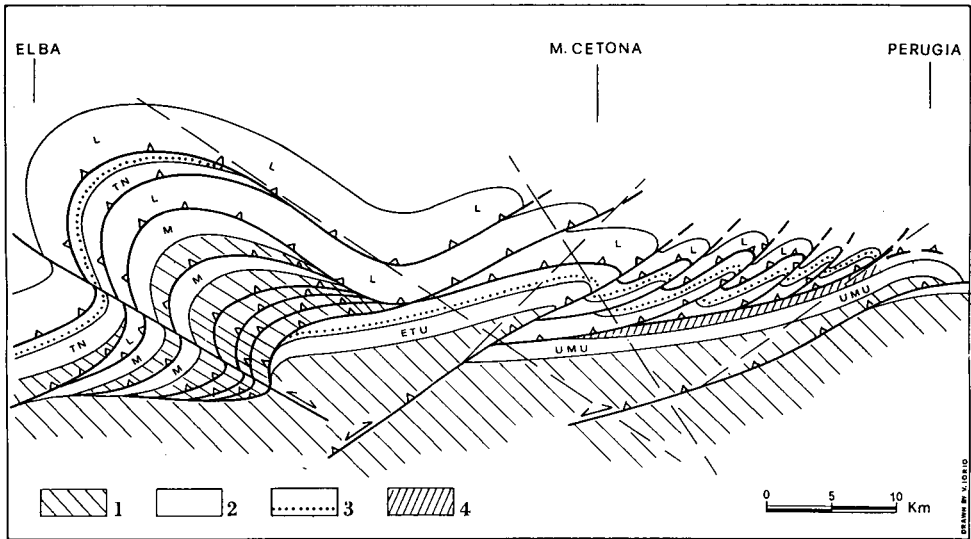


Fig. 6. Cross-section from Elba Island to Perugia massifs restored to compressive phases. Elba and Mid-Tuscany Range (left) are considered parts of the same orogenic chain formed during the early Burdigalian phase in a complex crustal shear zone underneath the inner part of the Macigno foredeep. First the Ligurids l.s. were emplaced onto the Macigno, then the Tuscan sequence along with its basement overthrust the Ligurids l.s. already emplaced. With continued compression an antiformal stack was created; eventually all the structure was refolded and rethrust westward by shear zones connected to the obducted Adriatic slab. The next (toward the foreland) thrust system is hypothesized to reach the upper crust on the basis of refraction seismic data of Fig. 3 beneath the Tuscan nappe front. It is responsible at shallow levels of the imbricate system of the Cervarola-Falterona-Trasimeno nappe during the Serravallian. The easternmost crustal shear zone of the figure, based on refraction seismics and borehole data, shows a duplication of Umbrian basement, Middle Tortonian in age, that refolds the Cervarola-Falterona-Trasimeno nappe previously emplaced. 1 = basements; 2 = (white) L = Ligurids l.s.; M = metamorphic cores of Elba (Trevisan's complexes I and II) and Mid-Tuscany Range; TN = Tuscan nappe; ETU = external Tuscan unit; UMU = Umbria-Marche unit; 3 = Macigno flysch; 4 = Marnoso-Arenacea flysch. Dashed lines symbolize the main systems of normal faults and related crustal shear zones that will stretch the compressive construction during later extensional phases. Scale is indicative only.

and the northern Adriatic Sea; subsurface data, however, indicate thicknesses of more than 6000 m, i.e. about three times as great as the Macigno. Between the Macigno and the Pliocene troughs, the foredeep thicknesses are 3500 m for the Marnoso-Arenacea and around 4000 m for the Laga. This is surprising because the weight of the nappe pile that was built up beside the inner and more ancient foredeeps was surely greater than that of the nappe piles adjacent to the external foredeeps for at least two reasons: (1) in the external tectonic piles Ligurids are lacking, and (2) in the inner piles thrusts are deeper and involve basement. If the lithospheric bending that creates a foredeep were proportional to the weight of the adjacent nappe pile then the Macigno thickness should be greater than that of the Marnoso-Arenacea and even more so for the Pliocene deposits. Apparently, as Royden et al. (1987) have pointed out, the effect of the weight of the nappe piles is not dominant and the cause of lithosphere bending has to be different. In agreement with these authors, we hypothesize that bending of the

lithosphere occurred through its progressive rolling back and retreating under its own weight after the cessation of the active early Burdigalian subduction. The increase in thickness of the Middle Miocene–Pliocene foredeeps reflects either a progressive verticalization of the Apulian lithosphere (as seismic tomography seems to show), or its length increases at depth due to the progressive incorporation of sectors of the foreland in the nappe pile–foredeep system. We hypothesize that in both cases an important role is played at depth by the eclogitization of lower crust, as discussed below.

## THE PERI-TYRRHENIAN AND INTRA-APENNINIC EXTENSIONAL BASINS

Since the late Burdigalian (Bartole et al., 1991) the area encompassing the NTS and the NA Ridge has undergone strong extension. This activity started in the Corsica basin and has propagated eastward, forming a sequence of marine and continental basins elongated NW–SE. Passive seismics show that at the present time extensional stresses are acting in the NA Ridge.

The principal events in the propagation of extension in the NA region, following the formation of the Corsica basin and the emplacement of the Sisco lamproitic body at about 15 Ma (Serri et al., 1991), are: (a) the second Apuane deformational phase, which occurred during the Langhian (Carmignani and Kligfield, 1990); (b) the formation of lacustrine basins in western Tuscany during the Late Tortonian–Messinian (Bertini et al., 1991); (c) the development of marine basins in all of Tuscany and western Umbria in the Early Pliocene and their termination due to uplift in the Middle Pliocene (Bartolini et al., 1982); (d) the formation of continental basins in eastern Tuscany–Umbria during the Late Pliocene–Pleistocene (Boccaletti et al., 1991).

As in the case of the compression, extension occurred in the NA in more than one event. In western Tuscany, which is the most extended area of the NA, three events are recognizable: (1) a first event, not well dated but surely pre-late Tortonian, was characterized by low-angle normal faults that caused a stretching of both basement and cover of the order of 120% (Bertini et al., 1991); (2) a second event, of late Tortonian and Lower Pliocene age, produced the lacustrine and marine basins; it was accommodated by high-angle normal faults with minor extension (5–7%) (Bertini et al., 1991); (3) a third event, from Middle Pliocene onward, uplifted all of western Tuscany in a generalized way, again by means of high-angle normal faults.

The propagation of extensional stresses was contemporaneous with thrust nucleation and deformation of the nappe pile–foredeep system so that at any given time during Middle Miocene–Pliocene, adjacent sectors of the NA were subjected to compression (external) and to extension (internal) according to many authors (e.g., Elter et al., 1975; Lavecchia et al., 1984; Lavecchia, 1988; Alvarez and Pialli, 1989). In addition, recent data from passive seismics in the NA Ridge (Amato and Selvaggi, 1991) show that present-day extension at upper crustal levels is concurrent with shortening at depth. If applicable also to the Mio–Pliocene Apenninic phases, this means that while extension was acting in a given sector there was compression both underneath it and in the adjacent external sector.

## AN EXPLANATORY MODEL

*Sinking of lower crust after inversion to eclogite*

The simultaneous deformation of the NA by extension and compression in adjacent belts presents a significant tectonic problem. Clearly it implies that the tectonic stresses were not applied from the front and rear of the NA and transmitted through the lithosphere. It seems to require lateral motion of the axial belt of the NA crust itself, from southwest to northeast. This would generate the stresses, compressional in front of the moving belt and extensional in the rear, and it agrees with the direction in which the foredeep basins migrated. To first approximation, the boundaries of the NA region, on the southwest and northeast, need not have moved relative to one another.

What could drive this inferred northeastward motion of the medial portion of the NA relative to both lateral margins? It is unlikely to be driven by drag from the mantle beneath, because the belt of possible coupling to the mantle is only 100–200 km across. An alternative possibility is that some fraction of the lithosphere is negatively buoyant and is sinking into the upper mantle, with a rolling hinge line advancing from southwest to northeast and drawing the median belt of the NA along behind it. This situation would produce the observed compression along the northeast margin of the NA and the extension to the southwest, and the areas affected by the two kinds of stresses would migrate in the observed direction. The NA and adjacent areas have evidently acted in this way since the late Burdigalian.

As a mechanism to produce this sinking, we suggest that, when the oceanic lithosphere of the Apulian plate had been eliminated by subduction under the Corsica–Sardinia microplate, compressional suturing forced the Apulian plate (upper mantle and crust) to obduct over the already formed Corsican chain, initiating backthrusting with Adriatic vergence. About at the level of the present position of Monte Cetona, the obducted indenter was broken and the Tuscan mafic lower continental crust and upper mantle were pushed down underneath the early Burdigalian chain to a depth of 50–60 km, where the gabbro–eclogite phase change would take place, with a density increase of 15% (Artyushkov and Sobolev, 1982; Anderson, 1987).

If mafic rocks made up a sufficient fraction of the Apulian lower continental crust, the density increase would change the lower continental crust from positively to negatively buoyant with respect to peridotitic mantle (Fig. 7). Because of temperature differences, cold peridotite in the mantle portion of the Apulian lithosphere would be slightly denser than the warm asthenospheric peridotite beneath, and than the hot asthenosphere which laterally intrudes from below, and this density contrast would not inhibit, and might slightly enhance, the tendency of the eclogitic lower crust to sink.

As the eclogitic lower crust began to fall under its own weight, it would initiate a self-sustaining process which would continue even after the initiating collision ceased, with each increment of densified lower crust pulling the next increment to the depth where it also would invert to eclogite. The sinking process would roll back the lithosphere in the lower plate, drawing the upper plate in the direction of rollback, thus producing a situation where a leading wave of compression and a trailing wave of extension migrate in the direction of rollback, toward the foreland, as observed in the NA. This process would continue beyond the termination of the original continental



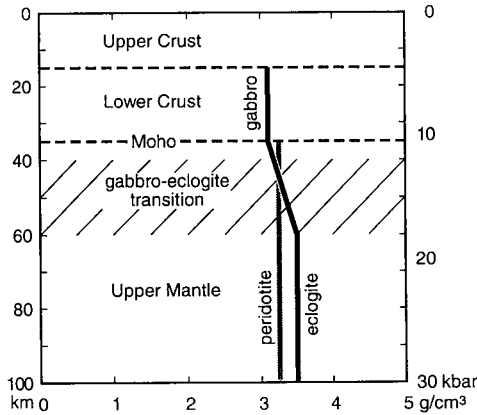


Fig. 7. Conceptual density curves to explain sinking of A- subducted lower continental crust and showing the density increase during the eclogitization of the lower crust gabbroic rocks.

collision between Corsica and Italy which initiated the orogeny, and could produce the sharply curving pattern of the circum-Tyrrhenian orogenic belts.

#### *Support for the lower-crust sinking model*

Viewed in one way, the present model explains many features of the Apennine–Tyrrhenian region. Viewed in another way, it links together several previous partial explanations and shows why each was the correct answer to some part of the Apennine–Tyrrhenian puzzle.

Recent studies of the thrust geometry of the Apennine fold-and-thrust belt (Bally et al., 1986; Lavecchia et al., 1989) favor a structure with superimposed thrust sheets representing at least a doubling of the Mesozoic–Lower Tertiary stratigraphic sequence and thus at least a 50% shortening of the continental crust beneath this cover. Bally (1981) has long recognized that this situation, common in thrust belts, requires the disappearance of widths of continental crust of the order of 100 km. He has named this process ‘A-subduction’ (after Amferer), in contrast to B-subduction (after Benioff) in which wide belts of ocean crust, of the order of 1000–10,000 km, are consumed.

Merla (1951) first recognized that a compressional wave had migrated northeast across the Northern Apennines. Elter et al. (1975) stressed that a wave of extension had followed the wave of compression. Reutter et al. (1978, 1980) explained the northeastward migration of compression by the splitting off and sinking of a slab which included only the sub-continental mantle of the lithosphere, but otherwise closely resembles our model. Castellarin et al. (1982) suggested detachment and sinking of the lower continental crust, as we do. Malinverno and Ryan (1986) proposed that most or all of the continental crust previously thinned during the passive-margin phase splits off and sinks during orogenesis, thus explaining the associated migrating waves of compression and extension. Our principal contribution to this line of thought is the concept that lower continental crust depressed to about 50 km would invert to eclogite and become negatively buoyant; we thus provide a physical mechanism to

explain a pattern of movement which other geologists have inferred from studies of the NA.

All of these studies are generally compatible with our model of sinking, A-subducted, lower continental crust. For the first time Spakman's (1990) and, subsequently, Amato's et al. (1991) tomographic studies image a seismically fast (cold, dense) body in the position predicted by the A-subduction model, and the gabbro–eclogite inversion provides an explanation for why this should happen. This inversion, in addition, may explain the distribution of stress tensors evidenced by Channell and Marechal (1989) across the southern Tyrrhenian subducted slab. The model accounts for the missing crust required by balancing considerations (Bally, 1981; Bally et al., 1986). It also agrees with calculations indicating that the weight of the Apennine fold-and-thrust belt is not sufficient to explain the depth of the foredeep, and that some additional downward force on the lower plate, such as negative slab buoyancy, is required (Royden and Karner, 1984a, b). Partial melting of the A-subducted body offers a possible source for the puzzling calc-alkaline and potassic volcanics of the western coastal regions of Italy, a possibility briefly suggested by Bally et al. (1986).

If A-subduction has removed a segment of crust 100–200 km wide, that body should be present at depth. Spakman (1986, 1990) carried out a detailed seismic tomographic study of the lithosphere and upper mantle beneath the Mediterranean region. His maps inspire confidence, as they image both the warm region (slow P-wave velocity) to be expected beneath the extending, volcanic coastal area of Tuscany and Lazio and the known seismic slab beneath the southeastern Tyrrhenian Sea. Spakman's velocity anomaly maps show a large, unexpected high-velocity body (cold, dense) beneath the Apennines at depths of 250–500 km. In fact, the entire system of Alpine-age mountain belts from the Atlas through the Apennines, Alps, Carpathians, and Hellenides, is marked by deep, fast bodies on Spakman's (1990) tomographic maps. Spakman's early interpretation of this system of fast bodies was that they represent Tethyan oceanic crust subducted long ago (Spakman, 1986).

In order for the gabbro–eclogite phase transition to be effective, the lower continental crust of the Adriatic promontory would have to be of largely mafic composition. Lower crust is actually exposed in both northern Italy (the Ivrea Zone of the Alps) (Schmid, 1967; Fountain, 1976; Zingg, 1983) and southern Italy (southern Calabria) (Schenk, 1981, 1984). In both cases, the lower crustal rocks are indeed largely of mafic composition. In fact, although there is good reason to consider the continental crust to be complex and heterogeneous (Oliver, 1982), studies of high-pressure xenoliths argue for dominantly mafic lower continental crust on a worldwide basis (Griffin and O'Reilly, 1987).

The seismic zone beneath Calabria and the southeastern Tyrrhenian Sea, with frequent earthquakes within a range of 250–300 km and rare events down to 500 km (Anderson and Jackson, 1987), marks oceanic lithosphere which was formerly continuous with the Ionian Sea. Its narrow width (200 km along strike) has long suggested that it is a local region descending beneath Calabria as the latter microplate migrates to the east-southeast (Alvarez et al., 1974). In the light of the present model, it may alternatively be interpreted as a small part of a long, curving A-subducted body underlying the Apennines and the Sicily–Atlas orogenic belts. In that case the Calabrian sector would be the only place along the subducting belt where the downgoing material

is oceanic lithosphere which is cold and brittle enough to permit earthquakes; elsewhere along the subducting body, the material was originally lower continental crust, which has always been too warm and ductile to fracture.

Migration of the compressional and extensional waves outward, in the direction of rollback, explains the region of extension in the middle of the arc which is now the Tyrrhenian Sea (Malinverno and Ryan, 1986; Kastens et al., 1988). The Tyrrhenian Sea grew by continental stretching and subsequent oceanic spreading moving from west to east (Kastens et al., 1986, 1988; Wang et al., 1989). This spreading continued synchronously with the inferred A-subduction surrounding the Tyrrhenian Sea. Van Bemmelen (1969, 1972) and Wezel (1982) have invoked vertical upwelling and doming to explain the circular tectonic pattern in the southeastern Tyrrhenian Sea; this pattern is well explained if the upwelling needed to balance the sinking, A-subducted bodies occurs within the arcuate A-subduction zone, as would be expected.

## GENERALIZATIONS AND APPLICATIONS

A-subduction of lower continental crust in which gabbro has inverted to eclogite accounts for a wide variety of observations and previous hypotheses on the Apennine–Tyrrhenian region, and it may be applicable elsewhere. Bally (1981) argued that balancing considerations require A-subduction to be widespread in fold-and-thrust belts. We contend that the density increase of the gabbro–eclogite phase transition, occurring not far beneath the usual depth of the continental Moho, makes sinking of lower crust, and thus A-subduction, a likely consequence of continent–continent collision. Detailed seismic tomography now offers the possibility of imaging the A-subducted bodies. This technique will be increasingly important as a tool for tectonic geology, although detailed tomographic mapping will only be possible in regions with many seismic stations and widespread earthquakes.

Finally, the self-sustaining character of A-subduction, with recently densified lower continental crust dragging neighbouring crust to the depth where it too will be densified, can explain the mysterious continuation of fold-and-thrust belt deformation long after the apparent driving collision has ceased. For example, Tempelman-Kluit (1979) attributes the northern Canadian Cordillera fold-and-thrust belt to a collision in the Late Jurassic and Early Cretaceous, but notes that the mountain belt continued to grow eastward for 60 million years after the collision terminated. This behaviour would be well explained by the type of A-subduction we propose here.

## SOMMAIRE — CADRE TECTONIQUE DU MIOCÈNE DES APENNINS SEPTENTRIONAUX: LE PROBLÈME DU SYNCHRONISME COMPRESSION-EXTENSION

*(Manuscrit soumis: Février 1995, révisé: Juin 1995; rédacteurs responsables: AM et RC)*

Les chaînes de montagne jeunes qui flanquent le triangle de la Mer Tyrrhénienne sont difficiles à interpréter par le modèle de tectonique des plaques. Ces chaînes apennine et sicilienne ont été déformées en compression pendant le Tertiaire supérieur

et le Récent alors même que la région tyrrhénienne adjacente subissait une extension. Comme exemple particulier, citons l'extension en Toscane qui suit immédiatement un raccourcissement dans les Apennins du nord puisque les deux régions migrent vers le nord-est. D'abondantes données géophysiques ont été récemment mises à disposition et ont éclairé la géométrie et la cinématique de la croûte inférieure et du manteau supérieur situé sous les Apennins du nord. Plusieurs chercheurs ont suggéré que la simultanéité de la compression et de l'extension dans des chaînes adjacentes implique enfoncement et plongée d'une portion de la lithosphère dans le manteau. La tomographie sismique du manteau supérieur sus-jacent révèle des corps qui peuvent représenter la lithosphère plongeante. Nous suggérons ici que la subduction avortée de la croûte continentale durant la collision entre les deux plaques Apulie et Corse–Sardaigne aurait provoqué un enfoncement de la croûte continentale inférieure de quelques dizaines de km, à une profondeur où les roches mafiques auraient subi un changement de phase vers l'éclogite. Cet enfoncement du matériel dense serait à l'origine de la plongée de la plaque sus-jacente. La plongée de la croûte inférieure éclogitique par augmentation de la densité explique de nombreuses observations faites dans les Apennins du nord et peut constituer une explication généralisée pour les chaînes orogéniques comme les Rocheuses canadiennes et les Alpes qui ont poursuivi leur déformation longtemps après que la collision initiale continent–continent soit terminée.

*(Sommaire proposé par les rédacteurs d'après résumé anglais des auteurs, GSO)*

#### ACKNOWLEDGEMENTS

We would like to thank T. Atwater for having reviewed the original manuscript.

This Page Intentionally Left Blank

*Chapter B3*

**GEOLOGY, TECTONICS, AND INTEGRATED STRATIGRAPHY POTENTIAL OF JAPAN**

M. Takahashi and M. Oda

**INTRODUCTION**

A succession of evolutionary events in planktonic microfossils has made possible the construction of a biostratigraphic model which is commonly employed for long-distance correlations. Recent advances in the biostratigraphy of planktonic foraminifera, calcareous nanofossils, radiolarians, and diatoms enable the combination of a set of datum levels useful for correlating Middle to Upper Miocene onshore sections in central and northeast Japan (Oda et al., 1984). Some of these important datum levels have been geochronologically calibrated by K–Ar and fission-track dates on intercalated tuff beds (Shibata et al., 1984). Radioisotope dates from numerous biostratigraphically controlled tuff layers using several methods provides not only the age ranges for individual datum levels but also the means for estimating the reliability of the geochronology data taken from these continuous and complete sedimentary sequences. In this paper, we present a brief introduction of Neogene geologic evolution and setting in Japan, and describe the most promising Miocene sequences for detailed integrated stratigraphic research.

**GEOGRAPHIC AND STRATIGRAPHIC DISTRIBUTIONS OF NEOGENE IN JAPAN**

The Japanese islands constitute an elongated archipelago extending from 46°N (north of Hokkaido) to 31°N, including the main four islands, and to about 24°N including the extreme Nansei Shoto islands (Fig. 1). The entire length of the main island archipelago is roughly 2000 km, whereas the entire archipelago exceeds 3500 km in length. The width of the main islands ranges from about 300 to 400 km. By comparison with Europe, Italy is geographically comparable; the northern part of Japan (Hokkaido) is approximately at the same latitude as the Swiss/Italian border, and the southern main islands would correspond to the Mediterranean north coast of Egypt, and southernmost part of the Japanese archipelago would be the equivalent of Assouan, on the Nile River in Egypt.

Neogene strata are well represented in northeastern Japan, while their distribution is rarer in southwestern Japan (Fig. 1). Stratigraphic distributions of Neogene sedimentary rocks throughout the Japanese islands are shown in Figs. 2 and 3. It can be recognized that the Neogene strata in northern Japan extend continuously from the Middle Miocene to the Recent, while those in southern Japan are more limited. This is likely caused by the difference in the tectonic regimes between southwest and northeast Japan.

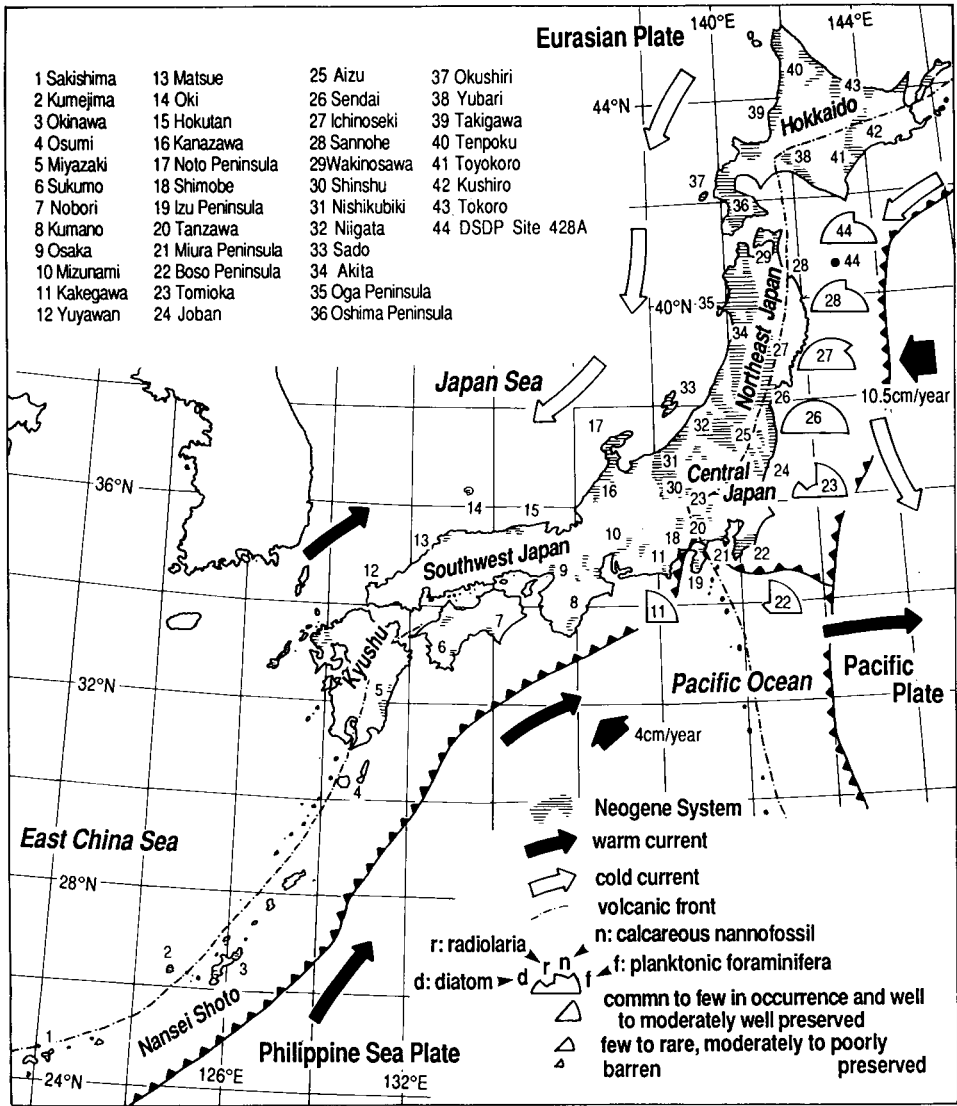


Fig. 1. Location map of selected stratigraphic sections in Japan. Neogene, predominantly bio-silicic sedimentary rocks are mainly developed in northeastern Japan. Each fan-shape diagram represents the abundance and preservation of microfossils (from Oda et al., 1984).

The type of microfossils contained in these rocks is also different between northern and southern Japan. While calcareous microfossils are dominant in the southern part of the Japanese islands, siliceous microfossils dominate in northern Japan. This difference is probably caused by different temperatures in these two regions, as revealed by studies of living planktonic foraminifera which clearly show a distribution at least partially dependent on temperature and climate.

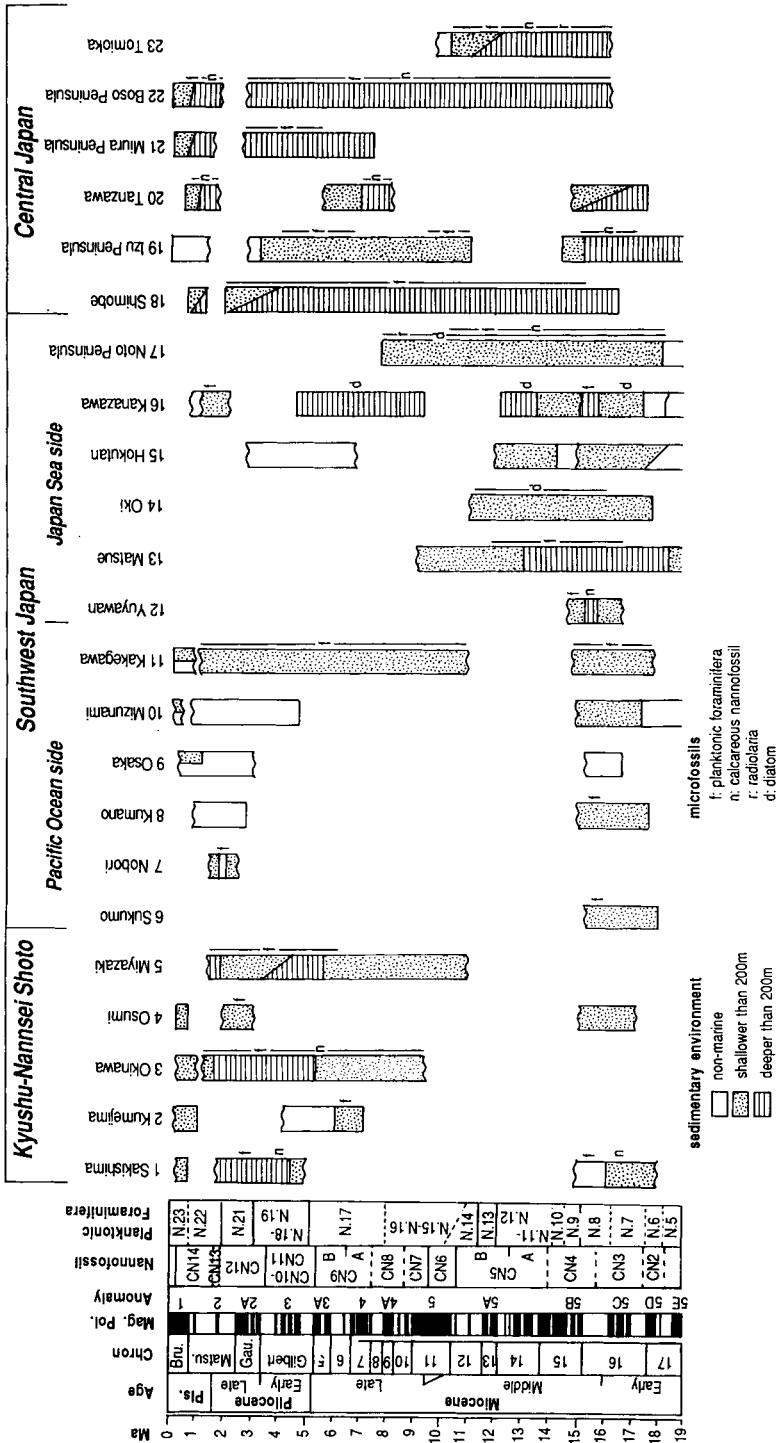


Fig. 2. Stratigraphic distribution of late Neogene sedimentary rocks in southern Japan modified from Kano et al. (1991). Magneto-biostratigraphic interpretation is modified from Oda (1986). Calcareous microfossils are dominant in the southern part of the Japanese islands, while Middle and Late Miocene strata are lacking there.



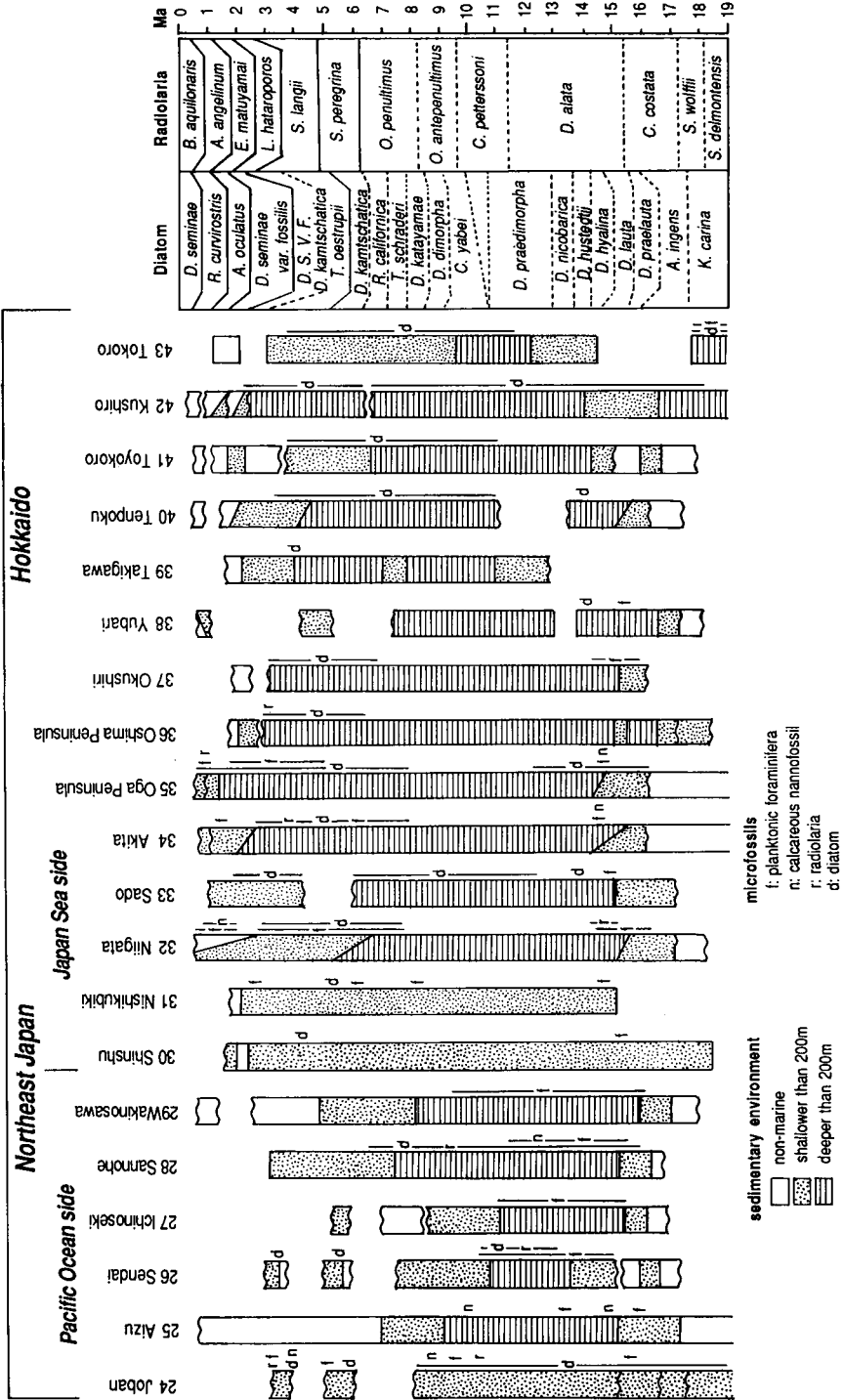


Fig. 3. Stratigraphic distribution of late Neogene sedimentary rocks in northern Japan modified from Kano et al. (1991). Siliceous microfossils are abundant in northern Japan, where late Neogene sediments are completely preserved.

NEOGENE TECTONICS OF THE JAPANESE ISLANDS

A brief introduction to the tectonic development of the Japanese islands is necessary because the stratigraphic distribution of Neogene strata was strongly affected by the tectonic history of this region. On the other hand, stratigraphic and geographic

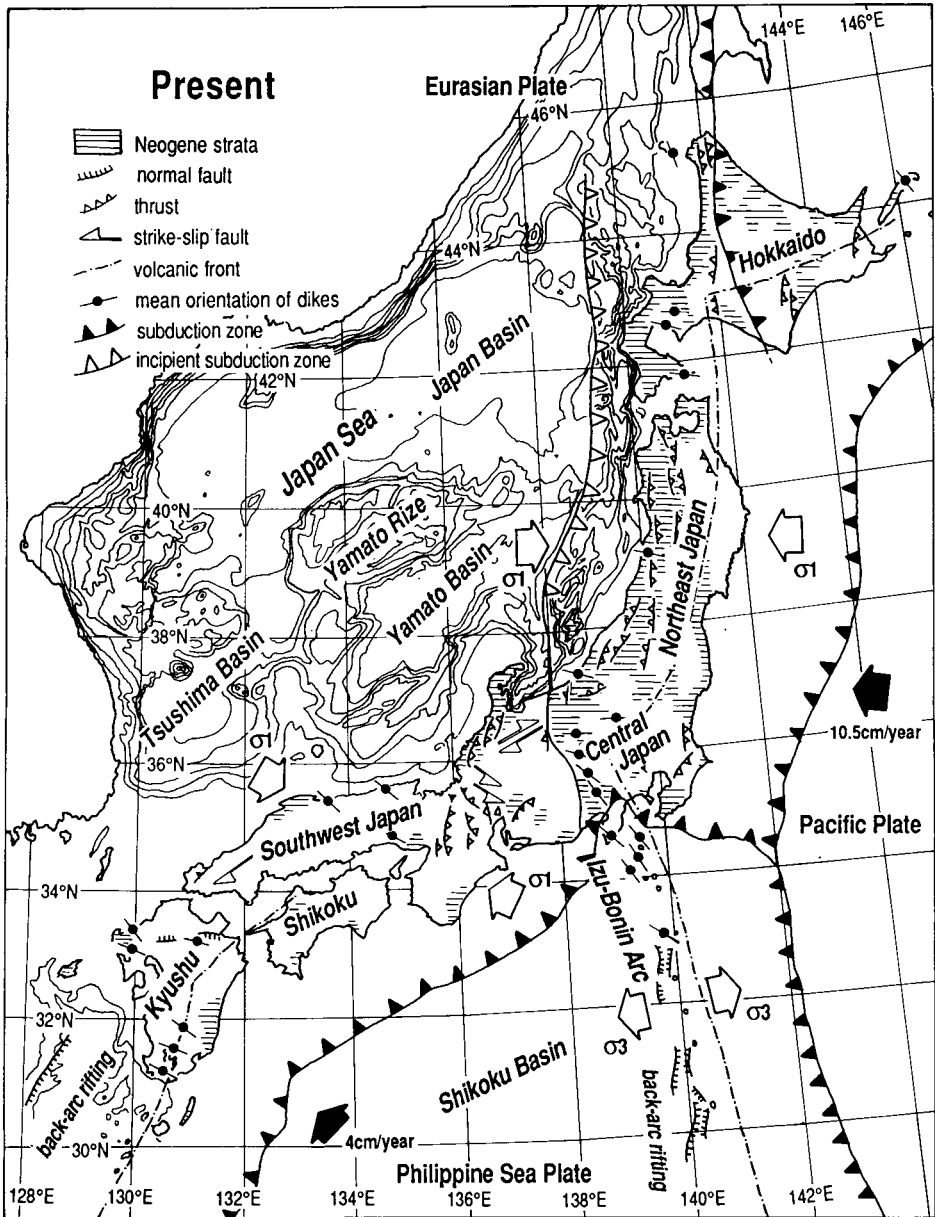


Fig. 4. Tectonic sketch of the Japanese islands, and bathymetric chart of the Japan Sea.

distributions of fossil species have also been affected by global climate changes. Thus, an awareness of the geodynamic and climatic histories of this rather active Pacific area, is fundamentally important for the development of integrated stratigraphic research in Japan.

### *Opening of the Japan Sea*

Fig. 4 illustrates the present tectonic setting of the Japanese islands located along the western Pacific subduction zones. The Japanese island arc itself consists of two main arc systems: the northeastern Japan and southwestern Japan arcs, each having contrasting tectonic features.

The tectonic regimes of the northeastern and southwestern Japan arcs have been related to the subducting Pacific and Philippine Sea Plates, respectively. In central Japan, where both northeast and southwest Japan arcs meet, tectonic development is further complicated by the Izu–Bonin arc collision with central Japan since the Miocene.

One of the most important events in understanding the tectonics of Japan is the opening of the Japan Sea which occurred in the Early Miocene. The Sea of Japan is comprised of three major basins: the Japan Basin, the Yamato Basin, and the Tsushima Basin with the continental Yamato Bank in the middle. The Japan Basin has a normal oceanic crust and is believed to be of a back-arc spreading origin.

Since 1980, extensive palaeomagnetic investigations have been carried out in this region, and have focused mainly on the rotational movement of the Japanese islands (Otofujii and Matsuda, 1983, 1984, 1987; Hayashida and Ito, 1984; Otofujii et al., 1985a, b, c, 1991, 1994). A large number of palaeomagnetic data show that southwestern Japan has undergone a clockwise rotation, which is thought to have been associated with the breakup of the continental crust and subsequent back-arc spreading of the Japan Sea. Based on a data set obtained from Southwest Japan since 1982, Otofujii et al. (1985a) estimated the amount of clockwise rotation relative to stable Eurasia to be 47°, and processed the rotation data using best-fitting curves for the rotation deduced from declination versus age data; the climax of rotation was around 15 Ma (Fig. 5). Recently, Otofujii et al. (1994) obtained additional palaeomagnetic data from northeastern Japan, which provide a best-fit curve for the rotation process, with the counterclockwise rotation reaching a climax at around 15 Ma, and a net rotation change of 46°. Thus the 500 km long northeast Japan block was rotated counterclockwise by more than 45°, and accompanied a 47° clockwise rotation of the 600 km long southwest Japan block at about 15 Ma. The differential rotation of northeast and southwest Japan arcs peaked around 15 Ma, indicating that the Japanese islands have migrated southeastward in the fashion of a double-door, following the opening of the Japan Sea.

### *Intra-arc rifting in Miocene northeastern Japan*

Stratigraphic analyses of the sedimentary basins provide age constraints for the back-arc rifting. Yamaji (1990) described the short-lived, and rapid intra-arc rifting in Early Miocene northeastern Japan, using on-land stratigraphic records (Fig. 6).

The syn-rift sediments are well exposed in the Uetsu district of northeastern Japan, where small, elongate, and tilted basins were bounded by normal faults trending NNE–

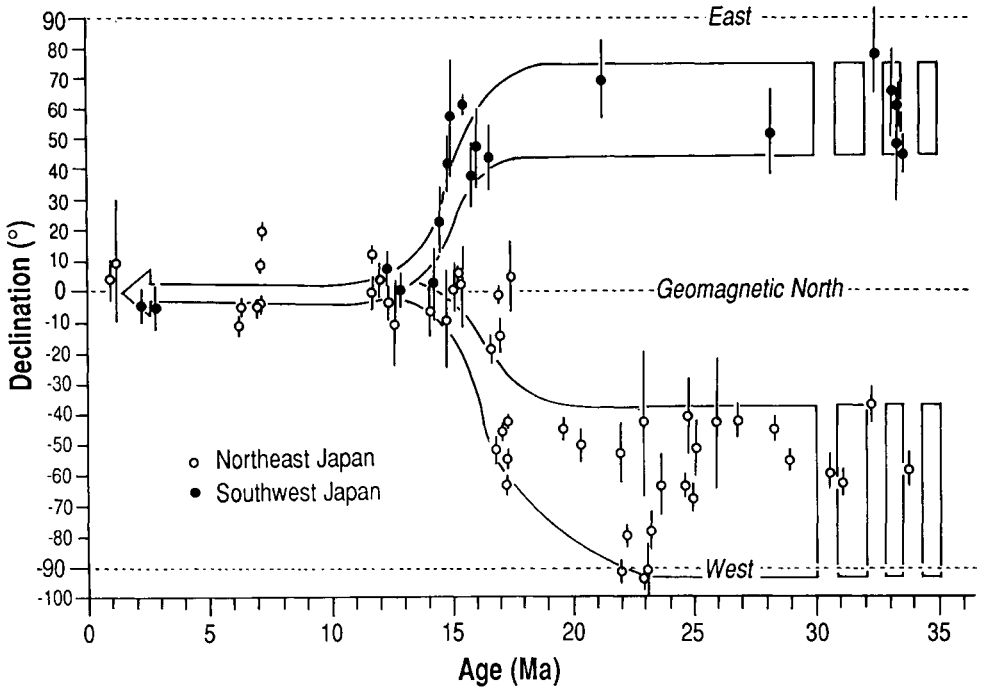


Fig. 5. Declination versus age for northeastern Japan (Otofujii et al., 1985c, 1994; Nishitani and Tanoue, 1988), and southwestern Japan (Otofujii et al., 1985a). Differential rotations between northeast and southwest Japan arcs took place around 15 Ma, and was most likely caused by the back-arc spreading of the Japan Sea.

SSW to NE–SW. The Lower Miocene sequence in this area shows a rapid change in thickness from 0 km to 2 km within the district, and also exhibits localized internal unconformities. Yamaji (1989) showed that the rapid change in thickness was controlled by the syn-depositional fault movements.

After the beginning of syn-rift sedimentation around 18 Ma in the nonmarine environments, the depositional environment abruptly became shallow marine and then deep marine from 16 to 15 Ma. Consequently, the deposition of black muds occurred in the inner-arc region until 14 Ma, and siliceous shale subsequently filled the basin (Fig. 6). Extensional tectonics lasted from about 18 Ma until 15 Ma in northeastern Japan. However, as most of the syn-rift sediments of the early stage are nonmarine, and therefore undatable, the exact timing of the initiation of rifting is uncertain. The rifting began after the eruption of the pre-rift ignimbrite (22–23 Ma), and before the climate change represented by fossil plant assemblages (17.5 Ma), which provides an upper and lower time range for the rifting. As for the termination of the extensional process, the uppermost horizon showing differential thickness is correlated with the N8 or the base of N9 of planktonic foraminiferal zones (i.e., around 15 Ma).

Sea water transgressed the inner-arc region around 16 Ma, and rapidly increased in depth. Based on the fossil assemblages of benthic foraminifera, Yamaji (1990) showed that the inner-arc region of northeastern Japan subsided from shallow marine to middle

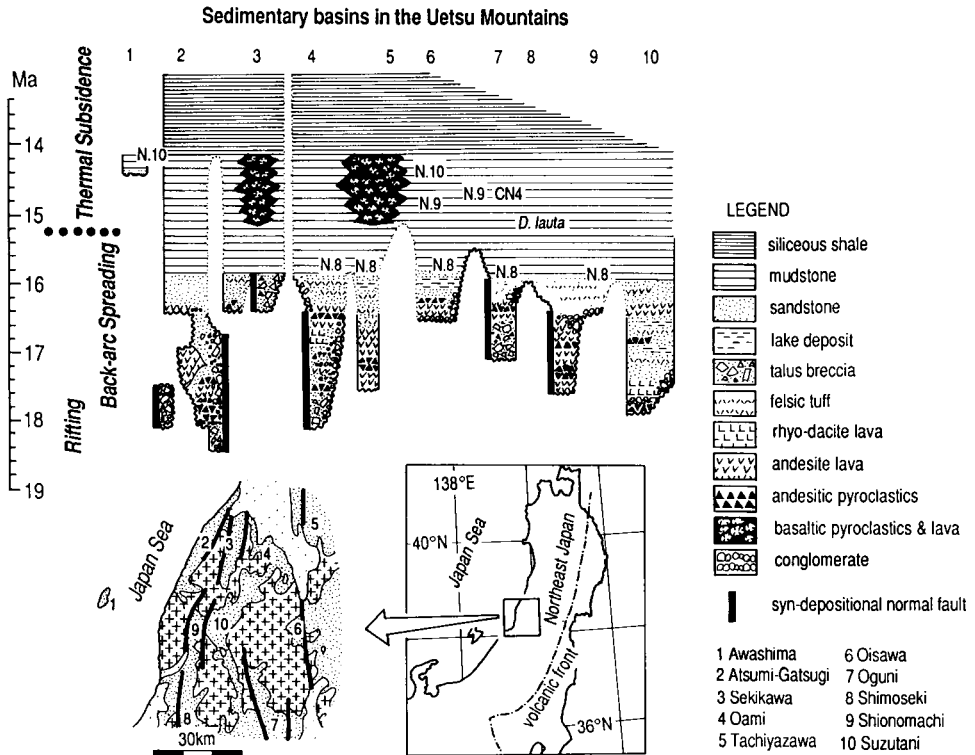


Fig. 6. Chronostratigraphic sections in ten localities of the Uetsu district, northeastern Japan, modified from Yamaji (1990). Syn-depositional tectonics under extensional stress field occurred between 18 Ma and 15 Ma, and represent the Early Miocene intra-arc rifting of northeastern Japan.

or lower bathyal depths in a million years. This rapid subsidence of a few kilometres within only one million years was produced by tectonic rather than eustatic causes since sea-level fluctuations during the Miocene were smaller than 200 m (Haq et al., 1987).

The total subsidence during rifting was calculated to be 2–3 km in the Uetsu district (Yamaji, 1990). On the other hand, the outer-arc region subsided only on the order of 100 m during the rifting stage. This contrast may be attributed to the localization of the extensional deformation along the back-arc side.

*Early Miocene back-arc spreading of the Japan Sea*

Based on the palaeomagnetic, geologic and palaeontological data, the Neogene tectonic development of the Japanese islands is summarized as follows. Reconstructions are partly modified from Takahashi (1994a, b), with the additional zoogeographical data of Chinzei (1991).

Until the Early Miocene, Japan was located along the eastern margin of the Asian continent, and a marginal basin was not yet present behind the Japan arcs. The inception of intra-arc rifting occurred in the Early Miocene, and many half-grabens were formed

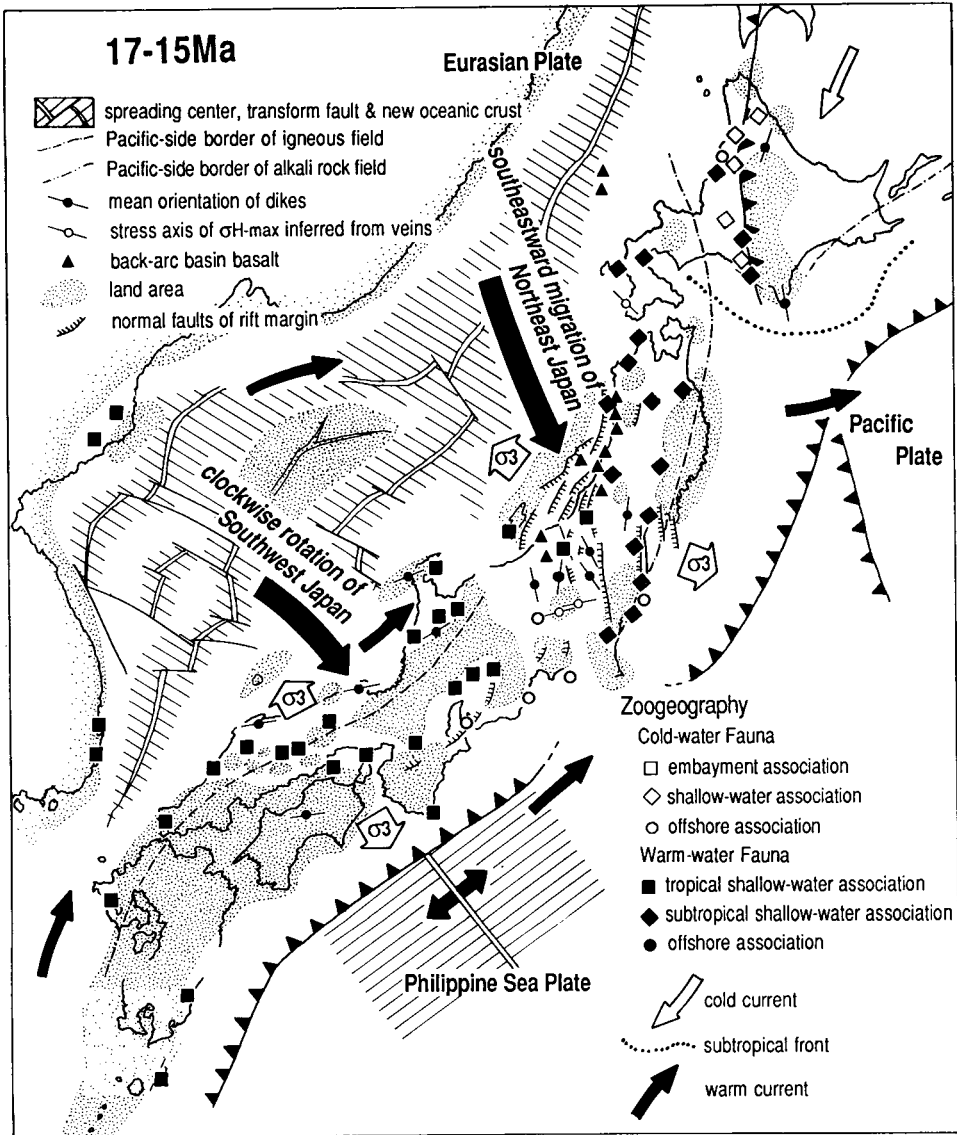


Fig. 7. Palaeogeographic map of Japan in the latest Early Miocene. Both Northeast and Southwest Japan rotated like a double-door in association with the Japan Sea opening. Northeast Japan broke into a number of blocks, and subsided rapidly under extensional stress field. On the other hand, Southwest Japan rotated without major intra-arc deformation, and subsided slightly.

under an extensional stress field perpendicular to the arc axis (Fig. 7). Both the northeast and southwest Japan arcs migrated with a counterclockwise rotation in response to the back-arc spreading of the Japan Sea. The extensional deformation and abrupt subsidence probably represent a stretching of the lithosphere of northeastern Japan. On the other hand, the subsidence of southwestern Japan during this stage was small.

There are few Early Miocene half-grabens, suggesting that southwestern Japan rotated as a block without extensional deformation within the arc. Therefore, the lithosphere of southwestern Japan was not stretched, and mechanical subsidence did not occur.

The fauna during this stage is remarkable in its tropical and subtropical nature as shown in Fig. 7. The molluscan associations in southwestern Japan include strictly tropical mangrove-swamp elements, and subtidal forms (Chinzei, 1991). Larger foraminifera, common in calcareous sediments, also indicate the tropical nature of the marine climate (Matsumaru, 1981).

## TECTONIC CONTROL ON THE PALAEOONTOLOGICAL AND SEDIMENTOLOGICAL RECORDS IN JAPAN

### *The Middle Miocene subsidence phase*

In the Middle Miocene, while most of southwestern Japan was uplifted and emerged, the northeast Japan arc subsided gently, and diatomaceous mud accumulated in a deep sea (Fig. 8). Compressional deformation occurred along the Japan Sea side of southwestern Japan at the end of its rotation (15–14 Ma), while northeastern Japan did not undergo this tectonic deformation. The decrease in volcanic activity was remarkable. In central Japan, the Early Miocene formations were exceedingly deformed during this stage, suggesting that the Izu–Bonin arc was already colliding with central Japan.

With regard to the fauna, the tropical molluscs and larger foraminifera disappeared from northern Japan at about 15 Ma, in the upper part of Zone N9. The abrupt change in the benthic foraminiferal fauna is also observed at the same time in the Sea of Japan. This faunal assemblage changes from a highly diversified, warm-water type to a limited arenaceous assemblage (Chinzei, 1991). The planktonic foraminiferal fauna also decreased from this horizon upward, and was replaced within Zone N11 by cold-water species (Maiya and Inoue, 1981; Maiya, 1988).

Siliceous sediments composed mainly of planktonic diatoms started to accumulate at about 15 Ma in the Sea of Japan basin and along the coastal areas of the main islands. The resulting sediments, which are lithologically similar to the Miocene Monterey Formation of California, U.S.A., are barren of benthic megafossils, and are considered to be the deposits of an isolated and stagnant marine basin. All these changes in molluscan and foraminiferal faunas, as well as in the sedimentary facies, were most probably related to the rapid opening of the Japan Sea, and to slow marine transgression associated with post-rifting thermal subsidence.

### *The Late Miocene to Pliocene incipient compressional phase*

This stage is characterized by numerous caldera swarms along the axis of the northeast Japan arc (Fig. 9). During this interval, the stress field was neutral or, at most, characterized by a weak compression, and marine sediment deposition was limited. The present Backbone Ranges of northeastern Japan started to uplift in the latest Middle Miocene, and formed emerging islands at the beginning of this period. Numerous caldera structures related to subaerial volcanism formed along this uplifting zone (Sato and Amano, 1991).

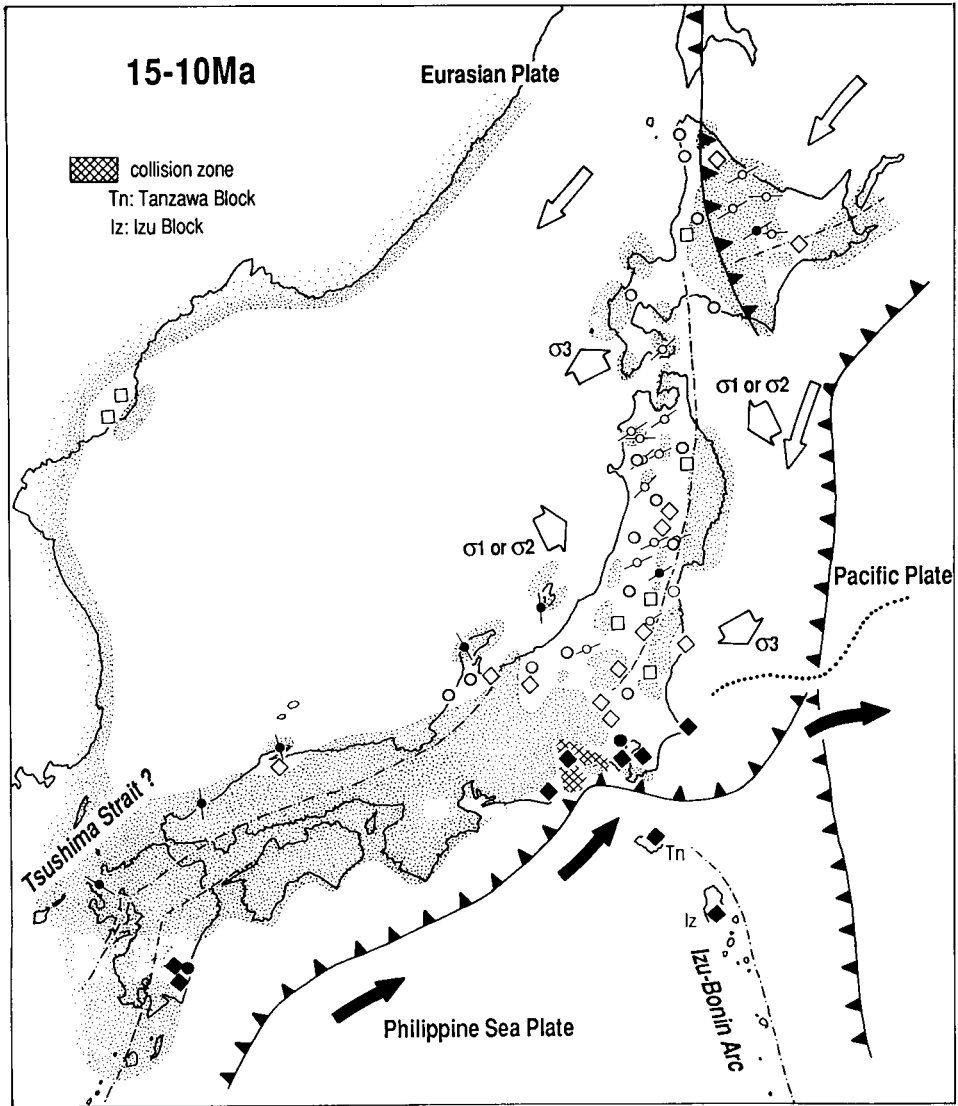


Fig. 8. Palaeogeographic map of Japan in the Middle Miocene. The major rotations of northeast and southwest Japan ceased at 14 Ma, and northeast Japan subsided gently. The tectonic regime during this time is characterized by a relative tectonic quiescence throughout Japan, except for the central part where the Izu-Bonin arc collided.

During the Late Miocene, the deposits throughout the Sea of Japan area are dominated by diatomaceous mudstones; shallow-marine sediments are rare. These deposits contain a very limited arenaceous foraminiferal fauna, suggesting a stagnant condition on the floor of the Sea of Japan. The planktonic diatom flora is comparable to that of the northwest Pacific, which indicates the presence of a main water connection toward the north (Kanaya, 1959).



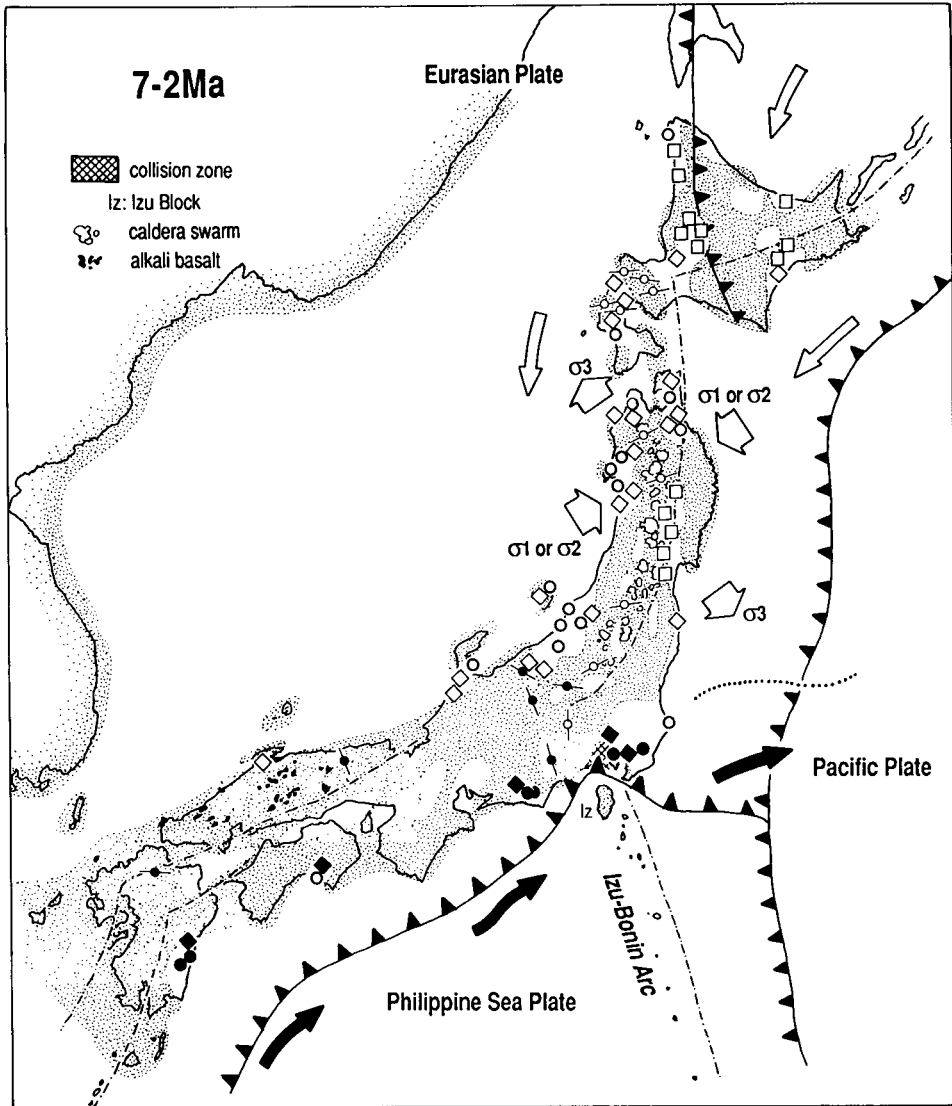


Fig. 9. Palaeogeographic map of Japan from the latest Miocene to Pliocene. Many calderas were formed along the uplifting zone in Northeast Japan. Deposition of marine sediments was scarce during this time interval.

On the fore-arc side of northeastern Japan, vertical movements were relatively small in comparison to the back-arc side. In this mild tectonic regime, shallow-marine sequences accumulated mainly under the influence of eustatic sea-level fluctuations (Ishii, 1989; Yanagisawa et al., 1989).

*Recent shortening deformation phase*

The Japanese islands have been deformed under a compressional stress field since the latest Pliocene (Fig. 4). A large number of reverse faults with a general trend parallel to the arc axis were formed in northeastern Japan. The reconstructed stress field from these reverse faults suggests that the maximum and minimum principal stresses were oriented horizontally, normal, and vertical with respect to the Japan trench. The  $\sigma_1$  direction in northeastern Japan (see Fig. 4) is almost parallel to the present motion of the Pacific Plate relative to the Eurasian Plate, which implies that the present tectonism in northeastern Japan is related to the converging plates. Southwestern Japan also has been under a compressional tectonic regime in recent times, since strike-slip faults are dominant. The stress field in southwestern Japan is also well defined by the motion of the Philippine Sea Plate. The compressional stress field in central Japan is a mixture of E–W-trending stress in northeastern Japan, and a NW–SE trend in southwestern Japan.

## POTENTIAL OF JAPAN FOR INTEGRATED STRATIGRAPHY

Since the Japanese islands were submerged in the latest Early Miocene during the back-arc spreading of the Japan Sea, marine sequences suitable for integrated stratigraphic studies are restricted to the Middle Miocene through the Pleistocene. However, the sequences with a high potential for integrated stratigraphic studies, including calcareous microfossil biostratigraphy (planktonic foraminifera and calcareous nannofossils), and other physical–chemical stratigraphic approaches (i.e., magnetostratigraphy, chemostratigraphy, etc.), are mostly limited to the southern part of the Japanese islands. On the other hand, sequences with abundant siliceous microfossils are dominant in northern Japan.

The Japanese islands are located at a middle-latitude area in the northwestern Pacific domain where cold and warm currents may have influenced the spatial distribution of planktonic microfossils (Fig. 1). As shown in Figs. 2 and 3, Middle Miocene sediments are almost absent in the Pacific side of southwestern Japan, owing to uplift under the compressional deformation in the Middle Miocene. A complete Late Miocene through Pliocene sedimentary sequence is preserved in the Kakegawa area (11 in Fig. 2), and planktonic foraminiferal events conducive to a world-wide correlatable biostratigraphic zonation have been recognized (Ibaraki, 1986). Although eight key tuffs, some of which were fission-track-dated offering a high potential for integrated stratigraphy studies, are intercalated in this sequence, we did not adopt it because of the poor exposure of the strata.

Middle Miocene sediments were better developed in the Japan Sea side of southwestern Japan where siliceous microfossils are dominant.

Neogene sequences of some areas in central Japan include the Middle Miocene through Pliocene of the Boso Peninsula (22 in Fig. 2) which represent the best field case for integrated stratigraphic studies thanks to the well exposed sedimentary rocks containing abundant calcareous microfossils and more than 200 interbedded key tuff layers.

Rock magnetism in this sequence was studied by many workers (e.g., Kimura, 1974; Niitsuma, 1976). However, because of the magnetic instability of these rocks, a resolv-

able magnetic polarity sequence conducive to a magnetostratigraphic interpretation was established only for the last 6 Ma. The details of the integrated stratigraphy in the Boso Peninsula is presented by Takahashi et al. (Chapter E8).

Biostratigraphic work on the Middle Miocene sequence in the Tomioka area (23 in Fig. 2) further indicates a high potential for integrated stratigraphic studies since many important planktonic microfossil 'datums' have been recognized in this sequence. The preliminary data for integrated stratigraphy on the Tomioka and adjacent areas (Iwadono and Karasuyama areas) are presented in the papers by Takahashi and Oda (Chapter D5), Takahashi and Saito (Chapter D6), and Odin et al. (Chapter D7) in this volume. The volcanoclastic Shimobe sequence (18 in Fig. 2) also covers the Middle Miocene through Pliocene time interval, but it is not suitable for detailed integrated stratigraphic studies.

The Neogene strata along the Japan Sea side of northeastern Japan exceeds 5000 m in thickness, and constitutes a major source for petroleum and natural gases. A large number of micropalaeontological studies reveal that planktonic foraminifera are missing in the interval represented by the biostratigraphic zones N15 and N18 of Blow (1969). Therefore this sequence is not suitable for integrated stratigraphic research. The Miocene sequence on the Pacific side of northeastern Japan is not as thick as the one along the Japan Sea side, where microfossils are well preserved enough to permit a biostratigraphic zonation (Fig. 1).

The sedimentary rocks in the Joban area (24 in Fig. 3) are mostly diatomaceous, and the calcareous microfossils are rare there. The Sendai, Ichinoseki, and other sedimentary sequences in northern Japan are similar to the Joban sequence. As shown in Figs. 1 and 3, the Neogene rocks in northern Japan yield mainly siliceous microfossils, predominantly diatoms, which favoured cold water in this mid-latitude area. In general, Miocene strata are well developed but calcareous microfossils are rare or absent in northeastern Japan and Hokkaido.

Since the stratigraphic and geographic distributions of fossil species have been affected by world-wide changes in climate, it is most likely that northern Japan may have been under the influence of local cold currents favouring the blooming of diatoms. Consequently, although well preserved, the bio-siliceous Miocene sequences in northeastern Japan and Hokkaido are not suitable for integrated stratigraphic studies requiring a combination of physical-chemical data, geochronologic dates, and a biostratigraphic zonation based on calcareous microfossils.

In summary, the biostratigraphy based on calcareous microfossils (planktonic foraminifera and calcareous nannofossils) was established mainly in central Japan. Integrated stratigraphic data from the Miocene sequences in the Tomioka, Iwadono, Karasuyama, and Boso areas (including Miura Peninsula) are presented in the other technical papers about Japan contained in this volume. These four representative sequences were selected as potentially suitable for integrated stratigraphic studies on the basis of calcareous microfossil content and the possibility of dating interbedded volcanic tuffs by geochronological approach. An integrated stratigraphic study has already been performed in the Tomioka and Boso sequences, whereas the Iwadono and Karasuyama still await further high-resolution integrated stratigraphic studies.

## SUMMARY

In summary, some selected Miocene sequences currently under study in Japan exhibit excellent potential for integrated stratigraphic studies. Past experience has shown that  $^{40}\text{Ar}/^{39}\text{Ar}$  may be a better technique than the traditional K/Ar technique for dating the numerous volcanic tuffs interbedded in these fossiliferous marine sequences. Ultimately, geochronological study of biostratigraphically controlled tuff layers will provide a precise and accurate geochronologic calibration for important 'datums', and magnetic polarity sequences. The results of these integrated stratigraphic studies will hopefully produce the means for a world-wide correlation of Miocene strata, and a refinement of the Miocene stratigraphic time scale.

## SOMMAIRE — GÉOLOGIE, TECTONIQUE ET POTENTIEL POUR LA STRATIGRAPHIE INTÉGRÉE DU JAPON

*(Manuscrit soumis: Novembre 1993; révisé: Mai 1994; rédacteur responsable: GSO)*

Les îles japonaises recouvrent aujourd'hui une large bande latitudinale de 3.500 km. Le Néogène marin y est localement exposé, notamment au nord depuis le début du Miocène Moyen jusqu'au Récent, avec des microfossiles variés, selon les paléolatitudes, plutôt calcaires au sud, plutôt siliceux au nord: Foraminifères planctoniques, coccolithes, Radiolaires, et Diatomées. Au nord-est et au sud ouest, ces îles ont constitué deux arcs se rencontrant au Japon Central actuel et liés à la subduction des plaques Pacifique et Mer des Philippines respectivement. Initialement collé à la marge est de l'Asie, le Japon subit une histoire tectonique fortement marquée par l'ouverture de la Mer du Japon au Miocène Inférieur. Des rotations ont été mises en évidence par études paléomagnétiques au début du Miocène Moyen. Un rifting intra-arc a été identifié au NE créant de petits bassins de dépôt allongés bordés de failles et se remplissant, dès la fin du Burdigalien, de sédiments marins côtiers puis profonds de caractère tropical par une subsidence tectonique atteignant 2 à 3 km au NE, plus faible au SO. Au Miocène Moyen, le SO est émergé, l'arc NE subit une faible subsidence; les faunes déposées passent de microfossiles calcaires à des microfossiles siliceux. L'émission d'un abondant volcanisme accompagne les phases initiales de cette histoire; ce volcanisme diminue au Miocène Moyen tandis que le Miocène Supérieur voit se développer des groupes de calderas qui, émergées, émettent des produits dont les traces sont nombreuses dans les sédiments marins. Les îles japonaises constituent une région clé pour l'intégration des approches et caractérisations stratigraphiques depuis la base du Miocène Moyen. Elles permettent la combinaison de niveaux repères — biorepères — de différents groupes fossiles qui sont utiles pour repérer l'âge des sédiments de sections à terre déposées durant le Miocène Moyen et Supérieur au Japon Central spécialement. Quelques-uns de ces biorepères importants ont été calibrés géochronologiquement par des âges K-Ar et traces de fission sur des niveaux de tufs. Ces derniers sont abondants, souvent riches en minéraux pyroclastiques bien préservés. Par ces qualités, cette région complète idéalement les possibilités rencontrées dans la région méditerranéenne pour l'établissement de corrélations à l'échelle globale.

*(Sommaire proposé par les rédacteurs, GSO)*

**ACKNOWLEDGEMENTS**

We would like thank Prof. G.S. Odin of the Université P. & M. Curie for his helpful comments on the contents of the original paper, and G. Michel (Carleton College) for improving the English.

**Part C**

**STUDIES RELEVANT TO THE LOWER MIOCENE SUBSERIES**

This Page Intentionally Left Blank

*Introduction to Part C*

**INTRODUCTION: THE LOWER MIOCENE**

A. Montanari and R. Coccioni

In the western Tethys domain, the beginning of the Miocene is characterized by widespread explosive volcanism accompanying the uplifting of the Apennine and Alpine orogens. Volcanism was actually active in Sardinia and in the southeastern Venetian Alps (Monti Lessini, Monti Berici, Colli Euganei) since the Late Eocene, but it was mainly characterized by mafic magmatism represented by thick andesite sequences in western Sardinia, and basaltic to trachytic sequences in the Venetian area.

Numerous biotite-rich volcanosedimentary layers interbedded with Upper Eocene and Oligocene pelagic marls throughout the northeastern Apennines represent the distal air-fall products of this Mediterranean mafic volcanism, although their provenance (i.e., Sardinia vs. Alpine or other volcanic sources) remains unknown (Mattias et al., 1987, 1989). Nevertheless, these volcanosedimentary layers provided excellent material for a direct radioisotopic age calibration of the Late Eocene and Oligocene with unprecedented accuracy and precision (e.g., Montanari et al., 1985, 1988d; Odin et al., 1991a, b).

During the Miocene, the western Mediterranean volcanism evolves to a progressively more sialic, explosive magmatism. In western Sardinian, Palaeogene andesites underlay pyroclastic deposits including dacite and rhyolite tuffs which prelude the Early Miocene rifting of the Corso-Sardinian microplate from the southwestern European margin, and its counterclockwise rotation with consequent opening of the Balear Sea (e.g., Alvarez et al., 1974; Assorgia et al., 1994). Once again, the pelagic and hemipelagic basins of the Apennines functioned as relatively tranquil depositional sites for the distal wind-blown tephra produced by the western Mediterranean syntectonic volcanism.

Plagioclase-rich volcanosedimentary layers were found and dated by Odin et al. (Chapter C1) in the Carrosio section (northwestern Apennines), and yielded  $^{40}\text{Ar}$ - $^{39}\text{Ar}$  ages around 22.4 Ma, therefore consistent with a lowermost Miocene age inferred from the planktonic foraminiferal record.

Several Lower Miocene, marine, fossiliferous sections in the northeastern Apennines of the Emilian region contain volcanosedimentary layers with plagioclase and biotite suitable for radioisotopic dating (Odin et al., Chapter C2), and yielded preliminary  $^{40}\text{Ar}$ - $^{39}\text{Ar}$  ages ranging between 22 and 19 Ma. Thus, these sections bear a strong potential for the calibration of the Early Miocene chronostratigraphic scale although they require further studies for improving the precision of both radioisotopic ages and biostratigraphic determinations.

In the northeastern Apennines of the Umbria and Marche regions, the Lower Miocene is represented by the Bisciario formation, and the lower part of the overlying Schlier formation. The general mafic to sialic evolutive trend of the Miocene Mediterranean volcanism is reflected by the mineralogy of the volcanosedimentary layers interbedded



with these pelagic units. In the Bisciario formation, sanidine is totally absent and the felsic fraction is represented mostly by andesine (plagioclase: An<sub>36–52</sub>), quartz, and traces of anorthoclase. Amphiboles and heavy minerals are rare, and biotite is present only in a very few ash layers. Rare sanidine first occurs in a biotite-rich layer which marks the boundary between the Bisciario and the Schlier formations (mid-Burdigalian). Sanidine is then found as an accessory mineral in practically all the volcanosedimentary layers in the upper Burdigalian to Tortonian Schlier formation.

The Bisciario in the Contessa Valley, near Gubbio, is exposed in continuity with the underlying Palaeogene and Cretaceous pelagic carbonate sequence which has been the object of various stratigraphic and geochronologic studies (e.g., Lowrie et al., 1982; Montanari et al., 1985, 1988a,b, 1991; Nocchi et al., 1986). A first integrated stratigraphic study of the Bisciario section at Contessa was carried out by Montanari et al. (1991) who produced a detailed biostratigraphy based on planktonic Foraminifera and calcareous nannofossils, a magnetostratigraphy, a strontium isotopic profile throughout the Oligocene and Lower Miocene, and <sup>40</sup>Ar–<sup>39</sup>Ar single-crystal laser fusion dates on plagioclase from two volcanoclastic layers bracketing the Aquitanian/Burdigalian boundary. In Chapter C3, Montanari et al. present new data from Bisciario exposures at Contessa improving the magnetostratigraphy, biostratigraphy (planktonic Foraminifera, calcareous nannofossils, and dinoflagellates), chemostratigraphy (Sr, O, and C isotopes, and trace elements), and geochronology of the upper Chattian to mid-Burdigalian interval previously studied by Montanari et al. (1991).

New <sup>40</sup>Ar/<sup>39</sup>Ar step heating analyses on plagioclase originally dated with the single-crystal laser fusion technique permit a tightly interpolated age estimate of 20.5 Ma for the first occurrence of *Globigerinoides trilobus* which constitutes a useful biomarker for the identification of the Aquitanian/Burdigalian boundary. However, the lower part of the Bisciario and the uppermost part of the underlying Scaglia Cinerea in the Contessa section are strongly condensed and may contain one or more hiatuses compromising the accuracy for the age estimate of biostratigraphic boundaries. For the same reason, the recognition of the Oligocene/Miocene boundary in this incomplete interval remains uncertain. Nevertheless, new palaeomagnetic data, which permit the identification of Chron 6C, and the refinement of the planktonic foraminiferal biostratigraphy, restrict the location of this within a geochronologically calibrated interval ranging from 25 Ma to 23.5 Ma.

Combined biostratigraphic and magnetostratigraphic analyses of a new stretch of the Bisciario section exposed along the Contessa highway permit the identification of the N6/N7 planktonic foraminiferal zonal boundary in the lower part of Chron 5Cr. This allows the correlation of the upper part of the Contessa section with the lower part of the Moria section described by Deino et al. in Chapter D1, and provides stratigraphic continuity and completeness for the Lower Miocene sequence in the Umbria–Marche region.

The most continuous and complete section of Bisciario known at present in the Umbria–Marche Apennines is located at Santa Croce di Arcevia, about 35 km northwest of Gubbio. This section bears a great potential for high-resolution integrated stratigraphy of the Lower Miocene. The only drawback is that it is located in a private backyard and the access for sampling requires permission from the land lord. Nevertheless, Coccioni et al. in Chapter C4, produce a detailed lithostratigraphy and biostratigraphy

based on planktonic Foraminifera, calcareous nannofossils, and dinoflagellate cysts. These results help to implement the condensed and incomplete Contessa section, and permits correlation with the upper Burdigalian portion of the Moria section described in Chapter D4.

In the Ebro basin of northern Spain, the Early Miocene is mostly represented by continental deposits. In Chapter C5, Odin and co-workers describe the floral and mammal biostratigraphy of this vast basin reporting the presence of a conspicuous volcanoclastic layer which can be recognized in several distant sections. Fresh sanidine contained in this volcanoclastic marker yielded a  $^{40}\text{Ar}$ - $^{39}\text{Ar}$  plateau age of 19.4 Ma which constitutes a strong geochronologic tight point for correlating Lower Miocene (Ramblian) continental biostratigraphy with Tethyan marine biostratigraphy which is well calibrated in the Italian sections.

This Page Intentionally Left Blank

*Chapter C1*

**INTEGRATED STRATIGRAPHY NEAR THE OLIGOCENE/MIOCENE  
BOUNDARY IN THE PIEDMONT BASIN (ITALY): BIOSTRATIGRAPHY AND  
GEOCHRONOLOGY**

G.S. Odin, A. d'Atri, F. Tateo, M. Cosca and J.C. Hunziker

INTRODUCTION

Geologists working in Italy have suspected the presence of volcanoclastic layers within sediments assumed to be near to the Oligocene/Miocene boundary (Guerrera and Veneri, 1989), for example, in the Piedmont Basin (Bersani et al., 1987; Minguzzi et al., 1987; d'Atri, 1990; Tateo, 1992 and references therein), the northern Apennines (Bologna area, Selli, 1948; Cati, 1974; Borsetti et al., 1983) and more to the south in the Marche Region (section of Casa di Tosi: Cati et al., 1981). This situation is rare in the world. We have undertaken studies aimed at characterizing by isotopic dating sediments correlated to near the Oligocene/Miocene boundary according to biostratigraphical control.

The Piedmont Tertiary Basin (northern Italy) is a well suited area for location of the Oligocene/Miocene boundary. The search for the definition of a Global Stratotype Section and Point (GSSP) has been undertaken for a long time, and special attention has been focused on the Lemme section, near Carrosio (Piedmont basin, northwestern Italy; Cati et al., 1981; see also Steininger et al., Chapter A9), and in the surrounding palaeobasin where volcanoclastic layers have been found. We have also investigated other sections particularly promising for an integrated stratigraphic study (Selli, 1948; Cati, 1974; Borsetti et al., 1984) in the Monte Arligo area (near Bologna, in the Emilia Region). However, the stratigraphic location has been revised during our study (see Odin et al.). In this paper we present our first results on the Bosio section (Piedmont basin).

LITHOSTRATIGRAPHY AND LOCATION OF THE SECTIONS

*Lithostratigraphy*

The sections discussed in this paper are located in the southeastern margin of the Tertiary Piedmont Basin (Fig. 1) where an Oligocene/Miocene, mainly terrigenous succession unconformably overlying some pre-Oligocene Apenninic and Alpine structural units is well exposed.

These sections were measured in a lithostratigraphic unit locally named 'Marne di Rigoroso' formation (Boni and Casnedi, 1970). This unit is time-equivalent to the Rocchetta formation of Gelati (1968) or the Antognola Marl unit of Gelati (1977) deposited in adjacent areas. The Marne di Rigoroso formation consists of slope-to-basin

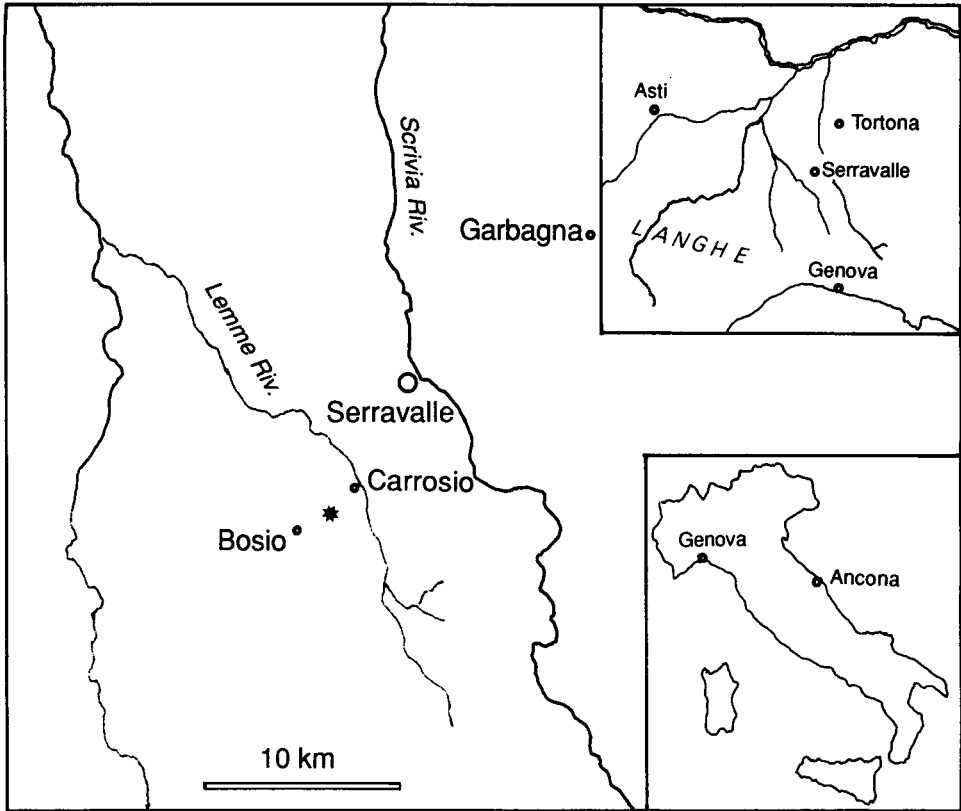


Fig. 1. Location of the studied area. The dated section is shown (\*) between Carrosio and Bosio. Note that the area hosts a number of type location for Cenozoic stages.

hemipelagic marls with interbedded arenitic turbiditic layers (Andreoni et al., 1981) deposited during the Oligocene to Early Miocene time. This unit overlies Oligocene fan delta conglomerates with sandy, shallow-water intercalations and are followed by Early Miocene basinal plain turbidites. The lithology comprises silty to clay-rich marls and rare 1–10 cm thick sandstone beds which denote periods of steady deposition in an unchanged environment. The Bosio section and the nearby Lemme section are located in the upper part of the formation. They are bound at the top by a discontinuity surface overlain by a calcareous marl of late Burdigalian age in Bosio (d'Atri, 1990).

In the whole region surrounding the Lemme Valley, an erosional hiatus is present at the top of Marne di Rigoroso formation. Usually, early or late Burdigalian sediments directly overlie the Marne di Rigoroso formation (Gelati, 1968; d'Atri, 1990). A smaller hiatus is present in a restricted sector near Carrosio where the Aquitanian portion of the Marne di Rigoroso was not eroded. Otherwise, this chronostratigraphic interval is totally missing in adjacent areas. Therefore, the site near Carrosio is exceptional compared to the surrounding outcrops.

### Location

The so-called Lemme section is located west of the village of Serravalle Scrivia, to the north of the River Lemme, about 300 m from and to the east-northeast of the church of Carrosio. The measured section includes the hemipelagic marls of the Marne di Rigoroso formation, and it is considered for the definition of the Oligocene/Miocene boundary following a preliminary research by Cati et al. (1981). More recent studies suggest that this section is the best available (IUGS Palaeogene–Neogene Working Group (WG), Borsetti, 1992; Steininger, 1992; Steininger et al., Chapter A9).

The Bosio section is located 2.5 km to the southwest of Carrosio. On the left side of the small road from Carrosio to Bosio, about 3 km after leaving the first and 2 km before reaching the second village, there is a trail going up. This section is exposed along the side of the trail, it is about 1 m high and several tens of metres long.

### BIOSTRATIGRAPHIC INFORMATION

According to Steininger (1992) “the measured part of the (Lemme) section spans the time interval from the Late Oligocene (below the last occurrence of *Sphenolithus ciperoensis*, to the Early Miocene (above the first occurrence of *Globigerinoides altiaperturus*).” On the basis of recent data including bio- and magnetostratigraphic investigation, the Palaeogene–Neogene WG proposed the epoch boundary to be located at metre level 35, in correspondence with what is supposed to be the reversal between Chron 6Cn.2r and Cn.2n, and which, in this section, may be correlated to other signals such as: (1) the first occurrence (FO) of *Paragloborotalia kugleri*, (2) the FO of *Globoquadrina dehiscens* (both planktonic Foraminifera), (3) the last occurrence (LO) of *Dictyococcites bisectus* (calcareous nannofossils), and other bio-signals (Borsetti, 1992; Steininger, 1992).

Replicated sampling for calcareous nannofossils and planktonic foraminiferal biostratigraphy (28 samples were collected with a 1 m spacing) was carried out by one of us (A. d’Atri) in the Bosio section. For calcareous nannofossils, a quantitative approach collecting of data was used following methods discussed in Backman and Shackleton (1983), and Rio et al. (1990a).

Both planktonic foraminiferal and calcareous nannofossil contents are quite abundant and diversified, and the preservation is fairly good. The planktonic foraminiferal assemblage is characterized by the presence of *Paragloborotalia pseudokugleri* and *P. gr. kugleri* throughout the section. The specimens of *P. gr. kugleri* have the following features: plano-convex test, only 5–6 chambers in the last whorl and straight to slightly arched sutures on spiral and umbilical sides. These features do not permit to refer the specimens present in the Bosio section to *P. kugleri* s.s. as originally described by Bolli (1957). For this reason they are indicated as *P. gr. kugleri*. The taxon *Globoquadrina sellii* (very rare) is discontinuously present at the base of the section and seems to disappear 1 m above the volcanoclastic layer. This observation is interpreted as the result of reworking of a taxon which becomes extinct during the Late Oligocene.

The first occurrence of *P. gr. kugleri* has been considered the lower boundary of the *Paragloborotalia kugleri* Zone in the Lemme section, Early Miocene in age according to the Palaeogene–Neogene Working Group (A.M. Borsetti, pers. commun., 1994).

Thus, the Bosio section is referable to the *Paragloborotalia kugleri* Zone (i.e., Lower Miocene).

The presence of a gap at the top of the section does not permit to recognize the FO of *Globoquadrina dehiscens* and the other bio-signals present in the Lemme section (Borsetti, 1992; Steininger, 1992).

The calcareous nannofossil assemblage is characterized by the absence of the Late Oligocene *Sphenolithus ciproensis* and *S. distentus*. The presence of *Dictyococites bisectus* allows to refer the volcanoclastic layer to the lower part of subzone CN1a of Okada and Bukry (1980).

*D. bisectus* has its last common occurrence (LCO) just above the volcanoclastic layer (Fig. 2). The significance of this bioevent is not known with certainty. According to the zonal model of Okada and Bukry (1980), the LO of *D. bisectus* is used as an alternative criterion to define the CP19/CN1 boundary primarily defined by the LO of *Sphenolithus ciproensis*. This zonal boundary is generally correlated to the Oligocene/Miocene boundary. In the Mediterranean area, the LO of *D. bisectus* does not appear to be a time-significant event. On the contrary, the drop in frequency (LCO) of the taxon seems

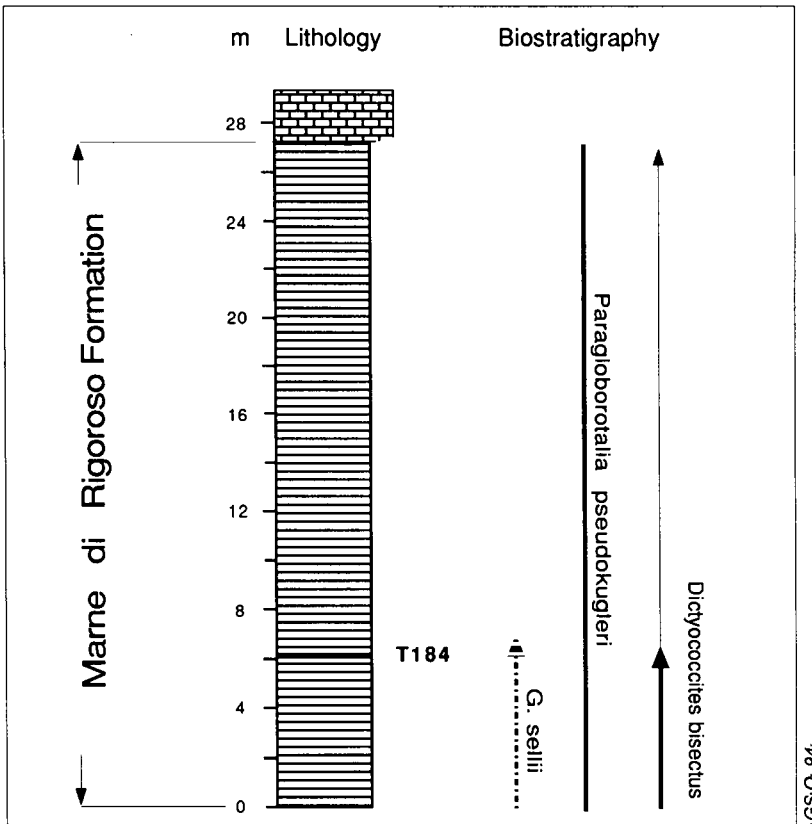


Fig. 2. The Bosio section (near the road from Carrosio to Bosio). The last common occurrence of the nannofossil *D. bisectus* is just above the volcanoclastic layer (original data by A. d'Atri).

to be a regional correlation criterion (E. Fornaciari and D. Rio, pers. commun., 1994). The LCO of *D. bisectus* is reported in the literature (Montanari et al., 1991; Fornaciari and Labaume, 1992). In the Contessa section, Montanari et al. (1991) located the FO of *P. kugleri* below both the FO of *S. ciproensis* and the LO of *Dictyococcites bisectus*. In the same section, Coccioni and Monechi (1992), and Montanari et al., Chapter C3), instead report the FO of *P. kugleri* above (after) the LCO of *D. bisectus*. However, Monechi clearly indicates that this bio-signal, being a question of relative abundance, can only be located tentatively. In the present work, the LCO of *D. bisectus* is observed to be after both the LO of *S. ciproensis* and the FO of *P. gr. kugleri*.

The LCO of *D. bisectus* may probably be recognized in the Lemme section (cf. Cati et al., 1981, fig. 13: in that figure, the taxon is called *D. dictyodus*). Therefore, the location of the volcanoclastic layer from Bosio may be precisely correlated to the nearby proposed GSSP-bearing section, and could be compared to the epoch boundary. However, G. Villa (pers. commun., March, 1996) informed us about her results on the variation of abundance of *D. bisectus* (*R. bisecta*) in the Lemme section. The drop in abundance from values of about 3–4% to values smaller than 1.5% occurs between samples collected at metre levels 49 and 50. This has been considered a last common occurrence and corresponds to about 15 metres below the level proposed for locating the Oligocene/Miocene boundary at metre level 35. There is a second drop in abundance from 1 to 1.5% to less than 0.5% between metre levels 34 and 35 in the same section.

## GEOCHRONOLOGY

### *Petrography and mineralogy of the geochronometers*

*Search for volcanoclastic layers in the Lemme section.* A sample from the Lemme section assumed to be a lapilli was provided by Dr. F. Rögl in 1990. Following mineral separation, it was concluded to be a partly altered pyritic nodule. The section was later sampled by one of us (GSO) to consider particular layers well marked in the outcrop. These layers are thin, often wet and thus favourable for vegetation growth, and distinctly different in lithology from the rest of the marly suite. Some are rich in dense ellipsoidal nodules. The optical composition of the silt–sand fraction ultrasonically cleaned is from dominant to rare: carbonate debris, pyrite, foraminifers, white mica flakes, altered biotite flakes.

Five other samples collected independently by another one of us (FT) from the same section were analyzed using X-ray diffraction and thermal analyses. Their appearance in the field is distinctive (red colour, water content, S-rich nodules, hardness). However, the mineralogical composition was similar to that of the rest of the succession (abundant quartz, calcite, terrigenous clay minerals, and other minor phases). A detailed account will be given elsewhere (Tateo, 1997).

In summary, a significant volcanic input, free of detrital contamination and suitable for age calibration was never detected in this section.

*Search for other favourable sections in the vicinity of Carrosio.* The Garbagna section is considered to be of Late Oligocene age by Gelati (1977), and Guerrerra and Veneri (1989). One sample collected for petrographic study represents the base of a volcanoclastic composite bed (about 2 m thick) first described by Sersale et al. (1963).



In the field, hand specimens are light and the colour is distinctive (light yellow to light pink). Details on the mineralogy and geochemistry are quoted by Minguzzi et al. (1987, 1990, sample 90). The most common mineral is Ba-phillipsite (phillipsite is usually a Ba-free zeolite), minor amounts of other zeolites (heulandite and chabazite) are admixed; smectite, feldspars, quartz, and calcite are also present. Geochemical data based on 'immobile' element ratios display alkaline affinity to parental magma confirmed by the sanidine occurrence reported by Bersani et al. (1987).

Mineral separation from the sample was undertaken following gentle crushing of the tuff with a large hammer. Biotite crystals (0.2% of the W-R) are brilliant, thin, brown, idiomorphic flakes, 0.1–0.2 mm in diameter. Feldspar is present (less than 1% of the W-R). Idiomorphic short crystals of apatite (less than 0.08%) and short, pink crystals of zircon (about 80 crystals per kg) have been identified. A small proportion of probable amphibole, 0.1–0.2 mm thin, heavy, magnetic, green–brown, is also present. X-ray diffraction shows that biotite is well preserved with no 14 Å peak, but the feldspar, probably sanidine, is poorly crystallized. Therefore, the search for datable minerals was successful and the layer would be favourable for age calibration. However, following recent biostratigraphic study (d'Atri and Tateo, 1994) the section usually ascribed to the Late Oligocene is now correlated to the Early Oligocene and cannot be used to calibrate the Oligocene/Miocene boundary.

In the Bosio section, the habit of the material from the Marne di Rigoroso formation (d'Atri, 1990), is that of hard lenses, about 10 cm thick, white when fresh, generally rusty and partly oxidized (Fig. 3). The layer is only visible at a distance of 2 m. In the field, the hard layer is clearly different from the rest of the section, an homogeneous marly facies, grey–yellow in surface. Under binocular microscope, the sawed white rock shows small black dots identified as amphibole crystals which are irregularly distributed (with sedimentation figures). The rock also contains a few centimetre-large pieces of the surrounding sedimentary matrix with its fresh grey–green colour.

The petrographic study undertaken in Bologna using thin-sections and X-ray diffraction allowed identification of abundant and clear feldspars, zeolites (including wellsite–harmotome), amphibole, less abundant pyroxene, rare volcanic quartz. A calcite matrix and locally abundant ferric oxi-hydroxides are also present. Therefore, the hard layer appears pyroclastic in origin and can be related to orogenic calc-alkaline magmatism of andesitic–dacitic composition according to geochemical and mineralogical data (d'Atri and Tateo, 1994).

Purification of the geochronometers was undertaken on a 5 kg sample. The hard sample was sawed for selection of non-oxidized pieces, then crushed and soaked in 15% HCl for two days. An abundant and pure fraction of clear feldspar was obtained from the 0.25–0.10 mm size fraction. A small quantity of amphibole was also purified. According to the X-ray diffraction study, the feldspar is a well crystallized (high peaks) plagioclase with a (131) (131) distance of 2.07° (Ca plagioclase). Hornblende is pure.

The presence of zeolites in these layers is diagnostic and needs comment. The phillipsite–wellsite–harmotome group is characterized by the increasing content of barium (from 0–1 to 19–22% BaO for phillipsite and harmotome, respectively; Cherny et al., 1977). The problems are (1) the reason for the presence of zeolite which is not a pyroclastic mineral, and (2) the reason for an abundance of barium which is not so common in volcanic rocks. These problems would need a long discussion. In short,

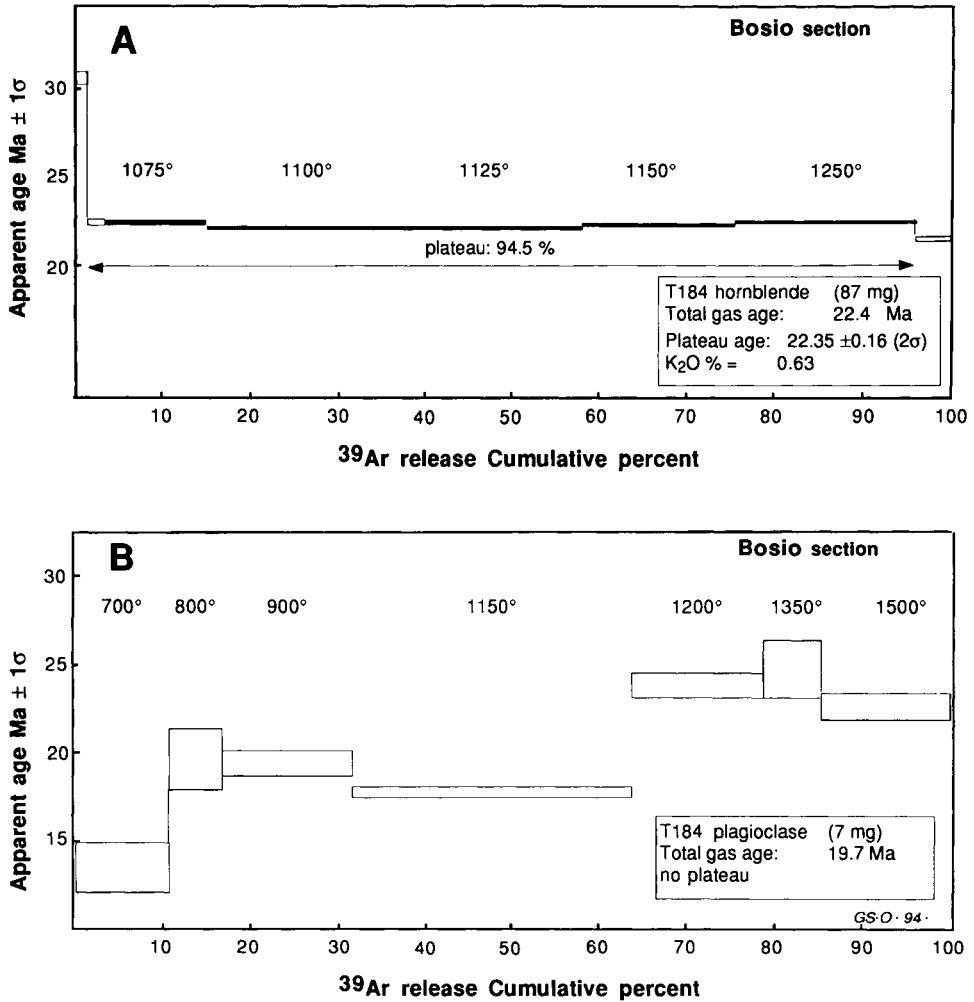


Fig. 3. <sup>40</sup>Ar/<sup>39</sup>Ar analytical results for the hornblende (A) and plagioclase (B) from the Bosio section

zeolites testify for hydrothermal activity with interaction between volcanic material and water. This may occur during the eruptive phase (before explosion) but possibly (?) also within the marine basin. In our study, this is important because the presence of zeolite may be interpreted as the source for two contrary disturbances. (1) If zeolites have formed following initial eruption of the magma and before later explosion, then the dated minerals have crystallized 'some time' before their inclusion in the stratigraphic column and, especially for the stable ones such as amphiboles, the measured radiometric ages will be older than the time of deposition. (2) If zeolites have mainly formed within the marine basin, the measured ages will be able to give the actual age of crystallization near that of explosion and deposition in the basin; however, because zeolite genesis denotes a significant geochemical activity in the deposited volcanigenic layer, then, the fragile pyroclastic minerals (such as biotite or plagioclase) may be

geochemically disturbed; their apparent age will result, modified in different ways depending on whether K will be lost or enriched and radiogenic argon will be lost. This actually results in a complex situation as far as the reliability of the geochronometers is concerned.

#### $^{40}\text{Ar}/^{39}\text{Ar}$ isotopic analyses

The  $^{40}\text{Ar}/^{39}\text{Ar}$  analytical technique was applied using the incremental heating procedure in Lausanne (Cosca et al., 1992). Irradiation was made in the Triga reactor in Denver using HD-B1 biotite as the monitor with a K–Ar age of 24.21 Ma. The hornblende was first backed under vacuum at 600°C. Nine heating steps were measured independently on 87 mg of purified mineral. There was no measurable gas in the last step at 1600°C. The results are shown in Table 1 and Fig. 3.

The integrated total gas age is 22.42 Ma. The spectrum in Fig. 3A shows one deviating step at 950°C. Five successive heating steps representing 94.5% of the gas released define a plateau with the criterion that the independently calculated ages are not different at the 95% confidence level. The calculated weighted mean plateau age is  $22.35 \pm 0.16$  Ma ( $2\sigma$  analytical precision including intralaboratory calibration of neutron flux).

The plagioclase was first backed at 600°C for 25 min and then eight heating steps were measured independently on 7 mg of pure plagioclase (a small quantity). Results are shown in Table 2 and Fig. 3B. The age spectrum is disturbed. Step ages are spread, with a group of 3 at 18–20 Ma, and another group at 23–25 Ma for high-temperature heating steps. The apparent total gas age is calculated at 19.7 Ma. The total gas age is younger compared to the age calculated for the hornblende separate. This situation is in contrast to that encountered when dating pairs of minerals including plagioclase during this project: usually, plagioclase separates gave significantly older apparent ages compared to the other dated phase and the known stratigraphic age.

Possible interpretations of these results are: (1) non-meaningful ages, (2) an analytical disturbance (gas lost during irradiation), or (3) a mixture of presence of extraneous argon as suspected from the high-temperature steps and of loss (recrystallization following

Table 1  
Isotopic results on hornblende T184 from the Bosio section

°C	Apparent age	$\pm 2\sigma$	% $^{39}\text{Ar}$	% Rad.	K/Ca
950	31.6	1.4	1.32	18	0.025
1050	22.5	0.6	1.94	66	0.051
1075	22.52	0.30	11.61	88	0.051
1100	22.13	0.28	20.08	91	0.051
1125	22.15	0.28	22.88	93	0.051
1150	22.33	0.28	17.43	93	0.052
1250	22.62	0.28	20.58	88	0.050
1400	21.5	0.4	4.16	78	0.046

Sample weight = 87.51 mg; error in  $J=0.5\%$ ; calculated apparent ages (total gas age) =  $22.42 \pm 0.17$  Ma; (plateau age 1050–1250: 94.5%) =  $22.35 \pm 0.16$  ( $2\sigma$ ).

Table 2

Isotopic results on plagioclase T184 from Bosio (preliminary data)

°C	Apparent age	$\pm 2\sigma$	% <sup>39</sup> Ar	% Rad.	K/Ca
700	13.3	2.8	10.6	5	0.14
800	19.9	3.4	6.0	28	0.10
900	19.3	1.4	14.7	58	0.06
1150	17.7	0.6	32.2	74	0.04
1200	23.8	1.4	15.2	56	0.02
1350	25.0	3.2	6.6	41	0.02
1500	22.4	1.4	14.6	43	0.02

The sample weight = 7.34 mg; calculated apparent age (total gas age) = 19.7 ± 0.6 Ma; disturbed spectrum.

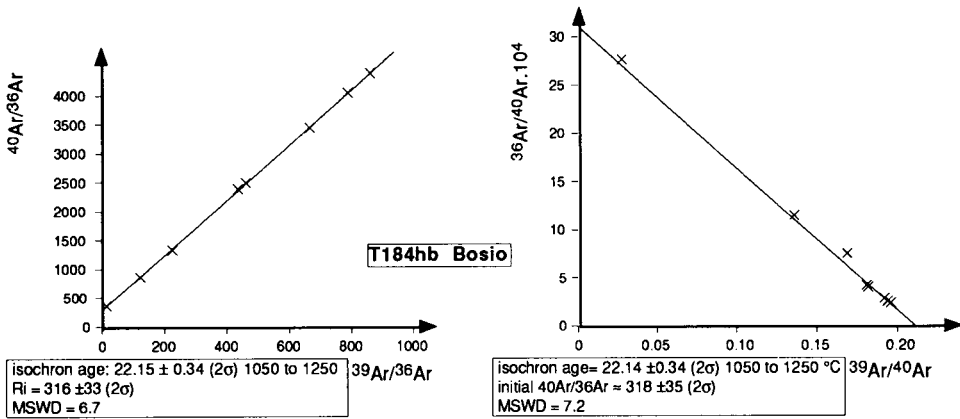


Fig. 4. Isochron plots of the <sup>40</sup>Ar/<sup>39</sup>Ar measurements on hornblende from Bosio.

eruption) as evidenced by low-temperature heating steps. We suggest that the presence of abundant zeolite may be related to and explain this unusual analytical observation. The volcanogenic material would have been submitted to important geochemical transformation after deposition significantly modifying the isotopic equilibrium within the plagioclase.

Using steps on the plateau (1050–1250°C), isochron calculations on the age results obtained from the hornblende lead to similar ages using either plot (Fig. 4). The resulting isochron ages are similar to the plateau age considering the larger analytical errors for the former ( $22.15 \pm 0.34$  and  $22.14 \pm 0.34$  Ma, respectively). The corresponding initial Ar isotope ratios ( $316 \pm 32$  and  $318 \pm 34$ , respectively) are consistent with an initial atmospheric composition. The MSWD (6.7 and 7.2, respectively) suggest that the points representative for the different steps are not perfectly colinear but the deviation remains reasonably small.

In summary, well crystallized hornblende and plagioclase are present and demonstrate a pyroclastic origin of the layer. Sedimentary evidence observed in the layer invalidate the hypothesis that the layer could be of laccolitic origin; the <sup>40</sup>Ar/<sup>39</sup>Ar isotopic analysis indicates that the geochemical equilibrium has been disturbed in the plagioclase but

probably not in the geochemically more stable hornblende (good plateau). A geological age may be derived from the hornblende.

## STRATIGRAPHICAL DISCUSSION AND CONCLUSIONS

### *Biostratigraphical constraints*

The biostratigraphic study of some sections in the SE margin of the Tertiary Piedmont Basin has permitted to select the single section suitable for numerical age calibration of the Oligocene/Miocene boundary. The isotopically dated volcanoclastic layer of Bosio is located near to a biostratigraphic signal (LCO of *Dictyococcites bisectus*). The section shows everywhere the presence of a taxon first referred to as *P. pseudokugleri* (and then correlated to the Oligocene) but later combined to a *P. kugleri* group (and then correlated to the Miocene). The LCO of *D. bisectus* is commonly considered more recent (but sometimes quoted older) than the FO of *P. kugleri* (present in the nearby Lemme section). The chronostratigraphical age is assumed to be younger but potentially very near to the epoch boundary.

### *Geochronological constraints*

The analytically precise age of the hornblende at  $22.35 \pm 0.16$  Ma is related to the accepted value of 24.21 Ma for the monitor allowing calibration of the neutron flux. However, the age of the monitor biotite HD-B1 is only known with a large error bar ( $\pm 2.5\%$ ,  $2\sigma$ ) which should be incorporated into the analytical age to derive a realistic geological age of  $22.3 \pm 0.7$  Ma.

### *Time-scale calibration*

The present age estimate of the Oligocene/Miocene boundary is between 22.5 and 23.5 Ma (Odin, 1994). According to Montanari et al. (1991), interpolation between Mid-Oligocene and late Aquitanian isotopically dated levels from the Contessa area (Umbria) would suggest an age of 22.0 e.Ma (e.Ma = estimated Ma) for the local first occurrence of *G. dehiscens* and 23.4 e.Ma for the local first occurrence of *Paragloborotalia kugleri*.

Our age is obtained from a layer interbedded with layers apparently (biostratigraphically) located in between the two bio-signals dated by interpolation by Montanari et al. (1991), if the key fossil marker horizons are contemporaneous in the two distant areas (Umbria: Contessa; and Piedmont: Carrosio). The face value at 22.3 Ma suggests (1) that the two key fossils *G. dehiscens* and *P. kugleri* are in similar succession and age in the two areas; (2) that the dated volcanic event is in between the bio-signals dated in Umbria, and (3) that the Oligocene/Miocene boundary is slightly older than 22.3 Ma and was correctly estimated by the previous authors (Montanari et al., 1991; Odin, 1994) although possibly slightly younger than the age of 23.4 Ma proposed by the former.

The new data reported in this volume indicate: (1) that the younger volcanic event used for interpolation (Raffaello Level) may be older by 0.6 to 0.8 Ma than was accepted in 1991; (2) that the location of the Palaeogene/Neogene boundary in the

Contessa section is inconsistent by 3 m (or about 1 Ma) depending on the use of either the magnetotratigraphic control or the biostratigraphic control. In this situation, numerical ages resulting from a sedimentary interpolation is debatable.

**SOMMAIRE — STRATIGRAPHIE INTÉGRÉE PRÈS DE LA LIMITE OLIGOCÈNE/MIOCÈNE DANS LE BASSIN DU PIÉMONT (ITALIE): BIOSTRATIGRAPHIE ET GÉOCHRONOLOGIE**

*(Manuscrit soumis: Décembre 1993; révisé: Janvier 1995; rédacteur responsable: GSO)*

La section type proposée à Carrosio (Piémont, Italie) pour la limite Oligocène/Miocène ne semble pas contenir de niveau utilisable en géochronologie. Cependant, dans les environs immédiats, un affleurement a montré la présence d'un tuf compact à biotite, hornblende et plagioclase. D'abord attribué à l' Oligocène, ce tuf a ensuite été rapporté au Miocène basal par la présence de *Paragloborotalia pseudokugleri* notamment. Deux géochronomètres extraits du tuf ont été soumis à une analyse isotopique préliminaire par la technique  $^{39}\text{Ar}/^{40}\text{Ar}$  et chauffage par paliers. Le spectre d'âge du plagioclase ne présente pas de plateau et cette phase ne paraît pas digne de confiance. La hornblende a livré un plateau acceptable dont l'âge de  $22,35 \pm 0,16$  Ma (incertitude analytique interne) est identique à l'âge total et proche des âges sur isochrones. Ce résultat est en accord avec la localisation géochronologique de la limite entre 22,5 et 23,5 Ma, peut-être vers 23 Ma.

*(Sommaire des auteurs)*

**ACKNOWLEDGEMENTS**

Isotopic measurements for this study by G.S. Odin were achieved thanks to facilities made available by the Fonds National Suisse in Lausanne. The authors acknowledge improvement of the English by A. Montanari. No funding was provided by French Organizations for this research.

This Page Intentionally Left Blank

*Chapter C2*

**INTEGRATED STRATIGRAPHY (BIOSTRATIGRAPHY AND GEOCHRONOLOGY) OF THE EARLY MIOCENE SEQUENCE FROM THE EMILIAN APENNINES (ITALY)**

G.S. Odin, A. Amorosi, F. Tateo, R. Coccioni, M. Cosca, A. Negri, G.A. Pini and J.C. Hunziker

**INTRODUCTION**

Volcaniclastic layers interlayered within marine sediments of Early Miocene age have been reported from many sections of the Emilia and Marche Apennines. Ten sections are considered by Borsetti et al. (1979a, 1979b) who emphasize the common explosive volcanic activity 'at the Oligocene/Miocene boundary'. These volcaniclastic layers were studied during elaboration of doctoral theses dealing with the sedimentology (Amorosi, 1993) and petrography (Tateo, 1992) of Oligocene and Miocene deposits in northern Italy. The presence of volcanic layers within a marine sedimentary sequence and the general goals of the Miocene Columbus Project (Integrated Stratigraphy with particular emphasis on the geochronological–biostratigraphical connection) led us to focus on gathering information on selected sections relevant for integrated stratigraphy.

**GEOLOGICAL SETTING, LITHOSTRATIGRAPHY, AND SAMPLE LOCATION**

The studied sections are located to the south of the Po River, on the northern edge of the Apennines (Fig. 1). The regional lithostratigraphy in Emilia Apennines defines three units: (1) the Antognola Marls (lower portion of the Antognola Formation); (2) the Marne Selciose (Siliceous Marls) (higher portion of the Antognola Formation); and (3) the Bismantova Formation. There is a similar time-equivalent lithologic succession in the Umbria–Marche Apennines (to the south) and the Piedmont Basin (to the west) with a common siliceous unit called 'Bisciaro' in Umbria–Marche, as shown in Fig. 2.

The three units are all part of the semi-allochthonous complex (Ricci-Lucchi, 1987). This structural unit is composed of slabs of various size, made up of Eocene to Pliocene deposits, overlying the strongly tectonized clayey formations of the Ligurian nappe ('Argille scagliose'). The sedimentological study of the semi-allochthonous units (Ricci-Lucchi, 1986; Amorosi, 1992) shows that an abrupt facies change occurs between Eocene to Early Miocene deep-water (turbidite) facies and Miocene shallow-water (shelf to marginal marine) deposits. This facies change, corresponding to the boundary between the marly Antognola Formation and the overlying arenaceous Bismantova Formation in the Emilia Apennines, marks a tectonic phase known as the Burdigalian phase (Boccaletti et al., 1990).

The studied sections are located in the upper member of the Antognola Formation which is composed of highly siliceous marls and associated volcaniclastic layers, form-



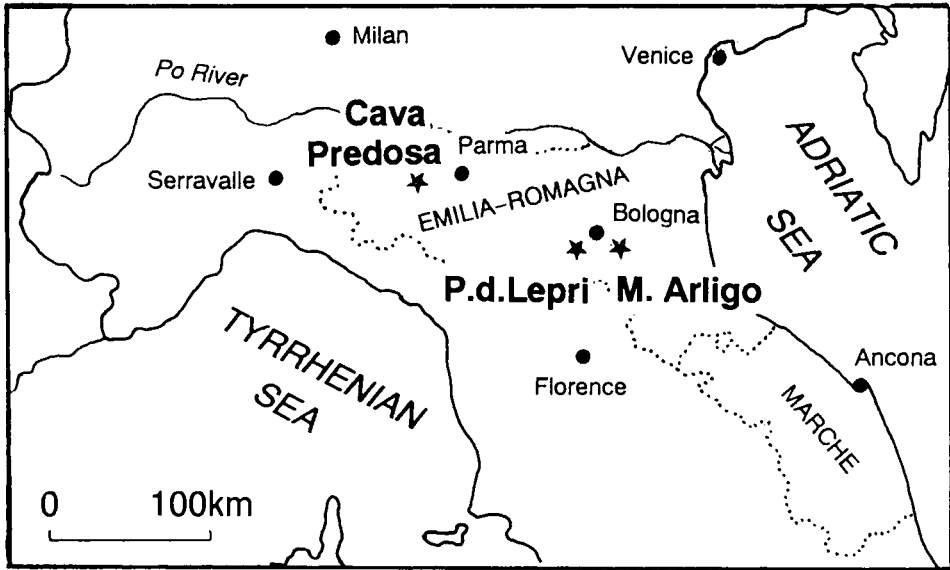


Fig. 1. General location of the studied sections in the Emilia-Romagna region.

ing a distinctive unit in the Lower Miocene of the Emilia Apennines, locally known as 'Contignaco Tripoli' (Parma Apennines), 'Siliceous Marls' (Bologna Apennines), and 'Campaolo Formation' (Romagna Apennines). Lithologically time-equivalent successions have been reported in different structural basins (Fig. 2) such as the Piedmont Basin, the foredeep area (Cervarola, Falterona, and Vicchio formations), and the foreland ramp (Bisciaro Formation). All of these units have been recently reported as part of a distinct Lower Miocene 'Siliceous lithozone' (Amorosi et al., 1992), which finds coeval analogs in the whole Mediterranean area (Didon et al., 1969; Wezel, 1977; Lorenz, 1984).

### *Cava Predosa*

The first section considered in this paper is located southwest of Parma, 2 km south of Salsomaggiore, near Contignaco (Fig. 3), in an abandoned quarry: the Cava Predosa. The Early Miocene Siliceous lithozone is here represented by the Contignaco Tripoli (Pieri, 1961), whose thickness in the Parma area ranges between 35 and 100 m (Sestini, 1970). The Contignaco Tripoli is mainly composed of diatomaceous marls locally containing abundant volcanic material. The occurrence of volcanoclastic layers within this unit was first recognized by Selli (1948); detailed studies were then carried out by Mezzetti and Olivieri (1964). The studied section displays a fresh exposure of two thick tuff layers, mainly glassy cinerite, white, generally poor in pyroclastic minerals, and obviously composed of a series of graded layers. Several samples were collected from the base of the second and main volcanoclastic unit. The mineral-rich level selected for dating was collected from the very base: a mm-thin level (T163) with a local occurrence of biotite-rich material.

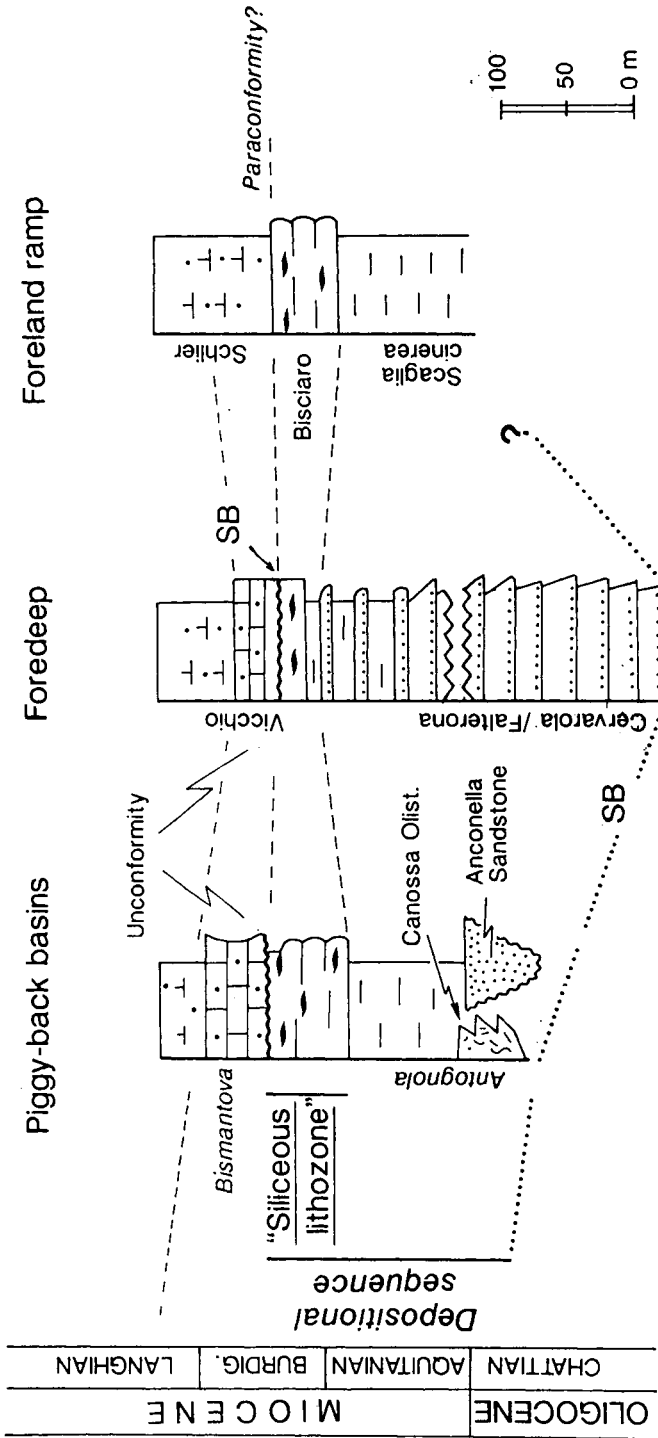


Fig. 2. Lithostratigraphy of the studied area. Volcaniclastic and silica-rich layers are common in the Siliceous lithozone.

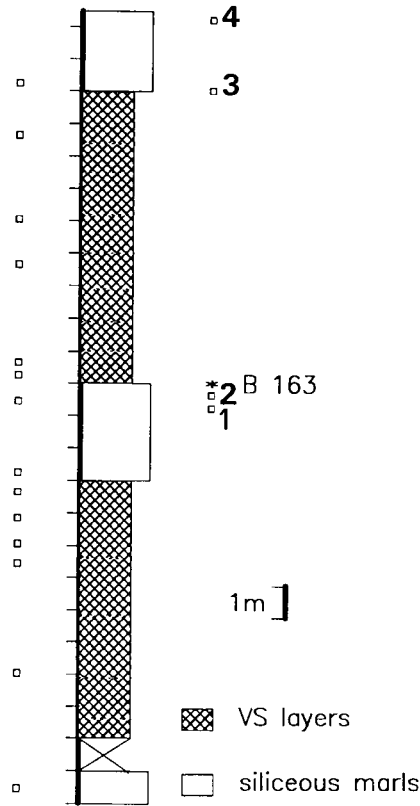


Fig. 3. Schematic section of the Cava Predosa locality. Samples collected for mineralogy (left) and biostratigraphy (right) are shown.

According to X-ray diffraction, the clay fraction of the volcanoclastic beds is 100% smectite with high stacking order; the siliceous marls instead contain smectite with low stacking order, illite, chlorite, and serpentine.

#### *Ponte delle Lepri section*

The Ponte delle Lepri section (Mezzetti, 1969; Guerrera, 1979) is located 12 km southwest of Bologna (Fig. 1). It has been studied along the Torrente Olivetta; outcrops are present on both banks of the river, both upstream and downstream of the bridge (Fig. 4). The measured section, about 80 m thick, represents the thickest outcrop of the Siliceous Marls in the Bologna area. It exposes the upper part of the Antognola Marls showing an obvious transition to the overlying Siliceous Marls. In spite of the thickness of the succession, the sharp, unconformable, upper boundary of the Bismantova Formation is lacking in this outcrop due to the deep erosive truncation by Pliocene fan delta conglomerates.

Many volcanoclastic layers are present. They are diversified in nature, including cream-coloured, unaltered tuffs composed mainly of glassy particles, or mineral-rich

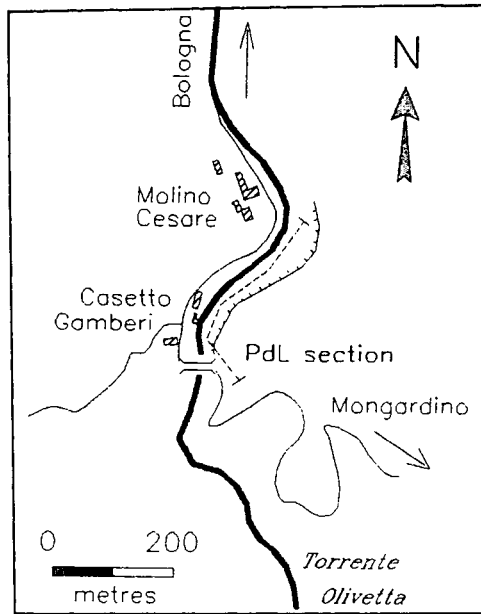


Fig. 4. Location of the major outcrop near Ponte delle Lepri.

clay layers. The latter are easily recognized by their rusty colour and their propensity of remaining wet when the rest of the section is dry. Their thickness ranges from more than 7 m (thick white tuff at the top of the section) to few centimetres (layers a–d in Fig. 5).

A systematic petrographical (65 samples) and geochemical study (10 samples) has been completed. The volcanoclastic beds display different sedimentological features and textures (grain size, sorting, relative amount of glass and crystals, etc.; Tateo, 1992). According to these parameters, different mechanisms of deposition are likely (Mezzetti et al., 1991). One of the main problems with the thickest layers is that their grain size (within the sand fraction) and thickness suggest a short distance from volcanic source but no other observation supports this hypothesis. A pyroclastic origin of many volcanoclastic beds can be readily inferred from their monogenic composition. However, they are clearly reworked, and cannot be considered pyroclastic deposits *sensu stricto*. Resedimentation, which probably occurred immediately after the pyroclastic deposition, led to the formation of these lenticular and often very thick volcanoclastic bodies (Amorosi et al., 1995).

A Sardinian provenance for Early Miocene volcanoclastic layers in the North Apennines was first inferred by Mezzetti et al. (1991) on the basis of contemporaneity of paroxysmal volcanic activity in Sardinia, compositional affinity of Sardinian and Apenninic material, and widespread distribution of volcanoclastic deposits in Sardinian basins similar in texture to those in the Apennines. A Sardinian provenance was also inferred by Montanari et al. (1994) on the basis of the geographical distribution and grain size of felsic crystals contained in an Aquitanian volcanic ash found in numerous outcrops throughout the Umbria–Marche region, and by Assorgia et al. (1994) who remarked a compositional similarity between biotites from Lower and Middle Miocene

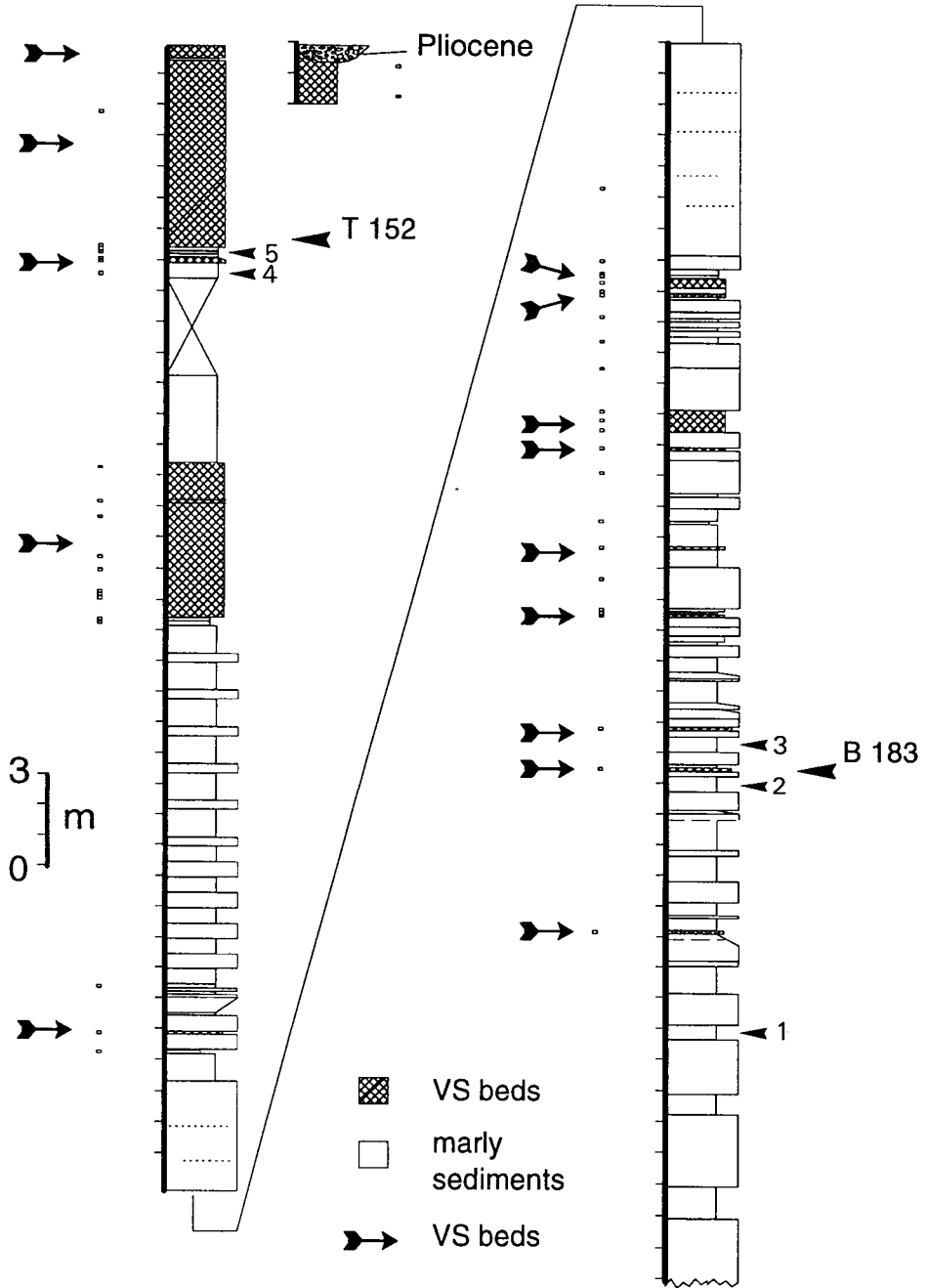


Fig. 5. Portion of the Ponte delle Lepri section. Volcanogenic layers are indicated by arrows; samples studied for petrography (left), biostratigraphy (1 to 5), and geochronology (T152 and B183) are shown.

Appennine volcanoclastic layers, and in coeval proximal tuffs in central-western Sardinia.

In the Ponte delle Lepri section, about fifteen discrete and almost pure volcanogenic beds were identified. Their composition is characterized by glass shards with minor amounts of plagioclase and mafic minerals (pyroxene, amphibole, biotite). Their provenance from different magma chambers is evident from the wide range of glass compositions (from about 61 to 75% SiO<sub>2</sub>, water-free basis, EDS technique) and the variable occurrence of mafic minerals and plagioclase chemistry.

Non-volcanic beds are pelitic sediments with enrichment in free silica (opal-CT is the most abundant phase, but rare beds with opal-A are present as well). Quartz, feldspar, and calcite are present with clay minerals (smectite, illite, chlorite, serpentine and rare talc).

Two samples were selected from the right bank of the river and within the Siliceous Marls (stars in Fig. 5) according to the quality of the pyroclastic mineral separates and the X-ray diffraction crystallographical properties of these separates. These are the mineral-rich layer  $\delta$  (B183, Fig. 6) located about 15 m above the top of the Antognola Marls and the base of the major tuff (T152) at the top of the Siliceous Marls (about 70 m above the lower boundary with the Antognola Marls). Layer  $\delta$  is altered on the surface (rusty colour, oxidization of pyrite to gypsum).

#### *Monte Arligo section*

The Monte Arligo section is part of an outcrop of semi-allochthonous deposits of the Epiligurian sequence located above the Ligurian nappe (Fig. 7B). The locality is known for long for the presence of a volcanoclastic layer (Selli, 1948).

In general agreement with Selli (1948), Cati (1974) describes the section (probably A in Fig. 7A) as consisting "entirely of marls overlying the Argille scagliose" and locates his "milk-white volcanic ash, 1.5 m thick between green clayey marls below (11 m thick) and green then whitish with manganese coating marls above (thickness 11.5 m)".

Within the section visited in 1992 (C in Fig. 7A), we have recognized the following lithostratigraphical succession: an Upper Oligocene–Lower Miocene (?) olistostrome below, covered by Antognola Marls, then 'Marne Selciose' Member above with, at the very top, a brown-black layer which may correspond to the Mn coating quoted by Cati. Two tuff-like layers suspected to be volcanogenic were collected; one is located within the Marne Selciose Member (T181 is a blackish 'tuff' collected from 3 m below the top of the section) and the other is about 12 m below within the top of the underlying Antognola Marls (Amorosi, 1993). The latter sample (T182) is a whitish 'tuff'.

These observations led to the question: how is it possible to locate the Oligocene/Miocene boundary in a sequence mostly corresponding with the Marne Selciose lithofacies which, everywhere else in the Apennines, is late Aquitanian to early Burdigalian in age? In order to answer this question, the section was cleaned and sampled in 1993 for biostratigraphy (A.N., G.A.P and F.T., Fig. 7). During this field research, it appeared that: (1) sample T182 is from a layer which is no longer in place but had slid over a short distance; (2) laterally, the suspected tuff layers cannot be followed due to tectonic disturbances; and (3) the tuff layers were interpreted as thin lenses rather than continuous layers (Amorosi, 1993).

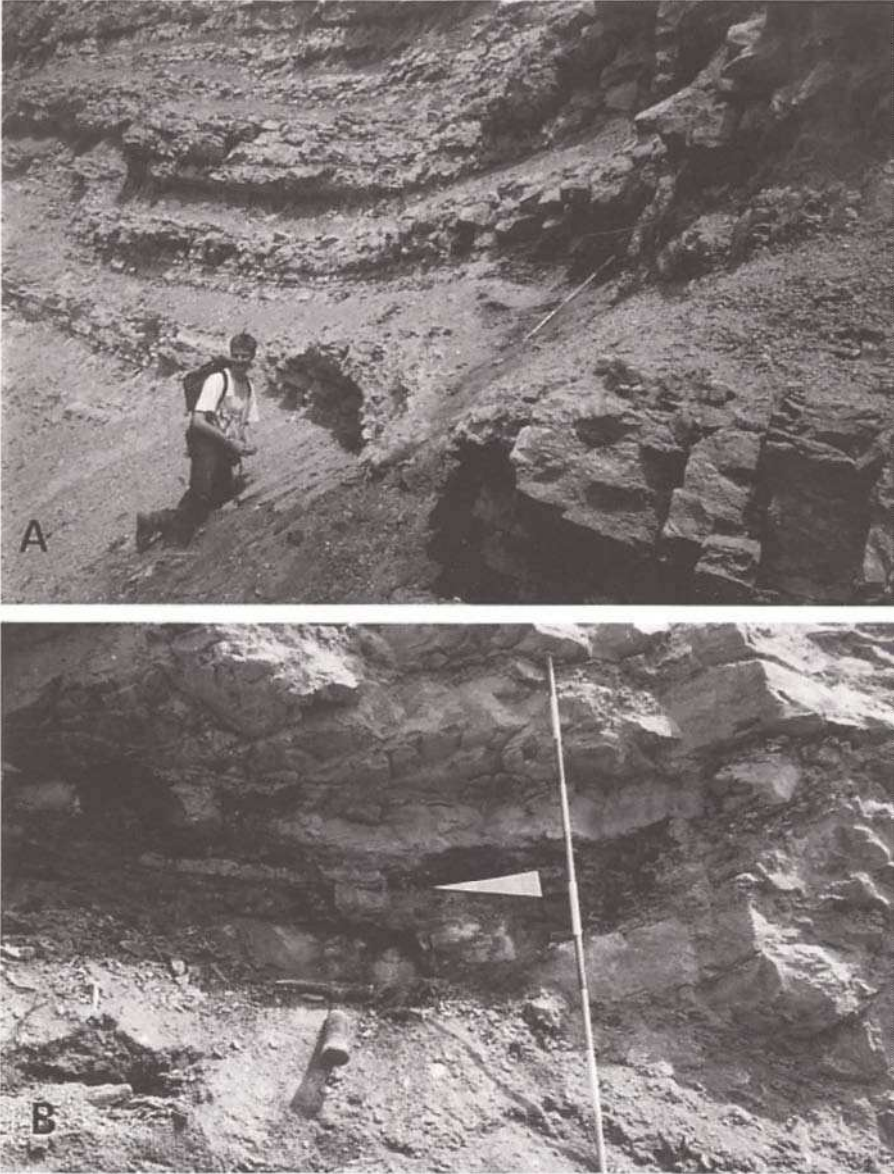


Fig. 6. Photographs of the Ponte delle Lepri section: (A) the mid part of the cliff (bar is 1 m); (B) layer B183; white arrow shows the base of the dated 3 cm thick volcaniclastic bed, 0.2 m above hammer.

## BIOSTRATIGRAPHY

Planktonic Foraminifera were studied from the Cava Predosa and Ponte delle Lepri sections (R.C.). Samples were washed (grain size  $>63$   $\mu\text{m}$ ). We largely adopted generic and specific concepts of Bolli and Saunders (1985), Iaccarino (1985), Loeblich and

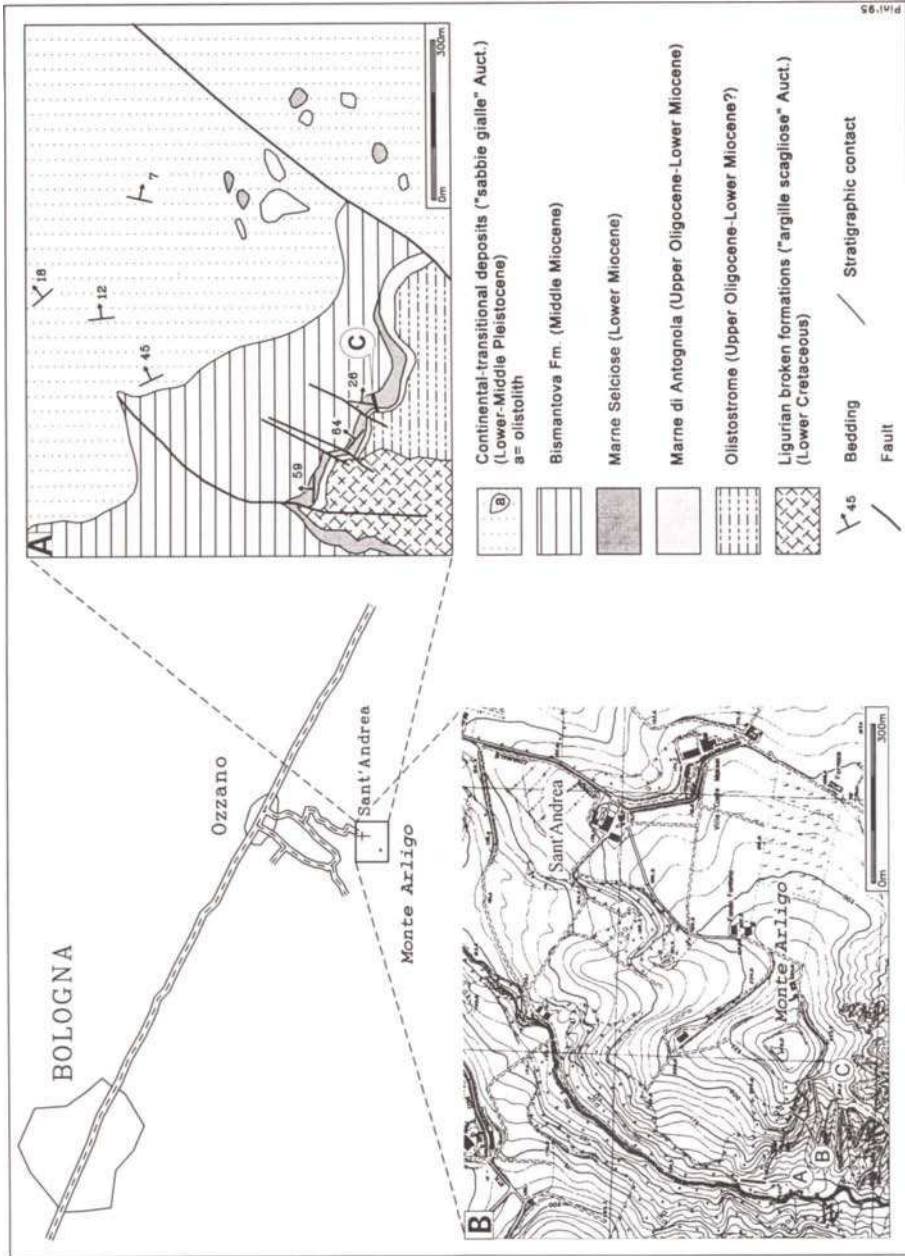


Fig. 7. (A) Geologic map of the Monte Arligo area, and (B) in the topographic map, the locations of the best exposed sections; (A) presumed location of the section known from Cati and Selli; (B) another section with the best potential for future research; (C) section sampled in this study (from Carta Tecnica Regionale Regione Emilia-Romagna, with permission of the Geological Survey of the Emilia-Romagna Region).



Tappan (1988) and Spezzaferri (1992, 1994) but in some instances we deviated from these and used additional documentation.

### *Cava Predosa section*

In the Cava Predosa section, four samples were collected for biostratigraphic analysis from above and below the tuff layers (Fig. 3). The four samples from this section yield a rich microfauna except for sample 2 which is barren. The microfauna consists mainly of planktonic Foraminifera and Radiolaria, and subordinately of benthonic Foraminifera. Very rare fish teeth are also present. The planktonic foraminiferal assemblages have a low diversity and preservation ranges from moderate to very poor with dissolution effects. The following taxa have been identified: *Catapsydrax dissimilis ciperensis* (Blow and Banner) 1962; *C. dissimilis dissimilis* (Cushman and Bermudez) 1937; *C. unicavus* (Bolli, Loeblich and Tappan) 1957; *Dentoglobigerina baroemoenensis* (LeRoy) 1939; *Globigerina praebulloides* (Blow, 1959); '*Globigerina*' *venezuelana* (Hedberg) 1937; *Globoquadrina dehiscens* (Chapman, Parr and Collins) 1934; *Paragloborotalia continuosa* (Blow) 1959; *P. siakensis* (LeRoy) 1939.

This assemblage can be referred to the N4 biozone of Blow (1969) corresponding to the N4b biozone of Spezzaferri (1992, 1994) or to the *Globoquadrina dehiscens dehiscens* Subzone of the *Globoquadrina dehiscens dehiscens*–*Catapsydrax dissimilis* biozone of Iaccarino and Salvatorini (1982) and Iaccarino (1985). All these biozones indicate an early Aquitanian age.

### *Ponte delle Lepri section*

According to preliminary biostratigraphic analysis (see Coccioni, in Amorosi, 1993) sample B183 would be latest Aquitanian, and sample T152 early Burdigalian in age. Five more samples were collected for additional study (see Fig. 5). They yield a rich microfauna consisting mainly of planktonic Foraminifera and subordinately by benthonic Foraminifera and Radiolaria, the latter usually rare but frequent to common in samples 1 and 5. Very rare fish teeth also occur. The planktonic foraminiferal assemblages are well diversified and preservation ranges from moderate to very poor with dissolution effects. The following taxa have been identified: *Cassigerinella chipolensis* (Cushman and Ponton) 1932; *Catapsydrax dissimilis ciperensis* (Blow and Banner) 1962; *C. dissimilis dissimilis* (Cushman and Bermudez) 1937; *C. unicavus* (Bolli, Loeblich and Tappan) 1957; *Dentoglobigerina baroemoenensis* (LeRoy) 1939; *D. larmeu* (LeRoy) 1939; *Globigerina eamesi* (Blow) 1959; *G. falconensis* (Blow) 1959; *G. officinalis* (Subbotina) 1953; *G. ouachitaensis* (Howe and Wallace) 1932; *G. praebulloides* (Blow) 1959; '*Globigerina*' *euapertura* (Jenkins) 1960; '*G.*' *quinteloba* (Natland) 1938; '*Globigerina*' *venezuelana* (Hedberg) 1937; *Globigerinella obesa* (Bolli) 1957; *Globigerinita incrusta* (Akers) 1955; *Globigerinoides immaturus* (LeRoy) 1939; *G. quadrilobatus* (d'Orbigny) 1846; *G. subsacculifer* (Cita, Premoli Silva and Rossi) 1965; *G. trilobus* (Reuss) 1850; '*Globigerinoides*' *primordius* (Blow and Banner) 1962; '*G.*' *altiaperturus* (Bolli) 1957; *Globorotalia birnageae* (Blow) 1959; *Globorotaloides* sp.; *Globoquadrina dehiscens* (Chapman, Parr and Collins) 1934; *Paragloborotalia continuosa* (Blow) 1959; *P. siakensis* (LeRoy) 1939; *Sphaeroidinellopsis* sp.; *Tenuitellina angustiumbilitata* (Bolli) 1957;

*Zeaglobigerina brazieri* (Jenkins) 1966; *Z. connecta* (Jenkins) 1964; *Z. druryi* (Akers) 1955; *Z. labiacrassata* (Jenkins) 1966; *Z. woodi* (Jenkins) 1960.

These assemblages can be referred to the N5 (upper part)–N6 Zones of Blow (1969) corresponding to the *Globigerinoides altiapertura*–*Catapsydrax dissimilis* Subzone of the *Globoquadrina dehiscentis dehiscentis*–*Catapsydrax dissimilis* Zone of Iaccarino and Salvatorini (1982) and Iaccarino (1985). All these biozones indicate an early Burdigalian age.

### Monte Arligo section

Based on the abundant planktonic Foraminifera, Cati (1974) shows the Oligocene/Miocene boundary (based on first appearance of the *Globigerinoides* genus in the section, is base of his *Globigerinita dissimilis* biozone) 1 m below their volcanogenic layer. However, the bio-signal is commonly considered diachronous because *Globigerinoides* are found in pre-Aquitainian sediments from several sections including the type area in Aquitaine (Scott, 1972). Borsetti et al. (1983) show the boundary based on the local first occurrence of *Globorotalia kugleri* in the same section slightly above the volcanogenic layer of Cati (1974).

Three pilot samples collected from the section available in 1992 yielded no Foraminifera (A.M. Borsetti, pers. commun., 1993). Nevertheless, a calcareous nannofossil association was observed. About fifteen more samples were collected (Fig. 8) for biostratigraphy. Foraminiferal assemblages were too poorly preserved for biostratigraphic determination but nannofossil data have been gathered for five samples (Table 1). Calcareous nannofossils are moderately preserved; indicative taxa are shown in Table 1. The lacking of

Table 1

Calcareous nannofossils from the Monte Arligo section C (original data by A.N.)

Taxa	Samples				
	1	5	6	7	13
<i>Cyclicargolithus abisectus</i>	F	F	F	F	F
<i>Cyclicargolithus floridanus</i>	F	F	C	F	F
<i>Coccolithus miopelagicus</i>	F	R	R	R	F
<i>Coccolithus pelagicus</i>	C	F	F	F	C
<i>Discoaster deflandrei</i>	F	F	F	RF	C
<i>Dictyococcites</i> spp.	A	A	A	A	A
<i>Helicosphaera carteri</i>	F	F	R	F	F
<i>Pontosphaera</i> spp.		R	R		
<i>Reticulofenestra</i> spp.		A	A	A	A
<i>Reticulofenestra daviesii</i>	C		F		C
<i>Pirocyclus orangensis</i>			R		
<i>Sphenolithus moriformis</i>	F		R	R	R
Siliceous fragments	A	A	A	A	A
Okada and Bukry (1980)	←		CN1		→
chronostratigraphy:	←		Early Miocene		→

A = abundant ( $\geq 1$  specimen every field of view); C = common (1 specimen every 2–10 fields of view); F = few (1 specimen every 11–50 fields of view); R = rare (1 specimen every 51–200 fields of view).

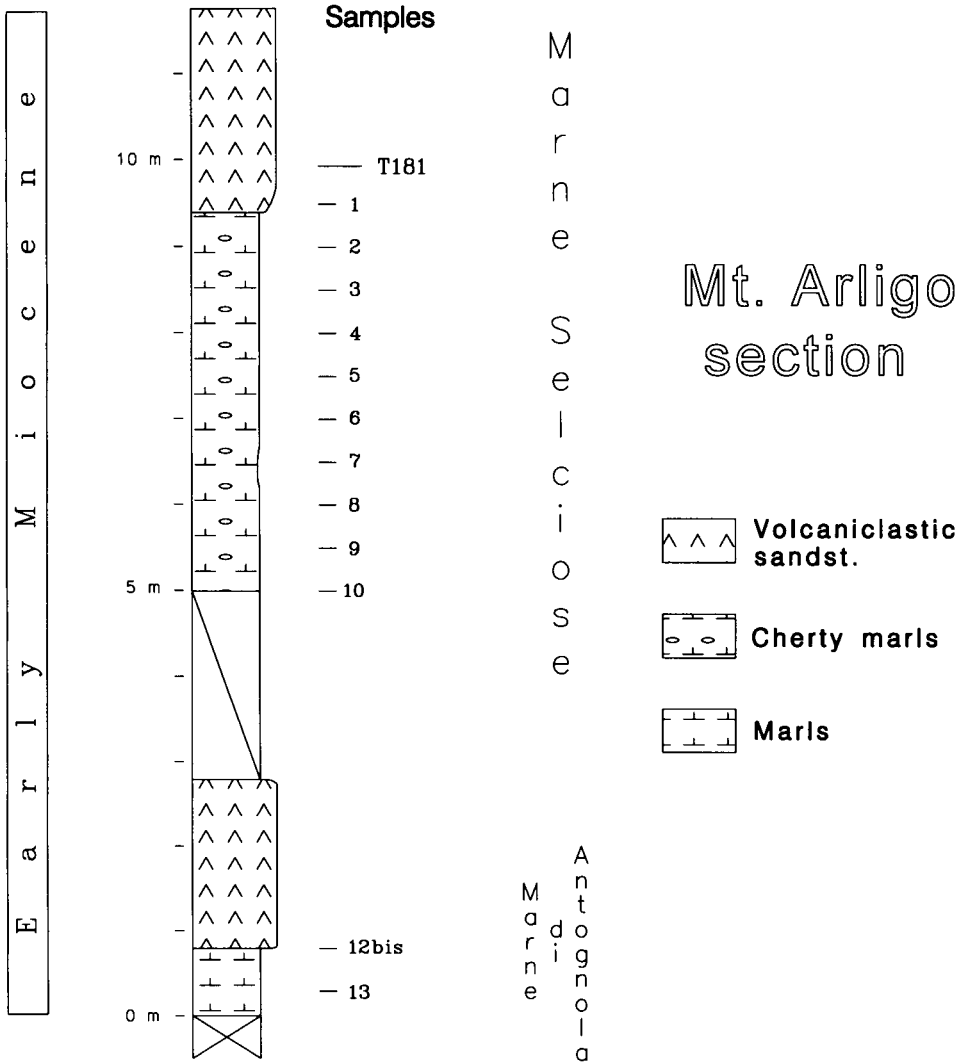


Fig. 8. The Monte Arligo section as observed in 1993 (A.N., G.A.P., F.T.). Sample T181 and the dated sample T182 were collected in 1992 from levels equivalent to about +10 m and -2 m, respectively, in a parallel section.

*Sphenolithus ciperoensis* and *Dictyococcites bisectus* as well as the absence of *Sphenolithus belemnus* suggest that the samples correspond to the CN1 biozone of Okada and Bukry (1980): the last occurrence of *S. ciperoensis* and *D. bisectus* is indicative of the base of the CN1 biozone while the first occurrence of *S. belemnus* is supposed to 'define' the younger boundary of the same unit. Moreover, the occurrence of *Helicosphaera carteri* in the whole section is diagnostic because its Mediterranean first occurrence appears to follow the last occurrence of *D. bisectus*, thus indicating an age younger than the base of the Aquitanian in the Monte Arligo section.

GEOCHRONOLOGY

*Petrography and mineralogy of the geochronometers*

Clay-rich layers have been disaggregated first with refined petroleum and then water. The usual separation procedure for tuff samples is a gentle crushing using a large hammer on a wooden board, followed by sieving for removal of large composite grains, ultra-sonic cleaning in water, magnetic and heavy liquid (bromoform, 3:5 bromoform-acetone mixtures, and ethylene iodide) separation and fractioning. The latter treatment is accompanied by systematic X-ray diffraction analyses when binocular microscope examination does not allow identification of the fraction where the useful geochronometer is located.

*Cava Predosa section.* The best samples from the Cava Predosa section contain an assortment of pyroclastic minerals comprising plagioclase (about 10% versus whole-rock), biotite (>5%), abundant idiomorphic zircon crystals (0.1%), and traces of apatite.

X-ray diffraction patterns of the preliminary T163 biotite separate show a significant vermiculite peak at 14.5 Å. However, the final separate (heavy in bromoform, gently crushed in acetone and sieved, cleaned with 30% acetic acid for 10 min, and hand-picked for removal of orange-red flakes) was purely brown biotite with no 14 Å peak and a (001) reflection at 10.08 Å; that thickness indicates a slight opening of the mica sheets.

The final biotite separate was submitted for geochemical EDS analyses (EDS-SEM EDAX PV9100, technique described by Gasparotto, 1988; see Table 2) following the approach pioneered by A. Montanari (Montanari, 1988; Odin et al., 1991). The results (Fig. 9) indicate: (1) heterogeneity in FeO and MgO contents (three flakes with FeO ≈ 26% and MgO ≈ 8% and the remaining ones with FeO ranging from 27 to 31% and MgO ≈ 5%); the FeO/MgO ratios are widespread between 3.0 and 6.4; (2) TiO<sub>2</sub> contents vary between 3.5 and 4.7; and (3) a reasonably high K content (between 8.2% and 9.3%; mean 8.8% K<sub>2</sub>O) but lower than in pure, fresh biotite. These properties suggest an a-priori polygenic nature of the volcanoclastic material (sub-syn depositional

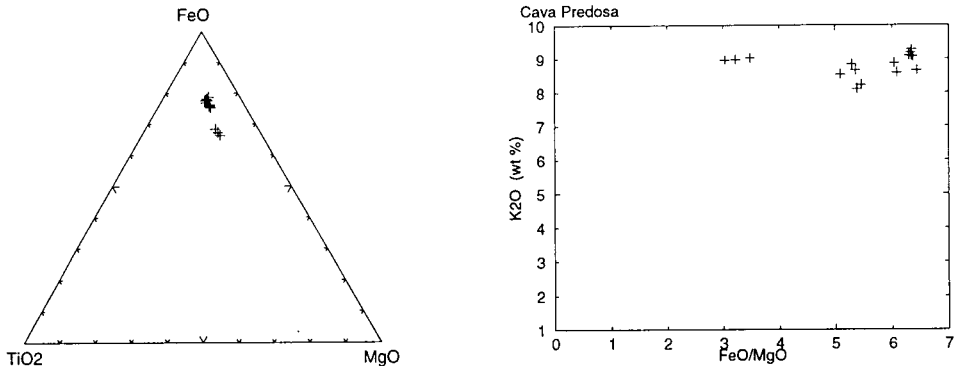


Fig. 9. Results of geochemical (EDS-SEM) analyses on fifteen biotite flakes from the sample T163, Cava-Predosa section, Italy (recalculated on an anhydrous basis; original data by F.T.).

Table 2

Geochemical analyses (EDS–SEM technique, Gasparotto, 1988) of 15 biotite flakes from T163, Cava Predosa (recalculated on an anhydrous basis; original analyses from Bologna, Institute of Mineralogy by F.T.)

SiO <sub>2</sub>	TiO <sub>2</sub>	Al <sub>2</sub> O <sub>3</sub>	FeO*	MnO	MgO	CaO	Na <sub>2</sub> O	K <sub>2</sub> O	FeO*/MgO
36.90	4.54	15.42	25.32	0.12	8.35	0.04	0.36	8.96	3.03
36.61	4.59	15.41	25.77	0.17	8.00	0.06	0.41	8.98	3.22
36.57	4.71	15.18	26.48	0.20	7.60	0.00	0.22	9.03	3.48
39.49	3.53	15.52	27.05	0.17	5.31	0.32	0.06	8.54	5.10
39.32	3.55	15.13	27.19	0.29	5.14	0.15	0.39	8.84	5.29
39.82	3.47	15.33	27.31	0.19	5.10	0.09	0.02	8.66	5.36
38.43	3.73	15.67	27.86	0.34	5.18	0.32	0.35	8.11	5.38
37.44	3.63	15.51	28.48	0.36	5.22	0.67	0.46	8.23	5.46
36.05	3.72	15.09	30.38	0.39	5.03	0.09	0.37	8.88	6.04
36.22	4.10	15.05	29.90	0.28	4.91	0.19	0.76	8.59	6.09
35.91	3.45	15.22	31.00	0.34	4.92	0.00	0.05	9.10	6.30
35.98	3.75	15.17	30.52	0.32	4.82	0.02	0.23	9.19	6.34
35.87	4.04	14.76	30.89	0.37	4.87	0.02	0.08	9.09	6.34
36.03	3.85	14.99	30.60	0.32	4.82	0.03	0.08	9.28	6.35
36.05	3.78	14.92	30.69	0.43	4.82	0.03	0.20	9.07	6.36
36.05	4.08	15.16	30.52	0.34	4.74	0.06	0.39	8.66	6.44
Average ± 1σ									
37.05	3.91	15.22	28.75	0.29	5.55	0.13	0.28	8.83	5.41
1.37	0.39	0.23	1.95	0.09	1.19	0.17	0.19	0.33	1.13

FeO\* = total iron; σ: standard deviation.

material suspected to be associated with previously crystallized material). In addition, an alteration occurred and a portion of the mica flakes will be able to lose argon during irradiation (Hess and Lippolt, 1986).

*Ponte delle Lepri section.* The choice of samples B183 and T152 for geochronological investigation was suggested by their locations not far from the base and the top of the Siliceous lithozone (Fig. 2), respectively. The thin layer δ (B183) is composed of two sublevels (two volcanic events). The thick tuff layer, from the base of which we collected T152, appears to represent a single sedimentary event of extraordinary thickness

Petrographically, the mineral-rich layer (B183) contains feldspar, amphibole, ortho- and clino-pyroxenes and quartz as pyroclastic components. The base of the youngest thick tuff (T152) is dominantly made of glass with admixed feldspar, quartz and pyroxene. The geochemical compositions of some components from the layers from where the geochronological samples were collected is shown in Table 2. The plagioclase composition of the two layers is analytically distinct, as well as the composition of glass. EDS analyses of plagioclase indicate a labradoric composition for both samples (B183 and T152), and a subgroup with bytownitic affinity in sample T152. This compositional heterogeneity is quite common for zoned plagioclase.

The two layers have strong affinity based on their similar plagioclase composition (labradoritic), the occurrence of both hypersthene and augite, and the composition of shards which resemble that of rhyolitic rocks (the chemical compositions of glass are also similar but not quite overlapping). The phenocryst paragenesis is typical for

andesitic rocks *sensu lato* but glass shards are markedly more evolved, representing a differentiated phase in the magma chambers.

Following the usual separation technique, we obtained diversified pyroclastic minerals from sample B183 which disaggregates easily in water as a bentonite indicating the presence of a significant amount of expandable (smectitic) clay derived from glass alteration. The main component is xenomorphic feldspar (>15% of the whole rock). Idiomorphic biotite (brown and red flakes), amphibole (about 3%), and pyroxene (hypersthene according to X-ray diffraction, more than 5%) are also present. Very well preserved apatite elongated crystals (100 to 200/kg, 0.1 to 0.25 mm long), rare zircon crystals (10/kg), and ilmenite confirm the volcanogenic origin of this layer. Pyrite is also present together with biogenic phosphate and rare microfossils.

The B183 amphibole was separated from equally magnetic pyroxene using methylene iodide–acetone mixtures within the size fraction larger than 0.1 mm. B183 feldspar (grain size larger than 0.16 mm) was cleaned with a nitric–acetic acid mixture for 7 min. X-ray diffraction patterns of the selected light fraction show the presence of pure anorthite-rich, well crystallized plagioclase (distance  $(\bar{1}\bar{3}1)$   $(131) = 2.0^\circ K\alpha Cu 2\theta$ ).

The tuff sample T152 allowed separation of more than 30% feldspar, 2% pyroxene, 0.3% apatite, and about 50 zircon crystals per kg of bulk rock. The facies of the rock and its composition with abundant glass shards indicate a 100% volcanogenic material. The single potential geochronometer is plagioclase which was cleaned using a diluted nitric–acetic acid mixture for 14 h, and ultrasonic treatment (T152-1). A second portion of the sample was similarly separated but cleaned using cold 10% hydrochloric acid for 20 min (T152-2). In both cases, we obtained a 100% pure, transparent mineral separate.

X-ray diffraction patterns of the two plagioclase separates are similar to those from the plagioclase separated from B183.

*Monte Arlago section.* T181 is a tuff-like light rock, black in colour, and without clay. Under the binocular microscope the rock is mainly composed of silt- to sand-sized pumice grains, a few transparent grains, and bottle-green crystals in addition to grey and black grains including brown glass. Most of the grains, ash or vitric in aspect, black and grey in colour, are magnetic. X-ray diffraction patterns indicate that the transparent non-magnetic grains are made of anorthite-rich plagioclase with possibly very small peaks related to quartz. Intense, magnetic separation removes a large proportion of the plagioclase fraction due to the presence of black inclusions in them. The final purely transparent plagioclase separate constitutes less than 1% of the rock, too small an amount for further treatment.

The T182 tuff is mainly composed of pumice fragments and it is similar for aspect and hardness to tuff T181 from which it differs only for its light-cream colour. The sample contains abundant transparent and brilliant calcite spherules, irregular in shape, 0.3 to 0.8 mm in diameter. These spherules were also observed in other volcanoclastic layers from the Apennines, and were interpreted as the result of diagenetic replacement of gas bubbles in vesicular glass shards.

The single magnetic idiomorphic fraction of sample T182 comprises light bottle-green pyroxene crystals, 0.1 to 0.3 mm in length with acicular ends. The main non-magnetic, light component is plagioclase (about 1% of the whole rock). X-ray diffraction patterns reveal well crystallized anorthite-rich plagioclase (interval  $(\bar{1}\bar{3}1)$   $(131) = 2.0^\circ 2\theta$ ). The plagioclase separate was submitted to 10% hydrochloric acid

treatment for 45 min in an ultra-sonic bath, followed by magnetic treatment for removal of inclusion-rich crystals. Hand-picked transparent or sometimes slightly milky, about 0.1-mm crystals were used for isotopic analysis.

Heavy grains include abundant transparent, brilliant, and idiomorphic barrel-like apatite crystals, generally 0.1 to 0.2 mm and rarely up to 0.5 mm in length. No zircon crystals were observed. In addition to the pyroclastic components, some ten fish teeth less than 1 mm in length were separated from the heavy fraction concentrated with bromoform.

In summary, the two layers sampled from the Monte Arligo section are volcanic in origin, exhibit a restricted array of pyroclastic minerals, and contain scarce biogenic material (in T182) but no detrital components. They represent suitable rocks for geochronological study.

#### $^{40}\text{Ar}/^{39}\text{Ar}$ isotopic analyses

$^{40}\text{Ar}/^{39}\text{Ar}$  step heating datings of selected samples were performed at Lausanne (Cosca et al., 1992) using biotite HD-B1 as the monitor for calibration of the neutron flux in the TRIGA reactor of Denver.

All samples were baked in vacuum before the increment heating procedure in order to eliminate a large portion of atmospheric gas contamination before measurement of  $^{40}\text{Ar}/^{39}\text{Ar}$  ratios for higher temperature steps. The analytical conditions for all samples are summarized in Table 3. At the time of measurement, our facility used an electron multiplier for small quantities of gas. Precise ratio measurements were obtained for a signal smaller than 1 V but contributions from previous blanks may become significant, and quantities of gas between 2 and 9 V were more appropriate.

The recommended age value for the monitor biotite HD-B1 is 24.21 Ma with a  $2\sigma$  analytical uncertainty of  $\pm 2.5\%$ . All ages given below quote the internal analytical error bar. This error is propagated to the analytical ages of other samples to derive realistic geological ages comparable to data obtained using other monitors or analytical techniques and methods. All ages given with this restricted error bar are consistent and significant

Table 3

Geochemical composition of some minerals from samples equivalent to B183 and T152 (recalculated on an anhydrous basis; from Tateo, 1992).

Sample	SiO <sub>2</sub>	TiO <sub>2</sub>	Al <sub>2</sub> O <sub>3</sub>	FeO*	MnO	MgO	CaO	Na <sub>2</sub> O	K <sub>2</sub> O	N
183 plagio	54.9	0.01	28.3	0.4	0.02	0.21	10.8	5.0	0.30	7
± 1σ	0.5	0.01	0.4	0.1	0.03	0.06	0.4	2.3	0.04	
Glass shard	69.9	0.26	13.0	1.6	0.05	0.34	1.64	2.0	3.2	22
± 1σ	1.6	0.06	0.4	0.3	0.05	0.12	0.15	0.4	0.2	
Amphibole	46.4	1.7	8.7	14.9	0.45	13.5	10.9	1.6	0.47	6
± 1σ	0.5	0.4	0.4	0.4	0.13	0.2	0.3	0.3	0.04	
152 plagio	52.6	0.07	30.3	0.6	0.03	0.27	13	3.7	0.4	8
± 1σ	3.9	0.05	2.7	0.1	0.04	0.05	3	1.7	0.2	
Glass shard	67.4	0.3	13.6	2.6	0.09	0.3	1.5	2.5	4.2	15
± 1σ	1.8	0.1	0.5	0.7	0.05	0.3	0.7	0.6	0.4	

FeO\* = total iron. N = number of analyses.

Table 4

Analytical conditions used for isotopic analysis

Sample	Weight (mg)	Preheating in vacuum	Quantity of gas <sup>a</sup>
T163 biotite	58	500°C, 25 min	≈ 100–300 V
B183 hornblende	32	500°C, 20 min	0.4–2.3 V
B183 plagioclase	21.7	550°C, 30 min	0.3–0.8 V
T152-1 plagioclase	18.6	550°C, 15 min	0.4–0.7 V
T152-2 plagioclase	74	450°C, 10 min	1.5–10 V
T182 plagioclase	18.1	600°C, 30 min	0.3–0.6 V

<sup>a</sup> The quantity of gas is the analytical signal obtained on the electron multiplier of the mass spectrometer (ideal measurements are obtained for signals between 2 and 20 V).

Table 5

Results of <sup>40</sup>Ar/<sup>39</sup>Ar incremental heating measurements on biotite T163 (58 mg): Cava Predosa (by G.S.O. in Lausanne)

Temp. (°C)	Apparent age	± 2σ	% <sup>39</sup> Ar	% radiogenic	K/Ca
650	6.8	1.1	4.8	10	13.2
800	12.0	0.8	7.8	23	20.9
925	14.8	0.8	18.4	33	16.9
1000	21.1	0.3	12.2	70	27.5
1050	20.6	0.5	18.2	73	20.8
1090	20.9	0.5	20.2	82	24.3
1130	21.4	0.2	12.0	91	31.5
1180	21.4	0.3	6.1	94	16.8
1300	21.4	0.3	0.2	–	8.3

Apparent ages: (total gas age) = 18.4 ± 0.3 Ma; (pseudo-plateau 1000–1300°C) = 21.17 ± 0.20 Ma; monitor HD-B1 = 24.21 Ma; error on *J* = 0.5%.

within this work as well as with external works using the same monitor. Comparison with dates obtained with other monitors or dating methods should be made by taking into consideration an increased error bar of ±2.5% for the age. 2σ error bars (95% confidence level) are given everywhere in this work except when otherwise specified.

*Cava Predosa section.* Nine heating steps were measured for biotite T163. A split was done for each step (large amount of gas released, see Table 4), and the corresponding ages calculated (Table 5). The age spectrum in Fig. 10A shows low apparent ages for the three low-temperature heating steps, a situation similar to that observed by Lippolt et al. (1986) for comparatively low K biotite. The later six steps are generally consistent with ages between 21.0 Ma and 21.8 Ma. The calculated ages for these six steps are analytically different at the 95.5% confidence level, and the spectrum does not show a true plateau. However, a weighed mean age of the five main successive steps can be calculated for a 'pseudo-plateau' at 21.2 ± 0.2 Ma (2σ). The total gas age obtained is about 18.4 Ma with a somewhat uncertain determination of the analytical error bar.

*Ponte delle Lepri.* Sample B183 amphibole gives five significant analytical results (the steps including less than 1.5% of the total <sup>39</sup>Ar released are not considered significant). The age spectrum is disturbed (Fig. 10B) with, amongst the significant steps, three ages at 19.5 Ma, one low age at 18.3, and a high age at 20.9 Ma (Table 6).



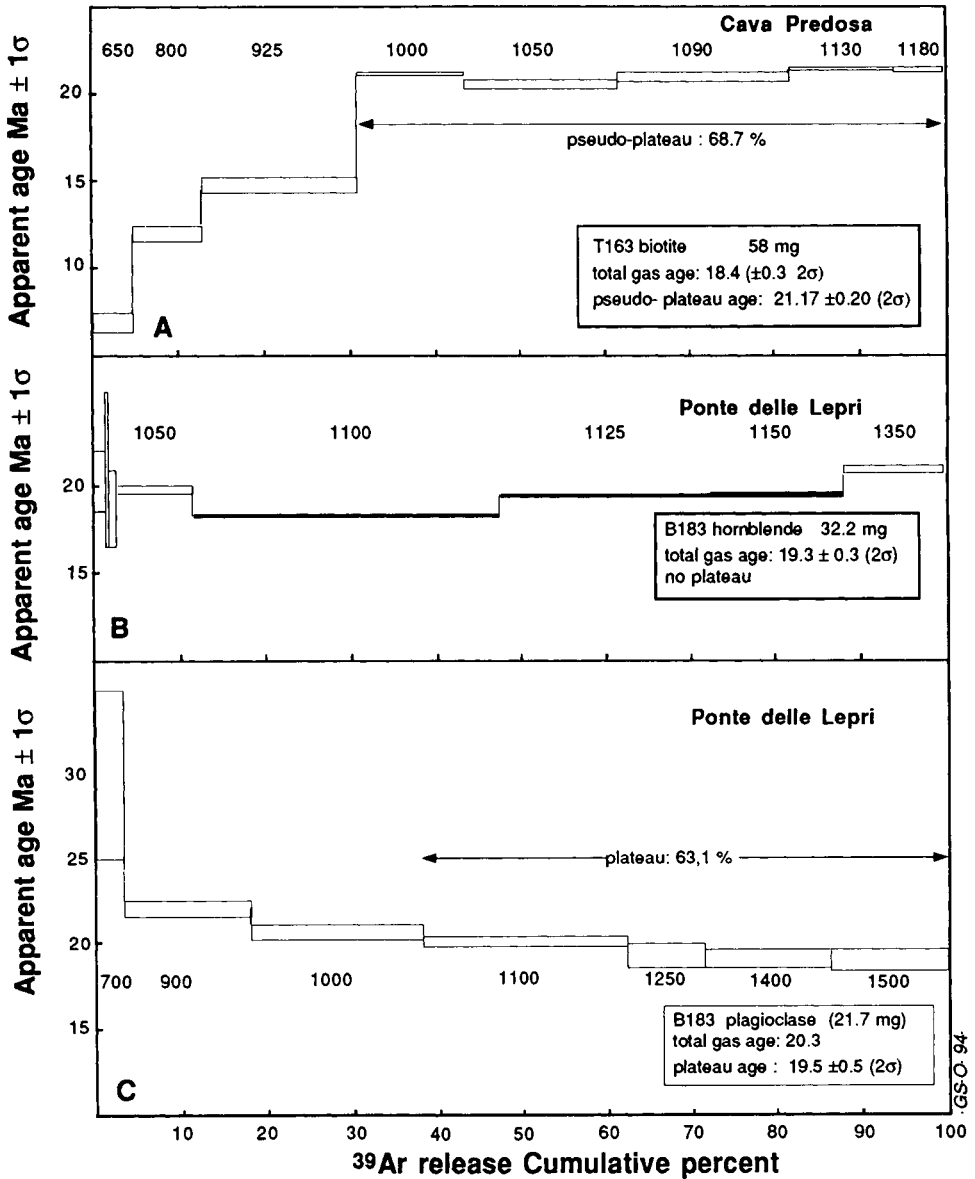


Fig. 10.  $^{40}\text{Ar}/^{39}\text{Ar}$  age spectra for samples of the Marne Selciose unit. (A) T163 biotite (Cava Predosa); (B) B183 hornblende; (C) B183 plagioclase (Ponte delle Lepri).

The total gas age is 19.3 ( $\pm 0.3$ ) Ma. Isochron ages at 19.2 Ma can be calculated for this hornblende (Table 6 and Fig. 12).

From sample B183 plagioclase, we obtained less precise analytical ages than for the amphibole (small signals, Table 4). Three low temperature heating steps show analytical ages seemingly older than the time of deposition. A reasonably good plateau follows at 19.5  $\pm 0.5$  Ma for the next four steps (Table 7 and Fig. 10C).

Table 6

Results of  $^{40}\text{Ar}/^{39}\text{Ar}$  incremental heating measurements on hornblende B183 (32.18 mg): Ponte delle Lepri (preliminary data by G.S.O. in Lausanne)

Temp. (°C)	Apparent age	$\pm 2\sigma$	% $^{39}\text{Ar}$	% rad.	K/Ca
850	20.4	3.4	1.4	5	0.20
950	21	9	0.4	7	0.08
1000	18.7	4.4	0.9	28	0.06
1050	19.8	0.5	8.9	79	0.043
1100	(18.3)	0.3	35.9	86	(0.040)
1125	19.5	0.3	25.2	92	0.043
1150	19.5	0.3	15.8	91	0.043
1350	(20.9)	0.4	11.5	84	(0.029)

Apparent ages: (total gas age) = 19.28 ( $\pm 0.25$ ) Ma; no plateau age; steps 1000°C and 1350°C are analytically suspect; monitor HD-B1 = 24.21 Ma; error on  $J = 0.5\%$ ; isochron ages for steps 850–1150:

( $^{40}\text{Ar}/^{36}\text{Ar}$  versus  $^{39}\text{Ar}/^{36}\text{Ar}$ ) = 19.26  $\pm$  0.56 Ma;  $^{40}\text{Ar}/^{36}\text{Ar}(i)$  = 293  $\pm$  26; MSWD = 49  
 ( $^{36}\text{Ar}/^{40}\text{Ar}$  versus  $^{39}\text{Ar}/^{40}\text{Ar}$ ) = 19.18  $\pm$  0.54 Ma;  $^{40}\text{Ar}/^{36}\text{Ar}(i)$  = 296  $\pm$  26; MSWD = 47.

Table 7

Results of  $^{40}\text{Ar}/^{39}\text{Ar}$  incremental heating measurements on plagioclase B183 (21.7 mg): Ponte delle Lepri (by G.S.O. in Lausanne)

Temp. (°C)	Apparent age	$\pm 2\sigma$	% $^{39}\text{Ar}$	% rad.	K/Ca
700	30.0	10	3.1	2.6	0.024
900	22.1	1.0	14.5	36	0.015
1000	20.6	0.8	19.4	86	0.010
1100	19.9	0.6	24.5	78	0.017
1250	19.2	1.5	9.2	74	0.019
1400	19.1	0.9	14.9	68	0.020
1500	19.1	1.0	14.5	33	0.012

Preliminary data. Apparent ages: (total gas age) 20.34 ( $\pm 0.48$ ) Ma; error in  $J = 0.5\%$ ; plateau age 1100–1500 = 63%; 19.51  $\pm$  0.46 Ma; monitor HD-B1 = 24.21 Ma.

The data obtained from T152-1 and T152-2 plagioclase separates (Tables 8 and 9) are mostly spread within a restricted range of apparent ages between 19 and 21 Ma. Excluding the slightly older low-temperature age at 22.3 Ma, the age spectrum for T152-1 plagioclase (Fig. 11A) is nearly flat. A plateau age at 20.4  $\pm$  0.3 Ma (or another at 21.0  $\pm$  0.3 Ma) can be calculated. They bracket the total gas age at 20.7 ( $\pm 0.3$ ) Ma.

The age spectrum for the hydrochloric acid treated plagioclase (T152-2) also shows a nearly flat pattern (Fig. 11C). The low-temperature heating step age is younger than the others in contrast to that of sample T152-1. It is followed by four consistent step ages including more than 50% of the total  $^{39}\text{Ar}$  gas released. A plateau age can be calculated at 19.7  $\pm$  (0.3) Ma. The corresponding isochron ages are slightly younger, 19 Ma (Fig. 12).

In summary, sample T152 does not give reproducible spectra nor apparent ages (total gas or plateau). It is not yet known whether this is due to the different acid treatment, and this aspect will have to be considered in the future. However, the geological age is most probably comprised in the interval 19 to 21 Ma within which all calculated ages are included.

Table 8

Data and results of  $^{40}\text{Ar}/^{39}\text{Ar}$  incremental heating measurements on plagioclase T152-1 (18.6 mg) from Ponte delle Lepri (preliminary data by G.S.O. in Lausanne)

Temp. (°C)	Apparent age (Ma)	$\pm 2\sigma$	% $^{39}\text{Ar}$	% rad.	K/Ca
700	(22.3)	1.6	7.4	14	0.09)
900	21.2	0.7	12.5	64	0.033
1000	20.9	0.5	16.4	80	0.024
1100	20.8	0.5	18.7	92	0.029
1200	20.0	0.6	15.1	88	0.043
1300	20.4	0.9	9.0	83	0.044
1400	20.0	0.7	12.3	81	0.044
1500	20.4	0.9	8.6	84	0.026

Temp. (°C)	40*	$\pm$	39	$\pm$	38	$\pm$	37	$\pm$	36	$\pm$	Ar/K	$\pm$
700	135.3	0.3	3.923	0.008	0.354	0.001	21.24	0.07	0.403	0.002	4.80	0.17
900	46.88	0.09	6.675	0.013	0.258	0.001	99.5	0.2	0.083	0.002	4.55	0.07
1000	48.67	0.10	8.81	0.02	0.140	0.001	177.6	0.4	0.079	0.002	4.49	0.05
1100	47.88	0.10	9.97	0.02	0.147	0.001	165.0	0.3	0.056	0.002	4.48	0.05
1200	39.23	0.08	8.06	0.02	0.128	0.001	91.2	0.2	0.040	0.002	4.31	0.06
1300	25.06	0.05	4.79	0.01	0.087	0.001	53.21	0.11	0.028	0.002	4.33	0.09
1400	34.77	0.07	6.55	0.01	0.137	0.001	76.97	0.15	0.043	0.002	4.30	0.07
1500	23.95	0.05	4.621	0.009	0.136	0.001	84.98	0.17	0.035	0.002	4.40	0.10

*Upper part.* Apparent ages: (total gas age) 20.7 ( $\pm 0.3$ ); plateau age 1100–1500 = 63.7%; 20.4  $\pm$  0.3 Ma; plateau age 700–1100 = 55.0%; 21.0  $\pm$  0.3 Ma. *Lower part.* Analytical details of the  $^{40}\text{Ar}/^{39}\text{Ar}$  increment heating measurements on plagioclase T152-1;  $J = 0.00259$ ; gas in  $10^{-15}$  moles; errors  $1\sigma$  in this table; (Ar/K) =  $^{40}\text{Ar rad}/^{39}\text{ArK}$ .

*Monte Arligo section.* The quantities of gas extracted during eight heating steps from the T182 plagioclase separate are small (Table 4). The analytical results (Table 10) are plotted in an age spectrum in Fig. 11C, and are very similar to the one obtained from plagioclase T152-2 (Fig. 11B), but with additional extraneous argon at low temperature. Three nearly consistent large steps are present with apparent ages between 21.6 to 22.8 Ma (65.6% of the spectrum). There are two steps with an old age followed by two high-temperature steps with apparent ages similar to the pseudo-plateau age at  $22.0 \pm 0.3$  Ma. The latter number is able to represent the age of the plagioclase. For plagioclases T152-2 and T182 it is suspected that inclusions (or attached impurities degassed at about 1200–1300°C) tend to increase the apparent age.

## DISCUSSION AND CONCLUSIONS

### *Cava Predosa section*

The chronostratigraphic age of tuff T163 is thought to be near the Aquitanian/Burdigalian Stage boundary according to the lithostratigraphic correlation, or early Aquitanian based on foraminiferal biostratigraphy.

The quality of the geochronometers separated is questionable. We did not analyze the poorly crystallized plagioclase. Biotite combines probability for both inheritance

Table 9

Results of  $^{40}\text{Ar}/^{39}\text{Ar}$  incremental heating measurements on plagioclase T152-2 (74.28 mg) from Ponte delle Lepri (by G.S.O. in Lausanne)

$(^{40}\text{Ar}/^{36}\text{Ar}$ vs. $^{39}\text{Ar}/^{36}\text{Ar})$	$(^{36}\text{Ar}/^{40}\text{Ar}$ vs. $^{39}\text{Ar}/^{40}\text{Ar})$	$^{40}\text{Ar}/^{36}\text{Ar}(i)$	MSWD
<i>Isochron ages for steps 900 to 1150</i>			
18.94 ± 0.54 Ma		304 ± 8 (2σ)	1.0
	19.00 ± 0.56 Ma	305 ± 8 (2σ)	1.2
<i>For all steps</i>			
19.5 ± 0.8 Ma		296.4 ± 5.4	24
	19.5 ± 0.8 Ma	296.8 ± 5.4	25

Detail of the  $^{40}\text{Ar}/^{39}\text{Ar}$  increment heating measurements on plagioclase T152-2;  $(\text{Ar}/\text{K}) = ^{40}\text{Ar rad}/^{39}\text{Ar}/\text{K}$ ;  $J = 0.00259$ ; gas in  $10^{-15}$  moles; error 1σ for Ar isotopes.

Temp. (°C)	Apparent age (Ma)	± 2σ	% $^{39}\text{Ar}$	% rad.	K/Ca
750	18.1	1.2	15.5	13	0.053
900	19.7	0.4	13.2	51	0.021
1025	19.5	0.4	18.2	55	0.015
1100	19.5	0.4	20.1	48	0.020
1150	20.5	0.8	4.5	33	0.030
1200	22.9	1.0	4.2	25	0.033
1250	23.1	1.4	2.8	15	0.031
1350	21.0	2.0	5.2	9	0.033
1450	18.9	2.0	10.4	8	0.032
1580	21.2	2.2	6.0	8	0.016

Temp. (°C)	40*	±	39	±	38	±	37	±	36	±	(Ar/K)	±
750	2866	6	93.5	0.2	7.786	0.016	866.3	1.7	8.70	0.02	3.89	0.13
900	181.1	0.4	21.99	0.04	0.836	0.002	511.9	1.0	0.438	0.001	4.23	0.04
1025	226.7	0.5	30.45	0.06	0.568	0.001	949.1	1.9	0.594	0.002	4.199	0.04
1100	285.4	0.6	33.54	0.07	0.599	0.001	902.7	1.6	0.708	0.002	4.198	0.04
1150	97.8	0.2	7.412	0.015	0.191	0.001	119.5	0.2	0.253	0.002	4.396	0.08
1200	135.4	0.3	6.913	0.014	0.190	0.001	102.99	0.21	0.372	0.002	4.909	0.09
1250	148.8	0.3	4.565	0.009	0.165	0.001	71.56	0.14	0.446	0.002	4.97	0.15
1350	437.9	0.9	8.645	0.017	0.437	0.001	126.7	0.3	1.387	0.003	4.43	0.21
1580	546.8	1.1	10.14	0.02	0.659	0.001	304.1	0.6	1.777	0.004	4.56	0.23

Apparent ages: (total gas age) = 19.7 (± 0.4) Ma; plateau age 900–1150 = 19.67 ± 0.28 Ma.

(heterogeneous geochemistry) and slight alteration which may not have modified the isotopic geochemical equilibrium during geological history but has certainly disturbed in part the analytical procedure.

Using the pseudo-plateau age and taking into account the error bar on the monitor for irradiation, a plateau age for T163 biotite can be calculated at 21.2 ± 0.7 Ma. Due to probable extraneous argon, and possible loss of  $^{39}\text{Ar}$  during irradiation (Hess and Lippolt, 1986), 21.2 Ma is a maximum age for the time of deposition of the dated layer. The chronostratigraphical location of this age is not precise enough for time-scale calibration. Compared to the data obtained elsewhere in this volume, an age younger than 21.6 Ma suggests a middle to late Aquitanian age of deposition.

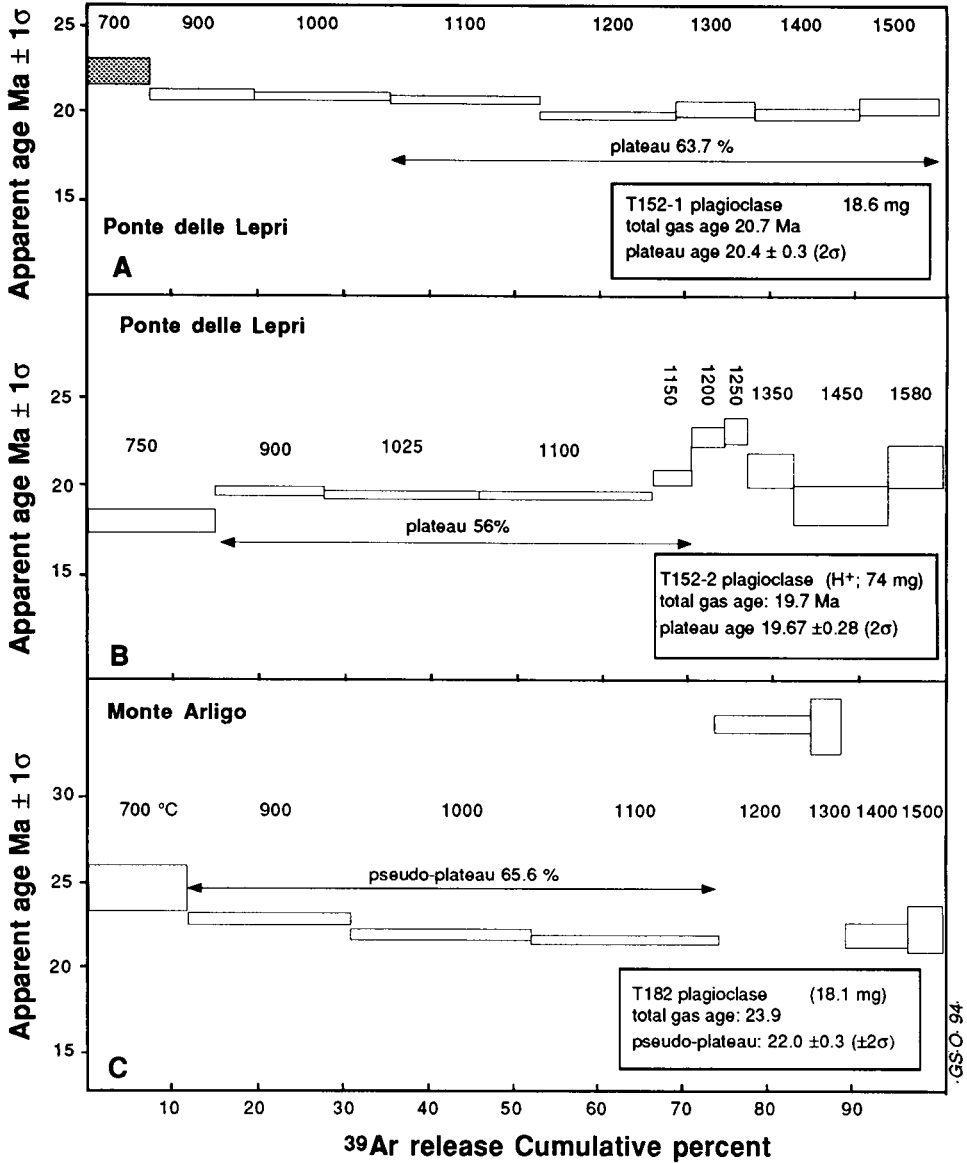


Fig. 11. <sup>40</sup>Ar/<sup>39</sup>Ar age spectra for two plagioclase separates. (A) T152-1 and (B) T152-2 from Ponte delle Lepri; (C) T182 from Monte Arligo.

*Ponte delle Lepri section*

This section is the thickest available from the area and is consequently supposed to be the best potential for the record of the marine events throughout this stratigraphic interval. Additional stratigraphic research is planned using other fossil groups including calcareous nannofossils, as well as magneto- or chemostratigraphic analyses (i.e.,

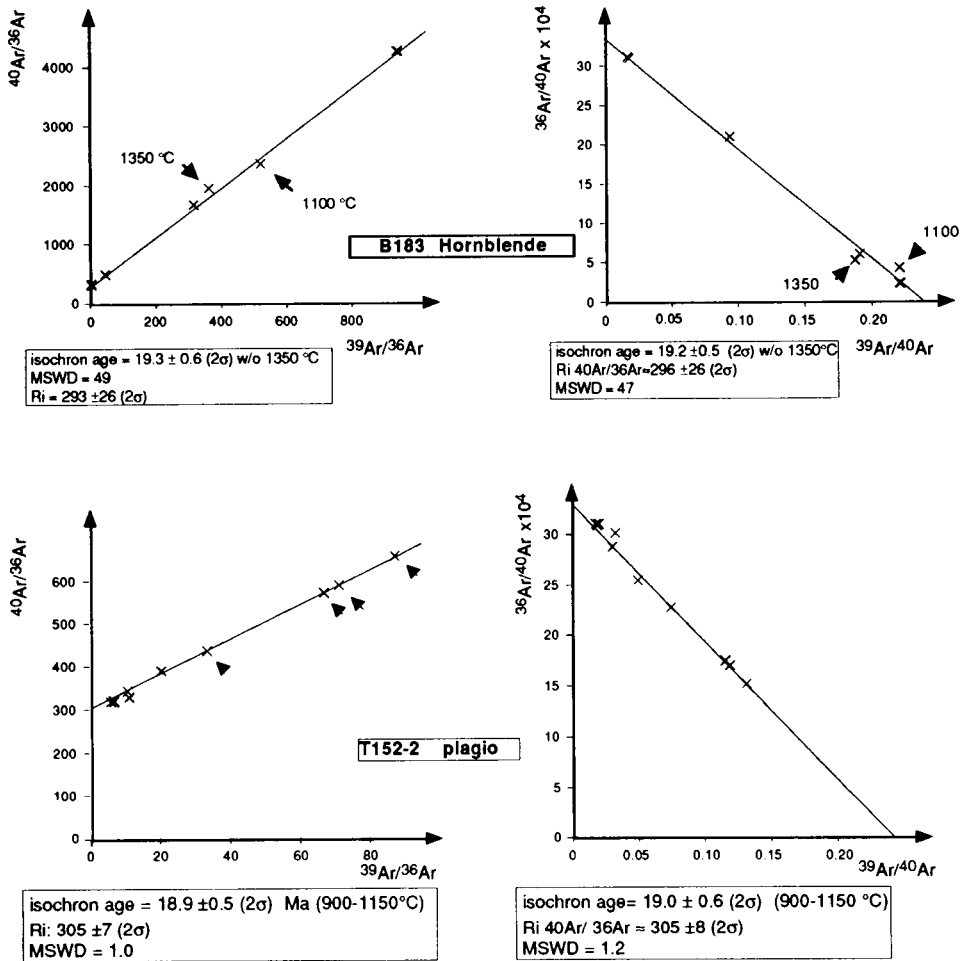


Fig. 12. Isochron plots of samples B183 hornblende and T152-2 plagioclase. Note the poor mean standard weighted deviation (MSWD calculated from all but the 1350°C step) for sample B183 (disturbed spectrum).

Sr isotopes). On lithostratigraphical ground, the ‘Siliceous lithozone’ is inferred to encompass the Aquitanian/Burdigalian boundary. Foraminiferal biostratigraphy suggests an early Burdigalian age.

From the methodological point of view, the two age spectra obtained from the same material (plagioclase T152) have different aspects: an old age for the low-temperature heating step and a slightly younger age for the 1200°C heating step in separate T152-1, and the reverse for the separate T152-2. This behaviour may be due to different acid treatments which will have to be studied further.

From the geological point of view, and within sample B183, the hornblende of the older sample from Ponte delle Lepri indicates a total gas age at 19.3 Ma which is a mixture of heating step ages between 18.3 Ma and 19.8 Ma. This does not represent a plateau; the data suggest an imprecise age between 19.2 Ma (isochron age and total gas

Table 10

Results of  $^{40}\text{Ar}/^{39}\text{Ar}$  incremental heating measurements on plagioclase T182 (18.1 mg) from Monte Arligo (by G.S.O. in Lausanne)

Temp. (°C)	Apparent age (Ma)	$\pm 2\sigma$	% $^{39}\text{Ar}$	% rad.	K/Ca
700	24.9	2.7	12.0	8	0.045
900	22.8	0.6	20.1	84	0.023
1000	21.8	0.5	22.3	100	0.022
1100	21.6	0.5	23.2	97	0.028
1200	34.3	1.2	9.3	85	0.031
1300	(34.1)	3.2	3.1	76	(0.028)
1400	21.8	1.7	6.2	55	0.024
1500	22.2	2.8	3.8	63	0.014

Apparent ages: (total gas age) 23.9 ( $\pm 0.4$ ) Ma; pseudo plateau age: 900–1100 = 65.6%: 22.0  $\pm$  0.3 Ma.

age) and 19.6 Ma (most step ages). The plagioclase separate reinforces this age with a plateau age at 19.5  $\pm$  0.5 Ma. Within sample T152, there is no perfect agreement between T152-1 (plateau and total gas ages at about 20.5 Ma) and T152-2 (plateau and total gas ages at 19.7 but isochron age as young as 19.0 Ma). This plagioclase has a crystallization age apparently between 19.5 Ma and 20.5 Ma.

Comparison between data from the two distinct layers suggests that there is no significant difference of analytical ages between them, with face values for the younger layer older than those for the other layer. An overall age of 19.5 Ma may be recommended for the section. This is considered as an early Burdigalian age in this volume. However, the conclusion for this section is that a better geochronometer should be found for more precise and accurate radioisotopic age determinations.

### Monte Arligo section

According to previous works, the Monte Arligo section was promising for geochronological calibration of the stratigraphic series on the Aquitanian side of the Oligocene/Miocene boundary. In fact, although volcanogenic layers are present in fossiliferous sediments, the outcrop shows a complex exposure. The tectonic setting does not insure continuity of the depositional succession. The biostratigraphical control is not perfect. The single tuff layer previously quoted near the Oligocene/Miocene boundary is different from the one we studied. Finally, a single type of geochronometer (i.e., plagioclase) is available from the tuffs.

Lithostratigraphical control suggests an age slightly older than a late Aquitanian–early Burdigalian age ('Marne Selciose' of the Siliceous lithozone). Biostratigraphical (calcareous nannofossils) data suggest a strictly Early Miocene age (within the interval Aquitanian plus Burdigalian p.p.) for sample T182.

Samples from the same area (Fig. 7) were submitted to geochronological study in the past. Cati (1974) quotes unpublished K–Ar ages (isotope dilution technique, recalculated for modern conventional decay constants) from Dymond at 24.1  $\pm$  1.0 Ma (originally 23.5 Ma), confirmed by Savelli in Bologna with dates on glass, and later improved by Dymond to 23.4  $\pm$  1.0 Ma (originally 22.8 Ma). Unprecise apparent ages

obtained from glass separates at 26 and 27 Ma are also documented in Borsetti et al. (1983). Glass fraction is generally considered a poorly reliable geochronometer and we have dated the plagioclase fraction of a layer most certainly younger than those studied before. The selected sample (T182) does not provide a good age spectrum. However, the pseudo-plateau age may be proposed as representative of the time of crystallization ( $22.0 \pm 0.3$  Ma). This is a typically Aquitanian age according to the knowledge gathered in this volume, and is consistent with the stratigraphical control.

### *General conclusions*

In the northern and central Apennines, volcanoclastic layers are common in Aquitanian and early Burdigalian marine deposits. Due to the variable number of layers in different sections, they cannot be used as individually correlatable lithological markers on a regional scale. Moreover, these volcanoclastic layers lack specific characteristics, geochemical or mineralogical, which would permit their identification in distant sections. Nevertheless, the association of numerous layers appears regionally diagnostic. The section in Ponte delle Lepri is important because it contains more volcanoclastic layers than other studied sections in the area. This abundant volcanoclastic material would suggest per se a proximal volcanic source (no more than a few tens of km away) during Early Miocene time. However, this section is much thicker than other coeval sections in the area, suggesting that it may represent a deeper basin hosting a thicker and more complete sedimentary sequence in respect to adjacent palaeobasinal, perhaps shallower areas. In short, other than the number and thickness of volcanoclastic layers, no additional geological evidences presently support the hypothesis of a proximal volcanic source for the Ponte delle Lepri tephra.

In addition to the Ponte delle Lepri section, we have investigated many other coeval outcrops in the Emilian Apennines. Only three were considered suitable for integrated stratigraphic studies either because they contained several potentially datable geochronometers or because they exhibited apparently more interesting stratigraphical situations. As it turned out, the Ponte delle Lepri section is the only one which yielded diversified and yet consistent data insuring some geologic reliability of radioisotopic age determinations.

The geochronological results of this study are summarized in Table 11. Despite their overall disturbed spectra, the four plagioclase samples dated in this study yielded significant geochronologic results. All plagioclase age spectra display a restricted flat portion which yield ages consistent with the known stratigraphic position of the analyzed samples. The low-temperature heating step ages are discrepant, and in three of the four studied cases tend to be too old. Significant age information can only be obtained following removal of the gas fraction released from plagioclase at temperatures below 750°C.

The numerical age of the biotite-rich tuff from the Cava Predosa section is poorly constrained and most is probably between 18.4 Ma and 21.2 Ma. The two samples from Ponte delle Lepri indicate similar ages around 19.5 Ma which are consistent with a late Aquitanian–early Burdigalian stratigraphic age for some part of the ‘Marne Selciose’ lithostratigraphic unit. The age of the plagioclase from the Monte Arligo section is at about 22 Ma, thus older than the plagioclase separates from the other two sections



Table 11

Summary of geochronological ages obtained in this study

Sample	Total gas age	Plateau age (Ma)	Geological age
<i>Cava Predosa</i>			
163 biotite	18.4 ± 0.3	(21.2 ± 0.2) 68.7%	→ 18.4 < probable age < 21.2 Ma
<i>Ponte delle Lepri</i>			
152-1 plagioclase	20.7 ± 0.3	20.4 ± 0.3	→ about 20.5 Ma?
152-2 plagioclase	19.7 ± 0.4	19.7 ± 0.3 56.0%	isochron: 19.0 ± 0.5 → 19.0 to 19.5 Ma
183 hornblende	19.3 ± 0.3	(3 steps at ≈ 19.6)	isochron: 19.2 ± 0.5 → 19.2 to 19.6 Ma
183 plagioclase	20.3 ± 0.5	19.5 ± 0.5 63.0%	→ 19.5 ± 0.5 Ma
<i>Monte Arligo</i>			
182 plagioclase	23.9 ± 0.4	(pseudo-plateau 22.0 ± 0.3)	→ ≈ 22 Ma

Error bar estimates are given at the 95% confidence level (internal analytical precision including error in flux calibration but not on the monitor age).

studied. In fact, the Monte Arligo section comprises the Antognola Marl Formation which is stratigraphically located below the units exposed in the Ponte delle Lepri and Cava Predosa sections.

All numerical ages calculated here must include an additional 2.5% error bar when compared to data from other sources using a different monitor.

#### SOMMAIRE — STRATIGRAHIE INTÉGRÉE (BIOSTRATIGRAPHIE, GÉOCHRONOLOGIE) DE SECTIONS DANS LE MIOCÈNE INFÉRIEUR DES APENNINS D'ÉMILIE (ITALIE)

(Manuscrit soumis: Décembre 1993; révisé: Janvier 1995; rédacteur responsable: GSO)

Nous avons recherché dans les Apennins d'Emilie-Romagne (Italie) des coupes géologiques fossilifères comprenant des niveaux volcanoclastiques favorables à l'étude géochronologique. Les trois sections de Cava Predosa, Ponte delle Lepri et Monte Arligo ont finalement été datées. La première a été attribuée à l'Aquitanién inférieur et la seconde au Burdigalien inférieur (d'après les foraminifères planctoniques); la troisième est plus jeune que l'Aquitanién basal d'après les nannofossiles calcaires. La biotite de la Cava Predosa a livré un spectre d'âge  $^{40}\text{Ar}/^{39}\text{Ar}$  avec un pseudo-plateau à 21,  $17 \pm 0$ , 20 Ma. Au Ponte delle Lepri, le niveau inférieur a été daté par la hornblende entre 19,2 et 19,6 Ma et par un plagioclase: plateau à  $19,5 \pm 0,5$  Ma; le niveau supérieur a livré un plagioclase montrant des âges compris entre 19 et 20 Ma. Au Monte Arligo, le plagioclase extrait permet de déduire un âge de cristallisation de l'ordre de 22 Ma. Ces résultats présentent un bon accord avec les attributions données par la biostratigraphie. Au plan du calibrage de l'échelle chronostratigraphique, ils doivent pourtant être considérés comme préliminaires car soit la biostratigraphie soit les résultats isotopiques manquent encore de précision.

(Sommaire des auteurs)

## ACKNOWLEDGEMENTS

We thank A.M. Borsetti for her information on the planktonic Foraminifera of the Monte Arligo area. Isotopic measurements for this study by G.S. Odin were achieved thanks to facilities made available by the Fonds National Suisse in Lausanne. X-ray diffraction patterns were obtained thanks to the facility made available by the Laboratory of Geology of the Muséum National d'Histoire Naturelle. This work was also supported by a grant from the Italian Ministry of University and Research (MURST 60%, R. Coccioni responsible). The careful reviews of the original version of this paper by Kewin Steward and Alessandro Montanari are deeply acknowledged. No funding was provided by French organizations for this research.

This Page Intentionally Left Blank

*Chapter C3*

**INTEGRATED STRATIGRAPHY OF THE CHATTIAN TO  
MID-BURDIGALIAN PELAGIC SEQUENCE OF THE CONTESSA VALLEY  
(GUBBIO, ITALY)**

A. Montanari, D.M. Bice, R. Capo, R. Coccioni, A. Deino, D.J. DePaolo, L. Emmanuel,  
S. Monechi, M. Renard and D. Zevenboom

**INTRODUCTION**

The pelagic sequence exposed in active quarries and along road cuts in the Contessa Valley, near Gubbio in the Umbrian region of central Italy, represents a remarkably continuous stratigraphic record from the Upper Jurassic to the Mid-Miocene. The numerous volcanoclastic layers within the Eocene to Miocene portion of this sequence present the rare opportunity to radioisotopically date magnetostratigraphic, biostratigraphic, and chemostratigraphic events. Premoli Silva et al. (1988) summarize the studies that have accomplished this task for the Upper Eocene and Oligocene in the Contessa sequence, and in other sections in the Umbria–Marche region.

An integrated stratigraphic study focused on the interval across the Oligocene/Miocene boundary in the Contessa Valley, was carried out by Montanari et al. (1991), and included calcareous microplankton biostratigraphy, magnetostratigraphy, strontium isotope stratigraphy, and  $^{40}\text{Ar}/^{39}\text{Ar}$  geochronology on two interbedded volcanoclastic layers. In this study, we have carried out further interdisciplinary analytical work to improve the biostratigraphic, magnetostratigraphic, chemostratigraphic, and geochronologic resolutions of this sequence, and propose an integrated stratigraphic model for the Chattian to lower Burdigalian interval.

**LITHOLOGIC AND SEDIMENTOLOGIC FRAMEWORK (A. Montanari and  
R. Coccioni)**

The stratigraphic interval comprising the upper Chattian, Aquitanian, and lower Burdigalian in the Contessa sequence, is represented by the upper part of the Scaglia Cinerea formation, and the overlying lower part of the Bisciaro formation. This sequence has been studied in three sections, namely the Contessa Quarry (CQ), the Contessa Testimone (CT) and the Contessa Valderchia (CV), the locations of which are shown in Fig. 1.

The sharp contact between the Scaglia Cinerea and the Bisciaro formations is marked by the so-called ‘Raffaello Level’, a 18 cm thick bentonite layer which represents a regional marker bed easily recognizable in the field (Coccioni et al., 1989; Montanari et al., 1991). This lithostratigraphic boundary is well exposed along the NE face of the CQ quarry which belongs to the ‘Cementerie Aldo Barbetti’ (Fig. 2), and at the base of the CT section exposed along the Contessa Highway (Fig. 3).

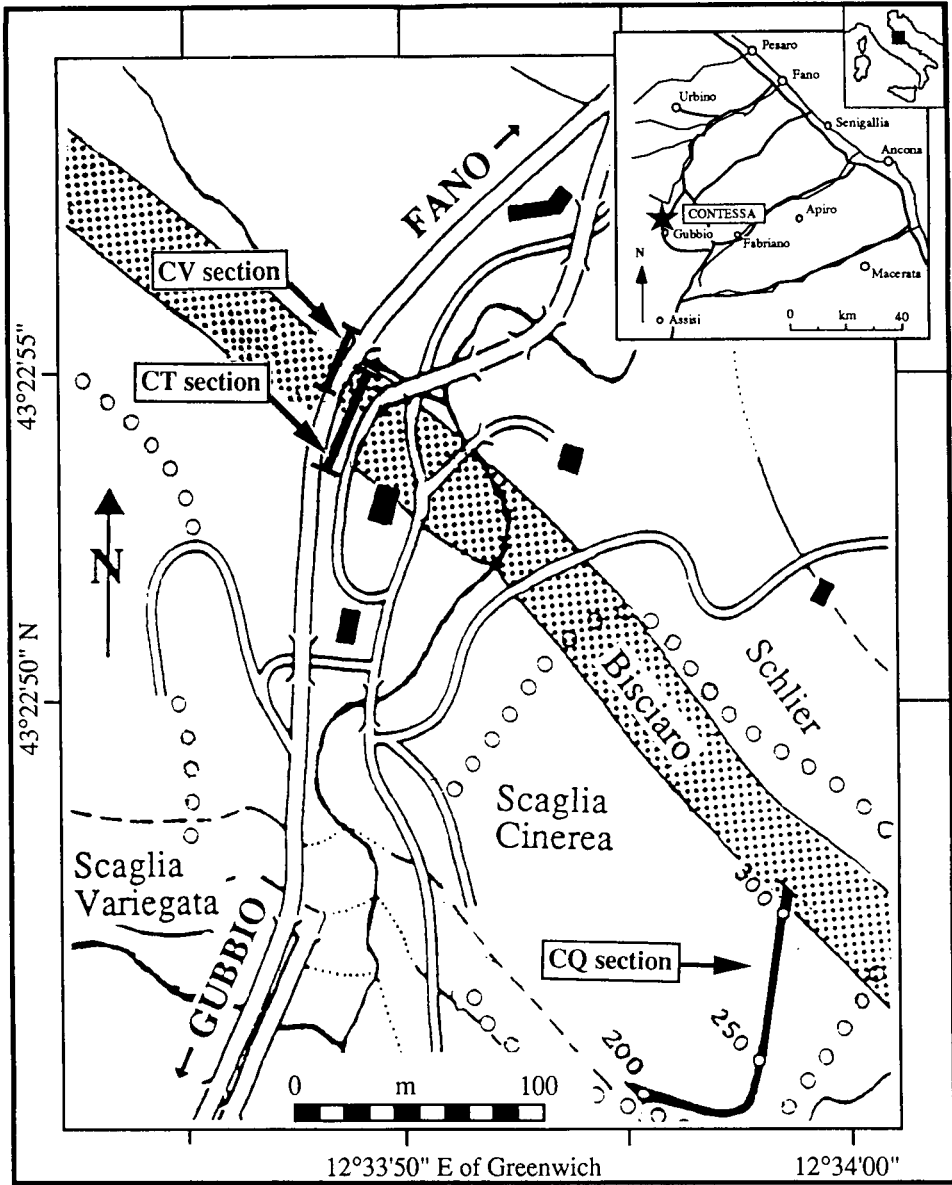


Fig. 1. Location map of the studied sections in the Contessa Valley.

The Scaglia Cinerea is a 100 m thick, homogeneous sequence of well bedded, blue-grey, biomicritic marly limestones containing sporadic biotite-rich distal volcanoclastic layers deposited in a deep-water pelagic basin (Cati et al., 1981; Lowrie et al., 1982; Montanari et al., 1985, 1988; Odin et al., 1991). By contrast, the Bisciario formation is made of an alternation of different rock types representing hard pelagic marly limestones (i.e., the silicic limestones in Morandi and Tateo, 1992), pelagic calcareous marls, vol-

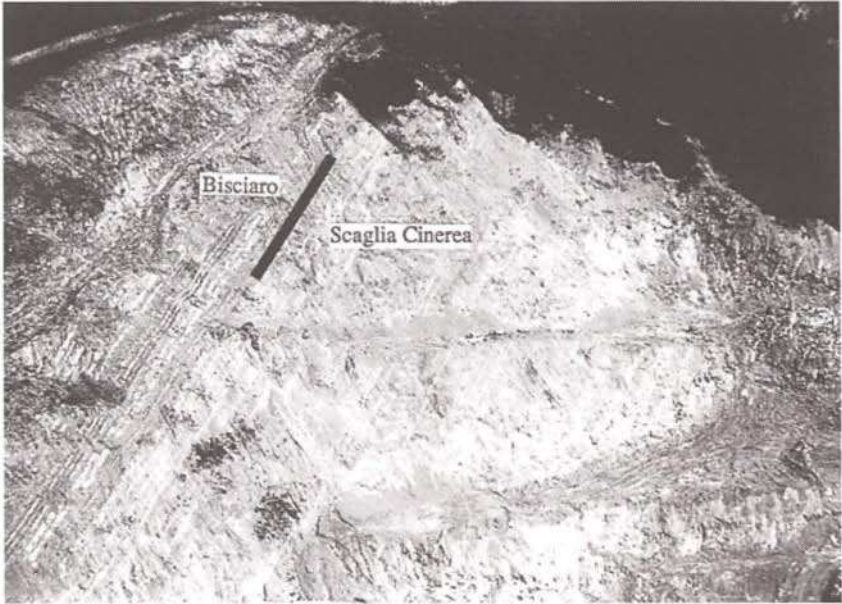


Fig. 2. Panoramic view of the Contessa CQ quarry showing the Scaglia Cinerea/Bisciario boundary.



Fig. 3. The Contessa CT outcrop exposing the Scaglia Cinerea/Bisciario boundary.

caniclastic layers, and glauconitic–sandy limestones occurring in the lowermost part of the formation. The lithostratigraphy of the Bisciario is consistently represented, at Gubbio as well as in the surrounding Umbria–Marche region, by a lower marly member, a middle calcareous–siliceous–tuffitic member, and an upper marly member representing the gradual passage to the overlying Schlier formation (Coccioni and Montanari, 1994).

An exhaustive documentation of the Bisciario lithostratigraphy and petrography is reported by Balogh et al. (1993) who recognized a wide variety of volcanic products representing a rather conspicuous syndepositionary calc-alkaline volcanism (mainly andesitic to rhyolitic–dacitic). On the basis of detailed mineralogic and petrographic analyses, and regional sedimentologic relations, Balogh et al. (1993) inferred a WSW distant source for the Bisciario tephra. This has been confirmed by Montanari et al. (1994) by means of a regional grain size analysis of the felsic fraction from the Raffaello Level which shows a marked decrease in the mean grains size from southwest to northeast throughout the basin. Montanari et al. (1994) proposed the explosive Miocene volcanism of western Sardinia as the possible source for the Bisciario tephra. This hypothesis finds some support from a comparative geochemical analysis of biotite samples from several Sardinian volcanic sequences, and volcanoclastic layers in the upper Bisciario and lower Schlier formations from the Apennine basin (Assorgia et al., 1994). In particular, Assorgia et al. (1995) showed that biotites from the Bisciario and Schlier volcanoclastic layers are geochemically identical to those from the calc-alkaline sequence of Bosa, on the western coast of Sardinia, but significantly different from biotites in other Sardinian sequences.

The Bisciario in the CT–CV section is exposed continuously for about 21 m, and is then truncated by a low angle fault which puts it in direct contact with the overlying Schlier formation.

In summary, as Alvarez and Montanari (1988) point out, the Scaglia Cinerea, Bisciario, and Schlier formations represent a transition from dominantly pelagic carbonate deposition to siliciclastic, synorogenic turbidite deposition in the Apennine foredeep, which is represented by the Langhian Marnoso Arenacea flysch. This foredeep, created by the advancing Apennine fold-and-thrust belt, migrated from the southwest to the northeast; it is now located in the Adriatic Sea. At the time of deposition of the calcareous marls of the Scaglia Cinerea, the Umbria–Marche basin was presumably receiving clays and fine silt that represent the distal edge of the siliciclastic deposition within the foredeep trough. Sporadic biotite-rich volcanoclastic layers interbedded in the Scaglia Cinerea formation are the distal products of andesitic volcanism occurring in the western Mediterranean at the beginning of the Alpine–Apennine main orogenic phase. With the inception of explosive volcanism in Sardinia, the Umbria–Marche basin became the receptacle of frequent volcanic fallout products which were incorporated in the Bisciario formation. In the late Burdigalian, sedimentation returned predominantly marly with the deposition of the Schlier formation, whereas volcanoclastic deposition became more sporadic.

## BIOSTRATIGRAPHY

### *Planktonic Foraminifera (R. Coccioni)*

The biostratigraphy of the Palaeogene carbonate sequence of the Contessa Valley was originally determined by Lowrie et al. (1982) on the basis of planktonic Foraminifera

and calcareous nannoplankton. Later on, Montanari et al. (1991) and Coccioni and Monechi (1992) carried out a biostratigraphic analysis of the Upper Oligocene–Lower Miocene composite CQ–CT–CV section by defining the first (FO) and last (LO) occurrence of the most significant planktonic foraminiferal and calcareous nannofossil in order to provide a biostratigraphic calibration of polarity reversals, and of the radioisotopically dated Raffaello Level, and CT–WAL volcanoclastic layers. At the International Geology Congress in Kyoto (1992), the Working Group (WG) on the Palaeogene/Neogene (P/N) boundary, equated to the Oligocene/Miocene (O/M) boundary, after several years of study and debate, recommended the Carrosio–Lemme section (Tertiary Piedmont Basin, northwestern Italy) to the International Commission on Stratigraphy as the Global Boundary Stratotype Section and Point (GSSP) for the P/N boundary. The WG will propose to place the boundary at metre level 35 in the Carrosio–Lemme section, in correspondence with a magnetic polarity reversal interpreted as the base of the magneto-Chronozone C6C2n (Steininger et al., 1994). Consequently, a revision of the planktonic foraminiferal stratigraphy became necessary to compare the events recognized near the O/M boundary in the composite Contessa section, with those identified in the Carrosio–Lemme section.

Planktonic Foraminifera were studied mainly in washed residues (grain size fraction  $>40 \mu\text{m}$ ), and subsequently in thin section, from a total of 94 samples. The generic and specific concepts of Spezzaferri (1994) were largely adopted. Poor preservation due to recrystallization and deformation was the major problem in this study. The Oligocene Scaglia Cinerea contains abundant and moderately well-preserved planktonic foraminiferal tests, whereas foraminiferal abundance and preservation in the overlying Bisciaro vary greatly from moderately good to very poor. Samples with a high volcanogenic component contain the most scarce and poorly preserved foraminiferal assemblages. Volcanoclastic layers are almost barren of Foraminifera, whereas iron-rich layers contain poorly preserved, often limonitized or pyritized tests. Occasional reworking represented by sporadic Oligocene specimens was recognized in the uppermost part of the Scaglia Cinerea, and in the lower part of the Bisciaro.

Notwithstanding the generally poor preservation of planktonic Foraminifera in the Bisciaro, the close sampling made it possible to recognize some well-differentiated and sequential events allowing a reliable biostratigraphic zonation of the studied sequence. In terms of the Blow (1969) and Spezzaferri (1994) biozonations it was possible to recognize five zones, and four zones subdivided into two subzones, respectively. Following the Mediterranean zonal model of Iaccarino and Salvatorini (1982) and Iaccarino (1985), two zones and two subzones were recognized (Fig. 4).

'*Globigerinoides primordius*' whose first occurrence (FO) defines the P22/N4 zonal boundary of Blow (1969) is already present at m 296 in the CQ section where the lowest sample was collected. This study confirms previous results by Lowrie et al. (1982) who placed the FO of *Paragloborotalia kugleri* a few metres above the top of Chron 7, that is at 298 m in the CQ section. The FO of *P. kugleri* is used by Spezzaferri (1994) to place the P22/N4 zonal boundary. According to Steininger et al. (1994) the FO of *P. kugleri* in the Carrosio–Lemme section is found about 2 m above magneto-Chronozone C6C2n.

The next significant event is the FO of *Globoquadrina dehiscens* at 301.5 m in the CQ section. This event occurs at the diversification level of the genus *Globigerinoides* (i.e., the *Globigerinoides* event of Spezzaferri, 1994), where *Globigerinoides immaturus*



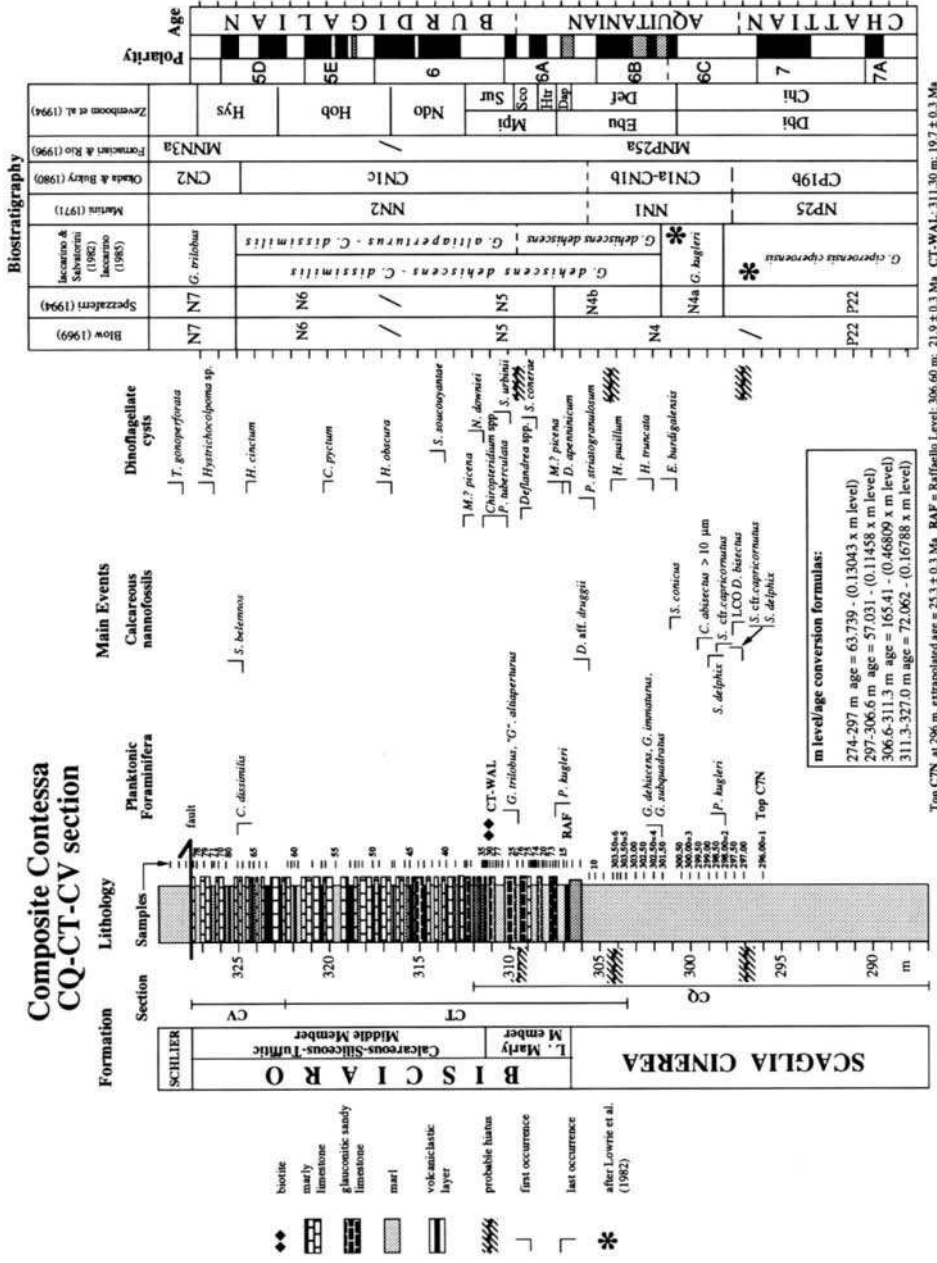


Fig. 4. Litho-, bio- and magnetostratigraphic synthesis of the composite CQ-CT-CV section.

and *Globigerinoides subquadratus* first appear. The *Globigerinoides* event defines the boundary between Subzones N4a and N4b of Spezzaferri (1994).

According to all the biozonations followed herein, the FO of *G. dehiscens* is recognized within the range of *P. kugleri*, and precedes the entrance of '*Globigerinoides*' *altiaperturus* and *Globigerinoides trilobus*. Following Blow (1969) the FO of *G. dehiscens* takes place in the upper part of Zone N4. This event defines the lower boundary of the *G. dehiscens dehiscens* Subzone of the *G. dehiscens dehiscens*–*Catapsydrax dissimilis* Zone of Iaccarino and Salvatorini (1982) and Iaccarino (1985). Therefore, the *G. dehiscens dehiscens* Subzone of Iaccarino and Salvatorini (1982) and Iaccarino (1985) seems correlatable with the upper part of Zone N4 and the basal part of Zone N5 of Blow (1969). However, Spezzaferri (1994) showed the diachronous character of the FO of *G. dehiscens* which is found from the middle of Zone P22 in the Pacific Ocean to the lower third of Zone N4 in the North Atlantic and Mediterranean.

The LO of *P. kugleri* which is used by Blow (1969) and Spezzaferri to define the N4/N5 zonal boundary, is found at 307.4 m.

The FO of *Zeaglobigerina woodi* is recognized at 308.4 m in the CQ–CT section. According to most biostratigraphers, this event occurs between the FO of *G. dehiscens* and the FOs of *G. altiaperturus* and *G. trilobus* (Jenkins, 1981; Biolzi et al., 1981; Chaproniere, 1988). Furthermore, *Z. woodi* seems to appear after the LO of *P. kugleri* (Jenkins, 1966, 1971, 1985; Biolzi et al., 1981; Biolzi, 1985; Iaccarino, 1985), in the lowermost part of the N5 Zone of Blow (1969), that is in the uppermost part of *G. dehiscens dehiscens* Subzone of Iaccarino (1985). In terms of Blow's (1969) zonal model, *Z. woodi* first appears within the uppermost part of Zone N4, above the FO of *G. dehiscens*, and within the range of *P. kugleri* but below the FOs of '*G.*' *altiaperturus* and *G. trilobus*. Molina (1979) recognized the FO of *G. woodi* at the same level of the FO of *G. dehiscens dehiscens*. Keller (1981, 1984) documented that in deep-sea sediments from the equatorial Pacific, *Z. woodi* appears before *G. dehiscens*, whereas Bizon and Müller (1981), studying deep-sea sediments from the same area, found just the opposite. However, according to Chaproniere (1988), the FO of *G. dehiscens* at DSDP 192 (southwest Pacific) does not represent an evolutionary event but rather an environmental one. Moreover, in the Upper Oligocene–Lower Miocene sections from Victoria, Australia, the FO of *Z. woodi* is below the FO of '*G.*' *altiaperturus* which precedes that of *G. trilobus* (Chaproniere, 1988). Recently, Spezzaferri (1994) showed that in the Indian Ocean *Z. woodi* first occurs in the lower part of Zone P22.

'*G.*' *altiaperturus* and *G. trilobus*, the former extremely rare in the CQ–CT section, first occur at 309.6 m, about 2 m above the LO of *P. kugleri*. There is no unanimous agreement on the relative stratigraphic positions of the FOs of '*G.*' *altiaperturus* and *G. trilobus*, the former defining the lower boundary of the *G. altiaperturus*–*Catapsydrax dissimilis* Subzone of Iaccarino and Salvatorini (1982) and Iaccarino (1985), and also considered as marker for the Aquitanian/Burdigalian boundary (Bizon and Bizon, 1972; Demarcq et al., 1974; Bizon, 1984; Iaccarino and Salvatorini, 1982; Iaccarino, 1985). However, for the Aquitanian/Burdigalian boundary there is no definitive consensus on the datum that ought to be used for recognition. In fact, in the biostratigraphic scheme of Blow (1969), the Aquitanian/Burdigalian boundary is within Zone N6. The *G. altiaperturus*–*C. dissimilis* Subzone correlates with part of Zone N5 and the entire Zone N6 of Blow (1969) and Spezzaferri (1994). According to several authors (Blow, 1969;

Demarcq et al., 1974; Borsetti et al., 1979a; Biolzi et al., 1981; Bizon and Müller, 1981; Iaccarino, 1985, among others), '*G.* *altiaperturus*' appears before *G. trilobus*, whereas according to Bolli and Saunders (1985), Molina (1979), and Biolzi (1984, 1985), the FO of *G. trilobus* is stratigraphically lower than the FO of '*G.* *altiaperturus*'.

According to Keller (1984), the FO of *G. trilobus* precedes not only that of '*G.* *altiaperturus*' but also that of *G. dehiscens*. According to Spezzaferri (1994) the FO of '*G.* *altiaperturus*' is followed slightly above by the FO of *G. trilobus* in the upper part of Zone N4 in the equatorial Atlantic, eastern South Atlantic and South Pacific whereas these two species first occur together within the upper third of Zone N4 in the western South Atlantic, and in the lower part of Zone N5 in the Indian Ocean, respectively. It is worth mentioning, however, that in the stratotype of the Burdigalian, '*G. altiaperturus*' and *G. trilobus* first occur at the same level. An almost similar biostratigraphic situation is found in the Carrosio–Lemme section where the FO of *G. trilobus* slightly precedes the FO of '*G.* *altiaperturus*', both these events occurring slightly below the LO of *P. kugleri* (Steininger et al., 1994; S. Spezzaferri, pers. commun., February, 1995). In the Santa Croce di Arcevia section Coccioni et al. (1992b, and Chapter C4) recognized the FO of '*G.* *altiaperturus*' slightly below the LO of *P. kugleri*, the latter event taking place just before the FO of *G. trilobus*.

As mentioned above, in the CQ–CT section the lowest finding of *G. trilobus* is associated with that of '*G.* *altiaperturus*'. Therefore, following the zonal model of Iaccarino and Salvatorini (1982) and Iaccarino (1985) the concurrence of the two taxa should be indicative of incompleteness of the lowermost part of the *G. altiaperturus*–*C. dissimilis* Subzone.

In the CQ–CT section, it was not possible to biostratigraphically distinguish Zone N5 from Zone N6 of Blow (1969) and Spezzaferri (1994) because *Globigerinatella insueta*, the FO of which defines the N5/N6 zonal boundary, is lacking in the Mediterranean area.

The last significant event is the LO of *C. dissimilis* at 325 m in the CV section (Fig. 4). This event defines the N6/N7 zonal boundary of Blow (1969) and the boundary between the *G. dehiscens dehiscens*–*C. dissimilis* and the *G. trilobus* zones of Iaccarino and Salvatorini (1982) and Iaccarino (1985).

#### *Calcareous nannofossils (S. Monechi)*

A revision of the calcareous nannofossil stratigraphy of the composite Contessa section has been carried out in order to better define the O/M boundary, and to compare the recognized events with the proposed O–M GSSP section of Carrosio–Lemme (Steininger et al., Chapter A9).

The Contessa composite section is characterized by abundant, poorly preserved calcareous nannofossil assemblages. Nevertheless, it has been possible to further refine the biostratigraphy and to detect some well-differentiated and sequential events which are herein briefly discussed (Fig. 4). The LO of *Dictyococcites bisectus* has been used as a secondary criterion by Bukry (1973) to define the top of Subzone CP19b, and it has been used by many authors to approximate the top of Zone NP25 (Martini, 1971) when *Helicosphaera recta* is missing. Few and discontinuous *D. bisectus* occurs in the lower part of the CQ section, thus making difficult to define the exact extinction level.

The LO of *D. bisectus* has been tentatively located at 297.5 m where the percentage of relative abundance decreases, even if few *D. bisectus* are found up to 302 m. The next significant data are the FOs of *Sphenolithus* cfr. *S. capricornutus* and *Sphenolithus delphix* both occurring at 297 m and getting extinct at 298.5 m and 299 m, respectively. The poor preservation biases the correct taxonomic assignment to *S. capricornutus*, in fact the specimens recognized are characterized by two diverging but not very prominent spines. *Sphenolithus conicus* is continuously present up to 301 m where the LO is fixed; few scattered specimens have been found up to 307 m, just preceding the FO of *G. dehiscens*.

According to these new findings (FO and LO of *S. delphix* and *S. capricornutus*), the presence of *S. delphix* and *S. capricornutus* previously found at sample CT15/306.9 (Coccioni and Monechi, 1992) can be explained inferring reworking or different taxonomic concepts. *S. capricornutus* could be assigned to *Sphenolithus multispinatus*; according to Fornaciari et al. (1990) this species seems to be restricted to a short interval above the LO of *S. conicus*. From 306.9 m upward in the CQ–CT section, small sphenoliths (intermediate between *S. compactus* and *S. neoabies*) become a constant component of the nannofossil assemblage, besides intermediate specimens of *S. dissimilis*–*S. belemnos*. The FO of *S. belemnos* is confirmed at 324.8 m.

The previous recognized events have been compared with calcareous plankton events and magnetostratigraphy of the Carrosio–Lemme section. The calcareous plankton events from both sections match fairly well, even if few discrepancies are noted in the stratigraphic distribution of *D. bisectus*, *S. delphix* and *S. capricornutus*.

#### *Dinoflagellate cysts (D. Zevenboom)*

Brinkhuis et al. (1992) recently presented the first detailed dinoflagellate cyst (dinocyst) zonal scheme for the O/M transition in Italy, calibrated against calcareous microfossil distributions and magnetostratigraphic interpretations where possible. The authors defined three zones (subdivided into six subzones) on the basis of the Carrosio–Lemme section from the Piedmont Basin (northwestern Italy) and the Contessa Quarry section from the Umbria–Marche Basin (northeastern Apennines). However, Brinkhuis et al. (1992) reported on the distribution of selected taxa only, used by the authors to define and characterize their three-fold zonation. Subsequent studies by the present author were aimed at further enhancing and refining this zonal scheme, and at documenting the entire dinoflagellate cyst distribution. For this purpose, new sample sets from the Carrosio–Lemme section, the composite Contessa section, and a new section at Santa Croce di Arcevia (Coccioni et al., Chapter C4) in the Umbria–Marche Basin have been investigated.

With regard to the dinocyst, results of these activities are presented in a series of papers. Firstly, Zevenboom (in press) relocated all the proposed zones of Brinkhuis et al. (1992) to the Carrosio–Lemme section. Secondly, within the framework of the MICOP project, the present paper is one of two contributions in this volume by the author, reporting on the Contessa and Santa Croce di Arcevia sections, respectively. This paper is concerned with samples from the Contessa section (Montanari et al., 1990) and aims at giving a detailed documentation of the dinoflagellate cyst distribution and a recognition of the previously established dinocyst zones and subzones.

Most samples yield excellently preserved and rich dinocyst assemblages. Only in the upper part of the sequence preservation and richness decreases, possibly due to weathering. The main dinocyst events in the Contessa composite section are shown in Fig. 4. The various zones and subzones of Brinkhuis et al. (1992) and Zevenboom (in press) can readily be recognized and suggest a complete O/M transition. In the Lower Miocene part, however, a hiatus is assumed on the basis of the quantitative and qualitative dinocyst data and a comparison with calcareous plankton of the Carrosio-Lemme and the Contessa sections (Zevenboom et al., 1994). It is proposed that the hiatus coincides with the (Def/Dap) boundary, located near the top of the Scaglia Cinerea formation, around metre level 305. The *Hystrichokolpoma truncata* Subzone of the *Membranilarnacia? picena* Zone, previously thought to be missing at the Contessa site (Brinkhuis et al., 1992), can now be recognized. The following extension of the zonal model of Brinkhuis et al. (1992) and Zevenboom (in press) is proposed:

*Membranilarnacia? picena* (Mpi) Interval Zone (lowest Miocene to middle Lower Miocene) emend.

*Definition.* The interval from the FO of *Membranilarnacia? picena* to the FO *Nematosphaeropsis downiei*.

*Calibration.* Basal N5 (LO of *P. kugleri*) to basal N6 (FO of '*G. altiapertura*'), magnetic polarity chronozone C6An to basal 6.

*Age.* Earliest Miocene to middle Early Miocene.

*Thickness.* In the Contessa section 5.65 m; samples CT 16-CT 35.

*Remarks.* The base of the zone was defined in the Lemme section (Brinkhuis et al., 1992; Zevenboom, in press). However, these authors did not define the top of this zone. It is here proposed to subdivide this zone into three subzones, viz. the earlier proposed *Hystrichokolpoma truncata* (Htr), *Stoveracysta conerae* (Sco), and the new *Systematophora urbinii* (Sur) Subzone. The former two subzones were defined in the Lemme section. Similar to the top of the *Membranilarnacia? picena* Zone, also the top of the *Stoveracysta conerae* Subzone has not yet been defined. This is now resolved by the introduction of the *Systematophora urbinii* (Sur) Subzone, defined below.

*Stoveracysta conerae* (Sco) Interval Subzone emend.

*Definition.* The interval from the FO of *Stoveracysta conerae* to the FO of *Systematophora urbinii*.

*Calibration.* Magnetic polarity chronozone C6An.

*Age.* Middle Early Miocene.

*Thickness.* At the Contessa site 1.85 m; samples CT 20-CT 24.

*Remark.* The base of the subzone was defined in the Lemme section. Brinkhuis et al. (1992) did not recognize the base of this subzone in the Contessa section and a hiatus was inferred.

*Systematophora urbinii* (Sur) Interval Subzone.

*Definition.* The interval from the FO of *Systematophora urbinii* to the FO of *Nematosphaeropsis downiei*.

*Calibration.* Planktonic foraminiferal uppermost N5 to basal N6 zones, magnetic polarity chronozone 6.

Age. Middle Early Miocene.

Thickness. 3.85 m; samples CT 25–CT 35.

*Nematosphaeropsis downiei* (Ndo) Interval Zone (Lower Miocene).

*Definition.* The interval from the FO of *Nematosphaeropsis downiei* to the FO of *Hystrichosphaeropsis obscura*.

*Calibration.* Planktonic foraminiferal N5 Zone, calcareous nannoplankton NN2, magnetic polarity chronozone 6 to 5Er

Age. Early Miocene.

Thickness. 4.35 m; samples CT 37–CT 48.

The interval overlying the FO of *Hystrichosphaeropsis obscura*, contains only poorly preserved and less diversified dinocyst assemblages. Zevenboom (in Deino et al., Chapter D1) presenting results from the Santa Croce di Arcevia section proposes an additional two new zones representing this interval, viz. the *Hystrichosphaeropsis obscura* (Hob) and *Hystrichokolpoma* sp. B of Powell (1986) (Hys) zones. These can be recognized (albeit tentatively) in the Contessa section. One may note that, as discussed by Zevenboom (in Deino et al., Chapter D1), the top of the Hys Zone is again defined on the basis of the samples from the Contessa section.

#### *Taxonomic notes*

A reference is given for species not included in Lentin and Williams (1993):

*Cerebrocysta* sp. A Biffi and Manum (1988).

*Cerebrocysta* sp. B Biffi and Manum (1988).

*Distatodinium* sp. A Williams and Brideaux (1975).

*Homotryblium* sp. cf. *H. oceanicum* Brinkhuis et al. (1992).

*Hystrichokolpoma* sp. B Powell (1986).

*Hystrichosphaeropsis* sp. cf. *H. obscura* Brinkhuis et al. (1992).

*Incertae sedis* sp. Edwards (1984).

*Palaeocystodinium* sp. A Powell (1986).

*Pyxidiella* sp. A. It was depicted by Manum et al. (1989) as “*Pyxidiella* sp. 1”.

The ‘*Spiniferites* complex’ (cpx). Remark: this ‘complex’ represents all species attributable to either *Achomosphaera* or *Spiniferites* spp.

*Thalassiphora gonoperforata* Strauss (1991).

*Trinovantedinium* sp. cf. *T. capitatum*. Remark: this species is similar to *Trinovantedinium capitatum*, but is larger in size and has longer spines than those described for *T. capitatum*. It also differs in the less dense distribution of the spines.

#### MAGNETOSTRATIGRAPHY (D.M. Bice and A. Montanari)

In view of the fact that the Oligocene/Miocene boundary in the recently proposed GSSP of the Carrosio–Lemme section (Steininger et al., 1994, Chapter A9) is established at metre level 35 in correspondence with a polarity reversal interpreted as Chron boundary 6Cn2r–6Cn2n, we found it necessary to refine the magnetostratigraphy of the Contessa sequence, previously defined by Montanari et al. (1991). Thus, we have measured the remanent magnetization of 38 new samples, which, when combined with the previous

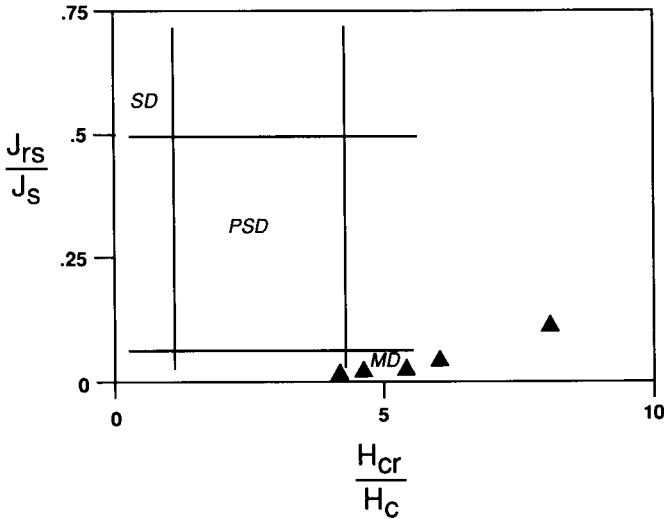


Fig. 5. Hysteresis experiment results from Bisciario in the Contessa CT section, shown relative to the fields for single-domain (*SD*), pseudo single-domain (*PSD*) and multi-domain (*MD*) synthetic magnetites as determined by Day et al. (1976).

work of Montanari et al. (1991), provide a much more complete polarity record for the interval across the uppermost Chattian, the Aquitanian, and the lower Burdigalian.

The intensity of natural remanent magnetization in these samples ranged from about  $5 \times 10^{-5}$  to  $5 \times 10^{-3}$  A/m, probably reflecting variations in the concentrations of magnetic minerals. The behaviour of these rocks during thermal demagnetization and hysteresis experiments indicates that the magnetic mineralogy of most samples consists largely of multi-domain magnetite, with lesser amounts of hematite, and some unidentified paramagnetic mineral, whose presence shows up in the hysteresis experiments. Multi-domain magnetite is indicated by the results of hysteresis experiments.  $H_{cr}/H_c$  values from five representative samples yield a mean of 5.6, while  $J_{rs}/J_r$  values have a mean of 0.043. Applying the results of Day et al. (1976), these hysteresis results place our samples within the region of multi-domain magnetite, close to the region of pseudo single-domain magnetite (Fig. 5).

The demagnetization behaviour of samples from the Scaglia Cinerea and Bisciario at Contessa is somewhat variable, indicating variations in the relative abundance of different magnetic minerals (Fig. 6). Demagnetization in alternating fields of 50 to 70 mT or thermal demagnetization at temperatures of 300–350°C was generally sufficient in removing a weaker secondary component of magnetization that in many cases is aligned with the present field. Thermal demagnetization beyond 350°C often resulted in erratic behaviour that could be attributed to the creation of some new magnetic mineral (possibly magnetite from the oxidation of pyrite). The ChRM directions were determined by visual analysis of orthogonal vector diagrams of the demagnetization (see examples in Fig. 6).

The resulting ChRM directions from both the new collection of samples, and the samples previously analyzed by Montanari et al. (1991), are generally in agreement

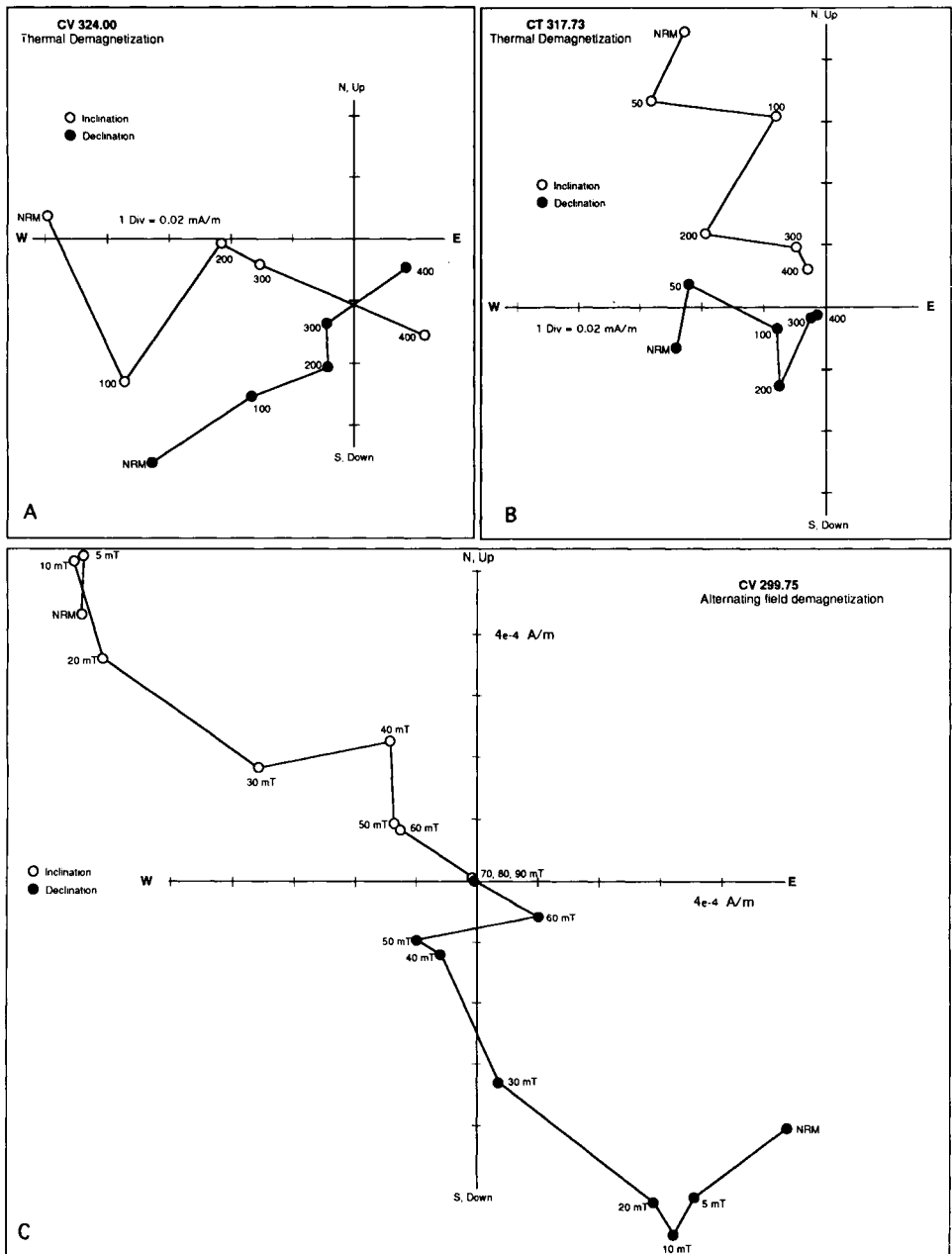


Fig. 6. Demagnetization plots of representative sample from the Scaglia Cinerea in the Contessa CQ section (CQ 299.75), and two representative samples from Bisciaro in the CT section.

with expected directions for this part of the Apennines in the Upper Oligocene–Lower Miocene and are also roughly antipodal (Fig. 7), leading us to believe that most of these ChRM directions are indeed primary. In some cases, however, the ChRM is anomalous



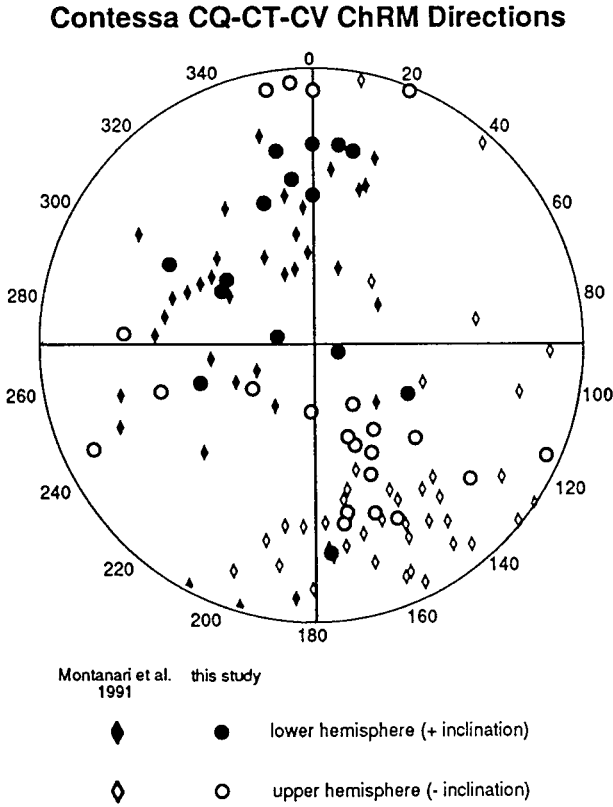


Fig. 7. Lower-hemisphere stereonet plot of NRM directions from uppermost Scaglia Cinerea and Bisciaro samples from the Contessa CQ and CT sections.

(e.g., a northeastern declination and a negative inclination or a westerly declination and a very shallow positive inclination), adding some uncertainty to the resulting polarity sequence. A possible explanation for some of these anomalous directions is that they were acquired while the magnetic field reversed during the lithification process — which is undoubtedly delayed in these rocks by extensive bioturbation. Alternatively, the anomalous directions could be due to unsuccessful demagnetization.

Fig. 8 shows the variation of the VGP latitude with the stratigraphic level at Contessa, along with the new interpreted polarity sequence which is compared to the older sequence from Montanari et al. (1991). The new data enable us to identify several polarity events that were previously not recognized. One or more reversals have been found in the uppermost Scaglia Cinerea; these are most likely Chrons 6B and 6C. We also see new reversals above and below the previously interpreted Chron 6A, which may include Chrons 6A1 and 6AA. Other short normal-polarity events have been found below Chron 5E, and in the uppermost part of the sequence in the newly studied CV section. The latter is here interpreted as Chron 5D.

Fig. 9 illustrates a tentative correlation between the Harland et al. (1990), and Cande and Kent (1992) magnetic polarity sequence models, and the polarity sequence

### Composite CQ-CT-CV section

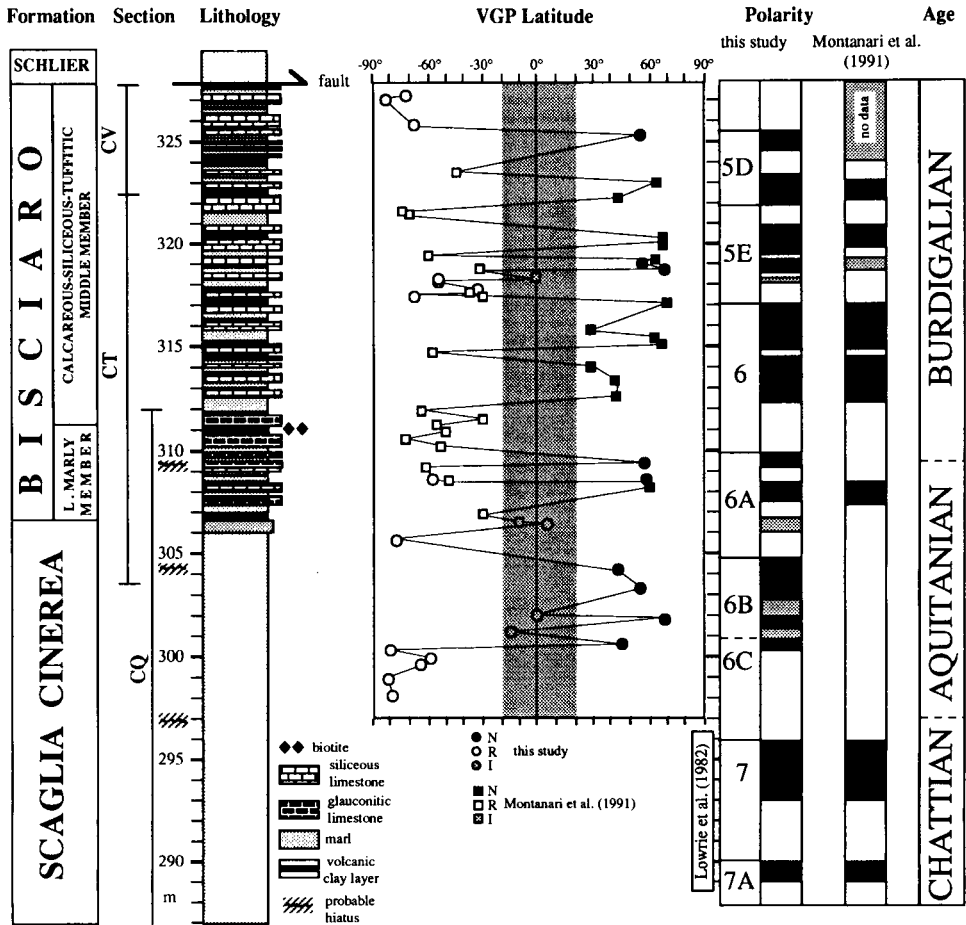


Fig. 8. VGP plot and magnetostratigraphic interpretation of the composite CQ-CT-CV section.

determined in the Contessa composite CQ-CT-CV section (Fig. 8), and the Moria section (see Deino et al., Chapter D1). As correlation horizon between the Contessa and Moria sections, we have chosen the LO of *Catapsydrax dissimilis* which is used to place the N6/N7 foraminiferal zonal boundary. This bioevent is generally found in the upper part of Chron 5Dn (e.g., Miller et al., 1991). In constructing the time scale in Fig. 9, we have utilized the radioisotopic ages of interbedded volcanoclastic layers in the Contessa CT section (i.e., the Raffaello and CT-WAL levels), reported below, and the Piero della Francesca Level in the Moria section (Deino et al., Chapter D1).

Although we have made improvements in the previously determined polarity sequence from Contessa, it is still somewhat difficult to correlate our sequence with that of the marine magnetic anomalies. The apparent miscorrelation between the two could be due to several factors. As a first general problem, variable rates of sedimentation,

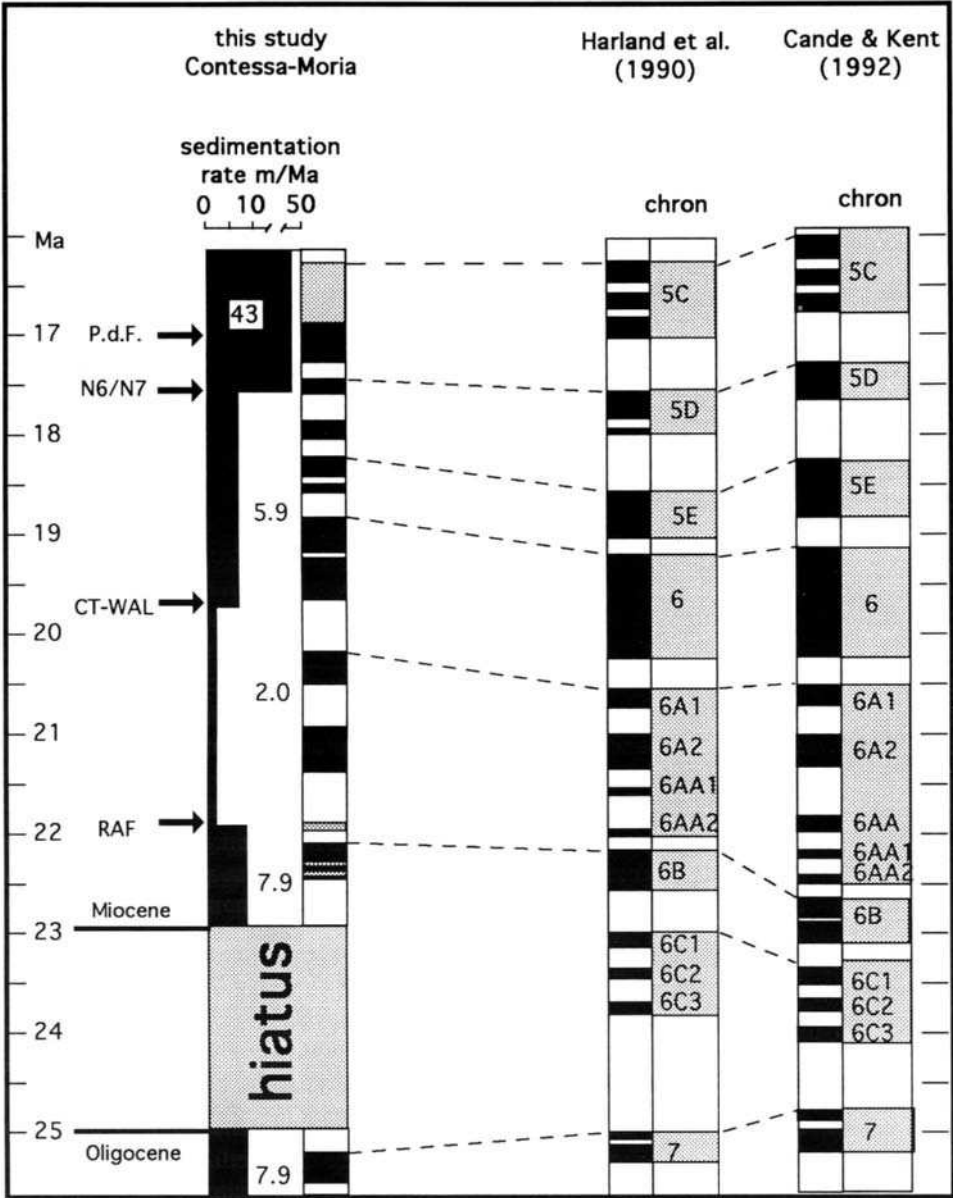


Fig. 9. Interpreted upper Chattian through Burdigalian magnetostratigraphic sequence from the Contessa and Moria sections (see Deino et al., Chapter D1), correlated against variations in sedimentation rates, and the magnetic polarity reversal models of Harland et al. (1990), and Cande and Kent (1992). The time scale is derived from geochronologic data from this paper, and the paper on the Moria section by Deino et al. (Chapter D1).

and uncertainties in accurately dating marine magnetic anomalies make it difficult to compare these sequences. Secondly, the numerical age estimates proposed by Harland et al. (1990), and Cande and Kent (1992) for magnetic polarity reversals were indirectly

derived from a few, and distantly interpolated radioisotopic calibration points, and are primarily dependent on biostratigraphic correlation criteria.

On the other hand, the Contessa–Moria polarity sequence is directly calibrated by several dated volcanoclastic layers contained in these sections (see also Deino et al., Chapter D1), and thus it represents the real radioisotopically dated magnetostratigraphic record for this span of time in this particular palaeobasin. However, the problem remains that slow sedimentation rates (Fig. 9), and strong bioturbation in the Contessa sequence, conspire to complicate the locking-in of a magnetization, especially in the case of particularly short and closely spaced magnetic reversal events, and may lead to the preservation of a magnetic polarity record which can appear significantly different from the polarity sequence recorded in expanding oceanic crust. Moreover, detailed biostratigraphic analysis based on planktonic Foraminifera and calcareous nannofossils described above, suggest the presence of a major hiatus at 297 m, which may represent a time gap as big as 2 Ma (see discussion at the end of this paper).

In conclusion, our magnetostratigraphic interpretation herein described, must be still considered somewhat tentative. Additional detailed bio- and magnetostratigraphic analyses in other coeval sections in this region, and anywhere else in the world, which would permit direct radioisotopic dating of a geomagnetic polarity sequence is, in our view, the most viable way to further improve the resolution of the Lower Miocene magnetostratigraphic polarity sequence.

## CHEMOSTRATIGRAPHY

### *Stable isotopes and trace elements (L. Emmanuel and M. Renard)*

Stable isotopes and trace element analyses on carbonate samples from the composite CQ–CT section do not show any major geochemical anomaly across the lithostratigraphic boundary between the Scaglia Cinerea and the Bisciaro, nor across the biostratigraphically identified interval containing the Aquitanian/Burdigalian boundary. Nevertheless, subtle shifts and clear trends are recognizable through the studied stratigraphic interval, and can be indicative of particular palaeoclimatic conditions. The results of our study are synthesized in Fig. 10, and reported in Table 1.

*Stable isotopes.* Despite the sparse sampling, the  $\delta^{13}\text{C}$  and  $\delta^{18}\text{O}$  through the composite CQ–CT section shows a relatively marked decrease (i.e., about 1.5‰ from bottom to top). It seems that this general decreasing trend is interrupted by a positive break (around 0.5–0.8‰) around or just above the Aquitanian/Burdigalian boundary (Fig. 10). This subtle signal may indicate a temporary cooling during the generally warm Aquitanian time, and would be associated with oxidation or to an increased production of organic matter.

*Strontium.* The general whole Sr trend in the studied section shows a progressive decrease of concentration (from 1600 to 1150 ppm), but no geochemical breaks are obvious near the Aquitanian/Burdigalian boundary (Fig. 10). Nevertheless, the lithological change between the Scaglia Cinerea and the Bisciaro formations is characterized by a well marked negative shift.

*Magnesium.* The evolution curve displays fairly wide fluctuations. Nevertheless, both the Scaglia Cinerea/Bisciaro boundary, and the Aquitanian/Burdigalian boundary are characterized by major negative shifts.

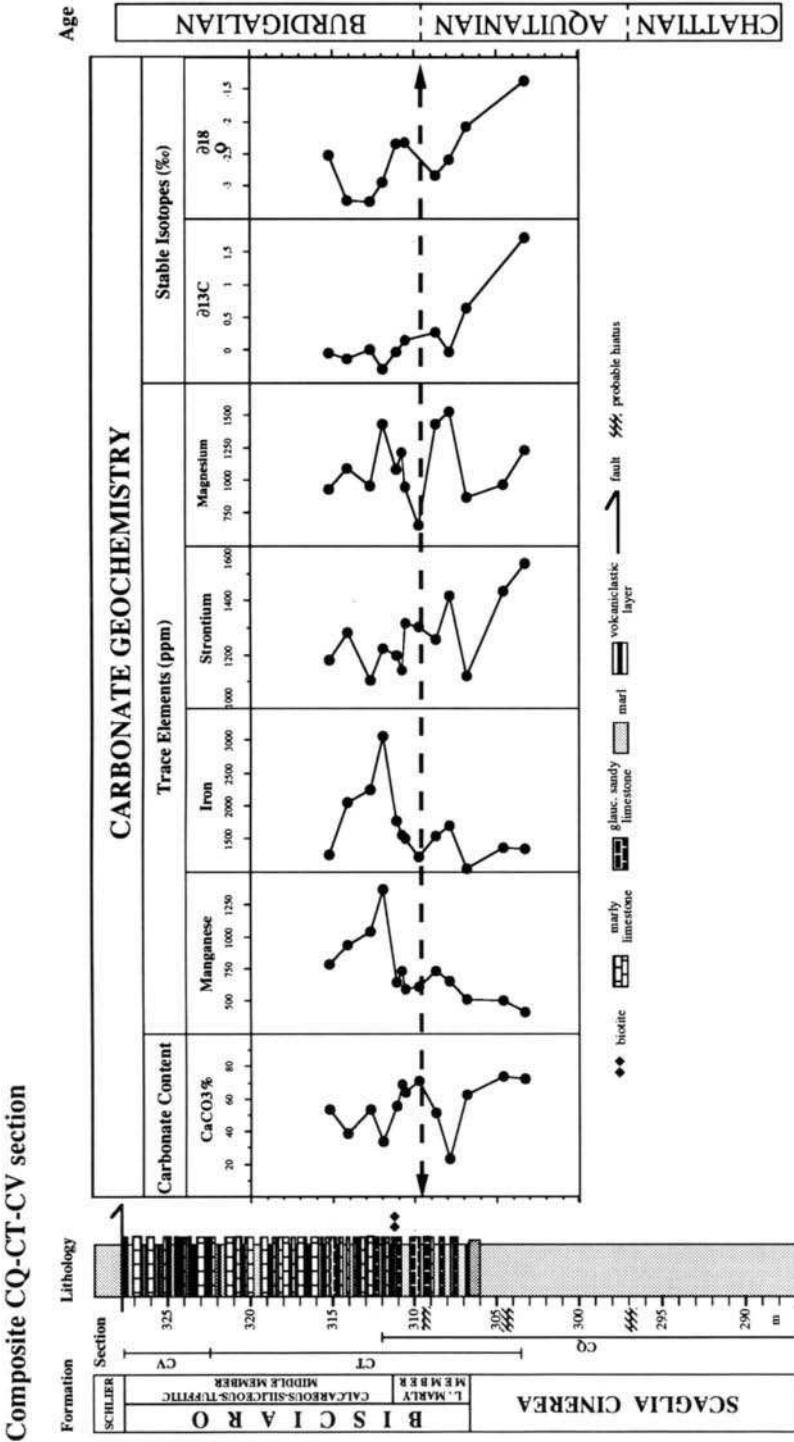


Fig. 10. Stable isotopes and trace element chemostratigraphy across the Scaglia Cinerea/Bisciaro boundary in the Contessa CQ-CT composite section.

Table 1

Strontium isotope analysis of carbonate and phosphate samples from the Contessa CQ and CT sections

Sample/ m level	Material Material	Foram. zone <sup>a</sup>	Nanno. zone <sup>b</sup>	Chron Chron	<sup>87</sup> Sr/ <sup>86</sup> Sr average <sup>c</sup>	± 2σ	Nr. analyses
CT/322.2	bulk carbonate + shell	N6	CN1c	5Dn	0.708381	0.000014	4
CT/311.3	bulk carbonate	N5/6	CN1c	6Rr	0.708299	0.000015	4
CT/306.6	fish teeth	top N4	CN1c	6An1?	0.708322	0.000004	6
CQ/306.5	bulk carbonate	top N4	CN1c	6An1?	0.708330	0.000014	8
CQ/304.0	bulk carbonate	N4	CN1a/b	6Bn2?	0.708309	0.000019	4
CQ/302.0	bulk carbonate	N4/P22	CN1a/b	6Bn?	0.708300	0.000018	4
CQ/298.0	bulk carbonate	P22	CP19b	6Cr	0.708268	0.000027	1
CQ/296.0	bulk carbonate	P22	CP19b	top 7n	0.708236	0.000012	4
CQ/292.4	bulk carbonate	P22	CP19b	base 7n	0.708193	0.000003	1

<sup>a</sup> Planktonic foraminiferal zone after Blow (1969).<sup>b</sup> Calcareous nannofossil zone after Okada and Bukry (1980).<sup>c</sup> Corrected for sea water <sup>87</sup>Sr/<sup>86</sup>Sr = 0.70925.

*Manganese and iron.* The evolution curves of these two elements are very similar, and show low values in the Aquitanian followed by a straightforward increase in the lower Burdigalian. Using the geochemical model proposed Emmanuel and Renard (1993), which is based on the manganese marker, it is possible to recognize a third-order cycle (*sensu* Vail) in this evolution. According to this model, low values of Mn contents are recorded in lowstand systems intervals. Increasing values occur in the transgressive intervals with the maxima corresponding to the maximum flooding surface, whereas decreasing values characterize highstand systems intervals. For example, a maximum surface would be located near the sample MIOK 17 (311.93 m) (Table 1), and could be linked with the TB 2.1 cycle of the eustatic chart (Haq et al., 1987).

#### *Strontium isotopes (R. Capo, D.J. Depaolo and A. Montanari)*

A continuous <sup>87</sup>Sr/<sup>86</sup>Sr profile of the Upper Eocene through the Burdigalian Contessa sequence was produced by Montanari et al. (1991) who recognized a clear isotopic curve flexure in the mid-Chattian (i.e., around 26 Ma) represented by a decrease in the rate of isotopic ratio change from  $5 \times 10^{-5}/\text{Ma}$  to  $2 \times 10^{-5}/\text{Ma}$ . This flexure was interpreted as a delayed effect of the great Mid-Oligocene sea-level drop (Schlanger and Premoli Silva, 1986) which would have caused erosion and recycling of newly exposed carbonate shelves, including Tertiary and Mesozoic carbonate rocks.

The data by Montanari et al. (1991) covering the transition between the Scaglia Cinerea and the Bisciaro formations are herein repropoed in Table 2, and corrected for a standard seawater Sr isotopic ratio of 0.70925. The Sr curve for the Oligocene–Miocene Apennine sequence is plotted in Fig. 11, recalibrated with the new radioisotopic dates from the Raffaello Level and CT–WAL volcaniclastic layers, and compared with the general oceanic curve. While the oceanic and Apennine strontium isotopic values are consistent throughout the Upper Eocene and Oligocene, in the Lower Miocene (i.e., around 21 Ma) the Apennine <sup>87</sup>Sr/<sup>86</sup>Sr trend seems to deviate from the oceanic one. This deviation, which results from a relative decrease in <sup>87</sup>Sr in the Apennine samples,

Table 2

$^{40}\text{Ar}/^{39}\text{Ar}$  analytical data, incremental furnace step-heating of plagioclase from the Raffaello (RAF) and CT-WAL volcanoclastic layers

Lab ID#	<i>T</i> (°C)	Ca/K	$^{36}\text{Ar}/^{39}\text{Ar}$	$\%(^{36}\text{Ar}/^{39}\text{Ar})_{\text{Ca}}$	$^{40}\text{Ar}^*/^{39}\text{Ar}$	$\%^{40}\text{Ar}^*$	Age (Ma) $\pm 1\sigma$
<i>Sample CT-RAF (5670/2B-01), 0.042 g</i>							
A	800	3.30	0.4862	0.1	1.320	0.9	5.0 $\pm$ 6.5
B	850	6.43	0.2124	0.4	3.648	5.5	13.8 $\pm$ 2.1
C	900	11.07	0.5976	0.2	3.646	2.0	13.8 $\pm$ 5.0
D	950	19.62	0.1036	2.5	4.976	14.2	18.83 $\pm$ 0.86
E	1000	23.22	0.0103	29.5	5.521	71.7	20.88 $\pm$ 0.27
F	1050	23.18	0.0100	30.5	5.613	73.0	21.23 $\pm$ 0.31
G	1100	21.51	0.0099	28.4	5.408	71.8	20.46 $\pm$ 0.19
H	1150	20.44	0.0083	32.4	5.493	76.7	20.78 $\pm$ 0.18
I	1200	21.10	0.0102	27.3	5.507	71.4	20.83 $\pm$ 0.20
J	1250	22.76	0.0121	24.7	5.723	67.7	21.65 $\pm$ 0.22
K	1300	22.18	0.0155	18.8	5.793	60.7	21.91 $\pm$ 0.22
L	1350	22.10	0.0349	8.3	5.814	37.9	21.99 $\pm$ 0.38
M	1400	21.36	0.0717	3.9	5.740	21.9	21.71 $\pm$ 0.74
N	1450	21.25	0.0781	3.6	5.549	19.8	20.99 $\pm$ 0.75
O	1500	21.44	0.0620	4.6	5.470	23.7	20.69 $\pm$ 0.66
P	1550	21.51	0.0611	4.6	5.663	24.6	21.42 $\pm$ 0.68
Q	1600	21.37	0.0935	3.0	5.438	16.8	20.6 $\pm$ 1.1
R	1650	21.88	0.0727	4.0	5.371	20.5	20.32 $\pm$ 0.95
<i>Sample CT-WAL (5662/2B-01), 0.026 g</i>							
A	600	2.05	0.1144	0.2	4.109	10.8	15.5 $\pm$ 2.1
B	700	2.49	0.2092	0.2	3.137	4.8	11.9 $\pm$ 3.8
C	750	4.08	0.5808	0.1	-5.738	-3.5	-21.9 $\pm$ 9.1
D	800	3.08	0.5450	0.1	-4.592	-2.9	-17.5 $\pm$ 7.4
E	850	4.11	0.3681	0.1	1.564	1.4	5.9 $\pm$ 4.1
F	900	6.93	0.6970	0.1	4.014	1.9	15.2 $\pm$ 6.2
G	950	10.00	0.0841	1.6	4.661	15.8	17.60 $\pm$ 0.89
H	1000	12.52	0.0637	2.6	4.866	20.9	18.38 $\pm$ 0.62
I	1050	12.86	0.0374	4.5	5.156	32.7	19.47 $\pm$ 0.42
J	1100	12.42	0.0273	6.0	5.275	40.8	19.91 $\pm$ 0.28
K	1150	12.91	0.0119	14.2	5.194	63.0	19.61 $\pm$ 0.20
L	1200	11.92	0.0147	10.6	5.063	56.3	19.12 $\pm$ 0.23
M	1250	12.31	0.0166	9.8	5.147	53.6	19.43 $\pm$ 0.23
N	1300	12.42	0.0250	6.5	5.173	42.7	19.53 $\pm$ 0.29
O	1350	12.44	0.1584	1.0	4.501	8.8	17.0 $\pm$ 1.4
P	1400	11.94	0.1143	1.4	4.919	12.8	18.6 $\pm$ 1.0
Q	1250	12.04	0.1319	1.2	4.133	9.7	15.6 $\pm$ 1.2
R	1500	12.11	0.1320	1.2	4.403	10.2	16.6 $\pm$ 1.3

Notes. Lab ID#'s highlighted in italic are the plateau steps. Errors in age quoted for individual runs are  $1\sigma$  analytical uncertainty. Weighted averages are calculated using the inverse variance as the weighting factor (Taylor, 1982), while errors in the weighted averages are  $1\sigma$  standard error of mean (Samson and Alexander, 1987). Ca/K is calculated from  $^{37}\text{Ar}/^{39}\text{Ar}$  using a multiplier of 1.96.  $^{40}\text{Ar}^*$  refers to radiogenic argon.  $\lambda = 5.543 \times 10^{-10} \text{ y}^{-1}$ . Isotopic interference corrections:  $(^{36}\text{Ar}/^{37}\text{Ar})_{\text{Ca}} = (2.59 \pm 0.06) \times 10^{-4}$ ,  $(^{39}\text{Ar}/^{37}\text{Ar})_{\text{Ca}} = (6.7 \pm 0.3) \times 10^{-4}$ ,  $(^{40}\text{Ar}/^{39}\text{Ar})_{\text{K}} = (8 \pm 7) \times 10^{-4}$ .  $J = (2.109 \pm 0.010) \times 10^{-3}$  for CT-RAF and  $(2.104 \pm 0.010) \times 10^{-3}$  for CT-WAL. Sanidine from the Fish Canyon Tuff was used as the neutron fluence monitor, with a reference age of 27.84 Ma (Cebula et al., 1986) recalculated based on Samson and Alexander (1987). Samples were irradiated for 3 h in the hydraulic rabbit facility of the Omega West reactor of the Los Alamos National Laboratory.

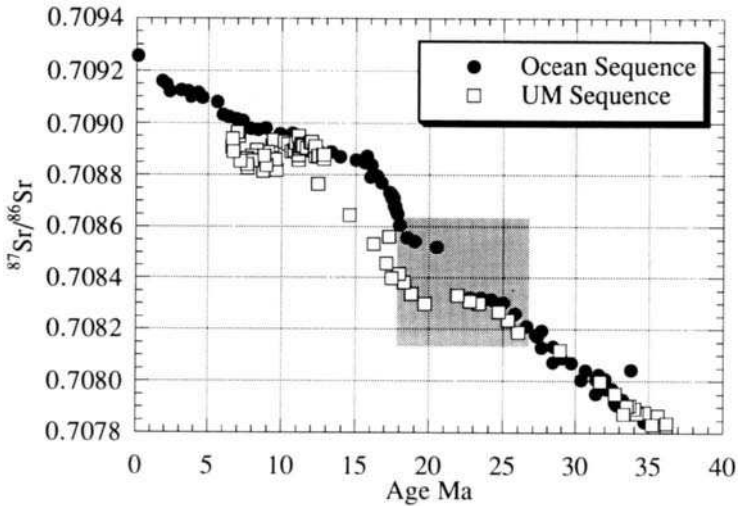


Fig. 11. Upper Eocene to Miocene  $^{87}\text{Sr}-^{86}\text{Sr}$  curve of the Umbria–Marche (U–M) sequence compared with that of oceanic sequences. Shaded area represents the uppermost Oligocene to lower Burdigalian interval covered by the CQ, CT and CV sections in the Contessa Valley.

is also observed in the Burdigalian–Langhian Moria section (see Deino et al., Chapter D1), and in the Serravallian–Messinian Cònero Riviera sequence (see Montanari et al., Chapter E1). A similar deviation has been observed also in Miocene Paratethys sections (Sharbert and Steiniger, 1994).

This deviation of the Tethyan and Paratethyan Sr curve from the oceanic trend leads to the inference that the closing, synorogenic early Burdigalian Tethyan ocean started to develop a seawater Sr isotopic composition different from that of the rest of the world’s oceans. One possible explanation for this is that the orogenic uplifting of thick Cenozoic and Mesozoic carbonate sequences throughout the Alpine–Himalayan system, have discharged into the Tethys recycled Sr with lower isotopic ratios, and at the same time the water exchange and re-balancing with the open ocean was inhibited by the partial closure of the Gibraltar Strait and eastern Tethyan sea ways (see Vrienlinck et al., Chapter B1). This working hypothesis encourages further testing through additional Sr isotope analyses in other Tethyan sequences. However, the data by Montanari et al. (1991) summarized herein indicate that Sr isotope analysis is not a viable numerical tool for correlating marine Tethyan sequences with those of the open ocean realm.

GEOCHRONOLOGY (A. Deino and A. Montanari)

Previously we reported on single-crystal  $^{40}\text{Ar}-^{39}\text{Ar}$  ages for plagioclase from volcanogenic levels ‘Raffaello’ (RAF), and CT–WAL (CT-311.0 m) in the Contessa section (metre levels 306.7 and 310.5, respectively), and obtained ages of  $21.17 \pm 0.46$  Ma ( $2\sigma$  error, as in all other ages reported hereafter) and  $19.81 \pm 0.52$  Ma (Montanari et al., 1991). We have re-prepared plagioclase separates from new samples from these levels to



Table 3

Geochemistry of whole-carbonate samples from the CQ and CT sections

Samples	Meter level	%CaCO <sub>3</sub>	Mn (ppm)	Fe (ppm)	Sr (ppm)	Mg (ppm)	δ <sup>13</sup> C	δ <sup>18</sup> O
MIOK 22	315.2	53.79	786	1258	1180	929	-0.04	-2.52
MIOK 20	314.11	38.54	934	2053	1282	1091	-0.13	-3.23
MIOK 18	312.76	53.57	1039	2254	1105	958	0.01	-3.24
MIOK 17	311.93	33.9	1368	3052	1225	1437	-0.29	-2.94
MIOK 15	311.13	55.5	646	1779	1198	1076	-0.03	-2.34
MIOK 14	310.79	68.72	735	1562	1142	1213		
MIOK 13	310.55	64.31	596	1511	1315	944	0.14	-2.32
MIOK 12	309.75	71.28	608	1230	1303	659		
MIOK 9	308.67	51.21	729	1550	1257	1429	0.28	-2.84
MIOK 7	307.87	22.87	652	1702	1416	1529	-0.02	-2.58
MIOK 6	306.83	62.43	514	1052	1123	870	0.65	-2.08
MIOK 3	304.63	74.01	505	1366	1433	965		
MIOK 1	303.25	72.45	413	1355	1536	1232	1.72	-1.37

date by the bulk-heating resistance-furnace incremental-release <sup>40</sup>Ar/<sup>39</sup>Ar technique as a test of our earlier results. The incremental-release method was considered appropriate since the earlier single-crystal plagioclase age populations contained outliers which were thought to be due to incipient alteration.

The results of the incremental-release experiments are given in Table 3, and illustrated as age spectra in Fig. 12. The first 10–20% of the gas release (cumulative %<sup>39</sup>Ar) in both cases was generally lower in percent radiogenic argon (%<sup>40</sup>Ar\*), lower in Ca/K ratio, and younger in age than the remainder of the gas release, suggesting that indeed this early gas release may have originated from loosely held argon in zones of incipient alteration and from grain surfaces. The more tightly held 80–90% of the gas formed single plateaus in the loose sense of the term. Using plateau criteria such as that of Fleck et al. (1977), however, in which at least three contiguous steps comprising at least 50% of the cumulative %<sup>39</sup>Ar released cannot mutually be distinguished using a 95% confidence value test, the 'true' plateaus are confined to about 55–65% of the gas release. The weighted-mean plateau age for samples of CT-RAF and CT-WAL are 21.71 ± 0.38 and 19.42 ± 0.36 Ma, respectively. Inverse isochron analyses of the plateau steps for CT-RAF give ages of 21.88 ± 0.32 Ma (MSWD = 1.2, (<sup>40</sup>Ar/<sup>36</sup>Ar)<sub>trapped</sub> = 293.0 ± 1.4, n = 9), while CT-WAL gives 19.61 ± 0.18 Ma (MSWD = 1.6, (<sup>40</sup>Ar/<sup>36</sup>Ar)<sub>trapped</sub> = 292.3 ± 2.1, n = 6). While both the plateau and isochron ages are concordant for both samples, isochron ages are preferred as the final age result as they are more robust against potential errors in assuming an internal argon composition of precisely atmospheric <sup>40</sup>Ar/<sup>36</sup>Ar ratio of 295.5 (Steiger and Jäger, 1977).

A *t*-test suggests that the new bulk-sample incremental-heating results for CT-RAF are statistically distinguishable at the 95% confidence level from the previous single-crystal mean age. Because the furnace results are better able to look through possible alteration effects on the age of this plagioclase, and noting the high quality of the age spectrum for this sample, we prefer to use the new date of 21.88 ± 0.32 Ma as the representative <sup>40</sup>Ar–<sup>39</sup>Ar age for level CT-RAF.

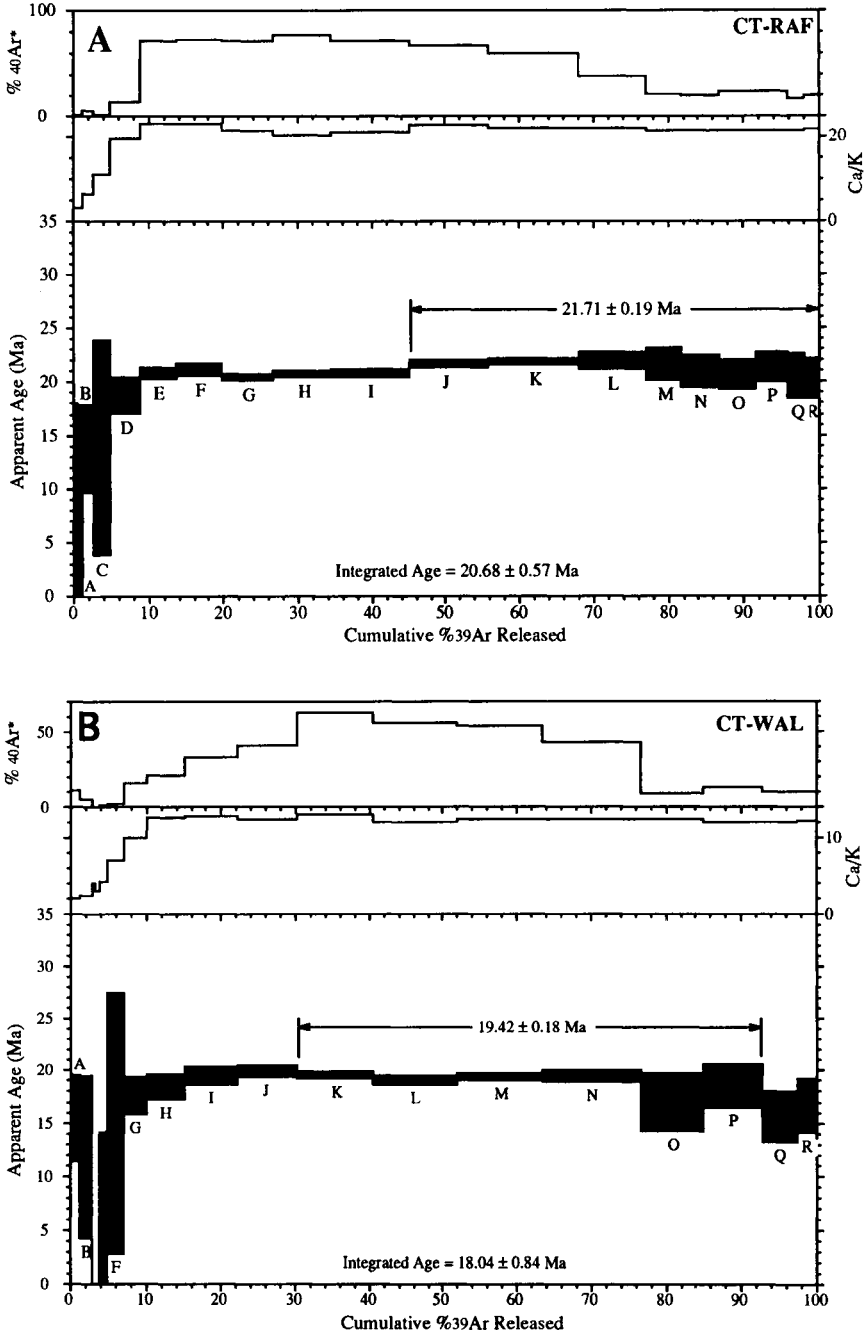


Fig. 12. Step-heating <sup>40</sup>Ar/<sup>39</sup>Ar plateau diagrams of plagioclase from the Livello Raffaello (CT-RAF) and the CT-WAL level in the Contessa CT section.

Conversely, the single-crystal and bulk incremental-heating ages for CT–WAL are not statistically distinguishable at the 95% confidence level. We therefore take the final age as the weighted mean of the ages of the two methods, giving an overall result of  $19.67 \pm 0.30$  Ma for CT–WAL.

## SUMMARY AND CONCLUSIONS (A. Montanari)

### *Integrated stratigraphy of interstage boundaries*

The composite stratigraphic sequence of the CQ, CT, and CV sections in the Contessa Valley contains the boundaries between the Chattian, the Aquitanian, and the Burdigalian stages. This stratigraphic interval is well exposed in the CQ section, and is easily accessible in various points despite the fact that quarrying activity changes frequently the shape and quality of exposure of this section. No problems of outcrop accessibility and preservation are affecting the CT and CV sections which are well exposed on road cuts along the Contessa Highway.

Dated volcanoclastic layers in these sections permit to assign numerical ages to biostratigraphic, magnetostratigraphic, and chemostratigraphic events across these interstage boundaries. However, detailed biostratigraphic analyses based on planktonic Foraminifera, calcareous nannofossils, and dinoflagellate cysts, reveal the probable presence of hiatuses in the stratigraphic interval across the Scaglia Cinerea and Bisciaro lithostratigraphic contact. This states some problems in the stratigraphic location and geochronologic age assignment for the Chattian/Aquitanian interstage boundary. On the other hand, the interval covering the Aquitanian/Burdigalian boundary seems to be more continuous and complete allowing a certain degree of confidence in placing biostratigraphic boundaries and interpreting the magnetic polarity sequence.

### *Chattian/Aquitanian*

In order to interpret the biostratigraphic and magnetostratigraphic record of the interval across this interstage boundary at Contessa, we attempted a correlation with the proposed GSSP of Carrosio–Lemme (see Steininger et al., Chapter A9), utilizing all possible correlation tools available in both sections which include planktonic Foraminifera, calcareous nannofossils, dinoflagellate cysts, and magnetic polarity reversals. A synthesis of this correlation is shown in Fig. 13, and discussed below.

*Biostratigraphy.* In the Carrosio–Lemme section, the proposed O/M boundary, which corresponds to the Chattian/Aquitanian interstage boundary, is located at metre level 35, in close correspondence to the FO of calcareous nannofossil *S. capricornutus*, and a magnetic polarity reversal interpreted by Steininger et al. (Chapter A9) as the chonal boundary 6Cn2r–6Cn2n. Other bioevents are found in the immediate vicinity of these markers; the FO of dinoflagellate cyst *E. burdigalensis* is found 3 m below the boundary, the LOs of nannofossils *S. capricornutus* and *S. delphix* are located 1 and 4 m above the boundary, respectively, and the FO of planktonic foraminifer *P. kugleri* is located 2 m above the boundary. In respect to existing and commonly used biostratigraphic models, the interstage boundary is located near the planktonic foraminiferal zonal boundary N4a/N4b of Spezzaferri (1994), corresponding to the *G. kugleri*/*G. dehiscens dehiscens*

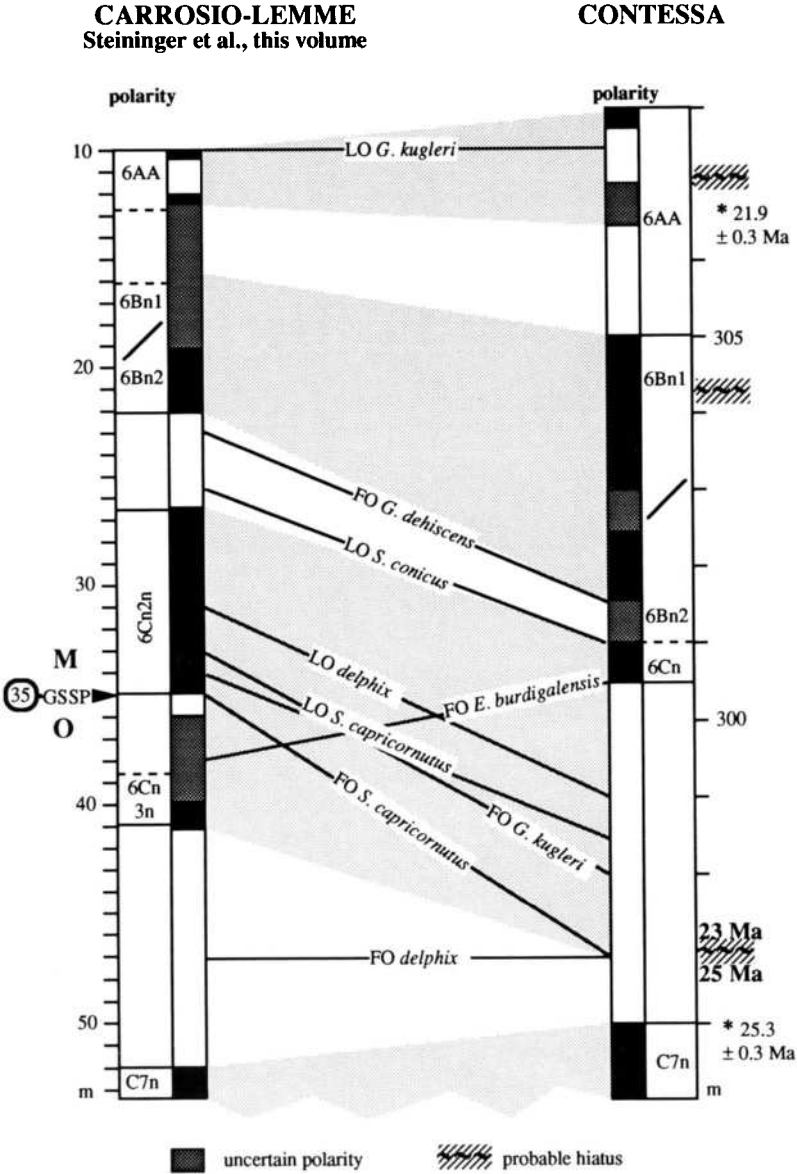


Fig. 13. Bio- and magnetostratigraphic correlation between the proposed GSSP for the O/M boundary Carrosio-Lemme, and the Contessa composite section.

zonal boundary of Iaccarino and Salvatorini (1982) and Iaccarino (1995). In respect to calcareous nannofossil stratigraphy, the boundary is located in the middle part of NN1 and CN1a–CN1b zones of Martini (1971), and Okada and Bukry (1980), respectively, which are defined by the LCO of *D. bisectus*. As for dinoflagellate cysts, the O/M boundary is located near the base of Zone Ebu, Subzone Def (Zevenboom et al., 1994).

The biostratigraphic correlation in Fig. 13 shows that most of the calcareous microfossil events occur in the same succession in both sections, whereas the FO of dinoflagellate cyst *E. burdigalensis* appears strongly diachronous. Moreover, the FOs of *S. capricornutus* and *S. delphix*, which are widely separated in the Carrosio–Lemme section, appear contemporaneous at 297 m in the Contessa section. This fact suggests the presence of a hiatus immediately below these occurrences. In summary, on the basis of calcareous plankton stratigraphy of the proposed GSSP of Carrosio–Lemme, the O/M boundary (i.e., the Chattian/Aquitania interstage boundary) in the Contessa section has to be located at metre level 297, in correspondence to a probable hiatus. Because of its apparent diachroneity between the two sections, *E. burdigalensis* cannot be confidently taken as a useful biomarker for the identification of the O/M boundary.

**Magnetostratigraphy.** In the proposed GSSP section of Carrosio–Lemme (Steininger et al., Chapter A9), the O/M boundary is placed at metre level 35 in correspondence to a magnetic polarity reversal interpreted as the 6Cn2r/6Cn2n magnetozone boundary. This magnetic polarity boundary is located immediately below the FO, and subsequent closely spaced LO, of calcareous nannofossil *S. capricornutus*. The lower part of the normal magnetic polarity interval 6Cn2n in the Carrosio–Lemme section is punctuated by the succession of the FO of planktonic foraminifer *P. kugleri* and the LO of calcareous nannofossil *S. delphix*. In the Contessa section, these bioevents are found well within a densely sampled reversed polarity interval which can be interpreted as magnetozone 6Cr. However, in the Contessa section the FOs of *S. delphix* and *S. capricornutus* appear together at 297 m, while in the Carrosio–Lemme section the FO of *S. delphix* is found a dozen metres below the FO of *S. capricornutus* (Fig. 13). This suggests the presence of a hiatus at 297 m in the Contessa section which would cut out the interval comprising magnetozones 6Cn2n, 6Cn2r, and 6Cn3n. Despite the fact that we cannot confirm this on a strictly magnetostratigraphic basis since we did not sample below 298 m (the CQ section was originally analyzed by Lowrie et al., 1982), such an explanation is plausible considering the very short stratigraphic interval which separates the top of magnetozone 7n at 296 m from the boundary biomarkers at 297 m.

On the other hand, the presence of a hiatus in the Contessa section cannot fully explain the fact that the four most significant calcareous plankton bioevents above metre level 35 in the proposed GSSP of Carrosio–Lemme (FO and LO of *S. capricornutus*, FO of *P. kugleri*, and LO of *S. delphix*), are all found in a normal-polarity zone, whereas the same events at Contessa are found in a similar succession but in an undoubtedly, densely sampled, and relatively long reversed interval (Fig. 13). This may indicate that the remanent magnetization in the Carrosio–Lemme is strongly overprinted by a normal viscous component not cleaned by laboratory demagnetization procedures. In any case, whatever the reasons are for such a poor magnetostratigraphic correlation, it may be concluded that palaeomagnetism is not a viable tool for the recognition of the O/M boundary in the Contessa section, and correlation with the proposed GSSP of Carrosio–Lemme.

**Chemostratigraphy.** Trace elements and stable isotopes were not analyzed in the studied sections. As for Sr isotopes, the Chattian/Aquitania boundary is located near a point of inflection of the  $^{87}\text{Sr}$ – $^{86}\text{Sr}$  curve, defined by a decrease in the rate of isotopic ratio change from  $5 \times 10^{-5}/\text{Ma}$  (Oligocene) to  $2 \times 10^{-5}/\text{Ma}$  (Lower

Miocene). The  $^{87}\text{Sr}/^{86}\text{Sr}$  values near the boundary, and through the Aquitanian, are around  $0.70835 \pm 0.0005$ , and are similar to the isotopic ratios measured in oceanic carbonates. Because of this flattening of the  $^{87}\text{Sr}$ – $^{86}\text{Sr}$  curve, strontium isotopic ratios in biogenic carbonate and phosphate (i.e., fish teeth) may not represent a precise and efficient numerical tool for recognizing the interstage boundary. Nevertheless, the isotopic inflection near Chron 7n (i.e., around 25 Ma) is a clear feature which may be useful for the identification of the uppermost Oligocene.

*Geochronology.* In the Contessa sequence, the Chattian/Aquitian boundary is bracketed by the biotite-rich CQ–GAR marker at 274 m, which has been dated with the K/Ar and Rb/Sr methods at  $28.0 \pm 0.3$  Ma (Montanari et al., 1988a), and the Raffaello Level with a plagioclase  $^{40}\text{Ar}$ – $^{39}\text{Ar}$  age of  $21.88 \pm 0.32$  Ma (Deino and Montanari, this work). However, a straightforward geochronologic interpolation between these two age calibration points to derive an age for the interstage boundary would be erroneous.

In fact, detailed integrated stratigraphic analyses of the homogeneous, complete, and continuous Scaglia Variegata–Scaglia Cinerea pelagic sequence (Montanari et al., 1985, 1988a) indicate a constant sedimentation rate of about 7.9 m/Ma throughout the sequence up to the top of Chron 7n, at 296 m in the CQ section (see also Lowrie et al., 1982). Therefore, an age of 25.3 Ma for the top of Chron 7n can be extrapolated considering the underlying homogeneous pelagic sequence. On the other hand, the uppermost 10.6 m of the Scaglia Cinerea appear disturbed by strong pressure solution, and tectonic fracturation (Lowrie et al., 1982), and may represent a condensed interval (Montanari et al., 1991). Moreover, as discussed above, detailed calcareous microplankton biostratigraphy indicates the presence of a hiatus immediately below the FOs of *S. delphix* and *S. capricornutus*, at 297 m.

Another probable hiatus of unknown amplitude is inferred at 304 m from anomalies in the sequence of dinoflagellate cysts events (see section by Zevenboom in this work). The facts that the pelagic, biomicritic marly limestone facies of this interval is identical to the rest of the underlying Scaglia Cinerea, and that angular unconformities or steep faults were not noted in the field, suggest that the hiatuses may be due to low-angle faults, such as the one found at the Bisciario–Schlier contact in the CV section, or removal of unconsolidated sediment by syndepositional slumping and/or winnowing. With these premises, the assignment of meaningful numerical ages to bio- and magnetostratigraphic events in the uppermost part of the Scaglia Cinerea (i.e., between 297 m and 306.6 m) entirely depends on a fair estimate of the duration of these hiatuses.

By supposing a constant sedimentation rate of 7.9 m/Ma for the homogeneous uppermost part of the Scaglia Cinerea, we would expect a total thickness of 48.2 m between the actual biotite-rich level at 274 m, and the Raffaello Level at 306.6 m, taking into consideration that the actual age difference between these two markers is about 6.1 Ma. Following this reasoning, the difference between the actual thickness and the expected thickness of this interval is 15.6 m, corresponding to a time span of about 2 Ma, which corresponds to the cumulative time gap represented by the hiatuses. The dinocyst hiatus mentioned above is probably of small amplitude as suggested by the conspicuous thickness of magnetozone 6Bn. On the other hand, the hiatus indicated by the anomalously contemporaneous FOs of *S. delphix* and *S. capricornutus*, and the exiguous thickness of Chron 6C, probably represents most of the deduced time gap.

This leads to the inference that the age of the O/M boundary is comprised between 25 and 23 Ma, and most likely placed toward the younger end of this time span.

### *Aquitanian/Burdigalian*

This interstage boundary is located in the CT section, between the Raffaello Level (306.6 m), and the CT–WAL biotite-rich volcanic ash (311.3 m), and is easily accessible. However, this interval is strongly condensed with a sedimentation rate of 2.0 m/Ma, and may contain a hiatus (see section by Coccioni, this work).

*Biostratigraphy.* The FO of *G. altiaperturus* at 309.6 m, is here used to approximate the interstage boundary according to the biostratigraphic models of Iaccarino and Salvadorini (1982) and Iaccarino (1985) (i.e., *G. dehiscens dehiscens*–*G. altiaperturus*–*C. dissimilis* zonal boundary). This foraminiferal event is located in the lower part of the calcareous nannofossil zones NN2 (Martini, 1971) and CN1c (Okada and Bukry, 1980). In respect to dinoflagellate biostratigraphy, the LO of '*G.*' *altiaperturus* is found, in the CT section, within Zone Mpi, at the boundary between Subzones Sco and Sur. Because of the strong stratigraphic condensation in the interval between the Raffaello Level and CT–WAL, and the probable existence of a hiatus, the precise recognition of the Aquitanian/Burdigalian boundary in the CT section is uncertain.

*Magnetostratigraphy.* The interstage boundary in the CT section, which is approximated to the FO of '*G.*' *altiaperturus*, is located within a short normal-polarity interval here interpreted as Cron 6A1.

*Chemostratigraphy.* Subtle positive shifts of the  $\delta^{13}\text{C}$  and  $\delta^{18}\text{O}$  near or just above the approximated Aquitanian/Burdigalian boundary may indicate a temporary cooling during the generally warm Aquitanian time, and would be associated with oxidation or increased production of organic matter. Clear positive shifts immediately above the boundary are also recognized in the iron and magnesium curves, whereas magnesium exhibits a strong negative minimum right at the boundary. In respect to the  $^{87}\text{Sr}$ – $^{86}\text{Sr}$  curve, the approximated Aquitanian/Burdigalian boundary is found in a negative trend track around a value of  $0.70830 \pm 0.00005$ . This isotopic ratio is significantly lower than values around  $0.70850 \pm 0.00005$  measured in oceanic carbonates. Although we do not have a definitive explanation for the Sr isotopic difference between the CT section, and the oceanic sequence, we may conclude that the  $^{87}\text{Sr}/^{86}\text{Sr}$  ratio cannot be used as a reliable numerical criterion of correlation for the Aquitanian/Burdigalian boundary between Tethyan and open-ocean sequences.

*Geochronology.* The FO of '*G.*' *altiaperturus* at 309.6 m in the CT section, has a tightly interpolated  $^{40}\text{Ar}$ – $^{39}\text{Ar}$  age of  $20.5 \pm 0.3$  Ma, and we estimate that the Aquitanian/Burdigalian boundary is not far from this age although probably slightly younger (see synthesis Chapter by Odin et al.).

In summary, because of the problematic condensed interval bracketed by the Raffaello Level and CT–WAL volcanoclastic layers, which probably contains a hiatus, the CT section in the Contessa Valley may not be considered as a suitable case for the establishment of the GSSP for the Aquitanian/Burdigalian boundary. Nevertheless, the integrated stratigraphic work presented here permits to assign numerical ages to most of the important biostratigraphic, chemostratigraphic, and magnetostratigraphic events characterizing the uppermost Chattian, Aquitanian, and lower Burdigalian interval.

SOMMAIRE — STRATIGRAPHIE INTÉGRÉE DE LA SÉQUENCE PÉLAGIQUE DU CHATTIEN AU BURDIGALIEN MOYEN DE LA VALLÉE DE LA CONTESSA (GUBBIO, ITALIE)

(Manuscrit soumis: Juin 1995, révisé: Juillet 1995; rédacteurs responsables: AM et RC)

Les sédiments de la section de la vallée de la Contessa ont été soumis à de nouvelles études biostratigraphiques (foraminifères planctoniques, nannofossiles calcaires, kystes de Dinoflagellés), magnéto- et chimiostratigraphique ainsi que géochronologique pour affiner notre connaissance antérieure. Dans cette section, le sommet de la formation Scaglia Cinerea et la formation Bisciaro affleurent représentant les Étages Chattien, Aquitaniien et Burdigalien. Un tableau détaillé de la stratigraphie de cette séquence a été obtenu. Les corrélations bio- et magnétostratigraphiques entre la coupe synthétique de la Vallée de la Contessa et la section où le point stratotypique global a été récemment proposé pour la limite Oligocène/Miocène à Carrosio–Lemme révèlent la présence de hiatus dans l'intervalle critique entre les formations Scaglia Cinerea et Bisciaro. Ceci limite notre possibilité d'estimer l'âge numérique de la limite Oligocène/Miocène qui, dans les limites de nos incertitudes, peut cependant être située entre 23 et 25 Ma et plus probablement vers le côté jeune de cet intervalle. D'après l'apparition des foraminifères planctoniques *G. altiapertura* et *G. trilobus* usuellement placée près de la limite Aquitaniien/Burdigalien, cette dernière peut être localisée dans la partie supérieure de la magnétozone interprétée comme 6A mais, là encore, un hiatus est sans doute présent dans la séquence. De plus, cette même limite a été encadrée par les âges obtenus par la technique par irradiation sur deux niveaux volcanoclastiques proches le niveau Raffaello daté à  $21,88 \pm 0,32$  Ma et le niveau WAL daté à  $19,67 \pm 0,30$  Ma (incertitude analytique  $2\sigma$  exclue l'incertitude sur l'âge du dosimètre). Ces âges permettent de situer les apparitions contemporaines de *G. altiapertura* et *G. trilobus* à la Contessa dans l'intervalle  $20,5 \pm 0,3$  Ma.

(Sommaire proposé par les rédacteurs d'après un résumé des auteurs, GSO)

ACKNOWLEDGEMENTS

This work has been supported, through past years, by grants from the United States National Science Foundation, Exxon Oil Co., and Armines (A. Montanari) and a grant from the Italian Ministry of University and Scientific Research (MURST, 60%; responsible R. Coccioni). We would like to thank Paul Kopsick for improvements of the English text.



This Page Intentionally Left Blank

Chapter C4

**POTENTIAL INTEGRATED STRATIGRAPHY OF THE AQUITANIAN TO UPPER BURDIGALIAN SECTION AT SANTA CROCE DI ARCEVIA (NE APENNINES, ITALY)**

R. Coccioni, A. Montanari, E. Fornaciari, D. Rio and D. Zevenboom

INTRODUCTION

The Santa Croce di Arcevia exposure is located about 1 km southwest of the hilltop town of Arcevia, on the road to Sassoferrato, near the intersection with the secondary country road to Serra San Quirico (central Marche region, coordinates 43°29'20"N 12°55'52"E, Fig. 1). The actual section is located in the backyard of a recently built house, and it is necessary to obtain permission from the land lord in order to visit it. Nevertheless, while the house was still in construction, the still fresh section was studied and sampled by Coccioni et al. (1988) who provided a detailed account on the lithostratigraphy, and preliminary biostratigraphic analysis.

In the context of the MICOP working group, the original sample collection from the

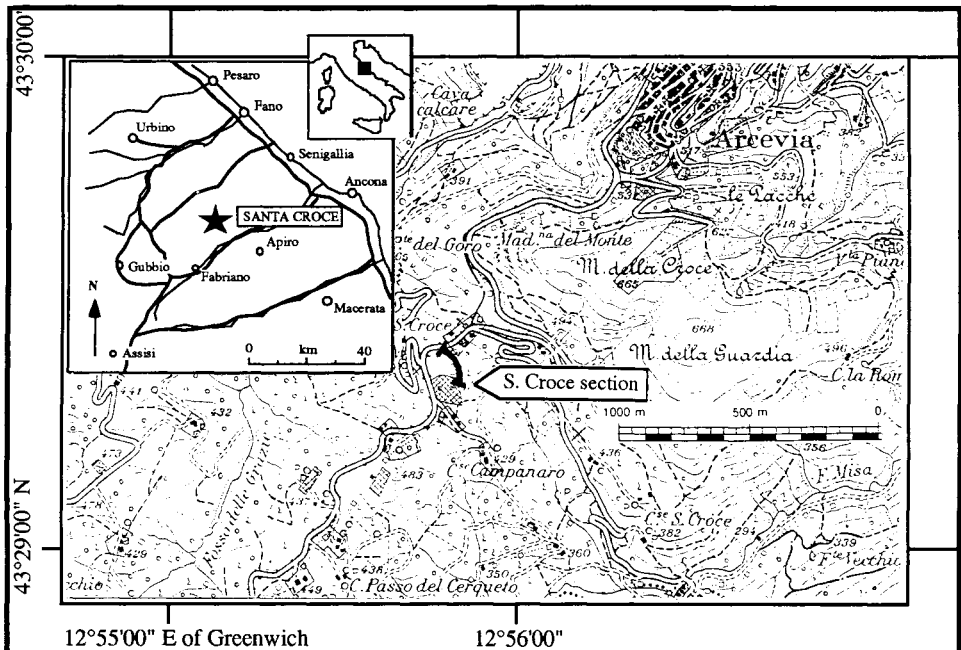


Fig. 1. Location map of the Santa Croce di Arcevia section.



Fig. 2. Panoramic view of the Santa Croce di Arcevia section, and location of the Raffaello, Mega P, and Arcevia volcanoclastic marker levels.

Santa Croce di Arcevia section was analyzed in detail for calcareous microplankton, and dinoflagellate biostratigraphy (Coccioni et al., 1992b; Zevenboom and Brinkhuis, 1992), and attempts have been made to obtain biostratigraphically controlled geochronologic and magnetostratigraphic data. Unfortunately, preliminary radioisotopic analyses on biotite and sanidine separates from the Arcevia Level in the uppermost part of the section, yielded inconsistent results (Deino and Montanari, 1992; see also below), and several pilot samples analyzed for palaeomagnetism by Victoria E. Langenheim (U.S.G.S., Menlo Park, pers. commun., 1993) appeared too weak and unstable to be used for magnetostratigraphy. However, abundant biostratigraphic data covering a nearly continuous interval from the lowermost Aquitanian to the middle Burdigalian, and the presence of several interbedded volcanoclastic layers, make the Santa Croce di Arcevia section a potential case for integrated stratigraphic work. In this paper, we report on the state of knowledge, and integrated stratigraphic potentials of this section.

## LITHOSTRATIGRAPHY

The Santa Croce di Arcevia section is 52 m thick, and comprises 11.5 m of the Scaglia Cinerea formation, about 35 m of the overlying Bisciaro formation, and at the top, about 5 m of the Schlier formation. The Bisciaro exhibits all three of its lithologic members, which were defined by Coccioni and Montanari (1994) as follows: (1) a lower marly member; (2) a middle calcareous–siliceous–tuffitic member; and (3) an upper marly member. The base of the Bisciaro is marked, in this section as everywhere else in the Umbria–Marche basin, by the Raffaello Level (Fig. 2), which yielded a  $^{40}\text{Ar}/^{39}\text{Ar}$  plagioclase age of  $21.88 \pm 0.32$  ( $2\sigma$ ) Ma in the classic Contessa section, near Gubbio (see Chapter C3).

The top of this formation is marked by a 15-cm-thick, biotite-rich, volcanoclastic clay layer, originally named ‘Arcevia Level’ by Montanari et al. (1988b) (Fig. 2). At the time the preliminary study of this section was carried out, Coccioni et al. (1988) did not recognize the Arcevia Level as a potential regional marker for the definition of the boundary between the Bisciaro and the overlying Schlier formation. Further studies revealed a similar biotite-rich layer, named Piero della Francesca Level, at approximately the same biostratigraphic position in several other sections

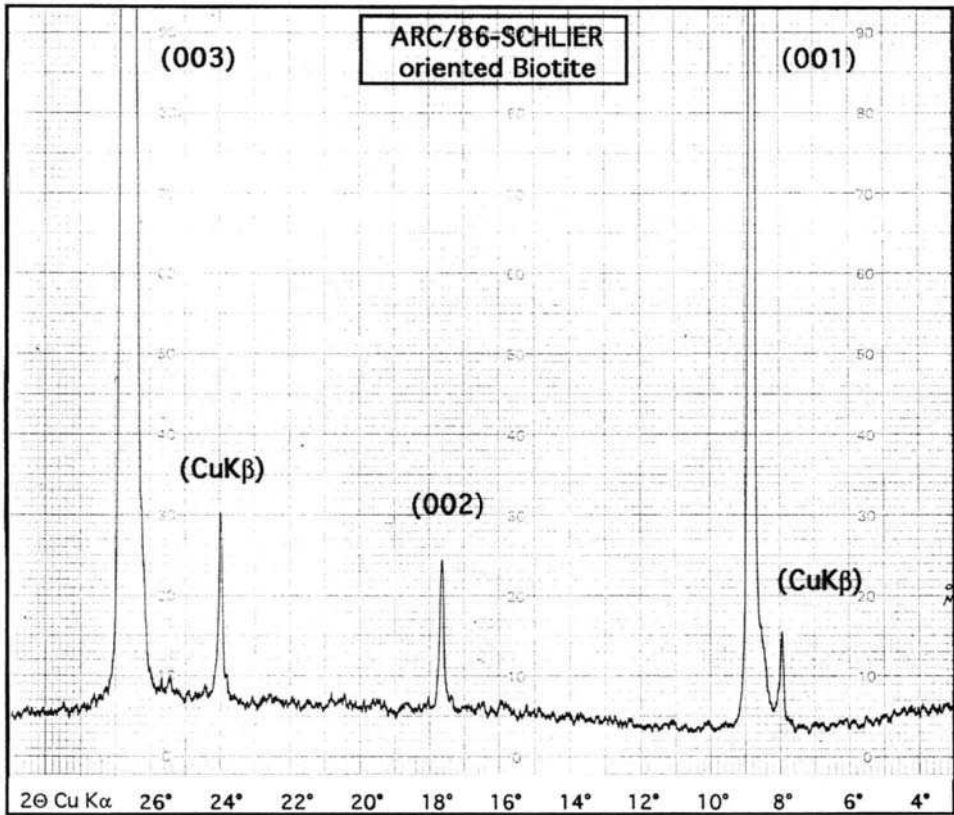


Fig. 3. XRD diffractogram of oriented biotite from the Arcevia Level.

throughout the region, and it was proposed by Coccioni and Montanari (1992) as a potential regional marker for the recognition of this intraformational boundary. In fact, the Piero della Francesca Level exposed at 19.5 m in the Moria section (see Chapter D1) can be confidently correlated with the 'Arcevia Level' on the basis of lithostratigraphic, biostratigraphic, petrographic, and biotite-geochemistry criteria. Therefore, this volcanoclastic marker in the Santa Croce di Arcevia section will be called Piero della Francesca hereafter.

The Piero della Francesca contains abundant, fresh, and unaltered biotite flakes (see X-ray diffractogram in Fig. 3), often exhibiting euhedral contours. Its chemical composition is very similar to that of the Piero della Francesca Level at Moria (Table 1; see also Table 1 in Chapter D1). Moreover, like at Moria, this biotite-rich volcanic marker contains minor amounts of pristine sanidine which appears to be absent in the underlying volcanoclastic layers of the Bisciario and Scaglia Cinerea formations. Sanidine in the Piero della Francesca Level suggests that the volcanic source for the Eocene to Miocene Apennine distal tephra evolved to more acidic terms through time. Montanari et al. (1994) and Assorgia et al. (1994) showed several lines of evidence suggesting that this source may have been the volcanic province of western Sardinia.

Table 1

Chemical compositions in weight percent of biotite flakes from the Piero della Francesca Level in the Santa Croce di Arcevia section compared with the average composition of biotite from the same level in the Moria section (MOR-19.5 m)

Analysis	SiO <sub>2</sub>	TiO <sub>2</sub>	Al <sub>2</sub> O <sub>3</sub>	FeO*	MgO	CaO	Na <sub>2</sub> O	K <sub>2</sub> O	Total
(1) 9 points analyzed	35.41	4.00	13.46	26.09	8.20	0.00	0.37	8.65	96.17
(2) 4 points analyzed	34.48	4.06	13.62	25.55	8.06	0.00	0.41	8.69	94.86
(3) 4 points analyzed	34.98	4.03	13.17	25.80	7.99	0.01	0.40	8.51	94.90
(4) 4 points analyzed	35.40	4.03	12.88	25.54	8.00	0.01	0.42	8.49	94.76
(5) 5 points analyzed	35.04	3.96	13.24	26.69	7.55	0.01	0.40	8.46	95.35
(6) 4 points analyzed	34.99	4.13	12.93	26.48	8.11	0.08	0.42	8.37	94.52
(7) 4 points analyzed	34.61	4.08	13.22	26.07	8.02	0.01	0.44	8.41	94.95
(8) 4 points analyzed	35.12	3.92	13.97	25.31	7.96	0.00	0.41	8.46	94.19
(9) 4 points analyzed	35.59	3.85	12.62	23.65	7.88	0.01	0.40	8.63	94.64
Average (Santa Croce)	35.06	4.01	13.93	25.69	7.97	0.01	0.41	8.52	94.93
Average(MOR-19.5)	34.39	3.41	14.00	24.00	7.56	0.08	0.36	8.65	92.49

FeO\* = total iron.

The typical calcareous–siliceous–tuffitic member of the Bisciario in the Santa Croce di Arcevia section is characterized by a 8-m-thick, whitish, composite volcanoclastic horizon reported as the ‘Mega P’ (P is for pyroclastite) by Coccioni et al. (1988) (Fig. 2), and described in detail by Amorosi et al. (1992, 1994). This composite mega-layer is present, with similar characteristics, in numerous other Bisciario sections throughout the region, and analogous volcanoclastic intervals in coeval epiligurian basins of the Emilian Apennines are possibly correlated with the Umbro–Marchean Mega P (Amorosi et al., 1992, 1994). The Mega P is apparently absent in the classic CT section of the Contessa valley which, in fact, probably contains a hiatus (Amorosi, 1992, 1994; Chapter C3). According to Amorosi et al. (1992, 1994) the Mega P contains an abundant, fine to very fine vitric component of dacitic–rhyolitic composition. The crystal fraction is mostly concentrated at the base of the mega-layer, and is dominated by usually untwinned plagioclase grains. Accessory biotite, and/or pyroxene, and/or amphibole are also present. The Mega P has been interpreted as the product of decelerating submarine flows after remobilization and transport into deeper parts of the palaeobasin of volcanoclastic ash debris (Amorosi et al., 1992, 1994).

## BIOSTRATIGRAPHY

A summary of the lithostratigraphy and biostratigraphy of the Santa Croce di Arcevia section, including planktonic Foraminifera, calcareous nannofossils, and dinoflagellates, is shown in Fig. 4. Detailed biostratigraphic accounts for each of these microfossil groups are reported as follows.

### *Planktonic Foraminifera (R. Coccioni)*

A total of 112 samples were analyzed using mainly washed residues (grain size fraction >40 µm) and occasionally thin sections. Most of the samples contain very

## Santa Croce di Arcevia section

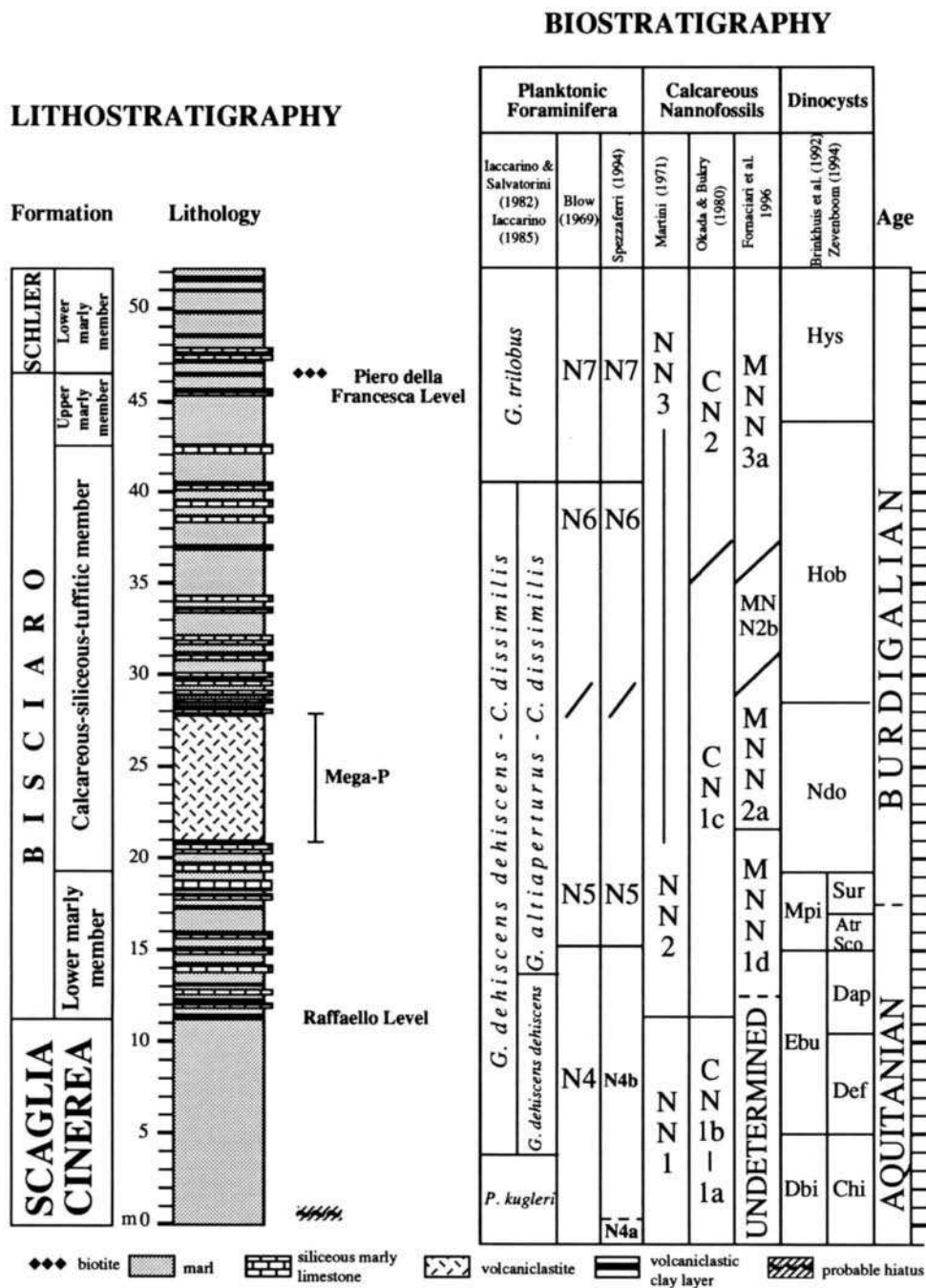


Fig. 4. Lithostratigraphic and biostratigraphic synthesis based on planktonic Foraminifera, calcareous nannofossils, and dinoflagellate cysts of the Santa Croce di Arcevia section.

abundant and well diversified assemblages. Preservation varies from sample to sample from moderately good to very poor: some specimens are crushed and show evidence of dissolution and strong recrystallization. Samples with a high volcanogenic component usually contain scarce and poorly preserved foraminiferal assemblages. Volcaniclastic layers are almost barren of Foraminifera. Occasional reworking represented by sporadic Oligocene specimens was recognized mainly across the boundary between the Scaglia Cinerea and the Bisciaro.

The generic and specific concepts of Spezzaferri (1994) were largely followed. All the events useful for the Lower Miocene in the Mediterranean zonation of Iaccarino and Salvatorini (1982) and Iaccarino (1985) were recognized, whereas only some events used by Blow (1969) and Spezzaferri (1994) to define their zonal boundaries were identified. According to the zonal models of Blow (1969) and Spezzaferri (1994) it was possible to recognize five foraminiferal zones, and four zones and two subzones based on calcareous nannofossils. In terms of the Iaccarino and Salvatorini (1982) and Iaccarino (1985) biozonations, two zones and two subzones were recognized. The main foraminiferal events and derived biostratigraphic zonation for the Santa Croce di Arcevia section are shown in Fig. 5.

'*Globigerinoides primordius*', whose first occurrence (FO) defines the P22/N4 zonal boundary of Blow (1969), is already present at the base of the section in association with *Paragloborotalia pseudokugleri* and *P. pseudokugleri/Paragloborotalia kugleri* transitional forms.

The FO of *Paragloborotalia kugleri* which is used by Spezzaferri (1994) to place the P22/N4 zonal boundary is found at 0.9 m where *Globigerinoides quadrilobatus*, *G. sacculifer* and *G. subsacculifer* also first appear. In the Carrosio–Lemme section (Tertiary Piedmont Basin, northwestern Italy), which was recommended by the Working Group on the Palaeogene/Neogene (P/N) (i.e., the Oligocene/Miocene (O/M) boundary; see Chapter A9), to the International Commission on Stratigraphy as the Global Boundary Stratotype Section and Point (GSSP) for the P/N boundary, this event is found just above a magnetic polarity reversal interpreted as the base of the magneto Chronozone C6C2n, where the same Working Group proposed to place the O/M boundary (Steininger et al., 1994; Chapter A9).

In the Santa Croce di Arcevia section, the diversification of the genus *Globigerinoides* (i.e., the *Globigerinoides* event of Spezzaferri, 1994), which defines the boundary between the Subzones N4a and N4b of Spezzaferri (1994), seems therefore to occur at the same stratigraphic level of the FO of *P. kugleri*. The diversification of the genus *Globigerinoides* goes on with the FO of *Globigerinoides parawoodi* and *G. immaturus* at 1.9 m and 6.9 m, respectively. However, according to Spezzaferri (1994) the *Globigerinoides* event occurs well above the FO of *P. kugleri*, these two events defining the N4a Subzone. The available data from the Santa Croce di Arcevia section suggest therefore that the N4a Subzone is missing, probably due to a hiatus.

The FO of *Globoquadrina dehiscens* takes place at 3.9 m and defines the lower boundary of the *G. dehiscens dehiscens* Subzone of the *G. dehiscens dehiscens*–*Catapsydrax dissimilis* Zone of Iaccarino and Salvatorini (1982) and Iaccarino (1985). According to all the zonal models followed herein, the FO of *G. dehiscens* occurs within the range of *P. kugleri*, predating the appearance of *Globigerinoides altiapertura* and *Globigerinoides trilobus*. Blow (1969) places the FO of *G. dehiscens* in the upper part

# Santa Croce di Arcevia section

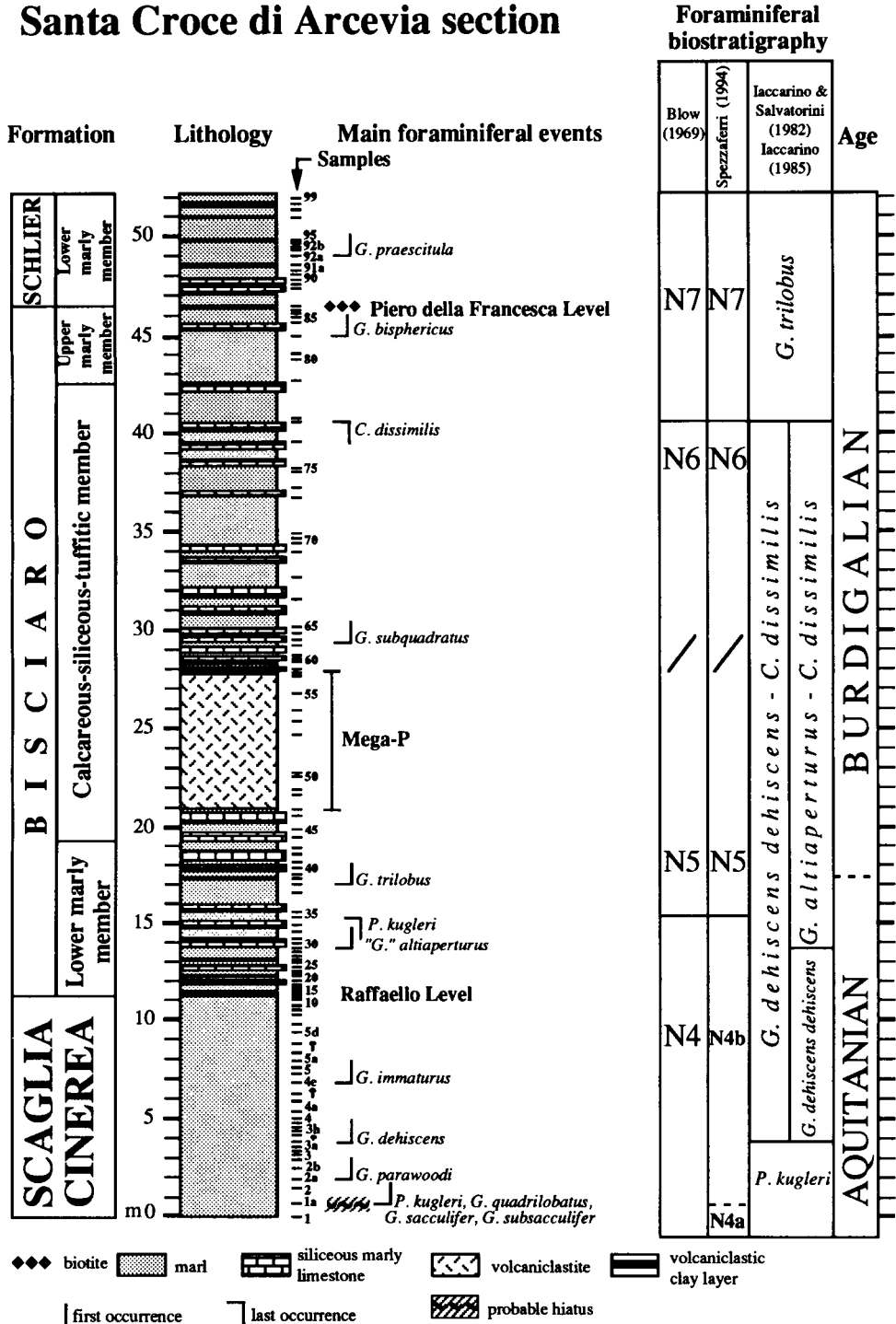


Fig. 5. Main planktonic foraminiferal events and biostratigraphy of the Santa Croce di Arcevia section.



of Zone N4. Therefore, the *G. dehiscens dehiscens* Subzone of Iaccarino and Salvatorini (1982) and Iaccarino (1985) seems to correlate with the upper part of Zone N4 and the basal part of Zone N5 of Blow (1969). However, the diachronous character of the FO of *G. dehiscens* which is found from the middle of Zone P22 to the lower part of Zone N4, has been shown by Spezzaferri (1994).

The FO of '*G.*' *altiaperturus* occurs at 13.78 m which defines the lower boundary of the *G. altiaperturus*–*Catapsydrax dissimilis* Subzone of Iaccarino and Salvatorini (1982) and Iaccarino (1985). This event is followed by the last occurrence (LO) of *P. kugleri* and the FO of *G. trilobus* at 15.3 m and 17.12 m, respectively. The LO of *P. kugleri* is used by Blow (1969) and Spezzaferri (1994) to define the N4/N5 zonal boundary.

There is no unanimous agreement on the relative stratigraphic positions of the FOs of '*G.*' *altiaperturus* and *G. trilobus*, the former often used for the recognition of the Aquitanian/Burdigalian boundary (Bizon and Bizon, 1972; Demarcq et al., 1974; Iaccarino and Salvatorini, 1982; Bizon, 1984; Iaccarino, 1985). However, for the Aquitanian/Burdigalian boundary there is no definitive consensus on the datum that ought to be used for its recognition. In fact, according to Blow (1969), the Aquitanian/Burdigalian boundary is within the N6 Zone. The *G. altiaperturus*–*C. dissimilis* Subzone correlates with part of Zone N5 and the entire N6 of Blow (1969) and Spezzaferri (1994). According to several authors (e.g.: Blow, 1969; Demarcq et al., 1974; Borsetti et al., 1979a,b; Biolzi et al., 1981; Bizon and Müller, 1981; Iaccarino, 1985), '*G.*' *altiaperturus* appears before *G. trilobus*, whereas according to Molina (1979), Biolzi (1984, 1985) and Bolli and Saunders (1985) the FO of *G. trilobus* is stratigraphically lower than the FO of '*G.*' *altiaperturus*. According to Keller (1984), the FO of *G. trilobus* precedes not only that of '*G. altiaperturus*' but also that of *G. dehiscens*. According to Spezzaferri (1994) the FO of '*G.*' *altiaperturus* slightly precedes the FO of *G. trilobus* in the upper part of Zone N4 in the Equatorial Atlantic, eastern South Atlantic and South Pacific; in contrast, these two species first occur associated within the latter third of Zone N4 in the western South Atlantic and in the lower part of Zone N5 in the Indian Ocean, respectively. It is worth mentioning, however, that in the stratotype of the Burdigalian, '*G. altiaperturus*' and *G. trilobus* first occur at the same level. An almost similar biostratigraphic situation is found in the Carrosio–Lemme section where the FO of *G. trilobus* occurs just before the FO of '*G.*' *altiaperturus*, both these events taking place slightly before the LO of *P. kugleri* (Steininger et al., 1994; S. Spezzaferri, pers. commun., February 1995). In the composite Contessa section the lowest finding of '*G.*' *altiaperturus* is associated with that of *G. trilobus*, both these events occurring just above the LO of *P. kugleri* (Coccioni and Monechi, 1992).

It has been known that *Globigerinatella insueta*, the FO of which defines the N5/N6 zonal boundary, is lacking in the Mediterranean area. Therefore, in the Santa Croce di Arcevia section it was not possible to biostratigraphically distinguish Zone N5 from Zone N6 of Blow (1969) and Spezzaferri (1994).

*Globigerinoides subquadratus*, which according to Iaccarino and Salvatorini (1982) and Iaccarino (1985) first appears in the middle of the *G. dehiscens dehiscens*–*C. dissimilis* Zone and following Blow (1969) in the middle Zone N5, is firstly recognized at 29.3 m.

The next significant event is the LO of *C. dissimilis* at 40.5 m which defines the

N6/N7 zonal boundary of Blow (1969), and the boundary between the *G. dehiscens*–*C. dissimilis* and the *G. trilobus* Zones of Iaccarino and Salvatorini (1982) and Iaccarino (1985).

The FOs of *Globigerinoides bisphericus* and *Globorotalia praescitula* are recognized respectively at 45.13 m and 49 m, within the N7 Zone of Blow (1969) and the *G. trilobus* Zone of Iaccarino and Salvatorini (1982) and Iaccarino (1985). According to Blow (1969) *G. praescitula* first occurs at the lower boundary of Zone N5 whereas following Iaccarino and Salvatorini (1982) and Iaccarino (1985) the FO of *G. praescitula* is found close to the lower boundary of the *G. trilobus* Zone, slightly predating the FO of *G. bisphericus*. The discrepancy between the succession of these events as recognized in the Santa Croce di Arcevia section and that shown by Iaccarino and Salvatorini (1982) and Iaccarino (1985) could be related to a relatively sparse sampling in the lower part of the *G. trilobus* Zone.

#### Calcareous nannofossils (*E. Fornaciari* and *D. Rio*)

The calcareous nannofossil biostratigraphic analysis was carried out by polarizing light microscopy on smear slides prepared from 89 samples. A close-spaced sample collection was available starting from the upper exposed part of the Scaglia Cinerea, at metre level 10; in the interval below, only six samples were available.

Calcareous nannofossils are common to abundant, but show a moderate to poor preservation state. Eight samples (mainly from volcanoclastic layers) are barren. The taxonomic concepts adopted herein are after Perch-Nielsen (1985), Rio et al. (1990a), and Fornaciari et al. (1990).

The calcareous nannofossil assemblages are dominated by placoliths (*Dictyococcites*, *Reticulofenestra*, *Coccolithus*, and *Cyclicargolithus*). Helicoliths and sphenoliths are well represented while discoasterids and triquetrorabdulids are generally rare.

After a qualitative analysis, the distribution patterns of stratigraphically important forms have been established by quantitative counting methods following Backman and Shackleton (1983) and Rio et al. (1990c). Specifically, we counted the number of the index species of helicoliths, of sphenoliths, and of discoasterids relative to a fixed number of 50 helicoliths, of 100 sphenoliths, and of 200 discoasterids, respectively.

For the biostratigraphic classification of the investigated section, we have made reference to the standard zonations of Martini (1971) and of Okada and Bukry (1980) and to the recently established regional mediterranean lower Miocene zonation of Fornaciari and Rio (1996). The counting of marker species and the resulting biostratigraphic classification are reported in Fig. 5, and briefly commented below.

The basal 10 m of the section, where only six samples were available, cannot be constrained with precision. However, *Sphenolithus ciperoensis* (the LO of which defines the CP19/CN1 boundary) is missing throughout, *Dictyococcites bisectus* (the LCO of which is a secondary criterion for recognizing the CP19/CN1 boundary) is present up to 3.0 m, *Helicosphaera recta* (the LO of which is the original definition of the NP25/NN1 boundary) is present as scattered up to 12.0 m, and large forms of *Cyclicargolithus abisectus* (the acme end of which is the original definition of the CN1a/CN1b boundary) are virtually missing. These data suggest that this lower part of the section must be referred to the lower part of Zone CN 1 (Subzones CN1a and CN1b) of Okada and

Bukry (1980) and to Zone NN1 of Martini (1971) as emended by Fornaciari et al. (1996), to which the reader is referred for issues related to the NP25/NN1 boundary.

The biostratigraphic classification of the remaining part of the section is straightforward in terms of Okada and Bukry (1980), and Fornaciari and Rio (1996) zonations, as documented in Fig. 6. Martini's NN2/NN3 boundary, defined by the LO of *Triquetrorhabdulus carinatus*, cannot be recognized because the species is rare and scattered and unreliable in the Mediterranean stratigraphic record (Fornaciari and Rio, 1993).

In summary, the 52-m-thick Santa Croce d'Arcevia section is comprised between the LO of *Sphenolithus ciperoensis* and the LO of *Sphenolithus belemnos*. Both these biohorizons are considered as reliable for long-distance correlations in low- and mid-latitude sediments (see Fornaciari and Rio, 1993, for a review). Considering the presence of rapidly deposited volcanoclastic sediments, hiatuses below the resolution power of biostratigraphy are probably present.

#### *Dinoflagellate cysts (D. Zevenboom)*

Within the framework of the MICOP project the dinoflagellate cyst (dinocyst) assemblages from the Santa Croce di Arcevia section (Coccioni et al., 1992b) are used to extend the biozonation model for the Contessa section (see Zevenboom in Chapter C3).

In general, the palynological associations consist of well preserved bisaccate pollen, other pollen and spores, and dinocysts. The qualitative dinocyst distribution is depicted in Fig. 7, and the resulting biostratigraphic zonation is correlated with the foraminiferal and calcareous nannofossil zonations in Fig. 4. The results readily allow recognition of the Upper Oligocene–Lower Miocene zonal models of Brinkhuis et al. (1992), Zevenboom (in press, and in Chapter C3), viz. the *Chiropteridium* acme Subzone of the *Distatodinium biffii* (Dbi) Zone, the *Ectosphaeropsis burdigalensis* (Ebu) Zone, subdivided into the *Deflandrea* acme (Def) Subzone and the *Distatodinium apenninicum* (Dap) Subzone. These (sub)zones are all based on the Lemme section (Zevenboom, 1993). The overlaying *Membranilarnacia? picena* (Mpi) Zone and the *Nematosphaeropsis downiei* are defined on basis of the Contessa section (Zevenboom, in Chapter C3). The *Hystrichokolpoma truncata* (Htr) Subzone and *Stoveracysta conerae* (Sco) Subzone of the Mpi Zone could however not be distinguished, due to the apparently delayed first occurrence (FO) of the index species *S. conerae*. The *Systematophora urbinii* (Sur) Subzone of the Mpi Zone is recognized between samples SC 38 and SC 43. Moreover, as discussed by Zevenboom (in Chapter C3), the rich associations of the interval above the Ndo Zone allow even further subdivision of the upper Lower Miocene at the Santa Croce di Arcevia site. The following new biozones are herein proposed:

#### *Hystrichosphaeropsis obscura* (Hob) Interval Zone (lower Miocene).

Definition: The interval from the FO of *Hystrichosphaeropsis obscura* to the LO of *Caligodinium pychnum*.

Calibration: Planktonic foraminifers: upper part N6 Biozone through lower part N7 (to LO of *G. bisphaericus*); calcareous nannoplankton: top MNN2a through base MNN3a Biozone.

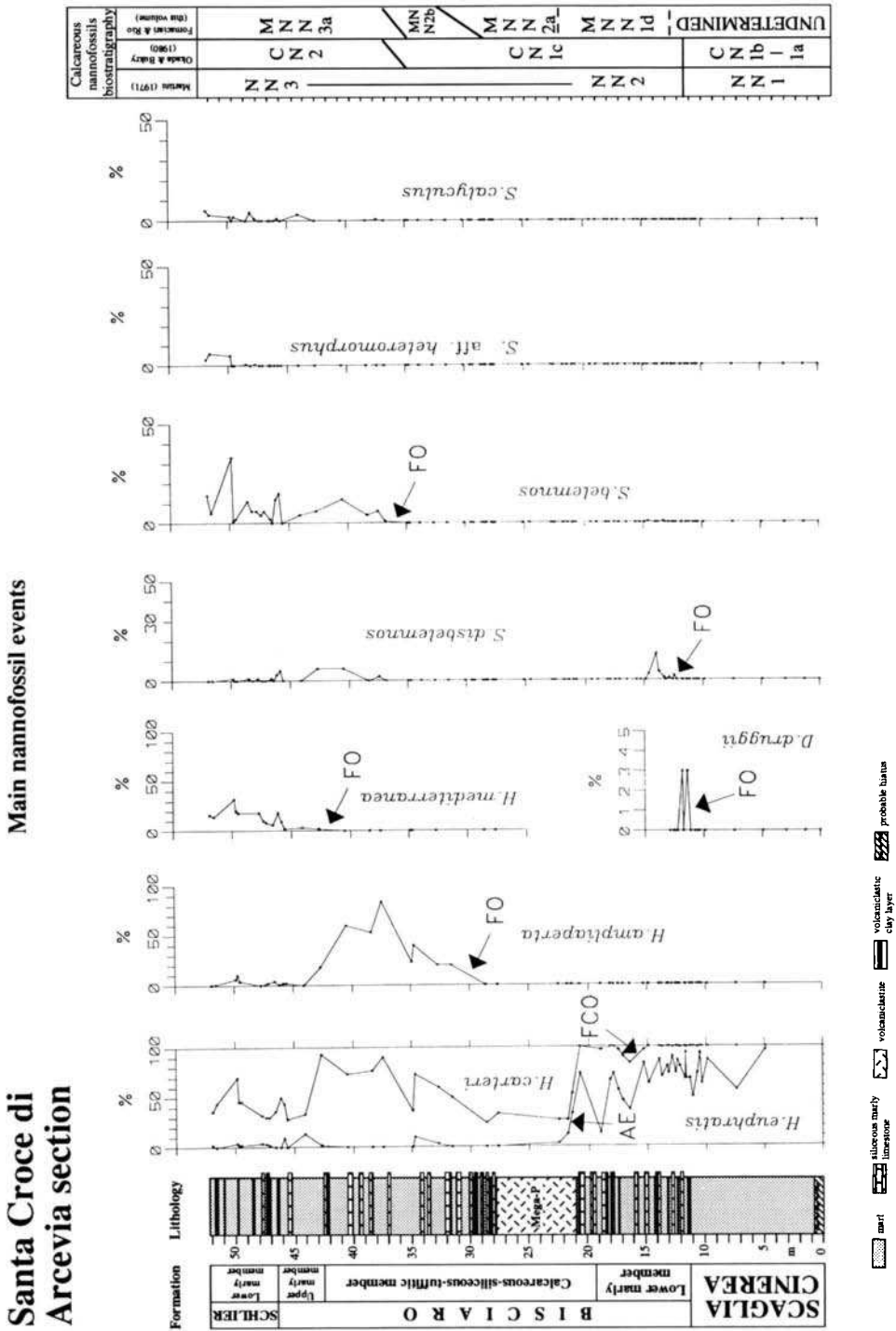
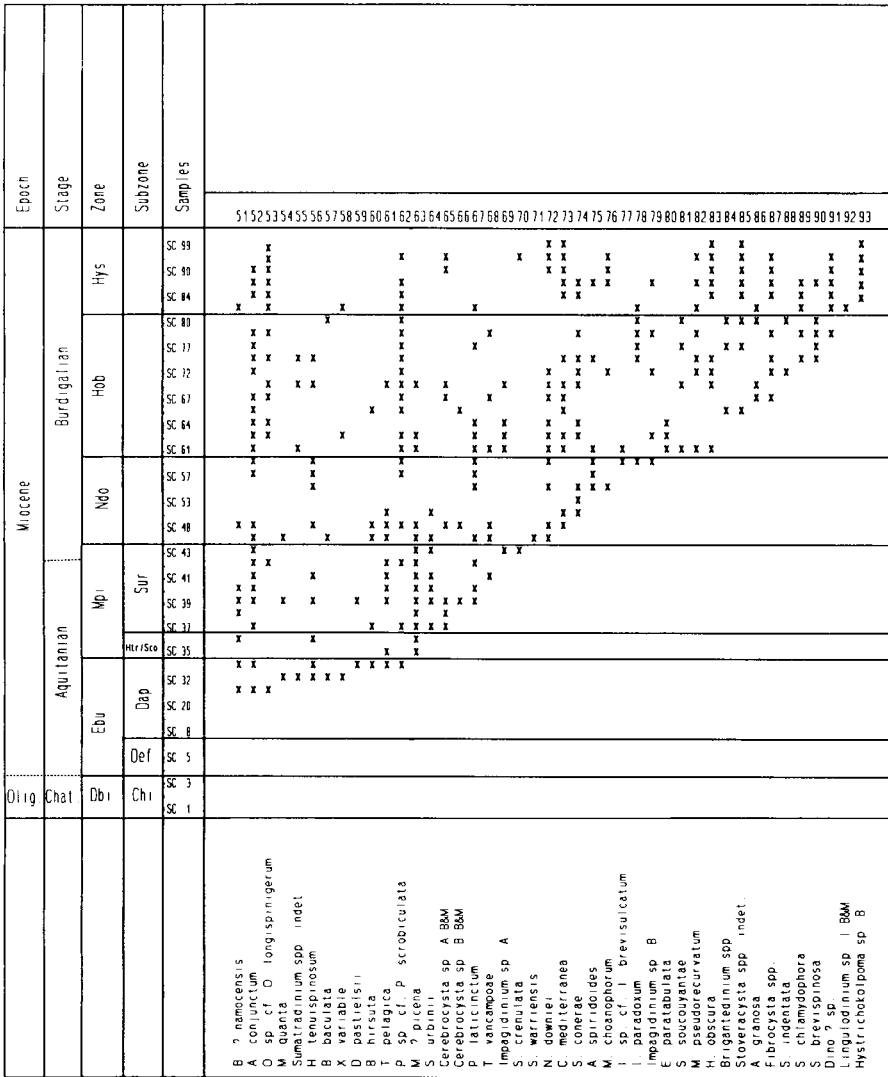


Fig. 6. Main calcareous nannofossil events and biostratigraphy of the Santa Croce di Arcevia section. AE = acme zone end; FCO = first common occurrence; FO = common occurrence.



(a)

Fig. 7. +Fig. 7 (continued). Range chart of dinocysts by lowest appearance in the Santa Croce di Arcevia section. For metre level location of these samples, see Fig. 5.

Age: Early Miocene.

Thickness: 16.15 m; samples SC 61–SC 80.

*Hystrichokolpoma* sp. B (Hys) of Powell, 1986 Interval Zone (lower Miocene).

Definition: The interval from the LO of *Caligodinium pychnum* to the FO of *Hystrichokolpoma inflata*.



### Taxonomic notes

A reference is given for species not included in Lentin and Williams (1993):

*Cerebrocysta* sp. A Biffi and Manum (1988).

*Cerebrocysta* sp. B Biffi and Manum (1988).

Dinocyst? sp. Remark: a possible dinocyst, with an inferred epicystal (?) archaeopyle and fibrous processes.

*Homotryblium* sp. cf. *H. oceanicum* Brinkhuis et al. (1992).

*Hystrichokolpoma* sp. B Powell (1986).

*Hystrichosphaeropsis* sp. cf. *H. obscura* Brinkhuis et al. (1992).

*Impagidinium* 'small' spp. indet. Remark: a complex of extremely small *Impagidinium* species with, apparently, a variable paratabulation and smooth septa, probably belonging to the informally described *Impagidinium* species of Mudie (1989).

*Impagidinium* sp. A. Remark: an extremely small species of *Impagidinium*, probably also belonging to the complex of small *Impagidinium* species informally described by Mudie (1989). This species may be recognized by the presence of small spines on the septa.

*Impagidinium* sp. B. Remark: an extremely small species of *Impagidinium*, probably also belonging to the complex of small *Impagidinium* species informally described by Mudie (1989). This species may be recognized by the consistent presence of perforate septa.

*Incertae sedis* sp. Edwards (1984).

*Lingulodinium* sp. 1 Biffi and Manum (1988).

*Pyxidiella* sp. A. It was depicted by Manum et al. (1989) as '*Pyxidiella* sp. 1'.

The '*Spiniferites* complex' (cpx). Remark: this 'complex' represents all species attributable to either *Achomosphaera* or *Spiniferites* spp.

### DISCUSSION

The Santa Croce di Arcevia is perhaps the most complete and continuous exposure comprising the lowermost Aquitanian and lower Burdigalian currently known in the Umbria–Marche Apennines. All the useful planktonic foraminiferal, calcareous nannofossil, and dinoflagellate biozones through this stratigraphic interval have been recognized and precisely correlated. However, some inconsistency in the sequence of diagnostic dinoflagellate cyst events also in respect to the main planktonic foraminiferal events, emerged after a tentative correlation of the lower part of this section with the Contessa section, as it is shown in Fig. 8. In this figure, the Raffaello Level is chosen as a correlation time line between the two sections. Above this volcanoclastic horizon, the tree common bioevents represented by the LO of *P. kugleri* (planktonic foraminifer), and the FOs of dinocysts *M. ?picena* and *S. conerae* are widely spaced in a 5-m interval in the Santa Croce di Arcevia section but are almost synchronous in the Contessa section. This is probably due to a hiatus and/or strong stratigraphic condensation in the Contessa section, as discussed by Montanari and co-workers in Chapter C3. On the other hand, the FO of '*G.* *altiaperturus*', which is often used to approximate the Aquitanian/Burdigalian boundary, is found 1.2 m below the FO of *G. trilobus* at Santa Croce di Arcevia, and about 2 m above it at Contessa, where it coincides with a probable hiatus. Therefore,

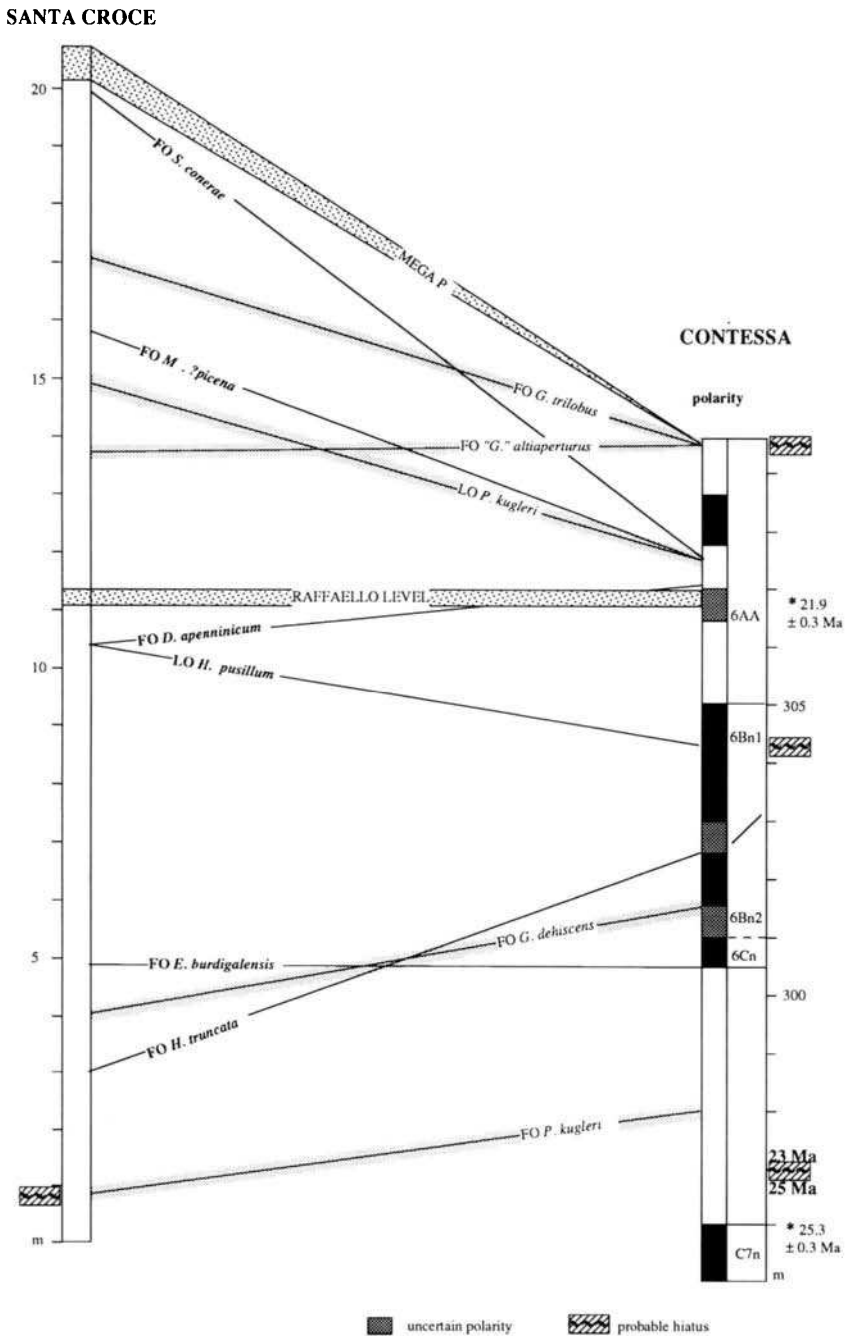


Fig. 8. Biostratigraphic correlation between the Santa Croce di Arcevia and Conessa section based on main planktonic foraminiferal events (shaded lines), and dinocyst events. Stratigraphic and geochronologic data for the Conessa section are from Chapter C3.



these foraminiferal bioevents have to be considered as slightly dyachronous between the two sections.

Below the Raffaello Level, the correlation shown in Fig. 8 appears somewhat more problematic. While the foraminiferal biomarkers represented by the FOs of *G. dehiscentis* and *P. kugleri* correlate very well between the two sections (in either case they are separated by about 3 m of Scaglia Cinerea sediment), none of the four dinoflagellate cysts events seem to occur at the same time in the two sections. The FO of *D. apenninicum* is located below the Raffaello Level at Santa Croce di Arcevia, and above it in the Contessa section. Moreover, this event occurs in the same level as the FO of *H. pusillum* in the Santa Croce di Arcevia, while the same events are separated by about 3 m of section at Contessa. Finally, the sequence of consecutive FOs of *H. truncata* and *E. burdigalensis* at Santa Croce di Arcevia is inverted at Contessa. This suggests that dinoflagellate cysts do not provide a precise and accurate means for stratigraphic correlation among Lower Miocene sections of the Umbria–Marche pelagic sequence. On the other hand, planktonic foraminiferal events seem to be more consistent as correlation tools at least at a regional scale. Unfortunately, nothing can be said about calcareous nannofossils because none of the biomarkers used for biostratigraphic determinations in the Contessa section were found in the Santa Croce di Arcevia section.

An unpublished pilot study by V.E. Langenheim revealed that Bisciario samples from this section are not conducive to magnetostratigraphy due to palaeomagnetic weakness and instability.

Preliminary radioisotopic dating of the biotite-rich Piero della Francesca Level, found in the uppermost part of the Santa Croce di Arcevia section, yielded  $^{40}\text{Ar}/^{39}\text{Ar}$  single crystal, laser fusion ages around  $17.6 \pm 0.6$  ( $2\sigma$ ) Ma from three sanidine grains, which were too small to be considered as reliable geochronometers, and two very imprecise biotite ages around 18.5 Ma. A second run on biotite from the Piero della Francesca Level was rejected because of a laboratory preparation error (Deino and Montanari, 1992). Nevertheless, the biotite in this marker bed is compositionally pure and homogeneous, and constitutes a potentially reliable geochronometer. Moreover, other volcanic layers are present in the section, promoting further geochronologic analysis for an accurate and precise calibration of Lower Miocene interstage boundaries.

The major drawback of the Santa Croce di Arcevia section is that it is located in a private property, and its accessibility is limited. However, on a road cut immediately outside of this property, the Scaglia Cinerea/Bisciario boundary is well exposed, and may constitute a suitable situation for future integrated stratigraphic studies on the therein comprised interstage boundaries between the Aquitanian and Burdigalian, and possibly between the Chattian and the Aquitanian.

#### SOMMAIRE — POTENTIEL POUR LA STRATIGRAPHIE INTÉGRÉE DE LA SECTION D'ÂGE AQUITANIEN–BURDIGALIEN À SANTA CROCE DI ARCEVIA (NE APENNINS, ITALIE)

(Manuscrit soumis: Juin 1995, révisé: Juillet 1995; rédacteurs responsables: AM et RC)

La section de Santa Croce di Arcevia, épaisse de 52 m, constitue l'affleurement le plus complet et continu de la Formation Bisciario dans les Apennins de Marches–

Ombrie. Pour la biostratigraphie, on a observé la présence des taxons indice des biozones usuelles pour les foraminifères planctoniques, les nannofossiles calcaires et les kystes de Dinoflagellés. Ceci permet d'envisager des corrélations précises pour tout l'Aquitainien et l'essentiel du Burdigalien. Les études préliminaires ont révélé l'impossibilité d'aboutir à une caractérisation magnétostratigraphique. La section renferme les niveaux volcanoclastiques régionaux dénommés Raffaello (daté à la Contessa) qui marque la limite inférieure de la formation Bisciario à la cote 11,3 m et le niveau Piero della Francesca (daté à Moria) qui marque la limite supérieure de la même formation à la cote 46,5 m mais aussi d'autres niveaux qui pourraient être caractérisés géochronologiquement. Ainsi, la section de Santa Croce di Arcevia est susceptible de livrer d'intéressantes informations stratigraphiques qui compléteront avantageusement celles obtenues à partir des autres sections de Marches–Ombrie lesquelles se sont souvent révélées insuffisantes de par la présence de niveaux condensés et de hiatus dans l'intervalle considéré.

*(Sommaire proposé par les rédacteurs d'après un résumé anglais des auteurs, GSO)*

#### ACKNOWLEDGEMENTS

Financial support has been provided by a grant from the Italian Ministry of University and Scientific Research (MURST, 60%; responsible R. Coccioni.), and grants from Armines and Exxon Oil Co. (A. Montanari). D. Zevenboom thanks H. Brinkhuis for carefully reading and reviewing the manuscript, which substantially improved it. Furthermore this author acknowledges support from The Netherlands Foundation for Earth Science Research (AWON) and financial aid from The Netherlands Organization for the Advancement of Scientific Research (NWO). This is a publication of The Netherlands Research School of Sedimentary Geology (NSG), 950204.

This Page Intentionally Left Blank

*Chapter C5*

**BIOSTRATIGRAPHY AND GEOCHRONOLOGY OF A MIOCENE  
CONTINENTAL VOLCANICLASTIC LAYER FROM THE EBRO BASIN,  
SPAIN**

G.S. Odin, G. Cuenca Bescós, J.I. Canudo, M. Cosca and M. Lago

**INTRODUCTION**

The Tertiary Ebro Basin in Spain is a large continental basin filled with Miocene fluvial to lacustrine sediments. In the Lanaja–Peñalba area (Zaragoza Province) a volcanoclastic layer has been found in 1989 within these Miocene sediments. The biostratigraphic age has been characterized using Charophyta and micromammals. This makes this material promising for correlation of continental and marine biostratigraphic and chronostratigraphic scales.

This study reports new findings related to the presence of this unique volcanoclastic layer in five sections. A new biostratigraphic mammal site immediately overlying the layer has also been investigated.

**LITHOSTRATIGRAPHY**

*Geology and sediments*

The study area is located in the Ebro Basin (Aragón Province) in the northeastern part of the Iberian Peninsula (Fig. 1). This basin is limited by the Pyrenean Range to the north and the Iberian Range to the south. The nearest continental basin is the well-known Catalayud–Teruel Basin in the Iberian Range.

The triangular Ebro Basin is one of the largest continental Cenozoic basins of western Europe, extending over nearly 45,000 km<sup>2</sup> and containing sediments of Middle Eocene to Quaternary age. The infilling is asymmetrical, with the northern part locally reaching a thickness of 5 km. Overthrust marine Mesozoic and Palaeocene nappes cover the area. In the southern part, the continental sediments unconformably overlap the margin of the basin; in the central part, the sediments are well-exposed and nearly horizontal (Riba et al., 1983).

Extensively studied by the Spanish geologists, the Ebro Basin has generated a number of unit names partly depending on the methodological approach. The unit containing the studied layer has been named: (1) as a lithologic unit: Formación Sariñena–Calizas de Peñalba (Quirantes, 1978); (2) a facies unit: Huesca fluvial system (Hirst, 1989); (3) a sequential analysis unit: Sistema Deposicional de los Monegros (Cabrera, 1983); (4) a tectosedimentary unit: N1 (Arenas and Pardo, 1991); and (5) a genetic sedimentary unit: Unidad de Zuera (Hernandez et al., 1991). The deposits of the Huesca fluvial system and the Formación Sariñena consist of geometrically distinct channel sandstone

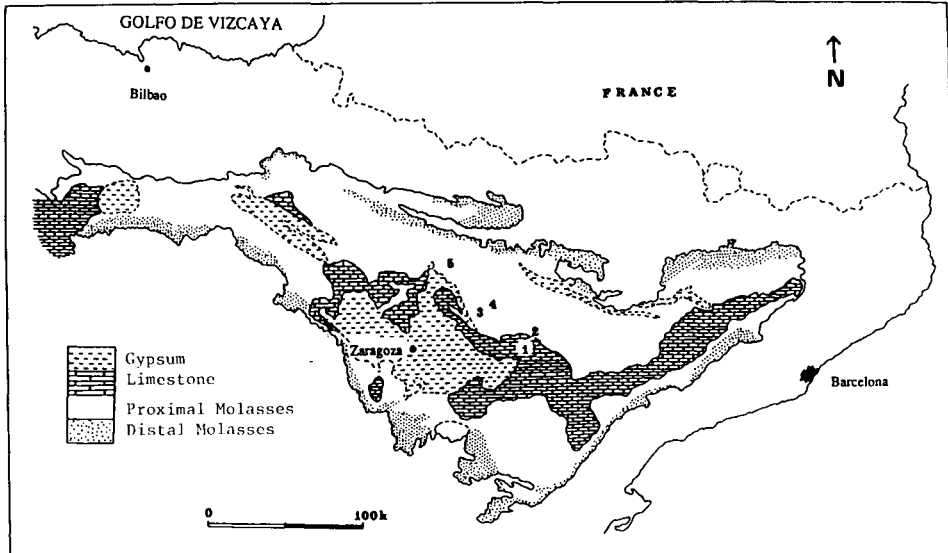


Fig. 1. Schematic map of the lithological facies of the Tertiary Ebro Basin (after Riba et al., 1983, modified). 1 = Peñalba, 2 = Sigena, 3 = Lanaja, 4 = El Tejar, 5 = Tardienta.

bodies enclosed within fine-grained floodplain deposits. Flow was mainly through a network of well defined channels within which a bulk of the sandy bedload material was deposited (Hirst, 1989). The Calizas de Peñalba and Sistema Depositional de los Monegros were deposited mainly in lake to lake-margin environments. Lacustrine sediments predominated in the centre of the Oligocene–Miocene Ebro Basin.

#### *The volcaniclastic layer*

The volcaniclastic layer studied in this work extends over nearly 100 km. From northwest to southeast, the layer has been observed in five sites at Tardienta, Lanaja, El Tejar, Peñalba, and Sigena (Fig. 2).

The first report of volcanogenic sediments in the Ebro Basin is recent (Hirst, 1989). This author interpreted a horizon at Tardienta as a volcanic ash layer. The layer consists of a lower white, sandine-rich sandstone, about 2 cm thick, and overlain by about 10 cm of pure smectite clay. The clay is pinkish with a soapy texture. Canudo et al. (1993) first reported the ash layer as a 45 km wide more or less continuous horizon in the Lanaja–Peñalba area. The wide distribution, independent of the facies, is a good criterion for truly aerial transportation of the volcanic material. The layer displays two levels of different colour. The base is characterized by a lithological change between fine-grained sedimentary material below: clay in Lanaja or limestone in Peñalba and white volcaniclastic material above for the lower level. The colour of the upper level varies from red in Lanaja to green in Peñalba. The thickness generally varies between 0.15 m to the northwest and 0.30 m to the southeast. The white level is present alone in Sigena but absent in El Tejar.

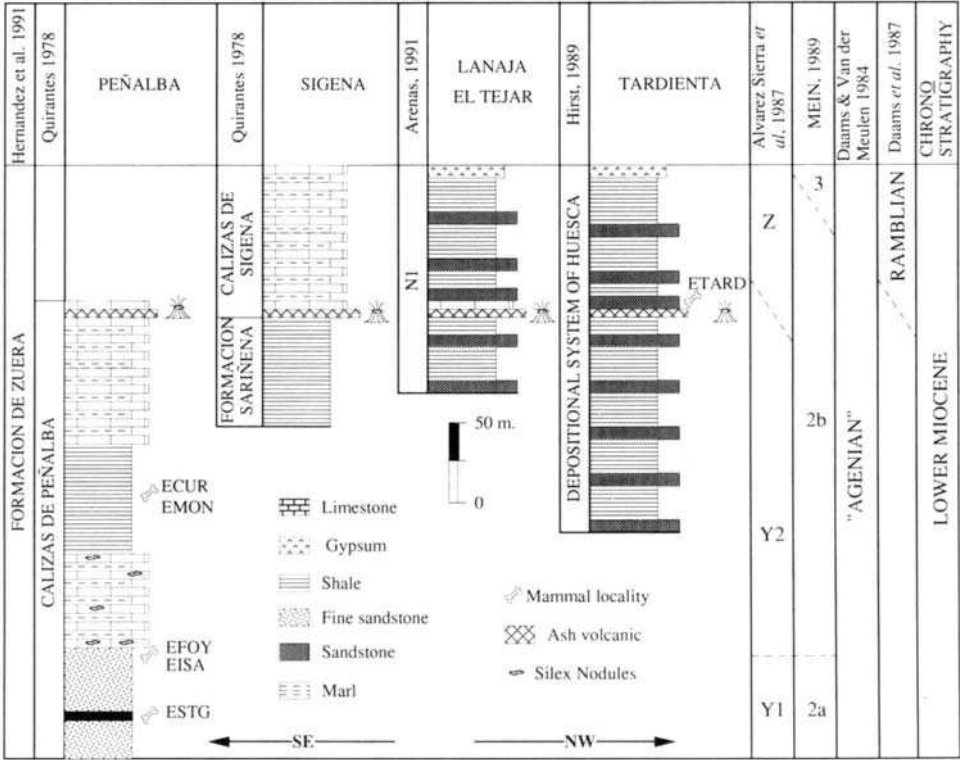


Fig. 2. Lithologic succession in five sections from the Ebro Basin where a volcanioclastic layer has been observed.

BIOSTRATIGRAPHY

Biozonation with mammals

Miocene continental biostratigraphy is primarily based on the evolution of mammals. Limits of large units (continental stages) are traditionally marked with large mammals, and smaller units (biozones) commonly use micromammals. For instance, the Aragonian unit (of stage or superstage ranking) was originally identified as the interval between the first appearance of the horse *Anchiterium* below and the first appearance of the horse *Hipparion* above (Daams et al., 1977). The unit was formally established and characterized for sediments and mammals in the Catalayud–Teruel Basin; it comprises two land mammal stages: Orléanian and Astaracian which would cover MN zones 3 to 8 of Mein (1989). The approximate marine equivalent would be Early (pp) and Middle Miocene (Table 1).

Subsequent work (Daams and Freudenthal, 1981, 1989) improved the biostratigraphy but revealed that the base of the Aragonian unit (first appearance of *Anchiterium*) could not be identified confidently in the type area and the event could not serve as a marker horizon in absence of the key fossil. Daams et al. (1987) redefined the base of

Table 1

Schematic relation between continental and marine subdivisions (partly after Mein, 1989, and Steininger et al., 1989)

OLIGOCENE		AQUITAN.		BURDIGALIAN		LANGH.		SERRAVALLIAN	
AGENIAN		ORLEANIAN				ASTARACIAN			
2a	2b	3	4	5	6	7	8		
Y2	Z	A	B	C	D	E	F	G	
"AGENIAN pp"		RAMBLIAN		ARAGONIAN					
	↑ (2)				↑ (1)				

(1) initially presumed location of the dated layer; (2) newly established location according to the fauna discovered in the section at Tardienta.

the Aragonian in correspondence with the first appearance of modern cricetid rodents and created the Ramblian regional stage for strata underlying the Aragonian ones. This revision places the 'biozone A' of their previous study (Daams and Freudenthal, 1981) in the Ramblian. They also define the base of their Ramblian stage in correspondence with extinction of the *Rhodanomys*–*Ritteneria* group of eomyd rodents. However, this level is not concretely represented in the type area of the Ramblian (Calamocha–Navarrete del Río in the Catalayud–Teruel Basin). Daams et al. (1987) identified two local biozones in the Ramblian stage: (1) zone Z would be characterized by the presence of cricetids and large number of glirids (Rodentia); and (2) zone A would show the predominance of the Eomyidae (an extinct family of rodents) with genera *Ligerimys* and *Pseudotheridomys*. However, the zonal limit is difficult to identify both in the Catalayud–Teruel and the Ebro basins (Hernandez et al., 1987; Cuenca et al., 1993). The distribution of the significant taxa is shown in Fig. 3.

*Biostratigraphic location of the volcanoclastic layers*

Our first study of the ash layer (Canudo et al., 1993) used the information available from Hernandez et al. (1991) who located the corresponding beds within the Zuera Formation accepted to be Aragonian in age. According to Hernandez et al. (1991) the Zuera Formation is stratigraphically above the Calizas de Peñalba unit which contains a diagnostic 'pre-Ramblian' fauna including the eomyd *Ritteneria* (Cuenca et al., 1989). However, following our recent studies, the Calizas de Peñalba unit appears to be at the very bottom of the Zuera unit. In addition, the age of the ash has been documented with a newly discovered fauna in the Tardienta section (Fig. 2) and this new fauna is pre-Aragonian.

The fauna comes from a fluvial silt bed overlaying the ash bed in Tardienta. The age is considered Ramblian based on (1) the presence of the glirids *Peridyromys murinus* and *P. turbatus*, *Pseudodryomys ibericus* and *Quercomys daamsi*, and the lagomorph *Prolagus* aff. *vasconiensis fortis*, and (2) the absence of *Ritteneria* and cricetids. The

UPPER	STAGES		LOCAL BIONAZONATION	Rodent genera and species	Mammals of dominion	CRICETIDAE										GLIRIDAE										EOMYIDAE										SCIURIDAE										CASTORIADAE																																																																																																																																																																																																																																																																																																																																																																																																																																																																																																																																																																																																																																																																																																																																																																																																																																																																																																																																																																																																																																																																																																																																																																																																																																																																																																																																																																																																																																																																													
	VALLES	CONTINENTAL				LOCALITIES	1	2	3	4	5	6	7	8	9	10	11	12	13	14	15	16	17	18	19	20	21	22	23	24	25	26	27	28	29	30	31	32	33	34	35	36	37	38	39	40	41	42	43	44	45	46	47	48	49	50	51	52	53	54	55	56	57	58	59	60	61	62	63	64	65	66	67	68	69	70	71	72	73	74	75	76	77	78	79	80	81	82	83	84	85	86	87	88	89	90	91	92	93	94	95	96	97	98	99	100	101	102	103	104	105	106	107	108	109	110	111	112	113	114	115	116	117	118	119	120	121	122	123	124	125	126	127	128	129	130	131	132	133	134	135	136	137	138	139	140	141	142	143	144	145	146	147	148	149	150	151	152	153	154	155	156	157	158	159	160	161	162	163	164	165	166	167	168	169	170	171	172	173	174	175	176	177	178	179	180	181	182	183	184	185	186	187	188	189	190	191	192	193	194	195	196	197	198	199	200	201	202	203	204	205	206	207	208	209	210	211	212	213	214	215	216	217	218	219	220	221	222	223	224	225	226	227	228	229	230	231	232	233	234	235	236	237	238	239	240	241	242	243	244	245	246	247	248	249	250	251	252	253	254	255	256	257	258	259	260	261	262	263	264	265	266	267	268	269	270	271	272	273	274	275	276	277	278	279	280	281	282	283	284	285	286	287	288	289	290	291	292	293	294	295	296	297	298	299	300	301	302	303	304	305	306	307	308	309	310	311	312	313	314	315	316	317	318	319	320	321	322	323	324	325	326	327	328	329	330	331	332	333	334	335	336	337	338	339	340	341	342	343	344	345	346	347	348	349	350	351	352	353	354	355	356	357	358	359	360	361	362	363	364	365	366	367	368	369	370	371	372	373	374	375	376	377	378	379	380	381	382	383	384	385	386	387	388	389	390	391	392	393	394	395	396	397	398	399	400	401	402	403	404	405	406	407	408	409	410	411	412	413	414	415	416	417	418	419	420	421	422	423	424	425	426	427	428	429	430	431	432	433	434	435	436	437	438	439	440	441	442	443	444	445	446	447	448	449	450	451	452	453	454	455	456	457	458	459	460	461	462	463	464	465	466	467	468	469	470	471	472	473	474	475	476	477	478	479	480	481	482	483	484	485	486	487	488	489	490	491	492	493	494	495	496	497	498	499	500	501	502	503	504	505	506	507	508	509	510	511	512	513	514	515	516	517	518	519	520	521	522	523	524	525	526	527	528	529	530	531	532	533	534	535	536	537	538	539	540	541	542	543	544	545	546	547	548	549	550	551	552	553	554	555	556	557	558	559	560	561	562	563	564	565	566	567	568	569	570	571	572	573	574	575	576	577	578	579	580	581	582	583	584	585	586	587	588	589	590	591	592	593	594	595	596	597	598	599	600	601	602	603	604	605	606	607	608	609	610	611	612	613	614	615	616	617	618	619	620	621	622	623	624	625	626	627	628	629	630	631	632	633	634	635	636	637	638	639	640	641	642	643	644	645	646	647	648	649	650	651	652	653	654	655	656	657	658	659	660	661	662	663	664	665	666	667	668	669	670	671	672	673	674	675	676	677	678	679	680	681	682	683	684	685	686	687	688	689	690	691	692	693	694	695	696	697	698	699	700	701	702	703	704	705	706	707	708	709	710	711	712	713	714	715	716	717	718	719	720	721	722	723	724	725	726	727	728	729	730	731	732	733	734	735	736	737	738	739	740	741	742	743	744	745	746	747	748	749	750	751	752	753	754	755	756	757	758	759	760	761	762	763	764	765	766	767	768	769	770	771	772	773	774	775	776	777	778	779	780	781	782	783	784	785	786	787	788	789	790	791	792	793	794	795	796	797	798	799	800	801	802	803	804	805	806	807	808	809	810	811	812	813	814	815	816	817	818	819	820	821	822	823	824	825	826	827	828	829	830	831	832	833	834	835	836	837	838	839	840	841	842	843	844	845	846	847	848	849	850	851	852	853	854	855	856	857	858	859	860	861	862	863	864	865	866	867	868	869	870	871	872	873	874	875	876	877	878	879	880	881	882	883	884	885	886	887	888	889	890	891	892	893	894	895	896	897	898	899	900	901	902	903	904	905	906	907	908	909	910	911	912	913	914	915	916	917	918	919	920	921	922	923	924	925	926	927	928	929	930	931	932	933	934	935	936	937	938	939	940	941	942	943	944	945	946	947	948	949	950	951	952	953	954	955	956	957	958	959	960	961	962	963	964	965	966	967	968	969	970	971	972	973	974	975	976	977	978	979	980	981	982	983	984	985	986	987	988	989	990	991	992	993	994	995	996	997	998	999	1000	1001	1002	1003	1004	1005	1006	1007	1008	1009	1010	1011	1012	1013	1014	1015	1016	1017	1018	1019	1020	1021	1022	1023	1024	1025	1026	1027	1028	1029	1030	1031	1032	1033	1034	1035	1036	1037	1038	1039	1040	1041	1042	1043	1044	1045	1046	1047	1048	1049	1050	1051	1052	1053	1054	1055	1056	1057	1058	1059	1060	1061	1062	1063	1064	1065	1066	1067	1068	1069	1070	1071	1072	1073	1074	1075	1076	1077	1078	1079	1080	1081	1082	1083	1084	1085	1086	1087	1088	1089	1090	1091	1092	1093	1094	1095	1096	1097	1098	1099	1100	1101	1102	1103	1104	1105	1106	1107	1108	1109	1110	1111	1112	1113	1114	1115	1116	1117	1118	1119	1120	1121	1122	1123	1124	1125	1126	1127	1128	1129	1130	1131	1132	1133	1134	1135	1136	1137	1138	1139	1140	1141	1142	1143	1144	1145	1146	1147	1148	1149	1150	1151	1152	1153	1154	1155	1156	1157	1158	1159	1160	1161	1162	1163	1164	1165	1166	1167	1168	1169	1170	1171	1172	1173	1174	1175	1176	1177	1178	1179	1180	1181	1182	1183	1184	1185	1186	1187	1188	1189	1190	1191	1192	1193	1194	1195	1196	1197	1198	1199	1200	1201	1202	1203	1204	1205	1206	1207	1208	1209	1210	1211	1212	1213	1214	1215	1216	1217	1218	1219	1220	1221	1222	1223	1224	1225	1226	1227	1228	1229	1230	1231	1232	1233	1234	1235	1236	1237	1238	1239	1240	1241	1242	1243	1244	1245	1246	1247	1248	1249	1250	1251	1252	1253	1254	1255	1256	1257	1258	1259	1260	1261	1262	1263	1264	1265	1266	1267	1268	1269	1270	1271	1272	1273	1274	1275	1276	1277	1278	1279	1280	1281	1282	1283	1284	1285	1286	1287	1288	1289	1290	1291	1292	1293	1294	1295	1296	1297	1298	1299	1300	1301	1302	1303	1304	1305	1306	1307	1308	1309	1310	1311	1312	1313	1314	1315	1316	1317	1318	1319	1320	1321	1322	1323	1324	1325	1326	1327	1328	1329	1330	1331	1332	1333	1334	1335	1336	1337	1338	1339	1340	1341	1342	1343	1344	1345	1346	1347	1348	1349	1350	1351	1352	1353	1354	1355	1356	1357	1358	1359	1360	1361	1362	1363	1364	1365	1366	1367	1368	1369	1370	1371	1372	1373	1374	1375	1376	1377	1378	1379	1380	1381	1382	1383	1384	1385	1386	1387	1388	1389	1390	1391	1392	1393	1394	1395	1396	1397	1398	1399	1400	1401	1402	1403	1404	1405	1406	1407	1408	1409	1410	1411	1412	1413	1414	1415	1416	1417	1418	1419	1420	1421	1422	1423	1424	1425	1426	1427	1428	1429	1430	1431	1432	1433	1434	1435	1436	1437	1438	1439	1440	1441	1442	1443	1444	1445	1446	1447	1448	1449	1450	1451	1452	1453	1454	1455	1456	1457	1458	1459	1460	1461



glirids are the most abundant mammal group in the locality. They are usually considered poor for correlation (Alvarez-Sierra et al., 1990; Daams, 1990). Nevertheless, because other small mammals are scarce in the Ebro Basin (Cuenca et al., 1993), glirids are used in this study.

*Quercomys daamsi* represents a more primitive morphological stage compared to Ramblian representatives such as *Quercomys parsani*; this would suggest a pre-Ramblian age. The Tardienta fauna is almost identical to the close San Juan and La Galocha (1, 2, 3) faunas (Alvarez-Sierra et al., 1990). The San Juan fauna contains a tooth of *Rhodanomys* or *Ritteneria* which may be a vestigial form of the pre-Ramblian (Agenian) assemblage. For this reason, the authors included the San Juan locality in the Y2 mammal biozone. About 10 and 20 m above are the localities La Galocha 1 and La Galocha 2 and 3, respectively. Alvarez-Sierra et al. (1990) group the three localities within the same mammal zone (Y2 = MN2b) of the Agenian stage because they share *Peridyromys turbatus* which is also present in Tardienta. The lack of *Rhodanomys* or *Ritteneria* in Tardienta could be caused either by local ecological or by regional biostratigraphical factors. In short, Tardienta should be included in biozone Y2 based on glirid assemblage, or in the Z zone (Ramblian) based on the absence of *Ritteneria* and cricetids.

Lagomorpha could be very useful for local correlation; unfortunately, the material collected from Tardienta is poor. Nevertheless, the taxon identified is closer to *Prolagus vasconiensis fortis* from San Juan and La Galocha than to any other *Prolagus* species. The reference level of Mein's zone MN2a in Spain is Cetina de Aragón (Zaragoza, Duero Basin; Mein, 1989) which contains *Ritteneria molinae* (Alvarez-Sierra, 1990) and *Quercomys bijmai* (Daams, 1990) among other rodents. They represent more primitive morphological stages than *Ritteneria manca* and *Quercomys daamsi*, respectively. The reference level for Mein's zone MN2b in Spain is Navarrete del Rio in the Catalayud-Teruel Basin. It contains no *Ritteneria* nor *Rhodanomys* being thus a Ramblian locality and no hypsodont glirids as *Quercomys*. In the correlative Ramblar 1 locality, *Quercomys parsani* is the hypsodont glirid present according to Daams (1990).

In summary, the presently known constraints allow us to place the Tardienta locality either in mammal biozone Y2 or in biozone Z and the immediately underlying ash layer is at the limit Agenian/Ramblian or at the very bottom of the Ramblian.

## GEOCHRONOLOGY

### *Petrography and mineralogy of the geochronometers*

Study of the ash layer was undertaken using microscopy, microchemistry (microprobe), and X-ray diffraction. The layer shows sporadic clinopyroxene (0.01 to 1.0 mm) and abundant sanidine and plagioclase as the main crystallized phases. The chemical composition of clinopyroxene (between  $\text{En}_{42.5} \text{Wo}_{44} \text{Fs}_{13.5}$  and  $\text{En}_{16.5} \text{Wo}_{40.5} \text{Fs}_{43}$ ) suggests a tholeiitic affinity. Plagioclase composition is near the anorthite end member. These minerals have a planar orientation and follow continuous levels with respect to the partly devitrified matrix. SEM analysis of pyroxene and feldspars shows fragmentation structures. Zircon and apatite crystals are present, idiomorphic (Fig. 4) but scarce in Tardienta. X-ray diffraction of the matrix shows the presence of analcime, rodocrosite (?) and clay minerals: corrensite, illite, smectite, and saponite. Two samples

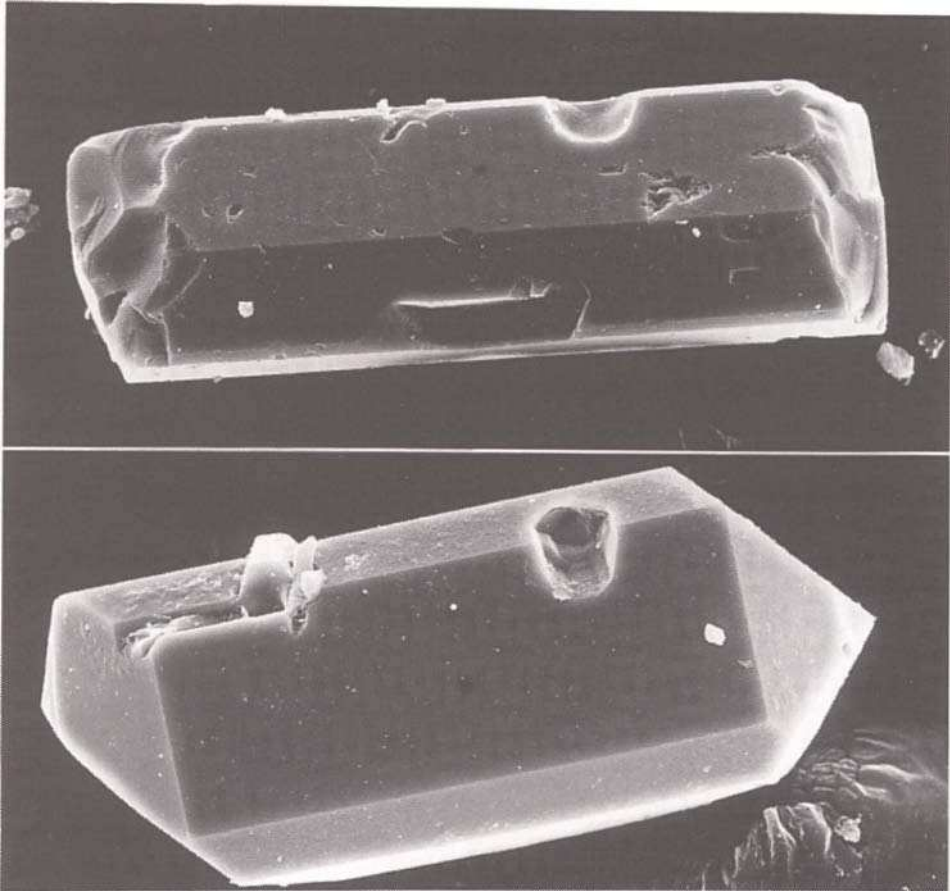


Fig. 4. Scanning electron microscopic views of idiomorphic pyroclastic heavy minerals; apatite crystal (top, length is 200  $\mu\text{m}$ ) and zircon crystal (bottom, length is 140  $\mu\text{m}$ ) (pictures: Dto Ciencias de la Tierra, Zaragoza).

collected from Lanaja (T157) and Peñalba (T172) were used for separation of datable minerals.

The Lanaja sample is pink in colour, and binocular microscope examination shows essentially white milky minerals, some transparent, and common oxy-hydroxides which give the colour to the rock. The sample was treated following the usual procedure for separation of pyroclastic components using washing, sieving, magnetic fractionation, and heavy liquids (bromoform, mixtures bromoform–acetone, methylene iodide).

The single magnetic mineral observed is bottle-green, transparent pyroxene (about 1% versus whole-rock = /WR). The non-magnetic fraction includes feldspar (about 3% /WR) and quartz including common bipyramidal idiomorphic crystals. Apatite is rare and pink zircon crystals (>0.05% /WR) are short, 0.15 to 0.3 mm long, idiomorphic, commonly poorly shaped, and contain black inclusions. The array of pyroclastic minerals confirms the volcanic origin of the sample.

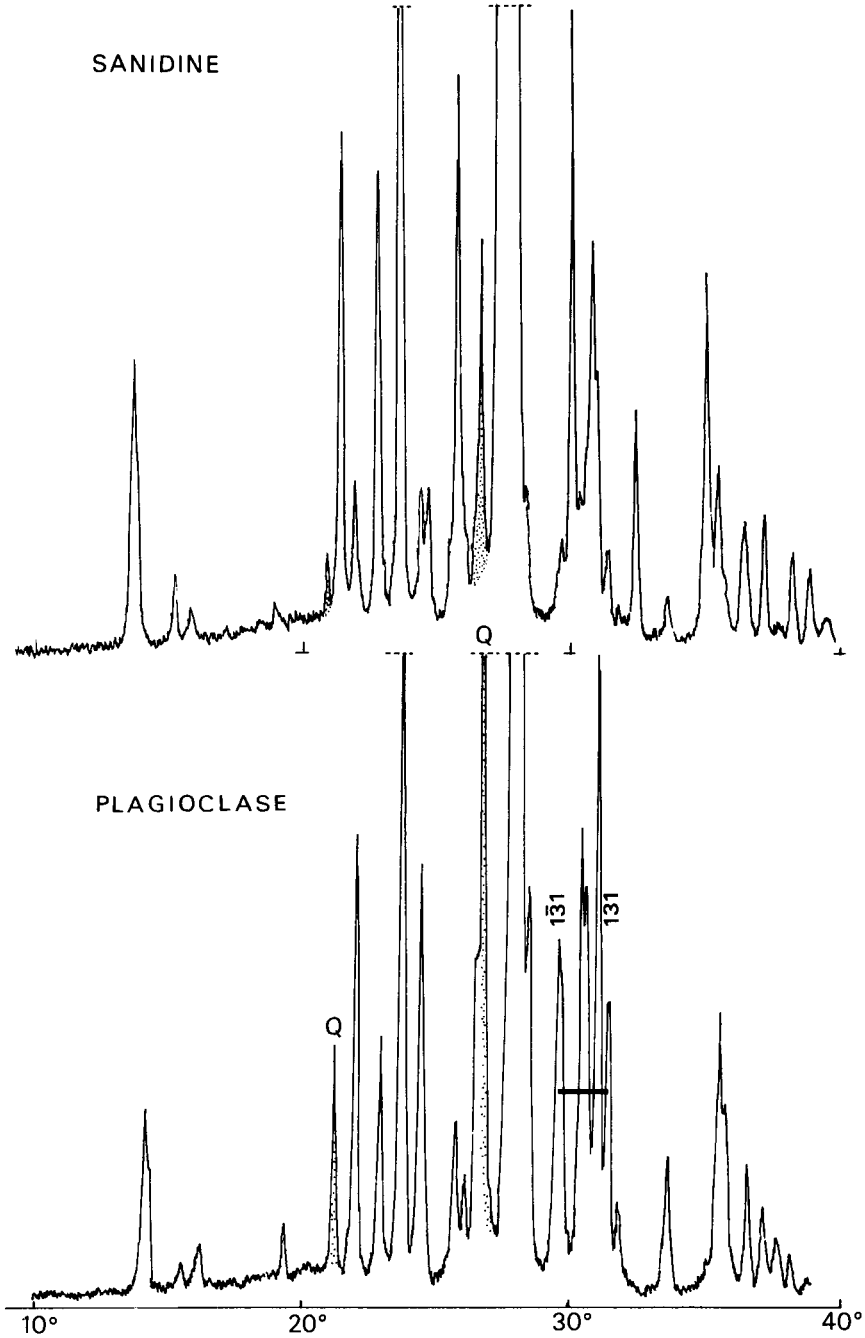


Fig. 5. X-ray diffraction patterns of the feldspars separated from the Lanaja volcanoclastic sample. The interval (1 $\bar{3}$ 1)–(131) is emphasized; quartz (Q) is present. Diagrams obtained in the Laboratoire de Géologie of the Muséum National d'Histoire Naturelle, Paris using K $\alpha$  Cu ray; abscissa units are in  $^{\circ}2\theta$ ).

X-ray diffraction allowed recognition of two different feldspars (admixed with a small proportion of quartz): a denser calcic plagioclase with a peak interval (131) (131) of  $1.85^\circ$  ( $2\theta$ ) and a lighter sanidine (Fig. 5). The fractions were cleaned using 10% hydrochloric acid during 1 h and purified by hand-picking for selection of the clear (non-milky) crystals.

A similar study has been undertaken for the sample from Peñalba (T172). In contrast to the Lanaja sample, mica flakes are present in Peñalba, commonly idiomorphic in shape but altered with brown, green and white crystals mixed. Amphibole (?) is also present (small 0.1 mm long, brown to smoked glass needles). Heavy minerals include both idiomorphic (commonly 0.08 mm and up to 0.25 mm long, short to elongated crystals) and slightly rounded zircon crystals; apatite is uncommon. The light non-magnetic fraction comprises quartz and probable feldspar crystals which are milky to white. The sample was not considered suitable for  $^{40}\text{Ar}/^{39}\text{Ar}$  dating. Considering the two distinct assemblages in preserved pyroclastic minerals in the two samples in Peñalba and Lanaja, they cannot be shown to correspond to a single volcanic event.

*$^{40}\text{Ar}/^{39}\text{Ar}$  isotopic analyses*

The purest sanidine fraction was used for irradiation (Triga reactor in Denver) and  $^{40}\text{Ar}/^{39}\text{Ar}$  dating using the HD-B1 biotite as the monitor. The sanidine was first heated under vacuum at  $550^\circ\text{C}$  for 20 min. Thirteen heating steps were then measured on 125 mg of purified mineral with large quantities of gas available for each step; splits 4 to 60 times smaller than the extracted gas were measured. The analytical results are shown in Table 2.

The integrated total fusion age is 19.36 Ma. The spectrum in Fig. 6 is essentially undisturbed with very precise apparent ages. Seven successive steps representing 91.8% of the gas released define a plateau with the criterion that the independently calculated ages for each step are not different at the 95% confidence level. The calculated weighted

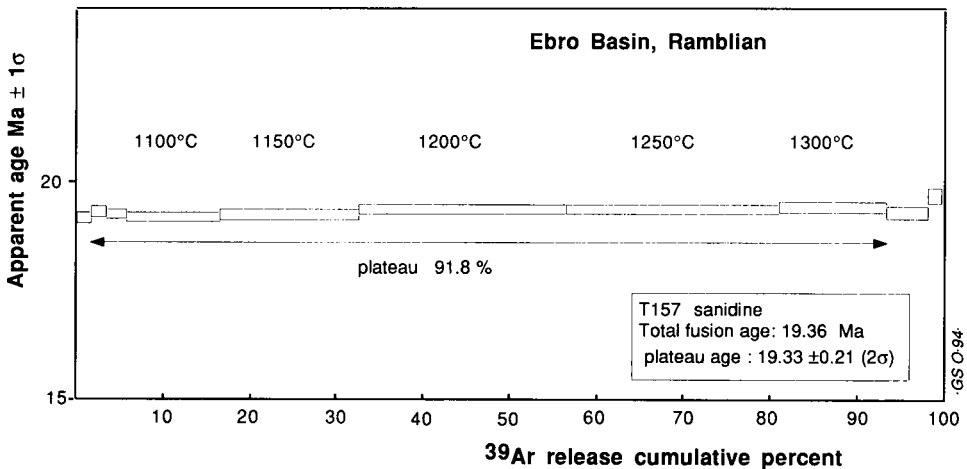


Fig. 6. Spectrum of argon release from sanidine T157 from Lanaja.

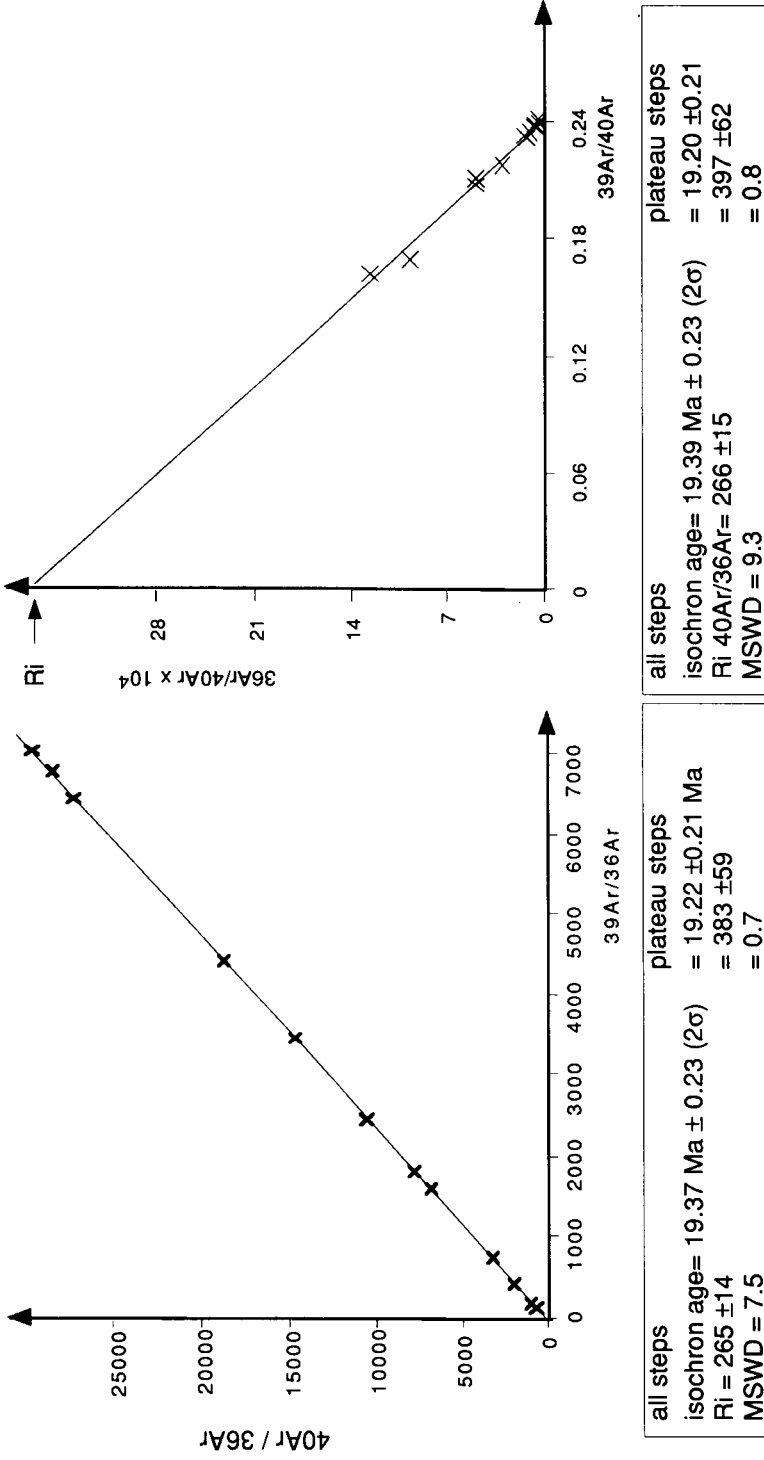


Fig. 7. Isochron plots of the step-heating results from sanidine T157 from Lanaja.

Table 2

Results of the <sup>40</sup>Ar/<sup>39</sup>Ar incremental heating measurements on sanidine from Lanaja

°C	Apparent age Ma	±2σ	% <sup>39</sup> Ar	% Rad.	K/Ca	
650	18.11	0.28	0.1	63	1.4	
800	18.80	0.24	0.3	85	1.3	
950	19.19	0.22	1.7	96	1.4	
1000	19.34	0.22	1.8	99	1.8	
1050	19.28	0.22	2.2	99	2.3	
1100	19.19	0.22	10.5	99	3.0	
1150	19.28	0.22	16.2	98	3.2	
1200	19.37	0.22	24.0	98	5.5	
1250	19.38	0.22	24.5	97	6.0	
1300	19.46	0.22	12.6	96	5.3	
1375	19.52	0.24	4.6	91	4.4	
1450	19.34	0.24	1.3	85	2.5	
1600	19.69	0.28	0.2	71	4.4	

°C	40*	39	38	37	36	40/39
650	732.4 ± 1.5	117.9 ± 0.1	2.059 ± 0.005	42.49 ± 0.28	0.936 ± 0.05	3.887 ± 0.02
800	283.4 ± 0.6	59.64 ± 0.12	0.883 ± 0.002	21.68 ± 0.08	0.149 ± 0.002	4.037 ± 0.02
950	6426 ± 13	1490 ± 3	20.79 ± 0.04	521.5 ± 1.0	1.074 ± 0.005	4.122 ± 0.01
1000	6243 ± 12	1485 ± 3	20.06 ± 0.04	403.9 ± 0.8	0.337 ± 0.005	4.153 ± 0.01
1050	7667 ± 15	1831 ± 4	24.44 ± 0.05	385.0 ± 0.8	0.361 ± 0.005	4.141 ± 0.01
1100	171400 ± 300	41100 ± 100	544.8 ± 1.1	6659 ± 13	7.81 ± 0.03	4.122 ± 0.01
1150	988200 ± 2000	234600 ± 500	3196 ± 6	35480 ± 70	62.35 ± 0.12	4.141 ± 0.01
1200	1479500 ± 3000	347900 ± 700	4697 ± 9	30730 ± 60	109.4 ± 0.2	4.161 ± 0.01
1250	1520400 ± 3000	354600 ± 700	4778 ± 10	28750 ± 60	152.4 ± 0.3	4.162 ± 0.01
1300	791600 ± 1600	181900 ± 400	2490 ± 5	16720 ± 30	106.3 ± 0.2	4.180 ± 0.01
1375	82500 ± 165	17910 ± 40	250.5 ± 0.5	2532 ± 5	25.45 ± 0.05	4.192 ± 0.01
1450	25220 ± 50	5170 ± 10	78.12 ± 0.16	995.5 ± 2.0	12.84 ± 0.03	4.153 ± 0.01
1600	220.2 ± 0.4	36.98 ± 0.07	0.596 ± 0.001	4.14 ± 0.08	0.216 ± 0.002	4.230 ± 0.02

HD-B1 = 24.21 Ma; error on J curve = 0.5%; T (total fusion age): 19.36 (± 0.21) Ma; (plateau age 1000–1300°C): 19.33 ± 0.21 Ma. J = 0.00259; 40/39 = <sup>40</sup>Ar radiogenic/<sup>39</sup>ArK; gas in 10<sup>-15</sup> moles; analytical precision 1σ in lower table. Sample weight: 125 mg. (Analytical data G.S.O. in Lausanne.)

mean plateau age is 19.33 ± 0.21 Ma (2σ intralaboratory analytical uncertainty). The plateau age is similar to the total age; this is a priori an excellent age result which is both precise and well qualified by the obtained spectrum.

The isochron plots of the step-heating analytical results were then calculated. If one uses the seven steps forming the plateau, the <sup>40</sup>Ar/<sup>36</sup>Ar versus <sup>39</sup>Ar/<sup>36</sup>Ar plot gives an apparent age at 19.22 ± 0.21 Ma with an excellent mean standard weighted deviation (MSWD) of 0.7 and an initial <sup>40</sup>Ar/<sup>36</sup>Ar ratio at 383 ± 59; the <sup>36</sup>Ar/<sup>40</sup>Ar versus <sup>39</sup>Ar/<sup>40</sup>Ar plot gives similar results with an apparent age at 19.20 ± 0.21 Ma, a MSWD of 0.8, and an initial ratio at 397 ± 62 apparently higher than the atmospheric ratio. However, the isochron plot of all steps (see Fig. 7) would suggest a ratio smaller than atmospheric and it is assumed that the information given by the isochron plots is not significant from this point of view.

## DISCUSSION AND CONCLUSIONS

The peculiar layer recently discovered in several localities in the Ebro Basin is purely volcanic in origin in Lanaja and probably in other sections too. This is shown in the field and the laboratory by the sedimentologic and petrographic characteristics; the variety of pyroclastic minerals and their shape also confirm the volcanic origin following air transport in Lanaja.

The biostratigraphic age has been improved during the study from mid-Aragonian to earliest Ramblian or pre-Ramblian following discovery of a new site for mammal fauna in a section presumably time-equivalent to the one dated (see Table 1).

Geologically, the apparent age measured is most probably connected to the time of crystallization of the sanidine at the time of eruption of the volcanic material. As discussed above, the purely volcanoclastic nature of the layer which results from aerial transport of the erupted material and sub synchronous deposition indicates that the age of the sanidine is reasonably similar to that of the deposition.

The age at  $19.3 \pm 0.2$  Ma may be compared directly to the other ages obtained in this volume using the same reference material. For use by comparison to external data, the intralaboratory analytical error bar must be combined with the error on the known age of the monitor ( $\pm 2.5\%$  of the age,  $2\sigma$ ) which should be propagated to the analytical age in order to derive a realistic geological age of  $19.3 \pm 0.7$  Ma.

This age corresponds to a moment within the first quarter of the Burdigalian global stage and may be used for connection between the continental and marine chronostratigraphic scales.

The Aragonian continental stage is sometimes shown as Middle Miocene in age in the Spanish literature. In terms of Ma, this would correspond to an interval between 16 and 11 Ma. However, Hernandez et al. (1991), among others, locate the Zuera Formation in the Early Miocene; Steininger et al. (1985) show the Aragonian in correspondence to the entire Burdigalian to Serravallian Stage interval which would correspond to the interval between about 20.5 Ma and 11 Ma. Introduction of the Ramblian has modified this picture in Steininger et al. (1989).

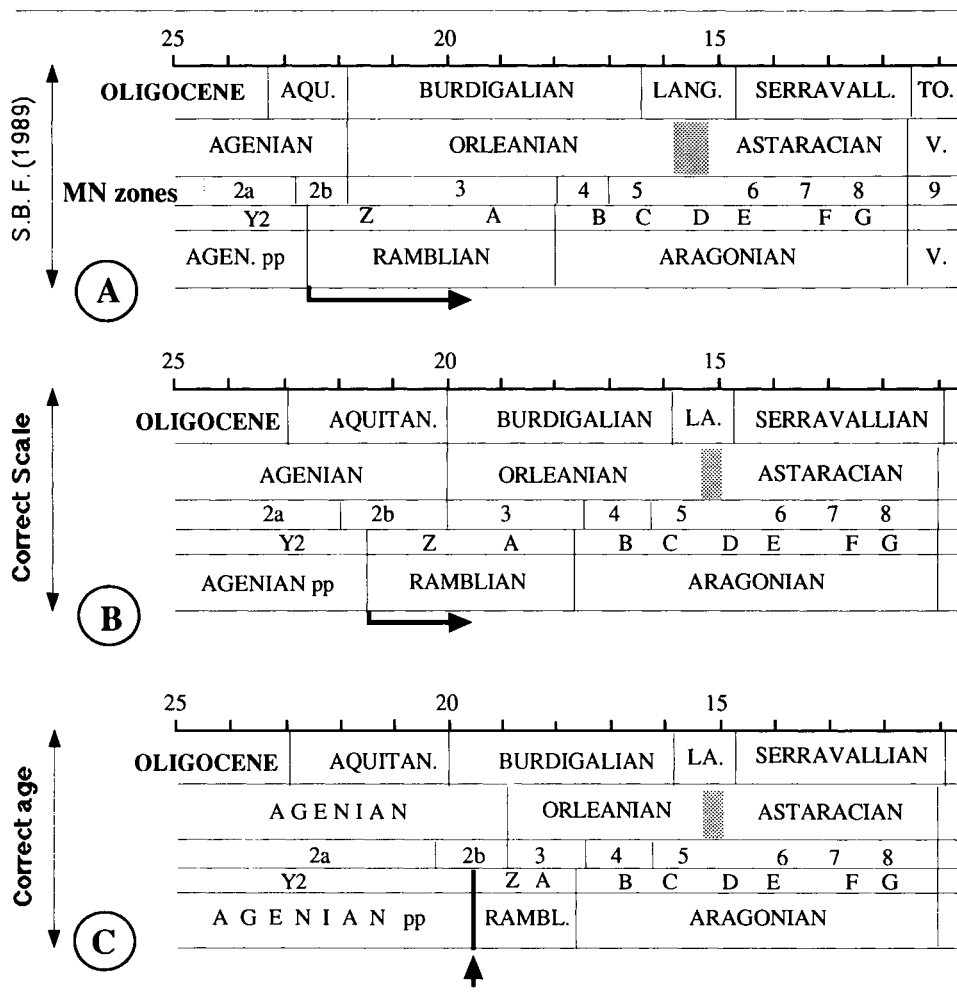
The present study reports data documenting the isotopic age of a level which is not Aragonian in age, as originally accepted, but practically coincident with the Ramblian/Agenian limit of the Ebro Basin (= within Mein's zone MN2b, = somewhere within local mammal zonal units Y2–Z). According to evolutionary criteria, the entire regional Ramblian 'stage' would comprise only a small interval of time (local zonal units Z + A or a portion of Mein's mammal zone MN2b). Compared to the Aragonian, this would probably represent about 1 Ma. The brevity of this interval may lead to question the necessity to create a 'stage' which is not (or difficult to be) subdivided on the basis of faunal units.

The age of 19.3 Ma obtained in the present study suggests the pre-Ramblian/Ramblian limit about 0.5 Ma above the base of the Burdigalian. We have shown in Table 3 the influence of our new result on the previously proposed relations between chronostratigraphic units. In Table 3A, we show the proposal by Steininger et al. (1989). However, the numerical scale used by these authors is not correct as far as marine stages are concerned.

As a first improvement, we have redrawn the columns keeping unchanged the

Table 3

Time relation between chronostratigraphic and biostratigraphic units around the Ramblian Spanish mammal stage



A) Scale proposed by Steininger et al. (1989); B) Scale A kept unchanged but for application of a better numerical scale to the marine Stages; C) Scale B improved to agree with an age of about 19.3 Ma for the basal boundary of the Ramblian stage. Note that Agenian stage does not go into the Oligocene (S. Sen: personal communication)

relations between marine and continental units but using an up-to-date numerical scale (see Odin and Odin, 1990; Odin 1994). Proposal B is obtained; it is still inconsistent with our new geochronological study. In a second improvement, we have thus drawn a third proposal (Table 3C) by disconnecting the relationship between the continental units and the marine stage column. Relations within the continental units are kept unchanged because these units are interrelated by their comparable faunas, and thus the relations



are assumed to be correct. Compared to the initial scheme, the final picture shows: (1) a short 'Ramblian' unit; (2) MN zones of quite comparable apparent durations; (3) an Agenien/Orléanien boundary about 3 Ma younger than supposed before. The validity of these conclusions depends on the three hypotheses done (i) in changing the direct relation between time and continental units assumed to be poorly known; (ii) in changing the geometric relation between marine and continental units also known to be uncertain; and (iii) in accepting that the correct relation between Spanish and European MN faunal zones is known.

With our new geochronological results, we have established with an acceptable reliability that the base of the Ramblian unit in the Tertiary Ebro Basin, is located near and slightly younger than the Aquitanian/Burdigalian global stage boundary.

#### SOMMAIRE — BIOSTRATIGRAPHIE ET GÉOCHRONOLOGIE D'UN NIVEAU VOLCANOCLASTIQUE MIOCÈNE DU BASSIN CONTINENTAL DE L'ÈBRE, ESPAGNE

(Manuscrit soumis: Décembre 1993; révisé: Décembre 1994; rédacteur responsable: GSO)

Le Bassin tertiaire de L'Èbre est un grand bassin montrant une succession fossilifère continentale. Un niveau volcanoclastique a été découvert, caractérisé et repéré dans plusieurs sections ainsi qu'une faune de Mammifères très proche. Ce niveau correspondrait à un horizon voisin de la limite entre les étages continentaux Agenien et Ramblien. Grâce à la présence, notamment, de sanidine en excellent état d'après les analyses minéralogiques, la datation isotopique a été réalisée par la technique  $^{39}\text{Ar}/^{40}\text{Ar}$  et chauffage par paliers. Le spectre d'âge obtenu révèle un plateau très bien individualisé dont l'âge de  $19, 36 \pm 0, 21$  (incertitude analytique interne,  $2\sigma$ ) Ma est identique à l'âge total et aux âges déduits des isochrones.

Cet âge permet de revoir et de modifier de façon appréciable, les corrélations entre la succession des unités biostratigraphiques continentales vis à vis de l'échelle chronostratigraphique. D'après cette datation directe, la base de l'«étage» Ramblien se situerait dans le Burdigalien inférieur et cette unité ramblienne serait très courte.

(Sommaire des auteurs)

#### ACKNOWLEDGEMENTS

Preliminary steps of mineral separation were undertaken by A. Amorosi (Univ. Bologna and Univ. P. & M. Curie, Paris) as part of his thesis. S. Sen (Muséum, Paris) is thanked for his comment on this paper. Isotopic measurements for this study by G.S. Odin were achieved thanks to facilities made available by the Fonds National Suisse in Lausanne and permission of the responsible of the University. X-ray diffraction analyses were achieved in the Laboratoire de Géologie du Muséum, Paris. Field and palaeontological studies were partially supported by the Spanish DGCYT Project No. PB 92-0013. No funding was provided by French Organizations for this research.

**Part D**

**STUDIES RELEVANT TO THE MIDDLE MIOCENE SUBSERIES**

This Page Intentionally Left Blank

*Introduction to Part D*

## **INTRODUCTION: THE MIDDLE MIOCENE**

A. Montanari and R. Coccioni

During the Middle Miocene (Langhian and Serravallian), the Alpine–Himalayan orogenesis reached its paroxysmic phase while the Tethyan Ocean approached its definitive closure. This major tectonic event deeply affected the world palaeoclimate and ecology with important repercussions on regional biological rearrangements in both marine and terrestrial environments. On the other hand, this widespread tectonism caused interruption of pelagic sedimentation in most of the epeiric and oceanic basins throughout the Tethyan domain, and the onset of copious synorogenic detrital sedimentation (i.e., flysch and molasse) in tectonically active foredeep basins. For these reasons, continuous and complete pelagic sequences covering the Middle Miocene, and potentially suitable for detailed integrated stratigraphic studies, are rare throughout the Tethyan domain.

Rare cases of open sea, essentially hemipelagic mid-Miocene basins are found in the external (eastern) foothills of the northern Apennines which were involved in the northeasterly migrating orogenic deformation only in the Pliocene. A well-exposed, continuous section located near the village of Moria, in the northwestern Marche region, contains all the essential qualities for high-resolution integrated stratigraphic studies throughout the upper Burdigalian and lower Langhian (Deino et al., Chapter D1). Three volcanic ashes have been dated in this section yielding very precise  $^{40}\text{Ar}/^{39}\text{Ar}$  plateau ages of 17.1 Ma (biotite), 16.2 Ma (sanidine), and 15.5 Ma (sanidine), respectively. The upper two dates bracket the Burdigalian/Langhian boundary identified on the basis of the first occurrence (FO) of *Praeorbulina glomerosa sicana*, here recognized within magnetic Chron 5Br. The tightly interpolated radioisotopic age for this event is 15.9 Ma. The planktonic foraminiferal biostratigraphy is also integrated with a detailed calcareous nannofossil biozonation. Trace elements chemostratigraphic analyses exhibit significant excursions of Mg, Fe, Sr and Mn just prior to, or at the Burdigalian/Langhian boundary, coinciding also with a considerable negative shift of the  $\delta^{18}\text{O}$ . Strontium isotope analyses on fish teeth indicate a monotonic increase of the  $^{87}\text{Sr}/^{86}\text{Sr}$  values throughout the Moria section. However, the isotopic ratios in this section are significantly lower than ratios measured in coeval oceanic carbonates outside the Mediterranean domain. This may indicate that during the Middle Miocene, the proto-Mediterranean had already a limited water exchange with the rest of the world's oceans. If confirmed in other sections, this differentiation will command caution in using geochemical criteria for correlating mid-Miocene Tethyan sequences with oceanic ones.

In the northeastern Apennines, Langhian sections potentially suitable for detailed integrated stratigraphic analyses are found near Apiro (about 50 km southeast of Moria; see Montanari et al., Chapter D2), and in the Cònero Riviera near Ancona. The latter exhibits a continuous hemipelagic sequence from the upper Langhian to the lower Messinian, and is described by Montanari et al. in Chapter E1. A strong potential

for integrated stratigraphy is found in central Sicily where a Serravallian section is well calibrated with planktonic foraminiferal biostratigraphy, and contains a biotite-rich volcanoclastic layer which yielded a  $^{40}\text{Ar}/^{39}\text{Ar}$  age of 13.5 Ma (Odin et al., Chapter D3).

Widespread volcanism in the Betic Cordilleras produced abundant volcanoclastic material which is preserved in Langhian to upper Tortonian marine sequences throughout southeastern Spain (Montenat et al., Chapter D4). This Spanish situation certainly bears a strong potential for high-resolution integrated stratigraphy of the Miocene Epoch and encourages further detailed interdisciplinary studies.

A particularly promising situation for detailed integrated stratigraphic studies outside the Tethyan domain is found in Japan. Serravallian sections containing well-preserved calcareous (Foraminifera and nannofossils), and siliceous (Radiolaria and diatoms) planktonic microfossils are located in central Japan, and promote detailed studies for biostratigraphic intercorrelation among these fossils groups (Takahashi and Oda, Chapter D5). Moreover, the mid-Miocene Japanese sections contain volcanic tuffs which yielded preliminary fission-track ages from zircon ranging from 13 to 12 Ma, and a biotite K/Ar age of 11.6 Ma, with analytical uncertainties as large as 1.5 Ma. More precise K/Ar and  $^{40}\text{Ar}/^{39}\text{Ar}$  ages were obtained by Takahashi and Saito (Chapter D6) from two key tuff beds which bracket the N13/N14 foraminiferal zonal boundary marked by the FO of *Globigerina nepenthes*. Additional  $^{40}\text{Ar}/^{39}\text{Ar}$  dates from biotite and sanidine in the upper tuff key bed were obtained by Odin et al. (Chapter D7) allowing a precise age estimate of  $11.76 \pm 0.1$  Ma for the FO of *G. nepenthes*. An equally precise  $^{40}\text{Ar}/^{39}\text{Ar}$  plateau age of 11.48 Ma from volcanoclastic biotite in the Cònero Riviera section leads to an age estimate of 11.3 Ma for the same foraminiferal event. Thus, the integrated stratigraphic study by Odin and co-workers reveals a slight diachronism for the FO of *G. nepenthes* between Japan and Italy. Nevertheless, on the basis of these precise geochronologic data, an age between 11.0 and 11.5 Ma can be estimated for the Serravallian/Tortonian boundary which shortly postdates the FO of *G. nepenthes*.

*Chapter D1*

**INTEGRATED STRATIGRAPHY OF THE UPPER BURDIGALIAN–LOWER LANGHIAN SECTION AT MORIA (MARCHE REGION, ITALY)**

A. Deino, J. Channell, R. Coccioni, G. De Grandis, D.J. DePaolo, E. Fornaciari, L. Emmanuel, M.A. Laurenzi, A. Montanari, D. Rio and M. Renard

**INTRODUCTION**

The 100 m thick Moria section (coordinates: 43°30'13.9"N; 12°35'39.1"E of Greenwich) is exposed along a mountain road between the villages of Palcano and Moria (Pontedazzo exit of the State Highway No. 3, near Cantiano), on the west side of Monte Petrano, in the Marche region of Italy (Fig. 1). This section exposes in continuity the transition between the Bisciario Formation and the overlying Schlier Formation, as well as the stratigraphic interval containing the Burdigalian/Langhian boundary. Moreover, several intercalations of volcanoclastic horizons permit direct radioisotopic age calibration of relevant biostratigraphic, magneto-stratigraphic, and chemostratigraphic events. Thus, the Moria section represents an advantageous circumstance for the comprehensive definition of the Lower/Upper Miocene boundary in a representative Tethyan pelagic facies.

**LITHOSTRATIGRAPHY**

The top part of the Bisciario Formation is exposed in the lower 20 m of the Moria section. The formation is characterized in the lower half of this interval by the greyish-beige 'siliceous–calcareous–tuffitic member', which is overlain by the 'upper marly member' (Guerrera, 1977; Morandi and Tateo, 1992). The siliceous component of these foraminiferal and nannofossil-rich marls and marly limestones is mainly of biogenic origin (i.e., radiolarians and diatoms), although diagenesis has transformed the original opal-CT to microcrystalline quartz (Morandi and Tateo, 1992). The lesser competence of the soft marls is due to a relatively lower concentration of biogenic silica compared to the indurated siliceous–calcareous marls, and to a higher content of clay minerals mostly represented by smectite with minor illite and chlorite components (Morandi and Tateo, 1992).

The lithology of the upper marly member of the Bisciario Formation and the overlying lower marly member of the Schlier Formation are virtually identical and characterized by soft grey–blue marls. Nevertheless, Coccioni and Montanari (1992) describe a conspicuous biotite-rich volcanoclastic clay layer located about 4 m above the uppermost hard marl of the Bisciario Formation (at 19.6 m). A similar layer has been recognized in several other sections in the region, and precisely located in the lower part of Zone N7 of Blow (1969) or the *Globigerinoides trilobus* Zone of Iaccarino and Salvatorini (1982) and Iaccarino (1985). Because this layer is easily recognizable in the

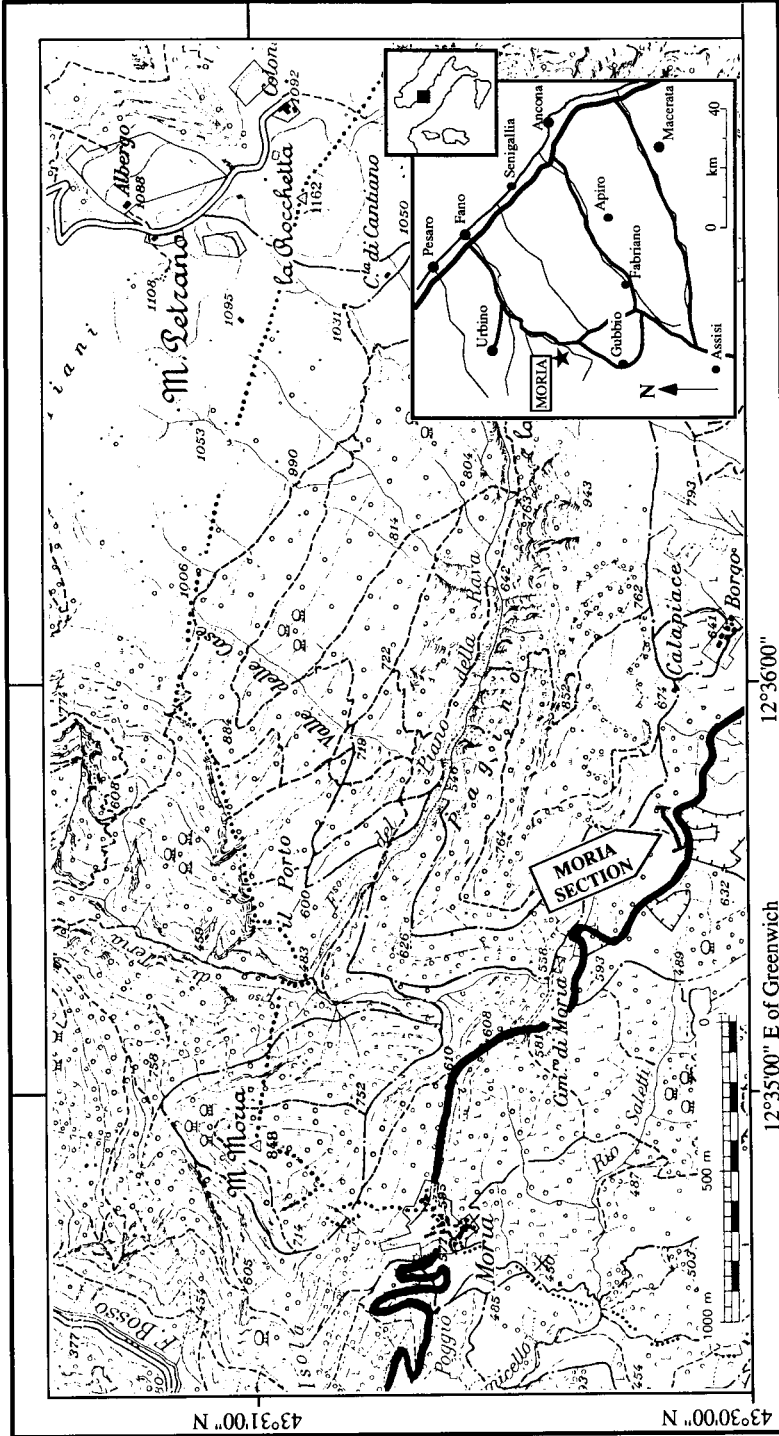


Fig. 1. Location map of the Moria section.

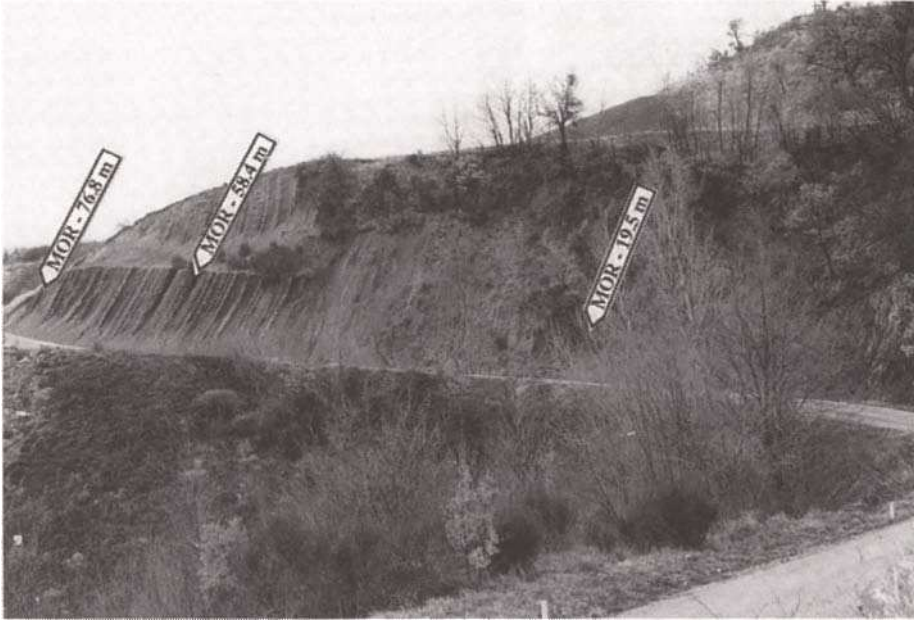


Fig. 2. Panoramic view of the Moria section, and location of the dated volcaniclastic layers.

field throughout the region, Coccioni and Montanari (1992) proposed it as the lithologic marker for the definition of the Bisciaro/Schlier boundary, and named it the 'Livello Piero della Francesca'.

The Schlier Formation at Moria is characterized by a 40 m thick middle member (from 48 m to 88 m) of alternating siliceous–calcareous marly limestones and soft marls (Fig. 2). This interval also contains several biotite-free bentonitic layers, and is therefore similar to the middle member of the underlying Bisciaro Formation. As in the Bisciaro, this well bedded and indurated member is sandwiched between marly members. Morandi and Tateo (1992) found variable amounts of quartz (~10%), plagioclase, biogenic carbonate, diagenetic gypsum, traces of heavy minerals, and in one case zeolite in these volcaniclastic beds which are primarily smectite (up to 85% of the bulk rock) derived from diagenetic alteration of volcanic glass. Unlike the bentonites and cinerites of the underlying Bisciaro Formation, sanidine is present in small amounts in the volcaniclastic layers of the Schlier Formation. Montanari et al. (1994) and Assorgia et al. (1994) have inferred western Sardinia as the volcanic source for the tephra in the Bisciaro and Schlier of the Umbria–Marche Apennines on the basis of a general eastward decrease of the grain size of the felsic fraction contained in these distal volcaniclastic layers, and a geochemical affinity between the Schlier biotites and those found in the Lower to Mid-Miocene ignimbrites of Bosa (mid-western Sardinia).



## BIOSTRATIGRAPHY

### *Planktonic Foraminifera (R. Coccioni)*

A total of 188 samples were analyzed using mainly washed residues (grain-size fraction  $>63 \mu\text{m}$ ), and occasionally thin-sections. Most of the samples contain very abundant and well diversified assemblages. Preservation varies from sample to sample, from good to very poor, the planktonic foraminiferal tests being better preserved in the Schlier than in the Bisciario. Samples with a high volcanogenic component usually contain scarce and poorly preserved foraminiferal assemblages. Volcaniclastic layers are almost barren of Foraminifera.

The generic and specific concepts of Bolli and Saunders (1985), Iaccarino (1985), Loeblich and Tappan (1988), and Spezzaferri (1994) were largely adopted. All the biohorizons utilized in the standard zonation of Blow (1969) were recognized as well as all the events useful for the Lower–Middle Miocene in the Mediterranean zonal models of Iaccarino and Salvatorini (1982) and Iaccarino (1985). According to the biozonation of Blow (1969), it was possible to recognize three zones whereas in terms of the Iaccarino and Salvatorini (1982) and Iaccarino (1985) zonal model three zones and two subzones were identified (Fig. 3).

The first significant event is the last occurrence (LO) of *Catapsydrax dissimilis* at m 4.24 which defines the N6/N7 zonal boundary of Blow (1969) and the boundary between the *G. dehiscens dehiscens*–*C. dissimilis* and the *G. trilobus* zones of Iaccarino and Salvatorini (1982) and Iaccarino (1985). The first occurrences (FOs) of *Globorotalia praescitula* and *Globigerinoides bisphericus* are found at m 7.52 and m 14, respectively. In agreement with Iaccarino and Salvatorini (1982) and Iaccarino (1985), this succession of events takes place close to the lower part of the *Globigerinoides trilobus* Zone. *Praeorbulina glomerosa sicana* first occurs at m 66.2 defining the lower boundary of the *P. glomerosa* s.l. Zone of Iaccarino and Salvatorini (1982) and Iaccarino (1985) and, practically, the N7/N8 zonal boundary of Blow (1969). According to Rio et al. (Chapter A5), the first evolutionary appearance of *P. glomerosa* s.l. is considered as a marker for the recognition of the Burdigalian/Langhian boundary which, in agreement with the historical stratotype, should be located slightly above this bio-event (see Odin et al. Chapter F2). The FO of *P. glomerosa sicana* is followed by the FOs of *P. glomerosa curva*, *P. glomerosa glomerosa*, and *P. glomerosa circularis* which, respectively, take place at m 71.69, m 79.8, and m 94, within the *P. glomerosa* s.l. Zone of Iaccarino and Salvatorini (1982) and Iaccarino (1985), and the N8 Zone of Blow (1969).

### *Calcareous nannofossils (E. Fornaciari and D. Rio)*

The calcareous nannofossil biostratigraphic analysis on the Moria section was carried out on 115 samples by polarizing light microscopy in smear slides. Calcareous nannofossils are common to abundant but show a moderate to poor preservation state. Only seven samples (mainly from volcanoclastic intervals) are barren. The taxonomic concepts adopted herein are after Perch-Nielsen (1985), Rio et al. (1990a) and Fornaciari et al. (1990).

The calcareous nannofossil assemblages are dominated by placoliths (*Reticulofen-*

# Moria Section

## Planktonic foraminiferal biostratigraphy

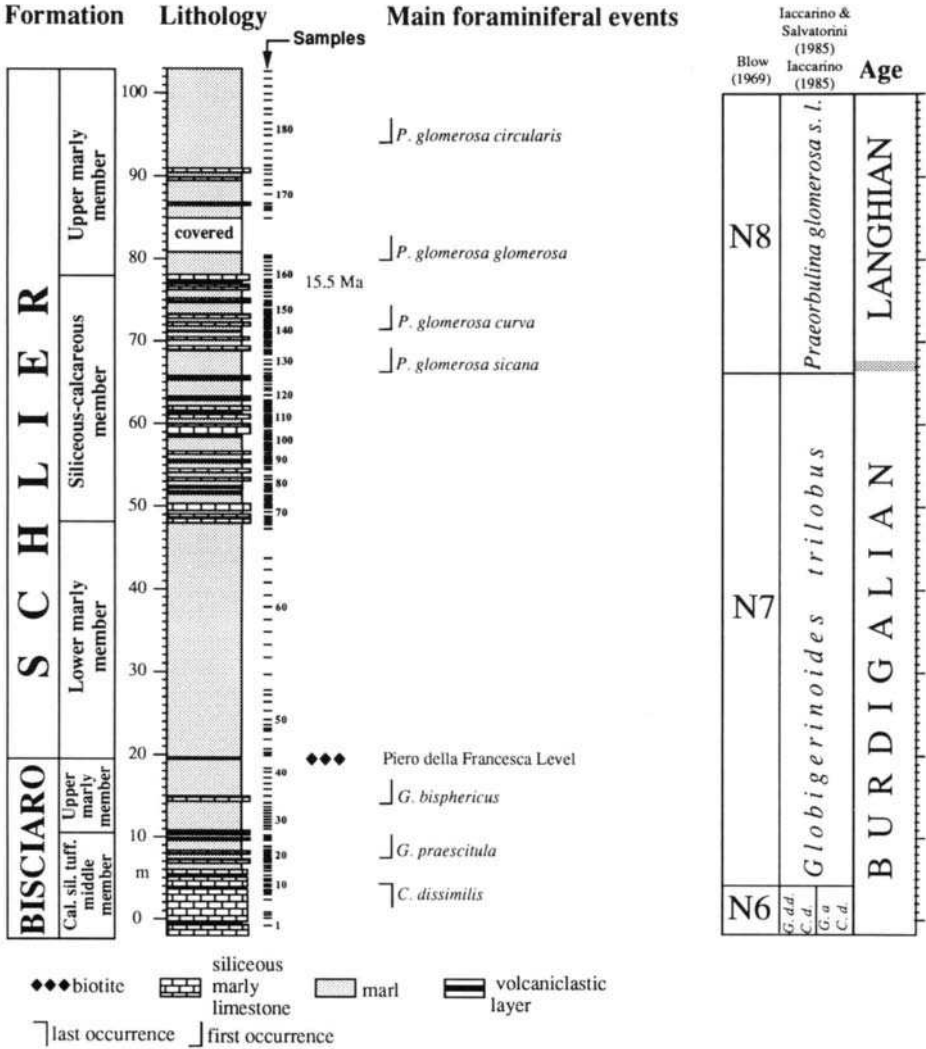


Fig. 3. Main planktonic foraminiferal events and biostratigraphy of the Moria section.

estra, *Coccolithus*, *Cyclicargolithus*). Helicoliths and sphenoliths are also well represented, while discoasterids are generally rare. After a preliminary qualitative analysis, the distribution patterns of stratigraphically important forms have been established by quantitative counting methods following Backman and Shackleton (1983) and Rio et al. (1990b). Specifically, we counted the number of the index species of helicoliths

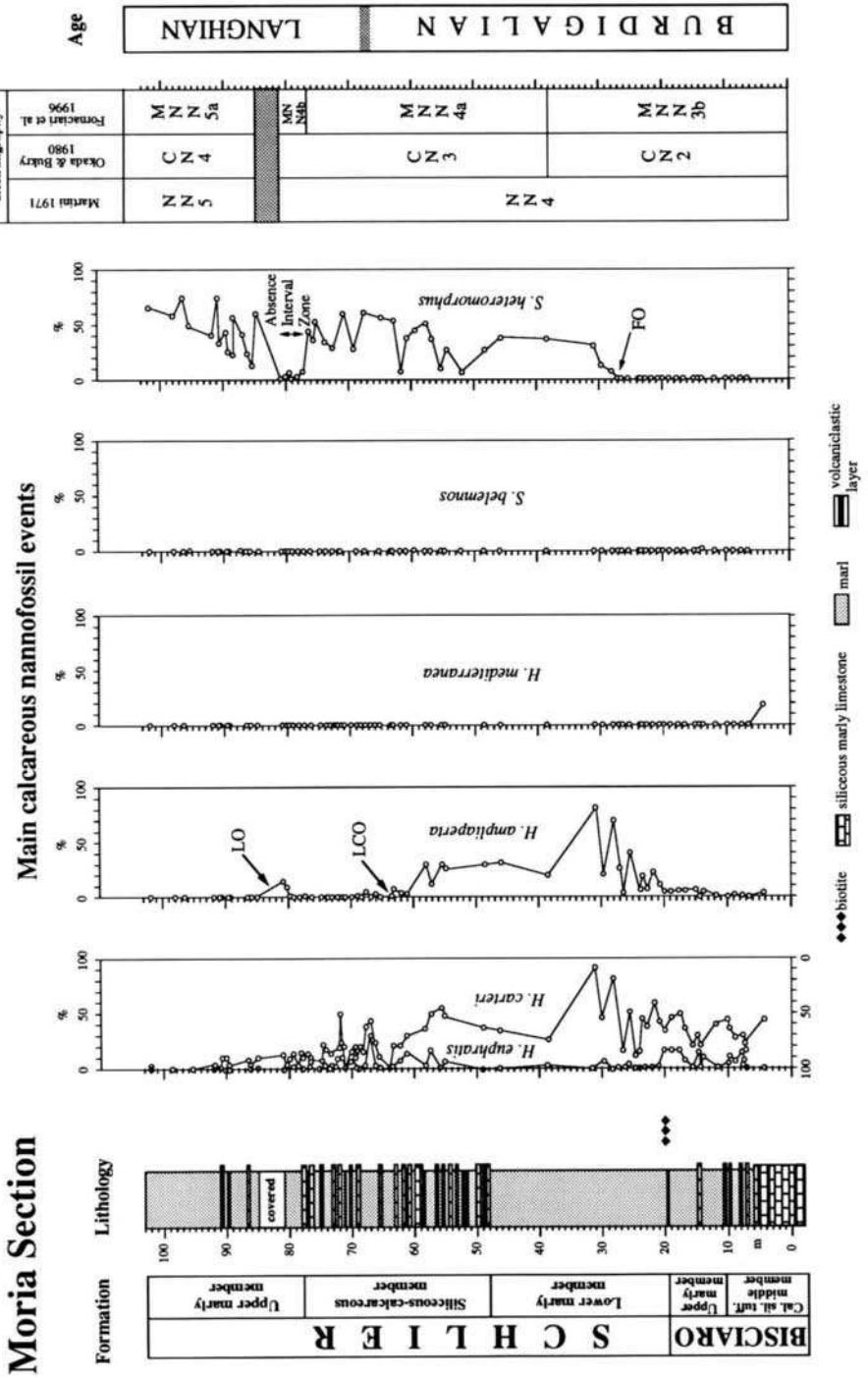


Fig. 4. Main calcareous nanofossil events and biostratigraphy of the Moria section.

and of sphenoliths relative to a fixed number of 50 helicoliths and of 100 sphenoliths, respectively.

For the biostratigraphic classification of this section, we have made reference to the standard zonations of Martini (1971), and Okada and Bukry (1980), as well as to the recently established regional Mediterranean Miocene zonation of Fornaciari and Rió (1996), and of Fornaciari et al. (1996). The countings of marker species and the resulting biostratigraphic classification are reported in Fig. 4, and briefly commented upon as follows.

The basal 28 m of the section is characterized by the absence of both *Sphenolithus belemnos* (the LO of which is the definition of the top of Zone NN3) and of *Sphenolithus heteromorphus* (the FO of which defines the top of Zone CN2), and they are therefore assigned to Zone NN3 and Zone CN2. An interval of absence of *S. heteromorphus* above the LO of *S. belemnos* is a general feature in the Mediterranean stratigraphic record, and defines the '*S. belemnos*–*S. heteromorphus* Interval Zone' (MNN3b) of Fornaciari and Rio (1996). *Helicosphaera ampliaperta*, the LO of which defines the top of Zones NN4, is continuously present above the FO of *S. heteromorphus* up to metre level 63.69 (LCO in Fig. 4). Above it occurs discontinuously and in low abundance, but its presence is probably genuine and not related to reworking (Fig. 4). Picking the absolute last occurrence of this species, and hence drawing the NN4/NN5 (CN3/CN4) boundary, is difficult in the section as it is in general in the Mediterranean region (Fornaciari et al., 1996).

*S. heteromorphus* is abundant in the upper part of the section, which is therefore ascribed to Zone NN5 (CN4) (Fig. 4). It is noteworthy that *S. heteromorphus* is strongly reduced in abundance for a short interval between the LCO and the absolute LO of *H. ampliaperta*. An interval of reduced abundance or absence of this species in the same stratigraphic position is a general feature observed in the Mediterranean region by Fornaciari et al. (1996), which based their *S. heteromorphus* Absence Interval Zone (MNN4b) upon it. Fornaciari et al. (1993) recognized the first common and continuous presence of *H. walbersdorfensis* as a useful subzonal boundary (base of *H. walbersdorfensis*–*S. heteromorphus* Interval Subzone, MNN5b) above the LO of *H. ampliaperta* and below the LO of *S. heteromorphus*. *H. walbersdorfensis* has not been observed in Moria section, the upper part of which is therefore to be assigned to Zone MNN5a of Fornaciari et al. (1996).

#### MAGNETOSTRATIGRAPHY (J. Channell and A. Montanari)

Forty-nine oriented cores were collected from the lower 76 m of the Moria section, excluding a sampling gap in the 24–43 m interval due to difficulties in obtaining fresh, coherent samples in the portion of the section characterized by soft marls.

Each sample was thermally demagnetized in 25°C increments from 100°C to 400°C. Magnetization component directions could be resolved in 23 samples. The remainder of the samples showed unstable behaviour during thermal demagnetization. Component directions were determined by picking (by eye from orthogonal projections of demagnetization data; Fig. 5) the temperature range in which the component is defined, and applying standard principle component analysis. Virtual geomagnetic pole (VGP) latitudes were calculated from the component directions; these form the basis

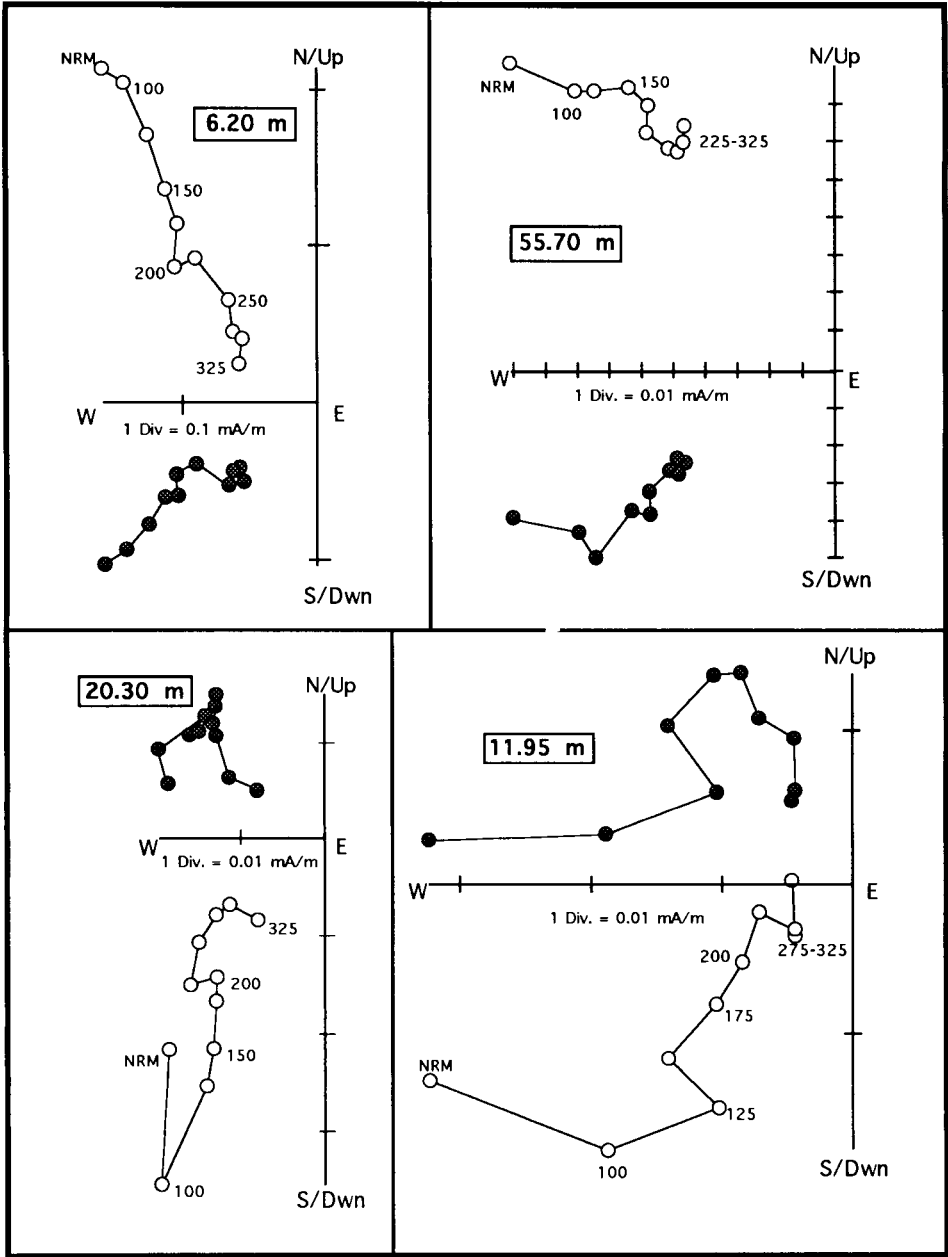


Fig. 5. Demagnetization plots of four representative samples from the Moria section.

for the tentative polarity sequence shown in Fig. 6. There is considerable scatter in the component directions and this scatter is reflected in the scatter in VGP latitude.

We tentatively associate the blocking temperature spectra reflected in the demag-

# Moria Section

## Lithostratigraphy

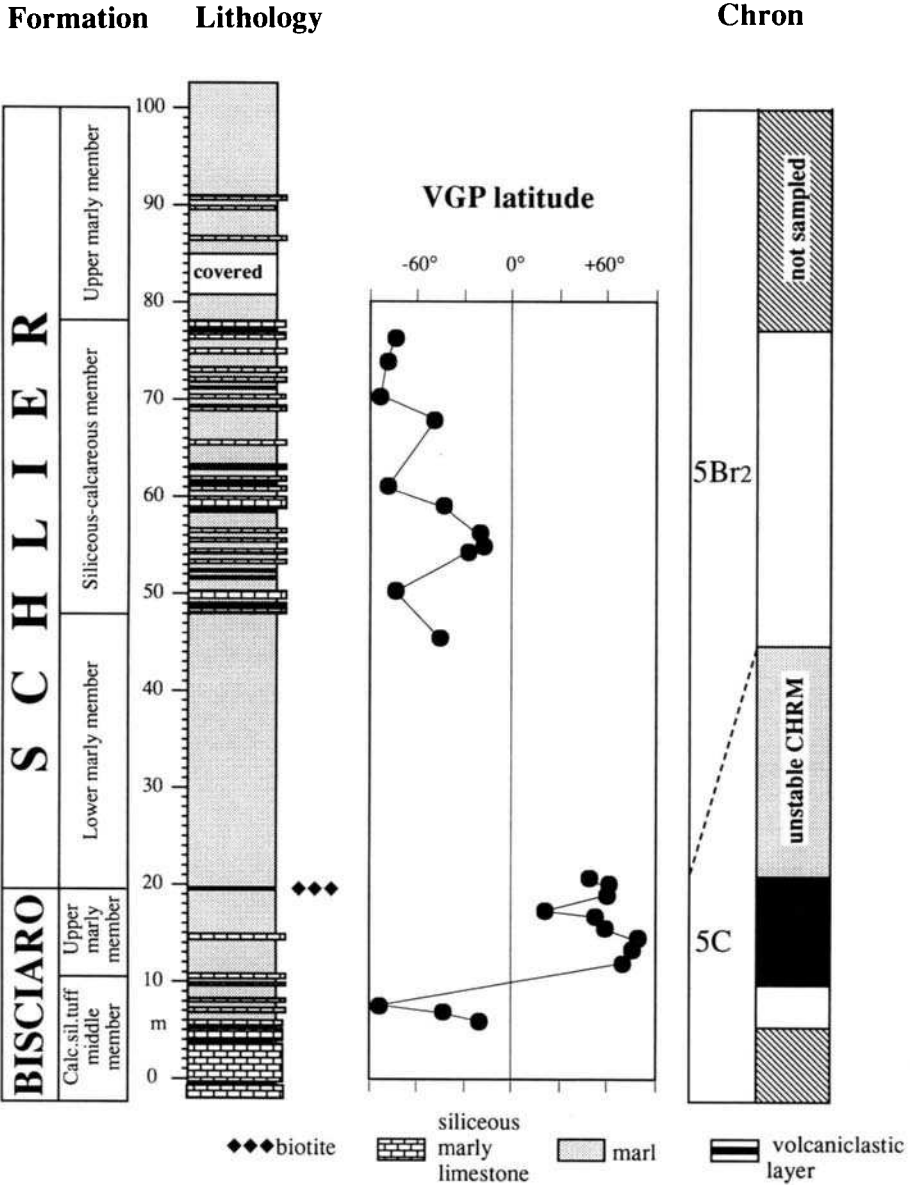


Fig. 6. VGP plot and integrated bio-magnetostratigraphic synthesis of the Moria section.

# Moria Section

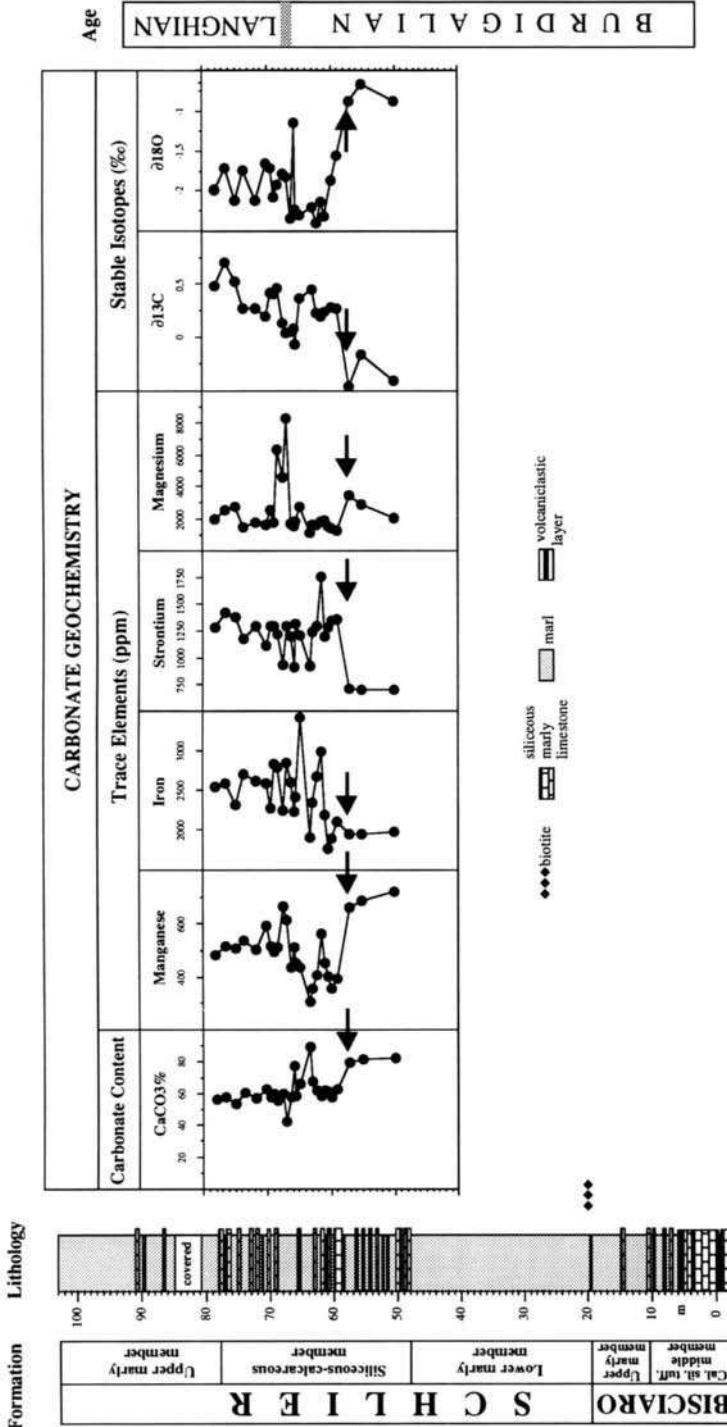


Fig. 7. Stable isotopes and trace element chemostratigraphy of the Moria section.

netization data (Fig. 5) with a titanomagnetite remanence carrier. Above 325°C, the remanence directions often became erratic due possibly to the oxidation of pyrite (and consequent formation of magnetite) during the thermal demagnetization procedure. In many cases (e.g., sample 55.70 in Fig. 5), the component has maximum unblocking temperatures above that expected for an iron sulphide remanence carrier.

The directional scatter in the magnetization components is attributed to the variable degree of weathering in the section. During sample collection, considerable effort was made to procure fresh samples. However, even with digging and trenching, it is not always possible to obtain samples with the characteristic bluish colour of fresh material.

Nevertheless, the data obtained from our analysis are sufficient to attempt a magnetostratigraphic interpretation of the Moria section. In fact, biostratigraphic and radioisotopic data allow the placement of the Burdigalian/Langhian boundary slightly above 66 m, with an interpolated radioisotopic age of about 15.9 Ma. This interstage boundary is located, in the Moria section, within a palaeomagnetically reversed interval which we interpret as Chron 5Br2.

The base of the Moria section (Fig. 6) is within a reversed zone that may correlate with the uppermost reversal seen at the Contessa section. The overlying normal zone found at about 10 m above the base of the Moria section, in the lower part of the foraminiferal Zone N7, taken together with the uppermost normal zone at Contessa (assigned to Chron 5C) may represent two of the three closely spaced normals that appear in the marine magnetic anomaly record of Cande and Kent (1992). The remainder of the Moria section is thus interpreted as belonging to Chron 5Br2 of Cande and Kent (1992).

## CHEMOSTRATIGRAPHY

### *Trace element and stable isotope chemostratigraphy (L. Emmanuel and M. Renard)*

Analyses on major trace elements in whole-carbonate have been carried out in samples from the upper Burdigalian–lower Langhian Moria section. Mn, Fe, Sr, and Mg trace element contents were measured in acetic acid soluble fraction by atomic absorption spectrophotometry (Instrumentation Laboratory 551 video and Hitachi Z8100 apparatus) according to the method described by Richebois (1990).

Carbon and oxygen isotopic ratios were measured on a VG mass spectrometer and the results are given in ‰ with respect to the PDB1 standard. The precision of the measurements, as standard deviation of the mean calculated from replicated analyses, is  $\pm 0.02\text{‰}$ . Our results are summarized in Fig. 7 and Table 1. A major geochemical event (between samples MO 57.2 and MO 61) is recorded by nearly all the geochemical markers, and is located about 10–8 m below the biostratigraphically defined Burdigalian/Langhian stage boundary (i.e., between samples MO 66.3 and MO 67).

*Stable isotopes.* An important shift of the  $\delta^{18}\text{O}$  (more than 1‰) occurs between samples MO 57.2 ( $-0.88\text{‰}$ ) and MO 61 ( $-2.32\text{‰}$ ). Ratios still remain negative in the upper Burdigalian. A slight increase is observed across the Burdigalian/Langhian boundary. In the lower Langhian,  $\delta^{18}\text{O}$  values fluctuate between  $-2.12\text{‰}$  and  $-1.71\text{‰}$ .

The evolution curve of the  $\delta^{13}\text{C}$  shows a clear general increasing trend from  $-0.41\text{‰}$



Table 1

Trace elements (ppm) and stable isotopes concentrations in samples from the Moria section

Samples	m Level	%CaCO <sub>3</sub>	Manganese	Iron	Strontium	Magnesium	$\delta^{13}\text{C}$	$\delta^{18}\text{O}$
MO 78.00	78	56.44	483	2541	1282	1977	0.48	-1.98
MO 76.50	76.5	57.6	519	2579	1417	2557	0.71	-1.71
MO 74.90	74.9	53.59	508	2315	1372	2771	0.52	-2.12
MO 73.60	73.6	60.75	539	2694	1172	1481	0.27	-1.74
MO 71.80	71.8	57.28	515	2618	1296	1728	0.27	-2.12
MO 70.15	70.15	62.5	595	2591	1108	1615	0.2	-1.65
MO 69.50	69.5	57.47	518	2273	1288	2518	0.42	-1.71
MO 68.90	68.9	59.8	494	2826	1293	1744	0.14	-2.08
MO 68.35	68.35	55.36	511	2782	1221	6363	0.46	-1.93
MO 67.50	67.5	59.66	667	2247	928	4601	0.13	-1.78
MO 67.00	67	41.96	613	2842	1297	8320	0.04	-1.83
MO 66.30	66.3	57.68	435	2603	1194	1696	0.05	-2.34
MO 65.80	65.8	77.77	514	2235	909	1565	0.08	-1.15
MO 65.60	65.6	58.66	455	2420	1313	1833	-0.07	-2.24
MO 64.90	64.9	65.92	536	3416	1212	2735	0.37	-2.3
MO 63.30	63.3	89.63	306	1905	918	1134		
MO 63.00	63	67.5	356	2341	1237	1629	0.45	-2.2
MO 62.30	62.3	61.65	408	2669	1290	1631	0.23	-2.4
MO 61.50	61.5	58.41	565	2981	1754	1859	0.2	-2.14
MO 61.00	61	61.86	453	2190	1197	1898	0.24	-2.32
MO 60.50	60.5	61.52	403	1771	1277	1569		
MO 59.95	59.95	58.00	358	1892	1348	1415	0.28	-1.86
MO 59.00	59	63.05	396	2102	1354	1271	0.27	-1.56
MO 57.20	57.2	79.96	663	1946	708	3464	-0.46	-0.88
MO 55.10	55.1	81.94	685	1944	700	2905	-0.16	-0.67
MO 50.00	50	82.16	720	1980	697	2025	-0.41	-0.88

(MO 50) to +0.71‰ (MO 76.5). A positive shift appears between 57.2 and 59 m, while the Burdigalian/Langhian boundary is characterized by a smooth negative trend.

*Strontium.* A major break is observed between samples under 57.2 m (with Sr contents around 700 ppm), and samples above 59 m (with Sr contents ranging between 1200 and 1300 ppm). This break corresponds to the main shift of carbon and oxygen isotopic evolution curves. On the other hand, no anomalies occur at the Burdigalian/Langhian boundary.

*Magnesium.* A decrease of the Mg contents appears between 57.2 m (ranging between 2000 and 3000 ppm) and 59 m (ranging between 1200 and 1900 ppm). The Burdigalian/Langhian boundary is well characterised by a positive shift (from 4000 to 8000 ppm) in the early Langhian and could be due to occurrence of dolomite.

*Manganese.* There is a sharp decrease between 57.2 m (663 ppm) and 59 m (396 ppm). Then, the values remain relatively low through the upper Burdigalian, and is interrupted only by a positive shift (565 ppm) near 61.5 m. Mn contents increase progressively through the upper Burdigalian and the lowermost Langhian with a maximum at 67.5 (667 ppm). A more fluctuating but decreasing trend is observed up to the top of the section.

*Iron.* There is an opposite relationship between relatively low Fe contents in the

Table 2

Strontium isotope analysis of fish teeth from the Moria section

Sample-m level	Foram. Zone <sup>a</sup>	Nanno. Zone <sup>b</sup>	Chron	<sup>87</sup> Sr/ <sup>86</sup> Sr	± 2σ average	Number
MOR-4.6	Top N6	CN2	5Cr1?	0.708398	0.000005	2
MOR-12.0	Base N7	CN2	5Cn1	0.708563	0.000015	2
MOR-19.4	N7	CN2	5Cn1	0.708455	0.000005	2
MOR-58.2	Top N7	Mid CN3	5Br2	0.708533	0.000005	2
MOR-101.8	N8	CN4	No data	0.708645	0.000015	2

<sup>a</sup> Planktonic foraminiferal zone after Blow (1969).<sup>b</sup> Calcareous nannofossil after Okada and Bukry (1980).

Burdigalian (ranging from 1700 to 2100 ppm), and high contents around 2500 ppm in the Langhian. This gradual change occurs in the upper Burdigalian, and is characterized by a high variability, and a positive shift zone contemporaneous with the manganese negative excursion.

#### *Sr isotopes (D.J. DePaolo and A. Montanari)*

We have analyzed the <sup>87</sup>Sr/<sup>86</sup>Sr composition of five fish teeth samples from the Moria section following the same sample preparation and analytical procedures used for samples from the Sardella section in the Conero Riviera (Montanari et al., Chapter E1). The results are reported in Table 2.

We consider fish teeth as an excellent material for determining the original <sup>87</sup>Sr/<sup>86</sup>Sr composition of sea water firstly because biogenic phosphate is less soluble in sea water than carbonate (Schmitz et al., 1991), and secondly because diagenesis in a clay-rich sediment, such as the soft marl of the Moria section (Morandi and Tateo, 1992), may have altered the original composition of biogenic carbonate (Richter and DePaolo, 1987).

The Sr isotopic ratios of the Moria fish teeth plotted against time are shown in Fig. 8 and compared with the <sup>87</sup>Sr/<sup>86</sup>Sr values measured in carbonate and phosphate samples from the Contessa section (see Montanari et al., 1991, Chapter C3), and with the Sr composition of oceanic sea water obtained from deep-sea cores, and the Miocene Monterey formation in California (DePaolo and Finger, 1991).

With the exception for sample MOR-12.0, which appears slightly deviant from the general trend of the other analyzed samples, the strontium isotopic values of the Moria fish teeth are consistent with the <sup>87</sup>Sr/<sup>86</sup>Sr trend of the Contessa CT section obtained from bulk limestone and bivalve shell samples (Fig. 8A). However, the <sup>87</sup>Sr/<sup>86</sup>Sr values in these Apennine sections are consistently lower than coeval oceanic values by a factor of about 0.0002. This geochemical difference cannot be attributed simply to diagenetic alteration of the Apennine samples for two main reasons: (1) the Sr leached from continent-derived clay contained in the marl would increase, rather than decrease, the Sr isotopic ratio in fish teeth in case of recrystallization of the latter, and (2) it is unlikely that diagenetic alteration and remobilization of Sr would affect in an equal manner the <sup>87</sup>Sr/<sup>86</sup>Sr composition of fish teeth, mollusc shells, and whole-rock. This leads us to speculate that the Sr composition of the sea water of Umbria–Marche

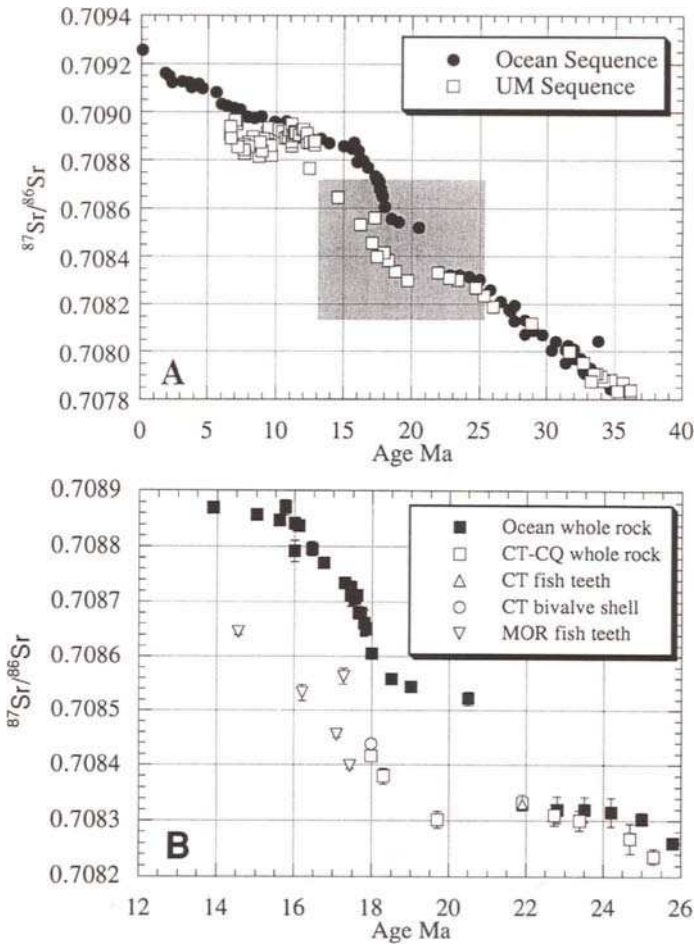


Fig. 8. (A) Upper Eocene to Miocene  $^{87}\text{Sr}/^{86}\text{Sr}$  curve of the Umbria–Marche (*U–M*) sequence compared with that of oceanic sequences. Shaded area represents the uppermost Oligocene to lower Langhian interval exposed in the Contessa and Moria sections. (B) Detailed Sr isotope chemostratigraphy of the Contessa and Moria sections.

basin, and therefore of the proto-Mediterranean, was different from that of the world's oceans during the Mid-Miocene. Similar Sr isotopic deviations were observed also in well-preserved mid-Lower Miocene aragonitic bivalve and gastropod shells from the Parathetys (Scharber and Steininger, 1994).

A lowering of the  $^{87}\text{Sr}/^{86}\text{Sr}$  composition in the proto-Mediterranean could have resulted from orogenic uplifting and erosion of Mesozoic and Cenozoic carbonates in the western Apennine, Dinaride, and Alpine orogens, with consequent recycling of extra  $^{86}\text{Sr}$ , and the progressive tectonic closure and isolation of the basin from oceanic water circulation.

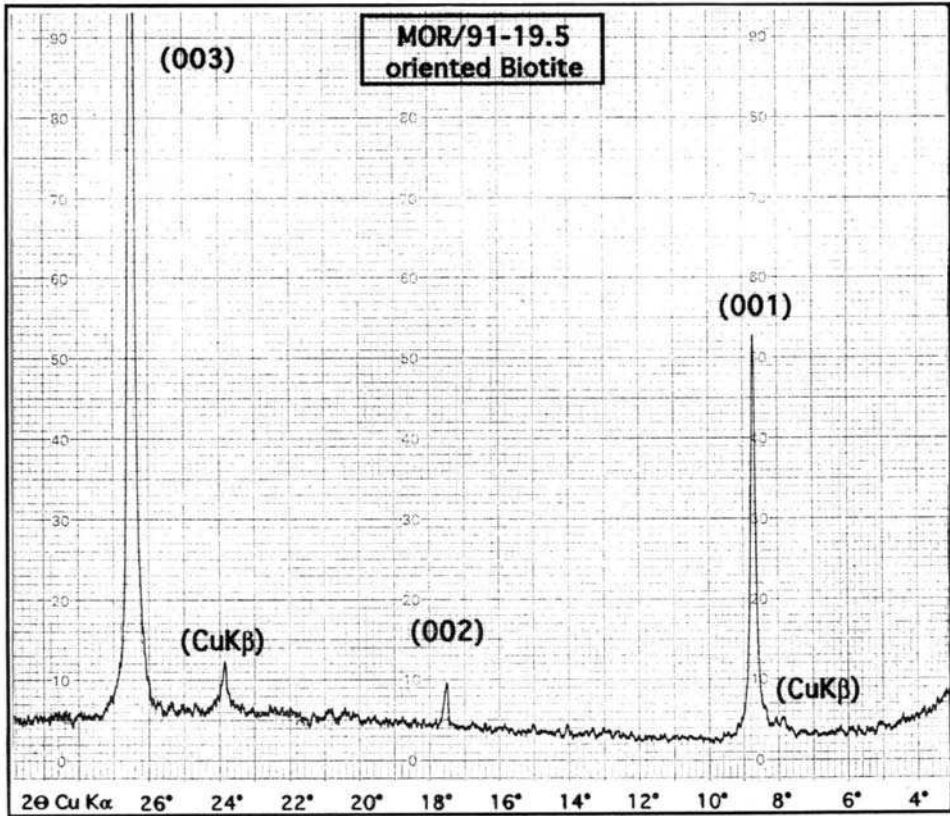


Fig. 9. XRD diffractogram of oriented biotite from the Piero della Francesca Level (MOR 19.5 m).

GEOCHRONOLOGY (A. Deino, M. De Grandis, M. Laurenzi and A. Montanari)

*K/Ar and  $^{40}\text{Ar}/^{39}\text{Ar}$  dating of the Livello Piero della Francesca*

The abundant, lustrous, black, often euhedral biotite contained in the Piero della Francesca Level appears macroscopically to be suitable material for accurate radioisotopic dating. However, in order to assess in more detail its potential reliability as a geochronometer, a sample of this biotite was analyzed with X-ray diffractometry and electron microprobe, following the recommendations of Montanari (1988), and Odin et al. (1991). Biotite was separated from the bulk-rock by wet-sieving, and concentrated using a Franz isomagnetic separator. Residual impurities were hand-picked, and the  $>225 \mu\text{m}$  fraction washed in distilled water in an ultrasonic bath.

The X-ray diffractogram shown in Fig. 9 exhibits only biotite peaks indicating that the separate is mineralogically pure and free of vermiculite, the diagenetic clay mineral often found in altered volcanic biotites of the Umbria–Marche Tertiary sequence (Odin et al., 1991).

Electron microprobe analyses on thirteen individual biotite grains, along transects of

Table 3

Chemical compositions (in wt%) of biotite flakes from sample MOR/91-19.5

Analysis, flake	SiO <sub>2</sub>	TiO <sub>2</sub>	Al <sub>2</sub> O <sub>3</sub>	FeO*	MgO	CaO	Na <sub>2</sub> O	K <sub>2</sub> O	Total
(1) 5 points analyzed	34.23	3.18	14.02	23.92	7.73	0.08	0.32	8.68	92.16
(2) 5 points analyzed	34.28	3.68	13.70	23.74	7.42	0.05	0.30	8.68	91.86
(3) 5 points analyzed	34.76	3.46	13.88	23.79	7.61	0.11	0.36	8.63	92.60
(4) 4 points analyzed	34.25	3.45	14.07	23.63	7.54	0.10	0.48	8.44	91.95
(5) 4 points analyzed	34.16	3.30	14.10	24.27	7.61	0.05	0.38	8.70	92.57
(6) 5 points analyzed	34.33	3.30	14.07	24.17	7.58	0.11	0.36	8.65	92.57
(7) 5 points analyzed	34.58	3.56	13.97	24.31	7.45	0.08	0.37	8.71	93.01
(8) 5 points analyzed	34.33	3.30	14.17	24.47	7.55	0.08	0.37	8.72	92.98
(9) 6 points analyzed	34.43	3.53	13.97	23.47	7.98	0.13	0.39	8.45	92.34
(10) 3 points analyzed	34.61	3.76	13.85	24.02	7.41	0.06	0.35	8.72	92.77
(11) 5 points analyzed	34.20	3.18	14.23	24.18	7.77	0.06	0.35	8.76	92.74
(12) 8 points analyzed	34.42	3.23	14.03	24.16	7.50	0.11	0.35	8.67	92.47
(13) 4 points analyzed	34.50	3.39	13.89	23.86	7.63	0.08	0.34	8.70	92.39
Average	34.39	3.41	14.00	24.00	7.56	0.08	0.36	8.65	92.49

FeO\* = total iron.

five or more points per grain, reveal a homogeneous chemical composition and a K<sub>2</sub>O content almost always higher than 8.5%. The microprobe data therefore suggest that this biotite sample is unaltered and is made of a compositionally homogeneous population of grains (Table 3). A split of the same sample was utilized for <sup>40</sup>Ar/<sup>39</sup>Ar dating at the Berkeley Geochronology Center.

Another sample of biotite collected from the Piero della Francesca Level in the Moria section, was dated by traditional K/Ar as well as step-heating <sup>40</sup>Ar/<sup>39</sup>Ar techniques at the CNR Geochronology Lab in Pisa. The results from these two laboratories are consistent, as reported below.

*Berkeley Geochronology Center (A. Deino and A. Montanari).* One biotite concentrate extracted from the Piero della Francesca Level (designated as MOR/91-19.5) was analyzed by the incremental-heating <sup>40</sup>Ar/<sup>39</sup>Ar dating technique, using a defocused Ar-ion laser beam as the heat source. Two aliquots of this biotite of approximately 1–2 mg each were analyzed separately, yielding the analytical results as tabulated in Tables 4 and 5. Step-heating spectra for these experiments are shown in Fig. 10. The spectra show good reproducibility in the percentage of radiogenic argon of total argon (%<sup>40</sup>Ar\*), chemical parameters (atomic K/Ca, K/Cl), and in the shape of the age spectra. The %<sup>40</sup>Ar\* rises steadily from less than 20% to eventually more than 90% after about half of the total %<sup>39</sup>Ar release. There are also fairly systematic but enigmatic changes in K/Ca, which increases in the first 10–20% of the %<sup>39</sup>Ar released, then falls steadily throughout the rest of the experiment. K/Cl responds similarly in one aliquot (5806/2-01) but is steady throughout the other aliquot.

These responses suggest some degree of marginal alteration of the biotite that influences the adsorption or incorporation of atmospheric argon into the crystal in the lower-temperature steps. However, apart from a slightly lower age in some of the earliest steps, the spectra in both aliquots form a plateau that extends across more than 90% of the cumulative %<sup>39</sup>Ar release, suggesting good preservation of the K/Ar

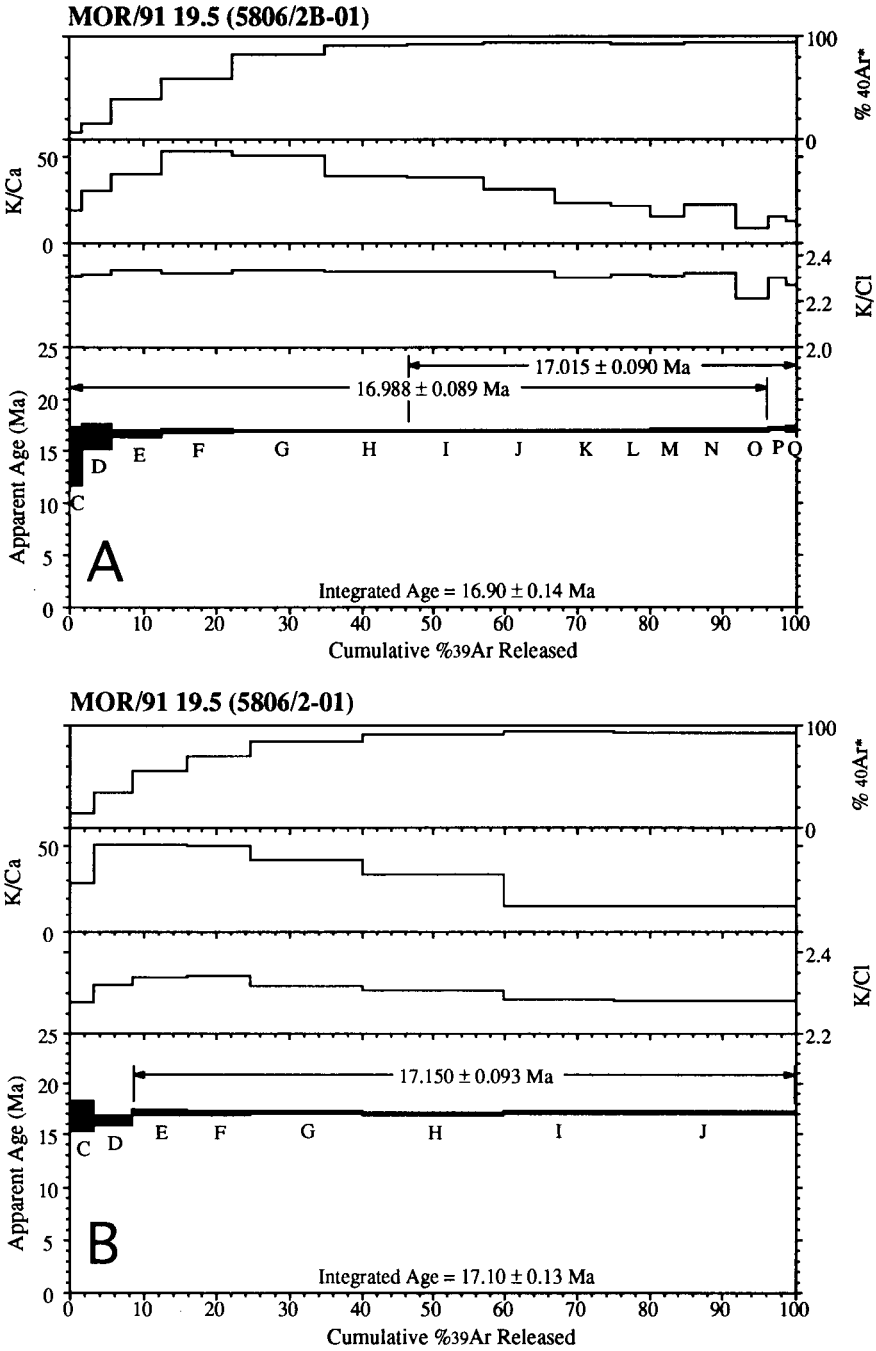


Fig. 10.  $^{40}\text{Ar}/^{39}\text{Ar}$  plateau diagrams of biotite from the Piero della Francesca Level (MOR 19.5 m) dated at Berkeley Geochronology Center.

Table 4

$^{40}\text{Ar}/^{39}\text{Ar}$  analytical data of laser incremental-heating experiments for biotite from level MOR/91-19.5 (Berkeley Geochronology Center)

Lab ID#	Power (W)	Ca/K	$^{36}\text{Ar}/^{39}\text{Ar}$	$^{40}\text{Ar}^*/^{39}\text{Ar}$	% $^{40}\text{Ar}^*$	Age (Ma) $\pm 1\sigma$
<i>Sample MOR/91-19.5:</i>						
5806/2-01C	15.0	0.0351	0.01855	0.952	14.8	16.83 $\pm$ 0.73
5806/2-01D	17.0	0.0196	0.00596	0.927	34.5	16.38 $\pm$ 0.27
5806/2-01E	19.0	0.0199	0.00257	0.971	56.2	17.16 $\pm$ 0.16
5806/2-01F	21.0	0.0203	0.00143	0.968	69.7	17.10 $\pm$ 0.13
5806/2-01G	24.0	0.0236	0.00064	0.975	83.8	17.23 $\pm$ 0.11
5806/2-01H	27.0	0.0299	0.00031	0.966	91.4	17.07 $\pm$ 0.10
5806/2-01I	30.0	0.0644	0.00022	0.972	94.0	17.17 $\pm$ 0.10
5806/2-01J	50.0	0.0652	0.00025	0.971	93.3	17.16 $\pm$ 0.10
<i>5806/2B-01:</i>						
5806/2B-01C	15.0	0.0523	0.03910	0.820	6.6	14.50 $\pm$ 1.42
5806/2B-01D	17.0	0.0338	0.01659	0.926	15.9	16.37 $\pm$ 0.61
5806/2B-01E	19.0	0.0252	0.00478	0.942	40.0	16.65 $\pm$ 0.21
5806/2B-01F	21.0	0.0189	0.00222	0.962	59.4	17.00 $\pm$ 0.14
5806/2B-01G	23.0	0.0197	0.00070	0.960	82.3	16.96 $\pm$ 0.10
5806/2B-01H	25.0	0.0260	0.00033	0.959	90.8	16.94 $\pm$ 0.10
5806/2B-01I	27.0	0.0268	0.00027	0.961	92.5	16.98 $\pm$ 0.10
5806/2B-01J	29.0	0.0324	0.00022	0.962	93.7	17.01 $\pm$ 0.10
5806/2B-01K	31.0	0.0430	0.00023	0.962	93.6	17.01 $\pm$ 0.10
5806/2B-01L	33.0	0.0470	0.00024	0.961	93.4	16.97 $\pm$ 0.10
5806/2B-01M	35.0	0.0652	0.00024	0.963	93.5	17.01 $\pm$ 0.11
5806/2B-01N	37.0	0.0450	0.00023	0.964	93.6	17.02 $\pm$ 0.10
5806/2B-01O	40.0	0.1208	0.00023	0.964	93.8	17.03 $\pm$ 0.11
5806/2B-01P	45.0	0.0640	0.00018	0.971	95.0	17.16 $\pm$ 0.12
5806/2B-01Q	50.0	0.0792	0.00021	0.971	94.2	17.15 $\pm$ 0.17

Notes. Runs at the beginning of incremental-heating experiments which comprise less than 1% of the total percent of  $^{39}\text{Ar}$  released have been omitted from this table and elsewhere as these are essentially blanks. Italic-type indicates steps included in the plateau. The plateau definition is that of Fleck et al. (1977) wherein at least three contiguous steps comprising at least 50% of the cumulative % $^{39}\text{Ar}$  released cannot mutually be distinguished using a 95% confidence value test. Errors in age quoted for individual runs are  $1\sigma$  analytical uncertainty. Ca/K is calculated from  $^{37}\text{Ar}/^{39}\text{Ar}$  using a multiplier of 1.96.  $^{40}\text{Ar}^*$  refers to radiogenic argon.  $\lambda = 5.543 \times 10^{-10} \text{ y}^{-1}$ . Isotopic interference corrections:  $(^{36}\text{Ar}/^{37}\text{Ar})_{\text{Ca}} = (2.58 \pm 0.06) \times 10^{-4}$ ,  $(^{39}\text{Ar}/^{37}\text{Ar})_{\text{Ca}} = (6.7 \pm 0.3) \times 10^{-4}$ ,  $(^{40}\text{Ar}/^{39}\text{Ar})_{\text{K}} = (2.17 \pm 0.08) \times 10^{-2}$ .  $J = (9.840 \pm 0.05) \times 10^{-3}$ .

systematics. The plateau ages (sample 5806.2B-01 actually contains two broadly overlapping plateaus) are statistically indistinguishable between aliquots. Isotope correlation analysis in both cases yields good isochrons (Table 4), with trapped  $^{40}\text{Ar}/^{36}\text{Ar}$  compositions that are indistinguishable from atmospheric argon in one case or, in the other case, just slightly less than two standard deviations below atmospheric composition ( $(^{40}\text{Ar}/^{36}\text{Ar})_{\text{atm}} = 295.5$ ; Steiger and Jäger, 1977). Isochron ages are indistinguishable between aliquots and are also indistinguishable from the plateau ages. The isochron ages are preferred over the plateau age calculations since the isochron approach is inherently more correct in performing the  $^{40}\text{Ar}/^{36}\text{Ar}$  correction. For the final age of this biotite the weighted mean of the isochron ages for the two aliquots is calculated, giving  $17.08 \pm 0.18 \text{ Ma}$  ( $2\sigma$ ). Note that this age is determined using the Fish Canyon Tuff

Table 5

Summary incremental-heating ages — integrated, plateau, and isochron plateau age calculations

Sample	n (integr.)	Integrated age	n (plat. or isoch.)	Plateau age	MSWD	( <sup>40</sup> Ar/ <sup>36</sup> Ar) <sub>trapped</sub>	Isochron age
<i>MOR/91-19.5:</i>							
5806/2-01	8	17.10 ± 0.13	6(E–J)	17.15 ± 0.09	1.2	296.7 ± 2.8	17.15 ± 0.09
5806/2B-01	15	16.90 ± 0.14	13(C–O)	16.99 ± 0.09			
			8(I–Q)	17.02 ± 0.09			
			15(C–Q)		0.7	292.4 ± 1.1	17.02 ± 0.09

Notes. All ages are in units of Ma with an indicated uncertainty of 1σ. Isochron fitting is by the ‘inverse’ isochron (<sup>36</sup>Ar/<sup>40</sup>Ar vs. <sup>39</sup>Ar/<sup>40</sup>Ar). MSWD = mean square of weighted deviates, a goodness of fit parameter that provides a measure of the scatter of the data about the line.

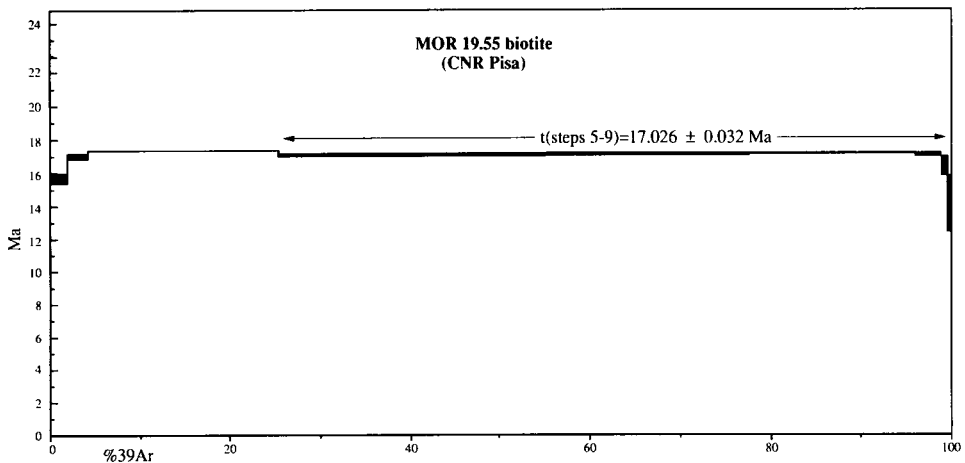


Fig. 11. <sup>40</sup>Ar/<sup>39</sup>Ar plateau diagrams of biotite from the Piero della Francesca Level (MOR 19.5 m) dated at the CNR Institute of Geochronology and Isotope Geochemistry at Pisa.

(FCT) sanidine as the neutron flux monitor mineral, with an age of 27.84 Ma (Cebula et al., 1986, modified for Samson and Alexander, 1987).

*CNR Geochronology Lab, Pisa (M. Laurenzi and M. De Grandis).* The volcanoclastic marker Piero della Francesca Level (19.55 m) contains abundant biotite grains, with an average K content determined by AAS of 7.09%, a normal value for unweathered biotites. A preliminary K/Ar measure on a biotite separate yielded an age of 17.09 ± 0.40 Ma (Laurenzi and De Grandis, 1992). An <sup>40</sup>Ar/<sup>39</sup>Ar determination was done on a split of the same separate: the spectrum is slightly disturbed on the first 25% of gas release (Fig. 11) but for the remaining 75% it defines a plateau (steps 5–9) yielding an age of 17.026 ± 0.064 Ma. The same steps, on an isochron plot (Table 6, Fig. 12), define an age of 17.060 ± 0.096 Ma, with an atmospheric intercept (286 ± 22). The integrated age of 17.06 Ma is equivalent, within the analytical uncertainty, to the plateau and isochron age, and to the K–Ar age.

All the forementioned errors are ±2σ derived from in-run 1σ analytical errors.



Table 6

Step-heating Ar release from biotite separate MOR-19.55 (Istituto di Geocronologia e Geochimica Isotopica, CNR, Pisa)

$T$ (°C)	$^{40}\text{Ar}_{\text{tot}}$ (ml/g)	$^{39}\text{Ar}$ (ml/g)	$^{38}\text{Ar}$ (ml/g)	$^{37}\text{Ar}$ (ml/g)	$^{36}\text{Ar}$ (ml/g)	Age (Ma)
700	$7.83 \times 10^{-8}$	$5.49 \times 10^{-10}$	$9.80 \times 10^{-11}$	$9.05 \times 10^{-11}$	$2.48 \times 10^{-10}$	7.824
1 $\sigma$	$\pm 1.3 \times 10^{-10}$	$\pm 5.9 \times 10^{-12}$	$\pm 2.1 \times 10^{-12}$	$\pm 2.8 \times 10^{-11}$	$\pm 4.1 \times 10^{-12}$	$\pm 1.900$
870	$1.76 \times 10^{-7}$	$3.84 \times 10^{-9}$	$3.36 \times 10^{-10}$	$2.19 \times 10^{-10}$	$3.61 \times 10^{-10}$	15.671
1 $\sigma$	$\pm 3.1 \times 10^{-10}$	$\pm 8.9 \times 10^{-12}$	$\pm 4.1 \times 10^{-12}$	$\pm 2.5 \times 10^{-11}$	$\pm 4.1 \times 10^{-12}$	$\pm 0.280$
930	$1.64 \times 10^{-7}$	$5.89 \times 10^{-9}$	$4.55 \times 10^{-10}$	$1.73 \times 10^{-10}$	$1.63 \times 10^{-10}$	16.962
1 $\sigma$	$\pm 2.9 \times 10^{-10}$	$\pm 1.6 \times 10^{-11}$	$\pm 2.2 \times 10^{-12}$	$\pm 3.6 \times 10^{-11}$	$\pm 3.1 \times 10^{-12}$	$\pm 0.140$
980	$1.21 \times 10^{-6}$	$4.98 \times 10^{-8}$	$3.58 \times 10^{-9}$	$3.49 \times 10^{-10}$	$7.01 \times 10^{-10}$	17.335
1 $\sigma$	$\pm 2.1 \times 10^{-9}$	$\pm 8.4 \times 10^{-11}$	$\pm 1.6 \times 10^{-11}$	$\pm 5.8 \times 10^{-11}$	$\pm 8.5 \times 10^{-12}$	$\pm 0.060$
1030	$1.49 \times 10^{-6}$	$7.03 \times 10^{-8}$	$4.93 \times 10^{-9}$	$4.71 \times 10^{-10}$	$3.33 \times 10^{-10}$	17.074
1 $\sigma$	$\pm 7.3 \times 10^{-9}$	$\pm 1.5 \times 10^{-10}$	$\pm 1.5 \times 10^{-11}$	$\pm 3.4 \times 10^{-11}$	$\pm 4.2 \times 10^{-12}$	$\pm 0.092$
1080	$1.10 \times 10^{-6}$	$5.34 \times 10^{-8}$	$3.73 \times 10^{-9}$	$3.46 \times 10^{-10}$	$1.60 \times 10^{-10}$	17.082
1 $\sigma$	$\pm 1.8 \times 10^{-9}$	$\pm 1.4 \times 10^{-10}$	$\pm 1.5 \times 10^{-11}$	$\pm 2.8 \times 10^{-11}$	$\pm 3.1 \times 10^{-12}$	$\pm 0.054$
1130	$8.89 \times 10^{-7}$	$4.35 \times 10^{-8}$	$3.01 \times 10^{-9}$	$3.38 \times 10^{-10}$	$1.14 \times 10^{-10}$	16.990
1 $\sigma$	$\pm 9.6 \times 10^{-10}$	$\pm 1.0 \times 10^{-10}$	$\pm 9.9 \times 10^{-12}$	$\pm 3.4 \times 10^{-11}$	$\pm 3.3 \times 10^{-12}$	$\pm 0.048$
1160	$1.59 \times 10^{-7}$	$7.03 \times 10^{-9}$	$5.00 \times 10^{-10}$	$2.51 \times 10^{-10}$	$6.74 \times 10^{-11}$	17.050
1 $\sigma$	$\pm 2.5 \times 10^{-10}$	$\pm 1.5 \times 10^{-11}$	$\pm 4.8 \times 10^{-12}$	$\pm 3.2 \times 10^{-11}$	$\pm 2.8 \times 10^{-12}$	$\pm 0.110$
1200	$4.94 \times 10^{-8}$	$1.51 \times 10^{-9}$	$1.23 \times 10^{-10}$	$1.30 \times 10^{-10}$	$7.03 \times 10^{-11}$	16.356
1 $\sigma$	$\pm 6.5 \times 10^{-11}$	$\pm 9.6 \times 10^{-12}$	$\pm 1.9 \times 10^{-12}$	$\pm 2.4 \times 10^{-11}$	$\pm 3.0 \times 10^{-12}$	$\pm 0.510$
1350	$3.82 \times 10^{-8}$	$4.65 \times 10^{-10}$	$5.25 \times 10^{-11}$	$4.16 \times 10^{-11}$	$1.04 \times 10^{-10}$	14.116
1 $\sigma$	$\pm 6.1 \times 10^{-11}$	$\pm 2.8 \times 10^{-12}$	$\pm 1.8 \times 10^{-12}$	$\pm 3.0 \times 10^{-11}$	$\pm 3.1 \times 10^{-12}$	$\pm 1.700$
$t_{\text{tot}}$						18.030

Note.  $J = 4.8097 \times 10^{-4}$ ; sample weight = 39.83 mg. Concentration data are corrected for instrumental background, isotopic fractionation, and  $^{37}\text{Ar}$  decay, but not for nuclear interferences, except for  $^{40}\text{K}$  on  $^{40}\text{Ar}$ . Ages are corrected for all nuclear interferences due to K, Ca, and Cl. All reported errors are  $\pm 2\sigma$  in-run analytical errors, and they do not take into account uncertainty on neutron flux variation, and on monitor age.

Adding the uncertainty due to the vertical neutron flux variation and to the monitor age they become:

$$\text{Plateau age } (t_{\text{pl}}) = 17.03 \pm 0.28 \text{ Ma}$$

$$\text{Isochron age } (t_{\text{is}}) = 17.06 \pm 0.30 \text{ Ma}$$

All data are referred to an age of the FCT biotite of 27.55 Ma (Lanphere et al., 1990). We recalculated the obtained ages using the other published values of 27.84 Ma (see Izett et al., 1991, for a detailed discussion on the age of FCT), the  $t_{\text{pl}}$  and  $t_{\text{ps}}$  will be 17.21 and 17.25 Ma, respectively.

#### Comparison of biotite $^{40}\text{Ar}/^{39}\text{Ar}$ dating

In  $^{40}\text{Ar}/^{39}\text{Ar}$  geochronology, there is no universally accepted age reference material, so to compare the results from one lab with another it is necessary to recalculate ages

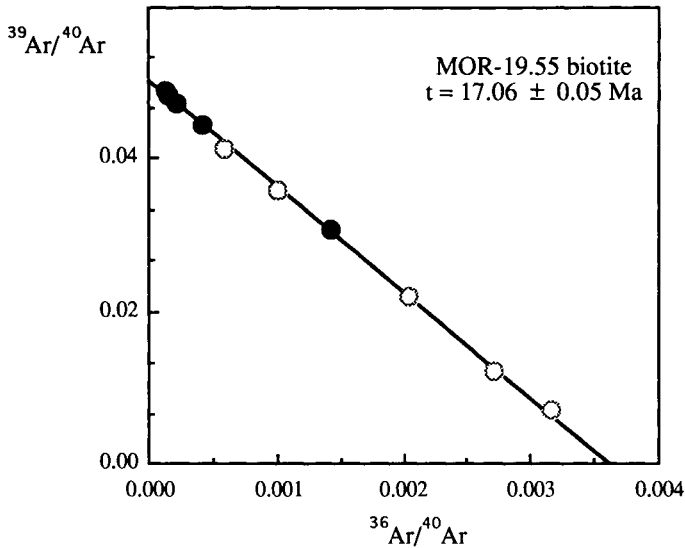


Fig. 12. Isochron diagram from  $^{40}\text{Ar}/^{39}\text{Ar}$  thermal increment experiments on biotite from the Piero della Francesca Level (MOR 19.5 m) dated at the CNR Institute of Geochronology and Isotope Geochemistry at Pisa.

to a consistent reference age. For the purposes of this comparison, the Pisa  $^{40}\text{Ar}$ – $^{39}\text{Ar}$  ages can be recalculated to a reference age of 27.84 Ma, assuming that the FCT biotite records the same age as the FCT sanidine, taken above to be 27.84 Ma, yielding  $17.24 \pm 0.30$  for the isochron age. This age is within ( $2\sigma$ ) error of the Berkeley isochron age for this biotite of  $17.08 \pm 0.18$  Ma. An overall weighted mean age of the K–Ar ( $17.09 \pm 0.40$  Ma) and  $^{40}\text{Ar}$ – $^{39}\text{Ar}$  isochron ages for this biotite (using the 27.84 Ma FCT sanidine reference age) is  $17.1 \pm 0.2$  Ma. This value should be taken as the reference age for the Piero della Francesca biotite.

#### Sanidine $^{40}\text{Ar}/^{39}\text{Ar}$ dating (A. Deino and A. Montanari)

Sanidine extracted from two volcanoclastic horizons in the Moria section at metre levels 58.4 (MOR/91-58.4) and 76.8 (MOR/91-76.8), respectively, were analyzed by the single-crystal  $^{40}\text{Ar}/^{39}\text{Ar}$  method (Table 7). Fifteen analyses from the stratigraphically lower sample (MOR/91-58.4) yielded a fairly symmetrical age-probability distribution with a single mode (Fig. 13). Ca/K ratios of individual grains from this sample are also markedly reproducible, suggesting that all are cognate grains from a single eruptive source. A weighted mean age of all analyses gives  $16.18 \pm 0.16$  Ma (error is reported as  $2\sigma$  standard error of the mean, incorporating error in the neutron flux parameter,  $J$ ). This age is corroborated by an inverse isochron least-squares fit to the data, which produces the identical age of  $16.18 \pm 0.16$  Ma, with an acceptable MSWD of 1.9 and a ‘trapped’  $^{40}\text{Ar}/^{36}\text{Ar}$  composition of  $295.7 \pm 4.0$  Ma, well within error of the expected atmospheric composition of 295.5. The modal age of 16.16 Ma is also well within error of the arithmetic mean and isochron ages, as is the median age of 16.18 Ma.

Table 7

$^{40}\text{Ar}/^{39}\text{Ar}$  analytical data of incremental-heating experiments for sanidine from levels MOR-58.1 and MOR-76.8 (Berkeley Geochronology Center)

Lab ID#	Ca/K	$^{36}\text{Ar}/^{39}\text{Ar}$	$^{40}\text{Ar}^*/^{39}\text{Ar}$	% $^{40}\text{Ar}^*$	Age (Ma) $\pm 1\sigma$
<i>Sample MOR/91-58.4:</i>					
5798/2-02	0.0297	0.00046	0.9100	85.4	16.07 $\pm$ 0.07
5798/2-10	0.0264	0.00037	0.9110	87.5	16.09 $\pm$ 0.05
5798/2B-05	0.0258	0.00006	0.9120	95.9	16.11 $\pm$ 0.06
5798/2B-03	0.0298	0.00006	0.9134	95.9	16.13 $\pm$ 0.05
5798/2-07	0.0261	0.00014	0.9139	93.8	16.14 $\pm$ 0.05
5798/2B-02	0.0233	0.00004	0.9147	96.7	16.15 $\pm$ 0.05
5798/2-08	0.0272	0.00073	0.9156	79.4	16.17 $\pm$ 0.11
5798/2B-06	0.0265	0.00005	0.9161	96.2	16.18 $\pm$ 0.06
5798/2-05	0.0243	0.00011	0.9161	94.5	16.18 $\pm$ 0.05
5798/2-09	0.0249	0.00051	0.9168	84.2	16.19 $\pm$ 0.06
5798/2-06	0.0495	0.00134	0.9186	68.9	16.22 $\pm$ 0.08
5798/2-03	0.0213	0.00032	0.9195	88.8	16.24 $\pm$ 0.05
5798/2-04	0.0239	0.00009	0.9212	95.1	16.27 $\pm$ 0.05
5798/2-01	0.0267	0.00034	0.9212	88.5	16.27 $\pm$ 0.06
5798/2B-04	0.0268	0.00004	0.9226	96.6	16.29 $\pm$ 0.06
Weighted average, $1\sigma$ error without error in $J$ :					16.18 $\pm$ 0.02
$1\sigma$ error with error in $J$ :					$\pm 0.08$
<i>Sample MOR/91-76.8:</i>					
5799/2-03	0.0157	0.00183	0.8574	60.5	15.15 $\pm$ 0.16
5799/2-02	0.0168	0.00230	0.8647	55.2	15.27 $\pm$ 0.14
5799/2-07	0.0563	0.00092	0.8664	74.9	15.30 $\pm$ 0.13
5799/2B-01	0.0316	0.00012	0.8693	94.1	15.36 $\pm$ 0.06
5799/2B-08	0.2330	0.00032	0.8698	89.0	15.36 $\pm$ 0.08
5799/2B-03	0.0117	0.00009	0.8733	94.9	15.43 $\pm$ 0.06
5799/2-06	0.0447	0.00061	0.8747	81.4	15.45 $\pm$ 0.10
5799/2B-02	0.0142	0.00011	0.8754	94.3	15.46 $\pm$ 0.06
5799/2B-04	0.0378	0.00010	0.8772	94.5	15.49 $\pm$ 0.06
5799/2-05	0.0080	0.00080	0.8781	77.3	15.51 $\pm$ 0.24
5799/2-04	0.0086	0.00117	0.8811	70.6	15.56 $\pm$ 0.10
5799/2B-06	0.0147	0.00011	0.8833	94.3	15.60 $\pm$ 0.06
5799/2B-07	0.0546	0.00011	0.8846	94.6	15.62 $\pm$ 0.04
5799/2B-05	0.0517	0.00009	0.8850	95.0	15.63 $\pm$ 0.07
5799/2-01	0.2147	0.00143	0.9009	67.3	15.91 $\pm$ 0.30
Weighted average, $1\sigma$ error without error in $J$ :					15.50 $\pm$ 0.03
$1\sigma$ error with error in $J$ :					$\pm 0.08$

Notes. Errors in age quoted for individual runs are  $1\sigma$  analytical uncertainty. Weighted averages are calculated using the inverse variance as the weighting factor (Taylor, 1982), while errors in the weighted averages are  $1\sigma$  standard error of the mean (Samson and Alexander, 1987). Ca/K is calculated from  $^{37}\text{Ar}/^{39}\text{Ar}$  using a multiplier of 1.96.  $^{40}\text{Ar}^*$  refers to radiogenic argon.  $L = 5.543 \times 10^{-10} \text{ y}^{-1}$ . Isotopic interference corrections:  $(^{36}\text{Ar}/^{37}\text{Ar})_{\text{Ca}} = (2.58 \pm 0.06) \times 10^{-4}$ ,  $(^{39}\text{Ar}/^{37}\text{Ar})_{\text{Ca}} = (6.7 \pm 0.3) \times 10^{-4}$ ,  $(^{40}\text{Ar}/^{39}\text{Ar})_{\text{K}} = (2.17 \pm 0.08) \times 10^{-2}$ .  $J = (9.833 \pm 0.050) \times 10^{-3}$ .

Concurrence of all these approaches to determining the age of a suite of single-crystal  $^{40}\text{Ar}$ - $^{39}\text{Ar}$  data testifies to the robustness of the data.

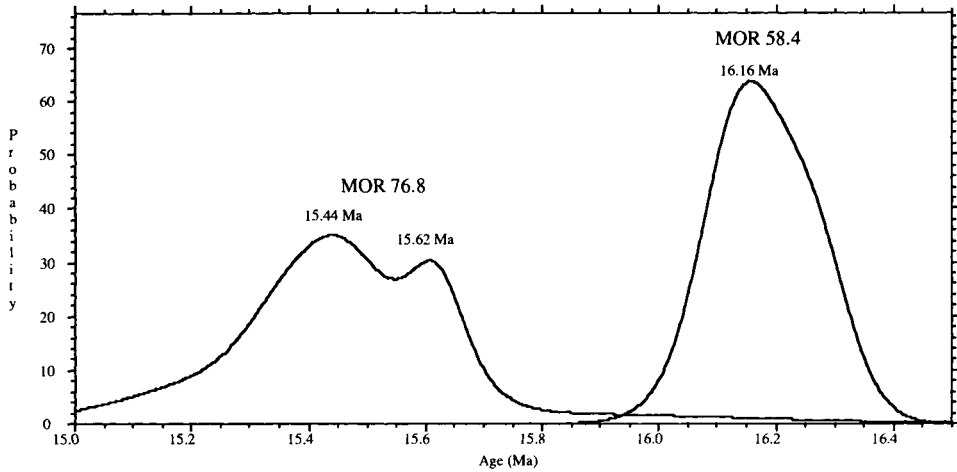


Fig. 13.  $^{40}\text{Ar}$ – $^{39}\text{Ar}$  age probability diagrams for sanidine samples from the volcaniclastic layers MOR 58.5 m, and MOR 76.8 m.

However, the sanidine single-crystal age results for the stratigraphically higher sample are not as simple. Two overlapping modes are apparent in the age-probability spectrum (Fig. 13), at 15.44 and 15.61 Ma. Also, Ca/K ratios are much more variable than the lower sample; however, the Ca/K variation does not correlate with age and may simply represent an originally heterogeneous magma. An attempt to fit the age data for this sample to an inverse isochron yielded an age of  $15.53 \pm 0.16$  Ma, a ‘trapped’  $^{40}\text{Ar}/^{36}\text{Ar}$  composition of  $289.7 \pm 4.2$  Ma, but a high MSWD (3.0) suggesting the presence of more scatter than the analytical errors alone can account for. The additional scatter could be due to unaccounted analytical errors, or to geologic error (age inhomogeneity). It is unclear at this point whether unknown analytical variations or geologic factors such as xenocrystic contamination may be responsible for the poor isochron and bimodality. If xenocrystic contamination is to blame, then the eruption age of this level will be closer to that of the younger mode at 15.44 Ma than the overall weighted mean age of  $15.50 \pm 0.16$ . The difference between the two possibilities is only 0.15%. Since the younger mode lies well within  $2\sigma$  uncertainty of the overall weighted mean age, this latter value ( $15.50 \pm 0.16$ ) is taken as the age of MOR/91-76.8.

## SUMMARY AND CONCLUSIONS

The Moria section is a rare case in the Umbria–Marche pelagic basin where the transition between the Bisciaro and the Schlier formations is well exposed. The three lithologic members comprising the Schlier with its typical Umbrian facies (i.e., the lower marly member, the middle siliceous–calcareous member, and the upper marly member) are well represented in this section, although the uppermost part of the Schlier is covered.

The Moria section contains several interbedded volcaniclastic layers, three of which were dated with the traditional K/Ar, and the  $^{40}\text{Ar}/^{39}\text{Ar}$  incremental heating techniques.

**Moria Section**

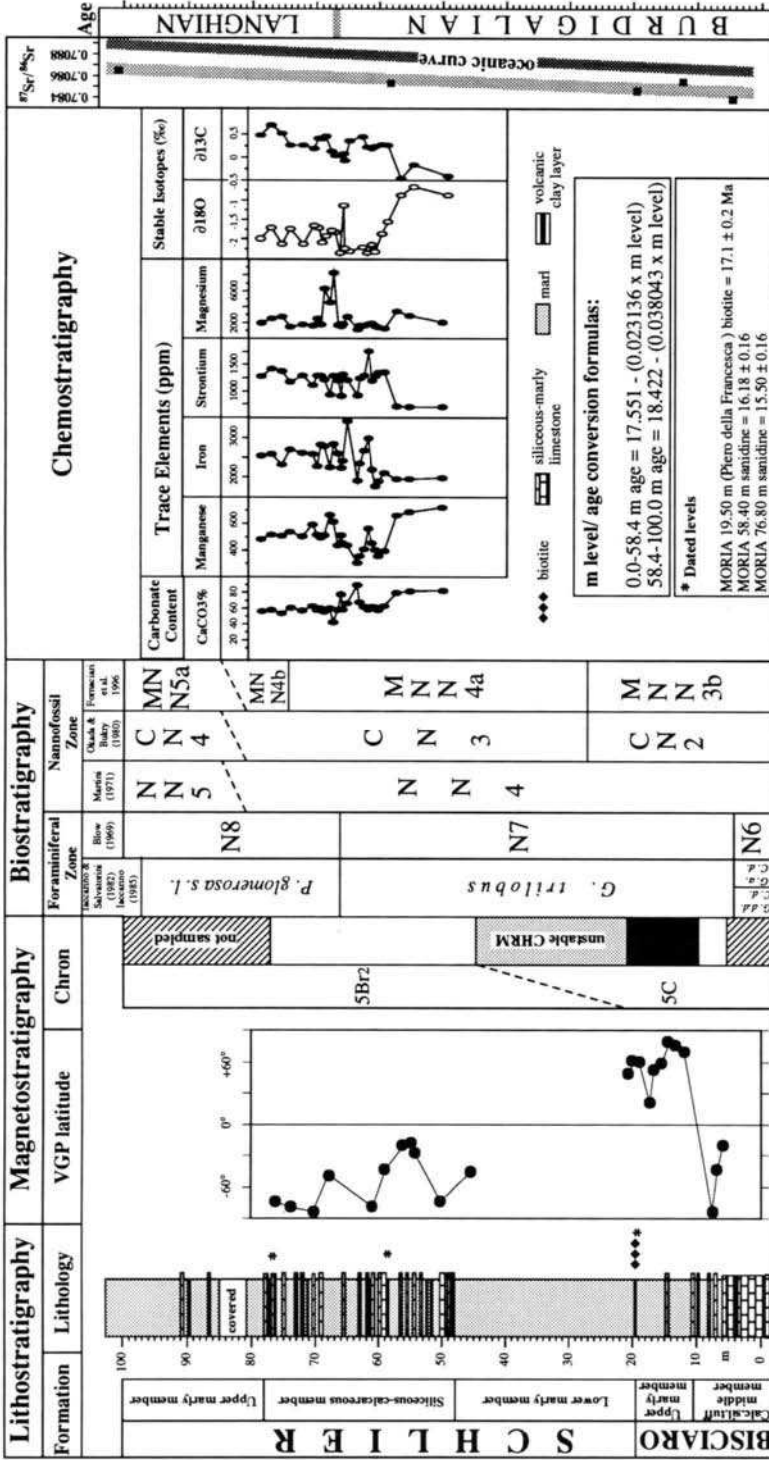


Fig. 14. Integrated stratigraphic synthesis of the Moria section.

These dated levels permit precise and accurate numerical age assignments to calcareous microplankton, magnetostratigraphic, and chemostratigraphic events. In particular, this section permits a precise integrated stratigraphical definition of the Burdigalian/Langhian boundary, and bears all the qualities for a proponible GSSP for this interstage boundary. A summary of the integrated litho-, bio-, magneto-, and chemostratigraphy of the Moria section is shown in Fig. 14, and summarized below.

#### *Integrated stratigraphy of the Burdigalian/Langhian boundary*

*Accessibility, location, and preservation.* Being a mountain road cut, the Moria section (coordinates: 43°30'13.9"N; 12°35'39.1"E of Greenwich) is easily accessible through most of the year. The competent middle member of the Schlier, and the upper part of the Bisciario do not risk to be covered by detritus or vegetation in the close future. On the contrary, the softer marly members of these formations tend to be covered by soil and vegetation. Cleaning of the section from time to time will be required in order to keep it exposed. Nevertheless, the Burdigalian/Langhian boundary is located within the siliceous–calcareous member of the Schlier, and there is no risk of it being covered.

*Calcareous microplankton biostratigraphy.* The FO of *P. glomerosa sicana* is located at 66.20 m, and corresponds to the *G. trilobus*/*P. glomerosa* s.l. zonal boundary of Iaccarino and Salvatorini (1982) and Iaccarino (1985), and the N7/N8 zonal boundary of Blow (1969). This planktonic foraminiferal event is located in the upper parts of calcareous nannofossil zones NN4, CN3, and MNN3b of Martini (1971), Okada and Bukry (1980), and Fornaciari et al. (1996), respectively. On the basis of this biostratigraphic information, the Burdigalian/Langhian boundary has to be placed slightly above the FO of *P. glomerosa sicana* (see Odin et al., Chapter F2).

The recognition of the N6/N7 zonal boundary at 4.24 m ( $17.5 \pm 0.1$  Ma), as defined by the LO of *C. dissimilis*, allows a biostratigraphic correlation with the upper part of the Contessa section (Montanari et al., Chapter C3).

*Magnetostratigraphy.* In the Moria section, we have identified only one definite reversal, from reverse to normal traversing upsection at about metre level 10. This normal interval occurs within the lower–middle part of nannofossil Zone NN4, in the upper part of nannofossil Zone CN2, and in the lower part of planktonic foraminiferal Zone N7. Based on Harland et al. (1990), this normal interval can only be attributed to Chron 5Cn, while the lower reversed interval containing the N6/N7 zonal boundary in both Contessa and Moria must be the lowest reversed interval of Chron 5C corresponding to 5C3r. The uppermost reversed interval at Moria, which contains the Burdigalian/Langhian boundary, most likely corresponds to Chron 5Br.2r. It is worthwhile comparing the timing of reversals with the palaeomagnetic time scale of Cande and Kent (1992). Their estimated age range for 5Br.2r does not conflict greatly with our geochronologic calibration of the Moria section, although our precise date for the volcanoclastic layer at 58.4 m ( $16.18 \pm 0.16$  Ma,  $2\sigma$ ), which is located within this reversed polarity zone, indicates that the lower boundary of 5Br.2r should be older than their age assignment of 16.014 Ma. However, our biotite age of  $17.1 \pm 0.2$  for the upper part of the normal interval we identify as 5Cn strongly conflicts with the age for the base of 5CN given by Cande and Kent (1995) as 16.726 Ma. When our radiometrically calibrated sedimentation rates are projected downward to the R/N transition at 10 m at Moria, we calculate a minimum

age for the transition of 17.3 Ma, about 0.6 Ma (~3.5%) older than that given by Cande and Kent (1995). Even without extrapolation, our age of  $17.1 \pm 0.2$  Ma for near the upper part of the normal interval at Moria indicates a discrepancy of at least 0.4 Ma.

**Chemostratigraphy.** Stable isotopes and trace elements show significant shifts at 58 m (16.2 Ma), and sharp anomalies at or near the interstage boundary. The  $\delta^{18}\text{O}$  exhibits a conspicuous negative shift at 58 m, and a sharp positive shift right at the boundary, whereas the  $\delta^{13}\text{C}$  shows a positive shift at 58 m, and a lesser negative shift at the interstage boundary. Major negative shifts in the Mn and Mn curves, and positive shifts in the Fe and Sr curves are localized at 58 m (16.2 Ma). Mn and Mg show maximum values just above the interstage boundary, whereas Fe exhibits a maximum peak just below it.

These stable isotopes and trace elements signals may constitute precise tools for chemostratigraphic correlations among Burdigalian–Langhian sections in the Mediterranean domain. Uncertainty remains on whether these signals exist also in coeval oceanic sequences. On the other hand, the  $^{87}\text{Sr}/^{86}\text{Sr}$  curve through the Moria section shows a monotonic decrease from 0.7084 in the lower part of the section, to 0.70865 in the upper part. These values differ from the oceanic curve by a factor of  $-0.0003$ . For instance, a fish teeth sample from 58.2 m (i.e., slightly below the Burdigalian/Langhian boundary) yielded a  $^{87}\text{Sr}/^{86}\text{Sr}$  value of  $0.708533 \pm 0.000005$  which is significantly lower than ratios around 0.70880 measured in coeval oceanic whole carbonate samples. Therefore, Sr isotopic chemostratigraphy cannot be considered a reliable tool for correlating Tethyan and oceanic Burdigalian–Langhian sequences, although it may constitute a valuable means for infra-Tethyan and Paratethyan correlation. Additional analyses on other sections in the Mediterranean domain are necessary for confirming these results.

**Geochronology.** The biostratigraphically approximated Burdigalian/Langhian boundary (i.e., located slightly above the FO of *P. glomerosa sicana*) is closely bracketed by two well dated volcanoclastic layers at 58.40 m, and 76.8 m respectively. Pristine sanidine crystals from these two layers yielded  $^{40}\text{Ar}$ – $^{39}\text{Ar}$  ages of  $16.18 \pm 0.16$  Ma, and  $15.50 \pm 0.16$  Ma, respectively which, by tight interpolation, permit to determine an accurate and precise age of  $16.0 \pm 0.2$  Ma for the FO of *P. glomerosa sicana*; this can be considered as a maximum age for the Burdigalian/Langhian boundary.

Unaltered and homogeneous biotite from the Piero della Francesca Level at 19.5 m was dated independently at the Berkeley Geochronology Center, and the Institute of Geochronology at Pisa. Both labs obtained remarkably consistent K–Ar and  $^{40}\text{Ar}$ – $^{39}\text{Ar}$  ages yielding an overall weighted mean age of  $17.1 \pm 0.2$  Ma for this level. An age of  $17.4 \pm 0.1$  Ma can be assigned to calcareous nannofossil zonal boundaries MNN3b/MNN4a (Fornaciari et al., 1993), and CN2/CN3 (Okada and Bukry, 1980) by tight interpolation between the age of the Piero della Francesca Level with the dated volcanoclastic layer at 58.4 m.

**SOMMAIRE — STRATIGRAPHIE INTÉGRÉE DE LA SECTION DU BURDIGALIEN SUPÉRIEUR-LANGHIEN INFÉRIEUR À MORIA (RÉGION DES MARCHES, ITALIE)**

(Manuscrit soumis: Juin 1995, révisé: Octobre 1995; rédacteurs responsables: AM et RC)

La section de Moria, dans les Apennins du NE, présente une série épaisse de 100 m, continue, complète, en milieu de dépôt pélagique. L’affleurement de bonne qualité a été soumis à des études bio-, chimio-, magnétostratigraphique et géochronologique. L’étude biostratigraphique a mis en évidence 7 apparitions ou disparitions de foraminifères planctoniques permettant l’identification des biozones N6, N7 et N8 de Blow. Les limites de la biozone N7 sont localisées aux cotes 4,24 (disparition de *C. dissimilis*) et 66,20 (apparition de *P. glomerosa sicana*). Les nannofossiles calcaires permettent aussi de proposer une biozonation. La magnétostratigraphie a été fructueuse sur une portion de la section en caractérisant en partie 2 magnétozones interprétées successivement comme 5Cn et 5Br. La caractérisation chimiostratigraphique a mis en jeu les éléments en trace, les isotopes stables et le rapport isotopique du Sr. Pour le strontium, l’influence du facteur régional n’a pas permis de trouver des rapports compatibles avec ceux des eaux océaniques contemporaines limitant l’utilisation de cet outil pour des corrélations à longue distance. Trois niveaux volcanoclastiques situés aux cotes 19,50, 58,5 et 76,8 ont été datés par les techniques de dilution isotopique et d’irradiation au centre de Géochronologie de Berkeley et au Laboratoire de Géochronologie de Pise. Dans ces deux laboratoires, des biotites extraites du niveau 19,50, baptisé Piero della Francesca, ont livré un âge de  $17,1 \pm 0,2$  Ma (incertitude analytique intralaboratoire  $2\sigma$ ). A Berkeley, la sanidine extraite des niveaux 58,4 et 76,8 a été analysée et les âges de  $16,18 \pm 0,16$  Ma et  $15,50 \pm 0,16$  Ma sont proposés pour ces éruptions. Par corrélation biostratigraphique, elles se sont produites de part et d’autre de la limite entre le Miocène Inférieur et le Miocène Moyen telle qu’elle est définie dans les stratotypes historiques du Burdigalien et du Langhien. Une interpolation sédimentaire de courte durée permet de calculer un âge de  $16,0 \pm 0,2$  Ma pour l’apparition de *P. sicana* qui est légèrement plus ancienne que cette limite laquelle se situerait dans la magnétozone interprétée comme 5Br2, et dans les biozones de nannoflore NN4, CN3 et MN4a.

(Sommaire proposé par les rédacteurs d’après un résumé des auteurs, GSO)

**ACKNOWLEDGEMENTS**

This work was partially supported by a grant from the Italian Ministry of University and Scientific Research (MURST, 60%; responsible R. Coccioni.), a grant from Armines (to A. Montanari), and a grant from Exxon Co. (to A. Deino and A. Montanari).



This Page Intentionally Left Blank

## Chapter D2

### **POTENTIAL INTEGRATED STRATIGRAPHY IN THE LANGHIAN L'ANNUNZIATA SECTION NEAR APIRO (MARCHE REGION, ITALY)**

A. Montanari, R. Coccioni, E. Fornaciari and D. Rio

#### INTRODUCTION

The Langhian in the Umbria–Marche basin of the northeastern Apennines is represented by the Schlier formation, a soft marly unit which is usually covered by thick soil and bushy vegetation, or is deeply eroded in badlands-like landscapes locally known as ‘*calanchi*’ which are frequently subjected to landsliding. In the western areas of the Umbria–Marche Apennines (i.e., around Gubbio), the sequence of hemipelagic marls of the Schlier is interrupted by the Marnoso Arenacea flysch, whereas in the easternmost areas of this region, along the Adriatic coast, the Schlier facies stretches up to the Messinian, and underlies the Euxinic Shale formation (i.e., in the Cònero Riviera sequence described by Montanari et al., Chapter E1).

The contrast in lithologic competence between the softer Schlier, the underlying Bisciario marly limestones, and overlying Marnoso Arenacea sandstones, often favour low-angle faulting, as it is the case in the Contessa section (Montanari et al., Chapter C3). For all these reasons, it is difficult to find complete and continuous sections of Schlier in the Umbria–Marche region, and the few ones which permitted some detailed stratigraphic studies are located either in fresh road cuts (i.e., the Moria section described by Deino et al., Chapter D1) or on the cliffs of the Cònero Riviera which are repeatedly washed by sea-wave action (Montanari et al., Chapter E1).

In the late 1980s, road works on the country dirt road near the L'Annunziata chapel of Apiro (Fig. 1), have exposed a short stretch of the upper marly member of the Schlier containing an 8 cm thick biotite-rich, olive-green, clay layer (Fig. 2) named Michelangelo Level by Montanari et al. (1988b). This volcanoclastic layer may constitute a regional marker bed suitable for radioisotopic age calibration of the Langhian.

#### LITHOSTRATIGRAPHY

The 2.35 m thick L'Annunziata section consists of greenish-grey to blue-grey hemipelagic marls representing the upper marly member of the Schlier formation (Coccioni and Montanari, 1992). On the basis of calcareous nannofossil stratigraphy (see below), this short exposure may be correlated with the partially covered base of the same Schlier member in the Moria section (Deino et al., Chapter D1). In fact, the biotite-rich Michelangelo Level in the Moria section may be hidden beneath the soil cover, between 81 m and 85 m. A similar biotite-rich clay layer was recently discovered in the Vedova section (Cònero Riviera sequence, see Montanari et al., Chapter E1), at metre level 24.10.

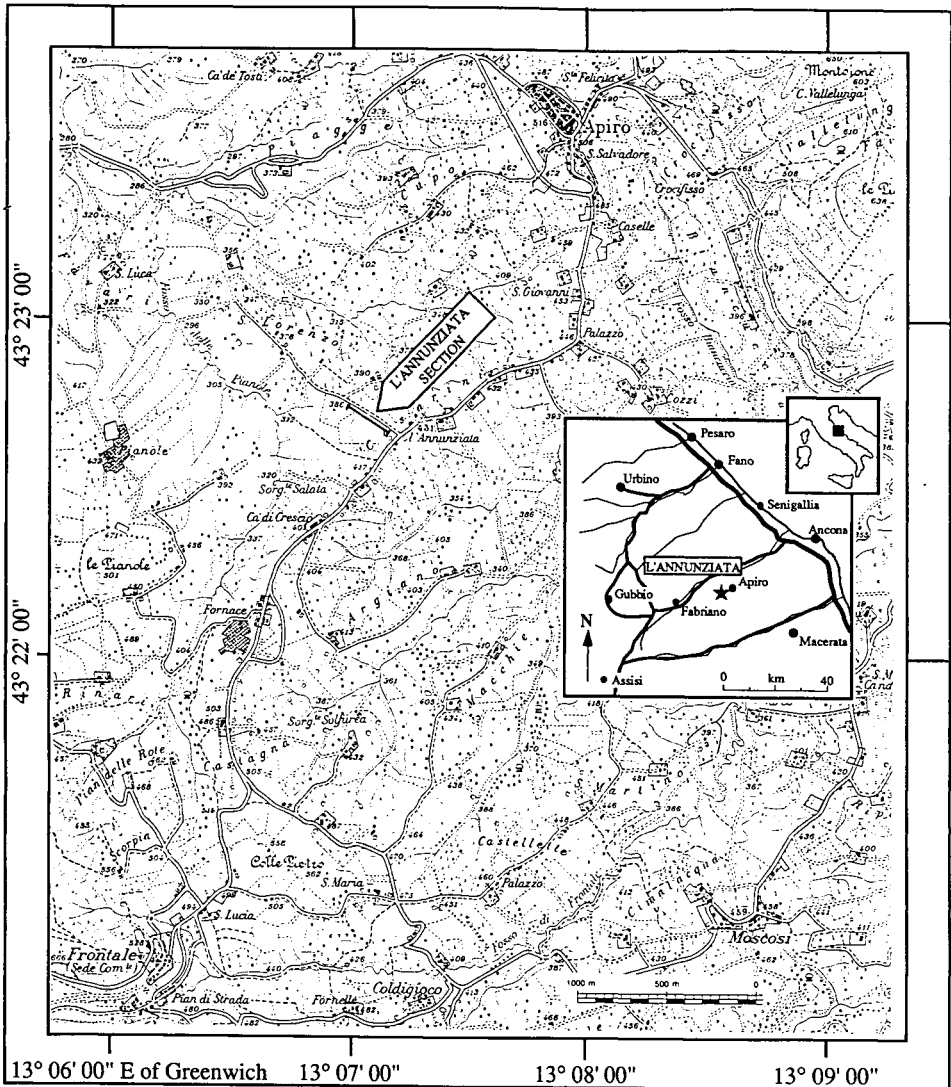


Fig. 1. Location map of the L'Annunziata section.

### CALCAREOUS PLANKTON BIOSTRATIGRAPHY (R. Coccioni, E. Fornaciari and D. Rio)

Four samples collected in the L'Annunziata section were analyzed for planktonic foraminiferal and calcareous nannofossil biostratigraphic determinations. The biostratigraphic results of these analyses are illustrated in Fig. 3.

Planktonic Foraminifera are abundant and moderately to well preserved. The occurrence of *Praeorbulina sicana*, *P. transitoria*, *P. glomerata curva*, and *P. glomerata*



Fig. 2. The l'Annunziata exposure in 1988. The dark, tectonically deformed horizon is the volcanoclastic biotite-rich Michelangelo Level. Horizontal field is about 3 m.

*glomerosa* within the foraminiferal assemblages indicate that this section belongs to the N8 Zone of Blow (1969) and/or to the lower part of the *Praeorbulina glomerosa* s.l. Zone of Iaccarino and Salvatorini (1982) and Iaccarino (1985). Thus, this section is definitively early Langhian in age, although the absence of relevant foraminiferal events does not permit to establish which part of the N8 Zone it represents.

Calcareous nannofossil are common in the investigated samples, although they are in a moderate to poor preservation state. Assemblages are dominated by placoliths. Helicoliths are well represented. Discoasterids and sphenoliths are scarce to rare. We counted helicolith and sphenolith index species as reported in Fig. 3. Because of the absence of *Helicosphaera ampliaperta* and the presence of *Sphenolithus heteromorphus*, the entire section is to be ascribed to zones NN5 and CN4 of Martini (1971) and Okada and Bukry (1980), respectively. In the lowermost sample (0.05 m level), sphenoliths are very rare and *S. heteromorphus* is virtually missing (one specimen in a counting of 30 sphenoliths). This feature (together with the absence of *H. ampliaperta*) may indicate that the lowermost part of the section belongs to the '*Sphenolithus heteromorphus* Absence Interval Zone' (MNN4b) of Fornaciari et al. (1993), which has been recognized also in the Moria section (Deino et al., Chapter D1). The section interval above the lowermost sample, may be ascribed to the '*Sphenolithus heteromorphus*–*Helicosphaera walbersdorfensis* Interval Subzone' (MNN5a) of Fornaciari et al. (1996) because of the absence of *H. ampliaperta* and *Helicosphaera walbersdorfensis* and the presence of *S. heteromorphus*. In summary,

# L'Annunziata Section

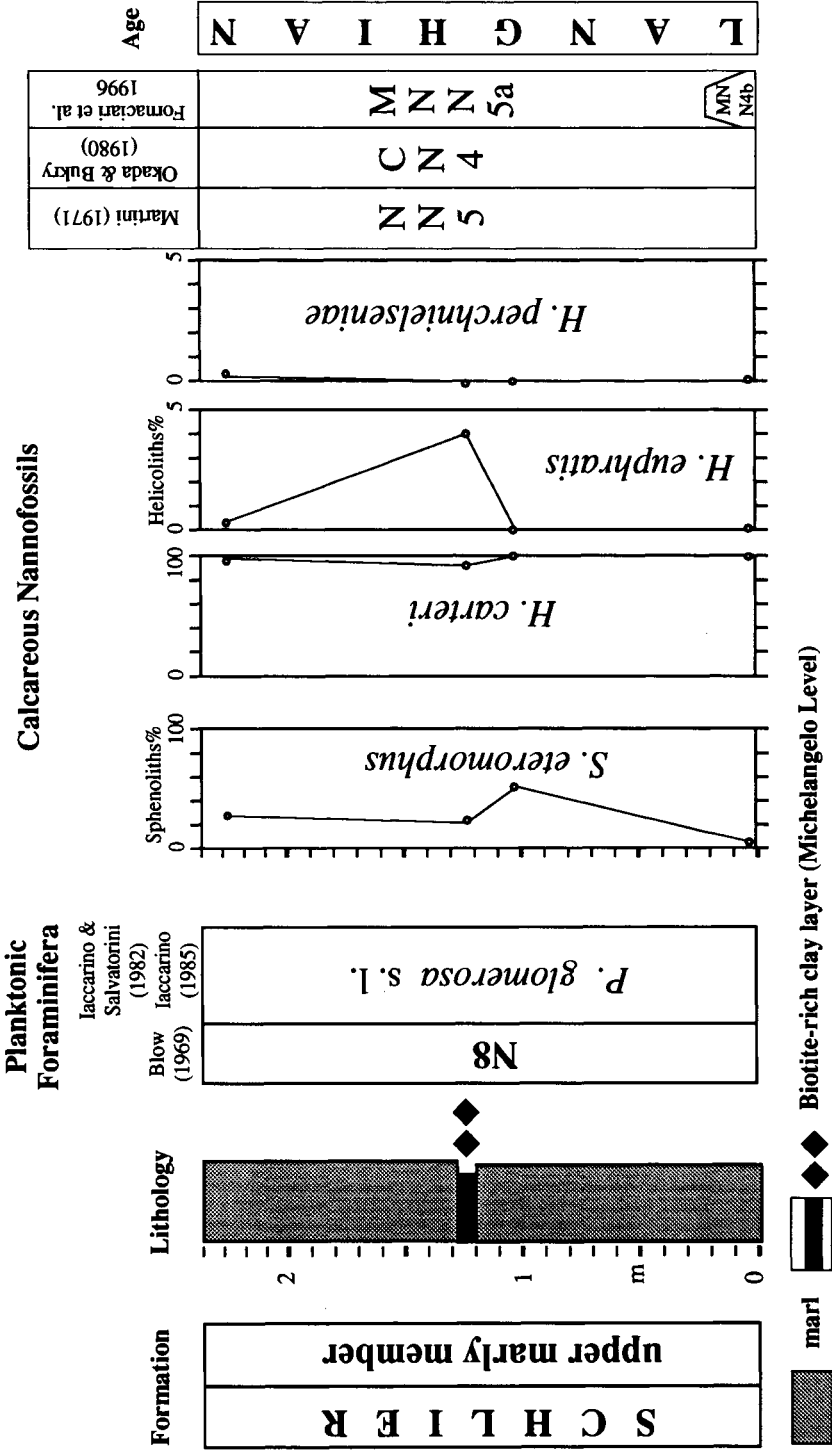


Fig. 3. Calcareous microplankton litho-, and biostratigraphy of the L'Annunziata section.

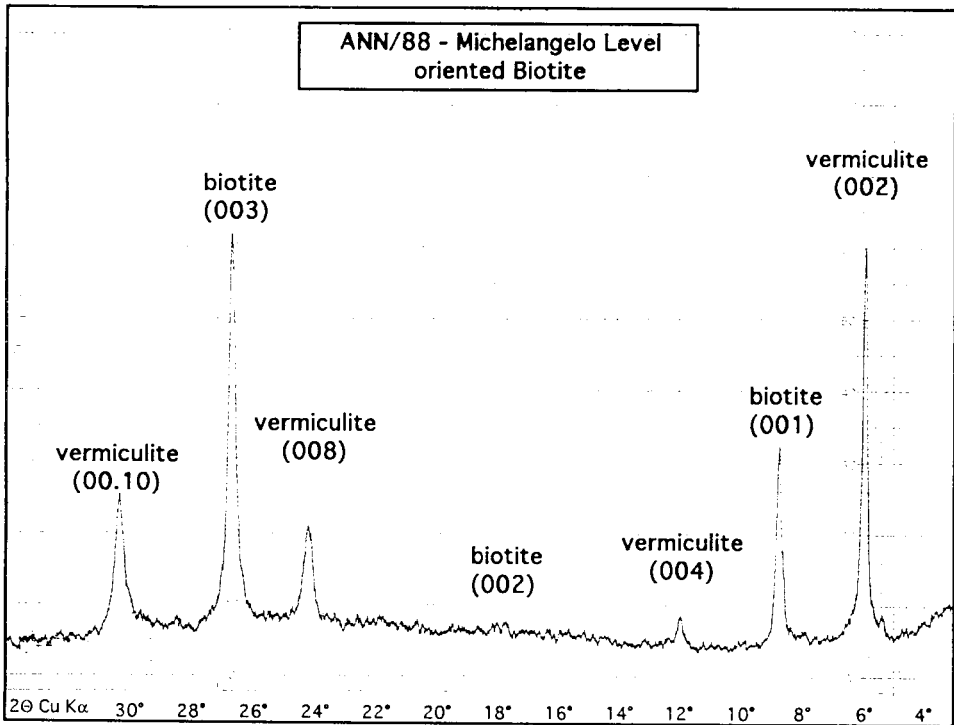


Fig. 4. X-ray diffractogram of biotite from the Michelangelo Level in the L'Annunziata section.

calcareous nannofossils indicate that the base of the section is early Langhian in age.

#### GEOCHRONOLOGIC POTENTIAL (A. Montanari)

A sample of the Michelangelo Level collected in 1987 contains apparently pristine biotite but X-ray diffractometry has shown the presence of vermiculite (Fig. 4). Therefore, following the recommendations of Odin et al. (1991), this altered biotite cannot be considered a priori as a potentially reliable geochronometer.

Microprobe analyses on Michelangelo biotite flakes (Table 1) yielded, in some cases, relatively low totals probably due to the presence of water and/or vermiculite. Nevertheless, the mean MgO/Fe ratio of 0.34 is similar to the 0.31–0.32 ratios found in biotites from the Piero della Francesca Level in the Santa Croce di Arcevia and Moria sections (upper Burdigalian; see Coccioni and Montanari, 1992; Deino et al., Chapter D1), and slightly higher than the mean ratio of 0.19 measured in the biotite from the Respighi Level in the Monte dei Corvi section (lower Serravallian). All these Mid-Miocene biotites exhibit MgO/FeO ratios (0.2–0.3) significantly lower than those found in the overlying uppermost Serravallian Ancona and uppermost Tortonian and Rossini levels (1.03 and 0.57, respectively), the underlying Oligocene biotites which range from 0.8 to 1.1, and the Eocene biotites with MgO/FeO ratios ranging from 0.45

Table 1

Chemical composition (in wt%) of biotite flakes from the Michelangelo Level in the L'Annunziata section

Analysis/flake	SiO <sub>2</sub>	TiO <sub>2</sub>	Al <sub>2</sub> O <sub>3</sub>	FeO*	MgO	CaO	Na <sub>2</sub> O	K <sub>2</sub> O	Total
(1) 3 points analyzed	34.43	3.42	12.45	22.80	7.00	0.15	0.06	7.87	89.18
(2) 5 points analyzed	35.00	3.28	12.35	22.26	6.90	0.27	0.04	7.32	87.42
(3) 4 points analyzed	35.80	3.32	11.63	22.74	7.61	0.16	0.04	7.80	88.45
(4) 5 points analyzed	33.83	3.39	13.58	25.13	6.91	0.15	0.38	8.32	91.70
(5) 5 points analyzed	35.06	3.30	12.46	21.47	7.26	0.18	0.09	7.80	87.62
(6) 5 points analyzed	35.12	4.47	14.07	19.93	9.63	0.12	0.57	8.70	92.60
(7) 5 points analyzed	35.76	3.39	12.65	20.12	8.68	0.38	0.13	7.76	88.87
(8) 4 points analyzed	34.62	4.12	13.97	22.17	8.41	0.26	0.45	7.77	91.76
(9) 5 points analyzed	35.00	3.31	12.94	22.47	7.14	0.23	0.11	8.09	89.30
(10) 4 points analyzed	34.97	3.42	12.80	22.74	6.92	0.31	0.11	7.35	88.63
Average	34.96	3.54	12.89	22.18	7.64	0.22	0.20	7.88	89.51

FeO\* = total iron.

to 0.65 (Montanari, 1988). This may suggest that the volcanic source was probably the same for all these Mid-Miocene (upper Burdigalian, Langhian, and lower Serravallian) biotite-rich levels (Assorgia et al., 1994).

Preliminary <sup>40</sup>Ar/<sup>39</sup>Ar laser-fusion analyses on nine individual sanidine grains from the Michelangelo Level were carried out at the Berkeley Geochronology Center (Montanari et al., 1988b), yielding a mean ideogram age of about 15.0 Ma. However, although the sanidine crystals seemed pristine, the analyzed grains were too few and small for technically accepting the analytical results as indicative to reliable age determination. Thus, further radioisotopic analyses on larger and coarser-sanidine samples are necessary to establish a precise and accurate age for this volcanoclastic layer.

## CONCLUSIVE REMARKS

Despite the exiguous thickness of this section, the exposure of the lower part of the upper marly member of the Schlier formation at L'Annunziata permitted the discovery of the biotite-rich Michelangelo Level which may constitute a precise lithologic marker for the recognition of the lower Langhian in other exposures throughout the Umbria-Marche Apennines. The presence of biotite and sanidine in this volcanoclastic layer, and the good calcareous microplankton record in the layers surrounding it, promote further integrated stratigraphic studies in this and other coeval sections in the region as well (i.e., the Vedova section in the Cònero Riviera: see Montanari et al., Chapter E1) which would be useful for a better calibration of the (often elusive) Langhian chronostratigraphic interval.

SOMMAIRE — POTENTIEL POUR LA STRATIGRAPHIE INTÉGRÉE DE LA SECTION LANGHIENNE DE L'ANNUNZIATA PRÈS D'APIRO (RÉGION DES MARCHES, ITALIE)

(Manuscrit soumis: Juin 1995, révisé: Juillet 1995; rédacteurs responsables: AM et RC)

Le petit affleurement situé près de la chapelle de l'Annunziata à Apiro (Marches, Italie) expose 2,3 m de sédiments. L'étude biostratigraphique de l'association de foraminifères planctoniques (*Praeorbulina sicana*, *P. transitoria*, *P. glomerosa curva*, *P. glomerosa glomerosa*) indique que ces sédiments peuvent être attribués à la biozone N8 de Blow (1969) et à la partie inférieure de la biozone à *P. glomerosa* s.l. de Iaccarino (1985). Ces dépôts sont ainsi en corrélation avec le Langhien. Les nannofossiles calcaires permettent de préciser que la partie basale de la section appartient à la biozone MNN4 et, par corrélation, à la partie inférieure mais non basale de la biozone N8. Un niveau volcanoclastique à biotite (altérée) et sanidine (de qualité acceptable) est visible dans la section et une étude géochronologique préliminaire a montré que ce dernier minéral pouvait être daté avec confiance. Cet affleurement indique qu'il est possible de trouver, là ou dans un affleurement proche, une série sédimentaire susceptible de permettre une intéressante recherche de stratigraphie intégrée pour l'intervalle chronostratigraphique souvent insaisissable que constitue le Langhien.

(Sommaire proposé par les rédacteurs d'après un résumé anglais des auteurs, GSO)

ACKNOWLEDGEMENTS

This work has been supported, through past years, by grants from the United States National Science Foundation, a grant from Exxon Oil Co., Armines (to A. Montanari), and a grant from the Italian Ministry of University and Scientific Research (MURST, 60%; responsible R. Coccioni.).



This Page Intentionally Left Blank

Chapter D3

**BIOSTRATIGRAPHY AND GEOCHRONOLOGY OF AN EARLY  
SERRAVALLIAN VOLCANICLASTIC LAYER FROM SICILY**

G.S. Odin, P. Miculan, M. Cosca, F. Tateo, A. Amorosi and J.C. Hunziker

INTRODUCTION

The presence of volcanoclastic deposits has been repeatedly reported from the Middle Miocene of south-central Sicily (e.g., Ogniben, 1969; Romeo, 1969; Spadea and Carmisciano, 1974; Carveni et al., 1982). They consist of rhyo-dacitic tuffs which form lenticular bodies up to several metres thick (about 5.5 m thick at Case Liardo near Enna), and some hundreds of metres wide.

These tuffs are usually included in the lower part of the so called 'marne a globigerine' of Burdigalian to Messinian age. This informal lithostratigraphic unit is referred to as '*Globigerina* marl formation' in the present work. Estimates of the age of the volcanoclastic deposits range from uppermost Burdigalian (base of biozone N8 of Blow, 1969) to middle (?) Serravallian (N12–N14 zones, Carveni et al., 1982). The tuffs are poorly exposed in short sections which show faulting and tectonic disturbance including reversed series or possible duplication (Spadea and Carmisciano, 1974).

A thin volcanoclastic layer, first reported by Romeo (1969) from the Monte Giammoia section is a conspicuous exception. The reasonably well documented biostratigraphical situation of the layer (Miculan, 1994) and the presence of a-priori favourable material led us to consider that level for geochronological investigation.

LITHOSTRATIGRAPHY

The study area is located in southern-central Sicily (Fig. 1), along the eastern margin of the so-called Caltanissetta Basin. The Miocene deposits mainly consist of hemipelagic marls covered by Messinian evaporitic deposits. The following informal lithological units can be distinguished, from bottom to top: (1) the Burdigalian to early Messinian *Globigerina* marl formation ('marne a globigerine' of Italian authors) which consists of grey marls with regular intercalations of thin bedded, organic-rich, brown clays; (2) Messinian 'Tripoli' composed of laminated diatomites and diatomaceous clays; (3) Messinian limestones ('Calcare di base'); (4) Messinian gypsum.

The Miocene succession unconformably overlies multicoloured scaly clays containing a chaotic mixture of various dismembered lithotypes ('argille scagliose variegata', Cretaceous to Palaeogene in age).

The *Globigerina* marl extensively crops out on the southern slope of the Monte Giammoia. The area shown in the map (Fig. 1) falls within sheet 272 I SE 'Passo di Piazza' of the Carta d'Italia, scale 1 : 25,000, edited by the Istituto Geografico Militare.

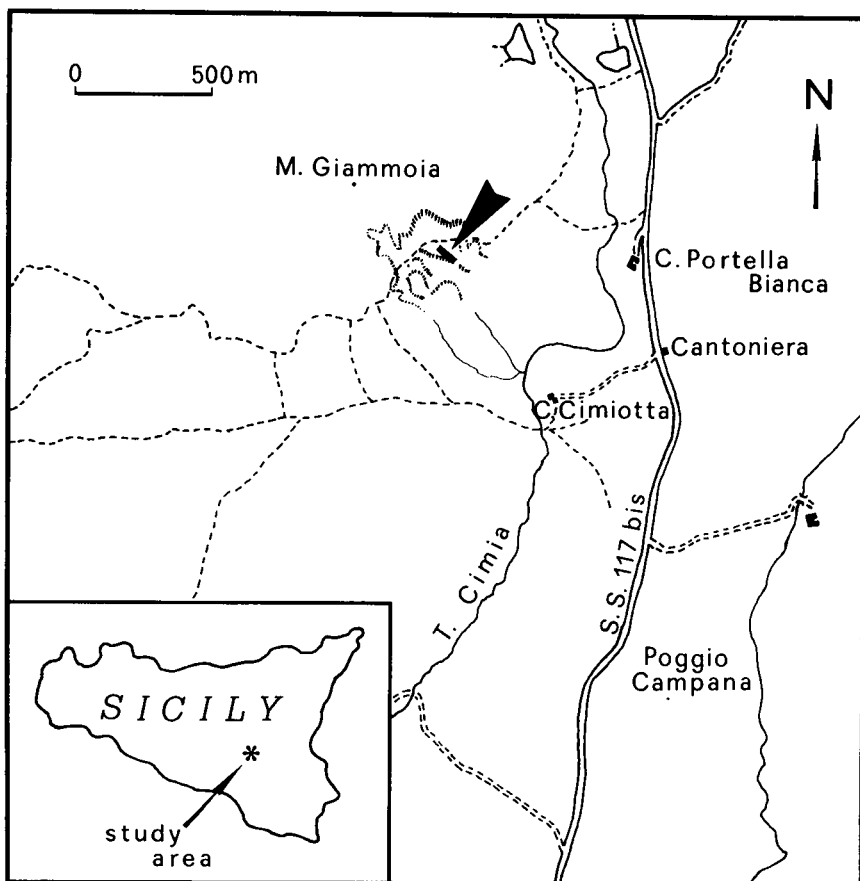


Fig. 1. Geographical location of the Monte Giammoia section (star) in Sicily.

The section was first described by Romeo (1969) and subsequently was the subject of several investigations (Colalongo et al., 1979b; Zachariasse and Spaak, 1983; Theodoris, 1984; Chamley et al., 1986; Miculan, 1994; Suc and coworkers, in prep., among others).

According to G.B. Vai and M. Grasso (pers. commun., following a visit in 1993), the precise succession of deposits is locally complex due to faulting which is poorly evidenced in the outcrop and the section is not favourable for detailed stratigraphy in the deposits younger than the Serravallian ones considered here.

In the lower portion of the Monte Giammoia section, the *Globigerina* marl contains a thin sandy layer of probable pyroclastic nature (Romeo, 1969; Carveni et al., 1982; Miculan, 1994). This layer, 1 or 2 cm thick, is pale grey in colour (when fresh) and is diagnostically marked by abundant biotite flakes. This layer turns yellow to rusty on weathered surfaces which makes it easy to follow. It is overlain and underlain by green-grey clays which are around 40 cm thick. The lower clay bed yields rare and poorly preserved microfossil tests, whereas the upper bed (above the volcanoclastic layer) is almost devoid of microfossils. X-ray diffraction analysis shows

that the dominant fraction is composed of poorly ordered clay minerals including illite-smectite, smectite, chlorite and kaolinite. This complex association suggests a detrital origin and the absence of Foraminifera might be related to a high sedimentation rate or to a particular chemistry during that time interval.

Around 2.5 m above the volcanoclastic layer is a lens of apparently similar composition. It is about 1 m wide and 0.15 m at its maximum thickness in the outcrop. About 0.3 m immediately above the lens, the stratigraphic record is truncated by an unconformity.

The carbonate content of the rock is generally between 40% and 50% and decreases to less than 10% around the cinerite and within the two dark clay layers (Fig. 2).

The stratigraphic interval encompassing the biotite-rich layer (Fig. 2) has been closely sampled and is shown in Fig. 3.

## BIOSTRATIGRAPHY

Within the Monte Giammoia section, the *Globigerina* marl yields rich, highly diversified, and very well preserved planktonic foraminiferal assemblages. A precise biostratigraphic zonation has been established by Miculan (1994).

In the lower part of the section, the foraminiferal assemblages (Fig. 4) are characterized by *Globorotalia peripheroronda*, *Globorotalia praemenardii*, *Globorotalia praescitula*, *Orbulina universa*, *Orbulina suturalis*. This association correlates to the *G. praemenardii*-*G. peripheroronda* Subzone (*O. suturalis*-*G. peripheroronda* Zone) of Iaccarino and Salvatorini (1982) and Iaccarino (1985).

The last recognized occurrence of *G. peripheroronda* is in sample MGE17, less than 2 m below the 'unconformity'. Up to level MGE17 the species is abundant in the studied samples (except for MGE12-MGE14). Conversely, it is missing in samples MGE18-MGE20 in the upper part of the measured section.

Advanced specimens of *G. peripheroronda*, transitional to *Globorotalia peripheroacuta*, have been recognized in the uppermost part of the local range of *G. peripheroronda*. They commonly occur immediately before the last Mediterranean occurrence of *G. peripheroronda* (Martinotti, 1981). Consequently, we assume that level MGE17 correlates with the Mediterranean last occurrence of the taxon.

*Paragloborotalia partimlabiata* was first recorded in sample MGE21, immediately above the unconformity. *Globigerina decoraperta* first occurs in sample MG14.

The last Mediterranean occurrence of *G. peripheroronda* is commonly considered a reliable marker event for regional correlation (Bizon, 1979; Martinotti, 1981, 1990; Iaccarino and Salvatorini, 1982; Iaccarino, 1985; Miculan, 1994). This event probably predates the extinction of *G. peripheroronda* at lower latitudes. Following Martinotti (1981, 1990), Miculan (1994) assumed that the species disappeared from the Mediterranean immediately before the first evolutionary appearance of *G. peripheroacuta* which marks the lower boundary of Blow's zone N10. However, this later event is not recognizable in the Mediterranean since the presence of typical specimens of *G. peripheroacuta* was never documented exhaustively in this area and the correlation is rather speculative.

The micropalaeontological analysis reveals an important hiatus in the record, corresponding to the unconformity. As a matter of fact, *P. partimlabiata* first occurs immediately above the unconformity and the *Globoquadrina altispira* Zone (Iaccarino

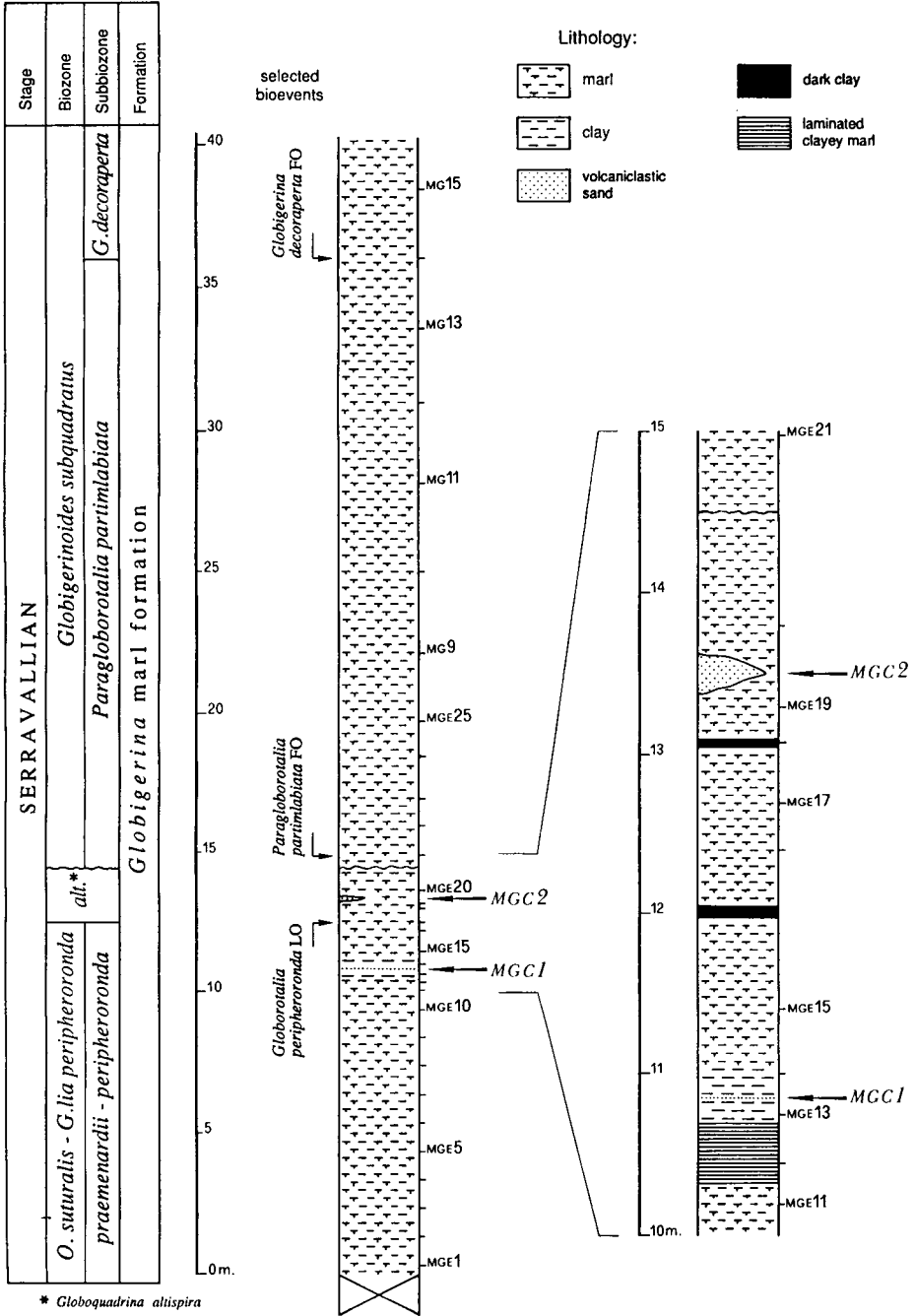


Fig. 2. Lithostratigraphy and biostratigraphy of the Monte Giammoia section. The dated sample (MGC1) is a layer. Volcaniclastic material is also present as lenses above, less than 1 m below the unconformity.



Fig. 3. Photograph of the measured section. The white bar shows the lower part of the measured section (MG1 to MG25 in Fig. 2); arrow locates the change in colour from darker below to lighter grey above; it is interpreted as an unconformity (photo by P. Miculan, 1992).

and Salvatorini, 1982) is only a few metres thick in the Monte Giammoia section. Miculan (1994) tentatively correlates the *G. altispira* Zone with Blow's Zones N10 to N12 (pars). According to Salvatorini and Cita (1979), *P. partimlabiata* appears in Zone N12.

The biotite-rich layer, which is the main subject of the present work, belongs to the uppermost part of the *O. suturalis*-*G. peripheroronda* Zone (Iaccarino and Salvatorini, 1982; Iaccarino, 1985) and to the upper part of Blow's Zone N9 on the basis of the proposed correlation. The age is early Serravallian.

## GEOCHRONOLOGY

### *Petrography and mineralogy of the geochronometers*

It was not easy to collect a fresh sample from the biotite-rich layer alone. A portion of the sample selected contained some of the surrounding green clay. After washing, the remaining sand-size fraction was submitted to the usual procedures for mineral separation (see Chapter F1).

The rock contains well-preserved biotite, elongated green crystals of amphibole are common, and plagioclase is abundant. The silt-size fraction of the sediment contained a single zircon crystal but no estimate of zircon and apatite proportions was possible



Table 1

Geochemical data from biotite flakes in samples T180 (original data by F.T.)

	SiO <sub>2</sub>	TiO <sub>2</sub>	Al <sub>2</sub> O <sub>3</sub>	FeO*	MnO	MgO	CaO	Na <sub>2</sub> O	K <sub>2</sub> O	FeO*/MgO
	39.06	4.58	15.98	12.70	0.11	16.98	0.09	0.80	9.70	0.75
	39.77	3.13	15.96	15.46	0.08	15.45	0.14	0.79	9.21	1.00
	39.47	3.19	15.97	15.67	0.08	15.48	0.11	0.74	9.28	1.01
	39.81	2.80	15.50	15.82	0.08	15.61	0.04	0.66	9.67	1.01
	39.96	3.20	15.50	15.74	0.02	15.52	0.04	0.52	9.49	1.01
	39.65	3.20	15.89	15.65	0.11	15.32	0.07	0.48	9.63	1.02
	38.86	3.82	15.90	15.83	0.00	15.33	0.04	0.77	9.43	1.03
	38.73	3.00	16.52	16.00	0.07	15.38	0.09	0.68	9.52	1.04
	38.80	3.57	15.90	16.12	0.13	15.24	0.07	0.59	9.57	1.06
	39.28	3.26	16.16	16.13	0.00	15.20	0.01	0.44	9.51	1.06
	38.39	3.83	15.91	16.22	0.03	15.15	0.04	0.88	9.55	1.07
	39.18	3.20	15.93	16.29	0.09	15.20	0.12	0.43	9.57	1.07
	38.73	3.17	15.80	16.44	0.21	15.30	0.10	0.68	9.56	1.07
	38.56	3.33	16.11	16.47	0.13	15.06	0.03	0.63	9.68	1.09
Average	39.16	3.38	15.93	15.75	0.08	15.44	0.07	0.65	9.53	1.02
±1σ	0.49	0.43	0.24	0.90	0.05	0.45	0.04	0.14	0.14	0.08

FeO\* = total iron: ±1σ: standard deviation.

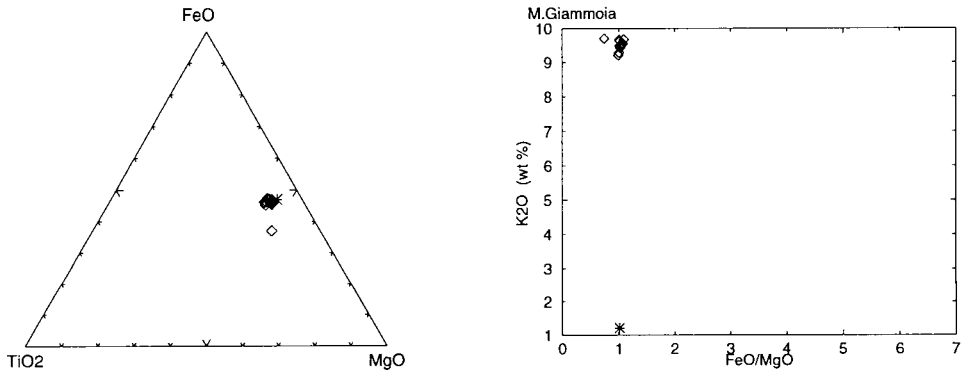


Fig. 5. Geochemical homogeneity of biotite flakes from sample T180 (original data by F.Tateo).

1.02. Interestingly, the single amphibole crystal analyzed has a similar FeO, MgO and TiO<sub>2</sub> signature. A single biotite flake shows significantly high TiO<sub>2</sub> and MgO, and low FeO contents which cannot be accounted for by instrumental errors (Fig. 5). Nevertheless, Na<sub>2</sub>O content is significantly high in all flakes (Table 1) and, for this reason, we believe the ‘anomalous’ crystal can hardly be considered as an extra source component.

The plagioclase was separated from the non-magnetic fraction using bromoform acetone mixtures, and cleaned with 50% acetic acid in an ultrasonic bath for 3 h. The final separate still showed a rusty surface pointing to a surface alteration of the original sample in the outcrop. X-ray diffraction patterns indicate the plagioclase to be anorthite-rich and poorly crystallized as evidenced by low peaks.



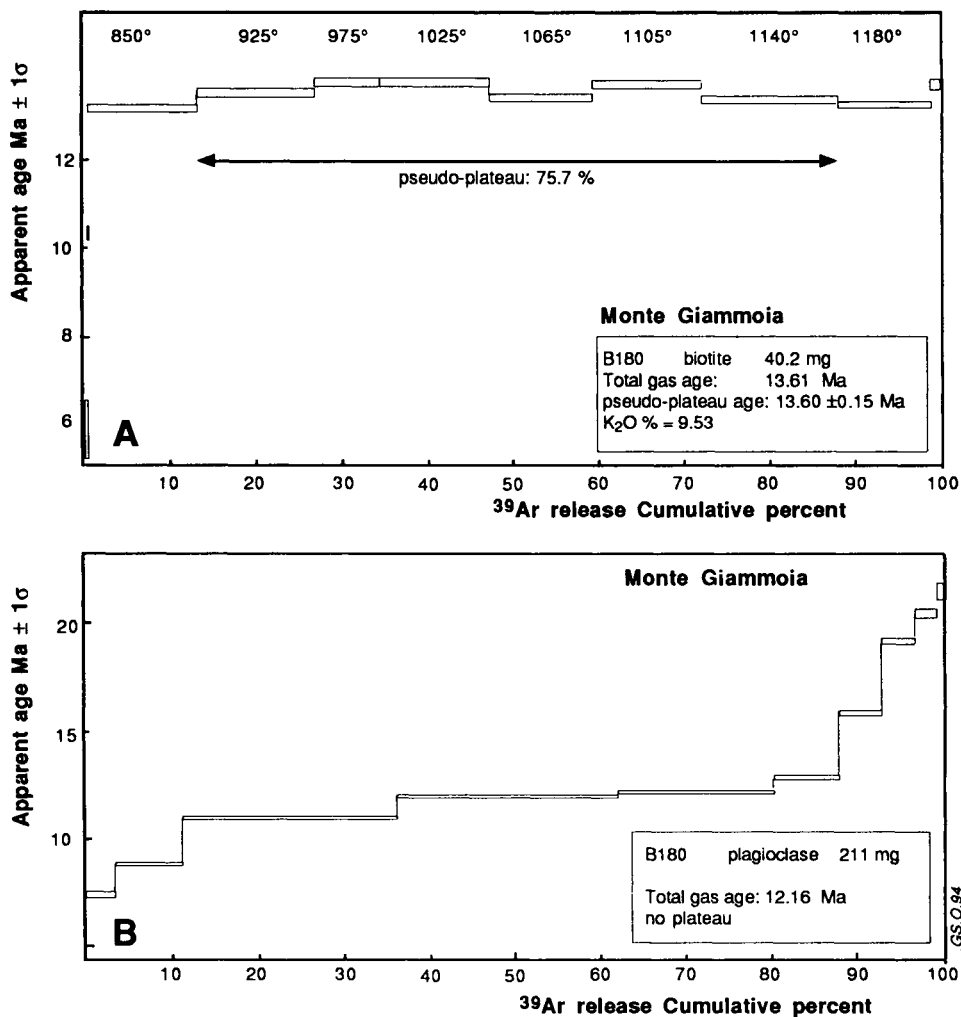


Fig. 6. Spectra of age results obtained from  $^{40}\text{Ar}/^{39}\text{Ar}$  incremental heating measurements on biotite (A) and plagioclase (B) separated from sample T180, Monte Giammoia, Sicily.

#### $^{40}\text{Ar}/^{39}\text{Ar}$ isotopic results

The biotite and plagioclase were analyzed by the stepwise  $^{40}\text{Ar}/^{39}\text{Ar}$  technique. The samples were irradiated in the Triga reactor in Denver together with subsamples of the biotite HD-B1 standard. The isotope ratios were measured using the standard procedure developed in Lausanne (Cosca et al., 1992).

Sample T180 biotite (40.24 mg) was analyzed in thirteen heating steps following preliminary heating in a vacuum at  $500^{\circ}\text{C}$  for 30 min. Fig. 6A and Table 2 present the results. Analytically significant ages were obtained for nine steps. They are spread between 13.2 and 13.8 Ma and there is no series of successive ages with an analytically

Table 2

Results of  $^{40}\text{Ar}/^{39}\text{Ar}$  step heating measurements on B180 biotite (40.24 mg) from Monte Giammoia (by GSO in Lausanne)

°C	Apparent age (Ma)	$\pm 2\sigma$	% $^{39}\text{Ar}$	%rad.	K/Ca
650	5.9	1.4	0.4	4	5.5
750	10.4	0.6	0.2	14	10.8
850	13.2	0.2	12.4	47	24.3
925	13.54	0.20	13.5	55	25.5
975	13.77	0.20	8.0	63	18.9
1025	13.80	0.20	13.1	63	21.0
1065	13.43	0.18	12.2	70	10.5
1105	13.74	0.18	13.0	75	6.1
1140	13.38	0.18	15.9	79	8.1
1180	13.29	0.16	9.8	81	16.0
1230	13.8	0.2	1.4	58	9.3
1300	9.7	2.8	0.1	11	2.2
1550	7.3	2.6	0.1	4	0.6

Apparent ages: (total gas age) = 13.61 ( $\pm 0.15$ ) Ma; (pseudo plateau age 925–1140°C) = 13.60  $\pm$  0.15 Ma ( $2\sigma$ ); calibration with biotite HD-B1 = 24.21 Ma.

Table 3

Results of  $^{40}\text{Ar}/^{39}\text{Ar}$  step heating measurements on B180 plagioclase (211.8 mg) from Monte Giammoia (by G.S.O. in Lausanne)

°C	Apparent age (Ma)	$\pm 2\sigma$	% $^{39}\text{Ar}$	%rad.	K/Ca
650	7.21	0.22	3.5	28	0.26
800	8.76	0.14	7.8	63	0.16
950	10.97	0.14	24.8	87	0.074
1050	12.09	0.16	26.0	92	0.056
1150	12.30	0.16	18.6	81	0.064
1250	12.96	0.22	7.6	53	0.070
1350	15.9	0.2	4.9	64	0.049
1450	19.2	0.3	3.9	49	0.045
1500	20.5	0.4	2.4	54	0.043
1580	21.7	0.8	0.5	44	0.048

Apparent age (total gas): 12.16 ( $\pm 0.11$ ) Ma.

similar apparent age (no plateau). However, minimum and maximum ages are not very different from each other and a weighted mean age of 13.60  $\pm$  0.15 (steps 925 to 1140°C) can be proposed as a representative age of the biotite phase; this is similar to the total gas age at 13.61 Ma (with similar  $2\sigma$  error bar estimate).

Isochron plots were calculated from the seven steps in between 925 and 1140°C (Fig. 7). The  $^{40}\text{Ar}/^{36}\text{Ar}$  versus  $^{39}\text{Ar}/^{36}\text{Ar}$  plot gives an apparent age at 13.52  $\pm$  0.64 Ma, an initial  $^{40}\text{Ar}/^{36}\text{Ar}$  ratio at 301  $\pm$  28 and a MSWD of 20. The  $^{36}\text{Ar}/^{40}\text{Ar}$  versus  $^{40}\text{Ar}/^{39}\text{Ar}$  plot gives similar results with an apparent age of 13.53  $\pm$  0.65,  $^{40}\text{Ar}/^{36}\text{Ar}$  ratio at 301  $\pm$  26 and MSWD of 26. Similar calculations using all steps lead to a more precise age of 13.85  $\pm$  0.25 Ma, with a low initial ratio of 283  $\pm$  7, and a similar MSWD.

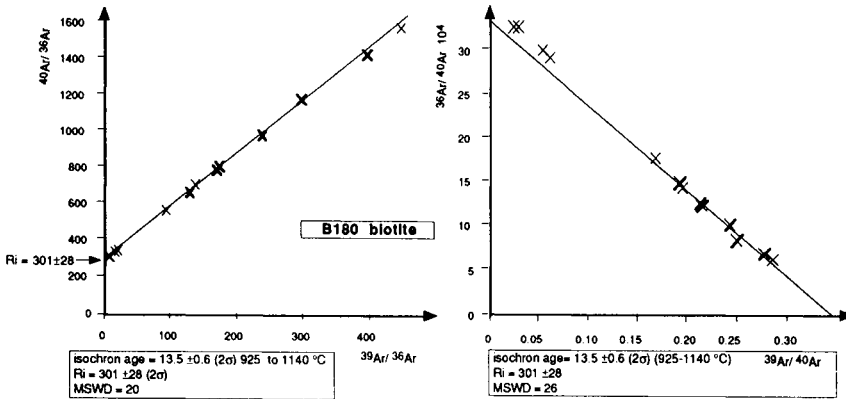


Fig. 7. Isochron plots of biotite from the Monte Giammoia section. Thicker crosses distinguish the seven main steps.

Sample T180 plagioclase (211.8 mg) was heated first in a vacuum at 550°C for 30 min. The  $^{40}\text{Ar}/^{39}\text{Ar}$  spectrum (Fig. 4B) displays a wide range of consistently increasing ages from 7.2 to 21.7 Ma (Table 3). There is no plateau and the total gas age at 12.16 Ma is not similar to that of the biotite separate.

## DISCUSSION AND CONCLUSIONS

In the present work, we assume that the base of the Serravallian Stage may be approximated biostratigraphically by the first evolutionary appearance of *O. universa*. In fact, the local first occurrence of this taxon in the Serravallian historical stratotype proposed by Vervloet (1966) along the Scrivia Valley at Serravalle is recognizably below the base of the Serravallian type section (Chapter A5). It is also located immediately below the upper limit of the Langhian historical stratotype proposed by Cita and Premoli Silva (1960) according to Iaccarino (1985), Bossio et al. (1992), and Miculan (1994). The two type sections are therefore consistent from this point of view (Chapter A5). To help in correlating the first occurrence of *O. universa* appears to be the biostratigraphical criterion nearest to, yet older than, the Langhian/Serravallian boundary. It significantly predates the last Mediterranean occurrence of *G. peripheroronda* (Cita, 1976; Bizon, 1979; Martinotti, 1981, 1991; Iaccarino and Salvatorini, 1982; Iaccarino, 1985; among others). The latter event has been recognized immediately above the dated layer which is therefore early Serravallian in age.

The biotite-rich layer is assumed to result from an ash fall. The biotite crystals exhibit euhedral shapes suggesting a pyroclastic origin, a high proportion of inclusions, favourable X-ray diffraction patterns showing a weak admixture of apparently well-preserved amphibole, and a high K content. The geochemical homogeneity suggests a single volcanic event and no sedimentary detrital admixture.

The slightly disturbed spectrum of the biotite suggests some heterogeneity of the dated material which is probably related to the inclusions and the admixture of amphibole. Fortunately, the apparent ages calculated for most steps vary within close

limits: 13.2 to 13.8 Ma with a weighted mean and a total gas age of  $13.6 \pm 0.15$  Ma. These ages may be considered reliable geological indications of the time of crystallization, and the time of deposition. The analysis of the plagioclase was not able to give any significant geological data.

The analytical ages of the biotite separate are related to the accepted value of 24.21 Ma for the monitor allowing calibration of the neutron flux. However, the actual age of HD-B1 is known with an error of  $\pm 2.5\%$  ( $2\sigma$ ) which should be combined with the analytical age to derive realistic geological ages that are comparable to data obtained using other monitors or analytical techniques and methods. Accordingly, the radiometric age of biotite from T180 can be proposed at  $13.6 \pm 0.5$  Ma ( $2\sigma$ ).

Our study is a preliminary one; additional samples from the same section may prove useful for additional research. In particular, we suspect that the material collected from the lens below the unconformity contains some K-feldspar which represents a good potential for additional study. Sediments from Sicily may therefore provide further evidence to document the biostratigraphic scale with geochronological ages for not only the Serravallian Stage but for younger sediments as well.

#### SOMMAIRE — BIOSTRATIGRAPHIE ET GÉOCHRONOLOGIE D'UN NIVEAU VOLCANOCLASTIQUE SERRAVALLIEN INFÉRIEUR DE SICILE

(Manuscrit soumis: Janvier 1994; révisé: Juin 1994; rédacteur responsable: GSO)

En Sicile, comme dans le reste de la Péninsule italienne, les traces d'activité volcanique interstratifiées dans la série sédimentaire sont communes. Nous avons porté notre attention sur un des rares niveaux d'origine volcanique connu dans le Serravallien inférieur. La biostratigraphie des Foraminifères planctoniques indique le sommet de la biozone à *O. suturalis*-*G. peripheroronda*. L'étude géochronologique a consisté à caractériser la nature de ce niveau (d'origine volcanique, il révèle la présence de biotite — géochimiquement homogène — de hornblende et de plagioclase essentiellement). L'analyse isotopique préliminaire a utilisé la technique  $^{39}\text{Ar}/^{40}\text{Ar}$  avec chauffage par paliers.

Le spectre d'âge obtenu pour le plagioclase est en escalier et n'apporte pas d'information d'âge très précise. Le spectre d'âge de la biotite est plus régulier et permet de proposer un âge de  $13,60 \pm 0,15$  Ma (incertitude intralaboratoire) pour l'éruption des minéraux pyroclastiques séparés. Cet âge caractérise un moment déjà franchement situé dans l'Étage Serravallien.

(Sommaire des auteurs)

#### ACKNOWLEDGEMENTS

M. Grasso and G.B. Vai are thanked for their comments on the Monte Giammoia section. A. Montanari is thanked for improvement of the English in the original manuscript. The radiometric measurements were done in Lausanne thanks to the facilities made available in the Institute of Mineralogy by the Swiss National Funds. No funding was provided by French Organizations for this research.

This Page Intentionally Left Blank

*Chapter D4*

**POTENTIAL INTEGRATED MIDDLE MIOCENE STRATIGRAPHY IN  
SOUTHEASTERN SPAIN**

Ch. Montenat, F. Serrano and J.A. Martin-Perez

**INTRODUCTION**

The eastern segment of the Betic Cordilleras includes three major geological zones, from the north to the south: (1) the prebetic autochthonous domain linked to the Iberian Meseta; (2) the subbetic allochthonous units, overthrusting the Prebetic northward; Prebetic and Subbetic are referred to the external sedimentary zones of the Betics; (3) the internal allochthonous zone, composed of a pile of large alpine nappes including sedimentary and various metamorphic rocks. This domain is separated from the External zone by a major ENE–WSW-trending wrench-fault.

The Miocene sedimentary sequences discussed below are located within the Internal zone, between Almeria and Alicante (Fig. 1). The Internal nappes recorded a complex polyphase structural evolution, from Mesozoic to Oligocene–Early Miocene times (review in Diaz de Federico et al., 1990).

From the Early Miocene (Burdigalian) onwards, the pile of nappes was torn into small blocks by faulting which developed within a large transcurrent fault zone, the Trans-Alboran shear zone, trending NE–SW through the Eastern Betics. Faulting is related to a compressional stress field caused by the Iberia–Africa collision (N–S- to NW–SE-trending direction of compression; Ott d’Estevou and Montenat, 1985).

Wrench tectonics, including large-scale lateral movements (Montenat and Ott d’Estevou, 1992), directly controlled the development of Miocene sedimentary basins (Montenat, 1990).

A first generation of basin filling, late Burdigalian to Serravallian in age, with an intra-Langhian minor structural phase, was severely deformed and eroded before Tortonian time. The second generation, ranging from Tortonian to Plio–Pleistocene time, is widely distributed in a variety of intra-mountain depressions (Fig. 1). Miocene deposits are predominantly deep marine, planktonic fossils-rich sediments. Near-shore and continental deposits, sometimes abundant with micromammals (de Bruijn et al., 1975; Mein and Agustí, 1990), are present in the well-preserved Late Miocene palaeogeographic sequence.

A diversified Neogene magmatic sequence is closely related to the Trans-Alboran shear zone (Hernandez et al., 1987). It includes plutonic, volcanic and metallogenic events which interfered with the tectonic and sedimentary processes.

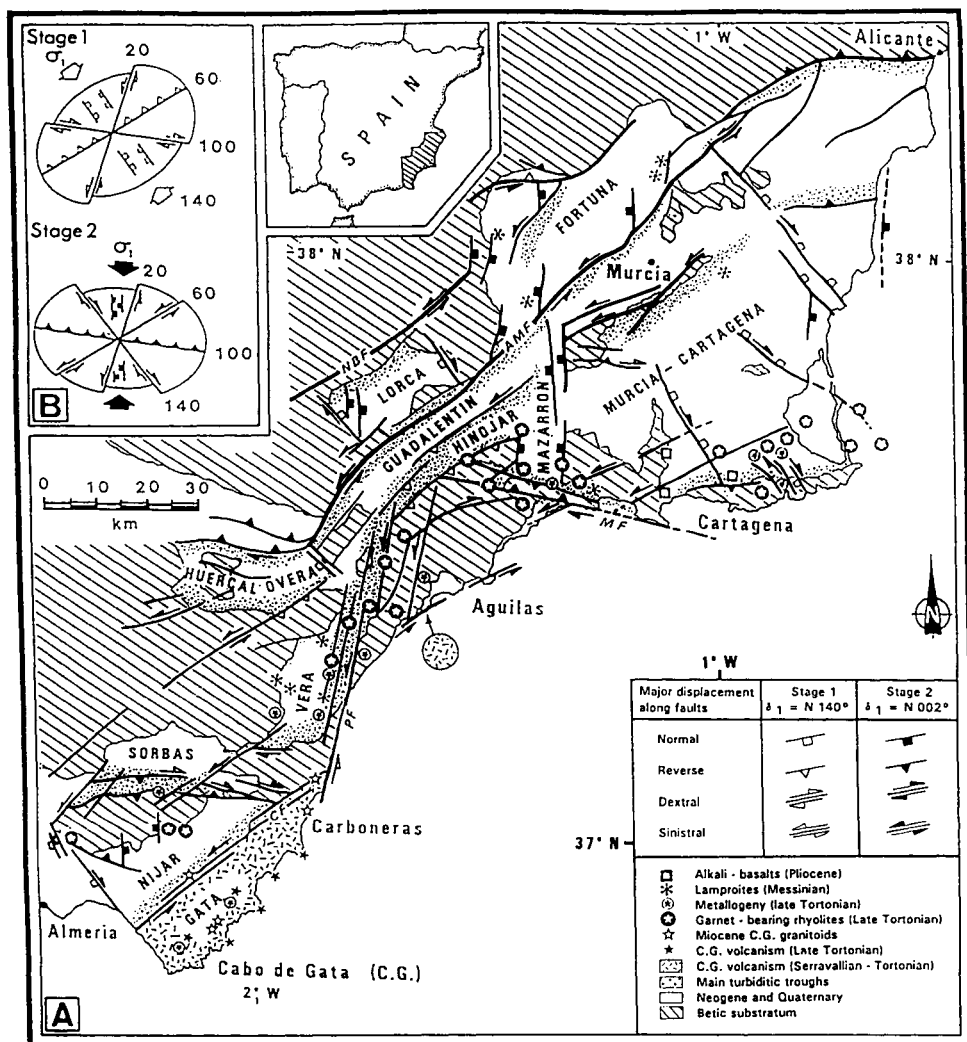


Fig. 1. (A) Neogene structural framework of the Eastern Betic domain and relationships with location of volcanics. (B) Variations of stress field during the late Neogene (stage 1: Serravallian–early Tortonian; stage 2: late Tortonian–Early Pliocene).

## VOLCANIC SERIES AND RELATED MIOCENE SEDIMENTS

The Miocene volcanism is basically restricted to the easternmost part of the Betic Cordilleras and can be split into three major belts. For each of them the stratigraphic correlations, radioisotopic dates, and biostratigraphic data from the associated sediments, make possible a quite confident chronological framework for the magmatic activity (Bellon et al., 1983; Serrano, 1992) (Fig. 2).

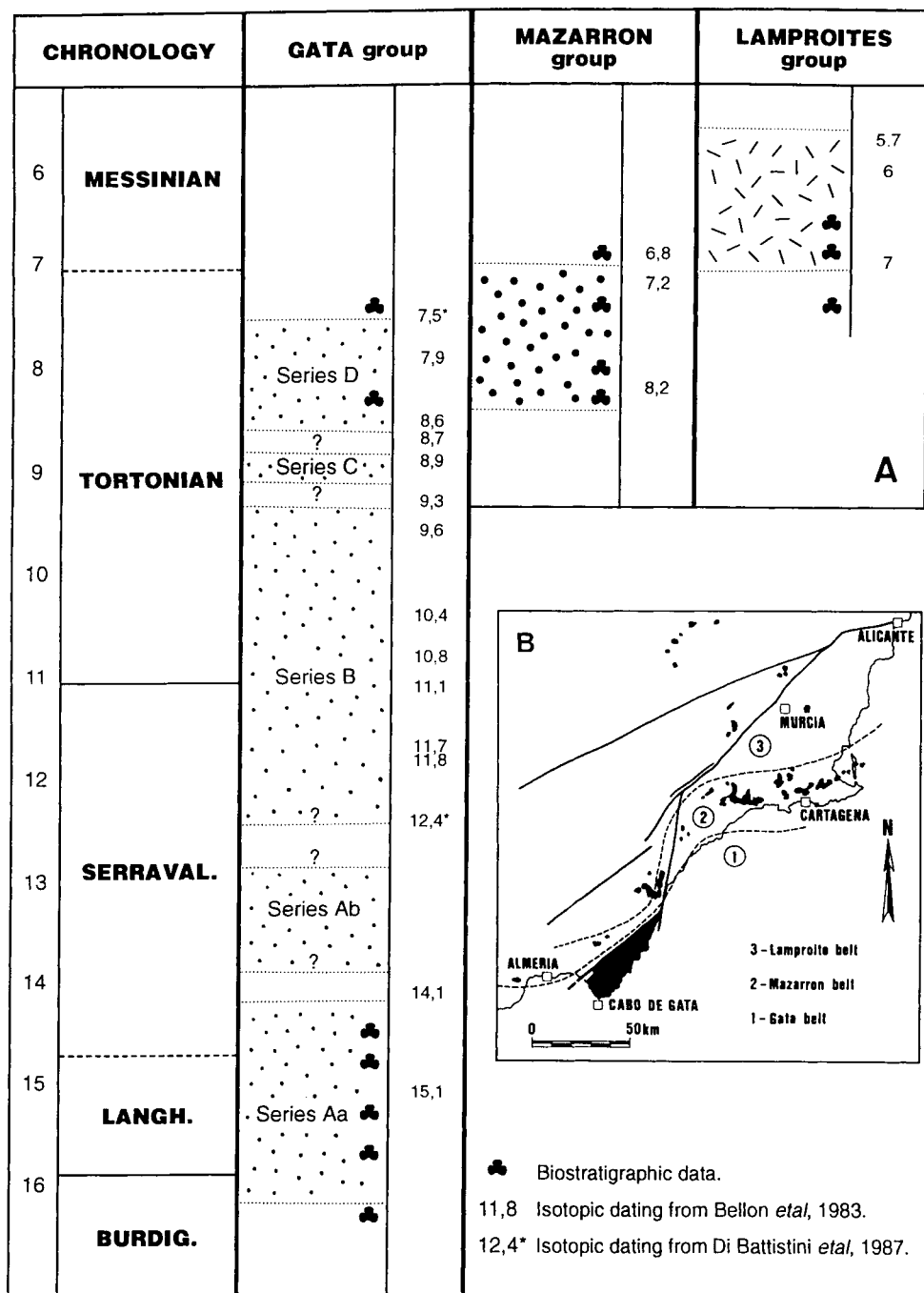


Fig. 2. (A) Stratigraphic range of the different volcanic groups. (B) Location of the Miocene volcanic belts.



### *Cabo de Gata group*

The Cabo de Gata group is located in the Cabo de Gata massif (northeast of Almeria), including the off-shore extensions to the east and the southwest. This group represents one of the most important Miocene volcanic complexes of the Mediterranean which includes about 500 km of outcrop, and more than 1000 m of drilled volcanics below sea level. The volcanics were piled up on the eastern side of a large left lateral fault, the Carboneras fault, trending NE–SW (Fig. 1).

The Cabo de Gata group includes a series of calc-alkaline sequences referred as sequences A to D (Bellon et al., 1983; see regional mapping of these different units in Bordet, 1985).

*Sequence A.* This sequence is composed of two different petrochemical suites: low-K andesites (Aa suite) overlain by a thick pile of dacites, and rhyolites and ignimbrites enriched in  $K_2O$  (Ab suite, outcropping in the southern part of the Gata massif). The first manifestations of the Aa member are found in the NW approaches of the Gata massif (north and northwest of the city of Carboneras) where several andesitic flows are interbedded with pelagic marls and turbidites, late Burdigalian–early Langhian in age (see below). About 50 km to the northeast of Carboneras, volcanics referred to as the Aa suite outcrop in the Aguilas area along the beach of Los Terreros. Andesitic agglomerates are interbedded within plankton-rich marls at the Langhian/Serravallian boundary (Montenat et al., 1978; see description below). The Ab suite is not yet dated and is tentatively referred to the Serravallian, but without precise correlation with any sedimentary series.

*Sequence B.* Sequence B is composed of low- $K_2O$  and  $Na_2O$  rocks ranging from frequent andesites to more rare dacites and rhyolites. It is characterized by a thick pile of breccias and domes, widely outcropping in the Gata mountains. Nine K–Ar dates of whole-rocks spread out within the series gave ages ranging from  $11.83 \pm 0.60$  ( $2\sigma$  interlaboratory) Ma to  $9.34 \pm 0.45$  Ma (late Serravallian to early Tortonian; Bellon et al., 1983). Rocks presumably correlated to the lower part of the same sequence are dated to between 12.4 Ma and 10.8 Ma (late Serravallian) by Di Battistini et al., (1987). Sediments interbedded within series B are calcarenites abundant with *Heterostegina* (Los Escullos near San José). In some places, like El Plomo, the volcanics, dated at  $9.62 \pm 0.50$  Ma (Bellon et al., 1983) are covered by marls with planktonic Foraminiferas, indicative of the base of the upper Tortonian (Serrano, 1992; Montenat and Serrano, Chapter E8).

*Sequence C.* This sequence is an acid suite of ignimbritic rhyolites some of which are locally enriched in  $K_2O$  and hydrothermalized, that are located in the central part of the massif in what is referred to as the gold ore deposits of Rodalquilar. Whole-rock rhyolite samples taken outside of the altered zone are K–Ar dated at  $8.90 \pm 0.45$  Ma, and  $8.75 \pm 0.45$  Ma, late Tortonian (Bellon et al. 1983). Sequence C is capped by Messinian reefs (Bordet, 1985).

*Sequence D* This sequence corresponds to low-K and Na andesites (similar to sequence B) grouped in several volcanoes located close to the coast (near San José, Roldan, and other localities). No stratigraphic relationships between sequences C and D have been observed. Available K–Ar dates from whole-rock samples indicate ages of  $8.67 \pm 0.45$  to  $7.90 \pm 0.45$  Ma (Bellon et al., 1983), and 8.6 Ma to 7.5 Ma (Battistini

et al., 1987). These volcanic rocks are located within the late Tortonian as evidenced by *Neogloboquadrina* with dextral and sinistral coiling, below and above the volcanics, respectively.

The plutonic equivalents of these volcanic granodiorites to gabbros units are evidenced by the way of erupted pebble-dikes (Montenat et al., 1984).

#### *The Mazarrón group*

This is another calc-alkaline sequence with high Al content, derived from shallow crustal anatexis from the Betic metamorphic basement (Zeck, 1970; Venturelli et al., 1986). It includes a variety of dacitic to rhyolitic volcanoes (domes and breccias) located in an outer position (westwards to northeastwards) with regard to the Gata massif (Almería, Vera, Hinojar, Mazarrón, Cartagena) (Fig. 2).

The volcanics cut through early Tortonian pelagic deposits in the Cartagena area. In the Hinojar and Mazarrón basins, the breccias and tuffites are interbedded within late Tortonian plankton-rich marls with *Neogloboquadrina humerosa*. In any case the volcanics were emplaced prior to the Tortonian/Messinian boundary.

Only a few reliable radioisotopic K–Ar whole-rock dates are currently available (see Chapter E8):  $6.62 \pm 0.30$  Ma, and  $7.20 \pm 0.35$  Ma (Cartagena);  $8.31 \pm 0.40$  Ma (Vera) (Bellon et al., 1983),  $7.6 \pm 0.30$  Ma (Vera, K–Ar dating of biotites from rhyolite, Nobel et al., 1981).

#### *The lamproites group*

Lamproites are uncommon ultra-K and magnesium-rich volcanic rocks of deep mantle origin. They are generally found as small pipes, dikes, sills, cones and flows, scattered over a large area to the west and northwest of the preceding groups. Lamproitic intrusions are found in marine Tortonian or Messinian basin deposits at Fortuna, Jumilla, and Murcia, and other locations. In some places like Barqueros and Vera, the volcanic flows are interbedded within marine or continental Messinian deposits (see Chapter E8).

Available data indicate K–Ar isotope ages on whole-rock ranging from  $7.0 \pm 0.3$  Ma to  $6.2 \pm 0.3$  Ma at Barqueros (Montenat et al., 1975,) and at Fortuna from  $6.16 \pm 0.30$  Ma (Bellon et al., 1983) to  $5.67 \pm 0.30$  Ma (Bellon et al., 1981).

### POTENTIALLY USEFUL MIDDLE MIOCENE SECTIONS

Two sections belonging to the Gata group suitable for integrated stratigraphy, are described below (Fig. 3).

#### *North of Carboneras (Rambla Granadilla and Torre del Peñon)*

Various outcrops of a late Burdigalian–early Langhian succession are preserved within the Carboneras fault zone. They suffered significant deformations due to wrench tectonics prior to the Late Miocene (Tortonian). This sequence consists of pelagic planktonic microfossil-rich deposits, often associated with volcanic flows (especially to the north of Carboneras).

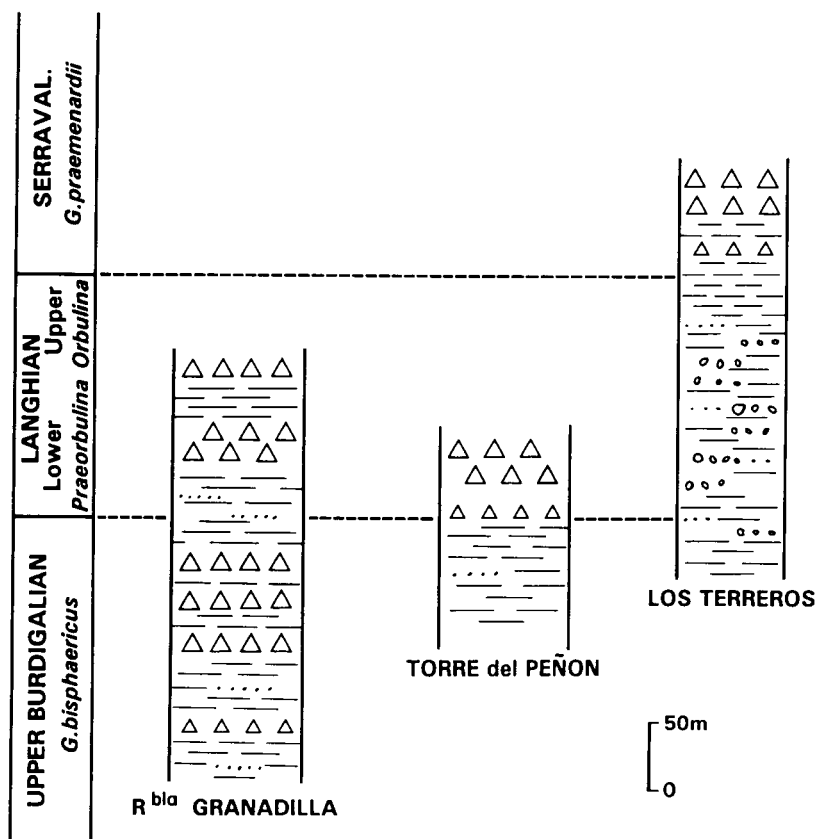


Fig. 3. Correlation of stratigraphic sections discussed in the text.

*Rambla Granadilla (Cerro del Marques)*. A large strip of Miocene rocks, trending NE–SW, appears faulted within dark crystalline schists of the Betic basement. It is a succession of light-grey to green silty marls and brownish turbidite sandstones alternating with andesitic flows some of which are 5 to 20 m in thickness. The total thickness of this sequence is about 200 m.

Most of the marls yield a late Burdigalian microfauna including *Globigerinoides bisphaericus*, *G. altiapertura*, *G. subquadratus*, *G. gr. trilobus*, *Globoquadrina dehiscens*, *G. baroemoensis*, *G. langhiana*, *Glorotalia (Fohsella) peripheroronda*, *Praeorbulina glomerosa sicana*, etc., which probably indicate the uppermost part of the Burdigalian.

Nannoplankton assemblages contain *Coccolithus miopelagicus*, *C. pelagicus*, *Cycliargolithus abisectus*, *C. floridanus*, *Dictyococcites productus*, *D. scrippsae*, *Discoaster deflandrei*, *D. druggi*, *D. variabilis*, *Helicosphaera ampliapertura*, *H. carteri*, *H. euphratis*, *Pontosphaera multipora*, *Reticulofenestra daviesii*, *R. gartneri*, *Sphenolithus heteromorphus*. The presence of *Sphenolithus heteromorphus* and *Helicosphaera ampliapertura*, and the absence of *Reticulofenestra pseudoumbilica*, further indicate that these levels belong to the latest Burdigalian.

The uppermost part of the series contains an early Langhian microfauna, including

the preceding species (with the exception of *G. altiapertura*), and *P. glomerosa*. The primitive form of *P. glomerosa* (*P. glomerosa curva* type), seems to indicate an earliest Langhian age. In the calcareous nannoplankton assemblages *Reticulofenestra pseudoumbilica* is present, indicating a Langhian age.

Isotopic dating of the volcanic rocks (andesite and amphiboles) has not been carried out. It is important to note that a southwestern part of the same faulted zone in La Serrata, at the Archidona quarry, basaltic andesite related to the same sedimentary sequence yielded a Langhian age ( $15.15 \pm 0.75$  Ma, K–Ar on whole-rock; Bellon et al., 1983).

*Torre del Peñon*. The Miocene grey marls exposed near the coastline include the previously quoted calcareous microfauna (late Burdigalian and earliest Langhian). They are capped by massive andesitic volcanic rocks (suite Aa). Volcanic debris and tuffites with amphiboles, interbedded within the uppermost part of the marls, make it possible to radioisotope-date the lower Langhian near its basal boundary.

#### *South of Aguilas (Los Terreros beach)*

The northernmost extension of the Gata group volcanics may be found in some islets located near the shoreline, to the south of Aguilas along the beach at Los Terreros.

In the Los Terreros area, outcrops of a thick Miocene sequence, including pelagic marls, turbidite sandstones, and debris-flows, contain planktonic microfaunas indicative of early and late Langhian ages (*Praeorbulina* and *Orbulina* zones; Montenat et al., 1978).

The top of the sequence is made of grey marls and includes volcanic debris of andesite, tuffites with amphiboles, and conglomerates. In these levels, the Langhian/Serravallian boundary is located at the first appearance of *Globorotalia praemenardii* (Serrano, 1992).

The nannoplankton assemblages contain *Sphenolithus heteromorphus*, *Reticulofenestra pseudoumbilicus* and *Calcidiscus macintyreii*, which characterize zone NN5 of *S. heteromorphus* (Martini, 1971). The disappearance of *Discoaster kugleri* occurs in the same level as the appearance of *G. praemenardi*.

These volcanoclastics mark the beginning eruptions of massive andesitic volcanics (breccias and domes) which crop out in the islets and on the shoreline at Cuatro Calas north of Los Terreros. Radioisotope dating of the andesite of Cuatro Calas (K–Ar whole-rock) give an age of  $14.1 \pm 0.7$  Ma for the lowermost Serravallian.

## CONCLUSIONS

This short review on the chronology of Betic Miocene volcanic rocks, and related sediments, points out the good correlation of available radioisotope datings in a robust chronological framework. Nevertheless, it is important to note that most of these dates were produced ten or fifteen years ago using the K–Ar isotope dilution technique applied to whole-rock samples. Additional interdisciplinary studies taking into consideration the recent progress in radioisotopic analysis, regional geology, and biostratigraphy, will certainly lead to a more accurate and precise determination of the integrated stratigraphy of this important volcano-sedimentary sequence.

As for the Middle Miocene interval, several different sections in the Gata–Aguilas area contain suitable sections (volcaniclastic layers and volcanic flows with amphiboles, associated with plankton-rich sediments) to bracket the Burdigalian/Langhian and Langhian/Serravallian boundaries (Fig. 3).

#### SOMMAIRE — POTENTIEL POUR LA STRATIGRAPHIE INTÉGRÉE DU MIOCÈNE MOYEN EN ESPAGNE DU SE

*(Manuscrit soumis: Février 1994; révisé: Juin 1994; rédacteur responsable: GSO)*

Le segment oriental des Cordillères bétiques se compose de trois unités géologiques du nord au sud: (1) le domaine prébétique autochtone; (2) les unités subbétiques allochtones charriées vers la nord; (3) la zone interne allochtone composée de nappes empilées comprenant des roches sédimentaires et diverses roches métamorphiques. Les séquences sédimentaires miocènes situées dans cette zone interne remplissent des bassins en deux temps: (1) du Burdigalien supérieur au Serravallien; les sédiments ont ensuite été déformés et en partie érodés avant le Tortonien; (2) du Tortonien au Plio–Pléistocène; elles sont alors largement réparties dans des dépressions intramontagneuses. Les faciès représentés sont marins, profonds et riches en fossiles planctoniques mais on rencontre aussi d'intéressants bassins continentaux parfois riches en micromammifères. La présence commune de roches volcaniques interstratifiées depuis le Burdigalien supérieur jusqu'au Messinien constitue le caractère le plus remarquable pour une étude de stratigraphie intégrée. Au Miocène moyen, le 'Groupe' volcanique de Gata subdivisé en 'Séries' paraît être un bon objectif de recherche. Les profils les plus prometteurs concernent la partie inférieure du Miocène moyen: les deux limites du Langhien pourraient ainsi être caractérisées à la base dans les profils de Rambla Granadilla et Torre del Peñon, au sommet dans celui de la plage de Los Terreros. Ces études modernes permettant de préciser les connaissances déjà acquises pour localiser dans le temps des événements biostratigraphiques marins et continentaux.

*(Sommaire proposé par les rédacteurs, GSO)*

*Chapter D5*

**THE POTENTIAL FOR INTEGRATED STRATIGRAPHIC STUDIES OF  
MIDDLE MIOCENE SEQUENCES IN CENTRAL JAPAN**

M. Takahashi and M. Oda

**INTRODUCTION**

A geologic map of central Japan, with the localities of selected areas, is shown in Fig. 1. The Neogene sequence in the Boso Peninsula almost completely spans the interval from latest Early Miocene to the Recent, and is described by Takahashi et al. in Chapter E10. The Upper Miocene sequence in the Miura Peninsula is also reviewed by Saito et al. in Chapter E9.

Middle Miocene strata are well exposed in the Tomioka area, and the biostratigraphy is well established. A Middle Miocene sedimentary sequence is also exposed in the Iwadono area, in the vicinity of the Tomioka area, and is correlated to the upper half of the Tomioka sequence. This sequence, which contains four groups of calcareous and siliceous microfossils, has strong potential for high-resolution integrated stratigraphic studies. The Karasuyama area is situated in the northern part of central Japan, and the Middle Miocene is completely represented in this area. Preliminary results show that this sequence contains both calcareous and siliceous microfossils, and is intercalated with more than 100 tuff layers.

**GEOLOGY, AND INTEGRATED STRATIGRAPHY**

*Tomioka area*

The Tomioka area is located about 100 km northwest of Tokyo, and is characterized by a sedimentary sequence which exceeds 3000 m in thickness (Figs. 1, 2 and 3). This Miocene sequence is divided into the following seven formations, in ascending order: Ushibuse, Obata, Idozawa, Haratajino, Niwaya, Haraichi, and Itahana formations (Oishi and Takahashi, 1990). The contacts between each formation are conformable except for the Niwaya Formation which rests on the underlying formations with partial unconformity (Niwaya Unconformity). These formations consist mainly of siltstone and sandstone containing microfossils, except for the Ushibuse (the lowest in the sequence), and the Itahana (the uppermost) which are sterile. A roughly homoclinal geologic structure, and frequent intercalations of key tuff beds promoted numerous biostratigraphic studies in this area (e.g., Saito, 1963; Matsumaru, 1967; Kurihara, 1974; Takayanagi et al., 1976, 1978; Oda, 1977; Chiji and Konda, 1978; Konda, 1980; Honda, 1981).

Planktonic microfossils in more than 100 samples were analyzed by several workers, and many important events were recognized (Fig. 3). Radiometric ages from the

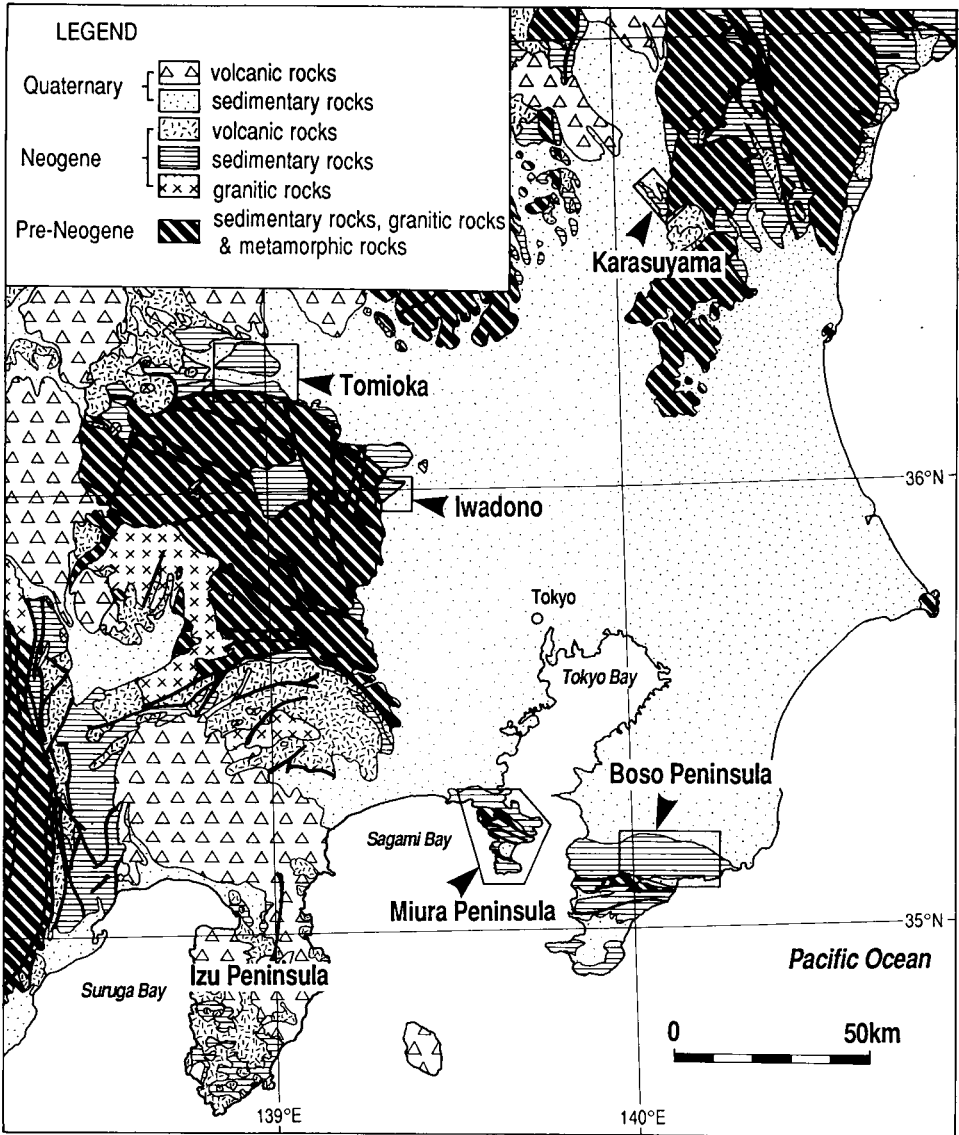


Fig. 1. Geologic map of Central Japan with the localities of key areas for integrated stratigraphic studies. Preliminary data for integrated stratigraphy in the Miura and Boso Peninsula are shown in Chapters E9 and E10.

Kitamura and Baba Tuffs are also shown in Fig. 3. Foraminiferal and nannofossil events in this sequence, in ascending order, are the first occurrence (FO) of *Praeorbulina glomerosa curva* and of *Orbulina suturalis*, the last occurrence (LO) of *Sphenolithus heteromorphus*, the FO of *Globorotalia peripheroacuta*, the LO of *Cyclicargolithus floridanus*, the FO of *Sphaeroidinellopsis subdehiscens* and of *Globigerina nepenthes*, and the LO of *Discoaster deflandrei*.

Among the twenty tuffs in this sequence, only the Kitamura and Baba tuffs were

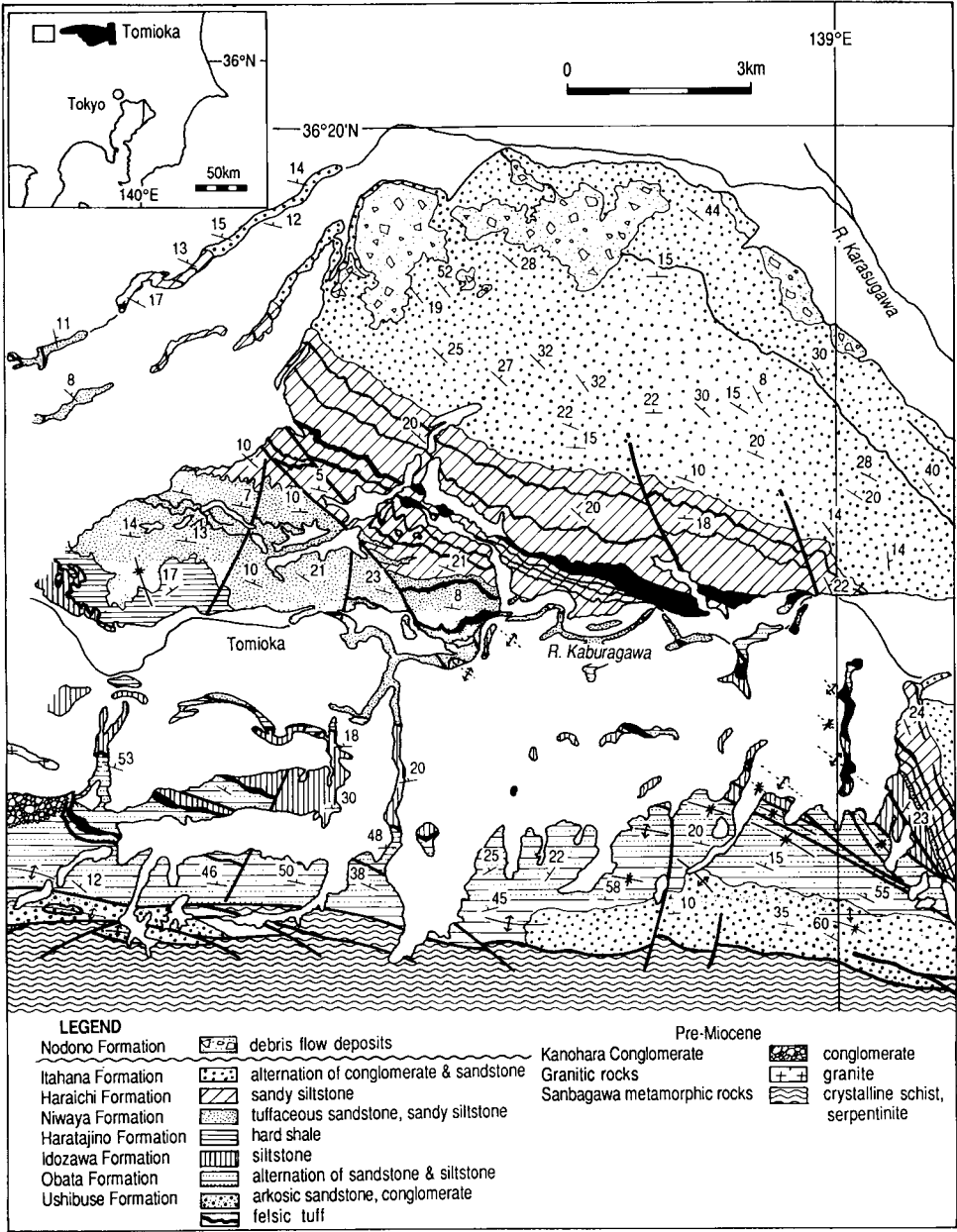


Fig. 2. Geological map of the Tomioka area modified from Oishi and Takahashi (1990). The lower half of this sequence is deformed under a NE-SW compressional stress field which occurred at the end of the opening of the Japan Sea (i.e., around 15 Ma).



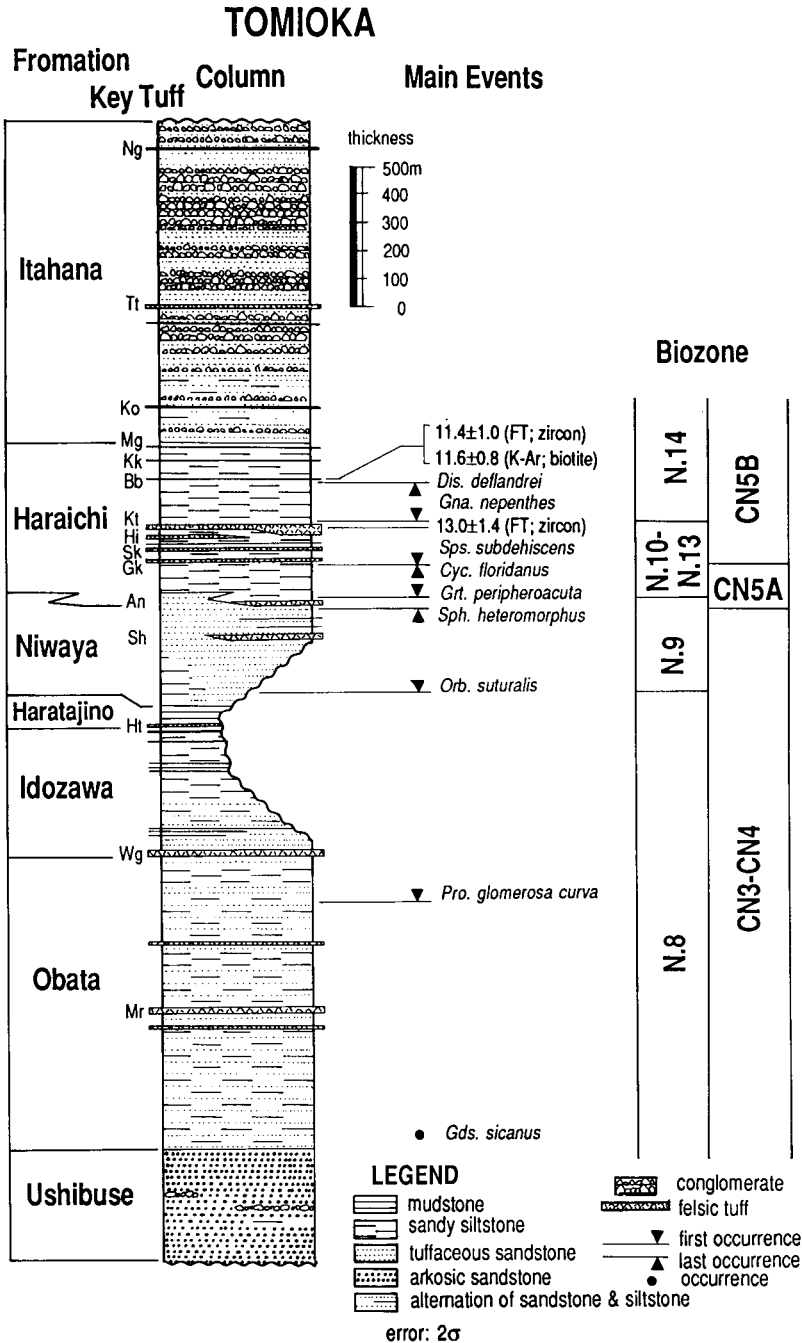


Fig. 3. Stratigraphy of the Tomioka sequence with the positions of biostratigraphically important events. The succession from the Obata Formation through the lowest Niwaya Formation, which indicates a very high sedimentation rate (1600 m/Ma), is correlated to foraminiferal Zone N8 of Blow (1969). The high sedimentation rate during N8 is caused by rifting as mentioned by Takahashi and Oda in Chapter B3. N.B.: the *Gds. sicanus* quoted in the figure is a synonym of *Praeorbulina sicana* quoted in the Italian sections.

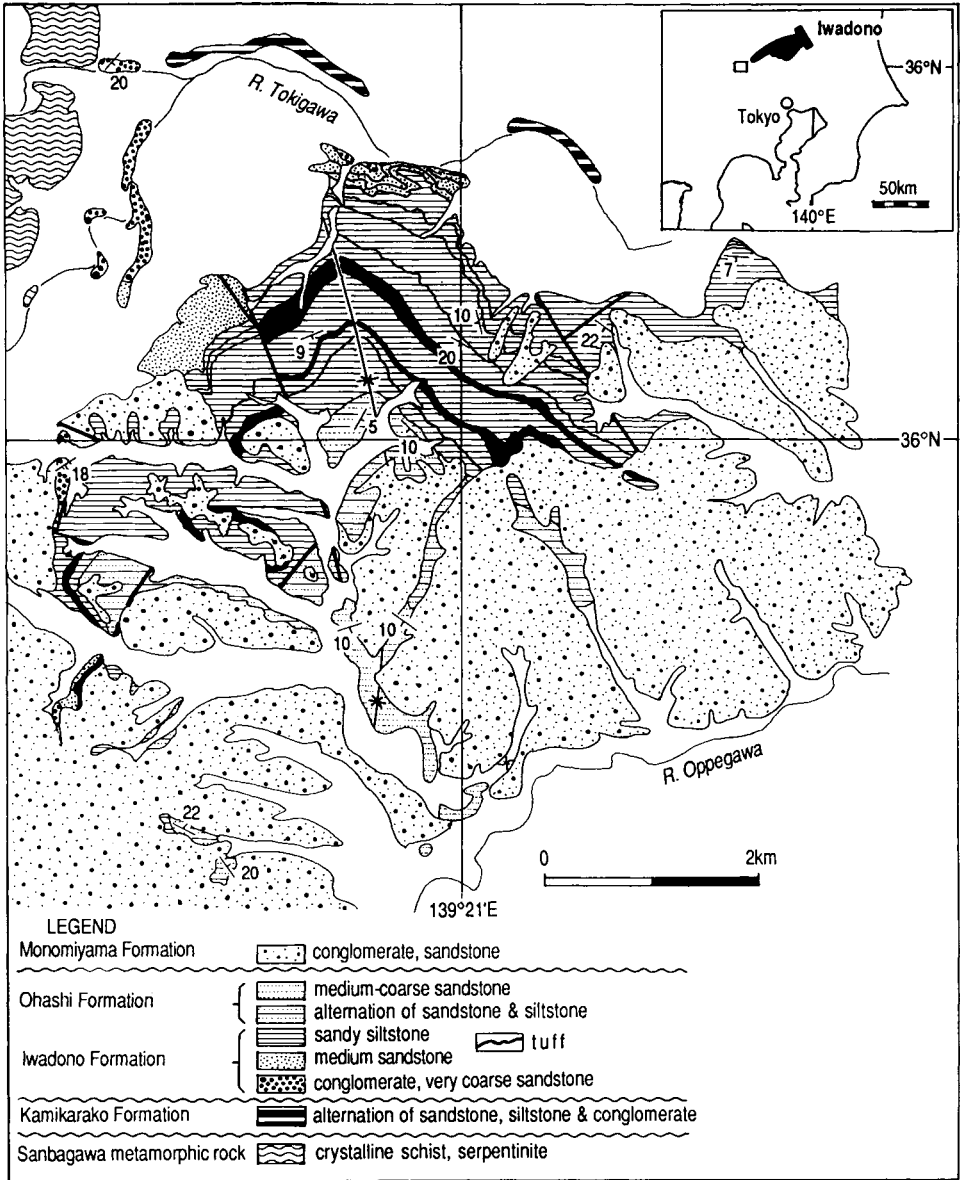


Fig. 4. Geologic map of the Iwadono area partly modified from Koike et al. (1985).

dated, the former with fission-track on zircon, and K–Ar on biotite, yielding a mean age of  $11.5 \pm 0.4$  Ma ( $2\sigma$  interlaboratory), and the latter with fission-track on zircon, yielding an age of  $13.0 \pm 0.7$  Ma (Shibata et al., 1979; Kasuya, 1987; Takahashi et al., 1992; Fig. 3). The most important potential event in the Tomioka sequence is the FO of *G. nepenthes*, which defines the local planktonic foraminiferal N13/N14 zonal boundary of Blow (1969). Since this FO level is located a few metres above the Kitamura Tuff,

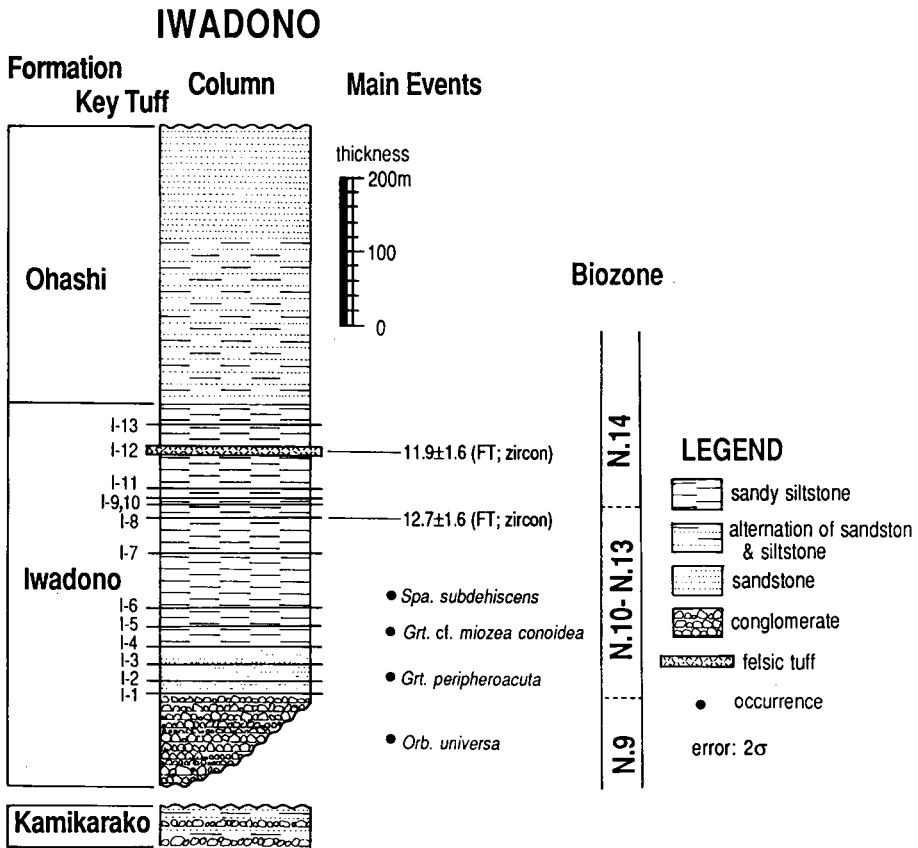


Fig. 5. Stratigraphy of the Iwadono sequence. The stratigraphic break between the Kamikarako and Iwadono formations represents the analog of the Niwaya Unconformity in the Tomioka area. This sequence is important because it yields both siliceous and calcareous microfossils.

and about 200 m below the Baba Tuff, the ages of these two tuffs bracket the boundary age. The newly obtained radiometric results from these two tuff beds, and discussions in reference to the magneto-biostratigraphic time scale, are presented by Takahashi and Saito (Chapter D6), and Odin et al. (Chapter D7). As the other tuff layers lack biotite and hornblende crystals, they will have to be dated, hopefully in a near future, using the <sup>40</sup>Ar-<sup>39</sup>Ar technique on feldspars. Magnetostratigraphy of this sequence will be also established in a near future.

*Iwadono area*

A correlative sequence of the upper part of the Tomioka is well exposed in the Iwadono area (Fig. 4), where it is represented by the Iwadono and Ohashi formations. The lower unit consists of sandy siltstone with thirteen interbedded key tuff layers, as shown in Fig. 5. Two of these tuff beds have been dated by the fission-track method, and correlated directly with those of the Tomioka sequence. The key tuffs I-8 and I-12 are

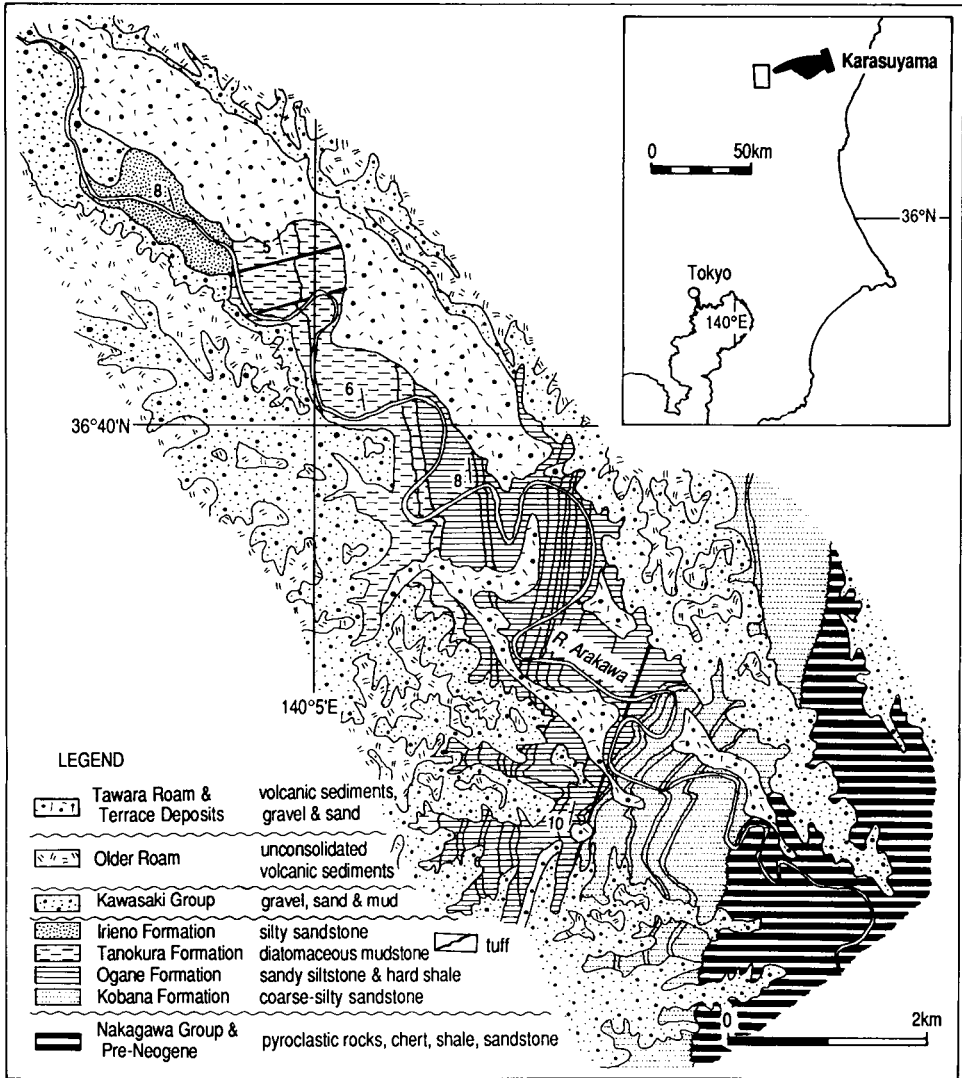


Fig. 6. Geologic map of the Karasuyama area, modified from Sakai (1986). Miocene strata are exposed only along the Arakawa River, and are gently dipping toward the west. A few faults, which are a rare occurrence in the active island arc of Japan, are present in this area.

correlated with the Kitamura and Baba tuffs, respectively, on the basis of zircon crystal morphology (Takahashi, and Hayashi, 1991). Radiometric results from tuff I-8 yielded an age of  $12.7 \pm 1.6$  Ma, whereas tuff I-12 yielded a fission-track age of  $11.9 \pm 1.6$  Ma (Kasuya, 1987), thus supporting the correlation of this formation with the Haraichi Formation in the Tomioka sequence. A preliminary micropalaeontological study showed that the Miocene sediments in the Iwadono area contain well preserved calcareous microfossils, which offer the opportunity for further integrated stratigraphic work.

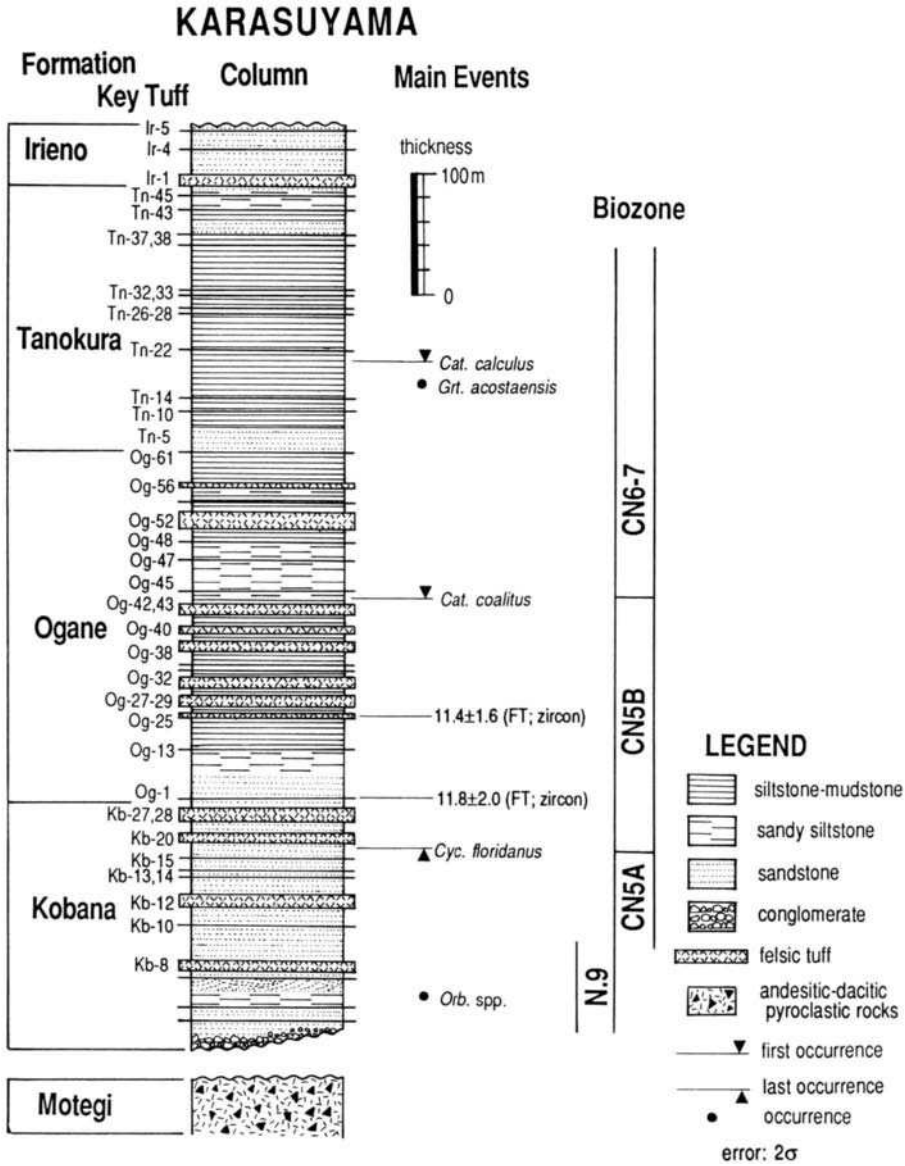


Fig. 7. Stratigraphy of the Karasuyama sequence modified from Sakai (1986). This sequence is characterized by numerous intercalations of tuff layers. Siliceous microfossils are present in the upper half of the sequence, while well preserved calcareous fossils are present all the way throughout the sequence.

*Karasuyama area*

The Karasuyama area is located in the northern part of central Japan. The local Middle to Late Miocene sedimentary sequence is represented by four formations, in ascending order: Kobana, Ogane, Tanokura, and Irieno formations. This sequence is

characterized by numerous interbedded tuff layers. Detailed columnar sections including more than 100 key tuff layers are reported by Sakai (1986).

Preliminary studies show that the Miocene strata in the Karasuyama area contain both foraminifera and calcareous nannofossils throughout the entire sequence, and siliceous microfossils predominantly in its upper part. Only two tuff beds were dated by the fission-track method (Kasuya, 1987), yielding ages of  $11.4 \pm 1.6$  Ma, and  $11.8 \pm 2.0$  Ma, respectively (Fig. 7, while there are many other datable tuff layers which are awaiting conventional K–Ar, and  $^{40}\text{Ar}/^{39}\text{Ar}$  radioisotopic analyses.

Integrated stratigraphic studies were mainly devoted to the geochronological and biostratigraphic calibration of this sequence. More than 350 samples have been collected for micropalaeontologic analyses, and about 30 tuffs for high-resolution radioisotopic analysis, some of which are currently under preparation for fission-track dating. More than 20 tuff layers contain fresh biotite and/or hornblende making high-resolution radioisotopic age calibration of this sequence likely. Palaeomagnetic analyses are also under way.

In summary, the Middle Miocene sedimentary sequences of Central Japan all exhibit the required characteristics for developing detailed integrated stratigraphic analyses, including calcareous and siliceous marine microplankton biostratigraphy, magnetostratigraphy, and geochronology.

## SOMMAIRE — POTENTIEL POUR L'ÉTUDE DE STRATIGRAPHIE INTÉGRÉE DE SÉQUENCES DU MIOCÈNE MOYEN DU JAPON CENTRAL

(Manuscrit soumis: Novembre 1993; révisé: Mai 1994; rédacteur responsable: GSO)

Du fait de différences marquées dans le paléoclimat et la température, les microfossiles siliceux sont prédominants dans le Japon méridional, par contre, au Japon Central, la confluence de courants chauds et froids a favorisé la prolifération de microorganismes à la fois calcaires et siliceux représentés par des Foraminifères bien préservés, des coccolithes, des Radiolaires et des Diatomées. Un objectif très important pour la stratigraphie japonaise est d'élucider les relations entre ces quatre groupes d'organismes. Dans ce travail, on décrit des séquences du Miocène Moyen dans trois régions clé du Japon Central: Tomioka (qui expose une grande partie reconnue du Langhien et du Serravallian), Iwadono (exposant une grande partie du Serravallian) et Karasuyama (exposant une grande partie du Serravallian ainsi que la base du Tortonien) qui ont un bon potentiel pour de nouvelles recherches de stratigraphie intégrée. La combinaison possible d'études biostratigraphiques (déjà bien avancées) et géochronologiques avec un abondant matériel volcanoclastique disponible, ouvre d'intéressantes perspectives confirmées par des datations préliminaires significatives. L'enregistrement magnétostratigraphique paraît, en outre, plus prometteur qu'en Italie.

(Sommaire proposé par les rédacteurs d'après un résumé des auteurs, GSO)

## ACKNOWLEDGEMENTS

We would like to thank K. Stewart (University of North Carolina) for improving the English in the original manuscript.

This Page Intentionally Left Blank

Chapter D6

**RADIOMETRIC AGE OF THE FIRST OCCURRENCE OF *GLOBIGERINA*  
*NEPENTHES* IN THE TOMIOKA SEQUENCE, CENTRAL JAPAN**

M. Takahashi and K. Saito

INTRODUCTION

The correlation between the marine Middle and Late Miocene magnetic anomaly pattern, and the magnetostratigraphy defined in sediment sections, has been a vexing topic for the past 20 years. The controversy lies, in essence, in the choice of two alternative correlation models: one is the Anomaly 5–Chron 9 model proposed by Ryan et al. (1974) and Theyer and Hammond (1974), and the second is the Anomaly 5–Chron 11 model of Foster and Opdyke (1970) and Hsü et al. (1984). These two models differ in the correlation approach of Chrons 7 through 14 (Fig. 1). Lack of reliable radioisotopic ages calibrating magneto-biostratigraphic time scales has prevented the solution of this problem.

In this work, we obtained the K–Ar and  $^{40}\text{Ar}/^{39}\text{Ar}$  ages from two Miocene tuff layers (Kitamura Tuff and Baba Tuff) in the Tomioka area, with the primary objective of bracketing the local first appearance datum (local FAD) of *G. nepenthes* in Japan. *G. nepenthes* is one of the most important species of planktonic foraminifera for this time interval because its first appearance defines the boundary between Zone N13 and Zone N14 (Blow, 1969). In the Tomioka sequence, the first occurrence (FO) of *G. nepenthes* has been recognized by several micropalaeontological studies (e.g., Takayanagi et al., 1978; Chiji and Konda, 1978). Recent field studies have indicated that the FO of *G. nepenthes* was located below the Baba Tuff, and a few metres above the Kitamura Tuff. Consequently, radiometric dating of these two tuff layers would control the timing of the local planktonic foraminiferal N13/N14 zonal boundary.

In this chapter we document in detail the stratigraphic positions of the local FAD of *G. nepenthes*, and of the radioisotopically dated tuff samples in the Miocene Tomioka sequence. In addition, we also discuss the validity of the two models of correlation between magnetic anomaly patterns and magnetostratigraphy, on the basis of the comparison between radiometric ages of the two dated tuff layers, and the numerical ages of the N13/N14 boundary estimated by these two models.

GEOLOGY AND BIOSTRATIGRAPHY OF THE TOMIOKA SEQUENCE

The Miocene sedimentary rocks are extensively exposed in the Tomioka area of central Japan. Separated from the pre-Miocene basement rocks by unconformities or faults, the Miocene strata are developed in a roughly homoclinal structure with an east–west strike, and a north dip (Fig. 2). This sequence is divided into the following



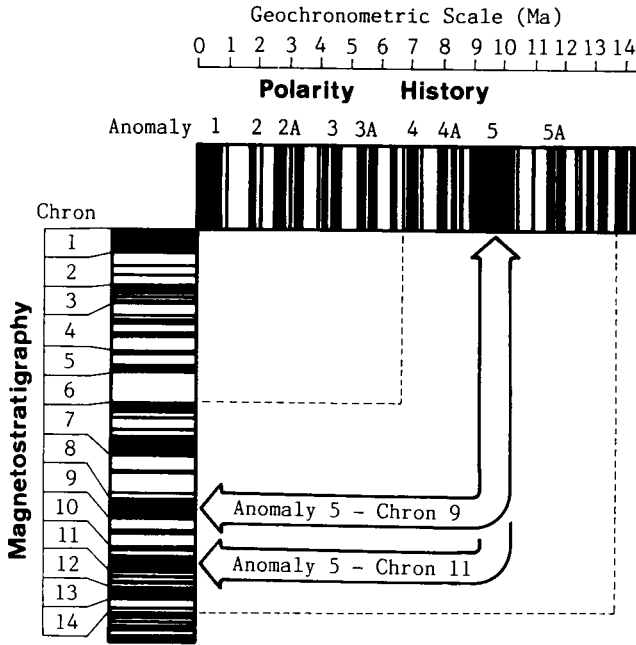


Fig. 1. Correlation of the marine magnetic anomaly pattern (Anomalies; Berggren et al., 1985a) with the magnetostratigraphy in deep-sea sediments (Chron; Ryan et al., 1974), considering two alternative models (i.e. Anomaly 5 vs Chron 9, and Anomaly 5 vs Chron 11).

seven units by Oishi and Takahashi (1990), in ascending order: the Ushibuse Formation (>400 m thick), Obata Formation (900 m), Idozawa Formation (450 m), Haratajino Formation (40 m), Niwaya Formation (400 m maximum), Haraichi Formation (550 m), and the Itahana Formation (1200 m). These units are conformable in respect to each other, except for the Niwaya Formation which is partially unconformable in respect to the underlying formations (Fig. 3).

These Miocene strata through the Obata to Haraichi formations contain abundant microfossils including planktonic and benthonic foraminifera, calcareous nannofossils, and radiolarians (e.g. Saito, 1963; Kurihara, 1974; Takayanagi et al., 1976, 1978; Chiji and Konda, 1978; Konda, 1980), and are interbedded with numerous tuff layers. The relations between the stratigraphic ranges of some important species of planktonic foraminifera and key tuff layers are also shown in Fig. 3. The following eight potential datums of planktonic foraminiferal species have been found (in ascending order): FO of *Praeorbulina glomerosa curva*; FO of *P. glomerosa glomerosa*; FO of *Orbulina suturalis*; FO of *O. universa*; FO of *P. glomerosa circularis*; FO of *Globorotalia peripheroacuta*; FO of *Sphaeroidinellopsis subdehiscens*; FO of *Globigerina nepenthes*.

The FO of *G. nepenthes* is the most important among these eight horizons, as its stratigraphic position is located between the Baba and the Kitamura tuffs which contain suitable minerals for radiometric dating.

The collection sites of the examined samples, and the routes for each columnar section, are shown in Fig. 2. Fig. 4 exhibits each columnar section of the Tomioka

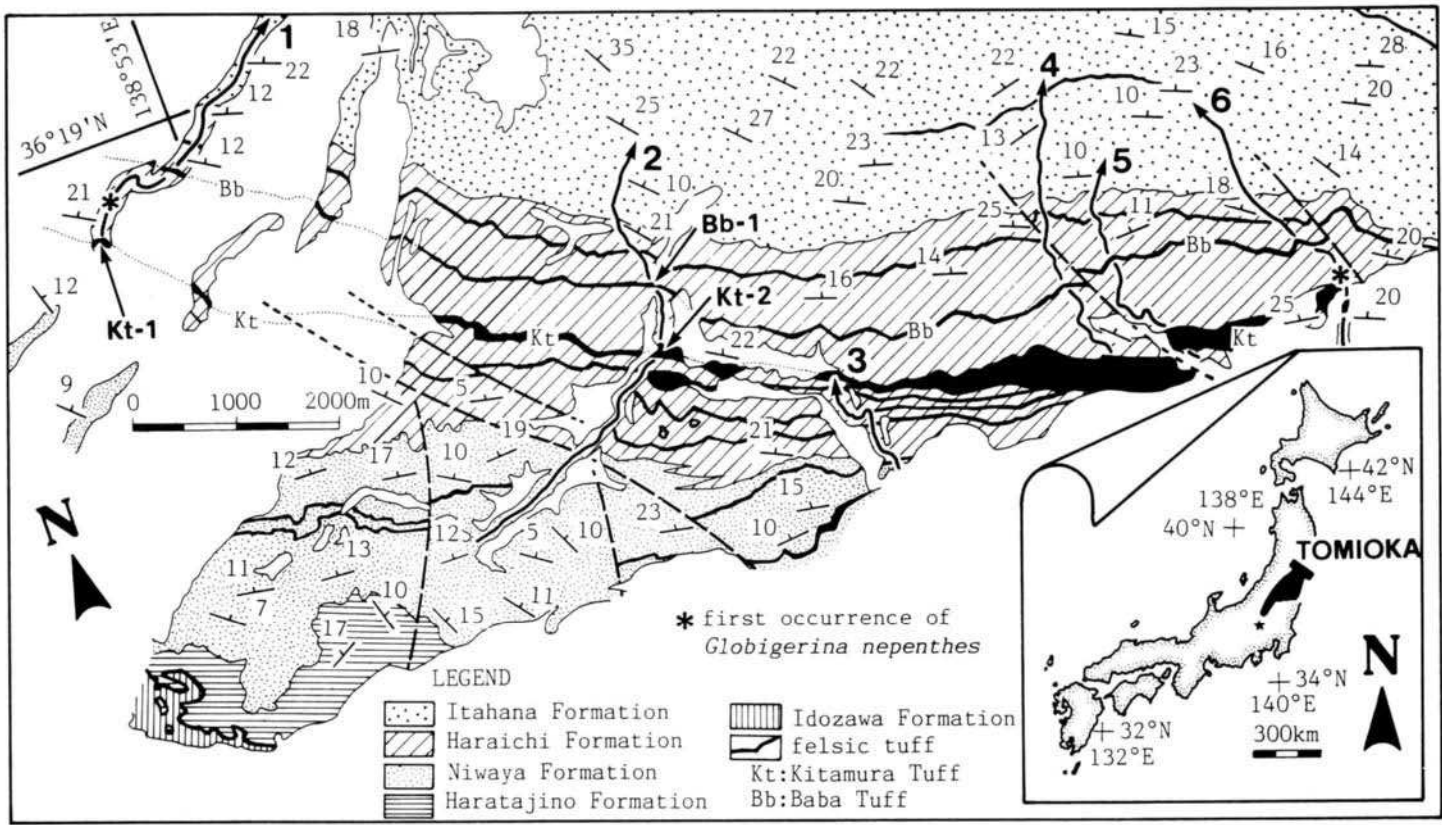


Fig. 2. Geological map of the Tomioka area partly modified from Oishi and Takahashi (1990). Routes of columnar sections, and locations of tuff samples used for radiometric dating are also shown (as in Fig. 4).

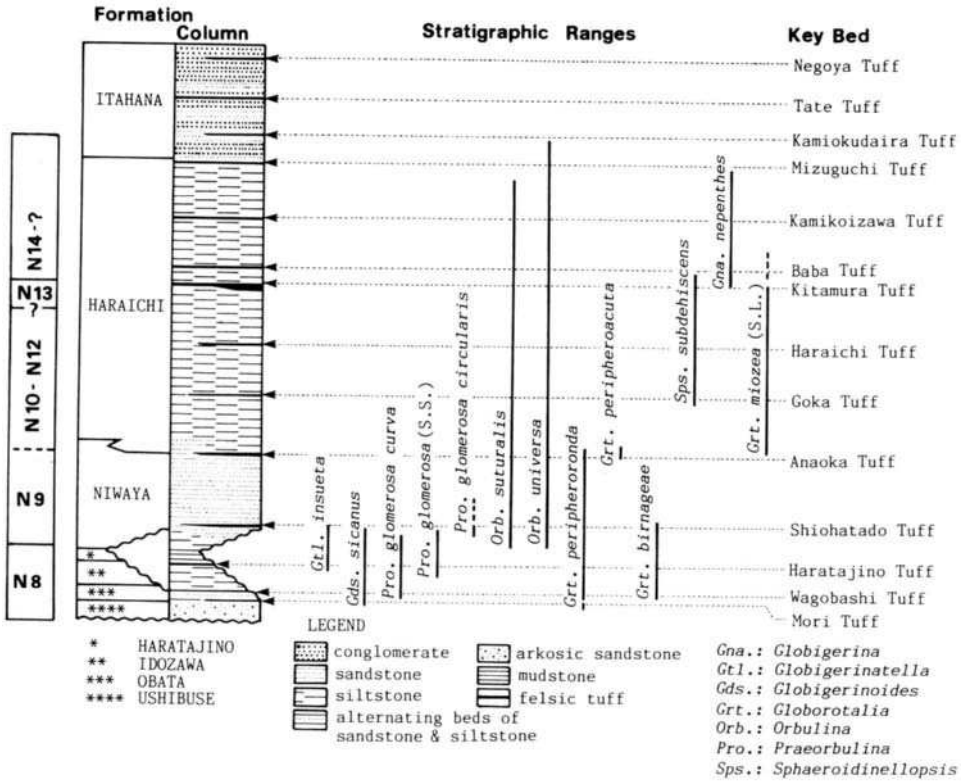


Fig. 3. Generalized stratigraphic column of the Miocene sedimentary sequence in the Tomioka area, also showing the relationships between stratigraphic ranges of selected planktonic foraminifera, and the location of key tuff layers.

sequence with the stratigraphic positions of tuff samples. The relation between the horizons of the FO of *G. nepenthes*, and each key tuff bed are also shown. As shown in both Figs. 2 and 4, the FO of *G. nepenthes* has been recognized along section 1 by Takayanagi et al. (1978), and along section 6 by Chiji and Konda (1978). While the horizon of the FO of the *G. nepenthes* in section 1 lies in the middle between the two key tuff beds (i.e., Baba Tuff and Kitamura Tuff), Chiji and Konda (1978) show that the position of the same event along section 6 is a few metres above the Kitamura Tuff. The thickness between the Kitamura Tuff and the Baba Tuff along each section is almost the same, suggesting that the difference of the stratigraphic positions of each FO is not due to the existence of hiatus just above the Kitamura Tuff along section 6. We adopted the lower horizon between the two as the local first appearance datum (local FAD) of *G. nepenthes* in this sequence. Consequently, the regional planktonic foraminiferal zonal boundary N13/N14 lies 150–190 m below the Baba Tuff, and just above the Kitamura Tuff in this area. Therefore, the radiometric datings of these two tuff beds impose a constraint on the age of the local FAD of *G. nepenthes*, that is, the local N13/N14 zonal boundary in Japan.

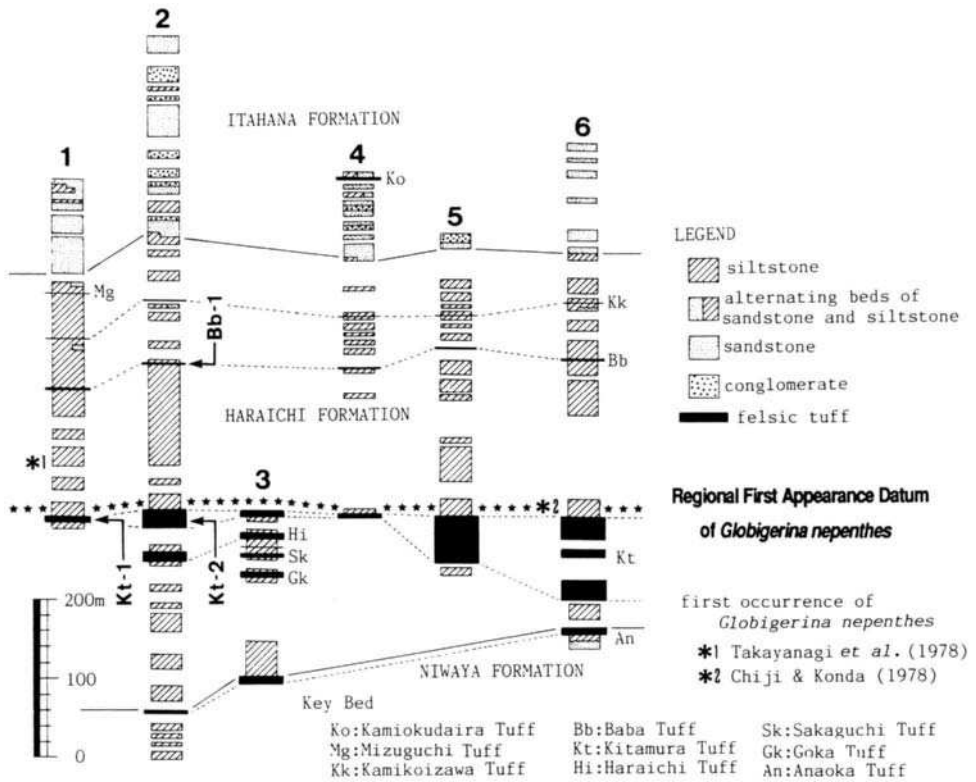


Fig. 4. Columnar sections along the six routes. Kt-1, Kt-2 and Bb-1 indicate the points of radiometric dating.

**GEOCHRONOLOGY**

*Sampling*

We collected tuff samples from one site (Bb-1) for the Baba Tuff, and from two sites (Kt-1 and Kt-2) for the Kitamura Tuff (Fig. 2). These tuff samples were crushed in a stainless steel mortar and sieved to a grain size of 150–300 mm. Biotite was first concentrated using an isodynamic separator, then by tapping. Purity of the biotite samples is 99% or higher.

*K–Ar isotope dilution technique*

Concentrations of K were determined by flame photometry. The basic technique is described by Nagao et al. (1984). Results are listed in Table 1. In every series of K analyses, JGS standards (JF-1, JG-1a, JG-2 and JGb-1) were analyzed as references. K-concentration of the standards analyzed together with one of the Kitamura Tuff samples (Kt-1) gave lower K concentrations. Assuming that some troubles in preparing alkali solution was responsible for this discrepancy, we calculated K contents for this series by multiplying a correction factor defined by the analysis of standard samples.

Table 1

K contents in biotite from the Baba (Bb) and Kitamura (Kt) tuffs

Sample	No.	K (wt%)	Standard sample	Literature value <sup>a</sup>
Bb-1	(1)	6.46		
	(2)	6.48		
	(3)	6.68	JG-2 3.93	3.93 ± 0.02
	(4)	6.70	JF-1 9.29	8.29 ± 0.02
	(5)	6.55	JGb-1 0.19	0.190 ± 0.001
	(6)	6.54		
	(7)	6.51		
	average	6.56 ± 0.18		
Kt-1	(1)	6.45	JF-1 7.82 (5.7%)	8.29 ± 0.02
	(2)	6.23	JG-1a 3/21 (3.9%)	3.34 ± 0.02
	(3)	5.99		
	(4)	5.91	JG-1 7.63 (7.9%)	8.29 ± 0.02
	(5)	6.15	JG-1a 3/15 (5.7%)	3.34 ± 0.02
	(6)	6.18		
	average	6.15 ± 0.34 → corrected 6.50 ± 0.34		
Kt-2	(1)	6.46	JF-1 8.32	8.29 ± 0.02
	(2)	6.14	JG-2 3.92	3.93 ± 0.02
	(3)	5.81		
	average	6.14 ± 0.66		

<sup>a</sup> Matsumoto (1989). In the case of Kt-1, we list the corrected contents as well as the original ones because the K content for the GSJ standard measured together with Kt-1 showed values significantly lower than the reported values, which are also listed here.

Error on averages  $2\sigma$ .

The K contents of the Kitamura and Baba Tuffs are not as high as it is expected for pure and unaltered biotite, which suggests presence of altered phases.

The samples for the Ar analysis were fused in a Mo crucible at 1600°C. The extracted gases were purified twice on hot Ti sponge and, on the last stage, by a Sorb Ac<sup>®</sup> getter pump. Ar analyses were carried out at Yamagata University with a 25-cm radius, 60° deflection, metal mass spectrometer. About  $0.8 \times 10^{-6}$  cm<sup>3</sup> STP of <sup>38</sup>Ar was used as a spike. An amount of the spike <sup>38</sup>Ar was occasionally calibrated by Bern 4B Biotite (Flisch, 1982) several times during a series of analyses. Correction for a mass discrimination of the machine was applied by determining a correction factor based on measurements of the <sup>40</sup>Ar/<sup>36</sup>Ar ratio of the atmospheric argon. Effects of hot blank Ar were also corrected. Results are listed in Table 2.

The K–Ar ages of two tuff biotites are listed in Table 3. Here, we emphasize that, if we use the face value of K for calculating the age of the Kt-1, the resulting age appears older. Hence, the age of Kt-1 biotite listed in Table 3 has to be considered an upper limit.

#### <sup>40</sup>Ar/<sup>39</sup>Ar technique

About 0.3 g of Baba biotite was wrapped in aluminum foil, and vacuum sealed in a quartz tube (10 × 70 μm) together with the standard Bern 4B. Neutron irradiation was performed by the JMTR at Tohoku University for 12 h. The total fast neutron dose was

Table 2

Ar isotope analyses of biotite from the Baba (Bb) and Kitamura (Kt) tuffs (Middle Miocene, central Japan)

Sample	No.	$^{36}\text{Ar}$ ( $10^{-3}$ nl/g)	$^{40}\text{Ar}^*$ (nl/g)	Atm. $^{40}\text{Ar}$ (%)
Bb-1	(1)	2.50	2.96	20.0
	(2)	0.56	3.08	5.1
	(3)	5.44	2.77	36.8
	(4)	2.51	2.97	20.0
	(5)	15.38	3.10	59.4
	(6)	4.28	2.97	29.9
	(7)	4.13	2.96	29.2
	(8)	1.16	2.89	10.7
	(9)	1.10	2.94	9.9
$^{40}\text{Ar}^*$ average			$2.96 \pm 0.20$	
Kt-1	(1)	0.78	3.27	6.6
	(2)	0.93	3.41	7.5
	(3)	1.34	3.34	10.6
$^{40}\text{Ar}^*$ average			$3.34 \pm 0.12$	
Kt-2	(1)	0.68	3.16	6.0
	(2)	0.87	3.20	7.4
	(3)	0.36	3.26	3.2
	(4)	0.68	3.04	6.2
	(5)	0.44	2.95	4.1
$^{40}\text{Ar}^*$ average			$3.12 \pm 0.22$	

Error  $2\sigma$ .

Table 3

K-Ar analyses of the Baba and Kitamura tuffs

Sample	Mineral	K (wt%)	$^{40}\text{Ar}^*$ (nl/g)	Age (Ma)
Bb-1	biotite	$6.56 \pm 0.18$	$2.96 \pm 0.20$	$11.6 \pm 0.8$
Kt-1	biotite	$6.50 \pm 0.34$	$3.34 \pm 0.12$	$13.2 \pm 1.0$
			(corrected mean)	
Kt-2	biotite	$6.14 \pm 0.66$	$3.12 \pm 0.22$	$13.0 \pm 1.6$

Error  $2\sigma$ .

estimated to be  $3 \times 10^{17}$  n/cm<sup>2</sup>, and the thermal to fast neutron ratio was about 0.08. Ar degassing was done at Yamagata University by using an extraction line off the mass spectrometer. A sample was heated from 600°C to 1400°C with temperature increments of 100°C. The biotite sample was completely fused at 1400°C. The temperature of each step was previously calibrated with the output power of the induction heater, and the temperature of the sample in the extraction was estimated from the output. After purification on hot Ti sponge, Ar was collected on a charcoal finger at the liquid nitrogen temperature. Then the Ar sample in a glass ampoule was sealed off from the extraction line. The same procedure that was applied to the conventional K-Ar technique, was also used in Ar analyses.

Because the Ar analyses took place 10 months after the irradiation, most of  $^{37}\text{Ar}$  had decayed. Hence, we did not apply corrections for Ca-induced  $^{39}\text{Ar}$  and  $^{36}\text{Ar}$  based

Table 4

<sup>40</sup>Ar/<sup>39</sup>Ar stepwise heating analysis results from Baba (Bb-1) and Kitamura (Kt-1) biotites

Step	Temp. (°C)	<sup>39</sup> Ar (%)	<sup>36</sup> Ar/ <sup>40</sup> Ar (×10 <sup>-3</sup> )	<sup>39</sup> Ar/ <sup>40</sup> Ar (×10 <sup>-3</sup> )	Apparent age <sup>a</sup> (Ma)
<b>Bb</b>					
1	600	0.1	3.47 ± 0.47	2.7 ± 0.4	
2	700	1.2	2.84 ± 0.19	41.9 ± 0.7	10.3 ± 0.5
3	800	14.8	0.99 ± 0.02	186.3 ± 2.7	11.6 ± 0.5
4	900	9.0	1.17 ± 0.05	166.1 ± 2.9	12.0 ± 0.5
5	1000	23.1	0.63 ± 0.02	212.4 ± 1.6	11.7 ± 0.5
6	1100	48.5	0.32 ± 0.02	228.4 ± 1.6	12.1 ± 0.5
7	1200	2.7	1.98 ± 0.13	106.3 ± 1.4	11.9 ± 0.5
8	1300	0.4	3.06 ± 0.34	19.3 ± 0.6	15.1 ± 0.5
9	1400	0.2	3.10 ± 0.26	9.5 ± 0.2	26.8 ± 1.3
<i>J</i> = (1.69 ± 0.07) × 10 <sup>-3</sup> ; plateau age: 11.9 ± 0.9 Ma (700–1200°C)					
<b>Kt 1A</b>					
1		0.1	2.27 ± 1.00	7.7 ± 5.8	254 ± 198
2		0.2	2.82 ± 0.34	14.1 ± 3.0	74 ± 44
3		0.2	2.52 ± 0.52	20.8 ± 3.0	77 ± 44
4		0.2	2.45 ± 0.96	28.3 ± 4.0	61 ± 62
5		0.9	2.27 ± 0.46	75.0 ± 2.8	27.8 ± 11.4
6		24.5	0.62 ± 0.05	378.2 ± 2.6	13.8 ± 0.4
7		17.2	0.27 ± 0.11	433.4 ± 4.8	13.5 ± 0.4
8		12.1	0.49 ± 0.12	387.3 ± 6.4	14.1 ± 0.6
9	fuse	44.6	0.20 ± 0.06	453.5 ± 5.8	13.2 ± 0.2
<i>J</i> = (3.54 ± 0.10) × 10 <sup>-3</sup> ; weighted mean age: 13.4 ± 0.7 Ma (step 6 –fuse)					
<b>Kitamura 1B</b>					
1	700	0.7	3.32 ± 0.20	49.3 ± 3.0	2.5 ± 7.8
2	800	17.0	0.69 ± 0.07	424.4 ± 6.8	12.2 ± 0.4
3	900	8.1	0.71 ± 0.01	434.2 ± 6.0	11.9 ± 0.2
4	1000	5.6	1.07 ± 0.13	399.0 ± 5.2	11.1 ± 0.6
5	1100	49.1	0.16 ± 0.03	506.6 ± 3.4	12.2 ± 0.4
6	1200	19.5	0.40 ± 0.04	479.5 ± 4.0	12.0 ± 0.2
7	fuse	0.1>	4.32 ± 0.54	14.2 ± 7.8	
<i>J</i> = (3.62 ± 0.10) × 10 <sup>-3</sup> ; weighted mean age: 12.2 ± 0.4 Ma (800–1200°C)					

<sup>a</sup> Uncertainty of apparent ages for each temperature step does not include uncertainty in the *J*-value. Errors in plateau and weighted mean ages include uncertainty in the *J*-value.

Error 2σ.

on <sup>37</sup>Ar. Lack of correction would not make any significant difference in the results, however, because Ca concentration in biotite is low relative to K. A correction for K-induced <sup>40</sup>Ar was not applied either, because we had some problems in analyzing K<sub>2</sub>SO<sub>4</sub>. A previously reported correction factor was 7.0 × 10<sup>-2</sup> (Kaneoka et al., 1979), and our determination (by the other series of irradiation) was 8.37 × 10<sup>-2</sup> (unpublished data) for similar irradiation conditions.

The data for the stepwise degassing are listed in Table 4. The Baba biotite shows a good isochron, and defines a plateau age of 11.9 ± 0.9 Ma (2σ interlaboratory) (Fig. 5). The results agree well with the conventional K–Ar age of 11.6 ± 0.8 Ma.

The same procedures of the <sup>40</sup>Ar/<sup>39</sup>Ar analysis were applied to the Kitamura biotite.

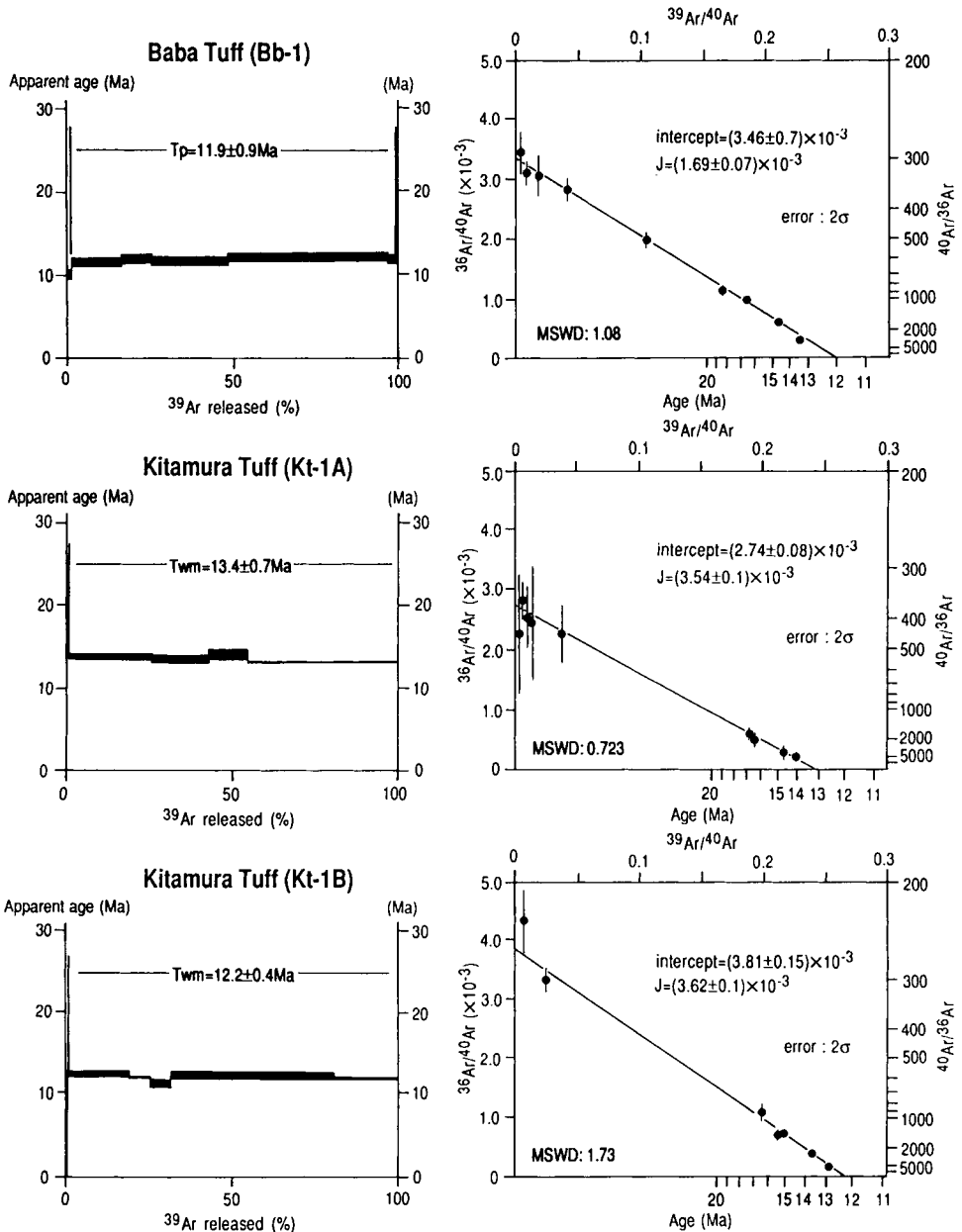


Fig. 5. A  $^{36}\text{Ar}/^{40}\text{Ar}$ - $^{39}\text{Ar}/^{40}\text{Ar}$  inverse isochron plot and age spectra for Bb-1 and Kt-1 biotites. An isochron age can be calculated from the intercept value with the  $^{39}\text{Ar}/^{40}\text{Ar}$  axis  $F$  by using the equation:  $T = (1/\lambda) \ln(J/F + 1)$ ,  $\lambda = 5.543 \times 10^{-10}/\text{year}$

Two samples separated from the Kt-1 biotite were analyzed together with the Bern 4B and the Baba biotite as monitor samples. The results of a  $^{40}\text{Ar}/^{39}\text{Ar}$  stepwise heating



analysis of the Kitamura biotites are listed in Table 4. Kitamura-A and Kitamura-B showed fairly well defined isochrons, whose trapped  $^{40}\text{Ar}/^{36}\text{Ar}$  ratios, respectively  $365 \pm 10$  and  $263 \pm 10$ , are considerably different from the atmospheric ratio. Even if we exclude five lower temperature fractions of Kitamura-A, and lowest and highest temperature fractions of Kitamura-B from the calculation of the isochrons, we still obtain identical age and trapped Ar ratios. It could be possible to argue that Kitamura-A trapped inherited Ar, but the trapped ratio as low as 265 found in the Kitamura-B is difficult to explain. Whether such a good isochron as that for Kitamura-A can be obtained only by chance would be a problem for a future study. The facts are: (1) that the trapped Ar ratios of two Kitamura samples are considerably different from the atmospheric ratio, and (2) that two samples show largely different ratios suggest that the K–Ar systematics in these samples experienced some kind of disturbance. Hence, although the choice of different trapped Ar ratios had little effect on their ages, the ages of Kitamura samples have a limited geological significance.

### Results

The K–Ar ages obtained from the Kitamura Tuff and the Baba Tuff are  $13.1 \pm 0.9$  Ma ( $2\sigma$  interlaboratory) and  $11.6 \pm 0.8$  Ma, respectively. The fission-track age of the Kitamura Tuff ( $13.0 \pm 1.4$  Ma) determined by Kasuya (1987) is consistent with our result ( $13.1 \pm 0.9$  Ma), demonstrating the high reliability of these radiometric ages. As for the Baba Tuff, a  $11.4 \pm 1.0$  Ma fission-track age was obtained by Kasuya (1987), whereas a  $11.6 \pm 0.8$  Ma K–Ar age was obtained by Shibata et al. (1979). An agreement between these ages and our new K–Ar dates, as well as the  $^{40}\text{Ar}/^{39}\text{Ar}$  analyses, assure the reliability of these geochronologic results. Therefore, we consider the K–Ar dates of  $13.1 \pm 0.9$  Ma for the Kitamura Tuff, and of  $11.6 \pm 0.8$  Ma for the Baba Tuff, the final, most reliable radioisotopic ages for the eruption of these tuffs.

As mentioned above, the regional FAD of *G. nepenthes* lies about 150–190 m below the Baba Tuff, and a few metres above the Kitamura Tuff (Fig. 4). Consequently, the timing of the first appearance of *G. nepenthes* is constrained between the age of the Baba Tuff, and that of the Kitamura Tuff. Strictly speaking, as the horizon of the local FAD of *G. nepenthes* in the Tomioka sequence is very close to the level of the Kitamura Tuff (Fig. 4), we can consider the age of the local FAD of *G. nepenthes* to be almost identical to that of the Kitamura Tuff (i.e.,  $13.1 \pm 0.9$  Ma). For these reasons, the age of the local FAD of *G. nepenthes*, that is, the regional N13/N14 planktonic foraminiferal zonal boundary, in the Tomioka sequence can be represented by the age of the Kitamura Tuff (i.e.,  $13.1 \pm 0.9$  Ma).

### DISCUSSION

The relationship between marine magnetic anomalies and the magnetostratigraphic division based on the Anomaly 5–Chron 9 or, alternatively, Chron 11 correlation models is shown in Fig. 6. The planktonic foraminiferal zonation, corresponding to the relative magnetostratigraphic chron (Ryan et al., 1974), and radiometric ages of the Baba and Kitamura tuffs, are also shown in Fig. 6. These two models differ only in the Anomaly–Chron correlation. We can estimate the numerical ages of a given datum level

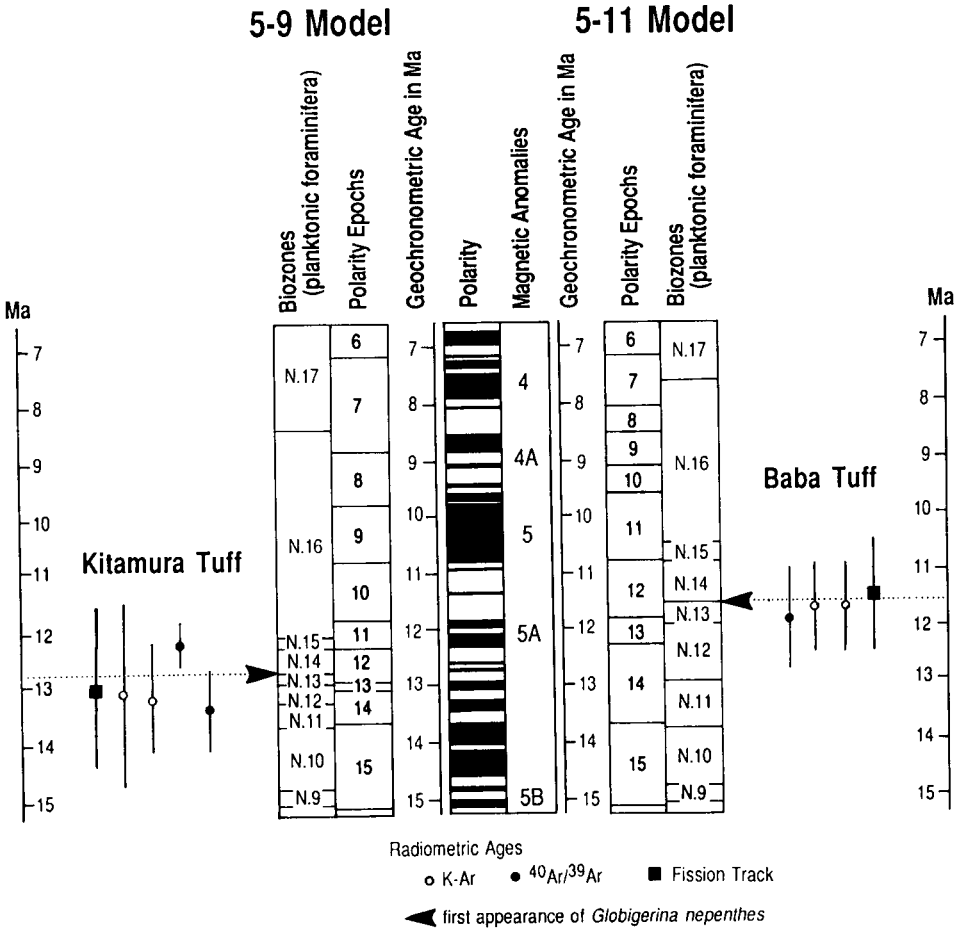


Fig. 6. Two correlation models of the magneto-biochronology scales for the Middle and Late Miocene (the plotted radiometric ages are from the Kitamura and Baba tuffs).

by examining these two correlation models, and assess the preference of one of these two models by comparing the ages of the Baba and Kitamura tuffs with the alternative numerical ages of the N13/N14 boundary.

The age of the N13/N14 boundary must be both older than the age of the Baba Tuff, and close to that of the Kitamura Tuff. As shown in Fig. 6, the age N13/N14 boundary appears older than the Baba Tuff, and within the error of the age of the Kitamura Tuff in the Anomaly 5–Chron 9 correlation model. On the other hand, the age of the N13/N14 boundary in the Anomaly 5–Chron 11 model is estimated considerably younger than that of the Kitamura Tuff, and undistinguishable from the age of the Baba Tuff. Therefore, the Anomaly 5–Chron 9 correlation seems to be preferable to the Anomaly 5–Chron 11 model.

Magneto-biochronologic scales are primarily constructed in low latitudes. In this

work, the radiometric ages of the Baba and the Kitamura tuffs were not directly compared with magnetostratigraphy. Therefore, it is necessary to assume a synchronism of the FAD of *G. nepenthes* between low latitudes and Japan, for the discussion mentioned above. This assumption is supported by the stratigraphic consistency of the datum levels between the two regions. However, a close scrutiny done by Johnson and Nigrini (1985) revealed the significant non-synchronicities for numerous microfossil biomarkers within and between latitudinal zones. The above-mentioned assumption needs to be cross-checked by magnetostratigraphic analysis in the Tomioka sequence. Datum levels will be directly connected to magnetic anomalies in the future by accumulating biostratigraphic, magnetostratigraphic, and radiometric data from the same section on land, as well as biostratigraphic data of cored deep-sea sediments.

## CONCLUSIONS

The geochronologic study of the Miocene Baba and Kitamura tuffs in the Tomioka sequence, central Japan, leads to the following conclusions.

(1) Newly obtained K–Ar ages of the Kitamura and Baba tuffs are  $13.1 \pm 0.9$  Ma, and  $11.6 \pm 0.8$  Ma, respectively. The  $^{40}\text{Ar}$ – $^{39}\text{Ar}$  ages of the Baba Tuff ( $11.9 \pm 0.9$  Ma), and the Kitamura Tuff ( $13.4 \pm 0.7$  Ma,  $12.2 \pm 0.4$  Ma) suggest that the Baba and Kitamura biotites are suitable for K–Ar measurement, and well determined K–Ar ages are reliable.

(2) The first occurrence of *G. nepenthes* is recognized a few metres above the Kitamura Tuff, and 150–190 m below the Baba Tuff, which implies that the age of the regional N13/N14 boundary in central Japan is almost coeval to the Kitamura Tuff ( $13.1 \pm 0.9$  Ma).

(3) Conclusion 2 also suggests that the Anomaly 5–Chron 9 correlation model appears preferable to the Anomaly 5–Chron 11 model, if we assume a synchronism of the FAD of *G. nepenthes* between low latitudes and Japan.

## SOMMAIRE — AGE RADIOMÉTRIQUE DE LA PREMIÈRE MANIFESTATION DE *GLOBIGERINA NEPENTHES* DANS LA SÉQUENCE DE TOMIOKA, JAPON CENTRAL

(Manuscrit soumis: Décembre 1993; révisé: Juillet 1994; rédacteur responsable: GSO)

L'apparition de *Globigerina nepenthes* qui définit la limite interzone N13/N14 de Blow a été reconnue entre deux niveaux de tufs (tufs de Kitamura et de Baba) de la région de Tomioka, au Japon Central. Elle se situe quelques m au dessus du tuf de Kitamura et 150 à 190 m au dessous du tuf de Baba. Les âges radiométriques des deux tufs (techniques par dilution isotopique et irradiation) ont été déterminés à Yamagata sur biotite. Dans l'ordre stratigraphique, les âges par dilution isotopique nouvellement obtenus se succèdent correctement à  $13,1 \pm 0,9$  Ma ( $2\sigma$ ) et  $11,6 \pm 0,8$  Ma. Le chauffage par étape d'échantillons irradiés conduit à un âge plateau de  $11,9 \pm 0,9$  Ma pour le tuf de Baba et à deux âges moyens pondérés de  $13,4 \pm 0,7$  et  $12,2 \pm 0,4$  Ma pour le tuf de Kitamura. Pour ce dernier, les spectres d'âge sont légèrement perturbés et les rapports isotopiques de l'argon initial calculés sur les représentations isochrones

sont assez différents des rapports normaux de l'atmosphère. La signification géologique de ces âges est assurée pour le tuf de Baba et probablement pas très éloignée de la réalité pour le tuf de Kitamura. On a retenu l'âge de  $13,1 \pm 0,9$  Ma pour caractériser le biorepère sélectionné.

*(Sommaire proposé par les rédacteurs, GSO)*

#### ACKNOWLEDGEMENTS

We would like to thank Drs. M. Oda and M. Kasuya for their helpful advices. We also appreciate the staffs of Tohoku University (Oarai branch) for irradiating samples by JMTR. Prof. Oba of Yamagata University helped us in the K-analyses. The manuscript was improved with suggestions by G.S. Odin of the P. et M. Curie University in Paris, and A. Montanari of the Osservatorio Geologico di Coldigioco.

This Page Intentionally Left Blank

*Chapter D7*

**GÉOCHRONOLOGIE DE NIVEAUX SITUÉS AUTOUR DE L'APPARITION  
DE *GLOBIGERINA NEPENTHES* AU JAPON ET EN ITALIE: ÂGE DE LA  
LIMITE SERRAVALLIEN/TORTONIEN**

G.S. Odin, M. Takahashi, R. Coccioni et M. Cosca

**INTRODUCTION**

Dans la plupart des tentatives de calibrage de l'échelle stratigraphique, le repérage chronostratigraphique est effectué à l'aide d'un ou deux groupes fossiles en admettant la validité chronologique d'un nombre restreint de biorepères. Nous abordons, dans ce travail, une approche différente qui est de dater un biorepère dans deux régions éloignées afin d'estimer à la fois son âge numérique mais aussi sa validité chronologique à l'échelle globale.

La succession sédimentaire miocène japonaise, comme celle d'Italie, est riche de niveaux pyroclastiques utilisés comme repères lithostratigraphiques régionaux avec des noms appropriés (cf Takahashi et Oda Chapitre B3 de ce volume). Parmi ces niveaux, les tufs de Kitamura et de Baba ont déjà fait l'objet d'études géochronologiques (Kasuya, 1987; Shibata et al., 1979; Takahashi et al., 1992) ayant montré la qualité du matériel analysé. Les techniques d'analyse isotopique appliquées jusqu'ici n'étaient pas assez précises et nous avons tenté d'obtenir de nouveaux résultats. Mais l'objectif de ce travail était d'abord d'obtenir des résultats comparables afin de discuter concrètement et précisément de l'âge d'un même biorepère parmi ceux communément utilisés pour la corrélation chronologique de deux régions éloignées. La technique  $^{39}\text{Ar}/^{40}\text{Ar}$  avec chauffage par palier est bien adaptée à cette comparaison puisqu'elle est remarquablement précise lorsqu'il s'agit de comparer deux événements; la difficulté qu'est le calibrage analytique n'entre pas en ligne de compte.

Dans ce travail, nous présentons de façon résumée les résultats que nous avons obtenus d'un côté au Japon central dans la région de Tomioka, de l'autre en Italie dans la coupe du Monte dei Corvi près d'Ancône; une étude détaillée a été publiée par ailleurs (Odin et al., 1995a, 1995b).

**GÉOLOGIE DES ÉCHANTILLONS**

*La région de Tomioka*

La présentation de la géologie et des profils datés situés à près de 80 km au NO de Tokyo sont faites dans le travail précédent de MM Takahashi et Saito. Rappelons que l'apparition du foraminifère planctonique considéré ici se situe dans une succession de biorepères que l'on peut qualifier de normale puisqu'ont été observées successivement (Takayanagi et al., 1978; Chiji and Konda, 1978) les apparitions, de bas en haut, de

*Praeorbulina glomerosa curva*, *Praeorbulina glomerosa glomerosa*, *Orbulina suturalis* et *Orbulina universa*, *Praeorbulina glomerosa circularis*, *Globorotalia peripheroacuta*, *Sphaeroidinellopsis subdehiscens*, *Globigerina nepenthes* suivie de la disparition de *Zeaglobigerina druryi* que l'on considère comme l'ancêtre de *G. nepenthes*; de fait, les deux formes sont citées dans presque tout l'intervalle entre les deux tufs.

Plus précisément, l'apparition locale de *G. nepenthes* a été reconnue dans une première coupe pratiquement à équidistance des deux tufs datés (Kitamura et Baba); dans une seconde coupe, l'apparition locale se situe seulement une dizaine de mètres au dessus du tuf inférieur (Kitamura); elle paraît donc plus ancienne si l'on tient compte du fait que ces deux coupes ont la même épaisseur d'environ 180 m et donc qu'il n'y a pas de différence apparente au plan des dépôts représentés. On a donc considéré comme l'âge de l'apparition régionale de *G. nepenthes*, le niveau situé un dizaine de mètres au dessus du tuf de Kitamura. Cette interprétation régionale a été rendue nécessaire par le fait que les niveaux les plus frais sélectionnés pour la datation ont été prélevés dans une troisième coupe située entre les deux précédentes. La succession est, par ailleurs, bien adaptée pour des corrélations à longue distance grâce à la présence de nannofossiles calcaires.

#### *La falaise du Monte dei Corvi*

Au sud d'Ancône la falaise qui borde la mer Adriatique expose une série pélagique fossilifère de l'ensemble du Miocène et du Pliocène. Ce remarquable affleurement de la Riviera del Cònero a fait l'objet de plusieurs travaux exposés plus loin dans ce volume (Chapter E1) et l'on se reportera à cet exposé pour les généralités. Le présent travail concerne l'étude d'un niveau riche en biotite de 15 cm d'épaisseur qui fut nommé niveau 'Ancône'. Il se situe à la cote 150,0 de la section du Monte dei Corvi (MDC) et est plus jeune que le niveau 'Respighi' (étudié à Berkeley par Deino et Montanari, 1992, en même temps que le niveau Ancône) qui est situé à la cote 101,3 dans la même falaise et est d'âge Serravallien plus ancien (voir Chapter E1).

L'étude biostratigraphique de la portion Serravallien supérieur-Tortonien inférieur (Coccioni et al., 1992c) a été complétée pour ce travail. La première observation de *G. nepenthes* peut être située à la cote 148,5. La disparition de *Z. druryi* a été observée légèrement au dessus, à la cote 149,9. En outre, la première observation de *Neogloboquadrina acostaensis*, souvent utilisée pour approcher la limite Serravallien/Tortonien, est située à la cote 157,6. En bref, le niveau 'Ancône' est situé 1,5 mètre au dessus de la première observation de *G. nepenthes* et moins de 8 mètres sous un biopère suggérant la limite entre Serravallien et Tortonien. On notera que l'intervalle sédimentaire considéré (entre 148,5 et 157,6) comprend deux biozones classiques de foraminifères planctoniques (biozones N14 et N15 de Blow, 1969).

La signification chronologique du biopère: émergence de *G. nepenthes*, a été débattue (Kennett, 1973; Cita, 1978; Cati et al., 1981; Kennett and Srinivasan, 1983; Bolli and Saunders, 1985); ceci pourrait conduire à remettre en question ce signal. Pourtant il s'agit fondamentalement d'une transition dans une lignée qui, lorsque l'ancêtre et le descendant sont tous deux reconnus dans une succession, a un potentiel chronologique certain. Au sud d'Ancône, l'apparition de *G. nepenthes* a été placée au niveau de l'apparition des formes qui sont complètement semblables à l'holotype.

Le chevauchement des formes *G. druryi* et *G. nepenthes* est ici apparemment moins important qu'au Japon.

## ÉTUDE GÉOCHRONOLOGIQUE

### *Etude du matériel daté: les géochronomètres*

Les tufs japonais sont connus depuis longtemps et leur nature de dépôt d'origine volcanique primaire est reconnue. Nous avons sélectionné un échantillon du tuf inférieur dit de Kitamura (T217) et un du tuf supérieur dit de Baba (T215), tous les deux le long de la même coupe mise à jour par la rivière Fujiki. Les minéraux extraits par les techniques traditionnelles ont une belle apparence (automorphes) et la diffraction des rayons X indique une bonne préservation. Pour le tuf inférieur, seule la biotite a été utilisée; pour le tuf supérieur la biotite, la sanidine et le plagioclase ont tous trois été purifiés et analysés isotopiquement.

Le niveau Ancône comporte à la fois des composants volcaniques (verre argilisé, biotite et feldspath) et sédimentaires pélagiques (carbonate, glauconie, test de foraminifères et dents de poisson). Le mélange est probablement lié à l'activité d'organisme fouisseurs. La biotite, de bonne qualité minéralogique et géochimiquement homogène (Montanari, 1988), est un géochronomètre digne de confiance.

### *Analyses isotopiques*

La technique  $^{40}\text{Ar}/^{39}\text{Ar}$  avec chauffage par paliers a été utilisée selon les mêmes procédures que celles employées pour les autres travaux présentés dans ce volume. Les incertitudes analytiques internes sont données pour un intervalle de confiance de 95%. Pour l'ensemble des échantillons, les résultats analytiques sont rassemblés dans le Tableau 1. Les spectres d'âges présentent tous des plateaux ayant permis de calculer des âges plateaux résumés dans le Tableau 2.

Concernant les résultats obtenus sur les échantillons japonais, on soulignera la bonne cohérence des âges calculés pour le tuf de Baba sur trois phases différentes (T215, Tableau 2). Les âges isochrones calculés indépendamment sont identiques aux âges plateau et aux âges totaux pour chaque phase datée. Nous retiendrons, pour le tuf de Baba, l'âge plateau sur la biotite à  $11,26 \pm 0,09$  Ma, l'âge plateau sur la sanidine à  $11,29 \pm 0,12$  Ma et l'âge total sur le plagioclase autour de 11,3 Ma. Nous avons réalisé, dans une seconde série de mesures, un nouvel âge par fusion totale sur la biotite et celui-ci s'est révélé légèrement plus élevé que lors de la première série à  $11,48 \pm 0,14$  Ma. Le spectre d'âge du plagioclase (Fig. 1) est légèrement en escalier depuis 11,0 jusqu'à 11,6 Ma. On peut indifféremment calculer un âge plateau sur les paliers initiaux (âge à  $11,21 \pm 0,12$  Ma pour les paliers 875 à 1325°C, Tableau 2) ou sur les paliers de haute température (âge à près de  $11,4 \pm 0,1$  Ma pour les paliers 1175 à 1475°C et 64,1% des gaz extraits). L'âge total à 11,26 Ma paraît plus proche de l'âge des deux autres phases. Pour le tuf de Kitamura, l'âge plateau de  $11,79 \pm 0,08$  est solidement fondé (Fig. 1).

Concernant la biotite du niveau 'Ancône' analysé en même temps que les échantillons japonais, le spectre d'âge (Fig. 2) est entièrement plat et les âges total, plateau et isochrones sont parfaitement identiques à  $11,48 \pm 0,13$  Ma



Tableau 1

Résultats des analyses  $^{40}\text{Ar}/^{39}\text{Ar}$  avec chauffage par palier sur les échantillons du Japon: Analyses G.S. Odin à Lausanne.

°C	Âge apparent (Ma)	$\pm 2\sigma$	% $^{39}\text{Ar}$	%rad.	K/Ca
T217 biotite (poids utilisé: 12,62 mg)					
700	11,4	1,0	1,7	46	67
850	11,78	0,20	7,8	88	180
950	11,76	0,15	21,8	96	240
1050	11,85	0,16	7,1	94	140
1095	11,77	0,15	7,5	96	180
1135	11,78	0,15	15,1	97	255
1200	11,76	0,14	36,9	99	505
1350	11,93	0,23	2,1	100	290
T215 biotite (poids utilisé: 13,83 mg)					
700	11,3	0,3	5,6	46	51
850	11,45	0,24	7,5	74	88
950	11,45	0,22	11,3	83	95
1020	11,40	0,15	14,0	92	101
1075	11,22	0,14	22,6	96	116
1120	11,19	0,14	21,2	97	80
1190	11,24	0,14	16,5	99	31
1350	11,1	0,7	1,3	100	15
T215 sanidine (poids utilisé: 11,4 mg)					
900	10,6	0,6	1,7	62	39
1050	10,89	0,21	4,5	86	56
1150	11,18	0,15	8,2	98	69
1185	11,35	0,15	5,9	99	82
1230	11,31	0,16	9,4	98	84
1270	11,29	0,14	16,4	98	88
1320	11,25	0,14	34,2	99	87
1370	11,35	0,14	15,8	99	83
1410	non analysé				
1570	11,54	0,22	3,9	95	104
T215 plagioclase (poids utilisé: 74,56 mg)					
730	9,5	1,0	3,5	43	0,10
875	10,8	0,4	5,6	57	0,08
1025	10,97	0,22	20,2	86	0,07
1175	11,25	0,16	23,8	94	0,08
1325	11,39	0,18	16,1	93	0,08
1475	11,59	0,26	24,2	54	0,07
1600	12,0	0,4	6,5	53	0,06
T220 biotite (poids utilisé: 15,67 mg)					
700	11,6	2,5	1,5	18	27
870	11,55	0,18	7,0	88	71
970	11,51	0,14	22,0	95	145
1050	11,46	0,15	17,9	92	110
1100	11,48	0,15	15,0	90	30
1140	11,41	0,21	6,9	88	15
1190	11,48	0,15	17,0	88	17
1350	11,48	0,16	12,5	81	26
1600	10	11	0,1	25	

°C: température de chauffage; incertitude sur le flux  $J = 0,5\%$ ; dosimètre: biotite HD-B1 = 24,21 Ma.

T215 (uf de Baba); T217 (uf de Kitamura); T220 (niveau Ancône).

Tableau 2

Âges apparents calculés d'après les chauffages par paliers réalisés sur les échantillons japonais (T215 et T217) et italien (T220)

Échantillon	Âge (gaz total) (Ma)	Gaz extrait	Paliers	Âge plateau (Ma)
T217 bio	11,77( ± 0,09)	98,3%	0850–1350°C	11,79 ± 0,08
T215 bio	11,29( ± 0,09)	75,7%	1020–1350°C	11,26 ± 0,09
T215 bio re	11,48( ± 0,14)			
T215 san	11,26( ± 0,12)	89,9%	1150–1370°C	11,29 ± 0,12
T215 plag	11,26( ± 0,12)	65,8%	0875–1325°C	11,21 ± 0,12
T220 bio	11,48( ± 0,13)	99,9%	0700–1350°C	11,48 ± 0,13

## DISCUSSION

### Géochronologie

Les analyses isotopiques ont confirmé la qualité des géochronomètres sélectionnés sur la base de la pétrographie et de la minéralogie. Ceci est évident à l'examen des spectres d'âge qui dénotent des phases homogènes n'ayant apparemment pas subi d'altération depuis leur émission au cours d'un événement volcanique.

La cohérence stratigraphique est respectée pour les deux échantillons japonais dont la différence d'âge apparente ( $0,5 \pm 0,1$  Ma) semble compatible avec les données biostratigraphiques alliées aux épaisseurs de sédiment. Nos résultats diffèrent un peu de ceux rassemblés par Shibata et al. (1979), Kasuya (1987) ou Saito et Takahashi (1992, et rappelés dans ce volume au Chapter D6) à  $13,1 \pm 0,8$  Ma (tuf de Kitamura) et  $11,6 \pm 0,8$  Ma (tuf de Baba) mais ceci concerne essentiellement la question de la précision des résultats. Nous avons aussi pris soin, dans la présente étude, de purifier avec attention les extraits de biotite qui, particulièrement pour T217, montraient une abondance d'inclusions ainsi que de faibles proportions de hornblende et pyroxène qui sont susceptibles de piéger, dans le magma, de l'argon enrichi en isotope radio-génique.

En résumé, nos résultats indiquent un âge de 11,28 Ma pour le tuf de Baba et de 11,79 Ma pour le tuf de Kitamura. Si l'on tient compte des incertitudes sur le dosimètre HD-B1 les incertitudes analytiques doivent être portées à  $\pm 0,37$  Ma (tuf de Kitamura) et 0,36 Ma (tuf de Baba) mais ce qui importe maintenant est la comparaison avec l'âge du niveau 'Ancône' daté dans les mêmes conditions à 11,48 Ma.

### Biostratigraphie

Au Japon, l'âge de l'apparition régionale de *G. nepenthes*, localisée environ 10 m au dessus du tuf de Kitamura et 170 au dessous du tuf de Baba, peut être suggéré par une simple extrapolation sédimentaire dans un dépôt dont le taux épaisseur/durée de dépôt est de l'ordre de 360 m/Ma si l'on se réfère aux âges mesurés. Dans cette hypothèse d'un taux régulier, l'âge du biopère est d'environ 11,76 Ma.

Dans les Apennins, le niveau 'Ancône' est situé 1,5 m au dessus de la première observation de *G. nepenthes* (Coccioni et al., 1992c; Montanari et al., Chapter E1). Dans cette section, le taux moyen épaisseur/durée de dépôt peut être estimé d'après

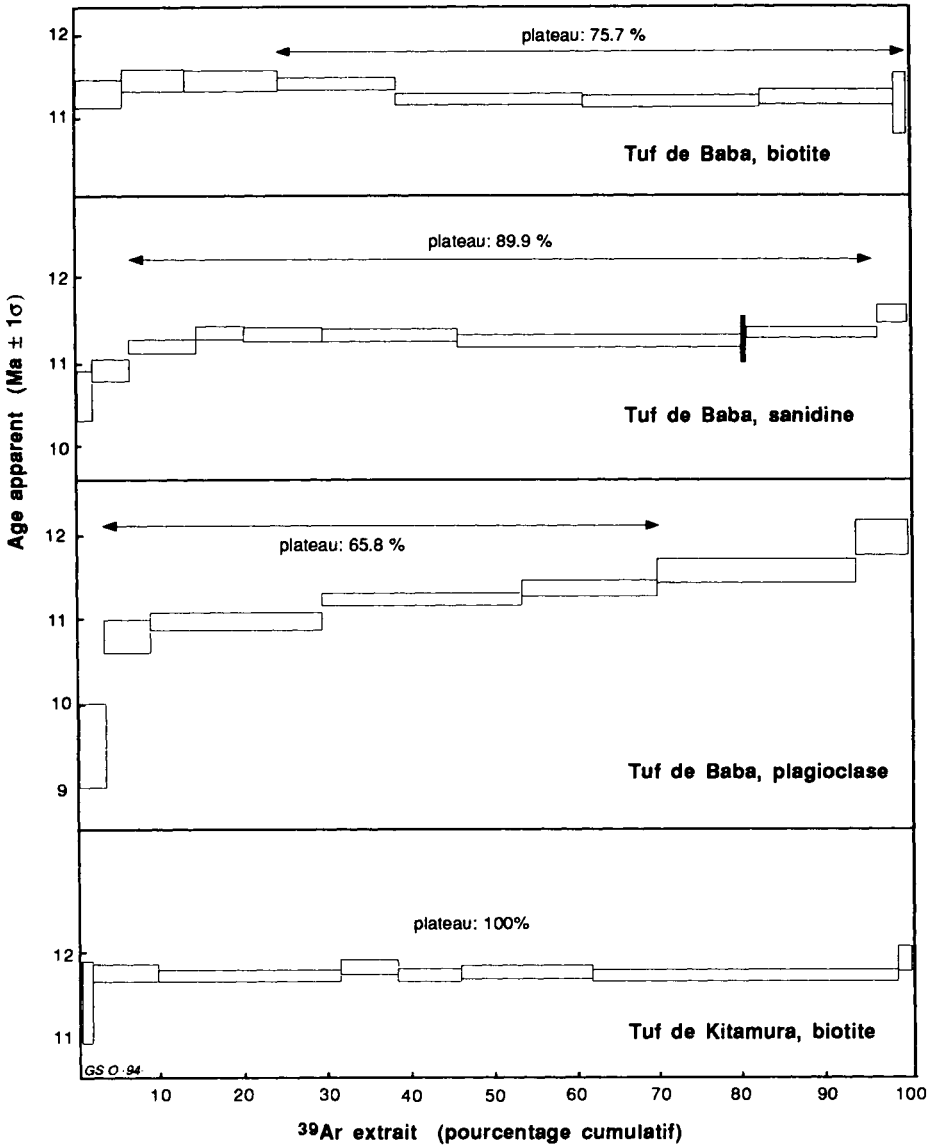


Fig. 1. Spectres d'âge des minéraux séparés des tufs de Kitamura et de Baba au Japon.

le fait qu'entre la moitié et les deux tiers de l'Étage Serravallien sont représentés par 60 m de dépôt; or cet Étage dure probablement entre 3,5 et 4,0 Ma (Odin, 1994); le taux déduit est alors situé entre 25 et 35 m/Ma. Par une autre approche combinant les résultats géochronologiques préliminaires obtenus à Berkeley dans cette coupe (Deino and Montanari, 1992) et l'épaisseur des sédiments, on observe que deux tufs espacés de 48,5 m présentent une différence d'âge mesurée de 1,5 Ma soit un taux moyen situé autour de 30 m/Ma, une bonne estimation établie directement. Si l'on utilise notre âge

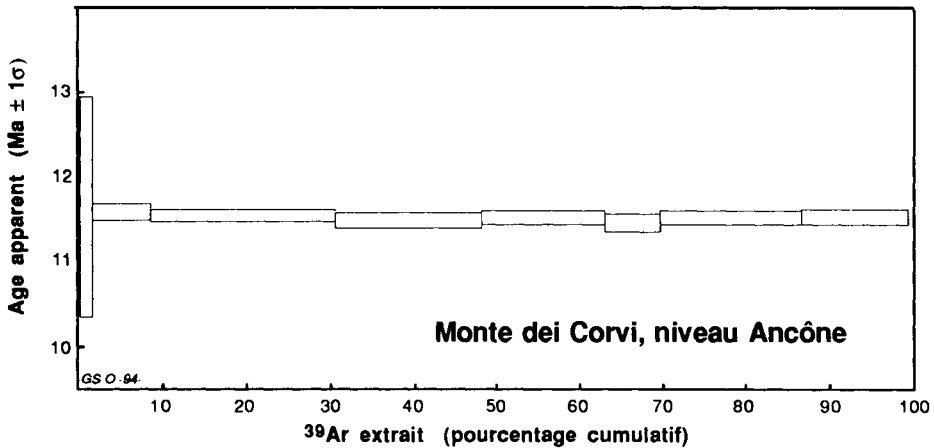


Fig. 2. Spectre d'âge de la biotite du niveau 'Ancône' de la falaise du Monte dei Corvi.

de 11,48 ( $\pm 0,13$ ) Ma pour le niveau Ancône, l'âge de l'apparition de *G. nepenthes* est de 11,48 + (1,5/30) = 11,53 Ma en Italie.

La différence d'âge entre les deux régions est d'environ 0,23 Ma (11,76–11,53) avec une incertitude du même ordre de grandeur autour de 0,20 Ma. Ainsi, en tenant compte d'une marge d'incertitude maximale, nous n'avons pas démontré de diachronisme ce qui suggère une bonne validité chronologique pour ce biorepère. Pourtant, si la différence moyenne de 0,23 Ma est correcte, alors l'arrivée de *G. nepenthes* serait plus ancienne au Japon. La différence serait du même ordre que la durée des deux biozones N14 et N15 (entre l'émergence de *G. nepenthes* et celle de *Neogloboquadrina acostaensis*) représentées par environ 9 m de sédiments dans la coupe du Monte dei Corvi soit à peu près 0,3 Ma au taux calculé de 30 m/Ma.

### Chronostratigraphie

Comme dit plus haut, la limite Serravallien/Tortonien est souvent approchée par l'apparition de *N. acostaensis*. En Italie, dans le stratotype historique du Tortonien (Piémont) seul valide en l'absence de définition plus précise, ce biorepère était classiquement situé près mais au dessus de la base de la section type (Iaccarino, 1985). D'après Miculan (Chapter A7) l'apparition du fossile marqueur se fait sous la base du stratotype Tortonien. On ne dispose pas de critère susceptible d'apprécier le caractère isochrone ou non du biorepère entre les deux coupes de Tortona et d'Ancône. Mais, faisant l'hypothèse d'un synchronisme entre les deux régions italiennes, l'âge de l'apparition de *N. acostaensis* près d'Ancône peut être proposé comme l'âge maximum (légèrement plus ancien) de la limite d'après les observations de Miculan. Par une extrapolation limitée utilisant le taux de 30 m/Ma et le fait que le biorepère est situé 7,6 m (environ 0,25 Ma) au dessus du niveau Ancône, son âge pourrait être estimé à 11,25 ( $\pm 0,20$ ) Ma. Ainsi, d'après notre étude, la limite Serravallien/Tortonien serait assez probablement située entre 11,0 et 11,5 Ma.

**ABSTRACT — GEOCHRONOLOGY OF LAYERS LOCATED NEAR THE FIRST OCCURRENCE OF *GLOBIGERINA NEPENTHES* IN JAPAN AND ITALY: AGE OF THE SERRAVALLIAN/TORTONIAN BOUNDARY**

*(Manuscript submitted: March 1994; revised: March 1994; responsible editor: GSO)*

Two biotite-rich tuffs of Central Japan were dated using the incremental heating  $^{40}\text{Ar}/^{39}\text{Ar}$  technique. The Kitamura tuff, located 10 m below the regional first occurrence (FO) of the planktonic Foraminifera *Globigerina nepenthes* yielded a biotite age of  $11.79 \pm 0.08$  Ma. The Baba tuff, located 180 m above the previous one yielded ages of  $11.26 \pm 0.09$  (biotite),  $11.29 \pm 0.12$  Ma (sanidine) and  $\approx 11.3$  Ma (plagioclase). The first occurrence of *G. nepenthes* is concluded at  $11.76 (\pm 0.10)$  Ma in Japan. Similarly precise results obtained from Central Apennines (biotite:  $11.48 \pm 0.13$  Ma) lead to an age of 11.53 Ma for the same first occurrence in the Italian section. The age difference between sections is of the same magnitude as the analytical errors. However, the potential diachronism of the biostratigraphic signal has been independently estimated at 0.25 Ma. According to these data, the Serravallian/Tortonian boundary located near the dated layers can be estimated to be 11.0 to 11.5 Ma old.

*(Authors' summary)*

**REMERCIEMENTS**

Nous sommes redevables envers Monsieur A. Montanari pour nous avoir conduit sur les remarquables falaises d'Ancône. Monsieur K. Saito (Univ. de Yamagata) a contribué à l'étude géochronologique préliminaire des tufs japonais; nous avons eu une utile discussion biostratigraphique avec Mr S. Galeotti (Univ. d'Urbino); l'aide de Mr G. Venturini a été appréciée durant les analyses isotopiques à Lausanne. L'étude minéralogique a été rendue possible grâce au laboratoire de Géologie du Muséum de Paris (diffraction des rayons X) et les analyses isotopiques grâce à l'Institut de Géologie de l'Université de Lausanne financé par le Fonds National Suisse. Cette recherche a disposé de fonds par le Ministère Italien Université et Recherche (MURST 60%, R. Coccioni responsable). Nous n'avons pas obtenu de fonds de recherche de la part d'organismes français pour cette étude.

**Part E**

**STUDIES RELEVANT TO THE UPPER MIOCENE SUBSERIES**

This Page Intentionally Left Blank

*Introduction to Part E*

## **INTRODUCTION: THE UPPER MIOCENE**

A. Montanari and R. Coccioni

During the Late Miocene (Tortonian and Messinian), the Tethyan Ocean was definitively closed as a result of syn-orogenic collisional tectonism, and its Mesozoic and Cenozoic sedimentary sequences were deformed and uplifted along the emerging Alpine–Himalayan orogenic system. Here and there in the proto-Mediterranean basin, deep-water, open-sea environments persisted through the Late Miocene, and were involved in the orogenic deformation only later on, in the Pliocene. However, the dominant Late Miocene sedimentary deposits throughout the Alpine–Himalayan domain are represented by thick flysch and molasse sequences which quickly filled tectonic foredip troughs immediately before being deformed and obducted on the emerging orogens.

Tectonic upheaval accompanied by violent and widespread volcanism affected also areas outside the Alpine–Himalayan domain, as well as marine basins which were still open to the rest of the world's oceans. Finally, the Messinian witnessed two other extraordinary events which are currently the focus of heated debates and fascinating scientific research: the temporary desiccation of the Mediterranean basin, and the appearance of the first hominids in Africa.

From this flash overview of the Late Miocene scenario, it clearly appears that this exceptionally active time of geologic history offers subjects for scientific research in the most disparate fields of earth sciences which will be absorbed by generations of geoscientists for many years to come. However, if in the one hand the Late Miocene is generous in rocks, phenomena, and tectonic structures, on the other hand it is parsimonious of those marine sedimentary deposits which allow an integrated stratigraphic approach for a much needed improvement of the geologic time scale. Moreover, the actual chronostratigraphy of this sub-Epoch is currently based on Mediterranean stratigraphic sections which do not necessarily bear fossil records reliable for time-correlations among distant sequences throughout the world.

The first seven chapters in Part D of this book report the results of integrated stratigraphic studies in several sections located along the eastern side of the northern Apennine foreland palaeobasin, namely the Apennine foothills near Faenza (Emilia region), and the coastal cliffs of the Cònero Riviera near Ancona (Marche region). The latter constitute a rare, perhaps unique case in which the entire Miocene Epoch is represented by a nearly complete and continuous sequence of pelagic and hemipelagic sediments.

In Chapter E1, Montanari and co-workers document the results of their interdisciplinary stratigraphic studies on the Cònero Riviera sequence covering the time interval from the mid-Langhian to the lower Messinian. These include detailed bio-event determinations based on planktonic Foraminifera and calcareous nannofossils which allow precise correlations with well established biostratigraphic models. Unfortunately, a



detailed palaeomagnetic study of a rich sample collection from the Serravallian and lower Tortonian portion of this sequence was not conducive to magnetostratigraphic determinations due to the magnetic weakness and/or altered conditions of these marly sediments.

The interval comprising the upper Serravallian and the lowermost Tortonian in the Cònero sequence was analyzed in detail for geochemical determinations of trace elements. Significant shifts of the total iron, strontium, and magnesium values found near the Serravallian/Tortonian boundary may constitute a viable tool for the recognition of this interstage boundary among western Tethyan sections. Stable isotopes were also measured in this interval but they show fairly uniform trends. On the other hand, both oxygen and carbon isotope curves exhibit significant trend shifts just above the Tortonian/Messinian boundary, which may very likely be related to the initiation of the Messinian salinity crisis.

$^{87}\text{Sr}/^{86}\text{Sr}$  ratios in biogenic carbonate and fish teeth throughout the Serravallian, Tortonian, and lower Messinian interval of the Cònero Riviera sequence show considerable scattering and are overall deviant from isotopic ratios measured in coeval oceanic sequences. A quick negative trend inversion of the  $^{87}\text{Sr}/^{86}\text{Sr}$  values is recorded in the upper Tortonian and it is followed by an equally rapid trend inversion to higher values in the lower Messinian. Again, these geochemical signatures are indicative of the particular palaeoenvironmental conditions which developed in the Apennine palaeobasin at a time when the western Tethyan was no longer exchanging deep-marine waters with the rest of the world's oceans (see also Chapter B1). An organic geochemistry study was also carried out on black shales from the Cònero sequence indicating, in fact, that the organic matter preserved in Serravallian shales is predominantly of open-marine origin, whereas the Messinian black shales carry a clear terrestrial organic signature. In summary, geochemical trends shifts in the Cònero Riviera sequence may be useful tools for correlating sections within the Tethyan domain but also indicate that this palaeobasin was developing its own geochemical equilibria already in the Serravallian and had restricted water-mass exchange with the open ocean at least since then. This would prevent the use of chemostratigraphic tools for correlating Middle and Upper Miocene Tethyan sections with oceanic ones.

Unaltered biotite from two volcanoclastic layers located in the lower, and uppermost Serravallian, respectively, were dated with the  $^{40}\text{Ar}/^{39}\text{Ar}$  incremental heating technique yielding very precise ages. From these, Montanari and co-workers derived a tightly interpolated age of  $11.0 \pm 0.2$  Ma ( $2\sigma$ ) for the Serravallian/Tortonian boundary.

The next five chapters of this book (Chapters E2–E6) report detailed integrated stratigraphic data from several sections in the Faenza area of the Romagna Apennines. These sections contain the Tortonian/Messinian boundary, and exhibit a sedimentary facies characterized by open-marine marls interbedded with black shales, practically devoid of turbiditic and/or siliciclastic deposits. Moreover, these sections contain several biotite-rich volcanoclastic layers which permit precise and accurate geochronologic dating of the Tortonian/Messinian boundary. In Chapter E2, Odin and co-workers present new litho- and biostratigraphic data from the Pieve di Gesso section which can be easily correlated with more complete and continuous sections exposed in the nearby Monte del Casino and Monte Tondo areas (see Chapters E3–E5). A number of new radioisotopic dates from biotite and plagioclase obtained by Odin and co-workers are

consistent with a suite of dates from volcanoclastic layers presented in the following chapters, and confirm an age slightly older than 7 Ma for the Tortonian/Messinian boundary. Using the rich geochronologic documentation of these northern Apennine sections, Vai in Chapter E3 examines the cyclostratigraphy of the Messinian finding a good consistency between geochronologic data and cyclostratigraphic sequence. It appears that orbital precession cycles (about 20 ka) are dominant throughout this stage, whereas obliquity cycles (about 40 ka) are prevalent in the upper Messinian. The cyclostratigraphic approach appears, in this case, a viable means for calibrating Messinian stratigraphic and geologic events with extreme precision and accuracy, and leads to an estimate of about 2 Ma for the duration of this stage. Details about nannofossil biostratigraphic and palaeomagnetic analyses of the Monte del Casino and Monte Tondo sections are presented by Negri and Vigliotti in Chapter E4, whereas a complete account on the integrated stratigraphy of these sections are given by Laurenzi and co-workers in Chapter E5, and Odin and co-workers in Chapter E6. From these studies, an age of 7.2 Ma is derived from the Tortonian/Messinian boundary.

In Chapter E7, Odin and co-workers present new data about the integrated stratigraphy of the Maccarone section, located in the eastern Marche region of Italy. This is a rare, perhaps unique situation in which the interval across the Messinian/Zanclean (i.e., Miocene/Pliocene) boundary is represented by a continuous sequence post-evaporitic, fossiliferous, marine pelitic sediments which contain, in the upper part of the Messinian, a prominent volcanic tuff layer. Two  $^{40}\text{Ar}/^{39}\text{Ar}$  incremental heating dates from pristine biotite from this tuff yield an age of 5.5 Ma. Thus, Odin and co-workers estimate an age younger than 5.5 Ma for the Miocene/Pliocene boundary, in good agreement with previous estimates slightly older than 5 Ma.

An interesting stratigraphic situation, very promising for integrated stratigraphic studies, is represented by the sedimentary basin of southeastern Spain, and described by Montenat and Serrano in Chapter E7. In this region, the Tortonian is genuinely marine while the Messinian records the evolution of the basin from open-marine, to evaporitic, and finally to terrestrial environments. Both marine and terrestrial sediments are fossiliferous and contain volcanic rocks such as rhyodacites and lamproites which may be suitable for radioisotopic dating.

Detailed calcareous nannofossil data from several Middle to Upper Miocene sections in the Miura Peninsula of Central Japan are presented by Saito and co-workers in Chapter E9. These sections contain several key tuff beds which yielded reliable mid-Tortonian and Messinian K–Ar ages. The stratigraphy, mineralogy and petrography of these tuffs are described in detail by Saito and co-workers, and constitute a great potential for a numerical calibration of the Late Miocene calcareous nannofossil biostratigraphy in an oceanic setting. This permits to test the consistency of correlation, on the basis of robust geochronologic dates, among stratigraphic sections representing open-ocean environments, and isolated Tethyan environments described in the preceding chapters of this book. Similarly, a great potential for integrated stratigraphic study of the entire Miocene Epoch is found in the fossiliferous, volcanic tuff-bearing sequence of the Boso Peninsula of central Japan. A geologic description and discussion of preliminary biostratigraphic data from this sequence are presented by Takahashi and co-workers in Chapter E9.

This Page Intentionally Left Blank

*Chapter E1*

**INTEGRATED STRATIGRAPHY OF THE MIDDLE TO UPPER MIOCENE  
PELAGIC SEQUENCE OF THE CÒNERO RIVIERA (MARCHE REGION,  
ITALY)**

A. Montanari, B. Beaudoin, L.S. Chan, R. Coccioni, A. Deino, D.J. DePaolo, L. Emmanuel, E. Fornaciari, M. Kruge, S. Lundblad, C. Mozzato, E. Portier, M. Renard, D. Rio, P. Sandroni and A. Stankiewicz

**INTRODUCTION**

In the western Tethyan domain, the Middle to Upper Miocene is usually represented by thick flysch and post-flysch sequences. In the northern Apennines, turbiditic sandstones, conglomerates and molasses derived from the denudation of the emerging Alpine–Apennine orogenic system, and collected in various minor basins with complex topography and facies characteristics (Cantalamesa et al., 1986), interrupt thick sequences of pelagic carbonate rocks which were deposited in a subsiding epeiric basin since the Early Jurassic. The orogenic deformation of this basin started in the westernmost part of the region (i.e., Tuscany) in the Eocene, and proceeded eastward with the formation of NE-verging foreland thrusts. Syndeformational deposition of turbiditic sandstones and marls began in the Umbria–Marche (U–M) region in the Langhian (i.e., Gubbio area), and then ‘migrated’ toward the east in the Marche region filling NW–SE-elongated troughs to form the thick flysch sequence of the Marnoso–Arenacea formation. Thus, syntectonic pelagic and hemipelagic sedimentation occurring in the external (eastern) areas of the thrust belt were successively interrupted by flysch deposits as the basin was being deformed by the advancing orogenic front.

In this geodynamic scenario of the northeastern Apennines, pelagic and hemipelagic carbonate sequences representing the Middle and Late Miocene are found along the Adriatic coast, since this area was the last to be involved in the orogenic deformation. In particular, the cliffs between the city of Ancona and the locality called Il Trave (Monte Cònero Riviera, Fig. 1), which includes the Aquitanian to Langhian Bisciario formation, the Langhian to Tortonian Schlier formation, and the Messinian Euxinic Shale and Gessoso Solifera formations, is the most continuous and complete (see also Fig. 2).

While synorogenic flysch and postflysch sequences preclude the possibility for detailed biostratigraphy, and the application of other stratigraphic approaches for the precise definition of chronostratigraphic time, the pelagic sequence of the Cònero Riviera is a fortunate, perhaps unique situation in the western Tethyan domain because it permits the interdisciplinary stratigraphic and geochronologic calibration of the Miocene time scale, particularly for the continuous interval including the Langhian, Serravallian, Tortonian, and lower Messinian.

In this paper, we expose the results of an integrated stratigraphic analysis covering the Langhian to lower Messinian portion of the Cònero Riviera sequence. This

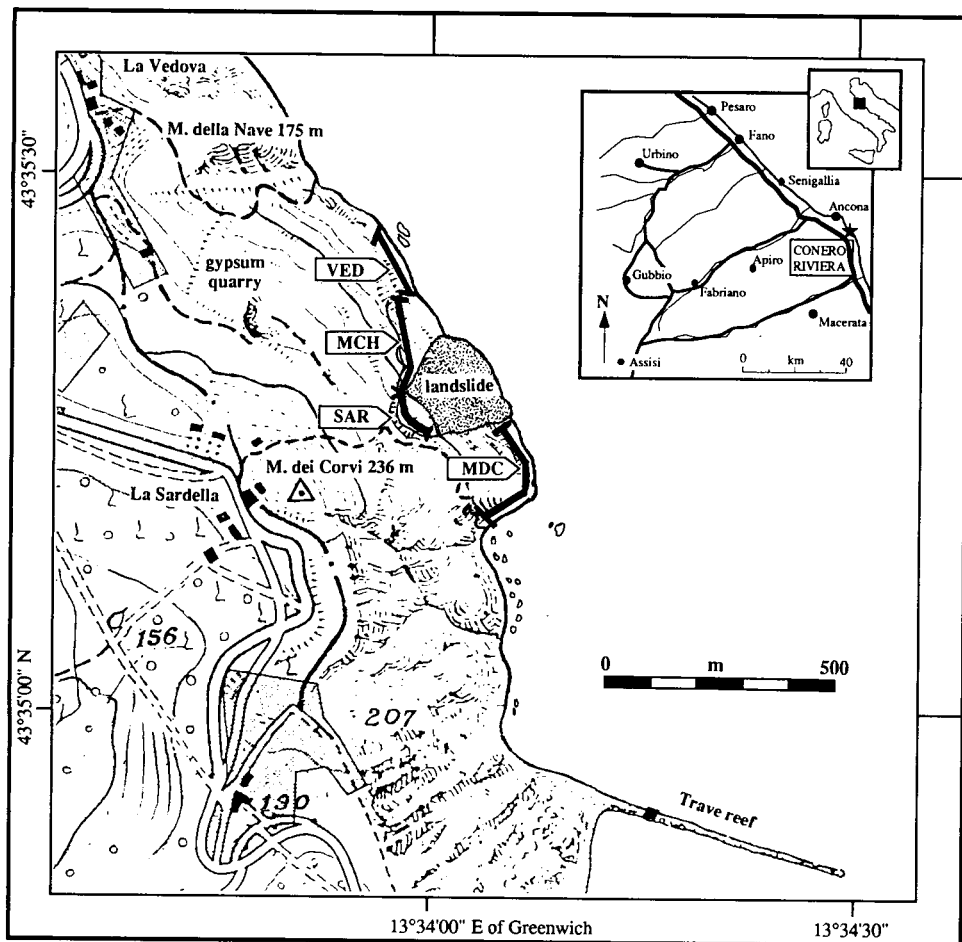


Fig. 1. Location map of the section studied at Monte dei Corvi: VED = La Vedova; MCH = Monte dei Corvi High cliff; MDC = Monte dei Corvi beach; SAR = La Sardella).

includes a biostratigraphic zonation based on planktonic Foraminifera and calcareous nannofossils, a detailed chemostratigraphic analysis based on O, C, and Sr isotopes, and the geochronologic calibration of the sequence based on  $^{40}\text{Ar}$ - $^{39}\text{Ar}$  dates from two distal volcanic ashes found in the lower Serravallian and near the Serravallian/Tortonian boundary. Other biotite-rich volcanoclastic layers are also found in the uppermost part of the sequence, a few metres below the biostratigraphically approximated Tortonian/Messinian boundary. However, at the time this paper was written, these layers were still in the process of being dated at the Berkeley Geochronologic Center. Nevertheless, similar biotite-rich ashes located just below the base of the Messinian in several sections near Faenza (Romagna Apennines, 200 km NE from Ancona), have been dated by Vai et al. (1993) yielding ages around 7.2 Ma.

Several oriented samples from the Serravallian-Tortonian portion of this sequence

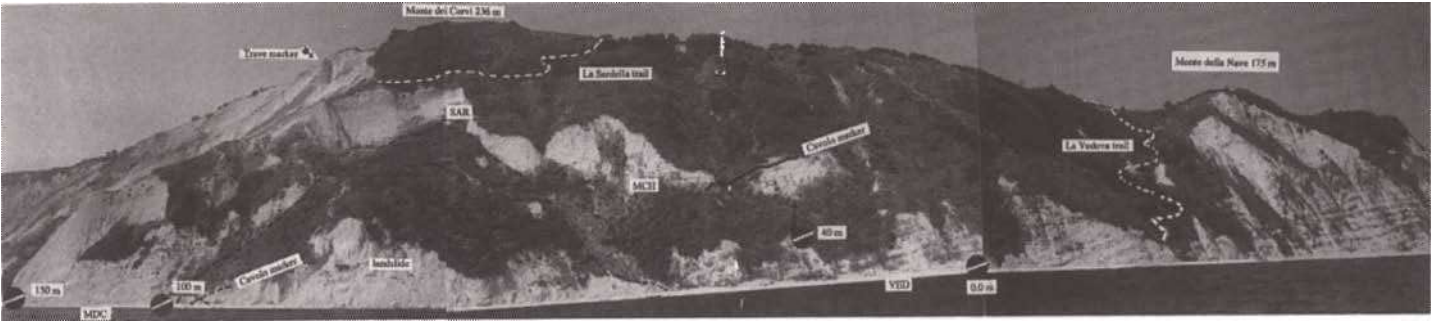


Fig. 2. Panoramic view of the Monte dei Corvi cliffs, and location of the sections studied. Section abbreviations as in Fig. 1.

were analyzed for rock magnetic properties which, however, were found non-conducive to magnetostratigraphic determinations due to the weakness of the magnetic signature and surficial alteration of the outcrop studied.

The principal aim of this work is to calibrate the boundaries between the Langhian, Serravallian, Tortonian, and Messinian stages recognized on the basis of biostratigraphic criteria, by interpolating from radioisotopically dated volcanoclastic layers contained in this pelagic sequence. This leads to the compilation of an integrated stratigraphic model for the Late Miocene time scale which, being derived from an apparently complete and continuous sequence, may serve as a reference for the proposal of integrated stratigraphic definitions of Serravallian/Tortonian, and Tortonian/Messinian boundaries.

## LITHOSTRATIGRAPHY (A. Montanari, P. Sandroni and E. Portier)

### *Section location*

The Middle to Upper Miocene sequence of the Cònero Riviera exposed along the coastal cliffs of Monte dei Corvi, comprises the upper part of the Schlier formation, the Euxinic Shale unit, and the base of the Gessoso Solifera formation. The boundaries between these lithostratigraphic units were never clearly defined in previous works, and their lithologic characteristics are somewhat different from those of the homonym formations exposed elsewhere in the Umbria–Marche Apennines. Due to the synsedimentary orogenic deformation in the western part of the Umbria–Marche basin, the pelagic sedimentation of the Schlier is usually interrupted, in the Langhian, by the arrival of sandy turbidites of the Marnoso Arenacea flysch. Synorogenic detrital sedimentation reaches the Cònero Riviera area only in Pliocene time, and consequently the Schlier is much thicker than anywhere else in the region, and extends stratigraphically up to the lowermost Messinian.

Our attention is here focused on the upper Langhian through the lower Messinian portion of the sequence which is continuously exposed on the eastern slopes and cliffs of the Monte dei Corvi. A general lithostratigraphic scheme of this sequence, and the location of the principal outcrops studied and discussed below, are shown in Figs. 2 and 3. In summary, the sequence of Monte dei Corvi is exposed on three main outcrops: (1) along the beach (MDC section); (2) up high on the cliff, along the scarp of a large landslide (SAR–MCH composite section); and (3) along the seashore bluffs and cliffs stretching from the locality known as 'La Vedova' (VED section), to the port of Ancona towards the north.

The coastal cliff exposures of the Monte dei Corvi area were first measured and studied in detail by Sandroni (1985), and subsequently re-measured and sampled by Montanari et al. (1988b). In the original log by Montanari, the section was called TRA/87 (after the locality Trave (= beam, from the characteristic bio-calcareous marker bed that from the base of the Colombacci formation, stretches out in the sea as a natural reef; Fig. 1) with its base marked as metre level 100.00, and located at the first marly limestones outcropping from the southern edge of a large landslide along the seashore (Figs. 2 and 4). The foraminiferal biostratigraphy was defined by Coccioni in the following years (Coccioni et al., 1992c), after further refinement of the original

### Monte dei Corvi Sequence

#### COMPOSITE VED-MCH-MDC-SAR SECTION

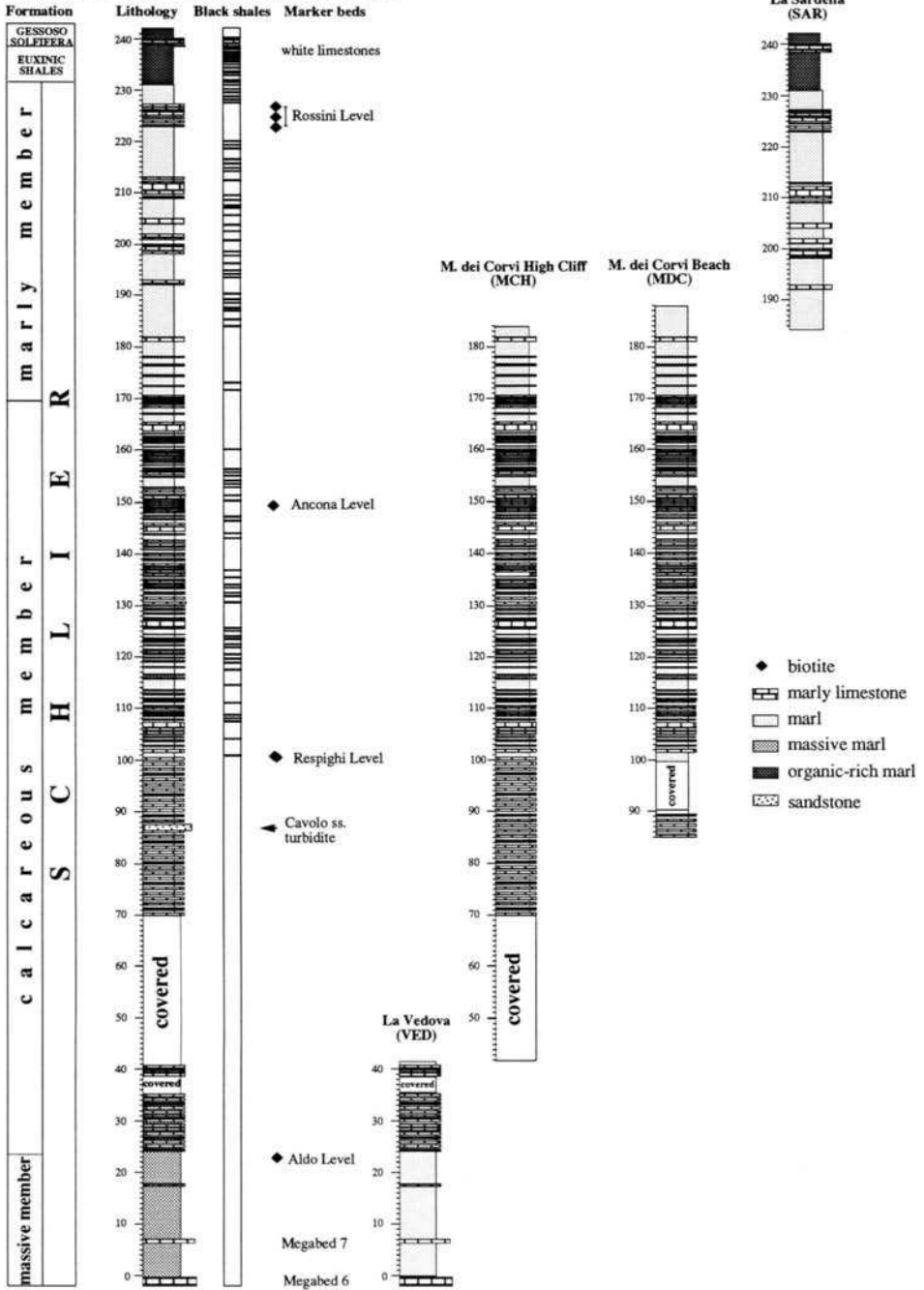


Fig. 3. Lithostratigraphy of the sections studied at Monte dei Corvi.



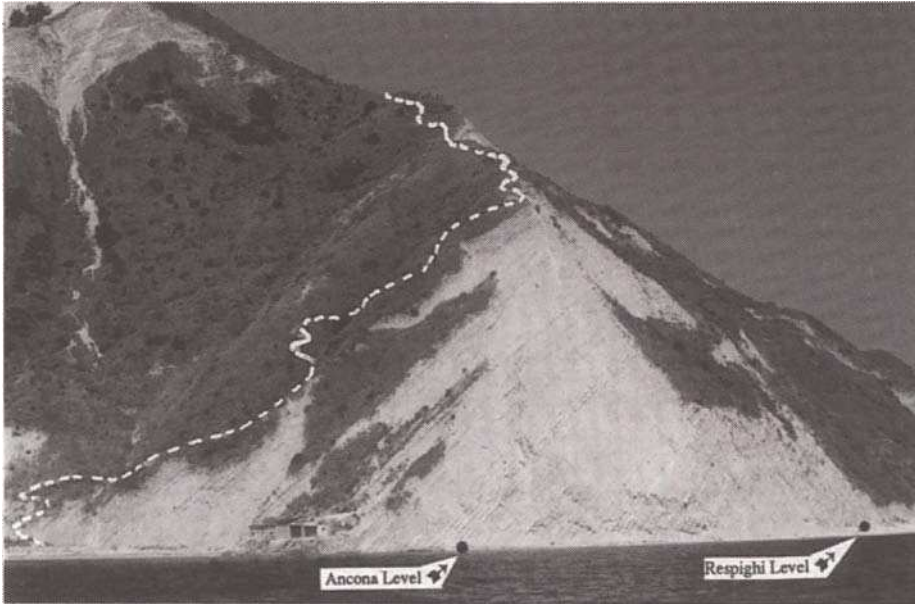


Fig. 4. The MDC section as seen from the sea, with the locations of the Respighi and Ancona biotite-rich volcanoclastic layers.

lithostratigraphic log. The section was re-named MDC from Monte dei Corvi, and its base marked as metre level 100.00 (i.e., MDC-100).

The MDC section is continuously exposed along the seashore for about 90 m, and contains two biotite-rich volcanoclastic markers named Respighi Level (MDC-101.35), and Ancona Level (MDC-149.86; Fig. 4). The latter is located near the Serravallian/Tortonian boundary (Coccioni et al., 1992c, 1994d).

The Sardella section (SAR) is located up high on the Monte dei Corvi cliff, and is exposed on a landslide scarp (Fig. 5). Coccioni et al. (1992) defined a foraminiferal zonation of this section based on a preliminary lithostratigraphic log, recognizing the Tortonian/Serravallian boundary (which is approximated to the *Globorotalia suturae*/*Globorotalia conomiozea* zonal boundary) just above a biotite-rich horizon called the Rossini Level.

As a first step to produce a comprehensive lithostratigraphic log of the Monte dei Corvi sequence, we have examined and measured the landslide scarp exposure, which we called MCH section (Monte dei Corvi High), from the uppermost marls of the La Vedova (VED) section exposed along the beach, hiking up to the La Sardella (SAR) section. In so doing, we have identified on the MCH section some characteristic lithologic markers (i.e., the 'Cavolo' sandstone, the Respighi Level, and the Ancona Level; see Figs. 2 and 3) which allowed a direct correlation with the measured MDC section, thus maintaining a consistent stratimetric criterion.

The Cavolo marker — from the wild cabbage (cavolo) plants growing on the outcrop — is a 10 cm thick calcareous sandstone turbidite discovered by A. Montanari and P.

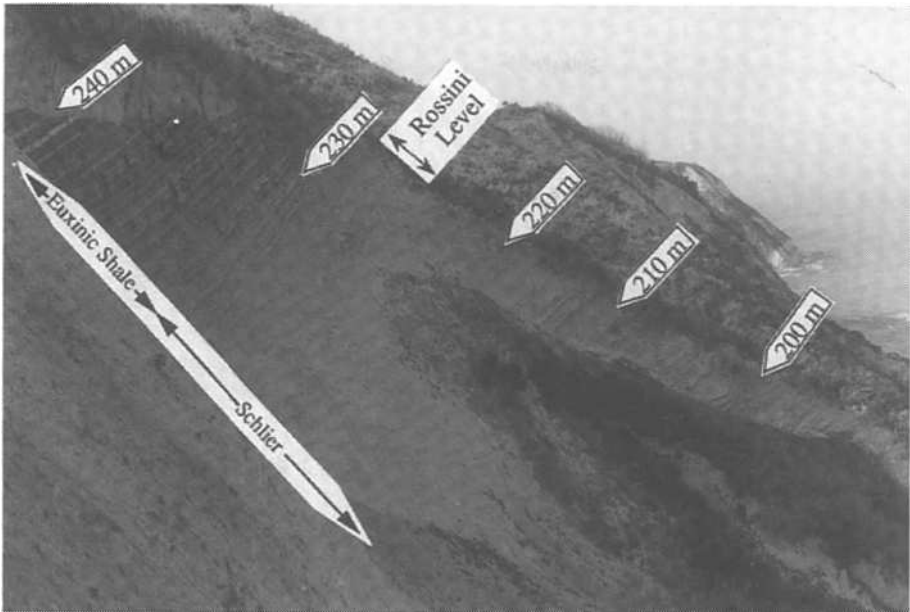


Fig. 5. Panoramic view of the Sardella section.

Sandroni (February 1993, unpublished), on a short stretch of new exposure below metre level MDC-100.00 (Fig. 2). This new exposure was created by a winter storm which removed some material from the foot of the landslide covering the base of the MDC section. It is worth to point out that this thin sandstone turbidite is the only one ever found in the Burdigalian to Messinian, ~400 m thick carbonate sequence exposed along the Cònero Riviera cliff. The Cavolo marker, which is located at metre level 86.85, has flute casts indicating a westerly palaeocurrent flow.

The MCH section on the high cliff is fairly continuous, although in some intervals it is qualitatively inferior to the MDC section exposed along the beach, and difficult to reach. From the Ancona Level, which we marked as MCH-150.00 m, we measured up-section until reaching the base of the original Sardella section at metre level 184. From this point to the top of the exposure, we have marked the Sardella section every metre with 35 cm steel rods driven into the rock, and welded to steel discs with engraved numbers indicating the metre levels. In summary, the MCH-SAR sequence measured along the high cliff landslide scarp is continuously exposed from metre level 70.2 m up to metre level 241.5.

Below the base of the MCH section, the sequence is covered for an interval of about 28.7 m (Fig. 2). Its thickness has been estimated after measuring a transect across the bushy slope from the lowermost layer exposed at MCH-70.15 m to the uppermost marly layer of the VED section exposed on the beach bluff, and corresponding to metre level 41.3 (Fig. 2). Nevertheless, this covered stratigraphic interval is well exposed in other localities on the sea cliffs stretching from the Monte dei Corvi to Ancona.

### Lithology

The overall lithologic evolution of the Monte dei Corvi sequence reflects a clear change in sedimentation mode following the gradual transition from an open-sea environment in the Langhian, to a closed, euxinic basin in the Messinian. The standard member subdivision of the Schlier formation exposed in the Umbria–Marche Apennines (Deino et al., Chapter D1), cannot be applied to the Cònero sequence because here the Schlier stretches up to the base of the Messinian, and this Upper Miocene interval is never represented in the region's hinterland.

The lower portion of the Schlier in the Cònero Riviera, which is exposed on the coastal cliffs between Monte dei Corvi and Ancona, is characterized by a 35 m thick sequence made of 7 composite but apparently massive layers ('megabeds') of hemipelagic marls (Sandroni, 1985), and covers most of the Langhian (Fig. 2). This interval is here referred as the Massive Member, and may correspond to the middle Calcareous–Siliceous Member in the standard Schlier of the Umbria–Marche basin (see Deino et al., Chapter D1).

The Schlier exposed at Monte dei Corvi in the composite VED–MCH–MDC–SAR section, comprises the upper part of the formation, and can be subdivided into two lithologic members: a lower Calcareous Member, and an upper Marly Member (Fig. 3).

The Calcareous Member is characterized by a rhythmic sequence of foraminiferal marly limestones (75% CaCO<sub>3</sub> average, 87% maximum) and marls (50% average, 35% minimum), with average bedding thickness of about 30 cm (Fig. 4). Black shale layers 10–13 cm thick (25–30% CaCO<sub>3</sub>) are found interbedded with the marls and marly limestones in the upper half of the member.

Except for the Cavolo sandstone marker at 86.85 m, the Schlier in the Cònero Riviera sequence is virtually devoid of turbidites, slumping, or any other sedimentological feature indicating a high-energy depositional environment. Light grey calcareous marls, and interbedded darker grey marls are intensely bioturbated. The most common ichnofossils traces are *Planolites* and *Zoophycos*. The finely laminated black shales interbedded with the grey marlstones represent brief, sudden anoxic events. Anoxia was probably caused by eutrophication of the seafloor following massive algal blooms (Kruge et al., 1994), leading to almost complete suppression of benthic activity (Bromley and D'Alessandro, 1992).

The Marly Member of the Schlier is dominated by marlstones with fewer marly limestone intercalations. Black shales are rare in the lower part of this member, more frequent in the upper part. The average sedimentation rate is 16.7 m/Ma, about a factor of two lower than in the underlying Calcareous Member. The uppermost part of the Marly Member is characterized by a 3 m thick, more calcareous interval containing biotite-rich marly layers; this is the so-called Rossini Level, and represents several volcano-sedimentary events which have been reported at approximately the same stratigraphic level in the sequences of Pesaro (northern Marche; Coccioni et al., 1992a), and Faenza (Romagna Apennines; Vai et al., 1993; Vai and Laurenzi et al., Chapter E5).

The Gessoso Solifera formation is extensively exposed in the northeastern Apennines, and is characterized by thick sequences of evaporitic gypsum deposited during the Mediterranean Messinian Salinity Crisis. It is usually preceded by a bituminous, well stratified unit of shales and marls known as Ghioli di Letto, but more properly referred

to as Euxinic Shale (or Euxinic Pelites) by Vai (Chapter E3). This unit represents the initial, euxinic stage of closure of the Mediterranean basin. In the Monte Cònero area, as well as in other localities of the eastern Marche region, Messinian gypsum is found as isolated bodies and lenses contained in stratified sequences of marine shales and marls. In these cases, gypsum is often found as reworked gypsum–arenite. In the Cònero Riviera, these lenses of gypsum are found a few tens of metres above the base of the Messinian but are not exposed in continuity with the underlying Schlier marls; the soft bituminous marls of the Euxinic Shale are usually covered by thick Mediterranean vegetation.

The SAR section can be reached from the Monte dei Covi beach climbing up the landslide, or taking off from the trail that descends from the La Sardella bar-restaurant (near a Navy post along the Cònero Riviera road) down to the sea (Fig. 1). However, the upper part of the section comprising the Tortonian/Messinian boundary and the Euxinic Shale unit, is difficult to reach because it is exposed on a nearly vertical landslide scarp. We have overcome this problem using a rock-climbing nylon rope fastened to a *Genista* tree at the edge of the scarp, and repelling down on the outcrop with a descendeur. In this way, we were able to measure and sample the section in detail, compiling a layer-by-layer lithologic log.

In the SAR section, the upper part of the Marly Member of the Schlier comprises the typical highly fossiliferous grey marls interbedded with fewer, more competent marly limestones. The preservation of these rocks is locally poor due to tectonic fracturing and weathering. Likewise, black shale layers are deeply altered (oxidized), and exhibit light brown or beige colours. Rock preservation improves greatly at around 223 m (Fig. 5).

The first appearance of shiny, euhedral biotite flakes marks the base of the Rossini Level at metre level 224.60. Biotite flakes are present also in the interval between 225.45 m and 227.93 m, and between 226.48 m and 228.18 m.

We have located the base of the Euxinic Shale unit at 231.0 m, corresponding with a prominent 30 cm thick black shale layer. Below this level, black shales never exceed 20 cm in thickness (they are rarely thicker than 15 cm), and above this level, the typical grey marls and marly limestones of the Schlier formation are absent.

The Black Shales unit comprises three main lithologies: (1) very dark green, almost black, finely laminated shales, with a strong hydrocarbon odour when fresh, odourless and brown in colour when altered (~20–25% CaCO<sub>3</sub>); (2) brown or dark-grey clayey marls (~40% CaCO<sub>3</sub>); and (3) light-green marls which turn whitish when weathered (~50% CaCO<sub>3</sub>). Glauconitic pellets and pyrite crystals are common in the green marls, but rare or absent in the organic-C-rich layers. The green marls are usually mottled by bioturbation whereas the organic-C-rich layers exhibit very fine, dense laminations with lamina in the range of 1 mm. The green mottled marls usually have a sharp lower contact, only slightly disturbed by burrows which penetrate the underlying black shales for a short depth. On the other hand, the contacts between the green marls and overlying black shales are usually gradual over an interval of 1 cm.

Planktonic Foraminifera (globigerinids and orbulinids), and benthonic Foraminifera (mainly *Lenticulina*) are generally more abundant in the green marls than in the black shales. The benthonic/planktonic foraminiferal ratio ranges between 0.05 and 0.2 in the green marls, and is usually less than 0.03 in the black shales. Fish shales and teeth are common in the dark, organic-C-rich shales. Some light-green layers, especially in

VED-MDC-MCH-SAR composite section

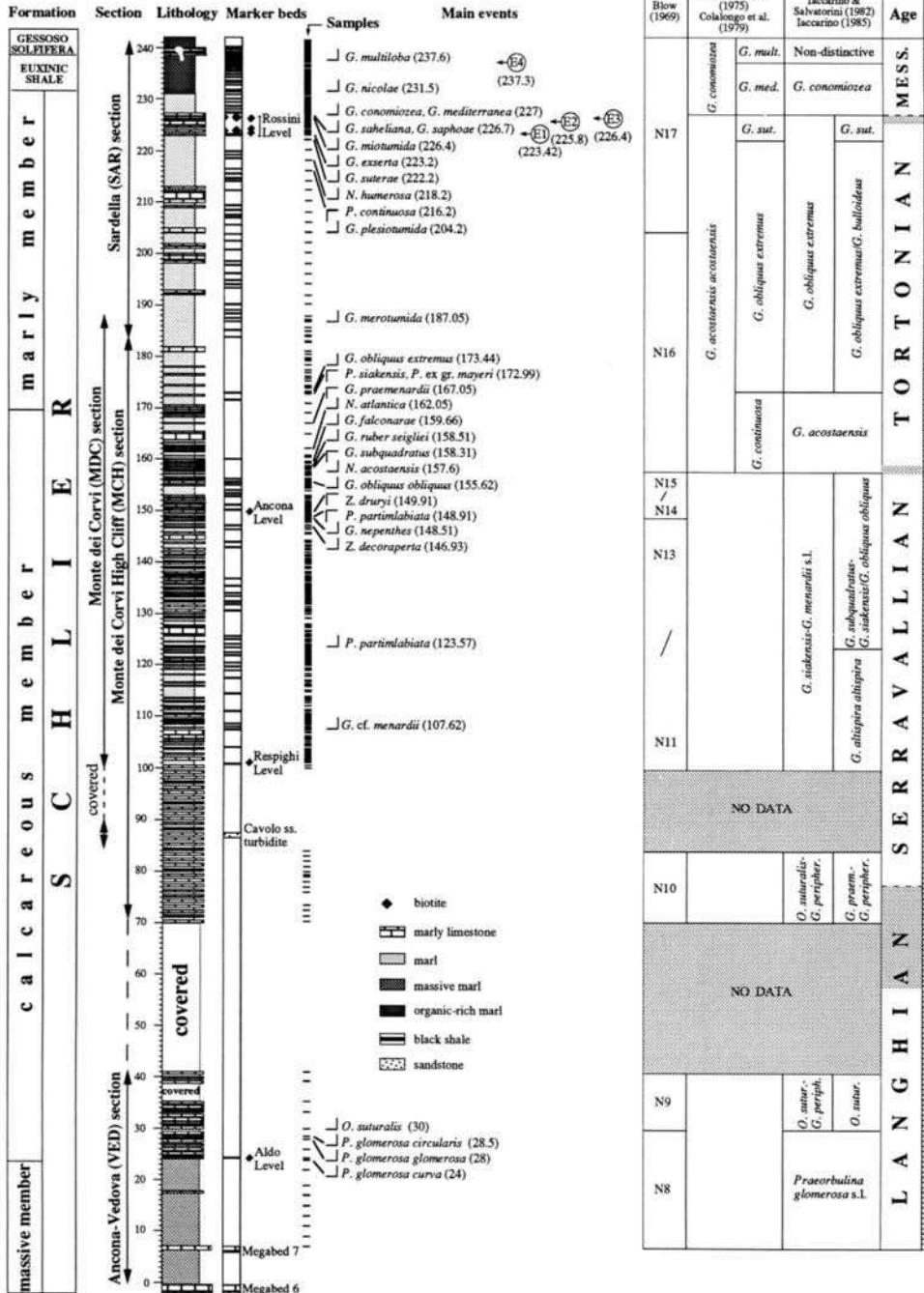


Fig. 6. Main planktonic foraminiferal events and interpreted biostratigraphy of the composite VED-MDC-MCH-SAR sequence.

the upper part of the unit, are characterized by rich, apparently mono- or oligospecific populations of small bivalves, and ostracodes.

The top boundary of the Euxinic Shale has been located at 238.67 m, corresponding with a 10 cm thick, white, granular, finely laminated marly limestone (75% CaCO<sub>3</sub>). Two similar layers are located at 239.27 m and 239.90 m, and are 25 cm and 15 cm thick, respectively (Fig. 5). These peculiar marly limestones may be of evaporitic origin. The thickest of these three marker beds underlies a thin layer of iron-oxide-rich marl. Other iron oxide layers and nodules are found in the uppermost part of the exposed section. Charcoal is found in a black shale in between the lower two white layers, and is associated with abundant bivalve shells.

The SAR section is interrupted at about 241.50 m by soil cover. A few metres above this level, on a ledge at the very top of the landslide scarp, there is a small outcrop of beige, deeply altered marls. Sporadic outcrops of evaporitic gypsum are found here and there on the mountain side above the Sardella trail, and in a couple of abandoned quarries in the vicinity (i.e., at Pietralacroce and at Monte della Nave, near La Vedova along the Riviera road), but the rest of the Messinian sedimentary sequence overlying the section studied is elsewhere covered by thick Mediterranean vegetation.

## BIOSTRATIGRAPHY

### *Planktonic Foraminifera (R. Coccioni)*

A total of 354 samples were studied using washed residues (grain-size fraction >63 µm). Most samples contain very abundant and well diversified assemblages. Preservation varies from sample to sample from good to very poor.

The generic and specific concepts of Bolli and Saunders (1985), Iaccarino (1985), Loeblich and Tappan (1988), and Spezzaferri (1994) were largely adopted. All the events useful for the Lower to Upper Miocene in the Mediterranean zonal models of Iaccarino and Salvatorini (1982) and Iaccarino (1985) were recognized, whereas only some events used by Blow (1969) to define his standard zonal model were identified. The biozonations of D'Onofrio et al. (1975) and Colalongo et al. (1979b) were followed for the latest Miocene where some distinctive events were found. On the whole, several zones and subzones were recognized. A comprehensive biostratigraphic synthesis of the composite VED–MDC–MCH–SAR section based on planktonic Foraminifera is shown in Fig. 6 and discussed below.

*Praeorbulina glomerosa sicana* is already present in the lowest samples of the Vedova (VED) section which therefore can be assigned to the N8 Zone of Blow (1969) and the *Praeorbulina glomerosa* Zone of Iaccarino and Salvatorini (1982) and Iaccarino (1985). *Praeorbulina glomerosa glomerosa* first occurs at 24 m followed by the first occurrences (FOs) of *Praeorbulina glomerosa curva* and *Praeorbulina glomerosa circularis* at 24.1 m and 28.5 m, respectively. All these events occur within the N8 Zone of Blow (1969) and the *P. glomerosa* s.l. Zone of Iaccarino and Salvatorini (1982) and Iaccarino (1985).

The FO of *Orbulina suturalis* is found at 30 m, defining the N8/N9 zonal boundary of Blow (1969) and the boundary between the *P. glomerosa* s.l. and the *O. suturalis*–*Globorotalia peripheroronda* zones of Iaccarino and Salvatorini (1982) and Iaccarino (1985).

The biostratigraphic analysis of the stratigraphic interval between 41.1 m and 70.15 m was impossible because this stretch of the section in the Monte dei Corvi cliff is covered by vegetation (see Fig. 2). Nevertheless, the same interval is continuously exposed in the cliffs near Ancona, and will be sampled in detail in the near future.

The assemblages from the stratigraphic interval between 70.15 m and 84 m (base of the MCH section) contain *Orbulina universa*, *Globorotalia praemenardii*, and *G. peripheroronda* which can be attributed to Zone N10 of Blow and to the *G. praemenardii*–*G. peripheroronda* Subzone of the *O. suturalis*–*G. peripheroronda* Zone of Iaccarino and Salvatorini (1982) and Iaccarino (1985).

Numerous events were recognized in the Monte dei Corvi (MDC) section (see also Coccioni et al., 1992c, 1994). They are listed as follows (from bottom to top): FO of *Globorotalia* cf. *menardii* (107.62 m), FO of *Paragloborotalia partimlabiata* (123.5 m), FO of *Zeaglobigerina decoraperta* (146.73 m), FO of *Globigerina nepenthes* (148.51), last occurrence (LO) of *P. partimlabiata* (148.91 m), LO of *Zeaglobigerina druryi* (149.91 m), FO of *Globigerinoides obliquus obliquus* (155.62 m), FO of *Neogloboquadrina acostaensis* (157.6 m), LO of *Globigerinoides suquadratus* (158.31 m), FO of *Globigerinoides ruber seigliei* (158.51 m), FO of *Globigerina falconarae* (159.66 m), FO of *Neogloboquadrina atlantica* (162.05 m), LO of *G. praemenardii* (167.05), LOs of *Paragloborotalia siakensis* and *P. ex gr. mayeri* (172.99 m), FO of *Globigerinoides obliquus extremus* (173.44 m), and FO of *Globorotalia merotumida* (187.05 m).

The assemblages of the lowest samples of the MDC section can be attributed to the *Globoquadrina altispira altispira* Subzone of the *G. siakensis* Zone of Iaccarino and Salvatorini (1982) and Iaccarino (1985), and most probably to Zone N11 of Blow (1969).

It was not possible to biostratigraphically distinguish the N11/N12 and N12/N13 zonal boundaries of Blow (1969) because of the lack of index species.

The FOs of *P. partimlabiata* and *G. nepenthes*, respectively, define the lower boundary of the *G. suquadratus* Subzone of the *G. siakensis* Zone of Iaccarino and Salvatorini (1982) and Iaccarino (1985) and the N13/N14 zonal boundary of Blow (1969).

Following Rio et al. (Chapter A5), the Serravallian/Tortonian boundary is recognized close to the evolutionary appearance of *N. acostaensis* which also defines the lower boundary of Zone N16 of Blow (1969). Some discrepancies exist with respect to the models of Iaccarino and Salvatorini (1982) and Iaccarino (1985), as *G. subquadratus* and *P. siakensis* whose LOs define the boundaries between the *G. subquadratus* and the *G. siakensis*–*G. obliquus obliquus* subzones, and the *G. siakensis* and the *Globorotalia menardii* s.l. zones, respectively, are still present within the *N. acostaensis* Zone, where only a few isolated specimens are found. The LOs of *G. subquadratus* and *P. siakensis* well above the FO of *N. acostaensis* do not allow the differentiation of the *G. siakensis* and the *G. menardii* s.l. zones, and the *G. subquadratus* and the *G. siakensis*–*G. obliquus obliquus* subzones of Iaccarino and Salvatorini (1982) and Iaccarino (1985). Moreover, the disappearance of *P. siakensis* well above the FO of *N. acostaensis* prevents from defining the lower boundary of Zone N15 of Blow (1969). In agreement with Iaccarino and Salvatorini (1982) and Iaccarino (1985) the LO of *P. mayeri* s.s. has been found just below the FO of *N. acostaensis*, but scattered, small and atypical specimens of this taxon were recognized throughout the *G. acostaensis* Zone and are here included

within the *P. ex gr. mayeri*. The last significant event is the FO of *G. obliquus extremus* which defines the lower boundary of the *G. obliquus extremus* Zone of Iaccarino and Salvatorini (1982) and Iaccarino (1985).

Several biohorizons were identified in the Sardella section (SAR) and are listed as follows (from bottom to top): FO of *Globorotalia plesiotumida* (204.2 m), LO of *Paragloborotalia continuosa* (216.2 m), FO of *Neogloboquadrina humerosa* (218.2 m), FO of *Globorotalia suterae* (222.2), FO of *Globorotalia exserta* (223.2 m), FO of *Globorotalia miotumida* (226.4 m), FO of *Globorotalia saheliana* and *Globorotalia saphoe* (226.7 m), FOs of *Globorotalia conomiozea* and *Globorotalia mediterranea* (227 m), FO of *Globorotalia nicolae* (231.5 m), and FO of *Globigerina multiloba* (237.6 m).

The FO of *G. plesiotumida* defines the lower boundary of Zone 17 of Blow (1969). According to Iaccarino and Salvatorini (1982) and Iaccarino (1985) the FOs of *G. suterae* and *G. conomiozea*, respectively, define the lower boundary of the *G. suterae* Subzone of the *G. obliquus extremus* Zone and the lower boundary of the *G. conomiozea* Zone. Following D'Onofrio et al. (1975) and Colalongo et al. (1979b) the Tortonian/Messinian boundary is placed in correspondence of the FO of *G. conomiozea*. However, this interstage boundary is actually defined, in the historical stratotype, on the basis of lithologic criteria, and the quoted biostratigraphic marker should be considered as an approximation for the recognition of the base of the Messinian (see comments by Odin et al., Chapter F2). The FO of *G. multiloba* is used by D'Onofrio et al. (1975) and Colalongo et al. (1979a, b) to distinguish the *G. multiloba* Subzone.

Following several authors (Sierro, 1985; Sierro et al., 1987, 1993; Glaçon et al., 1990; Flores et al., 1992; among others), additional useful stratigraphic events based on distribution and coiling changes of globorotaliids and neogloboquadrinids were recognized across the Tortonian/Messinian boundary. They are listed as follows (from bottom to top): (a) Event 1 at 223.42 m which is defined by the exit of sinistral keeled globorotaliids (i.e., *G. menardii* group I of Sierro et al., 1993); (b) Event 2 at 225.8 m which is characterized by the entrance of dextral keeled globorotaliids (i.e., *G. menardii* group II of Sierro et al., 1993) after an interval in which keeled globorotaliids are absent; (c) Event 3 at 226.4 m which consists of the replacement of *G. menardii* group II of Sierro et al. (1993) by the left-coiled planoconvex keeled globorotaliids of the *G. miotumida* group; (d) Event 4 at 237.3 m which consists of the change from sinistral to dextral coiling of *N. acostaensis*. The latter event defines the upper boundary of the *G. conomiozea* Zone of Iaccarino and Salvatorini (1982) and Iaccarino (1985).

#### *Calcareous nannofossil (E. Fornaciari, D. Rio and C. Mozzato)*

Calcareous nannofossil biostratigraphic analyses were carried out by polarised-light microscopy on smear slides representing 210 samples from the SAR, MDC, base of the MCH, and VED sections. The calcareous nannofossil are common to abundant but show a moderate to poor preservation state in the MDC section, whereas in the SAR, MCH, and VED sections the preservation is generally better. The taxonomic concepts adopted herein are after Perch-Nielsen (1985), Rio et al. (1990a), and Fornaciari et al. (1990). In all sections studied, the calcareous nannofossil assemblages are dominated by placoliths, in particular *Reticulofenestra* and *Coccolithus*, while *Calcidiscus* is subordinate.



**VED–MCH section.** Thirty samples covering the stratigraphic interval between 7.0 m and 84.0 m throughout the La Vedova section (VED) and the base of the Monte dei Corvi High cliff section (MCH) were studied, and the relative percentages of fifteen calcareous nannofossil species determined following the analytical methods by Backmann and Shackleton (1983), and Rio et al. (1990b). Specifically, we counted the number of the index species of helicoliths, discoasterids, *Coccolithus*, and *Calcidiscus* relative to a fixed number of 50 helicoliths and discoasterids, of 100 *Coccolithus*, and of 30 *Calcidiscus*. Among these, we have chosen five important species which permit a detailed biostratigraphic zonation of this sequence (Fig. 7). These are *Helicosphaera walberdorfensis*, *Sphenolithus heteromorphus*, *Calcidiscus premacintyreii*, *Reticulofenestra pseudoumbilicus*, and *Cyclicargolithus floridanus*. The most relevant event in this sequence is the disappearance of *S. heteromorphus* at metre level 78. This event has been considered by Rio et al. (Chapter A5) as a valid marker for the recognition of the Langhian/Serravallian boundary; however, the LO of *S. heteromorphus* is slightly, yet distinctly younger than the base of the Serravallian historical stratotype (see discussion by Odin et al., Chapter F2).

**MDC section.** Helicoliths and sphenoliths are well represented, while discoasterids are generally rare except in the upper part of the section where they are fairly common. After a preliminary qualitative analysis, the distribution patterns of stratigraphically important forms have been established by quantitative methods following Backmann and Shackleton (1983) and Rio et al. (1990b). The counting of the selected species and the biostratigraphic classification of the section in terms of the standard zonation of Martini (1971), of Okada and Bukry (1980) are shown in Fig. 8.

The bottom of the section is above the LO of *Sphenolithus heteromorphus* (defining the tops of zones NN5 and CN4). The top of the section, containing *Discoaster hamatus*, has been referred to zones NN9–CN7 notwithstanding that this species has not been observed in the topmost sample examined (Fig. 8). *Discoaster kugleri* and *Catinaster coalitus* utilized in standard zonations for subdividing the interval between the LO of *S. heteromorphus* and the FO of *D. hamatus* (zones NN6, NN7, NN9 and CN7 and CN8) are usually missing or atypically developed in the Mediterranean region (Müller, 1978; Theodoridis, 1984) and, indeed, they have not been observed in the MDC section. Hence, with reference to the standard zonations of Martini (1971) and Okada and Bukry (1980), the MDC section remains virtually unresolved (Fig. 8). Recently Fornaciari et al. (1996) in order to overcome problems associated with the application of standard zonations in the Mediterranean region, have proposed a zonal scheme based on Mediterranean biohorizons. All biohorizons utilized in the scheme of Fornaciari et al. (1993) have been recognized in the section (Fig. 8), which indeed has been chosen as a reference section for the proposed scheme.

**SAR section.** A preliminary analysis of the calcareous nannofossil content in 90 samples from the La Sardella section has been carried out using the criteria and methods reported above. Placoliths and helicoliths are the dominant forms, whereas discoasterids are generally scarce and in a poor state of preservation. In numerous samples, particularly in the upper part of the section (i.e., in the bituminous Euxinic Shale unit), rare to common diatoms and silicoflagellates have been observed.

In this preliminary analysis, we have looked for marker species used in Miocene standard zonations for a qualitative biostratigraphic determination of the section. We

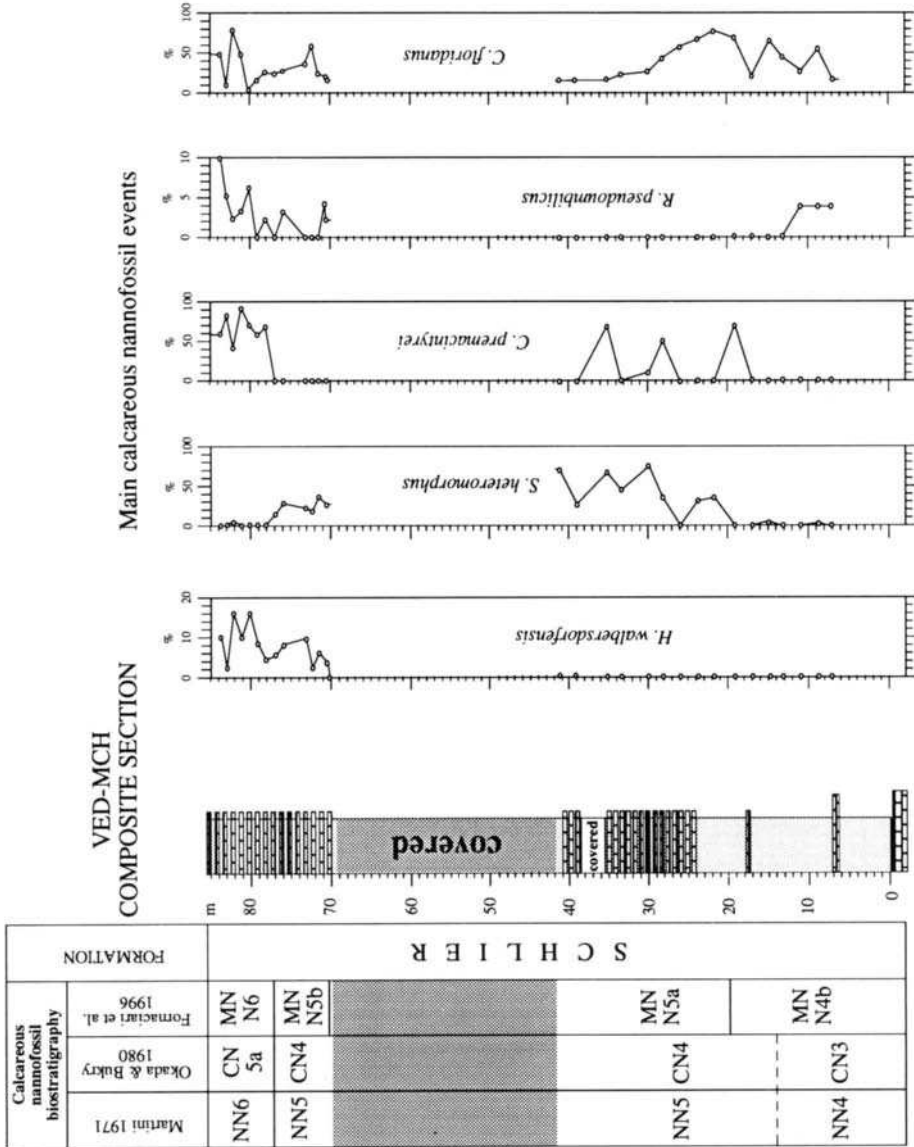


Fig. 7. Main calcareous nannofossil events and interpreted biostratigraphy of the composite VED-MCH sequence.

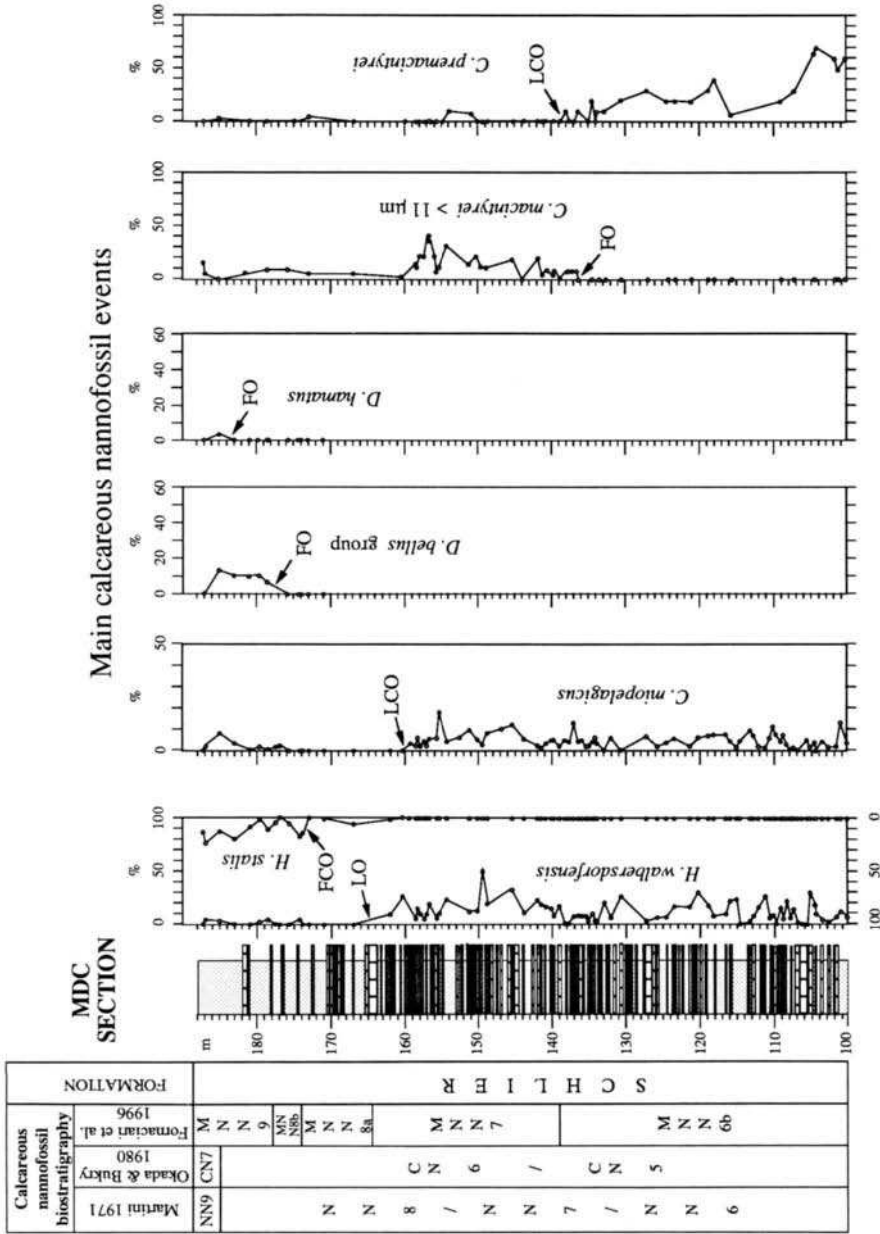


Fig. 8. Main calcareous nannofossil events and biostratigraphy of the MDC section. FO = first occurrence; LCO = last occurrence; FCO = first common occurrence; LCO = last common occurrence.

have not found *D. hamatus*, the LO of which defines the basal boundaries of zones NN10 and CN8, and *D. quinqueramus*, the LO of which defines the basal boundaries of zones NN11/CN9.

The virtual absence of these two biomarkers is not unexpected because they are known to be missing or atypically developed in the Mediterranean domain. The only 'standard' biohorizon we have identified with a certain confidence is the FO of *Amaurolithus* spp., occurring at 225.50 m. This event defines the base of Subzone CN9b of Okada and Bukry (1980), to which the upper part of the section is to be referred. The remaining lower part (i.e., the Marly Member of the Schlier formation), is most probably correlated to Zone CN8 and Subzone CN9a of latest Tortonian age.

#### PALAEOMAGNETISM (L.S. Chan and A. Montanari)

One hundred oriented samples covering most of the MDC section were subjected to palaeomagnetic analysis including measurement of NRM intensity and magnetic susceptibility, AF and thermal demagnetization, hysteresis experiments, anhysteresis remanent magnetism (ARM), and partial ARM analyses. The main purpose of this investigation was to determine the magnetic reversal stratigraphy of the section. As it turned out, the magnetic intensity is too weak to yield useful information on the magnetic polarity. The rock magnetic experiments, however, reveal some interesting information on the sedimentation process that may be crucial to the calibration of the time scale.

NRM intensity of the samples ranges from  $2 \times 10^{-4} \text{ Am}^{-1}$  to  $2 \times 10^{-5} \text{ Am}^{-1}$  with one exception at 117 m which yielded  $10^{-3} \text{ Am}^{-1}$ . Alternating field and thermal demagnetization (conducted by Vicki Langenheim, USGS at Menlo Park, unpublished data) isolated a component with a southwesterly declination at 200°C. In most samples, the NRM intensity at 200°C is already at the same magnitude as the background. The components after the removal of the southwesterly overprints do not form a conspicuous cluster.

The seafloor magnetic polarity record of Cande and Kent (1992) indicates that there are about twelve reversals during the equivalent 3 Ma stratigraphic interval of the MDC section, (i.e., from Chron 5AAn to Chron 5n). While several specimens show negative inclinations above 200°C, no unambiguous magnetic reversal can be determined. The lower hemisphere projection of the NRM from the MDC samples shown in Fig. 9, exhibits an average declination different from any of the known declinations from this part of the northern Apennines. In summary, the observed magnetic results from this study suggest that the MDC section does not carry an accurate record for the magnetic polarity history of this time interval.

Although the NRM results do not yield useful information for magnetostratigraphic determination, the magnetic properties of the samples reveal interesting variations within the section. Both magnetic susceptibility and ARM intensity increase gradually with stratigraphic level (Fig. 10). The darker marly layers generally show a stronger ARM intensity and magnetic susceptibility. The increase in these two magnetic properties may be due to differences in mineralogy, grain size, or abundance of the magnetic carrier. A partial ARM experiment was conducted to examine the nature of this variation. A set of samples was selected at 10 m intervals and the pARM experiment was carried out in 10

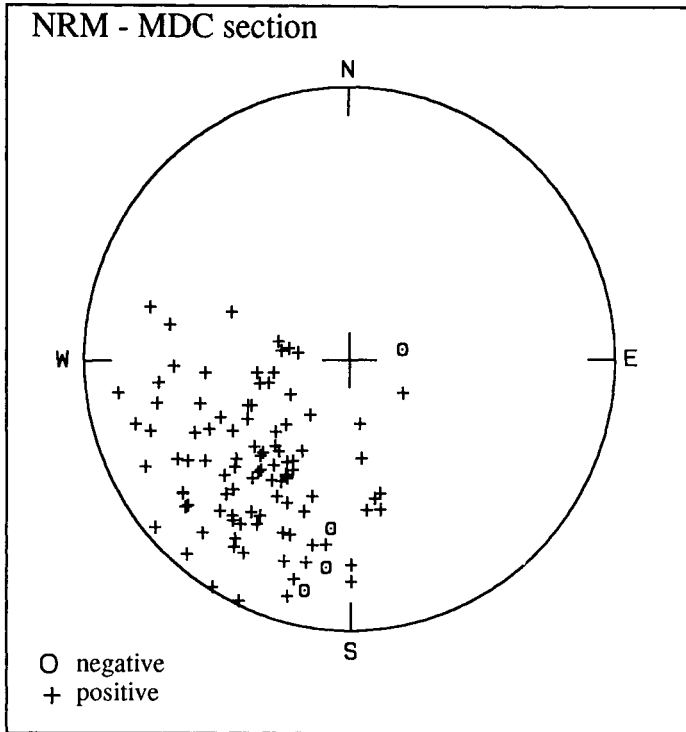


Fig. 9. Lower hemisphere stereonet plot of NRM directions from the MDC section.

mT increments. As shown in Fig. 11, the  $pARM$  curves for the seven samples studied were basically identical. The  $pARM$  results basically rule out differences in magnetic mineralogy or grain size as the cause of the variations. The increase in magnetic susceptibility and ARM therefore is probably due to a simple increase in abundance of the magnetic carrier towards the upper part of the section.

We measured the hysteretic properties of the samples in order to determine the origin of the magnetic minerals. In particular, we were interested to determine whether the magnetic carrier is diagenetic or volcanoclastic in origin. Six specimens were subjected to a peak field of 1 T and the  $H_{cr}/H_c$  and  $J_{rs}/J_s$  ratios were determined. Most of the samples acquired a saturation at about 0.3 T. As shown in Fig. 12, most of the samples show  $H_{cr}/H_c$  ratios below 4 and  $J_{rs}/J_s$  ratios of 0.1 to 0.2. Such ratios are not indicative of a diagenetic source which we would expect to show higher  $H_{cr}/H_c$  ratios.

The increase in magnetic intensity with stratigraphic level can perhaps be explained in terms of changes in the sedimentation rate towards the top of the section. If the magnetic carriers are of volcanogenic or detrital origin and if we assume a constant depositional influx of magnetic grains into the pelagic basin, the variation in the magnetic intensity may be due to an increase by a factor of two in the magnetic concentration. The increase in magnetic concentration could, in turn, be due to a decrease in the rate of carbonate deposition. Such variations in the sedimentation rate within the section could have important implications for the age calibration of the stratigraphic boundaries and

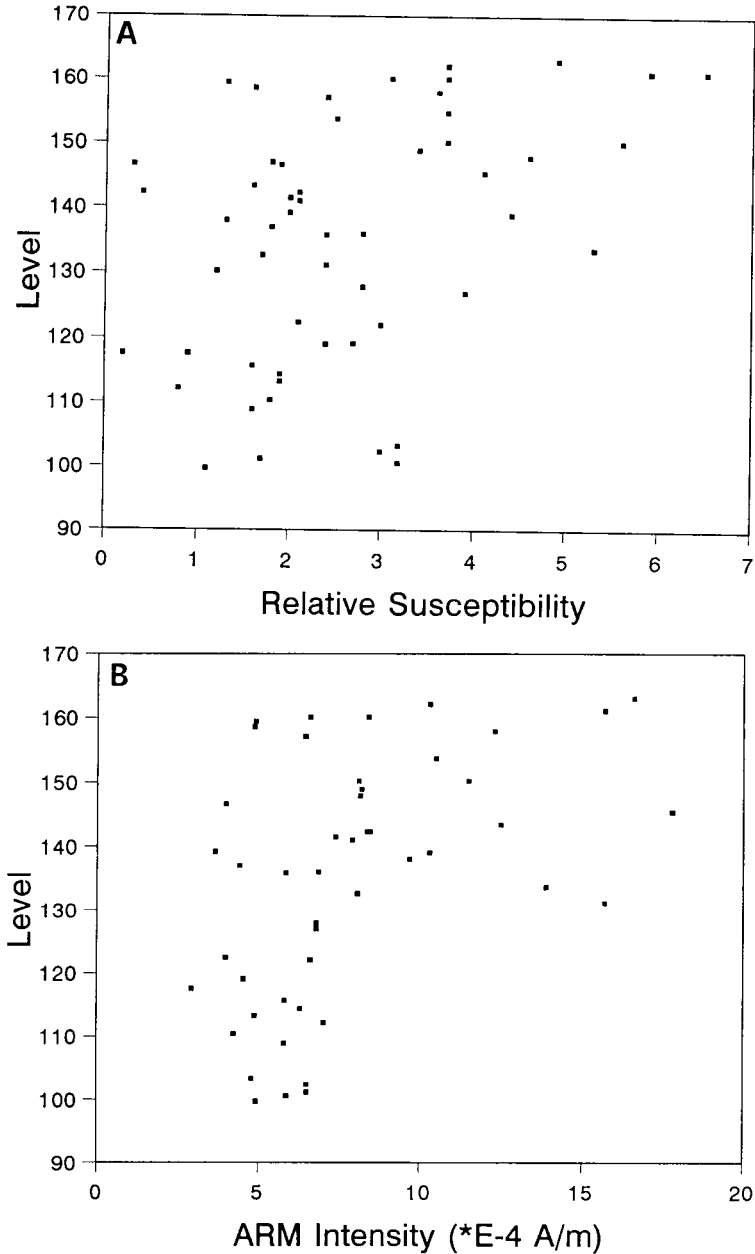


Fig. 10. Variation of relative (A) magnetic susceptibility and (B) anhysteretic remanent magnetization, ARM, with stratigraphic position in metres relative to datum 100 m at the base of the MDC section. Although there is considerable scatter, both parameters tend to increase towards the top of the section.

search for sedimentary cyclicality. Alternatively, the increase in magnetic concentration near the top of the section could be the result of an increase in volcanic activity during

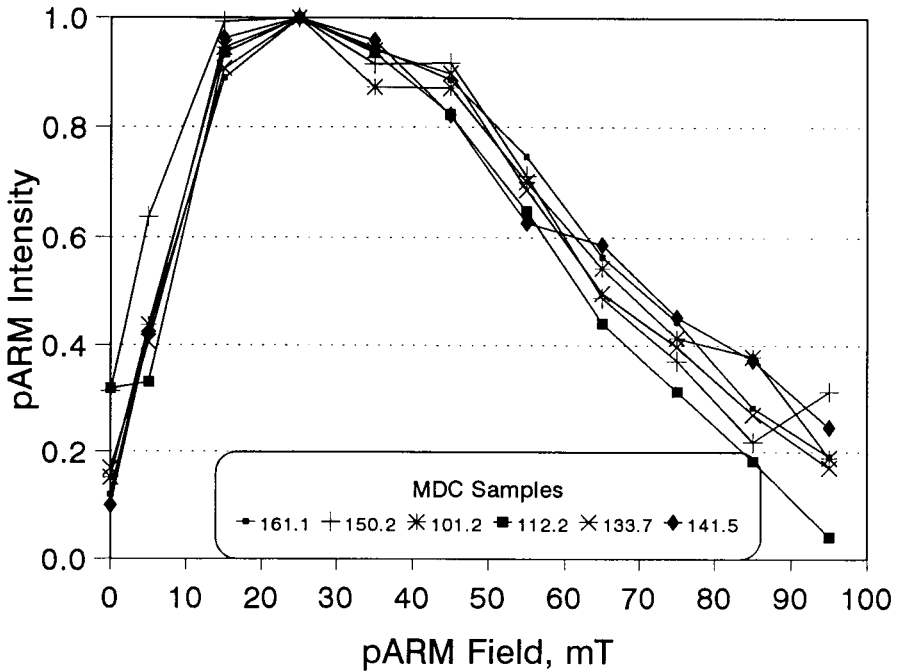


Fig. 11. Partial anhysteretic remanent magnetization (pARM) curves for seven samples from the MDC section. The key indicates the stratigraphic level of each sample. The fact that these curves are nearly identical rules out differences in magnetic mineralogy or grain size as the cause of the variations shown in Fig. 13.

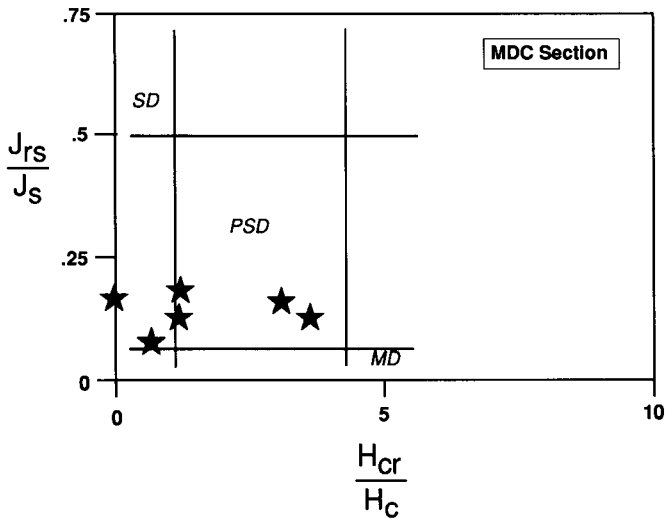


Fig. 12. Hysteresis experiment results from the MDC section, shown relative to the fields for single-domain (SD), pseudo single-domain (PSD) and multi-domain (MD) synthetic magnetites as determined by Day et al. (1976).

this time. This possibility, however, is not supported by an increase in the frequency of identifiable volcanic ashes within the section. Moreover, the overall sedimentation rate of 34.6 m/Ma for the Serravallian portion of the section is, in fact, about a factor of two higher than the rate of 16.7 m/Ma for the overlying Tortonian portion as it can be calculated assuming an age of 7.2 Ma for the Tortonian/Messinian boundary (Vai et al., 1994) which is located at 227 m in the SAR section. We are thus led to favour the hypothesis calling on a decrease in carbonate production toward the top of the section.

## CHEMOSTRATIGRAPHY

### *Trace element and stable isotope chemostratigraphy (L. Emmanuel and M. Renard).*

Analyses on major trace elements in whole carbonate have been carried out in samples from the Serravallian–Tortonian MDC section. Other samples from the Tortonian–Messinian SAR section will be analyzed in our lab in the near future. Trace element contents were measured on acetic acid soluble fraction by atomic absorption spectrophotometry (Instrumentation Laboratory 551 video and Hitachi Z8100 apparatus) according to the method described by Richebois (1990).

Carbon and oxygen isotopic ratios were measured on a VG mass spectrometer and the results are given in ‰ with respect to the PDB1 standard.

The precision of the measurements, as standard deviation of the mean calculated from replicate analyses, is  $\pm 0.02\%$ . Our results are summarized in Fig. 13 and Table 1.

*Strontium.* Despite a marked variability, total Sr concentrations show a clear increasing trend in the Serravallian. Values are ranging from 1200–1300 ppm, at the base of the section, to 1700–1900 ppm just below the Serravallian/Tortonian boundary. A negative shift appears at this stage boundary (1401 ppm at 159.4 m). Then, the values rise again during the early Tortonian reaching a maximum of 1677 ppm at 163.4 m (Fig. 13).

*Magnesium.* It is seemingly difficult to distinguish any trend in the Mg evolution curve in the MDC section. This is essentially due to a very high variability in the element concentrations. Nevertheless, a distinct negative excursion occurs below the Serravallian/Tortonian boundary with Mg values lower than 3000 ppm between 152.3 m and 157.4 m.

*Manganese.* The overall trend in the upper Serravallian is characterized by a decrease in Mn contents from 1324 ppm at 101.2 m, to 280 ppm at 154.9 m. The concentrations slightly increase during the Tortonian (502 ppm at 163.4 m) but this trend reversal is not centred at the Serravallian boundary.

*Iron.* The iron evolution curve shows a trend opposite to that of Mn, with values ranging from 500 to 800 ppm at the base of the MDC section, and reaching 2000 ppm at the top of the section (Fig. 13). A negative excursion contemporaneous with a low-Mg zone occurs below the Serravallian/Tortonian boundary. This positive trend may explain the overall increase in magnetic intensity throughout the MDC section recognized by L.S. Chan and A. Montanari from their detailed rock magnetism analysis (see below).

*Stable isotopes.* In the MDC section, oxygen isotopic ratios are more or less uniform in the upper Serravallian, and exhibit low-amplitude fluctuations ( $+0.79\%$  to  $-0.1\%$ ). A smooth decreasing trend is recognizable in the lower Tortonian but the sparse sampling does not ensure the reliability of this apparent evolution (Fig. 13, Table 1).



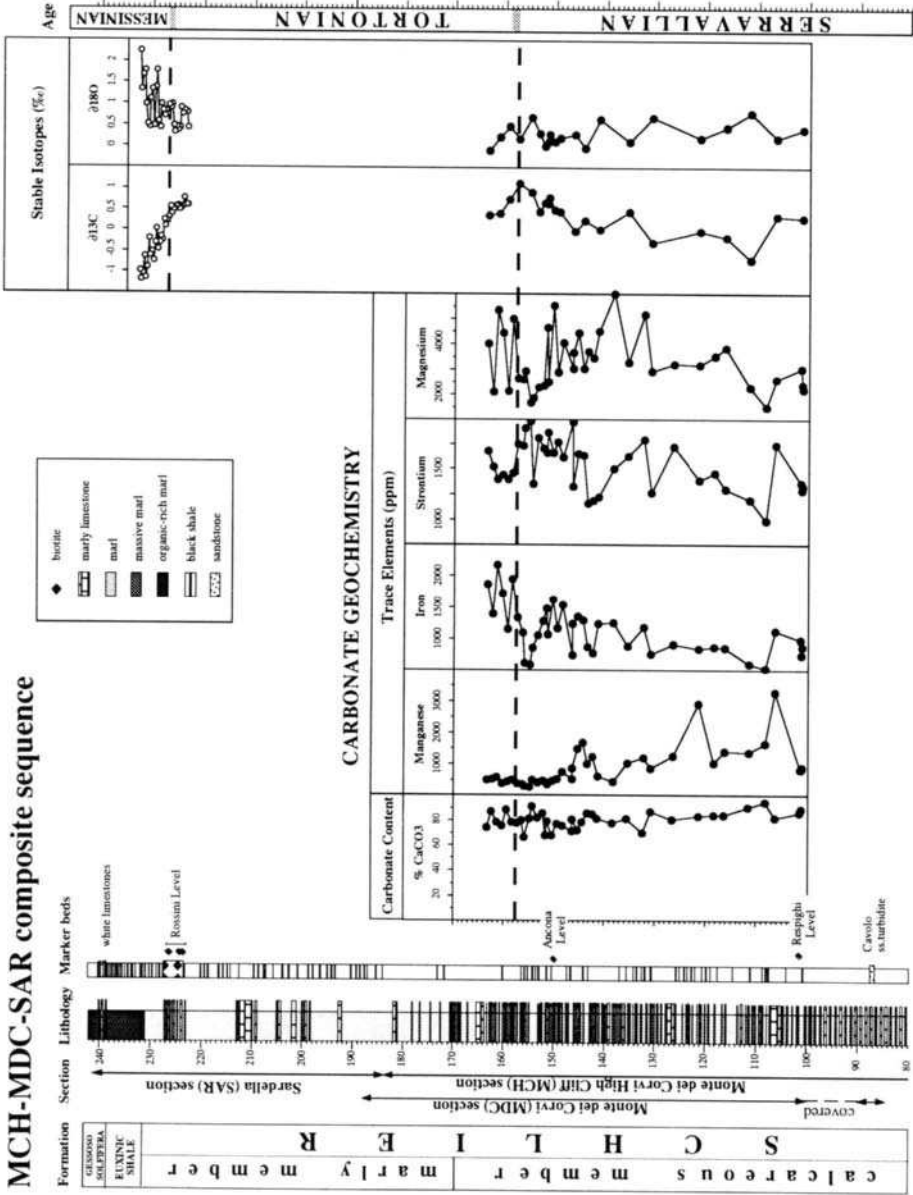


Fig. 13. Stable isotopes and trace element chemostratigraphy of the MDC and SAR sections.

In the Sardella section, the oxygen isotopic ratios remain constant in the upper Tortonian and the Messinian ranging from +0.3 and +0.8‰. From 229 m, there is a sharp overall increase reaching +2.24‰ at 232.7 m. Even if the major shift appears after the stage boundary, the Messinian oxygen isotopic ratios are particularly different from those of the Tortonian.

As for carbon isotope ratios, the lower part of the MDC section is characterized by a sharp decrease from +0.33‰ at 106.4 m to -0.7‰ at 111.6 m. (Fig. 13). Above this interval, the  $\delta^{13}\text{C}$  value strongly increases throughout the Serravallian, up to the Serravallian/Tortonian boundary (+1.12‰ at 157.4 m). This boundary is well marked in the  $\delta^{13}\text{O}$  curve, and corresponds to a trend reversal preceding a renewed oxygen isotopic ratio decrease in the lower Tortonian (-0.1‰ at 163.4 m).

Carbon isotopic ratios through the SAR section are very constant throughout the upper Tortonian with isotopic values around +0.5‰. Above the Tortonian/Messinian boundary, the carbon isotopic ratios progressively decrease down to -1.18‰ at 232.4 m. Both the carbon and oxygen isotopic ratios are very different between the Messinian and the Tortonian portions of the SAR section (Fig. 13).

In summary, although our analytical work is to be considered in a preliminary stage, the geochemical data documented in Fig. 13 and Table 1 indicate that some geochemical break may exist between the Serravallian and the Tortonian (i.e., iron, and  $\delta^{13}\text{C}$ ).

#### *Sr isotope chemostratigraphy (D.J. DePaolo, S. Lundblad and A. Montanari)*

We have analyzed the Sr isotopic composition in samples from the MDC and the SAR sections. Strontium isotopic analyses from whole-rock, isolated foraminiferal tests, and fish teeth from the SAR section were completed on a VG Sector 54 thermal ionization mass spectrometer at the University of North Carolina at Chapel Hill (S. Lundblad). Whole-rock samples were dissolved in approximately 1 M acetic acid and the insoluble (non-carbonate) material removed by centrifuging. The supernatant was dried and re-dissolved in 5 M nitric acid in preparation for column chemistry.

Fish teeth were leached in 1 M acetic acid for 30 min in an ultrasonic bath. They were then rinsed in deionized water and dissolved in 5 M nitric acid in preparation for column chemistry. Strontium was extracted from the samples using a Sr-selective resin. The samples were then loaded on single Ta or W filaments, and the strontium analyzed using the dynamic-multicollector mode with  $^{88}\text{Sr} = 3\text{V}$ . The analytical reproducibility based on analyses of the standard NBS-987 is better than 40 ppm ( $^{87}\text{Sr}/^{86}\text{Sr} \pm 0.000028, 2\sigma$ ). The average of 75 analyses of the NBS-987 standard over the previous six months was 0.0710248.

As for the MDC section, only whole-rock samples were analyzed at the University of California at Berkeley (D.J. DePaolo) using sample preparation and analytical procedure similar to the one described above for the SAR samples (see also Capo and DePaolo, 1988; Montanari et al., 1991, for further analytical and technical details). The analytical results from the analyses of the MDC and SAR samples are shown in Table 2.

The strontium isotopic composition of seawater for the time interval between 20 Ma and 0.1 Ma was determined by Richter and DePaolo (1987, 1988) in bulk pelagic carbonate sediments from DSDP Site 590B (Lord Howe Rise, between Australia, New Zealand, and New Caledonia), and DSDP Site 575 (Equatorial Central Pacific). The time

Table 1

Carbonate and stable isotope geochemistry of the MDC and SAR sections

Sample name	Metre level	%CaCO <sub>3</sub>	Manganese (ppm)	Iron (ppm)	Strontium (ppm)	Magnesium (ppm)	$\delta^{13}\text{C}$	$\delta^{18}\text{O}$
<i>Monte Dei Corvi section</i>								
MDC + 62	163.4	73.88	502	1855	4020	1677	0.36	-0.1
MDC + 61	162.4	87.1	531	1397	2125	1520		
MDC + 60	161.4	78.28	573	2168	5341	1398	0.4	0.22
MDC + 59	160.4	75.45	367	1723	4440	1439		
MDC + 58	159.4	88.35	434	1150	2132	1401	0.73	0.48
MDC + 57	158.4	78.43	480	1946	4999	1459		
MDC + 56	157.4	77.94	377	1332	2650	1750	1.12	0.18
MDC + 55	156.4	79.64	358	1103	2619	1730		
MDC + 54.50	155.9	66.79	299	619	2921	1906		
MDC + 53.50	154.9	81.34	280	588	1680	1981	0.9	0.69
MDC + 53	154.4	91.31	492	856	1855	1356		
MDC + 51.90	153.3	81.81	412	1059	2274	1812	0.44	0.31
MDC + 50.90	152.3	85.8	454	1287	2341	1704	0.66	0.01
MDC + 50MA	151.6	67.86	407	1482	4636	1665	0.64	0.17
MDC + 50	151.4	79.07	355	1065	2506	1866	0.78	0.27
MDC + 49	150.4	68.08	469	1628	5546	1664	0.49	0.1
MDC + 48	149.4	77.2	515	1163	2890	1769	0.44	0.2
MDC + 47	148.4	75.69	740	1542	4048	1619		
MDC + 46	146.4	80.74	858	1233	3678	1328	-0.03	0.29
MDC + 45	146.4	71.21	529	740	3041	1970		
MDC + 44	145.4	72.11	1475	1354	4444	1650		
MDC + 43	144.4	78.21	1690	1298	3042	1636	0.23	-0.04
MDC + 42	143.4	85.35	1010	878	3694	1157		
MDC + 41	142.4	85.09	1238	777	3439	1190		
MDC + 40	141.4	81.54	615	1245	4507	1223	0.03	0.64
MDC + 37	138.4	77.84	442	1258	5986	1503		
MDC + 34.20	135.6	81.15	1034	885	3267	1627	0.44	0.1
MDC + 31	132.4	70.33	1195	1181	5176	1792		
MDC + 29.50	130.9	87.24	866	756	2934	1269	-0.3	0.69
MDC + 25.20	126.6	80.66	1249	920	3211	1727		
MDC + 20	121.4	83.05	2920	842	3165	1388	-0.03	0.2
MDC + 17	118.4	83.81	1031	870	3509	1462		
MDC + 15	116.4	83.78	1382	861	3834	1302	-0.18	0.45
MDC + 10.20	111.6	90.48	1362	600	2295	1192	-0.7	0.79
MDC + 7	108.4	94.91	1658	534	1502	990		
MDC + 5	106.4	81.81	3279	1121	2593	1741	0.33	0.19
MDC respi + 20	101.6	86.24	838	982	3009	1361		
MDC 0	101.4	87.94	831	752	2386	1294	0.29	0.4
MDC respi - 20	101.2	89.13	900	878	2231	1324		
<i>Sardella section</i>								
223.2	223.20	68.00					0.6	0.42
223.45	223.42	44.00					0.6	0.78
223.95	223.95	64.00					0.76	0.82
224.3	224.30	68.00					0.55	0.74
224.6	224.62	74.50					0.5	0.89
224.9	224.90	64.50					0.49	0.43
225.2	225.20	80.00					0.57	0.36
225.5	225.50	67.00					0.54	0.45

Table 1

*Continued.*

Sample name	Metre level	%CaCO <sub>3</sub>	Manganese (ppm)	Iron (ppm)	Strontium (ppm)	Magnesium (ppm)	$\delta^{13}\text{C}$	$\delta^{18}\text{O}$
225.8	225.85	70.50					0.49	0.32
226.1	226.05	77.05					0.46	0.48
226.4	226.40	67.00					0.38	0.98
226.7	226.70	67.00					0.54	0.9
227	227.00	56.50					0.3	0.96
227.3	227.35	45.00					0.22	0.73
227.6	227.60	69.00					0.08	0.82
227.9	227.88	51.00					0.23	0.7
228.2	228.20	40.50					-0.26	0.82
228.5	228.50	36.50					-0.17	0.97
228.8	228.80	62.50					-0.32	0.43
229.1	229.15	33.50					-0.47	0.57
229.4	229.45	42.00					0.03	1.78
229.7	229.70	41.00					-0.32	1.39
230	230.00	31.00					-0.74	0.46
230.3	230.35	52.50					-0.53	1.33
230.6	230.61	66.50					-0.61	1.1
230.9	230.90	32.50					-0.21	0.45
231.15	231.15	72.00					-0.88	0.52
231.5	231.55	68.50					-1.15	0.98
231.7	231.77	49.50					-0.63	1.79
232.05	232.05	38.50					-1.03	1.68
232.4	232.40	21.00					-1.18	1.33
232.7	232.70	43.50					-0.97	2.24

interval from about 15 Ma to 6 Ma, which covers approximately the upper Langhian to lower Messinian, is characterized by a low gradient of  $^{87}\text{Sr}/^{86}\text{Sr}$  variation in oceanic water, from 0.70886 to 0.70904 (i.e.,  $2 \times 10^{-5}/\text{Ma}$ ), which is about a factor of four lower than the monotonic Sr isotopic variation in the preceding time interval between 19 Ma and 15 Ma (Burdigalian; see Fig. 14A).

By comparison, the isotopic compositions of whole-rock samples (marly limestones) from the MDC collection are in general consistent with the oceanic  $^{87}\text{Sr}/^{86}\text{Sr}$  in bulk pelagic carbonate sediments from DSDP Site 590B, although they show a wider scatter of values probably due to diagenetic, and/or outcrop alteration (Fig. 14B). On the other hand, the samples from the SAR section exhibit  $^{87}\text{Sr}/^{86}\text{Sr}$  ratios significantly lower than those obtained from deep-oceanic sediments (Fig. 14B). Except for two whole-rock samples from the lowermost, and most weathered part of the section, the Sr isotopic ratios from such different materials like fish teeth, planktonic and benthonic foraminiferal tests, and whole-rock samples from stratigraphically adjacent layers, show little scatter, and are consistent within the limits of analytical uncertainty. This suggests that the deviation of the  $^{87}\text{Sr}/^{86}\text{Sr}$  of these samples from oceanic values cannot solely be attributed to diagenetic alteration or outcrop weathering. A possible explanation is that in the Late Miocene, the Mediterranean basin was isolated, or partially so, from the rest of the world's oceans, and a relatively high influx of  $^{86}\text{Sr}$  recycled from Jurassic

Table 2

Sr isotope analyses of samples from the MDC and SAR sections

Sample name	Metre level	Material	Sr <sup>87</sup> /Sr <sup>86</sup> *	±2σ
<i>Monte Dei Corvi section</i>				
TRA 100.6	100.60	Whole carbonate	0.708879	0.000015
TRA 103.3	103.30	Whole carbonate	0.708879	0.000009
MDC 0.50	105.00	Whole carbonate	0.708863	0.000012
MDC 12.37	112.37	Whole carbonate	0.708875	0.000005
TRA 113.26	113.26	Whole carbonate	0.708870	0.000014
MDC 13.65	113.65	Whole carbonate	0.708766	0.000012
TRA 119.1(2)	119.10	Whole carbonate	0.708911	0.000007
MDC 22.15	122.15	Whole carbonate	0.708897	0.000005
TRA 127.9	127.90	Whole carbonate	0.708927	0.000033
TRA 131.1	131.10	Whole carbonate	0.708925	0.000007
TRA 137.95	137.95	Whole carbonate	0.708905	0.000028
TRA 146.6	146.60	Whole carbonate	0.708914	0.000013
MDC 49.51	149.51	Whole carbonate	0.708910	0.000005
TRA 153.65	153.65	Whole carbonate	0.708919	0.000007
MDC 55.57	155.57	Whole carbonate	0.708901	0.000005
MDC 90-57 F	157.00	Bivalve shell	0.708859	0.000007
MDC 90-57 M	157.00	Whole carbonate	0.708877	0.000010
TRA 157.05	157.05	Whole carbonate	0.708951	0.000013
TRA 160.1	160.10	Whole carbonate	0.708924	0.000016
MDC 62.00	162.00	Whole carbonate	0.708894	0.000009
TRA 165.3	163.30	Whole carbonate	0.708890	0.000007
TRA 169.0	169.00	Whole carbonate	0.708920	0.000016
MDC 74.00	174.00	Whole carbonate	0.708927	0.000013
MDC 87.15	187.15	Whole carbonate	0.708934	0.000005
MDC 88.99	188.99	Whole carbonate	0.708913	0.000005
<i>Sardella section</i>				
SAR 9.50	184.20	Whole carbonate	0.708820	0.000025
SAR 9.44	185.20	Fish teeth	0.708889	0.000025
SAR 8.94	194.20	Whole carbonate	0.708816	0.000025
SAR 8.82	196.40	Fish teeth	0.708896	0.000025
SAR 8.68	198.80	Fish teeth	0.708875	0.000025
SAR 8.61	200.20	Whole carbonate	0.708864	0.000025
SAR 8.16	208.20	Whole carbonate	0.708860	0.000025
SAR 7.82	214.20	Whole carbonate	0.708838	0.000025
SAR 7.81	214.30	Fish teeth	0.708874	0.000025
SAR 7.53	219.30	Fish teeth	0.708857	0.000025
SAR 7.48	220.20	Whole carbonate	0.708827	0.000025
SAR 7.48	220.30	Fish teeth	0.708841	0.000025
SAR 6.99	228.80	Whole carbonate	0.708854	0.000025
SAR 6.93	230.00	Planktic forams	0.708915	0.000025
SAR 6.82	232.05	Planktic forams	0.708908	0.000025
SAR 6.54	237.00	Benthic forams	0.708950	0.000025
SAR 6.49	237.90	Benthic forams	0.708965	0.000025
SAR 6.49	237.90	Fish teeth	0.708891	0.000025
SAR 6.47	238.20	Fish teeth	0.708941	0.000025

\*Corrected for seawater  $^{87}\text{Sr}/^{86}\text{Sr} = 0.709250$ .

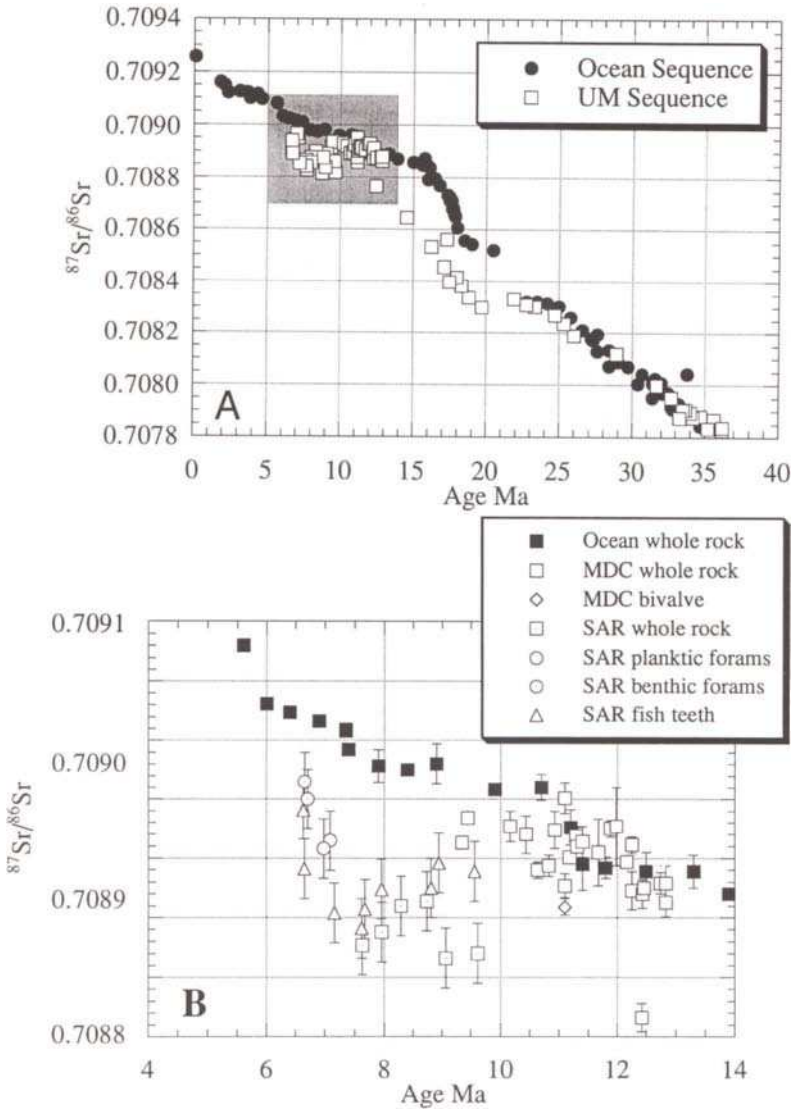


Fig. 14. (A) Upper Eocene to Miocene  $^{87}\text{Sr}/^{86}\text{Sr}$  curve of the Umbria–Marche (*U–M*) sequence compared with that of oceanic sequences. Shaded area represents the MCD and SAR sections at Monte dei Corvi. (B) Detailed Sr isotope chemostratigraphy of the MDC and SAR sections.

and Cretaceous limestones in the uplifting Alps, Apennines, and Dinarides would have lowered the  $^{87}\text{Sr}/^{86}\text{Sr}$  ratio in seawater. The  $^{87}\text{Sr}/^{86}\text{Sr}$  trend in the SAR section shows a clear positive shift near the Tortonian/Messinian boundary (i.e., at 230 m, 7.0 Ma in Fig. 14B). This level coincides with the base of the Euxinic Shale unit which was deposited at the bottom of a stagnant, euxinic marine basin already affected by strong evaporation and increasing salinity.

In summary, it appears that Sr isotopic signatures in biogenic calcite and phosphate in the MDC and SAR sections reflect local conditions of a palaeobasin somewhat isolated from the world oceans. Therefore, the  $^{87}\text{Sr}/^{86}\text{Sr}$  cannot be used as a geochemical marker for correlating this, and perhaps other Mediterranean stratigraphic sequences, with coeval open-ocean sediments in the world. However, further analytical work in other upper Tortonian and lower Messinian sections in the Mediterranean area is necessary to test whether the  $^{87}\text{Sr}/^{86}\text{Sr}$  trend revealed in the Cònero Riviera sequence is, in fact, a common feature at a regional scale reflecting the particular palaeogeographic and tectonic conditions of the synorogenic western Tethyan domain. This trend is characterized by an inflection of the  $^{87}\text{Sr}/^{86}\text{Sr}$  ratio in the terminal Tortonian, followed by a rapid increase at the base of the Messinian.

*Organic geochemistry (M. Kruge, A. Stankiewicz and A. Montanari)*

Both the Serravallian and Messinian intervals of the Cònero Riviera sequence are punctuated by the occurrence of thin, dark shales of variable organic richness. The kerogen or solid organic matter of representative samples from both intervals was examined by reflected-light microscopy and by analytical pyrolysis-gas chromatography/mass spectrometry (py-GC/MS), after removal of bitumen (mobile organic phase) by  $\text{CH}_2\text{Cl}_2$  extraction. The methods employed have been described previously (Krugé et al., 1994).

According to the petrographic data, the dominant organic matter types in the Serravallian are of marine origin, including several types of fossil algae and amorphous material. The latter is largely the product of bacterial reworking of primary organic matter (Tissot and Welte, 1984). The py-GC/MS data concur (Fig. 15), indicating that the samples contain Type II organic matter, i.e., they show a predominance of monoaromatic (benzene series) compounds, with secondary amounts of normal hydrocarbons (Krugé et al., 1994). Alkylthiophenes and alkylpyrroles, which are sulphur- and nitrogen-containing compounds, respectively, are also of secondary importance. Such occurrences of the thiophene series are characteristic of organic matter deposited in waters of normal-marine salinity and are among the key diagnostic features for Type II organic matter (Eglinton et al., 1992; Stankiewicz et al., 1993). A likely pathway for the incorporation of sulphur into organic matter is from dissolved sulfate via bacterial interaction during early diagenesis (Demaison and Moore, 1980). The occurrence of the pyrrole series as important compounds in a pyrolyzate is more unusual. These compounds may possibly derive from degradation of chlorophyll (Sinninghe Damsté et al., 1992) or from the by-products of bacterial or fungal activity. The prominence of prist-1-ene indicates that the samples have not experienced much thermal alteration during burial and are thermally immature with respect to petroleum generation (Larter, 1984). Overall, the Serravallian pyrolyzates are qualitatively very similar to one another, although they vary significantly in the amounts of organic matter that they contain (Krugé et al., 1994).

Petrographically, the kerogen of the Messinian shales resembles the Serravallian, in that it contains a mixture of alginite and amorphinite. The py-GC/MS analyses also indicate that they are broadly similar to the Serravallian kerogens, having a high concentrations of monoaromatic compounds and secondary amounts of normal hydrocarbons. However, the Messinian pyrolyzates are significantly enriched in sulphur compounds,

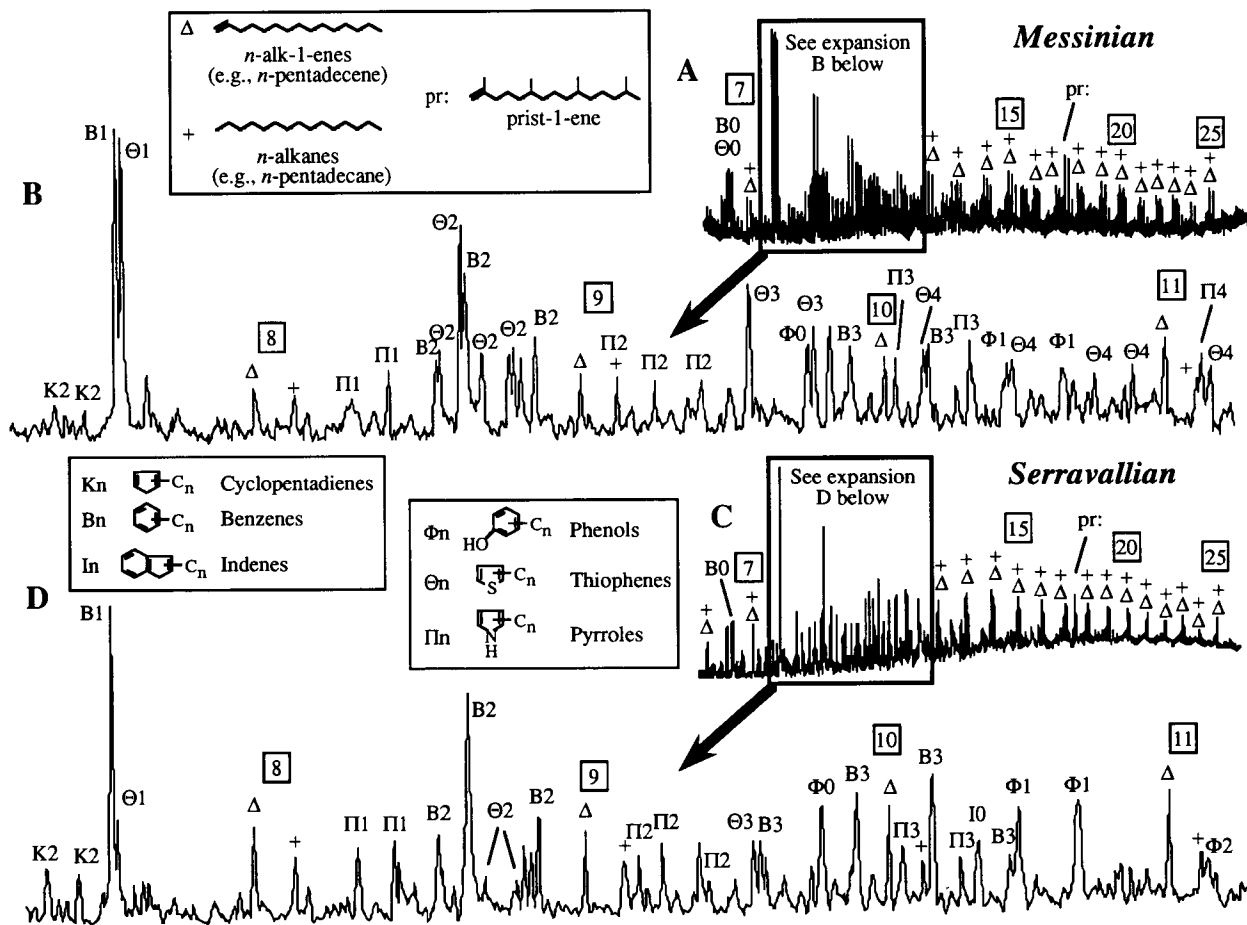


Fig. 15. Organic chemistry characterization of black shales from the MDC section (A, B), and the SAR section (C, D).



as the intensities of thiophene peaks rival or surpass those of the monoaromatic (Fig. 15). This indicates kerogen formation in a highly saline depositional and diagenetic environment, consistent with the mineralogical and sedimentological evidence. While there are variations in kerogen concentration, the Messinian shales all contain the same type of sulphur-rich organic matter, which can be classified as Type II-S (Sinninghe Damsté et al., 1989).

Aside from the typical dark shales, a single lensoid organic-rich body was noticed in the Messinian sequence. Its form and position in the outcrop suggested that it was fossil wood, possibly driftwood. Petrographic examination indicated that it was indeed different from the shale kerogen, being composed of degraded vitrinite and sclerotinite (fossil wood and fungal remains, respectively), consistent with an origin of rotting driftwood. Its pyrolyzate is dominated by phenols and methoxyphenols, which have been shown to be lignin derivatives (Hatcher, 1990), further supporting a land plant origin. Interestingly, the thiophene series is also dominant in this pyrolysis, most readily explained as a diagenetic overprint, due to the deposition of the wood in the highly saline environment.

#### GEOCHRONOLOGY (A. Deino and A. Montanari)

Biotite flakes contained in the Respighi and Ancona levels (at 101.35 m and 149.85 m, respectively), exhibit a fresh, shiny appearance and are often euhedral in shape. While the 1 cm Respighi Level can be considered as a true bentonite, mostly made of dark smectitic clay derived from alteration in situ of vitric volcanic ash, the Ancona Level is a strongly bioturbated clay-rich marl containing sparse biotite flakes. Plagioclase and sanidine grains in these layers are scarce and very small, thus not suitable for radioisotopic dating.

Two kilograms of bulk-rock samples from each of these two biotite-bearing layers, were washed with tap water using a 63  $\mu\text{m}$  polyester cloth, and dried under a heat lamp at a temperature less than 80°C. The indurated marl of the Ancona Level needed to be crushed before washing, whereas the Respighi bentonite broke apart after immersion in plain water. No acids were used in the preparation of these samples. Biotite was then separated from the washed residues using a Frantz isodynamic separator, and cleaned extensively in distilled water in an ultrasonic bath to remove adhered materials. Finally, the biotite samples were concentrated using Li-metatungstate at a density of 3.06 g/cm<sup>3</sup> to obtain the heavier fraction, which experience has shown us contains the most unaltered material.

The X-ray diffractograms shown in Fig. 16 exhibit only biotite peaks indicating that these separates are mineralogically pure and free of vermiculite, the diagenetic clay mineral often found in altered volcanic biotites contained in the Umbria–Marche Tertiary sequence (Odin et al., 1991).

Electron microprobe analyses on six individual biotite flakes from the Respighi Level, along transects of three or more points per flake, reveal a fairly homogeneous chemical composition of this separate, and an average K<sub>2</sub>O of 8.2% (Table 3). Similarly, we have analyzed nine individual biotite flakes from the Ancona Level (Table 3) which also show a fairly homogeneous composition, with an average K<sub>2</sub>O content of 8.4%. While the Respighi biotite, with a relatively low MgO/FeO ratio of 0.19, is compositionally

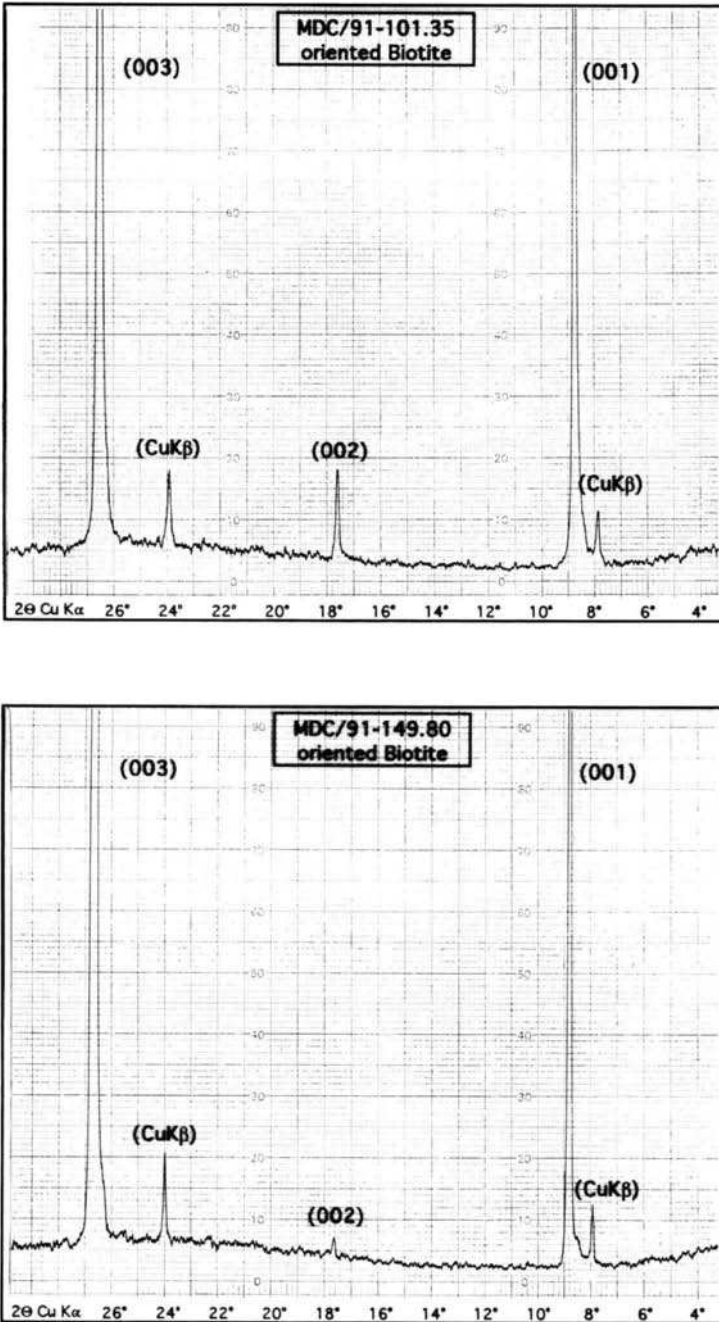


Fig. 16. XRD diffractograms of oriented biotite from the Respighi (A), and Ancona (B) volcanoclastic layers.

Table 3

Chemical compositions in wt% of biotite from the Respighi and Ancona volcanoclastic layers

Analysis	SiO <sub>2</sub>	TiO <sub>2</sub>	Al <sub>2</sub> O <sub>3</sub>	FeO*	MgO	CaO	Na <sub>2</sub> O	K <sub>2</sub> O	Total
<i>Respighi Level</i>									
(1) 3 points analyzed	32.70	3.38	12.78	27.33	5.22	0.24	0.36	7.72	89.76
(2) 5 points analyzed	33.48	3.15	13.26	27.48	5.22	0.15	0.36	8.33	91.79
(3) 4 points analyzed	33.45	4.38	13.06	27.57	5.08	0.13	0.41	8.51	92.60
(4) 4 points analyzed	34.42	3.66	13.42	27.90	5.37	0.12	0.39	8.69	93.98
(5) 4 points analyzed	32.88	3.31	12.88	27.23	5.31	0.05	0.46	8.10	90.50
(6) 3 points analyzed	32.48	3.30	12.82	26.73	5.27	0.12	0.36	8.11	89.18
Average	33.24	3.53	13.04	27.54	5.25	0.14	0.39	8.24	91.30
<i>Ancona Level</i>									
(1) 4 points analyzed	35.11	5.67	13.56	14.13	14.58	0.02	0.67	8.39	92.09
(2) 4 points analyzed	34.96	5.61	13.67	14.39	14.26	0.01	0.67	8.41	37.97
(3) 10 points analyzed	35.11	5.68	13.62	14.34	14.51	0.01	0.65	8.52	92.45
(4) 5 points analyzed	35.14	5.48	13.13	13.96	14.56	0.01	0.64	8.46	91.36
(5) 4 points analyzed	34.95	4.54	14.82	12.28	15.70	0.03	0.79	8.26	91.37
(6) 4 points analyzed	35.39	5.68	13.81	14.78	14.30	0.01	0.71	8.53	93.18
(7) 4 points analyzed	34.72	5.44	13.26	14.39	14.40	0.01	0.65	8.59	92.09
(8) 4 points analyzed	35.96	5.61	13.67	14.39	14.26	0.01	0.67	8.41	91.97
(9) 4 points analyzed	34.91	5.49	13.46	14.18	14.02	0.00	0.67	8.27	91.01
Average	35.14	5.47	13.67	14.09	14.51	0.01	0.68	8.43	91.94

\*Total iron as FeO.

similar to the biotites found in the underlying Bisciario formation (Deino et al., Chapter D1; Assorgia et al., 1994), the Ancona biotite, with a mean MgO/FeO ratio of 1.03, is more similar to the biotites found in the Upper Eocene–Oligocene Scaglia Cinerea formation (Montanari, 1988). This suggests that the chemistry of the volcanic source for the Respighi Level, which was probably the western Sardinian volcanic province (Montanari et al., 1994; Assorgia et al. 1994), or the source itself, was not the same as for the Ancona Level. Nevertheless, because of their compositional purity and homogeneity, the Respighi and Ancona biotites can be considered a priori as reliable geochronometers.

Biotite separates obtained from the Respighi and Ancona volcanoclastic layers were analyzed by the incremental-heating <sup>40</sup>Ar/<sup>39</sup>Ar dating technique, using a defocused Ar-ion laser beam as the heat source. All samples reported here were irradiated at the same time in the same aluminum sample irradiation disk (for more details of the analytical procedure, see the discussions in Deino and Potts, 1990; Deino et al., Chapter D1). The samples were irradiated for 14.2 h in the central thimble of the Omega West reactor without Cd shielding. Sanidine from the Fish Canyon Tuff was used as the neutron fluency monitor, with a reference age of 27.84 Ma (Cebula, 1986) recalculated based on Samson and Alexander, 1987). X Two aliquots each of two different grain sizes separates of the same sample from the Respighi Level were analyzed by this technique (laboratory numbers prefixed with 5804 were from the > 180 μm fraction while samples prefixed with 5809 were from the 150–180 μm range). Analytical results for these experiments are given in Table 3, and plotted as step-heating spectra in Fig. 17. All four spectra reveal similar behaviour in the evolution of the percentage of radiogenic

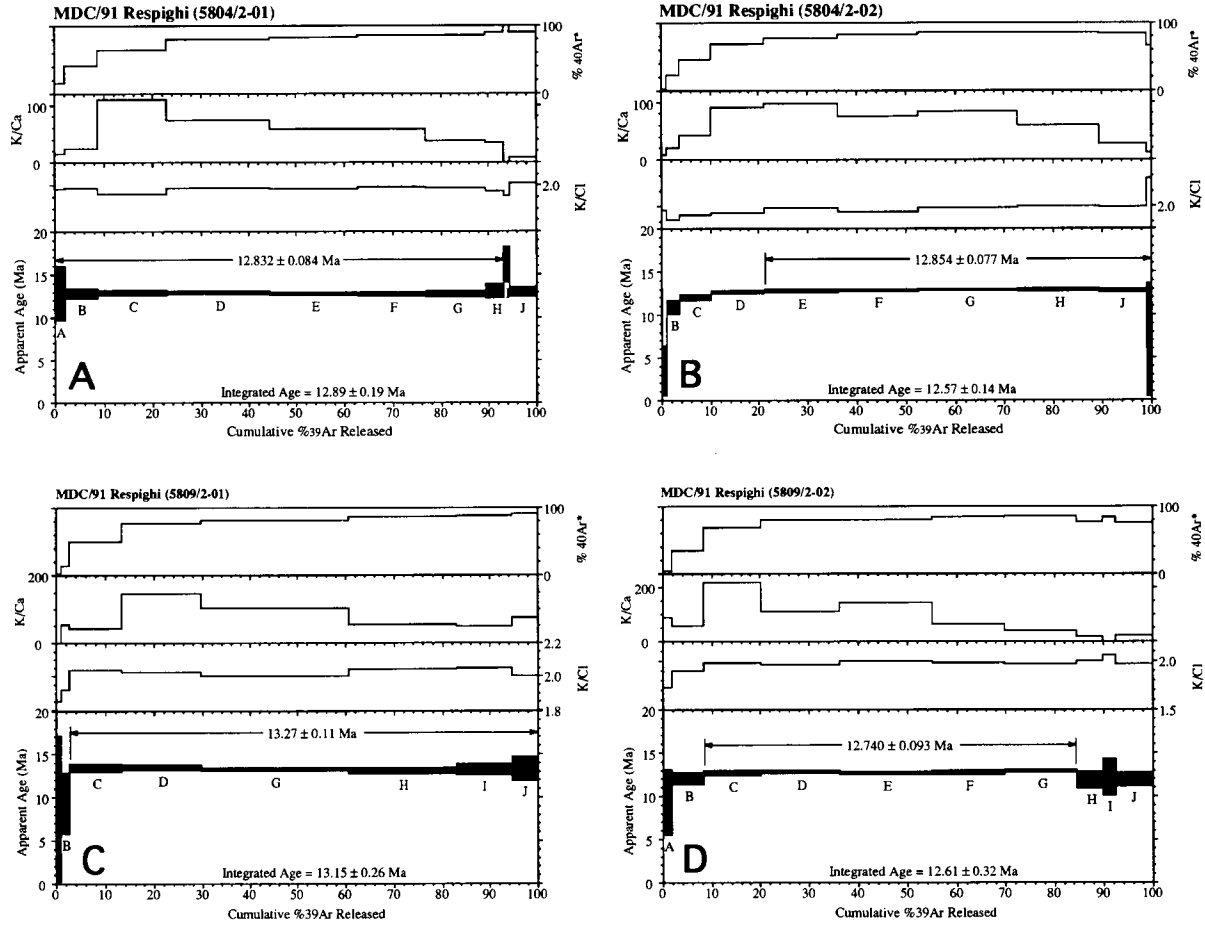


Fig. 17. <sup>40</sup>Ar/<sup>39</sup>Ar plateau diagrams of biotite from the Respighi Level.

Table 4

$^{40}\text{Ar}/^{39}\text{Ar}$  analytical data for laser incremental-heating experiments for levels Respighi and Ancona, Monte dei Corvi section

Lab ID#	Power (W)	Ca/K	$^{36}\text{Ar}/^{39}\text{Ar}$	$^{40}\text{Ar}^*/^{39}\text{Ar}$	% $^{40}\text{Ar}^*$	Age (Ma) $\pm 2\sigma$
<i>Sample MDC/91 Respighi (101.35 m)</i>						
5804/2-01A	11.0	0.0685	0.01372	0.727	15.2	12.86 $\pm$ 1.60
5804/2-01B	13.0	0.0411	0.00350	0.726	41.3	12.84 $\pm$ 0.28
5804/2-01C	15.0	0.0091	0.00138	0.731	64.1	12.93 $\pm$ 0.15
5804/2-01D	17.0	0.0135	0.00062	0.730	80.1	12.92 $\pm$ 0.10
5804/2-01E	19.0	0.0172	0.00050	0.722	83.2	12.78 $\pm$ 0.10
5804/2-01F	21.0	0.0172	0.00042	0.720	85.5	12.73 $\pm$ 0.11
5804/2-01G	24.0	0.0264	0.00043	0.722	85.1	12.77 $\pm$ 0.18
5804/2-01H	27.0	0.0287	0.00027	0.738	90.3	13.06 $\pm$ 0.38
5804/2-01I	30.0	0.0000	-0.00052	0.913	120.1	16.14 $\pm$ 1.05
5804/2-01J	50.0	0.1230	0.00029	0.733	90.1	12.96 $\pm$ 0.28
5804/2-02A	11.0	0.1281	0.02899	0.197	2.2	3.49 $\pm$ 1.45
5804/2-02B	13.0	0.0506	0.00702	0.618	23.0	10.93 $\pm$ 0.40
5804/2-02C	15.0	0.0231	0.00268	0.679	46.2	12.01 $\pm$ 0.18
5804/2-02D	17.0	0.0111	0.00110	0.714	68.7	12.63 $\pm$ 0.12
5804/2-02E	19.0	0.0102	0.00073	0.723	77.1	12.79 $\pm$ 0.10
5804/2-02F	21.0	0.0134	0.00049	0.725	83.5	12.83 $\pm$ 0.09
5804/2-02G	24.0	0.0118	0.00042	0.729	85.4	12.90 $\pm$ 0.09
5804/2-02H	27.0	0.0166	0.00042	0.729	85.6	12.89 $\pm$ 0.10
5804/2-02I	30.0	0.0278	0.00039	0.727	86.6	12.85 $\pm$ 0.10
5804/2-02J	40.0	0.0367	0.00045	0.726	84.7	12.83 $\pm$ 0.11
5804/2-02K	50.0	0.0791	0.00073	0.397	65.1	7.03 $\pm$ 3.29
5809/2-01A	10.0	0.0000	0.07275	0.489	2.2	8.67 $\pm$ 4.24
5809/2-01B	11.0	0.0188	0.01107	0.526	13.9	9.32 $\pm$ 1.75
5809/2-01C	13.0	0.0232	0.00258	0.757	49.8	13.40 $\pm$ 0.24
5809/2-01D	15.0	0.0069	0.00074	0.761	77.6	13.47 $\pm$ 0.16
5809/2-01G	18.0	0.0096	0.00056	0.748	81.9	13.23 $\pm$ 0.11
5809/2-01H	21.0	0.0181	0.00039	0.741	86.5	13.10 $\pm$ 0.18
5809/2-01I	26.0	0.0205	0.00032	0.748	89.0	13.23 $\pm$ 0.30
5809/2-01J	50.0	0.0133	0.00025	0.751	91.0	13.28 $\pm$ 0.69
5809/2-02A	11.0	0.0111	0.03531	0.524	4.8	9.27 $\pm$ 1.87
5809/2-02B	13.0	0.0177	0.00446	0.680	34.0	12.01 $\pm$ 0.33
5809/2-02C	15.0	0.0046	0.00110	0.715	68.8	12.65 $\pm$ 0.16
5809/2-02D	17.0	0.0091	0.00060	0.723	80.3	12.78 $\pm$ 0.12
5809/2-02E	19.0	0.0071	0.00059	0.714	80.4	12.63 $\pm$ 0.12
5809/2-02F	21.0	0.0155	0.00046	0.719	84.1	12.72 $\pm$ 0.13
5809/2-02G	24.0	0.0247	0.00044	0.729	85.0	12.89 $\pm$ 0.12
5809/2-02H	27.0	0.0590	0.00066	0.673	77.8	11.91 $\pm$ 0.48
5809/2-02I	30.0	0.0000	0.00044	0.690	84.2	12.21 $\pm$ 1.05
5809/2-02J	40.0	0.0434	0.00074	0.674	75.6	11.92 $\pm$ 0.41
<i>Sample MDC/91 Ancona (149.9 m)</i>						
5808/2-01B	13.0	0.0664	0.00043	0.732	85.4	12.95 $\pm$ 0.39
5808/2-01C	15.0	0.0103	0.00037	0.657	85.9	11.63 $\pm$ 0.12
5808/2-01D	17.0	0.0050	0.00023	0.652	90.4	11.54 $\pm$ 0.10
5808/2-01E	19.0	0.0072	0.00026	0.654	89.4	11.57 $\pm$ 0.10
5808/2-01F	21.0	0.0105	0.00027	0.644	89.0	11.39 $\pm$ 0.10

Table 4

Continued.

Lab ID#	Power (W)	Ca/K	$^{36}\text{Ar}/^{39}\text{Ar}$	$^{40}\text{Ar}^*/^{39}\text{Ar}$	% $^{40}\text{Ar}^*$	Age (Ma) $\pm 2\sigma$
5808/2-01G	24.0	0.0028	0.00025	0.641	89.6	11.34 $\pm$ 0.08
5808/2-01H	27.0	0.0027	0.00028	0.637	88.3	11.27 $\pm$ 0.11
5808/2-01I	30.0	0.0000	0.00021	0.647	91.1	11.44 $\pm$ 0.11

Notes. Runs at the beginning and end of the incremental-heating experiment which comprise less than 1% of the total percent of  $^{39}\text{Ar}$  released have been omitted in this table and elsewhere as these are essentially blanks. Samples in italic indicate steps included in plateau. The plateau definition is that of Fleck et al. (1977) where in at least three contiguous steps comprising at least 50% of the cumulative % $^{39}\text{Ar}$  released cannot mutually be distinguished using a 95% confidence value test. Errors in age quoted for individual runs are  $1\sigma$  analytical uncertainty. Ca/K is calculated from  $^{37}\text{Ar}/^{39}\text{Ar}$  using a multiplier of 1.96.  $^{40}\text{Ar}^*$  refers to radiogenic argon.  $\lambda = 5.543 \times 10^{-10} \text{ y}^{-1}$ . Isotopic interference corrections:  $(^{36}\text{Ar}/^{37}\text{Ar})_{\text{Ca}} = (2.58 \pm 0.06) \times 10^{-4}$ ,  $(^{39}\text{Ar}/^{37}\text{Ar})_{\text{Ca}} = (6.7 \pm 0.3) \times 10^{-4}$ ,  $(^{40}\text{Ar}/^{39}\text{Ar})_{\text{K}} = (2.17 \pm 0.08) \times 10^{-2}$ .  $J = (9.840 \pm 0.05) \times 10^{-3}$ .

$^{40}\text{Ar}$  (% $^{40}\text{Ar}^*$ ) with increased intensity of sample heating, starting at values below 15% and rising to 70–90%  $^{40}\text{Ar}^*$  after about a fourth of the cumulative  $^{39}\text{Ar}$ . K/Ca ratios are not as regular but in general show a similar pattern of rapidly rising K/Ca in the first 20% of % $^{39}\text{Ar}$  released, followed by a slow irregular drop through the rest of the spectrum. K/Cl in general is marked by a initial rise in the first 5–10% of the cumulative  $^{39}\text{Ar}$  release, succeeded by flat behaviour throughout the rest of the experiment. The behaviour of the % $^{40}\text{Ar}^*$  release curve is typical of other biotites we have analyzed in the Apennines, and we describe this to minor, marginal alteration of the biotite grains undetectable by X-ray diffractometry. This alteration could also explain the low K/Ca ratios in the early release as due to the presence of Ca-enriched alteration phases. However, apart from a slightly lower age in some of the earliest steps, the spectra in each of the four aliquots contain a plateau that extends across more than three-fourths of the cumulative % $^{39}\text{Ar}$  release, suggesting good preservation of the K–Ar systematics.

Three of the four plateau ages are statistically indistinguishable from one another at between 12.74–12.85 Ma, but one aliquot (5809/2-01) gives a significantly older plateau at 13.27 Ma ( $2\sigma$  errors are between 0.16 and 0.22 Ma, including the errors in  $J$  and in the dosimeter). In all cases, plateau ages are statistically indistinguishable from integrated ages, though the integrated ages are about twice as imprecise. Isotope correlation analysis yields good isochrons in all cases (Table 5), with trapped  $^{40}\text{Ar}/^{36}\text{Ar}$  compositions that are indistinguishable from atmospheric argon. Isochron ages encompass a similar range of ages but show considerably more overlap; nevertheless experiment 5809/2-01 is markedly old. Leaving this out, the mean isochron age is  $12.86 \pm 0.16$  Ma (including this aliquot would increase the age by 0.08 Ma). This final result is preferred as the reference age for this bentonite over the mean plateau age, since the isochron analysis technique is a better approach to performing the ‘trapped’  $^{40}\text{Ar}/^{36}\text{Ar}$  correction.

Analytical results from the Ancona biotite separate are shown in Table 4, and a step-heating spectrum for this experiment is shown in Fig. 18. Again, as is typical of biotites analyzed from this region, the initial lower-temperature steps show more

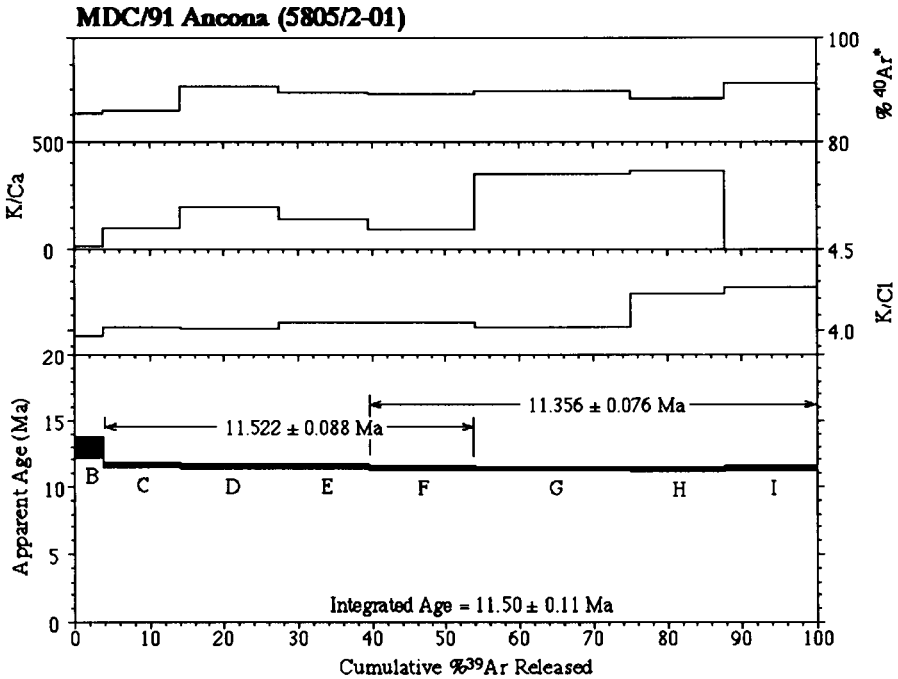


Fig. 18.  $^{40}\text{Ar}/^{39}\text{Ar}$  Ar plateau diagram of biotite from the Ancona Level.

atmospheric contamination of the total argon than later steps, in this case reaching the norm after only 14% of the cumulative  $^{39}\text{Ar}$  release. This pattern likely reflects slight marginal alteration of the biotite accompanied by atmospheric argon uptake by the crystal. However, apart from slightly older ages in the first few steps, the argon systematics may not have been significantly affected by alteration since the spectrum is quite flat. Using a common definition of a 'plateau' (see notes to Table 4), this spectrum in fact contains two overlapping plateaus encompassing a total of about 94% of the cumulative  $\%^{39}\text{Ar}$  release. The weighted mean ages of the two plateau sequences differ by only 0.16 Ma and are not statistically distinguishable. A weighted average of the two plateau ages gives  $11.43 \pm 0.20$  Ma. This mean of the plateau ages is very close to the integrated age of  $11.50 \pm 0.22$  Ma, reflecting the fact that so much of the gas release falls within the scope of the combined plateaus. Isotope correlation analysis of the combined plateaus (i.e., all steps except the first) revealed an isochron with a rather poorly defined value for the 'trapped'  $^{40}\text{Ar}/^{36}\text{Ar}$  composition of  $417 \pm 93$  that is indistinguishable from atmospheric argon [ $(^{40}\text{Ar}/^{36}\text{Ar})_{\text{atm}} = 295.5$ ; Steiger, 1977] (Table 5). Likewise the isochron intercept age of  $10.88 \pm 0.76$  Ma ( $2\sigma$  error) is also poorly defined, both as a consequence of the limited spread in the isotopic ratios of  $^{36}\text{Ar}/^{40}\text{Ar}$  and  $^{39}\text{Ar}/^{40}\text{Ar}$  data. With such a large uncertainty the isochron age is statistically indistinguishable at the 95% confidence level from the mean plateau age. However, because the isochron intercepts are so poorly determined, the reference age for this sample is taken to be the mean plateau age as given above.

Table 5

Summary incremental-heating ages: integrated, plateau, and isochron plateau age calculations

Sample	n (Integ.)	Integrated age	n (plat. or isoch.)	Plateau age	MSWD	( <sup>40</sup> Ar/ <sup>36</sup> Ar) <sub>trapped</sub>	Isochron age
<i>MDC/91 Respighi (101.35 m)</i>							
5804/2 01	10	12.89 ± 0.19	8 (A-H)	12.83 ± 0.08	0.7	297.8 ± 3.8	12.80 ± 0.09
5804/2 02	10	12.57 ± 0.14	6 (E-K)	12.85 ± 0.08	0.6	278.0 ± 4	13.00 ± 0.14
5804/2 01	8	13.15 ± 0.26	6 (C-J)	13.27 ± 0.11	0.7	301.5 ± 6.4	3.20 ± 0.12
5809/2 02	10	12.61 ± 0.32	5 (C-G)	12.74 ± 0.09	1.0	283.0 ± 14	12.87 ± 0.16
<i>MDC/91 Ancona (149.90 m)</i>							
5808/2 01	8	11.50 ± 0.11	4 (C-F)	11.52 ± 0.09			
			4 (F-I)	11.36 ± 0.08			
			7 (C-I)		1.8	417.0 ± 93	10.88 ± 0.38

Notes. All ages are in units of Ma with an indicated uncertainty of  $1\sigma$ . Isochron fitting is by the 'inverse' isochron (<sup>36</sup>Ar/<sup>40</sup>Ar vs. <sup>39</sup>Ar/<sup>40</sup>Ar). MSWD = mean square of weighted deviates; a goodness of fit parameter that provides a measure of the scatter of the data about the line.

## SUMMARY AND CONCLUSIONS

### *Integrated interstage boundary stratigraphy*

The complete and nearly continuous pelagic-hemipelagic sequence of the Cònero Riviera, exposed on sea cliffs between Ancona and Monte dei Corvi, contains the interstage boundaries between the Langhian, the Serravallian, the Tortonian, and the Messinian. These boundaries can be recognized on the basis of stratigraphic criteria including calcareous microplankton events (planktonic Foraminifera and calcareous nannofossils), geochemical signatures (Sr, C, and O isotopes, and Fe, Mg, Mn, and whole Sr trace elements), and calibrated with direct radioisotopic age dates from two interbedded biotite-rich volcanoclastic layers.

The rock magnetic properties of this sequence are not conducive to magnetostratigraphy due to the weakness and/or instability of the magnetic signatures in altered marls.

Organic carbon analyses from interbedded black shale layers show a clear differentiation between the Tortonian and the Messinian, the latter being characterized by an enrichment in sulphur compounds, as the intensities of thiophene peaks rival or surpass those of the monoaromatic. This indicates kerogen formation in a highly saline depositional and diagenetic environment, consistent with the mineralogical and sedimentological evidence for the great Messinian salinity crisis of the proto-Mediterranean.

The characterizations of the interstage boundaries exposed in the Cònero Riviera sequence are summarized as follow, and illustrated in Fig. 19.

### *Langhian/Serravallian*

*Location and accessibility.* This boundary is located in the lower part of the calcareous member of the Schlier formation (Cònero facies), characterized by an alternation of grey marl and marly limestone layers. In the Cònero Riviera, this lithostratigraphic



### Monte dei Corvi Sequence

**Formation**    **Section**    **Lithology**    **Marker beds**

GIUSSOSO SOLFEREA  
GHOLI DILETTO

massive member  
marly member  
S C H L I E R  
calcareous member

Monte dei Corvi (MDC) section  
Monte dei Corvi High Cliff (MCH) section  
Ancona-Vedova (VED) section

white limestones  
Rosini Level SAR 224 m  
L. Ancona 11.43 ± 0.20 Ma (MDC 149.9 m)  
Reapighi Level 12.86 ± 0.16 Ma (MDC 101.4 m)  
Cavolo ss. turbidite  
Aldo Level VED 24.0 m  
Megabed 7  
Megabed 6

covered

Legend:  
sandstone    massive marl  
marly limestone    organic-rich marl  
marl    black shale    biotite

Blow (1969)	Planktonic foraminiferal Zone		Nannofoossil Zone	Isotope chemostratigraphy		Age
	D'Onofrio et al. (1975) Colalongo et al. (1979)	Iaccarino & Salvatorini (1982) Iaccarino (1985)		δ13C	Sr87/Sr86	
N17	<i>G. conomiozea</i>	<i>G. mult.</i> <i>G. med.</i> <i>G. sut.</i>	Non-distinctive <i>G. conomiozea</i> <i>G. sut.</i>	CN9b CN9a	0.7088	Messinian
N16	<i>G. acostaensis acostaensis</i>	<i>G. obliqua extremus</i> <i>G. obliqua extremus</i>	<i>G. obliqua extremus</i> <i>G. obliqua extremus</i> <i>G. obliqua extremus</i> <i>G. bulboides</i>	CN8 CN8 CN8	0.7090	Tortonian
N15 / N14	<i>G. conomiozea</i>	<i>G. acostaensis</i>	<i>G. acostaensis</i>	CN7 CN7		Tortonian
N13		<i>G. nidicosis</i> <i>G. mercurii</i> s.l. <i>G. subquadrisulc.</i> <i>G. nidicosis</i> <i>G. obliqua obliqua</i>	<i>G. nidicosis</i> <i>G. mercurii</i> s.l. <i>G. subquadrisulc.</i> <i>G. nidicosis</i> <i>G. obliqua obliqua</i>	CN6 CN6 CN6 CN6		Tortonian
N11		<i>G. altopetra altopetra</i>	<i>G. altopetra altopetra</i>	CN5 CN5		Tortonian
N10		<i>O. australis</i> <i>G. peripher.</i> <i>G. prism.</i> <i>G. peripher.</i>	<i>O. australis</i> <i>G. peripher.</i> <i>G. prism.</i> <i>G. peripher.</i>	CN4 CN4 CN4 CN4		Tortonian
N9		<i>O. aur.</i> <i>G. periph.</i> <i>O. aur.</i>	<i>O. aur.</i> <i>G. periph.</i> <i>O. aur.</i>	CN3 CN3 CN3		Tortonian
N8		<i>Praeorbulina glomerata</i> s.l.	<i>Praeorbulina glomerata</i> s.l.	CN2 CN2 CN2		Langhian

m level/age conversion formulas:  
 0.00-149.9 m: age = 15.850 - (0.029485 x m level)  
 149.9-227.0 m: age = 19.537 - (0.054086 x m level)

Sr87/Sr86  
 Ocean curve  
 Cònero curve

Fig. 19. Integrated stratigraphy of the upper Langhian to lower Messinian sequence of the Cònero Riviera sequence.

interval is exposed on the cliffs near Pietralacroce and the municipal swimming pool of Ancona, and can be reached only by repelling down the cliff with a mountaineer rope. The same interval is partially exposed at the base of the MCH section al Monte dei Corvi.

**Biostratigraphy.** The LO of *G. peripheronda* (planktonic foraminifer) defines the N10/N11 zonal boundary of Blow (1969), and it is often used to approximate the interstage boundary. However, this event has not been recognized in the MCH section due to a covered interval. Nevertheless, the disappearance of *S. heteromorphus* (calcareous nannofossil) recognized at 78 m in the MCH section, has been considered as an equally valid marker for the biostratigraphic approximation of the Langhian/Serravallian boundary (Rio et al. 1995; Chapter A5).

**Geochronology.** An age of about 13.6 Ma for the LO of *S. heteromorphus*, which can be considered an upper limit for this interstage boundary, can be derived by extrapolating down-section from the  $^{40}\text{Ar}$ - $^{39}\text{Ar}$  date of  $12.86 \pm 0.16$  Ma for the Respighi Level (MDC 101.35 m). In the same way, an age of about 15 Ma is derived for the Aldo Level (VED-24.0 m), which may correspond to the Michelangelo Level in the L'Annunziata section (see Montanari et al., Chapter D2). In fact, sanidine in the Michelangelo Level yielded a preliminary  $^{40}\text{Ar}$ - $^{39}\text{Ar}$  age of 15 Ma (Montanari et al., 1988b). Direct radioisotopic dating of the Aldo Level will provide, in the future, a more precise and accurate age calibration for the stratigraphic interval across the Langhian/Serravallian boundary.

### *Serravallian/Tortonian*

**Location and accessibility.** This boundary is located in the upper part of the Calcareous Member of the Cònero Schlier formation, best exposed in the MDC section at metre level 157.55, about 7.5 m above the biotite-rich Ancona Level. It is easy to reach when the sea is calm. The action of sea waves during storms may change the preservation of the outcrop.

**Biostratigraphy.** This boundary is approximated to the FO of planktonic foraminifer *N. acostaensis* (MDC 157.55 m), corresponding to the N15/N16 zonal boundary of Blow (1969). The FO of *N. acostaensis* in the MDC section is found in the upper parts of calcareous nannofossil zones NN7, CN5b, and MNN7, of the biostratigraphic models of Martini (1971), Okada and Bukry (1980), and Fornaciari et al. (1993), respectively.

**Chemostratigraphy.** The  $\delta^{13}\text{C}$  curve exhibits a distinct maximum of +1.12‰ near the Serravallian/Tortonian boundary followed by a negative trend in the lower Tortonian. This boundary is well marked also in the  $\delta^{13}\text{O}$  curve, and corresponds to a trend reversal preceding a renewed isotopic ratio decrease in the lower Tortonian (−0.1‰ at 163.4 m). Major negative shifts in the iron and magnesium curves are found just below the boundary. The  $^{87}\text{Sr}/^{86}\text{Sr}$  in the region of the Serravallian/Tortonian boundary in the MDC section are similar to those of coeval oceanic carbonates, with average values around  $0.70895 \pm 0.0003$ .

**Geochronology.** A weighted average of two  $^{40}\text{Ar}$ - $^{39}\text{Ar}$  plateau dates from unaltered biotite of the Ancona Level (MDC 149.9 m) yields an accurate and precise numerical age of  $11.43 \pm 0.20$  Ma. Using the age of 7.26 Ma for the Tortonian/Messinian boundary (i.e., SAR 227.0 m) as it was determined by Laurenzi et al. in the Emilian sections of

the northern Apennines (Chapter E5), a tightly interpolated age of  $11.0 \pm 0.2$  Ma can be assigned to the Serravallian/Tortonian boundary.

### *Tortonian/Messinian*

*Location and accessibility.* This interstage boundary is located in the uppermost part of the Marly Member of the Schlier formation (Cònero facies), well exposed in the La Sardella section (SAR), just above the biotite-rich Rossini Level at metre level 227, and about 4 m below the base of the Euxinic Shale formation. It is difficult to reach because the SAR section is located on a nearly vertical landslide scarp. However, the authorities of the Monte Cònero national Park are considering to trace a trail for an easy access to this section, and arm it with a steel ladder in the near future.

*Biostratigraphy.* The boundary is approximated to the FO of the planktonic foraminifer *G. conomiozea* which is located at 227 m in the SAR section. This bioevent is located within foraminiferal Zone N17 of Blow (1969), and in the lower part of calcareous nannofossil Subzone CN9b of Okada and Bukry (1980) which is defined by the FO of *Amaurolithus* spp., occurring at 225.50 m in the SAR section.

*Chemostratigraphy.* The trends of carbon and oxygen isotopic ratios across the Tortonian/Messinian boundary in the SAR section show a monotonic decrease, and increase, respectively. Trace element analyses in this section have yet to be carried out. The  $^{87}\text{Sr}/^{86}\text{Sr}$  ratios from whole carbonate, and fish teeth at the boundary show values in the range of  $0.70890 \pm 0.00004$  which are considerably lower than the ratios around 0.70905 found in oceanic carbonates. The SAR low-Sr isotopic ratios sharply increase just above the interstage boundary, but they never reach values as high as those of coeval oceanic carbonates.

*Geochronology.* Vai, (Chapter E3) and Laurenzi et al. (Chapter E5), assign an age of 7.2 Ma to the Tortonian/Messinian boundary exposed in several sections in the Emilian Apennines, where it is approximated to the FO of the planktonic foraminifer *G. conomiozea*. Several biotite and sanidine samples from the Rossini Level of the SAR section are currently in the process of being dated at the Berkeley Geochronology Center (Deino and Montanari, in preparation), and will hopefully yield accurate and precise dates for further refining of the geochronology of this important interstage boundary.

## SOMMAIRE — STRATIGRAPHIE INTÉGRÉE DE LA SÉQUENCE PÉLAGIQUE DU MIOCÈNE MOYEN AU MIOCÈNE SUPÉRIEUR DANS LA RIVIERA DEL CÒNERO (RÉGION DES MARCHES, ITALIE)

(Manuscrit soumis: Juin 1995, révisé: Octobre 1995; rédacteurs responsables: AM et RC)

La séquence de la Riviera du Cònero, au sud du port d'Ancône (Italie), comprend 247 m de sédiments affleurant de façon presque continue pour une grande partie du Miocène. Ce remarquable affleurement de falaise de bord de mer expose des sédiments carbonatés méditerranéens pratiquement dépourvus de turbidites et de perturbation syntectonique. L'étude lithostratigraphique a été effectuée. La biostratigraphie a été décrite d'après le microplancton calcaire; elle a mis en évidence des âges de dépôt compris entre le

Langhien supérieur et le Messinien inférieur inclus. L'étude paléomagnétique a permis une certaine caractérisation des sédiments qui n'ont cependant pas encore fourni de résultats significatifs pour l'interprétation magnétostratigraphique du fait de la faible intensité magnétique, elle-même probablement liée à une altération de surface. La chimiostratigraphie a été appliquée avec l'étude des éléments en trace, des isotopes stables, des isotopes du strontium et de la matière organique. On a observé sur la courbe de  $\delta^{13}\text{C}$  un maximum distinct à +1, 12‰ près de la limite Serravallien/Tortonien laquelle est aussi marquée dans les courbes de teneur en fer et en magnésium (excursion négative nette sous la limite). Autour de cette même limite, les rapports isotopiques du strontium sont, en moyenne, semblables dans cette séquence à ceux connus pour les carbonates océaniques ( $^{87}\text{Sr}/^{86}\text{Sr}$  autour de  $0,70895 \pm 0,0003$ ). Autour de la limite Tortonien/Messinien, les courbes de  $\delta^{13}\text{C}$  et  $\delta^{18}\text{O}$  montrent de très nettes tendances vers des valeurs faibles pour la première et fortes pour la seconde ce qui est propre à cette séquence. Les rapports  $^{87}\text{Sr}/^{86}\text{Sr}$  de la fraction carbonatée totale et des dents de requin prélevées autour de cette même limite, ont des valeurs de l'ordre de  $0,70890 \pm 0,00004$  considérablement plus basses que celles des carbonates océaniques qui se situent près de 0,70905. Les analyses de chimie organique des niveaux noirs du Messinien basal indiquent une origine végétale continentale pour le carbone et un environnement de dépôt hypersalin. Ceci contraste avec une origine clairement algale et marine pour l'essentiel du carbone organique des niveaux noirs du Tortonien et du Serravallien. Ceci pourrait être un bon critère de reconnaissance et de corrélation pour la limite Tortonien/Messinien dans la région où elle est communément repérée par la première manifestation du foraminifère planctonique *Globorotalia conomiozea*, laquelle est connue pour se situer très légèrement au dessus de la base du Messinien stratotypique. Cette apparition tombe, dans cette séquence, dans la partie inférieure de la sous zone de nanofossiles calcaires CN9b définie par la première manifestation de *Amaurolithus* spp.

Quatre niveaux volcanoclastiques riches en biotite et susceptibles de caractérisation géochronologique ont été repérés. Le plus ancien niveau est situé à la base de la séquence, dans le Langhien; il pourrait relever du même épisode volcanique que le niveau observé à l'Annunziata. Les deux niveaux suivants ont été découverts aux cotes 101 (niveau Respighi) et 150 (niveau Ancône) vers la base et vers le sommet du Serravallien. L'épisode volcanique le plus récent (baptisé ici niveau Rossini) a laissé des traces vers la cote 225, dans le Tortonien terminal et est contemporain de celui qui a engendré les niveaux volcanoclastiques observés à Pieve di Gesso et dans la région de Faenza. Les deux niveaux serravalliens ont été datés par la méthode K-Ar, technique par irradiation et chauffage par étape sur biotite. Les âges dignes de confiance de  $12,86 \pm 0,16$  et  $11,43 \pm 0,20$  Ma (incertitude intralaboratoire  $2\sigma$ ) ont été obtenus. Cette nouvelle information géochronologique, combinée à celle obtenue dans d'autres sections et par d'autres laboratoires permet de proposer, pour un grand nombre de repères biostratigraphiques, des âges propres à cette séquence, déduits pratiquement directement et dignes de confiance grâce à un taux de dépôt relativement régulier. Par exemple, la dernière manifestation de *Sphenolithus heteromorphus* (nanofossiles calcaire), plus jeune que la limite Langhien/Serravallien définie par les stratotypes, permet de proposer un âge minimum pour la limite de 13,5 Ma; la première manifestation de *Neogloboquadrina acostaensis* (foraminifère planctonique), à peine plus ancienne

que la limite Serravallien/Tortonien dans les stratotypes historiques, est très proche de  $11,0 \pm 0,2$  Ma.

*(Sommaire proposé par les rédacteurs d'après un résumé des auteurs, GSO)*

#### ACKNOWLEDGEMENTS

This work has been supported, through past years, by grants from the United States National Science Foundation, Exxon Oil Co., and Armines (A. Montanari) and a grant from the Italian Ministry of University and Scientific Research (MURST, 60%; responsible R. Coccioni). We would like to thank V.E. Langenheim (U.S.G.S. Menlo Park), and S. Rutenfrans, E. Klinkenberg, J. Ton, and G.-J. Wijers (Utrecht University) for field work assistance. We would like to thank Paul Kopssock for reviewing the original manuscript.

## Chapter E2

### **INTEGRATED STRATIGRAPHY OF THE LATE TORTONIAN PIEVE DI GESSO SECTION (ROMAGNA, ITALY)**

G.S. Odin, M. Cosca, F. Tateo, A. Negri, G.B. Vai and J.C. Hunziker

#### INTRODUCTION

The first quotation of a volcanoclastic arenaceous layer near the Tortonian/Messinian boundary was made by Gandolfi et al. (1983) from the Marnoso-arenacea Formation sampled near Fontanelice (Romagna, Italy). The study of these authors emphasizes the volcanic origin of one layer. G.G. Zuffa (pers. commun., 1991) informed us that several similar layers were seen at the same locality but not analysed for petrology. The present study was undertaken with the aim to characterize the potential use of those layers for integrated mostly geochronological–biostratigraphical knowledge. Similar biotite-rich layers were described by Calieri (1992) from the same province pointing to a regional significance of these layers which can be seen along river valleys oriented SW–NE and crossing the general NW–SE strike of the deposits (Fig. 1). Farther to the southwest a probably equivalent layer has been found by D. Cosentino (Roma) in the ‘Valle del Salto’ (on the border between the Umbria and Latium regions).

The first results obtained from these layers sampled in the Monte Tondo and Monte del Casino sections were extremely positive (Vai et al., 1993); they were obtained from two groups of biotite-rich layers located about 5 m and about 10 to 13 m below what is considered the base of the Messinian Stage in the area; the present work intends to supplement those pioneer results.

#### LITHOSTRATIGRAPHY

The Pieve di Gesso section is located 25 km southeast of Bologna, 15 km southwest of Imola near Fontanelice (Fig. 1). The stratigraphy is generally similar to that of the Monte del Casino and Monte Tondo sections which are located 10 to 15 km farther to the east-southeast.

Three to six particular layers (2 to 4 cm thick) can be observed in the Pieve di Gesso section along the 100-m-long bank of the road (Fig. 2A). The base of the regional marker bed ‘Calcare di base’ can be seen 40 to 50 m above the section (Fig. 2B). The Calcare di base is a characteristic Messinian feature usually located 20 to 30 m above the base of the Messinian historical stratotype of Selli (1960). This means that the layers are lithostratigraphically correlated to near and below the Tortonian/Messinian boundary. In the field, these layers differ from the marly sequence by their hardness; they can be followed easily laterally and the presence of abundant biotite flakes is diagnostic. Sedimentologically, they are locally considered to be faint turbidite layers and contain

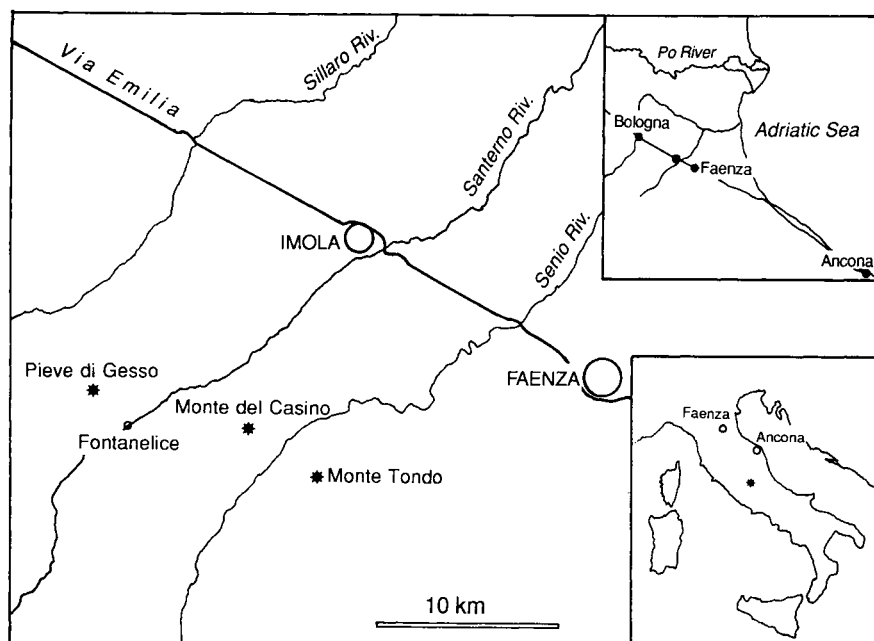


Fig. 1. Location of the Pieve di Gesso section in the Faenza area. The outcrop from the Valle del Salto is shown (star in the small map of Italy).

more or less abundant white mica flakes. The two layers richest in biotite were sampled for geochronological study and several samples were collected for biostratigraphy.

## BIOSTRATIGRAPHY

Five samples from the Pieve di Gesso section were analyzed for calcareous nannoplankton biostratigraphic purposes. The samples bracket the two biotite-rich layers studied in the present work. Calcareous nannofossils generally show high abundance but poor preservation.

The taxa identified are: *Calcidiscus leptoporus*, *Calcidiscus macintyreii*, *Helicosphaera carteri*, *Discoaster pentaradiatus*, *Discoaster brouweri*, *Discoaster variabilis*, *Reticulofenestra pseudoumbilica*, and *Amaurolithus* sp. The range chart for some selected species is shown in Table 1. The occurrence of *Amaurolithus* sp. is rare and discontinuous along the section. The first occurrence of the taxon commonly marks the boundary between subzones CN9a and CN9b of Okada and Bukry (1980) and falls in the youngest portion of the Tortonian.

In the extra-Mediterranean area, the boundary between subzone CN9a and CN9b is indicated by the first occurrence (FO) of *Amaurolithus primus*, the first horseshoe-shaped calcareous nannofossil in the Neogene. Another species appears shortly after *A. primus*, namely *Amaurolithus delicatus*. Since in the Mediterranean area, the genus *Amaurolithus* occurs very rarely, it appears difficult to discriminate whether or not the observed first occurrence of *A. primus* really predates the *A. delicatus* FO and it is thus

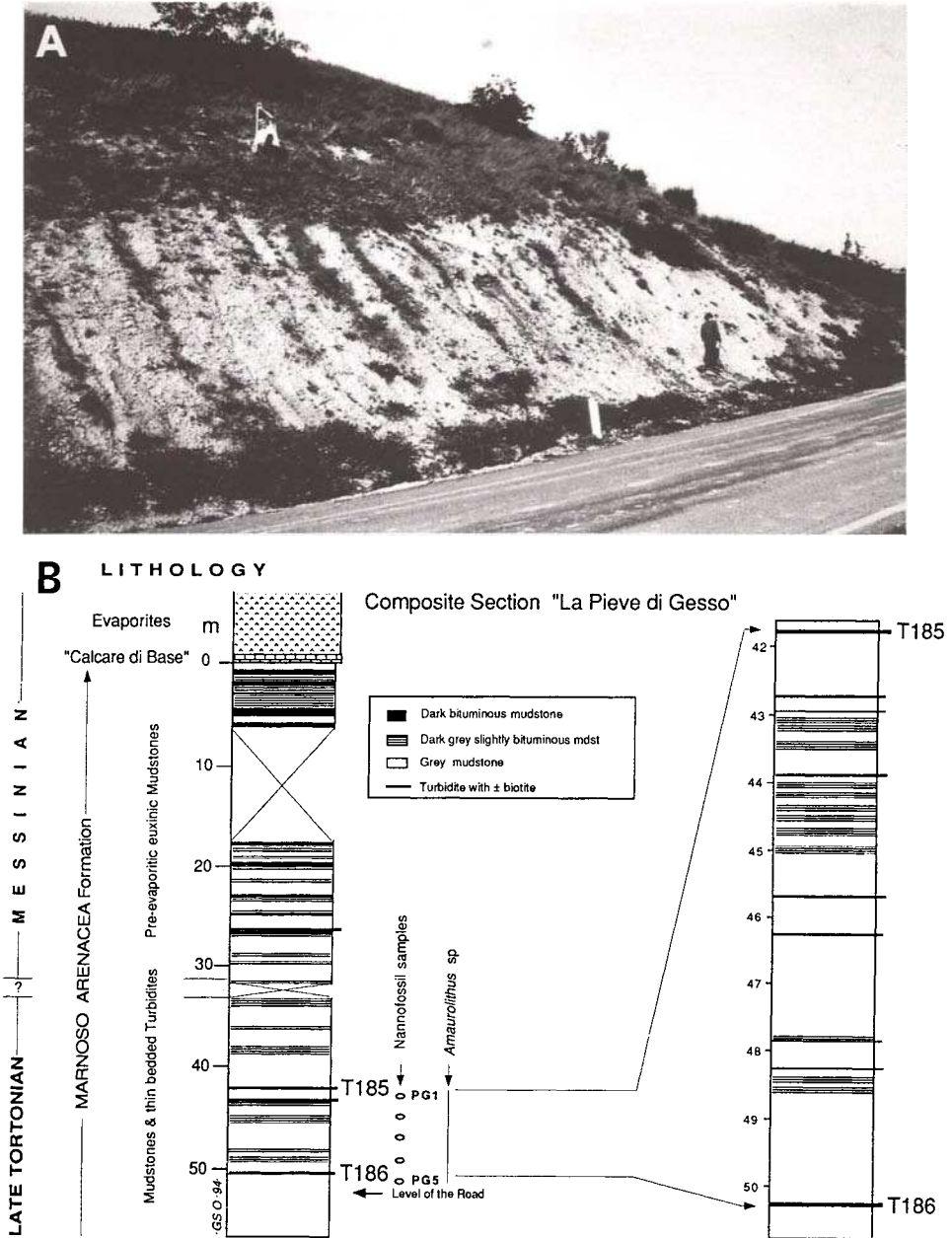


Fig. 2. (A) Photograph of the Pieve di Gesso section. The person to the bottom right of the figure (R. Calieri) stands on the lower sampled layer; the person to the top with a 1-m scale, is on the upper sampled layer. (Photo by GSO, 1992). (B) Schematic section at 'La Pieve di Gesso'. (Simplified from field observation and section by Ferretti, 1993). Note that the turbidite layers may or may not correspond to biotite-rich sediments. The section may be compared to the precise ones proposed by Vai et al. (1993, and in Chapter E3).



Table 1

Calcareous nannofossils from the Pieve di Gesso section (original data from A.N.)

Taxa	← young Samples old →					T186	PG5
	T185	PG1	PG2	PG3	PG4		
<i>Amaurolithus</i> sp.			R				R
<i>Calcidiscus leptoporus</i>		R	R	F	F		F
<i>Calcidiscus macintyre</i>		R	R	R			F
<i>Coccolithus pelagicus</i>		C	C	C	C		C
<i>Dictyococcites</i> spp.		A	A	A	A		A
<i>Discoaster</i> 5 rays spp.		R	C	R	R		R
<i>Discoaster</i> 6 rays spp.		F	C	C	R		C
<i>Helicosphaera carteri</i>		C	C	C	C		C
<i>Reticulofenestra</i> spp.		C	C	C	C		C
<i>Sphenolithus moriformis</i>		C	C	C	C		C

A = abundant, 1 or more specimen every field of view; C = common, 1 specimen every 2–10 fields of view; F = few, 1 specimen every 11–50 fields of view; R = rare, 1 specimen every 51–200 fields of view.

preferred to use the FO of the *Amaurolithus* group as a diagnostic key marker. The FO of *A. primus* is used in the extra-Mediterranean area, to approximate (by the old side) the Tortonian/Messinian boundary.

The planktonic foraminiferal study in the section (Colalongo, in Ferretti, 1993) points out the absence of the Messinian taxon *Globorotalia conomiozea* and the occurrence of *Globorotalia humerosa* and *Globorotalia praemargaritae*.

The accepted chronology from older to younger nannofossils and Foraminifera (Colalongo et al., 1979a) within this interval is as follows: FO of *G. humerosa*; FO of *Globorotalia suterae*; FO of *A. primus* followed by the FO of *A. delicatus*; and finally the Tortonian/Messinian boundary, contemporaneous or immediately followed by FO of *G. conomiozea*. Thus the dated section is slightly older than the Tortonian/Messinian boundary in terms of biostratigraphic control.

In summary, the layers collected from the Pieve di Gesso section may be contemporaneous with either the lower first cluster or the upper second cluster of those previously studied for integrated stratigraphy in the Monte Tondo and Monte del Casino sections (Vai et al., 1993).

## GEOCHRONOLOGY

### *Petrography and mineralogy of the geochronometers*

The volcanic origin of the material from the layers sampled was deduced from their distinctive nature compared to all neighbouring sediments (Gandolfi et al., 1983). These authors quote the presence of 100% of acidic volcanic elements in the rock fragments extracted from the sediment. For these authors, the spectrum of components is diagnostic with the total sand-sized sediment made of 25% of plagioclase and 34% of mica flakes (biotite); heavy minerals extracted following acid treatment, show a volcanic composition with 97% of opaques and, amongst transparent minerals, a unique assemblage of zircon (75%) and allanite (18%). The regional extent of

Table 2

Geochemical data from biotite flakes in samples T185 and T186 (original data from FT)

SiO <sub>2</sub>	TiO <sub>2</sub>	Al <sub>2</sub> O <sub>3</sub>	FeO*	MnO	MgO	CaO	Na <sub>2</sub> O	K <sub>2</sub> O	FeO*/MgO
Pieve di Gesso, upper layer T185:									
39.06	3.57	16.00	17.55	0.03	13.80	0.03	0.35	9.61	1.27
39.17	3.67	15.62	17.78	0.12	13.67	0.01	0.50	9.46	1.30
38.86	3.70	16.40	17.60	0.17	13.39	0.12	0.42	9.33	1.31
39.11	3.62	16.09	17.75	0.09	13.47	0.07	0.29	9.51	1.32
39.46	3.62	15.60	17.94	0.13	13.40	0.00	0.23	9.61	1.34
38.40	3.64	16.08	18.33	0.17	13.65	0.02	0.33	9.37	1.34
38.70	3.78	16.39	18.31	0.15	12.60	0.03	0.33	9.71	1.45
38.37	3.75	16.02	18.71	0.11	12.84	0.02	0.56	9.62	1.46
38.58	3.48	16.36	18.89	0.12	12.69	0.01	0.50	9.37	1.49
38.49	3.49	15.97	18.86	0.24	12.63	0.05	0.59	9.68	1.49
38.50	3.95	15.73	18.90	0.20	12.60	0.06	0.32	9.72	1.50
38.96	3.75	15.63	19.13	0.17	12.42	0.03	0.41	9.50	1.54
38.64	3.73	17.12	18.65	0.26	11.57	0.05	0.40	9.57	1.61
37.81	3.60	16.87	19.77	0.19	11.67	0.00	0.41	9.66	1.69
38.27	3.53	16.27	19.98	0.22	11.73	0.00	0.20	9.81	1.70
Average ( $\pm 1\sigma$ )									
38.69	3.66	16.14	18.54	0.16	12.81	0.03	0.39	9.57	1.46
0.41	0.12	0.43	0.72	0.06	0.72	0.03	0.11	0.14	0.14
Pieve di Gesso, lower layer T186:									
38.43	3.74	15.81	18.56	0.03	13.11	0.09	0.51	9.72	1.42
38.05	4.49	15.79	18.63	0.15	12.55	0.10	0.54	9.69	1.48
38.38	3.66	15.95	19.05	0.18	12.61	0.02	0.33	9.82	1.51
37.87	3.72	16.39	19.38	0.11	12.56	0.01	0.31	9.64	1.54
38.53	3.87	15.89	19.48	0.23	12.41	0.09	0.23	9.26	1.57
38.33	3.72	15.88	19.68	0.14	12.31	0.00	0.13	9.82	1.60
38.77	3.42	16.05	19.82	0.03	12.35	0.08	0.43	9.04	1.61
38.27	3.80	15.93	19.63	0.13	12.13	0.09	0.23	9.79	1.62
38.06	3.59	16.17	19.74	0.29	11.84	0.08	0.44	9.78	1.67
37.78	3.51	16.28	20.01	0.25	11.92	0.03	0.50	9.69	1.68
38.10	3.62	16.21	20.21	0.19	11.58	0.03	0.47	9.60	1.75
37.85	3.71	16.22	20.30	0.18	11.60	0.00	0.36	9.80	1.75
38.01	3.60	16.35	20.16	0.26	11.47	0.06	0.38	9.69	1.76
37.93	4.48	15.73	20.34	0.18	11.37	0.01	0.26	9.71	1.79
37.43	4.88	16.90	19.70	0.19	10.57	0.07	0.40	9.86	1.86
Average ( $\pm 1\sigma$ )									
38.12	3.86	16.10	19.65	0.17	12.03	0.05	0.37	9.66	1.64
0.33	0.40	0.30	0.54	0.07	0.62	0.04	0.12	0.22	0.12

FeO\* = total iron;  $\pm 1\sigma$ : standard deviation.

these thin biotite-rich layers is an additional criterion which suggests a dominantly aerial transport of the pyroclastic material because dominant hydrodynamic transport would have efficiently segregated the morphologically very different pyroclastic crystals.

Our samples T186 (base of the road bank) and T185 (Fig. 2) have been submitted to the usual procedure for mineral separation using water sedimentation, dry-sieving, magnetic and heavy liquids separation and fractionation; the latter work has been

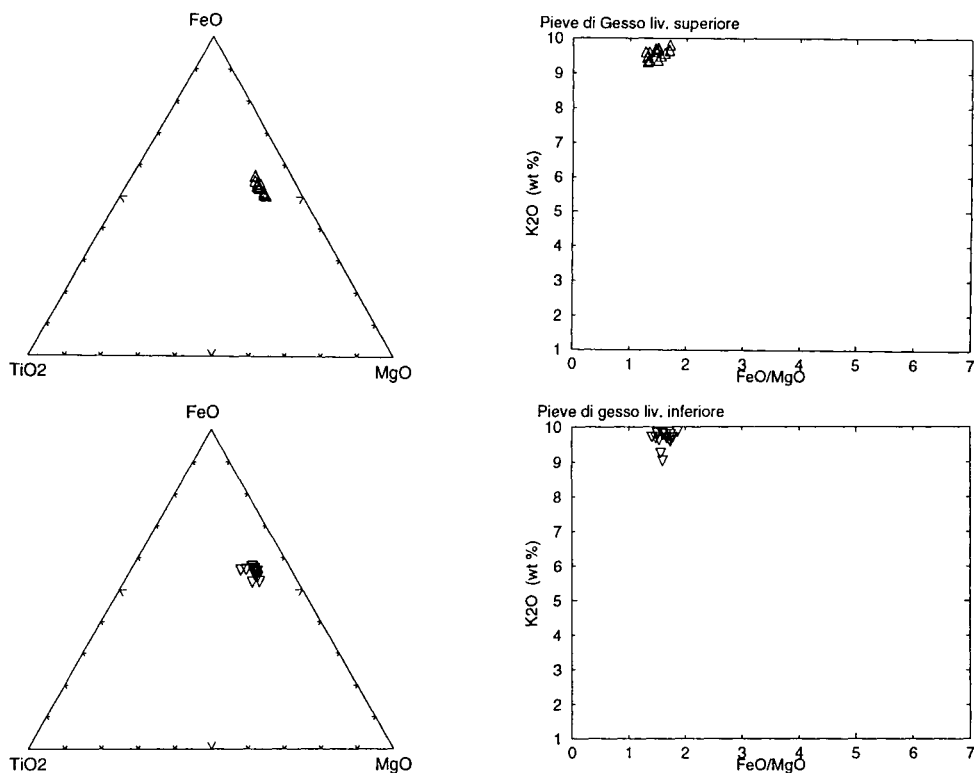


Fig. 3. Geochemical homogeneity of the biotite flakes purified from Pieve di Gesso (T186 lower layer, T185 upper layer). Note that the upper layer may be qualified as homogeneous but a few flakes from the lower layer have slightly less potassium than the others. This may be compared to the fact that the step-heating age spectrum for the upper layer shows a good plateau, while there is only a pseudo-plateau for the lower layer. (Original data by FT.)

monitored according to systematic and synchronous X-ray diffraction analyses for recognition of the most promising phases.

The two samples comprise a variety of pyroclastic minerals including diversely preserved biotite crystals (up to 90% versus whole-rock, WR), abundant plagioclase, rare and elongated apatite and zircon crystals suggesting a restricted submarine transportation (if any). The sampled sediments also contain muscovite, internally pyritized microforaminifers, and organic phosphate (including a fish tooth in T186) pointing to a triple origin (volcanic, detrital, and marine). In addition, diagenetic pyrite is also common.

The biotite fraction heavy in bromoform was first gently crushed in acetone and sieved (mesh 0.16 mm), then purified by hand-picking especially for sample T185 where a few % of the idiomorphic hexagonal flakes with a red colour was removed from the generally dark brown ones. X-ray diffraction patterns denote absence of alteration and well closed structure with (001) reflection at 10.03 and 9.99 Å for samples T185 and T186, respectively.

Due to the possibly mixed origin of the sediment (presence of suspected muscovite), a study of the geochemical homogeneity of the biotite flakes was undertaken. We

used the electron dispersive microprobe technique (Philips' SEM-EDS instrument) on polished surfaces and adopted the approach pioneered by Montanari (Montanari, 1988; Odin et al., 1991). The results (Table 2 and Fig. 3) for T185 are (1) that K content is large (9.66%  $K_2O$ ) and homogeneous with no alteration (K loss), and (2) that Mg, Fe and Ti contents are reasonably homogeneous. For biotite T186, K content is even greater as a mean (9.66%  $K_2O$ ) but two flakes of 15 are very slightly altered; Fe and Mg contents are more homogeneous than in T185 but the Ti content is significantly greater for three flakes of 15 in this sample.

If one removes those three flakes from T185, the mean Ti content becomes similar to that in T186. The biotite phase from the upper layer T185, shows a FeO/MgO ratio (1.45) smaller than the one from the lower layer T186 (1.63) suggesting two distinct eruptive events. However, because these ratios are near each other, taking into consideration the analytical error bars, this suggests a common, slightly evolving source compared to biotite phases from other Miocene volcanoclastic layers (the FeO/MgO ratio is 1.03 in the Serravallian Sicilian biotite from Monte Giammoia (Chapter D3) and 3.52 in the late Messinian biotite from Maccarone in the Marche Province (Chapter E10).

The overall geochemical homogeneity of the biotite selected for dating suggests both a volcanic origin of the mineral and, furthermore, a single volcanic event feeding the depositional unit in T185 and a possibly less obvious quality for T186.

The plagioclase fraction of T186 was selected using a series of bromoform-acetone mixtures and ultrasonically cleaned for 20 min using a nitric-acetic acid mixture. The obtained crystals were mostly transparent and about 0.1 mm in size. X-ray diffraction patterns indicate only a small proportion of quartz and a dominantly anorthitic composition.

#### <sup>40</sup>Ar/<sup>39</sup>Ar isotopic study

Two biotite and one plagioclase separates were analyzed by the <sup>40</sup>Ar/<sup>39</sup>Ar technique. The samples were irradiated in the Triga reactor in Denver together with a dozen of subsamples of the biotite HD-B1 monitor. This monitor has a recommended K-Ar age of 24.21 Ma according to Hess and Lippolt (1994). The isotopic ratios were measured using the usual procedure developed in Lausanne (Cosca et al., 1992).

Sample T186 biotite (3.48 mg) was heated for seven independent heating steps following preliminary heating in vacuum at 450°C for 10 min. The calculated integrated age is 7.34 Ma. The age spectrum indicates (Fig. 4 and Table 3): (1) younger apparent ages at low and high temperatures; (2) a small but significant (95% confidence level) difference of age between steps at 1000°C and 1050°C versus those at 1100°C and 1200°C pointing to an absence of a true plateau especially due to the heating step at 1100°C with a comparatively old age at 7.58 Ma; (3) a weighted mean age of  $7.47 \pm 0.08$  Ma ( $2\sigma$ ) for the four main steps (a near plateau) which includes 81.8% of the total <sup>39</sup>Ar released.

Sample T186 plagioclase (32.4 mg) was degassed for 10 heating steps (Table 4) following heating under vacuum at 600°C for 25 min. The resulting age spectrum (Fig. 5) shows a series of apparent ages between 8 Ma and 9 Ma followed by increasing apparent ages at higher temperatures (1250°C and 1560°C). The calculated integrated

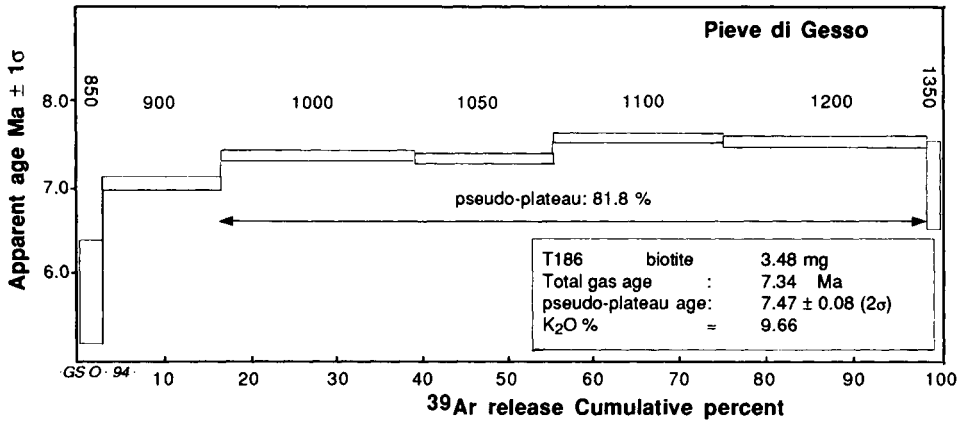


Fig. 4. <sup>40</sup>Ar/<sup>39</sup>Ar age spectrum for sample T186 biotite.

Table 3

Results of <sup>40</sup>Ar/<sup>39</sup>Ar step heating measurements on biotite T186 (3.48 mg) from Pieve di Gesso (by GSO in Lausanne)

°C	Apparent age (Ma)	±2σ	% <sup>39</sup> Ar	%rad.	K/Ca
750	5.7	1.2	2.9	4	6.2
900	7.06	0.16	13.6	40	20
1000	7.37	0.12	22.5	50	30
1050	7.33	0.12	16.4	60	32
1100	7.58	0.10	19.8	75	
1200	7.51	0.10	23.1	70	
1350	7.1	1.0	1.8	8	

°C = heating temperature. Irradiation ULRD 5, preheating 450°C for 10 min.

apparent age at 10.2 Ma (analytically similar to an age measured using the conventional isotope dilution technique) is higher than the biotite age and of no geological meaning.

Sample T185 biotite (92.6 mg) was degassed in twelve heating steps (Table 5) following heating under vacuum at 450°C for 10 min. The age spectrum (Fig. 6) is essentially flat for temperatures above 750°C. A good plateau age (more than three successive heating steps with similar analytical ages using 2σ error bars) can be calculated at 7.37 ± 0.06 Ma (2σ); this is the weighted mean age of eight steps including 87.7% of the <sup>39</sup>Ar released. That plateau age is near but slightly higher than the integrated (total gas) age at 7.20 Ma (error bar at about ±0.05 Ma).

### DISCUSSION AND CONCLUSIONS

Lithostratigraphic criteria useful for correlating the incompletely exposed Pieve di Gesso section with those already studied to the east (Vai et al., 1993) are: (1) the spacing of the dysoxic to anoxic layers; (2) the stratigraphic distance from the 'Calc-care di base' datum level; and (3) the first occurrence of a biotite-rich horizon. The

Table 4

Results of  $^{40}\text{Ar}/^{39}\text{Ar}$  step heating measurements on plagioclase T186 (32.4 mg) from Pieve di Gesso (data by GSO Lausanne)

°C	Apparent age (Ma)	$\pm 2\sigma$	% $^{39}\text{Ar}$	%rad.	K/Ca
750	7.4	0.4	12.8	14	0.19
900	8.5	0.2	14.1	64	0.087
1013	9.1	0.1	23.3	73	0.083
1085	8.3	0.2	14.9	75	0.094
1175	8.4	0.2	13.4	39	0.106
1250	11.4	0.4	6.5	42	0.085
1350	14.6	0.3	9.4	56	0.075
1440	24.2	0.7	3.6	50	0.050
1500	28.8	1.4	1.7	49	0.043
1560	21.6	5.0	0.5	9	0.056

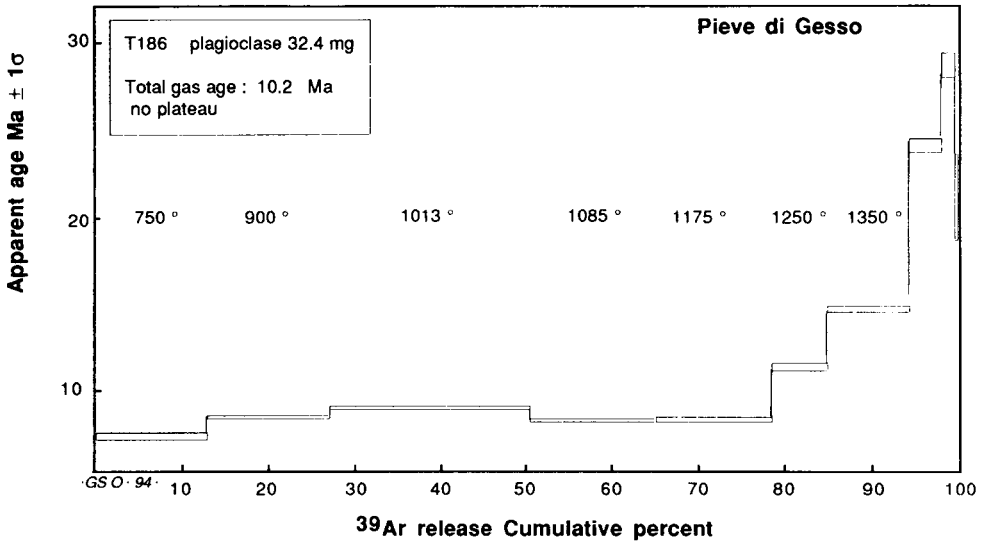


Fig. 5.  $^{40}\text{Ar}/^{39}\text{Ar}$  age spectrum for sample T186 plagioclase.

section corresponds to part of the pre-*conomiozea* wide-spaced anoxic interval, clearly distinguished from the overlying narrow-spaced ones in the eastern sections (Vai et al., 1993). In fact, only four dark-grey, partly anoxic, shaly layers are found here between the two dated samples, with a large portion of the interval characterized by reddish to maroon dysoxic pelites interlayered with the usual grey ones in agreement with observations in the lower part of the Monte del Casino I section (Vai et al., 1993).

The interval between samples T186 and T185 is about 8.5 m. The total thickness up to the 'Calcare di base' is slightly less than 50 m, to be compared to about 40 m totalling the distance from the first biotite-rich layer to the 'Calcare di base' in the Monte del

Table 5

Results of  $^{40}\text{Ar}/^{39}\text{Ar}$  step heating measurements on biotite T185 (92.6 mg) from Pieve di Gesso (data by GSO in Lausanne)

°C	Apparent age (Ma)	$\pm 2\sigma$	% $^{39}\text{Ar}$	%rad.	K/Ca
650	2.0	0.5	2.8	3	5
750	6.3	0.2	1.0	23	34
850	7.32	0.08	8.0	60	60
925	7.39	0.08	9.4	73	67
975	7.42	0.06	8.2	79	66
1025	7.36	0.08	13.4	77	72
1065	7.34	0.06	13.7	83	117
1100	7.38	0.06	12.5	87	106
1140	7.34	0.06	17.1	88	107
1170	7.4	0.3	6.3	93	61
1230	7.36	0.06	7.2	83	71
1300	7.1	0.2	0.6	29	

Step 1170°C is technically dubious due to gas lost during analysis (the apparent age is a maximum one). Preheating 450°C for 10 min under vacuum.

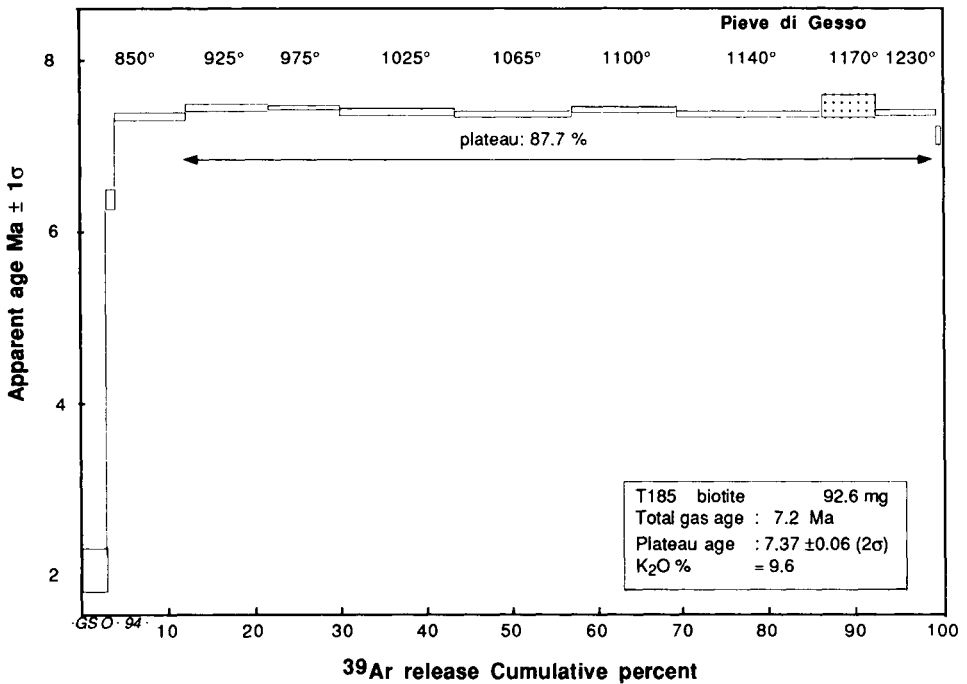


Fig. 6.  $^{40}\text{Ar}/^{39}\text{Ar}$  age spectrum for sample T185 biotite.

Casino–Monte Tondo area. Assuming a simultaneous occurrence of the first biotite-rich layer in the two nearby areas, the resulting 20% increase of the sedimentation rate would be consistent with (1) the regional increase of thickness of the Marnoso-arenacea

turbidite body NW-ward, (2) the regional pinch-out of many arenaceous turbidite layers SE-ward (Ricci Lucchi and Valmori, 1980), and (3) the local occurrence of faint, fine-grained turbidites in the Pieve di Gesso western (relatively depressed) area at higher stratigraphic levels as compared with the eastern (relatively raised) area.

The abrupt occurrence of volcanoclastic layers in about ten previously studied sections appears quite well confined within or close to the short biostratigraphic interval between *G. humerosa* (and/or *G. suterae*) and *Amaurolithus* sp. first occurrences. The local survey has shown that the first biotite-rich layer is found at sample T186; *Amaurolithus* sp. occurs immediately beneath; *G. praemargaritae* and *G. humerosa* are present in the upper T186–T185 interval together with *Amaurolithus* sp. Therefore, an assignment of both T186 and T185 layers to the ‘first cluster’ of similar horizons described by Vai et al. (1993) appears quite appropriate. Assignment to the second cluster cannot be excluded and closer correlation of individual layers on the base of pure biostratigraphic and field lithostratigraphic data is still difficult (Vai et al., 1993, p. 1411).

The separated phases appear reliable geochronometers according to their location in dominantly volcanogenic layers; the actual significance of the layers is not well understood, but we suspect a near contemporaneity between volcanic eruption and inclusion in the sedimentary succession and no mixture with extraneous pyroclastic components. Biotite shows a good shape, favourable X-ray diffraction patterns, generally good homogeneity and high K content. T185 biotite appears a priori better than T186 biotite concerning these criteria.

Geochronologically, the two successive layers give apparent ages at 7.47 ( $\pm 0.08$  Ma, pseudo plateau) and 7.37 ( $\pm 0.04$  Ma, excellent plateau). According to the age spectra and overall quality of the selected flakes, this is most probably representative of their respective crystallization age. The very good internal consistency of the apparent ages calculated from the heating steps measured for T185 and the external consistency of the two biotite separates versus the stratigraphical relation ( $7.47 \geq 7.37$ ) is an additional criterion for the geological meaning of the measured ages.

The comparison between the plagioclase and the biotite ages for sample T186 emphasizes both the inappropriate nature of the particular plagioclase separate as a geochronometer and the probable incorporation of extraneous argon in the mineral at the time of crystallization or eruption.

The analytically precise ages of the biotite separates are related to the accepted value of 24.21 Ma for the monitor allowing calibration of the neutron flux. However, the actual age of HD-B1 is known with an error bar ( $\pm 0.6$  Ma or  $\pm 2.6\%$  of the age,  $2\sigma$ ) which should be propagated to the analytical age to derive realistic geological ages comparable to data obtained using other monitors or analytical techniques and methods. Accordingly, the radioisotopic ages of biotite from T186 and T185 are  $7.47 \pm 0.28$  and  $7.37 \pm 0.26$  Ma ( $2\sigma$  interlaboratory), respectively.

Comparison with the study by Vai et al (1993) can be made via the proposed respective stratigraphic position of the dated layers. The new  $^{40}\text{Ar}/^{39}\text{Ar}$  ages obtained from biotite separates from samples T186 and T185 fall within the age range previously found for the group of biotite-rich layers close to the *suterae* FO (K–Ar conventional ages at  $7.29 \pm 0.76$  Ma,  $7.90 \pm 0.58$  Ma, and  $7.75 \pm 0.42$  Ma). The mean age value of this early group of volcanic events located 10 to 13 m below the FO of *G. conomiozea* ( $7.72 \pm 0.30$  Ma) is analytically consistent with our new analytical data. However, the



younger group of volcanic events located about 5 m below the FO of *G. conomiozea* in the Monte del Casino and Monte Tondo sections has a mean age at  $7.35 \pm 0.16$  Ma according to Vai et al. (1993) and is also consistent with our data from the Pieve di Gesso section.

The favourable crystallographical nature, the geochemical homogeneity, and the nearly undisturbed plateau of sample T185 points to an acceptable reliability of the measured ages. The Pieve di Gesso ages indicate that the FO of *G. humerosa* is older than 7.4 to 7.7 Ma in this section and that the FO of *Amaurolithus* sp. is about this age; this conclusion is not analytically distinct from that obtained from the previously dated sections and confirms that the Tortonian/Messinian boundary is older than 7 Ma.

#### SOMMAIRE — STRATIGRAPHIE INTÉGRÉE DU PROFIL TORTONIEN SUPÉRIEUR DE PIEVE DI GESSO (ROMAGNE, ITALIE)

(Manuscrit soumis: Février 1994; révisé: Février 1995; rédacteur responsable: GSO)

Nous avons travaillé sur la première section de la région de Faenza (Romagne, Italie) dans laquelle des niveaux volcanoclastiques ont été identifiés autour de la limite Tortonien/Messinien. Par comparaison lithostratigraphique et étude biostratigraphique, deux niveaux riches en biotite ont été localisés au sommet du Tortonien. L'étude géochronologique a d'abord permis de caractériser ces niveaux à biotite; ce sont des turbidites — c'est à dire des dépôts secondaires — renfermant encore plagioclase, apatite et zircon; la biotite est bien préservée et géochimiquement homogène. Les analyses isotopiques ont utilisé la technique  $^{39}\text{Ar}/^{40}\text{Ar}$  avec chauffage par étape appliquée à deux échantillons l'un avec plagioclase et biotite, l'autre avec biotite seule. Le spectre d'âge perturbé du plagioclase a révélé que ce géochronomètre n'était pas favorable. La biotite correspondante a donné un spectre plus régulier avec presque un plateau (âge  $7,47 \pm 0,08$  Ma). La deuxième biotite a livré un plateau acceptable permettant le calcul d'un âge de  $7,37 \pm 0,06$  Ma (incertitude analytique interne). Ces âges confortent les résultats géochronologiques de Vai et al. (1993) indiquant, pour la base du Messinien, dans sa définition originelle, un âge un peu supérieur à 7,2 Ma.

(Sommaire des auteurs)

#### ACKNOWLEDGEMENTS

The radiometric measurements were achieved in Lausanne thanks to the facilities made available in the Institute of Mineralogy by the Swiss National Funds. No funding was provided by French organizations for this research.

Chapter E3

**CYCLOSTRATIGRAPHIC ESTIMATE OF THE MESSINIAN STAGE  
DURATION**

G.B. Vai

INTRODUCTION

The duration of the Messinian Stage (Mayer, 1867, 1868; Selli, 1960) has fascinated a generation of geologists, especially when, in the early 1960s, some radiometric dates and the first magnetostratigraphic calibrations suggested a remarkably short time interval for this peculiar stage which is characterized, in the Mediterranean domain, by a pervasive 'salinity crisis' (Selli, 1960). An even shorter interval was estimated by Ogniben (1957, pp. 226–229) who used the classical cyclostratigraphic tool, the interpretation of evaporitic sediments laminated as varves. He estimated that the Messinian evaporitic formations in Sicily (i.e., the Tripoli, the Calcare di base, and the Gessi) accumulated in about 120 ka, 95 ka, and 500 ka, respectively (altogether from about 500 ka for the 'gypsum–sulphur' facies to about 900 ka for the 'gypsum–salt' facies; Ogniben, 1957). The estimate appeared considerably shorter than the chronologic estimates available at that time.

An important contribution to the definition of the problem came from the largely unexpected results of the DSDP leg 132 (Hsü et al., 1973, 1978; Adams et al., 1977). Since the very beginning, the dating of these samples was approached mainly in terms of correlation with oceanic geomagnetic polarity zones, and their chronometric calibration (Ryan et al., 1974; Berggren et al., 1985; Hsü, 1986b). This approach is especially appropriate here because other conventional tools used for estimating the durations of chronostratigraphic units (such as evolution rate, number of biozones, sedimentation rate, etc.) seemed unsuitable for the Messinian case. According to Hsü (1986b), "the Messinian Stage lasted about a million years. The salinity crisis had an even shorter duration of about half a million years, spanning the time interval from about 5.7 to 5.2 m.y. B.P."

Following the pioneering work of Emiliani (1966) and Shackleton and Opdyke (1973), in the last decade or so, significant advancements have been made in the establishment of an astronomy-based time scale derived from cyclic patterns observed on Pleistocene and Pliocene sedimentary successions. These were studied both in exposed sections and in subsurface (mainly oceanic) continuous cores (Berger, 1976, 1977; Hays et al., 1976; Imbrie and Imbrie, 1980; Ruddiman and McIntyre, 1981; Berger, 1984; Pisias and Shackleton, 1984; Ruddiman et al., 1986; Berger and Pestiaux, 1987; Hilgen, 1987, 1991a, b; Hilgen and Langereis, 1988, 1993; Shackleton et al., 1990, 1992; Berger and Loutre, 1991; Tiedemann et al., 1992). Attempts have also been made at extending this kind of time-scale analysis down to the early Messinian and

Tortonian, in similar sedimentary sequences exposed beneath the Messinian evaporites in the Mediterranean area (e.g., Krijgsman et al., 1994).

It is surprising that, as far as I know, after Ogniben's (1957) pioneering effort, no modern attempt has been made to use a cyclostratigraphic approach for the problem of the Messinian Stage duration. This is even more surprising if we consider the remarkable cyclic pattern of various formations within the Messinian, as noted by many authors (Selli, 1954; Ogniben, 1957; Vai and Ricci Lucchi, 1977; Colalongo et al., 1978; Casati et al., 1978; etc). However, to expect a reliable estimate for the duration of a chronostratigraphic unit on the basis of its cyclostratigraphic patterns, at least some direct geochronometric calibration points within an updated biostratigraphic and magnetostratigraphic correlation frame are needed. This is the primary reason why I have initiated a cooperative campaign of geochronometric research around the Tortonian/Messinian boundary.

The Northern Apennine stratigraphic sections provide excellent biostratigraphic resolution, and direct radiometric dates supporting an age of  $7.11 \pm 0.20$  Ma for the Tortonian/Messinian boundary (Vai et al., 1993; Odin, 1994). The magnetostratigraphic record in these sections is still incomplete but promising analytical work is currently in progress (see Chapter E4).

The aim of this chapter is to show the cyclostratigraphic potential of the Northern Apennine sections across the late Tortonian/early Messinian transition, and during a large part of the Messinian, and to discuss some of the sedimentary, radiometric, cyclic, and magnetostratigraphic constraints bearing on the possible duration of the Messinian Stage and of its component intervals (e.g., the evaporitic Messinian comprising the time interval of the Messinian salinity crisis s.str.).

#### CYCLOSTRATIGRAPHY OF THE MESSINIAN (NORTHERN APENNINES)

The peri-Adriatic Messinian (Fig. 1) is subdivided into three main intervals: a pre-evaporitic, an evaporitic or hyperhaline, and a post-evaporitic or hypohaline interval. This facies triplet is reflected in the three main lithostratigraphic units called: (1) euxinic shales; (2) Gessoso-Solfifera Formation; (3) Colombacci Formation, including several more or less locally distinct members. Cyclic patterns, developed at different hierarchic scales, characterize the three intervals as compared with the overlying (Pliocene), and immediately underlying (Tortonian) sequences (Selli, 1954, 1973; Borsetti et al., 1975; Vai and Ricci Lucchi, 1977; Colalongo et al., 1978; Savelli and Wezel, 1979; Cremonini and Farabegoli, 1982; Cremonini and Marabini, 1982; Marabini and Vai, 1985; Vai, 1988).

Similar cyclic patterns are found in the peri-Ionian and Sicilian Messinian, where three main lithostratigraphic units are also distinguished: (1) the Tripoli Formation and its equivalents; (2) the 'Gessi Inferiori' formation (in both sulphur-rich and salt-rich facies) and its equivalents; (3) the 'Gessi Superiori' and Arenazzolo Formations, and their equivalents (Ogniben, 1957; Roda, 1965; Decima and Wezel, 1971; Richter-Bernburg, 1973; Selli, 1973; Mascle and Heiman, 1978, McKenzie et al., 1979; Decima et al., 1988; Grasso et al., 1990; Grasso and Pedley, 1990; Pedley and Grasso, 1993; Grasso and La Manna, 1993).

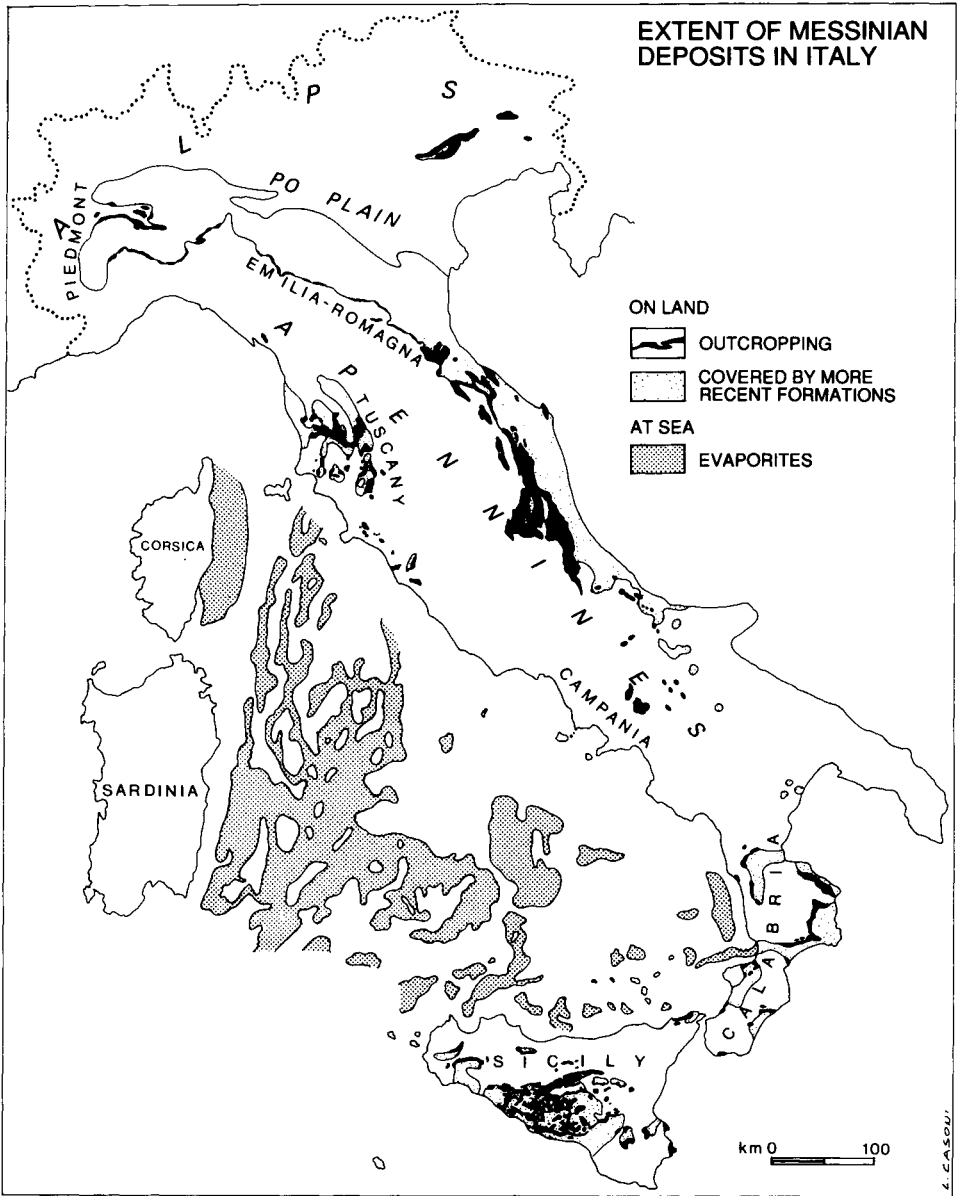


Fig. 1. Surface and subsurface extent of the Messinian deposits in Italy, with location of the major areas referred to in the text.

*The euxinic shale formation*

Historically known as ‘ghiola or Formazione di Letto’ (informal and incorrect names), this unit consists of transgressive pelagites overlapping different kinds of deposits, from transitional deltaic to deeper turbiditic and hemipelagic ones (Vai and

Castellarin, 1993). The term 'shale' is used to emphasize the prominent laminitic character of the unit, although the rock presents a low degree of induration. Regional equivalents in the Central and Southern Apennines are called 'Marne a Pteropodi', 'Marne Tripolacee', Tripoli Formation, or bear the name of local formations. In spite of apparently conspicuous facies segmentation (from black shales, to yellowish marls, to white 'tripoli'-like laminites), the maximum thickness of this sequence (about 30 to 50 m) is remarkably constant over large areas, and the palaeoenvironmental conditions are equivalent (mainly pelagic, more or less anoxic, starved basins). This unit represents a marine flooding event apparently synchronous across large areas of the Mediterranean, and was followed by a short-lived high stand of sea level, which is also recorded world-wide in the eustatic curves of Haq et al. (1988). This time interval within the Mediterranean is tectonically quiet, with a trend to increasing and propagating rifting conditions, suddenly inverted by the intra (late)-Messinian compressional event (Marabini and Vai, 1985; Vai, 1988; Patacca and Scandone, 1989; Patacca et al., 1992).

The cyclic stratigraphic pattern of this unit in the Northern Apennines has been previously neglected. Sedimentary cyclicity was first documented in detailed sections by Vai et al. (1993). A partially related palaeobiological cyclicity controlled by alternating palaeo-oceanographic conditions was also recognized from planktic foraminiferal assemblages (Calieri, 1992) showing a fine agreement with similar studies made in Sicily (R. Sprovieri pers. commun., 1992), and a good correlation with stable isotope cyclicity derived from oceanic cores (Vincent et al., 1985; Keigwin et al., 1987), and intra-Mediterranean sections on land (e.g., Van der Zwaan and Gudjonsson, 1986). Beside the original cyclic investigations by Ogniben (1957), a few studies on the sedimentary cyclicity of the Tripoli Formation in Sicily have been published (McKenzie et al., 1979; Grasso et al., 1990; Grasso and Pedley, 1990; Pedley and Grasso, 1993). Much more advanced are cyclostratigraphic studies of equivalent units in Greece, especially in Crete (Krijgsman et al., 1994). There, the integration of visual cycle counting with detailed palaeomagnetic analyses provided a suite of sections correlated with the same detail and reliability as in the Plio-Pleistocene surface exposures (Hilgen, 1987, 1991a, b; Hilgen and Langereis, 1993), and oceanic cores (Ruddiman et al., 1986; Shackleton et al., 1990, 1992; Tiedemann et al., 1992).

The preliminary results of our investigations show that the basic cyclic couple (light mudstones versus dark pelitic laminites) can be recognized throughout most of the euxinic shale formation, given appropriate wetness and lighting conditions (Fig. 2). Cycle counting in the field, however, may be hampered by strong lateral variations in colour and other cyclic features of this formation. Nevertheless, a conservative provisional recognition of slightly less than 40 cycles in the time interval between the first occurrence of *Globorotalia conomiozea* and the *Neogloboquadrina acostaensis* left to right coiling (L/R) inversion can be made (or possibly about 50 cycles up to the base of the gypsum evaporites, implying that the onset of the evaporites is coeval, at least across the peri-Adriatic basin). Some additional 20 cycles can be recognized downwards between the FO's of *G. conomiozea* and *G. suterae*, where this cyclicity vanishes (Figs. 2 and 3). These figures probably represent minimum values, and were reached using the assumption that the cycle spacing recognized in the Monte Tondo section can be transferred to the equivalent portions of the Monte del Casino section, where the colour pattern is less pronounced.

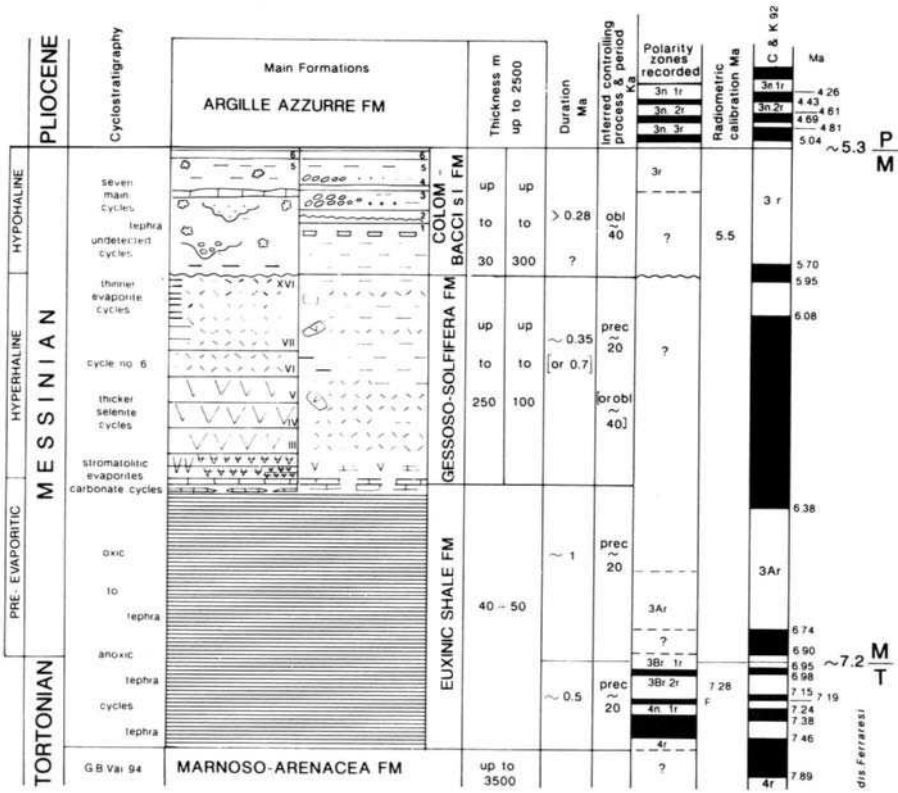
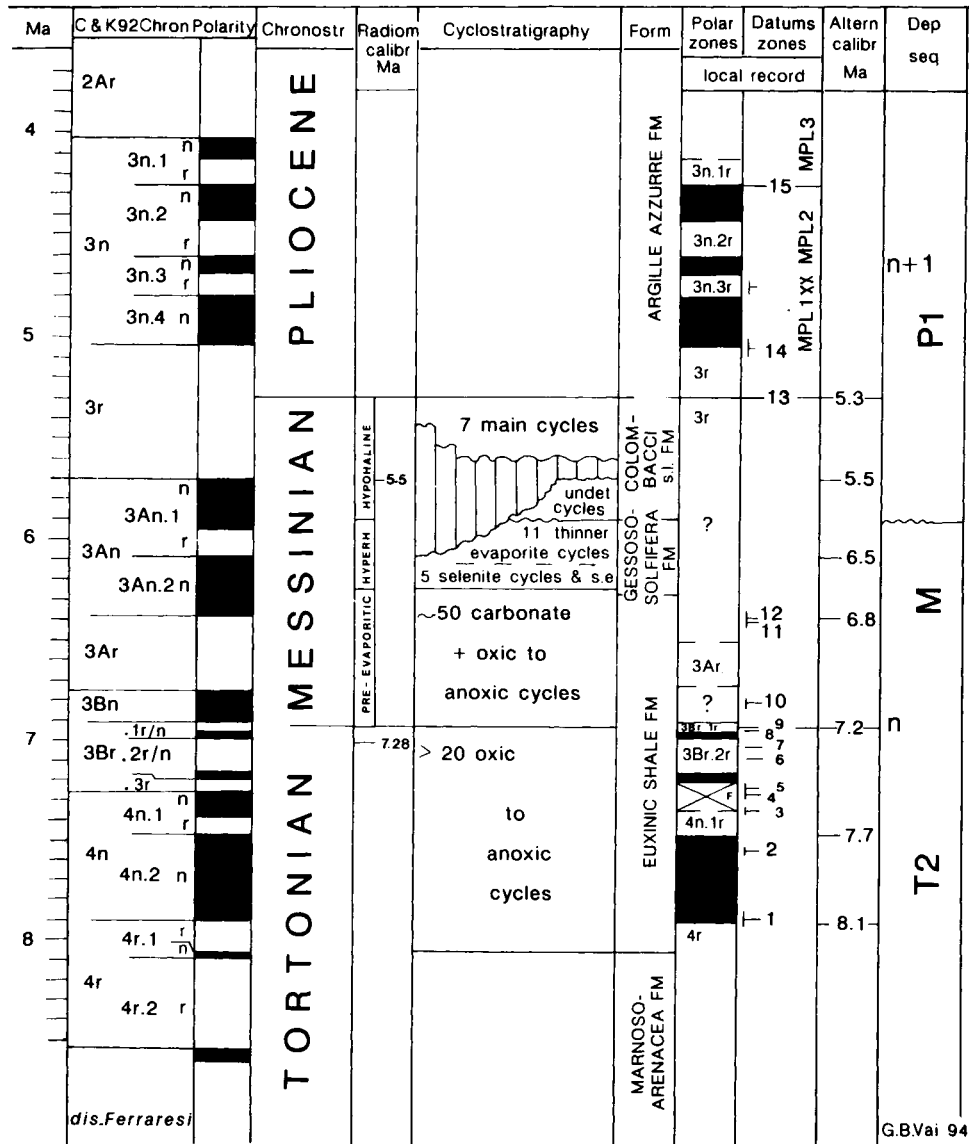


Fig. 2. Schematic lithostratigraphic framework of the Messinian formations in the Romagna Apennines.

In the Monte del Casino section, approximate rates of sedimentation have been calculated. Depending on some uncertain radiometric age determinations, the possible sedimentary rates range from 10–15 m/Ma to 30–60 m/Ma, the second figure being much more tenable. In fact, an independent cross-check based on the thickness of some polarity inversions in the range of the late Tortonian suggests sedimentation rates around 30–40 m/Ma (Figs. 2 and 3).

It can be confidently assumed that the sedimentation rate in the studied sections remained fairly constant during the time interval from slightly before the FO of *G. suterae* to the *N. acostaensis* L/R inversion. This assumption is based on the following observations. The facies does not change except for a relative increase of the dark laminated versus the lighter mudstones upwards. This is supported by the rather scarce benthic foraminifera, and by the abundant pteropods and pelagic bivalves present throughout the entire interval. This pelagic faunal component remains practically unchanged until just above the *N. acostaensis* L/R inversion. It seems, therefore, that the evaporative drop in sea level, and the related rapid shallowing, took place only in the last 5 to 10 m of the pre-evaporitic Messinian, after the *N. acostaensis* L/R inversion. Moreover, the fairly constant thickness of the observed lithologic cycles, especially during the interval bracketed by the FO's of *G. conomiozea*–*Globigerina multiloba*,



G.B.Vai 94

Fig. 3. Cronostratigraphic framework of the Messinian formations and marine depositional sequences (Northern Apennines). Direct biostratigraphic datums, magnetostratigraphic chrons and subchrons, and radiometric dates available from the Romagna Apennines are reported (sources: Marabini and Vai, 1988; Calieri, 1992; Vai et al., 1993; Vigliotti, 1988; Chapter E4). Key to datum numbers: 1 = *G. continuosa* LO; 2 = *G. humerosa* FO; 3 = *G. suterae* FO; 4 = *Amaurolithus* sp. FO; 5 = *G. menardi* form 4 FO; 6 = *G. saheliana* FO; 7 = *G. menardi* form 5 FO; 8 = *G. miotumida* FO; 9 = *G. conomiozea* FO; 10 = small *Helicosphaera* LO; 11 = *N. acostaensis* (L/R); 12 = *G. multiloba* FO; 13 = *Sphaeroidinellopsis* Acme FO; 14 = *G. seiglei* LO; 15 = *G. puncticulata* FO.

supports a uniformity of the sedimentation rate when the euxinic shale formation was deposited. The apparently thicker cycles in the interval preceding the FO of *G. conomiozea* in these sections are assumed to be clusters of individual cycles, difficult to distinguish in the field, when anoxic conditions were receding. This is easily understood by simple correlation of the two sections in an interval of a few metres just above the FO of *G. conomiozea* (Fig. 4).

With the assumed nearly stable sedimentation rate of about 30 m/Ma, the entire euxinic shale formation would have lasted slightly less than 2 Ma, and the pre-evaporitic Messinian slightly less than 1 Ma. The total number of cycles in the pre-evaporitic Messinian is about 50, which makes a periodicity in the order of 20 ka quite reasonable (Figs. 2 and 3).

Let us consider also the other scenario which, although less preferable, is not excluded by the still uncertain radiometric dates. With an assumed sedimentation rate of about 10–15 m/Ma, the duration of the entire formation would be about, or slightly more than, 3 Ma with a pre-evaporitic Messinian lasting slightly more than 2 Ma. These figures would exceed the total time ever assigned, or available for, the entire Messinian Stage. It seems, therefore, quite difficult to accept such a sedimentation rate, and the corresponding radiometric dates (Vai and Laurenzi, 1994).

In summary, pending further refinement in the radioisotopic age calibration of these sections, it is suggested that the duration of the pre-evaporitic Messinian should be about 1 Ma or slightly less, with a lithologic cyclicity mainly controlled by the orbital precession periods (about 20 ka).

### *The Gessoso–Solfifera Formation*

This formation has gained global recognition after the discovery of the equivalent Messinian Evaporite in the Mediterranean Sea (Hsü et al., 1973), and the related reconsideration of the Messinian salinity crisis (Selli, 1960, 1973; Drooger, 1973; Cita, 1982; Camerlenghi et al., 1983; Hsü, 1986b). The remarkable cyclicity of the sulphate-rich selenitic facies (or Vena del Gesso Basin) in the Northern Apennines was first outlined and discussed in detail by Vai and Ricci Lucchi (1977); a total of 15 to 16 evaporitic cycles was recognized by these authors in the Vena del Gesso Basin (Fig. 5), and correlated in Sicily with the ‘Gessi Inferiori’ Formation. Many intra-Mediterranean evaporitic Messinian sections of similar facies fit in this ideal cyclic model as far as number, composition, recurrence, and overall evolution of the cycles are concerned. The structure and facies sequence of each cycle imply evaporative draw down in sea level, shallowing up to desiccation, increasing concentration of the brines, transition from in-situ growing of V-shaped bottom crystals to prismatic crystals settled from the water column, and eventually cannibalistic reworking of gypsum. Each cycle was followed by flooding of almost normal marine water of possible Indian–Red Sea provenance (Vai, 1988), as suggested also by stenohaline fishes (especially Clididae) recently found in different cycles in the peri-Adriatic area (Sorbini, 1988). These marine floodings appeared to be prominent transgressions which extended to at least the whole eastern Mediterranean, but have lesser amplitudes and a definitely different character as compared to the ‘intra-Messinian transgression’ of Hsü (1986b).

It is still unclear which kind of mechanism controlled the recurrent pattern of





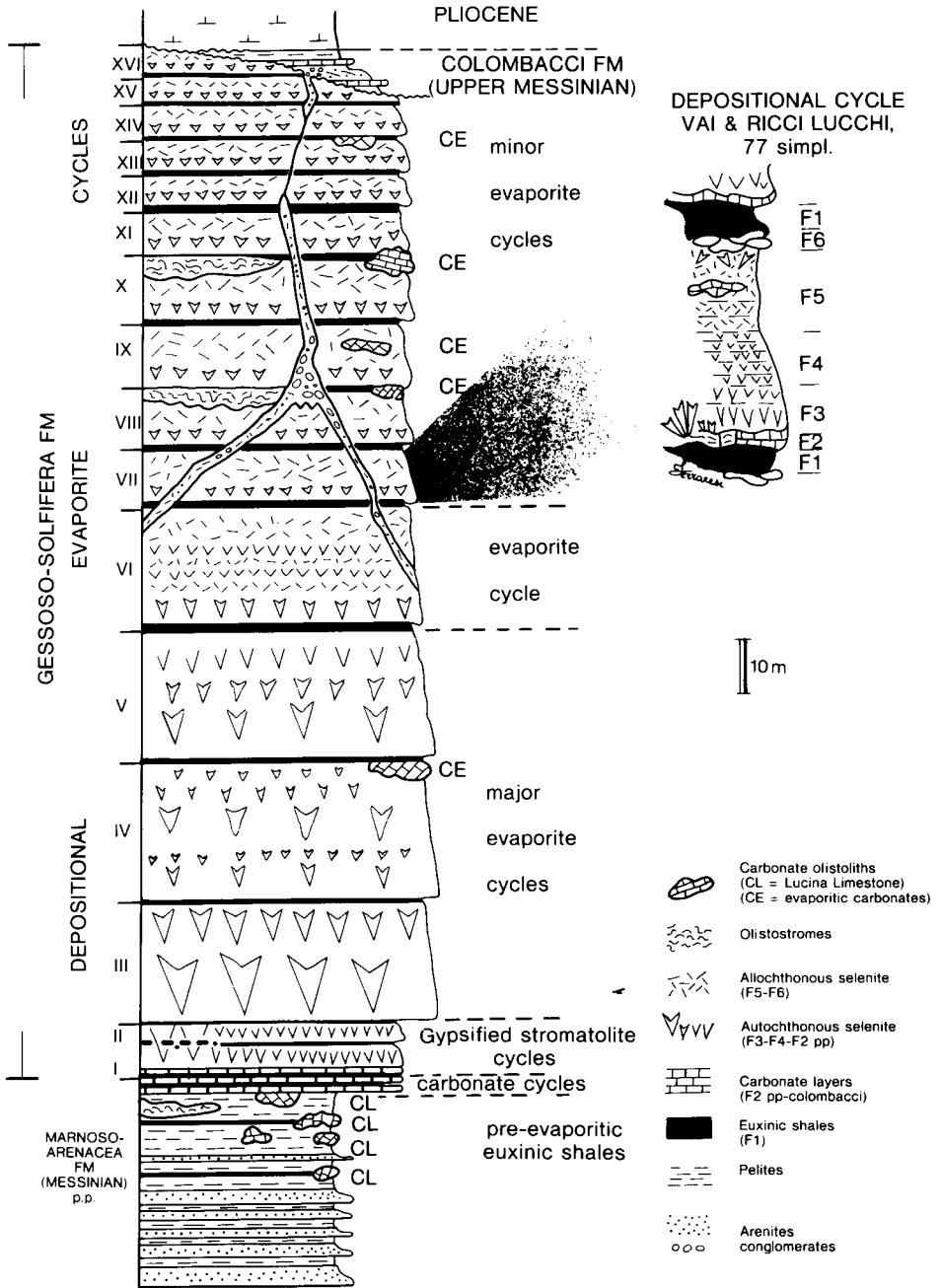


Fig. 5. Cyclostratigraphy of the Gessoso-Solfifera Formation, Vena del Gesso Basin, Romagna Apennines (modified from Vai, 1988).

these important marine floodings. Either moderate sea-level fluctuations over a narrow threshold or repeated tectonic break-down of discrete portions of a wider threshold area may account for it. At any rate, whatever controlling factor is assumed, the cycle synchronism, and the normal marine water type of floodings, seem certain.

Enclosed within this higher-rank cyclicity (tens of metres in wave length) there are at least three further orders of hierarchically shorter cycles: (1) thick laminae (metric wave length); (2) intermediate laminae (decimetric wave length); and (3) thin laminae (centimetric wave length). The smallest laminae are characterized by a relatively continuous axial growth of the V-shaped bottom of gypsum crystals. This growth, at a given time, is abruptly interrupted by a brine-water dilution, recorded by the deposition of a thin drape of mud and gypsum sand over the eroded and leached upper crystal edges.

The problem now is to recognize the process responsible for such different frequency levels in cyclicity. The only general assumption which can be made is that common allocyclic processes may be responsible for the different ranks of cyclicity, based on the great uniformity of these evaporitic cyclic patterns in the Mediterranean area. If we assume that the thin, elementary laminae have a seasonal control (alternating dry-warm crystal growth versus wet-cool break and relative dilution), the total duration per individual gypsum megabed will be on the order of some thousands of years. On the other hand, recalling that the duration of the Gessoso–Solifera Formation is an unknown fraction of the entire Messinian Stage (for instance, about 1/3 of the total or less than about 700 ka, see Fig. 3), we would get a possible theoretical duration of about 40 ka per megabed, which is the mean period of the orbital obliquity (also often recognized as one of the controlling factors of lithological cycles, especially in the glacial Pleistocene). However, is the resulting difference between some (3 to 5 ka) and 40 ka true or apparent? It should be apparent, because in the first case we have considered only the autochthonous facies of the gypsum megabed, whereas in the second case all the cycle components (including euxinic shales, stromatolitic limestone, and the reworked gypsum–mudstone interval) have been summed up.

From this comparison one can argue that the growing time of the autochthonous gypsum (in an individual megabed or in the entire Gessoso–Solifera Formation) is about 1/10 of the time required for the deposition of the corresponding complete cycle or cluster of cycles (Fig. 5). As a whole, one could also infer that the fraction of the Messinian time to be assigned to the evaporitic formation may be even shorter than 1/3 as assumed above (Fig. 3). In this case, the first-order evaporitic cycles of the Vena del Gesso Basin could be related to astronomical cycles of the precessional type (about 20 ka, see Fig. 3).

In conclusion, when the cyclicity of the Gessoso–Solifera formation in the Vena del Gesso type of evaporites is synchronous and astronomically controlled, two possible scenarios for the duration of the evaporitic Messinian can be suggested: either about 350 ka or about 700 ka, respectively. This is, of course, a pure working hypothesis to be tested.

#### *The Colombacci Formation s.l.*

The Colombacci Formation reflects a major palaeoclimatic change almost concurrent with, but independent from, an important compressional tectonic phase in many parts of the Mediterranean. This formation represents the hypohaline, alkaline-rich

Lagomare-type Messinian interval (Selli, 1954, 1973; Colalongo et al., 1978; Casati et al., 1978). The Colombacci Formation is still a response to the Messinian salinity crisis, even more schizoid in the peri-Adriatic regions, characterized by increasing fresh-water influx (Paratethyan realm), whereas the peri-Tyrrhenian areas still contain thick gypsum evaporites (the Sicilian 'Gessi Superiori' and equivalents). The main climatic signature of the Colombacci Formation is represented by cooler and definitely humid conditions as suggested by the occurrence of *Sciadopitys*, a tree of the present oceanic coastal forest requiring about 6 m of annual rainfall (Bertolani Marchetti and Marzi, 1988; Vai, 1988). The cyclic deposition of the Colombacci Formation was thoroughly investigated by Colalongo et al. (1978), Casati et al. (1978), and Cremonini and Farabegoli (1982). They have recognized up to eight cycles (with six Colombacci layers) following an interval lacking of cyclic evidence (the so-called 'Formazione di Tetto') (Fig. 6). This cyclicity is also clearly shown by palynological investigations (Bertolani Marchetti and Marzi, 1988; Bertini, 1992) in which relevant climatic oscillations are revealed by the pollen curves.

According to Marabini and Vai (1988) and Vigliotti (1988), the upper cycles of the Colombacci Formation are enclosed within the C3r reversed chron (Figs. 2 and 3) bridging the Messinian/Pliocene boundary. Following the Cande and Kent (1992) scale, this polarity interval should last about 660 ka (from 5.705 Ma to 5.046 Ma). Marabini and Vai (1988, p. 45) have suggested that the prominent climatic character of the six major Colombacci cycles (Fig. 6) might be controlled by an astronomical cycle of about 100 ka (orbital eccentricity), implying a duration of about 600 ka for this part of the formation. This assumption, however, is in conflict with the fact that at least 1/3 of the Colombacci Formation belongs to the C3r chron totalling a duration of about 660 ka, of which about 150 ka are assigned to the Pliocene (Hilgen and Langereis 1993). Therefore, no time would be available to accommodate the sedimentation of the initial, non-cyclically developed part of the Colombacci Formation s.l., and for the intervening, very important intra-Messinian tectonic phase (Marabini and Vai, 1985; Patacca and Scandone, 1989; Vai, 1989).

An alternative assumption would be to consider rather, that the controlling factor was an astronomical cycle of 40 ka (orbital obliquity). In this way, the cyclic part of the Colombacci Formation would last some 250 ka, leaving a reasonable time interval available. This solution would fit quite well also for the 'Gessi Superiori' formation, unanimously considered as the Sicilian equivalent of the Colombacci Formation. Up to seven major gypsum cycles are recognized within the 'Gessi Superiori' (M. Grasso, pers. commun., 1993) suggesting a total duration of at least slightly less than 300 ka for this unit and the equivalent Colombacci Formation s.l. There are no theoretical objections against a shorter periodicity, such as 20 ka (orbital precession). However, for having a minimum time available for the intra-Messinian (intra-Colombacci Formation s.l.) tectonic phase to develop, the longer period is preferred.

A characteristic volcanoclastic layer is found just beneath the first 'Colombaccio' marker bed from Abruzzi to eastern Romagna (Selli, 1954; Girotti and Parotto, 1969; Carloni et al., 1974a, b; Cremonini and Farabegoli, 1982), and frequent lava flows and ash layers are found in the equivalent Hyblean foreland of Sicily. These are expected to provide soon new radiometric calibration points for the cyclostratigraphic estimates above. A few previous attempts based on fission-track dating on glass from

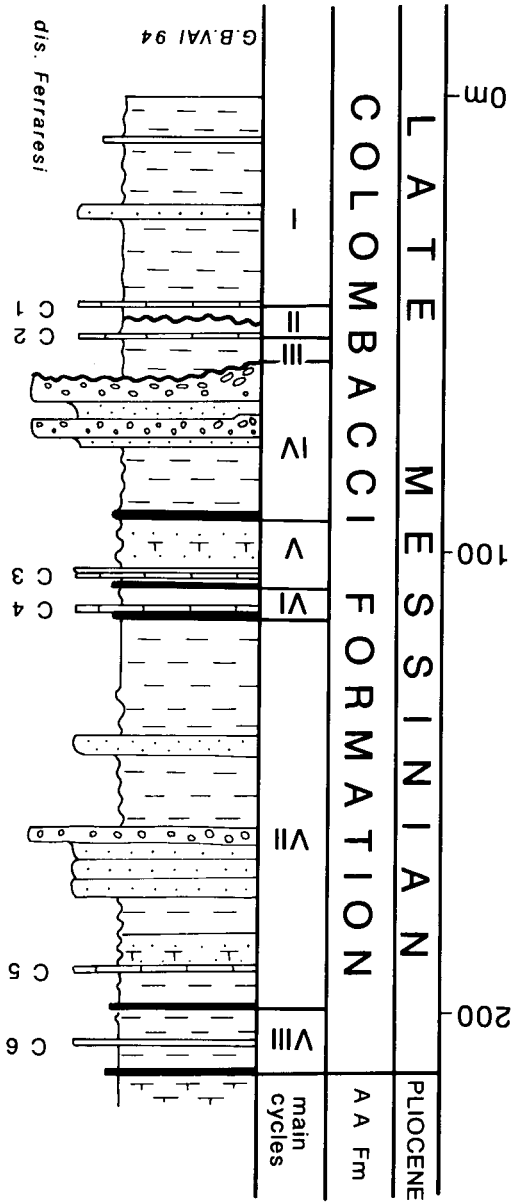


Fig. 6. First-order cyclostratigraphy of the Colombacci Formation s.l., Romagna-Marche Apennines.

the volcaniclastic layer yielded ages of approximately  $5.71 \pm 0.50$  Ma (Bernardes et al., 1986), contrasting with an anomalously younger age obtained by Artas et al. (1981). New  $Ar^{40}/Ar^{39}$  investigations by Odin et al. (Chapter E6) provide biotite ages of  $5.40 \pm 0.06$  Ma and  $5.51 \pm 0.05$  Ma for the same volcaniclastic layer in the Colombacci Formation s.l. in the Maccarone section, near Apiro (Marche region).

## CONCLUSIONS

Three hemipelagic to evaporitic, cyclically developed formations recording most of the Messinian, and spanning continuously both the Tortonian/Messinian and the Messinian/Pliocene boundaries, are well exposed in the Northern Apennines. They can be grouped into two main depositional sequences, the first of which includes the late Miocene portion of the turbiditic Marnoso-Arenacea Formation, and the second the mainly pelagic early Pliocene portion of the Argille Azzurre Formation (Ricci Lucchi, 1986). The two sequences are separated by an unconformity laterally becoming a paraconformity (Figs. 2 and 3), implying a possibly very short (some tens of ka?) undetectable depositional gap even over large parts of the depocentral areas, followed slightly later by a strong compressional tectonic phase in the internal areas of the palaeobasin (Vai, 1988, 1989a).

The cyclicity of the euxinic shale formation was interpreted as possibly related to precessional cycles (about 20 ka). The total duration of the pre-evaporitic Messinian enclosed within the euxinic shale should be slightly less than 1 Ma. This figure is supported by a cross-check with radiometric (Vai et al., 1993), magnetostratigraphic (Negri and Vigliotti in Chapter E4), and facies data from recently studied sections.

As for the cyclicity of the Gessoso-Solfifera Formation and the Colombacci Formation, two alternative scenarios have been discussed. The Gessoso-Solfifera cyclicity may be related either to orbital precession (about 20 ka) or to orbital obliquity (about 40 ka) periods resulting in a total duration of about 350 ka or 700 ka for this unit, respectively. In any case, the evidence suggests that the time required for the accumulation of the gypsum evaporites is in the order of 1/10 of the total time corresponding to any individual cycle (which includes also deposition of non-evaporitic components). The Colombacci cyclicity may be related, in a similar way, either to orbital obliquity (about 40 ka) or to orbital eccentricity (about 100 ka) periods, which means a total duration of about 280 ka or 700 ka for the cyclic part of the unit, respectively. A shorter period seems to be less likely.

Following the first direct radiometric dating close to the Tortonian/Messinian boundary in the Northern Apennines (Vai et al., 1993), and strongly supported by astronomical and magnetostratigraphic calibration in Crete (Krijgsman et al., 1994), the duration of the Messinian Stage is presently assumed to be much longer than previously thought, approaching almost 2 Ma (see also Odin, 1994). Within this frame, the shorter estimates for the duration of both the Gessoso Solfifera and the Colombacci units are more likely. It follows that, in spite of the remarkable vertical variation in the facies sequence from pelagic-anoxic, to hyperhaline evaporitic, to hypohaline brackish up to evaporitic-schizoid, a coherent cyclicity pattern appears, which is mainly controlled by precessional cycles before and during most of the Messinian (the first depositional sequence in Fig. 3). This pattern may have been replaced by cycles related to orbital obliquity in the latest Messinian (Colombacci and 'Gessi Superiori' formations or second depositional sequence in Fig. 3), as a response to a major climatic and/or tectonic change.

The main results of this general evaluation of the cyclostratigraphic potential (also in terms of duration) of the Messinian formations in the Northern Apennines, and more generally in Italy, are as follows.

(1) There is a basic consistency between the presently assumed duration of the Messinian Stage (about 2 Ma) based on both radiometric calibrations and magnetostratigraphic correlations, and the duration derived from the cyclically developed Messinian formations inferring an appropriate controlling cyclic process.

(2) The orbital precessional periods (about 20 ka) seem to play a major role for most of the Messinian. Only the late Messinian appears to be possibly controlled by an orbital obliquity period (about 40 ka).

(3) The pre-evaporitic Messinian should last slightly less than 1 Ma; the hyperhaline evaporitic Messinian (Gessoso–Solfifera Formation or ‘Gessi Inferiori’) about 0.3 Ma; the hypohaline Messinian (Colombacci s.l. or ‘Gessi Superiori’ and Arenazzolo) about 0.3–0.4 Ma.

(4) The few hundreds of ka left to reach about two Ma (duration of the Messinian Stage) would correspond to the boundary unconformity between the two depositional sequences (Fig. 3).

The tentative estimates of duration of the different parts of the Messinian Stage suggested above differ sharply from those proposed recently by Gautier et al. (1994) on a pure magnetostratigraphic basis.

It seems to me that there are adequate conditions, especially in the Romagna Apennines, to undertake detailed statistical analyses and test the reliability of the factors assumed here in controlling the cyclicity observed in the field, and to further refine the counting and identification of undetected cycles. This approach will hopefully provide a regional cyclostratigraphic scale for the Messinian Stage which can be compared with similar scales being currently established in different areas.

## SOMMAIRE — CYCLOSTRATIGRAPHIE ET ESTIMATION DE LA DURÉE DU MESSINIEN

*(Manuscrit soumis: Novembre 1994, révisé: Juin 1995; rédacteurs responsables: AM et RC)*

Notre connaissance de la durée de l'Étage Messinien s'est considérablement accrue grâce aux études géochronologiques et magnétostratigraphiques appliquées à des sections caractérisées biostratigraphiquement. Suite à nos recherches géochronologiques conformes aux nouvelles interpolations magnétostratigraphiques, la durée proche de 1 Ma admise auparavant est maintenant doublée. Ce travail examine la cyclicité sédimentaire remarquable des principales formations du Messinien sur les côtés ionien et adriatique des Apennins. Quelques 45 cycles anoxique–oxique (argile grise–laminite noire) et un petit nombre de cycles carbonatés sont observables dans la formation des argiles euxiniques (Messinien pré-évaporitique) remplacée par le faciès ‘Tripoli’ en Sicile. Dans la formation ‘Gessoso Solfifera’ (Messinien évaporitique), 15 à 16 cycles majeurs ont été corrélés depuis la région des Apennins d'Émilie–Romagne jusqu'à la Sicile. Dans le Messinien post-évaporitique (formations des ‘Colombacci’ au s.l. et ‘Gessi Superiori’) jusqu'à 7 cycles sont connus. Cependant, ici, un intervalle sans cycle, latéralement corrélé avec une disconformité majeure, rend le comptage des cycles incertain. On suggère dans ce travail la recherche d'une causalité climatique d'origine orbitale pour ces différents cycles lithologiques.

*(Sommaire adapté par les rédacteurs d'après un résumé de l'auteur, GSO)*

## ACKNOWLEDGEMENTS

The author thanks K. Stewart for reviewing the original manuscript.

Chapter E4

**CALCAREOUS NANNOFOSSIL BIOSTRATIGRAPHY AND  
PALAEOMAGNETISM OF THE MONTE TONDO AND MONTE DEL CASINO  
SECTIONS (ROMAGNA APENNINES, ITALY)**

A. Negri and L. Vigliotti

INTRODUCTION

Two sections at Monte Tondo and Monte del Casino (Romagna Apennines), spanning the Tortonian/Messinian boundary are exposed as badlands at the foot of the prominent cliff of the Vena del Gesso Messinian evaporites (see Chapter E3 for the lithological description).

The columnar logs of the two sections showing the schematic lithologies and the collected samples are represented in fig. 4 of Chapter E3. 141 samples were collected for calcareous nannofossil biostratigraphy (92 samples from the Monte Tondo section, and 49 samples from the Monte del Casino section). Both sections were also object of a palaeomagnetic sampling to establish the polarity record of the sequence, and to correlate it with the Geomagnetic Polarity Time Scale (GPTS). Fifty-three hand-oriented samples (thirty from the Monte Tondo section, and twenty-three from the Monte del Casino section) were collected in the field, and at least two cylindrical specimens (2.54 cm diameter) were drilled from each sample in the laboratory. With the exception of a few cases, most of the samples were collected from the light (more oxygenated) horizons recognized in the field, in order to avoid diagenetic processes which may have occurred in the dark, anoxic facies.

METHODOLOGY

Preparation of the calcareous nannofossil samples followed standard techniques, no centrifugation was done in order to retain the original composition, and a smear slide was mounted with Canada balsam.

Analyses were performed following the quantitative methodology described in Rio et al. (1990b). In order to define the first occurrence (FO) and last occurrence (LO) of the marker species, a count was done on a fixed number of specimens belonging to the taxonomically correlated group (i.e., the frequency of *Helicosphaera carteri* on 100 helicoliths).

In the case of the *Amaurolithus* spp., owing to the low frequency of this group in the whole assemblage, the number of specimens in every 1,000 fields of view was counted at a magnification of 1250 ×.

The palaeomagnetic investigations were carried out at the Palaeomagnetic Laboratory of the Istituto di Geologia Marina of the CNR of Bologna. Both thermal and



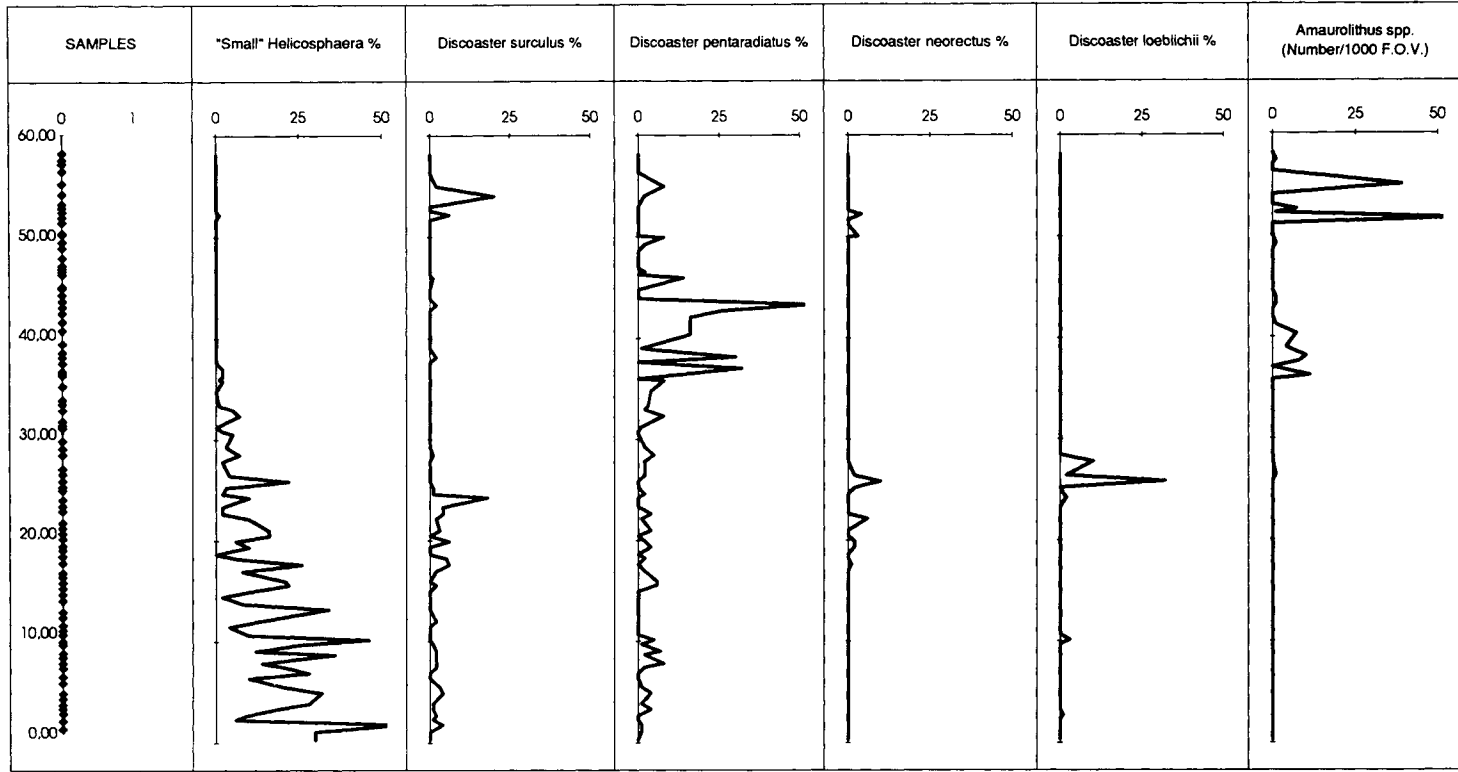


Fig. 1. Frequency diagrams of some selected species in the Monte Tondo section. Percentages are the result of counting of 100 specimens of *Discoaster* and *Helicosphaera*.

alternating field (AF) stepwise demagnetization treatments were used to reconstruct the palaeomagnetic vector of the rock. The remanence was measured by using a Jelinek Jr-4 spinner magnetometer; changes in the magnetic mineralogy during thermal treatment were monitored by measuring the susceptibility ( $K$ ) by a Bartington MS 2 susceptibility meter. Rock magnetic properties were investigated by isothermal remanent magnetization (IRM) experiments, and progressive thermal demagnetization of three orthogonal IRM (1 T to the  $z$ -axis, 0.4 T to the  $y$ -axis and 0.12 T to the  $x$ -axis) following the method proposed by Lowrie (1990). This procedure reveals an unblocking temperature spectrum of three different ranges of coercivities corresponding to different magnetic minerals.

## RESULTS

### *Calcareous nannofossil biostratigraphy*

All the samples show an abundant and moderate- to well-preserved nannoflora. The assemblages mainly consist of *Reticulofenestra* and *Dicryococcites* spp. *Coccolithus pelagicus*, *Reticulofenestra pseudoumbilicus*, *Sphenolithus moriformis*, *Sphenolithus abies* and *Syracosphaera pulchra* are commonly recorded, as well as *Scyphosphaera* spp., *Triquetrorhabdulus rugosus* and *Rhabdosphaera* spp. The genus *Discoaster* is very abundant in the studied sections, but the state of preservation rarely allows to distinguish the different species, especially in the case of the six rayed forms, very often showing secondary calcite overgrowth. Also abundant are the Helicoliths which are represented by at least five different species.

In the present chapter we discuss the occurrence of some selected species considered useful for biostratigraphic purposes. Three genera were analyzed in great detail: *Discoaster*, *Helicosphaera*, and *Amaurolithus*. The results are discussed in the following paragraphs.

*Discoaster*. Despite the frequent poor preservation state of these microfossils, a frequency evaluation of this genus was possible for most of the samples. Frequency diagrams of some selected species used as markers in the investigated interval are plotted in Fig. 1 (see also the biostratigraphic models of Martini, 1971, Colalongo et al., 1979b, and Okada and Bukry, 1980, Fig. 9).

Most of the specimens belong to the *Discoaster variabilis* species. *D. adamanteus* (a species recorded from the Lower Miocene) occurs in low percentages but consistently at the base of the Monte Tondo section, becoming more sporadic up-section. In the Monte del Casino section this species occurs discontinuously. *D. brouweri* is scattered throughout the sections. Few specimens of *D. brouweri triradiatus* were found in a single sample in the Monte del Casino section, and sporadically in the Monte Tondo section. Two samples of the Monte del Casino section also exhibited *D. asymmetricus*. It is noteworthy that this species defines the base of the Early Pliocene Zone NN 14 of Martini (1971), thus in this interval it appears to be at least anomalous. Few specimens of *D. calcaris*, *D. challengerii*, *D. icarus*, *D. mendomobensis*, *D. musicus*, *D. moorei*, *D. tamalis*, and *D. toralus* were also recorded in the two studied sections. *D. prepentaradiatus* occurs in a single sample of the Monte Tondo collection. *D. intercalaris* as well as *D. pentaradiatus* occur consistently, but with oscillating abundances in both sections (do they testify cyclicity in the productivity of the water

masses?). Toward the top at Monte Tondo section, *D. pentaradiatus* shows a drop in frequency while *D. intercalaris* shows an opposite trend in relative abundance.

In the Monte Tondo section, significant species such as *D. surculus* occurs from the bottom to the top with a negative trend. At the Monte del Casino section only few specimens are recorded in two samples at the base. *D. neorectus* and *D. loeblichii* are reported scattered in the Monte Tondo section, and appear to be rarer in the Monte del Casino section. A single specimen of *D. cf. quinquerramus* was found in the Monte del Casino section.

*Helicosphaera*. As far as the *Helicosphaera* genus is concerned, the potential of the group as a stratigraphic tool has never been investigated in this interval (Late Miocene), despite its common occurrence in the assemblage characterizing the Mediterranean sediments.

The vast majority of the *Helicosphaera* genus consists of *H. carteri*, commonly occurring with high-frequency values (often exceeding 80%) throughout the two sections. Subordinated but consistent is the occurrence of *H. intermedia* until the upper part of both sections.

Among the 'small' *Helicosphaera* the single species do not seem useful for biostratigraphic purposes, showing discontinuous occurrence in the upper part of the sections. If the 'small' *Helicosphaera* group is considered as a whole, a sharp drop in the frequency values can be placed 2.25 m above the base in the Monte del Casino section. Unfortunately the same observation cannot be drawn for the Monte Tondo section. Reduced frequency values (rarely exceeding 5%) have been observed up to 23.40 m above the base of the Monte del Casino section, and up to 37.35 m in Monte Tondo section.

Finally, rare specimens of *H. sellii* were recognized in the upper levels of the Monte Tondo section.

*Amaurolithus*. Among nannospecialists, the FO of the horseshoe-shaped *Amaurolithus* in the Mediterranean Neogene is considered the best approximating event for the definition of the T/M boundary (Colalongo et al., 1979b). Figures 1 and 2 document the results of a search expressed as the number of *Amaurolithus* every 1000 fields of view at a magnification of 1250 ×. The occurrence of the genus *Amaurolithus* is rare and discontinuous, especially in the first part of its range. In fact, in both sections it disappears after its FO suddenly for a long interval. After this, the frequency of the group increases but, soon after, the distribution is again discontinuous. This behaviour may reflect changes in the water masses (i.e., salinity productivity) to which the *Amaurolithus* genus was probably sensitive.

### *Palaeomagnetism*

The intensity of the natural remanent magnetization (NRM) does not appear constant in the two sections. At Monte Tondo, the NRM is generally well below 1 mA/m with most of the values in the range 0.1–0.2 mA/m. Only in the lower part of the section a couple of samples (Monte Tondo 28 and 30) exhibited a stronger magnetization about one order of magnitude above these values (Fig. 3). Not always NRM peaks correspond to higher magnetic susceptibility (K): the latter parameter shows a general decreasing trend from the Tortonian to the Messinian (Fig. 3). Samples collected at Monte del Casino exhibited a wider range of NRM. Generally the remanence is still

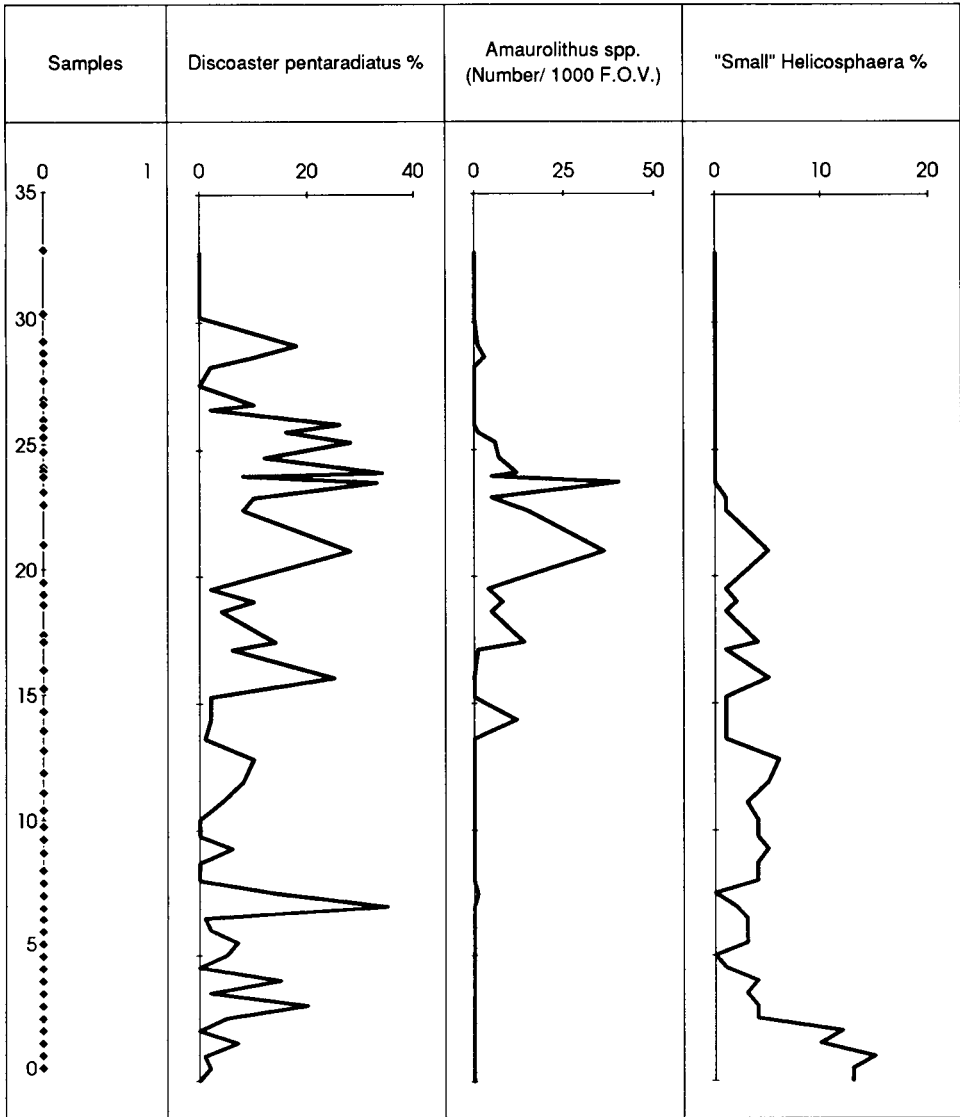


Fig. 2. Frequency diagrams of some selected species in the Monte del Casino section. Percentages are the result of counting of 100 specimens of *Discoaster* and *Helicosphaera*.

below 1 mA/m, but with higher values than at Monte Tondo. Differences of two orders of magnitude were measured between weaker and stronger samples. The observed differences in NRM and K suggest a change in the concentration, and in the nature of the magnetic minerals throughout the sections, which appear to be significant for the results. IRM experiments (Fig. 4) show that the rock is completely saturated with a DC field of 300 MT, suggesting that the magnetic mineralogy is dominated by ferromagnetic minerals (e.g. magnetite type). Experiments of thermal demagnetization of orthogonal

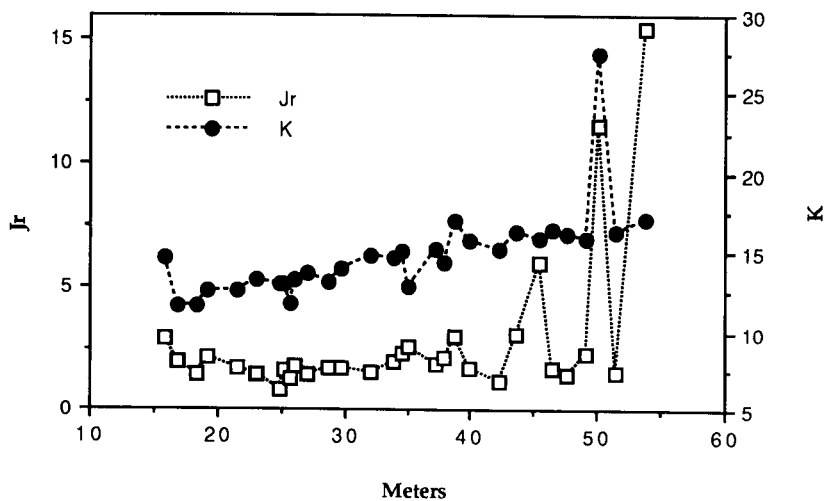


Fig. 3. NRM intensity ( $J_r$ ) and magnetic susceptibility ( $K$ ) for the samples collected at Monte Tondo section.  $J_r$  and  $K$  values are expressed respectively in  $10^{-7}$  A/m and  $10^{-5}$  SI units.

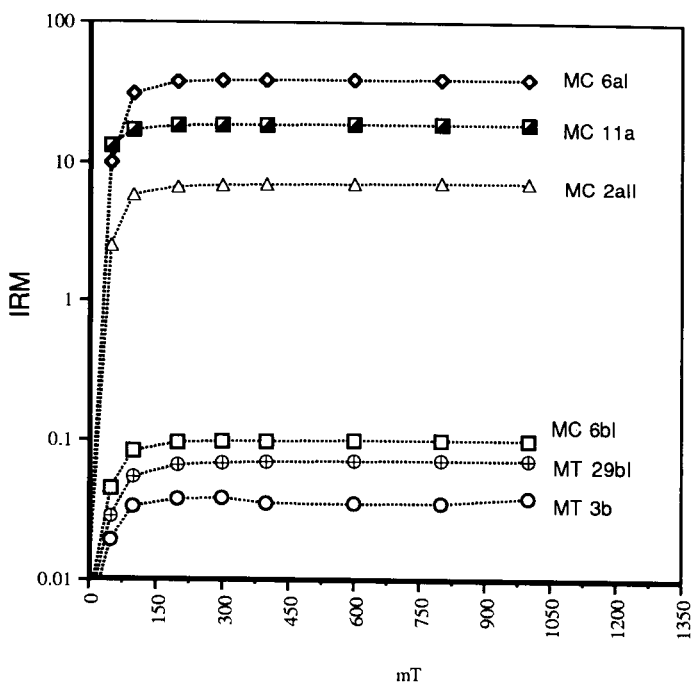


Fig. 4. Isothermal remanent magnetization measurements of some samples collected at Monte Tondo and Monte del Casino sections. Intensity of magnetization is expressed in A/m. Samples Monte del Casino 6aI and Monte del Casino 2aII were previously heated to 400°C.

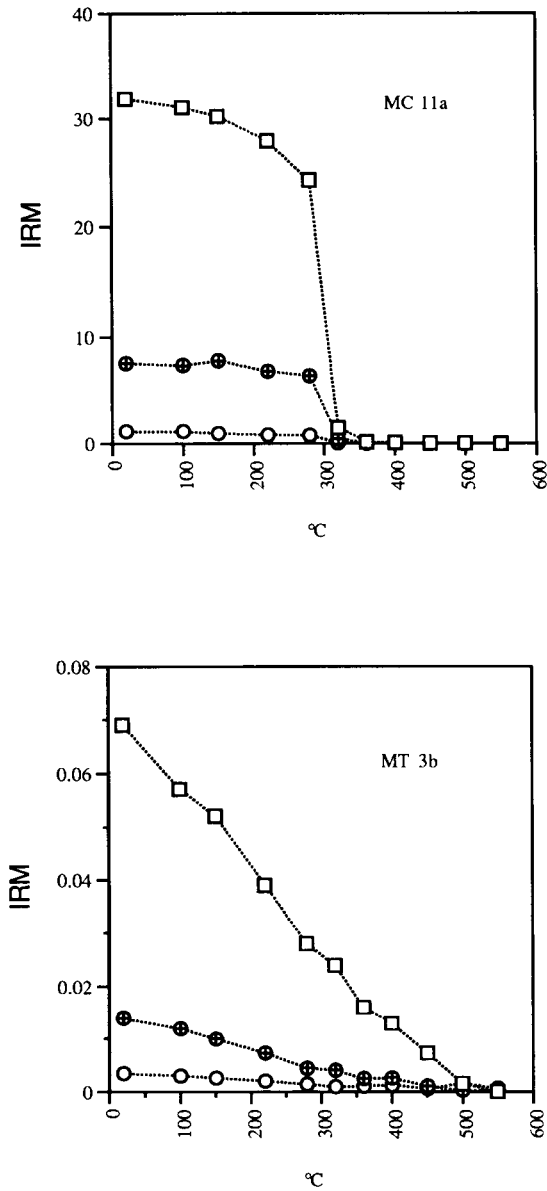


Fig. 5. Typical curves of thermal demagnetization of orthogonal IRM. Open squares indicate thermal decay of the soft component (0.12 T), closed circles and open circles represent medium (0.4–1 T) and hard (1 T) IRM's, respectively. IRM values are expressed in A/m.

IRM (Fig. 5) show that pyrrhotite is the only magnetic carrier of samples with stronger magnetization (sample Monte del Casino 11A).

The complex palaeomagnetic record hampered the possibility to resolve a coherent magnetostratigraphy. The rock is characterized by a low coercivity and palaeomagnetic

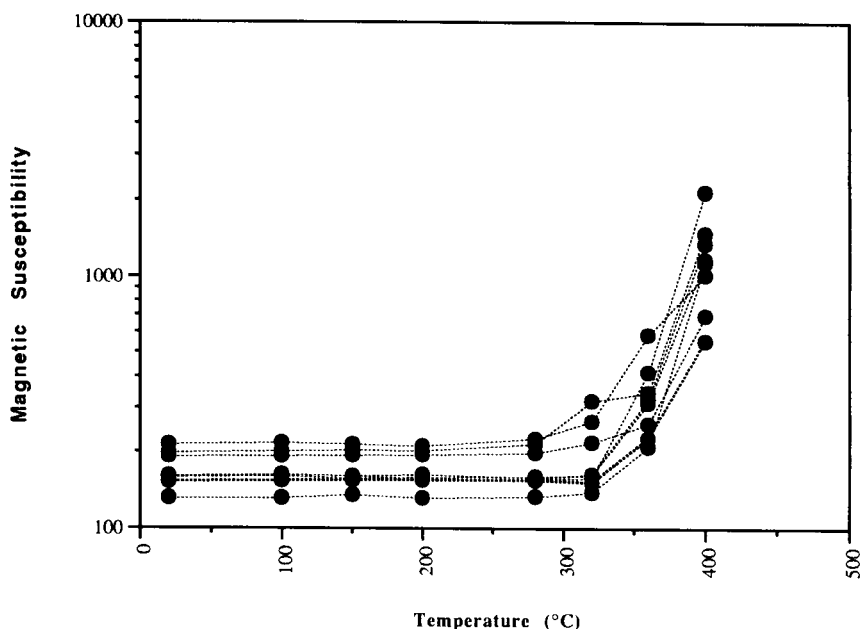


Fig. 6. Magnetic susceptibility ( $K$ ) measured after each step of thermal demagnetization for samples collected at Monte del Casino. Values are expressed in  $10^{-6}$  SI units.

directions strongly overprinted by a secondary component(s). During progressive demagnetization, an alternating field (AF) of 15 MT is effective to reduce, in many cases, the weak NRM of the rock in the range noise of the magnetometer ( $3 \times 10^{-5}$  A/m). Thermal treatment is not more successful: the Zijderveld plots show a confused pattern above  $350^\circ$  due to a viscous magnetization. This pattern corresponds to an increase in the magnetic susceptibility (Fig. 6) with production of very fine (superparamagnetic) magnetite during the heating. These characteristics did not allow to obtain a stable end-point on the demagnetization diagrams. So it has not been possible to identify the characteristic remanent magnetization (ChRM) of the rock. Nevertheless, an attempt was made at defining some polarity intervals in the samples from the Monte Tondo section by looking at the trend of the directions during the cleaning. The same observation does not hold for the samples from the Monte del Casino section which seem to suffer a stronger overprint.

A possible magnetostratigraphy of the Monte Tondo section is shown in Fig. 7. The data have been interpreted at two different levels (A and B in Fig. 7). Even the less speculative interpretation of the data (polarity pattern B in Fig. 7) recognized at least five polarity intervals in the section. They characterize two main polarity patterns. A R–N–R polarity pattern in the upper part of the section, and a N–R pattern in the middle of the section. Doubtful data separate these two main intervals and also characterize the lower part of the section. Here, both NRM and  $K$  exhibit spikes (Fig. 3) testifying that changes in the magnetic mineralogy play a role in this part of the section.

Especially the long reverse interval observed in the upper part of the section appears well established by the behaviour of the palaeomagnetic direction during the

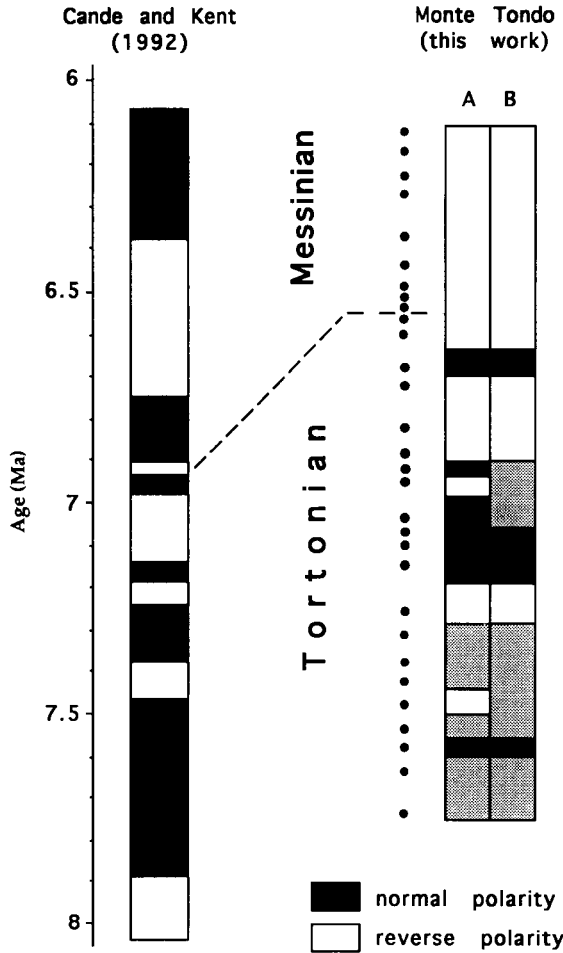


Fig. 7. Polarity pattern for the Monte Tondo section, and geomagnetic polarity time scale (Cande and Kent, 1992) for the interval spanning the T/M boundary. Magnetostratigraphy in column A represents a more speculative interpretation of the data. Shaded areas refer to uncertain data.

cleaning. NRM directions change progressively declinations and inclinations moving systematically toward a southeastern direction with negative inclination. This behaviour is reported in the stereonet plot in Fig. 8.

## DISCUSSION AND CONCLUSIONS

The data exposed in this paper document the peculiar distribution of some calcareous nannofossil species which are considered useful markers in the standard zonations of Martini (1971) and Okada and Bukry (1980). In Fig. 9, we compare the two above-mentioned standard zonations with the model derived from Bukry, and modified by Colalongo et al. (1979b). Microphotographs of the species described herein are shown in Fig. 10. As



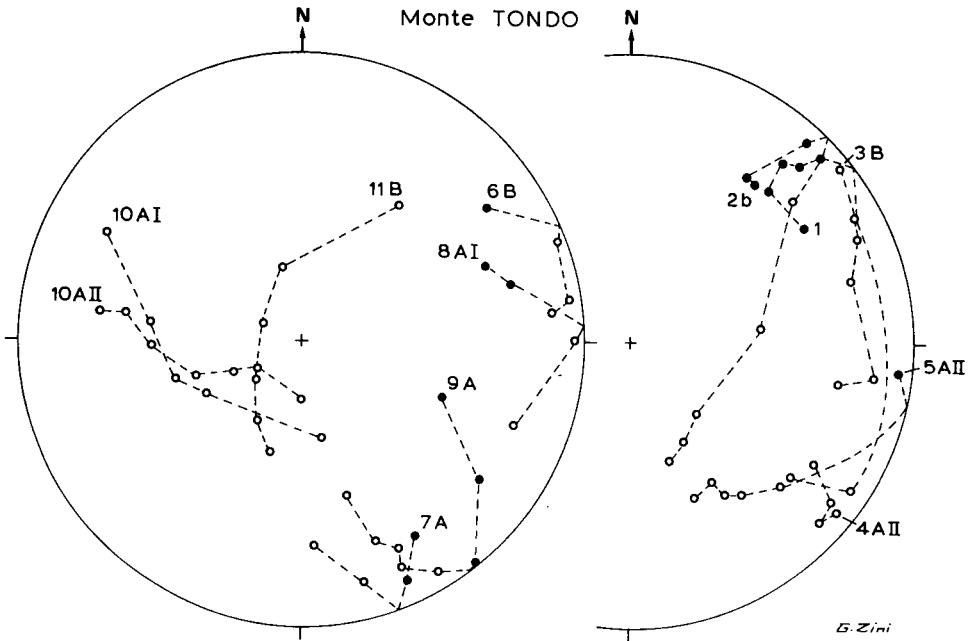


Fig. 8. Stereonet representing NRM direction change during thermal or AF cleaning for the samples collected in the upper part of the Monte Tondo section. Closed (open) circles for positive (negative) inclinations.

it can be seen in the correlation in Fig. 9, Martini's model considers the *D. quinquaramus* total range zone for the studied interval. In the analyzed samples, this species occurs only in one sample, thus the NN 10 Zone cannot be recognized.

In the Okada and Bukry's model, several events are proposed, based on the FOs and LOs of different *D.* species. The first couple of considered events regarding the Late Miocene is the FOs of *D. neorectus* and *D. loeblichii*. These two species are almost absent in the Monte del Casino section, and they occur very rarely in the Monte Tondo section. For this, it is impossible to recognize, in this section, the zonal boundary. On the other hand, no *D. bellus* nor *D. neohamatus* have been found in this section, while *D. surculus* occurs already at the base of the Monte Tondo section. Thus we could correlate the base of the section to the CN 9a Zone of Okada and Bukry, although this is not consistent with the range of *D. neorectus* which is restricted to the CN 8b Zone of Okada and Bukry (1980) (Aubry, 1984). On the contrary it fits well the model of Colalongo et al. (1979b) in which the FO of *D. surculus* is recorded together with the FO of *D. quinquaramus* at a level well below the one indicated by Okada and Bukry. As far as the model of Colalongo et al. (1979b) is concerned, many problems exist also in the application of this biozonation. In fact no *D. neohamatus* specimens were recorded, and *D. berggrenii* and *D. pseudovariabilis* appear so scattered that they cannot be adequately used for biostratigraphic purposes.

Furthermore, other problems still affect the *Discoaster* genus, in particular the bad preservation often characterizing this group. Therefore, the difficulties in the recognition

Chronostratigraphy	Martini, 1971		Bukry, 1973, 1975; Okada & Bukry, 1980			Bukry, 1973 modif. in Colalongo et al., 1979	
Messinian	<i>Amaurolithus</i>		<i>Amaurolithus</i>	<i>C. acutus</i> CN 10B	* <i>C. acutus</i> + <i>T. rugosus</i>		
	<i>tricorniculatus</i> NN 12	+ <i>Discoaster quinquaramus</i>	<i>tricorniculatus</i> CN 10	<i>T. rugosus</i> CN 10A	+ <i>D. quinquaramus</i>		* <i>A. delicatus</i>
	<i>Discoaster</i>		<i>Discoaster</i>	<i>A. primus</i> CN 9B	* <i>A. primus</i>	<i>A. primus</i>	* <i>A. primus</i>
Tortonian	<i>quinquaramus</i> NN 11	* <i>Discoaster quinquaramus</i>	<i>quinquaramus</i> CN 9	<i>D. berggreni</i> CN 9A	* <i>D. surculus</i> , <i>D. berggreni</i> * <i>D. quinquaramus</i> + <i>D. bellus</i> , <i>D. neohamatus</i>	<i>D. berggreni</i>	+ <i>D. pseudovariabilis</i> , <i>D. neohamatus</i> * <i>D. berggreni</i>
	<i>Discoaster</i>		<i>Discoaster</i>	<i>C. calyculus</i> CN 8B	* <i>D. neorectus</i> , <i>D. loeblichii</i>	<i>Discoaster</i>	* <i>D. quinquaramus</i> , <i>D. surculus</i>
	<i>calcaris</i> NN 10	+ <i>Discoaster hamatus</i>	<i>neohamatus</i> CN 8	<i>H. carteri</i> CN 8A	+ <i>D. hamatus</i>	<i>neohamatus</i>	+ <i>D. hamatus</i>

Fig. 9. Comparison of nannofossil biostratigraphic models of the Tortonian–Messinian interval.

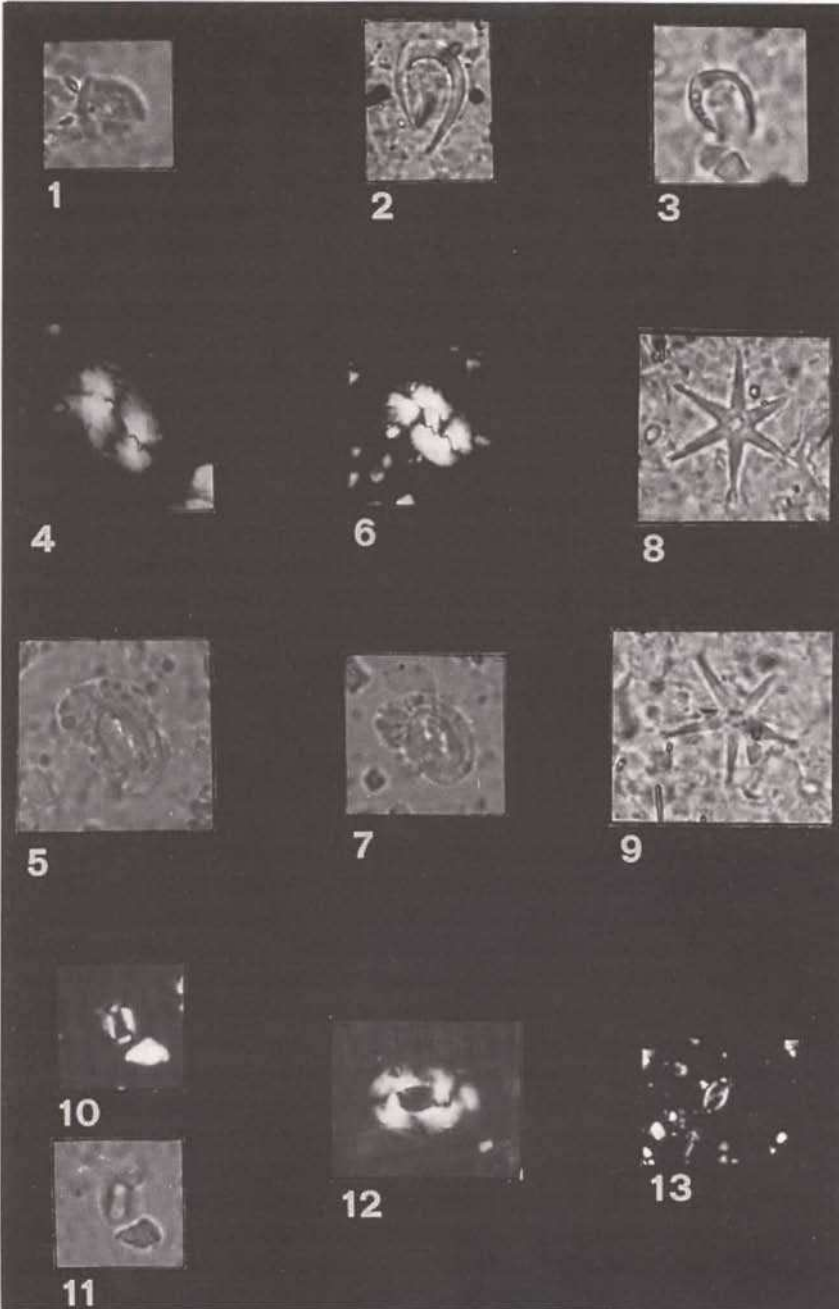


Fig. 10. Important calcareous nannofossil species from the Monte Tondo section described in this work: (1) *Amaurolithus primus* (Bukry and Percival, 1971; Gartner and Bukry 1975), specimen size  $5.6 \mu\text{m}$ , parallel nicols, sample MT 21; (2) *Amaurolithus delicatus* Gartner and Bukry (1975), specimen size  $6.4 \mu\text{m}$ , parallel nicols, MT 28; (3) *Amaurolithus delicatus* Gartner and Bukry (1975), specimen size  $6.4 \mu\text{m}$ , parallel nicols, MT 28; (4) *Helicosphaera carteri* (Wallich, 1877) Kamptner (1954), specimen size  $11.2 \mu\text{m}$ , cross-polarized

of the different species, and the discontinuous occurrence of the *Discoaster* marker species do not allow an accurate biostratigraphic determination.

The *Amaurolithus* group is also scarcely useful for the recognition of the zonal boundary. However, the FO of this genus is the only correlatable event between the Mediterranean and the open ocean. In fact, the model proposed by Okada and Bukry (1980) (Fig. 9) adopts the *A. primus* FO to define the lower boundary of the zone CN9B. Colalongo et al. (1979a, b) also utilize the FO of *A. primus* as zonal boundary. According to these authors, this event predates the FO of *A. delicatus*. However, this is not recorded in our collection of samples, and for this reason we preferred to utilize the FO of *Amaurolithus* spp. In fact, few and scattered specimens of this genus make it difficult to discriminate whether *A. primus* effectively predates *A. delicatus*. In the Monte del Casino section in particular, the first detected *Amaurolithus* is represented by *A. delicatus*, while in Monte Tondo *A. primus* is the first representative of this genus.

In the studied sections, the *Helicosphaera* genus, generally neglected as biostratigraphic marker for the Late Miocene, seems to help in the biostratigraphic resolution of this time interval with two new events: a drop in abundance of the 'small' *Helicosphaera* predates the FO of *Amaurolithus*, and the LO of this group follows this event.

Poor demagnetization characteristics did not allow to establish the ChRM of the rock. Diagenetic processes exerted a major control on the magnetic properties of the sediments collected in the two sections. Sulphur occurrence such as pyrrhotite may be responsible of the complex palaeomagnetic record. As said above, only in the Monte Tondo section was it possible to identify some polarity intervals. An interpretation of the polarity record, in terms of normal and reversed intervals, is shown in Fig. 7, which also shows a tentative correlation with the time scale of Cande and Kent (1992). Uninterpretable data are drawn as shaded areas.

Correlation of the polarity pattern with the GPTS is not straightforward. The Tortonian/Messinian (T/M) boundary (FO of *G. conomiozea*) occurs in a reverse interval recognized in the upper part of the section. This result seems to correlate with the data from several sections studied in Crete by Langereis et al. (1984), and Krijgsman et al. (1994). On the contrary, Channell et al. (1990) found the T/M boundary in a normal interval at ODP Site 654 in the Tortonian Sea. Krijgsman et al. (1994) correlate

One question which may arise by looking at our data concern the length of the interval containing the boundary. In the Cretan sections it invariably occurred in a short reversed interval contrasting with the length of the interval observed at Monte Tondo. If the data represent a primary magnetization, this would imply that either the boundary does not occur in the same chron, or that the long reversal interval recognized at Monte Tondo is not representative of a single chron. In the central part of this interval, the spacing of the sampling was quite scattered, so it is possible that we missed the recovery of Chron C3Bn. The hypothesis that the boundary occurs in a different chron cannot be completely discarded. It is well known that the FO of the *G. conomiozea* was considered as a migratory event in the Mediterranean (Zachariasse 1975, 1979; Scott 1980). However, biostratigraphic considerations may suggest a different interpretation. We take into account the interval existing between the FO of *G. conomiozea* and the LO of 'small' *Helicosphaera* (fig. 4 of Chapter E3) in both sections. At Monte del Casino this interval spans about 4 m, significantly thicker than the 1.5 m observed at Monte Tondo section. This consideration may suggest that some metres of succession are missing in the Monte Tondo section, just above the boundary. Thus Chron C3Bn of the GPTS (Cande and Kent, 1992) could be completely lacking.

The N–R magnetic polarity pattern recognized in the central part of the section can be confidentially correlated with Chron 4n.1 of the GPTS. In fact the FO of *Amaurolithus* spp. occurs few metres above the recognized pattern, in an interval which may be interpreted as reversed. This interpretation is in agreement with Young et al. (1993) who consider the FO of *Amaurolithus* spp. as occurring in Chron 3Br.3r of the time scale of Cande and Kent (1992).

In summary, biostratigraphic analysis of calcareous nannofossils in the studied sections indicates that the Helicoliths group is a very promising tool for the definition of a biostratigraphic sequence throughout this time interval, at least in the Mediterranean domain. In the studied samples, the LO of 'small' *Helicosphaera*, and a drop of the 'small' *Helicosphaera* predating the FO of *Amaurolithus* are clearly recorded events which, nevertheless, need to be tested in other sections, and may be useful even in extra-Mediterranean areas where this group is also documented (DSDP Site 369, Negri, 1989). If these two bioevents will be confirmed, they will improve the resolution of the Late Miocene biostratigraphy, and will constitute a valid means for a better

SOMMAIRE — BIOSTRATIGRAPHIE DES NANNOFOSSILES CALCAIRES ET PALÉOMAGNÉTISME DES PROFILS DU MONTE TONDO ET DU MONTE DEL CASINO (APENNINS DE ROMAGNE, ITALIE)

(Manuscrit soumis: Septembre 1994, révisé: Juin 1995; rédacteurs responsables: AM et RC)

Biostratigraphie des coccolithes et magnétostratigraphie ont été envisagées dans deux profils incluant la limite Tortonien/Messinien. Une analyse quantitative de l'abondante nannoflore met en évidence l'arrivée des *Amaurolithus* spp. et deux nouveaux biopères fondés sur le groupe des 'petits' *Helicosphaera* (*H. walbersdorfensis*, *H. stalis*, *H. orientalis*). Par contre, la rareté et la préservation insuffisante des *Discoaster* ne conduit pas à une biostratigraphie intéressante. Une faible intensité de magnétisation, une faible coercitivité et un enregistrement complexe a empêché la mise en évidence d'une séquence de polarité complète. La démagnétisation thermique suggère que, dans quelques niveaux, la pyrrhotite est l'unique porteur de la rémanence. Malgré cela, on a pu identifier dans la coupe du Monte Tondo quelques zones magnétiques distinctes par l'observation du comportement de la magnétisation durant le traitement. La limite Tortonien/Messinien tombe dans une intervalle inverse qui paraît anormalement long comparé à la séquence connue pour cet intervalle de temps. La combinaison des résultats bio- et magnétostratigraphiques suggère qu'il manque une partie de l'enregistrement sédimentaire près de la limite.

(Sommaire proposé par les rédacteurs d'après un résumé des auteurs, GSO)

This Page Intentionally Left Blank

Chapter E5

**NEW RADIOMETRIC DATINGS BRACKETING THE  
TORTONIAN/MESSINIAN BOUNDARY IN THE ROMAGNA POTENTIAL  
STRATOTYPE SECTIONS (NORTHERN APENNINES, ITALY)**

M.A. Laurenzi, F. Tateo, I.M. Villa and G.B. Vai

INTRODUCTION

The chronometric calibration of the standard global chronostratigraphic scale has undergone a major revolution during the first half of this Century, and is still showing substantial changes in the last few decades (e.g., Vai, 1975; Harland et al., 1982; Menning, 1988; Odin, 1994). Particularly relevant are the variations in chronometric estimates of Neogene stage boundaries such as the Tortonian/Messinian (T/M), and Miocene/Pliocene boundaries, which have resulted from improved high-resolution and interdisciplinary stratigraphic research. The most dramatic change occurred at the transition from the Kulp (1960, 1961) scale (with a figure of slightly more than 13 Ma) to the Phanerozoic Time Scale (PTS) 1964 of Harland et al. (1964) in which to the base of the Pliocene was assigned an age of about 7 Ma. This is remarkable when compared with the chronometric estimate for the base of the Miocene, which is practically unchanged since at least Holmes (1947) (see Harland et al., 1982).

The later stratigraphic use registered a trend toward even younger age estimates, up to 6.2 Ma, mainly based on both the assumption that the duration of the Messinian Age should be very short, and the first attempts at calibrating the T/M boundary, taken as the first appearance datum (FAD) of *Globorotalia conomiozea*, with the magnetostratigraphic time scale (Ryan et al., 1974; Hsü, 1986b). The youngest figure in this trend was reached by Langereis et al. (1984) with 5.6 Ma. The once widely used time scale of Berggren et al. (1985b) suggested an age estimate of 6.5 Ma.

In such a state we considered it to be highly desirable to search for possible direct dating of the T/M boundary in biostratigraphically well studied, continuous, and complete marine sections in the Italian Peninsula, which as a whole (Northern Apennines, Calabria and Sicily) is the place of all the historical stage stratotypes for the Middle Miocene and the Pleistocene. New, detailed stratigraphic and tectonic surveys of the Vena del Gesso Basin (Northern Apennines, Romagna region, Imola to Faenza area), aimed at resolving the still open problems of the Mediterranean salinity crisis (Selli, 1960; Vai and Ricci Lucchi, 1977), allowed the recognition of a sequence of thin volcanogenic biotite-rich horizons. They are intercalated within an increasingly anoxic mudstone sequence spanning the T/M boundary across the entire basin (Castellari, 1989; Calieri, 1992). Actually, the first record of a stratigraphically undifferentiated Tortonian volcano-sedimentary layer, found almost at the top of the Marnoso–Arenacea formation immediately west of the Faenza–Imola area, dates back to Gandolfi et al. (1983).



In this paper we report and discuss in some detail the preliminary results published by Vai et al. (1992, 1993), and compare them with some new measurements closely bracketing the T/M boundary, thus allowing a cross check of the original geochronologic results.

In the meantime similar volcano-sedimentary layers have been found in the same time interval some 100 km to the east (Coccioni et al., 1992) and some 300 km to the south (D. Cosentino, pers. commun., 1993), suggesting a regional importance for this volcanic cycle. Independent dating of biotite-rich horizons from the original locality of Gandolfi et al. (1983) showed a good agreement (Odin et al., Chapter E6) with the dating by Vai et al. (1993). Our radiometric results have been obtained in the frame of integrated and detailed litho- and cyclostratigraphic (Vai, Chapter E3), biostratigraphic (benthonic and planktonic Foraminifera, and calcareous nannofossils), mineralogic, isotopic, and magnetostratigraphic assessments (Negri and Vigliotti, Chapter E4).

Before listing our analytical results, we consider a present review of the previous, most important chronometric calibration of the T/M boundary, which we consider not only useful but crucial for a correct understanding of the new calibration provided by our measurements.

## CRITICAL EVALUATION OF PREVIOUS CALIBRATIONS

It is important to remark that until Charlot et al. (1967), and Choubert et al. (1968) no radiometric datings of the T/M boundary were performed neither in the type area (Northern Apennines and Sicily–Maghrebian foredeeps) nor in any other continuous marine sections. Even the term Messinian was neglected, being replaced by the unsuitable Paratethyan Pontian Stage, until Selli (1960, 1964) emphasized its priority and appropriateness, suggesting a neostratotype in central Sicily.

As for most of the Tertiary series prior to early 1960, the chronometric calibrations of this late Upper Miocene stage, and of the Miocene/Pliocene boundary, were based almost exclusively on radiometric dating of the North American mammal faunas. These faunas are often interposed between lava- and pyroclastic flows which provided the only adequate set of data available for constructing an independent physical time-scale at that time (Evernden et al., 1964).

Unfortunately, the stratigraphic correlation of the so-called North American Land Mammal Ages (a hybrid type of Parachronologie sensu Schindewolf) with the Standard Marine Stages and Series was made through the comparison with the mainly brackish, mammalian-rich, Paratethyan regional stages. In this way, the low mean-resolution-power of the Mammal ages (3 to 4 Ma) was summed up to the still unresolved problem of reliable correlation between regional Paratethyan and Standard Marine Stages of the Neogene (Rögl and Steininger, 1983; Vai, 1988). As a consequence, excellent radiometric datings of the North American faunas were tied in a poorly constrained correlation frame. The resulting effective chronostratigraphic error (Harland et al., 1990) of many Tertiary stage boundaries was too high (Funnell, 1964; Berggren, 1969; Page and McDougall, 1970; McDougall and Page, 1975). Especially difficult appeared the situation of the Tortonian/Messinian and the Miocene/Pliocene boundaries, both being included within the same Mammal 'Age' called 'Hemphillian'. It turned out, in fact, that the 'Hemphillian' possibly ranges from the late Tortonian to a large part of the

Table 1

Dated magnetic reversals ranging from 3 Ma to 10 Ma (simplified from Harland et al., 1990)

Magnetic anomaly	Chron/Subchron	Isotopic age (Ma)	References
C2A-2R (y)	Mammoth young	3.05	Mankinen and Dalrymple (1979)
C2A-2R (o)	Mammoth old	3.15	Mankinen and Dalrymple (1979)
C2AR (y)	Gauss/Gilbert	3.40	Mankinen and Dalrymple (1979)
C5N (y) <sup>a</sup>		8.87	Evans (1970)
C5N (y) <sup>a</sup>		9.64	McDouglas et al. (1984)

<sup>a</sup> Dated material is from a non-marine sequence.

Pliocene (Funnell, 1964; Berggren, 1969; Page and McDougall, 1970; McDougall and Page, 1975). With such premises, it is not surprising to find the following statement by McDougall and Page (1975, p. 75) which demonstrates how difficult it is to find a way of reliable dating when unsafe procedures in stratigraphic correlations are followed: "it seems firmly established from isotopic age data that earlier correlations of vertebrate-bearing continental succession with the marine sequences were considerably in error."

The substantial jump in age of the Miocene/Pliocene boundary from about 13–12 Ma to about 7 Ma was actually recognized in Italy, at the Elba island, by Eberhardt and Ferrara (1962), as a pre-Tabianian (Early Pliocene) minimum date of  $6.93 \pm 0.75$  Ma (Tongiorgi and Tongiorgi, 1964). Following this revolutionary date, the gate was open to any possible unconventionally young chronometric calibration for both the Miocene/Pliocene, and Tortonian/Messinian boundaries mainly derived from the application of the recently established magnetic polarity time scale.

However, with the exception of the too rarely considered dating provided by Charlot et al. (1967) and Choubert et al. (1968) (a K/Ar biotite date of  $7.44 \pm 0.75$  Ma within a set of dates ranging from 6.5 Ma to 8.0 Ma), no radiometric dates on marine successions from both oceanic cores or exposed sections were made in the critical Late Miocene–Early Pliocene interval. So any effort to improve the state of the earlier, poorly reliable, correlations of vertebrate-bearing continental sequences with the marine ones failed.

Up to 1991, the chronometric calibration of the T/M boundary by both the best statistical estimate of selected radiometric dates (Chronogram method), and best interpolated duration of magnetic polarity intervals was not satisfactory. Table 1 shows the isotopic dates available to calibrate the magnetostratigraphic scale in the age range of 3–10 Ma, updated from Harland et al. (1990). Direct geochronologic datings of magnetic reversals between 3.40 Ma and 8.87 Ma are lacking. Consequently, this time interval is calibrated by simple interpolation.

There is a large consensus among specialists in recognizing the FAD of *G. conomiozea* (together with the coeval FAD of *G. mediterranea*) within Chron 3Br (referred to as 6R1 or younger reversed interval of the equivalent Chron 6 recorded in sedimentary cores) (Ryan et al., 1974; Loutit and Kennett, 1979; Langereis et al., 1984; Berggren et al., 1985b; Hsü, 1986b) or even within subchron 3Br.1r (Calieri et al., 1992; Krijgsman et al., 1994). It means that the FAD of *G. conomiozea* seems consistently related to a reversed polarity interval in New Zealand (Loutit and Kennett, 1979), in much of the deep-sea regions cored outside the Mediterranean (Ryan et al.,

Table 2

Chronostratic rating of the isotopic database used for computing the Messinian chronogram (simplified and modified after Harland et al., 1990)

No.	Sample	Dated mineral	Radioisotopic date	Location	Quality rating
1	JEN4	WR	6.40 ± 0.60	Fort de France, Martinique	fair
2	MP4	Bi	6.93 ± 0.75	Elba Island, Italy	fair
3	MP5	Bi	7.44 ± 0.75	Melilla (Rif), Morocco	good
4	PTS253R	Sd	6.69 ± 0.09	Rattlesnake, OR USA	very bad
5	PTS254	Fl	8.30 ± 0.74	ALturas, CA USA	very bad
6	PTS255	Sd	9.12 ± 0.26	Drewsey, OR USA	very bad
7	PTS256	WR	9.43 ± 0.31	Teewinot, WY USA	very bad
8	PTS110	Gl	9.84 ± 0.43	Kadenberge, Germany	bad

1974; Hsü, 1986), in Crete (Langereis et al., 1984; Krijgsman et al., 1994), and in the Northern Apennines (Ryan et al., 1974; Calieri et al., 1992). However, different magnetostratigraphic ties for this biomarker's first occurrence have been suggested from uppermost Chron 4 (equivalent to 7) (Ryan et al., 1974) to possibly Chron 3A-1=3An.1r (or 5R1) (Langereis et al., 1984), and even in normal polarity intervals as done by Channel et al. (1990) in the Mediterranean and Benson and Rakic-El Bied (1991).

The acceptance of the last two data needs some caution, firstly in the light of problems in magnetic polarity assessment and fossil ranges (D. Rio, pers. commun., 1992), and secondly in reporting only a local 'abundant FAD of *G. conomiozea*'. Furthermore, following an old misinterpretation of Selli's suggestion for selecting the base of the Messinian Stage (see Ryan et al., 1974, p. 650, footnote), some authors place the T/M boundary below the FAD of *G. conomiozea* in a normal polarity interval (Ryan et al., 1974; Berggren et al., 1985b), but the magnetic polarity of the interval containing this bioevent is not always normal. This fact may explain why some authors preferred a 6.5–6.7 Ma as magnetostratigraphic calibration of the T/M boundary (Ryan et al., 1974; Berggren et al., 1985b; Harland et al., 1990) instead of  $6.2 \pm 0.1$  Ma (e.g., Hsü, 1986b), which is the original calibration of Ryan et al. (1974) for the FAD of *G. conomiozea*. This same argument is of no help in the case of Harland et al. (1990, p. 159) where the T/M boundary, palaeomagnetically calibrated at 6.7 Ma, is 'taken as mid-C3BN', viz. higher in the magnetostratigraphic scale than the FAD of *G. conomiozea*.

In this paper we follow the stratigraphic philosophy and procedures consolidated during the two last decades, and accept the suggestion made by D'Onofrio et al. (1975), in substantial agreement with the original requirements of Mayer-Eymar (1868), Seguenza (1868), and Selli (1960), to define the T/M boundary in relation to the FAD of *G. conomiozea* and associated faunal and floral elements, a proper Global Boundary Stratotype Section and Point (GSSP) still awaiting to be selected following an international agreement. Thus, on the basis of the geomagnetic polarity time scale (GPTS) published up to 1990, we should have expected a magnetically calibrated age of about 6.2–6.7 Ma for the T/M boundary.

Quite a different result in dating the T/M boundary was provided by the chronogram method aiming to improve the chronometric calibration of stage boundaries (Harland et al., 1990). Table 2 shows a critical review of the data used for constructing the

Table 3

Comparison between chronogram and interpolated magnetostratigraphic ages of Neogene stage boundaries in Ma (Modified after Harland et al., 1990)

Stratigraphic boundary	Piac/ Zanc	Zanc/ Mess	Mess/ Tort	Tort/ Serr	Serr/ Langh	Langh/ Burd	Burd/ Aqui	Aqui/ Chat
Chronogram	3.5	6.0	8.4	10.4	14.6	16.0	22.0	23.8
Magnetostratigr. interpolation	3.4	5.7	6.7	10.4	14.2	16.3	21.5	23.3
Difference	0.1	0.3	1.7	0.0	0.4	-0.3	0.5	0.5

Messinian chronogram, which gives a 'best age' of 8.4 Ma for the T/M boundary with a 'minimum age' of 6.0 and a 'maximum age' of 10.8 Ma. This chronogram has a gentle-sided error function (Harland et al., 1990, fig. A4.3), meaning that the dates used are sparse, and have large errors. Moreover, the error function is asymmetrical and flat bottomed because of a large time interval where no data were available.

A simple inspection of Table 3 shows that the T/M chronogram is the worst of all Neogene chronograms, because it shows the largest difference with the interpolated magnetostratigraphic boundary age. To explain this exceptionally erratic chronogram, a critical stratigraphic rating of the data base, which was selected for computing the chronogram, is useful (Table 2). We relate the rating to the chronostratic error (= fossil error) of 1 Ma assumed by Harland et al. (1990). We feel that such a very narrow condition is fulfilled only by item 3. Items 1 and 2 also may be partly useful for the chronogram, when better data are lacking; however, it is difficult to assess their chronostratic significance insofar they represent dates of intrusion-emplacement of subvolcanic bodies. Item 8 has a very poor stratigraphic resolution being generically assigned to the Late Miocene. Items 4 to 7 bear the largest chronostratic error. In fact, they come from North American mammalian-rich continental sequences which may be useful for land and ecostratigraphic correlations but are totally unsuitable for the needs of the Standard Chronostratigraphic Scale and its calibration (Hedberg, 1976; Salvador, 1994). Moreover, such mammal faunas are found in sites with poor stratigraphic resolution, severely tectonized, and extremely difficult to be correlated with the Standard Marine Stages. To assume that items 4 to 7 are bracketed by Tortonian and Messinian stratigraphic evidences, is not possible in the present state of knowledge.

It is not our intention to set doubts on the usefulness of the chronogram method. We simply remark that the data set used so far for the T/M boundary is too heterogeneous and largely unreliable. In fact, the T/M chronogram is the poorest of the set of Neogene chronograms, especially in the range difference between maximum and minimum age of the error function (see Harland et al., 1990, table 5.4). It may not be by chance that both T/M and Mess/Zanc chronograms show a 'best age' (minimum of the error function) systematically older than the '*best current geological estimate*' by 1 to 2 Ma. Such a deviation could be explained with a systematic error in correlation based on continental scales and 'mammal ages'.

As a conclusion, the only way to improve the present T/M chronogram is to reduce the chronostratic error with a critical integration of biostratigraphy, chronometric datings of different types, and magnetostratigraphic control in standard sections, providing

direct dating of boundary stratotypes (and auxiliary stratotypes) whenever possible. The preliminary results obtained with this approach in the frame of the MICOP and MIOMAR projects are encouraging (Vai et al., 1992, 1993; Coccioni et al., 1992; Deino and Montanari, 1992; Krijgsman et al., 1994; several papers in this volume). In a similar way, the improvement in the geomagnetic polarity time scale for the late Cenozoic recently accomplished by Cande and Kent (1992), and especially by Baksi (1993) is based partly on new and more accurately selected radiometric calibration points, and partly on ages derived from astronomical calibration. Further improvements of this scale are expected when the new Neogene radiometric dates published in the frame of MICOP will be used as additional calibration points.

## STRATIGRAPHIC SETTING

The set of original radiometric datings discussed in this paper include those preliminarily reported by Vai et al. (1993), and nine additional measurements on eight new samples from the Monte del Casino and Monte Tondo sections. All dated horizons are found in the two well-studied Monte del Casino and Monte Tondo areas of the Romagna Northern Apennines in Italy (Fig. 1).

### *Lithostratigraphy and cyclostratigraphy*

Both areas are physically connected to each other along strike, and consist of an apparently continuous, mainly hemipelagic, marine succession interposed between a large, thick Middle Miocene turbidite body (the Marnoso–Arenacea formation), and the well known shallow-marine blanket of the (mid-late) Messinian gypsum evaporites (the Gessoso–Solfifera formation) which is a part of the Mediterranean Evaporite (Marabini and Vai, 1985; Vai, 1989b).

At the regional scale of the Romagna Apennines, this transitional hemipelagic formation (called Euxinic Pelites) shows fairly regular evidence of bathyal bathymetry with rapid final upwards shallowing in the topmost metres, close to the ‘Calcare di Base’ of the Gessoso–Solfifera formation (Vai and Ricci Lucchi, 1977). These authors interpreted the shallowing as the evaporative sea-level drop of the Messinian salinity crisis in the Mediterranean (Selli, 1960). The Euxinic Pelites are characterized by a gradual upward increase in brown disoxic to black anoxic bituminous-rich layers, cyclically intercalated to normally oxygenated grey mudstones (see Vai et al., 1993 for details).

Minor lateral variations of this general lithostratigraphic pattern are represented by: (1) thin-bedded to faint fine-grained turbidites, which are more common in the western part of the area and in the lower portion of the succession; (2) eastward increasing hemipelagic to pure pelagic conditions in the Pesaro–Ancona region; and (3) slight eastward increase in anoxic intervals, thickness and frequency.

The cyclostratigraphic potential of the lithologically supported cycles is clearly represented by the lithologic logs derived from exclusive visual survey in the field (Fig. 1). Detailed measurements of magnetic susceptibility are now in progress to integrate the logs with cycles possibly overlooked during the field survey (Krijgsman et al., 1994). The aim is to look for a statistically significant correlation with astronomical types of

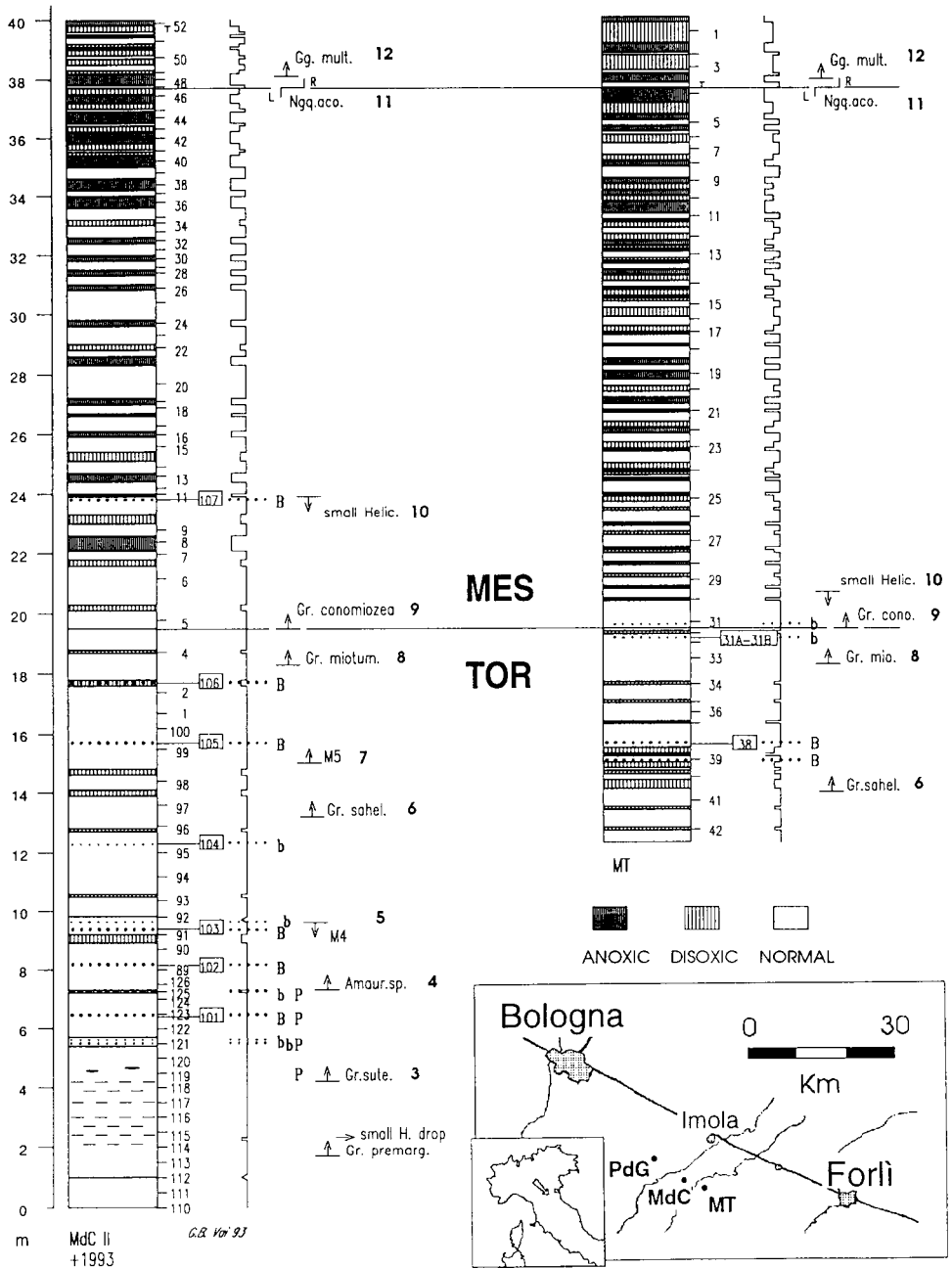


Fig. 1. Updated biostratigraphic correlation of the Monte del Casino (MdC II + 1993) and Monte Tondo (MT) sections spanning the T/M boundary (Imola–Faenza area, Northern Romagna Apennines). Samples labelled with boxes represent measured biotite-rich layers. The sinusoidal solid line to the right of the columns refers to oxio-anoxic cyclicality detected by visual inspection in the field. Bold numbers mark biostratigraphic datums.

periodicity (Berger, 1984; Shackleton et al., 1990; Hilgen, 1991a, b, etc.) providing an independent chronologic and chronometric tool (Vai, Chapter E3).

At the scale of the whole Apennines range, coeval (late Tortonian to early Messinian) hemipelagic equivalents of our Euxinic Pelites are usually found in almost all palaeotectonic domains, although they are associated with different lithologies (e.g., marls and diatomites, called Tripoli). This is interpreted as an effect of both marine flooding (and related transgressive highstand deposits), and tectonic stillstand between the mid-Tortonian and intra-Messinian deformation phases. It is important to notice that this transgressive trend is well recognized also in the historical stratotype sections of both the Tortonian (Tortona Northern Apennines), and the Messinian (Sicily) (Colalongo et al., 1979b; Grasso et al., 1990; Pedley and Grasso, 1993; Miculan, Chapter A7).

### Biostratigraphy

The Monte del Casino and Monte Tondo sections studied are excellent as far as abundance and preservation of microfossils are concerned, although perfect continuity and completeness of the fossil record is questioned (see Negri and Vigliotti, Chapter E4). The following most useful intra-Mediterranean and oceanic world-wide markers have been found above the *Globorotalia praemargaritae* occurrence (Fig. 1): (3) the *G. suteri* FAD, (4) the *Amaurolithus (delicatus and/or primus)* first occurrence datum (FOD), (5) the *G. menardii* form 4 last occurrence datum (LOD), (6) the *G. saheliana* FAD, (7) the *G. menardii* form 5 FOD, (8) the *G. miotumida* FAD, (9) the *G. conomiozea* (plus *G. mediterranea*) FAD, (10) the LOD of the small Helicoliths, (11) the sinistral to dextral shift in the *Neogloboquadrina acostaensis* shell coiling, and (12) the slightly younger FAD of *Globogerina multiloba* (Colalongo et al., 1979b; Zachariasse, 1979; Krijgsman et al., 1994).

Pending a formal definition of the Tortonian/Messinian boundary, the *G. conomiozea* FAD is taken as the most appropriate, widely used biostratigraphic criterion for correlating and defining the boundary (D'Onofrio et al., 1975; Colalongo et al., 1979b; Krijgsman et al., 1994).

The biostratigraphic correlation of the Monte del Casino and Monte Tondo sections is excellent. Particularly impressive is the perfect match in thickness of the interval between the *G. conomiozea* FAD to the *N. acostaensis* left–right coiling inversion (Fig. 1). It implies the same sedimentation rate for that interval in both sections. In the latest Tortonian the *G. saheliana* FAD suggests a sedimentation rate of the Monte del Casino section higher by about 12% with respect to the Monte Tondo one.

A further independent correlation tool is represented by high frequency palaeoclimatic cycles (including the equivalent of early Messinian  $\delta^{13}\text{C}$  negative shift) recognized on the basis of changing in relative abundance of different forms of Foraminifera; the cycles are positively correlated with  $\delta^{18}\text{O}$  cycles from well known sections, in and outside the Mediterranean (Calieri, 1992).

### Sedimentology

Composition, sedimentary structures and textures of the main recurring lithofacies types within the euxinic pelite formation have already been summarized in Vai et al.

(1993), together with the fine texture and content of the biotite-rich horizons. Some further information useful for understanding their depositional history is added here.

Most of the biotite-rich horizons are found in the light grey normally oxygenated mudstones, and the remaining ones in disoxic darker layers. They were never found enclosed within or associated to interlayered turbidites. Any type of detrital bed detectable in the outcrop is lacking in the measured parts of the two sections. However, some very subtle features (as faint gradation and sandy size of enclosed crystals) like those produced by nepheloid layers, are found in most of the biotite-rich horizons. They can be related exclusively to the settling of turbid clouds produced by volcanic eruptions and fall-out. Alternatively, they may be partly due also to a distal contribution of true turbidity currents supplied with terrigenous and volcanogenic material previously deposited in the internal, proximal part of the basin. This possibility is demonstrated by the fact that in the *Pieve di Gesso* section, some 12 km westward from *Monte Tondo*, a few biotite-rich horizons are found within faint turbidites (Odin et al., Chapter E6).

As to the biotite-rich horizons, the lowest ones are very thin with finer crystal size. The maximum crystal size is almost regularly increasing upwards, except for the *MdC104* sample which has a fine crystal size. The highest frequency or density of volcanogenic minerals was found in samples *MdC102*, *MdC103* and *MT38*.

It is important to give some explanation of the special architecture of a biotite-rich horizon. According to *Vai et al.* (1993, fig. 1A), it is composed in its core by a thin millimetre-thick parting marked by abundant biotite flakes, minor labradoritic plagioclase and quartz, and is also enriched in planktonic Foraminifera; large biotite flakes suspended in the mudstone matrix are found in a 4–6-cm-thick layer encompassing the parting. The thickness of individual partings range from 1 mm or less in sample *MdC101* up to 3–4 mm in *MdC103* and *MdC107*. The total thickness of the layer characterized by sparse biotite flakes is regularly increasing upwards from a few cm in *MdC102* to 7–10 cm in *MdC106* and *MdC107*. The frequency versus thickness distribution of volcanogenic minerals in a biotite-rich horizon, and especially the relevant amount of biotite flakes asymmetrically dispersed in a floating attitude within the mudstones facing the parting, can hardly be explained as a pure primary setting.

The original accumulation of a volcano-sedimentary layer can be viewed as an integrated result of discrete explosive pulses lasting some hundreds to thousand of years (i.e., a volcanic cycle) recurring sometimes after intervals of volcanic stasis over a time span of some hundreds of ka. On the other hand, a sequence of discrete volcano-sedimentary layers may derive from different, magmatically related or unrelated individual volcanoes. After the accumulation, the layer has undergone some changes following two main modifying factors: bioturbation, and extremely fine-scale mudflows (i.e., vertical mixing and reworking).

Bioturbation seems to be the most effective process able to modify the original distribution of volcanogenic minerals. The asymmetrical final distribution of the biotite flakes is explained with a burrowing activity preferentially oriented from bottom to top in the sedimentary layer. The apparent minor modification of isometric minerals is simply the consequence of their relative scarcity as compared with the abundance of biotite. Mini-flows of original millimetric mudstone laminae may have helped to reach the final floating to chaotic setting of the biotite flakes.



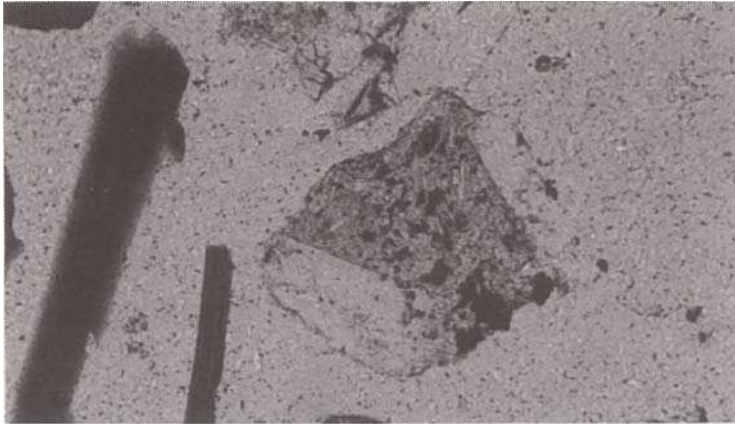


Fig. 2. Micrograph of sample MT38 showing a volcanic rock fragment (450  $\mu\text{m}$  long) with plagioclase and biotite crystals.

## QUALITY OF GEOCHRONOMETERS

In order to evaluate the most suitable minerals for geochronometrical investigations, two kind of analyses were run: diffractometrical (XRD, Philips diffractometer,  $\text{CuK}\alpha$  radiation) and chemical (SEM–EDS, details are described by Gasparotto, 1988). The use of these different methods was thought necessary, because the results from each one can be regarded with a different philosophy. In fact, while XRD gives synthetic results (a large amount of sample is analyzed), the SEM–EDS is an analytical method that enables detailed investigation of single crystals and within crystal (for example inclusions in biotites).

Preliminary optical and XRD investigations revealed the occurrence of feldspars, biotite, biogenic carbonates and quartz in all samples; the amount of each mineral varies from one sample to another. Volcanic rock fragments are present in all samples (Fig. 2), but their amount is low. The association of biogenic carbonates (detected by optical observations), and abundant quartz (detected by XRD) point out a dilute volcanoclastic input; in particular sample MdC104 is the richest in non-volcanogenic phases and was consequently excluded during preliminary radiometric measurements. Other phases extraneous to volcanoclastic contribution are gypsum (in samples MT38, MdC101, MdC103 and MdC107), and chlorite (sample MdC102). Gypsum can be considered as a diagenetic product due to the high sulfate content of circulating fluids (evaporite deposits are nearby), but it can also originate from weathering of pyrite and other sulphides that are abundant in the section (Dinelli and Tateo, 1993). Also some feldspar crystal with exsolution lamellae can be considered a signal of non-volcanoclastic origin, basically because this kind of texture was never observed in volcanoclastic materials of Miocene age in the Northern Apennines (Mezzetti et al., 1991). For these reasons plagioclase from the layers studied must be considered with caution when a geochronometric age determination is attempted, even if EDS data (36 analyses) display little dispersion (from about  $\text{An}_{40}$  to  $\text{An}_{70}$ , with 1 crystal  $\text{Or}_{90}$ ).

Table 4

XRD values of  $d$  001 of biotites from the Monte del Casino section

Sample (m level)	$d$ 001 (Å)
MdC101	10.0
MdC102	10.2
MdC103	10.0
MdC104	10.0
MdC105	10.0
MdC106	10.0
MdC107	10.1
MT31A -31B	10.1
MT38	9.9

The position of the 101 reflection of quartz is taken as internal standard; estimated error  $\pm 0.1$  Å.

Because the most peculiar feature of the selected samples is the occurrence of sand-sized biotite flakes, they were analyzed with special attention. Biotite crystals from all samples display sub-euhedral shapes, sometimes euhedral; inclusions are abundant (mainly apatite), but flakes look transparent and pristine. A definitive confirmation about possible crystal-chemical alteration of biotites can be achieved by the XRD technique which enabled to identify well crystallized biotite (sharp peaks) in all samples, without any significative shift of the  $d$  001 spacing (Table 4) from theoretical values (the  $d$  001 is very sensitive to hydration and vermiculitization).

A direct confirmation of crystal-chemical properties of biotites arises from chemical analyses by the SEM-EDS method. They were performed on about 15 biotite crystals for each sample (average data reported in Table 5). The analyses were run moving throughout the polished section avoiding to be restricted in selected portions only. In this way, the distribution of analyzed crystals was random, i.e., the possibility to detect the whole compositional spectrum is highest because the selection was not drawn by any physical criteria (this was not the case for the biotite fractions used for radiometric measurements). The quality of measurement was tested by computing crystal-chemical formulas for each crystal. Reasonable results were achieved for all; only one analysis of sample MT38 (the richest in MgO) has a number of ions in octahedral coordination (5.6 per formula unit) that is near the boundary of most common occurrences (Deer et al., 1992). More detailed evaluation of this analysis requires other information not available at the moment (for example the  $\text{Fe}^{2+}$  and  $\text{Fe}^{3+}$ , F, etc.). Because of low scattering of other analyses from the same sample, this particular one was excluded from the average calculation in Table 5.

As a general remark concerning the quality of these biotites as geochronometers, it is important to note that the  $\text{K}_2\text{O}\%$  content is always very high, and all samples can be considered reliable according to Odin et al. (1991). Nevertheless, some other considerations can be added. In Fig. 3, the chemical results are plotted in order to evaluate the compositional homogeneity within the same sample. To represent the situation as simple as possible, two groups of samples can be identified: the first group displays little dispersion around a medium point (MdC104, MdC103, MdC101, MT38); the second group displays some more scattering along an imaginary line parallel to

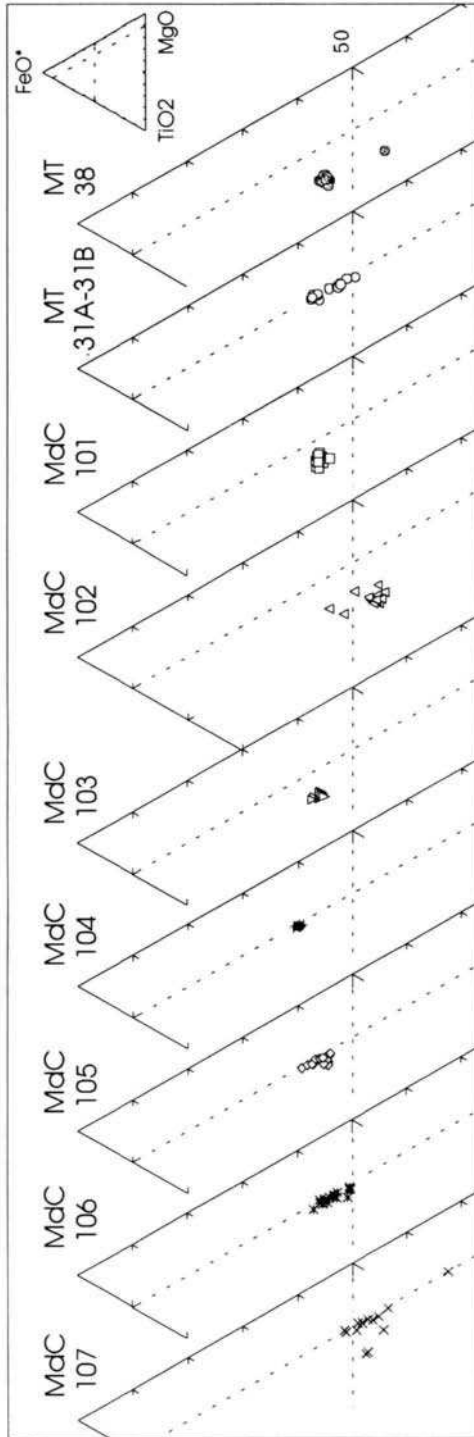


Fig. 3. Triangular diagrams showing the results of EDS analyses of biotite crystals (oxides %). Dotted lines are drawn to help comparisons.

Table 5

Chemical analyses of biotites (EDS) recalculated to anhydrous basis

Sample (Number of analyses)		SiO <sub>2</sub>	TiO <sub>2</sub>	Al <sub>2</sub> O <sub>3</sub>	FeO*	MnO	MgO	CaO	Na <sub>2</sub> O	K <sub>2</sub> O	FeO*/MgO
MdC 107 (15)	average	38.81	3.94	16.06	16.09	0.09	14.73	tr.	0.52	9.71	1.11
	± 1σ	0.42	0.73	0.26	1.72	0.07	1.42		0.11	0.14	0.19
MdC 106 (16)	average	38.24	3.80	16.04	18.92	0.19	12.61	tr.	0.41	9.70	1.51
	± 1σ	0.28	0.17	0.25	0.83	0.06	0.63		0.14	0.09	0.14
MdC 105 (15)	average	37.96	3.86	15.95	19.91	0.21	11.88	0.11	0.30	9.80	1.68
	± 1σ	0.31	0.24	0.40	0.53	0.09	0.48	0.04	0.10	0.10	0.11
MdC 104 (15)	average	37.22	3.59	17.84	20.72	0.21	10.26	tr.	0.27	9.84	2.02
	± 1σ	0.28	0.09	0.35	0.21	0.05	0.14		0.10	0.08	0.04
MdC 103 (15)	average	37.41	5.34	15.21	20.89	0.12	11.10	tr.	0.47	9.44	1.88
	± 1σ	0.20	0.13	0.12	0.29	0.09	0.18		0.13	0.09	0.05
MdC 102 (15)	average	37.87	6.35	15.33	17.23	0.08	13.17	tr.	0.56	9.39	1.32
	± 1σ	0.28	0.42	0.23	1.16	0.07	0.68		0.10	0.09	0.17
MdC 101 (15)	average	37.30	5.09	15.22	20.87	0.13	11.35	tr.	0.56	9.41	1.84
	± 1σ	0.39	0.28	0.31	0.29	0.08	0.29		0.10	0.05	0.06
MT 31A-31B (15)	average	38.26	3.65	15.94	19.25	0.16	12.51	tr.	0.44	9.75	1.55
	± 1σ	0.42	0.13	0.38	1.03	0.10	0.80		0.14	0.13	0.18
MT 38 (14)	average	37.35	5.82	15.07	20.64	0.14	11.06	tr.	0.51	9.36	1.87
	± 1σ	0.24	0.21	0.10	0.30	0.07	0.15		0.10	0.12	0.05

FeO\* = total iron.

the FeO–MgO side (MdC107, MdC106, MdC105, MdC102, MT31A–31B). With some more detail, the following evaluation of chemical heterogeneity of the analyzed biotites is possible: excellent (MdC104), excellent partly bimodal (MT38), good (MdC101, MdC103), poor (MdC102, MdC105, MdC106), poor and bimodal (MT31A–31B, MdC107). The chemical heterogeneity within a sample can be considered to reflect true different compositions or the result of alteration processes. To check this point the K<sub>2</sub>O% (assumed as an indicator of the degree of alteration) was plotted against the FeO\*/MgO ratio (Fig. 4). In all samples the scattered FeO\*/MgO values do not match any K<sub>2</sub>O variation; this feature points out a primary heterogeneity of crystal–chemical composition whose causes have to be found in the magmatic history or in a multiple source of the volcanic detritus. Sample MdC107 displays the most complex situation because the range of FeO\*/MgO values is very high, and the TiO<sub>2</sub> content of two samples is significantly higher than other crystals of the same sample (Fig. 2). These data, coupled with optical observations (feldspars with exsolution textures), depict a suspicious situation for geochronometrical use of this sample in particular, because the more heterogeneous is the composition, the most complex is the history of the sediment components. Similar considerations could be applied to all samples with scattered composition, but the high K<sub>2</sub>O content and the low *d* 001 values of all nine samples support an optimistic view concerning good potentialities of these biotites as geochronometers because no alteration effects are detected.

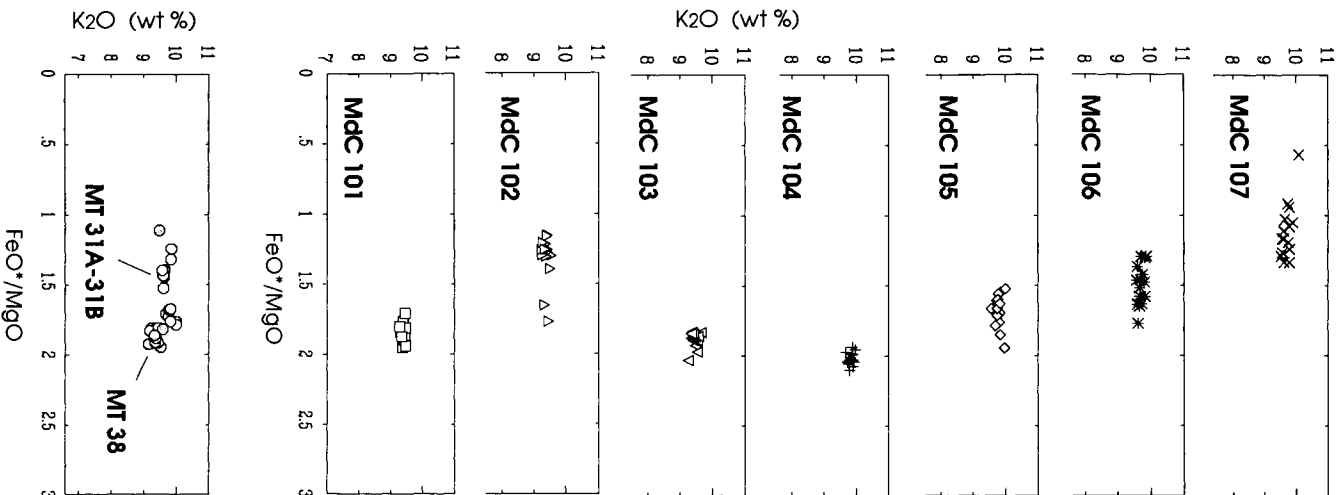


Fig. 4. K<sub>2</sub>O% vs. FeO\*/MgO ratio of biotite crystals (anhydrous EDS data).

Even though the analysis of the magmatic environment is not the aim of this work, simple considerations can be added based on the mineral assemblage, and composition of the feldspars. First of all, in all samples biotite is the exclusive mafic mineral; this is an indication of low Fe, Mg concentration. Feldspars display a plagioclase composition that can be due to sub-alkaline affinity of magmas. From these observations it is possible to conclude that the source of volcanoclastic materials was an intermediate-acidic volcanic suite with a calc-alkaline affinity.

An additional conclusive consideration must be put forward with regard to the comparison of biotite chemistry in the MdC and MT sections. One sample of the MT section (MT31A–31B) is comparable to samples MdC105 and MdC106, whereas sample MT38 displays chemical similarities with samples MdC101 and MdC103. However, these chemical affinities are not matched with stratimetric data (Fig. 1). This implies that the lateral continuity of these biotite-rich layers is very poor, and that the number of volcanoclastic layers is higher than suspected.

## RADIOMETRIC DATING

### Results

Seven volcanoclastic biotite-rich levels from a 17-m-thick clay deposit, on Monte del Casino II section '+ 1993', and one from the Monte Tondo section, were selected for  $^{40}\text{Ar}/^{39}\text{Ar}$  radiometric datings in order to constrain the Tortonian/Messinian boundary.

The age monitor used for this experiment was FCT#3 biotite: our laboratory currently uses an age of  $27.55 \pm 0.08$  Ma (Lanphere et al., 1990). Different ages for this standard are reported in the literature (Izett et al., 1991; Baksi, 1993). Renne et al. (1994) and Swisher et al. (1994) propose that the sanidine from the same rock has an age of 27.95 Ma and 28.05 Ma, respectively.

Samples were measured using conventional step-heating experiments and analytical data are reported in Table 6 (see also note in Table 7, and discussion in Chapter F1 for more details and explanations of the techniques and analytical procedures used). Errors quoted in this part and in displayed graphs are  $1\sigma$  in-run analytical errors only. Uncertainties related to monitor age measures and to neutron flux variations (which we may summarize as error in  $J$ ), are considered systematic in the frame of a single measure, and are added after plateau and isochron age calculations, forming what we call a total error, which is used in the general discussion and in the summary table. Biotite MdC101 has a slightly disturbed spectrum (Fig. 5A), and its plateau age ( $t_{\text{pl}}$  in the following discussion),  $7.32 \pm 0.02$  Ma ( $1\sigma$ ) is statistically unacceptable (MSWD = 4.6), while the same steps (3–5) give an acceptable isochron with a younger age of  $7.25 \pm 0.03$  (Fig. 5B). Its initial  $^{40}\text{Ar}/^{36}\text{Ar}$  dating is slightly radiogenic and it may account for the observed spectrum. MdC102 has an almost perfect spectrum (steps 3–8), with a  $t_{\text{pl}}$  of  $7.28 \pm 0.01$  (Fig. 5C), isochron age ( $t_{\text{is}}$  hereforth) of  $7.27 \pm 0.02$  (Fig. 5D), and an integrated total age ( $t_{\text{tot}}$  in the following discussion) of 7.31 Ma coincident with within error, and atmospheric intercept ( $299 \pm 3$ ).

From MdC103 we separated two mineral phases: plagioclase and biotite. The latter displays a fairly flat spectrum, but fails to identify a plateau or an isochron (Fig. 5E,F), and its total age is 7.30 Ma. The former has a gently saddle-shaped spectrum, with a minimum

Table 6

Analytical data from Ar/Ar step-heating experiments on samples from the Monte del Casino section

T(°C)	<sup>40</sup> Ar <sub>tot</sub>	<sup>39</sup> Ar	<sup>38</sup> Ar	<sup>37</sup> Ar	<sup>36</sup> Ar	Age (Ma)
<i>MT31, biotite, J = 4.400 · 10<sup>-4</sup>, p = 26.80 mg</i>						
700	3.864 · 10 <sup>-7</sup> ± 7 · 10 <sup>-10</sup>	1.437 · 10 <sup>-9</sup> ± 7	2.57 · 10 <sup>-10</sup> ± 4	6.37 · 10 <sup>-11</sup> ± 1.01	1.22 · 10 <sup>-9</sup> ± 1	15.04 ± 1.60
760	4.721 · 10 <sup>-7</sup> ± 11	1.930 · 10 <sup>-8</sup> ± 6	8.20 · 10 <sup>-10</sup> ± 8	1.29 · 10 <sup>-11</sup> ± 1.43	9.88 · 10 <sup>-10</sup> ± 8	7.39 ± 0.10
820	3.425 · 10 <sup>-7</sup> ± 8	2.821 · 10 <sup>-8</sup> ± 7	1.01 · 10 <sup>-9</sup> ± 1	bd.l.	2.97 · 10 <sup>-10</sup> ± 3	7.18 ± 0.04
900	2.341 · 10 <sup>-7</sup> ± 4	2.317 · 10 <sup>-8</sup> ± 7	7.88 · 10 <sup>-10</sup> ± 5	bd.l.	8.88 · 10 <sup>-11</sup> ± 20	7.10 ± 0.03
960	2.405 · 10 <sup>-7</sup> ± 6	2.360 · 10 <sup>-8</sup> ± 8	8.12 · 10 <sup>-10</sup> ± 6	4.84 · 10 <sup>-11</sup> ± 1.18	9.97 · 10 <sup>-11</sup> ± 20	7.08 ± 0.03
1020	6.074 · 10 <sup>-7</sup> ± 11	6.107 · 10 <sup>-8</sup> ± 13	2.10 · 10 <sup>-9</sup> ± 1	5.51 · 10 <sup>-11</sup> ± 1.91	1.88 · 10 <sup>-10</sup> ± 3	7.16 ± 0.02
1080	7.209 · 10 <sup>-7</sup> ± 14	6.879 · 10 <sup>-8</sup> ± 15	2.37 · 10 <sup>-9</sup> ± 1	1.11 · 10 <sup>-10</sup> ± 13	3.38 · 10 <sup>-10</sup> ± 4	7.15 ± 0.03
1150	8.890 · 10 <sup>-8</sup> ± 12	6.368 · 10 <sup>-9</sup> ± 20	2.40 · 10 <sup>-10</sup> ± 5	1.63 · 10 <sup>-10</sup> ± 11	1.04 · 10 <sup>-10</sup> ± 2	7.25 ± 0.06
1300	3.638 · 10 <sup>-8</sup> ± 7 · 10 <sup>-11</sup>	4.547 · 10 <sup>-10</sup> ± 38	3.73 · 10 <sup>-11</sup> ± 27	1.67 · 10 <sup>-11</sup> ± 1.20	1.02 · 10 <sup>-10</sup> ± 2	11.10 ± 0.96
Total age						
<i>MdC101, biotite, J = 4.133 · 10<sup>-4</sup>, p = 39.98 mg</i>						
640	1.072 · 10 <sup>-9</sup> ± 2	1.001 · 10 <sup>-11</sup> ± 12	1.13 · 10 <sup>-12</sup> ± 5	5.34 · 10 <sup>-13</sup> ± 1.50	3.11 · 10 <sup>-12</sup> ± 6	11.26 ± 1.40
760	1.940 · 10 <sup>-8</sup> ± 4	1.313 · 10 <sup>-9</sup> ± 3	6.96 · 10 <sup>-11</sup> ± 3	3.32 · 10 <sup>-12</sup> ± 25	2.09 · 10 <sup>-11</sup> ± 2	7.49 ± 0.04
820	2.891 · 10 <sup>-8</sup> ± 4	2.768 · 10 <sup>-9</sup> ± 6	1.38 · 10 <sup>-10</sup> ± 0	3.66 · 10 <sup>-12</sup> ± 14	6.23 · 10 <sup>-12</sup> ± 13	7.28 ± 0.02
880	1.053 · 10 <sup>-8</sup> ± 3	9.243 · 10 <sup>-10</sup> ± 26	4.71 · 10 <sup>-11</sup> ± 3	1.99 · 10 <sup>-12</sup> ± 19	4.98 · 10 <sup>-12</sup> ± 9	7.30 ± 0.04
930	7.658 · 10 <sup>-9</sup> ± 13	5.675 · 10 <sup>-10</sup> ± 12	2.99 · 10 <sup>-11</sup> ± 2	6.23 · 10 <sup>-12</sup> ± 19	6.82 · 10 <sup>-12</sup> ± 8	7.40 ± 0.04
1000	1.474 · 10 <sup>-8</sup> ± 2	1.194 · 10 <sup>-9</sup> ± 2	6.18 · 10 <sup>-11</sup> ± 4	1.36 · 10 <sup>-11</sup> ± 3	1.05 · 10 <sup>-11</sup> ± 2	7.26 ± 0.03
1070	1.900 · 10 <sup>-8</sup> ± 3	1.572 · 10 <sup>-9</sup> ± 3	7.96 · 10 <sup>-11</sup> ± 3	1.52 · 10 <sup>-11</sup> ± 5	1.20 · 10 <sup>-11</sup> ± 1	7.31 ± 0.02
1240	1.060 · 10 <sup>-9</sup> ± 2	2.260 · 10 <sup>-11</sup> ± 9	1.55 · 10 <sup>-12</sup> ± 7	2.69 · 10 <sup>-13</sup> ± 3.60	2.76 · 10 <sup>-12</sup> ± 7	7.99 ± 0.70
Total age						
						7.33

Table 6

*Continued.*

T(°C)	<sup>40</sup> Ar/ <sup>tot</sup>	<sup>39</sup> Ar	<sup>38</sup> Ar	<sup>37</sup> Ar	<sup>36</sup> Ar	Age (Ma)
<i>McCl02, biotite, J = 4.133 · 10<sup>-4</sup>, p = 42.32 mg</i>						
640	5.487 · 10 <sup>-9</sup> ± 9	3.419 · 10 <sup>-11</sup> ± 18	4.28 · 10 <sup>-12</sup> ± 7	1.77 · 10 <sup>-12</sup> ± 19	1.68 · 10 <sup>-11</sup> ± 2	11.19 ± 1.20
760	1.792 · 10 <sup>-8</sup> ± 3	1.254 · 10 <sup>-9</sup> ± 3	4.31 · 10 <sup>-11</sup> ± 2	3.54 · 10 <sup>-12</sup> ± 31	1.85 · 10 <sup>-11</sup> ± 2	7.39 ± 0.04
820	2.318 · 10 <sup>-8</sup> ± 4	2.197 · 10 <sup>-9</sup> ± 4	7.07 · 10 <sup>-11</sup> ± 4	3.49 · 10 <sup>-12</sup> ± 32	5.82 · 10 <sup>-12</sup> ± 10	7.27 ± 0.02
880	2.092 · 10 <sup>-8</sup> ± 3	1.973 · 10 <sup>-9</sup> ± 4	6.34 · 10 <sup>-11</sup> ± 3	2.68 · 10 <sup>-12</sup> ± 19	5.42 · 10 <sup>-12</sup> ± 11	7.29 ± 0.02
930	7.780 · 10 <sup>-9</sup> ± 20	5.956 · 10 <sup>-10</sup> ± 15	2.05 · 10 <sup>-11</sup> ± 2	3.74 · 10 <sup>-12</sup> ± 32	6.50 · 10 <sup>-12</sup> ± 8	7.32 ± 0.04
1000	1.167 · 10 <sup>-8</sup> ± 2	8.678 · 10 <sup>-10</sup> ± 23	2.99 · 10 <sup>-11</sup> ± 2	8.83 · 10 <sup>-12</sup> ± 19	1.06 · 10 <sup>-11</sup> ± 1	7.32 ± 0.04
1070	1.920 · 10 <sup>-8</sup> ± 3	1.602 · 10 <sup>-9</sup> ± 3	5.29 · 10 <sup>-11</sup> ± 3	1.24 · 10 <sup>-11</sup> ± 3	1.21 · 10 <sup>-11</sup> ± 1	7.25 ± 0.02
1240	4.552 · 10 <sup>-9</sup> ± 6	3.275 · 10 <sup>-10</sup> ± 9	1.13 · 10 <sup>-11</sup> ± 1	2.15 · 10 <sup>-12</sup> ± 21	4.56 · 10 <sup>-12</sup> ± 10	7.29 ± 0.71

Total age

7.31

*McCl03, plagioclase, J = 4.211 · 10<sup>-4</sup>, p = 163.0 mg*

700	1.113 · 10 <sup>-7</sup> ± 1	4.116 · 10 <sup>-10</sup> ± 15	6.94 · 10 <sup>-11</sup> ± 9	1.64 · 10 <sup>-9</sup> ± 2	3.51 · 10 <sup>-10</sup> ± 2	14.13 ± 1.20
830	6.107 · 10 <sup>-8</sup> ± 13	2.356 · 10 <sup>-9</sup> ± 6	5.48 · 10 <sup>-11</sup> ± 6	1.45 · 10 <sup>-8</sup> ± 1	1.34 · 10 <sup>-10</sup> ± 1	7.35 ± 0.12
900	2.858 · 10 <sup>-8</sup> ± 6	2.255 · 10 <sup>-9</sup> ± 8	3.57 · 10 <sup>-11</sup> ± 4	1.47 · 10 <sup>-8</sup> ± 1	2.96 · 10 <sup>-11</sup> ± 4	7.10 ± 0.05
960	2.976 · 10 <sup>-8</sup> ± 5	2.654 · 10 <sup>-9</sup> ± 8	4.04 · 10 <sup>-11</sup> ± 8	1.75 · 10 <sup>-8</sup> ± 1	2.34 · 10 <sup>-11</sup> ± 5	6.96 ± 0.04
1030	3.747 · 10 <sup>-8</sup> ± 7	2.514 · 10 <sup>-9</sup> ± 7	4.53 · 10 <sup>-11</sup> ± 8	1.63 · 10 <sup>-8</sup> ± 1	5.18 · 10 <sup>-11</sup> ± 7	7.11 ± 0.06
1100	3.342 · 10 <sup>-8</sup> ± 9	1.692 · 10 <sup>-9</sup> ± 4	3.94 · 10 <sup>-11</sup> ± 5	1.06 · 10 <sup>-8</sup> ± 0	6.15 · 10 <sup>-11</sup> ± 6	7.24 ± 0.08
1190	2.851 · 10 <sup>-8</sup> ± 5	1.529 · 10 <sup>-9</sup> ± 4	4.07 · 10 <sup>-11</sup> ± 6	9.72 · 10 <sup>-9</sup> ± 5	4.76 · 10 <sup>-11</sup> ± 9	7.58 ± 0.13
1280	1.606 · 10 <sup>-8</sup> ± 4	9.760 · 10 <sup>-10</sup> ± 30	3.74 · 10 <sup>-11</sup> ± 7	6.54 · 10 <sup>-9</sup> ± 3	2.44 · 10 <sup>-11</sup> ± 7	7.31 ± 0.15
1350	1.192 · 10 <sup>-8</sup> ± 2	5.754 · 10 <sup>-10</sup> ± 23	2.58 · 10 <sup>-11</sup> ± 7	3.93 · 10 <sup>-9</sup> ± 3	2.14 · 10 <sup>-11</sup> ± 5	7.83 ± 0.18
1400	5.477 · 10 <sup>-8</sup> ± 14	1.156 · 10 <sup>-9</sup> ± 5	5.49 · 10 <sup>-11</sup> ± 8	7.78 · 10 <sup>-9</sup> ± 4	1.44 · 10 <sup>-10</sup> ± 1	8.46 ± 0.23
1500	2.563 · 10 <sup>-8</sup> ± 5	6.563 · 10 <sup>-11</sup> ± 54	1.70 · 10 <sup>-11</sup> ± 3	4.30 · 10 <sup>-10</sup> ± 7	8.53 · 10 <sup>-11</sup> ± 8	5.21 ± 2.70
Total age						7.48



Table 6

*Continued.*

T(°C)	<sup>40</sup> Ar/ <sub>tot</sub>	<sup>39</sup> Ar	<sup>38</sup> Ar	<sup>37</sup> Ar	<sup>36</sup> Ar	Age (Ma)
<i>MaCl03, biotite, J = 4.209 · 10<sup>-4</sup>, p = 46.35 mg</i>						
700	3.132 · 10 <sup>-7</sup>	2.317 · 10 <sup>-9</sup>	2.94 · 10 <sup>-10</sup>	7.59 · 10 <sup>-11</sup>	9.60 · 10 <sup>-10</sup>	9.68
	± 7	± 6	± 3	±79	± 7	±0.69
830	7.874 · 10 <sup>-7</sup>	6.801 · 10 <sup>-8</sup>	3.66 · 10 <sup>-9</sup>	2.59 · 10 <sup>-10</sup>	4.44 · 10 <sup>-10</sup>	7.31
	± 10	± 13	± 1	±14	± 4	±0.02
900	5.467 · 10 <sup>-7</sup>	5.399 · 10 <sup>-8</sup>	2.85 · 10 <sup>-9</sup>	1.11 · 10 <sup>-10</sup>	1.07 · 10 <sup>-10</sup>	7.23
	± 8	± 9	± 1	± 7	± 1	±0.02
960	1.929 · 10 <sup>-7</sup>	1.598 · 10 <sup>-8</sup>	8.70 · 10 <sup>-10</sup>	1.08 · 10 <sup>-10</sup>	1.27 · 10 <sup>-10</sup>	7.37
	± 3	± 3	± 6	±13	± 2	±0.03
1030	1.985 · 10 <sup>-7</sup>	1.605 · 10 <sup>-8</sup>	8.83 · 10 <sup>-10</sup>	2.30 · 10 <sup>-10</sup>	1.52 · 10 <sup>-10</sup>	7.25
	± 5	± 3	± 6	±19	± 3	±0.05
1100	3.367 · 10 <sup>-7</sup>	2.884 · 10 <sup>-8</sup>	1.57 · 10 <sup>-9</sup>	4.19 · 10 <sup>-10</sup>	1.96 · 10 <sup>-10</sup>	7.32
	± 6	± 8	± 1	±13	± 2	±0.03
1160	3.289 · 10 <sup>-7</sup>	3.034 · 10 <sup>-8</sup>	1.61 · 10 <sup>-9</sup>	3.63 · 10 <sup>-10</sup>	1.38 · 10 <sup>-10</sup>	7.20
	± 4	± 5	± 1	± 8	± 2	±0.02
1350	1.546 · 10 <sup>-8</sup>	3.146 · 10 <sup>-10</sup>	2.29 · 10 <sup>-11</sup>	1.47 · 10 <sup>-11</sup>	4.41 · 10 <sup>-11</sup>	5.89
	± 3	± 19	±12	±1.20	±14	±0.97
Total age						
						7.30
<i>MaCl04, biotite, J = 4.209 · 10<sup>-4</sup>, p = 42.53 mg</i>						
700	2.100 · 10 <sup>-7</sup>	1.951 · 10 <sup>-9</sup>	1.63 · 10 <sup>-10</sup>	1.36 · 10 <sup>-10</sup>	5.59 · 10 <sup>-10</sup>	17.35
	± 5	± 8	± 2	±11	± 5	±0.59
770	4.833 · 10 <sup>-7</sup>	2.909 · 10 <sup>-8</sup>	1.03 · 10 <sup>-9</sup>	1.10 · 10 <sup>-10</sup>	4.62 · 10 <sup>-10</sup>	9.03
	± 4	± 6	± 1	±10	± 4	±0.04
830	5.537 · 10 <sup>-7</sup>	4.502 · 10 <sup>-8</sup>	1.50 · 10 <sup>-9</sup>	1.10 · 10 <sup>-10</sup>	2.04 · 10 <sup>-10</sup>	8.30
	± 11	± 10	± 1	±15	± 3	±0.03
900	4.132 · 10 <sup>-7</sup>	3.343 · 10 <sup>-8</sup>	1.10 · 10 <sup>-9</sup>	4.50 · 10 <sup>-11</sup>	1.35 · 10 <sup>-10</sup>	8.46
	± 4	± 7	± 1	±99	± 2	±0.02
960	3.337 · 10 <sup>-7</sup>	1.921 · 10 <sup>-8</sup>	6.44 · 10 <sup>-10</sup>	5.02 · 10 <sup>-11</sup>	1.80 · 10 <sup>-10</sup>	11.05
	± 4	± 4	± 3	±96	± 2	±0.04
1030	5.301 · 10 <sup>-7</sup>	4.118 · 10 <sup>-8</sup>	1.36 · 10 <sup>-9</sup>	6.48 · 10 <sup>-11</sup>	2.34 · 10 <sup>-10</sup>	8.48
	± 7	± 9	± 1	±2.40	± 4	±0.03
1100	5.204 · 10 <sup>-7</sup>	4.324 · 10 <sup>-8</sup>	1.42 · 10 <sup>-9</sup>	3.39 · 10 <sup>-11</sup>	2.31 · 10 <sup>-10</sup>	7.92
	± 6	± 9	± 1	±1.50	± 3	±0.02
1160	7.399 · 10 <sup>-8</sup>	5.508 · 10 <sup>-9</sup>	1.77 · 10 <sup>-10</sup>	4.34 · 10 <sup>-11</sup>	5.59 · 10 <sup>-11</sup>	7.91
	± 13	± 15	± 6	± 1.90	±49	±0.20
1350	1.217 · 10 <sup>-8</sup>	9.872 · 10 <sup>-11</sup>	9.53 · 10 <sup>-12</sup>	0.17 · 10 <sup>-11</sup>	3.56 · 10 <sup>-11</sup>	12.68
	± 2	±130	±2.00	±1.30	±13	±2.80
Total age						
						8.70

Table 6

*Continued.*

T(°C)	<sup>40</sup> Ar <sub>tot</sub>	<sup>39</sup> Ar	<sup>38</sup> Ar	<sup>37</sup> Ar	<sup>36</sup> Ar	Age (Ma)
<i>MaC105, biotite, J = 4.129 · 10<sup>-4</sup>, p = 60.23 mg</i>						
640	1.343 · 10 <sup>-8</sup> ± 2	1.228 · 10 <sup>-10</sup> ± 5	1.11 · 10 <sup>-11</sup> ± 1	5.52 · 10 <sup>-11</sup> ± 6	3.77 · 10 <sup>-11</sup> ± 3	13.91 ±0.46
760	3.126 · 10 <sup>-8</sup> ± 5	2.187 · 10 <sup>-9</sup> ± 4	7.74 · 10 <sup>-11</sup> ± 3	1.03 · 10 <sup>-11</sup> ± 4	2.85 · 10 <sup>-11</sup> ± 2	7.76 ±0.03
820	2.346 · 10 <sup>-8</sup> ± 3	2.191 · 10 <sup>-9</sup> ± 4	7.29 · 10 <sup>-11</sup> ± 4	5.56 · 10 <sup>-12</sup> ±20	5.76 · 10 <sup>-12</sup> ± 8	7.38 ±0.02
880	2.609 · 10 <sup>-8</sup> ± 3	2.373 · 10 <sup>-9</sup> ± 4	7.86 · 10 <sup>-11</sup> ± 3	8.21 · 10 <sup>-12</sup> ±20	8.09 · 10 <sup>-12</sup> ±12	7.42 ±0.02
930	2.512 · 10 <sup>-8</sup> ± 3	2.224 · 10 <sup>-9</sup> ± 5	7.43 · 10 <sup>-11</sup> ± 3	1.35 · 10 <sup>-11</sup> ± 3	9.96 · 10 <sup>-12</sup> ±14	7.41 ±0.02
1000	3.028 · 10 <sup>-8</sup> ± 4	2.714 · 10 <sup>-9</sup> ± 5	9.06 · 10 <sup>-11</sup> ± 4	2.05 · 10 <sup>-11</sup> ± 4	1.12 · 10 <sup>-11</sup> ±12	7.39 ±0.02
1070	1.454 · 10 <sup>-8</sup> ± 2	1.258 · 10 <sup>-9</sup> ± 4	4.26 · 10 <sup>-11</sup> ± 2	3.27 · 10 <sup>-11</sup> ± 5	7.28 · 10 <sup>-12</sup> ±12	7.32 ±0.03
1240	1.479 · 10 <sup>-9</sup> ± 3	1.669 · 10 <sup>-11</sup> ± 7	1.50 · 10 <sup>-12</sup> ± 7	5.02 · 10 <sup>-12</sup> ±41	4.15 · 10 <sup>-12</sup> ±8 · 10 <sup>-14</sup>	11.22 ±0.98
Total age						
<i>MaC106, biotite, J = 4.127 · 10<sup>-4</sup>, p = 49.27 mg</i>						
640	1.258 · 10 <sup>-8</sup> ± 2	7.376 · 10 <sup>-11</sup> ± 36	9.45 · 10 <sup>-12</sup> ±11	4.77 · 10 <sup>-12</sup> ±41	3.65 · 10 <sup>-11</sup> ± 3	17.94 ±0.87
760	3.260 · 10 <sup>-8</sup> ± 6	1.710 · 10 <sup>-9</sup> ± 3	6.67 · 10 <sup>-11</sup> ± 3	7.23 · 10 <sup>-12</sup> ±25	5.18 · 10 <sup>-11</sup> ± 4	7.52 ±0.05
820	1.809 · 10 <sup>-8</sup> ± 2	1.636 · 10 <sup>-9</sup> ± 3	5.56 · 10 <sup>-11</sup> ± 3	4.06 · 10 <sup>-12</sup> ±21	7.07 · 10 <sup>-12</sup> ± 9	7.27 ±0.02
880	1.640 · 10 <sup>-8</sup> ± 2	1.452 · 10 <sup>-9</sup> ± 3	4.96 · 10 <sup>-11</sup> ± 2	4.61 · 10 <sup>-12</sup> ±15	7.31 · 10 <sup>-12</sup> ±11	7.28 ±0.02
970	3.595 · 10 <sup>-8</sup> ± 7	3.234 · 10 <sup>-9</sup> ± 12	1.09 · 10 <sup>-10</sup> ± 1	1.63 · 10 <sup>-11</sup> ± 2	1.41 · 10 <sup>-11</sup> ± 1	7.30 ±0.03
1030	2.578 · 10 <sup>-8</sup> ± 2	2.306 · 10 <sup>-9</sup> ± 5	7.78 · 10 <sup>-11</sup> ± 4	1.59 · 10 <sup>-11</sup> ± 3	1.13 · 10 <sup>-11</sup> ± 2	7.23 ±0.02
1100	2.433 · 10 <sup>-9</sup> ± 4	1.344 · 10 <sup>-10</sup> ± 5	5.19 · 10 <sup>-12</sup> ±10	9.04 · 10 <sup>-12</sup> ±24	3.55 · 10 <sup>-12</sup> ± 8	7.65 ±0.14
1230	1.068 · 10 <sup>-9</sup> ± 2	5.535 · 10 <sup>-12</sup> ± 89	7.08 · 10 <sup>-13</sup> ±78	4.80 · 10 <sup>-13</sup> ±1.60	3.19 · 10 <sup>-12</sup> ± 8	16.65 ±3.10
Total age						7.40

Table 6

Continued.

T(°C)	$^{40}\text{Ar}_{\text{tot}}$	$^{39}\text{Ar}$	$^{38}\text{Ar}$	$^{37}\text{Ar}$	$^{36}\text{Ar}$	Age (Ma)
<i>MdC107, biotite, <math>J = 4.420 \cdot 10^{-4}</math>, <math>p = 34.44</math> mg</i>						
700	$1.977 \cdot 10^{-7}$ $\pm 5$	$1.369 \cdot 10^{-9}$ $\pm 4$	$1.42 \cdot 10^{-10}$ $\pm 2$	$2.09 \cdot 10^{-9}$ $\pm 5$	$5.69 \cdot 10^{-10}$ $\pm 5$	17.26 $\pm 0.83$
760	$2.699 \cdot 10^{-7}$ $\pm 4$	$9.468 \cdot 10^{-9}$ $\pm 32$	$4.11 \cdot 10^{-10}$ $\pm 3$	$3.65 \cdot 10^{-10}$ $\pm 12$	$6.08 \cdot 10^{-10}$ $\pm 4$	7.58 $\pm 0.10$
820	$3.036 \cdot 10^{-7}$ $\pm 7$	$2.350 \cdot 10^{-8}$ $\pm 5$	$8.04 \cdot 10^{-10}$ $\pm 7$	$1.40 \cdot 10^{-10}$ $\pm 11$	$3.17 \cdot 10^{-10}$ $\pm 3$	7.10 $\pm 0.04$
900	$3.016 \cdot 10^{-7}$ $\pm 5$	$2.960 \cdot 10^{-8}$ $\pm 7$	$9.51 \cdot 10^{-10}$ $\pm 7$	$9.21 \cdot 10^{-11}$ $\pm 62$	$1.34 \cdot 10^{-10}$ $\pm 2$	7.05 $\pm 0.03$
960	$3.435 \cdot 10^{-7}$ $\pm 6$	$3.394 \cdot 10^{-8}$ $\pm 10$	$1.10 \cdot 10^{-9}$ $\pm 7$	$1.36 \cdot 10^{-10}$ $\pm 10$	$1.54 \cdot 10^{-10}$ $\pm 2$	6.99 $\pm 0.03$
1020	$7.012 \cdot 10^{-7}$ $\pm 9$	$7.068 \cdot 10^{-8}$ $\pm 17$	$2.29 \cdot 10^{-9}$ $\pm 2$	$3.26 \cdot 10^{-10}$ $\pm 16$	$2.65 \cdot 10^{-10}$ $\pm 3$	7.02 $\pm 0.02$
1080	$5.786 \cdot 10^{-7}$ $\pm 13$	$5.256 \cdot 10^{-8}$ $\pm 15$	$1.76 \cdot 10^{-9}$ $\pm 1$	$4.07 \cdot 10^{-10}$ $\pm 15$	$3.90 \cdot 10^{-10}$ $\pm 5$	7.02 $\pm 0.03$
1150	$1.299 \cdot 10^{-7}$ $\pm 2$	$8.462 \cdot 10^{-9}$ $\pm 23$	$3.15 \cdot 10^{-10}$ $\pm 4$	$5.09 \cdot 10^{-10}$ $\pm 11$	$1.86 \cdot 10^{-10}$ $\pm 3$	7.04 $\pm 0.08$
1300	$3.886 \cdot 10^{-8}$ $\pm 8$	$5.211 \cdot 10^{-10}$ $\pm 37$	$3.74 \cdot 10^{-11}$ $\pm 19$	$6.60 \cdot 10^{-11}$ $\pm 92$	$1.17 \cdot 10^{-10}$ $\pm 2$	6.75 $\pm 0.78$
Total age						7.11

Isotope concentrations are in ml/g and are corrected for instrumental background, isotopic fractionation and  $^{37}\text{Ar}$  decay. Ages contain corrections for nuclear interferences, and displayed errors are  $1\sigma$  in-run analytical errors. b.d.l.: below detection limit

Table 7

Summary results of Ar/Ar analyses from selected MdC and MT samples

Sample	$t_{\text{pl}}$ (Ma)	$t_{\text{is}}$ (Ma)	$\%^{39}\text{Ar}_{\text{pl}}$	$t_{\text{tot}}$ (Ma)	$^{40}\text{Ar}/^{36}\text{Ar}_{\text{tr}}$	$t_1$ (Ma)	$t_2$ (Ma)
MdC107 biotite	$7.02 \pm 0.03$	$7.01 \pm 0.04$	(3–9) 95	7.11	$299 \pm 3$	7.09	7.12
MT31 biotite	$7.15 \pm 0.04$	$7.11 \pm 0.04$	(3–8) 91	7.22	$305 \pm 5$	7.18	7.21
MdC106 biotite	$7.28 \pm 0.04$	$7.23 \pm 0.19$	(3–5) 60	7.40	$311 \pm 55$	7.31	7.33
MdC105 biotite	$7.40 \pm 0.04$	$7.36 \pm 0.06$	(3–6) 73	7.52	$310 \pm 19$	7.44	7.47
MdC104 biotite				8.70			
MdC103 biotite				7.30			
MdC103 plagioclase		6.94	(2–6) 71	7.48	$307 \pm 3$	7.02	7.04
MdC102 biotite	$7.28 \pm 0.04$	$7.27 \pm 0.04$	(3–8) 85	7.31	$299 \pm 3$	7.34	7.37
MdC101 biotite		$7.25 \pm 0.04$	(3–5) 51	7.33	$313 \pm 6$	7.32	7.35

Plateau ages  $t_{\text{pl}}$  and isochron ages  $t_{\text{is}}$  are calculated in the same steps, and the displayed error is the total error, comprising uncertainties in monitor measures and age, and neutron flux variations.  $\%^{39}\text{Ar}_{\text{pl}}$  refers to the amount of gas released that forms the plateau and/or isochron, and the step numbers are given in brackets;  $t_{\text{tot}}$  is the integrated age.  $^{40}\text{Ar}/^{36}\text{Ar}_{\text{tr}}$  represents the isochron intercept on the axis  $^{36}\text{Ar}/^{40}\text{Ar}$ .  $t_1$  and  $t_2$  are isochron ages recalculated using different ages for the monitor biotite FCT:  $t_1$  is related to a value of 27.84 Ma (Deino and Potts, 1990),  $t_2$  is related to a value of 27.95 Ma (Baksi et al., 1993).

age of 6.96 Ma (Fig. 5G), and a fairly constant Ca/K. An isochron is obtained on 71% of the gas release with an age of  $6.94 \pm 0.04$  Ma (Fig. 5H), and a slightly radiogenic intercept ( $307 \pm 3$ ). Thus, the biotite of this sample is apparently affected by excess  $^{40}\text{Ar}$  or has a detrital contamination, so that a reliable age assignment is impossible.

Biotite MdC104, which displays the most homogeneous biotite population (see Figs. 3 and 4), yielded a very disturbed spectrum (Fig. 5I) and its total age, 8.70 Ma, is completely outside the range of other biotite ages, being about 1.3 Ma older than the oldest among the other samples. Biotite crystals from this sample were characterized by a smaller grain size, and a lower concentration in the volcanoclastic level compared to all other samples. Both MdC105 and MdC106 biotites display low-temperature steps with high ages, but the remaining part of the spectrum is quite regular in shape. The former has a plateau age of  $7.40 \pm 0.01$  Ma and  $t_{\text{is}} = 7.36 \pm 0.05$  Ma for steps 3–6 (Fig. 5J,K, respectively), the latter has  $t_{\text{pl}} = 7.28 \pm 0.014$  Ma (Fig. 5L) and  $t_{\text{is}} = 7.23 \pm 0.19$  Ma for steps 3–5 (Fig. 5M).

MdC107 is the only biotite-rich sample above what is considered the palaeontologic limit between the Tortonian and Messinian stages in the Monte del Casino section. Its biotite displays a regular spectrum, comprising 95% of gas release, with  $t_{\text{pl}} = 7.02 \pm 0.012$  Ma (Fig. 5N), and  $t_{\text{is}} = 7.01 \pm 0.02$  Ma (Fig. 5O). MT31A–31B comes from the nearby Monte Tondo section, and lies at the T/M palaeontologic boundary. Again the spectrum of its biotite is quite regular, and  $t_{\text{pl}}$  and  $t_{\text{is}}$  are, respectively,  $7.15 \pm 0.021$  Ma (Fig. 5P) and  $7.105 \pm 0.024$  Ma (Fig. 5Q), on 91% of gas release.

### Discussion

A summary of all data may be found in Table 7. There are no significant differences among plateau, isochron, and integrated total ages ( $t_{\text{pl}}$ ,  $t_{\text{is}}$ , and  $t_{\text{tot}}$ ) in the analyzed samples except for MdC103pl. The isotope correlation diagram confirms the plateau ages and atmospheric or slightly radiogenic intercepts which may account for the small observed differences, nevertheless within analytical error. On the other hand, we must recall that in biotites the existence of isochrons and plateaus does not guarantee the absence of a disturbance or of excess Ar as the different Ar components are homogenized when the crystal loses the OH-group during *in vacuo* heating (Foland, 1983; Phillips and Onstott, 1988; Hodges et al., 1994). No clear relationships were observed among ages and chemical parameters such as Ca/K (monitored by  $^{37}\text{Ar}/^{39}\text{Ar}$ ) and Cl/K (monitored by  $^{38}\text{Ar}/^{39}\text{Ar}$ ). The former (not displayed in graphs for biotites, whose ratio is very low) is relatively constant for steps with a high gas release, and is higher in the first and last steps ( $^{39}\text{Ar}$  release < 1%), where possible adhering contaminants and refractory mineral inclusions could play an important role.  $^{38}\text{Ar}/^{39}\text{Ar}$  is almost constant throughout the measurement.

Isochron ages will be used in the following discussion. To overcome the problem of different calibrations for the monitor and to make these data comparable with published data from other laboratories, Table 7 also contains isochron ages recalculated with FCT ages of 27.84 Ma (Deino and Potts, 1990), and 27.95 Ma (Baksi et al., 1993; Renne et al., 1994).

The dating of volcanoclastic layers may encounter problems. Both the presence of

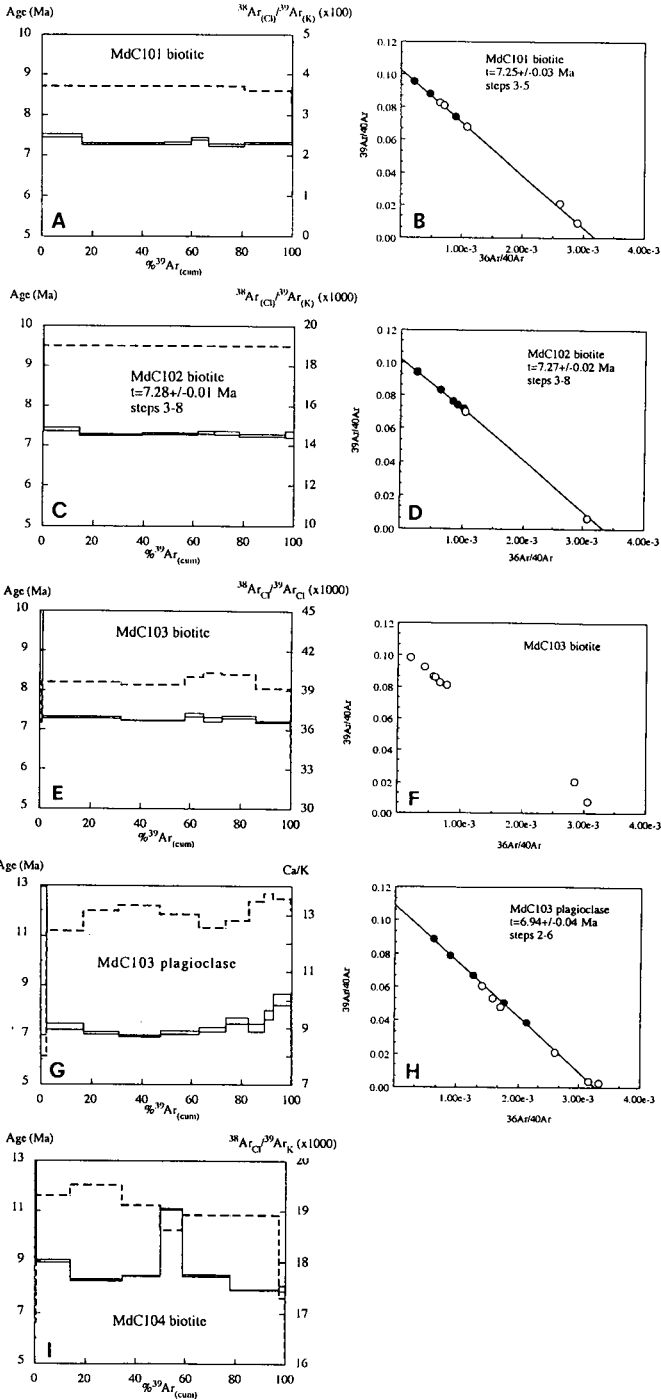


Fig. 5. For caption, see next page.

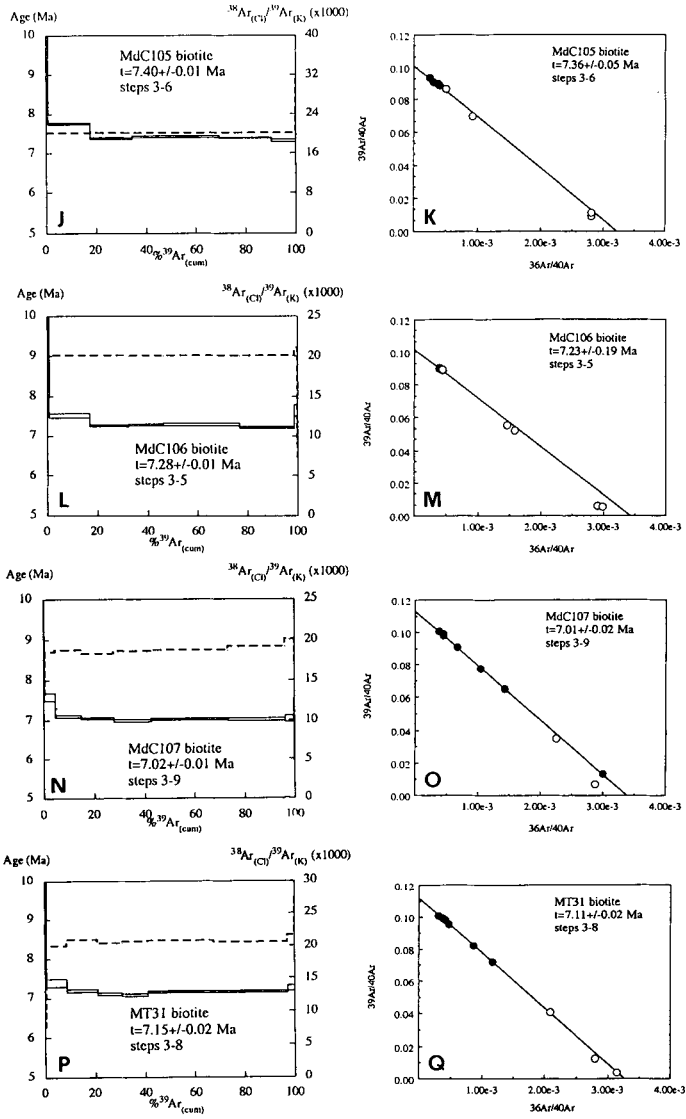


Fig. 5. *Continued.* Age spectra and isochron (or isotope correlation diagrams) of analyzed samples. All age spectrum graphs display a double y-axis, one refers to the age and the other to a chemical parameter, which is  $^{38}\text{Ar}(\text{Cl})/^{39}\text{Ar}(\text{K})$  for biotites and Ca/K for the plagioclase. Their variations are represented by a thick dashed line. In the isochron diagrams the points representative of the steps used for the age calculation are shown as dots, and circles represent all other points. Errors quoted are  $1\sigma$  in-run analytical errors.

contaminants and chemical alteration of the volcanic minerals are possible. The Monte del Casino section contains many volcanoclastic layers in a limited stratigraphic interval, and so it is a good section to study the Tortonian/Messinian boundary, check the vertical and lateral continuity of these type of deposits, and investigate their nature.

Table 7, compared with the stratigraphic column, clearly shows that obtained radiometric data do not match exactly the stratigraphic order, and the only couple of minerals available in the same level is discordant. There are three possible explanations for this: (1) contamination by a detrital component; (2) chemical alteration of volcanic minerals; (3) a non-ideal behaviour of biotite as geochronometer.

The first hypothesis is always possible in this type of sample, and the control is far from being easy. The typology of the level and the chemistry of different components may be of great help, but it is very difficult to check the ideality of the sample. Nevertheless, it is worth noting that in this investigation samples whose biotite displays the most homogeneous chemical compositions (Table 5 and Figs. 3 and 4) are the worst from a chronological point of view. MdC103 biotite and plagioclase are discordant, and MdC104 biotite has an unreasonably high age. So, it must be carefully borne in mind that, while it is always desirable to characterize every sample as thoroughly as possible, the diagnostic capability of tests based on chemical analyses is limited by the possibility that: (a) a series of temporally very close eruptions (for example,  $\Delta t < 0.05$  Ma, which is the analytical resolution) produce chemically heterogeneous biotite populations which are analytically coeval; (b) a series of temporally well distinct eruptions keep producing biotite populations that are chemically indistinguishable but have different ages. Detrital contributions are difficult to rule out in general, because of the presence of numerous volcanoclastic levels in the area. However, our analyses show that all these layers can be easily distinguished.

The potassium content is high in all samples (Table 5), so we can exclude that biotite was altered. As for the third possibility, we pointed out that micas may give good-looking plateaus and/or isochrons which are geologically meaningless. The discordance between MdC103 plagioclase and biotite seems to support this possibility. However, the biotite ages are all consistent among themselves, while the plagioclase age is lower than all other ages found in this and in the neighbouring sections (Monte del Casino I, Monte Tondo). The possible anomalous behaviour of this plagioclase contrasts with the plagioclase reported by Vai et al. (1993), and deserves to be investigated further.

### *Chronostratigraphy*

The radiometric data presented in this paper, and another group of data previously obtained in this area (Vai et al., 1993), are usefully compared with palaeontologic and palaeomagnetic results (Negri and Vigliotti, Chapter E4). Vai et al. (1993) reported K/Ar data on the Monte del Casino I section, and K/Ar data, in addition to one  $^{40}\text{Ar}/^{39}\text{Ar}$  datum on the Monte Tondo section. As for palaeomagnetism, no data are available for the two sections studied at Monte del Casino (one section is disturbed by a landslide and is no longer accessible, whereas the second seems to suffer from a strong magnetic overprint); nevertheless, some useful palaeomagnetic information was obtained from the Monte Tondo section (Negri and Vigliotti, Chapter E4).

In the two Monte del Casino sections, which are located 50 m from one another, the first group of data is clustered between the *G. suterae* and *G. saheliana* FADs (Fig. 6). The three pairs should tentatively be MdC21bis–MdC101, MdC30–MdC102, and MdC31bis–MdC103. With the only exception of sample 21bis, not reliable a

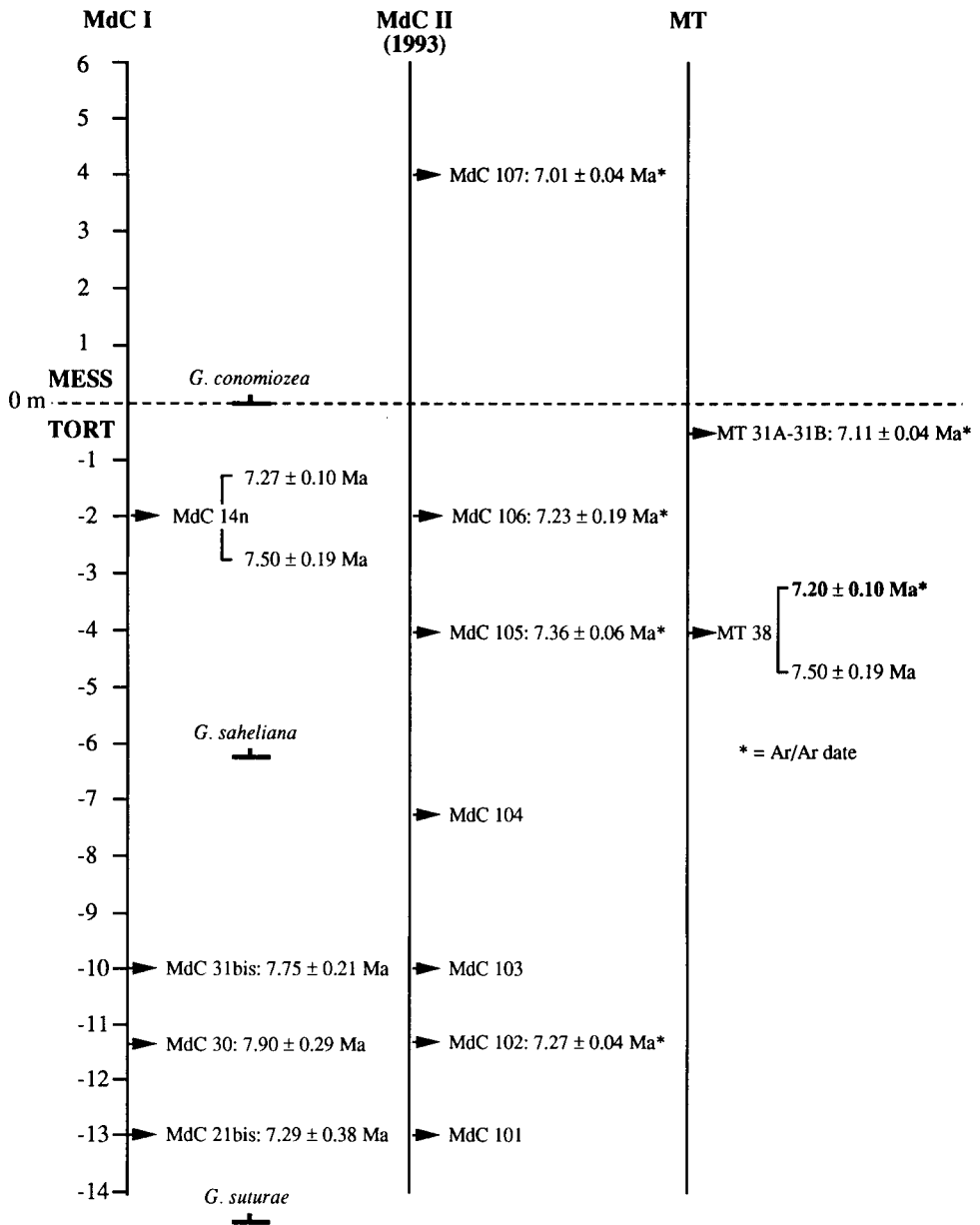


Fig. 6. Radiometric results from biotite (plain numbers) and plagioclase (bold face numbers) plotted on a stratigraphic frame. MdC I, MdC II (1993) and MT refer to the stratigraphic sections from which samples have been dated (Fig. 1 of this paper and fig. 2 in Vai et al., 1993).

priori for its low K content, K–Ar age values are apparently older than those obtained from integrated <sup>40</sup>Ar/<sup>39</sup>Ar analysis which, nevertheless, are indistinguishable at the 2σ confidence level.



The cluster of data from the stratigraphic interval bracketed by the *G. saheliana* and *G. conomiozea* FADs, from a purely metric point of view, are best represented by the pairs MdC105–MT38 and MdC106–MdC14n. The data are fairly consistent although the K–Ar ages have considerably high analytical errors. Moreover, according to chemical data on biotite, MdC105 and MT38 are different. Samples collected close to, or after the *G. conomiozea* FAD in both sections, display younger ages, namely 7.11 Ma for MT31, and 7.01 Ma for MdC107.

Due to the uncertainty on the lateral continuity of these levels, we can try to calculate the value of the limit using only the data from the Monte del Casino II section, and then compare the obtained values with the previous ones (Vai et al., 1993). We will use both set of data independently, at the bottom (MdC101 and MdC102), and at the top (MdC105 and MdC106) of the section, below the boundary, compared to the level above (i.e., MdC107). We cannot pool all samples below the boundary because the upper samples bear similar older dates than the lower ones. The interpolation using MdC101 and MdC102 will yield an age for the T/M boundary of about 7.08 Ma, and a sedimentation rate of 62 m/Ma; the interpolation using MdC105 and MdC106 will yield a T/M age of about 7.16 Ma, with a sedimentation rate of 23 m/Ma, thus consistent with that reported in Vai et al. (1993).

It is difficult to estimate an error, because the non-ideality of samples reveals a systematic error whose order of magnitude is unknown, nevertheless, the difference between the two calculated values is not statistically significant.

In the nearby Monte Tondo section, sample MT31 yields an age of 7.11 Ma; this sample is located at the palaeontologic T/M boundary but, unfortunately, available palaeomagnetic data (Negri and Vigliotti, Chapter E4) cast some doubts on the stratigraphic continuity of this section. It is important to note that this value is consistent with the data calculated in the Monte del Casino section, but its geologic reliability is compromised by the lack of clear palaeomagnetic data.

At the moment we have a range of new ages on the T/M boundary which span about 0.2 Ma, from 7.08 to 7.16 Ma (this paper) to 7.1 (astronomical calibration, Krijgsman et al., 1994) to 7.26 Ma (K/Ar and  $^{40}\text{Ar}/^{39}\text{Ar}$ , Vai et al., 1993).

## CONCLUSIONS

The aims of this paper are to bracket the age for the T/M boundary, and to control the preliminary radiometric datings obtained from volcanoclastic layers immediately below the T/M boundary (Vai et al., 1993). Our first purpose was accomplished insofar the T/M boundary in the Romagna Apennines is now confidently bracketed between  $7.28 \pm 0.10$  Ma, and  $7.01 \pm 0.04$  Ma, with an additional date of  $7.11 \pm 0.04$  at the *G. conomiozea* FAD. As for the second purpose, the new dates raised a series of problems affecting the reliability of the obtained results. These problems may be summarized as follows: (1) insufficient reproducibility of some data from the same sample, especially when comparing separate sample collections; this questions the lateral continuity and homogeneity of these levels; (2) poor lateral reproducibility; (3) less-than-perfect match between apparent ages and stratigraphic (super)position. The resulting age discrepancies range up to 200 ka.

These facts provide a good opportunity for approaching an interesting methodologic

problem concerning the confidence level of single crystal biotite and/or other mineral age measurements used to constrain the chronometric calibration of stratigraphic boundaries and datums.

Assuming *a priori* an adequate analytical procedure, a physical explanation for the discrepancies shown is needed. In general, contamination by detrital recycled micas, although present in amounts in the bulk rock, can be excluded when the same criteria of volcanic biotite selection are followed for both homogeneity test, and radiometric preparation. Unlike some biotite-rich layers which are associated with thin-bedded, fine-grained turbidites in the Pieve di Gesso section (Odin et al., Chapter E6), no turbidites were detected in the Monte del Casino and Monte Tondo sections studied. The regular superposition of the most important bioevents also exclude the possibility of reworking processes involving sedimentary intervals thicker than a few decimetres. The most effective mechanisms able to produce sediment transport and reorganization of such a magnitude are bioturbation and mini-mudflows. Both processes are confined to the given thickness threshold as shown by the fact that primarily laminated (and therefore undisturbed) black shale layers, alternating each for an interval of 1 or 2 m (or less), are physically traced at the large outcrop scale. However, one cannot exclude that in less distal parts of the basin mechanical reworking actually occurred and involved the upper few metres to decametres of the unconsolidated sedimentary blanket (via shelf storm suspensions or slope sedimentary failures and associated nepheloid layers). In this scenario, we should emphasize the high floating potential of the thin, large volcanic biotite flakes (including both the new airborne crystals related to the ongoing volcanic cycle, and those already formed during older volcanic cycles and incorporated into the same eruptive edifice). In this way, different populations of unaltered euhedral volcanic biotite having appreciable difference in composition and age, although derived from the same volcanic province, could be preserved within a single biotite-rich horizon of the distal sections studied (Montanari, 1988; Deino et al., 1988; Odin et al., 1991). Such a reworking mechanism, however, can only be assumed to explain measured dates older than the true age measured and/or expected at that stratigraphic level. For apparent ages younger than expected, different explanations have to be sought. We plan to further check our data set with different chronometers and methods in view of discriminating between all possible interpretative scenarios.

The chronostratigraphic potential of the western Romagna sections as possible site for placing the Global Stratotype Section and Point (GSSP) for the Tortonian/Messinian boundary was first suggested by Vai et al. (1993). The radiometric results presented in this Chapter, and the preliminary cyclo-, bio-, and magnetostratigraphic studies by Vai (Chapter E3), and Negri and Vigliotti (Chapter E4), as well as ongoing detailed magneto- and chemostratigraphic studies in this area, give priority to the Monte del Casino section as a potential GSSP choice. This section appears to be the most continuous among the several exposed sections in this area, and with a larger number of datable volcanoclastic layers bracketing the Tortonian/Messinian boundary. In view of this potential, a core was drilled recently with the aim of improving the resolution obtained in the close Monte del Casino section. We plan to submit a formal proposal for international consideration as soon as final results from both MICOP and MIOMAR projects will be published.

SOMMAIRE — NOUVELLES DATATIONS RADIOMÉTRIQUES AUTOUR DE LA LIMITE TORTONIEN/MESSINIEN DANS LES SECTIONS STRATOTYPIQUES POSSIBLES DE ROMAGNE (APENNINS DU NORD, ITALIE)

(Manuscrit soumis: Décembre 1994; révisé: Mars 1996; rédacteurs responsables: AM et RC)

Une étude précédente utilisant principalement la technique de dilution isotopique et portant sur les coupes du Monte Tondo et du Monte del Casino avait conclu aux âges K–Ar suivants:  $7,72 \pm 0,30$  Ma ( $2\sigma$ ): moyenne pondérée de 3 niveaux à biotite autour de l'apparition (émergence probable) de *Globorotalia suterae* et  $7,37 \pm 0,13$  Ma pour la meilleure biotite localisée entre l'apparition de *G. saheliana* et celle de *G. mediterranea* dans le Tortonien terminal. Ceci conduisait à estimer l'âge de ce dernier biosignal à  $7,26 \pm 0,20$  Ma. De nouvelles analyses par la technique d'irradiation et chauffage par étapes ont été réalisées sur huit niveaux. Les biotites sélectionnées ont généralement montré une assez bonne homogénéité géochimique (test Fe–Mg–K). Les niveaux MdC 101, 102, 103 et 104 sont encadrés par les apparitions de *G. suterae* et *G. saheliana*, MdC 105 et 106 par celles de *G. saheliana* et de *G. mediterranea*, MdC 107 est au dessus de ce dernier signal biostratigraphique et MT 31 légèrement au dessous. Des 4 premiers niveaux récoltés au Monte del Casino, seule la biotite de MdC 102 a permis d'obtenir un spectre d'âge régulier dont l'âge plateau:  $7,28 \pm 0,08$  Ma —  $2\sigma$  incertitude intralaboratoire — paraît jeune comparativement aux autres résultats disponibles. Il est proche des âges de la plupart des étapes de la biotite MdC 101 qui ne permet pas de calculer un plateau mais révèle un âge isochrone de  $7,25 \pm 0,08$  Ma. Les étapes principales de la biotite de MdC 103 donnent aussi des âges apparents voisins de 7,3 Ma tandis que le plagioclase correspondant donne des âges compris entre 7,0 et 7,6 Ma. Les biotites extraites de MdC 105 (âge plateau  $7,40 \pm 0,08$ ) MdC 106 (âge plateau  $7,28 \pm 0,08$ ), MdC 107 (âge plateau  $7,02 \pm 0,06$ ) sont cohérents et compatibles avec l'âge plateau de l'échantillon du Monte Tondo (âge plateau  $7,15 \pm 0,08$  Ma). D'après ces nouvelles données, l'apparition de *G. conomiozea*, serait estimée par extrapolation proche entre 7,08 et 7,16 Ma. La valeur de ces âges est fonction de celle adoptée pour le dosimètre pris comme référence (biotite FCT) qui est proposée avec une incertitude de 3% mais pour laquelle d'autres auteurs adoptent des valeurs pouvant vieillir l'ensemble de ces âges de près de 1,5%.

(Sommaire proposé par les rédacteurs, GSO)

#### ACKNOWLEDGEMENTS

Authors wish to thank C. Quercioli and G. De Grandis for mineral separations, O. Giuliani for laboratory maintenance and R. Calieri for field sampling support.

Chapter E6

**CONTRIBUTION TO THE GEOCHRONOLOGY OF THE  
TORTONIAN/MESSINIAN BOUNDARY IN THE FAENZA AREA (ROMAGNA,  
ITALY)**

G.S. Odin, G.B. Vai, M. Cosca, F. Tateo and J.C. Hunziker

INTRODUCTION

The purpose of this work is to document the Tortonian/Messinian boundary age by isotopic dating of biotite-rich layers in the Romagna Province (see Chapter E5).

The Monte del Casino II and Monte Tondo sections (see location in fig. 1 in Chapter E2) were described and dated by Vai et al. (1993). At that time, the layers dated were collected from two groups located about 5 m and 10 to 13 m below what is considered the base of the Messinian Stage in the area. In this study, we have selected two other layers located above the previously dated ones and bracketing the stage boundary. The samples B174 (Monte del Casino) and B189 (Monte Tondo) were collected during field trips with R. Calieri who studied the sections (Calieri, 1992).

STRATIGRAPHIC LOCATION

The biotite-rich layer B174 (collected between Calieri's 1992 marker beds 10 and 11) is located 23.5 m below the top of the 0.6 m thick 'Calcare di Base' distinctive limestone and 4.3 m above the contemporaneous first occurrences (FOs) of the taxa *G. conomiozea* and *G. mediterranea* in the Monte del Casino II section (Fig. 1). The biotite-rich layer B189 (collected near Calieri's 1992 marker bed 31) is located about 26 m below the 'Calcare di Base' limestone and is the lower of the two biotite-rich levels bracketing the first occurrence (FO) of the same two taxa in the Monte Tondo section.

The FOs of these two taxa are interpreted as corresponding to the Tortonian/Messinian boundary. This must be considered as an approximation for two reasons. Firstly, the absolute synchronism of the first occurrence of the two taxa over the area is a postulate which is only probable and difficult to demonstrate without more precise (litho- or magnetostratigraphic) criteria, and secondly the actual definition of the boundary in the historical stratotype is not a foraminiferal first occurrence but a lithological marker (first salinity index) which was precisely located by Selli (1960) in the historical stratotype section at Capodarso, and was found later to be about 2 m below the local first occurrence of *G. conomiozea* (cf. Chapter A8).

The presently studied layers are both stratigraphically younger than any of the samples dated in the pioneer work by Vai et al. (1993).



Fig. 1. Photograph of the upper part of the outcrop in the Monte del Casino section. The sampled layer B174 is shown (left hand of Pascal); the FO of *G. conomiozea* in the section is indicated by the vertical 1-m scale bar (photo by GSO, 1993).

## GEOCHRONOLOGY

### *Petrography and mineralogy of the geochronometers*

Sample B174 contains biotite (25‰ of the whole rock), plagioclase (more than 1‰), well-preserved, transparent idiomorphic apatite crystals (0.4‰) and about 250 short to elongated, brilliant, pink in color, zircon crystals per kg (size from  $20 \times 80$  to  $50 \times 400 \mu\text{m}$ ). The layer is not purely volcanogenic (gypsum, pyrite, biogenic phosphate including small fish teeth, microfossils and white mica flakes are present). The volcanic origin and dominant air transport is probable.

Sample B189 contains biotite (10‰), feldspars (15‰ with admixed quartz), a small proportion of apatite and zircon (about 0.02 to 0.03‰). Small fish teeth, microforaminiferal tests commonly filled with pyrite, and white mica are also present.

Biotite was separated by disaggregation, sedimentation in water, and magnetic

separation; the heavy fraction in bromoform was purified by gentle crushing in acetone and sieving (above 0.16 mm). The pure biotite fraction was ultrasonically cleaned with 10% acetic acid for 7 min. Plagioclase was similarly separated, purified in heavy liquid mixtures (bromoform–acetone) and treated with a diluted nitric–acetic acid mixture for 20 min before hand-picking the crystal fragments. According to X-ray diffraction, the separates were pure and the selected feldspar was a Ca-rich plagioclase.

#### <sup>40</sup>Ar/<sup>39</sup>Ar isotopic study

One biotite sample (B174bio, 2.7 mg) was irradiated together with samples from Pieve di Gesso and similar analytical conditions used (irradiation ULRD5). A second series of 5 samples (B174bio-re: 20.9 mg and 7.6 mg; B174plagio: 97.3 mg; B189bio: 23.7 and 8.3 mg) was irradiated 1 year later (irradiation ULRD7). Following preheating under vacuum at 450 to 600°C for 10 to 30 min, the separates were heated either step by step or by total gas procedure and the purified argon analyzed. The summarized analytical results are shown in Table 1; details are given in Table 4.

Biotite B174 first gave analytical results with large errors due to the small quantity of gas (no significant gas measured at steps 700 and 1600°C not shown in Table 1). In spite of the small quantity of gas, a significant plateau is present. The plateau age ( $7.2 \pm 0.2$  Ma) is apparently younger than the total gas age (Fig. 2 and Table 2).

The results obtained from a larger quantity of the same sample (B174re) are more precise with a broad (6 to 7 steps) plateau (more than 95% of the whole gas extracted). The plateau age at  $7.21 \pm 0.06$  Ma is similar to the total gas age (Table 2) suggesting absence of disturbance after crystallization.

An additional sample of B174bio (7.63 mg) was preheated at 550°C for 20 min, then heated at 700, 1350 and 1600°C. No significant quantities of gas were extracted for the two extreme temperatures but the one at 1350°C allowed calculation of a well defined age at  $7.14 \pm 0.11$  Ma (Table 2).

Although generally homogeneous as far as K/Ca ratios are concerned, the step heating ages of the plagioclase separated from B174 do not show a plateau pattern (Fig. 3). The total gas age is not consistent with the biotite age. Only one amongst the eight steps (1150°C) shows an apparent age nearly similar to that of the biotite. The analytical results do not seem to be useful for deriving any stratigraphically significant age information.

In spite of a technical problem during measurement of one step, the results obtained from biotite B189 are extremely convincing with seven steps overlapping in age within  $2\sigma$  (Fig. 4). The resulting plateau age at 7.44 Ma is similar to the total age (Table 2).

An additional sample of B189bio (8.34 mg) was preheated at 550°C for 25 min in vacuum, then heated at 700°C, 1350°C and 1600°C. An age of  $9.4 \pm 2.3$  Ma was obtained from the first step (1.3% of the total gas),  $7.55 \pm 0.10$  Ma from the second (98.7% of the gas released) and no significant quantity of gas was extracted at 1600°C. Unfortunately, the measurement of the second and main step was delayed during the mass spectrometric measurement, which tends to bias the results to slightly older ages (Table 2).

Isochron ages were calculated from the step heating data (Fig. 5, and Tables 3 and 4). Concerning biotite B174 (small sample), the results for the four steps contributing to

Table 1

Results of  $^{40}\text{Ar}/^{39}\text{Ar}$  step heating measurements on biotite and plagioclase from Monte del Casino (data by GSO in Lausanne)

$^{\circ}\text{C}$	Apparent age (Ma)	$\pm 2\sigma$	% $^{39}\text{Ar}$	%rad.	K/Ca
<i>B174bio, 2.7 mg, irradiation ULRD5</i>					
850	8.4	0.9	12.1	8	11.0
930	6.0	0.7	17.4	8	11.8
1000	7.3	0.5	15.7	28	11.4
1050	7.3	0.6	13.4	25	9.3
1100	7.0	0.5	14.9	30	
1200	7.4	0.4	20.4	30	
1350	6.1	1.2	6.2	6	
<i>B174bio-re, 20.94 mg, irradiation ULRD7</i>					
700	6.4	3.8	0.4	11	26
850	7.43	0.8	3.0	35	58
930	7.22	0.12	8.9	11	105
1000	7.25	0.10	14.7	67	140
1050	7.16	0.12	8.7	90	137
1100	7.20	0.10	14.0	93	76
1200	7.20	0.10	38.5	87	44
1350	7.22	0.10	11.2	9	62
1600	5.6	1.0	0.5	45	37
<i>B174plagio, 97.32 mg, irradiation ULRD7</i>					
800	7.7	0.7	4.6	19	0.09
950	7.74	0.14	12.2	71	0.09
1050	7.95	0.12	20.7	93	0.09
1150	7.39	0.13	21.0	95	0.09
1275	8.65	0.14	17.6	98	0.09
1400	13.82	0.20	17.9	93	0.09
1500	17.4	0.7	3.8	91	0.08
1600	17.7	1.2	2.2	84	0.08
<i>B189bio, 23.7 mg, irradiation ULRD7</i>					
700	5.8	2.0	0.3	12	19
870	7.42	0.15	4.3	73	55
980	7.47	0.10	16.3	93	68
1050	7.44	0.10	12.4	96	51
1100	7.42	0.10	10.8	95	30
1135	7.43	0.10	12.6	96	20
1190	7.42	0.10	29.5	96	19
1350	7.44	0.10	13.0	95	8
1600	10.2	0.9	0.7	79	27

B189 biotite from Monte Tondo (preheating 600°C for 25 min); the apparent age for the main step at 1350°C was affected by a technical problem: able to be biased toward increased  $^{40}\text{Ar}/^{39}\text{Ar}$  ratios; HD-B1 = 24.21 Ma; error on  $J = 0.5\%$ .

the plateau give a reasonable isochron age with increased error bars compared to those for the plateau age. The Ar initial ratios for the two isochrons are acceptable as well as the MSWD values ( $<1$ ). The use of all steps increases the MSWD value indicating analytically heterogeneous step ages in agreement to what is shown on the age spectrum.

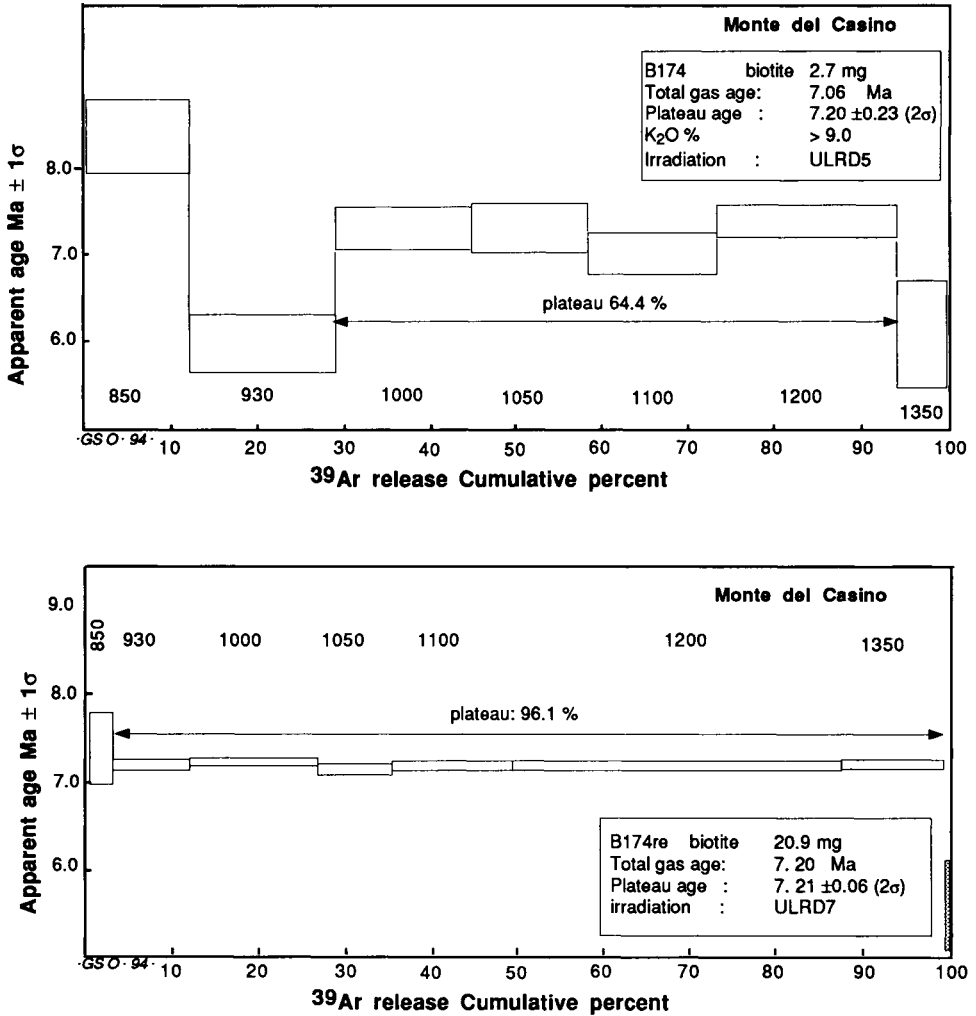


Fig. 2. <sup>40</sup>Ar/<sup>39</sup>Ar age spectrum for early Messinian sample B174 biotite. Irradiation ULRD5 contained too little sample for precise measurements; irradiation ULRD7; the well developed age spectrum suggests that the geochronometer is undisturbed since crystallization time.

The isochron plots for the heavier biotite sample B174re (Table 3) indicate precise and similar isochron ages ( $7.20 \pm 0.06$  Ma) with good colinearity of the points and 'atmospheric' <sup>40</sup>Ar/<sup>36</sup>Ar initial ratios.

The two isochron plots for biotite B189 also show similar results; the ages are also similar to that of the plateau age, the initial Ar isotopic ratio is consistent with an atmospheric composition and the MSWD are small and indicate good consistency of the diverse steps.



Table 2

Age data from separates from samples B174 and B189

Sample	mg	Apparent age (total gas) (Ma)	Steps on plateau	% <sup>39</sup> Ar	Apparent age (plateau, ±2σ) (Ma)
B174bio	2.7	7.06	(4) 1000–1200°C	64.4	7.20 ± 0.23
B174bio-re	20.9	7.20 (±0.07)	(6) 930–1350°C	96.1	7.21 ± 0.06
B174bio	7.63	7.14 ± 0.11	1 step from 700 to 1350°C		
B174plagio	97.3	9.5 (±0.9)	(0) no plateau; unreliable material		
B189bio	23.7	7.45 (±0.08)	(7) 870–1350°C	98.9	7.44 ± 0.08
B189bio	8.34	<7.55±0.10	1 step from 700°C to 1350°C (maximum age)		

The number of steps contributing to the plateau is shown in brackets. The 'single step' analysis for sample B189 was not entirely successful and the calculated age is slightly biased toward high value. The error bar given for each 'total gas age' is a tentative estimate.

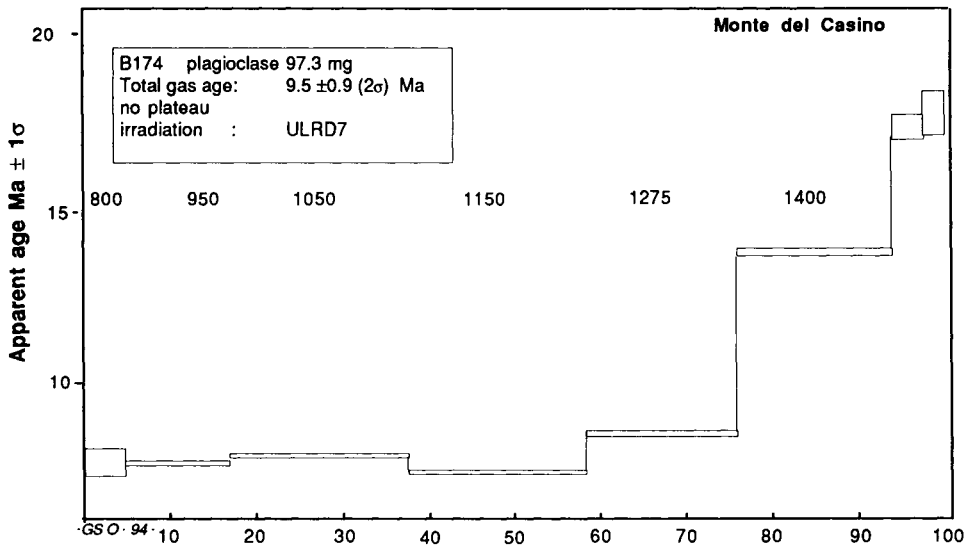


Fig. 3. <sup>40</sup>Ar/<sup>39</sup>Ar age spectrum for sample B174 plagioclase. Disturbed spectrum indicates unreliability of the analyzed separate.

## DISCUSSION AND CONCLUSIONS

We did not succeed in obtaining geologically meaningful ages from our separates of pyroclastic plagioclase. Amongst the similar materials studied by us during last two years, it seems that only the large (pieces of) crystals (more than 300 μm), perfectly clear and showing the highest peaks on the X-ray diffraction patterns, are able to give useful information.

Concerning biotite, we have tried to use several procedures and several sample weights for a methodological purpose. We have shown that preheating under vacuum up to 600°C for 30 min is a useful procedure for the kind of biotite concerned here which has a very homogeneous behavior.

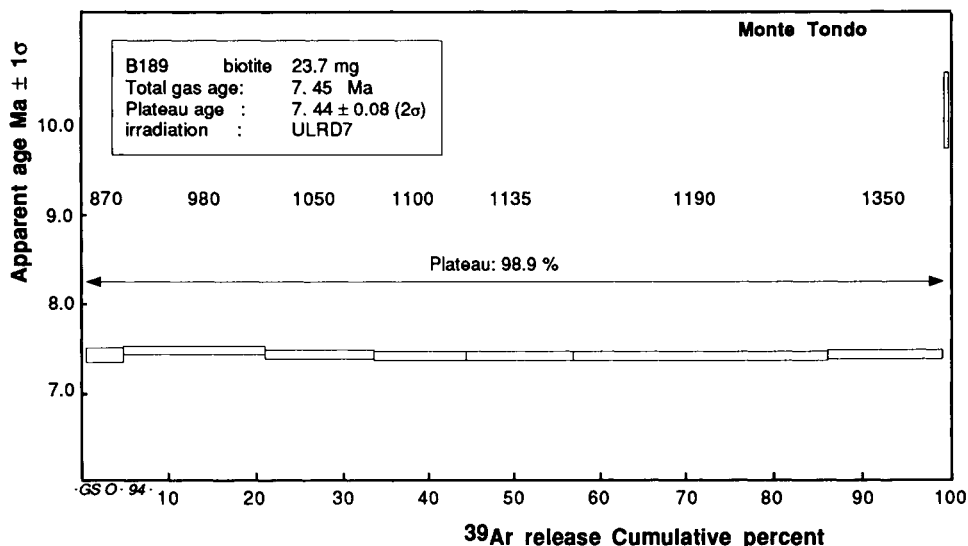


Fig. 4. <sup>40</sup>Ar/<sup>39</sup>Ar age spectrum for topmost Tortonian sample B189 biotite. The age spectrum suggests that the biotite was undisturbed since crystallization.

Table 3

Results from isochron treatment of analytical data for the two best biotite samples

Sample	Calculated age (Ma)	<sup>40</sup> Ar/ <sup>36</sup> Ar initial ratio	MSWD
<i>Sample B174bio (2.7 mg) for steps 1000 to 1200°C</i>			
<sup>40</sup> Ar/ <sup>36</sup> Ar versus <sup>39</sup> Ar/ <sup>36</sup> Ar isochron	7.32 ± 0.57	297 ± 13	0.8
<sup>36</sup> Ar/ <sup>40</sup> Ar versus <sup>39</sup> Ar/ <sup>40</sup> Ar isochron	7.34 ± 0.57	297 ± 15	0.8
<i>Sample B174bio (2.7 mg) for all steps</i>			
<sup>40</sup> Ar/ <sup>36</sup> Ar versus <sup>39</sup> Ar/ <sup>36</sup> Ar isochron	7.33 ± 0.74	294.7 ± 6.2	7.4
<sup>36</sup> Ar/ <sup>40</sup> Ar versus <sup>39</sup> Ar/ <sup>40</sup> Ar isochron	7.33 ± 0.74	294.9 ± 6.2	7.5
<i>Sample B174bio (2.7 mg) for steps 930 to 1350°C</i>			
<sup>40</sup> Ar/ <sup>36</sup> Ar versus <sup>39</sup> Ar/ <sup>36</sup> Ar isochron	7.20 ± 0.06	296.7 ± 8.7	1.2
<sup>36</sup> Ar/ <sup>40</sup> Ar versus <sup>39</sup> Ar/ <sup>40</sup> Ar isochron	7.20 ± 0.06	297.0 ± 8.6	1.2
<i>Sample B174bio (2.7 mg) for steps 870 to 1350°C</i>			
<sup>40</sup> Ar/ <sup>36</sup> Ar versus <sup>39</sup> Ar/ <sup>36</sup> Ar isochron	7.44 ± 0.04	292 ± 9	0.43
<sup>36</sup> Ar/ <sup>40</sup> Ar versus <sup>39</sup> Ar/ <sup>40</sup> Ar isochron	7.44 ± 0.04	291 ± 14	0.43

MSWD: mean standard weighted deviate.

The analytical age of B174 and B189 biotites are precisely located at 7.20 ± 0.06 Ma and 7.44 ± 0.04 Ma, respectively.

The two ages are in correct stratigraphic sequence. If the FOs of *G. mediterranea* and *G. conomiozea* are contemporaneous in the two dated sections, the distance between the two samples would be about 5 m. The mean sedimentary rate in the area is estimated between 20 and 30 m/Ma (according to Vai in Chapter E3, the pre-gypsum Messinian would represent about 1 Ma). Therefore, the analytical age difference of 0.25 Ma is fully

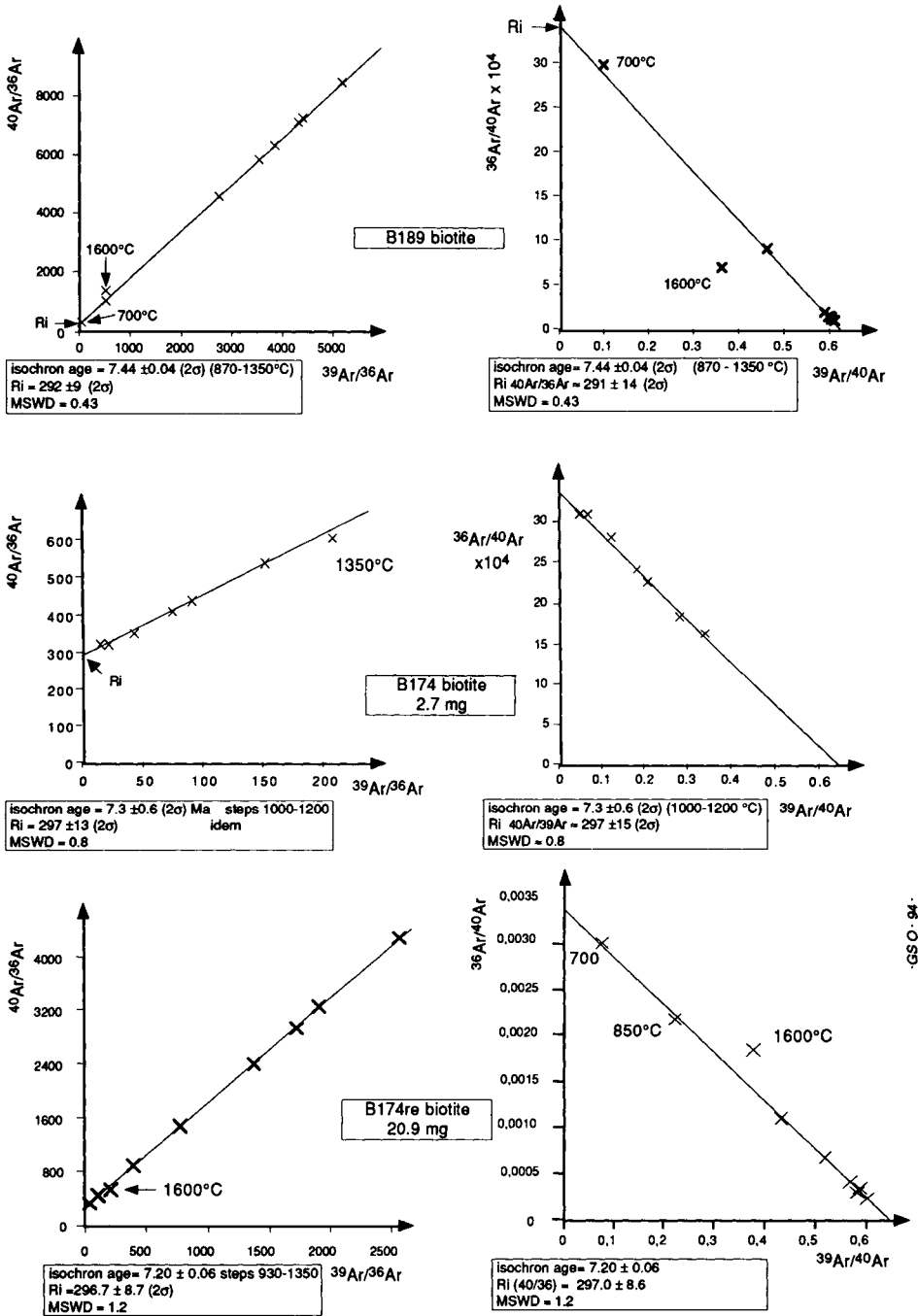


Fig. 5. Isochron data plots for the two biotite samples B174 and B189. Both  $^{40}\text{Ar}/^{36}\text{Ar}$  versus  $^{39}\text{Ar}/^{36}\text{Ar}$  and  $^{36}\text{Ar}/^{40}\text{Ar}$  versus  $^{39}\text{Ar}/^{40}\text{Ar}$  isochrons are shown.

Table 4

Analytical detail for the two best analyzed samples (data by GSO in Lausanne)

T (°C)	40*	±	39	±	38	±	37	±	36	±	40/39	±
<i>B174bio-re, ULRD7, J = 0.002584</i>												
700	72.0	1.0	5.65	0.10	0.244	0.004	0.107	0.010	0.217	0.004	1.4	0.4
850	174.5	0.4	38.7	0.6	1.45	0.02	0.327	0.022	0.381	0.020	1.60	0.08
930	267.2	0.5	115.4	0.2	4.02	0.02	0.540	0.016	0.296	0.002	1.551	0.01
1000	328.9	0.7	191.1	0.4	6.515	0.016	0.675	0.015	0.101	0.003	1.559	0.01
1050	194.3	0.4	113.2	0.2	3.888	0.016	0.405	0.010	0.066	0.003	1.539	0.01
1100	302.1	0.6	181.2	0.4	6.242	0.009	1.17	0.03	0.070	0.002	1.547	0.01
1200	884.9	1.8	499.6	1.0	17.50	0.04	5.62	0.05	0.369	0.006	1.548	0.01
1350	283.3	0.6	145.7	0.3	5.073	0.018	1.150	0.013	0.191	0.002	1.551	0.01
1600	16.0	0.4	6.01	0.05	0.225	0.003	0.080	0.013	0.029	0.002	1.20	0.11
<i>B189bio, ULRD7, J = 0.002584</i>												
700	49.5	0.6	4.80	0.06	0.334	0.003	0.126	0.018	0.147	0.001	1.25	0.21
870	131.3	0.3	60.10	0.13	3.65	0.01	0.530	0.013	0.119	0.002	1.596	0.01
980	389.5	0.8	226.7	0.5	13.62	0.04	1.63	0.02	0.083	0.003	1.605	0.01
1050	289.0	0.6	172.8	0.3	10.40	0.014	1.66	0.02	0.040	0.002	1.600	0.01
1100	251.6	0.5	149.9	0.3	9.156	0.025	2.43	0.03	0.040	0.001	1.595	0.01
1135	293.5	0.6	175.7	0.4	10.867	0.006	4.20	0.03	0.042	0.002	1.596	0.01
1190	680.8	1.4	410.6	0.8	25.28	0.02	10.31	0.03	0.081	0.003	1.596	0.01
1350	306.0	0.6	181.1	0.4	11.50	0.02	11.16	0.06	0.055	0.002	1.599	0.01
1600	28.7	0.4	10.31	0.08	0.245	0.07	0.187	0.016	0.020	0.003	2.20	0.09

Gas in  $10^{-15}$  mol; error bars analytical precision  $\pm 2\sigma$ ;  $40/39 = {}^{40}\text{Ar}$  radiogenic/ ${}^{39}\text{Ar}_K$ .

consistent with the 5 m distance. In this context, the age of the FO of *G. conomiozea* (30 cm above sample B189) should be only 10 ka younger than the measured age of 7.44 Ma.

Compared to other results from the same laboratory, we are led to conclude that samples from the Pieve di Gesso section are not significantly older than the base of the Messinian Stage dated in the Monte Tondo section.

In order to compare our results with those obtained in other laboratories, we should add to our internal analytical error the error on the monitor used (known to be  $\pm 2.6\%$ ). Therefore, our ages become  $7.20 \pm 0.25$  and  $7.44 \pm 0.23$  Ma, and the FO of *G. conomiozea* is  $7.43 \pm 0.23$  Ma old.

This age is consistent with the slightly extrapolated age of  $\leq 7.26 \pm 0.10$  Ma proposed by Vai et al. (1993). In fact, our results from the Monte Tondo and Monte del Casino sections would suggest that the boundary might be located on the old side of the interval of time proposed by the previous authors.

## SOMMAIRE — CONTRIBUTION À LA GÉOCHRONOLOGIE DE LA LIMITE TORTONIEN/MESSINIEN DANS LA RÉGION DE FAENZA (ROMAGNE, ITALIE)

(Manuscrit soumis: Février 1994, révisé: Février 1995; rédacteur responsable: GSO)

Déjà étudiées en 1993, les affleurements de la région de Faenza sont favorables à une définition de point stratotypique global pour la limite Tortonien/Messinien. Le

présent travail était destiné à la fois à assurer les premiers résultats géochronologiques par la datation de nouveaux niveaux (cohérence inter-échantillons) et à reproduire ceux de niveaux déjà caractérisés à Pise et Berne (cohérence inter-laboratoire). Deux niveaux riches en biotite situés de part et d'autre de l'apparition régionale des taxons *G. conomiozea* et *G. mediterranea* ont été datés à Lausanne par la technique  $^{39}\text{Ar}/^{40}\text{Ar}$  avec chauffage par étape.

Le niveau plus récent a été daté sur plagioclase (spectre perturbé) et sur biotite; 3 âges totaux indépendants sont compris entre 7,06 et 7,20 Ma; 2 âges plateau:  $7,20 \pm 0,23$  et  $7,21 \pm 0,06$  Ma sont cohérents avec les âges isochrone correspondants. Le niveau plus ancien, très proche de l'apparition des taxons cités a donné un excellent âge plateau à  $7,44 \pm 0,08$  Ma semblable à l'âge total et aux âges isochrone. Un âge nettement supérieur à 7 Ma est illustré une fois encore pour la limite Tortonien/Messinien.

*(Sommaire des auteurs)*

#### ACKNOWLEDGEMENTS

The radiometric measurements were achieved in Lausanne thanks to the facilities made available in the Institut of Mineralogy by the Swiss National Funds. No funding was provided by French Organizations for this research.

*Chapter E7*

**INTEGRATED STRATIGRAPHY OF THE MACCARONE SECTION, LATE MESSINIAN (MARCHE REGION, ITALY)**

G.S. Odin, F. Ricci Lucchi, F. Tateo, M. Cosca and J.C. Hunziker

**INTRODUCTION**

A few years ago, there was practically no direct geochronological calibration of the Messinian Stage. The search for datable material began in Italy where this stage is historically defined. In this country, the stage is composed essentially of three units referred to informally as: the pre-evaporitic 'Formazione di letto' or 'Euxinic Shale', the evaporitic 'Gessoso solfifera', and the post-evaporitic 'Formazione di tetto' and 'Colombacci' formation. This chapter is concerned with the last units from which a maximum age for the Miocene/Pliocene boundary could be documented.

A review of the literature dealing with supposed volcanoclastic layers in Italy is given by Guerrera and Veneri (1989). Additional information has been gathered in recent years in the course of new regional sedimentological studies. Within the Messinian, tuff layers occur within sediments located above the gypsum-bearing formation (Gessoso solfifera) and below the overlying, commonly transgressive Pliocene sediments (Selli, 1954). Along the Central Apennines, biotite-rich tuff layers crop out for about 120 km (Table 1, and Fig. 1). This suggests a regional phenomenon for which precise correlation is suspected but has not yet been confirmed.

The outcrops of evaporitic and post-evaporitic deposits of the area is schematically shown in Fig. 1 along with the locations of some sections from where biotite-rich tuffs are found. These outcrops extend along the general direction of Apennine folding (NNW–SSE) with the oldest pre-Messinian sediments to the west and the younger Plio–Pleistocene sediments to the east.

Table 1

Geographical locations of some post-evaporitic biotite-rich tuff layers: Candelara (60 km NW of Ancona); Maccarone (40 km SW of Ancona); Camporotondo (and nearby section at San Ginesio — 55 km SSW of Ancona; Colle Gallo, 80 km S of Ancona)

Section	Location	Lithology	Reference
Candelara,	Metauro Basin, near Pésaro	'volcanic sand'	Selli, 1954
Maccarone	near Apiro	glassy tuff (1.2 m)	Carloni et al., 1974a, b
Camporotondo	Tolentino, 30 km SSE of Apiro	glassy tuff	Carloni et al., 1974a
Force	15 km NNW of Ascoli	ash and marls (4–5 m)	Bassetti et al., 1993
Colle Gallo	4 km NE of Ascoli Piceno	2 glassy tuffs (0.4 m)	Girotti and Parotto, 1969

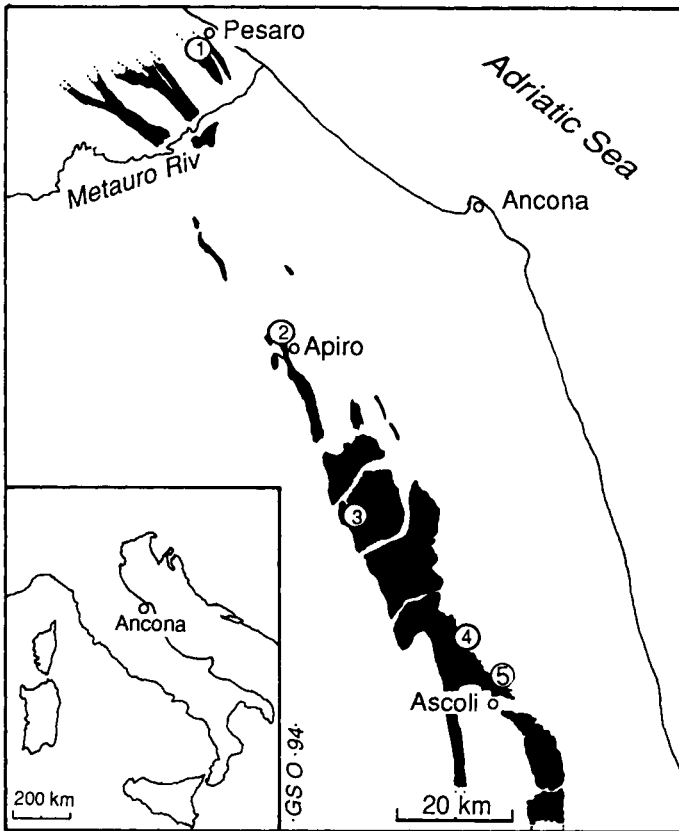


Fig. 1. Location of some sections including Messinian biotite-rich tuff in the Marche Province (simplified from Carloni et al., 1974b, and supplemented from Bassetti et al., 1993): 1 = Candelara; 2 = Maccarone; 3 = Camporotondo; 4 = Force; 5 = Colle Gallo. Black areas indicate gypsum and post-gypsum outcrops.

Two areas were investigated in this research: one 40 km southwest of Ancona, near Apiro (Carloni et al., 1974a, b), and the other 80 km south of Ancona, near Ascoli Piceno. The geologic map of the Ascoli Piceno area by Girotti and Parotto (1969) is accurate and allowed relocation of the outcrop at Colle Gallo (northeast of Ascoli Piceno) during a geologic mapping campaign by one of us (F.R.L.) in 1991. However, one year later, one of us (G.S.O.) tried to relocate the outcrop, and found it overgrown, thus unsuitable for a detailed stratigraphic study. In contrast, the section near Apiro (the Maccarone section) is remarkably well exposed on a large badland-like outcrop similar to the one pictured in Carloni et al. (1974b).

## LITHOSTRATIGRAPHY

The Maccarone section comprises about 250 m of marls; it was measured by Carloni et al. (1974b) according to whom we did our sampling (Fig. 2, left column). About 30 m above the base of the section, a distinctive more resistant 1.2 m thick tuff is exposed

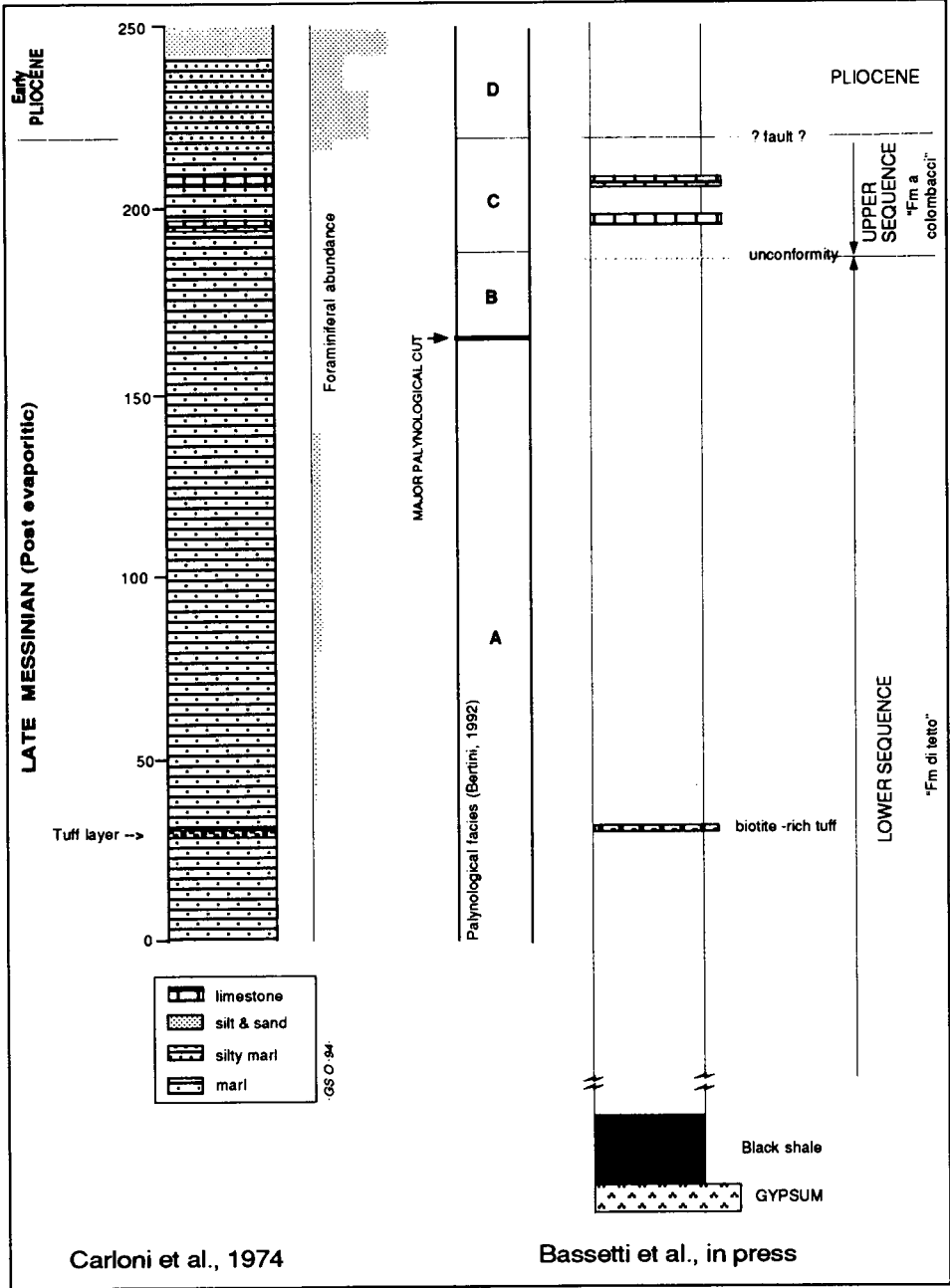


Fig. 2. Schematic section at Maccarone (Apiro). The interpretation taken from Carloni et al. (1974a) is shown to the left; the one by Bassetti et al. (1993) to the right. Note that planktonic foraminifers are rare within the hypohaline Messinian deposits. The palynofloral data (Bertini, 1992) are quoted to show environmental/depositional cuts.



between softer black (bituminous) clay layers. The top of the tuff exhibits a rusty colour. Biotite flakes are concentrated at different levels within this marker bed.

The section comprises Messinian hypohaline, post-evaporitic sediments, and Early Pliocene marine sediments. The hyperhaline evaporite unit is not exposed within the section but is present in the vicinity. The lower 220 m of clay-rich marls represent the post-evaporitic deposits ('Tetto' unit), the top of which is interbedded with thin limestone layers, light cream in colour; these are diagnostic for the formation with 'Colombacci'. These 'Colombacci' are regional lithologic marker beds for the topmost Messinian (Fig. 3).

In the composite section described by Borsetti et al. (1975) from the vicinity of Apiro, the base of the Maccarone section is not continuous with the rest of the series. However, from the map of the area and upon review of published information, it may be inferred that the lowermost layers exposed in the Maccarone section are either near the top of the local evaporite layers (arenitic gypsum) or about 100 m above the top of a 10 m thick gypsum-rich bed ('gessarenite') bracketed by two 25 m thick beds made of 'marne fogliettate' (flaky marls).

At that time, the sedimentary deposition was supposed to be continuous across the Miocene/Pliocene boundary by Carloni et al. (1974a, b). However, this interpretation of the section is now being questioned. On the one hand, G. Pasini (pers. commun.) suspects that a sedimentary break or a fault, more or less parallel to the sedimentary layers, is present at the top of the Messinian sediments. According to Pasini, this would explain why the layers correlated to the Pliocene begin with the *Globorotalia puncticulata* biozone, which is not lowermost Pliocene in age.

On the other hand, the new regional physical study of the Messinian post-evaporitic deposits in the area from Force to Apiro (Bassetti et al., 1994) suggests that the post-evaporitic deposits should be subdivided into two depositional sedimentary units informally named the 'di Tetto' formation at the bottom and the formation with 'Colombacci' at the top. The Maccarone section has been re-examined according to this new regional model, and an angular unconformity has been identified between the lower clayey unit which comprises the tuff layer, and the overlying sediments comprising both the 'Colombacci' unit and the later Pliocene Blue Clay formation.

In short, the biotite-rich tuff is located in the post-evaporitic Messinian deposits. Below it, there is a significant thickness of post-evaporitic sediments. Above it, there are even thicker still Messinian deposits (formation 'di Tetto'), then an angular unconformity (possibly representing a sedimentary break of unknown duration), then the 'Colombacci' unit, which is still Messinian, and then the fossiliferous marine layers of Pliocene age. For our purposes, one must conclude that the tuff is certainly late Messinian but not latest Messinian in age.

A realistic estimate of the time interval between the tuff and the Miocene/Pliocene boundary is difficult. The accumulation rate varies with the post-evaporitic marls which range in thickness between 100 and 1000 m from one location to another. The diagnostic tuff layer is sometimes in the lower portion, and sometimes in the upper portion of the unit. The unconformity at the top of the lower sequence makes it impossible to estimate the duration of the inferred hiatus. In short, the time between the deposition of the tuff layer and the deposition of the Early Pliocene may be several tens to a few hundreds ka long.



Fig. 3. The Maccarone section. (A) General view of the section with the tuff layer, nearly horizontal, marked on the left side (arrow; plant growing underlines the volcanoclastic horizon). The boundary and angular unconformity between the lower 'Tetto Formation' and the upper 'Colombacci Formation' can be seen on the upper right side: the clay becomes lighter than below. The Miocene/Pliocene boundary is in the topmost portion of the section. (B) Detail of the tuff layer. Note the black colored bituminous shale below the light cream colored tuff (scale is 1 m; photos by GSO).

The significance of the tuff layer can be understood by comparing it to 'equivalent' tuffs in other sections. In the southernmost area, the tuff unit is 4–5 m thick and occurs in the upper portion of the lower sequence. At Colle Gallo, it is observed as two successive metre thick layers intercalated with the usual marls. Bassetti et al. (1993) emphasize that at Force, it is made of resedimented material, with graded bedding and Bouma sequence, and because it is not laterally persistent, it cannot be used as a physical marker although it may derive from the same volcanic episode.

In the Camporotondo section, the tuff is still in the upper part of the post-evaporitic lower sequence but here it is not fully exposed and is represented by several volcanoclastic layers. In Maccarone, the tuff with graded bedding and Bouma sequence is thinner and lies in the lower portion of the post-evaporitic lower sequence.

In short, the continuity of this conspicuous tuff as a single post-evaporitic volcanic episode is clear, although, in some cases, it shows evidence of redeposition. Nevertheless, this marker bed is purely pyroclastic in nature in the studied outcrops suggesting that redeposition occurred shortly after the eruption.

## BIOSTRATIGRAPHY

The foraminiferal content of the Maccarone section was documented by Carloni et al. (1974b). The Miocene/Pliocene transition is rich in benthic and planktonic microfauna with more than 10,000 individuals per 100 g of sand fraction larger than 100  $\mu\text{m}$ . However, the first 40 m of the section and, more in general the 'di Tetto' formation, are scarcely fossiliferous (see Fig. 2).

According to the data by Borsetti (in Carloni et al., 1974b), from the base of the section to about 10 m above the tuff layer, the fauna is nearly absent. The foraminiferal assemblage becomes truly diagnostic 145 m above the base of the section. The beds bracketing the Miocene/Pliocene boundary were subdivided into the *Globigerinoides ruber parkeri* Zone (Messinian) followed by the *Globorotalia margaritae* Zone (Pliocene), itself comprising, from bottom to top, the *Sphaeroidinellopsis* spp., *Globorotalia hirsuta praehirsuta*, *G. puncticulata*, and the *G. bononiensis* subzones. However, according to Pasini (pers. commun.) this subdivision is tentative.

What is important to consider for this study is that no diagnostic pelagic foraminiferal faunas are present immediately above and below the tuff. Therefore, its biostratigraphic location cannot be precisely determined from present data.

## GEOCHRONOLOGY

### *Petrography and mineralogy of the geochronometers*

Mineral separation was done first to identify the overall composition of the tuff. Pumiceous glass is the major component, quartz and plagioclase (more than 5% of the whole-rock) are abundant; biotite makes locally more than 5% of the whole-rock. Short to elongated (up to 0.2 mm long) zircon crystals are also abundant (0.1% of the whole-rock), and they generally show irregular surfaces. Short idiomorphic crystals of apatite are rare. Pyrite is also present together with rock fragments. The layer is purely volcanic in origin which suggests either an instantaneous air transportation or reworking

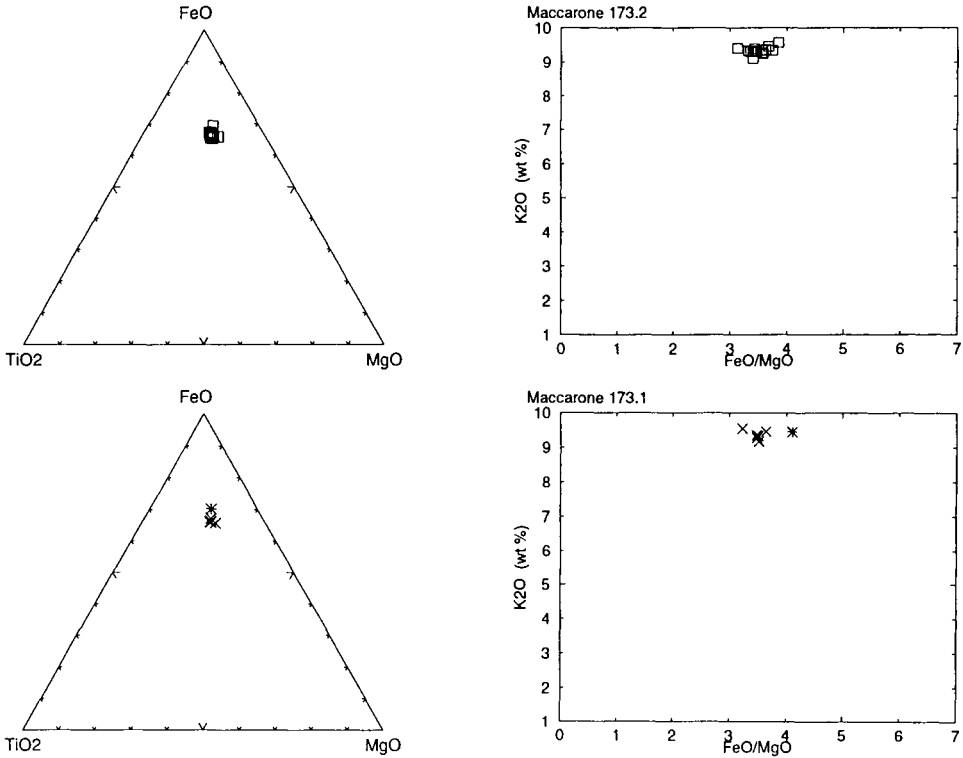


Fig. 4. Geochemical composition of the biotite mica flakes from two levels within the tuff layer of the Maccarone section. Note overall geochemical homogeneity. Asterisk indicates poorly polished small flake in separate T173-1 biotite, with resulting uncertain analysis.

and resedimentation immediately after the eruption and first air-fall deposition in a marine basin.

Biotite was magnetically separated from two different, millimetre thick mineral-rich horizons selected within the tuff at 0.1 dm (T173-1) and 0.3 dm (T173-2) above the base of the tuff layer. Most flakes are in the range of 0.1 mm although some idiomorphic hexagonal flakes are up to 1 mm wide and are often as thick as 0.5 mm. This mixture of sizes suggests a transportation without hydrodynamic winnowing. Some flakes contain many glass or zircon inclusions. The heavy fractions in bromoform, representing the two flake grain sizes, were purified by gently crushing the separates in acetone to remove inclusions. X-ray diffraction patterns of both purified biotite samples showed no trace of alteration and a (001) peak at 10.04 Å.

In order to assess the mineral homogeneity within and between each level, the geochemical composition of the two separates was studied using Energy Dispersive Spectrometer analyses (EDS-SEM EDAX PV9100, technique described by Gasparotto, 1988). The results are shown in Table 2 and Fig. 4, and indicate: (1) reasonably good homogeneity within both levels; (2) a similar composition of the two levels with the TiO<sub>2</sub> content near 5.6 (except for two of fifteen flakes with a lower content), and the FeO/MgO ratio at 3.5; and (3) a homogeneously high K content (9.35% K<sub>2</sub>O). These

Table 2

Geochemical composition of biotite flakes from the Maccarone section (SEM-EDS technique — Gasparotto, 1988; analyses by F.T. in Bologna)

SiO <sub>2</sub>	TiO <sub>2</sub>	Al <sub>2</sub> O <sub>3</sub>	FeO*	MnO	MgO	CaO	Na <sub>2</sub> O	K <sub>2</sub> O	FeO*/MgO
<i>Maccarone 173.2</i>									
37.42	5.03	14.69	25.17	0.03	8.05	0.02	0.18	9.41	3.13
36.96	5.76	15.12	24.81	0.07	7.48	0.05	0.40	9.35	3.32
37.16	5.43	14.94	25.36	0.07	7.55	0.00	0.18	9.32	3.36
36.62	5.99	15.08	25.31	0.16	7.45	0.05	0.21	9.11	3.40
36.69	5.64	15.18	25.43	0.00	7.47	0.00	0.26	9.33	3.40
37.11	5.45	15.01	25.13	0.06	7.33	0.06	0.44	9.39	3.43
36.75	5.87	14.96	25.33	0.17	7.34	0.06	0.20	9.32	3.45
36.48	5.83	15.00	25.40	0.11	7.36	0.02	0.48	9.31	3.45
36.64	5.50	15.11	25.51	0.22	7.37	0.03	0.28	9.32	3.46
36.87	5.55	14.76	25.90	0.06	7.29	0.00	0.21	9.35	3.55
36.50	5.53	14.85	25.97	0.12	7.28	0.08	0.41	9.26	3.56
36.74	5.88	15.02	25.73	0.00	7.20	0.00	0.16	9.28	3.58
36.54	5.57	15.08	25.90	0.19	7.15	0.01	0.18	9.37	3.62
36.28	5.69	15.33	25.82	0.15	7.03	0.01	0.23	9.47	3.67
36.42	5.71	15.10	25.83	0.26	6.90	0.06	0.35	9.36	3.74
37.06	4.91	14.61	26.60	0.19	6.91	0.06	0.08	9.58	3.85
Average $\pm 1\sigma$									
36.77	5.58	14.99	25.57	0.12	7.32	0.03	0.27	9.34	3.50
$\pm 0.30$	$\pm 0.28$	$\pm 0.18$	$\pm 0.41$	$0 \pm 8$	$\pm 0.27$	$\pm 0.03$	$\pm 0.11$	$\pm 0.10$	$\pm 0.17$
<i>Maccarone 173.1</i>									
36.58	5.34	14.75	25.46	0.15	7.90	0.00	0.27	9.55	3.22
36.58	5.91	14.64	25.66	0.14	7.38	0.03	0.29	9.37	3.48
36.59	5.76	15.17	25.39	0.09	7.30	0.06	0.34	9.28	3.48
36.58	5.86	15.03	25.60	0.11	7.30	0.00	0.19	9.34	3.50
36.71	5.69	15.25	25.41	0.04	7.24	0.02	0.47	9.18	3.51
36.35	5.58	14.85	26.10	0.13	7.18	0.00	0.33	9.46	3.63
36.76	4.98	14.46	27.31	0.11	6.66	0.02	0.23	9.46	4.10
Average $\pm 1\sigma$									
36.59	5.59	14.88	25.85	0.00	7.28	0.02	0.30	9.38	3.56
$\pm 0.12$	$\pm 0.12$	$\pm 0.27$	$10.64$	$\pm 0.03$	$\pm 0.34$	$\pm 0.02$	$\pm 0.08$	$\pm 0.12$	$\pm 0.25$

FeO\* = total iron;  $\sigma$  = standard deviation.

properties, in agreement with previous studies (Montanari, 1988; Odin et al., 1991), suggest a priori a good reliability (homogeneous provenance) for the selected biotite as a geochronometer.

The felsic phase, purified from quartz and mixed grains using bromoform-acetone mixtures monitored by systematic X-ray diffraction analyses, is mainly made of small fragments of clear, non-euhedral plagioclase. Cleaning involved a mixture of dilute nitric-acetic acids in ultrasonic bath for 1 h. The X-ray diffraction patterns of the purified felsic separate indicate an anorthite-rich plagioclase. The interval between reflections ( $1\bar{3}1-131$ ) is  $1.9^\circ 2\theta$ , and the relatively low peaks indicate a moderately preserved crystal structure of the plagioclase.

Table 3

Summarized analytical results of  $^{40}\text{Ar}/^{39}\text{Ar}$  step heating measurements on late Messinian tuff from Maccarone (by GSO in Lausanne)

°C	Age (Ma)	$\pm 2\sigma$	% $^{39}\text{Ar}$	%rad.	K/Ca
<i>Biotite T173 (46.2 mg), irradiation ULRD5</i>					
700	4.79	0.12	5.1	32	2.7
800	5.49	0.09	2.9	66	37
900	5.48	0.08	16.0	88	60
975	5.47	0.08	11.2	91	63
1050	5.45	0.08	14.7	87	33
1125	5.39	0.07	41.7	92	75
1185	5.36	0.08	7.8	91	26
1250	5.12	0.24	0.5	52	
1350	4.6	1.2	0.1	7	
<i>Biotite T173 (41.9 mg), irradiation ULRD7</i>					
700	5.73	0.26	3.0	56	82
850	5.55	0.10	6.6	75	164
970	5.88	0.08	23.8	90	257
1040	5.56	0.08	12.8	90	284
1075	5.54	0.08	14.1	89	268
1115	5.51	0.08	19.0	89	220
1175	5.46	0.08	16.8	90	46
1350	5.46	0.11	3.9	91	22
<i>Plagioclase T173 (26.26 mg), irradiation URLD5</i>					
750	7.6	0.4	13.2	13	0.27
900	7.02	0.24	13.1	49	0.12
1000	6.56	0.20	15.7	59	0.10
1100	6.23	0.16	20.8	57	0.11
1200	6.62	0.22	15.9	37	0.12
1300	7.31	0.30	11.1	36	0.11
1400	9.9	0.4	7.1	37	0.08
1500	19.2	1.2	2.9	39	0.06
1560	21	12	0.2	28	0.19

A technical problem with the step at 970°C led to measure a maximum age (*italics*). Age = apparent age; °C = heating temperature for given step.

#### $^{40}\text{Ar}/^{39}\text{Ar}$ isotopic analyses

Samples T173 biotite and T173 plagioclase were measured at the analytical facility designed in Lausanne (Cosca et al., 1992) using biotite HD-B1 as the monitor for calibration of the neutron flux in the TRIGA reactor in Denver. The revised age value of 24.21 Ma (Hess and Lippolt, 1994) was used for age calculation. All error bars quoted here correspond to a 95% confidence level (but for Table 4).

A first biotite sample was irradiated and measured in 1993. After preheating at 600°C for 55 min under a vacuum, 46 mg of the pure biotite T173 were heated step by step and nine successive apparent ages were calculated (Tables 3 and 4). The age spectrum at the top of Fig. 5 has a slightly disturbed shape with gently diminishing apparent ages from 800°C to 1185°C. There is no true plateau, and a weighted mean age of  $5.44 \pm 0.04$

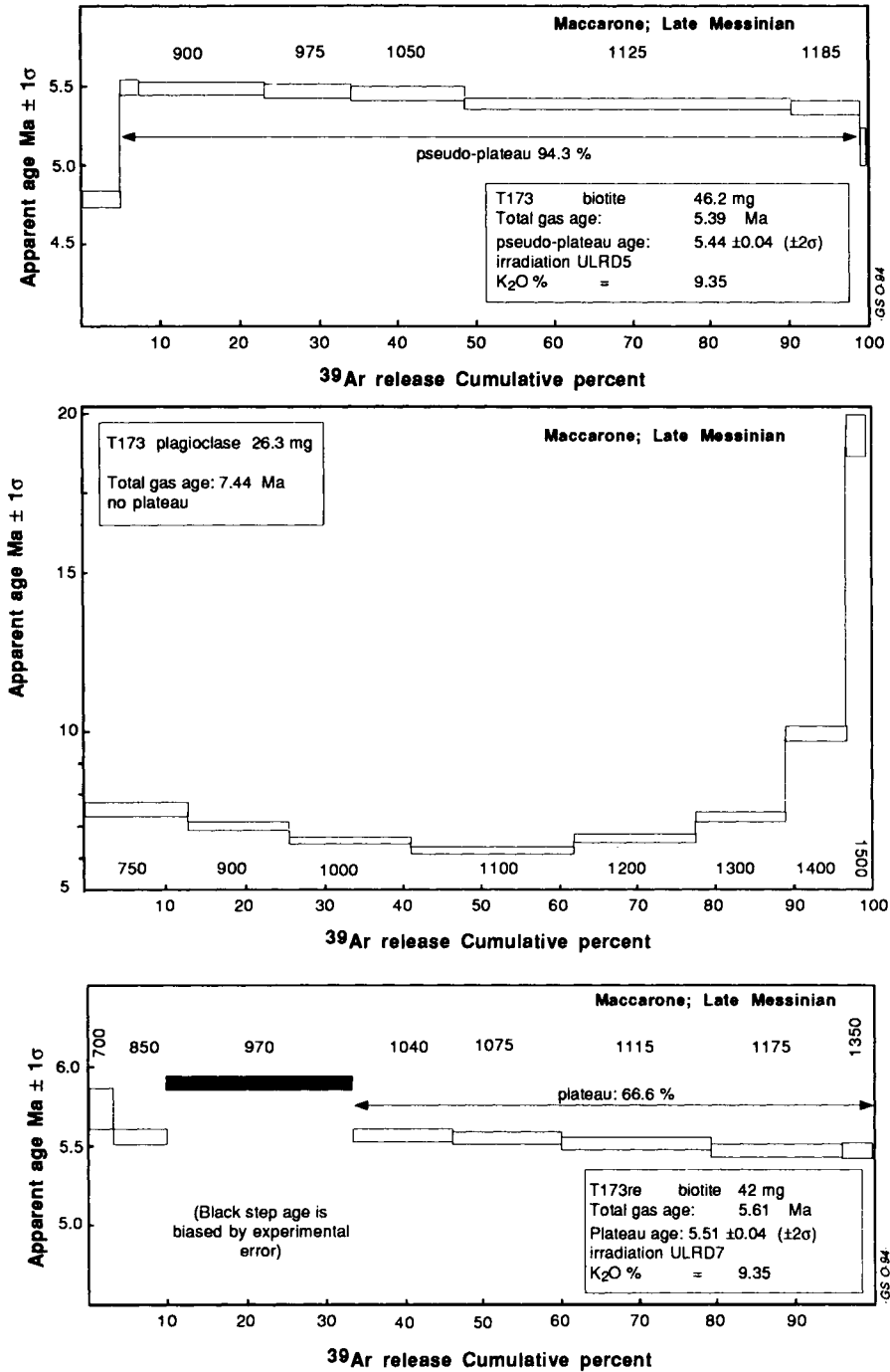


Fig. 5. <sup>40</sup>Ar-<sup>39</sup>Ar age spectra for biotite and plagioclase separates from tuff T173 (irradiation ULRD5, measured VI-1993; irradiation ULRD7, measured II-1994).

Table 4

Details of the analytical data for biotite from tuff T173 (by GSO in Lausanne)

°C	40*	±	39	±	38	±	37	±	36	±	40/39	±
<i>T173 biotite, irradiation ULRD5, J = 0.002588</i>												
700	9890	20	3.45	6	260.0	0.5	558.6	1.1	22.98	0.05	1.027	0.01
800	183.3	0.4	102.3	0.2	8.465	0.017	1.34	0.06	0.210	0.002	1.178	0.01
900	2739	5	2.55	4	164.0	0.3	16.76	0.22	1.055	0.005	1.176	0.01
975	511.4	1.0	395.0	0.8	30.78	0.06	3.09	0.06	0.156	0.002	1.173	0.01
1050	2561	5	1900	4	158.6	0.3	28.38	0.22	1.120	0.005	1.169	0.01
1125	6741	13	5382	11	420.3	0.8	35.38	0.22	1.656	0.006	1.156	0.01
1185	349.9	0.7	275.7	0.6	18.49	0.04	5.25	0.06	0.107	0.002	1.150	0.01
1250	39.18	0.08	18.72	0.04	1.160	0.002			0.062	0.002	1.100	0.02
1350	55.54	0.11	3.969	0.008	0.287	0.001			0.175	0.002	0.99	0.12
<i>T173-re biotite, irradiation ULRD7, J = 0.002584</i>												
700	157.0	0.3	71.0	0.5	5.91	0.03	0.425	0.020	0.234	0.004	1.231	0.03
850	253.9	0.5	159.9	0.3	13.09	0.05	0.478	0.012	0.211	0.003	1.193	0.01
970	809.8	1.6	574.0	1.1	45.41	0.08	1.093	0.017	0.274	0.004	1.265	0.01
1040	406.7	0.8	307.7	0.6	24.56	0.06	0.531	0.016	0.127	0.001	1.194	0.01
1075	454.2	0.9	339.8	0.7	28.76	0.06	0.621	0.018	0.161	0.003	1.191	0.01
1115	610.0	1.2	458.6	0.9	37.6	0.05	1.021	0.020	0.219	0.003	1.183	0.01
1175	529.8	1.1	404.3	0.8	30.27	0.08	4.34	0.06	0.181	0.003	1.173	0.01
1350	121.9	0.2	94.1	0.2	6.62	0.02	2.10	0.02	0.038	0.003	1.174	0.01

Gas in  $10^{-15}$  moles (errors are 1 standard deviation: analytical precision)  $40/39 = \text{ratio } ^{40}\text{Ar}_{\text{rad}}/^{39}\text{Ar}_{\text{K}}$ .

Ma can be calculated from the 6 main steps and another at  $5.40 \pm 0.09$  Ma using only the last three steps. The integrated (total fusion) age at 5.39 Ma, is not significantly different. However, we were not satisfied with this spectrum because it included a large proportion of gas released at 1125°C. A second irradiation was therefore performed using two splits of the same biotite.

The first split (about 15 mg) was preheated and then a first step at 700°C was measured but it did not allow calculation of a significant age because of the very small quantity of gas released which was mostly atmospheric in composition. The sample when heated at 1350°C, provided a large quantity of gas from which an age at  $5.50 \pm 0.07$  Ma was calculated. No more gas was released at 1600°C, therefore this age is considered a total gas age.

Following preheating for 25 min, the second biotite split (41.9 mg) was measured in a stepwise fashion (Fig. 5 bottom). One step measurement partly failed (970°C) due to late measurement following inlet in the mass spectrometer. Nevertheless, a plateau age at  $5.51 \pm 0.04$  Ma can be calculated from five steps with analytically consistent apparent ages. However, this age cannot be compared to the total gas age which is biased by the failed step. Isochron calculations including all five steps contributing to the plateau age are very close to each other (Fig. 6). The resulting apparent ages although poorly defined, are overall consistent with previously calculated ages, and the initial  $^{40}\text{Ar}/^{36}\text{Ar}$  ratios are not different from the atmospheric composition.

The plagioclase sample T173 (26.26 mg) was pre-heated at 450°C for 30 min under vacuum. Small quantities of gas were obtained for the nine measured steps (see Tables 3



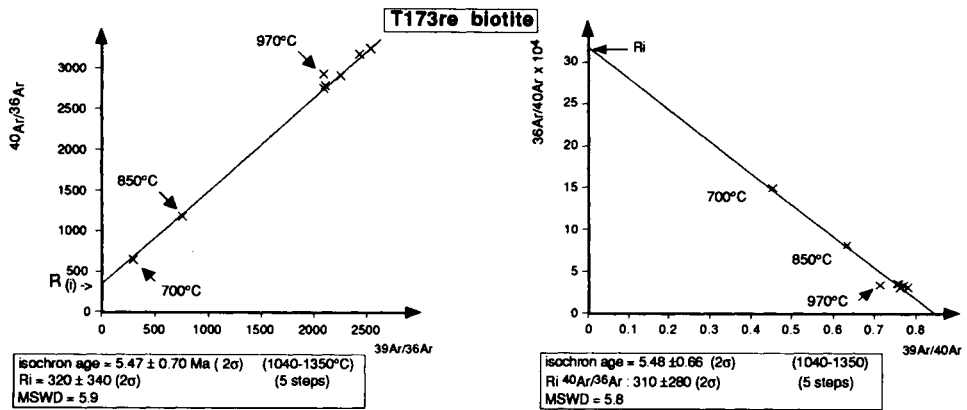


Fig. 6. Isochron ages of sample biotite T173-re. The five significant points (steps 1040°C to 1350°C) are so near that the resulting isochron ages and initial ratios are poorly defined.

and 4). The spectrum of calculated ages (Fig. 5) is 'saddle-shaped' with the lowest age at 6.23 Ma (step 1100°C) still older than the biotite age. The total fusion age of 7.44 Ma is significantly older than that of the biotite.

## DISCUSSION AND CONCLUSIONS

The stratigraphic location of the dated level is mainly based on lithostratigraphic relationships. According to the regional model, the dated layer is located in a late portion of the Messinian Stage, above the local gypsum depositional episode but not at the topmost of the Messinian series.

The tuff is a pure volcanoclastic layer although the precise origin and mechanism for transportation remain unclear. Some criteria suggest an aerial transport origin based on the widespread occurrence of the tuff in the Central Apennines. There is also a suggestion of a short distance transportation mechanism or 'en masse' deposition or redeposition with material of widely different nature and hydrodynamic sorting. The pyroclastic material has not been altered after deposition as shown by the good preservation of the glass fraction (Carloni et al., 1974b) and the quality of the biotite. The high K content and overall geochemical homogeneity of the biotite are additional criteria for substantiating that the unaltered dated material has a composition consistent with a single crystallization event.

Technically, the age data obtained from sample T173 are generally acceptable. The apparent ages calculated are summarized in Table 5. The consistency between ages obtained from several splits of the biotite during two different irradiations suggests that the measured ages are analytically significant.

The plagioclase phase may contain some extraneous argon and therefore, the calculated age for the youngest step might be considered to be a maximum age for the eruption.

Biotite is a more reliable geochronometer: (1) the age spectra are not perfect but

Table 5

Summary of calculated ages for tuff T173

Sample	Weight	Apparent age (Ma) (total gas)	Steps on pseudo-plateau	% <sup>39</sup> Ar	Apparent age (plateau) ±2σ (Ma)
<i>Age spectra</i>					
T173 biotite	46.2 mg	5.39 ± 0.05)	(6) 800 to 1185°C (3) 1050 to 1185°C	94.3% 64.3%	5.44 ± 0.04 5.40 ± 0.09
T173-re bio	41.9 mg	5.61 ± 0.04	(5) 1040 to 1350°C	66.6%	5.51 ± 0.04
T173 biotite	14.67 mg	5.50 ± 0.07	(1) 700 to 1350°C	>99.0%	
T173 plagio	26.26 mg	7.44 ± 0.12	disturbed spectrum		
<i>Isochron age for sample T173-re biotite</i>					
steps 1040–1350					
<sup>40</sup> Ar/ <sup>36</sup> Ar versus <sup>39</sup> Ar/ <sup>36</sup> Ar isochron: age 5.47 ± 0.70; Ri = 318 ± 336; MSWD = 5.9					
<sup>36</sup> Ar/ <sup>40</sup> Ar versus <sup>39</sup> Ar/ <sup>40</sup> Ar isochron: age 5.48 ± 0.66; Ri = 311 ± 276; MSWD = 5.8					
all steps					
<sup>40</sup> Ar/ <sup>36</sup> Ar versus <sup>39</sup> Ar/ <sup>36</sup> Ar isochron: age 5.53 ± 0.22; Ri = 309 ± 76; MSWD = 43					
<sup>36</sup> Ar/ <sup>40</sup> Ar versus <sup>39</sup> Ar/ <sup>40</sup> Ar isochron: age 5.56 ± 0.24; Ri = 309 ± 82; MSWD = 52					

The total gas age for sample T173-re biotite (*italics*) is not valid because one step was analytically biased. (Ri = initial <sup>40</sup>Ar/<sup>36</sup>Ar isotopic ratio).

acceptable; (2) most steps indicate precise ages between 5.36 and 5.56 Ma, and the sub-plateau and plateau ages (5.44 and 5.51 ± 0.04 Ma) are not significantly different from total gas ages (5.39 and 5.50 ± 0.07 Ma); and (3) isochron calculations are not totally convincing due to the fact that points on the plateau are not far from each other, and the MSWD value (about 6) is rather high. This is related to the slightly decreasing ages with increasing temperature on the spectra which possibly indicate a slight recoil phenomenon during irradiation. If this is true, total gas ages would be more representative than the 'plateau' ages. In any case, the age range of 5.40 to 5.50 Ma may be proposed as a good approximation of the time of biotite crystallization.

Previous geochronological studies from the S. Maria in the Carpineto area, near Pesaro, include a fission track age of 6.1 ± 0.6 Ma from glass shards (Arias et al., 1981). Carloni et al. (1974a) have reported radioisotopic data for the volcanic glass fractions from samples collected from Maccarone and Colle Gallo with apparent ages of 7.6 ± 0.9 Ma and 7.9 ± 0.9 (2σ) Ma, respectively. These ages recalculated using presently valid decay constants, were obtained using the K–Ar isotope dilution technique. These two series of ages, which are not internally consistent for the same material, suggest that the extraneous argon observed in our plagioclase separate may have been present also in the glass phase. Glass shards are not considered to be a reliable geochronometer. The biotite data obtained in this work are more reliable since they produce a more precise age strengthened by the good shape of several age spectra.

Our biotite ages correspond to the accepted value of 24.21 Ma for the monitor sample allowing calibration of the neutron flux. However, the actual age of HD-B1 is suggested with a 2σ error bar of ±0.6 Ma or ±2.5% of the age, which should be factored into the analytical age to derive the realistic geological ages that are comparable to data obtained using other monitors, analytical techniques, and methods. Because the analytical ages

of the biotite separated from T173 at 5.4 to 5.5 Ma is only proved with an error bar of  $\pm 0.2$  Ma, the Miocene/Pliocene boundary has to be younger than about 5.5 Ma based on direct geochronological data.

This correlates well with the pioneering work by H. Bellon, (results from his PhD. thesis 1976 presented in 1977) where he proposed a Miocene/Pliocene age of  $5.3 \pm 0.2$  Ma based on K–Ar whole-rock dates from Morocco. This was mostly based on a lava flow interlayered within Mio–Pliocene sediments which yielded an age of  $5.5 \pm 0.6$  Ma (Hernandez and Bellon, 1985).

Our results are also in agreement with a recent estimate derived from astronomical lithocyclicity, a procedure that sometimes disagrees with geochronology. We use here the abbreviated unit Ma(e.) for 'estimated Ma' for designation of a temporal unit different from true Ma, and resulting from an indirect dating procedure (extrapolated time deduced from any non-physical direct dating). For example, Hilgen (1991) applied the sedimentary cycle counting procedure to the Capo Rossello sections in southern Sicily, and found that the base of the Trubi Marls, which corresponds to the Miocene/Pliocene boundary, should be placed at about 5.32 Ma(e.) (with no estimated error bar). With this result for the boundary, Hilgen also concluded that the bottom of the *Sphaeroidinellopsis* acme observed by Borsetti in Maccarone, should be at 5.29 Ma(e.); the top of the *Sphaeroidinellopsis* acme would be at 5.20 Ma(e.); the *Globorotalia margaritae* FCO at 5.07 Ma(e.), and the first occurrence of *G. puncticulata* at 4.50 Ma(e.). This astronomical approach therefore can be very useful although Hilgen remembers that the same approach led to ages in between 4.86 and 4.93 Ma(e.) for the same boundary in previous years.

In this situation, the application of the geochronological approach is still the most efficient and other outcrops might now be investigated for additional information.

## SOMMAIRE — STRATIGRAPHIE INTÉGRÉE DU PROFIL DE MACCARONE, MESSINIEN SUPÉRIEUR (MARCHES, ITALIE)

(Manuscrit soumis: Février 1994, révisé: Février 1995; rédacteur responsable: GSO)

Dans les Apennins centraux, des traces d'activité volcanique sont présentes, interstratifiées dans les sédiments rapportés au Messinien supérieur par corrélation lithostratigraphique mais aussi par un contrôle biostratigraphique plus lâche. L'étude géochronologique a d'abord considéré la nature d'un tuf épais d'un mètre dans le profil de Maccarone. Le verre volcanique, le quartz, le plagioclase et la biotite sont abondants, zircon et apatite sont présents. La biotite sélectionnée pour la datation est homogène. La technique  $^{39}\text{Ar}/^{40}\text{Ar}$  avec chauffage par étape a été appliquée. Le plagioclase a montré un spectre d'âge en selle indiquant que ce géochronomètre n'était pas approprié. La biotite a été datée à 3 reprises. L'une a donné un spectre imparfait conduisant à un âge apparent de 5,44 à 5,40 Ma. L'autre a permis d'obtenir d'un côté un meilleur spectre avec un plateau dont l'âge calculé est de  $5,51 \pm 0,04$  Ma et de l'autre, un âge total similaire à  $5,50 \pm 0,07$  (incertitudes analytiques internes). Ces âges tournant autour de 5,5 Ma caractérisent un tuf déposé nettement avant la fin du Messinien tel qu'il est conçu en Italie, son pays de définition; alliés aux datations de la base de l'Étage à plus

de 7 Ma ils indiquent que la durée du Messinien est nettement supérieure à celle qui était admise jusqu'à ces travaux.

*(Sommaire des auteurs)*

#### ACKNOWLEDGEMENTS

We appreciated the information provided by A.M. Borsetti and G. Pasini about the Maccarone section. We also acknowledge the comments by G.B. Vai on the Messinian lithostratigraphy, and thank P. Myrow (Colorado College, Boulder) for improvement of the English of the original manuscript. The radiometric measurements were achieved in Lausanne thanks to the facilities made available in the Institute of Mineralogy by the Swiss National Funds. No funding was provided by French Organizations for this research.

This Page Intentionally Left Blank

Chapter E8

**POTENTIAL INTEGRATED UPPER MIOCENE STRATIGRAPHY IN  
SOUTHEASTERN SPAIN**

Ch. Montenat and F. Serrano

INTRODUCTION

The regional setting of the Eastern Betic Miocene series is presented by Montenat et al. (Chapter D4) who give a review of the chronology and regional distribution of Miocene volcanic rocks included in three major groups: the Cabo de Gata Group (early-Middle Miocene to late Tortonian), the Mazarrón Group (late Tortonian), and the lamproites complex (uppermost Tortonian/Messinian).

The relationships between the volcanics and biostratigraphically characterized sediments offer some opportunities for contributions to integrated stratigraphy of the Late Miocene sequence.

In this paper, we describe the state of knowledge on the following three main topics:

(1) The early/late Tortonian boundary. The partition of the Tortonian into two main biostratigraphic units is well documented by Serrano (1979). It corresponds to a notable eustatic event (late Tortonian transgression), well known in the Betics and surrounding domains, which in many places is documented by an unconformity (Montenat, 1990).

(2) The Messinian marine environment. The Messinian sediments include two distinct sequences, related to open-marine (lower part), and restricted evaporitic (upper part) environments, respectively. Datings of the establishment of the anoxic environment in different basins are useful for understanding the Messinian evaporitic event (the salinity crisis) in the Mediterranean domain in terms of duration of the evaporitic phase, and possible regional diachronism.

(3) Mammal biozonation. A mammal fauna is inserted in the Messinian succession.

ELEMENTS FOR LATE MIOCENE INTEGRATED STRATIGRAPHY

*Dating of the late Tortonian*

*Cabo de Gata.* In the coastal zone between Carboneras and San José (El Plomo, Caliguera, etc.) a marine sequence is locally inserted between volcanics related to Series B and Series D of the Gata Group, respectively (see figs. 1 and 2 in Montenat et al., Chapter D4).

The sediments are calcarenites including abundant volcanoclastic and marly layers, and contain a planktonic microfauna represented by *Globigerinoides extremus*, *Neogloboquadrina humerosa* (dextral), *N. acostaensis* (dextral), indicating the base of the upper Tortonian (Serrano, 1992). These deposits rest on altered volcanic rocks belonging to the Series B emplacement which ended around 9.3 Ma (Bellon et al.,

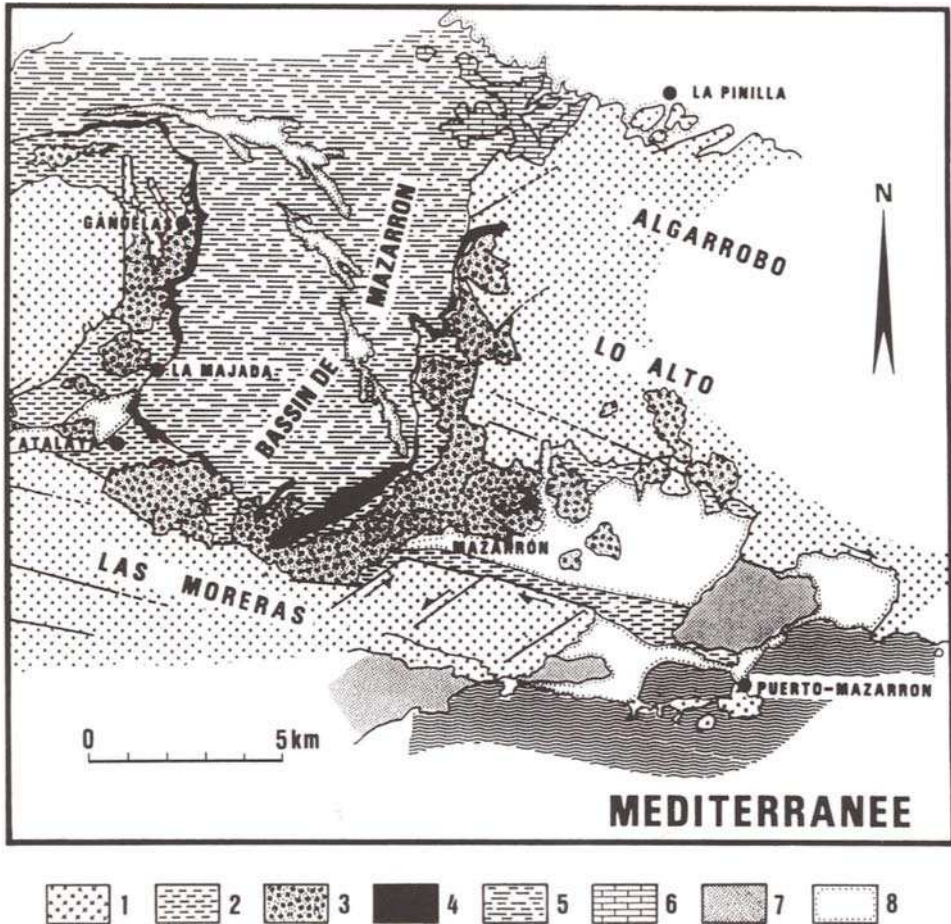


Fig. 1. Geologic map of the Mazarrón basin. 1 = basement; 2 = late Tortonian turbidites and marls; 3 = Rhyo-dacitic volcanics; 4 = 'Calcaire à Algues' (Tortonian/Messinian boundary); 5 = Messinian reefs; 7 = Pliocene deposits; 8 = Pleistocene.

1983). In some places (i.e., Caliguera), the sediments include volcanic breccias (not yet dated) related to the Series D which ranges in age from 8.6 Ma to 7.5 Ma (see Montenat et al., Chapter D4).

*Mazarrón basin.* (southwest of Murcia). This basin is a large quadrangular graben filled with late Tortonian and early Messinian marine deposits, mostly represented by planktonic-rich marls (Fig. 1). Numerous rhyo-dacitic domes (Mazarrón Group) are located along the basin's margins; large volumes of volcanic breccias and micaceous tuffites are interbedded within marls containing microfaunas indicating an earliest late Tortonian age.

Various sections yield suitable samples for radioisotopic dating (not yet carried out), and precise correlation with planktonic zonations. Near Mazarrón, marls below and above volcanic flows contain planktonic microfaunas with dextral and sinistral (50–60%

sinistral) specimens of *N. acostaensis*, and *N. humerosa*; also *G. extremus*, and forms close to *Globorotalia plesirotunda* are present. These assemblages characterize the lower part of the late Tortonian. The volcanic activity could be extended to the middle part of the late Tortonian and in the Mazarrón area; marls with *N. humerosa* (sinistral) show signs of hydrothermal alteration.

In the Cartagena area (Cabezo Baeza), marls below the volcanic sequence contain a planktonic assemblage with *N. acostaensis* (dextral), *N. continuosa* (dextral), and little-evolved *G. extremus*, indicating the upper part of the early Tortonian. In summary, the volcanic activity of the Mazarrón Group seems to range from the latest part of the early Tortonian to the earliest part of the late Tortonian.

Few radioisotopic dates related to the Mazarrón Group are available:  $6.62 \pm 0.30$  Ma, and  $7.20 \pm 0.35$  Ma (Cartagena area);  $8.30 \pm 0.40$  Ma, and  $7.60 \pm 0.30$  Ma (Vera basin) (Montenat et al., Chapter D4). The volcanic rocks of the Vera basin are not clearly associated with contemporaneous sediments. Radioisotopic dates from the Cartagena area are not useful for integrated stratigraphy purposes because the dated samples are not directly associated with Tortonian sediments. However, as mentioned above, it is possible to find some sections in this area possibly suitable for detailed integrated stratigraphic studies. One example is the Cabezo Baeza section, which contains biotite and sanidine-rich volcanic rocks associated with Tortonian marine sediments.

In summary, the Mazarrón basin provides the best sections for integrated stratigraphic studies, including: (1) suitable material for radioisotopic datings (i.e., unaltered rhyodacitic interbedded units, and numerous other volcanoclastic intercalations containing abundant biotite and sanidine; and (2) interbedded sediments containing distinctive Tortonian microfaunas. Thus, further geochronologic analyses in this sequence will hopefully provide accurate and precise age calibration points for the Tortonian planktonic biostratigraphic zonation (Fig. 2).

#### *Lamproitic volcanics associated with Messinian sediments*

**Geochronology.** Lamproitic lavas flowed out in the Vera basin (northeast of Almería) during the Messinian. Several flows spread out in submarine environments by the end of the still open-marine setting in the early Messinian (i.e., southeast of Antas). Several metres higher in the sequence, the deposition of laminated marls, impoverished in microfauna, marks the beginning of an anoxic environment (Fig. 3). Marls adjacent to the lamproitic lavas yield planktonic assemblages with *Globorotalia mediterranea* and *N. humerosa* (sinistral), which indicate an early Messinian age. Only in a site near Vera, marine marls contain a similar assemblage with dextral forms of *Neogloboquadrina* indicating an age close to the late Messinian evaporitic event.

These lamproitic volcanics have not yet provided reliable ages. Some radioisotopic analyses yielded the following ages:  $17.35 \pm 1.30$  Ma and  $11.10 \pm 1.60$  Ma (K–Ar from whole-rock, Bellon et al., 1983);  $7.60 \pm 0.30$  Ma (biotite), and  $8.60 \pm 0.30$  Ma (phlogopite) (K–Ar dates by Nobel et al., 1981). However, these ages are inconsistent with stratigraphic data (see discussion about  $^{40}\text{Ar}$  isotopic ratios in Bellon et al., 1983). Nevertheless, we have located several other sites for future sampling, and the potential for radioisotopic dating of unaltered biotite and phlogopite.

**Correlation with mammalian biozonation.** The lamproite volcano of Barqueros



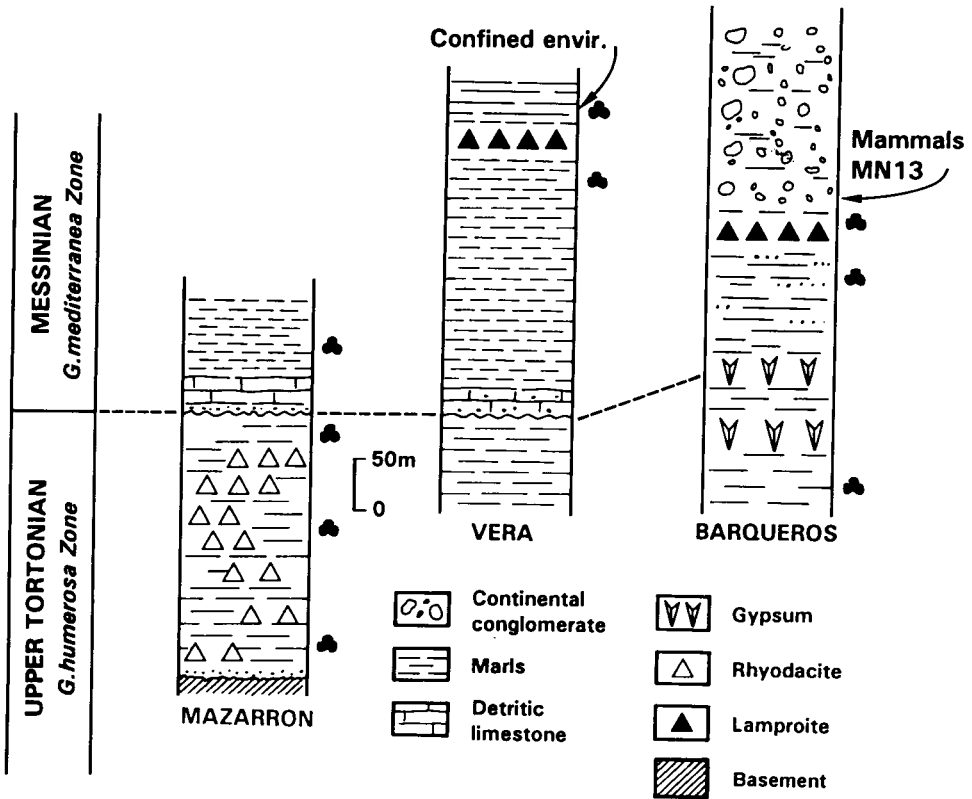


Fig. 2. Correlation of stratigraphic sections discussed in the text.

(southwest of Murcia), is emplaced within a thick Late Miocene sequence which displays the following succession, from bottom to top (Montenat, 1977, 1990) (Fig. 3):

(1) Grey-green silty marls with intercalations of nodular saccharoid gypsum in the lower half, and marly sandstone intercalations in the upper half of the unit (total thickness is about 250 m). The marls yield a late Tortonian microfauna (*N. humerosa*) enriched with Messinian species such as *Turborotalia multiloba* in the upper part (determination by G. Bizon). It is noteworthy that the classic Messinian *G. mediterranea* was not identified. Planktonic Foraminifera are absent in this area for ecological reasons because this area represents a shallow and restricted palaeoenvironment.

(2) Barqueros lamproitic volcanic edifice including cone, breccias and agglomerates, tuffites, and two main flows.

(3) The Barqueros volcanic rocks are locally overlain by sandy grey marls, about 30 m thick, which yield an impoverished Messinian microfauna including *Globorotalia* s.l. These small globorotalids, illustrated by Bizon et al. (1972a), display a regional extension in regressive beds at the top of the marine Messinian sequence.

(4) Several hundreds of metres of continental variegated sandy marls, sandstones, and conglomerates gradually replace the marine sediments. Close to the base of this continental sequence, grey and reddish sandy oncolitic marls contain abundant

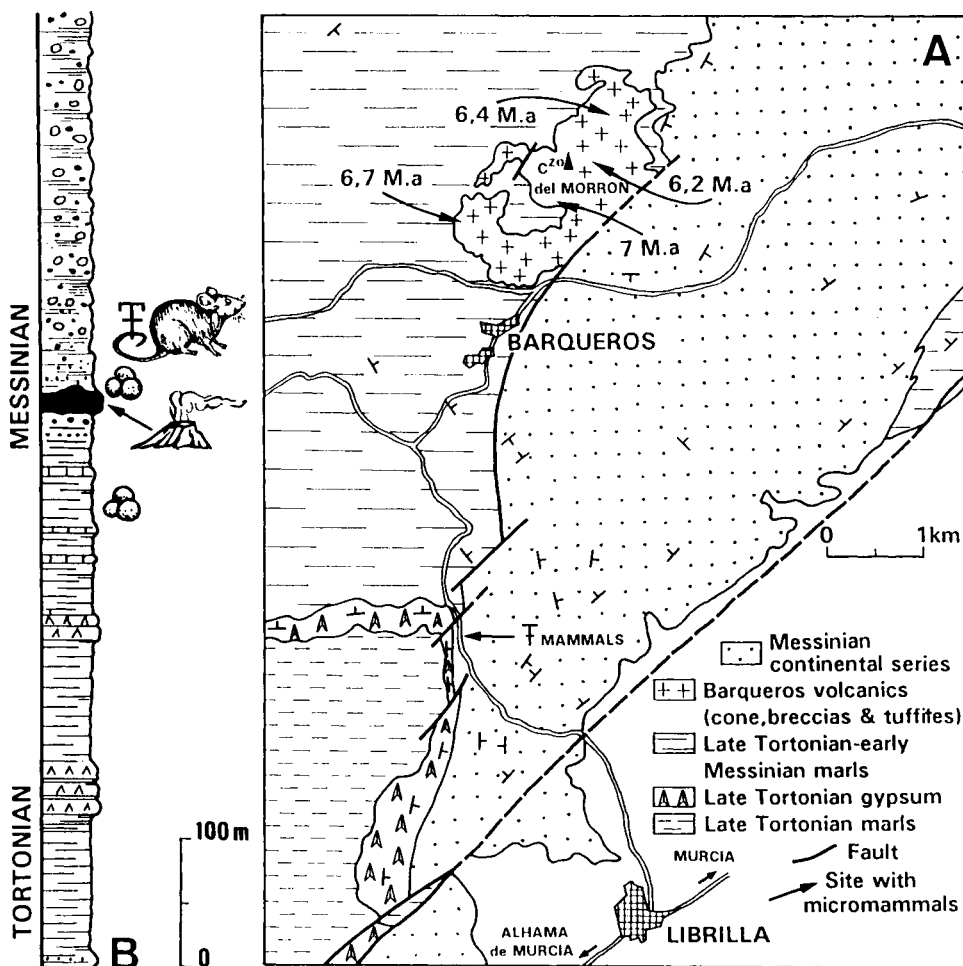


Fig. 3. Late Miocene series of Barqueros, near Murcia. (A) Geologic sketch map with indication of the dated volcanic samples. (B) Schematic stratigraphic column.

remains of various mammals (*Hipparion*, *Mastodon*, cervidae), and a rich fauna of micromammals including *Ruscinomys shaubi* (Vill. et Crus), *Cricetus* cf. *kormosi* (Shaub), *Occitanomys adroveri* (Thaler), *Apodemus primaevus* (Hugueney and Mein), *Stephanomys* sp., *Paraethomys miocenicus* (Jaeger, Muchaux, and Thaler) (Montenat et al., 1975). This is a typical association of upper Turolian age (upper half of the Mammalian Zone MN 13, Mein and Agustí, 1990). Four K–Ar dates from volcanic rocks (whole-rock; Drake and Curtis, Berkeley Geochronology Center, unpubl. data) yielded slightly discordant results (see location of these samples in Fig. 3A):  $6.20 \pm 0.30$  Ma,  $6.45 \pm 0.10$  Ma,  $6.79 \pm 0.03$  Ma, and  $7.00 \pm 0.03$  Ma.

In conclusion, we are confident that further efforts in refining these data using newly sampled, well preserved biotite and phlogopite, will yield accurate and precise age calibration of Late Miocene marine and terrestrial biostratigraphic events.

## SOMMAIRE — POTENTIEL POUR LA STRATIGRAPHIE INTÉGRÉE EN ESPAGNE DU SUD-EST

*(Manuscrit soumis: Février 1994; révisé: Juin 1994; rédacteur responsable: GSO)*

Dans le SE de l'Espagne, des roches volcaniques utilisables en géochronologie sont interstratifiées dans des sédiments contenant des microfaunes planctoniques. Des résultats préliminaires sont déjà disponibles. De nouvelles études permettraient de dater plus précisément des événements biostratigraphiques notamment dans le Tortonien (Cabo de Gata et Bassin de Mazarrón). Pour le Messinien, les résultats préliminaires sont moins prometteurs mais il se peut que de nouvelles datations permettent de meilleurs résultats dans le Bassin de Vera. Des événements biostratigraphiques continentaux (micromammifères, Zone MN13) pourraient aussi être datés géochronologiquement dans le Miocène Supérieur au SW de Murcie.

*(Sommaire proposé par les rédacteurs, GSO)*

## ACKNOWLEDGEMENTS

We would like to thank K. Stewart for reviewing the original paper.

Chapter E9

**A REVIEW OF GEOLOGICAL, BIOSTRATIGRAPHICAL, AND  
GEOCHRONOLOGICAL STUDIES OF THE MIURA PENINSULA (CENTRAL  
JAPAN)**

K. Saito, C. Inoue and Y. Kanie

INTRODUCTION

The Miura Peninsula is located south of the Tokyo metropolitan area. Because Yokosuka, in the southeastern part of the peninsula, was an important naval base, geological studies in this peninsula were restricted until the end of World War II. Therefore, no major report on the geology of this peninsula existed until 1945, despite it being located in the immediate vicinity of the metropolitan area, and its considerable geological importance.

After World War II, the Miura Peninsula became an affluent resort area, much appreciated by the public for its many small bays, often used for recreational activities. Thanks to the recent improvement and expansion of the rail and highway systems, the area can now be reached from downtown Tokyo in less than an hour and a half. This convenience is the major reason for large housing developments especially in the northern and central parts of the peninsula, and along the coast. In the course of the urban development many of the existing outcrops were destroyed or covered with concrete walls. For these reasons, it is somewhat difficult to carry out general field geological studies in this area today.

The southern part of the peninsula, however, still retains its natural coastline and it is possible to find good outcrops. Although the continuity of geological structures are often difficult to trace, the exposed outcrops provide a good opportunity for palaeontological and geochronological investigations.

Recently, several studies focusing on understanding the regional tectonic framework, were carried out in the South Fossa Magna region (e.g., Niitsuma, 1989; Koyama, 1989; and the other papers in *Modern Geology*, 1989, Vol. 14, 1–2). Because the Miura and Boso peninsulas form the eastern margin of this region, the geological evolution of the peninsulas is being discussed according to the existing tectonic framework.

The discovery of living *Calyptogena soyoae* communities in Sagami Bay, which is located on the west side of the Miura Peninsula (Fig. 1), provided important information on the depositional environments of the peninsula's major formations, in which occurrences of fossil *Calyptogena* species have been reported (Kanie et al., 1992).

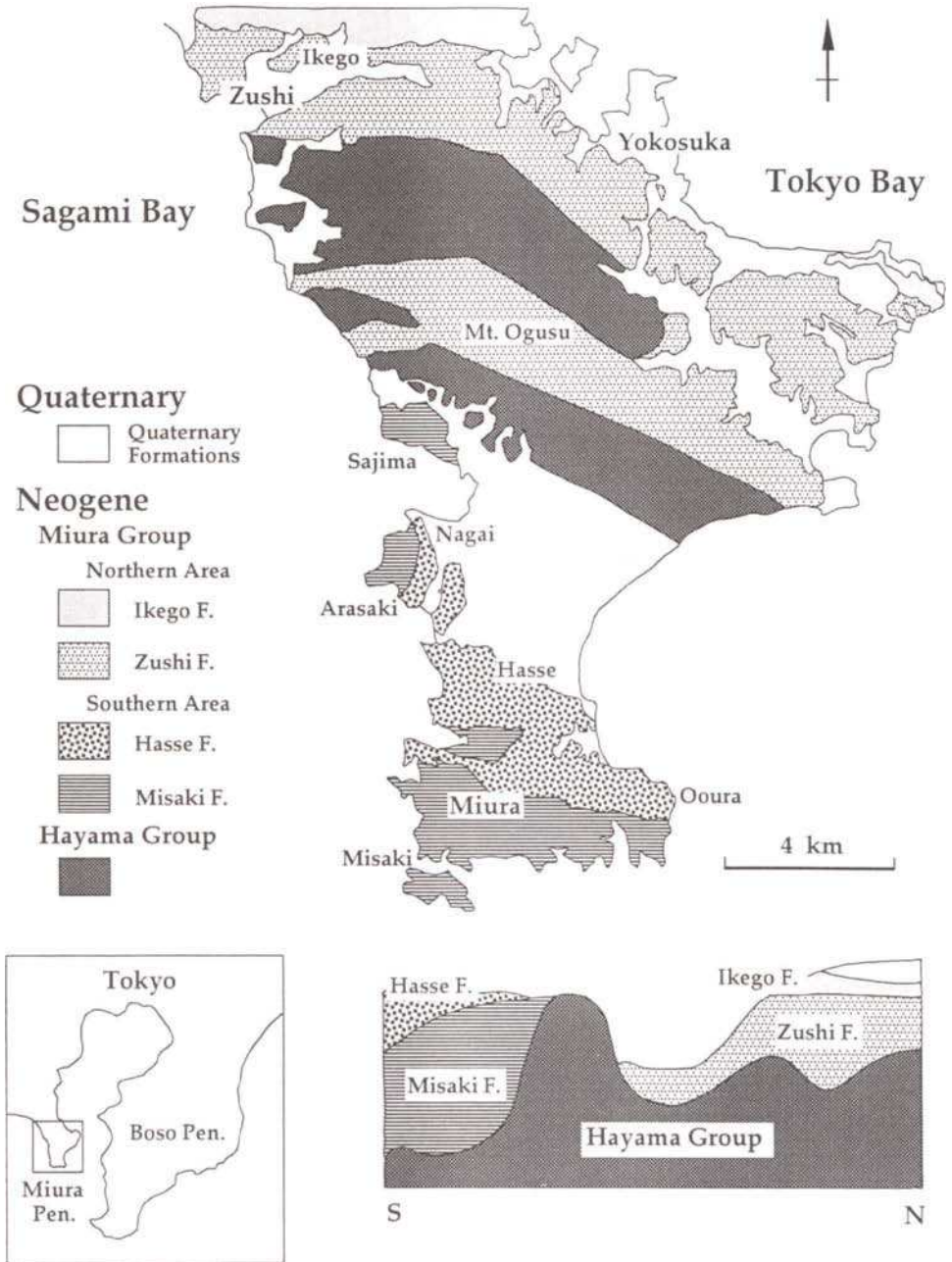


Fig. 1. Geological map of the Miura Peninsula. Modified from Mitsunashi and Yazaki (1968). Schematic cross section is redrawn from Kanie et al. (1991).

## GEOLOGIC SETTING AND VOLCANICS

### *Geology*

In 1956, Akamine et al. produced the first geological map of the Miura Peninsula including a report on the stratigraphy of the Miura Group. Later, Yazaki and Mitsunashi (1961) made a detailed geological map at the 1 : 20,000 scale of the northern part of the peninsula, showing the traceable tuff beds. Fig. 1 is a simplified version of their map with a schematic cross section (Kanie et al., 1991).

The Early to Middle Miocene Hayama Group divides the peninsula into northern, and southern areas. The Miocene–Pliocene Miura Group, unconformably covering the Hayama Group, is widely distributed in both areas. In the southern area, the group consists of the Misaki and Hasse formations, the latter overlying the former. In the northern area, the Zushi Formation, which was deposited simultaneously with the Misaki Formation, is overlain by the Ikego Formation.

The Misaki and Zushi formations consist of mudstone intercalated with numerous tuff beds. Most of these beds are scoria tuffs, several centimetres to several tens of centimetres thick. A study on benthonic foraminifera (Akimoto et al., 1991) suggests that most of this formation was deposited in situ at a depth of 1000–2500 m or more. The thickness of the Misaki Formation is more than 1300 m, whereas the Zushi Formation is about 2000 m thick.

The Hasse Formation consists of a 600 m thick tuff, whereas the Ikego Formation consists mainly of tuff breccia with some interbedded mudstone. The thickness of this formation is 150 m. *Calypptogena* species have been frequently reported in this formation (Hirata et al., 1991). Niitsuma et al. (1989) suggested, on the basis of oxygen isotope data, that the bivalve was living in an environment with a temperature around 2°C.

### *Key tuffs*

As mentioned above, the Miura Group contains numerous tuff beds most of which are made of scoria. Several well-traceable non-scoria key tuff beds are also present. The compositions of heavy mineral fractions extracted from these volcanic rocks are shown in Table 1. The description of important key tuffs follows below.

*Mk tuff.* The Mk tuff is described in detail by Mitsunashi and Yazaki (1968). This unit is considered to be ‘gomashio tuff’ (a fine-grained, light-coloured tuff including dark-coloured heavy mineral grains), and is intercalated in the lower part of the Misaki Formation (Fig. 2). The type locality is at Miyakawa in Miura City. The key Mk tuff can be traced intermittently in the southernmost part of the peninsula, and has a mean thickness of about 150 cm. As shown in Table 1, most of the tuff consists of quartz and plagioclase with secondary heavy minerals (hornblende, orthopyroxene and clinopyroxene). A small amount of opaque magnetic minerals and volcanic rock fragments is also present. The mean grain size ranges from 1 to 0.25 mm.

*So tuff.* This tuff was originally described by Mitsunashi and Yazaki (1968). Kanie et al. (1991) included some key tuff beds in more distant areas, which were classified as Hk tuff by Mitsunashi and Yazaki (1968). The So tuff is also a ‘gomashio tuff’ but, in some places, it can be defined as a pumice tuff with bedding structures. It is intercalated

Table 1  
Qualitative mineralogical composition of key tuff beds in the Miura Group

Mineral	Mk	Ok	So	Bg	Hk	Nt
Quartz	C	F	C	C	C	F
Plagioclase	A	C	C	A	C	C
Biotite	-	-	R	R	-	R
Hornblende	F	R	C	C	C	F
Orthopyroxene	F	C	C	F	C	A
Clinopyroxene	F	C	R	C	R	C
Olivine	-	R	-	R	-	R
Magnetite	F	C	F	F	R	F
Volcanic glass	F	R	F	F	A	C
Lithic fragments	F	F	F	F	R	F

Occurrence: A = abundant; C = common; F = few; R = rare; - = absent.

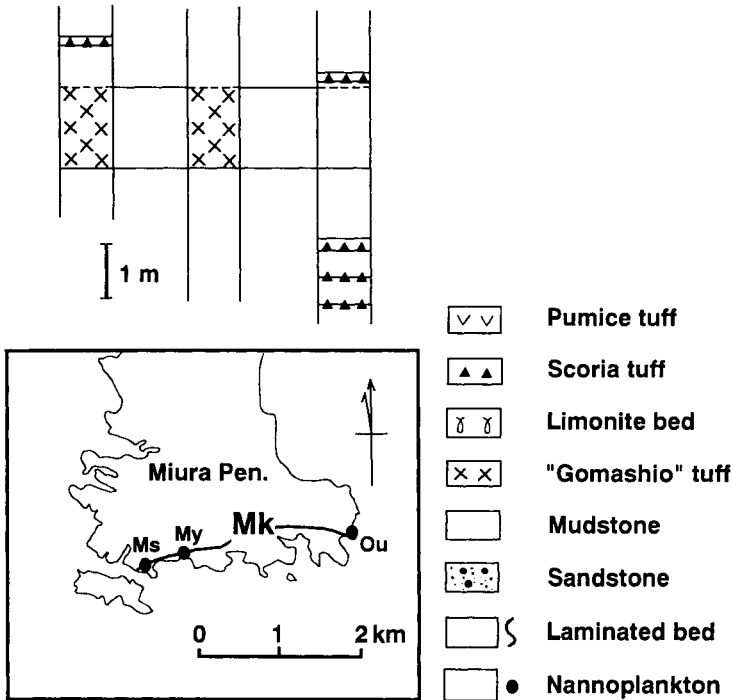


Fig. 2. Distribution of Mk tuff with columnar sections at several outcrops. Ms = Masaki; My = Miyakawa; Ou = Ooura.

in the upper part of the Misaki Formation (Fig. 3). The thickness is 550 cm on the western side of the peninsula, thinning to 150 cm on the eastern side. It is traceable intermittently in the southernmost part of the peninsula, and can also be observed in some remote areas. The type locality is at Nagai in Yokosuka City.

The So tuff is abundant in quartz, plagioclase, hornblende and orthopyroxene. Biotite

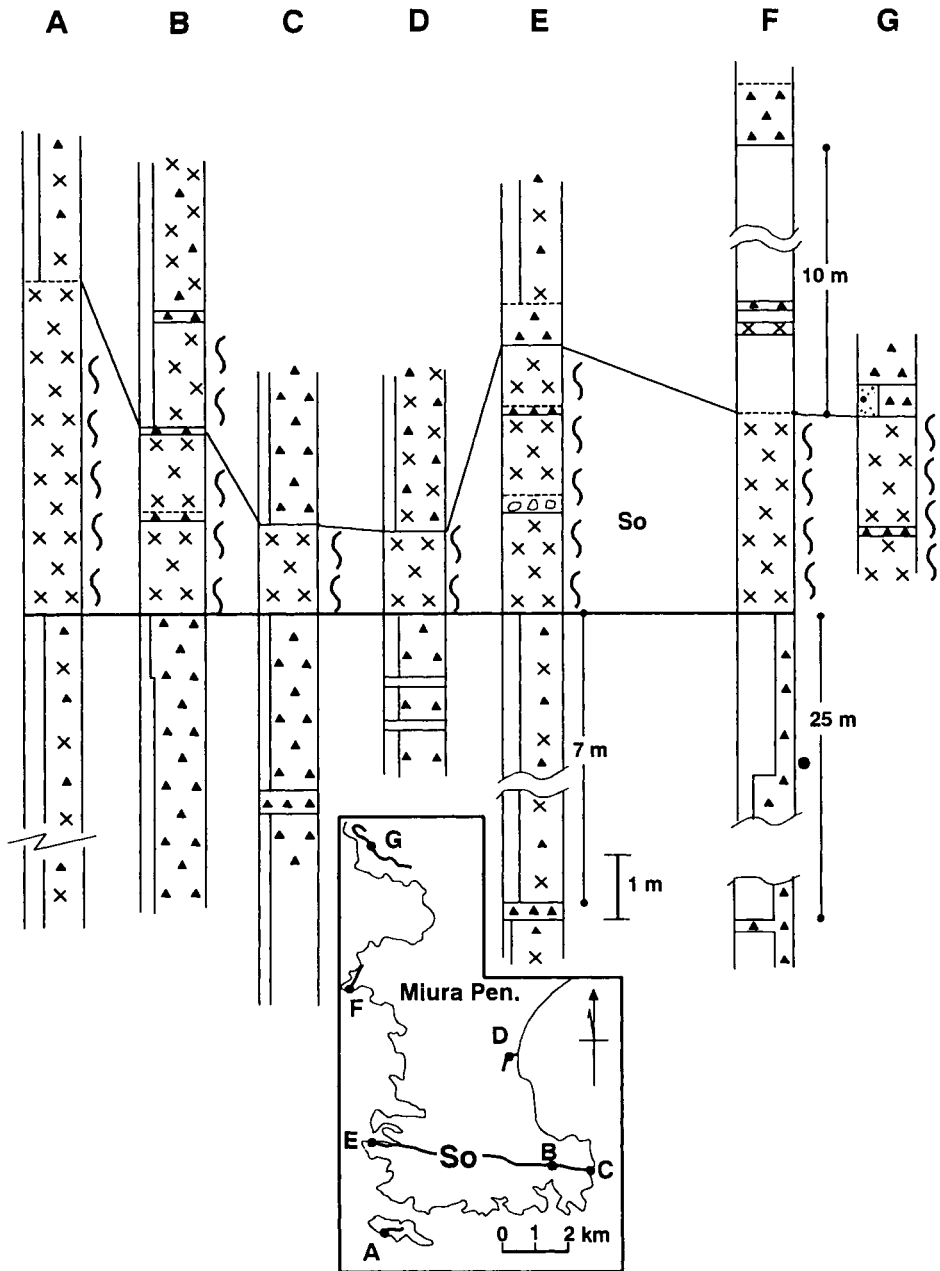


Fig. 3. Distribution of So tuff with columnar sections at several outcrops. See Fig. 2 for legend.

and clinopyroxene are rarely observed. Magnetic opaque minerals, volcanic glass, and volcanic lithic fragments are scarce. It is possible that the tuff experienced post-depositional transformation on the seafloor based on the following observations: (1) the mineral



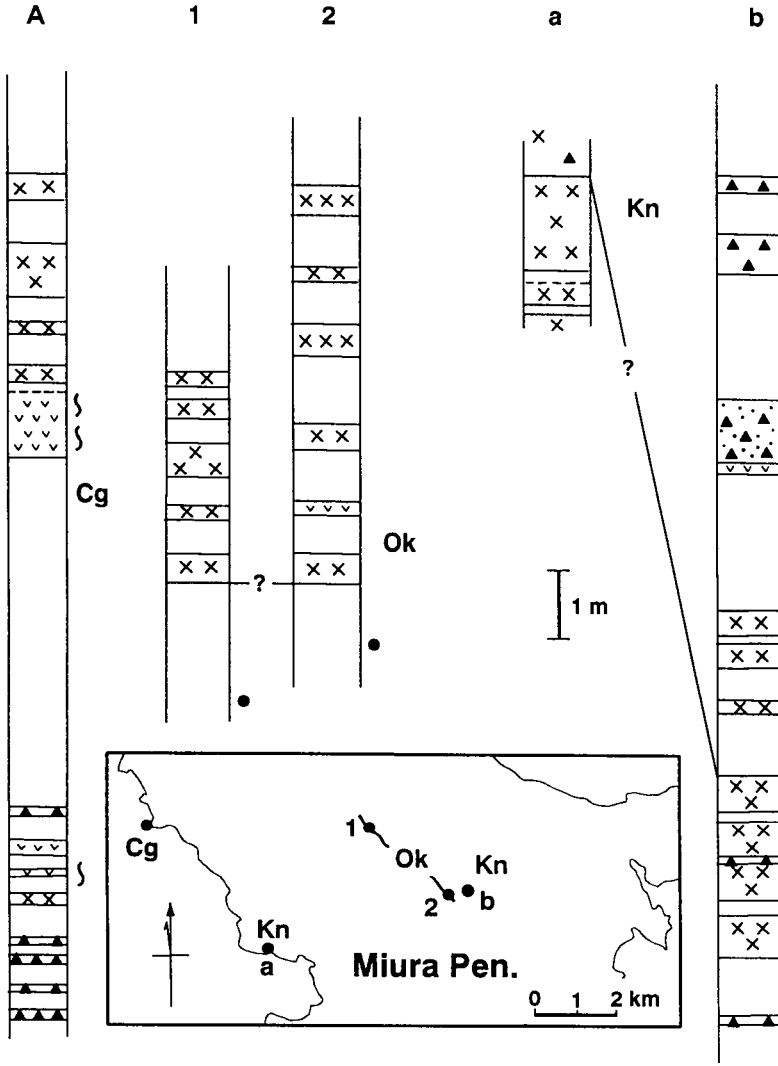


Fig. 4. Distribution of the Ok tuff with columnar sections at several outcrops. The Cg tuff was previously regarded a part of the Ok tuff (Mitsunashi and Yazaki, 1968), but Kanie et al. (1989) suggested that it lies below the Ok tuff. The stratigraphic relation of the Kn tuff with the Ok or Cg tuff has not been clarified. See Fig. 2 for legend.

grains in it are rounded; (2) more than 50% of the grains show a grain size ranging from 1 to 0.25 mm; and (3) the thickness of the tuff varies significantly from place to place.

*Ok tuff.* The Ok tuff was originally named by Yazaki and Mitsunashi (1961). In developing the stratigraphy of the peninsula, Mitsunashi and Yazaki (1968) used this tuff as one of the two most important key beds. Kanie et al. (1991) restricted its distribution in the peninsula, although Urabe (1992) correlated an Ok tuff layer between the Miura and Boso peninsulas.

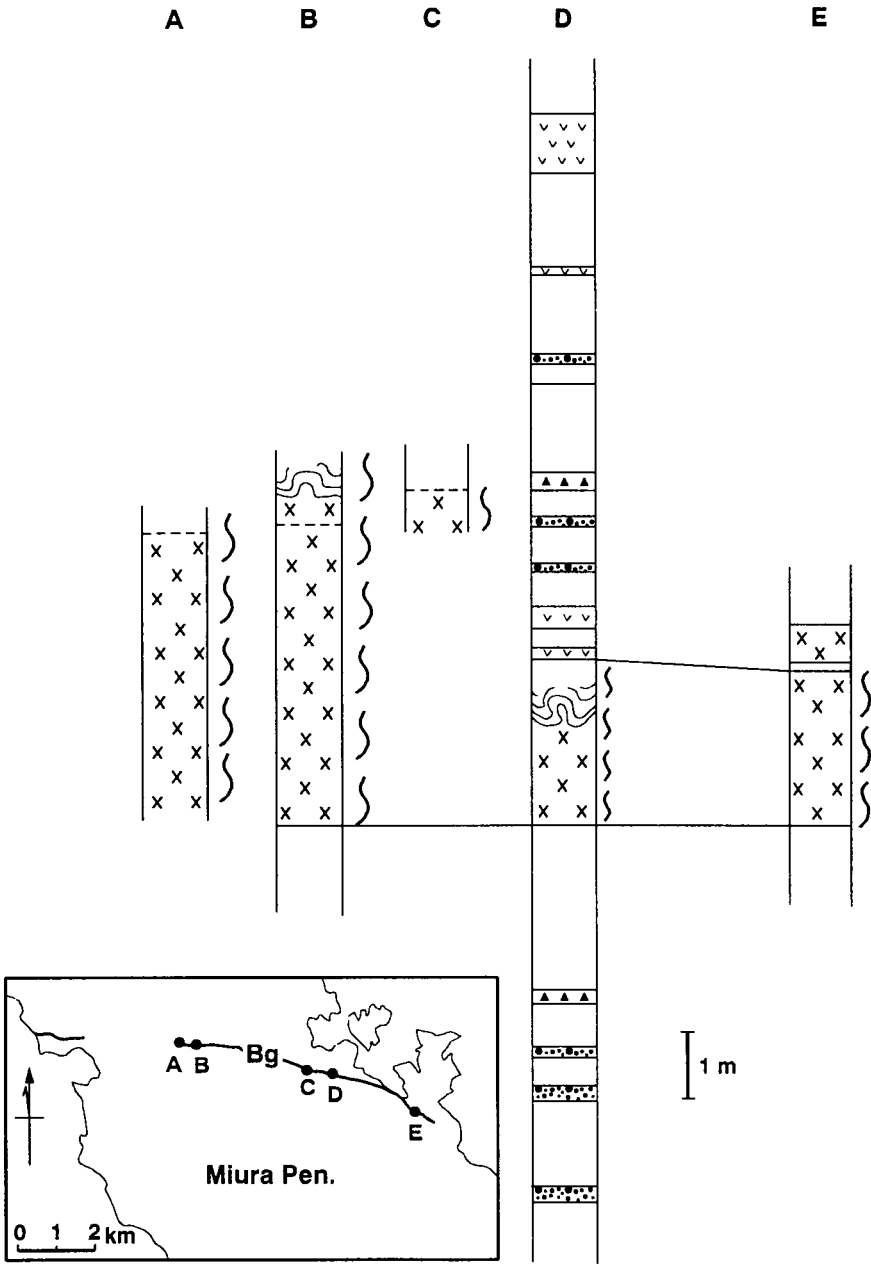


Fig. 5. Distribution of the Bg tuff with columnar sections at several outcrops. See Fig. 2 for legend.

The Ok tuff is intercalated in the lower part of the Zushi Formation, and consists of five tuff beds several tens of centimetres thick (Fig. 4). It is characterized by a mixture of transparent and dark mineral grains and is sandwiched between siltstone layers which

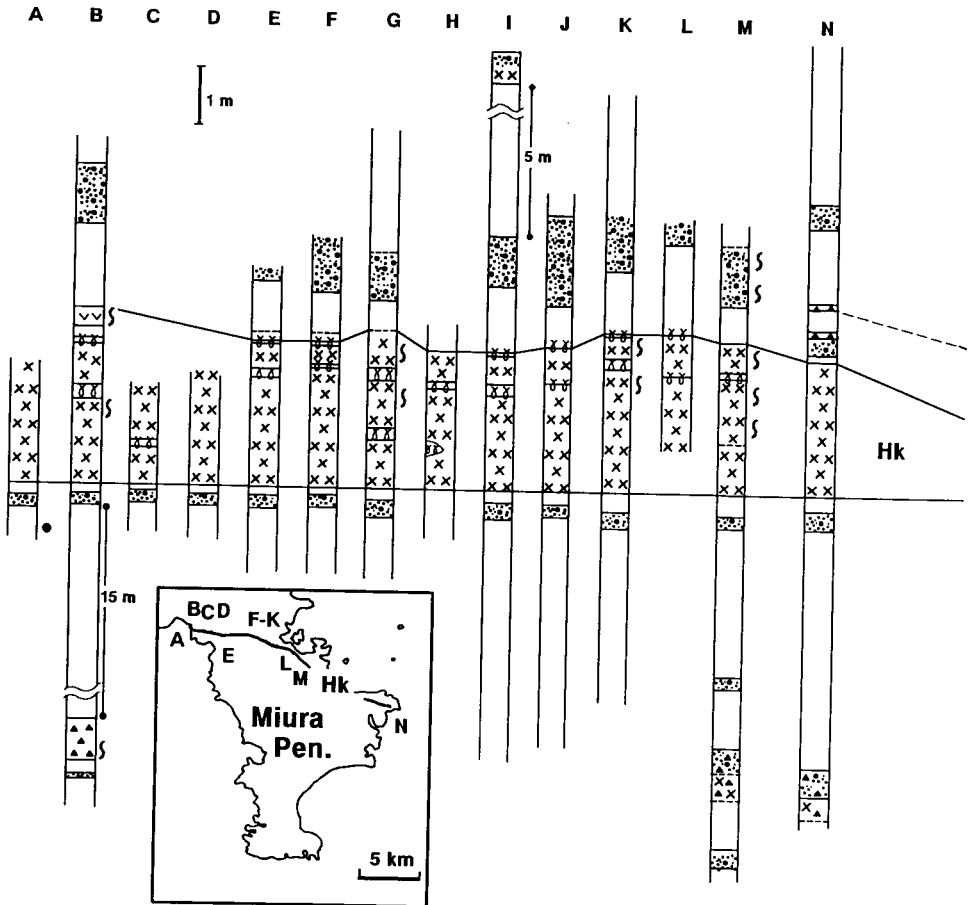


Fig. 6. Distribution of the Hk tuff with columnar sections at several outcrops. See Fig. 2 for legend.

include rare scoria beds. Clinopyroxenes and orthopyroxenes are abundant. In the upper beds, small amounts of hornblende are present, whereas volcanic glass is scarce. The grain size distribution shows a maximum in the 1–0.25 mm class. The type locality is on the northeastern flank of Mt. Ogusu in Yokosuka City.

*Bg tuff.* The Bg tuff was originally described by Yazaki and Mitsunashi (1961). It consists of a bedded pumice tuff, and it is intercalated in the middle part of the Zushi Formation (Fig. 5). The Bg tuff can be traced intermittently from coast to coast across the Miura Peninsula. It has a thickness of 600 cm on the west side of the peninsula, in the Zushi Bay, and 250 cm on the east side, in the Yokosuka promontory. The type locality is in Bango in the eastern part of Zushi City.

Convolute laminae of fine to very fine-grained volcanic glass are sometimes observed in the upper part of the tuff bed. The Bg tuff contains abundant transparent minerals with plagioclase being more abundant than quartz. The most common heavy minerals are hornblende, orthopyroxene and clinopyroxene. Small amounts of olivine and biotite

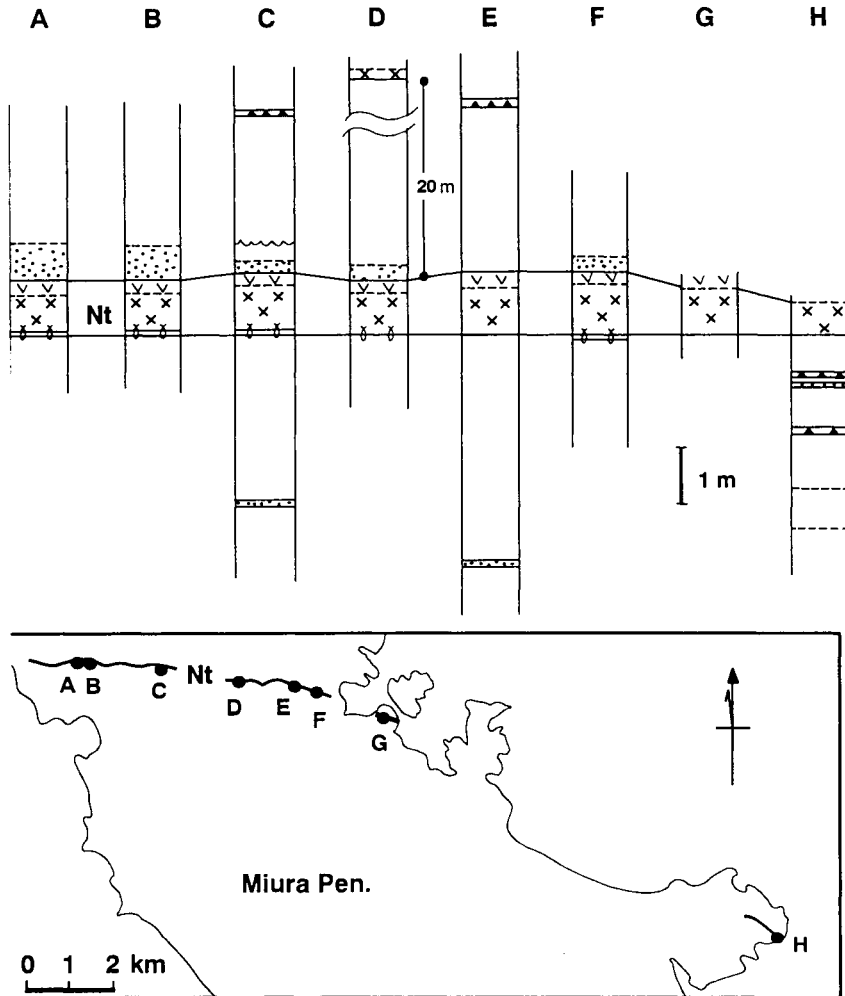


Fig. 7. Distribution of the Nt tuff with columnar sections at several outcrops. See Fig. 2 for legend.

are also observed, and magnetic minerals are rare. Fibrous volcanic glass is present and the pumice shows matured vesiculation.

The occurrence of rounded mineral grains suggests that the tuff accumulated on a seafloor and experienced post-depositional transportation.

*Hk tuff.* This tuff was used by Mitsunashi and Yazaki (1968) as a key bed in constructing their stratigraphy of the northern part of the Miura Peninsula. The Hk tuff is a 'gomashio tuff' contained in the upper part of the Zushi Formation (Fig. 6). Two limonite-rich layers are present in the upper part of the tuff bed and it is easily traceable across the peninsula. In the west side, at Zushi, its thickness is 290 cm, and in the east, at Yokosuka, it is 270 cm thick.

The most abundant minerals contained in this tuff are plagioclase, quartz, hornblende and orthopyroxene. Clinopyroxene is rarely observed. Volcanic glass is abundant

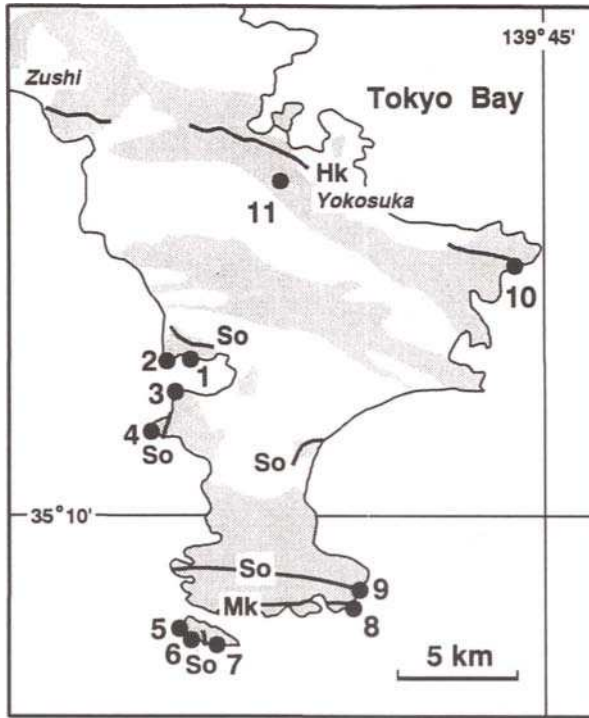


Fig. 8. Distribution of accretionary lapilli in the Miura Peninsula. Numbers 1 to 13 indicate sites where accretionary lapilli were observed.

whereas volcanic lithic fragments are rare. Magnetic minerals are rare in the eastern side of the peninsula, but are more abundant in the western side. The grain size distribution has a maximum in the 1–0.25 mm class.

*Nt tuff.* Yazaki and Mitsunashi (1961) named this tuff Hi, whereas Eto (1986) identified it as Nt-up. The Nt tuff is intercalated in the upper part of the Zushi Formation (Fig. 7). The lower part of this key bed is a 'gomashio tuff', 75–90 cm thick, whereas the upper part consists of a 30 cm thick volcanic glass unit. A layer of limonite-rich tuff several centimetres thick occurs at the base of the layer and is easily traced across the peninsula. The most abundant minerals are plagioclase, orthopyroxene and clinopyroxene. Small amounts of biotite and hornblende are also present.

There is still some disagreement in identifying these key tuff beds in the northern and southern areas. For example, Mitsunashi and Yazaki (1968) suggested that the So tuff, which is found in the southern area, is older than the Bg tuff exposed in the northern area of the peninsula. Recently, Kanie et al. (1991) showed that, on the basis of calcareous nannofossil biostratigraphy, these two key beds probably represent the same tuff bed (see below for further details).

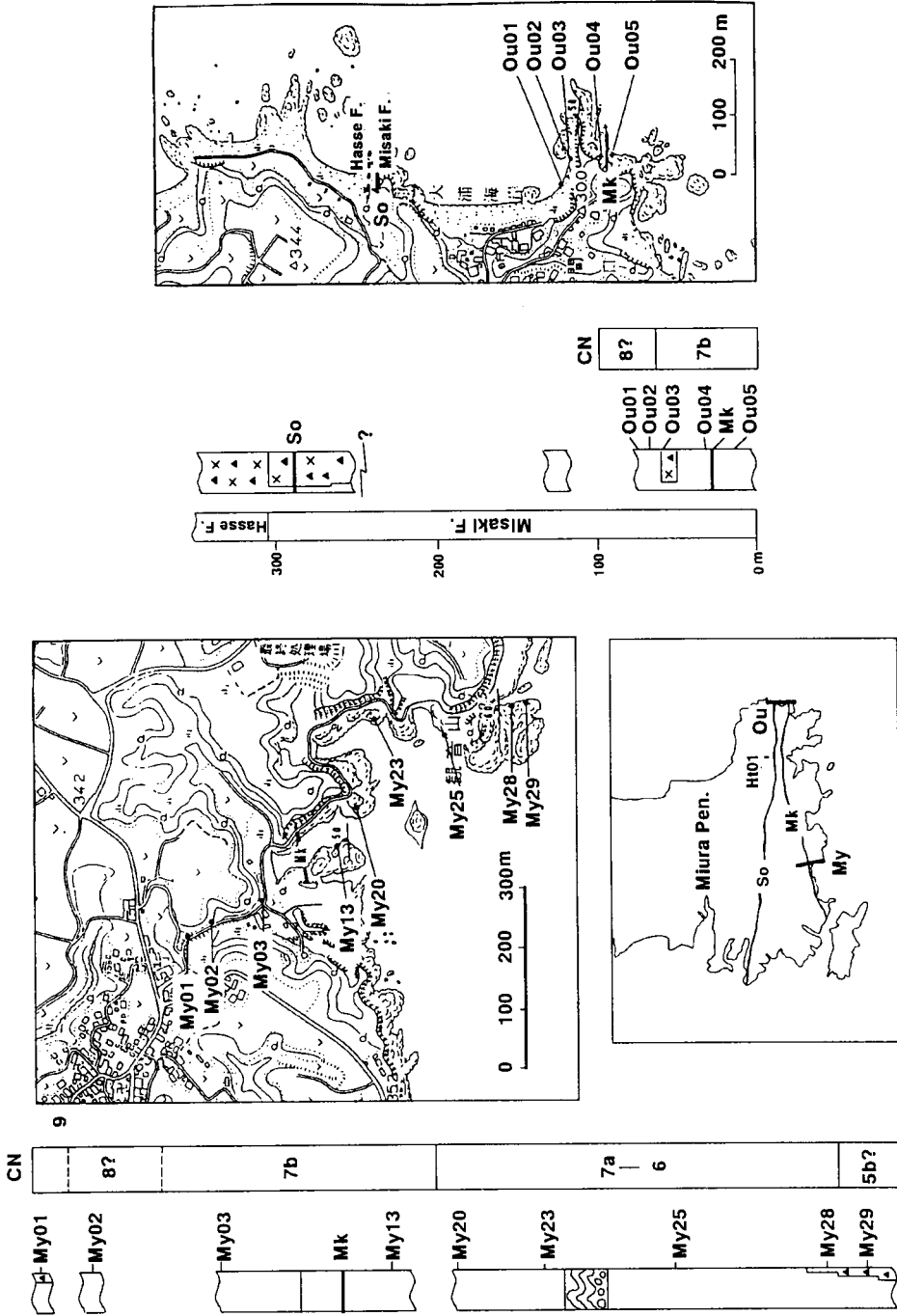


Fig. 9. Sampling sites of nannofossils along the Miyakawa and Ooura sections.

Table 2  
Calcareous nanofossils from the Miyakawa and Oora sections

Sample a:	Ma-29	28	25	23	20	13	03	02	01	Ou-05	04	03	02	01	Hf-01
Occurrence and preservation:	FM	RM	CM	AM	RP	CM	FM	FM	CM	CP	AM	AM	FM	CM	AM
Eching/overgrowth:	1/1	1/1	1/1	1/0	1/0	1/1	1/0	1/1	1/0	1/0	0/1	1/0	0/2	0/1	1/0
<i>Amaurolithus delicatus</i>	-	-	-	-	-	-	-	-	-	-	-	-	-	-	R
<i>Calcidiscus leptoporus</i>	F	-	F	F	-	R	R	R	F	R	R	R	R	R	C
<i>Calcidiscus macintyreii</i>	F	-	R	F	-	-	-	R	R	F	R	R	R	R	R
<i>Catinaster calyculus</i>	-	-	-	-	-	R	R	-	-	R	R	R	-	-	-
<i>Catinaster coalitus</i>	-	+	A	A	+	A	-	-	-	F	F	C	R	R	-
<i>Ceratolithus rugosus</i>	-	-	-	-	-	-	-	-	-	-	-	-	-	-	R
<i>Ceratolithus</i> sp.	-	-	-	-	-	-	-	-	-	-	-	-	-	-	F
<i>Coccolithus pelagicus</i>	C	+	C	A	+	C	C	A	-	C	F	C	F	C	C
<i>Dictyococcites perplexa</i>	A	-	A	C	+	C	F	C	C	C	A	C	C	C	-
<i>Dictyococcites productus</i>	-	-	C	-	-	-	-	-	-	F	F	F	F	F	A
<i>Discoaster adamanteus</i>	C	-	F	F	-	F	C	F	F	F	-	F	F	R	-
<i>Discoaster bellus</i>	-	-	-	-	-	-	R	-	F	F	F	F	-	F	-
<i>Discoaster berggrenii</i>	-	-	-	-	-	-	-	-	R	-	C	-	-	-	-
<i>Discoaster bollii</i>	F	+	R	F	+	F	-	-	F	-	-	C	-	-	-
<i>Discoaster braarudii</i>	-	-	-	-	-	-	F	-	F	-	-	-	F	F	-
<i>Discoaster brouweri</i>	-	-	-	-	-	-	-	R	C	-	-	-	R	F	C
<i>Discoaster calcaris</i>	R	-	-	R	-	-	-	-	-	-	-	-	-	-	-
<i>Discoaster challengerii</i>	F	-	-	-	+	F	-	-	F	F	F	R	R	F	R
<i>Discoaster decorus</i>	-	-	-	-	-	-	-	-	-	-	-	-	-	-	F
<i>Discoaster exilis</i>	-	-	R	F	-	-	-	-	R	-	-	-	-	-	-

<i>Discoaster hamatus</i>	-	-	-	-	-	F	R	-	-	-	R	R	-	-	-
<i>Discoaster intercalaris</i>	-	+	F	C	+	C	C	C	A	C	C	F	C	C	R
<i>Discoaster neohamatus</i>	-	-	-	-	-	-	R	-	-	R	F	-	-	-	-
<i>Discoaster pentaradiatus</i>	-	-	-	-	-	-	-	-	-	-	-	-	-	-	C
<i>Discoaster pseudovariabilis</i>	-	-	-	-	+	R	R	R	-	F	R	F	F	R	-
<i>Discoaster quinquemurum</i>	-	-	-	-	-	-	-	-	R	-	-	-	-	-	-
<i>Discoaster surculus</i>	-	-	-	-	-	-	-	-	-	-	-	-	-	-	C
<i>Discoaster variabilis</i>	C	+	F	C	-	C	C	C	C	C	C	F	C	C	F
<i>Florisphaera profunda</i>	-	-	-	-	-	-	-	-	-	-	-	-	-	-	A
<i>Helicosphaera carteri</i>	-	-	-	R	+	F	-	F	F	R	R	F	R	F	F
<i>Pontosphaera japonica</i>	-	R	-	-	-	-	-	-	-	-	-	-	-	-	-
<i>Pontosphaera multipora</i>	-	-	R	-	-	R	-	-	-	-	R	-	-	-	-
<i>Reticulofenestra gelida</i>	A	+	A	A	+	A	A	A	A	A	A	A	A	A	F
<i>Reticulofenestra haqii</i>	C	-	C	C	-	C	C	A	C	C	C	F	A	A	-
<i>Reticulofenestra minuta</i>	-	-	F	-	-	-	F	-	-	F	F	F	F	F	A
<i>Reticulofenestra minutula</i>	C	+	A	C	+	C	C	C	C	C	C	C	F	C	A
<i>Reticulofenestra pseudumbilica</i>	A	+	A	A	+	A	A	C	A	A	C	A	C	C	C
<i>Sphenolithus abies</i>	-	-	-	-	-	R	F	F	-	F	R	-	-	F	C
<i>Sphenolithus compactus</i>	-	-	F	-	-	-	R	-	-	F	-	-	-	-	-
<i>Sphenolithus neobabies</i>	-	-	-	-	-	R	-	F	-	R	R	-	-	-	-
Okada and Bukry Zonation (CN-)	/5b?/	6-7a	/	7b	/	8?	/	9	/	/	7b	/	8?	/	10c

Occurrence: A = abundant; C = common; F = few; R = rare. Preservation: G = good; M = moderate; P = poor. Etching/overgrowth: 1 = weak; 2 = moderate; 3 = strong.

<sup>a</sup> Sampling locations are shown in Fig. 9.



### *Accretionary lapilli*

Several accretionary lapilli layers have been found in the Miura Group (Kanie and Hattori, 1991), and some of them constitute key beds that are traceable throughout the peninsula (Fig. 8). Coarse lapilli layers are present on the western side of the Miura Peninsula, suggesting that their volcanic sources were nearby. Volcanic eruptions must have occurred in shallow water or even at sea level. However, at present no volcanoes are known that match these conditions. One possible explanation for this is that the volcanic edifice(s) that produced the accretionary lapilli collided with, and was accreted to, the main island of Honshu just before the end of its (their) eruptive activity.

### BIOSTRATIGRAPHY

Detailed investigations on calcareous nannofossils in six sections were reported by Kanie et al. (1991). Geological columnar sections of Miyakawa, Ooura, Sajima and Arasaki are illustrated, together with maps, in Figs. 9 and 10.

The Miyakawa and Ooura sections are located in the southernmost part of the peninsula and contain the Mk tuff. In addition, the Ooura section contains the So tuff. In the western part of the peninsula, the Sajima and Arasaki sections contain the So tuff, whereas in the central part, where the Ok tuff is exposed, nannofossils were sampled from seven sites (Fig. 11). The Yokosuka and Zushi sections are located in the north-northeastern part of the peninsula, and are distributed along the Hk, Bg and Nt tuff beds (Fig. 12). Tables 2–5 list the nannofossils from these sections (Kanie et al., 1991).

The calcareous nannofossil study revealed that the Ok tuff was deposited in Zone CN 9 and the Bg and So tuffs were deposited in Zone CN 10b. However, this differs with the stratigraphy of Mitsunashi and Yazaki (1968) who placed the So tuff layer below the Ok tuff bed.

Among these sections, the Miyakawa is the most promising for future studies on radiometric dating for the following reasons. Firstly, it is the only section which covers a considerably long period (from Zone CN 5b (Serravallian by correlation) to Zone CN 9 (Messinian by correlation)). Second, this section is devoid of major discontinuities, and can therefore be considered continuous. A slump structure observed in the middle part of the section is the only major disturbance. Third, the Miyakawa section contains numerous tuff layers, especially in the southernmost and northern areas of the peninsula. Unfortunately, most tuff beds are made of scoria and are not suitable for K/Ar dating. As mentioned above, there are no major discontinuities, but many minor faults are present, some of which have offsets as large as 10 m. This will make detailed sampling in the stratigraphic sequence somewhat difficult.

### GEOCHRONOLOGY

#### *Previous studies*

Fission track (FT) dates for two tuff beds (Yoshida et al., 1984), and preliminary K–Ar ages for four tuff beds (Okada et al., 1991) are currently available (Table 6). The FT works were performed on zircon crystals whereas the K–Ar dates were obtained from

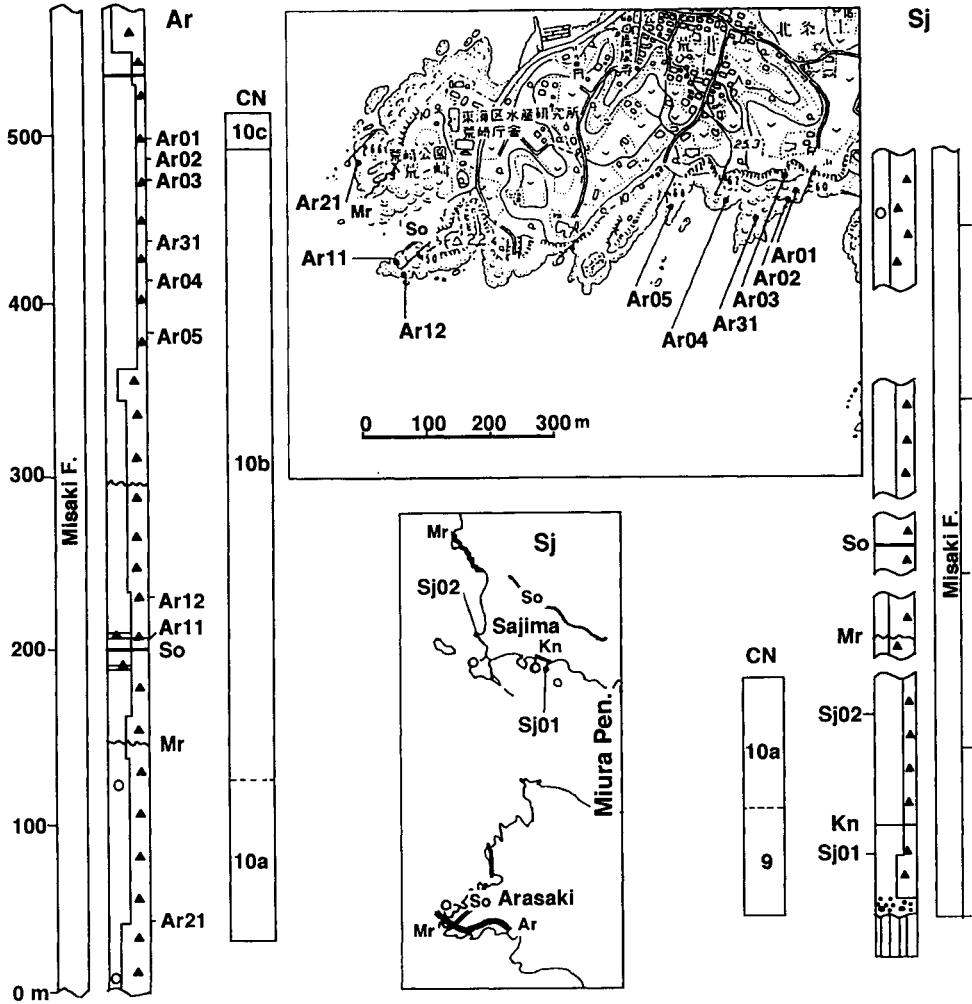


Fig. 10. Sampling sites of nannofossils along the Arasaki and Sajima sections.

hornblende separates. Both teams dated the Hk and So tuffs, and obtained consistent ages within acceptable error ranges for the So tuff, but discordant ages for the Hk tuff. Kanie et al. (1991) reported that the Hk tuff appears at the boundary of the CN 10b and CN 10c zones of Okada and Bukry's (1980) zonation, and assigned it an age of 4.4 Ma.

The K-Ar age for the Mk tuff (biozone CN7 = early or mid-Tortonian) is consistent with the biostratigraphy; however, the Bg tuff is older than its assumed Pliocene stratigraphic location.

*New K/Ar dates*

Since the So and Hk tuff samples which Okada et al. (1991) analyzed were still available, we carried out a second set of measurements on these samples. On

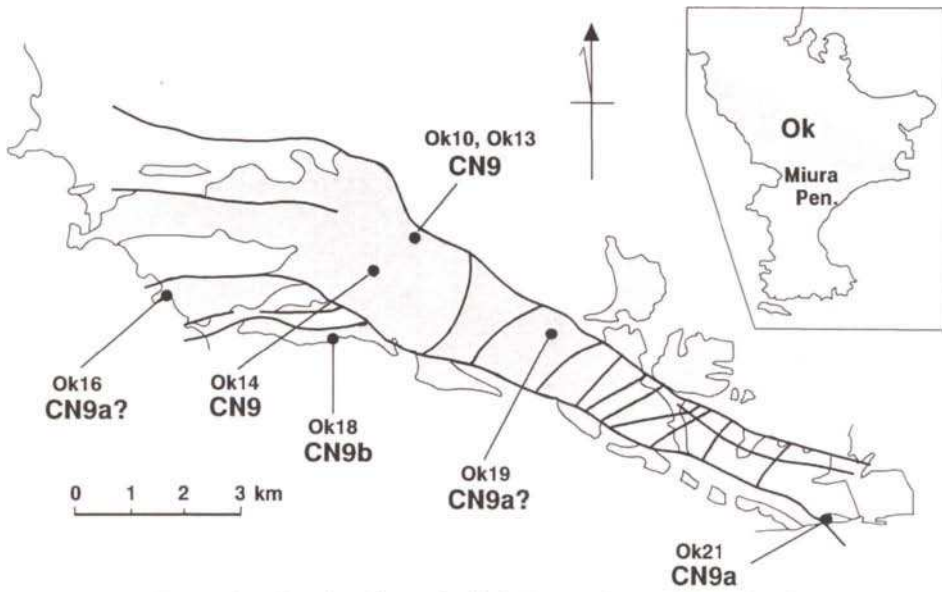


Fig. 11. Sampling sites of nannofossils in the central part of the peninsula.

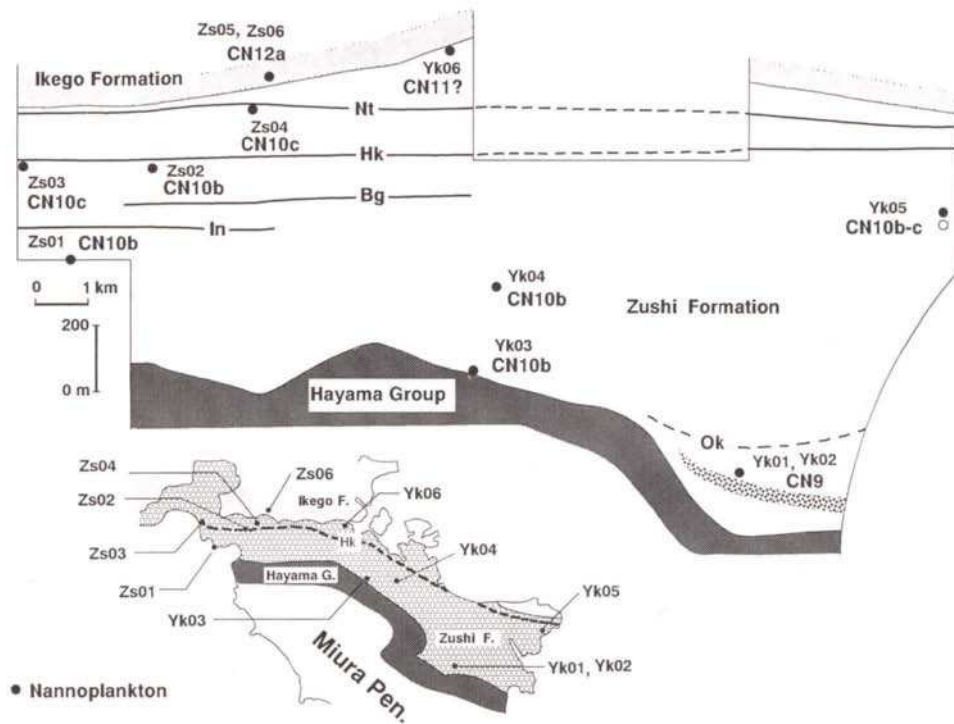


Fig. 12. Sampling sites of nannofossils along the Yokosuka and Zushi sections.

Table 3

Calcareous nannofossils from the Sajima (Sj) and Arasaki (Ar) sections

Sample <sup>a</sup> :	Sj-01	02	Ar-21	11	05	04	03	02	01
Occurrence and preservation:	CM	CM	CM	CM	CM	CM	AM	AM	AG
Etching/overgrowth:	1/0	1/0	1/0	0/1	0/1	0/1	0/1	0/1	0/0
<i>Amaurolithus delicatus</i>	–	–	–	–	R	R	–	–	–
<i>Amaurolithus tricorniculatus</i>	–	–	–	–	–	–	R	–	–
<i>Ceratolithus acutus</i>	–	–	–	–	R	–	–	–	–
<i>Ceratolithus rugosus</i>	–	–	–	–	–	–	–	–	R
<i>Ceratolithus</i> sp.	–	R	R	R	–	R	R	R	R
<i>Calcidiscus leptoporus</i>	F	F	F	F	F	C	C	C	C
<i>Calcidiscus macintyreii</i>	F	F	R	R	F	R	F	F	R
<i>Coccolithus pelagicus</i>	A	C	F	F	F	F	A	C	C
<i>Dictyococcites perplexa</i>	F	C	A	F	F	R	–	–	–
<i>Dictyococcites productus</i>	C	F	F	A	C	A	A	A	A
<i>Discoaster adamanteus</i>	R	R	F	–	–	R	R	–	–
<i>Discoaster asymmetricus</i>	–	–	–	–	–	–	–	–	R
<i>Discoaster berggrenii</i>	F	R	–	–	–	–	–	–	–
<i>Discoaster brouweri</i>	F	F	R	F	F	F	F	R	R
<i>Discoaster challengerii</i>	F	F	–	–	R	–	–	–	–
<i>Discoaster decorus</i>	–	–	–	–	–	R	F	F	R
<i>Discoaster intercalaris</i>	C	F	F	F	R	R	R	F	F
<i>Discoaster pansus</i>	–	–	R	–	R	–	R	R	F
<i>Discoaster pentaradiatus</i>	R	F	F	–	F	R	R	–	–
<i>Discoaster quinquemarus</i>	C	–	–	–	–	–	–	–	–
<i>Discoaster surculus</i>	–	F	F	F	F	F	F	F	F
<i>Discoaster variabilis</i>	A	F	F	F	F	C	C	C	F
<i>Florisphaera profunda</i>	F	C	F	C	C	F	–	–	–
<i>Helicosphaera carteri</i>	–	R	F	F	C	F	F	F	C
<i>Helicosphaera wallichii</i>	–	–	R	R	–	–	–	–	–
<i>Neosphaera coccolithomorpha</i>	–	–	R	–	R	–	–	–	–
<i>Pontosphaera japonica</i>	–	–	R	R	–	–	R	R	–
<i>Pontosphaera multipora</i>	–	–	–	R	R	–	R	R	R
<i>Reticulofenestra gelida</i>	A	C	A	A	A	A	F	C	–
<i>Reticulofenestra haqii</i>	A	A	C	F	F	R	–	–	–
<i>Reticulofenestra minuta</i>	C	F	C	C	A	A	A	A	A
<i>Reticulofenestra minutula</i>	C	A	C	C	F	C	F	F	F
<i>Reticulofenestra pseudoumbilica</i>	C	A	C	C	F	A	F	A	A
<i>Sphenolithus abies</i>	F	C	F	C	F	F	C	C	F
<i>Sphenolithus neoabies</i>	F	C	F	F	F	F	F	F	F
<i>Sphenolithus verensis</i>	–	–	R	–	–	–	–	–	–
<i>Triquetrorhabdulus rugosus</i>	–	R	–	R	–	–	–	–	–
Okada and Bukry Zonation (CN-)	9	/	10a	/		10b			/10c

Abbreviations as in Table 2.

<sup>a</sup> Sample locations are shown in Fig. 10.

investigating the remaining sample aliquots, we found that a considerable amount of pyroxene was included in the samples. This time, the samples were checked grain by

Table 4

Calcareous nannofossils from central Miura Peninsula

Sample <sup>a</sup> :	Ok-16	14	18	10	13	19	21
Occurrence and preservation:	CM	FM	AM	AM	CM	CM	CM
Etching/overgrowth:	0/1	1/0	1/0	0/1	1/0	1/0	2/0
<i>Amaurolithus primus</i>	–	R	R	R	–	–	–
<i>Calcidiscus leptoporus</i>	F	C	C	C	C	C	C
<i>Calcidiscus macintyreii</i>	R	R	R	R	R	R	–
<i>Coccolithus pelagicus</i>	F	F	F	F	C	F	C
<i>Dictyococcites perplexa</i>	C	A	C	A	A	F	R
<i>Dictyococcites productus</i>	A	A	A	A	A	A	A
<i>Discoaster adamanteus</i>	F	F	F	R	F	F	R
<i>Discoaster berggrenii</i>	F	F	F	R	F	F	F
<i>Discoaster blackstokae</i>	R	–	–	–	–	–	–
<i>Discoaster brouweri</i>	R	–	R	–	R	–	–
<i>Discoaster challengerii</i>	–	R	–	–	–	–	–
<i>Discoaster intercalaris</i>	F	F	F	F	F	R	R
<i>Discoaster pentaradiatus</i>	F	R	R	R	–	R	F
<i>Discoaster quinquerramus</i>	F	C	F	R	–	F	C
<i>Discoaster surculus</i>	R	F	R	R	R	R	F
<i>Discoaster variabilis</i>	F	F	F	–	F	F	F
<i>Florisphaera profunda</i>	F	F	C	–	R	C	–
<i>Helicosphaera carteri</i>	R	R	F	–	F	R	F
<i>Helicosphaera wallichii</i>	R	–	–	R	–	–	–
<i>Neosphaera coccolithomorpha</i>	R	–	–	R	–	–	–
<i>Pontosphaera multipora</i>	–	–	R	–	–	–	–
<i>Reticulofenestra gelida</i>	C	C	C	A	C	C	A
<i>Reticulofenestra haqii</i>	A	C	F	A	A	F	F
<i>Reticulofenestra minuta</i>	C	C	A	C	C	A	A
<i>Reticulofenestra minutula</i>	A	A	C	C	C	C	C
<i>Reticulofenestra pseudoumbilica</i>	C	C	C	A	C	C	F
<i>Sphenolithus abies</i>	F	F	C	C	C	C	C
<i>Sphenolithus neoabies</i>	F	F	F	C	F	F	F
<i>Sphenolithus verensis</i>	F	F	F	F	F	F	F
<i>Triquetrorhabdulus rugosus</i>	R	–	–	–	–	–	–
Okada and Bukry Zone (CN-)	9	9b	9b	9b	9	9	9

Abbreviations as in Table 1.

<sup>a</sup> Sampling locations are shown in Fig. 11.

grain under a binocular microscope and the purity of hornblende in separates was placed at more than 95%. The samples were dated using the conventional K/Ar technique with a <sup>38</sup>Ar spike (Table 6). The ages of both samples agree considerably well with the previously determined FT ages.

Fig. 13 appeared originally in Okada et al. (1989), and shows the summary of the K/Ar and biostratigraphic analyses of this area. In the same figure, K–Ar ages of the So and Hk tuffs are replaced by newly obtained ages.

Table 5

Calcareous nannofossils from the Yokosuca (YK) and Zushi (ZS) sections

Sample <sup>a</sup> :	YK-01	02	03	04	05	06	Zs-01	02	03	04	05	06
Occurrence and preservation:	CM	CM	CM	AM	AM	FP	AM	AM	CG	CM	AG	AG
Etching/overgrowth:	0/1	1/1	1/0	0/1	0/1	2/0	1/0	1/0	0/0	1/0	0/0	0/0
<i>Amaurolithus delicatus</i>	-	-	R	-	-	-	R	R	-	R	-	-
<i>Amaurolithus primus</i>	-	-	-	-	R	-	-	-	R	R	-	-
<i>Calcidiscus leptoporus</i>	C	F	C	F	C	C	C	C	C	F	C	C
<i>Calcidiscus macintyreii</i>	F	F	F	R	F	C	F	F	F	R	F	F
<i>Ceratolithus acutus</i>	-	-	R	R	-	-	R	-	-	-	-	-
<i>Ceratolithus armatus</i>	-	-	-	-	-	-	-	R	-	-	-	-
<i>Ceratolithus rugosus</i>	-	-	-	-	-	-	-	-	R	-	-	-
<i>Ceratolithus</i> sp.	-	-	-	-	-	R	-	-	R	R	-	-
<i>Coccolithus pelagicus</i>	C	A	C	C	C	F	C	F	F	F	C	C
<i>Dictyococcites perplexa</i>	F	F	A	A	A	F	C	F	F	F	-	-
<i>Dictyococcites productus</i>	A	A	C	A	C	A	C	A	C	C	C	C
<i>Discoaster adamanteus</i>	-	R	R	-	-	-	-	R	R	R	-	-
<i>Discoaster asymmetricus</i>	-	-	-	-	R	-	-	-	-	-	-	-
<i>Discoaster berggrenii</i>	R	R	-	-	-	-	-	-	-	-	-	-
<i>Discoaster brouweri</i>	-	-	F	F	F	F	F	F	F	F	R	R
<i>Discoaster challengerii</i>	R	-	-	F	-	R	-	-	-	-	-	-
<i>Discoaster decorus</i>	-	-	R	R	F	R	R	F	F	-	-	-
<i>Discoaster intercalaris</i>	-	F	R	F	F	R	R	F	R	F	R	-
<i>Discoaster pentaradiatus</i>	-	-	C	R	F	C	C	C	F	C	F	F
<i>Discoaster quinquermus</i>	R	R	-	-	-	-	-	-	-	-	-	-
<i>Discoaster surculus</i>	-	-	F	R	F	F	F	F	F	F	R	R
<i>Discoaster tamalis</i>	-	-	-	-	-	-	-	-	-	-	R	R
<i>Discoaster variabilis</i>	F	F	F	F	F	F	C	C	C	F	-	R
<i>Florisphaera profunda</i>	-	F	A	C	C	A	C	A	C	A	A	A
<i>Gephyrocapsa</i> spp. (small)	-	-	-	-	-	C	-	-	-	-	F	C
<i>Helicosphaera carteri</i>	R	R	F	F	F	F	F	F	F	F	R	F
<i>Helicosphaera sellii</i>	-	-	-	-	-	-	-	-	-	-	R	R
<i>Neosphaera coccolithomorpha</i>	-	-	-	R	-	-	R	R	-	R	R	R
<i>Pontosphaera japonica</i>	-	-	-	-	-	-	-	-	-	-	R	R
<i>Pontosphaera multipora</i>	-	-	R	R	-	-	R	-	R	-	-	-
<i>Pseudomilania lacunosa</i>	-	-	-	-	-	F	-	-	-	-	C	C
<i>Reticulofenestra gelida</i>	A	A	A	A	C	C	A	C	C	C	-	-
<i>Reticulofenestra haqii</i>	A	C	F	F	A	A	C	C	C	A	A	A
<i>Reticulofenestra minuta</i>	C	C	C	F	C	A	F	A	A	A	F	F
<i>Reticulofenestra minutula</i>	A	A	A	C	C	C	A	C	A	A	A	A
<i>Reticulofenestra pseudoumbilica</i>	A	A	A	A	C	C	A	A	A	C	-	-
<i>Sphenolithus abies</i>	F	F	F	C	C	R	F	C	F	F	-	-
<i>Sphenolithus neoabies</i>	R	R	R	F	F	F	F	C	R	F	-	-
<i>Sphenolithus verensis</i>	-	-	C	F	F	R	C	C	R	F	-	-
Okada and Bukry Zonation (CN-)	/ 9	/	10b	/10bc/	11?	/	/	10b	/	10c	/	12a

Abbreviations as in Table 2.

<sup>a</sup> Sample locations are shown in Fig. 12.

Table 6  
Radiometric dates from key tuffs of the Miura Group

Key tuff	FT dates age $\pm 2\sigma$ (Ma)	%K $\pm 2\sigma$	K-Ar dates age $\pm 2\sigma$ (Ma) $^{40}\text{Ar}(10^{-8} \text{ ml/g})$	Age $\pm 2\sigma$	Reference
Hk		$0.318 \pm 0.006$	$6.5 \pm 0.6$	$5.2 \pm 0.6$	Okada et al. (1991)
Hk		$0.356 \pm 0.018$	$5.7 \pm 0.6$	$4.1 \pm 0.6$	This work
Hk	$3.7 \pm 0.6$				Yoshida et al. (1984)
So		$0.360 \pm 0.016$	$8.3 \pm 1.0$	$6.0 \pm 1.0$	Okada et al. (1991)
So		$0.381 \pm 0.020$	$7.3 \pm 1.6$	$4.9 \pm 1.2$	This work
So	$5.1 \pm 1.0$				Yoshida et al. (1984)
Bg		$0.267 \pm 0.06$	$8.6 \pm 1.2$	$8.3 \pm 1.4$	Okada et al. (1991)
Mk		$0.245 \pm 0.16$	$8.1 \pm 0.6$	$8.5 \pm 0.8$	Okada et al. (1991)

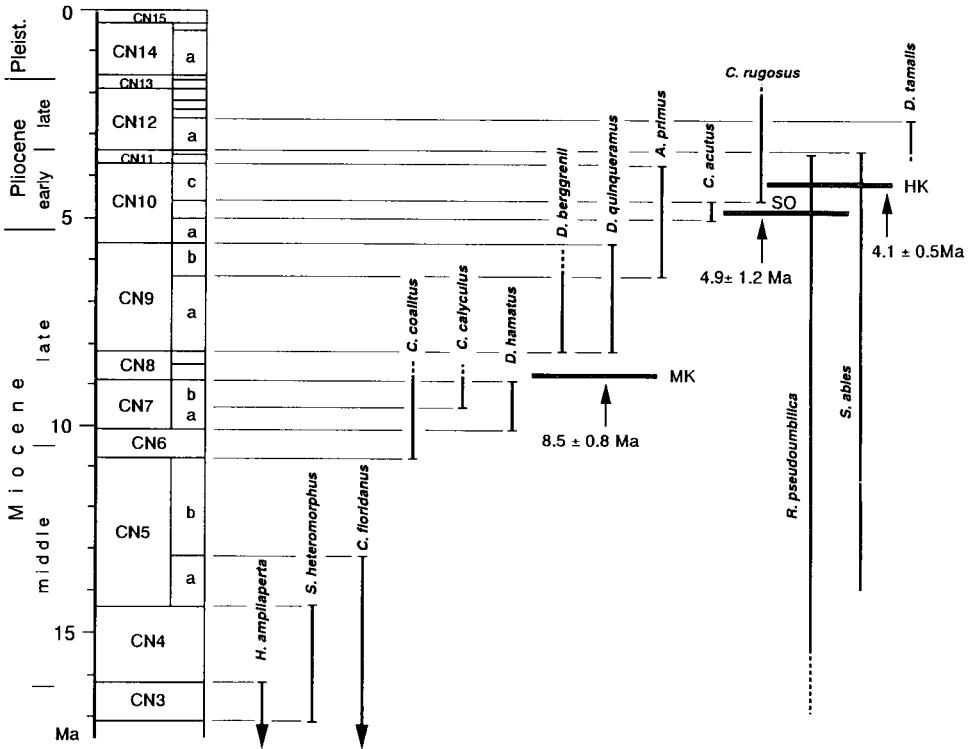


Fig. 13. Summary of the study of nannoplankton and K/Ar dating (after Okada et al., 1991). K-Ar ages for the Hk and So tuffs are replaced by new data.  $2\sigma$  errors are shown.

PALAEOMAGNETISM

In order to investigate the post-Miocene tectonic movements of this region, Yoshida et al. (1984) carried out palaeomagnetic measurements on tuffs and tuffaceous siltstone

layers. They reported a clockwise rotation of as much as 30° and suggested that this rotation occurred during the collision of the Izu block with the Honshu arc. Koyama (1989) reviewed recent palaeomagnetic work carried out in the South Fossa Magna, including the Miura and Boso peninsulas.

In the context of the arc–arc collision, the Miura itself has been interpreted as an accretional terrain. Taniguchi et al. (1991) proposed that the Miura Group may have formed about 100 km south of its present position.

## SUMMARY

Although located near a large housing development, and a dense population set certain limitations, numerous tuff beds interbedded in the Miura Group are potentially useful for the radiometric calibration of a critical position of Middle to Late Miocene biostratigraphic sequence. In particular, the Miyakawa Bay area, in the southern most part of the Miura Peninsula, is considered to be the most promising candidate for a detailed integrated stratigraphic study of this Miocene time interval.

## SOMMAIRE — REVUE DES ÉTUDES GÉOLOGIQUES, BIOSTRATIGRAPHIQUES ET GÉOCHRONOLOGIQUES DANS LA PÉNINSULE DE MIURA, JAPON CENTRAL

*(Manuscrit soumis: Décembre 1993; révisé: Juin 1994; rédacteur responsable: GSO)*

Le Groupe de Miura est formé de sédiments exposés dans les péninsules de Miura et de Boso, Japon Central. Il s'est déposé depuis le Miocène Moyen jusqu'au Pliocène Inférieur. Il est bien connu par plusieurs études biostratigraphiques sur les nannofossiles calcaires. Ces sédiments renferment de nombreux niveaux de tufs; certains d'entre eux peuvent être suivis sur de longues distances et servir de niveaux repères régionaux. Les quelques âges radiométriques disponibles sur ces tufs sont généralement cohérents avec les données biostratigraphiques. Les nombreux tufs intercalés dans la Formation de Misaki affleurant dans la partie la plus méridionale de la Péninsule de Miura pourraient servir pour une étude géochronologique détaillée permettant de calibrer les événements biostratigraphiques et magnétostratigraphiques bien qu'ils soient surtout composés de scories qui constituent un matériel volcanique difficile à dater par l'approche géochronologique.

*(Sommaire proposé par les rédacteurs d'après un résumé des auteurs, GSO)*

## ACKNOWLEDGEMENTS

We thank Prof. Okada for his kind permission to use his original tables of nannofossils. We also appreciate the help which Dr. R.W. Jordan and A. Montanari provided to improve the readability of the text.



This Page Intentionally Left Blank

Chapter E10

**PRELIMINARY RESULTS AND POTENTIAL FOR INTEGRATED STRATIGRAPHY OF THE VOLCANO-SEDIMENTARY SEQUENCE IN THE BOSO PENINSULA, CENTRAL JAPAN**

M. Takahashi, M. Oda and E. Uchida

NEOGENE GEOLOGY AND STRATIGRAPHY IN THE BOSO PENINSULA

The thick sequence of fossiliferous Neogene and Pleistocene marine sediments in the Boso Peninsula of Central Japan is one of the most promising sites in Japan for studies of Neogene geology and micropalaeontology. This sequence contains only one stratigraphic break (the Kurotaki Unconformity) and may provide a continuous stratigraphic record of the Miocene.

The Kamogawa area in the Boso Peninsula is located in the fore-arc basin of the Japanese Islands (Takahashi and Oda, Chapter B3), where a thick series of latest Early Miocene hemipelagic sediments were continuously deposited. This area is one of the most famous regions in Japan because Middle Miocene through Pliocene strata are extremely well exposed (Fig. 1). Many micropalaeontological studies in this area (e.g., Oda, 1977; Honda, 1981) have been carried out in the past 20 years. This 3000 m thick marine sedimentary sequence is divided into five formations (from oldest to youngest): (1) Kanigawa; (2) Kinone; (3) Amatsu; (4) Kiyosumi; and (5) Anno (Fig. 2). The lower half of this sequence is mainly composed of mudstones and siltstones, whereas sandstones are dominant in the Kiyosumi formation. The Anno formation is characterized by alternating beds of mudstone and sandstone.

Palaeomagnetic analyses in this sequence were originally carried out by Kawai (1951), who recognized only the present-day direction of the earth's magnetic field due to a strong component overprinting the remanent magnetization. Nakagawa et al. (1969) established a polarity reversal sequence of the detrital remanent magnetization of this sequence applying the alternating field (AF) demagnetization technique, and Kimura (1974) supplemented, and partly revised it. The latest revision of the magnetostratigraphy was made by Niitsuma (1976) who applied both thermal (Th) and AF demagnetization techniques; the results of this study are shown in Fig. 2.

In summary, magnetostratigraphic analyses were tried throughout this sequence but due to palaeomagnetic instability and/or overprints, a coherent magnetic polarity sequence was established only for the last 6 Ma history.

Calcareous nannofossil and planktonic foraminifera are present in almost all horizons in this sequence, and many potential bio-events are recognized throughout the Boso sequence as shown in Fig. 2. Important potential events recognized in the lower half of the sequence (i.e., the Kinone and Amatsu formations) in ascending order are the first occurrences of *Praeorbulina glomerosa*, *Orbulina suturalis*, and *Globorotalia*

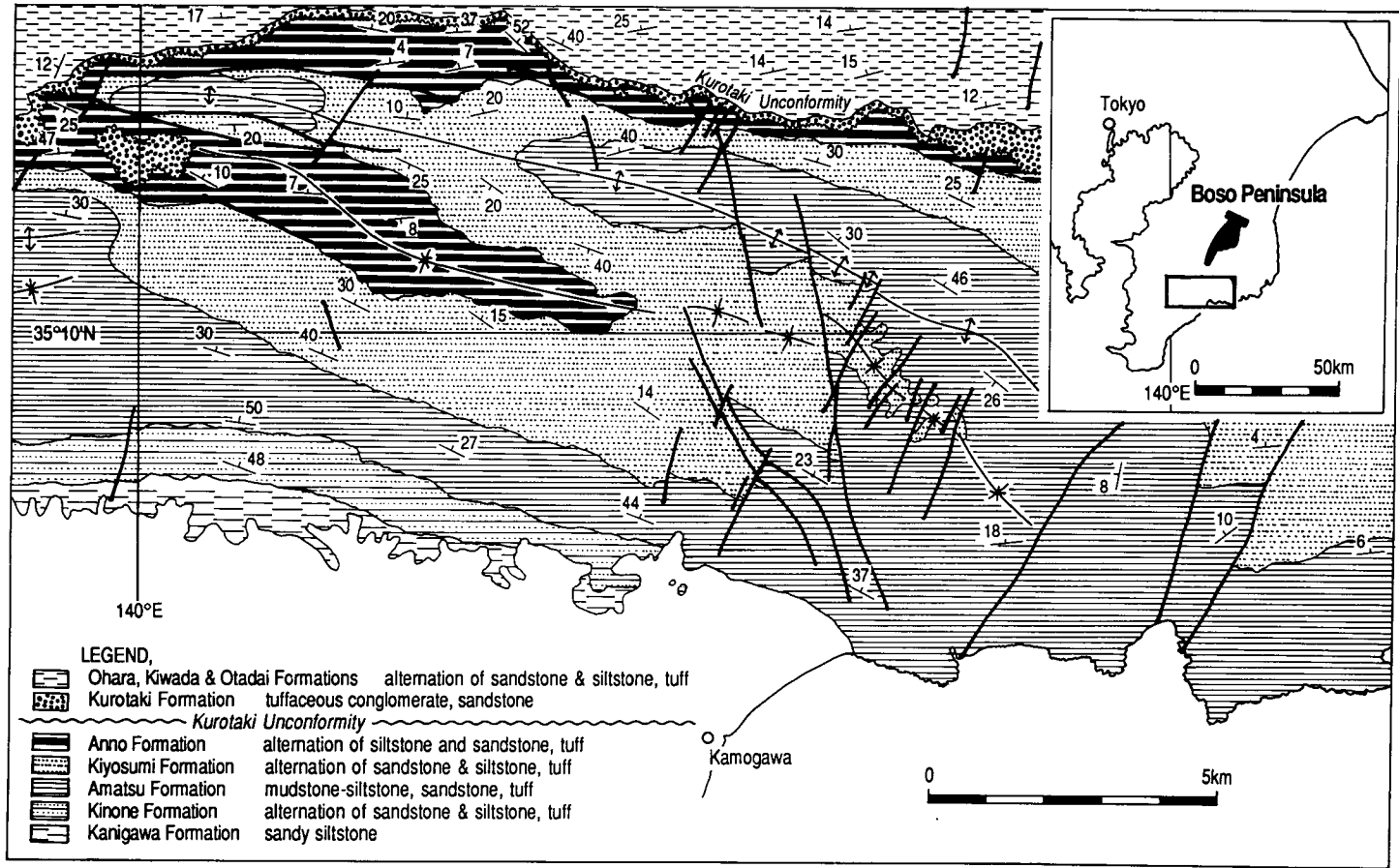


Fig. 1. Geologic map of the Neogene sedimentary rocks in the Boso Peninsula modified from Mitsunashi et al. (1979). The sedimentary sequence in this area extends from the latest Early Miocene to Recent, and is complete and continuous except for one short-lived unconformity (the Kurotaki Unconformity). Syn- and post-depositional folding and uplifting have provided numerous well exposed outcrops of this sequence throughout the Boso Peninsula.

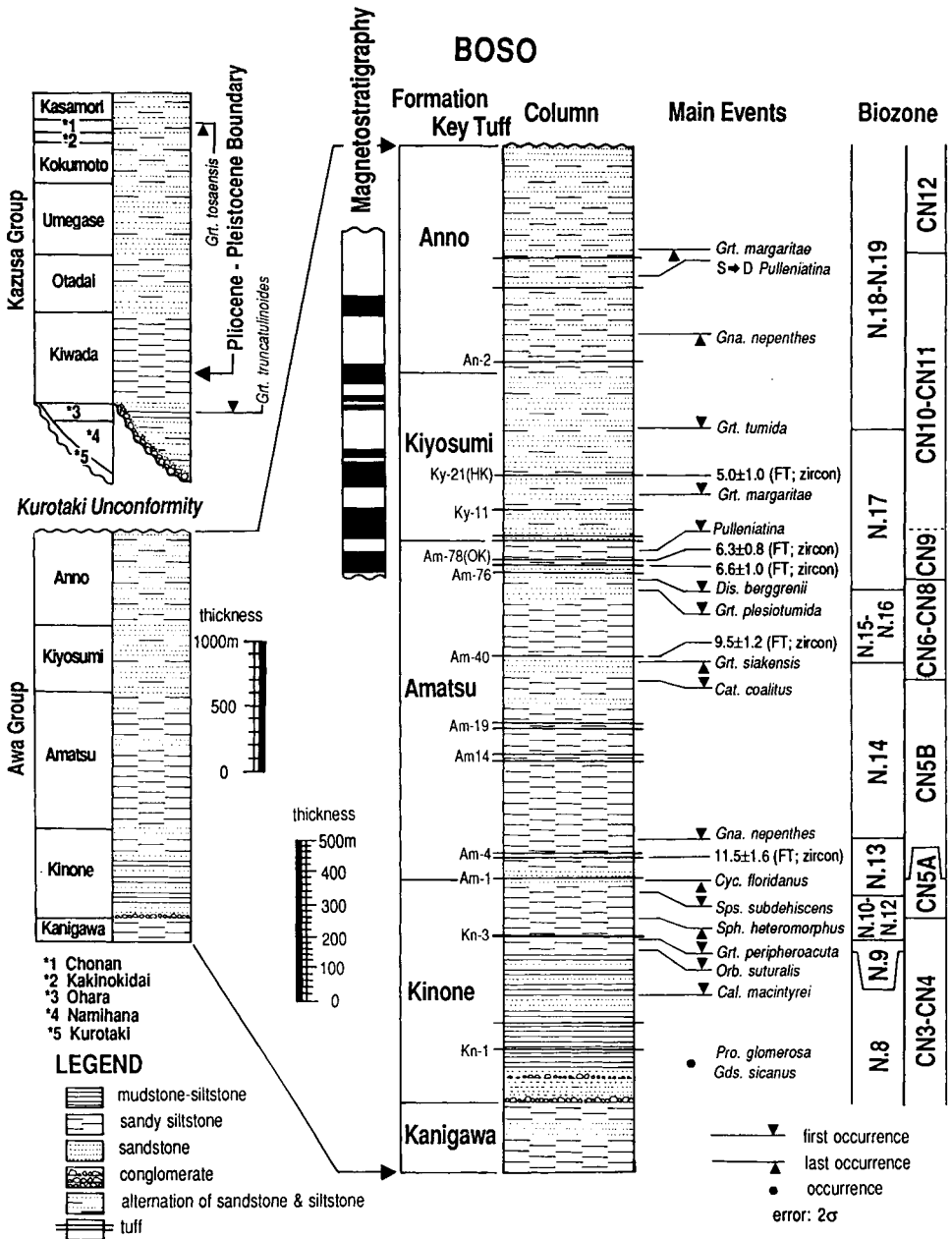


Fig. 2. Stratigraphic column of the sedimentary sequence in the Boso Peninsula. Stratigraphic positions of some important potential datum levels and key tuff layers are also shown.

*peripheroacuta*, the LO of *Sphenolithus heteromorphus*, FO of *Sphaeroidinellopsis subdehiscens*, the LO of *Cyclicargolithus floridanus*, the FOs of *Globigerina nepenthes* and of *Catinaster coalitus*, the LO of *Globorotalia siakensis*, the FOs of *Globorotalia plesiotumida* and of *Discoaster berggrenii*. The FO of *Pulleniatina* is recognized in the uppermost horizon of the Amatsu formation. The main bio-events recognized in the Kiyosumi and Anno formations are the following: FO of *Globorotalia margaritae*, FO of *Globorotalia tumida*, and the LOs of *Globigerina nepenthes* and *Globorotalia margaritae*. The coiling change of *Pulleniatina* from sinistral to dextral is observed in the middle part of the Anno formation.

Both the Amatsu and Anno formations contain more than 100 sets of key tuff layers, whereas the Kiyosumi formation contains more than 30 tuff sets. However, only very few radiometric dates were obtained from these tuff layers intercalated in this marine sequence. Fission tracks ages were reported by Kasuya (1987, 1990) for some of the layers.

Despite the abundance of volcanic intercalations, only some of the key tuffs are expected to be suitable for conventional K/Ar dating. In fact, about half of the volcanoclastic layers contained in this sedimentary sequence are basaltic scoria tuff, which is not suitable for dating. Although half of the volcanoclastic layers are felsic tuffs, biotite and/or hornblende, crystals suitable for radioisotopic dating are very rare.

In summary, only about 10% of the tuff beds in this sequence contain minerals suitable for conventional K/Ar dating. Among these tuffs, some are well controlled biostratigraphically by the planktonic microfossils. The pumice tuff Kn-3 in the Kinone Formation is located about 15 m above the FO of *G. peripheroacuta*. The mean sedimentation rate in this interval is about 100 m/Ma or more. We are currently in the process of dating the Kn-3 by counting fission tracks in zircon.

The key tuff Am-4 is a set of pumiceous tuffs containing both biotite and hornblende. The stratigraphic position of this key tuff is lower than the FO of *G. nepenthes*, which represents the local N13/N14 boundary. Am-19, located in the middle of zone N14, also contains biotite suitable for radioisotopic analysis. The FO of *G. siakensis* is recognized about 17 m below the Am-40, which contains datable hornblende.

Some fission tracks ages have been obtained from felsic tuffs around the Am-78 (OK tuff), while only Am-77 bears hornblende suitable for K/Ar dating. Detailed mineralogic studies on the volcano-sedimentary Kiyosumi and Anno formations are currently under way, and will hopefully serve to identify other key tuff layers with volcanogenic mineral phases suitable for radioisotopic dating.

A series of about 50 tuff samples from the Boso Peninsula sequence is presently under study, and some of them appear to contain minerals suitable for radioisotopic dating. Similarly, more than 140 samples have been analyzed by Dr. E. Uchida in an effort to establish a detailed planktonic foraminiferal biostratigraphy throughout this sequence. His co-worker, Dr. I. Mita is currently analyzing the calcareous nannofossils in the same samples. Recently, we collected about 80 samples of calcareous nodules in the sequence comprising the Kanigawa and the lower Amatsu formations, and more than 30% of the samples yield diatoms. This preliminary result strongly suggests that the stratigraphic interrelation between calcareous and siliceous microfossils will be clarified in the near future. The correlation between siliceous and calcareous microfossils bioevents is one of the most important targets for the definition of a robust biostratigraphic model in the mid-latitude areas of the Northwest Pacific region.

**SOMMAIRE — LA SÉQUENCE VOLCANO-SÉDIMENTAIRE DE LA PÉNINSULE DE BOSO (JAPON CENTRAL): POTENTIEL POUR LA STRATIGRAPHIE INTÉGRÉE**

*(Manuscrit soumis: Novembre 1993; révisé: Mai 1994; rédacteur responsable: GSO)*

Dans la Péninsule de Boso, la région de Kamogawa expose une épaisse (3.000 m) succession de sédiments fossilifères (foraminifères planctoniques, nannofossiles calcaires, diatomées) entrecoupée de niveaux volcanoclastiques. L'âge s'étend depuis le Miocène moyen jusqu'au Pléistocène avec seulement une coupure au niveau du Miocène terminal. Une faible proportion des niveaux dont l'origine volcanique est caractérisée contient des minéraux favorables à la datation (biotite, hornblende). Des prélèvements nombreux ont été réalisés pour compléter la connaissance biostratigraphique et repérer les niveaux les plus favorables à la datation. Cette succession apparaît comme très prometteuse pour coordonner les zonations biostratigraphiques et les résultats géochronologiques pour le Miocène; la magnétostratigraphie est aussi préservée pour les derniers 6 Ma.

*(Sommaire proposé par les rédacteurs, GSO)*

**ACKNOWLEDGEMENTS**

We would like to thank K. Stewart for revising the English of the original paper.

This Page Intentionally Left Blank

**Part F**



This Page Intentionally Left Blank

*Chapter F1*

**MIOCENE GEOCHRONOLOGY: METHODS, TECHNIQUES, AND RESULTS**

G.S. Odin, A. Deino, M. Cosca, M.A. Laurenzi and A. Montanari

**INTRODUCTION**

Prior to 1990, time scale syntheses for the Miocene Epoch were poorly documented with geochronological data. A few calibration points were obtained from glauconies and from a limited number of volcanoclastic layers found in sedimentary sequences. Often, these dated levels had scarce or imprecise stratigraphic attributions, and the resulting ages were more or less properly evaluated. However, in the past 10 years, geologists have shown that appropriate material for dating can be found in many areas worldwide in Alpine orogenic belts. This is one of the major reasons why the present research project has been undertaken, and this volume planned, when convincing results have begun to accumulate.

In this paper, we shortly review the methods, techniques, and results obtained in the laboratories which contributed to this study. This technical text is also for the use of non-experts who may sometimes be confused by the variety and apparent complexity of the information given in geochronological studies but who may also wish to have some basic information for judgement about the significance and reliability of results quoted in the literature. We have used here and in the volume, a terminology adapted from the one recommended under the aegis of the Subcommittee on Geochronology of IUGS (Odin, 1995).

**METHODS AND TECHNIQUES (G.S. Odin)**

*Tools used for numerical dating of the Miocene sequence*

*Methods and geochronometers.* The geochronological approach for the Miocene sequence can be accomplished using two main dating methods based on the decay of the two naturally radioactive isotopes  $^{40}\text{K}$  and  $^{87}\text{Rb}$ , which transform to the radiogenic isotopes  $^{40}\text{Ar}$  and  $^{87}\text{Sr}$ , respectively. Each pair of radioactive–radiogenic isotopes leads to the corresponding K–Ar and Rb–Sr dating *methods*. The applicability of these isotopes on the same geochronometer bears a great potential for testing the reliability of the resulting measured ages because their geochemical behaviour is different.

The fission track dating method has additionally been used for numerical dating of Japanese Miocene volcanic layers. This method uses the natural decay of isotope  $^{238}\text{U}$  by fission of the nucleus. This fission creates tracks which may be counted in U-bearing minerals such as zircon and apatite. This method, which is usually less precise than the K–Ar and Rb–Sr methods, is extremely sensitive to thermal disturbance, and is mainly

used to identify potential thermal disturbance in the dated layers more than for direct and precise calibration of the age of geological events.

In the works presented in this volume, the K–Ar method is the one almost exclusively used for dating volcanoclastic layers. This is partly because it is suitable for dating different kinds of geochronometers. K-bearing minerals such as biotite, sanidine, plagioclase, and hornblende are geochronometers representative of the time of their crystallization once they were erupted from a volcano, and then transported into marine sedimentary basins. Thus, these volcanoclastic minerals constitute the ideal material for measuring the age of geologic and biologic events recorded in the surrounding sediments.

In using a single dating method, the diversity of geochronometers plays a critically important role for a correct interpretation of the analytical results, which may be strongly constrained by geochemical problems such as: (1) the unknown initial isotopic composition (presence or absence of radiogenic isotopes at the time of crystallization); (2) the estimate of penecontemporaneity of the actual time of crystallization with deposition; and (3) the good preservation of the geochemical equilibria since crystallization time (closed systems vs exchanges with the exterior). While the first problem is difficult to resolve in a prioristic and easy way, the others can be partially solved through a careful sedimentological study of the outcrop, a petro-mineralogic analysis of the volcanoclastic layer hosting the geochronometer, and detailed X-ray and electron microprobe analyses of the separated and purified geochronometer. These analyses permit to document multiple provenance, inheritance or weathering of the potential geochronometer (Odin et al., 1991). Ultimately, consistency of results among geochronometers which are known to have different behaviours becomes perhaps the most efficient criterion for judging reliability.

*Extrapolation procedures.* Other approaches can be used to estimate the age of geological events. These involve extrapolation or interpolation between geochronologically documented tie points. The most powerful extrapolation procedure is the magnetokilometric principle which is based on the hypothesis of a constant seafloor-spreading rate between geochronologically calibrated tie points.

The accuracy of the resulting numbers increases with decreasing distances between tie points. However, this accuracy cannot be better than the accuracy of the tie points which were obtained from magnetostratigraphically calibrated sedimentary sequences. Nevertheless, the procedure may be helpful for judging the consistency of a series of geochronological results, and the combination of the two direct and indirect approaches has an interesting potential.

The climatostratigraphic procedure, which is somewhat comparable to tree-ring-dating, is particularly relevant for the end of the Miocene Epoch. Its power for direct dating is dependent on the possibility to count climatic cycles from the Present to the dated sediment. If disconnected from the Present, it becomes dependent on direct geochronologic datings of at least one point in the dated sequence. In fact, the procedure is also sensitive to other hypotheses such as the actual period recorded in the sedimentologic variations of the sequence which may be any of the Milankovich cycles. Then, some idea of the duration of the time interval under consideration is needed for application and geochronologic calibration cannot be avoided especially for ages older than a few Ma.

In this volume, our main purpose has been to follow the geochronologic approach described above documenting Miocene sedimentary sequences with direct numerical datings. These may later serve as tie points for calibrating the Time Scale as well as for indirect calibration of any other extrapolation procedure, or for the application of the climatostratigraphic approach.

*Modern techniques — dating techniques, principle, interest*

The most used method in this volume is the K–Ar method which can be applied using diverse analytical *techniques* and *procedures*. These are described and documented in several chapters of this book. Here is a summary on the analytical techniques used for dating Miocene volcanoclastic layers.

*The K–Ar conventional technique.* It allows measurement of the K content on the one hand, and the Ar content on the other hand, using the isotope dilution technique (a known volume of ‘artificial’  $^{38}\text{Ar}$  isotope is added to the sample, and the peak heights of this  $^{38}\text{Ar}$  spike and of the  $^{40}\text{Ar}$  are compared for deriving the  $^{40}\text{Ar}$  content).

*The irradiation technique (or  $^{40}\text{Ar}/^{39}\text{Ar}$  technique).* It is the other way to analyze the same isotopes and derive ages. In this technique, the natural  $^{39}\text{Ar}$  isotope is transformed to artificial  $^{39}\text{Ar}$  in a nuclear reactor, using irradiation by neutron flux. Then, the direct comparison of the  $^{40}\text{Ar}$  (radiogenic) of the sample to the  $^{39}\text{Ar}$  (artificially derived from K of the sample) allows to define a ratio which is related to the age of the measured sample. The irradiation technique is thus primarily a variety of the analytical technique which should lead to the same age as any other technique. However, this technique is extremely powerful because it allows to measure both K and Ar from the same sample, and it has been applied using a variety of procedures for obtaining significant information on the quality and behaviour of the geochronometer.

The analysis of any sample using the isotope dilution technique or the irradiation technique leads to the same information: the apparent age of the whole sample. However, sophisticated analytical procedures add information to the ages. The first sophisticated analytical procedure is by incremental *step-heating*. Instead of heating the sample up to fusion temperature, it is heated step by step at selected progressive temperatures: 800°, 900°, 1000°C, etc. ... and the gas extracted at each heating step is measured separately. In this way, five, ten or fifteen apparent ages may be obtained from a single sample. Comparison of these apparent ages, calculated from the ratios of isotopes extracted for each step, commonly leads to an effective estimate of the significance (and reliability) of the calculated ages as exemplified in this volume.

The previous procedure used a conventional furnace; a second interesting analytical procedure (following irradiation) is the *laser-heating* procedure. This usually involves heating a small sample (i.e., a portion of a large crystal, or several individual crystals, or even groups of small crystals) with a high-energy laser beam, and measuring the  $^{40}\text{Ar}/^{39}\text{Ar}$  ratios of the gas released after total fusion of the sample. It is also possible to use this laser-heating facility with a step-heating procedure (the incremental laser-heating procedure). As remembered above, the ages measured either using the laser or the conventional furnace will lead to similar apparent ages for a given material. Compared to the conventional furnace, the laser allows measuring smaller quantities of material, and does not require packing with metal foil which can be a source of contamination.

The common problem with the dating of small quantities of material is that it requires an extremely clean vacuum, and super highly sensitive detectors. The use of a multiplier is thus necessary to detect small quantities of gas.

The use of the irradiation technique allows to measure both K and Ar in the same sample avoiding problems of inhomogeneity in otherwise split sample aliquots used separately for K and Ar analyses in the conventional technique. In addition, the precision of the individual  $^{40}\text{Ar}/^{39}\text{Ar}$  measurements is commonly better than the sum of the precisions of the K and Ar measurements of the conventional technique. This means that, for a given irradiation, extremely precise comparisons are possible.

However, because the irradiation is a treatment which cannot be precisely calibrated in the absolute, it is necessary to use monitors of known ages (selected geochronometers) for analytical comparison. Since the actual age of these monitors can be derived only using the conventional technique, the current accuracy of the  $^{40}\text{Ar}/^{39}\text{Ar}$  ages is fundamentally not better than the accuracy of the conventional K–Ar ages.

## TECHNICAL DETAILS FOR INVOLVED LABORATORIES

Technological progress in radioisotopic dating has been significant in recent years, and the various analytical custom-built facilities are never identical. Consequently, the ages calculated in each laboratory depend on some factors which are not always standardized. It is therefore important to give some details on the analytical procedures and specifications of the diverse facilities used here and there to understand the actual meaning of the derived ages, and compare them properly. This question is summarized in the following paragraphs.

### *Analytical techniques in Berkeley (A. Deino and A. Montanari)*

*Mineral separation.* For extracting volcanoclastic biotite from relatively soft, marly samples, 2 kg of bulk-rock samples were washed with tap water using a 63 mm polyester cloth, and dried under a heat lamp at a temperature less than 60°C. Indurated marls needed to be crushed before washing, whereas clay-rich, softer samples broke apart after immersion in plain water. No acids were used in the preparation of samples. Biotite was then separated from the washed residues using a Frantz<sup>®</sup> isodynamic separator, and cleaned extensively in distilled water in an ultrasonic bath to remove adhered materials. Finally, the biotite samples were concentrated using Li-metatungstate at a density of 3.06 g/cm<sup>3</sup> to obtain the heavier fraction, which experience has shown to contain the most unaltered material.

X-ray diffractograms were run on oriented biotite separates to test whether they were mineralogically pure and free of vermiculite, the diagenetic clay mineral often found in altered volcanoclastic biotites in the Umbria–Marche Tertiary sequence (Odin et al., 1991). Homogeneity of the separates was tested by electron microprobe analyses on several individual flakes per sample, following the recommendations of Montanari (1988) and Odin et al. (1991).

For separating sanidine, the procedure used at Berkeley was the same as for biotite with the difference that the non-magnetic Frantz<sup>®</sup> separates coarser than 250  $\mu\text{m}$  were first studied at the microscope using clove-oil immersion to verify the presence of

sanidine (pale yellow) in contrast with pale blue plagioclase (Beke line for checking quartz and plagioclase vs sanidine). Sanidine was then separated with a graded density column of Li-metatungstate, rinsed two or three times in a ultrasonic bath in distilled water, and finally dried under an infrared lamp at temperatures less than 60°C. Impurities were picked using a binocular microscope and discarded. Before encapsulation for irradiation, the purified sanidine separates were washed for a few seconds in 2% diluted HF, rinsed again in an ultrasonic distilled water bath, and dried under an infrared lamp.

For separating plagioclase crystals, the procedure was essentially the same as the one used for sanidine with the difference that only the most pure, largest, and inclusion-free grains were hand-picked with a binocular microscope and utilized for radioisotopic dating. Hand-picked plagioclase grains from the same separate were also analyzed with the electron microprobe (Montanari et al., 1991).

*Irradiation and radioisotopic analysis.* Samples of purified mineral separates (sanidine, plagioclase, and biotite) were irradiated in the hydraulic rabbit facility of the Omega West reactor, Los Alamos National Laboratory, for between 3 and 14 h. Some samples were irradiated with cadmium shielding being used to reduce the thermal/fast neutron ratio, while others were not. The sample holders consisted of a stack of 14 mm diameter, 2.5 mm thick, 99.999% pure aluminum disks in which small wells were drilled to accept the <100-mg samples. Sanidine from the Fish Canyon Tuff was used as the monitor to chart vertical and lateral flux gradients, with a reference age of 27.84 Ma (Cebula et al., 1986), corrected for the updated age of monitor MMhb-1 of 520.4 Ma (Samson and Alexander, 1987).

After irradiation, the samples were transferred to a copper sample holder and loaded onto the extraction system for overnight bake-out at 250°C for biotite and 300°C for feldspars. Analyses of sanidine were all done by the total fusion of the grain using a 6-W continuous Ar-ion laser beam focused to a <100- $\mu$ m spot, applied for 15 s. Laser step-heating experiments on biotite and plagioclase were conducted using the Ar-ion laser, defocused to about 2.0 mm diameter. The laser power was raised incrementally through the course of the experiment, the samples being heated for 30–60 s, then allowed to cool during gas cleanup and spectrometer analysis. The gasses released from the crystals were scrubbed of reactive species by exposure to a 150°C Zr–Fe–V alloy getter for about 3 min. Argon was then measured in a Mass Analyzer Products Series 215 or 215-50 noble-gas mass spectrometer, operated in the static mode, using automated data collection procedures over a period of about 30 min. Peak intensities were measured on a Balzers electron multiplier operating at a gain of between 2 and  $5 \times 10^4$ . Typical volumes of  $^{40}\text{Ar}$  ranged from  $\sim 0.1$  to  $10 \times 10^{-10}$  cm<sup>3</sup>. Blanks for  $^{40}\text{Ar}$ ,  $^{39}\text{Ar}$ ,  $^{37}\text{Ar}$ , and  $^{36}\text{Ar}$  were  $\sim 1, 0.05, 0.02, 0.07,$  and  $0.02 \times 10^{-12}$  cm<sup>3</sup>, respectively.

Purified bulk plagioclase separates were also analyzed using the incremental-heating procedure with a resistance furnace as the heating source. Sample weights of plagioclase were between about 20 and 40 mg, and were wrapped in high-purity Al foil for irradiation and incremental heating.

*Isochron analysis.* ‘Inverse’ isochron analyses (Turner, 1971) have been used in this study to obtain the best age estimate from a suite of  $^{40}\text{Ar}/^{39}\text{Ar}$  determinations. In the inverse isochron,  $^{36}\text{Ar}/^{40}\text{Ar}$  is plotted against  $^{39}\text{Ar}/^{40}\text{Ar}$  for each analysis, after correction of the isotopic ratios for irradiation-produced interfering isotopes and mass spectrometer discrimination. Thus  $^{40}\text{Ar}$  is here composed of radiogenic  $^{40}\text{Ar}$  ( $^{40}\text{Ar}^*$ )

plus 'trapped'  $^{40}\text{Ar}$  ('trapped' argon is used here in the sense of argon incorporated within the feldspar at the time of crystallization, or adhering surficial argon),  $^{36}\text{Ar}$  is trapped argon, and  $^{39}\text{Ar}$  is produced from  $^{39}\text{K}$  in the reactor. The trapped  $^{40}\text{Ar}/^{36}\text{Ar}$  ratio ( $^{40}\text{Ar}_a/^{36}\text{Ar}_a$ ) is 295.5 where the source of this component is nonfractionated atmospheric argon (Steiger and Jäger, 1977). In the ideal case of unaltered cogenetic grains, the analyses form a linear isochron in which the ordinate gives  $^{40}\text{Ar}_a/^{36}\text{Ar}_a$  (the trapped component) and the abscissa yields  $^{39}\text{Ar}_K/^{40}\text{Ar}$  (thus the age). The isotope data set is fit with a York (1969) least-squares regression procedure that accommodates errors in both ratios and correlation of errors.

One of the advantages of the isochron plot of analytical data is that it makes no assumption concerning the composition of the trapped non-radiogenic component, whereas the straightforward computation of an age from a single  $^{40}\text{Ar}/^{39}\text{Ar}$  analysis assumes  $^{40}\text{Ar}_a/^{36}\text{Ar}_a = 295.5$ . In addition, the isochron plot provides a visual tool to help identify deviations from an ideal single population of analyses. For example, older contaminant grains will have lower  $^{39}\text{Ar}/^{40}\text{Ar}$  ratios and fall to the lower left of the main isochron trend. Alteration often causes an increase in atmospheric argon concentration accompanied by loss of  $^{40}\text{Ar}^*$ , such that these analyses occur to the upper left of the plot. Statistics of the York regression are helpful in identifying whether the population contains outliers.

#### *Analytical techniques in Yamagata*

Both the isotope dilution technique and the irradiation technique were used in Yamagata. The two techniques have involved the biotite Bern 4B as the reference mineral (see Flisch, 1982). According to Prof. K. Saito, and for several other reasons possibly including mineral purification, and certainly a long delay between irradiation and measurements, the apparent ages obtained at Yamagata for this volume were sometimes less precise than they could have been.

#### *Analytical techniques in Pisa (M. Laurenzi)*

*Mineral separation.* Samples were disaggregated in water and  $\text{H}_2\text{O}_2$ , and residues were repeatedly washed under running water, and further passed many times into an ultrasonic bath. Compositions of the washed fractions were checked both with diffractometric analyses and in thin sections. After sieving, proper fractions (generally 100, 150 and 250  $\mu\text{m}$ ) were passed through a Frantz<sup>®</sup> isodynamic separator, obtaining a concentration of magnetic and non-magnetic minerals.

The more widespread mineral in these volcanoclastic levels was biotite, so the main effort was concentrated on its separation. A combination of shaking table and Frantz<sup>®</sup> separator was used to obtain a good concentrate, which was delaminated in quartz mill with acetone, and then further sieved, shaken with paper and controlled under the microscope.

The non-magnetic fraction was processed in those few samples where diffractometric analyses revealed the presence of feldspar: plagioclase in our samples. A combination of Frantz<sup>®</sup> separator, shaking table and heavy liquids was used to obtain a good concentrate, followed by hand-picking.

*Isotopic measurements.* When the conventional technique was used, K determinations were done using a Elmer® 503 atomic absorption spectrophotometer. Ar isotopes were measured by isotope dilution, using a  $^{38}\text{Ar}$ -enriched spike. For analytical details and error calculations, see Del Moro et al. (1982).

When the  $^{40}\text{Ar}/^{39}\text{Ar}$  technique was used, samples were irradiated for 5 to 6 h in the thimble of the 250 kW TRIGA reactor, Pavia (for details, see Oddone and Villa, 1986). Samples were loaded in a unique column, interbedded with Ni wires to monitor vertical neutron flux variations and with FCT#3 biotite as age monitor. The value of 27.55 Ma, recommended by Lanphere et al. (1990) was used. Some detail about age calibration of this standard is given in Laurenzi et al. (Chapter E5). The use of a single sample column avoided any problem of lateral flux variation. Vertical neutron flux variation in the 7 cm long irradiation can, has a hyperbolic shape: an almost zero flux variation for 2.5–3 cm, about 2% per cm in the remaining part.

Samples were heated in about 8–10 temperature intervals, using an inductively heated furnace, in a molybdenum crucible. Intermediate- and high-temperature blanks were done before each sample. At 1300°C they were of the order of  $1.2 \times 10^{-9}$  ml STP (standard temperature and pressure) for  $^{40}\text{Ar}$  and  $2.0 \times 10^{-13}$  ml STP for  $^{39}\text{Ar}$  during measurements related to samples from Moria and to the first group of the Faenza sections. During a second set of samples, blanks were definitely lower, of the order of  $3.2 \times 10^{-10}$  and  $8.1 \times 10^{-14}$  ml STP for  $^{40}\text{Ar}$  and  $^{39}\text{Ar}$ , respectively. In both cases, the blank composition was atmospheric.

A pre-heating at a temperature of about 100°C under vacuum was done after loading samples on the Christmas tree, to remove adhering air. Evolved gas was cleaned from reactive gases using a hot Ti trap and two activated SAES® getters. Ar was then measured in the static mode, using peak jumping procedure, into a VARIAN-MAT® 240 mass spectrometer, using an electron multiplier as detector. Obtained data were corrected for instrumental background, mass discrimination,  $^{37}\text{Ar}$  decay, nuclear interferences due to K, Ca and Cl-derived Ar isotopes.

Ages were calculated using the two calculation procedures employed in Ar/Ar dating: the 'plateau' and the 'isochron' (or isotope correlation) approaches, taking into account only in-run analytical errors. Other sources of errors, which comprise error on neutron flux variation and uncertainty on monitor age, are added later. Plateau age calculation relies on the assumption that the trapped  $^{40}\text{Ar}/^{36}\text{Ar}$  component has an atmospheric composition, which is not always true. A weighted average was done on subsequent steps with the same age at the  $2\sigma$  level, containing at least 50% of gas release.

Age calculation using isotope correlation (or isochron) diagram does not make any type of assumption on the trapped component, whose isotopic composition is obtained as a by-product of the calculation. The obtained age is automatically corrected for the trapped component, whichever its composition. One problem related to this approach is that if points do not have a wide dispersion, the fit may be affected by a very large error.

#### *Analytical techniques in Lausanne (G.S. Odin and M. Cosca)*

$^{40}\text{Ar}/^{39}\text{Ar}$  analyses were performed at the University of Lausanne with a Mass Analyser Products® 215-50 mass spectrometer following the usual procedure in this laboratory for irradiation, sample treatment, correction for mass discrimination, interfering



derived isotopes of Ar, neutron flux gradient, and age calculation (Cosca et al., 1992; Cosca and O'Nions, 1993).

*Sample cleaning during analysis.* In addition to the usual heating of the line and samples at 150°C after storage of 30 to 50 samples, each sample has been heated in the crucible under vacuum for some time just before measurements (see below). This is intended for removing most of the adsorbed gas and other components such as water, traces of organic matter, etc., and for keeping the traps clean for better purification of argon.

Samples were heated from 10 to 50 min at 550°C (plagioclase); at 550° to 600°C for 15 to 50 min (sanidine, biotite); at 800°C for 15 to 45 min for hornblende. These conditions may affect some minerals. However, the truly pyroclastic (and well preserved) minerals are not significantly modified; in addition, our aim is to know whether or not the dated material has been 'disturbed' or not (i.e., whether  $^{40}\text{Ar}/^{39}\text{Ar}$  isotopic ratio is homogeneous for most steps, and shows a plateau). This simple criterion allows to reject (or question) the ages obtained from those geochronometers (our purpose is strictly to date the original volcanic event).

In spite of our carefulness, the gas extracted from some samples has been imperfectly cleaned. This may be inferred from the evolution of the peak intensities during the seven cycles of measurement of the gas. For unclean gas, ionization is not perfect at the time of inlet; the result is that, instead of decreasing regularly after introduction, the peak intensities for some isotopes increase following the first (or first and second) cycle of peak switching, and then decrease. This leads to uncertain extrapolation of the values for each peak at the time of inlet of the gas. The resulting apparent age may be biased by a few percents as we have checked by calculating the extrapolation using either all cycles or only the last five or six among the seven cycles recorded.

*Analytical procedure.* Practically, when the behaviour of the mineral used is well known (it is very homogeneous in our samples), and the quantity of sample has been correctly estimated, nine to ten steps were run for incremental heating procedure. We need two steps, one initial step at low temperature for removal of gas generally not clean, and one further step at high temperature for making sure that all the gas has been extracted. In between, we need two more steps for possibly mixed gas (altered material at low temperature and extraneous gas in foreign material at high temperature); then no more than five to six steps are needed to split the 'main gas' into steps which will demonstrate whether or not a plateau is present.

*Analytical calibration.* The samples were irradiated in the US Geological Survey's TRIGA reactor in Denver (Dalrymple et al., 1981) together with a dozen of subsamples of the biotite HD-B1 monitor (Figs. 1 and 2).

Analytical flux calibration was made using the monitor biotite HD-B1 (Fuhrmann et al., 1987) which has a recommended K–Ar age of 24.21 Ma according to Hess and Lippolt (1994). This interlaboratory comparison (based on conventional isotope dilution technique results) leads to an observed interlaboratory standard deviation of 0.32 Ma which means a ( $2\sigma$ ) error bar of 2.5% for the age. This error is not due to the sample itself which shows an acceptable intralaboratory reproducibility for both K and  $^{40}\text{Ar}$  in most laboratories (standard deviation of about 0.5% for each component).

*Blanks.* Blanks were measured for a series of temperatures for groups of 10 to 15 samples; intermediate analyses at mid and high temperature were undertaken each day

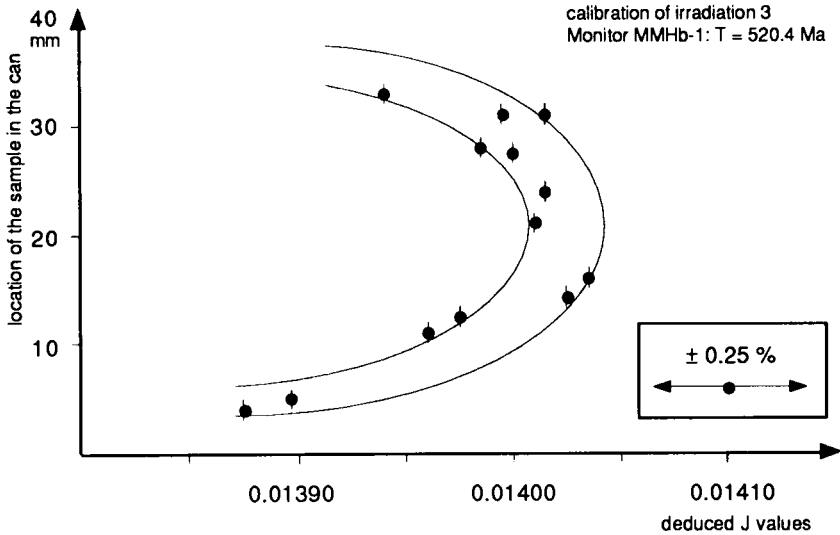


Fig. 1. Example of calibration of the neutron flux during one irradiation. Samples of the monitor are spread along the length of the storage can where unknown samples are put one above the other. The can is exposed perpendicular to the beam of neutron. Thirteen monitor samples were used for a can with samples on less than 4 cm. The neutron flux varies along the can with maximum and stable values in the middle of the beam. After irradiation the samples of the monitor are measured first to draw the reference domain for *J* values; these are then used to calculate the ages of the unknown samples according to their place along the can.

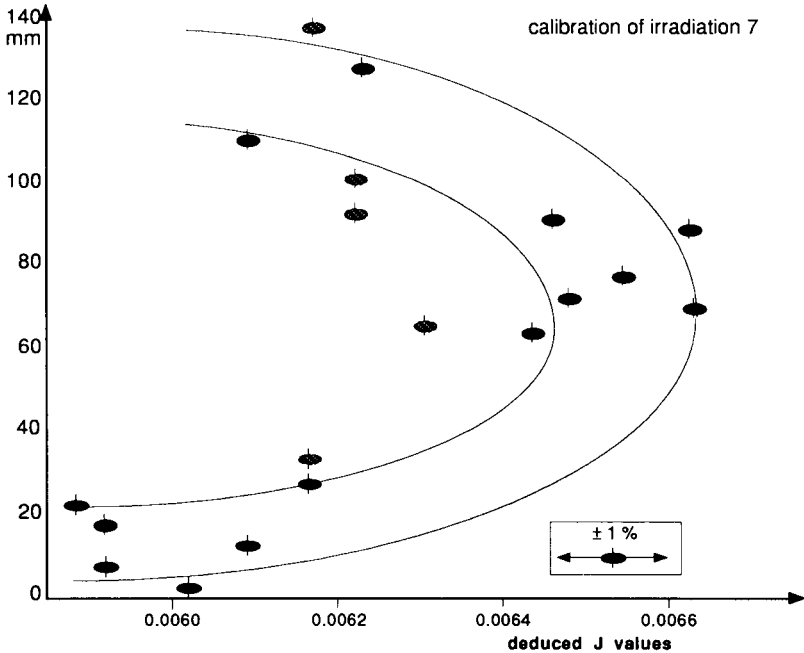


Fig. 2. Example of calibration of the neutron flux where the results obtained on the samples of the monitor are comparatively spread. Nineteen monitor samples were spread along a can full of samples on 14 cm.

for control of (possible) evolution of the blank. The blank values for mass 40 was about  $4 \times 10^{-15}$  moles at most temperatures up to 1350°C and increased to about  $10 \times 10^{-15}$  moles at 1600°C; for masses 39 and 36 the blanks remain at or less than  $0.02 \times 10^{-15}$  moles. Experience shows that precise analyses are obtained for radiogenic  $^{40}\text{Ar}$  quantities of  $100 \times 10^{-15}$  moles little contaminated with 'atmosphere'.

*Sample quantities.* With the extraction line employed in the years 1993–1994 using the multiplier detector, and for incremental heating procedure, ideal quantities of pyroclastic minerals were as follows. Plagioclase (0.4%  $\text{K}_2\text{O}$ ) 10 Ma old: 150 mg; hornblende 10 Ma old: 100 mg; biotite 10 Ma old: 15 mg; sanidine 10 Ma old: 10 mg. In principle, ten times older (or younger) samples would need ten times less (or more) material. The mean duration for a 10-step analysis is usually of about 5–6 h but absolute quantities of material above 100 mg may pose a problem for gas cleaning, and that duration should be increased by 2 or 3 h for large quantities due to the additional time for cleaning the trap after measurements (about 2 h). Thus, samples larger than 100 mg are not routinely analyzed.

*Analytical error bars.* The question is multiple and must be carefully considered in order to avoid common underestimation of the actual uncertainties in quoted ages. The experimental *intrasample* error margins for the (ratios of) gas measured (precision within the experiment or within run error) are calculated from a combination of the data obtained from the mass spectrometer. Commonly, when the gas is clean and the quantity large enough (compared to the line blank) the error margin is of the order of 1%. The uncertainty on ages calculated within the laboratory (*intralaboratory* error on ages) includes in addition the intralaboratory reproducibility which includes in turn (1) the short-term reproducibility, and (2) the long-term one mostly depending on the error margin on the calibration of the neutron flux (*J* curve). This latter is experimentally established from a series of analyses for each irradiation (see Fig. 1). This curve has a particular U shape which has been established in the reactor across the neutron flux. From the series of analyses on the monitor (commonly 10 to 15 of them per irradiation) the *J* values may usually be determined with a relative error of about 0.25%. However, comparisons of analytical results obtained from successive irradiations led us to prefer a relative error on *J* at 0.5%.

For intralaboratory age comparisons we can use the resulting  $\pm$  (usually equal or less than 1% of the age). However, for 'external' comparisons with other laboratories (*interlaboratory* errors) using different dating methods or monitors, the knowledge of the actual age of the monitor is involved. The whole set of ages obtained within a laboratory depends on this monitor, the age of which is only known worse than 1%.

In order to favour an actually significant meaning to the age numbers, we have followed the usual recommendation which is to discuss and conclude geological ages with a 95% confidence level.

## INTERLABORATORY COMPARISONS (G.S. Odin)

Comparison between geochronologically derived ages has been greatly facilitated since adoption of conventional values for decay constants. They are consistently used by all laboratories today since the recommendation has been made by the I.U.G.S. Subcommittee on Geochronology following the 1976 International Geology Congress

in Sydney. At that time, the isotope contents for the K–Ar dating method could be measured in a quasi absolute manner. Today, the development of the irradiation technique has made the problem of interlaboratory comparison more complex because this technique needs a calibration of the neutron flux which can only be achieved with some precision using natural rocks as monitors of known age during irradiation.

### *The age of the monitor*

The accuracy of the ages obtained using the irradiation technique is dependent on the age accepted for the monitors. The current situation regarding these monitors is that there is no internationally agreed convention for the age of any monitor. This is due to the fact that the decay constants of the naturally radioactive isotopes are already linked to a convention. In this situation, the numerical age of a rock or mineral is strictly dependent on a knowledge and cannot be assumed by a new convention which would interfere with the convention used for the decay constants. In addition, few reference materials are prepared in large enough quantities, and used routinely for quite a time by all laboratories. Therefore, the valid comparison between ages obtained from different laboratories can only be done either with a small (less than 0.5%) analytical uncertainty when the different laboratories use the same monitor or with a larger (about 1%) interlaboratory analytical uncertainty when ages are obtained by laboratories using different monitors.

Waiting for an improvement of this difficult situation, ages quoted by the various authors have to be related to a particular monitor and a particular age accepted for this monitor.

We may exemplify this situation with the case of the minerals from the Fish Canyon tuff (FCT) commonly used for monitoring the irradiations. Both biotite and sanidine are used. In 1985, Hurford and Hammerschmidt dated different minerals from this tuff using the isotope dilution technique. The biotite has been dated at  $27.01 \pm 0.50$  ( $2\sigma$ ) Ma and  $27.29 \pm 0.50$  Ma relative to Bern 4B biotite and Bern 4M muscovite for the  $^{38}\text{Ar}$  spike dose (Flisch, 1982), respectively. They also irradiated this FCT biotite, and found a total gas age at  $27.46 \pm 0.50$  Ma and a plateau (93% of the gas) at  $27.80 \pm 0.20$  relative to Bern 4M muscovite. The K–Ar age of the sanidine was 27.93 and  $28.04 \pm 0.50$  Ma. The plagioclase was dated at  $26.78 \pm 0.50$  Ma. The hornblende was dated at  $27.47 \pm 0.50$  Ma. All uncertainties are given  $2\sigma$  and include all analytical uncertainties. Except for the slightly younger plagioclase, the other ages are acceptably consistent given the analytical uncertainties quoted. However, it is suspected that the biotite may have a significantly younger (total) apparent age compared to the sanidine.

Lanphere et al. (1990) have accepted for the biotite (FCT 3 bio) a reference age of 27.55 Ma and this age is used in Pisa. In Berkeley, the sanidine from the same rock has been selected for monitor; an age of 27.84 Ma has been preferred in this work. The same sanidine has given an age of  $27.95 \pm 0.18$  Ma by inter comparison to the accepted ages of eight recent magnetic reversals within the last 3 Ma (Renne et al., 1994). Using either the age of 27.55 or that of 27.95 Ma for the tuff, the result is that the calculated central values for the age of sample MdC 102 of Laurenzi et al. (Chapter E5) are, respectively, either 7.28 or 7.39 Ma. The absolute difference of ages (0.11 Ma) is clearly larger than the precision of the analytical results at about 0.04 Ma. This demonstrates the need for

Table 1

Plateau ages on biotite from the Faenza area obtained using the irradiation technique

	Pisa		Lausanne
Early Messinian MdC107 plateau:	7.02 ± 0.03	B174: plateau:	7.21 ± 0.06 <sup>a</sup>
Late Tortonian MT31 plateau:	7.15 ± 0.04	B189: plateau:	7.44 ± 0.08 <sup>a</sup>
Age (Ma) interpolated for the correlation event	7.12 ± 0.04		7.4 ± 0.2 <sup>b</sup>

Former results obtained in Pisa using the isotope dilution technique resulted in the calculation of an age at  $7.26 \pm 0.20$  Ma for the FO of *G. mediterranea* (Vai et al., 1993).

<sup>a</sup>  $2\sigma$  Internal sample error and error on *J*.

<sup>b</sup> Total analytical and geological uncertainty (errors on ages from Pisa cannot be compared to those from other laboratories).

clear quotation of both the nature and the value accepted for the monitor used in these studies.

#### *Interlaboratory practical comparisons*

The nature and extent of analytical uncertainties ( $\pm$ ) on calculated apparent ages is complex. Out of the geological problems, there are three usual sources of errors: (1) the internal error (intrasample which is the precision of the analytical measurement plus the reproducibility of the sample itself) of about 1‰; (2) the uncertainty due to the irradiation procedure (factor *J*) of about 2‰ within a single irradiation or 5‰ between irradiations; and (3) the error on the age of the monitor which reaches 1% and is still higher for recently prepared monitors. Because the laboratories involved in the present work have used different monitors, interlaboratory comparisons between age results must consider all the above-quoted uncertainties.

*Berkeley–Lausanne.* The level Ancona has been analyzed both at Berkeley and Lausanne. In Berkeley, the biotite yielded a preferred mean from two plateau ages at  $11.50 \pm 0.11$  Ma (internal sample error and error on *J*). In Lausanne, the biotite separated from that level has given consistent total, good plateau and isochron ages at  $11.48 \pm 0.13$  Ma (internal error and error on *J*). In this case, a good consistency between the two laboratories is reached even when we do not take into account the uncertainty on the age of the different monitors used. This also suggests that the age values used for these two monitors are internally consistent.

*Pisa–Lausanne.* Similar levels have been independently sampled for age measurements in Lausanne and Pisa. The results quoted by the respective authors in this volume are shown in Table 1 (Chapters E5 and E6). In this interlaboratory comparison, it seems that the apparent ages calculated are significantly different if one takes into account the analytical precision alone. In other words, the ages accepted for the two different monitors used (FCT bio at 27.55 Ma and HD-B1 at 24.21 Ma) are not internally consistent.

*Pisa–Berkeley.* The two laboratories use the same rock but not the same mineral for monitoring the flux neutron dose during irradiation. Interlaboratory comparison has been provided during the study of level 19.55 of the Moria section (Deino et al., Chapter D1). Biotite separates have been dated in both laboratories.

In Pisa, an age of  $17.09 \pm 0.40$  ( $2\sigma$  analytical uncertainty) Ma has been obtained using the isotope dilution technique. The equivalent total gas age is not given for the irradiation technique and step-heating procedure. Nevertheless, a plateau age of  $17.03 \pm 0.06$  and an isochron age of  $17.06 \pm 0.10$  Ma, respectively, are calculated ( $2\sigma$  probably intrasample uncertainty) using the FCT biotite with a reference age at 27.55 Ma.

In Berkeley, the irradiation technique and step-heating procedure were used. The preferred age for the biotite separated from the same level as above is the weighted mean of two isochron ages:  $17.08 \pm 0.18$  ( $2\sigma$  including intrasample and  $J$  uncertainties). Monitoring of the irradiation was done using the FCT sanidine with a reference age of 27.84 Ma.

These results show a good interlaboratory consistency. This consistency would not be deteriorated if at Berkeley the same reference age would have been used in the two laboratories for both the biotite and the sanidine from the FCT: using an age of 27.55 Ma for the FCT sanidine in Berkeley would lead to a calculated age of  $16.90 \pm 0.18$  Ma which is still consistent with the ages calculated in Pisa.

## CONCLUSIONS

We have essentially discussed above the diverse analytical uncertainties which, combined, may be called as a *total analytical uncertainty*. However, the use of a calculated age for stratigraphy must consider also other uncertainties which have been reviewed previously (Odin, 1982). They comprise uncertainties on the qualities of the geochronometer such as those depending on the time of its genesis (genetical uncertainties), the locking time of the geochronometer versus its deposition in the dated sequence, and the history of the geochronometer after deposition (historical uncertainties): i.e., what may have happened to isotopic equilibria since the time of deposition up to the time of analysis. The total of the analytical, genetical and historical uncertainties — the estimate of which is an essential part of the geochronological study — leads to an estimate on the actual uncertainty on the age of the dated sediment. The results of the geochronologic studies presented in several chapters of this volume permit to calibrate the Miocene time scale with unprecedented precision and accuracy. We proposed a thorough review of the methods, techniques, and procedures used in the geochronology laboratories that contributed in this project because it is important that colleagues not directly involved in the geochronologic work, have at least a feeling of what a radioisotopic numerical age may entail, and be aware of its uncertainties, limitations, and problems.

With the ever-growing sophistication of analytical techniques, which almost always are independently developed in individual laboratories, and machineries which are assembled, custom-built or modified by the geochronologists in person in their laboratories (you cannot buy a standard Ar isotope dating machine in a Park-n-Shop store), one may expect difficulties in the comparison of results from different laboratories. However, the work presented in this volume, and the information summarized above, demonstrate that an acceptable consistency of the conclusions among laboratories may be achieved provided that a careful and rigorous consideration of the analytical uncertainties is made.

This is quite reassuring although from the present review it emerges that consistency may be further improved by means of constant scientific exchange among laboratories, acceptance of reliable standards, and sharing of procedures and technical information.

Finally, we would like to point out that the progress in refining technology, which leads to ever-increasing precision of age numbers, must keep pace with the progress in estimating the accuracy of age assignments, that is the 'closeness' between the analytical age and the unknown age of a given geological event. For this ultimate goal, the team work among specialists from different geological (physical and palaeontological) disciplines is a *sine qua non* requirement, and sharing of experience, information, and knowledge with mutual understanding of the problem, and critical cross-checking of diverse individual results, is what Integrated Stratigraphy consists of. We will conclude this remark by encouraging carefulness and exhaustive documentation of future integrated stratigraphic work "... the accuracy of the report being always tried by the most severe and detailed test possible" (Thucydides, 411 B.C.).

Chapter F2

**CHRONOSTRATIGRAPHY OF MIOCENE STAGES: A PROPOSAL FOR THE DEFINITION OF PRECISE BOUNDARIES**

G.S. Odin, A. Montanari and R. Coccioni

INTRODUCTION

Chronostratigraphy, which defines the units and common language for a subdivision of the Earth's history, has made significant progress thanks to the recommendation that sedimentary sequences should be characterized using multiple stratigraphic tools or, in other words, by applying the concept of *Integrated Stratigraphy*. This may be defined as the approach of characterizing sediments with two or more among the following five main tools: lithostratigraphy (including sequence stratigraphy), biostratigraphy, magnetostratigraphy, chemostratigraphy, and geochronology. Of these, at least one univocal tool, either biostratigraphy or geochronology, must be used in order to provide a chronologic attribution for the sedimentary sequence. Thus, Integrated Stratigraphy is an interdisciplinary team effort which can lead to a more reliable and cross-checked recognition of the time relations between samples collected vertically and horizontally.

The application of stratigraphical concepts depends on the nature of the available record (Odin, 1994). In short, in chronostratigraphy there are three main approaches which are relevant to as many main units: (1) for the geologic period characterized by a paucity or absence of fossils (i.e., from the origin of the Earth to about 540 Ma ago), chronostratigraphic units are defined on geochronologic basis only; (2) for rocks comprising most of the Phanerozoic (i.e., between 540 Ma and 7–4 Ma), biostratigraphy is the cardinal tool for the definition of *Stages* as fundamental chronostratigraphic units; (3) for younger rocks, the currently most followed approach may be called 'climatostratigraphy' and uses, as stratigraphic criterion, the various effects of climate changes linked to orbital cyclicity ( $^{18}\text{O}$  'stages'; palynologic changes, lithological rhythms, etc.). In this domain of the Earth's history, the fundamental units are or will be basically referred to 'Milankovich astronomic cycles'.

This general scheme basically depends on the fact that the younger the rocks are, the more they are approachable with diversified tools, allowing several parallel and all necessary, stratigraphic subdivisions such as climatically dependent cycles, magnetozones, biozones, etc., for precise and accurate correlations among distant sedimentary sequences.

The limit between recent deposits relevant for climatostratigraphy and older ones can be drawn within the Late Miocene Epoch. Working on the chronostratigraphy of the Miocene Epoch is, therefore, an interesting exercise because stratigraphy is here at the limit between two portions of the geological record which can be approached with both



multiple stratigraphy and integrated stratigraphy. The main difference between these approaches is the scale to which it becomes possible to distinguish with confidence two separate moments in the Earth's history.

It may be appropriate to remember here that the combinations of tools emphasized above are differently relevant for these two Phanerozoic stratigraphies. For instance, the combination of lithostratigraphic and/or chemostratigraphic and/or magnetostratigraphic and/or geochronologic data with biostratigraphic control allows definition of Stages. On the other hand, where Milankovich cycles are recognized, the combination of lithologic criteria (alternation of limestone and marls), and/or chemical criteria (fluctuations in organic matter content,  $^{18}\text{O}/^{16}\text{O}$  ratios, etc.), and/or magnetic properties (variations in magnetic intensity and susceptibility), and/or biologic abundance (i.e., cyclicity of pollens) with the known orbital history may lead to practical definitions of chronostratigraphic units.

In this volume, we have documented exemplar cases in which the relations between the two univocal tools used in stratigraphy (i.e., biostratigraphy and geochronology) were applied to sedimentary sequences in Europe and Japan. In this conclusive paper, we expose our view on how the rich body of information presented in the chapters of this volume are related to the definition of Stages.

## THE CHRONOSTRATIGRAPHIC MIOCENE UNITS

### *Foundation*

The units commonly recommended for the subdivision of the Miocene Epoch are six Stages which were originally defined in Europe. These are, from older to younger: the Aquitanian, the Burdigalian, the Langhian, the Serravallian, the Tortonian, and the Messinian. The recommendation for this chronostratigraphic subdivision is mostly based on historical grounds, and was promoted through conventions which have been established by European stratigraphers. The six Miocene Stages are grouped in couples constituting the three subunits of Lower, Middle and Upper Miocene. Outside Europe, this threefold chronostratigraphic subdivision is used more often than the Stages themselves.

There are two major reasons why the use of Miocene Stages on a global scale may be difficult. Firstly, their definition is insufficiently clear, and secondly (and perhaps consequently) they cannot be easily recognized. In this paper, we discuss this latter point in more detail trying to answer the following critical question: is it possible to easily recognize the Miocene Stages as currently defined?

We agree with Rio et al. (Chapter A5) that "it would be stultifying to maintain a unit only for historical reasons without considering their practical applicability." Indeed, the authors argue for a modification of the location of a Stage boundary compared to the historical stratotypes, and propose to substitute a near-biozonal limit to the actual content of the rock stratotype. Although biostratigraphy remains the key chronostratigraphic tool for this time interval of the Earth's history, the location of Stage boundaries exactly coinciding with biostratigraphic events would result in a misunderstanding by allowing confusion between biozonal boundaries, which simply serve as potential correlation criteria, and chronostratigraphic boundaries which are absolute-time, and

conventional, units. Therefore, a decoupling of these two substantially different systems is a pedagogical need.

However, we believe that the principle of questionability of the historical use for a particular chronostratigraphic Stage is valid for either or not maintaining the Stage itself. A major point for recognition of a Stage is its duration which is dependent on the key tool for correlation: evolution of fossils. The same tool is valid for the whole Phanerozoic (between 540 and about 5 Ma). Experience shows that the mean Stage duration is about 5 Ma all throughout the time scale (Odin and Odin, 1990). The Miocene, which lasted about 19 Ma, is subdivided into 6 Stages with a reasonable mean duration of 3 Ma. In reality, Miocene Stage durations are widely unequal. For a long time, the Messinian was considered very short (about 1 Ma) and sometimes its validity as chronostratigraphic unit has been questioned. Nowadays this does not constitute a problem any longer for the above-mentioned fact that the Messinian sedimentary record can be resolved with modern and very precise approaches (i.e., climatostratigraphy). In fact, it is now documented that the Messinian lasted about 2 Ma, and the Aquitanian, Burdigalian, Serravallian, and Tortonian Stages about 3–4 Ma each.

In contrast, the Langhian (as defined by its historical stratotype), with a duration of less than 2 Ma, is the shortest Stage of all (Odin, 1994). This point leads to question its validity as chronostratigraphic unit simply because its recognition is difficult in most sedimentary sequences throughout the world. It can be said with confidence that the uncertainty of the practical, and yet imperfect correlation tool based on planktonic fossil markers may be as large as 0.5 Ma. Therefore, a globally useful chronostratigraphic Stage must be at least 2 Ma long in order to be recognized with ease and internationally used. Following this reasoning, and trying to change as little as possible the current use for the subdivision of the Miocene, it may be recommended to consider the Middle Miocene as a single Stage.

### *The definition of Stages*

The fundamental chronostratigraphic units are based on bodies of rock which are at the origin of the units names. These historical stratotypes must therefore be taken as the reference for the content of the corresponding sediments: biostratigraphic characters as well as any other potential stratigraphic tool identify the content of Stages and, thus, define them. Our priority today is to define with more precision the limits between the Stages and this is now summarized according to the data made available by experts in Part A of this volume.

*The Chattian/Aquitanian (Oligocene/Miocene) boundary.* The difficulty in locating and correlating the Oligocene/Miocene boundary worldwide has been known for a long time. The main reason for this is that the Chattian historical stratotype lacks widely applicable correlation tools. According to Pognant et al. (Chapters A1 and A3), the Aquitanian stratotype contains fossil assemblages suggesting that almost all foraminiferal Zone N4 and a small portion of Zone N5 of Blow (1969) are present as well as calcareous nannofossil Zone NN1 of Martini (1981).

A recent proposal for a precise location of the GSSP for the Oligocene/Miocene boundary in the section of Carrosio–Lemme is summarized by Steininger et al. (Chapter A9). This is the result of a long-term research program during which a

number of sections studied in detail in the early 1980s did not yield a definitive, i.e., obvious, conclusion. Steininger and co-workers propose a number of observations and deductions. The biostratigraphic observations are diverse, and are the result of long scientific exchanges among many experienced stratigraphers. The authors note that the palaeoclimatic instability may be responsible for the apparent diachroneity of the range of several species in respect to other coeval sections elsewhere or in widely used biostratigraphic models.

These apparent discrepancies are documented in the light of the study of the nearby Bosio section (Odin et al., Chapter C1) which contains a volcanoclastic layer. At Bosio, the whole section bears a taxon first referred as *Paragloborotalia pseudokugleri* (and then correlated to the Oligocene) but which was combined later to a *Paragloborotalia kugleri* group (and then correlated to the Miocene). The volcanoclastic layer nearly coincides with the last common occurrence (LCO) of *Dicryococcites bisectus*, which is within the range of *P. kugleri*. The LCO of *D. bisectus* is commonly considered younger than the FO of *P. kugleri* although in some other cases it is quoted older. In the Carrosio–Lemme section, the LCO of *D. bisectus* is recognized at metre level 49, thus 14 m below the proposed GSSP at metre 35, and 16 m below the FO of *P. kugleri*. This 16 m interval represents about 1 Ma. Consequently, there seems to be a significant problem in the temporal relation between the two local events LCO of *D. bisectus* and FO of *P. kugleri* in sections a few kilometres apart.

In this difficult biostratigraphic context, the point where the boundary GSSP has been proposed coincides with a palaeomagnetic reversal. In contrast to many other coeval sections presented in this volume, the Carrosio–Lemme yielded a magnetostratigraphic record. Thus, the GSSP is proposed between the local magnetozone R-2, which has been interpreted by Steininger and co-workers as subchron C6Cn2r, and the overlying magnetozone N-3, interpreted as subchron C6Cn2n. However, we would like to point out that in the few Ma interval across the Oligocene/Miocene boundary, there should be sixteen palaeomagnetic reversals comprising Chrons 6C, 6B, 6AA, and 6A. These are further subdivided into a total of eight (normal polarity) subchrons. In the Carrosio–Lemme section, only six 'sure' reversals were recognized throughout this interval, and two relatively long stretches of section yielded uncertain polarity. In summary, the available magnetostratigraphic record in this section is difficult to be correlated point by point with the marine magnetic anomaly pattern.

*The Aquitanian/Burdigalian boundary.* The early Burdigalian Stage is defined in the Bordeaux area. The biostratigraphic conclusion proposed by Poignant et al. (Chapters A1 and A2) is that biozone N5 (excluding the basal portion of it) and a portion of biozone N6 of Blow (1969) are represented here, as well as the probably complete calcareous nannofossil biozone NN2 and the basal portion of NN3 of Martini (1981). The higher portion of the Stage is defined by the content of sections located in the Rhône Valley. Pouyet et al. (Chapter A4) note the presence of assemblages characterizing Martini's biozone NN2 at the base, and NN2–NN3 at the top. Planktonic Foraminifera characterizing biozones N5–N7 of Blow (1969) are also present according to the same experts. The overlying formation is already characterized by a fauna typical of biozone N8.

The precise foraminiferal information confirmed by A. Poignant (pers. commun., January 1996) indicates that taxa *Globigerinoides altiapertura* and *G. trilobus*, among others, are both present in the lowermost samples collected from the historical stratotype

section in the Bordeaux area. However, it is not known whether these first occurrences represent chronological equivalents of true phyletic appearances, or local appearances related to an unconformity found just below the stratotype. This means (1) that the deposition of the stratotype in the Bordeaux area began within the concurrent zone of these two taxa, and (2) that it is not known whether or not these two taxa appeared exactly at the same time in this area.

*The Burdigalian/Langhian (Lower/Middle Miocene) boundary.* The base of the Langhian historical stratotype was originally proposed by Cita and Premoli Silva (1960) in the 400 m thick Cessole Formation in an hilly area called 'Le Langhe' (southern Piedmont region of northwestern Italy), and has been further documented by several expert stratigraphers. Miculan (1994) recognizes the first occurrence of the planktonic foraminifer *Praeorbulina* (the marker for the base of biozone N8) with the taxon *Praeorbulina glomerosa sicana* 60 m below the base of the formation at Brico del Moro. Rio et al. (Chapter A5) also note that the historical stratotype of the Langhian begins above the evolutionary appearance of *Praeorbulina*. Finally, Fornaciari et al. (Chapter A6) report a similar observation: the base of the Cessole Formation is located some 100 m above the FO of *P. glomerosa sicana*. These authors also show the FO of *Praeorbulina glomerosa glomerosa* about 60 m above the base of the formation in the same section. The FO of *P. glomerosa curva* is not quoted by Fornaciari and co-workers, nor by Miculan (1994) but the former two observations allow to locate with confidence the Burdigalian/Langhian boundary within the evolutionary interval of the *Praeorbulina* group. Rio et al. (Chapter A5, fig. 8) give more information in this regard, and show the FO of *Praeorbulina glomerosa curva* about 30 m below the FO *P. glomerosa glomerosa*. Therefore, the Burdigalian/Langhian boundary (i.e., the Lower/Middle Miocene boundary) falls *within* planktonic foraminiferal Zone N8 of Blow (1969). According to Fornaciari et al. (Chapter A6), it is also located *within* calcareous nannofossil Zone NN4 of Martini (1981) the top of which is defined by the LCO of *Helicosphaera ampliapertura* observed 100 m above the base of the Cessole Formation. In summary, there seems to be good biostratigraphical consistency in regard to the Burdigalian/Langhian boundary as seen in Italian sections.

From the old side of the Burdigalian/Langhian boundary, the content of the upper portion of the historical stratotype of the Burdigalian is defined in the Rhône Valley. In Aquitaine, only the lower Burdigalian is represented by sediments in the type sections. Poignant et al. (Chapter A2) indicate that at La Sime there is a 4–5 Ma hiatus between the exposed Burdigalian sediment and the overlying deposits of the area of Serravallian age. In the Rhône Valley, planktonic foraminiferal biozones N5–N7 have been identified in the Burdigalian stratotype of Fontbonau, and the overlying rock unit is already characterized by a fauna of Zone N8 (Pouyet et al., Chapter A4). Demarq et al. (1974) also argue that, further to the south, in the rock unit corresponding to the uppermost portion of the stratotype section, some *P. glomerosa sicana* were identified, leading these authors to suggest that either the fossils are lacking in the uppermost portion of the type section due to adverse environmental conditions, or that *P. glomerosa sicana* first occurs above but very near the top of the sediments deposited in the stratotype.

Therefore, the two historical stratotypes are consistent between each other and, if any, there may be a small gap in between the two. We reached this conclusion from the data gathered in the Rhône Valley which not always have been taken into serious consideration in debates about the Burdigalian Stage. This Stage is peculiar in the

sense that it is defined in two different areas, and not only in the Bordeaux area (from *Burdigala*, Latin name for Bordeaux) as the name would suggest. The inferred small gap is most probably located within rocks containing *P. glomerosa sicana*. We may thus conclude that a good criterion for locating the boundary in a future conventional agreement is the FO of *P. glomerosa sicana*. This biosignal must be significantly below the proposed boundary to be fundamentally consistent with the definitions of the bracketing Burdigalian and Langhian Stages. At a significant distance above the boundary, the LO of the nannofossil *H. ampliaperta* is considered by all specialists as the next important biosignal. In summary, the Burdigalian/Langhian boundary can be recognized within the basal portion of foraminiferal Zone N8 of Blow (1969), and within the late portion of the calcareous nannofossil Zone NN4 of Martini (1981).

Other stratigraphic tools cannot be used with precision since scarce data are available for direct chemostratigraphy (Cahuzac and Turpin, Chapter A4) or magnetostratigraphy on the stratotype sections themselves. It is worth mentioning, however, that according to the observation made by Rio et al. (Chapter A5) the boundary is related to the beginning of a high sea-level stand.

*The Langhian/Serravallian boundary.* According to Miculan (1994), the FO of *Orbulina universa* is located about 45 m below the base of the Serravalle Sandstone unit exposed near the town of Serravalle in the Scrivia Valley (northwestern Apennines of Italy). This unit represents the historical stratotype for the Serravallian Stage (Vervloet, 1966). Miculan (1994) also emphasizes that the foraminiferal content of the basal stratotype corresponds to a level distinctly below the N10/N11 zonal boundary of Blow (1969), and falls within biozone N9. Rio et al. (Chapter A5) point out that there is no coincidence between the FO of *O. universa*, sometimes used as a taiteller for locating the Langhian/Serravallian boundary in the Mediterranean area, and the base of the Serravallian Stage which is younger: this boundary is either shown in correspondence with the base of biozone N10 or within biozone N9, depending on different authors' views. They also remark that the nearest bioevent located about 20 m above the base of the Serravalle Sandstone (Rio et al., fig. 14 in Chapter A5) is the LO of calcareous nannofossil *Sphenolithus heteromorphus* which is considered to be the evolutionary extinction. About 40 m below the same boundary, a zone of common occurrence of *H. walbersdorfensis* begins.

In regard to the old side of the boundary, in their study of the Langhian stratotype, Fornaciari et al. (Chapter A6) document that the top of the Cessole formation is slightly higher (about 10 m) than the FO of *O. universa* (the biomarker for the base of the *O. universa* biozone of Iaccarino and Salvatorini, 1982, and within Zone N9). This point is consistent with the observation of Miculan (1994) who found the first *O. universa* a few m below the top of the Cessole formation. Fornaciari et al. (Chapter A6) also document the fact that the nearest nannofossil event is the first common occurrence of *H. walbersdorfensis* practically at the top of the Cessole formation. According to the same authors, in this section this horizon "falls well within the range of *Sphenolithus heteromorphus*" the top of which defines the upper limit of Zone NN5 of Martini (1981). These data are similarly considered by Rio and co-workers in Chapter A5.

As for the consistency of the biosignals succession, and the comparative distance between them (FOs of *O. universa* and of *H. walbersdorfensis*, the LO of *S. heteromorphus*) Rio et al. (Chapter A5) conclude that there is a short gap in between the

top of the Langhian and the base of the Serravallian historical stratotypes (compare fig. 14 of Rio et al. in Chapter A5 with fig. 3 of Fornaciari et al. in Chapter A6). The location of a precise limit may, therefore, be achieved with complete consistency with the historical stratotypes, i.e., within rocks containing *O. universa* or within the *O. universa* Zone of Iaccarino and Salvatorini (1982), and within the top portion of rocks with *S. heteromorphus* or in the youngest portion of Zone NN5 of Martini (1971).

*The Serravallian/Tortonian (Middle/Upper Miocene) boundary.* The data gathered by Miculan (Chapter A7) in the section of Rio Mazzapiedi–Castellania led this author to document the base of the Sant’Agata Fossili formation, which may be considered as the historical stratotype for the Tortonian Stage, and the top of the underlying Serravalle Sandstone. The most relevant planktonic foraminiferal biomarker documented therein is *Neogloboquadrina acostaensis*, a taxon which is *already present* in the topmost sample(s) of the Serravalle Sandstone, very near the limit between the two formations. Miculan (Chapter A7), and Rio et al. (Chapter A5) document that this fossil marker is considerably older than observed in early studies some 20 years ago when it was reported about 30 m higher in the section (see fig. 18 in Chapter A5). Consequently, the Serravallian/Tortonian boundary is presently documented in *N. acostaensis*-bearing rocks, although in the Tortonian stratotype, it falls very near the FO of this taxon which is assumed to document its evolutionary appearance. This corresponds to the lowermost part of Zone N16 of Blow (1969).

As pointed out by Rio et al. in Chapter A5, this bioevent is commonly used to correlate the Serravallian/Tortonian boundary but it is also obvious: (1) that the precise connection between the chronostratigraphic boundary and the biostratigraphic signal is not necessary; and (2) that the precise boundary between the two Stages should preferably be located slightly above the observed evolutionary appearance when recognized.

As quoted by Rio and co-workers, the boundary is poorly constrained with calcareous nannofossils, and the available direct magnetostratigraphic information quoted by Miculan in Chapter A7 needs to be supplemented with new data.

*The Tortonian/Messinian boundary.* Colalongo and Pasini (Chapter A8) locate the historical stratotype for the Messinian in the Pasquasia–Capodarso section of Sicily. Following the original proposal of Selli, the (lithological) definition for the base of the Messinian Stage is the first lithosignal indicating a change from a genuine marine facies to a more confined facies which would evolve to the salinity crisis and gypsum deposition in the Mediterranean domain. In Sicily, this change is located 25 m below the transition between a grey–blue marl unit and the Tripoli facies. The nearest biosignal is located 2 m above the defining lithological criterion, and is the FO of planktonic foraminifer *Globorotalia conomiozea* (Colalongo et al., 1979a). A rough estimate of the time interval represented by these two levels can be made using sedimentary thickness in the Capodarso section in Sicily (50 m) and a duration of less than 1 Ma for the pre- evaporitic Messinian (Vai, Chapter E3). The resulting duration is less than 40 ka.

Rio et al. (Chapter A5) emphasize the observation that the base of the Messinian Stage as defined in Sicily, clearly correlates within the upper part of the Tortonian stratotype section: the Sant’Agata Fossili formation is 330 m thick, and the biosignals recognized in the Sicilian section near the base of the Messinian are located more than 100 m below the top of the original Tortonian of the Rio Mazzapiedi–Castellania section.

This is in contrast with the otherwise fair consistency between historical stratotypes below and above the boundaries for other Miocene Stages, and it is necessary to choose between the two possibilities which are to show the boundary at the top of the Tortonian historical stratotype or at the base of the Messinian stratotype. The common use is that the Tortonian/Messinian boundary is located at the base of the body of rocks defining the Messinian historical stratotype.

*The Miocene/Pliocene boundary.* The historical location of the end of the Miocene Epoch is presented by Colalongo and Pasini (Chapter A8). In the Pasquasia section of Sicily, the authors remember that it must be located between the Gessosso Solfifera formation and the Trubi unit. This contact is better exposed in other Sicilian sections such as at Capo Rossello (near Realmone, province of Agrigento; Cita, 1975). This contact corresponds also to a palaeogeographic event which led to a return of open-sea conditions usually indicated by a drastic lithologic change in Mediterranean and oceanic deposits.

The work undertaken by a Working Group of the IUGS-Subcommission on Neogene Stratigraphy is aimed at proposing a GSSP for this boundary. The most recent tendency on the matter is summarized by Suc et al. (Chapter A10) who present diverse solutions including: (1) deletion of the Messinian (partly comprised in the historical Tortonian); or (2) inclusion of a Messinian (at least in part) within the Pliocene, or (3) reduction of the Messinian to its saline deposits (covering less than 1 Ma), or (4) practical maintenance of the traditional sense. At present, the latter solution seems to be the most advocated one. The boundary would then be located in correspondence with the significant sea-level rise between the Miocene and the Pliocene, which may be traced in the  $^{18}\text{O}/^{16}\text{O}$  isotopic curve. The known shift of the curve is reasonably supposed to be contemporaneous with the return of open-sea conditions in the Mediterranean, and this solution is consistent with the historical definition of the chronostratigraphic units.

### *Biostratigraphic data and the definition of Stage boundaries*

There is a common tendency to locate chronostratigraphic boundaries in coincidence with some biostratigraphic signals. There are several reasons why some of us refrain to encourage such coincidences.

One reason is that local coincidence in a particular section is not a criterion for coincidence everywhere. The currently widely accepted view that the criteria used for recognition of biozone boundaries may be diachronous does not satisfy the necessity for chronostratigraphic boundaries to be isochronous everywhere. The coincidence in a reference section may thus lead to confusion between the fundamentally different nature of the two kinds of concepts and to improperly define a chronostratigraphic boundary by a diachronous criterion.

A second reason is that the common use of LOs and FOs of planktonic micro- or nanofossils for locating biozone boundaries in the Miocene, leads to the situation that one side of the limit is 'defined' by the absence of a particular fossil. This means that, in case of coincidence with a chronostratigraphic boundary, one of the two Stages is not characterised by a concrete content. This is a poor solution. Obviously, this comment is restricted to the practice of overemphasizing a single LO or FO, thought to be an evolutionary event indeed, for locating a given chronostratigraphic boundary. In this

situation, it is more preferable to locate a chronostratigraphic boundary slightly below a LO or slightly above a FO. The amount of time represented by the distance between the criterion of correlation and the boundary is a matter of both documentation in the field and, above all, convention.

Finally, a third reason is that the historical stratotypes show that there is generally no coincidence between the bodies of rocks defining the Stages and the presently used biosignals to approach the boundaries. Therefore, there is no reason to put in correspondence factors which do not coincide: this would modify the definitions instead of making them more precise which is the aim of integrated stratigraphy. The Burdigalian/Langhian and the Serravallian/Tortonian boundaries are well constrained *above* the FOs of the genus *Praeorbulina* and of the taxon *N. acostaensis*, respectively. The Langhian/Serravallian boundary coincides with a level slightly *below* the LO of *S. heteromorphus*; Rio et al. recommend to locate the limit near that LO. In fact this would be better expressed as near and below that LO. Given this, both sides of the chronostratigraphic boundary result characterized by the presence of a fossil, the actual position of the boundary being approached by the LO signal given by the fossil near and above in the section used for definition.

The Tortonian/Messinian boundary drawn at the base of the Messinian corresponds to slightly below the FOs of *Globorotalia mediterranea* and *G. conomiozea*. However, the Tortonian side of the boundary is concretely characterized by the presence of foraminifer *Globorotalia suterae* and of the nannofossil *Amaurolithus* group, the FO of which are not far from below the boundary.

As a last comment on this point, we wish to emphasize that the total duration of at least two Stages following their precise definitions, would be modified by making biosignals and boundaries coincident, as illustrated in fig. 19 of Rio et al. (Chapter A5). The Langhian would be increased both at the bottom (Burdigalian portion of rocks above the FO of *Praeorbulina*), and at the top (Serravallian portion of rocks below the LO of *S. heteromorphus*). In contrast, the Serravallian would be shortened at both limits: at the base, the Serravallian portion of rocks below the LO of *S. heteromorphus*, and at the top, the Serravallian portion of rocks above the FO of *N. acostaensis*.

It may be argued that the historical definitions of Stages must not be impediments to progress in the refinement of the chronostratigraphic time scale. In the case of the Miocene Epoch, however, it is our feeling that a perfect knowledge of the concrete record in the stratotypes is the best way for founding progress. The latter will consist in reaching more precise boundaries in selecting GSSPs in agreement with what should be the use as defined by our historical conventions. In addition, such considerations help in making more independent and fruitful the different concepts of Stage and biozone.

## AGES OF THE BOUNDARIES AND DURATION OF THE MIOCENE STAGES

The question of the age of the boundaries and duration of the Stages of the Miocene Epoch can be discussed in the light of the new geochronological information presented in this volume. Boundary ages were usually obtained directly from sections biostratigraphically correlated with the historical stratotypes in the same or nearby palaeogeographic domain; this is supposed to reduce the problem of potential diachronism of biosignals.



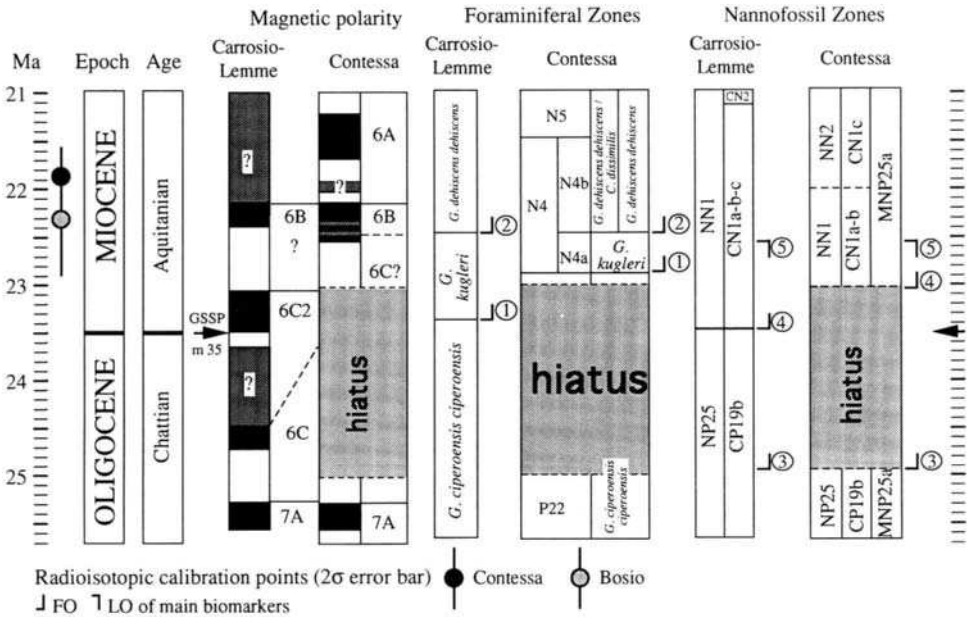


Fig. 1. The Oligocene/Miocene boundary. Data from the proposed Global Stratotype Section and Point of Carrosio-Lemme for the Oligocene/Miocene boundary are synthesized from Steininger et al. (Chapter A9). Calcareous plankton stratigraphy, and radioisotopic calibration point for the Contessa section are from Montanari et al. (Chapter C3). Radioisotopic date for the Bosio section is from Odin et al. (Chapter C1). Main biostratigraphic markers (circled numbers) are: 1 = *G. kugleri*; 2 = *G. dehiscens*; 3 = *S. delphix*; 4 = *S. capricornutus*; 5 = *S. conicus*.

It is explained in the previous contribution that the numbers deduced from geochronological investigation depend on several factors which must be considered for appropriate comparisons. Some results of this synthesis are summarized as follows: (1) the numerical ages quoted are not all similarly founded depending on the criterion of consistency; the quality of this criterion can be deduced either from multiple data obtained from a single sample or from intercomparisons between independently obtained data; (2) the numerical ages also depend on analytical calibration which may be different for different sets of data; (3) the numerical ages have no meaning if they are not exhaustively supplemented by realistic error bars (analytical uncertainties including intrasample, intralaboratory, and interlaboratory errors — combined as a total analytical uncertainty — as well as uncertainties due to the geochronometer), the value of which is commonly more difficult to estimate than the numerical age itself (as shortly exposed in Chapter F1).

*Numerical ages*

*The Oligocene/Miocene boundary* (Fig. 1). Our previous estimate of the numerical age of the Oligocene/Miocene boundary is the interval between 22.5 and 23.5 Ma (Odin and Odin, 1990; Odin, 1994). New data were obtained from two areas in Italy: the Piedmont and the Umbrian Apennines.

In the Piedmont, the presence of a volcanoclastic bed at Bosio, a few kilometres from the section proposed for definition of the GSSP of the boundary (Carrosio–Lemme section), is a potentially valuable new feature. The analytically precise age of hornblende contained in this layer at  $22.35 \pm 0.16$  Ma has been documented by Odin co-workers in Chapter C1 of this volume. As far as we may be sure that no alteration of the original isotopic equilibrium occurred, this date allows to derive a realistic geological age of  $22.3 \pm 0.7$  Ma (95% confidence level; total analytical uncertainties). The chronostratigraphic age of the dated level is made uncertain due to inconsistency between the two biosignals FO of *P. kugleri* followed by the LCO *D. bisectus* at Bosio, and the reverse in the Carrosio–Lemme section (as well as in the Umbrian Contessa section described by Montanari and co-worker in Chapter C3). If we assume that the nannofossil signal is diachronous, then the age at 22.35 may be interpreted to be close, yet younger, than the Epoch's boundary.

In Umbria, the nearest point geochronologically calibrated in the Contessa section is the Raffaello Level located (at metre level 306.7) above the boundary. It was previously dated using single-crystal  $^{40}\text{Ar}/^{39}\text{Ar}$  laser fusion dating on plagioclase crystals at  $21.20 \pm 0.50$  ( $2\sigma$ ) Ma and is now better constrained with a bulk mineral plagioclase age at  $21.71 \pm 0.38$  Ma ( $2\sigma$ ) and a preferred isochron age at  $21.88 \pm 0.32$  Ma (Montanari et al., Chapter C3). The latter is a minimum age for the Oligocene/Miocene boundary. The use of this point for interpolation to the boundary in the Contessa section is made difficult by the fact that the location of this boundary is different if one uses the biostratigraphic or the magnetostratigraphic control. Biostratigraphically, some biosignals such as the FO of *P. kugleri* (metre level 298), the FOs of *Sphenolithus delphix* and *S. capricornutus* at metre level 297 and the LO of *S. delphix* at metre level 299, should be found above (thus younger than) the boundary. These four signals are in similar sequence in the Carrosio–Lemme section and the boundary could then be located at about metre level 297. However, in terms of magnetostratigraphic control, the boundary is located within what is interpreted as Chron 6Cn in Carrosio–Lemme; the suspected corresponding interval is in between metre levels 300.5 and about 302 in Contessa. In the Contessa section, the boundary may thus be located either 6 m or 10 m below the dated level. An interpolation using the younger hypothesis leads Montanari and co-workers (Chapter C3) to suggest an age near 23.7 Ma; with the same procedure, the older correlation hypothesis would lead to an age at about 25.0 Ma. We can hardly reach a reliable and precise conclusion with the presently available data.

The new balance of evidence is either an age near and older than 22.4 according to the study from Bosio, or an age between 25 and 23 Ma according to the datings and sedimentological interpolation in Contessa. One result would suggest that the younger portion of the estimate by Odin (1994) would be more correct, the other would suggest that the older portion would be more correct. We thus propose to maintain the previous estimate as long as additional direct information will be provided. As a matter of fact, the problem lies more in the difficulty in using various correlation means to trace the chronostratigraphic boundary than to the geochronological measurements. They may also, in other circumstances, lead to poorly precise conclusions; the correlation at the Oligocene/Miocene boundary remains problematic.

*The Aquitanian/Burdigalian boundary* (Fig. 2). Our previous estimate of the numer-

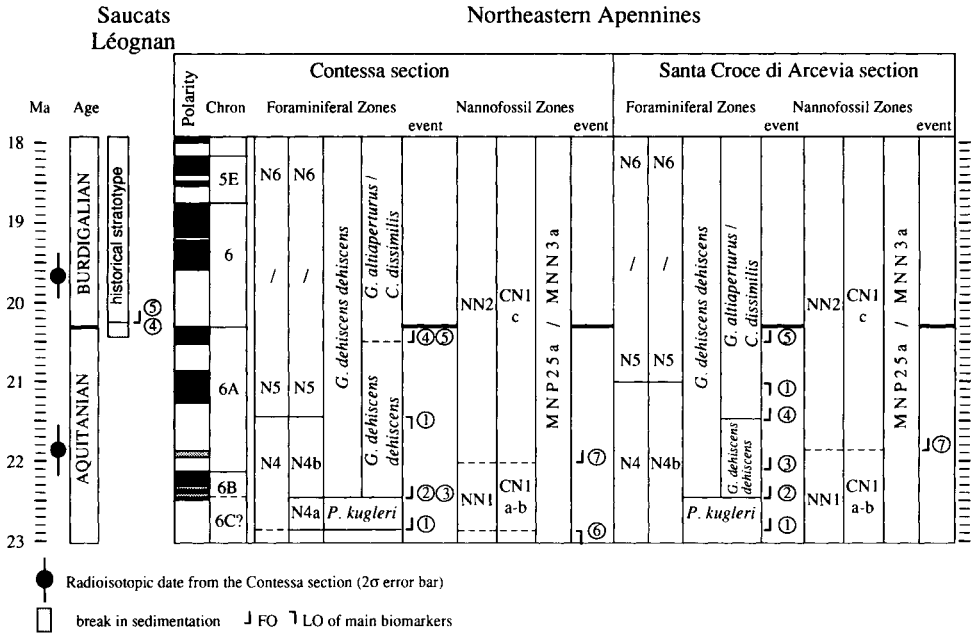


Fig. 2. The Aquitanian/Burdigalian boundary. Biostratigraphic information for the Saucats–Léognan historical stratotype are from Poignant et al. (Chapters A1 and A2). Calcareous plankton and magnetostratigraphy for the Contessa and Santa Croce di Arcevia sections are from Montanari et al. (Chapter C3), and Coccioni et al. (Chapter C4), respectively. Radioisotopic dates for the Contessa section are from Montanari et al. (Chapter C3). Main biostratigraphic markers (circled numbers) are: 1 = *P. kugleri*; 2 = *G. dehiscentis*; 3 = *G. immaturus*; 4 = '*G.* *altiaperturus*'; 5 = *G. trilobus*; 6 = *D. bisectus* (LCO); 7 = *D. aff. druggii*. The apparent diachrony of the sequence of main biomarkers between the two Apennine sections are probably due to hiatuses and/or strong condensation in the Contessa section (see Montanari et al., Chapter C3).

ical age of the Aquitanian/Burdigalian boundary is the interval between 19.8 and 20.8 Ma (Odin and Odin, 1990; Odin, 1994).

Geochronological calibration of the boundary may be additionally documented with the data obtained from the Contessa CT section presented by Montanari et al. (Chapter C3). The two volcanoclastic levels Raffaello ( $21.88 \pm 0.32$  Ma,  $2\sigma$ , at metre level 306.7), and CT-WAL (at metre level 310.5), most probably bracket the boundary. The latter level has been dated using plagioclase on single crystals at  $19.80 \pm 0.50$  ( $2\sigma$ ), and on bulk mineral leading to a plateau age at  $19.42 \pm 0.36$  with a corresponding isochron age of  $19.61 \pm 0.36$  Ma; the preferred age is a well documented weighted mean of the single crystal and the isochron ages at  $19.67 \pm 0.30$  Ma.

Derivation of the age of the Stage boundary has been deduced by Montanari et al. (Chapter C3) by estimating the interpolated age of the FOs of *Globigerinoides altiaperturus* and *Globigerinoides trilobus* which are contemporaneous in the Contessa section, and located at metre level 309.6. The resulting age is  $20.5 \pm 0.4$  Ma. It precisely concerns the level where the quoted biosignals are known in the dated section. These biosignals have commonly been used for approaching the location of the Stage boundary in geological sections. However, the precise point where the Burdigalian Stage begins

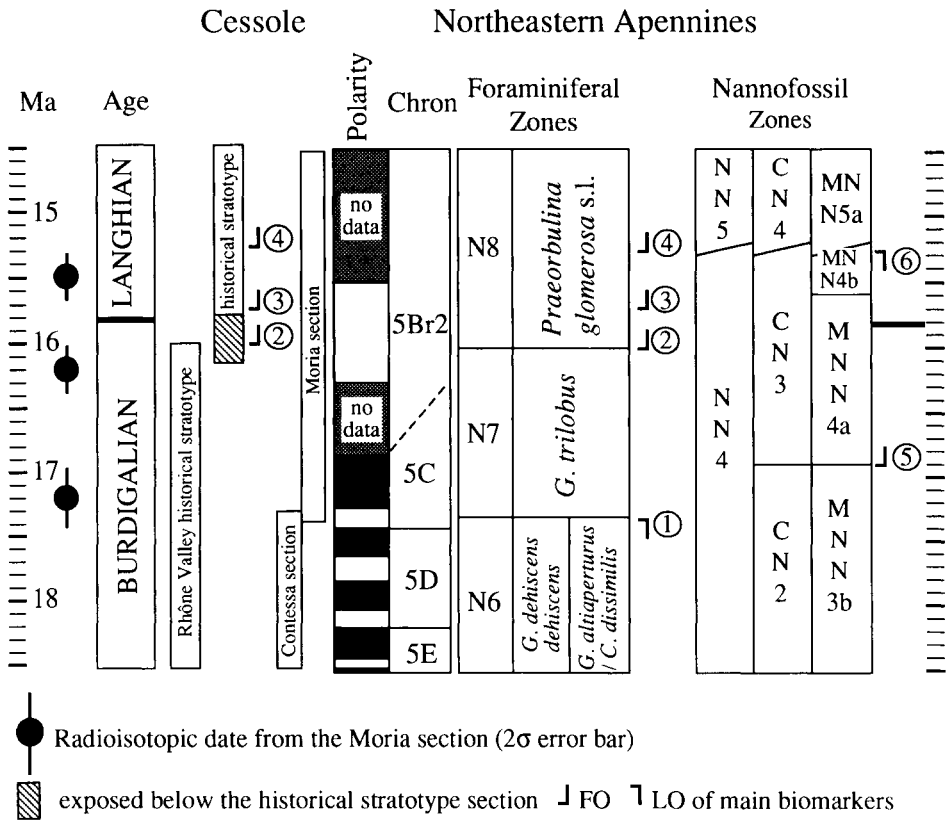


Fig. 3. The Burdigalian/Langhian boundary. Biostratigraphic information for the Cessole historical stratotype is from Rio et al. (Chapter A5) and Fornaciari et al. (Chapter A6). Magneto and biostratigraphic synthesis for the Contessa and Moria sections (northeastern Apennines) is derived from Montanari et al. (Chapter C3) and Deino et al. (Chapter D1), respectively. Radioisotopic dates are from Deino et al. (Chapter D1). Main biostratigraphic markers (circled numbers) are: 1 = *C. dissimilis*; 2 = *P. glomerosa sicana*; 3 = *P. glomerosa curva*; 4 = *P. glomerosa glomerosa*; 5 = *S. heteromorphus*; 6 = *H. ampliaptera*.

is still to be defined. The information available from the historical stratotype leads us to conclude that these FOs may coincide to a level located near yet below the base of the Burdigalian. The age at  $20.5 \pm 0.4$  Ma is thus an age most probably very near but slightly older than the base of the Burdigalian, as it is defined in the historical stratotype.

*The Burdigalian/Langhian boundary* (Fig. 3). Odin (1994) estimated the Burdigalian/Langhian boundary between 16.2 and 15.4 Ma. Direct additional geochronological information about this time interval has been obtained in a preliminary form from L'Annunziata section, and from two sandine-bearing volcanoclastic layers bracketing the interstage boundary in the Moria section.

From L'Annunziata, Montanari et al. (Chapter D2) have shown that the Langhian Michelangelo Level (not at the base and not at the top of the Stage in terms of foraminiferal biostratigraphic control) would be able to provide an age around 15.0 Ma. An age of about 15 to 15.5 Ma is typically given for the '*Orbulina datum*' in the

literature, and this datum (FO of the genus) refers to a well documented moment in the evolutionary trend of the phylum *Globigerinoides*–*Praeorbulina*–*Orbulina* which is actually within the Langhian Stage.

From Moria, Deino et al. (Chapter D1) have documented the interval of time comprising the Early/Middle Miocene boundary and the corresponding evolutionary lineage of *Praeorbulina*. The FOs of *P. glomerosa sicana* and *P. glomerosa curva* are bracketed between a sanidine age at  $16.18 \pm 0.16$  Ma ( $2\sigma$  intralaboratory error) below, and a sanidine age at  $15.50 \pm 0.16$  Ma above. The biotite from the Piero della Francesca Level is dated at  $17.08 \pm 0.18$  Ma at Berkeley, and  $17.24 \pm 0.30$  Ma (isochron age) and  $17.09 \pm 0.40$  Ma (isotope dilution,  $2\sigma$  interlaboratory) at Pisa, the weighted mean of these latter two results being  $17.20 \pm 0.24$  Ma according to us. These data are consistent with the above ones and allow calculation of mean rates of sedimentation. According to Deino et al., this set of data yields a tightly interpolated age of  $16.02 \pm 0.16$  ( $2\sigma$ ) for the FO of *P. glomerosa sicana*. This is a maximum age for the Early/Middle Miocene boundary. If we take into consideration the situation in the historical stratotype, where the boundary is located near the *P. glomerosa curva*, and above the FO of *P. glomerosa sicana* and, the age estimate for the boundary falls between 15.6 and 16.0 Ma.

*The Langhian/Serravallian boundary* (Fig. 4). Odin (1994) proposed to locate this boundary in the interval of time  $14.7 \pm 0.5$  Ma on the basis of geochronological data. New results were obtained from Sicily and the Cònero Riviera sequences.

In the Monte Giammoia section in Sicily, (Odin et al., Chapter D3), the geochronological age of biotite from sample T180 is proposed at  $13.6 \pm 0.5$  Ma ( $2\sigma$  interlaboratory). In this section, we assumed that the base of the Serravallian Stage may be approached by the first evolutionary appearance of *O. universa*. The first occurrence of this taxon in the Serravallian historical stratotype is recognizably below the base of the type section. It is also located immediately below the upper limit of the Langhian historical stratotype. The two type sections are therefore consistent; the first occurrence of *O. universa* appears to be the biostratigraphical criterion nearest to, yet older than, the Langhian/Serravallian boundary. It significantly predates the LO of *Globorotalia peripheroronda* in the Mediterranean. The latter biosignal has been recognized immediately above the dated layer in the Monte Giammoia section. Therefore, the biotite-rich layer belongs to the uppermost part of the *O. suturalis*–*G. peripheroronda* Zone (Iaccarino and Salvatorini, 1982), and to the upper part of Zone N9 on the basis of the proposed correlation. The correlative chronostratigraphic age is lower Serravallian. Therefore, the above quoted age of  $13.6 \pm 0.5$  Ma is a minimum age for the boundary.

In the Monte dei Corvi section on the Cònero Riviera, geochronological information has been obtained by Deino and Montanari (Montanari et al., Chapter D1) from the biotite-rich Respighi Level at metre level 101.35. The four isochron ages calculated are statistically consistent and allow calculation of a mean isochron age at  $12.94 \pm 0.16$  Ma ( $2\sigma$ , intralaboratory on the four dates). This age is in good sequence with the date from Monte Giammoia discussed above. It is reinforced by the age obtained from the Ancona Level located higher up in the same section at metre level 150 (11.43 Ma at metre level 149.86, see below).

In the Cònero Riviera sequence, the foraminiferal content allowed the following observations. The FO of *O. universa* is located in the covered interval between levels 41.10 m and 70.15 m. Above this covered interval, 14 m of section are attributed

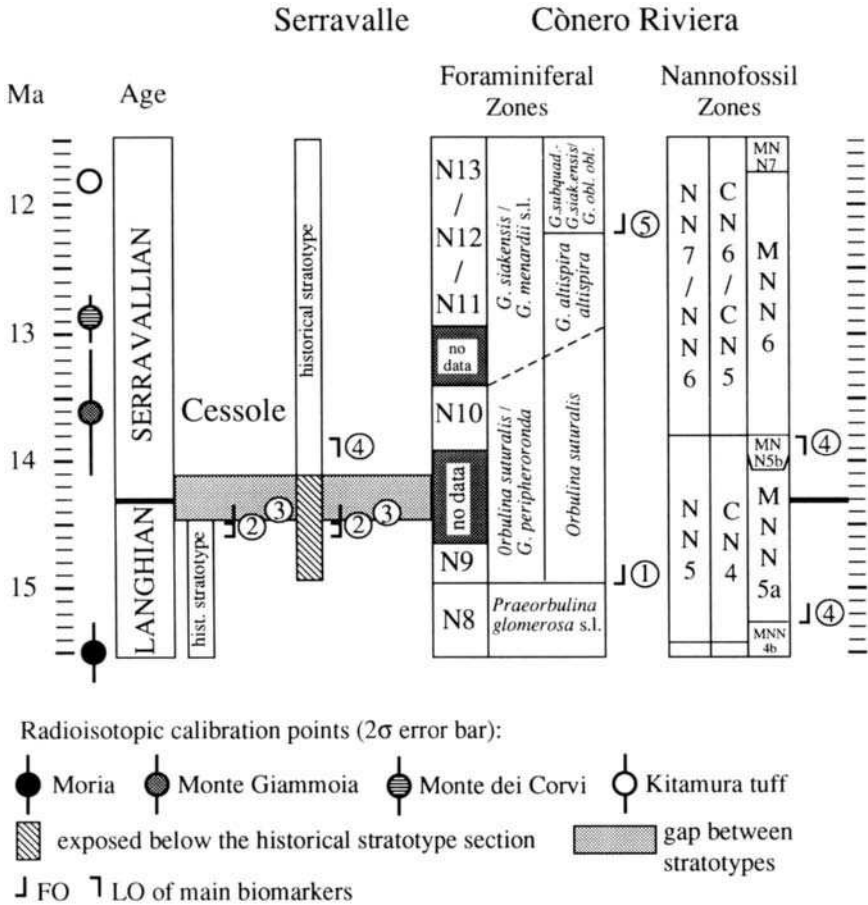


Fig. 4. The Langhian/Serravallian boundary. Biostratigraphic information for the Cessole and Serravalle historical stratotypes is from Rio et al. (Chapter A5). Biostratigraphic synthesis and radioisotopic date from the Cònero Riviera sequence are from Montanari et al. (Chapter E1). Radioisotopic dates from Moria, Monte Giammoia, and the Kitamura tuff are from Deino et al. (Chapter D1), Odin et al. (Chapter D3), and Takahashi and Saito (Chapter D6), respectively. Main biostratigraphic markers (circled numbers) are: 1 = *O. suturalis*; 2 = *O. universa*; 3 = *H. walbersdorfensis* (FCO); 4 = *S. heteromorphus* (LCO); 5 = *P. partimlabiata*.

to Zone N10 of Blow (1969). The Respighi Level is located immediately above the base of the Monte dei Corvi section at metre level 101.35 which, on the basis of the fossil assemblage, indicates Zone N11. The calcareous nannofossil record gives good independent information especially on the two taxa *H. walbersdorfensis* and *S. heteromorphus* (Fornaciari et al., in Montanari et al., Chapter D1). The LO of the latter is the first Serravallian biosignal known from slightly above (about 20 m) the base of the Serravallian stratotype section, and the FO of the former is the last biosignal seen in the topmost Langhian stratotype section. The observed common occurrence of the two taxa, between 71 and 77 m in the Cònero Riviera sequence, is therefore a good criterion

for correlating the Langhian/Serravallian boundary interval. In fact, it is worth noting that the available record above the covered interval shows a single sample without *H. walbersdorfensis* at the base of the younger portion of the section and it would be interesting to confirm in the future the actual FO of this taxon at this level, and not below, looking somewhere else along the Cònero Riviera as suggested by Montanari and co-authors in Chapter D1.

The location of the Langhian/Serravallian boundary in the Cònero Riviera sequence may be summarized as follows. In terms of calcareous nannofossil correlation, it is below 77 m and above 71 m — let us say for simplicity at level  $74 \pm 3$  m if the FO of *H. walbersdorfensis* may be confirmed (if not it would be within the covered interval below). In terms of foraminiferal correlation, it is located below level 71 m because we are yet in biozone N10 there, and above level 41 which is older than the FO of *O. universa*.

The two ages at 12.94 Ma and 11.43 Ma allow calculation of a 'mean rate of sedimentation'. An extrapolated age at 13.7 Ma is obtained for level 77.5 which is the location of the LO of *H. heteromorphus* in the section (in between the 2 samples with and without the taxon) and an age of 13.9 Ma for level 70.5 m which is the possible FO of *H. walbersdorfensis*. The foraminiferal recognition of the Langhian/Serravallian boundary would place it in the covered interval, the age of which may be estimated by extrapolation in between 13.9 and 14.8 Ma.

The minimum age of the Langhian/Serravallian boundary thus results at about 13.8 Ma and must be younger than 14.8 Ma according to data gathered in this volume (this may be written as  $14.3 \pm 0.5$ ). But the two extreme ages are known only approximately due to extrapolation procedures. It may be concluded that the previous estimate at  $14.7 \pm 0.5$  Ma for the boundary seems to need revision toward the younger side of the interval formerly proposed.

*The Serravallian/Tortonian boundary* (Fig. 5). According to Odin (1994), the interval of time  $11.0 \pm 0.3$  Ma derived from geochronological studies including those gathered in this volume, should include the age of the Stage boundary. Results have been obtained from the Cònero Riviera cliff and Japan.

Geochronological information has been obtained from two biotite-rich volcanoclastic layers in the Monte dei Corvi section: the Respighi Level ( $12.94 \pm 0.16$ , at metre level 101.35; see above), and the Ancona Level (metre level 149.85) by Deino and Montanari (in Montanari et al., Chapter E1). The biotite extracted from the latter shows two overlapping plateaux at  $11.52 \pm 0.18$  and  $11.35 \pm 0.16$  Ma ( $2\sigma$ ) the weighted mean of which is calculated at  $11.43 \pm 0.20$  Ma. In this sample, this mean age is preferable to the isochron age which, according to the authors, is poorly defined.

In Chapter D3, Odin and co-workers have independently dated a biotite extracted from another sample collected from the same level in the same Monte dei Corvi section. The spectrum of ages obtained from the biotite following step heating procedure, shows a 100% plateau and, for this reason, the total age, the plateau age, and the isochron age are similar at  $11.48 \pm 0.13$  Ma. This uncertainty is significantly increased to 0.4 Ma by adding the uncertainty in the age of the monitor used by Odin and co-workers. However, the good consistency between the results obtained in two different laboratories using different monitors suggests that the values accepted for the two monitors are consistent.

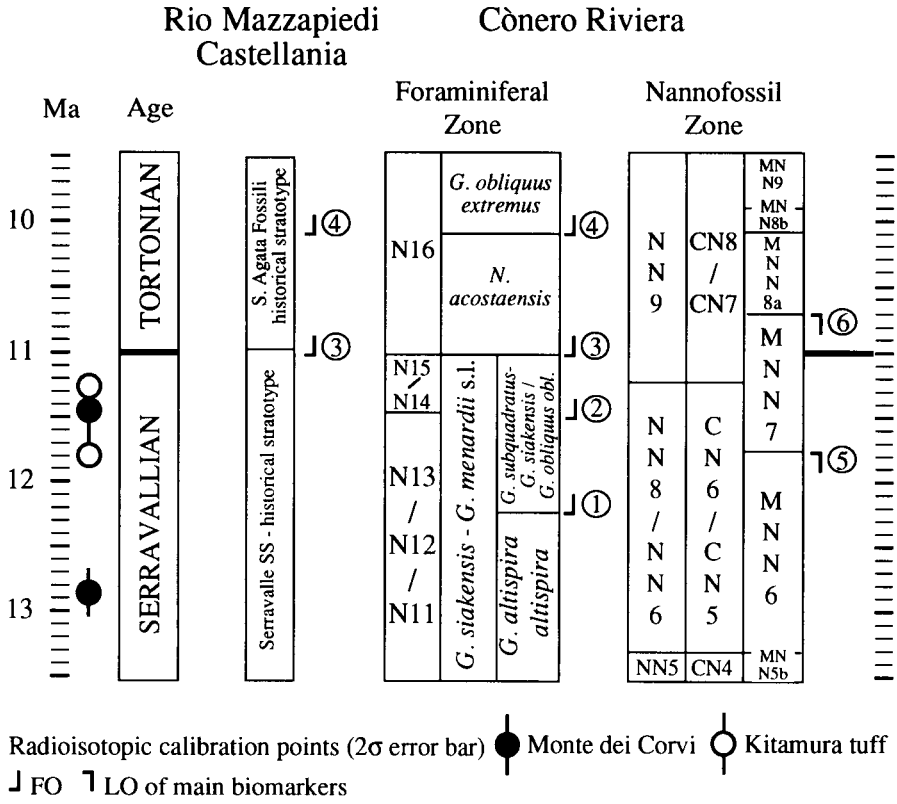


Fig. 5. The Serravallian/Tortonion boundary. Biostratigraphic information for the Serravallian and Tortonion historical stratotypes are from Rio et al. (Chapter A5). Biostratigraphic synthesis and radioisotopic dates from the Cònero Riviera sequence are from Montanari et al. (Chapter E1). Radioisotopic dates from the Kitamura tuff are from Takahashi and Saito (Chapter D6). Main biostratigraphic markers (circled numbers) are: 1 = *P. partimlabiata*; 2 = *G. nepenthes*; 3 = *N. acostaensis*; 4 = *G. obliquus extremus*; 5 = *C. premacintyreii* (LCO); 6 = *H. walbersdorfensis*.

In Japan, the geochronological study by Takahashi and Saito (Chapter D6) led the authors to document the age of the FO of *Globigerina nepenthes* in the Tomioka area with the analyses of two biotite-rich levels. One of them, the Kitamura tuff, is near and slightly below the biosignal; the other is far above. The Kitamura biotite has been dated at  $13.1 \pm 0.9$  Ma using the isotope dilution technique applied to biotite. The younger biotite yielded an age of  $11.6 \pm 0.9$  Ma. These two ages are the best information available from Japan where a number of other datings have been obtained from volcanoclastic samples collected in Serravallian sequences (Takahashi and Oda, Chapter B3).

The same two levels of the Tomioka sequence were submitted to a geochronological study by Odin and co-workers (Chapter D3). The age spectra obtained from several mineral phases following the step-heating procedure, show acceptable plateaux for biotite and sanidine. The biotite of the Kitamura tuff yields an age of  $11.79 \pm 0.08$  Ma ( $\pm 0.37$   $2\sigma$  intralaboratory). The biotite and sanidine ages of the other tuff give plateaux



ages of 11.26 Ma and 11.29 Ma, respectively. The deduced interpolated age for the FO of *G. nepenthes* in Japan is near 11.76 Ma.

The above information permits to calibrate biosignals versus numerical ages in widely separated areas. In the Cònero Riviera, the FO of *G. nepenthes* is located at metre level 148.51, very near the dated Ancona Level. This biosignal bears a strong potential for correlation because its chronologic significance is insured by the close LO of its presumed ancestral form *Zeaglobigerina druryi* which is located at metre level 149.9 in the Monte dei Corvi section. The FO of *N. acostaensis* is found at metre level 157.6. The calculated mean sedimentation rate of stratigraphic interval bracketed by the Respighi and Ancona levels (12.94 and 11.43 Ma, respectively) is about 32 m/Ma. Using this rate, the ages of the FO of *G. nepenthes* and of *N. acostaensis* in the Monte dei Corvi section can be estimated at 11.5 Ma, and extrapolated at 11.2 Ma, respectively, with an uncertainty of 0.2 Ma or slightly more if the deposition rate is assumed inconstant. Another calculation may be proposed using the age derived from direct geochronological datings of the FO of *G. conomiozea* (located at metre level 227 in the Cònero Riviera sequence). This age was estimated in the Faenza area at 7.26 Ma by Vai et al. (1993). It is documented again at 7.43 Ma by Odin et al. (Chapter E6), and close to 7.17 Ma by Laurenzi et al. (Chapter E5, recalculated with a value of 27.84 Ma for the monitor). In the Cònero Riviera sequence, the stratigraphic interval bracketed by a mean age of 7.29 Ma for the FO of *G. conomiozea* at metre level 227, and an age of 11.43 Ma for the Ancona Level, yields an average sedimentation rate of about 19 m/Ma. From this rate, the ages of the FOs of *G. nepenthes* and of *N. acostaensis* can be extrapolated at 11.5 Ma and interpolated at 11.0 Ma, respectively, with an uncertainty of about 0.2 Ma. Thus the two exercises lead to acceptably similar age estimates for these two important biosignals. From these data, it was concluded that the age of the FO of *G. nepenthes* is not demonstrably different in the two sections in Japan ( $11.75 \pm 0.40$ ) and Italy ( $11.5 \pm 0.2$ ). These ought to be considered as maximum ages for the Serravallian/Tortonian boundary because the FO of *G. nepenthes* is known to be slightly older than the Stage boundary in the historical stratotype. Concerning the FO of *N. acostaensis*, this biosignal has been shown to be latest Serravallian in age in the historical stratotype of Tortona. Its estimated age in the Cònero Riviera sequence (either 11.0 or  $11.2 \pm 0.2$  Ma, depending on the assumed sedimentation rate) is thus a maximum but very near age for the Stage boundary, and it is in agreement with the estimate proposed by Odin in 1994.

*The Tortonian/Messinian boundary* (Fig. 6). The direct geochronological documentation of the Tortonian/Messinian boundary has done significant progress during the past 4 years. According to Odin (1994), the interval of time between 6.8 and 7.4 Ma derived from geochronological studies, including a portion of those presented in this volume, should include the age of the Stage boundary with a mean value of 7.1 Ma. The improvement of a previous younger estimate at 6.5 Ma (Odin and Odin, 1990) was strongly influenced by new geochronological studies in the Apennines pioneered by Vai et al. (1993) who dated late Tortonian volcanoclastic layers discovered in the marine pelagic sequence extensively exposed in the Faenza area (Romagna region of Italy). Three biotite-rich layers bracketing the late Tortonian FO of planktonic foraminifer *G. suterae* led to a weighted mean age of  $7.72 \pm 0.30$  Ma ( $2\sigma$ ). The best preserved biotite

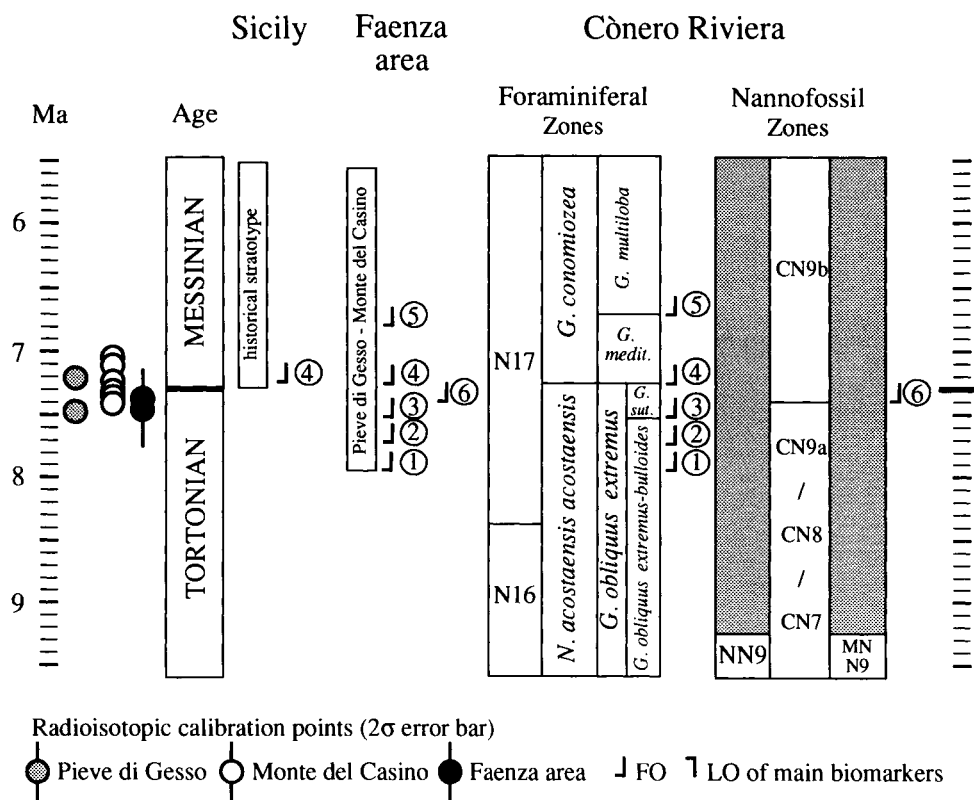


Fig. 6. The Tortonian/Messinian boundary. Biostratigraphic information for the Messinian historical stratotype is from Colalongo and Pasini (Chapter A8). Biostratigraphic information and radioisotopic dates for the Faenza area are from Vai (Chapter E3) and Negri and Vigliotti (Chapter E4). Biostratigraphic information for the Cònero Riviera sequence is from Montanari et al. (Chapter E1). Radioisotopic dates for the Pieve di Gesso and Monte del Casino sections are from Odin et al. (Chapter E6), and Laurenzi et al. (Chapter E5), respectively. Main biostratigraphic markers (circled numbers) are: 1 = *P. continua*; 2 = *N. humerosa*; 3 = *G. sutur.*; 4 = *G. conomiozea*; 5 = *G. multiloba*; 6 = *Amaurolithus* spp.

extracted from a younger level bracketed by the latest Tortonian FO of *Globorotalia saheliana* and the earliest Messinian contemporaneous FOs of *G. conomiozea* and *G. mediterranea* led to an age of  $7.37 \pm 0.13$  Ma.

Additional results on coeval volcanoclastic levels are presented in this volume from another outcrop: the Pieve di Gesso section (Odin et al., Chapter E2). Biotite ages of  $7.47 \pm 0.28$  ( $2\sigma$  intralaboratory; poor plateau) and  $7.37 \pm 0.36$  Ma (good plateau) were obtained for layers located above the FOs of *G. suterae*, and calcareous nannofossils belonging to the *Amaurolithus* group, and below the FO of *G. conomiozea*.

Laurenzi et al. (Chapter E5) have supplemented the data from the Faenza area. The sequence of dated volcanoclastic layers and biosignals is as follows: FO *G. suterae*, MdC 101, FO *Amaurolithus* group, MdC 102, FO *G. saheliana*, MdC 105, MdC 106, MT 31 immediately below the FO of *G. conomiozea*, and MdC 107 (4 m above the latter). These six dated biotite separates led to ages as follows: MdC 101 isochron  $7.32 \pm 0.08$

Ma (intralaboratory analytical uncertainty:  $2\sigma$  monitor FCT bio taken as 27.84 Ma), MdC 102 isochron  $7.34 \pm 0.08$  Ma, MdC 105 isochron  $7.40 \pm 0.12$  Ma, MdC 106 plateau  $7.35 \pm 0.08$  Ma and isochron  $7.31 \pm 0.38$  Ma, MT 31 plateau  $7.22 \pm 0.08$  Ma and isochron:  $7.18 \pm 0.08$  Ma, MdC 107 isochron  $7.09 \pm 0.08$  Ma. The first two biotite separates yielded ages much younger than the corresponding levels dated in Vai et al. (1993), and this has no explanation in the study. However, the last four levels display ages consistent with previous dates, and are reasonably ordered internally.

An additional study has been undertaken on the two best biotite samples extracted from the volcanoclastic levels located in the immediate vicinity of the Stage boundary in the Faenza area by Odin et al. (Chapter E6). The analytical ages of the early Messinian biotite B174 (Monte del Casino = MdC 107 of Laurenzi et al., Chapter E5) and the latest Tortonian biotite B189 (Monte Tondo = MT 31) are precisely measured at  $7.20 \pm 0.06$  Ma and  $7.44 \pm 0.04$  Ma ( $2\sigma$  intralaboratory analytical uncertainty on plateau ages), respectively.

The biostratigraphic characterization of the sediments containing the Tortonian/Messinian boundary is well documented. As emphasized by Negri (in Odin et al., Chapter E6), the biostratigraphic control near the Tortonian/Messinian boundary comprises a series of biosignals which, in the Mediterranean domain, are found in the following order: FO *Neogloboquadrina humerosa*, FO *G. suteræ*, FO *Amaurolithus* group, and finally FO *G. conomiozea*. A similar order is found in other areas such as: (1) the Faenza area where the biosignal FO of *G. saheliana* is observed between the FO of *Amaurolithus* group and the FO of *G. conomiozea* (Vai, Chapter E3); (2) the La Sardella section of the Cònero Riviera by Coccioni (in Montanari et al., Chapter E1): FO *N. humerosa*, FO *G. suteræ*, FO *G. saheliana*, then FO *G. conomiozea* and *G. mediterranea*; and (3) the Sicilian Falconara section described by Colalongo and Pasini in Chapter A8: FO *N. humerosa*, FO *G. suteræ*, FO *Amaurolithus primus*, FO of *A. delicatus*, and then FO *G. conomiozea* and *G. mediterranea*. The chronologic significance of these data is well documented by their good reproducibility. Colalongo and Pasini (Chapter A8) emphasize the fact that the beginning of the 'salinity crisis' of Selli, and thus the present definition of the base of the Messinian Stage, is located 2 m below the FO of *G. conomiozea*. Therefore, the documentation with directly measured numerical ages of this key biosignal observed in Italian sections, allows to closely approach — although slightly on the younger side — the age of the Stage boundary.

The age data gathered may be summarized as follows. The data by Vai et al. (1993) led these authors to propose a slightly extrapolated age (by sedimentation rate calculation) of  $7.26 \pm 0.20$  Ma for the FO of *G. conomiozea* in the two dated sections (Monte Tondo and Monte del Casino). At Pieve di Gesso, the two biotite ages of  $7.47 \pm 0.28$  and  $7.37 \pm 0.36$  Ma are maximum ages for the same biosignal which is probably located above the studied outcrop. Using the data produced by Laurenzi and co-workers, the FO of *G. conomiozea* can be tightly interpolated between the ages bracketing the biosignal at  $7.2 \pm 0.1$  Ma ( $2\sigma$  intralaboratory analytical uncertainty; monitor age at 27.84 Ma). The two ages of 7.44 and 7.20 Ma obtained by Odin and coworkers (Chapter E6) are in correct stratigraphic sequence. If the common biosignal FO of *G. conomiozea* is contemporaneous in the two separately dated sections of Monte Tondo and Monte del Casino, the vertical distance between the two samples is about 5 m. The mean accumulation rate in the area is estimated between 20 and

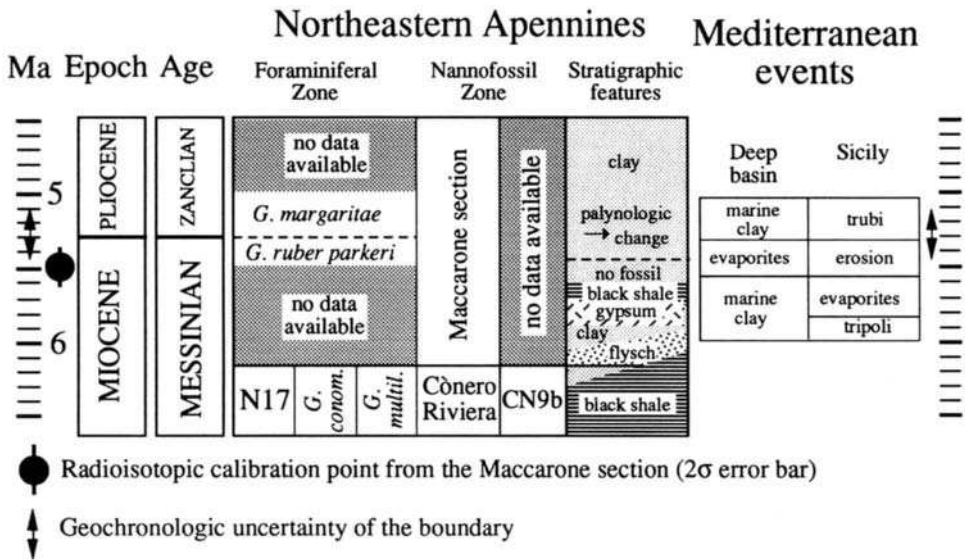


Fig. 7. The Miocene/Pliocene (Messinian/Zanclian) boundary. Bio- and lithostratigraphic synthesis of the Cònero Riviera and Maccarone sections are from Montanari et al. (Chapter E1) and Odin et al. (Chapter E7), respectively. Synthesis of Mediterranean events is from Suc et al. (Chapter A10).

30 m/Ma (according to Vai, Chapter E3, the pre-gypsum Messinian would represent about 1 Ma); a rate comprised between 23 and 62 m/Ma is also derived by Laurenzi and co-workers (Chapter E5). The analytical age difference of about 0.25 Ma is fully consistent with the 5 m distance using Vai's rate. On the other hand, the two ages obtained during the same irradiation and using similar other analytical conventions, lead to a calculated sedimentation rate of about 25 m/Ma between the two samples. The FO of *G. conomiozea* (30 cm above sample B189) should be only 10 ka younger than the measured age of 7.44 Ma, resulting in an age of  $7.43 \pm 0.04$  Ma ( $2\sigma$  intralaboratory) Ma for this biosignal. For comparison with other laboratories, the uncertainty on the age of the monitor (known to be  $\pm 2.6\%$ ) should be added. Therefore, the age of the FO of *G. conomiozea* is  $7.43 \pm 0.23$  Ma in the Faenza area according to this study. This is consistent with the slightly extrapolated age of  $7.26 \pm 0.20$  Ma proposed by Vai et al. (1993).

*The Messinian/Zanclian (Miocene/Pliocene) boundary* (Fig. 7). The name of the first Pliocene Stage comes from an Italian locality 'Zancla', which is an ancient name of the city of Messina. Seguenza (1869) created the word 'Zancléen' (in French) following the study of sediments in the Sicilian area, and in other Italian regions. This derivation is unusual given the fact that, at that time, a common suffix for Stage names was already accepted as '... ian', like Burdigala → Burdigalian, Tortona → Tortonian, and so on. Therefore, we propose to normalize also this global Stage name to *Zanclian* which appears more rigorous to one of us.

According to Odin (1994), the age of the boundary may be estimated at about 5.3 Ma but little direct geochronological evidence was available then. One age was taken

from the pioneering work of H. Bellon (results from his 1976 Ph.D. thesis presented in 1977) where he proposed a Miocene/Pliocene boundary age at  $5.3 \pm 0.2$  Ma based on K–Ar whole-rock dates from Morocco. Indirect climatostratigraphic dating (Earth orbital hypothesis) in the Mediterranean domain was proposed by Hilgen (1991) who applied the sedimentary cycle counting procedure to the Capo Rossello sections in southern Sicily. He found that the base of Trubi Marls, which corresponds to the Miocene/Pliocene boundary historical definition, should be placed at about  $5.32$  Ma<sub>e</sub>. (subscript 'e.' = estimate) without error bar.

The late Messinian section in Maccarone (Marche region of Italy) contains a volcanoclastic tuff from which several biotite separates were dated using the  $^{40}\text{Ar}/^{39}\text{Ar}$  technique. The step-heating procedure yielded age spectra indicating precise ages between 5.36 and 5.56 Ma. Sub-plateau and plateau ages are at 5.44 and 5.51 Ma ( $\pm 0.04$  Ma,  $2\sigma$  intralaboratory), and are not significantly different from total gas ages (5.39 and  $5.50 \pm 0.07$  Ma). Taking into account the uncertainty on the age of the monitor, the mean age of the Maccarone tuff may be proposed at  $5.47 \pm 0.17$  Ma.

The chronostratigraphic location of the dated level is mainly based on lithostratigraphic relationships but this procedure is reliable in this site where the depositional environment is directly related to the area from where the unit definitions are taken. According to the regional model, the dated layer is located in a late portion of the Messinian Stage, above the gypsum depositional episode but not at the topmost of the Messinian series. Therefore, the Miocene/Pliocene boundary has to be slightly younger than 5.5 Ma on direct geochronological data, and the estimate at  $5.30 \pm 0.15$  Ma would be acceptable in the light of our present geochronological knowledge.

### *Duration of Miocene Stages*

In contrast to the search for numerical ages of stratigraphic moments, the duration of deposition of rock bodies characterized between significant stratigraphic signals may be undertaken using a variety of tools in addition to straightforward geochronological characterization. The magnetokilometric extrapolation procedure across the ocean floors is one possibility. However, the actual connection between the known oceanic record and the definition of Stages is poorly documented by magnetostratigraphic studies, especially for the Miocene interval. In this situation, the necessity of using a long-distance biostratigraphic intermediate correlation tool does not lead to precise estimates due to potential diachronism of biosignals. More confidence may be given, in some cases, to climatostratigraphy or sedimentary cyclicity related to orbital constants, at least for the younger Stage of the Miocene Epoch.

Our present work has been focused on geochronological calibration which may lead to precise information at least when the question of the calibration of the K/Ar dating method using the irradiation technique may be turned by calibrating both limits of a Stage during a single series of measurements (Table 1).

The base of the Aquitanian Stage is documented in this volume by somewhat inconsistent or unclear bio- and magnetostratigraphic characterizations with a resulting age probably located in the interval  $23.0 \pm 0.5$  Ma. Other results indicate an age as old as 24 Ma. For the top boundary of this Stage, the new data obtained from the Contessa section are consistent with a previous estimate at  $20.3 \pm 0.5$  Ma: the interpolated age

Table 1

Proposal for the numerical time scale of the Miocene Epoch according to geochronological data (in Ma)

Miocene Epoch	Palmer (1981)	Harland et al. (1990)	Odin and Odin (1990)	Odin (1994)	This work
Messinian	5.3 (1.2)	5.2 ± 0.2 1.5	5.3 (1.2)	5.3 (1.8)	5.30 ± 0.15 (6) (2.0)
	6.5 (4.7)	6.7 ± 0.3 (3.7)	~6.5 (4.5)	7.1 ± 0.3 (3.9)	7.30 ± 0.15 (5) (3.7)
Tortonian	11.2 (3.9)	10.4 ± 0.1 (3.8)	~11 (3.5)	11.0 ± 0.3 (3.7)	11.0 ± 0.3 (4) (3.3)
	15.1 (1.5)	14.2 ± 0.3 (2.1)	14.5 ± 0.5 (1.5)	14.7 ± 0.5 (1.1)	14.3 ± 0.5 (3) (1.5)
Langhian	16.6 (5.2)	16.3 ± 0.2 (5.2)	~16 (4)	15.8 ± 0.4 (4.5)	15.8 ± 0.2 (2) (4.5)
	21.8 (1.9)	21.5 ± 0.2 (1.8)	~20 (3.5)	20.3 ± 0.5 (3.2)	20.3 ± 0.4 (1) (3?)
Aquitanian	23.7	23.3 ± 0.1	23.5 <sup>+0.5</sup> <sub>-1.0</sub>	23.0 ± 0.5	22.5 to 24.5

Approximate Stage durations in brackets. The major change documented during the past years concerns the Tortonian/Messinian boundary which is significantly older than thought before according to tuff levels dated from the Apennines. The Oligocene/Miocene is the least clearly documented boundary.

(1) slightly above FO of *G. altiapertura* and *G. trilobus*; (2) significantly above FO of *P. sicana* (base of biozone N8); significantly below LO of *H. ampliaptera*; (3) between the FCO of *H. walbersdorfensis* and the LO of *S. heteromorphus*: within the top of biozone NN5; above the FO of *O. universa*: within biozone N9; (4) slightly above the FO of *N. acostaensis*; (5) slightly below the FO of *G. conomiozea* and *G. mediterranea*; (6) in correspondence with the Mio–Pliocene sea-level rise and relevant shift in O isotope ratio in Mediterranean.

at 20.5 ± 0.4 Ma is most probably very near, and slightly older than the base of the Burdigalian as defined in the historical stratotype. The duration of the Stage results longer than 2.5 Ma and may be up to 3.5 Ma, a mean duration among the Miocene Stages.

The Burdigalian Stage has been convincingly documented in this volume between slightly less than 20.5 Ma (±0.4), and about 15.8 Ma (±0.3, 2σ interlaboratory). These ages, obtained in similar analytical conditions, determine a well constrained duration of 4.5 to 5.0 Ma.

The younger boundary of the Langhian Stage is constrained in the Cònero Riviera sequence. The newly documented age between 14.8 and 13.8 Ma is generally younger than what we estimated previously (14.7 ± 0.5). It may be located in the interval 14.3 ± 0.5 Ma with still good potential for improvement. Taking into account the mean face values at 15.8 and 14.3 Ma, the duration of the Stage would be of about 1.5 Ma. The geochronologic data presented in this volume are sufficiently precise for confidently confirm that the Langhian Stage is the shortest Miocene unit.

The Serravallian unit ends slightly after the FO of *N. acostaensis* which, in the Cònero Riviera sequence is dated between 11.0 and 11.2 Ma (±0.3, 2σ interlaboratory). This age is derived consistently from data obtained in two laboratories. It is consistent with our previous estimate at 11.0 ± 0.3 Ma for the boundary, and the duration of the Stage results comprised between 3.0 and 3.5 Ma.

The age of the upper boundary of the Tortonian Stage has been documented by four separate studies connected to consistent biostratigraphical control in Italy. The FO of *G. conomiozea*, which is located slightly above the limit of the historical stratotype, is estimated at: (1)  $7.26 \pm 0.20$  Ma (Vai et al., 1993); (2) younger than 7.37 and 7.47 Ma ( $\pm 0.30$ , Odin et al., Chapter E2); (3)  $7.2 \pm 0.1$  Ma (Laurenzi et al., Chapter E5); and (4)  $7.43 \pm 0.23$  Ma (Odin et al., Chapter E6). A well documented compromise age may be proposed at  $7.30 \pm 0.15$  Ma. The Tortonian Stage is thus approximately 3.7 Ma long.

The Messinian Stage, located between geochronological ages of  $7.30 \pm 0.15$  and  $5.30 \pm 0.15$  Ma is about 2 Ma long. This geochronologically derived duration is consistent with the opinion of experts in climatostratigraphy who, on the basis of the magnetostratigraphic record, now consider a Stage duration of about 1.8 Ma (see for example Krijgsman et al., 1994). The use of the latter procedure is sometimes made difficult by the presence of very diversified facies in the Mediterranean area, and the fact, emphasized by Vai (Chapter E3), that sedimentary 'cycles' may represent either the period of 20 or 40 ka in the deposits of this particular interval.

The above conclusions need to be considered in the light of the fact that, outside the Mediterranean domain, the use of Miocene Stage names is commonly poorly followed. For example, it is very rare to find these chronostratigraphic units related to sections described from areas around the Pacific. This is not due to the absence of common (bio)stratigraphic control but probably to the fact that the subdivision is locally too thin.

#### *Calibration of the continental Miocene*

*Agenian/Aragonian limit (intermediate Ramblian Spanish stage within the Burdigalian).* Odin et al. (Chapter C5) documented the age of the Ramblian — a Spanish mammal stage — at its lower boundary common with the underlying Agenian mammal stage. The study led to the following most relevant conclusions: (1) The Agenian/Ramblian boundary identified within mammal Zone MN2b, formerly located somewhere within the Aquitanian Stage, is  $19.3 \pm 0.2$  Ma (sanidine plateau age), and should preferably be shown within the lower Burdigalian; (2) the so-called Ramblian mammal stage is probably very short; its geological usefulness is questioned, and it might be incorporated as a regional substage into the overlying Aragonian Spanish mammal stage; (3) if the coincidence between the Spanish mammal stages and the 'European' Agenian and Orleanian mammal stages is correct, the Agenian/Orleanian stage boundary needs to be better shown within the Burdigalian than at the Aquitanian/Burdigalian boundary as proposed previously (i.e., Steininger et al., 1985).

*Late Vallesian (contemporaneous with mid-Tortonian).* Anadon et al., (1995) published a geochronological study on a 1 cm thick volcanoclastic layer lying within a mammal-bearing lacustrine sequence of eastern Spain (Bicorp Basin, to the north of the area studied by Montenat and Serrano in Chapter E8). This layer is located 19 m above a level with mammal remains and is therefore younger than the fauna 'which may be attributed to the late Vallesian' or mammal biozone MN10. The mineral separates dated are composed of sanidine-anorthoclase (a K-feldspar with noticeable amounts of Na; their K contents range between 4.9% and 5.4%. K/Ar dating using the isotope dilution technique leads the authors to derive an age of  $9.6 \pm 0.2$  Ma ( $2\sigma$ ). This age is consistent with a mid-Tortonian age as calibrated in this volume.

*Late Turolian (Messinian)*. Still in Spain, Montenat and Serrano (Chapter E8) point out that in the Eastern Betic domain, fossils of mammal Zone MN13 found between Librilla and Barqueros (about 20 km WSW of Murcia) within the upper Turolian mammal stage, are underlain by dated Messinian volcanics although they would need further, more detailed geochronological and stratigraphical studies. Another interesting feature of this area is the close presence of marine fossiliferous deposits. Finally, an additional relevant environmental aspect is the presence of evaporitic deposits indicating that gypsum is locally forming already during Tortonian time in the Mediterranean domain.

In short, there are promising sections in Spain for inter-calibration of continental and marine biostratigraphic records, and geochronological calibration of both.

#### POTENTIAL SECTIONS FOR LOCATING STRATOTYPES (GSSP)

As emphasized in the introduction to Part A of this volume, a major contribution to progress in stratigraphy can be obtained by careful definition of boundaries between Stages defined in their historical stratotype. During the search for integrating biostratigraphical and geochronological information in the sections studied in this volume, we have considered for each of them their possible use for definition of Stage boundaries using the concept of GSSP.

In the next paragraph, we review the sections for possibly locating a GSSP, as well as those preferably relevant for use as auxiliary sections. The need for auxiliary section(s) often emerged in recent attempts for proposing GSSPs. Designation of auxiliary sections may solve different kinds of problems. The first is the diversity of stratigraphical tools able to characterize an instant in the geological history; it is too wide for a single section to include all useful criteria. In addition, the factor of provincialism may be better constrained when using the now accepted concept of auxiliary section.

We remember shortly the current knowledge, advantages, and problems, and suggest the additional studies to be undertaken following the recommendation summarized in the introduction to Part A of this volume. The precise location of a possible GSSP is discussed when relevant.

#### *Aquitanian/Burdigalian boundary*

At Contessa, near Gubbio, Montanari et al. (Chapter C3) point to an easy access to the outcrop containing the transition between the Oligocene and the Miocene. The marine character of the deposits responds to the requirement for the placement of a GSSP. No major faults are visible in this section, and although the lithology is differentiated (alternation of marls and siliceous limestones) the overall sedimentary facies throughout the section can be considered homogeneous. However, the preservation of this section may be problematic in the still active quarry face. Moreover, the interval across the Oligocene/Miocene boundary seems to contain significant paracomformable hiatuses, and the lower portion of the Burdigalian is strongly condensed, preventing the use of this outcrop for locating the GSSP. This is particularly lamentable because the section has given significant information from the four biostratigraphic, chemostratigraphic, magnetostratigraphic, and geochronological points of view.



At Santa Croce di Arcevia, Coccioni et al. (Chapter C4) emphasize the problem of accessibility to this section which is located in a private home backyard. This limitation, together with the fact that it will be difficult to preserve the section and place a permanent marker in it, is sufficient to prevent placement of the GSSP. This situation may eventually be improved if an equivalent section could be cleaned and studied in the same hill. The open-marine character of the sediments is well documented and the stratigraphic record seems continuous and complete. Tectonic disturbances are moderate, and the overall sedimentary facies does not change throughout the exposure although lithology is diversified. Biostratigraphy has been successfully applied using planktonic Foraminifera, calcareous nannofossils, and dinoflagellate cysts. Magnetostratigraphy is not applicable due to weakness of the (probably altered) magnetic carrier. Chemostratigraphy still remains to be explored, and applicability of geochronology is probably possible. In short, a favourable sedimentary sequence is present in this site which has strong potentials for further studies. To be consistent with the historical stratotypes of the Aquitaine basin, the boundary is to be placed in the lower marly member of Coccioni et al. (Chapter C4), near metre level 18. This level is characterized by the presence of both *G. altiapertura* and *G. trilobus*, is located slightly above their FOs, and corresponds to the lower portion of biozone N5 of Blow (1969).

The Ponte delle Lepri section, near Bologna, has been preliminarily investigated by Odin et al. (Chapter C2). Accessibility and permanency of the outcrop along the Torrente Olivetta are as good as possible. The open-marine character is documented by the rich microfauna including planktonic and benthonic Foraminifera, and some radiolarians. The continuous deposition and relative thickness of the deposits is favourable for a high stratigraphic resolution, and the sequence analysis has been investigated. Tectonic disturbances are negligible, and the sedimentary facies is homogeneous. Biostratigraphy has been documented in a preliminary study. Chemostratigraphy remains to be investigated on calcareous and phosphatic remains. The magnetostratigraphic potential is not yet documented. Applicability of geochronology has been verified, and may be extended to several not yet studied tuff layers. In short, this section has a great potential for the definition of the GSSP for the Aquitanian/Burdigalian boundary.

#### *Lower Miocene/Middle Miocene boundary*

The Moria section is easily accessible along a paved mountain road. Preservation of this exposure may be endangered, in the future, mainly due to the softness of marly layers which tend to be eroded and recessed. Sampling will have to be performed carefully in order to prevent rocks and boulders from falling on the roadway. The facies is homogeneous although lithology is diverse, deposition appears continuous, and the section is sufficiently thick for high-resolution stratigraphic studies. Despite the nearly vertical bedding attitude, tectonic disturbances are negligible. Abundant and diversified foraminiferal assemblages and nannofossils ensure detailed biostratigraphic correlation. Elementary and isotopic chemostratigraphy has been applied successfully, and shows interesting features in the vicinity of the boundary although they may reflect regional rather than global marine palaeoenvironmental conditions. Magnetostratigraphy has been partly successful, and the section is moderately favourable for this tool. The presence of fresh sanidine-bearing volcanoclastic layers tightly bracketing this interstage

boundary permitted precise and accurate direct radioisotopic dating of the boundary. In short, the Moria section responds to most of the requirements for an candidate GSSP for the Lower Miocene/Middle Miocene boundary.

In order to be consistent with the historical stratotype sections of both the Burdigalian and the Langhian, the level where to place the GSSP must be selected in the upper portion of the siliceous–calcareous member of the Schlier formation, within the evolutionary lineage of *Praeorbulina* which, in the Moria section, is found at about metre level 70. This boundary falls within a reverse magnetic polarity interval interpreted by Deino and co-workers (Chapter D1) as Chron 5Br2.

Search for equivalent (possibly auxiliary) sections might be fruitful in Spain in the Rambla de Granadilla and Torre del Peñon sections (Montenat et al., Chapter D4), and possibly in the Cònero Riviera sequence.

#### *Langhian/Serravallian (Mediterranean-based substages)*

The High Cliff of the Monte dei Corvi section in the Cònero Riviera (Montanari et al., Chapter E1) may be considered for the search of the GSSP for this boundary. The section is accessible with some effort. The cliff is fairly stable and in the future its access may be made easier, and preservation insured, by the intervention of the Administration of the Cònero Regional Park. The marine character of the sediments is well documented with planktonic micro- and nannofossils. The continuous hemipelagic deposition characterized by a rhythmic alternation of more or less marly limestones, virtually devoid of siliciclastic sediments, insure a continuous and precise record of the evolution of the deep-marine palaeoenvironment. The sedimentary facies does not change throughout the section although the lithology is diverse. The preservation of the palaeontologic record is fair and not seriously affected by tectonic disturbances or diagenesis. Applicability of biostratigraphy is therefore possible with commonly abundant forms; fossil preservation ranges from good, to moderate, to poor. Magnetostratigraphy and Chemostratigraphy have not been applied yet.

A biotite-rich layer in the lower Serravallian has been dated successfully by  $^{40}\text{Ar}/^{39}\text{Ar}$  incremental heating technique, and a recently discovered biotite-rich volcaniclastic in the upper Langhian promotes further geochronologic study which may lead to a precise and accurate interpolated age assignment to this boundary.

In order to be consistent with the Langhian and Serravallian historical stratotype sections, the level where to place the GSSP can be found as a function of several correlation criteria, many of which are common in the sections of the Marche region and the historical stratotypes. Among others, the LO of calcareous nannofossil *S. heteromorphus* is well documented in the lowermost Serravallian, and must be kept slightly above the GSSP. A rough idea of the time separation between the biosignal and the GSSP may be inferred from the sedimentary thickness observed in the Serravalle Formation: this nannofossil bioevent can be estimated to be about 0.15 Ma younger than the base of the Serravallian stratotype. According to the calcareous nannofossil record, the GSSP should be placed somewhere within the stratigraphic interval between metre levels 71 and 77 of the High Cliff section of the Cònero Riviera. However, on the basis of planktonic foraminiferal stratigraphy, an older level should be preferred with the largest portion of the *O. universa* Zone pertaining to the Serravallian, and the FO of this

taxon being taken as correlating into the late Langhian. In this case, the boundary should probably be located within the covered interval between 41 m and 70 m in this particular section. Other exposures along the Cònero Riviera cliffs (see Montanari et al., Chapter E1) may be more favourable for documenting more completely the succession of events and for a better integration of biostratigraphic data from both sides of the boundary.

Other possibilities for documenting the Langhian/Serravallian boundary could be considered in Japan. In the Tomioka area, the Niwaya Formation is a thick sedimentary series where both planktonic Foraminifera and calcareous nannofossils (Takahashi and Oda, Chapter D5) would allow a correlation with the historical stratotypes, and place a level consistent to that of the GSSP in Italy. Similarly, the Boso Peninsula (Kinone Formation) contains good biostratigraphic and sedimentologic records allowing integrated stratigraphy to be applied (Takahashi et al., Chapter E8). Japanese sections may be used preferably as practical auxiliary sections because their permanency is not insured due to the rather rapid alteration of the outcrops.

#### *Serravallian/Tortonian (Middle Miocene/Upper Miocene)*

The Cònero Riviera is the most promising area for proposing a GSSP for the Middle Miocene/Upper Miocene boundary. The Monte dei Corvi section is recommended by Montanari et al. (Chapter E1). The access to the base of the cliff is fairly easy through a trail periodically maintained by local fishermen. A reasonable preservation could be favoured by locating the GSSP high enough in the cliff to avoid erosion by the sea. Other sedimentological criteria are similar to those discussed above for the nearby, and stratigraphically equivalent High Cliff section, as well as the applicability of biostratigraphy and geochronology. A detailed palaeomagnetic analysis was not conducive to magnetostratigraphic determinations due to instability and weakness of the magnetic carrier. Chemostratigraphical tools, including major and trace elements, Sr isotopes, stable isotopes, and organic geochemistry, have been applied successfully.

The unanimous choice for selecting a level for the GSSP for the Serravallian/Tortonian boundary is to consider the correlation criterion given by the FO of *N. acostaensis*. This bioevent occurs at 157.6 m in the Monte dei Corvi section. For the sake of consistency with the historical stratotypes and definition of the Stages, this biosignal must be formally kept in the Serravallian portion of the series (Rio et al., Chapter A5; Miculan, Chapter A7). We suggest herein to place the boundary level 1 m above the FO of *N. acostaensis* (i.e., 20 to 30 ka after the FO considered to be the evolutionary appearance of the taxon). This would make the biostratigraphic characterization of the GSSP consistent with the definitions of both the Serravallian and the Tortonian Stages.

Japan has also potential sections for documenting the Serravallian/Tortonian boundary in the Tomioka and Karasuyama sequences (Takahashi and Oda, Chapter D5). In the Miura Peninsula, some sections may be useful for testing the validity of the correlation criteria for the Serravallian and Tortonian Stages in another area. However, discontinuity of the outcrops due to faulting, and the possibility of imminent urbanization of the exposures in the near future, strongly limit the suitability of these outcrops for the placement of the GSSP (Saito et al., Chapter E9). The same is valid for outcrops in the Boso Peninsula (Takahashi et al., Chapter E10). In general, these Japanese sections are

potentially useful for integrated stratigraphy and merit particular attention for reaching a global application of the chronostratigraphic boundaries under discussion. Consideration for their selection as auxiliary sections is therefore relevant.

### *Tortonian/Messinian*

The northern foothills of the Apennines, near Faenza, are presently the most promising area for locating the GSSP of the Tortonian/Messinian boundary (Vai et al., 1993; Vai, Chapter E3; Negri and Vigliotti, Chapter E4; Laurenzi et al., Chapter E5; Odin et al., Chapter E6). Accessibility to the stratigraphically equivalent sections of Monte Tondo and Monte del Casino is easy. Both outcrops expose clay-rich sediments which are not favourable for preserving a stable and unaltered section for more than a few years. Trenching is needed for collecting clean and fresh samples, and section preservation will require either periodical cleaning and/or durable reference flags (or posts) to indicate metre levels. The Monte Tondo section is probably better preservable and more stable than the Monte del Casino section.

The sedimentary sequence exhibits a genuine marine facies although the main criterion for locating the boundary is the transition from an open-marine facies to a facies representing a restricted, euxinic environment poorly connected with oceanic, extra-Mediterranean oceanic environments. The Monte del Casino section appears continuous and bears a complete and precise record of marine events. On the other hand, according to Negri and Vigliotti (Chapter E4), the Monte Tondo section contains a gap of a few metres right near the boundary. There are neither significant tectonic disturbances, nor general facies changes around the boundary although the detailed description of the lithology shows alternate normal, disoxic, and anoxic events (Vai, Chapter E3). Biostratigraphy has been applied successfully on both sections as well as magnetostratigraphy in some portions of the Monte Tondo section. Chemostratigraphy has not yet been applied in this area but results obtained from the Falconara section in Sicily (Colalongo and Pasini, Chapter A8) indicate that useful information of global (palaeoclimatic) significance is possibly available in spite of the relative closure of the basin. Geochronology is applicable thanks to a number of volcanoclastic layers present on both sides of the boundary.

In summary, the Faenza area may yield a section suitable for placing the GSSP. The correlation with the historical stratotype is easy via the many planktonic foraminiferal events known from near the boundary in both Sicily and the Faenza area. In particular, the GSSP should be located at a short distance immediately below the FOs of *G. conomiozea* and *G. mediterranea*. The Pasquasia–Capodorso section in Sicily may serve to approximate the time span between FO of *G. conomiozea* and the first evidence of the salinity crisis. In the Faenza area, where deposition rate ranges between 20 and 30 m/Ma, this would correspond to an interval less than 1 m. From this estimate, the horizon for the GSSP in the Monte Tondo section may be recommended at metre level 19, about 0.5 m below and 20 ka older than the presently documented FO of *G. conomiozea* (Vai et al., Chapter E3, fig. 4)

In the Cònero Riviera, the Marly Member of the Schlier Formation, which contains the Tortonian/Messinian boundary, is exposed on a steep landslide scarp near the locality called La Sardella (Montanari et al., Chapter E1, fig. 16), and can be precisely

correlated with the sequences near Faenza and in Sicily. However, the access to the La Sardella section is difficult and prevents it to be considered for the GSSP unless the Administration of the Cònero Regional Park will intervene (following a proposal by A. Montanari) by tracing a new access trail, and building a permanent steel ladder on the side of landslide scarp where the section is already marked every metre with numbered steel rods. Nevertheless, stratigraphic documentation of the La Sardella section using interdisciplinary approaches is promising, and all tools may be applied for reaching a more global characterization of the rocks bracketing the Tortonian/Messinian boundary.

## CONCLUSIVE REMARKS

Most historical Stage stratotypes are unconformity-bounded rock units. This leaves some place to locate the future GSSPs in between them with full consistency with regard to previous definitions. According to a current general consensus, the Tortonian/Messinian boundary constitutes an exception and must be located within the historically defined Tortonian. The original definition of Selli was clearly documented sedimentologically, and may be applied in Italy for correlating the original base of the Messinian Stage and define the Tortonian/Messinian boundary which can be correlated with a level within the historical stratotype of the Tortonian.

It is proposed here to simplify the chronostratigraphic column for easier global applicability. The subdivision of the Miocene into three sub-Epochs is well established worldwide, and reasonably justified in time spans with durations of about 7.5 Ma, 4.8 Ma, and 5.7 Ma, respectively, for the Early, Middle, and Late Miocene. However, this observation leaves little room for two Middle Miocene Stages, and the interval represented by the historical stratotype shows that the Langhian is more of regional (Mediterranean) than global applicability. In this situation, the best solution would be to define a single 'mesomiocenic' global Stage covering the whole time represented by the Langhian and Serravallian units. The latter, which are commonly used in the Mediterranean domain, would thus become useful substages wherever they may be recognized. An appropriate section for a new designation of the proposed 'mesomiocenic' single Stage would be in the Cònero Riviera, and a possible name would be the 'Anconian' after the name of the nearby city. The two lower and upper boundaries located at levels roughly 10–20 and near 158.5, respectively, as well as the internal substage boundary could be proposed in this area which would make an interesting reference section.

In carrying out this work, we were able to document biosignals with direct numerical calibrations. It would have been important to similarly document the sections studied with the nowadays popular sequence stratigraphy interpretation, continuous and unequivocal magnetostratigraphic data, and more complete chemostratigraphic determinations. Sequence stratigraphic interpretation remains to be done on most sections. Magnetostratigraphy is generally important for global correlations, but palaeomagnetic characteristics in most sections studied were not conducive to magnetostratigraphy. The absence of a good palaeomagnetic record is particularly deplorable because the actual interpretation of the magnetic record in time intervals characterized by the sequence of numerous reversals, such as the Oligocene/Miocene transition, is often debatable. This is because the resolution of the unequivocal biostratigraphical control is locally much

poorer (i.e., wider) than the duration of many reversals; this makes the assignment of magnetozones versus the oceanic record necessarily ambiguous, and often a matter of inconclusive circular reasoning. In this sense, there is probably no solution for solving this problem in a large portion of the Miocene series studied in the world.

Chemostratigraphy, in turn, may be influenced by regional factors. This is particularly true for the Miocene deposits in the Mediterranean, a basin which had a limited water exchange with the rest of the world oceans during most of the (Middle and Late) Miocene. Some major events may have a global relevance, and a priority for further study would be to obtain additional geochemical information (i.e., light isotopes, trace elements) which can be calibrated with already available radioisotopic dates.

Finally, the application of climatostratigraphic criteria (Milankovich astronomic cycles) has not yet been thoroughly applied in the sections studied in this volume. At least for the younger portion of the Miocene, the consideration of sections with a significant rhythmic deposition would help in obtaining a high-resolution control which could be fruitfully combined with the integrated stratigraphic data presented in this volume.

Among the potentially useful other areas where good sections might be searched for in the future, Algeria, Slovenia, Cyprus are possible (Odin et al., 1992). Farther on, the palaeogeographic maps proposed by Cahuzac et al. (1992), show additional series for calibrating the planktonic biostratigraphic record with geochronologically founded ages in the Betic–Rifian Basin (former Alboran sea), for which sediments are preserved in South Spain and North Morocco. In this domain and for the entire Middle and Late Miocene, volcanic activity occurred at a time when oceanic sediments were deposited. Lesser Antilles on the west, Philippines on the East would also be favourable for the same purpose. Finally, although the present project is now finished and the relevant WG of the Subcommittee of Geochronology disbanded, we may emphasize that a new project has been established by Dr. Takahashi, who is actively working on new series in Japan.

## SOMMAIRE — CHRONOSTRATIGRAPHIE DES ÉTAGES DU MIOCÈNE, PROPOSITION POUR LA DÉFINITION DE LIMITES PRÉCISES

Le point des résultats principaux rassemblés dans ce volume est fait. Les unités chronostratigraphiques examinées sont fondées sur le contenu des corps de roche désignés historiquement (les stratotype historiques). L'étude de ces stratotypes historiques a montré une bonne cohérence des corrélations biostratigraphiques. Ces éléments permettent de déduire qu'entre chaque unité existe un intervalle qui permet de proposer des Points Stratotypiques Globaux précis compatibles avec les définitions présentes. La limite Aquitanien/Burdigalien est repérable, notamment, à l'intérieur et près du début de l'intervalle de coexistence des foraminifères *Globigerinoides altiaperturus* et *G. trilobus*. La limite Burdigalien/Langhien est repérable, en particulier, dans le continuum évolutif des Préorbulines entre les émergences des formes *P. glomerosa sicana* et *P. glomerosa curva*. La limite Langhien/Serravallien se repère au dessus de l'émergence langhienne du foraminifère *Orbulina universa*, très près de la première manifestation commune langhienne terminale du nannofossile *Helicosphaera walbersdorfensis* et bien au dessous de l'extinction serravallienne du nannofossile *Sphenolithus hetero-*

*morphus*. La limite Serravallien/Tortonien peut être corrélée au moyen de l'émergence de *Neoglobobadrina acostaensis*, un biosignal situé dans le Serravallien terminal. La limite Tortonien/Messinien est prise à la base du stratotype historique de ce dernier Étage qui se situe, en particulier, au dessus de l'émergence du foraminifère *Globorotalia suterae* et de celle du groupe de nannofossiles du genre *Amaurolithus*, quelques ka sous le niveau d'émergence des foraminifères *Globorotalia conomiozea* et *G. mediterranea*. La fin du Miocène est aisément repérée par le retour de conditions marines due à une élévation générale du niveau des mers coïncidant avec une variation nette du rapport isotopique de l'oxygène des eaux atlantiques. Ces limites d'unités ont été situées dans le temps par l'étude géochronologique; Aquitainien/Burdigalien:  $20,3 \pm 0,4$  Ma, Burdigalien/Langhien:  $15,8 \pm 0,2$  Ma, Langhien/Serravallien:  $14,3 \pm 0,5$  Ma, Serravallien/Tortonien:  $11,0 \pm 0,3$  Ma, Tortonien/Messinien  $7,30 \pm 0,15$  Ma. Les durées d'unité déduites de ces résultats conduisent à proposer un Étage global unique pour le Miocène Moyen, le Langhien, court et mal identifiable hors de la Méditerranée et le Serravallien devenant des sous étages méditerranéens. Les meilleures coupes étudiées sont discutées dans l'optique d'une localisation de Points Stratotypiques Globaux. On souligne enfin quelques possibilités d'amélioration des connaissances.  
(Sommaire des auteurs)

## ACKNOWLEDGEMENTS

We would like to express our most sincere gratitude to the experts who presented the state of the knowledge of the historical stratotype sections in this volume. Following their knowledgeable elaborations made it possible to progress toward a better understanding of the foundation of the stratigraphy of the Miocene Epoch. Our synthesis would not have been possible without the help of field geologists who worked in areas other than Italy. Their contribution has been critical for a broader view of the available stratigraphic record in the best known Miocene sections throughout the world, and this will be necessary for the proper selection and evaluation of candidate GSSPs. This matter remains to be considered more thoroughly in the near future, and we would like to encourage additional stratigraphic work in countries around the Mediterranean basin as well as in other distant areas around the world.

Although this work has been first undertaken under the aegis of the Subcommittee of Geochronology, the biostratigraphic input has been essential, and the experts who contributed in this are acknowledged; we can only recognize that biostratigraphy is still a fundamental discipline in earth sciences and, despite a recent tendency in underestimating and minimizing the painstaking work of palaeontologists and biostratigraphers, we want to stress that it constitutes the major basis of Phanerozoic stratigraphy, and hope that it will be properly supported in the future.

With the recent development and application of elaborated analytical techniques, experts in organic matter, trace elements, and isotope geochemistry, have brought to this work a significant amount of information investing considerable time, technical, and financial resources. To them goes our sincere gratitude.

Our main purpose has been to combine and, in some cases, coordinate the information provided by the many contributors to this volume, and come up with a synthesis for a comprehensive understanding of the Miocene time sequence recorded in sedimentary

rocks. We may have partially reached this purpose but we also recognize that we may have come short in emphasizing the high value of each contribution, properly exploiting their conclusions in this synthesis. Our strongest hope is that this work as a whole will be considered as a generous group effort, and understood not just for its specific contents and particular information, but as a suggestive encouragement for further developing the approach of Integrated Stratigraphy in other portions of the Earth's geologic record.



This Page Intentionally Left Blank

## REFERENCES

- Adams, C.G., Benson, R.H., Kidd, R.B., Ryan, W.B.F. and Wright, R.H., 1977. The Messinian Salinity Crisis and evidence of Late Miocene eustatic changes in the world ocean. *Nature*, 269: 383–386.
- AGIP S.p.A., 1983. Carta Magnetica d'Italia. Servizi Centrali per l'Esplorazione. Met. Appl., Geofis., San Donato Milanese.
- Agusti, J., Barberà, X., Cabrera, L., Parés, J.M. and Llenas, M., 1994. Magnetobiostratigraphy of the Oligocene–Miocene transition in the Ebro Basin (Eastern Spain): state of the art. *Münchner Geowiss. Abh.*, (A), 26: 161–172.
- Akimoto, K., Uchida, E. and Oda, M., 1991. Benthic foraminiferal assemblages from the Miura Group. *Chikyū Mon.*, 13: 3–52 (in Japanese).
- Alvarez, W., 1991. Tectonic evolution of the Corsica–Apennines–Alps region studied by the method of successive approximations. *Tectonics*, 10: 936–947.
- Alvarez, W. and Montanari, A., 1988. Geologic framework of the Northern Apennines pelagic carbonate sequence. In: I. Premoli Silva, R. Coccioni and A. Montanari (Editors), *The Eocene–Oligocene Boundary in the Marche–Umbria Basin (Italy)*, I.U.G.S. Spec. Publ., F.lli Anibaldi Publishers, Ancona, pp. 13–30.
- Alvarez, W. and Piali, G.P., 1989. Driving of thrust belts by sinking of densified (eclogitic) lower continental crust: the Apennine–Tyrhenian system. *Geol. Soc. Am., Abstr. Progr.*, 21: A318.
- Alvarez, W., Cocozza, T. and Wezel, F.C., 1974. Fragmentation of the Alpine orogenic belt by microplate dispersal. *Nature*, 248: 309–314.
- Alvarez-Sierra, M.A., Daams, R., Lacomba, J.I., López-Martinez, N., van der Meulen, A.J., Sesé, C. and Visser, J., 1990. Paleontology and biostratigraphy (micromammals) of the continental Oligocene–Miocene deposits of the north-central Ebro Basin (Spain). *Scripta Geol.*, 94: 1–77.
- Alvinerie, J., 1969. Contribution sédimentologique à la connaissance du Miocène aquitain. *Interprétation stratigraphique and paléogéographique*. Thèse, Université de Bordeaux, offset, 457 pp.
- Alvinerie, J., Hunziker, J.C., Odin, G., Poignant, A. and Pujol, C., 1974. Sur l'âge radiométrique des glauconies miocènes d'Aquitaine. *Bull. Inst. Géol. Bassin d'Aquitaine*, Bordeaux, 16: 159–166.
- Alvinerie, J., Anglada, R., Caralp, M. and Catzigras F., 1977. Stratotype and parastratotype de l'Aquitainien. *Les stratotypes français, Comité Français de Stratigr.*, Ed. du CNRS, Paris, 4, 105 pp.
- Alvinerie, J., Antunes, M.T., Cahuzac, B., Lauriat-Rage, A., Montenat, C. and Pujol, C., 1992. Synthetic data on the paleogeographic history of Northeastern Atlantic and Betic–Rifian basin, during the Neogene (from Brittany, France, to Morocco). *Palaeogeogr., Palaeoclimatol., Palaeoecol.*, 95: 263–286.
- Amato, A. and Selvaggi, G., 1991. Terremoti crostali e subcrostali nell'Appennino settentrionale. *Stud. Geol. Camerti*, vol. spec. 1991/1: 75–82.
- Amato, A., Cimini, G.B. and Alessandrini, B., 1991. Struttura del sistema litosfera–astenosfera nell'Appennino Settentrionale da dati di tomografia sismica. *Stud. Geol. Camerti*, vol. spec. 1991/1: 83–90.
- Amorosi, A., 1992. Stratigrafia e sedimentologia del Miocene epiligure tra le valli del Panaro e del Marecchia (Appennino settentrionale) Tesi di Dottorato, IV ciclo, Univ. Bologna, 205 pp.
- Amorosi, A., 1993. Intérêt des niveaux glauconieux et volcano-sédimentaires en stratigraphie: exemple de dépôts de bassins tectoniques miocènes des Apennins; comparaison avec quelques dépôts de plate-forme. Thèse Doctorat, label européen, Université Pierre et Marie Curie, Paris, 194 pp.
- Amorosi, A., Ricci Lucchi, F. and Tateo, F., 1992. The lower Miocene siliceous lithozone: a palaeogeographic divide in the evolution of the northern Apennines. In: A. Montanari, R. Coccioni and G.S. Odin (Editors), *Volume of Abstracts and Field Trips, Interdisciplinary Geological Conference on the Miocene Epoch with emphasis on the Umbria–Marche sequence (I.U.G.S., Subcommission on Geochronology, Miocene Columbus Project)*, Ancona, November 11–15, 1992, pp. 8–9.
- Amorosi, A., Coccioni, R. and Tateo, F., 1994. The volcanoclastic bodies in the lower Miocene Bisciaro Formation (Umbria–Marche Apennines, Italy). In: R. Coccioni, A. Montanari and G.S. Odin (Editors),

- Miocene Stratigraphy of Italy and Adjacent Regions. *G. Geol.*, 56(1): 33–46.
- Amorosi, A., Ricci Lucchi, F. and Tateo, F., 1995. The lower Miocene siliceous lithozone: a paleogeographic divide in the evolution of the northern Apennines. *Palaeogeogr., Palaeoclimatol., Palaeoecol.*, 3.
- Anadon, P., Mitjavila, J.M., Utrilla, R., Vasquez, A. and Lopez-Martinez, N., 1995. Radiometric dating and geochemistry of a tuff horizon from a mammal-bearing lacustrine sequence, Miocene Biscop Basin, Eastern Spain. *Rev. Soc. Geol. Esp.*, 8: 91–98.
- Anderson, D.L., 1987. Thermally induced phase changes, lateral heterogeneity of the mantle, continental roots and deeper slab anomalies. *J. Geophys. Res.*, 92: 13968–13980.
- Anderson, H. and Jackson, J., 1987. The deep seismicity of the Tyrrhenian Sea. *Geophys. J. R. Astron. Soc.*, 91: 613–637.
- Andreoni, C., Galbiati, B., Maccabruni, A. and Vercesi, P.L., 1981. Stratigrafia e paleogeografia dei depositi oligocenici sup. Miocenici inf. nell'estremità orientale del Bacino Liguro-Piemontese. *Riv. Ital. Paleontol. Stratigr.*, 87: 245–282.
- Anelli, L., Gorza, M., Pieri, M. and Riva, M., 1992. Dati di pozzi profondi dell'Appennino Settentrionale. *Soc. Geol. Ital.*, 76ma Riunione Estiva, Firenze, 21–23 settembre 1992, Riassunti, p. 191.
- Arenas, C. and Pardo, G., 1991. Significado de la ruptura entre las nidades tectosedimentarias N2 y N3 en el centro de la Cuenca del Ebro. *Geogaceta*, 9: 67–70.
- Arias, C., Bigazzi, G. and Bonadonna, F.P., 1981. Size correction and plateau age in glass shards. *Nucl. Tracks*, 5: 129–136.
- Artyushkov, E.V. and Sobolev, S.V., 1982. Mechanism of passive margins and island seas formation. In: J.S. Watkins and C.L. Drake (Editors), *Studies in Continental Margin Geology*. Am. Assoc. Pet. Geol. Mem., 34: 689–701.
- Ascoli, P., 1968. Preliminary report on the Ostracoda of the type-Tortonian. *G. Geol.*, Ser. 2, 35(2): 31–54.
- Assorgia, A., Chan, L.S., Deino, A., Garbarino, C., Montanari, A., Rizzo, R. and Tocco, S., 1994. Volcanogenic and paleomagnetic studies on the Cenozoic calc-alkalic eruptive sequence of Monte Furrù (Bosa, mid-western Sardinia). In: R. Coccioni, A. Montanari and G.S. Odin (Editors), *Miocene Stratigraphy of Italy and Adjacent Regions*. *G. Geol.*, 56(1): 17–29.
- Aubry, M.P., 1984. *Handbook of Cenozoic Calcareous Nannoplankton*, Book 1. *Ortholithae (Discoasters)*. Micropaleontology Press: American Museum of Nat. Hist., N.Y., 266 pp.
- Backman, J. and Shackleton, N.J., 1983. Quantitative biochronology of Pliocene and Early Pleistocene calcareous nannoplankton from the Atlantic, Indian and Pacific Oceans. *Mar. Micropaleontol.*, 8: 141–171.
- Backman, J., Schneider, D.A., Rio, D. and Okada, H., 1990. Neogene low-latitude magnetostratigraphy from Site 710 and revised age estimates of Miocene nannofossil datums events. *Proc. ODP Sci. Results*, 115: 71–276.
- Baksi, A.K., 1993. A geomagnetic polarity time scale for the period 0–17 Ma, based on  $^{40}\text{Ar}/^{39}\text{Ar}$  plateau ages for selected field reversals. *Geophys. Res. Lett.*, 20: 1607–1610.
- Baldauf, J.G. and Barron, J.A., 1994. Diatom biostratigraphy: Kerguelen Plateau and Prydz Bay region of the Southern Ocean. *Proc. ODP Sci. Results*, 119: 547–598.
- Bally, A.W., 1981. Thoughts on the tectonics of folded belts. In: K.R. McClay and N.J. Price (Editors), *Thrust and Nappe Tectonics*. Geological Society Special Publication. No. 9, Blackwell Scientific Publications, Oxford (UK), pp. 13–32.
- Bally, A.W., Burbi, L., Cooper, C. and Ghelardoni, R., 1986. Balanced sections and seismic reflection profiles across the Central Apennines. *Mem. Soc. Geol. Ital.*, 35: 257–310.
- Balogh, K., Delle Rose, M., Guerrero, F., Ravasz-Baranyai, L. and Veneri, F., 1993. New data concerning the inframiocenico 'Bisciaro volcanoclastic event' (Umbro–Marche Apennines) and comparison with similar occurrences. *G. Geol.*, 55: 83–104.
- Barron, J.A., 1983. Latest Oligocene through early Miocene diatom biostratigraphy of the eastern tropical Pacific. *Mar. Micropaleontol.*, 7: 487–515.
- Barron, J.A., Keller, G. and Dunn, D.A. 1985a. A multiple microfossil biochronology for the Miocene. In: T.P. Kenneth (Editor), *The Miocene Ocean: Paleooceanography and Biogeography*. *Mem. Geol. Soc. Am.*, 163: 21–36.
- Barron, J.A., Nigrini, C.A., Pujos, A., Saito, T., Theyer, F., Thomas, E. and Weinreich, N., 1985b. Synthesis of biostratigraphy, Central Equatorial Pacific, DSDP Leg 85: refinement of Oligocene to Quaternary biochronology. *Init. Rep. DSDP*, 85: 905–934.

- Barry, J.C., Lindsay, E.H. and Jacobs, L.L., 1982. A biostratigraphic zonation of the middle and upper Siwaliks of the Potwar Plateau of northern Pakistan. *Palaeogeogr., Palaeoclimatol., Palaeoecol.*, 37: 95–130.
- Bartole, R., Torelli, L., Mattei, G., Peis, D. and Brancolini, G., 1991. Assetto stratigrafico-strutturale del Tirreno Settentrionale: stato dell'arte. *Stud. Geol. Camerti*, vol. spec. 1991/1: 115–140.
- Bartolini, C., Bernini, M., Carloni, G.C., Costantini, A., Federici, P.B., Gasperi, G., Lazzarotto, A., Marchetti, G., Mazzanti, R., Papani, G., Pranzini, G., Rau, A., Sandrelli, F., Vercesi, P.L., Castaldini, D. and Francavilla, F., 1982. Carta neotettonica dell'Appennino settentrionale. Note illustrative. *Boll. Soc. Geol. Ital.*, 101: 523–549.
- Basseti, M.A., Ricci Lucchi, F. and Roveri, M., 1994. Physical stratigraphy of the Messinian post-evaporitic deposit in Central-Southern Marche Area (Apennines, Central Italy). *Mem. Soc. Geol. Ital.*, 48: 275–285.
- Beatrizotti, G., Bellinzona, G., Boni, A. and Braga, G., 1965. Carta Geologica d'Italia, Foglio 59, Pavia (2nd ed.). Servizio Geologico d'Italia, Roma.
- Bellardi, L. and Sacco, F., 1872–1904. I molluschi dei terreni terziari del Piemonte e della Liguria. Pt. 1-30, Torino.
- Bellon, H., 1976. Séries magmatiques néogènes et quaternaires du pourtour de la Méditerranée occidentale comparées dans leur cadre géochronométrique; implications géodynamiques. Thèse Univ. Paris Sud (Orsay), offset, 367 pp.
- Bellon, H., 1977. Chronostratigraphy of Neogene around western Mediterranean; micropaleontology and geochronology. *Vth Eur. Coll. Geochronology*, Pisa, September 1977, Abstracts.
- Bellon, H., Bizon, G., Calvo, J.P., Elizaga, E., Gaudant, J., Lopez-Martinez, N.L., 1981. Le volcan du Cerro del Monagrillo (Province de Murcia): âge radiométrique et corrélations avec les sédiments néogènes du bassin de Hellin (Espagne). *C.R. Acad. Sci., Paris*, 292(2): 1035–1038.
- Bellon, H., Bordet, P. and Montenat, C., 1983. Le magmatisme néogène des Cordillères Bétiques (Espagne): chronologie et principaux caractères géochimiques. *Bull. Soc. Géol. Fr.*, 7, 25(2): 205–218.
- Benda, L. and Meulenkamp, J.E., 1990. Biostratigraphic correlations in the Eastern Mediterranean Neogene. *Newsl. Stratigr.*, 23: 1–10.
- Benda, L., Meulenkamp, J.E., Schmidt, R.R., Steffens, P. and Zachariasse, J., 1977. Biostratigraphic correlations in the Eastern Mediterranean Neogene, 2. Correlation between sporomorph associations and marine microfossils from the Upper Oligocene–Lower Miocene of Turkey. *Newsl. Stratigr.*, 6(1): 1–22.
- Bender, M.L. and Graham, D.W., 1981. On Late Miocene abyssal hydrography. *Mar. Micropaleontol.*, 6: 451–464.
- Bender, M.L. and Keigwin, L.D., Jr., 1979. Speculations about the Upper Miocene change in abyssal Pacific dissolved biocarbonate <sup>13</sup>C. *Earth Planet. Sci. Lett.*, 43: 383–393.
- Benson, R.H. and Hodell, D.A., 1994. Comment on 'A critical re-evaluation of the Miocene/Pliocene boundary as defined in the Mediterranean' by F.J. Hilgen and C.G. Langereis. *Earth Planet. Sci. Lett.*, 124: 245–250.
- Benson, R.H. and Rakic-el-Bied, K., 1991. The Messinian parastratotype at Cuevas del Almanzora, Vera Basin, SE Spain: refutation of the deep-basin, shallow water hypothesis? *Micropaleontology*, 37(3): 289–302.
- Benson, R.H., Rakic-el-Bied, K. and Bonaduce, G., 1991. An important current reversal (influx) in the Rifian corridor (Morocco) and the Tortonian–Messinian boundary: the end of Tethys Ocean. *Paleoceanography*, 6(1): 164–192.
- Benson, R.H., Rakic-El Bied, K., Bonaduce, G., Berggren, W.A., Aubry, M.-P., Hodell, D.A., Napoleone, G., Kent, D., Flores, J.A., Mazzei, R. and Semenenko, V.N., 1996. The Bou Regreg Section, Morocco: Proposed Global Boundary Stratotype Section and Point of the Pliocene, Notes et Mém. Serv. Géol. Maroc (Rabat), 383: 51–150.
- Berger, A., 1976. Obliquity and precession for the last 5,000,000 years. *Astron. Astrophys.*, 51: 127–135.
- Berger, A., 1977. Support for the astronomical theory of climatic change. *Nature*, 268: 44–45.
- Berger, A., 1984. Accuracy and frequency stability of the Earth's orbital elements during the Quaternary. In: A. Berger et al. (Editors), *Milankovitch and Climate*. Reidel, Dordrecht, pp. 3–40.
- Berger, A.L. and Loutre, M.F., 1991. Insolation value for the climate of the last 10 million years. *Quat. Sci. Rev.*, 10: 297–317.
- Berger, A. and Pestiau, P., 1987. Astronomical frequencies in paleoclimatic data. In: Ye Duzheng et al. (Editors), *The Climate of China and Global Climate*. China Ocean Press, Springer-Verlag, Berlin, pp.

- 106–114.
- Berggren, W.A., 1969. Cenozoic chronostratigraphy, planktonic foraminiferal zonation and the radiometric time-scale. *Nature*, 224: 1072–1075.
- Berggren, W.A., 1971. Tertiary boundaries and correlations. In: B.M. Funnell and W.R. Riedel (Editors), *The Micropaleontology of the Oceans*. Cambridge University Press, Cambridge, pp. 693–809.
- Berggren, W.A., 1972. A Cenozoic time scale: some implications for regional geology and paleobiogeography. *Lethaia*, 5: 195–215.
- Berggren, W.A., Kent, D.V., Flynn, J.J. and Van Couvering, J.A., 1985a. Cenozoic geochronology. *Bull. Geol. Soc. Am.*, 96: 1407–1418.
- Berggren, W.A., Kent, D.V. and Van Couvering, J.A., 1985b. The Neogene, Part 2. Neogene geochronology and chronostratigraphy. In: N.J. Snelling (Editor), *The Chronology of the Geological Record*. Mem. Soc. Geol., London, 10, pp. 211–259.
- Berggren, W.A., Kent, D.V., Swisher, C., III, and Aubry, M.P., 1995. A revised Cenozoic geochronology and chronostratigraphy. In: W.A. Berggren, D.V. Kent, M.P. Aubry, and J. Hardenbol (Editors), *Geochronology, Time Scales and Global Stratigraphic Correlations: A Unified Temporal Framework for an Historical Geology*. SEPM Spec. Publ., 54, 129–212.
- Bernades, C., Bigazzi, G., Bonadonna, F.P., Centamore, E., Lattes, C.M.G and Hadler, J.C., 1986. Fission track dating on glass from 'Flysch della Laga' Formation: a very interesting and problematic application. *Nucl. Tracks*, 12: 901–904.
- Bersani, A., Dondi, M., Failla, A., Mezzetti, R., Minguzzi, V. and Morandi, N., 1987. Mineralogia e chimismo dei livelli a zeoliti di Ba nella Formazione di Antognola (Appennino Settentrionale). *Miner. Petrogr. Acta*, 30: 13–48.
- Bertini, A., 1992. Palinologia ed aspetti ambientali del versante adriatico dell'Appenninio centro-settentrionale durante il Messiniano e lo Zancleano. Doctorat Thesis, Università di Bologna.
- Bertini, G., Cameli, G.M., Costantini, A., Decandia, F.A., Di Filippo, M., Dini, I., Elter, M., Lazzarotto, A., Liotta, D., Pandeli, E., Sandrelli, F. and Toro, B., 1991. Struttura geologica fra i Monti di Campiglia e Rapolano Terme (Toscana Meridionale): stato attuale delle conoscenze e problematiche. *Stud. Geol. Camerti*, vol. spec. 1991/1: 155–178.
- Bertolani Marchetti, D., 1984. Some paleoclimatical and paleovegetational features of the Messinian on palynological basis. 4th OPTIMA Meeting, Palermo, Webbia, 38: 417–426.
- Bertolani Marchetti, D. and Marzi, L., 1988. Palynological data on the Monticino quarry sequence. In: C. De Giuli and G.B. Vai (Editors), *Fossil Vertebrates in the Lamone Valley, Romagna Apennines*. Field Trip Guidebook, Faenza, pp. 63–64.
- Bessedik, M., 1985. Reconstitution des environnements miocènes des régions nord-ouest méditerranéennes à partir de la palynologie. Thèse Univ. Sci. Tech. Languedoc, Montpellier, 162 pp.
- Biffi, U. and Manum, S.B., 1988. Late Eocene–Early Miocene dinoflagellate cyst biostratigraphy from the Marche Region (Central Italy). *Boll. Soc. Paleontol. Ital.*, 27(2): 162–212.
- Biolzi, M., 1984. The Oligocene/Miocene boundary in selected Atlantic, Mediterranean and Paratethys section based on biostratigraphic and stable isotope evidence. Inaugural Diss. Philos. Fak. Univ. Zürich, 107 pp.
- Biolzi, M., 1985. The Oligocene/Miocene boundary in selected Atlantic, Mediterranean and Paratethyan sections based on biostratigraphic and stable isotope evidence. *Mem. Soc. Geol. Ital.*, 37: 303–378.
- Biolzi, M., Bizon, G., Borsetti, A.M., Cati, F., Radovisc, R., Rögl, F. and Zachariasse, W.J., 1991. Biostratigraphic results of the Italian sections: planktonic Foraminifera. In: F. Cati, F.F. Steininger, A.M. Borsetti and R. Gelati (Editors), *In Search of the Paleogene/Neogene Boundary Stratotype, Part 1. Potential Boundary Stratotype Sections in Italy and in Greece and Comparison with Results from the Deep-Sea*. *G. Geol.*, 44: 167–172.
- Birck, J.L., 1986. Precision K–Rb–Sr isotopic analysis: application to Rb–Sr chronology. *Chem. Geol.*, 56: 73–83.
- Bizon, G., 1979. Planktonic Foraminifera. In: G. Bizon and C. Muller, Report of the Working Group on Micropaleontology. VII Int. Congr. Mediterranean Neogene, Athens 1979. *Ann. Geol. Pays Hellén.*, spec. iss., 3: 1335–1364.
- Bizon, G., 1984. Changes in planktonic Foraminifera and their environmental meaning. In: R. Gelati and F.F. Steininger (Editors), *In Search of the Paleogene/Neogene Boundary stratotype, Part 2. Potential Boundary Stratotype Sections in Italy and Spain*. *Riv. Ital. Paleontol. Stratigr.*, 89(4): 557–560.

- Bizon, G. and Bizon, J.J., 1972. Atlas des principaux foraminifères planctoniques du bassin méditerranéen Oligocène à Quaternaire. Editions Technip, Paris, 316 pp.
- Bizon, G. and Müller, C., 1979. Report on the working group on Micropaleontology. Ann. Géol. Pays Hellén., 3: 1335–1364.
- Bizon, G. and Müller, C., 1981. Remarks on the Paleogene/Neogene boundary based on results obtained from the Pacific and Indian oceans. In: F. Cati, F.F. Steininger, A.M. Borsetti and R. Gelati (Editors), In Search of the Paleogene/Neogene Boundary Stratotype, Part I. Potential Boundary Stratotype Sections in Italy and in Greece and Comparison with Results from the Deep-Sea. G. Geol., 44: 197–203.
- Bizon, G., Bizon, J.J. and Montenat, C., 1972a. Le Miocène terminal dans le Levant espagnol. Rev. IFP, 27(6): 831–863.
- Bizon, G., Bizon, J.J. and Ricou, L.E., 1972b. Etude stratigraphique et paléogéographique des formations tertiaires de la région de Neyriz (Fars interne, Zagros iranien). Rev. IFP, 27(3): 369–395.
- Blanc, G., Vitali, F. and Stille, P., 1995. Unusual diagenetic alteration of volcanoclastic sediments in the Tonga fore-arc: evidence from chemical and strontium isotopic compositions of interstitial waters. Geochim. Cosmochim. Acta, 59: 4633–4644.
- Blow, W.H., 1956. Origin and evolution of the foraminiferal genus *Orbulina* d'Orbigny. Micropaleontology, 2: 57–70.
- Blow, W.H., 1969. Late Middle Eocene to Recent planktonic foraminiferal biostratigraphy. Proc. Int. Conf. Planktonic Microfossils, Geneva, 1967, 1: 199–442.
- Boccaletti, M., Ciaranfi, N., Cosentino, D., Deiana, G., Gelati, R., Lentini, F., Massari, F., Moratti, G., Pescatore, T., Ricci Lucchi, F. and Tortorici, L., 1990. Palinspastic restoration and paleogeographic reconstruction of the peri-Tyrrhenian area during the Neogene. Palaeogeogr., Palaeoclimatol., Palaeoecol., 77, 41–50.
- Boccaletti, M., Cerrina-Feroni, A., Martinelli, P., Moratti, G., Plesi, G. and Sani, F., 1991. L'alternanza distensione–compressione nel quadro evolutivo dei bacini neogenici dell'Appennino Settentrionale. Stud. Geol. Camerti, vol. spec. 1991/1: 187–192.
- Bolli, H.M., 1957. Planktonic foraminifera from the Oligocene–Miocene Cipero and Lengua formations of Trinidad. U.S. Nat. Mus. Bull., 215: 97–123.
- Bolli, H.M., 1966. Zonation of Cretaceous to Pliocene marine sediments based on planktonic Foraminifera. Bol. Inf. Assoc. Venezol. Geol. Miner. Petrol., 9: 3–32.
- Bolli, H.M. and Saunders, J.B., 1985. Oligocene to Holocene low latitude planktic foraminifera. In: H.M. Bolli, J.B. Saunders and K. Perch-Nielsen (Editors), Plankton Stratigraphy. Cambridge Univ. Press, Cambridge, pp. 155–262.
- Boni, A., 1967. Notizie sul Serravalliano tipo. In: R. Selli (Editor), Guida alle escursioni del IV Congresso. C.M.N.S., Bologna, pp. 47–63.
- Boni, A. and Casnedi, R., 1970. Note illustrative della carta geologica d'Italia, Fogli 69 e 70 Asti–Alessandria. Poligrafica and Cartevalori, Ercolano, Napoli, 64 pp.
- Boni, A. and Selli, R., 1971. Stratotypes of Mediterranean Neogene Stages: Serravallian. G. Geol., 37(2): 181–188.
- Bordet, P., 1985. Le volcanisme miocène des Sierras de Gata et de Carboneras. Doc. et Trav. IGAL., Paris 8, 70 pp.
- Borsetti, A.M., 1992. Activity and results of the Working Group on the Palaeogene–Neogene Boundary Stratotype. In: A. Montanari, R. Coccioni and G.S. Odin (Editors), Volume of Abstracts and Field Trips, Interdisciplinary Geological Conference on the Miocene Epoch with emphasis on the Umbria–Marche sequence (I.U.G.S., Subcommittee on Geochronology, Miocene Columbus Project), Ancona, November 11–15, 1992, pp. 24–25.
- Borsetti, A.M., Carloni, G.C., Cati, F., Ceretti, E., Cremonini, G., Elmi, C. and Ricci Lucchi, F., 1975. Paleogeografia del Messiniano nei bacini periadriatici. G. Geol., 40(1): 21–72.
- Borsetti, A.M., Cati, F., Colalongo, M.L. and Sartoni, S., 1979a. Biostratigraphy and absolute ages of the Italian Neogene. Ann. Geol. Hellen., 7th Congr. Med. Neog. Athens, 1: 183–197.
- Borsetti, A.M., Savelli, C., Carloni, G.C., Cati, F., Ceretti, E., Toni, G.C. and Mezzetti, R., 1979b. Evidence of explosive volcanic activity at the Oligocene–Miocene boundary from the Tyrrhenian Sea area. Abstracts, Rapport Commission internationale Explor. Mer Méditerranée, 25/26: 57–59.
- Borsetti, A.M., Cati, F., Mezzetti, R., Savelli, C. and Toni, G.C., 1983. The influence of tectonics on stratigraphy. Newsl. Stratigr., 12(1): 54–67.

- Borsetti, A.M., Cati, F., Mezzetti, R., Savelli, C. and Toni, G.C., 1984. Le intercalazioni vulcanoclastiche nei sedimenti oligo-miocenici dell'Appennino settentrionale. *G. Geol.*, 45: 159–198.
- Borsetti, A.M., Curzi, P.V., Landuzzi, V., Mutti, M., Ricci Lucchi, F., Sartori, R., Tomadin, L. and Zuffa, G.G., 1990. Messinian and pre-Messinian sediments from ODP Leg 107 sites 652 and 654 in the Tyrrhenian sea: sedimentologic and petrographic study and possible comparisons with Italian sequences. *Proc. ODP Sci. Results*, 107: 169–186.
- Bossio, A., Giannelli, L., Mazzei, R., Rakic-el-Bied, K. and Russo, A., 1977. Biostratigraphy and chronostratigraphy of some stratigraphic sections from western Andalusia (Spain) including the stratotype of the Andalusian Stage. IGCP Proj. 96, Messinian Seminar 3, Malaga 1977, pp. 9–12.
- Bossio, A., Fornaciari, E., Iaccarino, S., Mazzei, R., Monteforti, B., Rio, D. and Salvatorini, F., 1992a. Integrated calcareous plankton stratigraphy from the Langhian stratotype section (Piedmont Tertiary Basin Italy). In: A. Montanari, R. Coccioni and G.S. Odin (Editors), Volume of Abstracts and Field Trips, Interdisciplinary Geological Conference on the Miocene Epoch with emphasis on the Umbria–Marche sequence (I.U.G.S., Subcommittee on Geochronology, Miocene Columbus Project), Ancona, November 11–15, 1992, p. 26.
- Bossio, A., Mazzei, R., Monteforti, B. and Salvatorini, G., 1992b. Notizie preliminari sul Miocene di S. Maria al Bagno–S. Caterina, presso Nardò (Lecce). *Paleopelagos*, 2: 99–107.
- Braud, J., 1989. La suture du Zagros au niveau de Kermanshah (Kurdistan Iranien): reconstitution paléogéographique, évolution géodynamique, magmatique et structurale. Thèse d'Etat, Univ. Orsay 1987, *Mém. Géodiffusion*, Paris, 5, p. 489.
- Brinkhuis, H., Powell, A.J. and Zevenboom, D., 1992. High-resolution dinoflagellate cyst stratigraphy of the Oligocene/Miocene transition interval in northwest and central Italy. In: M.J. Head and J.H. Wrenn (Editors), Neogene and Quaternary Dinoflagellate Cysts and Acritarchs. AASP, Dallas, pp. 219–258.
- Bromley, R.G. and D'Alessandro, T., 1992. Ichnology of oxygen crises in Miocene pelagic marls. In: A. Montanari, R. Coccioni and G.S. Odin (Editors), Volume of Abstracts and Field Trips, Interdisciplinary Geological Conference on the Miocene Epoch with emphasis on the Umbria–Marche sequence (I.U.G.S., Subcommittee on Geochronology, Miocene Columbus Project), Ancona, November 11–15, 1992, p. 28.
- Bronn, H.G., 1838. *Lethea Geognostica, oder Abbildungen und Beschreibungen der für die Gebirgsformationen bezeichnensten Versteinerungen*. Stuttgart, 2: 545–1356.
- Brown, G.F., Schmidt, D.L. and Huffman, A.C. Jr., 1989. Geology of the Arabian Peninsula. Shield area of western Saudi Arabia. *U.S. Geol. Surv. Prof. Pap.*, 560A: 188.
- Brujin, H. De, Mein, P., Montenat, C. and Van De Weer, D., 1975. Les gisements de Mammifères du Miocène supérieur d'Espagne méridionale (Provinces d'Alicante et de Murcia). Corrélations avec les formations marines du Miocène terminal. *Proc. K. Ned. Akad. Wet.*, B, 78(4): 1–32.
- Brujin, H. De, Daams, R., Daxner-Höck, G., Fahlbusch, V., Ginsburg, L., Mein, P. and Morales, J., 1992. Report of the RCMNS working group on fossil mammals, Reimsburg 1990. *Newsl. Stratigr.*, 26: 65–118.
- Bukry, D., 1973. Low latitude coccolith biostratigraphic zonation. *Init. Rep. DSDP*, 15: 685–703.
- Bukry, D., 1975. Silicoflagellate and coccolith stratigraphy, Deep-Sea Drilling Project Leg 29. *Init. Rep. DSDP*, 29: 845–872.
- Bukry, D., 1981. Pacific coast coccolith stratigraphy between Point Conception and Cabo Corrientes, Deep Sea Drilling Project Leg 63. *Init. Rep. DSDP*, 63: 445–471.
- Burbank, D.W., Engesser, B., Matter, A. and Weidmann, M., 1992. Magnetostratigraphic chronology, mammalian faunas and stratigraphic evolution of the Lower Fresh-water Molasse, Haute-Savoie, France. *Eclogae Geol. Helv.*, 85: 399–431.
- Cabrera, L., 1983. Estratigrafia y sedimentología de las formaciones lacustres del tránsito Oligoceno–Miocene del SE de la Cuenca del Ebro. Doctoral Tesis, Univ. de Barcelona, 443 pp.
- Cahuzac, B. and Chaix C., 1996. Structural and faunal evolution of Chattian–Miocene reefs and corals in Western France and Northeastern Atlantic Ocean. In: E. Franseen, M. Esteban, W. Ward and J.M. Rouchy (Editors), Models for Carbonate Stratigraphy from Miocene Reef Complexes of the Mediterranean Regions. S.E.P.M. (Soc. Econ. Paleontol. Mineral.), Concepts in Sedimentology and Paleontology, 5, p. 105–127.
- Cahuzac, B. and Pognant, A., 1988. Les foraminifères benthiques de l'Oligocène terminal du vallon de Poustagnac (Landes, Bassin d'Aquitaine, SW de la France). Découverte de *Cycloclypeus* et de *Pararotalia* à loges équatoriales supplémentaires. *Rev. Paléobiol.*, Genève, vol. spec. 2 (Benthos '86), pp. 633–642.

- Cahuzac, B. and Roman, J., 1994. Les Echinoïdes de l'Oligocène supérieur (Chattien) des Landes (Sud-Aquitaine, France). *Rev. Paléobiol.*, Genève, 13/2: 349–371.
- Cahuzac, B., Alvinerie, J., Lauriat-Rage, A., Montenat, C. and Pujol, C., 1992. Paleogeographic maps of the Northeastern Atlantic Neogene and relation with the Mediterranean sea. *Paleontol. Evol.*, 24–25: 279–293.
- Cahuzac, B., Janin, M.C. and Steurbaut, E., 1995. Biostratigraphie de l'Oligo-Miocène du Bassin d'Aquitaine fondée sur les nannofossiles calcaires. Implications paléogéographiques. *Géologie de la France, Orléans (B.R.G.M., and Soc. Géol. Fr. (Editors))*, 2: 57–82.
- Cahuzac, B., Carbonel, P., Cluzaud, A., Colin, J.P., Faury, B., Gilly, Y., Lesport, J.F., Londeix, L., Martin, N. and Rocher, P., 1996. La Réserve Naturelle Géologique de Saucats–La Brède (Gironde). *Sud-Ouest Nature, Bordeaux, (SEPANSO: Soc. Etude, Prot., Aménag. Nature Sud-Ouest, édit.)*, 92, 64 pp.
- Calcagnile, G. and Panza, G.F., 1990. The main characteristics of the lithosphere–asthenosphere system in Italy and surrounding regions. *Pure Appl. Geophys.*, 199: 865–879.
- Calieri, R., 1992. Stratigrafia, analisi paleoclimatica e radiometria del Tortoniano superiore–Messiniano preevaporitico in Appennino Romagnolo (M. del Casino–M. Tondo). Unpubl. thesis, Univ. of Bologna, 79 pp.
- Calieri, R., Vai, G.B., Villa, I.M. and Colalongo, M.L., 1992. Potential boundary stratotype sections, Tortonian/Messinian Northern Apennines, Imola area. In: A. Montanari, R. Coccioni and G.S. Odin (Editors), Volume of Abstracts and Field Trips, Interdisciplinary Geological Conference on the Miocene Epoch with emphasis on the Umbria–Marche sequence (I.U.G.S., Subcommission on Geochronology, Miocene Columbus Project), Ancona, November 11–15, 1992, pp. 111–115.
- Camerlenghi, A., Cita, M.B., Leoni, C., Malinverno, A., Malinverno, P. and Miranda, P., 1983. Progetto Messiniano. Banca dati, logs e carte varie sul Messiniano d'Italia. *Pubbl. 514 PF Geod. CNR, Esa*, 467 pp.
- Camoin, G., Bellion, Y., Dercourt, J., Guiraud, R., Lucas, J., Poisson, A., Ricou, L.E. and Vrielynck, B., 1993. Late Maastrichtian (69.5–65 Ma). In: J. Dercourt, L.E. Ricou and B. Vrielynck (Editors), *Atlas Tethys Palaeoenvironmental Maps. Explanatory Notes*. Gauthier Villars, Paris, pp. 179–196.
- Cande, S.C. and Kent, D.V., 1992. A new geomagnetic Polarity Time Scale for Late Cretaceous and Cenozoic. *J. Geophys. Res.*, 97: 13,917–13,951.
- Cande, S.C. and Kent, D.V., 1995. Revised calibration of the geomagnetic polarity time scale for the late Cretaceous and Cenozoic. *J. Geophys. Res.*, 100, B4: 6093–6095.
- Cantalamesa, G., Centamore, E., Chiocchini, U., Micarelli, A. and Potetti, M., 1986. Il Miocene delle Marche. In: E. Centamore and G. Deiana (Editors), *La Geologia delle Marche. Stud. Geol. Camerti, spec. vol.*, 73° Congr. Soc. Geol. Ital., pp. 35–55.
- Canud, J.I., Lag, M., Cuenc, G. and Odin, G.S., 1993. Setting, petrology and geochemistry of a new magmatism of Middle Miocene age (Basin of the Ebro, Spain). *E.U.G. 7th Meeting, Strasbourg, Terra Abstracts*, 1(6): 528.
- Capo, R. and DePaolo, D.J., 1990. Strontium isotopic analysis of marine carbonates from the Massignani section across the Eocene/Oligocene boundary. In: I. Premoli Silva, R. Coccioni and A. Montanari (Editors), *The Eocene–Oligocene Boundary in the Marche–Umbria Basin*. I.U.G.S. Spec. Publ., F.Ili Anibaldi Publishers, Ancona, pp. 189–192.
- Caprara, L., Garzanti, E., Gnaccolini, M. and Mutti, L., 1985. Shelf-basin transition: sedimentology and petrology of the Serravallian of the Tertiary Piedmont Basin (Northern Italy). *Riv. Ital. Paleontol. Stratigr.*, 90: 545–564.
- Caratini, C. and Sivak, J., 1971. Etude palynologique des stratotypes de l'Aquitainien et du Burdigalien. 5ème Congr. Int. Néogène Méditerranéen, Lyon, *Mém. BRGM*, 2, 78: 489–495.
- Carbonnel, G., 1969. Les Ostracodes du Myocène rhodanien. *Doc. Lab. Géol. Fac. Sci. Lyon*, 32, 469 pp.
- Carloni, G., Marks, P., Rutsch, R.F. and Selli, R. (Editors), 1971. Stratotypes of Mediterranean Neogene stages. *G. Geol.*, 37, 266 pp.
- Carloni, G.C., Cati, F., Borsetti, A.M., Francavilla, F., Mezzetti, R. and Savelli, C., 1974a. Il limite Miocene–Pliocene nelle Marche Centro-meridionali. *Boll. Soc. Geol. Ital.*, 93: 823–836.
- Carloni, G.C., Francavilla, F., Borsetti, A.M., Cati, F., D'Onofrio, S., Mezzetti, R. and Savelli, C., 1974b. Ricerche stratigrafiche sul limite Miocene–Pliocene nelle Marche. *G. Geol.*, 39(2): 363–394.
- Carmignani, L. and Kligfield, R., 1990. Crustal extension in the Northern Apennines: the transition from compression to extension in the Alpi Apuane core complex. *Tectonics*, 9: 1275–1303.



- Carmignani, L., Barca, S., Disperati, L., Fantozzi, P., Funedda, A., Oggiano, G. and Pasci, S., 1994. Tertiary compression and extension in the sardinian basement. *Boll. Geofis. Teor. Appl.*, 34/141–144, 45–62
- Carveni, P., Di Grande, A. and Romeo, M., 1982. Ulteriori dati geologici e stratigrafici sulle cineriti inframioceniche della Sicilia Centro-meridionale. *Boll. Soc. Geol. Ital.*, 101: 43–56.
- Casati, P., Bertozzi, P., Cita, M.B., Longinelli, A. and Damiani, V., 1978. Stratigraphy and paleoenvironment of the Messinian 'Colombacci' Formation in the Periadriatic trough. A pilot study. *Mem. Soc. Geol. Ital.*, 16: 173–195.
- Cassano, E., 1991. Dati magnetici lungo il profilo CROP 03. *Stud. Geol. Camerti*, vol. spec. 1991/1: 49–53.
- Cassinis, R., Piali, G., Broggi, M. and Prosperi, M., 1991. Dati gravimetrici a grande scala lungo la fascia del profilo CROP 03: interrogativissull'assetto della crosta e del mantello. *Stud. Geol. Camerti*, vol. spec. 1991/1: 41–47.
- Castellari, M., 1989. Rilevamento geologico e studio stratigrafico strutturale della Vena del Gesso tra il fiume Santerno e il fiume Senio. Unpubl. thesis, Univ. Bologna, 153 pp.
- Castellarin, A., Colacicchi, R., Praturlon, A. and Cantelli, C., 1982. The Jurassic–Lower Pliocene history of the Anzio–Ancona Line (Central Italy). *Mem. Soc. Geol. Ital.*, 24: 325–336.
- Cati, F., 1974. The Oligocene–Miocene boundary in the Monte Arligo section. *G. Geol.*, 39(2): 481–502.
- Cati, F., Steininger, F.F., Borsetti, A.M. and Gelati, R. (Editors), 1981. In search of the Palaeogene–Neogene boundary stratotype. I.U.G.S., CNR spec. publ., *G. Geol.*, 44(1–2), 210 pp.
- Cavelier, C., Butterlin, J., Clermonte, J., Colchen, M., Guennoc, P., Guirau, R., Lorenz, C. and Ricou, L.E., 1993. Late Burdigalian (18–16.5 Ma). In: J. Dercourt, L.E. Ricou and B. Vrielynck (Editors), *Atlas Tethys Palaeoenvironmental Maps. Explanatory Notes*. Gauthier Villars, Paris, pp. 225–242.
- Cebula, G.T., Kunk, M.J., Mehnert, H.H., Naeser, C.W., Obradovich, J.D. and Sutter, J.F., 1986. The Fish Canyon Tuff, a potential standard for the  $^{40}\text{Ar}/^{39}\text{Ar}$  and fission-track methods. *Terra Cognita*, 6(2): 139–140.
- Chamley, H., Meulenkamp, P.E., Zachariasse, W.J. and Van der Zwaan, G.J., 1986. Middle to Late Miocene marine ecostratigraphy: clay minerals, planktonic Foraminifera and stable isotopes from Sicily. *Oceanol. Acta*, 9(3): 227–238.
- Channell, J.E.T. and Marechal, J.C., 1989. Delamination and asymmetric lithospheric thickening in the development of the Tyrrhenian Rift. In: M.P. Coward, D. Dietrich and R.G. Park (Editors), *Alpine Tectonics*. *Geol. Soc. Spec. Publ.*, 45: 285–302.
- Channell, J. and Montanari, A., 1992. Paleomagnetic analysis of the Burdigalian–Langhian section of Moria in the Marche region (Italy). UGS–SOG Miocene Columbus Project, Ancona (Italy), October 1992, Abstract and Field Trips, pp. 35–37.
- Channell, J.E.T., Torii, M. and Hawthorne, T., 1990. Magnetostratigraphy of sediments recovered at Sites 650, 651, 652 and 654 (Leg 107, Thyrrhenian Sea). *Proc. ODP Sci. Results*, 107: 335–346.
- Channell, J., Poli, S., Rio, D., Sprovieri, R. and Villa, G., 1994. Magnetic stratigraphy and biostratigraphy of Pliocene 'Argille azzurre' (Northern Apennines, Italy). *Palaeogeogr., Palaeoclimatol., Palaeoecol.*, 110: 83–102.
- Chaproniere, G.C.H., 1988. *Globigerina woodi* from the Late Oligocene and Early Miocene of Southeastern Australia. *J. Foraminiferal Res.*, 18(2): 124–129.
- Charlot, R., Choubert, G., Faure-Muret, A., Hottinger, L., Marçais, J. and Tisserant, D., 1967. Note au sujet de l'âge isotopique de la limite Miocène–Pliocène au Maroc. *C.R. Acad. Sci. Paris*, 264, Sér. D, pp. 222–224.
- Cherny, P., Rinaldi, R. and Surdam, R.D., 1977. Wellsite and its status in the phillipsite–harmotome Group. *Neues Jahrb. Mineral. Abh.*, 128: 312–330.
- Chiji, M. and Konda, I., 1978. Planktonic foraminiferal biostratigraphy of the Tomioka Group and the Nishiyatsushiro and Shizuoka Groups, central Japan, with some considerations on the Kaburan stage (Middle Miocene). In: *Cenozoic Geology of Japan* (Prof. Nobuo Ikebe Memorial Volume). Osaka, pp. 74–92 (in Japanese with English abstract).
- Chinzei, K., 1991. Late Cenozoic zoogeography of the Sea of Japan area. *Episodes*, 14: 231–235.
- Choubert, G., Charlot, R., Faure-Muret, A., Hottinger, L., Marçais, J., Tisserant, D. and Vidal, P., 1968. Note préliminaire sur le volcanisme messinien–(pontien) au Maroc. *C.R. Acad. Sci. Paris*, 266, Sér. D, pp. 197–199.
- Ciampo, G., 1986. Ostracodi del limite Tortoniano-Messiniano in alcune sezioni italiane. *Boll. Soc. Paleontol. Ital.*, 24(1): 29–110.

- Cita, M.B., 1964. Considérations sur le Langhien des Langhe et sur la stratigraphie du Miocène du bassin tertiaire du Piémont. Proc. II Sess. C.M.N.S. Sabadell, Madrid, 1962, Inst. 'Lucas Mallada', 9: 203–210.
- Cita, M.B., 1967. Notizie sul Tortoniano-tipo. In: R. Selli (Editor), Guida alle escursioni del IV Congr. C.M.N.S., Bologna, pp. 39–45.
- Cita, M.B., 1971a. Stratotypes of Mediterranean Neogene Stages: Langhian. *G. Geol.*, 37(2): 107–116.
- Cita, M.B., 1971b. Stratotypes of Mediterranean Neogene Stages: Tortonian. *G. Geol.*, 37(2): 199–208.
- Cita, M.B., 1975. Studi sul Pliocene e sugli strati di passaggio dal Miocene al Pliocene, VIII. Planktonic foraminiferal biozonation of the Mediterranean Pliocene deep-sea record. A revision. *Riv. Ital. Paleontol. Stratigr.*, 81(4): 527–544.
- Cita, M.B., 1976. Planktonic foraminiferal biostratigraphy of the Mediterranean Neogene. In: Y. Takayanagi and T. Saito (Editors), *Progress in Micropaleontology*. Micropaleontology Press Spec. Publ., Am. Mus. Nat. Hist., pp. 47–68.
- Cita, M.B., 1978. Biostratigraphy of Miocene deep-sea sediments (sites 372 and 375). *Init. Rep. DSDP*, 42(1): 671–685.
- Cita, M.B., 1982. The Messinian salinity crisis in the Mediterranean: a review. In: H. Berckhemer and K. Hsü (Editors), *Alpine–Mediterranean Dynamics*, 7: 113–140.
- Cita, M.B. and Blow, W.H., 1969. The biostratigraphy of the Langhian, Serravallian and Tortonian stages in the type-sections in Italy. *Riv. Ital. Paleontol. Stratigr.*, 75: 549–603.
- Cita, M.B. and Elter, P., 1960. La posizione stratigrafica delle Marne a Pteropodi delle Langhe e della Collina di Torino ed il significato cronologico del Langhiano. *Accad. Naz. Lincei, Rend. Cl., Sci. Fis. Mat. Nat.*, 29: 241–246.
- Cita, M.B. and Gartner, S., 1973. The stratotype Zanclean. Foraminiferal and nannofossil biostratigraphy. *Riv. Ital. Paleontol. Stratigr.*, 79: 503–558.
- Cita, M.B. and McKenzie, J.A., 1986. The terminal Miocene event. In: K.J. Hsü (Editor), *Mesozoic and Cenozoic Oceans*. Am. Geophys. Union, Geodyn. Ser., 15: 123–140.
- Cita, M.B. and Premoli Silva, I., 1960. Pelagic foraminifera from the type Langhian. *Proc. Int. Paleontol. Union, Norden*, 1960, XXII: 39–50.
- Cita, M.B. and Premoli Silva, I., 1968. Evolution of the planktonic foraminiferal assemblages in the stratigraphical interval between the type Langhian and the type Tortonian and the biozonation of the Miocene of Piedmont. *G. Geol.*, 35: 1051–1082.
- Cita, M.B., Premoli Silva, I. and Rossi, R., 1965. Foraminiferi planctonici del Tortonian-tipo. *Riv. Ital. Paleontol. Stratigr.*, 71: 217–308.
- Cita, M.B., Premoli Silva, I. and Rossi, R., 1966. Biostratigraphie du Tortonien Type (Foraminifères Planctoniques). In: Drooger, C.W., Reiss, Z., Rutsch, R.F. and Marks, P. (Editors). *Proceedings of the third Session CMNS*. Brill, Leiden, pp. 216–222.
- Cita, M.B., Stradner, H. and Ciaranfi, N., 1973. Studi sul Pliocene e sugli strati di passaggio al Miocene al Pliocene, III. Biostratigraphical investigations on the Messinian stratotype and on the overlying 'Trubi' Formation. *Riv. Ital. Paleontol.*, 79(3): 393–446.
- Cita, M.B., Rio, D. and Sprovieri, R., in press. The Pliocene series: chronology of the type Mediterranean record and standard chronostratigraphy. *Am. Ass. Stratigr. Palynol. Contrib. Ser.*
- Clari, P. and Ghibaudo, G., 1979. Multiple slump scars in the Tortonian type area (Piedmont Basin, Northwestern Italy). *Sedimentology*, 26: 719–730.
- Clauzon, G., Suc, J.-P., Gautier, F., Berger, A. and Loutre, M.-F., 1996. An alternate interpretation of the Messinian Salinity Crisis: controversy resolved? *Geology*, 24: 363–366.
- Coccioni, R. and Monechi, S., 1992. New biostratigraphic data based on calcareous plankton of the uppermost Oligocene–lower Miocene of the Contessa section (Gubbio, Italy). In: A. Montanari, R. Coccioni and G.S. Odin (Editors), *Volume of Abstracts and Field Trips, Interdisciplinary Geological Conference on the Miocene Epoch with emphasis on the Umbria–Marche sequence (I.U.G.S., Subcommittee on Geochronology, Miocene Columbus Project)*, Ancona, November 11–15, 1992, pp. 38–40.
- Coccioni, R. and Montanari, A., 1992. The 'Livello Piero della Francesca' in the Umbria–Marche Apennines, Italy: a regional volcanoclastic marker bed at the boundary between the Bisciaro and the Schlier/Marne con Cerrognà formations (Lower Miocene). In: A. Montanari, R. Coccioni and G.S. Odin (Editors), *Volume of Abstracts and Field Trips, Interdisciplinary Geological Conference on the Miocene Epoch with emphasis on the Umbria–Marche sequence (I.U.G.S., Subcommittee on Geochronology, Miocene Columbus Project)*, Ancona, November 11–15, 1992, pp. 41–42.

- Coccioni, R. and Montanari, A., 1994. L'orizzonte del Bisciario. In: *Guide Geologiche Regionali, Appennino umbro-marchigiano*. BE-MA Editrice, pp. 36–38.
- Coccioni, R., Guerrera, F. and Veneri, F., 1988. Segnalazione di un intervallo piroclastico ('Mega-P') di notevole spessore nel Bisciario inframiocenico di Arcevia (Appennino marchigiano). *Boll. Soc. Geol. Ital.*, 107(1): 25–32.
- Coccioni, R., Langenheim, V.E. and Montanari, A., 1989. The 'Livello Raffaello' in the Umbria–Marche Apennines: a regional volcanoclastic marker bed at the boundary between the Scaglia Cinerea and the Bisciario Formations (Lowermost Miocene). 28th Int. Congr., Washington, D.C., 1: 308–309.
- Coccioni, R., Capuano, N., D'Antonio, G., Di Leo, C., Galeotti, S. and Perugini, M., 1992a. Litho- and biostratigraphy of the Casteldimezzo, S. Marina and La Sardella sections across the Tortonian–Messinian boundary (Northeastern Apennines, Italy). In: A. Montanari, R. Coccioni and G.S. Odin (Editors), *Volume of Abstracts and Field Trips, Interdisciplinary Geological Conference on the Miocene Epoch with emphasis on the Umbria–Marche sequence (I.U.G.S., Subcommittee on Geochronology, Miocene Columbus Project)*, Ancona, November 11–15, 1992, pp. 43–47.
- Coccioni, R., Di Leo, C., Fornaciari, E., Galeotti, S. and Rio, D., 1992b. Integrated calcareous plankton biostratigraphy from the S. Croce and Moria sections (Northeastern Apennines, Italy). In: A. Montanari, R. Coccioni and G.S. Odin (Editors), *Volume of Abstracts and Field Trips, Interdisciplinary Geological Conference on the Miocene Epoch with emphasis on the Umbria–Marche sequence (I.U.G.S., Subcommittee on Geochronology, Miocene Columbus Project)*, Ancona, November 11–15, 1992, pp. 48–50.
- Coccioni, R., Di Leo, C. and Galeotti, S., 1992c. Planktonic foraminiferal biostratigraphy of the upper Serravallian–lower Tortonian Monte dei Corvi section (NE Italy). In: A. Montanari, R. Coccioni and G.S. Odin (Editors), *Volume of Abstracts and Field Trips, Interdisciplinary Geological Conference on the Miocene Epoch with emphasis on the Umbria–Marche sequence (I.U.G.S., Subcommittee on Geochronology, Miocene Columbus Project)*, Ancona, November 11–15, 1992, pp. 53–56.
- Coccioni, R., Galeotti, S. and Di Leo, R., 1994a. The first occurrence of *Neoglobobulimina atlantica* (Berggren) in the Mediterranean. In: R. Coccioni, A. Montanari and G.S. Odin (Editors), *Miocene Stratigraphy of Italy and Adjacent Regions*. *G. Geol.*, 56(1): 127–138.
- Coccioni, R., Montanari, A. and Odin, G.S. (Editors), 1994b. *Miocene Stratigraphy of Italy and Adjacent Regions*. *G. Geol.*, 56(1), 212 pp.
- Colalongo, M.L., 1970. Appunti biostratigrafici sul Messiniano. *G. Geol.*, 36(2): 515–542.
- Colalongo, M.L., Cremonini, G., Farabegoli, E., Sartori, R., Tampieri, R. and Tomadin, L., 1978. Palaeoenvironmental study of 'Colombacci' Formation in Romagna (Italy): the Cella section. *Mem. Soc. Geol. Ital.*, 16: 197–216.
- Colalongo, M.L., Di Grande, A., D'Onofrio, S., Giannelli, L., Iaccarino, S., Mazzei, R., Poppi Brigatti, M.F., Romeo, M., Rossi, A. and Salvatorini, G., 1979a. A proposal for the Tortonian–Messinian boundary. *Ann. Géol. Pays. Hellén.*, 1: 285–294 (7th Int. Congr. Mediterranean Neogene, Athens).
- Colalongo, M.L., Di Grande, A., D'Onofrio, S., Giannelli, L., Iaccarino, S., Mazzei, R., Romeo, M. and Salvatorini, G., 1979b. Stratigraphy of Late Miocene Italian sections straddling the Tortonian–Messinian boundary. *Boll. Soc. Paleontol. Ital.*, 18: 258–302.
- Coradossi, N. and Corazza, E., 1980. Geochemistry of Messinian evaporitic marls. A comparison between results of DSDP and some Italian basins. *Géol. Méditerr.*, 7(1): 49–56.
- Cosca, M. and O'Nions, R.K., 1994. A re-examination of the influence of composition on argon retentivity in metamorphic calcic amphiboles. *Chem. Geol.*, 112: 39–56.
- Cosca, M.A., Hunziker, J.C., Huon, S. and Mason, H., 1992. Radiometric age constraints on mineral growth, metamorphism, an tectonism of the Gummfluh Klippe, Briançonais Domain of the Préalpes, Switzerland. *Contrib. Mineral. Petrol.*, 112: 439–449.
- Cossmann, M. and Peyrot, A., 1909–1933. *Conchologie néogénique de l'Aquitaine*. Actes Soc. Linn. Bordeaux, t. I–VI.
- Cowie, J.W., Ziegler, W., Boucot, A.J., Bassett, M.G. and Remane, J., 1986. Guidelines and statutes of the International Commission of Stratigraphy (I.C.S.). *Courier Forschungsinst. Senckenberg*, 83: 1–14.
- Cremonin, G. and Farabegoli, E., 1982. Carta geologica 1/25000 della Regione Emilia–Romagna, tavv. Cusercoli e Borello (con note illustrative). Pitagora, Bologna, 25 pp.
- Cremonini, G. and Marabini, S., 1982. La Formazione a Colombacci nell'Appennino Romagnolo. In: G. Cremonini and F. Ricci Lucchi (Editors), *Guida alla geologia del margine appenninico padano*. *Guide Geol. Reg. S.G.I.*, Bologna, pp. 167–169.

- Cuenca, G., Azanza, B., Canudo, J.I. and Fuentes, V., 1989. Los micromamíferos del Mioceno inferior de Peñalba (Huesca). Implicaciones bioestratigráficas. *Geogaceta*, 6: 75–77.
- Cuenca Bescós, G., Canudo, J.I., Andrés, J.A. and Laplana, C., 1992. Bio y cronostratigrafía con mamíferos en la Cuenca terciaria del Ebro. Ensayo de síntesis. *Acta Geol. Hisp.*, 27: 127–143.
- Daams, R., 1990. *Hypsodont Myomiminae (Gliridae, Rodentia) in the Oligocene–Miocene boundary interval and Miocene of Spain*. *Scripta Geol.*, 96: 1–62.
- Daams, R. and Freudenthal, M., 1981. Aragonian; the stage concept versus Neogene mammal zones. *Scripta Geol.*, 62: 17.
- Daams, R. and Freudenthal, M., 1988. Synopsis of the Dutch–Spanish collaboration program in the Aragonian tpe area, 1975–1985. *Scripta Geol.*, spec. iss., 1: 3–18.
- Daams, R. and Freudenthal, M., 1989. The Ramblian and Aragonian: limits, subdivision, geographical and temporal extension. In: E.H. Lindsay et al. (Editor), *European Neogene Mammal Chronology*. NATO ASI Series 180, Plenum Press, New York, pp. 51–60.
- Daams, R. and van der Meulen, A., 1984. Paleoenvironmental and paleoclimatic interpretation of micro-mammal faunal successions in the Upper Oligocene and Miocene of North Central Spain. *Paléobiol. Continentale*, 14(2): 241–257.
- Daams, R., Freudenthal, M. and van De Weer, A., 1977. Aragonian, a new stage for continental deposits of Miocene age. *Newsl. Stratigr.*, 6: 42–55.
- Daams, R., Freudenthal, M. and Alvarez-Sierra, M., 1987. Ramblian: a new stage for continental deposits of early Miocene age. *Geol. Mijnbouw*, 65: 297–308.
- Daguin, F., 1948. *L'Aquitaine occidentale*. Hermann et Cie, Paris, 227 p.
- Dalrymple, G.B., Alexander, E.C., Lanphere, M.A. and Kraker, G.P., 1981. Irradiation of samples for  $^{40}\text{Ar}/^{39}\text{Ar}$  dating using the Geological Survey TRIGA reactor. *U.S. Geol. Surv., Prof. Pap.*, 1176, 55 pp.
- Dalrymple et al., 1988. *Geophys. Res. Lett.*, 1(6): 589
- d'Atri, A., 1995. *Analisi sedimentologica, biostratigrafica e sequenziale della successione del Miocene inferiore tra le Valli Lemme e Bormida di Spigno (Margine sudorientale del Bacino Terziario Ligure–Piemontese)*. Tesi di Dottorato, Univ. di Torino, 143 pp.
- d'Atri, A. and Tateo, F., 1994. Volcano-sedimentary beds of Oligocene age in the Tertiary Piedmont Basin (NW Italy): biostratigraphy and mineralogy. In: R. Coccioni, A. Montanari and G.S. Odin (Editors), *Miocene Stratigraphy of Italy and Adjacent Regions*. *G. Geol.*, 56(1): 79–95.
- Day, R., Fuller, M.D. and Schmidt, V.A., 1976. Magnetic hysteresis properties of synthetic titanomagnetites. *J. Geophys. Res.*, 81: 873–880.
- Decima, A. and Wezel, F.C., 1971. Osservazioni sulle evaporiti messiniane della Sicilia centro-meridionale. *Riv. Min. Sic.*, 130–132, 172–187.
- Decima, A., McKenzie, J.A. and Schreiber, B.C., 1988. The origin of 'evaporative limestones': an example from the Messinian of Sicily. *J. Sediment. Petrol.*, 58(2): 256–272.
- Deer, W.A., Howie, R.A. and Zussman, S., 1992. *An introduction to rock-forming minerals*. Longman Scientific & Technical, 696 pp.
- Deino, A. and Montanari, A., 1992.  $^{40}\text{Ar}/^{39}\text{Ar}$  Geochronology of air fall ashes in the Miocene pelagic sequence of the Umbria–Marche Apennines (Italy). In: A. Montanari, R. Coccioni and G.S. Odin (Editors), *Volume of Abstracts and Field Trips, Interdisciplinary Geological Conference on the Miocene Epoch with emphasis on the Umbria–Marche sequence (I.U.G.S., Subcommittee on Geochronology, Miocene Columbus Project)*, Ancona, November 11–15, 1992, pp. 65–66.
- Deino, A. and Potts, R., 1990. Single-crystal  $^{40}\text{Ar}/^{39}\text{Ar}$  dating of the Ologesailie Formation, Southern Kenya Rift. *J. Geophys. Res.*, 95: 8453–8470.
- Deino, A., Drake, R.E., Curtis, G.H. and Montanari, A., 1988. Preliminary laser-fusion  $^{40}\text{Ar}/^{39}\text{Ar}$  dating results from Oligocene biotites of Gubbio, Italy. In: I. Premoli Silva, R. Coccioni and A. Montanari (Editors), *The Eocene–Oligocene Boundary in the Marche–Umbria Basin*, IUGS Spec. Publ., F.lli Aniballi Publishers, Ancona, pp. 229–238.
- Deino, A., Keller, J.V.A., Minelli, G. and Piali, G., 1994. Datazioni  $^{40}\text{Ar}/^{39}\text{Ar}$  del metamorfismo dell'Unità di Ortano–Rio Marina (Isola d'Elba): risultati preliminari. *Stud. Geol. Camerti*, vol. spec. 1992/2: 187–192.
- De Lapparent, A., 1906. *Traité de géologie: librairie de l'Académie de Médecine*. Masson, Paris, 2014 pp.
- Del Moro, A., Puxeddu, M., Radicati di Brozolo, F. and Villa, I.M., 1982. Rb/Sr and K/Ar ages on minerals at temperatures of 300–400°C from deep wells in the Larderello Geothermal Field. *Contrib. Mineral.*

- Petrol., 81: 340–349.
- Demaison, G.J. and Moore, G.T., 1980. Anoxic environments and oil source bed genesis. *AAPG Bull.*, 64: 1179–1209.
- Demarcq, G., 1962. Etude stratigraphique du Miocène rhodanien. Thèse Sciences, Paris. *Mém. B.R.G.M.*, 1970, 61, 257 pp.
- Demarcq, G., 1990. Pectinidés néogènes: proposition d'échelle biostratigraphique pour la Méditerranée. *Geobios*, 23(2): 149–159.
- Demarcq, G. and Carbonnel, G., 1975. Burdigalien (stratotype rhodanien) In: F.F. Steininger and L.A. Nevesskaya (Editors), *Stratotypes of Mediterranean Neogene Stages*. 2, C.N.M.S., Bratislava, pp. 51–56.
- Demarcq, G. et al., 1971. Le Néogène rhodanien. *Actes V<sup>o</sup> Congr. Néogène Méditerranéen*, 1, Doc. Lab. Géol. Univ. Lyon., 243 pp.
- Demarcq, G., Magné, J., Anglada, R. and Carbonnel, G., 1974. Le Burdigalien stratotypique de la vallée du Rhône, sa position biostratigraphique. *Bull. Soc. Géol. Fr.*, Paris, 7, XVI(5): 509–515.
- DePaolo, D.J., 1986. Detailed record of the Neogene Sr isotopic evolution of seawater from DSDP Site 590B. *Geology*, 14: 103–106.
- DePaolo, D.J. and Finger, K.L., 1991. High-resolution strontium-isotope stratigraphy and biostratigraphy of the Miocene Monterey Formation, central California. *Geol. Soc. Am. Bull.*, 103: 112–124.
- DePaolo, D.J. and Ingram, B.L., 1984. High resolution stratigraphy with strontium isotopes. *Science*, 227: 938–941.
- Depéret, M., 1892. Note sur la classification et le parallélisme du Système Miocène. *C.R. Somm. Soc. Géol. Fr.*, (3), 20, 13: 145–156.
- Dercourt, J., Ricou, L.E. and Vrielynck, B. (Editors), 1993. *Atlas Tethys Palaeoenvironmental Maps*. Gauthier Villars, Paris, 307 pp.
- Diaz De Federico, A., Torres-Roldan, R. and Puga, E., 1990. The rock-series of the Betic substratum. *Doc. Trav. IGAL Paris*, 12–13: 19–29.
- Di Battistini, G., Toscani, L., Iaccarino, S. and Villa, I., 1987. K/Ar ages and geological setting of calc-alkaline volcanic rocks from Sierra de Gata, SE Spain. *Neues Jahrb. Miner., Monatsh.*, H8: 369–383.
- Didon, J., Fernex, F., Lorenz, C., Magné, J. and Peyre, Y., 1969. Sur un niveau remarquable de silicite dans le Néogène inférieur d'Espagne méridionale et d'Italie du Nord. *Bull. Soc. Géol. Fr.*, 11(7): 841–853.
- Dieci, G. and Russo, A., 1965. Ostracodi tortoniani dell'Appennino settentrionale (Tortona, Montegibbio, Castelvetro). *Boll. Soc. Paleontol. Ital.*, 3(1): 38–88.
- Dinelli, E. and Tateo, F., 1993. Geochemistry and mineralogy of 'Monte del Casino' section: pre-evaporitic shales of Tortonian–Messinian age (Northern Apennines, Italy). *Mineral. Petrogr. Acta*, 36: 81–101.
- D'Offizi, S., Minelli, G. and Pialli, G., 1994. Foreland basins and thrust systems in the Northern Apennines. *Boll. Geofis. Teor. Appl.*, XXXVI(141–144), 91–102.
- Dollfus, G.F., 1909. Essai sur l'étage aquitanien. *Bull. Serv. Carte Géol. Fr.*, Paris, 19, 124: 379–495.
- Dollfus, G.F., 1920. Réunion extraordinaire de la Société Géologique de France à Bordeaux, du 23 au 28 août 1920. *C.R. Somm. Soc. Géol. Fr.*, Paris, Sér. 4, 20, 13: 141–160.
- D'Onofrio, S., 1964. I Foraminiferi del neostatotipo del Messiniano. *G. Geol.*, 32: 400–461.
- D'Onofrio, S., Giannelli, L., Iaccarino, S., Morlotti, E., Romeo, M., Salvatorelli, G. and Sprovieri, R., 1976. Planktonic foraminifera of the upper Miocene from some Italian sections and the problem of the lower boundary of the Messinian. *Boll. Soc. Paleontol. Ital.*, 14: 177–196.
- Drooger, C.W., 1964. Les transgressions du Miocène inférieur en Aquitaine. (2e Réunion du Comité du Néogène Méditerranéen, Sabadell–Madrid, 1961), *Cursillos y Conferencias del Instituto 'Lucas Mallada'*, Madrid, IX: 51–59.
- Drooger, C.W. (Editor), 1973. *Messinian Events in the Mediterranean*. *Geodyn. Sci. Rep.* 7, North-Holland Publishing Company, Amsterdam, London, 272 pp.
- Drooger, C.W., Kaasschieter, J.P.H. and Key, A.J., 1955. The microfauna of the Aquitanian–Burdigalian of southwestern France. *Verh. K. Ned. Akad. Wet.*, Ser. I, 21(2): 1–136.
- Eberhardt, P. and Ferrara, G., 1962. Confirmation of the absolute age of the granodiorite outcrop in Elba Island with potassium–argon measurements. *Nature*, 196: 665–666.
- Edwards, L.E., 1984. Miocene dinoflagellate cysts from Deep Sea Drilling Project Leg 81, Rockall Plateau, eastern North Atlantic Ocean. *Init. Rep. DSDP*, 81: 581–594.
- Eglinton, T.I., Sinninghe Damsté, J.S., Pool, W., de Leeuw, J.W., Eijkkel, G. and Boon, J.J., 1992. Organic sulfur in macromolecular sedimentary organic matter, II. Analysis of distribution of sulfur-containing

- pyrolysis products using multivariate techniques. *Geochim. Cosmochim. Acta*, 56: 1545–1560.
- Elderfield, H., Gieskes, J.M., Baker, P.A., Oldfield, R.K., Hawkesworth, C.J. and Miller, R., 1982.  $^{87}\text{Sr}/^{86}\text{Sr}$  and  $^{18}\text{O}/^{16}\text{O}$  ratios, interstitial water chemistry and diagenesis in deep-sea carbonate sediments of the Ontong Java Plateau. *Geochim. Cosmochim. Acta*, 46: 2259–2268.
- Elter, P., Giglia, G., Tongiorgi, M. and Trevisan, L., 1975. Tensional and compressional areas in the recent (Tortonian to Present) evolution of north Apennines. *Boll. Geofis. Teor. Appl.*, 17: 3–18.
- Emiliani C., 1966. Isotopic paleotemperatures. *Science*, 154 (3751): 851–857.
- Emmanuel, L., 1993. Apport de la géochimie des carbonates à la stratigraphie séquentielle. Application au Crétacé inférieur du domaine vocontien. Université P. et M. Curie, *Mém. Sci. Terre*, 93-5: 1–190.
- Emmanuel, L. and Renard, M., 1993. Carbonate geochemistry (Mn,  $\delta^{13}\text{C}$ ,  $\delta^{18}\text{O}$ ) of the late Tithonian–Berriasian pelagic limestones of the vocontian trough (SE France). *Bull. Cent. Rech. Explor. Prod. Elf-Aquitaine*, 17-1: 205–221.
- Erentöz, L. and Oztemür, C., 1964. Aperçu général sur la stratigraphie du Néogène de la Turquie et observations sur ses limites inférieure et supérieure. *Inst. 'Lucas Mallada', C.S.I.C. (España). Cursos y Conferencias*, IX: 259–266.
- Eto, T., 1986. Stratigraphy of the Miura and Kazusa Groups in the Miura peninsula, Japan. *Sci. Rep. Yocohama National Univ., Section II (Biology and Geology)*, 33: 107–132 (in Japanese with English abstr.).
- Evernden, J.F., Savage, D.E., Curtis, G.H. and James, G.T., 1964. Potassium-Argon dates and the Cenozoic mammalian chronology of North America. *Am. J. Sci.*, 262: 145–198.
- Falletti, P., Gelati, R. and Rogledi, S., 1994. Oligo–Miocene Evolution of episutural and perisutural basins at the Alps/Apennines boundary. *RCMNS Coll.* Rabat.
- Farrell, J.W., Clemens, S.C. and Gromet, L.P., 1995. Improved chronostratigraphic reference curve of Late Neogene seawater  $^{87}\text{Sr}/^{86}\text{Sr}$ . *Geology*, 23(5): 403–406
- Feist, M., Anadon, P., Cabrera, L., Choi, S.J., Colombo, F. and Saez, M., 1994. Upper Eocene–Lowermost Miocene charophyte succession in the Ebro Basin (Spain). Contribution to the charophyte biozonation in Western Europe. *Newsl. Stratigr.*, 30: 1–32.
- Fenner, J., 1985. Late Cretaceous to Oligocene planktic diatoms. In: H.M. Bolli, J.B. Saunders and K. Perch-Nielsen (Editors), *Plankton Stratigraphy*. Cambridge Univ. Press, Cambridge, pp. 713–762.
- Ferretti, S., 1993. Studio stratigrafico sedimentologico dei depositi clastici Tortoniano–Messiniani dell'Appennino settentrionale. Unpubl. Ph.D. Thesis, Univ. Bologna, 168 pp. (including the study of Foraminifera by M.L. Colalongo).
- Fleck, R.J., Sutter, J.F. and Elliot, D.H., 1977. Interpretation of discordant  $^{40}\text{Ar}/^{39}\text{Ar}$  age-spectra of Mesozoic tholeiites from Antarctica. *Geochim. Cosmochim. Acta*, 41: 15–32.
- Flishch, M., 1982. Potassium argon analysis. In: G.S. Odin (Editor), *Numerical Dating in Stratigraphy*. John Wiley and Sons, Chichester, pp. 151–158.
- Flores, J.A., Sierro, F.J. and Glaçon, G., 1992. Calcareous plankton analysis in the pre-evaporitic sediments of the ODP Site 654 (Tyrrhenian Sea, Western Mediterranean). *Micropaleontology*, 38(2): 279–288.
- Foland, K.A., 1983.  $^{40}\text{Ar}/^{39}\text{Ar}$  incremental heating plateaus for biotites with excess argon. *Isot. Geosci.*, 1: 3–21.
- Foresi, L.M., 1993. Biostratigrafia a foraminiferi planctonici del Miocene medio del Mediterraneo e delle basse latitudini con considerazioni cronostatigrafiche. PhD Thesis, Univ. of Parma, 146 pp.
- Fornaciari, E. and Labaume, P., 1992. Calcareous nannofossil biostratigraphy of the Bobbio Formation (NW Apennines, Italy). *Mem. Sci. Geol.*, 44: 109–126.
- Fornaciari, E. and Rio, D., 1996. Latest oligocene to early middle Miocene quantitative calcareous nannofossil biostratigraphy in the Mediterranean region. *Micropaleontology*, 42 (1): 1–36.
- Fornaciari, E., Raffi, I., Rio, D., Villa, G., Backman, J. and Olafson, G., 1990. Quantitative distribution patterns of Oligocene and Miocene calcareous nannofossils from the western equatorial Indian Ocean. *Proc. ODP, Sci. Results*, 115: 237–254.
- Fornaciari, E., Backman, I. and Rio, D., 1993. Quantitative distribution patterns of selected Lower to Middle Miocene calcareous nannofossils from the Ontong Java Plateau. *Proc. ODP Sci. Results*, 130: 245–256.
- Fornaciari, E., Di Stefano, E., Rio, D. and Negri, A., 1996. Middle Miocene quantitative calcareous nannofossil biostratigraphy in the Mediterranean region. *Micropaleontology*, 42(1): 37–63.
- Fornaciari, E., Ghibaudo, G., Iaccarino, S., Massari, F., Rio, D., submitted. Calcareous plankton biostratigraphy of the Serravallian (middle Miocene) stratotype section (Piedmont Tertiary basin NW Italy,

- submitted.
- Fornaciari, E., Iaccarino, S., Marzei, R., Rio, D., Salvatorini, G., Bossio, A. and Moteforti, B., 1997. Calcareous plankton biostratigraphy of the Langhian historical stratotype, Chapter A6, this volume.
- Foster, J.H. and Opdyke, N.D., 1970. Upper Miocene to Recent magnetic stratigraphy in deep-sea sediments. *J. Geophys. Res.*, 75: 4465–4473.
- Fountain, D.M., 1976. The Ivrea–Verbano and Strona–Ceneri zones, Northern Italy: a cross section of the continental crust. New evidence from seismic velocities of rock samples. *Tectonophysics*, 33: 145–165.
- Freeman, R., Giese, P. and Mueller, St., 1990. The European Geotraverse; integrative studies. Results from the Fifth Earth Science Study Centre. Rauschholzhausen, 26 March–7 April, 1990, 404 pp.
- Fuhrmann, U., Lippolt, H.J. and Hess, J.C., 1987. Examination of some proposed K–Ar standards:  $^{40}\text{Ar}/^{39}\text{Ar}$  and conventional K–Ar data. *Chem. Geol. (Isot. Geosci. Sect.)*, 7: 41–52.
- Funnell, B.M., 1964. The Tertiary period. In: W.B. Harland et al. (Editors), *The Phanerozoic Time Scale*. Q. J. Geol. Soc. London, 120: 179–191.
- Galbiati, B., 1976. La successione Oligo–Miocenica tra Rigoroso e Carrosio (Bacino Ligure–Piemontese). *Atti Ist. Geol. Univ. Pavia*, 26: 30–40.
- Gandolfi, G., Paganelli, L. and Zuffa, G.G., 1983. Petrology and dispersal pattern in the Marnoso–Arenacea Formation (Miocene, Northern Apennines). *J. Sediment. Petrol.*, 53: 493–507.
- Gartner, S., 1992. Miocene nannofossil chronology in the North Atlantic, DSDP Site 608. *Mar. Micropaleontol.*, 18: 307–331.
- Gasparotto, G., 1988. Evoluzione dei clinopirosseni in basalti e ‘Monzoniti’ di Cima Pape (Dolomiti Orientali). *Miner. Petrogr. Acta*, 31: 43–68.
- Gautier, F., Clauzon, G., Suc, J.-P., Cravatte, J. and Violanti, D., 1994. Age et durée de la crise de salinité messinienne. *C.R. Acad. Sci. Paris, Sér. 2*, 318: 1103–1109.
- Gelati, R., 1968. Stratigrafia dell’Oligo–Miocene delle Langhe tra le valli dei Fiumi Tanaro e Bormida di Spigno. *Riv. Ital. Paleontol. Stratigr.*, 74: 875–964.
- Gelati, R., 1977. La successione eo–oligocenica di Garbagna (Alessandria) al margine orientale del Bacino Terziario Ligure–Piemontese. *Riv. Ital. Paleontol. Stratigr.*, 83(1): 103–136.
- Gelati, R. and Gnaccolini, M., 1980. Significato dei corpi arenacei di conoide sottomarina (Oligocene–Miocene inferiore) nell’evoluzione tettonico-sedimentaria del Bacino Terziario ligure–piemontese. *Riv. Ital. Paleontol. Stratigr.*, 86: 167–186.
- Gelati, R. and Steininger, F.F. (Editors), 1984. In Search of the Palaeogene/Neogene Boundary Stratotype, Part 2. Potential Boundary Stratotype Sections in Italy and Spain. A comparison with results from the deep-sea and the environmental changes. *Riv. Ital. Paleontol. Stratigr.*, 89(4): 451–564.
- Gelati, R., Gnaccolini, M., Falletti, P. and Catrullo, D., 1993. Stratigrafia sequenziale della successione oligo–miocenica delle Langhe, Bacino terziario ligure–piemontese. *Riv. Ital. Paleontol. Stratigr.*, 98: 425–452.
- Ghibaud, G., Clari, P. and Perello, M., 1985. Litostratigrafia, sedimentologia ed evoluzione tettonico-sedimentaria dei depositi miocenici del margine sud-orientale del Bacino Terziario Ligure–Piemontese (Valli Borbera, Scrivia e Lemme). *Boll. Soc. Geol. Ital.*, 104: 349–397.
- Giannotti, A., 1953. Microfaune della serie tortoniana del Rio Mazzapiedi–Castellania (Tortona–Alessandria). *Riv. Ital. Paleontol. Stratigr., Mem.*, VI: 167–308.
- Giannotti, A. and Gino, G.F., 1958. Il Tortoniano classico di Tortona. *Coll. Int. Micropal., Guida alle escursioni*, pp. 13–21.
- Gignoux, M., 1950. *Géologie stratigraphique*. Masson, Paris, IV éd., VII, 735 pp.
- Gino, G.F., 1963. Osservazioni geologiche sui dintorni di S. Agata Fossili. *Riv. Ital. Paleontol. Stratigr., Mem.*, VI: 1–23.
- Girotti, O. and Parotto, M., 1969. Mio–Pliocene di Ascoli Piceno. *Atti Accad. Gioenia Sci. Nat. Catania*, 1: 127–174.
- Glaçon, G., Vergnaud-Grazzini, C., Iaccarino, S., Renault, J.-P., Randrianasolo, A., Sierro, J.F., Weaver, Ph., Channell, J., Torri, M. and Hawthorne, Y., 1990. Planktonic foraminiferal events and stable isotope records in the upper Miocene, Site 654. *Proc. ODP Sci. Results*, 107: 415–427.
- Gladenkov, A.Y. and Barron, J.A., 1993. Oligocene to Early Middle Miocene Diatom Biostratigraphy of ODP Hole 884B. *Proc. ODP Sci. Results*, 145.
- Gnaccolini, M., 1960. Contributo alla conoscenza della paleogeografia del Langhiano delle Langhe (tra Acqui e Bobbio). *Riv. Ital. Paleontol. Stratigr.*, 66: 589–603.

- Gnaccolini, M., 1968. Il bacino delle Langhe (Piemonte) durante il Miocene. *Riv. Ital. Paleontol. Stratigr.*, 74: 133–142.
- Gnaccolini, M., 1969. Caratteristiche principali dello stratotipo del Langhiano e delle formazioni adiacenti. *G. Geol.*, 95: 97–103.
- Gnaccolini, M., 1978a. L'Unità di S. Rocco' nella Formazione di Molare tra le valli del T. Stura e del T. Lemme. *Riv. Ital. Paleontol. Stratigr.*, 84: 411–442.
- Gnaccolini, M., 1978b. Depositi oligocenici di 'fan delta' nella regione compresa tra Bosio e la Costa Cravara (Bacino Terziario Ligure–Piemontese). *Riv. Ital. Paleontol. Stratigr.*, 84: 673–699.
- Gnaccolini, M., 1989. Il Langhiano–Serravalliano tra le valli del Tanaro e del Belbo. Confronti con i dintorni di Gavi e di Finale Ligure. *Riv. Ital. Paleontol. Stratigr.*, 95: 55–74.
- Gnaccolini, M., Gelati, R., Catrullo, D. and Falletti, P., 1990. Sequenze deposizionali nella successione oligo–miocenica delle 'Langhe': un approccio alla stratigrafia sequenziale del bacino Terziario Ligure–Piemontese. *Mem. Soc. Geol. Ital.*, 45: 671–686.
- Gnaccolini, M., Gelati, R., Falletti, P. and Catrullo, D., in press. Sequence stratigraphy of the 'Langhe', Oligo–Miocene succession, Piedmont Tertiary Basin, Northern Italy. *Int. Symp. Mesozoic and Cenozoic Sequence Stratigraphy of European Basins*, Dijon, 1992.
- Goldsmith, N.F., Martinell, J., Demarcq, G., Bohn-Havas, M. and Dockery, D.T., III, 1994. Sr-isotopic calibration of Cenozoic bivalvia and Early Miocene migrations: Eurasian carnivores to Africa (the Hazeva Formation, Israel) and African gazelles and proboscidea to Ipolytarnoc, Hungary. *Newsl. Stratigr.*, 31(3): 167–183.
- Grandjean, P., Cappetta, H., Michard, A. and Albarède, F., 1987. The assessment of REE patterns and  $^{143}\text{Nd}/^{144}\text{Nd}$  ratios in fish remains. *Earth Planet. Sci. Lett.*, 84: 181–196.
- Grasso, M. and La Manna, F., 1993. Lineamenti stratigrafici e strutturali del fronte della Falda di Gela affiorante a NW del Plateau ibleo (Sicilia sud-orientale). *Geol. Rom.*, 29: 55–72.
- Grasso, M. and Pedley, H.M., 1990. Neogene and Quaternary sedimentation patterns in the northwestern Hyblean Plateau (SE Sicily): the effects of a collisional process on a foreland margin. *Riv. Ital. Paleontol. Stratigr.*, 96: 219–240.
- Grasso, M., Pedley, H.M. and Romeo, M., 1990. The Messinian Tripoli Formation of north-central Sicily: palaeoenvironmental interpretations based on sedimentological, micropaleontological and regional tectonic studies. *Paliobiol. Continentale*, 17: 189–204.
- Griffin, W.L. and O'Reilly, S.Y., 1987. Is the continental Moho the crust–mantle boundary? *Geology*, 15: 241–244.
- Guerrera, F., 1979. Stratigrafia e sedimentologia dei livelli 'tripolacei' del Miocene inferiore–medio appenninico. *Boll. Serv. Geol. Ital.*, 99: 233–262.
- Guerrera, F. and Veneri F., 1989. Evidenze di attività vulcanica nei sedimenti neogenici e pleistocenici dell'Appennino. *Boll. Soc. Geol. Ital.*, 108: 121–159.
- Haq, B.U., Hardenbol, J. and Vail, P.R., 1987. Chronology of fluctuating sea levels since the Triassic. *Science*, 235: 1156–1167.
- Haq, B.U., Hardenbol, J. and Vail, P.R., 1988. Mesozoic and Cenozoic chronostratigraphy and cycles of sea level change. *SEPM Spec. Publ.*, 42: 71–108.
- Harland, W.B., Smith, A.G. and Wilcock, B. (Editors), 1964. The Phanerozoic Time-Scale. *Q. J. Geol. Soc. London*, 120, 458 pp.
- Harland, W.B., Cox, A.V., Llewellyn, P.G., Pickton, C.A.G., Smith, A.G. and Walters, R., 1982. A Geological Time Scale. Cambridge Univ. Press, Cambridge, 131 pp.
- Harland, W.B., Armstrong, R., Cox, A., Craig, L., Smith, A. and Smith, D., 1990. A Geological Time Scale 1989. Cambridge Univ. Press, Cambridge, 263 pp.
- Hatcher, P.G., 1990. *Org. Geochem.*, 16: 959–968.
- Haug, E., 1927. *Traité de Géologie*. Librairie Colin, Paris.
- Hayashida, A. and Ito, Y., 1984. Paleoposition of Southwest Japan at 16 Ma: implication from paleomagnetism of Miocene Ichishi Group. *Earth Planet. Sci. Lett.*, 68: 335–342.
- Hays, J.D., Imbrie, J. and Shackleton, N.J., 1976. Variations in the Earth's orbit: pacemaker of the ice ages. *Science*, 194: 1121–1132.
- Hedberg, H.D. (Editor), 1976. *International Stratigraphic Guide. A Guide to Stratigraphic Classification, Terminology and Procedure*. Wiley, New York, 200 pp.
- Hernandez, J. and Bellon, H., 1985. *Chronologie K–Ar du volcanisme miocène du Rif oriental (Maroc)*.



- Rev. Géol. Dyn. Géogr. Phys., 26: 85–94.
- Hernandez, A., Costa, J.M., Sola, J. et al., 1991. Evolución genético-sedimentaria de la Unidad de Zuera (Mioceno inferior, Cuenca del Ebro). I<sup>o</sup> Congreso del Grupo Español del Terciario, pp. 162–165.
- Hernandez, J., Larouzière, F.D., Bolze, J. and Bordet, P., 1987. Le magmatisme néogène bético-rifain et le couloir de décrochement 'trans-Alboran'. Bull. Soc. Géol. Fr., 8, 3, 2: 257–267.
- Hess, J.C. and Lippolt, H.J., 1986. Kinetics of argon isotopes during neutron irradiation: Ar loss from minerals as a source of error in  $^{40}\text{Ar}/^{39}\text{Ar}$  dating. Chem. Geol. (Isot. Geosci. Sect.), 59: 223–236.
- Hess, J.C. and Lippolt, H.J., 1994. Compilation of K–Ar measurements on HD-B1 biotite. In: G.S. Odin (Editor), Phanerozoic Time Scale. Bull. Liais. Inform. Subcomm. Geochronol., Paris, 12: 19–23.
- Hess, J., Bender, M.L. and Schilling, J.G., 1986. Evolution of the ratio of strontium-87 to strontium-86 in seawater from Cretaceous to Present. Science, 231: 979–984.
- Hess, J., Stott, L.D., Bender, M.L., Kennett, J.P. and Schilling, J.G., 1989. The Oligocene marine microfossil record: age assessments using strontium isotopes. Paleoceanography, 4(6): 655–679.
- Hilgen, F.J., 1987. Sedimentary rhythms and high resolution chronostratigraphic correlations in the Mediterranean Pliocene. Newsl. Stratigr., 17(2): 109–127.
- Hilgen, F.J., 1991a. Astronomical calibration of Gauss to Matuyama sapropels in the Mediterranean and implication for the Geomagnetic Polarity Time Scale. Earth Planet. Sci. Lett., 104: 226–244.
- Hilgen, F.J., 1991b. Extension of the astronomically calibrated (polarity) time scale to the Miocene/Pliocene boundary. Earth Planet. Sci. Lett., 107: 349–368.
- Hilgen, F.J. and Langereis, C.G., 1988. The age of the Miocene–Pliocene boundary in the Capo Rossello area (Sicily). Earth Planet. Sci. Lett., 91: 214–222.
- Hilgen, F.J. and Langereis, C.G., 1993. A critical re-evaluation of the Miocene/Pliocene boundary as defined in the Mediterranean. Earth Planet. Sci. Lett., 118: 167–179.
- Hill, P.R., 1987. Characteristics of sediments from Feni and Gardar drifts, Sites 610 and 611, Deep Sea Drilling Project Leg 94. Init. Rep. DSDP, 94: 1075–1084.
- Hirata, D., Matsushima, Y. and Asaga, M., 1991. Distribution and occurrence of fossil Clyptonogenas in the Miura and Boso peninsulas. Chikyu Mon., 13: 47–52 (in Japanese).
- Hirst, J.P.P., 1989. Pyrenean tectonic control of Oligocene–Miocene river systems, Huesca, Spain. In: P.F. Friend, J.P.P. Hirst, P.J. Hogan, E.J. Hogan, R. McEloy, G.J. Nichols and J. Rodriguez Vidal (Editors). Excursion Guidebook, 4th International Conference on Fluvial Sedimentology, offset, Sitges, Spain: 50–87.
- Hochuli, P., 1978. Palynologische Untersuchungen im Oligozän und Untermiozän der Zentralen und Westlichen Paratethys. Beitr. Paläontol. Österr., 4: 1–132.
- Hodell, D.A. and Kennett, J.P., 1986. Late Miocene–Early Pliocene stratigraphy and paleoceanography of the south Atlantic and southwest Pacific Oceans: a synthesis. Paleoceanography, 1: 285–311.
- Hodell, D.A. and Woodruff, F., 1994. Variations in the strontium isotopic ratio of seawater during the Miocene: stratigraphic and geochemical implications. Paleoceanography, 9(3): 405–426.
- Hodell, D.A., Mueller, P.A. and Garrido, J.R., 1991. Variations in the strontium isotopic composition of seawater during the Neogene. Geology, 19: 24–27.
- Hodell, D.A., Benson, R.H., Kent, D.V., Boersma, A. and Rakic-El Bied, K., 1994. Magneto-, bio-, and stable isotope stratigraphy of a Late Miocene drill core from the Salé Briqueterie (northwestern Morocco): A high-resolution chronology for the Messinian stage. Paleoceanography, 9(6): 835–855.
- Hodges, K.V., Hames, W.E. and Bowring, S.A., 1994.  $^{40}\text{Ar}/^{39}\text{Ar}$  age gradients in micas from a high temperature–low pressure metamorphic terrain. Evidence for very slow cooling and implications for the interpretation of age spectra. Geology, 22: 55–58.
- Honda, N., 1981. Upper Cenozoic calcareous nannofossil biostratigraphy of the Pacific side of Japan. Unpubl. Ph.D. dissertation, Tohoku University, 110 pp.
- Hörnes, M., 1853. Mitteilung an Prof. Bronn gerichtet: Wien, 3. Okt., 1853: Neues Jahrb. Mineral. Geol. Geogn. Petrefaktenkd., pp. 806–810.
- Hörnes, M., 1864. V. Die fossilen Mollusken des Tertiärbeckens von Wien. Jahrb. Geol. Reichsanst., 14: 509–514.
- Hsü, K.J. (Editor), 1986a. Mesozoic and Cenozoic Oceans. Am. Geophys. Union, Geodyn. Ser., 15, 216 pp.
- Hsü, K.J., 1986b. Unresolved problem concerning the Messinian salinity crisis. G. Geol., 47: 203–212.
- Hsü, K.J., Cita, M.B. and Ryan, W.B.F., 1973. The origin of the Mediterranean Evaporites. Init. Rep. DSDP, 13: 1203–1231.

- Hsü, K.J., Montadert, L., Bernoulli, D., Cita, M.B., Erickson, A., Garrison, R.E., Kidd, R.B., Milihres, X., Miller, C. and Wright, R., 1978. History of the Mediterranean Salinity Crisis. *Init. Rep. DSDP, 42A*: 1053–1078.
- Hsü, K.J., LaBrecque, J., Percival, S.F., Wright, R.C., Gombos, A.M., Pisciotto, K., Tucker, P., Peterson, N., McKenzie, J.A., Weissert, H., Karpoff, A.M., Carman, M.F., Jr. and Schreiber, E., 1984. Numerical ages of Cenozoic biostratigraphic datum levels: results of South Atlantic Leg 73 drilling. *Geol. Soc. Am. Bull.*, 95: 863–876.
- Hunziker, J.C. and Martinotti, G. 1987. Geochronology and evolution of Western Alps: a review. *Mem. Soc. Geol. Ital.*, 29: 43–56.
- Hurford A.J. and Hammerschmidt, K., 1985.  $^{40}\text{Ar}/^{39}\text{Ar}$  dating of the Bishop and Fish Canyon tuffs: calibration ages for fission track dating standards. *Chem. Geol. (Isot. Geosci. Sect.)*, 58: 23–32.
- Iaccarino, S., 1985. Mediterranean Miocene and Pliocene planktic foraminifera. In: H.M. Bolli, J.B. Saunders and K. Perch-Nielsen (Editors), *Plankton Stratigraphy*. Cambridge Univ. Press, Cambridge, pp. 283–314.
- Iaccarino, S. and Salvatorini, G., 1982. A framework of planktonic foraminiferal biostratigraphy for Early Miocene to Late Pliocene mediterranean area. *Paleontol. Stratigr. Evol.*, Quad., 2: 115–125.
- Ibaraki, M., 1986. Neogene planktonic foraminiferal biostratigraphy of the Kakegawa area on the Pacific coast of central Japan. *Rep. Fac. Sci. Shizuoka Univ.*, 20: 39–173.
- Imbrie, J. and Imbrie, J.Z., 1980. Modelling the climatic response to orbital variations. *Science*, 207: 943–953.
- Ingram, B.L. and DePaolo, D.J., 1992. Strontium isotopic composition of estuarine sediments as paleosalinity–paleoclimate indicator. *Science*, 255: 68–72.
- Ingram, B.L., Conrad, M.E. and Ingle, J.C., 1996. Stable isotope and salinity systematics in estuarine waters and carbonate: San Francisco Bay. *Geochim. Cosmochim. Acta*, 60: 455–467.
- Ishii, T., 1989. Tertiary geology and its geological development of the outer zone of Northeast Honshu Arc. *Mem. Geol. Soc. Jpn.*, 32: 113–132 (in Japanese with English abstr.).
- Issel, A., 1897. *Compendio di Geologia*. Unione Tipografica, Torino, 1046 pp.
- Izett, G.A., Dalrymple, G.B. and Snee, L.W., 1991.  $^{40}\text{Ar}/^{39}\text{Ar}$  Ar age of Cretaceous–Tertiary boundary tektites from Haiti. *Science*, 252: 1539–1542.
- James, G.A. and Wynd, J.G., 1965. Stratigraphic nomenclature of Iranian oil consortium agreement area. *AAPG Bull.*, 49, 12: 2182–2245.
- Jan du Chêne, R. and Londeix, L., 1987. Une rapide excursion sur les stratotypes néogènes du sud de Bordeaux (Aquitaine, France) et dans les vignobles voisins. *Livret-guide, Excursion Xe Symp. APLF (Assoc. Palymologues de Langue Française)*, Bordeaux 1987, 47 pp.
- Jarrige, J.J., Ott D'estevou, P., Burollet, P.F., Thiriet, J.P., Icart, J.C., Richert, J.P., Senans, P., Montenat, C. and Prat, P., 1986. Inherited discontinuities and Neogene structure: the Gulf of Suez and the northwestern edge of the Red Sea. *Philos. Trans. R. Soc. London, A*, 317: 129–139.
- Jenkins, D.G., 1966a. Planktonic foraminiferal zones and new taxa from the Danian to lower Miocene of New Zealand. *N.Z. J. Geol. Geophys.*, 8(6): 1088–1126.
- Jenkins, D.G., 1966b. Planktonic Foraminifera from the Aquitanian-Burdigalian of France. *Contrib. Cushman Found. Foram. Research*, Washington, vol. 17, 1, p. 1–15.
- Jenkins, D.G., 1971. New Zealand Cenozoic planktonic foraminifera. *N.Z. Geol. Surv., Paleontol. Bull.*, 42, 278 pp.
- Jenkins, D.G., 1981. Planktonic Foraminifera and the Paleogene/Neogene boundary in the southwest Pacific. In: F. Cati, F.F. Steininger, A.M. Borsetti and R. Gelati (Editors), *In Search of the Paleogene/Neogene Boundary Stratotype, Part 1. Potential Boundary Stratotype Sections in Italy and in Greece and Comparison with results from the Deep-Sea*. *G. Geol.*, 44: 205–210.
- Jenkins, D.G., 1985. Southern mid-latitude Paleocene to Holocene planktonic foraminifera. In: H.M. Bolli, J.B. Saunders and K. Perch-Nielsen (Editors), *Plankton Stratigraphy*. Cambridge Univ. Press, Cambridge, pp. 263–282.
- Jenkins, D.G., Saunders, J.B. and Cifelli, R., 1981. The relationship of *Globigerinoides bisphericus* Todd 1954 to *Praeorbulina sicana* (De Stefani) 1952. *J. Foraminiferal Res.*, 11: 262–267.
- Johnson, D.A. and Nigrini, C.A., 1985. Synchronous and time-transgressive Neogene radiolarian datum levels in the Equatorial Indian and Pacific Oceans. *Mar. Micropaleontol.*, 9: 489–523.
- Kanaya, T., 1959. Miocene diatom assemblages from the Onnagawa Formation and their distribution in the

- correlative formations in Northeast Japan. *Sci. Rep. Tohoku Univ.*, 2nd ser. (Geology), 30, 130 pp.
- Kaneoka, I., Ozima, M. and Yanagisawa, M., 1979.  $^{40}\text{Ar}$ - $^{39}\text{Ar}$  age studies of four Yamato-74 meteorites. *Mem. Natl. Inst. Polar Res.*, spec. iss., 12: 186-206 (in Japanese with English abstr.).
- Kanie, Y. and Hattori, M., 1991. Report of the symposium on Chronology and Paleoenvironmental Aspects of the Miura Group, Central Japan, held at the 97th annual meeting of the Geological Society of Japan in 1990. *J. Geol. Soc. Jpn.*, 97: 849-864 (in Japanese with English abstr.).
- Kanie, Y., Okada, H., Sasahara, Y. and Tanaka, H., 1991. Calcaceous nannoplankton age and correlation of the Neogene Miura Group between the Miura and Boso Peninsulas, southern-central Japan. *J. Geol. Soc. Jpn.*, 97: 135-155 (in Japanese with English abstr.).
- Kanie, Y., Hattori, M. and Sasahara, Y., 1992. Two types of white clam communities in Sagami Bay, Central Japan: geologic settings and the Tertiary records in the Miura and Boso Peninsulas. *Sci. Rep. Yokosuka City Mus.*, 40: 37-43. (In Japanese)
- Kano, K., Kato, H., Yanagisawa, S. and Yoshida, S. (Editors), 1991. Stratigraphy and geologic history of the Cenozoic of Japan. *Rep. Geol. Surv. Jpn.*, 274, 114 pp. (in Japanese with English abstr.).
- Kastens, K.A., 1992. Did glacio-eustatic sea level drop triggered the Messinian salinity crisis? New evidence from Ocean Drilling Program Site 654 in the Tyrrhenian Sea. *Paleoceanography*, 7(3): 333-356.
- Kastens, K., Mascle, J., Auroux, C., Bonatti, E., Broglia, C., Channell, J., Curzi, P., Emeis, K.-C., Glacon, G., Hasegawa, S., Hieke, W., Mascle, G., Mccoy, F., Mckenzie, J., Mendelson, J., Muller, C., Rehault, J.P., Robertson, A., Sartori, R., Sprovieri, R. and Torii, M., 1986. A microcosm of ocean basin evolution in the Mediterranean. *Nature*, 321: 383-384.
- Kastens, K., Mascle, J., Auroux, C., Bonatti, E., Broglia, C., Channell, J., Curzi, P., Emeis, K.-C., Glacon, G., Hasegawa, S., Hieke, W., Mascle, G., Mccoy, F., Mckenzie, J., Mendelson, J., Muller, C., Rehault, J.P., Robertson, A., Sartori, R., Sprovieri, R. and Torii, M., 1988. ODP Leg 107 in the Tyrrhenian Sea: insights into passive margin and back-arc basin evolution. *Geol. Soc. Am. Bull.*, 100: 1140-1156.
- Kasuya, M., 1987. Comparative study of Miocene fission-track chronology and magneto-biochronology. *Sci. Rep. Tohoku Univ.*, 2nd Ser. (Geology), 58: 93-106.
- Kasuya, M., 1990. Fission-track ages of tuff layers related to the Pliocene-Pleistocene boundary on the Boso Peninsula, Japan. *Quat. Res.*, 33: 86-93.
- Kawai, N., 1951. Magnetic polarization of Tertiary rocks in Japan. *J. Geophys. Res.*, 56: 73-79.
- Keigwin, L.D., 1987. Toward a high-resolution chronology for the latest Miocene paleoceanographic events. *Paleoceanography*, 2: 639-660.
- Keigwin, L.D. and Shackleton, N.J., 1980. Late Miocene-Early Pliocene stratigraphy and paleoceanography of the South Atlantic and Southwest Pacific: a synthesis. *Paleoceanography*, 1: 285-311.
- Keigwin, L.D., Aubry, M.-P. and Kent, D.V., 1987. North Atlantic late Miocene stable-isotope stratigraphy, biostratigraphy and magnetostratigraphy. *Init. Rep. DSDP*, 94: 935-963.
- Keller, G., 1981. Miocene biochronology and paleoceanography of the Northern Pacific. *Mar. Micropaleontol.* 6: 535-551.
- Keller, G., 1984. The Paleogene/Neogene boundary in the equatorial Pacific Ocean. In: R. Gelati and F.F. Steininger (Editors), *In Search of the Paleogene/Neogene Boundary Stratotype, Part 2. Potential Boundary Stratotype Sections in Italy and Spain*. *Riv. Ital. Paleontol. Stratigr.*, 89(4): 529-556.
- Keller, J.V.A. and Pialli, G., 1990. Tectonics of the Island of Elba: a reappraisal. *Boll. Soc. Geol. Ital.*, 109: 413-425.
- Kennett, J.P., 1973. Middle and late Cenozoic planktonic foraminifera biostratigraphy of the southwest Pacific, DSDP Leg 21. *Init. Rep. DSDP*, 21: 575-639.
- Kennett, J.P., 1985. Miocene to early Pliocene oxygen and carbon isotope stratigraphy in the southwest Pacific, Deep Sea Drilling Project Leg 90. *Init. Rep. DSDP*, 90: 1383-1411.
- Kennett, J.M. and Srinivasan, M.S., 1983. Neogene Planktonic Foraminifera. Dowden, Hutchinson and Ross, Stroudsbury, Penn., 265 pp.
- Kimura, K., 1974. Magnetic stratigraphy of late Cenozoic sedimentary sections in Boso Peninsula, Niigata area and Oga Peninsula, Japan. *J. Geol. Soc. Jpn.*, 80: 579-592.
- Koepnick, R.B., Burke, W.H., Denison, R.E., Hetherington, E.A., Nelson, H.F., Otto, J.B. and Waite, L.E., 1985. Construction of the seawater  $^{87}\text{Sr}/^{86}\text{Sr}$  curve for the Cenozoic and Cretaceous: supporting data. *Chem. Geol. (Isot. Geosci. Sect.)*, 58: 55-81.
- Koike, M., Takei, K., Shimono, T., Machida, J., Akimoto, K., Hashiya, I., Yoshino, H. and Hirakoso, S., 1985. Miocene formations of Iwadono Hills. *J. Geol. Soc. Jpn.*, 91: 665-677 (in Japanese with English

- abstr.).
- Konda, I., 1980. Benthonic foraminiferal biostratigraphy of the standard areas of Middle Miocene in the Pacific side province, central Japan. Mem. Fac. Sci. Kyoto Univ., Geol. Mineral., 47: 1–42.
- Koyama, M., 1989. Paleomagnetic studies in the south Fossa Magna and adjacent areas, Japan. Mod. Geol., 14: 69–86.
- Krijgsman, W., Hilgen, F.J., Langereis, C.G. and Zachariasse, W.J., 1994. The age of the Tortonian/Messinian boundary. Earth Planet. Sci. Lett., 121: 533–547.
- Kruege, M.A., Stankiewicz, B.A. and Montanari, A., 1994. Serravallian shales in the Monte dei Corvi pelagic sequence (Ancona, Italy): an organic geochemical perspective. In: R. Coccioni, A. Montanari and G.S. Odin (Editors), Miocene Stratigraphy of Italy and Adjacent Regions. G. Geol., 56(1): 173–182.
- Kurihara, K., 1974. Notes on the first appearance of *Orbulina* and the lower Middle Miocene planktonic foraminiferal zones in Japan. J. Jpn. Assoc. Pet. Technol., 39: 154–166.
- Langereis, C.G., 1984. Late Miocene Magnetostratigraphy in the Mediterranean. Ph.D. Thesis, Univ. of Utrecht, Geol. Ultraiectina, 34, 180 pp.
- Langereis, C.G. and Dekkers, M.J., 1992. Paleomagnetism and rock magnetism of the Tortonian–Messinian boundary stratotype at Falconara, Sicily. Phys. Earth Planet. Inter., 71: 100–111.
- Langereis, C.G. and Hilgen, F.J., 1991. The Rossello composite: a Mediterranean and global reference section for the Early to early Late Pliocene. Earth Planet. Sci. Lett., 104: 211–225.
- Langereis, C.G., Zachariasse, W.J. and Zijdeveld, J.D.A., 1984. Late Miocene magnetobiostratigraphy of Crete. Mar. Micropaleontol., 8: 261–281.
- Lanphere, M.A., Sawyer, D.A. and Fleck, R.J., 1990. High resolution  $^{40}\text{Ar}/^{39}\text{Ar}$  geochronology of Tertiary volcanic rocks, Western USA. Geol. Soc. Aust. Abstr., 27: 57.
- Larter, S.R., 1984. Application of analytical pyrolysis techniques to kerogen characterization and fossil fuel exploration/exploitation. In: K. Voorhees (Editor), Analytical Pyrolysis — Methods and Applications. Butterworth, London, pp. 212–275.
- Laurenzi, M.A. and De Grandis, G., 1992. K/Ar and  $^{40}\text{Ar}/^{39}\text{Ar}$  dating of volcanoclastic layers from the Miocene Umbria–Marche sequence. In: A. Montanari, R. Coccioni and G.S. Odin (Editors), Volume of Abstracts and Field Trips, Interdisciplinary Geological Conference on the Miocene Epoch with emphasis on the Umbria–Marche sequence (I.U.G.S., Subcommittee on Geochronology, Miocene Columbus Project), Ancona, November 11–15, 1992, p. 76.
- Lavecchia, G., 1988. The Tyrrhenian–Apennines system: structural setting and seismotectogenesis. Tectonophysics, 147: 263–296.
- Lavecchia, G., Minelli, G. and Piali, G., 1984. L'Appennino umbro–marchigiano: tettonica distensiva ed ipotesi di dismogenesi. Boll. Soc. Geol. Ital., 103: 467–476.
- Lavecchia, G., Minelli, G. and Piali, G., 1989. Contractural and extensional tectonics along the Lake Trasimeno, Pesaro transect (Central Italy). In: A. Boriani, M., Bonafede, G.B. Piccardo and G.B. Vai (Editors), The Lithosphere in Italy. Advances in Earth Science Research. Atti Convegni Lincei, 80: 177–194.
- Lentin, J.K. and Williams, G.L., 1993. Fossil Dinoflagellates: Index to Genera and Species, 1993 Edition. AASP Contrib. Ser., 28, 856 pp.
- Lesueur, J.L., Rubino, J.L. and Giraudmaillet, M., 1990. Organisation et structures internes des dépôts tidaux du Miocène rhodanien. Bull. Soc. Géol. Fr., 8(6): 49–65.
- Letz, H., Reichert, C., Wigger, P. and Giese, P., 1977. Seismic refraction measurements in the Ligurian Sea and in the Northern Apennines. In: H. Closs, D. Roeder and K. Schmidt (Editors), Alps, Apennines and Hellenides. Schweizerbart'sche, Stuttgart, pp. 215–220.
- Li, Z., 1990. Bryozoaires de Montbrison–Fontbonau (Drôme) et comparaison avec les autres faunes miocènes du bassin rhodanien méridional. Nouv. Arch. Hist. Nat. Lyon, 27, 126 pp.
- Lincoln, J.M. and Schlanger, S.O., 1987. Miocene sea-level fall related to the geologic history of Midway Atoll. Geology, 15: 454–457.
- Lincoln, J.M. and Schlanger, S.O., 1991. Atoll stratigraphy as a record of sea level change: problems and prospects. J. Geophys. Res., 96: 6727–6752.
- Lippolt, H.J. and Hess, J.C., 1988. HD-B1 biotite reference material for K–Ar chronometry. In: G.S. Odin (Editor), Calibration of the Phanerozoic Time Scale. Bull. Liais. Inf. IGCP Project 196, Paris, 7: 8.
- Lippolt, H.J., Hess, J.C., Holub, V.M. and Pesek, J., 1986. Correlation of Upper Carboniferous deposits in the Bohemian Massif (Czechoslovakia) and in the Ruhr District (FR Germany) — evidence from

- <sup>40</sup>Ar/<sup>39</sup>Ar ages of Tuff layers. Z. Dtsch. Geol. Ges., 137: 447–464.
- Loeblich, A.R., Jr. and Tappan, J.H., 1988. Foraminiferal Genera and Their Classification. Van Nostrand Reinhold, New York, Vol. 1, 970 pp.; Vol. 2, 212 pp.
- Londeix, L., 1991. Actualisation de quelques coupes classiques du Miocène inférieur et moyen bordelais (France). Bull. Soc. Linn. Bordeaux, 19(2): 59–74.
- Longinelli, A., 1979/1980. Isotope geochemistry of some Messinian evaporites: paleoenvironmental implications, geodynamic and biodynamics effects of the Messinian Salinity Crisis in the Mediterranean. Palaeogeogr., Palaeoclimatol., Palaeoecol. (spec. iss.), 29: 95–123.
- Lorenz, C., 1984. Les silexites et les tuffites du Burdigalien, marqueurs volcano-sédimentaires et corrélations dans le domaine de la Méditerranée occidentale. Bull. Soc. Géol. Fr., 26: 1203–1210.
- Lorenz, C., Butterlin, J., Cavelier, C., Clermonte, J., Colchen, M., Dercourt, J., Guiraud, R., Montenat, C.J., Poisson, A. and Ricou, L.E., 1993. Late Rupelian (30–28 Ma). In: J. Dercourt, L.E. Ricou and B. Vrielynck (Editors), Atlas Tethys Palaeoenvironmental Maps. Explanatory Notes. Gauthier Villars, Paris, pp. 211–223.
- Loutit, T.S. and Kennett, J.P., 1979. Application of carbon isotope stratigraphy to Late Miocene shallow marine sediments, New Zealand. Science, 204: 1196–1199.
- Lowrie, W., 1990. Identification of ferromagnetic minerals in a rock by coercitivity and unblocking temperature properties. Geophys. Res. Lett., 17: 159–162.
- Lowrie, W., Alvarez, W., Napoleone, G., Perch-Nielsen, K., Premoli Silva, I. and Toumarkine, M., 1982. Paleogene magnetic stratigraphy in Umbrian pelagic carbonate rocks: the Contessa sections, Gubbio. Geol. Soc. Am. Bull., 93: 414–432.
- Ludwig, K.R., 1992. ISOPLOT — A plotting and regression program for radiogenic-isotope data. U.S. Geol. Surv. Open-File Rep., pp. 91–445.
- Lyell, Ch., 1833. Principles of Geology, 3. Murray, London, 398 pp.
- Maiya, S., 1988. Neogene events as revealed by changes of foraminiferal assemblages from central and northern Japan. In: R. Tsuchi et al. (Editors), IGCP Project 246, Pacific Neogene Events in Time and Space. Osaka Mus. Nat. Hist., spec. publ., pp. 31–48 (in Japanese with English abstr.).
- Maiya, S. and Inoue, Y., 1981. Historical changes of Lower–Middle Miocene foraminiferal assemblages and paleogeography in Niigata Basin. Fossils, Paleontol. Soc. Jpn., 30: 73–78 (in Japanese with English abstr.).
- Malinverno, A. and Ryan, W.B.F., 1986. Extension in the Tyrrhenian Sea and shortening in the Apennines as a result of arc migration driven by sinking of the lithosphere. Tectonics, 5: 227–246.
- Malvesin-Fabre, M., 1939. Aperçu géologique sur Léognan et la vallée de l'Eau-Blanche. Proc. Verb. Soc. Linn. Bordeaux, CXI: 159–172.
- Manum, S.B., Boulter, M.C., Gunnarsdottir, H., Rangnes, K. and Scholze, A., 1989. Eocene to Miocene palynology of the Norwegian Sea (ODP Leg 104). Proc. ODP Sci. Results, 104: 611–662.
- Marabini, S. and Vai, G.B., 1985. Analisi di facies e macrotettonica della Vena del Gesso in Romagna. Boll. Soc. Geol. Ital., 104: 21–42.
- Marks, P. and Webb, P.N., 1966. Discussion to the 'Symposium on micropaleontological lineages and zones'. Proc. C.M.N.S. Berne, 1964: 140–145.
- Martini, E., 1968. Calcareous nannoplankton from the type Langhian. C.M.N.S., Proc. IV Sess. Bologna, 1967. G. Geol., 35: 163–172.
- Martini, E., 1970. Standard Neogene calcareous nannoplankton zonation. Nature, 225: 289–290.
- Martini, E., 1971. Standard Tertiary and Quaternary calcareous nannoplankton zonation. Proc. II Plankt. Conf., Roma, 1970: 739–786.
- Martini, E., 1975. Calcareous nannoplankton from the type Tortonian (upper Miocene). C.M.N.S., Proc. VI Regional Bratislava, 1975: 53–56.
- Martini, E., 1988. Late Oligocene and Early Miocene calcareous nannoplankton (Remarks on French and Moroccan sections). Newsl. Stratigr., 18(2): 75–80.
- Martini, E. and Müller, C., 1986. Current Tertiary and Quaternary calcareous nannoplankton stratigraphy and correlations. Newsl. Stratigr., 16: 99–112.
- Martinotti, G.M., 1981. Biostratigraphy and planktonic foraminifera of the Late Eocene to Pleistocene sequence in the Asqelon 2 well (S coastal plain, Israel). Rev. Esp. Micropaleontol., 13(3): 343–381.
- Martinotti, G.M., 1990. The stratigraphic significance of *Globigerinoides ruber* and *Globigerinoides obliquus obliquus* in the Mediterranean Middle Miocene. Micropaleontology, 36(1): 96–101.

- Masce, G. and Heimann, K.O., 1978. Geological observation from Messinian and lower Pliocene outcrops in Sicily. *Mem. Soc. Geol. Ital.*, 16: 127–140.
- Matsumaru, K., 1967. Geology of the Tomioka area, Gunma Prefecture, with a note on 'Lepidocyclina' from the Abuta Limestone Member. *Sci. Rep. Tohoku Univ., 2nd Ser. (Geology)*, 39: 39–63.
- Matsumaru, K., 1981. Consideration concerning larger foraminiferal zoogeography and ecology in Late Early Miocene to Early Middle Miocene. *Fossils, Paleontol. Soc. Jpn.*, 30: 59–66 (in Japanese with English abstr.).
- Matsumoto, A., 1989. Improvement for determination of potassium in K–Ar dating. *Bull. Geol. Surv. Jpn.*, 40: 65–70 (in Japanese with English abstract).
- Mattias, P., Mariottini, M. and De Casa, G., 1987. I minerali silicatici e gli altri minerali compresi nella sequenza eocenica–oligocenica della Valle della Contessa presso Gubbio (Appennino Centrale). *Miner. Petrogr. Acta*, 30: 113–139.
- Mattias, P., Crocetti, G., Barrese, E., Montanari, A., Coccioni, R., Farabollini, P. and Parisi, E., 1992. Caratteristiche mineralogiche e litostratigrafiche della sezione eo–oligocenica di Massignano (Ancona, Italia) comprendente il limite Scaglia Variegata–Scaglia Cinerea. *Stud. Geol. Camerti*, 12: 93–103.
- Mayer-Eymar, K., 1858. Versuch einer neuen Klassifikation der Teriär-Gebilde Europa's. *Verhandl. der Allgemeinen Schweiz. Ges. f. gesamt. Naturwissensch., Trogen*, (août 1857), p. 165–199.
- Mayer-Eymar, C., 1867. Catalogue systématique et descriptif des fossiles des terrains tertiaires qui se trouvent au Musée fédéral de Zürich, I: 1–37; II: 1–65. Librairie Schabelitz, Zurich.
- Mayer-Eymar, C., 1868. Tableau Synchronistique des terrains tertiaires supérieurs. *ETH Library, Zurich*.
- Mayer, K., 1877. Sur la carte géologique de la Ligurie centrale. *Bull. Soc. Geol. Fr., Sér. 6*, 5: 282–297.
- Mazzei, R., 1977. Biostratigraphy of the Rio Mazzapiedi–Castellania section (type section of the Tortonian) based on calcareous nannoplankton. *Atti Soc. Tosc. Sci. Nat. Mem.*, 84: 15–24.
- Mazzei, R., 1985. The Miocene sequence of the Maltese Islands: biostratigraphic and chronostratigraphic references based on nannofossils. *Atti Soc. Tosc. Sci. Nat. Mem., Ser. A*, 92: 165–197.
- McArthur, J.M., 1994. Recent trends in strontium isotope stratigraphy. *Terra Nova*, 6: 331–358.
- McCulloch, M.T., De Deckker, P. and Chivas, A.R., 1989. Strontium isotope variations in single ostracod valves from the Gulf of Carpentaria, Australia: a palaeoenvironmental indicator. *Geochim. Cosmochim. Acta*, 53: 1703–1710.
- McDougall, I. and Page, R.W., 1975. Toward a physical time scale for the Neogene. Data from the Australian region. In: I. Saito and L.H. Burckle (Editors), *Late Neogene Epoch Boundaries. Micropaleontology*, 1: 75–84.
- McKenzie, J.A. and Oberhänsli, H., 1985. Paleooceanographic expressions of the Messinian salinity crisis. In: K.J. Hsü and H.S. Weissert (Editors), *South Atlantic Paleooceanography*. Cambridge Univ. Press, Cambridge, pp. 99–123.
- McKenzie, J.A., Jenkyns, H.C. and Bennet, G.G., 1979. Stable isotope study of the cyclic diatomite–claystone from the Tripoli Formation, Sicily: a prelude to the Messinian salinity crisis. *Palaeogeogr., Palaeoclimatol., Palaeoecol.*, 29: 125–141.
- Mein, P., 1979. Rapport d'activité du Groupe de travail des Vertébrés; mise à jour de la biostratigraphie du Néogène basée sur les Mammifères. *Ann. Géol. Pays Hellén.*, 3: 1367–1372.
- Mein, P., 1989. Updating of MN zones. *European Neogene Mammal Chronology. Ser. A, Life Sci. Vol.*, 180: 73–90.
- Mein, P. and Agusti, J., 1990. Les gisements de Mammifères néogènes de la zone bétique. *Doc. Trav. IGAL, Paris*, 12–13: 81–84.
- Menning, M., 1988. Synopsis of numerical time scales 1917–1986. *Episodes*, 12(1): 3–5.
- Merla, G., 1951. Geologia dell'Appennino settentrionale. *Boll. Soc. Geol. Ital.*, 70: 95–382.
- Mezzetti, R., 1969. Studio petrografico di ceneri vulcaniche appenniniche. *Mineral. Petrogr. Acta*, 15: 9–34.
- Mezzetti, R. and Olivieri, R., 1964. Intercalazioni cineritiche di età oligocenica e miocenica dell'Appennino centro-settentrionale. *Mineral. Petrogr. Acta*, 10: 129–147.
- Mezzetti, R., Morandi, N., Tateo, F. and Dondi, M., 1991. Il contributo vulcano-derivato in successioni pelitiche oligo–mioceniche dell'Appennino settentrionale. *G. Geol.*, 53: 167–185.
- Miculan, P., 1992. Biostratigrafia a foraminiferi planctonici e cronostratigrafia del Miocene medio. PhD Thesis, Univ. di Bologna, 117 pp.
- Miculan, P., 1994. Planktonic foraminiferal biostratigraphy of the middle Miocene in Italy. *Boll. Soc. Paleontol. Ital.*, 33(2): 299–339.

- Miller, K.G., Aubry, M.-P., Kahn, M.S., Melillo, A., Kent, D.V. and Berggren, W.A., 1985. Oligocene–Miocene biostratigraphy, magnetostratigraphy and isotopic stratigraphy of the western North Atlantic. *Geology*, 13: 257–261.
- Miller, K.G., Fairbanks, R.G. and Mountain, G.S., 1987. Tertiary oxygen isotope synthesis, sea level history and continental margin erosion. *Paleoceanography*, 2: 1–19.
- Miller, K.G., Wright, J.D. and Fairbanks, R.G., 1991a. Unlocking the Ice House: Oligocene–Miocene oxygen isotopes, eustasy and marginal erosion. *J. Geophys. Res.*, 96: 6829–6848.
- Miller, K.G., Feigenson, M.D., Wright, J.D. and Clement, B.M., 1991b. Miocene isotope reference section, Deep Sea Drilling Project Site 608: an evaluation of isotope and biostratigraphic resolution. *Paleoceanography*, 6(1): 33–52.
- Milton, D.I., 1967. Geology of the Arabian peninsula, Kuwait. *Geol. Surv. Prof. Pap.*, 560 F, 7 pp.
- Minguzzi, V., Morandi, N. and Tateo, F., 1987. Significance of Ba-rich zeolitic sediments of the Oligo–Miocene sequences near Voghera (PV-AL Provinces), Italy. *Mineral. Petrogr. Acta*, 30: 253–270.
- Minguzzi, V., Morandi, N. and Tateo, F., 1990. Distinzione di termini Ba-zeolitici attraverso il loro comportamento diffrattometrico e termico dopo scambio con K e Ba. *Mineral. Petrogr. Acta*, 33: 205–218.
- Mitsunashi, T. and Yazaki, K., 1968. A map of petroleum and gas fields in Japan: The Miura Peninsula (Geological Map). Geological Survey of Japan.
- Mitsunashi, T., Kikuchi, T., Suzuki, Y., Hirayama, J., Nakajima, T., Oka, S., Kodama, K., Horiguchi, M., Katsurajima, S., Miyashita, M., Yazaki, K., Kageyama, K., Nasu, N., Kagami, H., Honza, E., Kimura, M., Nirei, H., Higuchi, H., Hara, Y., Furuno, K., Endo, T., Kawashima, S. and Aoki, S., 1979. Geological map of Tokyo Bay and adjacent areas. *Miscellaneous maps series (20)*, 1/100,000, *Geol. Surv. Jpn.*, 91 pp. (in Japanese with English abstr.).
- Molina, E., 1979. Oligoceno–Mioceno inferior por medio de foraminiferos planctonicos en el sector central de las Cordilleras Beticas (Espana). *Tesi doctoral, Publication Universidades de Granada y Zaragoza*, 342 pp.
- Mongelli, F. and Zito, G., 1991. Flusso di calore nella regione toscana. *Stud. Geol. Camerti*, vol. spec. 1991/1: 91–98.
- Mongereau, N., 1970. Les bryozoaires cyclostomes branchus du Miocène du bassin du Rhône (France). *Doc. Lab. Géol. Sci. Lyon*, 40, 95 pp.
- Montanari, A., 1988. Geochemical characterization of volcanic biotite from the Upper Eocene–Lower Miocene pelagic sequence of the Northern Apennines. In: I. Premoli Silva, R. Coccioni and A. Montanari (Editors), *The Eocene–Oligocene Boundary in the Marche–Umbria Basin (Italy)*. *Int. Subcomm. Paleogr. Strat.*, Ancona, Spec. Publ., II.1., F.Ili Anibaldi Publ., pp. 209–227.
- Montanari, A., Drake, R., Bice, M.D., Alvarez, W., Curtis, G.H., Turrin, B.D. and DePaolo, D.J., 1985. Radiometric time scale for the upper Eocene and Oligocene based on K/Ar and Rb/Sr dating of volcanic biotites from the pelagic sequence of Gubbio, Italy. *Geology*, 13: 596–599.
- Montanari, A., Deino, A., Drake, R., Turrin, B.D., De Paolo, D.J., Odin, S.G., Curtis, G.H., Alvarez, W. and Bice, D.M., 1988a. Radioisotopic dating of the Eocene–Oligocene boundary in the pelagic sequence of the Northern Apennines. In: I. Premoli Silva, R. Coccioni and A. Montanari (Editors), *The Eocene–Oligocene Boundary in the Marche–Umbria Basin (Italy)*. *Int. Subcomm. Paleogr. Strat.*, Ancona, Spec. Publ., II.1., F.Ili Anibaldi Publ., pp. 195–208.
- Montanari, A., Langenheim, V.E. and Coccioni, R., 1988b. Stratigraphy and geochronologic potential of the pelagic and hemipelagic sequence of the northeastern Apennines: a research note. *Bull. Liais. Inf.*, Project 196, 7: 17–23.
- Montanari, A., Deino, A., Coccioni, R., Langenheim, V.E., Capo, R. and Monechi, S., 1991. Geochronology, Sr isotope analysis, magnetostratigraphy and plankton stratigraphy across the Oligocene–Miocene boundary in the Contessa section (Gubbio, Italy). *Newsl. Stratigr.*, 23(3): 151–180.
- Montanari, A., Coccioni, R. and Odin, G.S. (Editors), 1992. *Interdisciplinary Geological Conference on the Miocene Epoch with emphasis on the Umbria–Marche sequence (I.U.G.S., Subcommittee on Geochronology, Miocene Columbus Project)*, Volume of Abstracts and Field Trips, Ancona, November 11–15, 1992, pp. 1–115.
- Montanari, A., Carey, S., Coccioni, R. and Deino, A., 1994. Early Miocene tephra in the Apennine pelagic sequence: an inferred Sardinian provenance and implications for western Mediterranean tectonics. *Tectonics*, 13(5): 1120–1134.

- Montenat, C., 1977. Les bassins néogènes du Levant d'Alicante et de Murcia. Stratigraphie, paléogéographie et évolution dynamique. Doc. Lab. Géol. Fac. Sci. Lyon, 69, 345 pp.
- Montenat, C. (Coord.), 1986. Etudes géologiques des rives du golfe de Suez et de la Mer Rouge nord-occidentale. Evolution tectonique et sédimentaire d'un rift néogène. Doc. Trav. IGAL, Paris, 10, 192 pp.
- Montenat, C. (Editor), 1990. Les bassins néogènes du domaine bétique oriental (Espagne). Tectonique et sédimentation dans un couloir de décrochement. Doc. Trav. IGAL, Paris, 12–13, 392 pp.
- Montenat, C. and Ott d'Estevou, P., 1992. Geodynamics of Eastern Betic late Neogene Basins. A review. In: Revisión de la geodinámica de las cuencas del Neogeno superior en las Béticas Orientales. Física de la Tierra, n° 4, Edit. Complut., Madrid, pp. 57–75.
- Montenat, C., Thaler, L. and Van Couvering, J.A., 1975. La faune de rongeurs de Librilla: corrélations avec les formations marines du Miocène terminal et les datations radiométriques du volcanisme de Barqueros (Province de Murcia, Espagne méridionale). C.R. Acad. Sci., Paris, 281: 519–522.
- Montenat, C., de Reneville, P. and Bizon, G., 1978. Le Néogène des environs d'Aguilas (province de Murcia et d'Almería), Cordillères bétiques (Espagne). Bull. Mus. Natl. Hist. Nat. Paris, 3, 511, 6: 37–54.
- Montenat, C., Bolze, J., Bordet, P. and Ott d'Estevou, P., 1984. Extrusions de type 'pebble dyke', à éléments plutoniques miocènes, dans le Tortonien des Cordillères bétiques orientales (Espagne). C.R. Acad. Sci., Paris, 299, Sér. II, 7: 343–346.
- Morandi, N. and Tateo, F., 1992. Mineralogy of the Santa Croce and Moria sections (Early–Middle Miocene, Marche region, Italy). In: A. Montanari, R. Coccioni and G.S. Odin (Editors), Volume of Abstracts and Field Trips, Interdisciplinary Geological Conference on the Miocene Epoch with emphasis on the Umbria–Marche sequence (I.U.G.S., Subcommittee on Geochronology, Miocene Columbus Project), Ancona, November 11–15, 1992, pp. 82–83.
- Mosna, S. and Micheletti, A., 1968. Microfaune del 'Serravalliano'. C.M.N.S. Proc. IV Sess., Bologna, 1967, pp. 183–189.
- Moyes, J., 1965. Les ostracodes du Miocène aquitain: essai de paléocologie stratigraphique et de paléogéographie. Thèse Doctorat Sciences, Drouillard imp., Bordeaux, 339 pp.
- Moyes, J., 1966. Les faluns néogènes du Bordelais. Bull. Inst. Géol. Bassin d'Aquitaine, Bordeaux, 1: 85–113.
- Mudie, P.J., 1989. Palynology and dinocyst biostratigraphy of the late Miocene to Pleistocene Norwegian Sea, ODP leg 104, Sites 642 to 644. Proc. ODP, Sci. Results, 104: 587–610.
- Müller, C., 1975. Calcareous nannoplankton from the type Serravallian. Proc. VI C.R.M.N.S., Bratislava, 1975, p. 4952.
- Müller, C., 1978. Neogene calcareous nannofossils from the Mediterranean Leg 42 of the Deep Sea Drilling Project. Init. Rep. DSDP, 42, 1: 727–752.
- Müller, C. and Mueller, P.A., 1991. Origin and age of the Mediterranean Messinian evaporites: implication from Sr isotopes. Earth Planet. Sci. Lett., 107: 1–12.
- Müller, C. and Pujol, C., 1979. Etude du nannoplancton calcaire et des Foraminifères planctoniques dans l'Oligocène et le Miocène en Aquitaine (France). Géologie Méditerranéenne, Marseille, VI, 2: 357–368.
- Müller, D.W. and Hsü, K.J., 1987. Event stratigraphy and paleoceanography in the Fortuna Basin (Southeast Spain): a scenario for the Messinian salinity crisis. Paleoceanography, 2: 679–696.
- Nagao, K., Nishido, H., Itaya, T. and Ogata, K., 1984. An age determination by K–Ar method. Bull. Hiruzen Res. Inst., 9: 19–38 (in Japanese with English abstr.).
- Nakagawa, H., Niitsuma, N. and Hayasaka, I., 1969. Late Cenozoic geomagnetic chronology of the Boso Peninsula. J. Geol. Soc. Jpn., 75: 267–280 (in Japanese with English abstr.).
- Nakagawa, H., Niitsuma, N., Kitamura, N., Matoba, Y., Takayama, T. and Asano, K., 1974. Preliminary results on magnetostratigraphy of Neogene stage stratotype sections in Italy. Riv. Ital. Paleontol. Stratigr., 80: 615–630.
- Naumann, C.F., 1858. Lehrbuch der Geognosie. Engelmann, Leipzig, 2nd ed., 3, 576 pp.
- Negri, A., 1989. Biostratigrafia del Miocene inferiore — medio Italiano e Mediterraneo. Ph.D. Thesis, University of Modena, National Libraries of Florence and Rome, 289 pp.
- Nely, G., 1978. Le Burdigalien stratotypique du bassin de Valréas (Drôme, Vaucluse) et ses abords. Thèse 3e cycle, Lyon, 3 vol., 368 pp.
- Nesteroff, W.D., 1973. Un modèle pour les évaporites messiniennes en Méditerranée: des bassins peu profonds avec dépôt d'évaporites lagunaires. In: C.W. Drooger (Editor), Messinian Events in the Mediter-



- ranean, Geodynamics Scientific Report 7 on the colloquium held in Utrecht, March 2–4, 1973. North-Holland Publishing Co., Amsterdam, pp. 68–81.
- Neveeskaja, L.A., Voronina, A.A., Goncharova, I.A., Iljina, L.B., Paramonova, N.P., Popov, S.V., Tchepalyga, A.L. and Babak, E.V., 1984. History of Paratethys: Palaeoceanography, Colloquium 03. 27th IGC, Moscow, 3: 113–128.
- Niitsuma, N., 1976. Magnetic stratigraphy in the Boso Peninsula. *J. Geol. Soc. Jpn.*, 82: 163–181.
- Niitsuma, N., 1989. Collision tectonics in the south Fossa Magna, central Japan. *Mod. Geol.*, 14: 3–18.
- Niitsuma, N., Matsushima, Y. and Hirata, D., 1989. Abyssal molluscan colony of Calyptogena in the Pliocene strata of the Miura Peninsula, central Japan. *Palaeogeogr., Palaeoclimatol., Palaeoecol.*, 71: 193–203.
- Nishitani, T. and Tanoue, S., 1988. Paleomagnetic study for the Oga Peninsula in Northeast Japan. *Rep. Res. Inst. Nat. Resour. Min. Coll., Akita Univ.*, 53: 69–75 (in Japanese with English abstr.).
- Nobel, F.A., Andriessen, P.A.M., Hebeda, E.H., Priem, H.N.A. and Rondeel, H.E., 1981. Isotopic dating of the post-Alpine Neogene volcanism in the Betic Cordilleras, Southern Spain. *Geol. Mijnbouw*, 60: 209–214.
- Nocchi, M., Parisi, G., Monaco, P., Monechi, S., Madile, M., Napoleone, G., Ripepe, M., Orlando, M. and Premoli Silva, I., 1986. In: Ch. Pomerol and I. Premoli Silva (Editors), Terminal Eocene Events, The Eocene/Oligocene Boundary in the Umbrian Pelagic Sequence. *Developments in Paleontology and Stratigraphy*, 9: 25–40. Elsevier, Amsterdam.
- Oda, M., 1977. Planktonic foraminiferal biostratigraphy of the late Cenozoic sedimentary sequence, Central Honshu, Japan. *Sci. Rep. Tohoku Univ., 2nd Ser. (Geology)*, 48, 72 pp.
- Oda, M., 1986. Some aspects and problems concerned with microfossil biochronology for the Neogene in Central and Northeast Honshu, Japan. In: H. Nakagawa et al. (Editors), *Essays of Geology. (Prof. Nobu Kitamura Commemorative Volume)*, Toko Insatsu, pp. 297–312 (in Japanese with English abstr.).
- Oda, M., Hasegawa, S., Honda, N., Maruyama, T. and Funayama, M., 1984. Integrated biostratigraphy of planktonic foraminifera, calcareous nannofossils, radiolarians and diatoms of Middle to Upper Miocene sequences of Central and Northeast Honshu, Japan. *Palaeogeogr., Palaeoclimatol., Palaeoecol.*, 46: 53–69.
- Oddone, M. and Villa, I.M., 1986. Neutron activation in geochronology: the  $^{40}\text{Ar}/^{39}\text{Ar}$  technique. *J. Radioanal. Nucl. Chem.*, 99: 153–159.
- Odin, G.S., 1982. Uncertainties in evaluating the numerical time scale. In: G.S. Odin (Editor), 1982. *Numerical Dating in Stratigraphy*. John Wiley, Chichester, pp. 3–18.
- Odin, G.S., 1992. New stratotypes for the Paleogene, the Cretaceous/Paleogene, Eocene/Oligocene and the Paleogene/Neogene boundaries. *Neues Jahrb. Geol. Paläontol., Abh.*, 168: 7–20.
- Odin, G.S., 1994. *Geological Time Scale*. C.R. Acad. Sci. Paris, 2, 318: 59–71.
- Odin, G.S., 1995. Géochronologie stratigraphique: de l'analyse à l'âge et à l'échelle numérique. In: G.S. Odin (Editor), *Bull. Liais. Inf. IUGS Subcomm. Geochronol.*, Paris, 13: 28–42.
- Odin, G.S. and Luterbacher, H.P., 1992. The age of the Paleogene stage boundaries. *Neues Jahrb. Geol., Paläontol., Abh.*, 186: 21–48.
- Odin, G.S. and Odin, C., 1990. Echelle numérique des temps géologiques, mise à jour. *Géochronique*, 25: 12–21.
- Odin, G.S., Montanari, A., Deino, A., Drake, R., Guise, P.G., Kreuzer, H. and Rex, D.C., 1991. Reliability of volcano-sedimentary biotite ages across the Eocene–Oligocene boundary. *Chem. Geol. (Isot. Geosci. Sect.)*, 86: 203–224.
- Odin, G.S., Amorosi, A., Takahashi, M., Cadet, J.-P., Cuenca, G., Guardia, P., Drobne, K., Jelen, B. and Orszag, F., 1992. Search for sections able to allow integrated stratigraphic calibration of the Miocene sequence, 1. Sections in Japan, Philippines, Lesser Antilles, Algeria, Spain, Cyprus and Slovenia. In: A. Montanari, R. Coccioni and G.S. Odin (Editors), *Volume of Abstracts and Field Trips, Interdisciplinary Geological Conference on the Miocene Epoch with emphasis on the Umbria–Marche sequence (I.U.G.S., Subcommission on Geochronology, Miocene Columbus Project)*, Ancona, November 11–15, 1992, pp. 84–85.
- Odin, G.S., D'Atri, A., Tateo, F., Cosca, M. and Hunziker, J.C., 1994. Integrated stratigraphy near the Oligocene–Miocene boundary: biostratigraphical and geochronological data from the Bosio section (Piedmont, Italy): contributions to the WG MISS. In: G.S. Odin (Editor), *Phanerozoic Time Scale*. *Bull. Liais. Inf. I.U.G.S. Subcomm. Geochronol.*, 12: 40–46.
- Odin, G.S., Coccioni, R., Cosca, M. and Montanari, A., 1995a. Geochronology of a Late Serravallian

- biotite-rich layer; dating of the FO of *Globigerina nepenthes* in Central Apennines (Italy). *Chem. Geol (Isot. Geosci. Sect.)*, 125: 118–121.
- Odin, G.S., Takahashi, M. and Cosca, M., 1995b.  $^{40}\text{Ar}/^{39}\text{Ar}$  geochronology of biostratigraphically controlled Miocene tuffs from Central Japan, comparison with Italy and age of the Serravallian–Tortonian boundary. *Chem. Geol (Isot. Geosci. Sect.)*, 125: 105–117.
- Ogniben, L., 1957. Petrografia della Serie Solfifera Siciliana e considerazioni geologiche relative. *Mem. Descr. Carta Geol. Ital.*, 33, 275 pp.
- Ogniben, L., 1969. Schema introduttivo alla geologia del confine calabro–lucano. *Mem. Soc. Geol. Ital.*, 8, 4: 453–763.
- Oishi, M. and Takahashi, M., 1990. Miocene formations in the Takasaki district, central Japan, with special reference to the developmental process of the Niwaya Unconformity. *Contrib. Inst. Geol. Paleontol., Tohoku Univ.*, 92: 1–17 (in Japanese with English abstr.).
- Okada, H. and Bukry, D., 1980. Supplementary modification and introduction of code numbers to the low latitude coccolith biostratigraphic zonation. *Mar. Micropaleontol.*, 5: 321–325.
- Okada, H., Saito, K. and Kaneko, M., 1991. Occurrence of calcareous nannoplankton and K–Ar ages measured for the intercalating tuff beds in the Miura Group. *Chikyū Mon.*, 13: 20–23 (in Japanese).
- Olafsson, G., 1991. Quantitative calcareous nannofossil biostratigraphy and biochronology of early through late Miocene sediments from DSDP 608. *Medd. Stockholm Univ. Inst. Geol. Geok.*, 203(4), 28 pp.
- Oliver, J., 1982. Probing the structure of the deep continental crust. *Science*, 216: 680–695.
- Olsson, R.K., 1964. *Praeorbulina* Olsson, a new foraminiferal genus. *J. Paleontol.*, 38: 770–771.
- Omboni, G., 1869. Nuovi elementi di storia naturale ad uso delle scuole superiori. *Geologia*, 870 pp., V. Maisner and Compagnia Editori-Librari, Milano.
- Orszag Sperber, F., Butterlin, J., Clermonte, J., Colchen, M., Guiraud, R., Poisson, A. and Ricou, L.E., 1993. Tortonian palaeoenvironments (11.5–6 Ma). In: J. Dercourt, L.E. Ricou and B. Vrielynck (Editors), *Atlas Tethys Palaeoenvironmental Maps. Explanatory Notes*. Gauthier Villars, Paris, pp. 243–258.
- Oslík, J.S., Miller, K.G., Feigenson, M.D. and Wright, J.D., 1994. Oligocene–Miocene strontium isotopes: stratigraphic revisions and correlations to an inferred glacioeustatic record. *Paleoceanography*, 9(3): 427–443.
- Otofujii, Y. and Matsuda, T., 1983. Paleomagnetic evidence for the clockwise rotation of Southwest Japan. *Earth Planet. Sci. Lett.*, 62: 349–359.
- Otofujii, Y. and Matsuda, T., 1984. Timing of rotational motion of Southwest Japan inferred from paleomagnetism. *Earth Planet. Sci. Lett.*, 70: 373–382.
- Otofujii, Y. and Matsuda, T., 1987. Amount of clockwise rotation of Southwest Japan: fan-shape opening of the southwestern part of the Japan Sea. *Earth Planet. Sci. Lett.*, 85: 289–301.
- Otofujii, Y., Hayashida, A. and Torii, M., 1985a. When was the Japan Sea opened? Paleomagnetic evidence from Southwest Japan. In: N. Nasu et al. (Editors), *Formation of Active Ocean Margins*. Terra Publ., Tokyo, pp. 551–556.
- Otofujii, Y., Matsuda, T. and Nohda, S., 1985b. Opening mode of the Japan Sea inferred from the paleomagnetism of the Japan Arc. *Nature*, 317: 603–604.
- Otofujii, Y., Matsuda, T. and Nohda, S., 1985c. Paleomagnetic evidence for the Miocene counter-clockwise rotation of northeast Japan, rifting process of the Japan Arc. *Earth Planet. Sci. Lett.*, 75: 265–277.
- Otofujii, Y., Itaya, T. and Matsuda, T., 1991. Rapid rotation of Southwest Japan, Paleomagnetism and K–Ar ages of Miocene volcanic rocks of Southwest Japan. *Geophys. J. Int.*, 105: 397–405.
- Otofujii, Y., Kambara, A., Matsuda, T. and Nohda, S., 1994. Counterclockwise rotation of northeast Japan: paleomagnetic evidence for regional extent and timing of rotation. *Earth Planet. Sci. Lett.*, 121: 503–511.
- Ott d'Estevou, P. and Montenat, C., 1985. Evolution structurale de la zone bétique orientale (Espagne) du Tortonien à l'Holocène. *C.R. Acad. Sci.*, Paris, 300, II, 8: 363–368.
- Page, R.W. and McDougall, I., 1970. Potassium–argon dating of the Tertiary f1–2 stage in New Guinea and its bearing on the geological time-scale. *Am. J. Sci.*, 269: 321–342.
- Pareto, L., 1865. Note sur les subdivisions que l'on pourrait établir dans les terrains tertiaires de l'Apennin septentrional. *Bull. Soc. Géol. Fr.*, sér. 2, 22: 210–217.
- Parona, C.F., 1903. *Trattato di geologia con speciale riguardo alla geologia d'Italia*. Biblioteca delle Scienze Fisiche e Naturali, F. Vallardi, 730 pp.
- Patacca, E. and Scandone, P., 1989. Post-Tortonian mountain building in the Apennines. The role of the passive sinking of a relic lithospheric slab. In: A. Boriani, M. Bonafede, G.B. Piccardo and G.B. Vai

- (Editors), *The Lithosphere in Italy*. Accad. Naz. Lincei, Atti Conv. Lincei, 80: 157–176.
- Patacca, E., Sartori, R. and Scandone, P., 1992. Tyrrhenian basin and Apenninic arcs: kinematic relations since late Tortonian times. *Mem. Soc. Geol. Ital.*, 45: 425–451.
- Pedley, H.M. and Grasso, M., 1993. Controls on faunal and sediment cyclicity within the Tripoli and Calcare di Base basins (late Miocene) of central Sicily. *Palaeogeogr., Palaeoclimatol., Palaeoecol.*, 105: 337–360.
- Perch-Nielsen, K., 1985. Silicoflagellates. In: H.M. Bolli, J.B. Saunders and K. Perch-Nielsen (Editors), *Plankton Stratigraphy*. Cambridge Univ. Press, Cambridge, pp. 811–846.
- Phillips, D. and Onstott, T.C., 1988. Argon isotopic zoning in mantle phlogopite. *Geology*, 16: 542–546.
- Pieri, M., 1961. Nota introduttiva al rilevamento del versante appennino padano eseguito nel 195-1959 dai geologi dell'AGIP Mineraria. *Boll. Soc. Geol. Ital.*, 80: 3–34.
- Pini, G.A., 1993. Geological map of the Bologna area foothills. C.T.F. s.n.c. and Grafiche STEP, Parma, July 1993.
- Pisias, N.G. and Shackleton, N.J., 1984. Modelling the global climate response to orbital forcing and atmospheric carbon dioxide changes. *Nature*, 310: 757–759.
- Poignant, A. and Pujol, C., 1976. Nouvelles données micropaléontologiques (foraminifères planctoniques et petits foraminifères benthiques) sur le stratotype de l'Aquitainien. *Géobios*, Lyon, 9(5): 607–663.
- Poignant, A. and Pujol, C., 1978. Nouvelles données micropaléontologiques (foraminifères planctoniques et petits foraminifères benthiques) sur le stratotype bordelais du Burdigalien. *Géobios*, Lyon, 11(5): 655–712.
- Poignant, A. and Pujol, C., 1979. Les stratotypes du bordelais (Bassin d'Aquitaine, France): Aquitainien et Burdigalien, le 'Sallomacien'. Leur microfaune et leur position biostratigraphique. VIIIth Int. Congr. R.C.M.N.S., Athens. *Ann. Géol. Pays Hellén.*, II: 993–1001.
- Ponziani, F., De Franco, R., Minelli, G., Biella, G., Federico, C. and Pialli, G., 1994. Caratteristiche della crosta dell'Appennino Settentrionale in base alla revisione dati dei profili N–C–S e B–C–A della campagna DSS 1978. *Stud. Geol. Camerti*, vol. spec. 1994/1, CROP 18: 151–162.
- Powell, A.J., 1986. A dinoflagellate cyst biozonation for the late Oligocene to middle Miocene succession of the Langhe region, northwest Italy. *Am. Assoc. Stratigr. Palynol. Contrib. Ser.*, 17: 105–128.
- Powers, R.W., Ramirez, L.F., Redmond, C.D. and Elberg, E.L., Jr., 1966. Geology of the Arabian Peninsula. *Sedimentary Geology of Saudi Arabia*. Geol. Surv. Prof. Pap., 560D, 147 pp.
- Premoli Silva, I. and Spezzaferri, S., 1990. Paleogene planktonic foraminifer biostratigraphy and paleoenvironmental remarks on Paleogene sediments from Indian Ocean sites, Leg 115. *Proc. ODP, Sci. Results*, 115: 277–314.
- Premoli Silva, I., Coccioni, R. and Montanari, A. (Editors), 1988. The Eocene–Oligocene Boundary in the Marche–Umbria Basin, I.U.G.S. Subcommission on Paleogene Stratigraphy, Spec. Publ., F.Ili Anibaldi Publ., Ancona, 268 pp.
- Pujol, C., 1970. Contribution à l'étude des foraminifères planctoniques néogènes dans le bassin aquitain. *Bull. Inst. Géol. Bassin d'Aquitaine*, Bordeaux, 9: 201–219.
- Purser, B.H. and Hotzl, H., 1986. The sedimentary evolution of the Red Sea rift: a comparison of the northwest (Egyptian) and northeast (Saudi Arabian) margins. *Tectonophysics*, 153: 193–208.
- Quirantes, J., 1978. Estudio sedimentológico y estratigráfico del Terciario continental de los Monegros. *Inst. Fernando el Católico*. CSIC, 200 pp.
- Raffi, I. and Rio, D., 1979. Calcareous nannofossil biostratigraphy of DSDP Site 132, Leg 13 (Tyrrhenian Sea, Western Mediterranean). *Riv. Ital. Paleontol. Stratigr.*, 85: 127–172.
- Raffi, I., Rio, D., d'Atri, A., Fornaciari, E. and Rocchetti, S., 1995. Quantitative distribution patterns and biomagnetostigraphy of middle and late Miocene calcareous nannofossils from equatorial Indian and Pacific oceans (Legs 115, 130 and 138). *Proc. ODP Sci. Results*, 138: 479–502.
- Rakic-El Bied, K., 1990. Stratigraphie à haute résolution et paléo-océanographie au Maroc à la fin du Miocène: apport des foraminifères planctoniques. Thesis, Univ. Bordeaux I, 121 pp.
- Renault, J.P., Moussat, E. and Fabbri, A., 1987. Structural evolution of the Tyrrhenian backarc basin. *Mar. Geol.*, 74: 123–150.
- Renne, P.R., Deino, A.L., Walter, R.C., Turrin, B.D., Swisher, C.C., III, Becker, T.A., Curtis, G.H., Sharp, W.D. and Jaouni, A.R., 1994. Intercalibration of astronomical and radioisotopic time. *Geology*, 22: 783–786.
- Reutter, K.J., Gunther, K. and Groscurth, J., 1978. An approach to the geodynamics of the Corsica–Northern Apennines double orogen. In: H. Closs, D. Roeder and K. Schmidt (Editors), *Alps, Apennines and*

- Hellenides. Schweizerbart'sche, Stuttgart, pp. 299–311.
- Reutter, K.J., Giese, P. and Closs, H., 1980. Lithospheric split in the descending plate: observations from the Northern Apennines. *Tectonophysics*, 64: T1–T9.
- Reyre, D. and Mohafez, S., 1970. Une première contribution des accords NIOC ERAP à la connaissance géologique de l'Iran. *Rev. Inst. Fr. Pétr.*, Pau, XXV, 9: 687–713, 979–1014.
- Riba, O., Reguant, S. and Villena, J., 1983. Ensayo de síntesis estratigráfica y evolutiva de la cuenca terciaria del ebro. In: *Libro Jubilar J.M. Rios*, IGME Publishers, pp. 131–157.
- Ricci Lucchi, F., 1986. The Oligocene to Recent foreland basins of the northern Apennines. *Spec. Publ. Int. Assoc. Sedimentol.*, 8: 105–139.
- Ricci Lucchi, F., 1987. Semi-allocthonous sedimentation in the Apenninic thrust belt. *Sediment. Geol.*, 50: 119–134.
- Ricci Lucchi, F. and Valmori, E., 1980. Basin-wide turbidites in a Miocene over-supplied deep-sea plain: a geometrical analysis. *Sedimentology*, 27: 241–270.
- Richter-Bernbur, G., 1973. Facies and paleogeography of the Messinian evaporites in Sicily. In: C.W. Drooger (Editor), *Messinian Events in the Mediterranean*. *Geodyn. Sci. Rep.*, 7: 125–141.
- Richter, F.M. and DePaolo, D.J., 1987. Numerical models for diagenesis and the Neogene Sr isotopic evolution of seawater from DSDP Site 590B. *Earth Planet. Sci. Lett.*, 83: 27–38.
- Richter, F.M. and DePaolo, D.J., 1988. Diagenesis and Sr isotopic evolution using data from DSDP 590B and 575. *Earth Planet. Sci. Lett.*, 90: 382–394.
- Richter, F.M. and Liang, Y., 1993. The rate and consequences of Sr diagenesis in deep-sea carbonates. *Earth Planet. Sci. Lett.*, 117: 553–565.
- Ricou, L.E., Braud, J. and Brunn, J.H., 1977. Le Zagros. *Mém. Soc. Géol. Fr.*, 8: 33–52.
- Riedel, W.R. and Sanfilippo, A., 1970. Radiolaria, Leg 4. *Init. Rep. DSDP*, 4: 503–575.
- Riedel, W.R. and Sanfilippo, A., 1971. Cenozoic Radiolaria from the western tropical Pacific, Leg 7. *Init. Rep. DSDP*, 7: 1529–1672.
- Riedel, W.R. and Sanfilippo, A., 1978. Stratigraphy and evolution of tropical Cenozoic radiolarians. *Micropaleontology*, 24: 61–96.
- Ringeade, M., 1978. Contribution à la biostratigraphie des faciès continentaux d'Aquitaine (Eocène supérieur-Miocène inférieur) par l'étude des micromammifères et des charophytes. Thèse, Université Bordeaux I, No. 572, offset, 318 pp.
- Rio, D., Sprovieri, R. and Raffi, I., 1984. Calcareous plankton biostratigraphy and biochronology of the Pliocene–Lower Pleistocene succession of the Capo Rossello area, Sicily. *Mar. Micropaleontol.*, 9: 135–180.
- Rio, D., Fornaciari, E. and Raffi, I., 1990a. Late Oligocene through early Pleistocene calcareous nannofossils from the western equatorial Indian Ocean (Leg 115). *Proc. ODP Sci. Results*, 115: 175–221.
- Rio, D., Raffi, I. and Villa, G., 1990b. Plio–Pleistocene calcareous nannofossil distribution patterns in the Western Mediterranean. *Proc. ODP Sci. Results*, 107: 513–553.
- Rio, D., Sprovieri, R. and Fornaciari, E., 1990c. Remarks on the middle-late Miocene boundary. IX Congr. C.R.M.N.S. (abstr.), Barcelona, 1990.
- Riveline, J., 1987. Les Charophytes du Paléogène et du Miocène Inférieur d'Europe occidentale. *Cah. Paléontol.*, 227 pp.
- Robba, E., 1968. Molluschi del Tortoniano tipo (Piemonte). *Riv. Ital. Paleontol. Stratigr.*, 74(2): 457–646.
- Robba, E., 1970. Otoliti del Tortoniano tipo (Piemonte). *Riv. Ital. Paleontol. Stratigr.*, 76(1): 89–172.
- Roda, C., 1965. Geologia della Tavolletta Belvedere di Spinello (Prov. Catanzaro, F. 237, I-SE). *Boll. Soc. Geol. Ital.*, 84(2): 159–285.
- Rögl, F. and Steininger, F., 1983. Vom Zerfall der Tethys zu Mediterran und Paratethys. *Ann. Naturhist. Mus. Wien*, 85/A: 135–163.
- Romeo, M., 1969. Stratigrafia e microfauna del Miocene di Monte Giammoia presso Gela (Caltanissetta). *Atti Accad. Gioenia Sci. Nat. Catania*, 7(1) (Suppl. Sci. Geol.): 239–245.
- Roure, F., Heitzmann, P. and Polino, R. (Editors), 1990a. Deep structure of the Alps. *Mém. Soc. Géol. Fr.*, Paris, 156; *Mém. Soc. Géol. Suisse, Zurich* 1; Vol. *Spec. Soc. Geol. Ital.*, Rome 1: 350 pp.
- Roure, F., Polino, R. and Nicolich, R., 1990b. Early Neogene deformation beneath the Po plain: constraints on postcollisional Alpine evolution. In: F. Roure, P. Heitzmann and R. Polino (Editors), *Deep Structure of the Alps*. *Mém. Soc. Géol. Fr.*, Paris 156; *Mém. Soc. Géol. Suisse, Zurich* 1; Vol. *Spec. Soc. Geol. Ital.*, Rome 1: 309–322.

- Royden, L. and Karner, G.D., 1984a. Flexure of lithosphere beneath Apennine and Carpathian foredeep basins: evidence for an insufficient topographic load. *AAPG Bull.*, 68: 704–712.
- Royden, L. and Karner, G.D., 1984b. Flexure of the continental lithosphere beneath Apennine and Carpathian foredeep basins. *Nature*, 309: 142–144.
- Royden, L., Patacca, E. and Scandone, P., 1987. Segmentation and configuration of subducted lithosphere in Italy: an important control on thrust–belt and foredeep–basin evolution. *Geology*, 15: 714–717.
- Ruddiman, W.F. and McIntyre, A., 1981. Oceanic mechanism for amplification of the 23,000-year ice-volume cycle. *Science*, 212: 617–627.
- Ruddiman, W.F., Shackleton, N.J. and McIntyre, A., 1986. North Atlantic sea-surface temperatures for the last 1.1 million years. In: C.P. Summerhayes and N.J. Shackleton (Editors), *North Atlantic Palaeoceanography*. *Geol. Soc. Spec. Publ.*, 21: 155–173.
- Ruggieri, G., 1956. Contributo alla conoscenza della geologia di San Marino. *G. Geol.*, Ser. 2, 25(1953): 49–80.
- Ruggieri, G., 1958. Gli esotoci neogenici della colata gravitativa della Val Marecchia. *Atti Accad. Sci. Lett. Art. Palermo*, Ser. 4(17) (1956–57), 169 pp.
- Ruggieri, G. and Sprovieri, R., 1976. Messinian salinity crisis and its paleogeographical implications. *Palaeogeogr., Palaeoclimatol., Palaeoecol.*, 20: 13–21.
- Ryan, W.B.F., Cita, M.B., Dreyfus-Rawson, M., Burkle, L.H. and Saito, T., 1974. A paleomagnetic assignment of Neogene stage boundaries and the development of isochronous datum planes between the Mediterranean, the Pacific and Indian Oceans in order to investigate the response of the world ocean to the Mediterranean 'salinity crisis'. *Riv. Ital. Paleontol. Stratigr.*, 80: 631–688.
- Sacco, F., 1890. Il bacino terziario e quaternario del Piemonte. *Bernardoni*, Milano, 634 pp.
- Saito, T., 1963. Miocene planktonic foraminifera from Honshu, Japan. *Sci. Rep. Tohoku Univ.*, 2nd Ser. (Geology), 35: 123–210.
- Saito, H.K. and Takahashi, M., 1992. Radiometric age of the first appearance datum of *Globigerina nepenthes* in Japan. In: A. Montanari, R. Coccioni and G.S. Odin (Editors), *Interdisciplinary Geological Conference on the Miocene Epoch. Abstracts and Field Trip*, Portonovo, 11–15 November, pp. 96–98.
- Sakai, T., 1986. Lithostratigraphy of Neogene Arakawa Group at the Type Section (Tochigi Prefecture, Japan). *Bull. Fac. General Education, Utsunomiya Univ.*, 19: 49–70 (in Japanese with English abstr.).
- Salvador, A. (Editor), 1994. *International Stratigraphic Guide*. 2nd ed. I.U.G.S. and Geological Society of America, Boulder, Colo., 214 pp.
- Salvatorini, G. and Cita, M.B., 1979. Miocene foraminiferal stratigraphy, DSDP site 397 (Cape Bojador, N. Atlantic). *Init. Rep. DSDP*, 47(1): 317–373.
- Sampo, M., 1969. Microfacies and microfossils of the Zagros area, southwestern Iran (from Pre Permian to Miocene). *Int. Sedimentol. Petrogr.*, Leiden, 102 pp.
- Samson, S.D. and Alexander, E.C.J., 1987. Calibration of the interlaboratory  $^{40}\text{Ar}/^{39}\text{Ar}$  dating standard, MMhb-1. *Chem. Geol. (Isot. Geosci. Sect.)*, 66: 27–34.
- Sandroni, P., 1985. Rilevamento geologico al 1:10.000 e litostratigrafia di alcune sezioni dello Schlier nel bacino marchigiano esterno e studio mineralogico e petrografico di una sezione ricostruita nell'anticlinale del Conero. Thesis, Univ. of Urbino, 188 pp.
- Sanfilippo, A. and Negrini, C., 1993. Radiolarian stratigraphy across the Oligocene/Miocene Transition. *Mar. Micropaleontol.*
- Sanfilippo, A., Burckle, L.H., Martini, E. and Riedel, W.R., 1973. Radiolarians, diatoms, silicoflagellates and calcareous nannofossils in the Mediterranean Neogene. *Micropaleontology*, 19: 209–234.
- Sato, H. and Amano, K., 1991. Relationship between tectonics, volcanism, sedimentation and basin development, Late Cenozoic, central part of Northern Honshu, Japan. *Sediment. Geol.*, 74: 323–343.
- Savelli, D. and Wezel, F.C., 1979. Schema geologico del Messiniano del Pesarese. *Boll. Soc. Geol. Ital.*, 97: 165–188.
- Scandone, P., 1979. Origin of Tyrrhenian Sea and Calabrian arc. *Boll. Soc. Geol. Ital.*, 98: 27–34.
- Scharber, S. and Steininger, F.F., 1994. Towards a Miocene strontium sea water curve for the central Paratethys. In: M.B. Cita and L.A. Ronchi (Editors), *I.U.G.S. Subcommission of Neogene Stratigraphy*. Newsletter, 1: 45.
- Schenk, V., 1981. Synchronous uplift of the lower crust of the Ivrea Zone and of Southern Calabria and its possible consequences for the Hercynian orogeny of Southern Europe. *Earth Planet. Sci. Lett.*, 56: 305–320.

- Schenk, V., 1984. Petrology of felsic granulites, metapelites, metabasics, ultramafics and metacarbonates from southern Calabria (Italy): Prograde metamorphism, uplift and cooling of a former lower crust. *J. Petrol.*, 25: 255–298.
- Schlanger, S.O. and Premoli Silva, I., 1986. Oligocene sea-level fall recorded in mid-Pacific and archipelagic apron settings. *Geology*, 14: 392–395.
- Schmid, R., 1967. Zur Petrographie und Struktur der Zone Ivrea–Verbano zwischen Valle d'Ossola und Val Grande (Prov. Novara, Italien). *Schweiz. Mineral. Petrogr. Mitt.*, 47: 935–1117.
- Schmitz, B., Åberg, G., Werdelin, L., Foey, P. and Bendix-Almgreen, S.E., 1991.  $^{87}\text{Sr}/^{86}\text{Sr}$ , Na, F, Sr and La in skeletal fish debris as a measure of the paleosalinity of fossil-fish habitats. *Geol. Soc. Am. Bull.*, 103: 786–794.
- Scotese, C.R., 1991. Jurassic and Cretaceous plate tectonic reconstructions. Paleomap Project Project Report, 6: 1–9.
- Scotese, C.R. and McKerrow, W.S., 1990. Revised world maps: an introduction. *Geol. Soc. Mem.*, 12: 1–21.
- Scott, G.H., 1972. *Globigerinoides* from Escornebéou (Aquitaine, France) and the basal Miocene *Globigerinoides* datum. *N.Z. Geol. Geophys.*, 15: 287–295.
- Scott, G.H., 1980. Upper Miocene biostratigraphy: does *Globorotalia conomiozea* occur in the Messinian? *Rev. Esp. Micropaleontol.*, 12: 489–506.
- Seguenza, M., 1868. La formation zancléenne, ou recherches sur une nouvelle formation tertiaire. *Bull. Soc. Géol. Fr.* (2), 25: 465–486.
- Selli, R., 1948. Una sabbia vulcanica oligocenica nel Subappennino Bolognese. *Rend. Accad. Naz. Lincei*, 8: 88–93.
- Selli, R., 1954. Il bacino del Metauro. *G. Geol.*, 24, 254 pp.
- Selli, R., 1957. Sulla trasgressione del Miocene nell'Italia meridionale. *G. Geol.*, 26(2): 1–54.
- Selli, R., 1960. Il Messiniano Mayer-Eymar 1867. Proposta di un neostratotipo. *G. Geol.*, 28: 1–33.
- Selli, R., 1964. The Mayer-Eymar Messinian 1867. Proposal for a neostratotipe. *Proc. 21st IGC Copenhagen 1960*, 28: 311–333.
- Selli, R., 1971. Messinian. *G. Geol.*, 37(2): 121–133.
- Selli, R., 1973. An outline of the Italian Messinian. Messinian events in the Mediterranean. *Geodyn. Sci. Rep.*, 7: 150–171.
- Serrano, F., 1979. Los Foraminiferos planctonicos del Mioceno superior de la Cuenca de Ronda y su comparacion con los de otras areas de las Cordilleras Béticas. *Thesis Univ. Malaga*, 272 pp.
- Serrano, F., 1992. Biostratigraphic control of Neogene volcanism in Sierra de Gata (South-East Spain). *Geol. Mijnbouw*, 71: 3–14.
- Serri, G., Innocenti, F., Manetti, P., Tonarini, S. and Ferrara, G., 1991. Il magmatismo neogenico–quaternario dell'area toscano-laziale–umbra: implicazioni sui modelli di evoluzione geodinamica dell'Appennino Settentrionale. *Stud. Geol. Camerti*, vol. spec. 1991/1: 429–463.
- Sersale, R., Atello, R. and Frignone, G., 1963. Sulla presenza di orizzonti zeolitici nella serie oligo–miocenica di Garbagna (AL). *Atti Accad. Sci. Torino*, 97: 620–634.
- Sestini, G., 1970. Sedimentation of the late geosynclinal stage. *Sediment. Geol.*, 4: 445–179.
- Shackleton, N.J. and Cita, M.B., 1979. Oxygen and carbon isotope stratigraphy of benthic foraminifers at Site 397: Detailed history of climatic change during the late Neogene. *Init. Rep. DSDP*, pp. 422–445.
- Shackleton, N.J. and Kennett, J.P., 1975a. Late Cenozoic oxygen and carbon isotopic changes at DSDP Site 284: Implications for glacial history of the Northern Hemisphere and Antarctica. *Init. Rep. DSDP*, 29: 743–755.
- Shackleton, N.J. and Kennett, J.P., 1975b. Paleotemperature history of the Cenozoic and initiation of the Antarctic glaciation: oxygen and carbon isotopic analyses in DSDP Sites 271, 279 and 281. *Init. Rep. DSDP*, 29: 801–807.
- Shackleton, N.J. and Opdyke, N.D., 1973. Oxygen isotope and paleomagnetic stratigraphy of equatorial Pacific core V28–238: Oxygen isotope temperatures and ice volumes on a  $10^5$  and  $10^6$  year scale. *Quat. Res.*, 3: 39–55.
- Shackleton, N.J., Berger, A. and Peltier, W.R., 1990. An alternative astronomical calibration of the lower Pleistocene timescale based on ODP Site 677. *Trans. R. Soc. Edinburgh, Earth Sci.*, 81: 251–261.
- Shackleton, N.J., Crowhurst, S.J., Pisias, N., Hagelberg, T., Schneider, D., Mix, A. and ODP Leg 138 Shipboard Scientific Party, 1992. An astronomically calibrated Pliocene time scale based on Leg 138 grape density records. *4th Int. Conf. Paleoceanography, Abstr. Vol.*, 260.

- Shackleton, N.J., Crowhurst, S.J., Pisias, N. and Schneider, D.A., 1993. A new late Neogene timescale: Application to ODP Leg 138 sites, Proc. Sci. Results, 138.
- Shackleton, N.J., Hall, M.A. and Pate, D., 1995. Pliocene stable isotope stratigraphy of Site 846. Proc. ODP Sci. Results, 138: 337–355.
- Shibata, K., Uchiyumi, S. and Nakagawa, T., 1979. K–Ar age results 1. Bull. Geol. Surv. Jpn., 30: 675–686 (in Japanese with English abstr.).
- Shibata, K., Nishimura, S. and Chinzei, K., 1984. Radiometric dating related to Pacific Neogene planktonic datum planes. In: N. Ikebe and R. Tsuchi (Editors), Pacific Neogene Datum Planes. Contributions to Biostratigraphy and Chronology, Univ. Tokyo Press, Tokyo, pp. 85–89.
- Sierro, F.J., 1985. The replacement of the '*Globorotalia menardii*' group by the *Globorotalia miotumida* group: an aid to recognizing the Tortonian/Messinian boundary in the Mediterranean and adjacent Atlantic. Mar. Micropaleontol., 9(6): 525–535.
- Sierro, F.J., Flores, J.A., Civis, J. and González Delgado, J.A., 1987. New criteria for the correlation of the Andalusian and Messinian stages. Ann. Inst. Geol. Publ. Hung., LXX: 355–361.
- Sierro, F.J., Flores, J.A., Civis, J., Gonzales Delgado, J.A. and Frances, G., 1993. Late Miocene globorotaliids event-stratigraphy and biogeography in the NE-Atlantic and Mediterranean. Mar. Micropaleontol., 21: 143–168.
- Signorini, R., 1941. Struttura dell'Appennino tra la val Tiberina e l'Urbinate. G. Geol., 2a s., 15: 17–29.
- Sinninghe Damsté, J.S., Eglinton, T.I., de Leeuw, J.W. and Schenck, P.A., 1989. Organic sulfur in macromolecular sedimentary organic matter: I. Structure and origin of sulfur-containing moieties in kerogen, asphaltenes and coal as revealed by flash pyrolysis. Geochim. Cosmochim. Acta, 53: 873–889.
- Sinninghe Damsté, J.S., Eglinton, T.I. and de Leeuw, J.W., 1992. Alkylpyrroles in a kerogen pyrolyzate: Evidence for abundant tetrapyrrole pigments. Geochim. Cosmochim. Acta, 56: 1743–1751.
- Smalley, P.C., Higgins, A.C., Howarth, R.J., Nicholson, H., Jones, C.E., Swinburne, N.H.M. and Bessa, J., 1994. Seawater Sr isotope variations through time: A procedure for constructing a reference curve to date and correlate marine sedimentary rocks. Geology, 22: 431–443.
- Sorbini, L., 1988. Biogeography and climatology of Pliocene and Messinian fossil fish of eastern-central Italy. Boll. Mus. Civ. St. Nat. Verona, 14: 1–85.
- Spadea, P. and Carmisciano, R., 1974. Nuovi dati sulle cineriti del Miocene medio della Sicilia centro-meridionale. Boll. Soc. Geol. Ital., 93: 1095–1126.
- Spakman, W., 1986. Subduction beneath Eurasia in connection with the Mesozoic Tethys. Geol. Mijnbouw, 65: 145–153.
- Spakman, W., 1990. Tomographic images of the upper mantle below central Europe and the Mediterranean. Terra Nova, 2: 512–553.
- Spezzaferri, S., 1991. Evolution and taxonomy of the *Paragloborotalia kugleri* (Bolli) lineage. J. Foramin. Res., 21: 313–318.
- Spezzaferri, S., 1992. Il limite Oligocene/Miocene nel 'record oceanico' (Atlantico, Indiano, sud Pacifico): biostratigrafia e paleontologia. Ph. Diss., Univ. Milano, 288 pp.
- Spezzaferri, S., 1994. Planktonic foraminiferal biostratigraphy and taxonomy of the Oligocene and lower Miocene in the oceanic record. An overview. Palaeontogr. Ital., 81, 187 pp.
- Sprovieri, R., 1975. Il limite Messiniano–Pliocene nella Sicilia centro-meridionale. Boll. Soc. Geol. Ital., 94: 51–91.
- Stainforth, R.M., Lamb, J.L., Luterbacher, H., Beard, J.H. and Jeffords, R.M., 1975. Cenozoic planktonic foraminiferal zonation and characteristics of index forms. Univ. Kansas Paleontol. Contrib., 62, 425 pp.
- Stankiewicz, B.A., Kruge, M.A. and Crelling, J.C., 1993. Density Gradient Centrifugation: Application to the Separation of Macerals of Type I, II and III Sedimentary Organic Matter. Energy Fuels.
- Staudigel, H., Doyle, P. and Zindler, A., 1985/86. Sr and Nd isotope systematics in fish teeth. Earth Planet. Sci. Lett., 76: 45–56.
- Steiger, R.H. and Jäger, E., 1977. Subcommission on Geochronology: Conventions on the use of decay constants in geo- and cosmochronology. Earth Planet. Sci. Lett., 36: 359–362.
- Steininger, F.F., 1992. A candidate for the Palaeogene/Neogene Global Stratotype Section and Point: the Lemme valley section, Piedmont Basin, Italy. 29th Int. Geol. Congr., Kyoto, p. 268 (abstr.).
- Steininger, F.F., Rabeder, G. and Rögl, F., 1985. Land mammal distribution in the Mediterranean Neogene. In: J. Stanley and F.C. Wezel (Editors), Geological Evolution of the Mediterranean Basin. Springer-Verlag, Berlin, pp. 559–571.

- Steininger, F.F., Bernor, R.L. and Fahlbusch, V., 1989. European Neogene marine/continental chronologic correlations. In: E.H. Lindsay, V. Fahlbusch and P. Mein (Editors), *European Neogene Mammal Chronology*. NATO ASI Series, 180, Plenum Press, New York, pp. 15–27.
- Steininger, F.F. and Cati, F. (Editors), in press. In search of the Palaeogene/Neogene Boundary Part III. The Palaeogene/Neogene Boundary and its Global Boundary Stratotype section and Point at meter 35 in the Lemme–Carrosio Section at Carrosio, 'Casa Carizziani', Piedmont Basin, Province of Alessandria, Italy. I.U.G.S. Commission on Stratigraphy, Subcommittee on Neogene Stratigraphy, Working Group on the Palaeogene/Neogene Boundary Report. *G. Geol.*
- Steininger, F.F., Berggren, W.B., Kent, D.V., Bernor, R.L., Sen, S. and Agusti, J., 1996. Circum Mediterranean Neogene (Miocene and Pliocene) Marine–Continental Chronologic Correlations of the European Mammal Units and Zones. In: R.L. Bernor, V. Fahlbusch and S. Rietschel (Editors), *Later Neogene European Biotic Evolution and Stratigraphic Correlation*. Columbia Univ. Press, pp. 7–46.
- Steininger, F.F., Aubry, M.P., Biolzi, M., Borsetti, A.M., Cati, F., Corfield, R., Gelati, R., Iaccarino, S., Napoleone, G., Rögl, F., Roetzel, R., Spezzaferri, S., Tateo, F., Villa, G. and Zevenboom, D., 1994. A Proposal for the Global Boundary Stratotype Section and Point (GSSP) of the Neogene. In: M.B. Cita and L.A. Ronchi (Editors), *Subcommission on Neogene Stratigraphy, Newsletter*, 1: 17–21.
- Stoppani, A., 1873. *Corso di geologia*, vol. 1; *Dinamica terrestre*, Vol. 2; *Geologia stratigrafica*, Vol. 3; *Geologia Endografica*. Bernardoni and Brigola, Milano.
- Stradner, H., 1959. First report on the disconformity of the Tertiary and their stratigraphic use. *Proceedings of the Fifth World Petroleum Congress*, New York, sect. I., 60: 1–12.
- Strauss, C., 1991. *Taxonomie und Biostratigraphie des marinen Mikroplanktons mit organischer Wandung im Oligo–Miozän Ostdeutschlands*. Diss., Bergakademie Freiberg.
- Suc, J.P. and Bessais, E., 1990. Pérennité d'un climat thermo-xérique en Sicile avant, pendant, après la crise de salinité messinienne. *C.R. Acad. Sci. Paris*, 310: 1701–1707.
- Suhadolc, P. and Panza, G.F., 1989. Physical properties of the lithosphere–asthenosphere system in Europe from geophysical data. In: A. Boriani, M. Bonafede, G.B. Piccardo and G.B. Vai (Editors), *The lithosphere in Italy*. *Advances in Earth Science Research*. Accad. Naz. Lincei, pp. 15–40.
- Swisher, C.C., III, DePaolo, D.J. and Owens, T., 1994. Age of Fish Canyon Tuff sanidine (FCTS): a single crystal  $^{40}\text{Ar}/^{39}\text{Ar}$  dating standard. *U.S. Geol. Surv. Circ.*, 1107: 312.
- Takahashi, M., 1994a. Miocene tectonic deformation of central Japan, Paleomagnetic evidence of intra-arc bending. *Geofis. Int.*, 33: 25–44.
- Takahashi, M., 1994b. Miocene lateral bending of central Japan, Intra-arc deformation at arc–arc collision zone. *Bull. Geol. Surv. Japan*, 45(8/9): 477–495.
- Takahashi, M. and Hayashi, M., 1991. Classification and correlation of Miocene tuffs in the Kanto area using zircon crystal morphology. *J. Geol. Soc. Jpn.*, 97: 451–459 (in Japanese with English abstr.).
- Takahashi, M., Saito, K., Umetsu, H. and Ichikawa, N., 1992. K–Ar and  $^{40}\text{Ar}$ – $^{39}\text{Ar}$  ages of the Miocene Kitamura and Baba Tuffs in the Tomioka area, Gunma Prefecture, central Japan. *J. Geol. Soc. Jpn.*, 98: 323–335 (in Japanese with English abstr.).
- Takayanagi, Y., Takayama, T., Sakai, T., Oda, M. and Kitazato, H., 1976. Microbiostratigraphy of some Middle Miocene sequences in northern Japan. In: Y. Takayanagi and T. Saito (Editors), *Progress in Micropaleontology: Selected Papers in Honor of Prof. Kiyoshi Asano*. Micropaleontology Press, New York, pp. 356–381.
- Takayanagi, Y., Takayama, T., Sakai, T., Oda, M., Kitazato, H., Oriyama, J. and Kaneko, M., 1978. Problems relating the Kaburan stage, in Cenozoic geology of Japan (Prof. Nobuo Ikebe Memorial Volume), Osaka, pp. 93–111 (in Japanese with English abstr.).
- Takayanagi, Y., Oda, M., Hasegawa, S., Honda, N., Maruyama, T. and Funayama, M., 1984. Some Middle Miocene planktonic microfossil datum planes in northern Honshu, Japan: Their paleoceanographic implications. *Palaeogeogr., Palaeoclimatol., Palaeoecol.*, 46: 71–84.
- Taniguchi, H., Soh, W. and Ogawa, Y., 1991. Discussions on the origin and tectonics of the volcanic rocks in the Misaki Formation. *Chikyu Mon.*, 13: 31–34 (in Japanese).
- Tateo, F., 1992. *Studio mineralogico–geochimico di sedimenti vulcanoderivati (Oligocene–Miocene inferiore) dell'Appennino settentrionale*. Tesi di Dottorato, Univ. Bologna, 216 pp.
- Tateo, F., 1997. Mineralogy of nodular and oxidized layers *Giorn. Geol.*, in press.
- Tauxe, L. and Opdyke, N.D., 1982. A time framework based on magnetostratigraphy for the Siwalik sediments of the Khaur area, northern Pakistan. *Palaeogeogr., Palaeoclimatol., Paleoecol.*, 37: 43–60.



- Tedford, R.H., 1987. Faunal succession and Biochronology of the Arikareean through Hemiphillian interval (Late Oligocene through earliest Pliocene Epochs) in North America. In: M.O. Woodburne (Editor), *Cenozoic Mammals of North America: Geochronology and Biostratigraphy*. Univ. California Press, pp. 153–210.
- Tempelman-Kluit, D.J., 1979. Transported cataclasite, ophiolite and granodiorite in Yukon; evidence of arc–continent collision. *Geol. Surv. Can. Pap.*, 79-14: 1–27.
- Theodoridis, S., 1984. Calcareous nannofossil biozonation of the Miocene and revision of the *Helicolithids* and *Discoasterids*. *Utrecht Micropaleontol. Bull.*, 32, 272 pp.
- Theyer, F. and Hammond, S.R., 1974. Paleomagnetic polarity sequence and radiolarian zones, Brunhes to polarity epoch 20. *Earth Planet. Sci. Lett.*, 22: 307–319.
- Thucydides, ca. 411 B.C. *History of the Peloponnesian War* (incomplete work).
- Tiedemann, R., Medelsee, M., Sarnthein, M. and Statterger, K., 1992. Astronomical tuning of high-resolution benthic  $\delta^{18}\text{O}$  records from ODP Sites 658 and 659 for the last 5 million years vs. non-linear climatic dynamics. 4th Int. Conf. Paleooceanography, Abstr. Vol., 282.
- Tissot, B.P. and Welte, D.H., 1984. *Petroleum Formation and Occurrence*. 2nd ed., Springer-Verlag, Berlin, 699 pp.
- Tongiorgi, E. and Tongiorgi, M., 1964. Age of the Miocene–Pliocene limit in Italy. *Nature*, 201: 365–367.
- Tournouer, R., 1862. Note stratigraphique et paléontologique sur les faluns du département de la Gironde. *Bull. Soc. Géol. Fr., Paris*, 19, Sér. 2: 1035–1088.
- Urabe, A., 1992. Correlation of some pyroclastic key beds in the Mio–Pliocene Miura Group, Miura and Boso Peninsulas, central Japan: reconsideration with additional data on heavy mineral composition and chemical composition. *J. Geol. Soc. Jpn.*, 98: 415–434 (in Japanese with English abstr.).
- Vai, G.B., 1975. Evento 'Caledoniano' nelle Alpi? Discussione sui rapporti tra radiocronometria e stratigrafia. *Boll. Soc. Geol. Ital.*, 94: 269–273.
- Vai, G.B., 1988. The Lamone Valley: A field trip guide to the Romagna Apennines. In: C. De Giuli and G.B. Vai (Editors), *Fossil Vertebrates in the Lamone Valley, Romagna Apennines*. F.T. Guidebook Int. Workshop Continental Faunas at the Mio–Pliocene Boundary, Faenza, pp. 7–37.
- Vai, G.B., 1989a. Migrazione complessa del sistema fronte deformativo-avanfossa-cercine periferico: il caso dell'Appennino Settentrionale. *Mem. Soc. Geol. Ital.*, 38: 95–105.
- Vai, G.B., 1989b. A field trip guide to the Romagna Apennine geology. The Lamone valley. *Boll. Soc. Paleontol. Ital.*, 28: 343–367.
- Vai, G.B. and Castellarin, A., 1993. Correlazione sinottica delle unità litostratigrafiche nell'Appennino Settentrionale. *Stud. Geol. Camerti*, vol. spec. 1992/2, CROP 1-1A, 171–185.
- Vai, G.B. and Laurenzi, M., 1994. Radiometric dating of the Tortonian Messinian boundary (N. Apennines, Italy). 8th Int. Conf. Geochron., Cosmochron. *Isot. Geol.*, Berkeley, USGS Circ., 1107: 333.
- Vai, G.B. and Ricci Lucchi, F., 1977. Algal crusts, autochthonous and clastic gypsum in a cannibalistic evaporite basin: A case history from the Messinian of the Northern Apennines. *Sedimentology*, 24: 211–244.
- Vai, G.B., Villa, I.M. and Colalongo, M.L., 1992. Radiometric age calibration of the latest Tortonian and Tortonian/Messinian Boundary from the North Apennine type area. 29th Int. Geol. Congr., Kyoto, Abstr., 1: 89.
- Vai, G.B., Villa, I.M. and Colalongo, M.L., 1993. First direct radiometric dating of the Tortonian/Messinian boundary. *C.R. Acad. Sci. Paris*, 316, II: 1407–1414.
- Vail, P.R., Colin, J.P., Jan du Chêne, R., Kuchly, J., Mediavilla, F. and Triflieff, V., 1987. La stratigraphie séquentielle et son application aux corrélations chronostratigraphiques dans le Jurassique du bassin de Paris. *Bull. Soc. Géol. Fr.*, 8(3): 1301–1321.
- Van Bemmelen, R.W., 1969. Origin of the Western Mediterranean basin. *Verh. K. Ned. Geol. Mijnbouw. Genoot.*, 26: 13–52.
- Van Bemmelen, R.W., 1972. Driving forces of Mediterranean orogeny. *Geol. Mijnbouw*, 51: 548–573.
- Van der Zwaan, G.J., 1982. Paleoecology of Late Miocene Mediterranean Foraminifera. *Utrecht Micropaleontol. Bull.*, 25: 5137.
- Van der Zwaan, G.J. and Gudjonsson, L., 1986. Middle Miocene–Pliocene stable isotope stratigraphy and paleoceanography of the Mediterranean. *Mar. Micropaleontol.*, 10: 71–90.
- Van Eysinga, F.W.B., 1975. *Geological Time table*, 3rd ed. Elsevier, Amsterdam.
- Vervloet, C.C., 1966. Stratigraphical and micropaleontological data on the Tertiary of Southern Piemont

- (Northern Italy). Schotanus, Utrecht, pp. 1–88.
- Vigliotti, L., 1988. Magnetostratigraphy of the Monticino Quarry section 1987 (Faenza, Italy). In: C. De Giuli and G.B. Vai (Editors), Fossil Vertebrates in the Lamone Valley, Romagna Apennines. F.T. Guidebook Int. Workshop on Continental Faunas at the Miocene/Pliocene Boundary, Faenza, pp. 61–62.
- Vigneaux, M., 1949. Révision des bryozoaires néogènes du Bassin d'Aquitaine et essai de classification. *Mém. Soc. Géol. Fr., Paris, N.S., XXVIII*, 1–3, 6, 155 pp.
- Vigneaux, M., 1971. Burdigalian. In: Stratotypes of Mediterranean Neogene Stages, CMNS. *G. Geol.*, 37(2): 49–54.
- Vigneaux, M. and Marks, P., 1971. Aquitanian. In: Stratotypes of Mediterranean Neogene Stages, CMNS. *G. Geol.*, 37(2): 23–31.
- Villa, I.M., 1992. Datability of Quaternary volcanic rocks: an  $^{40}\text{Ar}/^{39}\text{Ar}$  perspective on age conflicts in lavas from the Alban Hills, Italy. *Eur. J. Miner.*, 4: 369–383.
- Vincent, E., Killingley, J.S. and Berger, W.H., 1980. The magnetic epoch 6 — carbon shift: A change in the ocean's  $^{13}\text{C}/^{12}\text{C}$  ratio 6.2 million years ago. *Mar. Micropaleontol.*, 5: 185–203.
- Vincent, E., Killingley, J.S. and Berger, W.H., 1985. Miocene oxygen and carbon isotope stratigraphy of the tropical Indian Ocean. In: J.P. Kennett (Editor), *The Miocene Ocean: Paleooceanography and Biogeography*. *Mem. Geol. Soc. Am.*, 163: 103–130.
- Vrielynck, B., Dercourt, J. and Cottreau, N., 1994. Des seuils lithosphériques dans la Téthys. *C.R. Acad. Sci. Paris*, 318: 1677–1685.
- Anonymous, 1959. Résolution du comité du Néogène Méditerranéen à Vienne. *Mitt. Geol. Ges. Wien*, 1960, 52: 3–4.
- Anonymous, 1970. Reports of chairman of the session of the Working Teams. In: Results of the IVth Session of the C.M.N.S. (Bologna, 23–26 september 1967) *G. Geol.*, Ser. 2a, Vol. XXXV, 1: 41–47.
- Wang, C., Hwang, W. and Shi, Y., 1989. Thermal evolution of a rift basin: the Tyrrhenian Sea. *J. Geophys. Res.*, 94: 3991–4006.
- Wang, Q.M., Hishidai, T. and Coward, M.P., 1992. The Tarim basin, NW China: formation and aspects of petroleum geology. *J. Petrol. Geol.*, 15(1): 5–34.
- Wezel, F.C., 1977. Widespread manifestations of Oligocene–lower Miocene volcanism around western Mediterranean. In: B. Biju-Duval and L. Montadert (Editors), *Structural History of Mediterranean Basins*. Split, Edition Technip., pp. 287–302.
- Wezel, F.C., 1982. The Tyrrhenian Sea: a rifted krikogenic swell basin. *Mem. Soc. Geol. Ital.*, 24: 531–568.
- Wigger, P.J., 1984. Die Krustenstruktur des Nordappennins und angrenzender Gebiete mit besonderer Berücksichtigung der geothermischen Anomalie der Toskana. *Berl. Geowiss. Abh.*, B9: 1–87.
- Williams, G.L., 1975. Dinoflagellate and spore stratigraphy of the Mesozoic–Cenozoic, offshore eastern Canada. *Geol. Surv. Can.*, 74-30(2): 107–161.
- Williams, G.L., 1977. Dinocysts: their classification, biostratigraphy and paleoecology. In: A.T.S. Ramsay (Editor), *Oceanic Micropaleontology*. Academic Press, New York, pp. 1231–1325.
- Woodruff, F. and Savin, S., 1989. Miocene deep-water oceanography. *Paleoceanography*, 4: 87–140.
- Woodruff, F. and Savin, S., 1991. Mid-Miocene isotope stratigraphy in the deep sea: High-resolution correlation, paleoclimatic cycles and sediment preservation. *Paleoceanography*, 6: 755–806.
- Wright, J.D., Miller, K.G. and Fairbanks, R.G., 1992. Early and middle Miocene stable isotopes: Implications for deepwater circulation and climate. *Paleoceanography*, 7: 357–389.
- Yamaji, A., 1989. Geology of Atsumi area and Early Miocene rifting in the Uetsu district, northeast Japan. *Mem. Geol. Soc. Jpn.*, 32: 305–320 (in Japanese with English abstr.).
- Yamaji, A., 1990. Rapid intra-arc rifting in Miocene Northeast Japan. *Tectonics*, 9: 365–378.
- Yanagisawa, Y., Nakamura, K., Suzuki, Y., Sawamura, K., Yoshida, F., Tanaka, Y., Honda, Y. and Takahashi, M., 1989. Tertiary biostratigraphy and subsurface geology of the Futaba district, Joban Coalfield, northeast Japan. *Bull. Geol. Surv. Jpn.*, 40: 405–467 (in Japanese with English abstr.).
- Yazaki, K. and Mitsunashi, T., 1961. A map of petroleum and gas fields in Japan, Yokosuka. *Geol. Surv. Japan*.
- Young, J., Wei, W., incorporating workshop discussion contribution from Backman, J., Hamrsmid, B., van Heck, S.E., Krhowsky, Raffi, I., Di Stefano, A., Villa, G. and Wise, S.W., 1994. A summary chart of Neogene nannofossil magnetobiostratigraphy. *J. Nanoplankton Res.*, 16(1): 21–27.
- Zachariasse, W.J., 1975. Planktonic foraminiferal biostratigraphy of the Late Neogene of Crete (Greece). *Utrecht Micropaleontol. Bull.*, 21: 129–166.

- Zachariasse, W.J., 1979. The origin of *Globorotalia conomiozea* in the Mediterranean and the value of its entry level in biostratigraphic correlations. *Ann. Geol. Pays Hellen.*, Ser., 1979, III, pp. 1281–1292. 7th Int. Congr. Mediterranean Neogene, Athens.
- Zachariasse, W.J. and Spaak, P., 1983. Middle Miocene to Pliocene palaeoenvironmental reconstruction of the Mediterranean and adjacent Atlantic Ocean: planktonic foraminiferal record of S Italy. In: J.E. Meulenkamp (Editor), *Reconstruction of Marine Paleoenvironment*. Utrecht Micropaleontol. Bull., 30: 91–110.
- Zeck, H.P., 1970. An erupted migmatite from Cerro el Hoyazo, SE Spain. *Contrib. Mineral. Petrol.*, 26: 225–246.
- Zevenboom, D., Brinkhuis, H. and Visscher, H., 1994. Dinoflagellate-based palaeoenvironmental analysis of the Oligocene/Miocene transition in northwest and central Italy. *G. Geol.*, 56(1): 155–169.
- Zevenboom, D., in press. Late Oligocene–Miocene dinoflagellate cysts from the Lemme section (NW Italy): biostratigraphy and palaeoenvironmental interpretations. In: F.F. Steininger and F. Cati (Editors), *In search of the Palaeogene/Neogene Boundary. Part III, The Palaeogene/Neogene Boundary and its Global Boundary Stratotype section and Point at meter 35 in the Lemme–Carrosio Section at Carossio, “Casa Carizziani”, Piedmont Basin, Province of Alessandria, Italy*. IUGS Commission on Stratigraphy, Subcommission on Neogene Stratigraphy, Working Group on the Palaeogene/Neogene Boundary Report. *G. Geol.*
- Zhang, J., Miller, K.G. and Berggren, W.A., 1993. Neogene planktonic foraminiferal biostratigraphy of the northeastern Gulf of Mexico. *Micropaleontology*, 39(4): 299–326.
- Zingg, A., 1983. The Ivrea and Strona–Ceneri Zones (Southern Alps, Ticino and N Italy): a review. *Schweiz. Mineral. Petrogr. Mitt.*, 63: 361–392.

## AUTHOR INDEX

- Åberg, G., 659  
Adams, C.G., 463, 631  
AGIP S.p.A., 631  
Agusti, J., 144, 363, 551, 631, 651, 661  
Akimoto, K., 555, 631, 648  
Albarède, F., 645  
Alessandrini, B., 631  
Alexander, E.C.J., 268, 333, 336, 440, 587, 641, 658  
Alvarez, W., 180, 183, 205, 252, 631, 650, 652  
Alvarez-Sierra, M.A., 302, 631, 641  
Alvinerie, J., 14, 41, 53, 631, 637  
Amano, K., 196, 658  
Amato, A., 170, 172, 173, 180, 631  
Amorosi, A., 221, 222, 225, 227, 230, 282, 631, 632, 654  
Anadon, P., 620, 632, 643  
Anderson, D.L., 181, 632  
Anderson, H., 183, 632  
Andreoni, C., 129, 210, 632  
Andrés, J.A., 641  
Andriessen, P.A.M., 654  
Anelli, L., 178, 632  
Anglada, R., 631, 642  
Antunes, M.T., 631  
Aoki, S., 652  
Arenas, C., 297, 632  
Arias, C., 543, 632  
Armstrong, R., 645  
Artyushkov, E.V., 181, 632  
Asaga, M., 646  
Asano, K., 653  
Ascoli, P., 97, 632  
Assorgia, A., 205, 225, 252, 281, 317, 440, 632  
Atello, R., 659  
Aubry, M.P., 133, 486, 632, 633, 648, 652, 661  
Aubry III, M.P., 634,  
Auroux, C., 648  
Azanza, B., 641  
  
Babak, E.V., 654  
Backman, I., 643  
Backman, J., 69, 70, 77, 87, 93, 319, 422, 632, 643, 663  
Baker, P.A., 643  
Baksi, A.K., 69, 119, 498, 507, 512, 632  
Baldauf, J.G., 144, 632  
Bally, A.W., 175, 183, 184, 632  
  
Balogh, K., 252, 632  
Barberà, X., 631  
Barca, S., 638  
Barrese, E., 651  
Barron, J.A., 57, 144, 632, 644  
Barry, J.C., 85, 633  
Bartole, R., 171, 177, 180, 633  
Bartolini, C., 180, 633  
Bassett, M.G., 640  
Bassetti, M.A., 531–534, 536, 633  
Beard, J.H., 660  
Beatrizotti, G., 98, 633  
Becker, T.A., 656  
Bellardi, L., 61, 633  
Bellinzona, G., 633  
Bellion, Y., 637  
Bellon, H., 364, 366, 367, 369, 544, 547, 549, 618, 633, 645  
Benda, L., 41, 144, 633  
Bender, M.L., 120, 633, 646  
Bendix-Almgreen, S.E., 659  
Bennet, G.G., 651  
Benson, R.H., 111, 117, 122, 149–151, 496, 631, 633, 646  
Berger, A., 463, 500, 633, 639, 659  
Berger, A.L., 633  
Berger, W.H., 663  
Berggren, W.A., 14, 23, 48, 53, 66, 69, 70, 77, 82, 85, 87, 89, 94, 95, 97, 104, 125, 141, 144, 145, 152, 382, 463, 493–496, 633, 634, 652, 664  
Berggren, W.B., 661  
Bernades, C., 474, 634  
Bernini, M., 633  
Bernor, R.L., 661  
Bernoulli, D., 647  
Bersani, A., 209, 214, 634  
Bertini, A., 119, 533, 634  
Bertini, G., 180, 473, 634  
Bertolani Marchetti, D., 119, 473, 634  
Bertozzi, P., 638  
Bessa, J., 660  
Bessais, E., 119, 661  
Bessedik, M., 119, 634  
Bice, D.M., 652  
Bice, M.D., 652  
Biella, G., 656  
Biffi, U., 136, 144, 259, 292, 634  
Bigazzi, G., 632, 634

- Biolzi, M., 134, 255, 256, 286, 634, 661  
 Birck, J.L., 634  
 Bizon, G., 94, 125, 159, 163, 255, 256, 286, 353, 360, 550, 633–635, 653  
 Bizon, J.J., 125, 255, 286, 635  
 Blanc, G., 46, 69, 635  
 Blow, W.H., 21, 28, 41, 47, 48, 74, 75, 80, 82, 89, 94, 95, 97, 98, 103, 104, 125, 230, 231, 253, 255, 267, 284, 286, 287, 315, 318, 327, 339, 345, 352, 374, 375, 381, 396, 419–421, 447, 448, 600, 602, 603, 611, 622, 635, 639  
 Boccaletti, M., 59, 180, 221, 635  
 Boersma, A., 646  
 Bohn-Havas, M., 645  
 Bolli, H.M., 125, 144, 211, 228, 230, 256, 286, 318, 396, 419, 635  
 Bolze, J., 646, 653  
 Bonadonna, F.P., 632, 634  
 Bonaduce, G., 633  
 Bonatti, E., 648  
 Boni, A., 72, 84, 89, 209, 633, 635  
 Boon, J.J., 642  
 Bordet, P., 366, 633, 635, 646, 653  
 Borsetti, A.M., 100, 133, 209, 211, 212, 221, 231, 245, 256, 286, 464, 534, 634–638, 661  
 Borzonia, 159  
 Bossio, A., 96, 118, 360, 636, 644  
 Boucot, A.J., 640  
 Boulter, M.C., 650  
 Bowring, S.A., 646  
 Braga, G., 633  
 Brancolini, G., 633  
 Braud, J., 159, 163, 636, 657  
 Brinkhuis, H., 144, 257–259, 280, 288, 292, 636, 664  
 Broggi, M., 638  
 Broglia, C., 648  
 Bromley, R.G., 416, 636  
 Bronn, H.G., 142, 636  
 Brown, G.F., 161, 636  
 Bruijn De, H., 144, 636  
 Brunn, J.H., 657  
 Bukry, D., 93, 144, 212, 232, 267, 273, 276, 287, 288, 321, 327, 339, 340, 345, 422, 425, 447, 448, 452, 479, 485, 486, 488, 489, 567, 636, 655  
 Burbank, D.W., 144, 636  
 Burbi, L., 632  
 Burckle, L.H., 658  
 Burke, W.H., 648  
 Burkle, L.H., 658  
 Burolet, P.F., 647  
 Butterlin, J., 638, 650, 655  
 Cabrera, L., 297, 631, 636, 643  
 Cadet, J.-P., 654  
 Cahuzac, B., 35, 36, 40–42, 54, 602, 627, 631, 636, 637  
 Calcagnile, G., 170, 171, 637  
 Calieri, R., 112, 118, 451, 466, 468, 493, 495, 496, 500, 521, 637  
 Calvo, J.P., 633  
 Cameli, G.M., 634  
 Camerlenghi, A., 469, 637  
 Camoin, G., 157, 637  
 Cande, S.C., 50, 70, 83, 119, 141, 145, 149, 262, 264, 325, 339, 340, 425, 485, 489, 490, 498, 637  
 Cantalamessa, G., 409, 637  
 Cantelli, C., 638  
 Canud, J.I., 637  
 Canudo, J.I., 298, 300, 641  
 Capo, R., 431, 637, 652  
 Cappetta, H., 645  
 Caprara, L., 73, 637  
 Capuano, N., 640  
 Caralp, M., 631  
 Caratini, C., 14, 21, 637  
 Carbonel, P., 637  
 Carbonnel, G., 26, 30, 31, 637, 642  
 Carey, S., 652  
 Carloni, G., 59, 637  
 Carloni, G.C., 473, 531–534, 536, 542, 543, 633, 635, 637  
 Carman, M.F., Jr., 647  
 Carmignani, L., 168, 637, 638  
 Carmisciano, R., 351, 660  
 Carveni, P., 351, 352, 638  
 Casati, P., 464, 473, 638  
 Casnedi, R., 209, 635  
 Cassano, E., 169, 171, 638  
 Cassinis, R., 169, 172, 638  
 Castaldini, D., 633  
 Castellari, M., 493, 638  
 Castellarin, A., 182, 638, 662  
 Cati, F., 125, 209, 211, 213, 227, 231, 244, 250, 396, 634–638, 661  
 Catrullo, D., 644, 645  
 Catzigras F., 631  
 Cavalier, C., 158, 161, 638, 650  
 Cebula, G.T., 268, 440, 587, 638  
 Centamore, E., 634, 637  
 Ceretti, E., 635  
 Cerrina-Feroni, A., 635  
 Chaix C., 42, 636  
 Chamley, H., 352, 638  
 Chan, L.S., 429, 632  
 Channell, J., 638, 644, 648  
 Channell, J.E.T., 117–119, 122, 183, 321, 489, 496, 638

- Chaproniere, G.C.H., 255, 638  
 Charlot, R., 494, 638  
 Cherny, P., 638  
 Chiji, M., 371, 381, 382, 384, 395, 638  
 Chinzei, K., 194, 196, 638, 660  
 Chiocchini, U., 637  
 Chivas, A.R., 651  
 Choi, S.J., 643  
 Choubert, G., 494, 495, 638  
 Ciampo, G., 97, 638  
 Ciaranfi, N., 635, 639  
 Cifelli, R., 647  
 Cimini, G.B., 631  
 Cita, M.B., 61, 67, 69, 70, 74, 75, 79, 80, 82, 89,  
     91, 94, 97, 98, 100, 103, 104, 113, 120, 121,  
     149, 150, 230, 355, 360, 396, 469, 601, 604,  
     637–639, 646, 647, 658–660  
 Clari, P., 78, 79, 98, 639, 644  
 Clauzon, G., 152, 153, 639, 644  
 Clemens, S.C., 643  
 Clement, B.M., 652  
 Clermonte, J., 638, 650, 655  
 Closs, H., 657  
 Cluzaud, A., 637  
 Coccioni, R., 213, 230, 249, 252, 253, 257, 276,  
     279–282, 286, 288, 315, 317, 343, 344, 396,  
     399, 412, 414, 420, 494, 498, 608, 616, 622,  
     631, 639, 640, 651, 652, 654, 656  
 Coccozza, T., 631  
 Colacicchi, R., 638  
 Colalongo, M.L., 84, 102, 112–115, 117, 118,  
     121, 122, 150, 353, 419, 421, 454, 464, 473,  
     479, 480, 485, 486, 489, 500, 603, 604, 615,  
     616, 625, 635, 637, 640, 662  
 Colchen, M., 638, 650, 655  
 Colin, J.P., 637, 662  
 Colombo, F., 643  
 Conrad, M.E., 647  
 Cooper, C., 632  
 Coradossi, N., 120, 640  
 Corazza, E., 120, 640  
 Corfield, R., 661  
 Cosca, M., 589, 590, 640, 654, 655  
 Cosca, M.A., 216, 236, 358, 457, 539, 590, 640  
 Cosentino, D., 494, 635  
 Cossmann, M., 14, 20, 640  
 Costa, J.M., 646  
 Costantini, A., 633, 634  
 Cottereau, N., 663  
 Coward, M.P., 663  
 Cowie, J.W., 4, 57, 640  
 Cox, A., 645  
 Cox, A.V., 645  
 Craig, L., 645  
 Cravatte, J., 644  
 Crelling, J.C., 660  
 Cremonin, G., 640  
 Cremonini, G., 464, 473, 635, 640  
 Crocetti, G., 651  
 Crowhurst, S.J., 659, 660  
 Cuenc, G., 637  
 Cuenca, G., 300, 302, 641, 654  
 Cuenca Bescós, G., 641  
 Curtis, G.H., 641, 643, 652, 656  
 Curzi, P., 648  
 Curzi, P.V., 636  
  
 D'Alessandro, T., 416, 636  
 D'Antonio, G., 640  
 d'Atri, A., 209, 210, 214, 641, 654, 656  
 D'Offizi, S., 176, 642  
 D'Onofrio, S., 79, 80, 97, 100, 103, 112, 114,  
     118, 419, 421, 496, 500, 637, 640, 642  
 Daams, R., 299, 300, 302, 631, 636, 641  
 Daguin, F., 38, 641  
 Dalrymple, G.B., 590, 641, 647  
 Damiani, V., 638  
 Daxner-Höck, G., 636  
 Day, R., 260, 428, 641  
 De Casa, G., 651  
 De Deckker, P., 651  
 De Franco, R., 656  
 De Grandis, G., 333, 649  
 De Lapparent, A., 61, 78, 641  
 De Leeuw, J.W., 642, 660  
 De Reneville, P., 653  
 Decandia, F.A., 634  
 Decima, A., 464, 641  
 Deer, W.A., 503, 641  
 Deiana, G., 635  
 Deino, A., 176, 259, 263, 264, 280, 294, 335,  
     343–345, 400, 438, 440, 498, 512, 519, 586,  
     594, 609, 611, 612, 623, 632, 641, 652, 654  
 Deino, A.L., 656  
 Dekkers, M.J., 119, 649  
 Del Moro, A., 589, 641  
 Delgado, J.A., 660  
 Delle Rose, M., 632  
 Demaison, G.J., 436, 642  
 Demarcq, G., 26, 28, 31, 255, 256, 286, 601, 642,  
     645  
 Demarcq, G. et al., 642  
 Denison, R.E., 648  
 DePaolo, D.J., 14, 23, 38, 42–44, 49, 267, 327,  
     431, 637, 642, 647, 652, 657, 661  
 Depéret, M., 17, 36, 61, 69, 94, 97, 642  
 Dercourt, J., 157, 161, 637, 642, 650, 663  
 Di Battistini, G., 366, 642  
 Di Filippo, M., 634  
 Di Grande, A., 638, 640

- Di Leo, C., 640  
 Di Leo, R., 640  
 Di Stefano, A., 663  
 Di Stefano, E., 643  
 Diaz De Federico, A., 363, 436, 642  
 Didon, J., 222, 642  
 Dieci, G., 97, 642  
 Dinelli, E., 502, 642  
 Dini, I., 634  
 Disperati, L., 638  
 Dockery III, D.T., 645  
 Dollfus, G.F., 9, 17, 34, 642  
 Dondi, M., 634, 651  
 Doyle, P., 660  
 Drake, R., 652, 654  
 Drake, R.E., 641  
 Dreyfus-Rawson, M., 658  
 Drobne, K., 654  
 Drooger, C.W., 14, 21, 38, 41, 47, 112, 469, 642  
 Dunn, D.A., 632  
  
 Eberhardt, P., 495, 642  
 Edwards, L.E., 259, 292, 642  
 Eglinton, T.I., 436, 642, 660  
 Eijkel, G., 642  
 Elberg, E.L., Jr., 656  
 Elderfield, H., 46, 643  
 Elizaga, E., 633  
 Elliot, D.H., 643  
 Elmi, C., 635  
 Elter, M., 70, 634  
 Elter, P., 180, 182, 639, 643  
 Emeis, K.-C., 648  
 Emiliani C., 463, 643  
 Emmanuel, L., 267, 325, 643  
 Endo, T., 652  
 Engesser, B., 636  
 Erentöz, L., 161, 643  
 Erickson, A., 647  
 Eto, T., 562, 643  
 Evernden, J.F., 494, 643  
  
 Fabbri, A., 656  
 Fahlbusch, V., 636, 661  
 Failla, A., 634  
 Fairbanks, R.G., 652, 663  
 Falletti, P., 128, 643–645  
 Fantozzi, P., 638  
 Farabegoli, E., 464, 473, 640  
 Farabollini, P., 651  
 Farrell, J.W., 44, 643  
 Faure-Muret, A., 638  
 Faury, B., 637  
 Federici, P.B., 633  
 Federico, C., 656  
  
 Feigenson, M.D., 652, 655  
 Feist, M., 144, 643  
 Fenner, J., 144, 643  
 Fernex, F., 642  
 Ferrara, G., 495, 642, 659  
 Ferretti, S., 454, 643  
 Finger, K.L., 327, 642  
 Fleck, R.J., 270, 332, 443, 643, 649  
 Flisch, M., 386, 588, 643  
 Flores, J.A., 421, 633, 643, 660  
 Flynn, J.J., 634  
 Foey, P., 659  
 Foland, K.A., 643  
 Foresi, L.M., 74, 643  
 Fornaciari, E., 68–70, 74, 77, 78, 93, 213, 257, 287, 318, 321, 340, 344, 345, 421, 422, 447, 601–603, 609, 636, 640, 643, 644, 656, 657  
 Foster, J.H., 381, 644  
 Fountain, D.M., 183, 644  
 Francavilla, F., 633, 637  
 Frances, G., 660  
 Freeman, R., 177, 644  
 Freudenthal, M., 299, 300, 641  
 Frignone, G., 659  
 Fuentes, V., 641  
 Fuhrmann, U., 590, 644  
 Fuller, M.D., 641  
 Funayama, M., 654, 661  
 Funedda, A., 638  
 Funnell, B.M., 494, 495, 644  
 Furuno, K., 652  
  
 Galbiati, B., 129, 632, 644  
 Galeotti, S., 640  
 Gandolfi, G., 121, 451, 493, 644  
 Garbarino, C., 632  
 Garrido, J.R., 646  
 Garrison, R.E., 647  
 Gartner, S., 118, 150, 488, 489, 639, 644  
 Garzanti, E., 637  
 Gasparotto, G., 233, 502, 537, 644  
 Gasperi, G., 633  
 Gaudant, J., 633  
 Gautier, F., 149, 152, 476, 639, 644  
 Gelati, R., 59, 61, 65, 89, 125, 128, 209, 210, 213, 635, 638, 643–645, 661  
 Ghelardoni, R., 632  
 Ghibardo, G., 72, 73, 78, 79, 84, 98, 100, 639, 643, 644  
 Giannelli, L., 636, 640, 642  
 Giannotti, A., 78, 84, 97, 103, 113, 121, 644  
 Giese, P., 644, 649, 657  
 Gieskes, J.M., 643  
 Giglia, G., 643  
 Gignoux, M., 61, 644

- Gilly, Y., 637  
 Gino, G.F., 78, 80, 97, 98, 100, 113, 121, 644  
 Ginsburg, L., 636  
 Giraudmaillot, M., 649  
 Girotti, O., 473, 531, 532, 644  
 Glaçon, G., 648  
 Glaçon, G., 118, 120, 421, 643, 644  
 Gladenkov, A.Y., 644  
 Gnaccolini, M., 59, 61, 73, 89, 129, 637, 644, 645  
 Goldsmith, N.F., 50, 645  
 Gombos, A.M., 647  
 Goncharova, I.A., 654  
 Gonzales  
 González Delgado, J.A., 660  
 Gorza, M., 632  
 Graham, D.W., 120, 633  
 Grandjean, P., 46, 645  
 Grasso, M., 352, 464, 466, 473, 500, 645, 656  
 Griffin, W.L., 183, 645  
 Gromet, L.P., 643  
 Groscurth, J., 656  
 Guardia, P., 654  
 Gudjonsson, L., 119, 120, 466, 662  
 Guennoc, P., 638  
 Guerrero, F., 209, 213, 224, 315, 531, 632, 640, 645  
 Guirau, R., 638  
 Guiraud, R., 637, 650, 655  
 Guise, P.G., 654  
 Gunnarsdottir, H., 650  
 Gunther, K., 656
- Hadler, J.C., 634  
 Hagelberg, T., 659  
 Hall, M.A., 660  
 Hames, W.E., 646  
 Hammerschmidt, K., 647  
 Hammond, S.R., 381, 662  
 Hamrsmid, B., 663  
 Haq, B.U., 66, 142, 145, 146, 161, 163, 194, 267, 466, 645  
 Hara, Y., 652  
 Hardenbol, J., 645  
 Harland, W.B., 66, 262, 264, 339, 493, 494, 645  
 Hasegawa, S., 648, 654, 661  
 Hashiya, I., 648  
 Hatcher, P.G., 438, 645  
 Hattori, M., 648  
 Haug, E., 61, 78, 645  
 Hawkesworth, C.J., 643  
 Hawthorne, T., 638  
 Hawthorne, Y., 644  
 Hayasaka, I., 653  
 Hayashi, M., 377, 661  
 Hayashida, A., 192, 645, 655
- Hays, J.D., 463, 645  
 Hebeda, E.H., 654  
 Hedberg, H.D., 57, 230, 497, 645  
 Heimann, K.O., 464, 651  
 Heitzmann, P., 657  
 Hernandez, A., 298, 308, 646  
 Hernandez, J., 300, 363, 544, 645, 646  
 Hess, J., 47, 49, 539, 646  
 Hess, J.C., 234, 457, 590, 644, 646, 649  
 Hetherington, E.A., 648  
 Hieke, W., 648  
 Higgins, A.C., 660  
 Higuchi, H., 652  
 Hilgen, F.J., 149, 150, 463, 466, 473, 500, 544, 618, 646, 649  
 Hill, P.R., 646  
 Hirakoso, S., 648  
 Hirata, D., 555, 646, 654  
 Hirayama, J., 652  
 Hirst, J.P.P., 297, 298, 646  
 Hishidai, T., 663  
 Hochuli, P., 144  
 Hochuli, P., 646  
 Hodell, D.A., 44, 45, 47, 49, 120, 149, 150, 152, 153, 633, 646  
 Hodges, K.V., 646  
 Holub, V.M., 649  
 Honda, N., 371, 575, 646, 654, 661  
 Honda, Y., 663  
 Honza, E., 652  
 Horiguchi, M., 652  
 Hörnes, M., 125, 142, 646  
 Hottinger, L., 638  
 Hotzl, H., 656  
 Howarth, R.J., 660  
 Howie, R.A., 647  
 Hsü, K.J., 111, 381, 463, 469, 493, 495, 496, 646, 647, 653  
 Huffman, A.C., Jr., 636  
 Hunziker, J.C., 59, 631, 640, 647, 654  
 Huon, S., 640  
 Hurford A.J., 647  
 Hwang, W., 663
- Iaccarino, S., 48, 69, 74, 75, 94, 100, 102, 104, 144, 228, 230, 231, 253, 255, 256, 273, 276, 284, 286, 287, 315, 339, 345, 353, 355, 360, 401, 419–421, 603, 610, 636, 640, 642–644, 647, 661  
 Ibaraki, M., 199, 647  
 Icart, J.C., 647  
 Ichikawa, N., 661  
 Iljina, L.B., 654  
 Imbrie, J., 463, 645, 647  
 Imbrie, J.Z., 463, 647



- Ingle, J.C., 647  
 Ingram, B.L., 14, 23, 38, 43, 44, 642, 647  
 Innocenti, F., 659  
 Inoue, Y., 196, 650  
 Ishii, T., 198, 647  
 Issel, A., 78, 647  
 Itaya, T., 653, 655  
 Ito, Y., 192, 645  
 Izett, G.A., 507, 647  
  
 Jackson, J., 183, 632  
 Jacobs, L.L., 633  
 Jäger, E., 270, 332, 588, 660  
 James, G.A., 163, 647  
 James, G.T., 643  
 Jan du Chêne, R., 21, 647, 662  
 Janin, M.C., 637  
 Jaouni, A.R., 656  
 Jarrige, J.J., 163, 647  
 Jeffords, R.M., 660  
 Jelen, B., 654  
 Jenkins, D.G., 41, 48, 68, 94, 230, 231, 255, 647  
 Jenkyns, H.C., 651  
 Johnson, D.A., 647  
 Jones, C.E., 660  
  
 Kaasschieter, J.P.H., 642  
 Kagami, H., 652  
 Kageyama, K., 652  
 Kahn, M.S., 652  
 Kambara, A., 655  
 Kanaya, T., 197, 647  
 Kaneko, M., 655, 661  
 Kaneoka, I., 388, 648  
 Kanie, Y., 553–555, 558, 562, 566, 567, 648  
 Kano, K., 190, 648  
 Karner, G.D., 183, 658  
 Karpoff, A.M., 647  
 Kastens, K., 184, 648  
 Kastens, K.A., 112, 120, 648  
 Kasuya, M., 375, 377, 379, 390, 395, 399, 578, 648  
 Kato, H., 648  
 Katsurajima, S., 652  
 Kawai, N., 575, 648  
 Kawashima, S., 652  
 Keigwin, L.D., 120, 466, 648  
 Keigwin, L.D., Jr., 120, 633  
 Keller, G., 137, 255, 256, 286, 632, 648  
 Keller, J.V.A., 176, 641, 648  
 Kennett, J.M., 396, 648  
 Kennett, J.P., 77, 120, 495, 646, 648, 650, 659  
 Kent, D.V., 50, 70, 83, 119, 141, 145, 149, 262, 264, 325, 339, 340, 425, 485, 489, 490, 498, 633, 634, 637, 646, 648, 652, 661  
  
 Key, A.J., 642  
 Kidd, R.B., 631, 647  
 Kikuchi, T., 652  
 Killingley, J.S., 663  
 Kimura, K., 199, 575, 648  
 Kimura, M., 652  
 Kitamura, N., 653  
 Kitazato, H., 661  
 Kligfield, R., 637  
 Kodama, K., 652  
 Koepnick, R.B., 648  
 Koike, M., 648  
 Konda, I., 371, 381, 382, 384, 395, 638, 649  
 Koyama, M., 553, 573, 649  
 Kraker, G.P., 641  
 Kreuzer, H., 654  
 Krhowsky, Raffi, I., 663  
 Krijgsman, W., 119, 464, 466, 475, 489, 490, 495, 496, 498, 498, 500, 620, 649  
 Kruge, M.A., 416, 436, 649, 660  
 Kuchly, J., 662  
 Kunk, M.J., 638  
 Kurihara, K., 371, 382, 649  
  
 La Manna, F., 464, 645  
 Labaume, P., 213, 643  
 LaBrecque, J., 647  
 Lacomba, J.I., 631  
 Lag, M., 637  
 Lamb, J.L., 660  
 Landuzzi, V., 636  
 Langenheim, V.E., 640, 652  
 Langereis, C.G., 119, 149, 150, 463, 466, 473, 489, 490, 493, 495, 496, 646, 649  
 Lanphere, M.A., 334, 507, 589, 593, 641, 649  
 Laplana, C., 641  
 Larouzière, F.D., 646  
 Larter, S.R., 436, 649  
 Lattes, C.M.G., 634  
 Laurenzi, M., 333, 588, 662  
 Laurenzi, M.A., 416, 469, 589, 593, 614–617, 620, 625, 649  
 Lauriat-Rage, A., 631, 637  
 Lavecchia, G., 180, 182, 649  
 Lazzarotto, A., 633, 634  
 Lentini, J.K., 292, 649  
 Lentini, F., 635  
 Leoni, C., 637  
 Lesport, J.F., 637  
 Lesueur, J.L., 30, 649  
 Letz, H., 171, 172, 649  
 Li, Z., 31, 649  
 Liang, Y., 657  
 Lincoln, J.M., 120, 649  
 Lindsay, E.H., 633

- Liotta, D., 634  
 Lippolt, H.J., 234, 237, 457, 539, 590, 644, 646, 649  
 Llenas, M., 631  
 Llewellyn, P.G., 645  
 Loeblich, A.R., Jr., 228, 230, 318, 419, 650  
 Londeix, L., 11, 13, 20, 21, 637, 647, 650  
 Longinelli, A., 112, 638, 650  
 López-Martinez, N., 631–633  
 Lorenz, C., 159, 638, 642, 650  
 Loutit, T.S., 495, 650  
 Loutre, M.F., 463, 633, 639  
 Lowrie, W., 206, 250, 252, 274, 275, 479, 650  
 Lucas, J., 637  
 Ludwig, K.R., 48, 52, 650  
 Luterbacher, H., 660  
 Luterbacher, H.P., 145, 654  
 Lyell, Ch., 125, 142, 650
- Maccabruni, A., 632  
 Machida, J., 648  
 Madile, M., 654  
 Magné, J., 642  
 Maiya, S., 196, 650  
 Malinverno, A., 182, 184, 637, 650  
 Malinverno, P., 637  
 Malvesin-Fabre, M., 19, 38, 650  
 Manetti, P., 659  
 Manum, S.B., 136, 144, 259, 292, 634, 650  
 Marabini, S., 121, 464, 466, 468, 473, 498, 640, 650  
 Marcais, J., 638  
 Marchetti, G., 633  
 Marechal, J.C., 183, 638  
 Mariottini, M., 651  
 Marks, P., 70, 637, 650, 663  
 Martin, N., 637  
 Martinell, J., 645  
 Martinelli, P., 635  
 Martini, E., 23, 30, 31, 41, 48, 67, 69, 80, 82, 90, 91, 93–95, 97, 104, 125, 256, 273, 287, 288, 321, 339, 345, 369, 422, 447, 479, 485, 489, 599, 600, 602, 603, 650, 658  
 Martinotti, G., 59, 647  
 Martinotti, G.M., 353, 360, 650  
 Maruyama, T., 654, 661  
 Marzei, R., 644  
 Marzi, L., 473, 634  
 Mascle, G., 464, 648, 651  
 Mascle, J., 648  
 Mason, H., 640  
 Massari, F., 635, 643  
 Matoba, Y., 653  
 Matsuda, T., 192, 655  
 Matsumaru, K., 196, 371, 651  
 Matsumoto, A., 386, 651  
 Matsushima, Y., 646, 654  
 Mattei, G., 633  
 Matter, A., 636  
 Mattias, P., 205, 651  
 Mayer, K., 97, 463, 651  
 Mayer-Eymar, C., 9, 107, 122, 496, 651  
 Mayer-Eymar, K., 34, 61, 70, 84, 97, 113, 121, 651  
 Mazzanti, R., 633  
 Mazzei, R., 80, 82, 93, 96, 97, 104, 633, 636, 640, 651  
 McArthur, J.M., 43, 52, 651  
 Mccoy, F., 648  
 McCulloch, M.T., 44, 651  
 McDougall, I., 494, 495, 651, 655  
 McIntyre, A., 463, 658  
 Mckenzie, J., 648  
 McKenzie, J.A., 113, 120, 464, 466, 639, 641, 647, 651  
 McKerrow, W.S., 157, 659  
 Medelsee, M., 662  
 Mediavilla, F., 662  
 Mehnert, H.H., 638  
 Mein, P., 299, 302, 363, 551, 636, 651  
 Melillo, A., 652  
 Mendelson, J., 648  
 Menning, M., 493, 651  
 Merla, G., 175, 182, 651  
 Meulenkamp, J.E., 144, 633  
 Meulenkamp, P.E., 638  
 Mezzetti, R., 222, 224, 225, 502, 634–637, 651  
 Micarelli, A., 637  
 Michard, A., 645  
 Micheletti, A., 653  
 Miculan, P., 74, 75, 100, 351–353, 355, 356, 360, 500, 601–603, 624, 651  
 Milihres, X., 647  
 Miller, C., 647  
 Miller, K.G., 44, 45, 47, 52, 65, 69, 77, 82, 86, 104, 125, 141, 145, 263, 652, 655, 663, 664  
 Miller, R., 643  
 Milton, D.I., 161, 652  
 Minelli, G., 641, 642, 649, 656  
 Minguzzi, V., 209, 214, 634, 652  
 Miranda, P., 637  
 Mitjavila, J.M., 632  
 Mitsunashi, T., 554, 555, 558, 560–562, 566, 576, 652, 663  
 Mix, A., 659  
 Miyashita, M., 652  
 Mohafez, S., 161, 657  
 Molina, E., 255, 286, 652  
 Monaco, P., 654  
 Monechi, S., 213, 253, 257, 286, 639, 652, 654

- Mongelli, F., 171, 174, 652  
 Mongereau, N., 31, 652  
 Montadert, L., 647  
 Montanari, A., 48, 50, 53, 205, 206, 218, 225, 233, 249, 250, 252, 253, 259, 260, 262, 267, 269, 275, 280, 281, 294, 315, 317, 327, 329, 335, 339, 343, 344, 347, 356, 399, 412, 429, 431, 438, 440, 447, 457, 519, 538, 586, 587, 607–613, 615–617, 623–626, 631, 632, 638–641, 649, 651, 652, 654, 656  
 Monteforti, B., 636  
 Montenat, C., 163, 363, 366, 367, 369, 547–551, 620, 621, 623, 631, 633, 635–637, 647, 653, 655  
 Montenat, C.J., 650  
 Moore, G.T., 436, 642  
 Morales, J., 636  
 Morandi, N., 250, 315, 634, 651–653  
 Moratti, G., 635  
 Morlotti, E., 642  
 Mosna, S., 653  
 Moteforti, B., 644  
 Mountain, G.S., 652  
 Moussat, E., 656  
 Moyes, J., 14, 21, 653  
 Mudie, P.J., 292, 653  
 Mueller, C., 69  
 Mueller, P.A., 120, 646, 653  
 Mueller, St., 644  
 Muller, C., 648  
 Müller, C., 14, 20, 23, 36, 40, 41, 75, 77, 89, 93, 94, 120, 125, 255, 256, 286, 422, 635, 650, 653  
 Müller, D.W., 111, 653  
 Mutti, L., 637  
 Mutti, M., 636  
  
 Naeser, C.W., 638  
 Nagao, K., 385, 653  
 Nakagawa, H., 66, 74, 83, 97, 104, 575, 653  
 Nakagawa, T., 660  
 Nakajima, T., 652  
 Nakamura, K., 663  
 Napoleone, G., 633, 650, 654, 661  
 Nasu, N., 652  
 Naumann, C.F., 142, 653  
 Negri, A., 475, 494, 500, 516, 518, 615, 625, 643, 653  
 Negrini, C., 470, 658  
 Nelson, H.F., 648  
 Nely, G., 30, 653  
 Nesteroff, W.D., 112, 653  
 Neveškaja, L.A., 161, 654  
 Nicholson, H., 660  
 Nicolich, R., 657  
  
 Nigrini, C.A., 144, 632, 647  
 Niituma, N., 199, 553, 555, 575, 653, 654  
 Nirei, H., 652  
 Nishido, H., 653  
 Nishimura, S., 660  
 Nishitani, T., 193, 654  
 Nobel, F.A., 367, 549, 654  
 Nocchi, M., 206, 654  
 Nohda, S., 655  
  
 O’Nions, R.K., 590, 640  
 O’Reilly, S.Y., 183, 645  
 Oberhänsli, H., 120, 651  
 Obradovich, J.D., 638  
 Oda, M., 187–189, 371, 575, 613, 624, 631, 654, 661  
 Oddone, M., 589, 654  
 Odin, C., 309, 599, 606, 608, 654  
 Odin, G.S., 53, 145, 205, 218, 233, 250, 309, 318, 339, 376, 356, 395, 438, 457, 464, 475, 493, 494, 503, 519, 538, 583, 584, 586, 589, 595, 597, 599, 606–612, 614–617, 620, 622, 625, 627, 631, 637, 640, 652, 654, 655  
 Odin, S.G., 652  
 ODP Leg 138 Shipboard Scientific Party, 659  
 Ogata, K., 653  
 Ogawa, Y., 661  
 Oggiano, G., 638  
 Ogniben, L., 351, 463, 464, 466, 655  
 Oishi, M., 373, 382, 383, 655  
 Oka, S., 652  
 Okada, H., 90, 93, 212, 232, 267, 273, 276, 287, 321, 327, 339, 340, 345, 422, 425, 447, 448, 452, 479, 485, 486, 489, 566, 567, 570, 572, 632, 648, 655  
 Olafsson, G., 77, 655  
 Olafson, G., 643  
 Oldfield, R.K., 643  
 Oliver, J., 183, 655  
 Olivieri, R., 222, 651  
 Olsson, R.K., 655  
 Omboni, G., 61, 70, 78, 655  
 Onstott, T.C., 656  
 Opdyke, N.D., 85, 381, 463, 644, 659, 661  
 Oriyama, J., 661  
 Orlando, M., 654  
 Orszag, F., 162, 654  
 Orszag Sperber, F., 163, 655  
 Oslík, J.S., 43–45, 47, 52, 141, 655  
 Otofujii, Y., 192, 193, 655  
 Ott d’Estevou, P., 363, 647, 653, 655  
 Otto, J.B., 648  
 Owens, T., 661  
 Ozima, M., 648  
 Oztemür, C., 161, 643

- Paganelli, L., 644  
 Page, R.W., 494, 495, 651, 655  
 Pandeli, E., 634  
 Panza, G.F., 170, 171, 173, 637, 661  
 Papani, G., 633  
 Paramonova, N.P., 654  
 Pardo, G., 297, 632  
 Parés, J.M., 631  
 Pareto, L., 60, 61, 69, 70, 89, 97, 655  
 Parisi, E., 651  
 Parisi, G., 654  
 Parona, C.F., 78, 655  
 Parotto, M., 473, 531, 532, 644  
 Pasci, S., 638  
 Patacca, E., 100, 466, 473, 655, 656, 658  
 Pate, D., 660  
 Pedley, H.M., 464, 466, 500, 645, 656  
 Peis, D., 633  
 Peltier, W.R., 659  
 Perch-Nielsen, K., 93, 144, 287, 318, 421, 650, 656  
 Percival, S.F., 488, 647  
 Perello, M., 644  
 Perugini, M., 640  
 Pescatore, T., 635  
 Pesek, J., 649  
 Pestiau, P., 633  
 Peterson, N., 647  
 Peyre, Y., 642  
 Peyrot, A., 14, 21, 640  
 Phillips, D., 656  
 Piali, G., 176, 638, 641, 642, 648, 649, 656  
 Piali, G.P., 177, 180, 631  
 Pickton, C.A.G., 645  
 Pieri, M., 222, 632, 656  
 Pini, G.A., 656  
 Pisciotto, K., 647  
 Pisas, N., 463, 659, 660  
 Pisas, N.G., 656  
 Plesi, G., 635  
 Poignant, A., 11, 14, 17, 20, 21, 34, 36, 40, 41, 47, 94, 600, 608, 631, 636, 656  
 Poisson, A., 637, 650, 655  
 Poli, S., 638  
 Polino, R., 657  
 Ponziani, F., 169, 171, 172, 175, 178, 656  
 Pool, W., 642  
 Popov, S.V., 654  
 Poppi Brigatti, M.F., 640  
 Potetti, M., 637  
 Potts, R., 440, 512, 641  
 Powell, A.J., 259, 292, 636, 656  
 Powers, R.W., 161, 656  
 Pranzini, G., 633  
 Prat, P., 647  
 Praturlon, A., 638  
 Premoli Silva, I., 61, 67, 69, 72, 89, 91, 94, 230, 249, 267, 360, 601, 639, 650, 654, 656, 659  
 Priem, H.N.A., 654  
 Prosperi, M., 638  
 Puga, E., 642  
 Pujol, C., 11, 14, 17, 20, 21, 23, 24, 34, 40, 41, 47, 94, 631, 637, 653, 656  
 Pujos, A., 632  
 Purser, B.H., 163, 656  
 Puxeddu, M., 641  
 Quirantes, J., 297, 656  
 Rabeder, G., 97, 97, 660  
 Radicati di Brozolo, F., 641  
 Radovisc, R., 634  
 Raffi, I., 70, 77, 85, 87, 93, 643, 656, 657  
 Rakic-El-Bied, K., 117, 122, 149, 153, 496, 633, 636, 646, 656  
 Ramirez, L.F., 656  
 Randrianasolo, A., 644  
 Rangnes, K., 650  
 Rau, A., 633  
 Ravasz-Baranyai, L., 632  
 Redmond, C.D., 656  
 Reguant, S., 657  
 Rehault, J.P., 177, 648  
 Reichert, C., 649  
 Remane, J., 640  
 Renard, M., 267, 325, 643  
 Renault, J.-P., 644  
 Renault, J.P., 656  
 Renne, P.R., 507, 593, 656  
 Reutter, K.J., 177, 656, 657  
 Rex, D.C., 654  
 Reyre, D., 161, 657  
 Riba, O., 297, 298, 657  
 Ricci Lucchi, F., 100, 221, 461, 464, 469, 475, 498, 631–633, 635, 636, 657, 662  
 Richert, J.P., 647  
 Richter, F.M., 327, 431, 657  
 Richter-Bernbur, G., 657  
 Ricou, L.E., 163, 635, 637, 638, 642, 650, 655, 657  
 Riedel, W.R., 144, 489, 657, 658  
 Rinaldi, R., 638  
 Ringeade, M., 11, 657  
 Rio, D., 82, 85, 93, 97, 104, 150, 211, 213, 232, 287, 287, 288, 318, 319, 321, 344, 420–422, 447, 477, 496, 598, 601–603, 605, 609, 611, 613, 624, 632, 636, 638–640, 643, 644, 656, 657  
 Ripepe, M., 654  
 Riva, M., 632

- Riveline, J., 144, 657  
 Rizzo, R., 632  
 Robba, E., 97, 657  
 Robertson, A., 648  
 Rocchetti, S., 656  
 Rocher, P., 637  
 Roda, C., 464, 657  
 Roetzel, R., 661  
 Rögl, F., 133, 134, 494, 634, 657, 660, 661  
 Rogledi, S., 643  
 Roman, J., 40, 637  
 Romeo, M., 351, 352, 638, 640, 642, 645, 657  
 Rondeel, H.E., 654  
 Rossi, A., 640  
 Rossi, R., 230, 639  
 Roure, F., 130, 177, 657  
 Roveri, M., 633  
 Royden, L., 179, 183, 658  
 Rubino, J.L., 649  
 Ruddiman, W.F., 463, 466, 658  
 Ruggieri, G., 100, 111, 112, 658  
 Russo, A., 97, 636, 642  
 Rutsch, R.F., 637  
 Ryan, W.B.F., 97, 103, 111, 182, 184, 381, 382, 463, 493, 495, 496, 631, 646, 650, 658  
  
 Sacco, F., 61, 70, 78, 97, 633, 658  
 Saez, M., 643  
 Saito, H.K., 399, 658  
 Saito, K., 376, 611, 613, 624, 655, 661  
 Saito, T., 371, 382, 632, 658  
 Sakai, T., 377–379, 658, 661  
 Salvador, A., 497, 658  
 Salvatorini, F., 636  
 Salvatorini, G., 100, 102, 104, 144, 230, 231, 253, 255, 256, 273, 284, 286, 287, 315, 318, 339, 345, 353, 355, 360, 419–421, 602, 603, 610, 636, 640, 642, 644, 647, 658  
 Sampo, M., 159, 658  
 Samson, S.D., 268, 333, 336, 440, 587, 658  
 Sandrelli, F., 633, 634  
 Sandroni, P., 412, 416, 658  
 Sanfilippo, A., 137, 144, 657, 658  
 Sanfillipo, A., 658  
 Sani, F., 635  
 Sarnthein, M., 662  
 Sartoni, S., 635  
 Sartori, R., 636, 640, 648, 656  
 Sasahara, Y., 648  
 Sato, H., 658  
 Saunders, J.B., 144, 228, 256, 286, 318, 396, 419, 635, 647  
 Savage, D.E., 643  
 Savelli, C., 464, 635–637  
 Savelli, D., 658  
  
 Savin, S., 77, 87, 663  
 Sawamura, K., 663  
 Sawyer, D.A., 649  
 Scandone, P., 466, 473, 655, 656, 658  
 Scharber, S., 328, 658  
 Schenck, P.A., 660  
 Schenk, V., 658, 659  
 Schilling, J.G., 646  
 Schlanger, S.O., 120, 267, 649, 659  
 Schmid, R., 183, 659  
 Schmidt, D.L., 636  
 Schmidt, R.R., 633  
 Schmidt, V.A., 641  
 Schmitz, B., 327, 659  
 Schneider, D., 659  
 Schneider, D.A., 632, 660  
 Scholze, A., 650  
 Schreiber, B.C., 641  
 Schreiber, E., 647  
 Scotese, C.R., 157, 659  
 Scott, G.H., 118, 231, 490, 659  
 Seguenza, M., 496, 617, 659  
 Selli, R., 61, 84, 107–113, 121, 122, 209, 222, 227, 464, 469, 473, 494, 496, 498, 521, 531, 603, 635, 637, 659  
 Selvaggi, G., 170, 173, 180, 631  
 Semenenko, V.N., 633  
 Sen, S., 661  
 Senans, P., 647  
 Serrano, F., 364, 366, 369, 547, 620, 621, 659  
 Serri, G., 172, 174, 180, 659  
 Sersale, R., 659  
 Sesé, C., 631  
 Sestini, G., 222, 659  
 Shackleton, N.J., 77, 93, 119, 120, 211, 287, 319, 422, 463, 466, 500, 632, 645, 648, 656, 658–660  
 Sharp, W.D., 656  
 Shi, Y., 663  
 Shibata, K., 187, 375, 390, 395, 399, 660  
 Shimono, T., 648  
 Sierro, F.J., 103, 112, 117, 421, 643, 660  
 Sierro, J.F., 644  
 Signorini, R., 178, 660  
 Sinninghe Damsté, J.S., 436, 438, 642, 660  
 Sivak, J., 14, 21, 637  
 Smalley, P.C., 46, 52, 660  
 Smith, A., 645  
 Smith, A.G., 645  
 Smith, D., 645  
 Snee, L.W., 647  
 Sobolev, S.V., 181, 632  
 Soh, W., 661  
 Sola, J. et al., 646  
 Sorbini, L., 469, 660

- Spaak, P., 353, 664  
 Spadea, P., 351, 660  
 Spakman, W., 172, 183, 660  
 Spezzaferrì, S., 133, 137, 230, 253, 255, 256, 273, 284, 286, 318, 419, 656, 660, 661  
 Sprovieri, R., 108, 111, 113, 150, 466, 638, 639, 642, 648, 657, 658, 660  
 Srinivasan, M.S., 396, 648  
 Stainforth, R.M., 77, 660  
 Stankiewicz, B.A., 660  
 Stankiewicz, B.A., 436, 649  
 Stattegger, K., 662  
 Staudigel, H., 46, 660  
 Steffens, P., 633  
 Steiger, R.H., 270, 332, 444, 588, 660  
 Steininger, F., 494, 657  
 Steininger, F.F., 125, 128, 142, 144, 209, 211, 212, 253, 256, 259, 274, 284, 286, 308, 309, 328, 599, 606, 620, 638, 644, 658, 660, 661  
 Steurbaut, E., 637  
 Stille, P., 635  
 Stoppani, A., 61, 70, 78, 661  
 Stott, L.D., 646  
 Stradner, H., 93, 639  
 Straolner, H., 661  
 Strauss, C., 259, 661  
 Suc, J.P., 119, 352, 604, 617, 639, 644, 661  
 Suhadolc, P., 172, 661  
 Surdam, R.D., 638  
 Sutter, J.F., 638, 643  
 Suzuki, Y., 652, 663  
 Swinburne, N.H.M., 660  
 Swisher III, C.C., 507, 634, 656, 661
- Takahashi, M., 194, 373, 375–377, 382, 383, 395, 399, 575, 611, 613, 624, 654, 655, 658, 661, 663  
 Takayama, T., 653, 661  
 Takayanagi, Y., 371, 381, 382, 395, 661  
 Takei, K., 648  
 Tampieri, R., 640  
 Tanaka, H., 648  
 Tanaka, Y., 663  
 Taniguchi, H., 573, 661  
 Tanoue, S., 193, 654  
 Tappan, J.H., 230, 318, 419, 650  
 Tateo, F., 131, 209, 214, 221, 225, 236, 250, 315, 502, 631, 632, 641, 642, 651–654, 661  
 Tauxe, L., 85, 661  
 Tchepalyga, A.L., 654  
 Tedford, R.H., 144, 662  
 Tempelman-Kluit, D.J., 184, 662  
 Thaler, L., 653  
 Theodoridis, S., 352, 422, 489, 662  
 Theyer, F., 381, 632, 662
- Thiriet, J.P., 647  
 Thomas, E., 632  
 Thucydides, 662  
 Tiedemann, R., 463, 466, 662  
 Tisserant, D., 638  
 Tissot, B.P., 436, 662  
 Tocco, S., 632  
 Tomadin, L., 636, 640  
 Tonarini, S., 659  
 Tongiorgi, E., 495, 662  
 Tongiorgi, M., 495, 643, 662  
 Toni, G.C., 635, 636  
 Torelli, L., 633  
 Torii, M., 638, 648, 655  
 Toro, B., 634  
 Torres-Roldan, R., 642  
 Torri, M., 644  
 Tortorici, L., 635  
 Toscani, L., 642  
 Toumarkine, M., 650  
 Tournouer, R., 38, 662  
 Trevisan, L., 643  
 Trifilieff, V., 662  
 Tucker, P., 647  
 Turrin, B.D., 652, 656
- Uchida, E., 631  
 Uchiuni, S., 660  
 Umetsu, H., 661  
 Urabe, A., 558, 662  
 Utrilla, R., 632
- Vai, G.B., 114, 117, 119, 121, 122, 416, 417, 429, 448, 451, 453, 454, 458, 459, 464, 466, 468, 469, 473, 475, 493, 494, 498, 500, 516–519, 521, 529, 594, 603, 614–617, 620, 625, 637, 650, 662  
 Vail, P.R., 30, 461, 462, 471, 645, 662  
 Valmori, E., 461, 657  
 Van Bemmelen, R.W., 184, 662  
 Van Couvering, J.A., 634, 653  
 Van De Weer, D., 636, 641  
 Van der Meulen, A., 641  
 Van der Meulen, A.J., 631  
 Van der Zwaan, G.J., 116, 119, 120, 466, 638, 662  
 Van Eysinga, F.W.B., 66, 662  
 Van Heck, S.E., 663  
 Vasquez, A., 632  
 Veneri, F., 209, 213, 531, 632, 640  
 Veneri F., 645  
 Vercesi, P.L., 632, 633  
 Vergnaud Grazzini, C., 644  
 Vervloet, C.C., 61, 65, 72–74, 77, 78, 84, 89, 98, 129, 360, 602, 662

- Vidal, P., 638  
 Vigliotti, L., 468, 470, 473, 475, 494, 500, 516,  
     518, 615, 625, 663  
 Vigneaux, M., 14, 17, 94, 663  
 Villa, G., 133, 213, 638, 643, 657, 661, 663  
 Villa, I., 642  
 Villa, I.M., 589, 637, 641, 654, 662, 663  
 Villena, J., 657  
 Vincent, E., 466, 663  
 Violanti, D., 150, 644  
 Visscher, H., 664  
 Visser, J., 631  
 Vitali, F., 635  
 Voronina, A.A., 654  
 Vrielynck, B., 159, 269, 637, 642, 663  
  
 Waite, L.E., 648  
 Walter, R.C., 656  
 Walters, R., 645  
 Wang, C., 184, 663  
 Wang, Q.M., 163, 663  
 Weaver, Ph., 644  
 Webb, P.N., 70, 650  
 Wei, W., 663  
 Weidmann, M., 636  
 Weinreich, N., 632  
 Weissert, H., 647  
 Welte, D.H., 436, 662  
 Werdelin, L., 659  
 Wezel, F.C., 184, 222, 464, 631, 641, 658, 663  
 Wigger, P., 649  
 Wigger, P.J., 171, 663  
 Wilcock, B., 645  
 Williams, G.L., 144, 259, 292, 649, 663  
  
 Wise, S.W., 663  
 Woodruff, F., 44, 45, 47, 77, 87, 646, 663  
 Wright, J.D., 77, 86, 652, 655, 663  
 Wright, R., 647  
 Wright, R.C., 647  
 Wright, R.H., 631  
 Wynd, J.G., 163, 647  
  
 Yamaji, A., 192–194, 663  
 Yanagisawa, M., 648  
 Yanagisawa, S., 648  
 Yanagisawa, Y., 198, 663  
 Yazaki, K., 554, 555, 558, 560–562, 566, 652,  
     663  
 Yoshida, F., 663  
 Yoshida, S., 648  
 Yoshino, H., 648  
 Young, J., 490, 663  
  
 Zachariasse, J., 633  
 Zachariasse, W.J., 118, 353, 490, 500, 634, 638,  
     649, 663, 664  
 Zeck, H.P., 367, 664  
 Zevenboom, D., 137, 257–259, 274, 275, 280,  
     288, 636, 661, 664  
 Zhang, J., 47, 49, 664  
 Ziegler, W., 640  
 Zijderveld, J.D.A., 649  
 Zindler, A., 660  
 Zingg, A., 183, 664  
 Zito, G., 171, 174, 652  
 Zuffa, G.G., 451, 636, 644  
 Zushan, S., 641

## PALEONTOLOGIC INDEX

- Achomospaera*, 259, 292  
*Amaurolithus*, 448, 449, 454, 461, 462, 479, 489, 605, 615, 616  
*Amaurolithus amplificus*, 117  
*Amaurolithus delicatus*, 82, 117, 118, 452, 454, 489, 500, 564, 569–571, 616  
*Amaurolithus primus*, 82, 117, 452, 454, 489, 500, 571, 616  
*Amaurolithus* spp., 81, 82, 425, 452, 477  
*Amaurolithus tricorniculatus*, 569, 570  
*Ammonia*, 30  
*Anadara*, 36  
*Anadara cardiiformis*, 42  
*Anadara turonica*, 31  
*Anchiterium*, 299  
*Ancillaria glandiformis*, 78, 97  
*Anomia*, 31  
*Apodemus primaevus*, 551  
*Arca diluvii*, 31  
*Astrononion*, 30  
*Aurila cauditoiles*, 30  
*Aurila cicatricosa lauzea*, 31  
*Aurila vaclusi*, 30  
*Aurila ventroinflata*, 31
- Balanus tulipiformis*, 31  
*Barbatia*, 36  
*Braarudosphaera bigelowi*, 14  
*Brizalina*, 30  
*Bulimina echinata*, 112, 117
- Calcidiscus*, 421  
*Calcidiscus leptoporus*, 452, 564, 569–571  
*Calcidiscus macintyreii*, 369, 452, 564, 569–571  
*Caligodinium pychnum*, 288, 290  
*Calyptogena*, 553  
*Calyptogena soyoae*, 553  
*Calyptogena* sp., 555  
*Cardium*, 31, 42  
*Cassigerinella chipolensis*, 230  
*Catapsydrax dissimilis*, 126, 230, 231, 255, 256, 263, 276, 284, 286, 287, 318, 339, 341  
*Catapsydrax dissimilis ciperensis*, 230  
*Catapsydrax dissimilis dissimilis*, 230  
*Catapsydrax unicavus*, 230  
*Catinaster coalitus*, 81, 564, 578  
*Catinaster calyculus*, 564  
*Celleporaria palmata*, 31  
*Ceratolithus acutus*, 150, 569–571  
*Ceratolithus armatus*, 571  
*Ceratolithus rugosus*, 564, 569–571  
*Ceratolithus* sp., 564, 569–571  
*Cerebrocysta*, 292  
*Cerebrocysta* sp., 259  
*Cerithium*, 34  
Charophyta, 297  
Charophyte, 144  
*Chiropteridium*, 288  
*Chiropteridium* spp., 137  
*Chlamys davidi*, 31  
*Chlamys gentoni*, 32  
*Chlamys justiana*, 31  
*Chlamys multistriata*, 32  
*Chlamys palmaia*, 31  
*Chlamys pavonacea*, 32  
*Chlamys praescabriuscula*, 31  
*Chlamys subholgeri*, 32  
*Chlamys tournali*, 32  
*Cibicibes*, 30  
*Coccolithus*, 287, 319, 421  
*Coccolithus abisectus*, 30  
*Coccolithus miopelagicus*, 368  
*Coccolithus pelagicus*, 30, 368, 479, 564, 569–571  
*Conus canaliculatus*, 78, 97  
*Corbula*, 31  
*Cordosphaeridium canthaerellum*, 144  
*Coronocyclus nitescens*, 14  
Cortemilia Formation, 68  
*Cricetus* cf. *kormosi*, 551  
*Culicia parasitica*, 31  
*Cyclicargolithus*, 287, 319  
*Cyclicargolithus abisectus*, 14, 287, 368  
*Cyclicargolithus floridanus*, 14, 368, 372, 578  
*Cycloclypeus*, 40  
*Cyclococcolithus floredanus*, 30  
*Cyrena*, 34  
*Cytheridea acuminata caumontensis*, 30  
*Cytherideaourniei*, 30
- Deflandrea*, 137, 141, 288  
*Deflandrea* spp., 137  
*Dentoglobigerina baroemoenensis*, 230  
*Dentoglobigerina larnuei*, 230  
*Dictyococcites*, 287, 479  
*Dictyococcites bisectus*, 211–213, 218, 232, 256, 257, 273, 287, 600, 607



- Dictyococcites dictyodus*, 213  
*Dictyococcites perplexa*, 564, 569–571  
*Dictyococcites productus*, 118, 368, 564, 569–571  
*Dictyococcites scrippsae*, 368  
*Discoaster*, 479, 486, 489, 490  
*Discoaster adamanteus*, 479, 564, 569–571  
*Discoaster asymmetricus*, 479, 569–571  
*Discoaster bellus*, 85, 564  
*Discoaster berggrenii*, 81, 82, 486, 564, 569–571, 578  
*Discoaster bollii*, 564  
*Discoaster braarudii*, 564  
*Discoaster brouweri*, 452, 479, 564, 569–571  
*Discoaster brouweri triradiatus*, 479  
*Discoaster calcaris*, 479, 564  
*Discoaster challengerii*, 479, 564, 569–571  
*Discoaster decorus*, 564, 569–571  
*Discoaster deflandrei*, 93, 368, 372  
*Discoaster druggi*, 41, 126, 368  
*Discoaster exilis*, 93, 564  
*Discoaster hamatus*, 81, 82, 104, 425, 565  
*Discoaster icarus*, 479  
*Discoaster intercalaris*, 479, 565, 569–571  
*Discoaster kugleri*, 75, 81, 93, 369  
*Discoaster loeblichii*, 118  
*Discoaster mendomobensis*, 479  
*Discoaster moorei*, 479  
*Discoaster musicus*, 93, 479  
*Discoaster neohamatus*, 486, 565  
*Discoaster neorectus*, 486  
*Discoaster pansus*, 569, 570  
*Discoaster pentaradiatus*, 118, 452, 479, 565, 569–571  
*Discoaster pseudovariabilis*, 486, 565  
*Discoaster quinqueramus*, 81, 82, 425, 486, 565, 569–571  
*Discoaster sanmiguelensis*, 93  
*Discoaster surculus*, 118, 486, 565, 569–571  
*Discoaster tamalis*, 479, 571  
*Discoaster toralus*, 479  
*Discoaster variabilis*, 93, 368, 452, 479, 565, 569–571  
*Discolithina desueta*, 14  
*Discolithina enormis*, 14  
*Distatodinium apenninicum*, 137, 288, 294  
*Distatodinium biffii*, 288  
*Distatodinium* sp., 259  
*Distephanus speculum haliomma*, 144  
*Dorcadospyrus ateachus*, 144  
  
*Ectosphaeropsis burdigalensis*, 137, 272, 274, 288, 294  
*Elphidium*, 30  
*Eomyidae*, 300  
*Euthriofusus*, 36  
  
*Fasciolaria tarbelaria*, 31  
*Ficula condita*, 31  
*Flabellipecten burdigalensis*, 38  
*Flabellipecten galloprovincialis*, 32  
*Florilus*, 30  
*Florisphaera profunda*, 565, 569–571  
*Fron dipora verrucosa*, 32  
  
*Gephyrocapsa*, 118  
*Gephyrocapsa* spp., 571  
*Gigantoptecten latissima restitutusensis*, 32  
*Globigerina*, 106, 351–353  
*Globigerina apertura*, 105  
*Globigerina bulloides*, 105  
*Globigerina ciperoensis*, 22  
*Globigerina decoraperta*, 105, 353  
*Globigerina druryi*, 397  
*Globigerina euapertura*, 230  
*Globigerina falconarae*, 420  
*Globigerina falconensis*, 105  
*Globigerina foliata*, 105  
*Globigerina* gr. *Bulloides*, 22  
*Globigerina multiloba*, 117, 421, 467  
*Globigerina nepenthes*, 105, 314, 372, 375, 381, 382, 384, 390, 392, 396, 397, 399, 401, 420, 578, 613, 614  
*Globigerina officinalis*, 230  
*Globigerina praebulloides*, 31, 105, 230  
*Globigerina quinqueloba*, 230  
*Globigerina venezuelana*, 230  
*Globigerina woodi*, 14, 22, 105  
*Globigerina ouachitaensis*, 230  
*Globigerinatella insueta*, 256  
*Globigerinella obesa*, 106, 230  
*Globigerinella siphonifera*, 106  
*Globigerinita dissimilis*, 231  
*Globigerinita glutinata*, 106  
*Globigerinita incrusta*, 230  
*Globigerinita uvula*, 106  
*Globigerinoides*, 94, 137, 231, 253, 255, 610  
*Globigerinoides altiapertura*, 22, 48, 49, 131, 211, 230, 231, 255, 256, 258, 276, 284, 286, 368, 369, 600, 608, 622, 627  
*Globigerinoides bisphericus*, 287, 288, 318, 368  
*Globigerinoides bisphericus–Praeorbulina–Orbulina* lineage, 94  
*Globigerinoides bollii*, 106  
*Globigerinoides bulloideus*, 105  
*Globigerinoides ciperoensis*, 31  
*Globigerinoides dehiscens*, 255, 256, 276, 284, 286, 294  
*Globigerinoides dehiscens dehiscens*, 255, 273, 276, 284, 286, 287, 318  
*Globigerinoides event*, 253, 284

- Globigerinoides extremus*, 547, 549  
*Globigerinoides* genus, 231  
*Globigerinoides* gr. *trilobus*, 368  
*Globigerinoides immaturus*, 14, 230, 253  
*Globigerinoides obliquus*, 105, 120  
*Globigerinoides obliquus extremus*, 100, 102, 103, 420, 421  
*Globigerinoides obliquus obliquus*, 100, 420  
*Globigerinoides parawoodi*, 284  
*Globigerinoides primordius*, 14, 47, 230, 253, 284  
*Globigerinoides quadrilobatus*, 31, 230, 284  
*Globigerinoides quadrilobatus altiaptus*, 31  
*Globigerinoides quadrilobatus sacculifer*, 31  
*Globigerinoides quadrilobatus trilobus*, 31  
*Globigerinoides ruber parkeri*, 536  
*Globigerinoides ruber seigliei*, 420  
*Globigerinoides sacculifer*, 22, 284  
*Globigerinoides subquadratus*, 22, 103, 106, 255, 286, 368, 420  
*Globigerinoides subsacculifer*, 230, 284  
*Globigerinoides trilobus*, 22, 48, 106, 206, 230, 255, 256, 284, 287, 315, 318, 339, 600, 608, 622, 627  
*Globigerinoides-Orbulina* lineage, 67  
*Globigerionoides altiaptus*, 53  
*Globogenerina multiloba*, 500  
*Globogenerinoides dehiscens dehiscens*, 256  
*Globoquadrina altispira*, 31, 106, 353, 355  
*Globoquadrina altispira altispira*, 420  
*Globoquadrina baroemoensis*, 103, 106, 368  
*Globoquadrina dehiscens*, 14, 22, 31, 47, 106, 131, 141, 211, 212, 218, 230, 253, 257, 368  
*Globoquadrina dehiscens dehiscens*, 230  
*Globoquadrina globosa*, 22  
*Globoquadrina globularis*, 22  
*Globoquadrina langhiana*, 368  
*Globoquadrina sellii*, 211  
*Globorotalia*, 106, 550  
*Globorotalia* (Fohsella) *peripheroronda*, 368  
*Globorotalia birnageae*, 23, 230  
*Globorotalia bononiensis*, 536  
*Globorotalia* cf. *menardii*, 420  
*Globorotalia conomiozea*, 82, 84, 112–114, 117–122, 414, 421, 448, 449, 454, 461, 462, 466, 467, 469, 489, 493, 495, 496, 500, 518, 520, 521, 527, 529, 530, 603, 605, 614–617, 620, 625, 628  
*Globorotalia conomiozea* FAD, 518  
*Globorotalia continua*, 23  
*Globorotalia dehiscens*, 144  
*Globorotalia exserta*, 117, 421  
*Globorotalia hirsuta preahirsuta*, 536  
*Globorotalia humerosa*, 454, 461, 462  
*Globorotalia kugleri*, 14, 47, 141, 144, 231, 273  
*Globorotalia languensis*, 106  
*Globorotalia margaritae*, 149, 536, 544, 578  
*Globorotalia mayeri*, 84  
*Globorotalia mediterranea*, 117, 421, 495, 500, 520, 521, 527, 530, 549, 550, 605, 615, 616, 625, 628  
*Globorotalia menardii*, 103, 106, 117, 112, 421, 500  
*Globorotalia merotumida*, 103, 106, 420  
*Globorotalia miotumida*, 117, 118, 421, 500  
*Globorotalia nicolae*, 117, 421  
*Globorotalia obesa*, 23  
*Globorotalia opima opima*, 126  
*Globorotalia peripheroacuta*, 372, 382, 396, 575, 578  
*Globorotalia peripheroronda*, 353, 355, 360, 419, 420, 447, 610  
*Globorotalia peripheroronda* Zone, 24  
*Globorotalia plesiotumida*, 421, 549, 578  
*Globorotalia praemargaritae*, 454, 461, 500  
*Globorotalia praemenardii*, 75, 353, 369, 420  
*Globorotalia praescitula*, 287, 318, 353  
*Globorotalia puncticulata*, 534, 536, 544  
*Globorotalia sacculifer*, 120  
*Globorotalia saginata*, 23  
*Globorotalia saheliana*, 421, 500, 516, 518, 520, 615, 616  
*Globorotalia saphoe*, 421  
*Globorotalia scitula*, 106  
*Globorotalia siakensis*, 23, 84, 420, 578  
*Globorotalia suterae*, 103, 106, 117, 414, 421, 454, 461, 466, 467, 500, 516, 520, 605, 614–616, 628  
*Globorotalia tumida*, 578  
*Globorotaloides falconarae*, 102, 106  
*Globorotaloides* sp., 230  
*Glycymeris bimaculata*, 38, 42  
*Glycymeris cor*, 38, 42  
*Glycymeris jouanneti*, 42  
*Glycymeris* sp., 42  
*Granulolabium plicatum*, 46  
  
*Halicosphaera stalis*, 490  
*Helicosphaera*, 479, 489, 490  
*Helicosphaera ampliaptura*, 23, 41, 67, 69, 93, 321, 345, 368, 601, 602  
*Helicosphaera ampliaptura*, 30, 31  
*Helicosphaera carteri*, 14, 30, 232, 368, 452, 477, 565, 569–571  
*Helicosphaera euphratis*, 14, 368  
*Helicosphaera orientalis*, 490  
*Helicosphaera recta*, 256, 287  
*Helicosphaera sellii*, 571  
*Helicosphaera walbersdorfensis*, 69, 77, 93, 321, 345, 490, 602, 611, 612, 627

- Helicosphaera wallichii*, 569, 570  
*Helicosphaera waltrans*, 93  
*Hemicythere notata costulata*, 30  
*Hemicythere triangularis triangularis*, 30  
*Heterostegina*, 366  
*Hipparion*, 85, 299, 551  
*Homotryblium*, 292  
*Homotryblium oceanicum*, 259, 292  
*Homotryblium* sp., 259  
*Homotryblium truncata*, 294  
*Hornera dorsocavata*, 32  
*Hystrichokolpoma*, 290  
*Hystrichokolpoma inflata*, 290  
*Hystrichokolpoma* sp., 259  
*Hystrichokolpoma truncata*, 258, 288  
*Hystrichosphaeropsis*, 292  
*Hystrichosphaeropsis obscura*, 259, 288  
*Hystrichosphaeropsis* sp., 259  
  
*Impagidinium*, 137, 292  
*Impagidinium* sp., 292  
  
*Leguminocythereis elongata restitutensis*, 31  
*Lenticulina*, 417  
*Ligerimys*, 300  
*Limnaea*, 10  
*Lingulodinium* sp., 292  
*Loripes*, 36  
*Loxocochoa linearis*, 31  
*Loxocochoa linearis linearis*, 31  
*Lucina*, 34  
*Lychnocanoma elongata*, 144  
  
*Mactra*, 20  
*Mastodon*, 551  
*Membranilarnacia ?picena*, 137, 258, 288, 292  
*Minylitha convallis*, 118  
*Miogypsina globulina*, 41  
*Miogypsinidae*, 38, 41  
*Miogypsinoides*, 40  
  
*Natica*, 31  
*Naviculopsis biapiculata*, 144  
*Nematospaeropsis*, 137  
*Nematospaeropsis downiei*, 258, 259, 288  
*Neogloboquadrina acostaensis*, 103, 104, 421  
*Neogloboquadrina*, 367, 549  
*Neogloboquadrina acostaensis*, 81, 82, 84, 85, 100, 106, 117, 396, 401, 420, 447, 449, 466, 500, 547, 549, 603, 605, 614, 624, 628  
*Neogloboquadrina acostaensis* L/R, 467  
*Neogloboquadrina atlantica*, 420  
*Neogloboquadrina continua*, 549  
*Neogloboquadrina humerosa*, 367, 421, 547, 549, 550, 616  
  
*Neogloboquadrina praeumerosa*, 106  
*Neogloboquadrina acostaensis*, 619  
*Neosphaera coccolithomorpha*, 569–571  
*Nummulites bouillei*, 40  
  
*Occitanomys adroveri*, 551  
*Operculina*, 117  
*Orbulina*, 369, 609, 610  
*Orbulina datum*, 77, 94  
*Orbulina suturalis*, 67, 69, 77, 94, 106, 353, 355, 372, 382, 396, 419, 420, 575, 610  
*Orbulina universa*, 68, 74, 75, 77, 94, 96, 106, 353, 360, 382, 396, 420, 602, 603, 610, 612, 623, 627  
*Ostrea*, 36  
*Ostrea aginensis*, 42  
*Ostrea offreti*, 31  
*Ostrea ricardi*, 31  
  
*Palaeocystodinium* sp., 259  
*Panopea*, 31  
*Paraethomys miocenicus*, 551  
*Paragloborotalia continua*, 102, 106, 230, 421  
*Paragloborotalia* ex. gr. *mayeri*, 420, 421  
*Paragloborotalia kugleri*, 131, 142, 211–213, 218, 253, 255, 256, 258, 272, 284, 286, 292, 294, 600, 607  
*Paragloborotalia mayeri*, 103, 106  
*Paragloborotalia partimlabiata*, 103, 106, 353, 355, 420  
*Paragloborotalia pseudokugleri*, 284  
*Paragloborotalia pseudokugleri*, 211, 218, 600  
*Paragloborotalia siakensis*, 420  
*Pecten beudanti*, 11  
*Pecten josslingi*, 32  
*Pecten paulensis*, 32  
*Pecten praescabriusculus*, 17  
*Pecten pseudobeudanti*, 32  
*Pecten subbenedictus*, 31  
*Pecten zizinae*, 32  
*Pectinidae*, 38  
*Peridyromys murinus*, 300  
*Peridyromys turbatus*, 300, 302  
*Pinna*, 31  
*Planorbis*, 10  
*Pollen*, 144  
*Polymesoda brongniarti*, 46  
*Pontosphaera japonica*, 565, 569–571  
*Pontosphaera multipora*, 368, 565, 569, 570, 571  
*Potamididae*, 36  
*Praeorbulina sicana*, 94  
*Praeorbulina*, 66, 69, 369, 601, 605, 610, 623  
*Praeorbulina circularis*, 94  
*Praeorbulina curva*, 41  
*Praeorbulina datum*, 67, 69, 85, 94

- Praeorbulina glomerosa*, 67, 345, 369, 575  
*Praeorbulina glomerosa circularis*, 318, 382, 396, 419  
*Praeorbulina glomerosa curva*, 318, 344, 369, 372, 382, 396, 419, 601, 610, 627  
*Praeorbulina glomerosa glomerosa*, 94, 318, 344, 382, 396, 419, 601  
*Praeorbulina glomerosa s.l.*, 318  
*Praeorbulina glomerosa sicana*, 318, 340, 341, 419, 601, 602, 610, 627  
*Praeorbulina sicana*, 28, 41, 68, 344, 368  
*Praeorbulina transitoria*, 344  
*Praeorbulina glomerosa s.l.*, 339  
*Preorbulina*, 94  
*Preorbulina datum*, 96  
*Preorbulina glomerosa sicana*, 339  
*Prolagus aff. vasconiensis fortis*, 300  
*Prolagus vasconiensis fortis*, 302  
*Psammechinus dubius*, 31  
*Pseudodryomys ibericus*, 300  
*Pseudofrondipora davidi*, 32  
*Pseudomilania lacunosa*, 571  
*Psudotheridomys*, 300  
Pteropods, 61, 121  
*Pulleniatina*, 578  
*Pulvinulina*, 106  
*Pyloedexia*, 106  
*Pyxidiella* sp., 259, 292
- Quadracythere bavarica rhodanica*, 31  
*Quadracythere polygonata*, 31  
*Quercomys bijmai*, 302  
*Quercomys daamsi*, 300, 302  
*Quercomys parsani*, 302
- Radiolaria, 137  
*Rantzieniella nitida*, 144  
*Reticulofenestra*, 287, 318, 421, 479  
*Reticulofenestra bisecta*, 141, 213  
*Reticulofenestra daviesii*, 368  
*Reticulofenestra gartneri*, 368  
*Reticulofenestra gelida*, 565, 569–571  
*Reticulofenestra haqii*, 565, 569–571  
*Reticulofenestra minuta*, 565, 569–571  
*Reticulofenestra minutula*, 565, 569–571  
*Reticulofenestra pseudoumbilica*, 30, 368, 369, 452, 565, 569–571  
*Reticulofenestra pseudoumbilicus*, 479  
*Reticulofenestra* sp., 30  
*Reticulofenestra bisecta*, 143  
*Rhabdosphaera*, 479  
*Rhodanomys*, 302  
*Rhodanomys–Ritteneria* group, 300  
*Ritteneria*, 300, 302  
*Ritteneria manca*, 302  
*Ritteneria molinae*, 302  
*Rocella gelida*, 144  
Rodentia, 300  
*Ruggiera carinata fongolini*, 31  
*Ruscinomys shaubi*, 551
- Sciadopitys*, 473  
*Scutella*, 31  
*Scyphosphaera*, 479  
*Sphaeroidinella dehiscens subdehiscens*, 106  
*Sphaeroidinellopsis*, 230, 536, 544  
*Sphaeroidinellopsis Acme-Zone*, 149  
*Sphaeroidinellopsis subdehiscens*, 106, 372, 382, 396, 578  
*Sphenolithus abies*, 479, 565, 569–571  
*Sphenolithus belemnos*, 232, 257, 288, 321  
*Sphenolithus capricornutus*, 131, 141, 257, 272, 274, 276, 607  
*Sphenolithus cf. belemnos*, 30  
*Sphenolithus* cfr., 257  
*Sphenolithus ciperoensis*, 126, 141, 211–213, 232, 287, 288  
*Sphenolithus compactus*, 257, 565  
*Sphenolithus conerae*, 292  
*Sphenolithus conicus*, 141  
*Sphenolithus delphix*, 131, 257, 272, 274–276, 607  
*Sphenolithus dissimilis*, 257  
*Sphenolithus distentus*, 212  
*Sphenolithus heteromorphus*, 67, 69, 77, 78, 89, 93, 321, 345, 368, 369, 372, 447, 449, 578, 602, 603, 605, 611, 612, 623, 627  
*Sphenolithus moriformis*, 14, 30, 479  
*Sphenolithus multispinatus*, 257  
*Sphenolithus neoabies*, 141, 257, 565, 569–571  
*Sphenolithus verensis*, 570, 571  
*Sphenolithus capricornutus*, 275  
*Sphenolithus conicus*, 257  
*Spiniferites*, 259, 292  
*Stephanochara berdotensis*, 144  
*Stephanomys*, 551  
*Stoveracysta conerae*, 137, 258, 288  
*Syracosphaera pulchra*, 479  
*Systematophora urbinii*, 258, 288
- Tapes, 31  
*Tenuitellina angustiumbilicata*, 230  
*Thalassiosira spinosa*, 144  
*Thalassiphora gonoperforata*, 259  
*Trinovantedinium capitatum*, 259  
*Trinovantedinium* sp., 259  
*Triquetrorhabdulus carinatus*, 288  
*Triquetrorhabdulus rugosus*, 479, 569, 570  
*Turborotalia multiloba*, 550  
*Turborotalia quinqueloba*, 105

*Turritella*, 34

*Turritella terebralis*, 36

*Turritella vermicularis*, 31

*Uvigerina spinicostata*, 132

*Vernus verrucosa*, 42

*Zeaglobigerina brazieri*, 231

*Zeaglobigerina connecta*, 231

*Zeaglobigerina decoraperta*, 420

*Zeaglobigerina druryi*, 231, 396, 420, 614

*Zeaglobigerina labiocrassata*, 231

*Zeaglobigerina woodi*, 231, 255

*Zygrhablithus bijugatus*, 143

## GEOGRAPHY AND GEOLOGY INDEX

- A-subduction, 182–184
- Abesse river, 40
- Abruzzi, 473
- Acqui, 61
- Adria microplate, 59
- Adriatic, 171, 172, 175, 177, 343, 409, 464, 466, 469, 473
  - foreland, 168
  - promontory, 183
  - slope, 119
- Adriatic Sea, 168, 169, 174, 175, 178, 179, 252
- Adriatique, 396
- Aeolian arc, 172
- Afghanistan, 161
- Africa, 167, 168, 363, 405
  - convergence, 120
  - continental crust, 168
  - plate, 168
- Agenian, 302, 620
  - stage, 302
- Agenian/Orléanian boundary, 310
- Agenian/Ramblian boundary, 302
- Agrigento, 113, 604
- Aguilas, 366, 369, 370
- Alboran, 627
  - gate, 159, 164
- Alboran Sea, 153
- Aldo Level, 447
- Alessandria, 78, 128
  - province, 97
- Alfina, 171
- Algeria, 627
- Alicante, 363
- Almeria, 363, 366, 367
- Alpine, 205, 313, 328
  - chain, 168, 177
  - thrust, 172
- Alpine–Apennine, 409
  - orogenic phase, 252
- Alpine–Himalayan, 405
  - system, 269
- Alps, 167, 174, 183, 435
- Alps–Apennines system, 167, 177
- Amatsu, 575
- Amatusu formation, 578
- Ancona, 313, 347, 405, 409, 412, 414–416, 440, 443, 445, 447, 532
  - Level, 415, 438, 440, 610, 612, 614
- Ancône, 395–397, 399, 401
- Anconian, 626
- Andalusia, 122
- Anno, 575
  - formation, 575, 578
- Antas, 549
- Antognola Formation, 221
- Antognola Marl, 209, 221, 224, 227
- Antognola Marl Formation, 246
- Apennine, 173, 267, 327, 328, 405–407, 531
  - basin, 252
  - fold-and-thrust belt, 182, 183, 252
  - ridge, 173
  - sequence, 267
- Apennines, 59, 183, 184, 205, 225, 227, 235, 313, 343, 409, 416, 435, 448, 476, 477, 500, 602, 625
- Apennins, 399
- Apiro, 313, 343, 474, 532, 534
- Apuane Alps, 175
- Apulian, 172
  - lithosphere, 174, 177, 180, 181
  - plate, 177, 181
- Aquitaine, 3, 4, 9, 40, 41, 43, 44, 47, 52, 55, 231, 601
- Aquitaine Basin, 24, 33, 34, 41–43, 46, 49, 50, 53, 55, 61, 69, 94, 622
- Aquitania historical stratotype, 9
- Aquitanian, 3, 10, 14, 31, 33, 34, 38, 41, 48, 50, 52, 61, 176, 177, 210, 218, 225, 227, 230–232, 244, 245, 249, 260, 265, 267, 272, 277, 280, 292, 294, 409, 598, 599, 607, 608, 618
- Aquitanian boundary, 55
  - stratotype, 9, 14, 41, 43, 44, 47, 53, 55
- Aquitanian/Burdigalian boundary, 53, 286, 292
- Aquitanian Stage, 15, 41, 125, 145, 620
- Aquitanian–Burdigalian, 10, 621, 622
- Aquitanian/Burdigalian boundary, 13, 46, 206, 243, 255, 265, 272, 276, 310
- Aquitanian/Burdigalian Stage boundary, 240
- Aquitanian–Orleanian stage, 620
- Arabia, 157, 159
  - block, 161
  - gates, 161
- Arabian Platform, 161
- Arabian Shield, 161, 163
- Arabian–Persian Gulf, 163
- Aragón Province, 297

- Aragonian, 300, 308, 620  
   unit, 299  
 Aral Sea, 161  
 Arasaki, 566  
   section, 566  
 Arcevia, 279  
   Level, 280, 281  
 Archidona, 369  
 Arenacea, 176  
 Arenazzolo, 476  
   formation, 464  
 Argille Azzurre formation, 475  
 Argille scagliose, 114, 221, 227  
 Arguello, 72  
 Arguello-Lequio, 75  
 Arikareean, 144  
 Arno river, 174  
 Ascoli Piceno, 532  
 Asia, 157, 159  
 Assouan, 187  
 Astaracian, 299  
 Astian, 59, 107  
 At Bosio, 600  
 Athens, 125  
 Atlantic, 42, 47, 55, 84, 113, 120, 149, 151  
   super-basin, 157  
 Atlantic Ocean, 111, 117, 119, 149, 157, 164  
 Atlantic–East Pacific connection, 159  
 Atlas, 183  
 Australia, 157, 255, 431  
 Avignon, 34, 36  
  
 B-subduction, 182  
 Baba, 386, 388–392, 396, 397, 399, 402  
 Baba Tuff, 376, 377, 381, 382, 384–386  
 Backbone Ranges, 196  
 Balear Sea, 205  
 Bango, 560  
 Barqueros, 367, 549, 550, 621  
 Barrovian metamorphism, 176  
 Basin and Range, 175  
 Belbo, 61  
 Berkeley, 330, 340, 341, 348, 396, 400, 410, 431,  
   448, 586, 593, 594, 610  
 Bernachon, 34, 41, 46, 47  
   section, 47  
 Betic, 367–369  
 Betic Cordilleras, 314, 363, 364  
 Betic–Riff straits, 111  
 Betic–Rifian Basin, 627  
 Betics, 363  
 Bisciario, 221, 252, 253, 260, 265, 267, 272, 275,  
   282, 284, 317, 318, 337, 339, 343, 409  
 Bisciario Formation, 177, 205, 206, 222, 249, 250,  
   280, 281, 315, 317, 440  
  
 Bisciario-Schlier, 317  
 Bismantova Formation, 221, 224  
 Bistagno, 61  
 Black Sea, 161, 163  
 Black Shales, 417  
 Bollène–Pierrelatte, 25  
 Bollène–Saint–Restitut, 25  
 Bologna, 125, 209, 214, 222, 224, 244, 477,  
   622  
 Borbera, 75  
 Borbera–Staffora facies, 128  
 Bordeaux, 9, 17, 33, 40, 46, 600, 602  
   area, 601  
 Bordelais, 17, 24, 32  
 Borgo Tossignano, 120  
 Bormida, 61  
   river, 65, 90  
   valley, 61  
 Bormidian, 59, 61  
 Bosa, 317  
 Bosio, 213, 218, 607  
   section, 209–212, 214, 600  
 Boso, 553, 573  
   sequence, 575  
 Boso Peninsula, 199, 371, 407, 558, 575, 624  
   sequence, 578  
 Bou Regreg section, 149, 153, 154  
 Bratislava, 70, 73  
 Bricco del Moro, 61, 89, 93  
   section, 67, 90, 94  
 Bricco della Croce section, 61, 89, 90, 93, 94  
 Brico del Moro, 601  
 Bubbian, 59  
 Bucharest, 154  
 Budapest, 125  
 Burdigala, 17, 602  
 Burdigalian, 3, 11, 17, 20, 23, 24, 31–33, 36, 38,  
   42, 46, 48, 50, 59, 61, 66, 69, 70, 94, 159,  
   161, 171, 174–177, 180, 181, 206, 207, 210,  
   221, 227, 230, 244, 252, 256, 260, 267, 269,  
   277, 292, 294, 308, 313, 315, 325–327, 339,  
   340, 347, 348, 351, 363, 366–369, 415, 433,  
   598–602, 605, 607–609, 619–621  
   historical stratotype, 17, 25  
 Burdigalian/Langhian, 370  
 Burdigalian/Middle Miocene contact, 20  
 Burdigalian Saint Restitut Molasse, 30  
 Burdigalian Stage, 46, 53, 69  
 Burdigalian stratotype, 32, 36, 41, 48, 49, 53, 55  
 Burdigalian transgression, 28, 46  
 Burdigalian–Langhian, 315, 340  
 Burdigalian/Langhian boundary, 47, 313, 318, 339  
  
 Cabezo Baeza, 549  
 Cabo de Gata, 366

- Cabo de Gata Group, 366, 547  
 Calabria, 177, 183, 493  
 Calamocha, 300  
 Calcaire à Astéries, 13, 34  
 Calcare di Base, 116, 463, 498, 521  
 Calcareous Molasse, 30  
 California, 196, 327  
 Caliguera, 547, 548  
 Calizas de Peñalba, 297, 298  
     unit, 300  
 Caltanissetta, 107, 351  
 Cambridge, 43  
 Campaolo Formation, 222  
 Camporotondo section, 536  
 Canadian Cordillera, 184  
 Cantiano, 315  
 Capo Rossello, 113, 149, 544, 604  
     sections, 618  
 Capodarso, 521  
     section, 108, 112  
 Capodorso, 603  
 Carboneras, 366, 547  
     fault, 366, 367  
 Caribbean, 164  
 Caribbean Lithospheric Seuil, 159  
 Caribbean Seuil, 164  
 Carmona section, 153  
 Carosio–Lemme section, 286  
 Carpathians, 183  
 Carrosio, 128, 210, 218, 599, 600  
     section, 205  
 Carrosio–Lemme, 258  
     section, 253, 256, 257, 259, 272, 274, 284, 600,  
     607  
 Cartagena, 367, 549  
     area, 549  
 Casa di Tosi section, 209  
 Case Carrezzani, 128  
 Case Liardo, 351  
 Caspian Basin, 161, 163  
 Cassinasco Formation, 65, 77, 89, 90, 93  
 Castellania, 97  
 Castellania Formation, 98, 103  
 Castellania–Rio Mazzapiedi section, 82  
 Castellanian, 59  
 Castello di Falconara, 114  
 Catalayud–Teruel Basin, 297, 299, 300, 302  
 Caucasian Stage, 145  
 Cava Predosa, 222, 246  
     section, 228, 230, 233, 237, 245  
 Cavolo, 416  
     marker, 414, 415  
     sandstone, 414  
 Cenozoic, 59, 77, 157, 269, 297, 328, 405, 498  
 Central Afghanistan, 161, 163  
 Central Alps, 168  
 Central Apennines, 245, 402, 466, 531, 542  
 Central Italy, 126  
 Central Japan, 192, 575  
 Central-northern Apennines, 119  
 Cerro del Marques, 368  
 Cervarola formation, 222  
 Cervarola–Trasimeno thrust, 178  
 Cessole, 59, 61, 66, 69, 89  
 Cessole Formation, 61, 70, 89, 601, 602  
 Cessole Marls, 61, 67, 77, 89, 90, 93, 94  
 Cessolian, 59  
 Cetina de Aragón, 302  
 Ceva, 61  
 Chapel Hill, 431  
 Château Olivier, 38  
 Chattian, 34, 38, 40–44, 49, 50, 52, 125, 206, 249,  
     260, 267, 272, 277, 294, 599  
     series, 55  
     stratotype, 49  
 Chattian Stage, 145  
 Chattian/Aquitanian boundary, 43, 48, 53, 272,  
     274, 275  
 Chattian/Aquitanian Stage, 55  
 Chron 6Cn in Carrosio–Lemme, 607  
 Cinerea, 206  
 Circum-Tyrrhenian orogenic belts, 182  
 Colle Gallo, 536, 543  
 Colli Euganei, 205  
 Colombacci, 531, 534  
     formation, 412, 464, 472–475  
     s.l., 476  
 Colombine, 177  
 Cònero, 313, 314, 327, 343, 348, 396, 406, 416,  
     445, 448  
 Cònero River sequence, 269  
 Cònero Riviera, 405, 409, 412, 415–417, 436, 445,  
     610–612, 614, 616, 623–626  
     sequence, 619  
 Cònero Schlier formation, 447  
 Contessa, 177, 218, 258–260, 262, 294, 325, 327,  
     339, 621  
     composite section, 256, 258  
     section, 49, 50, 207, 213, 218, 258, 259, 274,  
     280, 286, 288, 291, 292, 607, 608, 618  
     sequence, 249, 265, 267, 275  
 Contessa Highway, 249, 272  
     section, 53  
 Contessa Quarry section, 249, 253, 256, 257, 272,  
     274  
 Contessa Quarry–Contessa Testimone section,  
     255–257, 265  
 Contessa Quarry–Contessa Testimone–Contessa  
     Valderchia section, 253, 263  
 Contessa Testimone section, 249, 263, 272, 608



- Contessa Testimone–Contessa Valderchia section, 252  
 Contessa Testimone–WAL, 267, 269, 276  
   levels, 263  
   volcaniclastic layers, 253  
 Contessa Valderchia, 249, 275  
   section, 256, 272  
 Contessa Valley, 206, 249, 252, 272, 276  
 Contignaco, 222  
 Contignaco Tripoli, 222  
 Coquillat, 17, 19, 20, 38  
   sands, 48  
 Corsica, 168, 172, 174, 181, 182  
   basin, 168, 177, 180  
 Corsica–Sardinia block, 168  
   174, 177  
 Corso–Sardinian microplate, 205  
 Cortemilia Formation, 65, 68, 89, 90, 94, 96  
 Cortemilian, 59  
 Costa Montada Formation, 129, 131  
 Coteau d'Avignon, 9  
 Cretaceous, 167, 206, 351, 435  
   Upper, 28  
 Crete, 466, 475, 489, 496  
 Cuatro Calas, 369  
 Cyprus, 627  
  
 Denver, 216, 236, 305, 358, 590  
 Di Tetto formation, 534, 536  
 Dinarides, 328, 435  
 Drôme, 25  
 DSDP  
   Hole 516 F, 53  
   Hole 608, 52  
   Leg 13, 149  
   Leg 132, 463  
   Site 289, 120  
   Site 575, 431  
   Site 590B, 431, 433  
   Site 608, 118  
   Site 610, 117  
   Site 611, 117  
 Duero Basin, 302  
 Duntroonian Stage, 145  
  
 Early Aquitanian, 240  
 Early Burdigalian, 243, 245  
 Early Cretaceous, 184  
 Early Miocene, 129, 168, 192–196, 199, 205, 207,  
   210, 211, 221, 225, 245, 258, 259, 299, 308  
 Early–Middle Miocene, 175  
 Early/Middle Miocene boundary, 66, 96, 161  
 Early Oligocene, 128, 214  
 Early Pliocene, 475, 479, 534  
 East Antarctic, 77  
 East Mediterranean basin, 161  
 Eastern Betic, 547, 621  
 Eastern Mediterranean, 163  
 Eastern Pontids, 161, 163  
 Eastern Tethyan sea ways, 269  
 Ebro Basin, 207, 297, 298, 300, 302, 308, 310  
 Egerian Stage, 145  
 Egypt, 187  
 El Plomo, 547  
 El Tejar, 298  
 Elba Island, 172  
 Elba–Mid-Tuscany Range, 175, 176  
 Elburz, 161  
 Elveziano, 103  
 Emilia, 112, 221  
   region, 209, 405  
 Emilia Apennines, 221, 222  
 Emilian, 447  
   region, 205  
 Emilian Apennines, 245  
 Enna, 351  
 Eocene, 142, 221, 249, 281, 347, 409  
 Epiligurid sequences, 174  
 Equatorial Atlantic, 256, 286  
 Equatorial Central Pacific, 431  
 Equatorial Pacific, 255  
 Eraclea Minoa sections, 149  
 Ethiopian, 163  
 Eurasia, 120, 161, 192  
 Eurasian Plate, 199  
 Europe, 3, 128, 167, 187, 598  
 European continental crust and cover, 167  
 European Continental Stage, 144  
 European lithosphere, 177  
 European Mammal Zonation, 144  
 Euxinic Pelites, 417, 498  
 Euxinic Shale, 412, 417, 464, 531  
   formation, 343, 448, 465, 466, 469, 475  
   unit, 422, 435  
 Evaporites, 469, 477  
  
 Faenza, 405, 406, 410, 416, 493, 521, 589, 614–  
   616, 625, 626  
   area, 617  
 Faenza–Imola, 493  
 Falconara section, 84, 114, 119, 122, 625  
   formation, 222  
 Falterona–Trasimeno tectonic unit, 175  
 Falun de Thibaudeau, 38  
 Faluns, 38  
 Faluns de Saucats, 36  
 Fars, 159  
 Fish Canyon Tuff, 440  
 Fontanelice, 451  
   member, 177

- Fontbonau, 601  
 Force, 534, 536  
 Formación Sariñena, 297  
 Formazione di Tetto, 473, 531  
 Fortuna, 367  
 Fossa Magna, 553  
 Fossanian, 59  
 France, 33, 69, 94  
 Fujiki, 397
- Garbagna section, 213  
 Gata, 366, 367, 369, 370  
 Gavi, 59, 74, 128  
 Gela, 114  
 Gela Nappe, 116  
 Genova, 60, 128  
 Geomagnetic polarity time scale (GPTS), 477, 496  
 German, 43  
 Germany, 49  
 Gessi, 463  
 Gessi Inferiori, 476  
     formation, 464, 469  
 Gessi Superiori, 473, 476  
     formation, 464, 473, 475  
 Gessoso Solfifera, 412, 531  
     formation, 113, 177, 409, 416, 464, 469, 472, 475, 476, 498, 604  
 Ghioli di Letto, 416  
 Ghioli or Formazione di Letto, 465  
 Gibraltar Strait, 269  
 Gironde, 9, 17  
 Global Boundary Stratotype Section and Point, 496  
 Global Stratotype Point (GSP), 6  
 Global Stratotype Section and Point (GSSP), 4–6, 57, 274, 496, 519, 600, 604, 605, 607, 621–625  
     Carrosio–Lemme, 256  
     Lemme–Carrosio section, 142  
     Miocene, 143  
     Miocene/Pliocene boundary, 153  
     Oligocene/Miocene boundary, 125, 126, 130, 143  
     Palaeogene/Neogene boundary, 126, 128, 130  
     Tortonian–Messinian, 121, 122  
 Gonfolite Group, 177  
 Gorgona–Pianosa Ridge, 171  
 Granada, 125  
 Great Caucasus, 161  
 Greece, 125, 126, 466  
 Greenwich, 315, 339  
 Guadalquivir basin, 153  
 Gubbio, 206, 249, 252, 280, 343, 409, 621  
 Gulf Coast, 145  
 Gulf of Aden, 163  
 Gulf of Mexico, 47, 49
- Gypsum, 116
- Hackberryian Stage, 145  
 Hadruk-Had Formation, 161  
 Haraichi, 371  
 Haraichi Formation, 377, 382  
 Haratajino, 371  
 Haratajino Formation, 382  
 Hasse Formation, 555  
 Hayama Group, 555  
 Hellenides, 183  
 Helvetian, 70  
 Himalayan, 313  
 Hinojar, 367  
 Hokkaido, 187  
 Huesca fluvial system, 297  
 Hyblean foreland, 473
- Iberia, 363  
 Iberian Peninsula, 297  
 Iberian Range, 297  
 Idozawa, 371  
 Idozawa Formation, 382  
 Ikego Formation, 555  
 Il Trave, 409  
 Imola, 120, 451, 493  
     area, 121  
 Indian, 157, 469  
     subcontinent, 85  
 Indian Ocean, 159, 161, 163, 256, 286  
 Indian–Mediterranean connection, 161  
     sea-ways, open, 163  
 Indonesian–Australian Lithospheric Seuil, 159  
 Indonesian–Australian Seuil, 164  
 Integrated stratigraphy, 597  
 Ionian, 464  
 Ionian Sea, 183  
 Iran, 161  
 Irieno, 378  
 Isthmus of Panama, 159  
 Itahana, 371  
 Italian, 601, 616, 617  
     continental crust, 167  
 Italian Peninsula, 172  
 Italie, 395  
 Italy, 3, 50, 55, 66, 70, 85, 89, 118, 125, 126, 149, 182, 183, 187, 249, 257, 314, 315, 343, 395, 401, 407, 409, 451, 475, 477, 493, 498, 521, 531, 601, 602, 606, 614, 618, 620, 624  
 IUGS-Subcommission on Neogene Stratigraphy, 604  
 Ivrea Zone, 183  
 Iwadono, 371, 376, 377  
 Izu-Bonin, 196  
     arc, 192

- Japan, 157, 187, 193–196, 198, 199, 314, 371, 378, 379, 381, 384, 392, 402, 407, 553, 575, 612–614, 624, 627  
   arc, 196  
   trench, 199  
 Japan Basin, 192  
 Japan Sea, 192, 195, 199  
 Japanese, 624  
   archipelago, 187  
   islands, 187, 188, 191, 192, 194, 199, 575  
 Japanese Miocene, 583  
 Japon, 395, 397, 399, 401  
 Jumilla, 367  
 Jurassic, 157, 409, 433  
  
 Kakegawa area, 199  
 Kamogawa area, 575  
 Kanigawa, 575  
   formation, 578  
 Karasuyama, 371, 378, 379  
   sequence, 624  
 Khur, 161  
 Kinone, 575  
 Kinone Formation, 624  
 Kitamura, 385, 388, 390–392, 395–397, 399, 402  
 Kitamura Tuff, 375, 377, 381, 382, 384, 386, 390, 613  
 Kiyosumi, 575  
   formation, 575, 578  
 Kobana, 378  
 Kopet Dagh, 161  
 Kurotaki Unconformity, 575  
 Kyoto, 125  
  
 L'Annunziata, 343, 348  
   Level, 447  
   section, 609  
 L'Arie, 9, 10, 14, 34, 36, 46, 47  
   section, 13  
 L'Eau Blanche, 17  
   river, 38  
   valley, 38  
 La Bourasse, 11  
   section, 36  
 La Brède, 9, 14, 33, 34, 36, 38  
 La Coquilleyre section, 36  
 La Galocha, 302  
   fauna, 302  
 La Sardella, 414, 417, 625  
   section, 422, 448, 616, 626  
 La Serrata, 369  
 La Sime, 20, 601  
 La Vedova, 412, 414, 419  
   section, 422  
 Lafaurie, 41  
  
 Laga, 179  
   flysch, 178  
 Laga Basin, 178  
 Lago mare, 112  
   biotope, 113  
 Lake of Van, 161  
 Lamproites complex, 547  
   group, 367  
 Lanaja, 298, 303, 305, 308  
 Lanaja–Peñalba area, 297  
 Landes, 40  
 Langhe, 61, 128  
   region, 59, 77, 89  
 Langhian, 3, 40, 41, 47, 61, 66, 69, 70, 77, 85, 89, 90, 93, 171, 175, 176, 178, 180, 252, 269, 313–315, 325–327, 339, 340, 343, 345, 347, 348, 360, 366, 367, 369, 405, 409, 412, 416, 421, 433, 445, 447, 598, 599, 601–603, 605, 609–612, 619, 623, 624, 626  
   GSSP, 66, 69, 96  
   historical stratotype, 89  
   Michelangelo Level, 609  
   stage, 67, 69, 89  
   stratotype, 57, 59, 66, 67, 89, 93, 94  
 Langhian–Serravallian, 360, 369, 370, 422  
 Langhian/Serravallian boundary, 73, 78  
 Larderello, 171  
 Lassime, 42  
 Lassus, 34, 41  
 Late Aquitanian, 241  
 Late Eocene, 59, 128, 175, 205  
 Late Jurassic, 184  
 Late Miocene, 84, 113, 117, 119, 128, 164, 171, 197  
 Late Oligocene, 34, 128, 175, 211, 213, 214  
 Late Oligocene–Early Miocene, 168  
 Late Pliocene, 180  
 Late Tortonian, 180  
 Late Turolian, 621  
 Late Vallesian, 620  
 Latium, 171, 451  
 Lausanne, 216, 236, 358, 361, 457, 539, 589, 594  
 Le Bragas, 41  
 Le Coquillat, 40  
 Le Langhe, 601  
 Lemme, 599, 600  
   section, 210–213, 218, 258  
 Lemme Valley, 210  
 Lemme–Carosio section, 126, 128, 138, 141, 142  
 Léognan, 17, 19, 20, 23, 33, 36, 38, 40, 42, 46  
 Lepri section, 230  
 Lequio, 72  
 Lesser Antilles, 627  
 Librilla, 621  
 Licata, 114

- Ligurian, 128
  - nappe, 221
  - phase, 59, 168
- Ligurian-Piedmont oceanic crust, 168
- Ligurid nappe, 176, 178
- Ligurids, 168, 175, 176, 179
- Limestone, 521
- Livello Piero della Francesca, 317
- Lord Howe Rise, 431
- Los Escullos, 366
- Los Terreros, 366, 369
- Louvière, 38
- Lower Miocene, 44, 49, 50, 53, 55, 117, 193, 206, 212, 222, 225, 227, 253, 255, 258, 265, 267, 275, 284, 288, 290, 294
- Lower Pliocene, 107, 117, 178
- Lower Tertiary, 182
- Lower–Middle Eocene, 168
- Lut, 161
  
- Maastrichtian, 157
- Maccarone, 457, 534, 536, 543, 544, 618
  - section, 474, 531, 532, 534
- Macigno, 176–179
  - foredeep, 175, 176
- Maghrebian, 494
- Makran subduction zone, 161
- Marche, 205, 294, 343, 407, 416, 417
  - region, 209, 279, 313, 315, 405, 409, 474, 531, 618
- Marche Apennines, 221
- Marche Province, 457
- Marche–Adriatic region, 171
- Marchean–Romagnan foredeep, 175
- Marne a Globigerine, 116
- Marne a Pteropodi, 466
- Marne di Rigoroso, 210
  - formation, 209, 211, 214
- Marne Selcirose, 221, 244, 245
- Marne Selcirose Member, 227
- Marne Tripolacee, 466
- Marnoso, 176
- Marnoso-Arenacea, 175, 178, 179, 343, 409, 460
  - flysch, 252, 412
  - basin, 177
  - formation, 451, 475, 493, 498
- Mazarrón, 367, 548, 549
  - basin, 548
- Mazarrón Group, 367, 547–549
- Mediterranean, 31, 49, 50, 57, 66, 69, 70, 73, 77, 82, 84, 96, 107, 111–113, 117–120, 122, 126, 137, 150–153, 157, 159, 164, 183, 212, 222, 232, 255, 256, 284, 286, 313, 318, 321, 328, 340, 353, 360, 366, 405, 416, 417, 419, 422, 425, 433, 436, 445, 452, 454, 463, 464, 466, 472, 480, 489, 493, 495, 496, 498, 500, 547, 602–604, 616, 618, 620, 621, 623, 625–627
  - area, 81, 100
  - basin, 120
  - mafic volcanism, 205
  - Neogene, 480
  - region, 93, 149, 157
  - salinity crisis, 111–113, 120, 121
  - zonal model, 253
- Mediterranean–Atlantic connection, 159
- Mediterranean/Atlantic passageways, 120
- Mediterranean Sea, 109, 149, 163, 469
- Mediterranean Seuil, 159
- Mediterranean Tethys, 163
- Mega P, 282
- Menlo Park, 280, 425
- Meseta, 363
- Mesozoic, 182, 267, 269, 297, 328, 363, 405
- Mesozoic–Palaeogene, 177
- Messina, 107
- Messinian, 3, 79, 82, 84, 111, 112, 119, 150, 159, 164, 175, 177, 178, 180, 269, 313, 343, 351, 366, 367, 405, 407, 410, 412, 415–417, 419, 421, 429, 431, 433, 435, 436, 445, 448, 451, 454, 457, 462–464, 466, 467, 469, 472, 473, 475–477, 480, 489, 493–498, 500, 507, 515, 519, 521, 527, 529, 531, 534, 536, 542, 547–550, 566, 598, 599, 603–605, 614–618, 620, 621, 625, 626
  - <sup>13</sup>C negative shift, 122
  - neostatotype, 112, 113
  - salinity crisis, 149, 152
  - seawater, 120
  - stratotype, 107
- Messinian Euxinic Shale, 409
- Messinian/Pliocene, 473, 475
- Messinian Stage, 107, 152
- Messinian–Zanclean, 407
- Michelangelo, 347, 348
  - Level, 343, 347, 348, 447
- MICOP, 519
  - projects, 498
- Mid-Burdigalian, 206, 249
- Mid-Miocene, 249
- Mid-Miocene event, 77
- Mid-Oligocene, 218
  - sea-level drop, 267
- Middle Early Miocene, 258, 259
- Middle Burdigalian, 280
- Middle East, 163
- Middle Eocene, 175, 297
- Middle Miocene, 59, 69, 70, 84, 89, 119, 164, 168, 169, 176, 180, 187, 196, 199, 225, 299, 308
- Middle Pliocene, 180

- Milano, 125
- Miocene, 10, 13, 15, 43, 52, 57, 61, 65, 78, 93,  
117, 125–127, 130, 141, 142, 145, 157, 159,  
163, 168, 177, 187, 192, 194, 196, 205, 218,  
221, 249, 281, 287, 297, 298  
volcanism, 252
- Miocene Epoch, 3, 5, 167
- Miocene Series, 55, 86
- Miocene/Pliocene boundary, 113, 122, 149–152,  
154
- MIOMAR, 519  
projects, 498
- Misaki Formation, 555, 556
- Miura, 555, 573
- Miura Group, 566, 573
- Miura Peninsula, 371, 407, 553, 555, 558, 560,  
561, 566, 573
- Miyakawa, 555, 566  
section, 566
- Miyakawa Bay area, 573
- Moesia, 163
- Moho, 171, 172, 178, 184
- Moirá, 339
- Molare Formation, 128, 129
- Molasse ossifère, 38
- Montbrison, 30
- Montbrison-Fontbonau, 25, 28, 31
- Monte Amiata, 171
- Monte Arligo  
area, 209  
section, 232, 235, 236, 240, 244, 245, 246
- Monte Cantigaglione, 114
- Monte Cervarola Formation, 176
- Monte Cetona, 175, 178, 181
- Monte Cònero, 417, 448
- Monte Cònero Riviera, 409
- Monte dei Corvi, 347, 395, 401, 412, 414–417,  
420, 445, 447, 612, 623  
high cliff section, 422 section, 610, 611,  
614, 624
- Monte del Casino, 118, 121, 122, 406, 407, 454,  
460, 462, 483, 484, 498, 518, 519, 616, 625  
section, 451, 466, 467, 477, 479, 480, 486, 489,  
500, 515, 518, 519, 521, 529, 625
- Monte del Casino I, 459, 516
- Monte del Casino II, 507
- Monte della Nave, 419
- Monte Falterona Formation, 176
- Monte Giammoia, 351–353, 355, 361, 457  
section, 610
- Monte Petrano, 315
- Monte Tondo, 118, 121, 122, 406, 407, 451, 454,  
460, 462, 481, 484, 489, 498, 501, 507, 516,  
519, 616, 625  
section, 466, 477, 479, 480, 486, 500, 516, 518,  
521, 529, 625
- Monterey Formation, 196, 327
- Monti Berici, 205
- Monti Lessini, 205
- Moria, 313, 315, 317, 318, 321, 325, 327, 330,  
335, 337, 340, 343, 345, 347, 589, 610  
section, 50, 206, 263, 269, 281, 594, 609, 622,  
623
- Morocco, 149, 152, 153, 544, 618
- Moulin d'Augéy, 34, 44
- Moulin de Bernachon, 9, 10, 14  
section, 13
- Moulin de l'Eglise, 9, 36, 47
- Moulin de la Maule, 34
- Moulin de la Mole, 34
- Moulin du Battant, 34
- Moulin du Bois Partus, 34
- Moulin du Malcomptant, 34
- Mouline de L'Ariey, 47
- Mt. Ogusu, Yokosuka City, 560
- Murcia, 367, 548, 550, 621
- Nagai, Yokosuka City, 556
- Nansei Shoto islands, 187
- Navarrete del Rio, 300, 302
- Neogene, 9, 57, 70, 85, 114, 116, 125, 126, 128,  
143, 149, 161, 175, 187, 191, 194, 199, 363,  
371, 452, 497, 575  
GSSP, 145
- New Caledonia, 431
- New Zealand, 145, 431, 495
- Nile River, 187
- Niwaya, 371
- Niwaya Formation, 382, 624
- North Africa, 159
- North America, 145, 157, 494, 497
- North American land mammal ages, 144
- North Atlantic, 47, 255
- North Atlantic Ocean, 118
- North Carolina, 431
- North Morocco, 627
- Northeastern Apennines, 257
- Northeastern Japan, 192, 199  
arcs, 192
- Northern Italy, 112
- Northern Apennine Ridge, 169, 180
- Northern Apennines, 120, 121, 128, 167, 168,  
171–174, 178, 181, 182, 209, 313, 425, 464,  
466, 469, 475, 493, 494, 496, 498, 500, 502
- Northern Europe, 145
- Northern Italy, 126, 128, 209, 221
- Northern Japan, 188, 199
- Northern Morocco, 118
- Northern Tyrrhenian Sea, 169, 172, 174, 180

- Northwest Pacific, 197, 578  
 Northwestern Italy, 97, 128, 253, 257, 284  
 Nyons, 25
- Obata, 371  
 Obata Formation, 382  
 Oceans, 157  
 ODP  
     Hole 608, 52  
     Hole 747A, 52  
     Site 654, 119, 120, 489  
     Site 846, 152  
 Ogane, 378  
 Ohashi, 376  
 Oligocene, 28, 49, 159, 175, 205, 206, 210, 218,  
     221, 253, 267, 284, 298, 363, 440, 599, 600,  
     606, 607, 621, 626  
 Oligocene–Miocene, 267  
     transition, 257, 258  
 Oligocene/Miocene boundary, 126, 127, 141, 142,  
     176, 206, 209, 211–214, 218, 221, 227, 231,  
     244, 253, 256, 259, 272, 274, 284  
     boundary GSSP, 145  
 Oman mountain belt, 161  
 Ooura, 566  
     section, 566  
 Orléanien, 299  
 Orogens, 205
- Pabdeh Formation, 159  
 Pacific, 47, 118–120, 620  
     oceans, 157  
     plates, 192  
     subduction zones, 192  
     super-basin, 157  
 Pacific Ocean, 159  
 Pacific Plate, 199  
 Pacific–Indian connection, 159  
 Palaeogene, 205, 206, 351  
 Palaeogene–Neogene, 125–127, 141–143  
     GSSP, 145  
 Palaeogene/Neogene boundary, 125, 218, 253  
     stratotype, 125  
 Palcano, 315  
 Paleocene, 297  
 Pangea, 157  
 Paratethyan, 340, 473  
 Paratethyan Pontian Stage, 494  
 Paratethys, 107, 111, 126, 145, 161, 163, 269, 328  
 Paris, 125  
 Parma, 125  
 Parma Apennines, 222  
 Pasquasia section, 113, 604  
 Pasquasia–Capodarso, 108  
 Pasquasia–Capodarso section, 107, 109, 111–113,  
     121, 122, 603, 625  
 Passo di Piazza, 351  
 Pavia, 589  
 Peloua, 10  
 Péloua section, 36  
 Pennidic, 128  
 Peñalba, 298, 303, 305  
 Peri-Adriatic area, 173  
 Perletian, 59  
 Perugia Mesozoic Massifs, 178  
 Pesaro, 416, 543  
 Pesaro–Ancona, 498  
 Pessac, 17  
 Pessac–Magonty section, 40  
 Phanerozoic, 597  
 Phanerozoic Time Scale (PTS), 493  
 Philippine Sea Plate, 199  
 Philippine Sea plates, 192  
 Philippines, 627  
 Pied Cros, 28  
 Piedmont, 4, 89, 113, 121, 218, 606, 607  
     region, 3, 59, 61, 601  
 Piedmont Basin, 59, 70, 72, 126, 209, 221, 257  
 Piedmont Tertiary Basin, 128  
 Piémont, 401  
 Piero della Francesca, 329, 330, 333, 335, 340,  
     341, 347  
     Level, 263, 281, 294, 610  
 Pierre du Midi, 30  
 Pietralacroce, 419, 447  
 Pieve di Gesso, 406, 462, 501, 519, 529, 616  
     section, 451, 452, 454, 458, 461, 615  
 Pirègues, 19  
 Pisa, 171, 333, 340, 593, 594, 610  
 Pise, 341  
 Pleistocene, 57, 180, 199, 463, 472, 493, 575  
 Plio-Pleistocene, 363, 466, 531  
 Pliocene, 57, 107, 111, 112, 125, 149, 150, 152,  
     153, 168, 171, 175, 177–180, 199, 221, 224,  
     396, 405, 407, 463, 464, 493–495, 531, 534,  
     536, 544, 555, 567, 575, 604, 617, 618  
     Blue Clay, 534  
     Series, 61  
     transgression, 111, 113  
 Po River, 221  
 Po Valley, 168, 178  
 Pont de Lassus, 34  
 Ponte delle Lepri, 237, 243, 245, 246, 622  
     section, 224, 227, 228, 234, 242, 245  
 Pontedazzo, 315  
 Ponti, 61  
 Pont-Pourquey, 17, 20, 23, 24, 42, 46  
     Lassime sections, 48  
 Premilcuore member, 177

- Present, 157  
 Prieuré, 28  
 Pteropod Marls, 61, 89  
  
 Quaternary, 297  
 Qum Basin, 161  
  
 Raffaello, 267, 269  
     Level, 218, 249, 253, 263, 275, 276, 280, 292,  
     294, 607  
 Rambla de Granadilla, 367, 368  
     section, 623  
 Ramblian, 207, 300, 302, 308, 310, 620  
 Ramblian Spanish, 620  
 Ramblian Stage, 144  
 Razak Formation, 163  
 Realmonte, 113, 604  
 Recent, 42, 187  
 Red Sea, 119, 161, 163, 469  
 Red Sea–Gulf of Aden corridor, 163  
 Respighi, 396, 438, 440  
     Level, 414, 438, 440, 447, 610–612, 614  
 Rhodanian, 25  
     basin, 31  
 Rhône Valley, 3, 4, 17, 32, 50, 55, 600, 601  
 Rifian, 111  
 Rigoroso Formation, 128, 129  
 Rio Castellania, 78, 97  
 Rio Mazzapiedi, 78, 97  
     section, 97  
 Rio Mazzapiedi–Castellania, 603  
     section, 74, 78, 82, 84, 97, 103, 104, 603  
     valley, 98  
 Rio Mazzapiedi–Rio Castellania section, 79  
 River Lemme, 211  
 Riviera, 419  
 Rocchetta formation, 209  
 Rodalquilar, 366  
 Roldan, 366  
 Romagna, 118, 121, 122, 178, 222, 451, 473, 476,  
     477, 493, 498, 519, 521  
     Apennines, 406, 410, 416, 498, 518  
     region, 614  
 Romagna–Marche Apennine, 168  
 Roman Magmatic Province, 171  
 Romania, 125, 126  
 Rome, 171  
 Rossini, 347  
     Level, 416, 417, 448  
 Rupelian, 34, 38, 159  
  
 S. Maria in de Carpineto, 543  
 Sagami Bay, 553  
 Sahelian Cycle, 100  
 Saint Restitut Greenish Molasse, 30  
 Saint-Jean-d'Etampes, 9, 17, 20  
 Saint-Paul-Trois-Châteaux, 25, 28, 30, 31  
     section, 132  
 Saint-Restitut, 28  
     greenish molasse, 32  
 Sajima, 566  
     section, 566  
 Salé, 153  
     section, 152  
 Salinity crisis, 152  
 Salles, 42  
     calcareous marls and sands, 30  
     formation, 31  
 Salles Calcareous Marls, 30  
 San José, 366, 547  
 San Juan, 302  
     fauna, 302  
 Sant'Agata Fossili, 78  
     formation, 98, 100, 102–104, 603  
 Sant'Agata Fossili Marls, 78, 82, 84, 100  
 Santa Croce di Arcevia, 206, 257, 279, 286, 287,  
     292, 294, 347, 622  
     Level, 281  
     section, 256, 259, 280, 282, 284, 288, 291  
 Sardella section, 414, 415, 421, 431  
 Sardella trail, 419  
 Sardinia, 177, 205, 227, 252, 317  
     microplate, 181  
 Sardinian basins, 225  
 Sardinian provenance, 225  
 Sassoferrato, 279  
 Saubrigues, 41  
 Saubrigues Gulf, 40  
 Saucats, 9, 10, 17, 20, 23, 33, 34, 36, 40, 42, 46,  
     53  
     Lassime outcrop, 47  
 Saucats–La Brède, 24, 53  
 Saucts–Léognan, 48  
 Scaglia Cinerea, 250, 253, 260, 262, 265, 267, 272,  
     275, 284, 287  
     formation, 249, 280, 281  
 Scaglia Cinerea/Bisciaro boundary, 265, 294  
 Scaglia Varietaga, 275  
 Scaglia-type limestones, 175  
 Scaglia Cinerea formation, 440  
 Schistes Lustrés, 168, 171  
 Schlier, 275, 317, 318, 337, 339, 343, 409, 412,  
     416, 417  
     formation, 177, 205, 206, 252, 280, 315, 317,  
     337, 343, 348, 412, 425, 445, 448, 623, 625  
 Scrivia river, 70  
 Scrivia Valley, 360, 602  
 Sea of Japan, 192, 197  
 Sequence stratigraphy, 145  
 Serra San Quirico, 279

- Serravalian, 42
- Serravalle, 59, 360, 602
- Serravalle Formation, 70, 623
- Serravalle Sandstone, 77, 82, 98, 100, 103, 602, 603
- Serravalle Scrvia, 70, 73, 84, 211
- Serravallian, 3, 20, 36, 47, 53, 59, 61, 70, 73, 77, 85, 103, 176–178, 269, 313, 314, 347, 348, 351, 352, 355, 360, 361, 363, 366, 402, 406, 409, 410, 412, 414, 420, 422, 429, 431, 436, 445, 447, 448, 457, 566, 598, 599, 601–603, 605, 610–613, 619, 623, 624, 626
  - GSSP, 74
  - stage, 77
  - stratotype, 57, 59, 72, 74, 77, 84
- Serravallian Sandstones, 73
- Serravallian Stage, 308
- Serravallian–Tortonian, 314, 401, 406, 429
- Serravallian/Tortonian boundary, 104
- Serravallien, 395, 396, 400
- Sibillini Mountains, 178
- Sicilian, 464, 604
  - area, 617
- Sicilian Falconara section, 616
- Sicilian Gessi Superiori, 473
- Sicilide Nappe, 114
- Sicily, 3, 4, 107, 112–114, 119, 122, 150, 153, 172, 314, 351, 361, 463, 466, 469, 473, 493, 494, 500, 544, 603, 604, 610, 618, 625, 626
- Sicily–Atlas orogenic belts, 183
- Sigena, 298
- Siliceous lithozone, 243, 244
- Siliceous marls, 222, 224
- Silvas Basin, 163
- Singa, 149
- Sisco basic dyke, 174
- Sisco lamproitic body, 180
- Sistema Depositional de los Monegros, 297, 298
- Sivas Basin, 161
- Slovenia, 627
- Son, 11
- South Alpine, 177
- South America, 157
- South Atlantic, 47, 256, 286
- South Fossa Magna, 573
- South Pacific, 256, 286
- South Spain, 627
- Southeastern Spain, 547
- Southern Apennines, 178, 466
- Southern France, 168
- Southern Indian Ocean, 47
- Southwest Pacific, 47, 49, 255
- Southwestern Alps, 177
- Southwestern Japan, 195, 196, 199
- Southwestern Japan arcs, 192
- Spain, 50, 118, 125, 126, 153, 159, 207, 297, 302, 314, 363, 407, 621
- Spanish, 310, 620
- St Etienne-d’Orthe, 44
- St-Jean-de-Marsacq, 41
- St-Paul-lès-Dax, 40, 42
- Stampian, 13, 34
- Stazione di Imera, 107
- Stazione Falconara, 119
- Strait of Sicily, 117
- Sydney, 125
- Tabianian, 495
- Tabiano, 107
- Tabiano beds, 107
- Tanokura, 378
- Tardienta, 298, 300, 302
  - fauna, 302
- Tertiary, 267, 297, 494
- Tertiary Piedmont Basin, 61, 85, 89, 218, 253, 284
- Tethyan, 313, 314, 315, 340, 406, 409
- Tethyan Ocean, 269, 313, 405
- Tethyan oceanic crust, 167, 183
- Tethyan sequences, 269
- Tethys, 205, 269
- Tethys basin, 159
- Tethys Ocean, 157, 161
- Tohoku, 386, 393
- Tokyo, 371, 395, 553
- Tomioka, 371, 376, 377, 381, 382, 390, 392, 395, 613, 624
  - sequence, 624
- Tongrian, 34
- Torre del Peñon, 367, 369
  - section, 623
- Torrente Olivetta, 224, 622
- Tortona, 78, 84, 107, 401, 500, 614
- Tortonian, 3, 59, 61, 70, 78, 82, 84, 85, 97, 103, 107, 109, 111–113, 121, 152, 159, 161, 163, 164, 175, 177, 178, 206, 314, 347, 363, 366, 367, 402, 405, 406, 409, 410, 412, 414, 420, 421, 429, 431, 435, 436, 445, 448, 451, 452, 454, 462, 464, 467, 480, 489, 493–495, 497, 500, 507, 515, 519, 521, 547–550, 567, 598, 599, 603–605, 612, 614, 616, 620, 621, 624–626
  - age, 425
  - GSSP, 85
- Tortonian stratotype, 57, 74, 78, 81, 82, 97, 103, 104
- Tortonian Stage, 97, 104
- Tortonian–Messinian, 406, 407, 417, 429, 475, 625
- Tortonian/Messinian boundary, 107–109, 112–114, 117, 118, 121, 122, 164
  - stratotype, 119



- Tortonien, 395, 396, 401  
 Tos Terreros beach, 369  
 Toulouse University, 43  
 Toulouzette, 42  
 Trans-Alboran, 363  
 Trave, 412  
 Triassic evaporites, 178  
 Tripoli, 114, 116, 150, 463, 500  
   facies, 603  
   formation, 109, 111, 112, 464, 466  
 Trubi, 109, 111, 113, 116  
   layers, 152  
 Trubi Marls, 544, 618  
 Trubi Formation, 113  
 Tsushima Basin, 192  
 Turkey, 163  
 Turolian, 551, 621  
 Tuscan coast, 171  
 Tuscan pre-Apennines, 173  
 Tuscan units, 168  
 Tuscany, 168, 171, 172, 174, 178, 180, 409  
 Tyrrhenian, 120, 177, 183, 473  
   lithosphere, 174  
   ODP Site 654, 117  
   region, 184  
 Tyrrhenian Sea, 168, 171, 173, 174, 177, 183, 184, 489  
  
 Uetsu district, 192, 194  
 Umbria, 171, 178, 180, 205, 294, 451, 607  
 Umbria-Marche, 252, 329, 337, 343, 409, 412, 416, 438  
   Apennines, 206, 221, 292, 317, 343, 348, 412, 416  
   basin, 257, 280, 327  
   region, 206, 225, 249, 252  
   Tertiary, 586  
 Umbria-Romagna, 177  
   area, 177  
 Umbrian, 173, 337  
   Apennines, 606  
   Contessa section, 607  
 Umbro-Marchean units, 168  
 Unidad de Zuera, 297  
 Upper Cretaceous, 175  
 Upper Eocene, 267, 440  
 Upper Jurassic, 249  
 Upper Miocene, 59, 117, 187  
 Upper Neogene, 119  
 Upper Oligocene, 227, 255, 288  
 Upper Oligocene–Lower Miocene, 261  
  
 Upper Pliocene, 119  
 Ushibuse, 371  
 Ushibuse Formation, 382  
 Utrecht, 125  
  
 Valle del Salto, 451  
 Valreas, 25  
   basin, 25  
 Vedova, 343, 348  
 Vena del Gesso, 472, 477  
 Vena del Gesso Basin, 121, 469, 493  
 Venetian Alps, 205  
 Vera, 367, 549  
 Vicchio Formation, 176, 222  
 Victoria, 255  
 Vienna, 17, 125, 126  
 Vignole, 74  
 Villafranchian, 59  
 Villalvernia, 98  
 Visone–Lemme facies, 128  
 Voltaggio, 128  
  
 Washington, 125, 126  
 West Pacific, 47  
 Western Alps, 59, 128, 168, 172  
 Western France, 3  
 Western Mediterranean, 111, 205, 252  
 Western Sardinia, 168, 281  
  
 Yamagata, 387, 393  
 Yamato Bank, 192  
 Yamato Basin, 192  
 Yemeni, 163  
 Yokosuka, 553, 561  
 Yokosuka promontory, 560  
  
 Zagros, 161, 163  
 Zagros–North Arabian Platform corridor, 163  
 Zanclean, 152, 153  
   stratotype, 153  
 Zanclian, 617  
 Zaragoza, 302  
 Zaragoza Province, 297  
 Zemorrian Stage, 145  
 Zuera Formation, 300, 308  
 Zuera unit, 300  
 Zurich, 78  
 Zushi, 561  
 Zushi Bay, 560  
 Zushi City, 560  
 Zushi Formation, 555, 559–562